NASA SP-456

B STARS
WITH and WITHOUT EMISSION LINES

MONOGRAPH SERIES ON NONTHERMAL PHENOMENA
IN STELLAR ATMOSPHERES

NASA

B STARS
WITH and WITHOUT EMISSION LINES

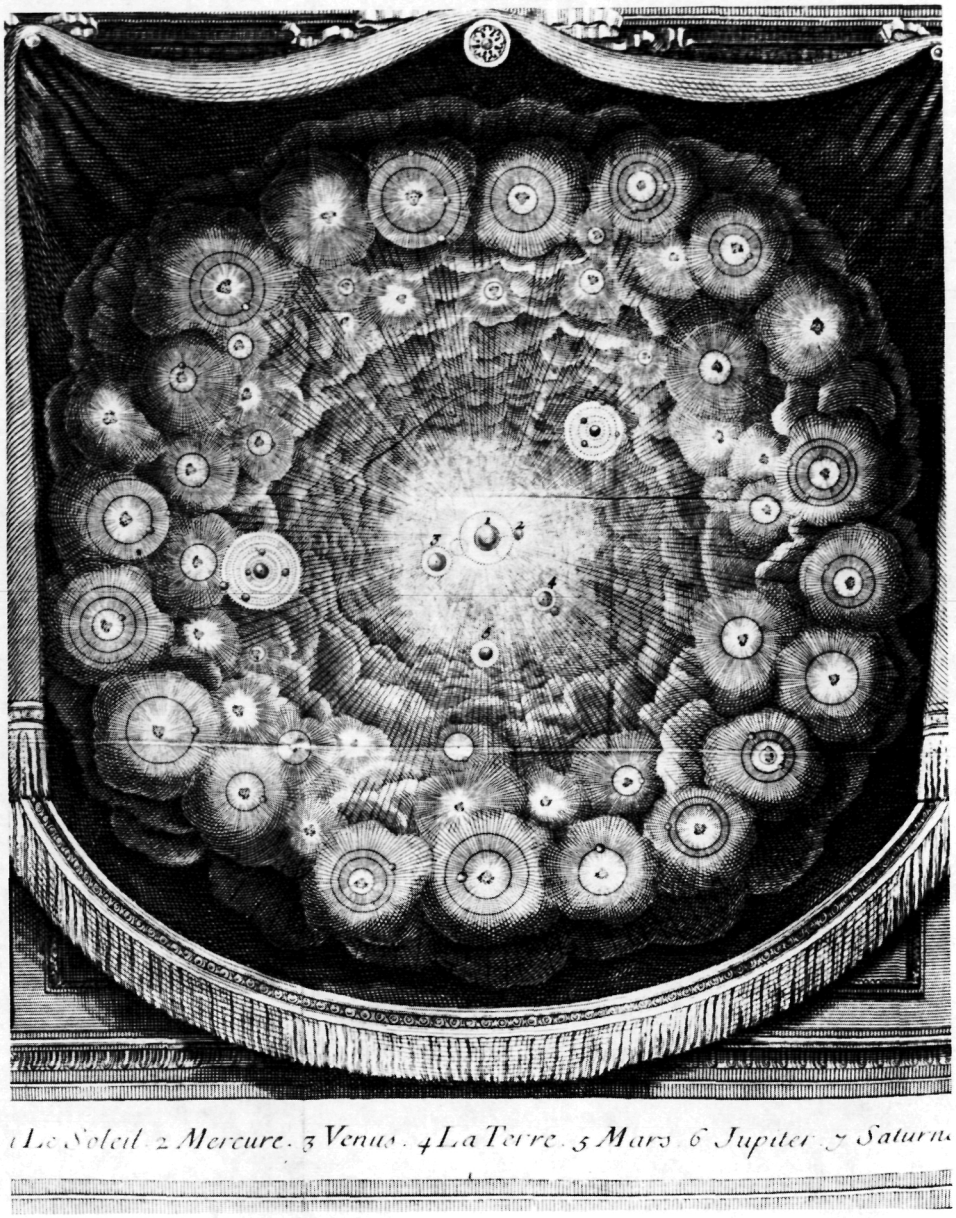

1 Le Soleil. 2 Mercure. 3 Venus. 4 La Terre. 5 Mars. 6 Jupiter. 7 Saturne

. . . Assurons-nous bien du fait, avant que de nous inquiéter de la cause. Il est vrai que cette méthode est bien lente pour la plupart des gens, qui courent naturellement à la cause, et passent par dessus la vérité du fait; mais enfin nous éviterons le ridicule d'avoir trouvé la cause de ce qui n'est point.

. . .
. . .

. . . De grands physiciens ont fort bien trouvé pourquoi les lieux souterrains sont chauds en hiver, et froids en été; de plus grands physiciens ont trouvé depuis peu que cela n'était pas.

–Fontenelle, Histoire des Oracles
Chapitre IV, pp. 20 et 23

NASA SP-456

B STARS
WITH and WITHOUT EMISSION LINES

Anne Underhill, Editor/Author Part I
Vera Doazan, Editor/Author Part II

MONOGRAPH SERIES ON NONTHERMAL PHENOMENA IN STELLAR ATMOSPHERES

Centre National de la Recherche Scientifique
Paris, France

1982

National Aeronautics and Space Administration
Scientific and Technical Information Branch
Washington, D.C.

Library of Congress Card Catalog No 82-2313

**For sale by the National Technical Information Service, Springfield, Virginia 22161*

DEDICATION

in grateful appreciation
we dedicate this series and these volumes

to *Cecilia Payne-Gaposchkin*, who, with Sergei, set the spirit of empirical-theoretical atmospheric modeling by observing the following:

> "All true variable stars have variable atmospheres, but a variable atmosphere is probably the property of all stars, whether obviously variable in brightness or not [as witness the solar envelope]";

and who, by her intimate knowledge of particular stars, pioneered in the recognition of the fundamental importance of "individuality of stellar atmospheric characteristics"

to *Daniel Chalonge*, who sought, by ingenious meticulous observations, to make quantitative the features of qualitative classical taxonomy, thereby laying the foundations for showing the inadequacy of its two-dimensional, single-region atmospheric, character,

and who always opposed the spirit of a distinguished theoretical colleague's remark

> "Don't show me those new observations of yours,
> they inhibit the range of my speculations."

Page Intentionally Left Blank

PREFACE

About one century has elapsed since the Henry Draper spectral classification scheme was introduced to try to identify physically alike kinds of stars from observational similarities in their visual spectra. The early one-letter classification has evolved into a very complex acronym with numerical subdivisions and symbols defining various kinds of peculiarity in stellar observations. During this time, our understanding of the variety of atmospheric regions which must exist to produce these peculiar spectral features has grown rapidly. The original classification was eventually interpreted in terms of an atmospheric model consisting of blackbody photosphere and a local-thermodynamic-equilibrium (LTE) reversing layer. Today, by analogy with the Sun, we recognize many layers above the photosphere which, although transparent to most visual wavelengths, have significant opacity in the far-UV, the X-ray, the infrared, and the radio spectral regimes. We recognize hot chromospheres, coronae and stellar winds, and even more extended regions such as cool emission envelopes, nebulae, and circumstellar dust clouds. Stellar classification and stellar atmospheric modeling are clearly in a stage of rapid continuing development. In particular, the farther the regions described here are found from the star, the more will their thermodynamic state be affected by nonthermal phenomena, and the less will they be controlled by the gravitational field of the star and by the local thermodynamic equilibrium associated with an extremely opaque medium.

More than two decades ago, the series *Stars and Stellar Systems* was generated under the general editorship of G.P. Kuiper. That series reviewed the status of astronomy and astrophysics at what we might call the beginning of a new era of extensive observations in the nonvisual wavelength regimes, many of them accessible only from space. We are now in the midst of this new era. These more recent observations continue to yield new insights into the outer atmospheric layers of the Sun and other stars. The new insights have forced us to reconsider the adequacy of the older HD system of classification and its classical successors, as well as of the assumptions underlying the classical theories for diagnosis and modeling of stellar atmospheres. All of these were reviewed in the Kuiper series' volume on *Stellar Atmospheres*. The present series will emphasize some of the current attempts to establish a new set of empirically based theoretical guidelines for treating stellar atmospheres. These new guidelines are intended as an elaboration of and also, where appropriate, as a revision of the classical guidelines, to permit a more comprehensive treatment which incorporates the recent new observations in a reasonable way.

To further put the current series, *Nonthermal Phenomena in Stellar Atmospheres*, in perspective in relation to the older series, *Stars and Stellar Systems*, the current series

is far less comprehensive, being restricted to stellar atmospheres and, in some cases, subatmospheric boundary conditions. However, the approach is deliberately more critical because the new ideas required to interpret the new data are still in an early and frankly controversial stage of development, while the older theories on which the Kuiper series focused were relatively "standard" at that time. These new volumes are intended primarily as a stimulus to researchers to probe the unknown, starting with the new data, and not mainly as a compendium of what was known at the inception of the space era. The earlier series served that function well. For this reason the first priority in these volumes will be a review of the highest quality data, particularly the more recent data which exhibit nonthermal phenomena. Observation of the full electromagnetic spectrum exposes to view regions of the atmosphere that are transparent to visible light. The UV spectrum reveals the structures of chromospheres and coronae, the X-ray spectrum is emitted from regions which are very hot, the IR spectrum comes from all layers, hot and cold, which are opaque to IR photons, and the radio spectrum gives evidence of both thermal emission and of energetic nonthermal processes.

In the light of these new extensions of the wavelength regimes covered by stellar spectra, conventional taxonomy provides only a very provisional labeling, useful in classical statistical studies, but insufficient to reflect the intricate nature of physical phenomena and the variety of physical parameters that control the appearance of many stellar spectra. It is also true that theoreticians had long ago generally exhausted the possibilities for modeling stellar atmospheres with only effective temperature and gravity. They have, of course, continued to introduce physical improvements in their models, such as taking account of departures from LTE, or of the ionization in convection zones, etc. But these models, which are barely adequate for unambiguous fitting of the visible spectra, fail completely when confronted by the various new features observed in other spectral regimes. Because of this failure, it is not at all clear that stars which astronomers have called peculiar in the past are, in fact, fundamentally different from stars classified as normal. Until superior models emerge, we cannot be sure that the statistically defined abnormalities are anything more than spectral signatures of large-amplitude nonthermal processes which exist with smaller amplitudes in many stars classified as normal.

In the early days of these recent observational developments, many theorists thought of the new features largely as perturbations modifying the basic classical description. For example, they tried to perturb their models slightly by adding a superficial hot layer labeled "chromosphere," and by representing parametrically the emission features at the centers of such intense spectral lines as Hα and K(Ca II). But adding layers ad hoc without considering their possible interactions with the lower regions is physically inconsistent. Whether we talk about shells, winds, or magnetic features, they must be compatible, in the framework of physical laws, with the values of the other parameters characterizing the star. It may well be, for example, that a star of $T_{\rm eff}$ equal to, say, 10^4 K cannot have a dust shell of high opacity; or perhaps it can. However, we cannot blindly accept that such dust shells can occur without full investigation of the processes by which dust grains condense, grow, and are destroyed in a given stellar environment. Nor can we accept them without asking whether the IR and radio excesses they were introduced to produce may not come from chromospheric-coronal emission instead.

Historically, the analysis of stellar spectra may be thought of as proceeding in three sequential stages. The first is based on taxonomy and rough modeling and leads to very approximate estimates of a few basic parameters, such as $T_{\rm eff}$, g, and chemical composition, while bypassing consideration of any anomalous features in the spectrum. The second is an attempt to explain each anomalous spectral feature in terms of some structural property

of the stellar atmosphere, e.g., a circumstellar shell of some temperature and density at a certain distance from the star, a warm chromosphere, or a hot corona. This leads to a provisional, parametric description of the atmosphere of a star which is often physically contradictory: one group of spectral features may require a low density shell, another a high density shell. The red supergiant α Orionis (M2 Iab) offers a good example of the anomalies that are found in this second stage of analysis. For instance, the interferometrically measured diameter is found to decrease with increasing wavelength, which is explained by dust scattering in the circumstellar shell, but this model requires that the dust be located 1-3 stellar radii from the star, whereas observations of emission at 11μ put the dust no closer than 10 stellar radii. Another example is given by the variability of some B stars, such as γ Cas, which appears at different times in three different guises—as a normal B star, as a Be star, and as a B-type shell star. Still another case is that of Sirius, which has been regarded as a bona fide A0 main-sequence star for years, but which now appears to show some spectral anomalies, possibly linked with metallicity.

The third and ultimate stage of analysis, which is an order of magnitude more difficult than the preliminary ones, aims at models of the atmosphere that will be compatible with all known facts about the star and with the laws of physics. Such models will clearly be neither in LTE nor static, and, therefore, we shall be obliged to take account of all physical processes that may be operating in the star, including some not now recognized as important by astrophysicists.

It is the intent of this series of books to help set the stage for this last step. At the very least, these monographs will try to define some types of observations to be made and some types of models to be constructed before we can approach a full understanding of stellar structure. A good example is the solar case in which we can foresee what new observational and theoretical vistas might emerge from the Solar Maximum Mission and the Solar Polar Mission. Certainly the coming of radioastronomy, infrared astronomy and space research have made it possible for us to handle the first two steps discussed above.

The principles of classical taxonomy are a necessary starting point for all parts of the HR diagram. In consequence, for each spectral type, the forthcoming volumes of this series will examine thoroughly those phenomena that are not included in the classical description. A typical problem that will be considered is the contrast between stars labeled B and Be respectively. What parameters or physical processes have been overlooked that might provide a connecting link between these two subclasses of stars? It will be argued that there may be no such thing as a peculiar B star when observed over the whole spectral range. Had we begun the analysis with the far-UV region of the spectrum, our notion of what is normal would have been quite different, and any attempt at one-or two-dimensional classification would have led to a labeling system incompatible with the HD system or its successors.

We hope that readers of these books will sense the emergence of a new point of view in stellar diagnosis and in stellar astrophysics, a global approach which assigns to the whole spectrum and to all its features the same a priori weight as a basis for diagnosis, a physical approach which tries to attract the theoretical astrophysicist to the interpretation of the observed spectra, no matter how elaborate they may be, and an approach which considers each star as a physical object to be understood, by itself, in a coherent way, not simply statistically. Because so many of the data which exhibit nonthermal phenomena have come from observations made from space, we also hope that the delineation of the above trends will be useful in planning observing programs from space in the 1980's, particularly in the UV, far-UV, and X-ray regimes, as well as in helping to coordinate these with ground-based

observing programs in the visual, IR, and radio regimes. We trust these observations will also stimulate relevant laboratory investigations.

In stressing the role of the principles of classical taxonomy above, it should be recognized that this classical taxonomy rests upon two stages of approximation. It is in these two stages that we find the clue to the distinction between thermal and nonthermal phenomena in the atmospheres of these stars. A first approximation orders the visual spectra of stars in terms of the strengths of absorption lines for any given ion, of line ratios, and essentially of the increasing degree of ionization, as one progresses from cold to hot stars. Essentially this is a temperature sequence. Assuming LTE conditions, one establishes an atmospheric model which represents these trends. Overlying a blackbody-like photosphere whose temperature is fixed by the radiative flux from the star, one has a cooler atmosphere, the reversing layer, which produces the absorption lines. This standard model underlies classical, first approximation taxonomic diagnostics. A second approximation simply separates the stars into luminosity classes being essentially an additional classification perpendicular to the first one, according to the gravity. The density in the reversing layer is fixed by the stellar gravity. A further approximation then separates all of these stars into two groups. That great majority of stars whose spectrum, under low dispersion, can be adequately classified by first-approximation taxonomy are called *normal* stars, the rest are called *peculiar* stars and characterized by a variety of peculiarities, which may differ from star to star within the same class. Most of the visual spectral features of a normal star are represented reasonably well by the standard model. Generally, the peculiar features of peculiar stars are not at all represented by the standard model. For a variety of reasons, summarized and illustrated throughout the series, many of these peculiar features are attributed to nonthermal properties of the stellar atmosphere and of the star as a whole. A knowledge of the effective temperature, the surface gravity, and the chemical composition apparently does not suffice to describe even the visual spectrum of such stars. Hence, the emphasis of this series is to contrast the normal and peculiar stars, to attempt to put into focus the nonthermal properties as contrasted to the thermal ones. The question is then asked, across the series as a whole, whether all stellar types have the same kind of nonthermal characteristics. To the extent that they do, one can then construct a model which is more encompassing than the standard one.

The preceding volume in this series was *The Sun as a Star*. The Sun is peculiar only by virtue of its proximity to the Earth, which permits the observation of relatively small scale nonthermal phenomena that would otherwise probably escape our attention. The Sun, therefore, puts into focus the kinds of nonthermal phenomena treated in this series. Because most of these peculiarites would not be easily observed if the Sun were at normal stellar distances, the Sun at such distances would undoubtedly be called a normal star.

One of the first stellar peculiarities to be observed in the visual spectrum of some stars was the presence of emission lines in place of some strong absorption lines, especially the Balmer lines of hydrogen, and particularly Hα. Such hydrogen emission lines are not confined to one classical spectral type; they are observed all across the HR diagram. It is, thus, essential to understand the implication of their presence and their relation to the occurrence of other peculiarities. The most naive interpretation of the presence of emission lines, their presence would demand that the standard model be perturbed by a temperature increasing, rather than decreasing, above the photosphere. However, such a model would demand that emission lines, rather than absorption lines, would be usually, rather than exceptionally, found, which is contrary to fact. Moreover, in hot stars like the B stars, an increase in temperature just above the photosphere decreases the number of neutral hydro-

gen atoms present, thus negating this simple viewpoint. Such an emission line anomaly was used to define an example of peculiarity in the B star class, namely the Be stars, almost at the same time that solar eclipse observations were giving evidence of the existence of a vastly extended outer atmosphere for the Sun, in about 1860. An intepretation of this B-star emission-line anomaly in terms of the existence of a similar, greatly extended atmosphere for the Be stars seems to be the first approximation to the changed atmospheric structure demanded by this stellar peculiarity. Thus a line-emitting area greater than the continuum-emitting area is required. One is thus faced with the question of why the Be stars have this characteristic and the normal B stars do not.

This volume, *B Stars With and Without Emission Lines*, is written to address these kind of issues. The normal B stars were early cited as those most directly illustrating the success of standard modeling; the few lines in their visual spectrum, following from the high atmospheric temperature, made analysis much easier than for the Sun, whose spectrum is crowded by lines from the lowly ionized atoms present there. The Be stars were early thought to illustrate a simple cause of extended atmospheres, a rotational instability which gave planetary-like circumstellar material. Early in the era of observations from space, both normal and peculiar B stars were found to exhibit that superionization and superthermic mass flow which demonstrated the need for nonthermal modeling of at least the outer atmosphere. By contrast, the Be stars put into focus the demand that some extended outer atmospheres must also have a region which is subionized relative to the photosphere and slowly moving. The hot superthermal regions accord with the solar picture; the cool slowly moving regions extend that picture to the Be stars, planetary nebulae, and possibly other stars.

B Stars With and Without Emission Lines is divided into two parts: Part I is about B stars for which emission lines do not occur on the main sequence, only among the supergiants. Part II is about those B stars for which the presence of emission in Hα is considered to be a significant factor in delineating atmospheric structure. The content of the book was planned by A.B. Underhill and V. Doazan.

This volume can also challenge the theorist to decide how to model a B star, whether he has to use the nonradial inhomogeneities, emphasized by Underhill, or a radial sequence consisting of both subionized and superionized regions, emphasized by Doazan or perhaps some combination of both, which will come closer to fitting the observations. It will also, and possibly in a more important way, challenge the observer to look for new measurements that may help to decide what is indeed the physics of a B star.

—Prepared by the Series' Senior Advisers
and the Organizers
Greenbelt, Paris, Tucson, January 1982

Page intentionally left blank

Page intentionally left blank

CONTENTS

Page intentionally left blank

Page intentionally left blank

RÉSUMÉ

La première partie

Depuis l'époque où le livre de A. B. Underhill *The Early Type Stars* a été rédigé, d'énormes progrès ont été faits dans les possibilités d'observation des étoiles B et dans l'interprétation de leur flux d'énergie par la physique du gaz et du rayonnement. Des observations ont été faites dans tous les domaines spectraux, depuis les rayons X jusqu'aux ondes radio, et des modèles détaillés ont été calculés pour la partie interne de l'étoile et pour son atmosphère. Les résultats de la théorie et de l'observation ont conduit à une révolution dans notre façon de comprendre les étoiles B. Beaucoup d'observations ont été faites en dehors de l'atmosphère terrestre. La mise au point de détecteurs électroniques et de moyens de calculs puissants ont révolutionné les techniques de l'observation et le développement de la théorie. Les résultats de ces progrès sont exposés dans le présent ouvrage, *Etoiles B avec et sans raies d'émission*, et l'on donne un schéma général de la nature des étoiles B et de la façon dont elles peuvent évoluer.

La première partie comporte 9 chapitres Les chapitres 1, 2, 3, 4, 6, 7, et 8 de la première partie ont été rédigés par A. B. Underhill avec l'aide de L. Divan pour la partie du chapitre 2 relative aux données de l'observation, et celle de M. Aizenman qui a préparé l'exposé fait au chapitre 7 sur les pulsations dans les modèles d'étoiles massives V. Doazan a collaboré à la préparation du chapitre 2 Le chapitre 5 a été rédigé par Janet Rountree Lesh.

Dans le chapitre 1, on pose de façon générale le problème de la définition et de la nature des étoiles B. On montre que la riche moisson des informations obtenues de l'espace conduit à penser que l'atmosphère des étoiles B est composée de deux parties distinctes: une photosphère et, entourant immédiatement la photosphère, une zone appelée *manteau* qui est définie plus loin.

L'atmosphère est constituée par l'ensemble des couches superficielles de l'étoile, celles dont le rayonnement s'échappe, du moins en partie, dans l'espace. Sa transparence est fonction de la longueur d'onde.

La photosphère forme la limite classique de l'étoile Nous montrons que dans le cas des étoiles B, on peut obtenir des modèles satisfaisants avec des couches plan-parallèles dans lesquelles le transfert de l'énergie est calculé dans l'hypothèse de l'équilibre radiatif et d'une stratification de la densité telle que l'équilibre hydrostatique soit réalisé. La composition chimique de l'atmosphère de la plupart des étoiles B est voisine de celle du soleil, dans ces

conditions deux paramètres, la température effective et la gravité superficielle, permettent de définir entièrement la photosphère lorsqu'on s'impose à la fois l'équilibre radiatif et l'équilibre hydrostatique.

Les observations faites de l'espace montrent que dans l'atmosphère d'une étoile B il existe aussi des régions où les températures électroniques sont beaucoup plus élevées que celles que pourraient produire le flux d'énergie traversant la photosphère. On voit dans beaucoup de cas des flux de matière, avec de très grandes vitesses dirigées vers l'extérieur, et le gaz apparaît inhomogène. De telles régions sont engendrées par la dissipation d'énergie non radiative qui s'ajoute au chauffage produit par le flux de rayonnement arrivant du centre de l'étoile, et par l'apparition, dans certaines parties du gaz au moins, d'une quantité de mouvement dirigée vers l'extérieur. Cette énergie supplémentaire et cette quantité de mouvement sont produites dans les couches extérieures de l'atmosphère, au delà de la région en équilibre radiatif. Cette partie de l'atmosphère est donc distincte de la photosphère et forme une zone bien individualisée que nous avons désignée par commodité du terme de "manteau"—les couches extérieurs de l'atmosphère.

L'ensemble chromosphère, couronne, vent solaire est l'équivalent, dans le cas du soleil, de la zone appelée "manteau" dans le cas de l'atmosphère d'une étoile B. On s'aperçoit maintenant que cette zone, mise en évidence dans le cas des étoiles B par les observations spatiales, se manifeste également dans le domaine visible, par exemple par la présence d'émissions dans les raies de l'hydrogène. Cependant la nécessité réelle de reconnaître l'individualité de cette zone dans l'atmosphère des étoiles B n'est apparue qu'après la découverte de l'émission X et de raies ultraviolettes correspondant à des éléments très fortement ionisés.

Dans le chapitre 8 un modèle simple est développé pour le "manteau." On suggère que des paramètres importants pour le "manteau" sont la densité de l'énergie qui apparaît dans cette région et l'efficacité du couplage entre la source d'énergie et le gaz présent. En particulier, on suggère que la valeur du champ magnétique moyen et la grandeur des mouvements différentiels seraient des paramètres utiles.

Dans toute cette première partie du livre le modèle de l'étoile a été conçu comme formé de quatre parties: (1) le noyau convectif où l'énergie est fournie par le combustibe nucléaire; (2) l'enveloppe qui s'étend entre le noyau et la photosphère et qui transmet l'énergie provenant du noyau; (3) la photosphère qui forme la limite classique de l'étoile et qui est la région d'où provient en général le spectre continu; (4) le "manteau" où l'apparition de l'énergie non radiative se manifeste et où le vent stellaire prend naissance.

La signature du noyau est constituée par l'énergie totale sortant de chaque cm^2 de l'étoile sous forme radiative. Cette énergie totale est représentée par le paramètre température effective. Les propriétés de l'enveloppe se manifestent surtout par le rayon de l'étoile et les variations de luminosité dues à des pulsations éventuelles. Les propriétés de la photosphère se déterminent principalement à partir de la distribution de l'énergie dans le spectre continu, de l'intensité des raies faibles et de la forme des ailes des raies de Balmer de l'hydrogène. Les propriétés du "manteau" sont révélées par la présence de raies d'émission et par le profil et l'intensité des raies de résonance. Ces raies de résonance sont observées dans l'ultraviolet spatial et seul un "manteau" très important peut être détecté à partir d'autres raies pour les élements plus lourds que l'hydrogène et l'hélium. La visibilité du "manteau" varie considérablement lorsqu'on passe des étoiles de la série principale aux supergéantes.

Le chapitre 2 donne, pour le lecteur novice, une description des propriétés générales des étoiles B. Dans la premier section, on trouve les principes de la classification des étoiles B ainsi que des indications concernant la calibration des divers critères spectroscopiques de

luminosité en magnitude absolue visuelle M_V. On a pris soin de relier les différents indices (ou combinaisons d'indices) de couleur de la photométrie photoélectrique aux types spectraux définis spectroscopiquement. Des tableaux de données concernant ce point sont fournis pour la photométrie à bandes passantes larges et intermédiaires. Le problème soulevé par les effets de l'extinction interstellaire sur la distribution de l'énergie dans le spectre continu est discuté et on donne la forme de la loi du rougissement interstellaire: les relations entre le système de classification de Barbier, Chalonge, et Divan (système BCD), et la classification MK sont décrites Le système de classification BCD repose sur des caractères liés à la distribution de l'énergie dans la spectre continu des étoiles pour le domaine spectral observable de la surface de la terre, et il est bien adapté à la classification des étoiles B en fonction des propriétés de leur photosphère.

Dans la deuxième section, on décrit les premières observations obtenues dans l'ultraviolet spatial. On remarque en particulier que les supergéantes B sont déficientes en lumière ultraviolette par rapport aux étoiles de la série principale ayant le même sous-type spectral.

Les troisième et quatrième sections sont consacrées aux observations dans les domaines infrarouge et radio. La photométrie à larges bandes passantes a été faite jusqu'à environ 10 μm pour un assez grand nombre d'étoiles B, et des spectres infrarouge à grande résolution ont été obtenus pour un petit nombre d'entre elles. Très peu d'étoiles B ont pu être détectées aux longueurs d'onde radio. Les plus faciles à observer sont celles qui ont des enveloppes gazeuses étendues telles que les étoiles BQ [ ] et quelques supergéantes. Les phénomènes physiques en relation avec le rayonnement infrarouge et radio des supergéantes B sont discutés dans le chapitre 4.

Dans la dernière section on a rassemblé des données sur les masses et les rayons. A partir des binaires à éclipses présentant un double spectre de raies, on trouve que les masses des étoiles B de classe de luminosité IV et V vont de environ 2,5 $M_\odot$ pour le type B9 à environ 17 $M_\odot$ pour le type B0. Les masses des géantes de classe de luminosité III sont moins bien connues. Elles semblent un peu plus grandes que pour les classes de luminosité IV et V. En ce qui concerne les masses des supergéantes, on peut obtenir des informations directes à partir du mouvement orbital de sources X dans lesquelles le compagnon optique est une supergéante B. Les masses ainsi obtenues sont de l'ordre de $20 \pm 5\ M_\odot$.

Les rayons des étoiles B peuvent être déduits de l'analyse de la courbe de lumière dans le cas des binaires à éclipses, si elles sont en même temps binaires spectroscopiques avec un double système de raies. Ils peuvent également être calculés à partir du diamètre angulaire et de la distance. Cette dernière méthode est discutée dans le chapitre 3. On montre que les rayons des étoiles B de classe de luminosité IV ou V vont de environ 3 $R_\odot$ pour le type B9 à environ 9 $R_\odot$ pour le type B0. Les géantes de luminosité II et III ont des rayons allant de environ 4 $R_\odot$ pour le type B9 à 12,5 $R_\odot$ pour le type B0. La Table 4-1 montre que les rayons des supergéantes vont de environ 30 $R_\odot$ pour le type B9 à environ 25 $R_\odot$ pour le type B0. Ainsi, les étoiles B de la série principale deviennent de plus en plus grandes lorsqu'on se déplace vers les types moins avancés, mais pour les supergéantes, cette tendance est inversée.

On montre que la vitesse d'échappement hors des photosphères des étoiles B de la série principale va de environ 580 km s^{-1} pour le type B9 à environ 880 km s^{-1} pour le type B1. Dans le cas des supergéantes ces vitesses sont moins élevées, mais les valeurs exactes ne peuvent être précisées car elles dépendent directement de la masse de ces supergéantes qui est très mal connue.

Le chapitre 3 donne des détails sur les spectres des étoiles B naines et géantes obtenus dans le visible et l'ultraviolet spatial. On montre que l'on peut rendre compte de la plupart des caractères observés par une photosphère classique, en utilisant les théories existantes des

spectres stellaires. Cependant quelques observations, dans le visible ou dans l'ultraviolet, ne peuvent s'interpréter que par la présence d'un "manteau" tel qu'il a été défini plus haut. En particulier, l'existence de rayons X provenant de certaines étoiles B de la série principale, exige la présence d'un "manteau" autour de ces étoiles B par ailleurs normales. Le "manteau" est très peu dense et difficile à détecter pour les étoiles B de la série principale. Il peut apparaître cependant de façon certaine pour toutes les classes de luminosité de II à V, la densité dans le vent stellaire, très faible pour les étoiles de la série principale, augmente lorsque la luminosité croit. Les observations sur les étoiles B normales présentées dans le chapitre 3 servent de base aux comparaisons faites ultérieurement avec des objets présentant un "manteau" très apparent comme les supergéantes et les étoiles Be/shell.

Dans la premier section du chapitre 3, on montre que les distributions d'énergie observées pour les étoiles B de la série principale sont bien représentées par des modèles en équilibre thermodynamique local et tenant compte de l'effet des raies d'absorption (modèles dits "ETL" et "line-blanketed") tels que ceux de Kurucz (1979). La valeur absolue des flux émis par les étoiles a également été mesurée. A titre d'exemple, la Table 3-2 donne, en unités absolues, la distribution de l'énergie entre 1200 Å et 12,6 μm pour l'étoile η UMa qui a été particulièrement bien étudiée. Les Figures 3-1 et 3-2 montrent l'allure de cette distribution d'énergie. Le bon accord entre toutes les données reportées sur la Figure 3-1 indique que les diverses calibrations absolues faites à partir de la surface de la terre forment un ensemble cohérent.

Les méthodes pour déterminer les températures effectives des étoiles B sont discutées dans la deuxième section. La méthode la plus directe fait usage des diamètres angulaires et des flux intégrés. Des méthodes indirectes permettent d'obtenir la température effective en comparant les valeurs observées de paramètres spectroscopiques bien choisis avec les valeurs prédites pour ces même paramètres, obtenues à l'aide de modèles classiques d'atmosphère. On montre que les méthodes qui font usage de la forme du spectre continu et/ou de la grandeur de la discontinuité de Balmer donnent des valeurs de la température effective en bon accord avec celles que l'on peut calculer directement à partir des flux intégrés et des diamètres angulaires. Par contre les températures estimées en comparant les intensités des raies d'un même élément dans deux ou plusieurs états d'ionisation différents ont tendance à être trop hautes. L'écart varie de 1500 à 3100 K pour les étoiles B des classes de luminosité IV et V, les plus grands écarts correspondant aux étoiles les moins avancées.

Les températures effectives de 37 étoiles B pour lesquelles au moins deux déterminations de température effective existent sont données dans la Table 3-4. Les valeurs de $\log g$ qui sont également données ont été obtenues en utilisant des modèles d'atmosphère. La Table 3-5 et la Figure 3-4 montrent comment varie la température effective des étoiles B en fonction du type spectral et de l'indice de couleur intrinsèque $(B - V)_0$. Ces relations permettent de déterminer la température effective d'une étoile B de la série principale avec une incertitude de $\pm$ 500 K à partir soit de son type spectral soit de sa couleur intrinsèque. Ces températures effectives vont de 10.900 K environ pour le type B9 à 30.900 K pour le type B0.

On a montré que les diamètres angulaires des étoiles B de la série principale obtenus en comparant les flux monochromatiques correspondant aux longueurs d'onde supérieures à 6000 Å aux flux prédits par les modèles d'atmosphère de Kurucz (1979) sont égaux aux diamètres angulaires mesurés directement par Hanbury Brown et al. (1974). Ce résultat fournit la preuve que les flux des modèles de Kurucz sont corrects en valeur absolue, au moins pour les longueurs d'ondes supérieures à 6000 Å utilisées pour déterminer les diamètres angulaires. Par ailleurs la forme de la distribution d'énergie du modèle de Kurucz

correspondant à l'étoile η UMa de type spectral B4 V est identique à celle que l'on observe entre 1200 Å et 12,6 μm. Nous conclurons donc que les modèles "ETL" et "line-blanketed" de Kurucz (1979) représentent correctement la photosphère des étoiles B de la série principale.

Le spectre d'absorption des étoiles B de la série principale est décrit dans la troisième section. L'aspect général de l'évolution des principales raies du domaine visible avec le type spectral est donné par les Figures 3-5 et 3-6. En comparant les profils et les largeurs équivalentes des raies des étoiles à raies fines aux prédictions des modèles on voit que la majeure partie du spectre d'une étoile B peut s'expliquer en adoptant une composition solaire et un modèle classique d'atmosphère. L'utilisation de la physique hors "ETL" améliore la représentation des intensités relatives des raies de He I, Si II, Si III, Si IV, Ne I, et Mg II. Il subsiste cependant quelques anomalies bien nettes qui indiquent que la contribution du "manteau" aux raies les plus intenses n'est pas totalement négligeable. Par exemple, les centres des premières raies des séries de He I ne sont pas représentés correctement, même en utilisant des modèles hors "ETL" et une théorie hors "ETL" de la formation des raies. De même, la raie He I à 3187 Å qui provient du niveau métastable 2^3S est environ deux fois plus intense que la raie prédite par les calculs hors "ETL" (d'après Dufton et McKeith, 1980). Nous en déduisons que les étoiles de la série principale sont entourées d'un "manteau" dans lequel les températures électroniques sont de l'ordre de 20.000 K, au moins dans certaines parties du volume. On peut encore signaler les anomalies qui subsistent dans les intensités relatives des raies de Si II, Si III, et Si IV malgré un traitement hors "ETL" fait par Kamp (1978). Ces anomalies pourraient sans doute s'expliquer par l'existence d'un "manteau."

Il résulte de tout ceci que les critères de type spectral et de luminosité utilisant les raies de He I, Si II, Si III et Si IV et sélectionnés par Walborn (1971) pour classer les étoiles de types B2,5 et antérieures, définissent les types spectraux non seulement d'après les propriétés de la photosphère mais aussi d'après les propriétés du "manteau."

On donne ensuite une description des principales raies du spectre ultraviolet pour les étoiles B de la série principale. Les Figures 3-8 à 3-12 montrent des profils typiques pour les raies de résonance de C II, C IV, Al III, Si II, et Si IV. Ces profils sont donnés pour HR 1861 (B1 V), ι Her (B3 IV), τ Her (B5 IV), π Cet (B7 IV), et ν Cap (B9, 5 V). Le profil des raies varie avec la luminosité; cette variation est illustrée par la Figure 3-14 où l'on montre la région située autour de 1300 Å, pour les classes de luminosité IV à Ia du type B5. On voit que les parties centrales des raies de résonance ultraviolettes ne sont en général pas déplacées vers les courtes longueurs d'onde et que c'est seulement pour un très petit nombre d'étoiles de la série principale qu'une asymétrie dans l'aile d'une raie de résonance suggère un vent stellaire, de faible densité et de forte température électronique.

On trouve que les raies du multiplet UV 13.04 de Si II à 1305. 59, 1309.46, et 1309.77 Å sont anormalement larges et intenses. Ceci implique que la constante d'amortissement pour ces raies est exceptionellement forte, par suite probablement de l'auto-ionisation qui intervient dans les niveaux $3s3p3d\ ^2F^\circ$. Ainsi, l'autoionisation et la recombinaison diélectronique pourraient être des facteurs importants pour l'équilibre d'ionisation entre Si^+ et Si^{++}.

Dans la quatrième section, on examine le problème des variations que l'on peut observer dans les étoiles B à raies fines avec une spectrophotométrie précise. Il semble que la plupart des étioles B à raies fines soient le siège de variations périodiques de faible amplitude concernant la magnitude, la vitesse radiale et le profil des raies. Ces variations pourraient être dues à des pulsations non radiales dans l'enveloppe de l'étoile. Pour les étoiles de type β Cep, on pense que les pulsations radiales jouent un rôle important. L'étoile à raies fines τ Sco possède des raies asymétriques avec des ailes suggérant une éjection de matière. Il

semble qu'elle ne soit pas variable. Elle diffère d'une étoile B typique de la série principale par son "manteau" qui apparaît plus important que dans la plupart des étoiles de classe de luminosité V.

L'ensemble des observations est discuté dans la dernière section. On a rassemblé les diverses indications en faveur de la présence d'un "manteau" de faible densité autour des étoiles de la séquence principale. En particulier le fait que π Cet, une étoile B7 V absolument normale sous tous les autres rapports, émette des rayons X est une preuve que du gaz à très haute température (environ 10^7 K) existe autour de cette étoile. Ainsi, le fait d'observer une photosphère absolument normale n'est pas du tout une garantie qu'aucun "manteau" ne pourra être décelé.

Le chapitre 4 traite des observations d'étoiles B supergéantes. On montre qu'un "manteau" doit être ajouté à la photosphère classique si l'on veut rendre compte de toutes les observations. La forme du spectre continu d'une étoile B supergéante et la valeur absolue du flux dans la majeure partie du domaine spectral observable (ultraviolet, visible, infrarouge) sont conformes aux prédictions des modèles classiques de la photosphère. On observe cependant un flux supplémentaire dans le continu de Balmer et la présence d'un excès de radiations infrarouge et radio. De plus beaucoup de détails du spectre de raies dans le visible et dans l'ultraviolet ne s'expliquent pas sans la présence d'un "manteau." Pour représenter correctement le spectre de raies des étoiles supergéantes, ce "manteau" doit avoir trois propriétés: (1) être le siège d'un chauffage par dissipation d'énergie nonradiative; (2) avoir un flux de masse dirigé vers l'extérieur; (3) présenter des inhomogénéités. Un modèle schématique du "manteau" est esquissé dans la huitième section de ce chapitre.

On connait douze étoiles B supergéantes qui présentent une polarisation intrinsèque. Ceci indique que leur atmosphère ne présente pas de symétrie sphérique et que la diffusion par les électrons est importante. Dans quatre cas, on a observé un changement du degré de polarisation avec le temps. Toutes les supergéantes B sont légèrement variables en magnitude et en vitesses radiales. Les variations ne sont pas réellement périodiques mais on peut en général définir une pseudo-période de quelques jours. Cette pseudo-période augmente lorsque le type spectral devient plus avancé.

La deuxième section traite de la détermination des températures effectives, des rayons et des corrections bolométriques pour les supergéantes B. La Table 4-1 donne les résultats pour 30 supergéantes et la Table 4-2 présente une échelle des températures effectives en fonction du type spectral. Les corrections bolométriques sont données dans la Table 4-3. Les températures effectives déterminées par la méthode directe (celle qui consiste à mesurer les diamètres angulaires et intégrer les flux observés pour toutes les longueurs d'onde) vont de environ 10.500 K pour le type B9 à environ 25.000 K pour le type B0. On montre que les températures effectives déduites de la forme du spectre continu sont en accord avec celles que donne la méthode directe. En particulier un indice de couleur défini par les régions du spectre située respectivement autour de 1600 Å et autour de 4000 Å est un bon indicateur de température effective. Par contre, la Figure 4-2 montre que les indices de couleur incluant les régions spectrales situées au début du continu de Balmer ne devraient pas être utilisées. De même, il convient d'éviter les indices de couleur incluant la région rouge du spectre pour les supergéantes B avancées car ces étoiles, surtout celles de type Ia, ont un excès d'infrarouge important. Celui-ci se manifeste parfois jusque vers 5000 Å.

Les températures effectives obtenues en comparant les intensités des raies d'absorption observées à celles des modèles d'atmosphère sont toujours trop grandes pour les supergéantes B. Par exemple pour le type B1, T_{eff} (raies) = T_{eff} (flux intégré) + 5000 K.

L'incertitude sur les températures effectives données dans la Table 4-1 est environ

± 500 K. Si l'on a une bonne classification spectrale, l'utilisation des données da la Table 4-2 devrait fournir la température effective d'une étoile B de luminosité Ib ou Ia avec une précision de ± 1000 K.

On remarque que pour les types O9,5 à B0,5 le type spectral n'est pas nécessairement un bon indicateur de température effective. Par exemple, les températures effectives de α Cam (09,5 Ia), 15 Sgr (09,7 Iab ou B0 Ia) et ϵ Ori (B0 Ia) sont respectivement 25.000, 29.700, et 25.090 K. Dans le même ordre d'idées, Underhill (1981) a montré que trois étoiles WN7 et une étoile WN8 avaient des températures effectives voisines de 25.000 K.

Il est probable que les diamètres angulaires sont connus avec une précision interne meilleure que 2 pour cent. La précision sur les valeurs des rayons des étoiles B supergéantes déduites des diamétres angulaires dépend donc principalement de la précision avec laquelle la distance est connue. L'incertitude sur le rayon est 0,2 ΔMod, ΔMod étant l'incertitude sur le module de distance de l'étoile. En général cette incertitude ne dépasse pas 0,5 magnitude. Les rayons des supergéantes B sont donnés dans la Table 4-1 et discutés également dans le chapitre 2.

Le spectre visible des supergéantes B est décrit dans la troisième section. Les raies d'absorption sont élargies et présentent un profil d'aspect rectangulaire qui est attribué à la macroturbulence. On observe également un élargissement du à la rotation de l'étoile, mais cette rotation est généralement faible par rapport à celles que l'on observe souvent dans la série principale. Dans la plupart des cas l'ensemble de ces deux types d'élargissement correspond à des vitesses inférieures à 50 km s^{-1}.

La composition chimique des supergéantes B ne semble pas différer de celle du soleil. Il n'existe pas de preuve réelle de sur-abondances ou de sous-abondances pour le carbone ou l'azote, bien que les intensités relatives de quelques raies de C, N, et O puissent varier d'une étoile à l'autre. Ces variations peuvent s'expliquer autrement qu'en admettant des différences dans les abondances.

Dans les supergéantes Ia des premiers types B, on voit souvent dans Hα, et quelquefois aussi dans He I 5876 et He I 6678, une émission faible avec une absorption centrale déplacée vers le violet. Ces émissions ne sont observées que rarement dans les supergéantes Ib. Les profils des raies intenses varient et il en est de même pour la vitesse radiale indiquée par le point le plus bas du profil. Dans les étoiles les plus lumineuses on note une progression de Balmer, les raies Hα et Hβ indiquant des vitesses qui, comparées aux vitesses radiales données par les autres raies de la série de Balmer, correspondent à un flux de matière dirigé vers l'extérieur de l'étoile. Les raies de He I et celles des ions des éléments légers ont les même vitesses que les raies d'ordre élevé de la série de Balmer L'étoile α Cam (09,5 Ia) a une émission Hα particulièrement intense et variable. On voit une émission Hα variable et faible dans ρ Leo de type B1 Ib. En général l'intensité dans l'émission à Hα ne dépasse pas le niveau du continu stellaire voisin de plus de 20 pour cent.

Le quatrième section traite du spectre ultraviolet des supergéantes B. On montre des profils typiques, donnés par les spectres à grande résolution de IUE, pour les raies de Si II, C II, Al III, Si IV et C IV dans 15 Sgr (B0 Ia), χ^2 Ori, (B2 Ia), η CMa (B5 Ia), et HD 21389 (A0 Ia). On montre aussi les changements du spectre pour le type B2 lorsque la classe de luminosité passe de IV (γ Peg, ζ Cas) à II (ϵ CMa) puis à Ib (9 Cep) et Ia (χ^2 Ori). Le profil des raies de résonance de C II, Al III, Si IV, C IV, N V, et O VI sont de type "P-Cygni" avec une absorption déplacée vers les courtes longueurs d'onde accompagnée parfois d'une composante faible en émission située du côté des grandes longueurs d'onde. La présence de fortes absorptions dans les raies de résonance qui correspondent à des ions ne pouvant être maintenus à ce niveau d'ionisation par le passage du rayonnement issu de la photo-

sphère, indique la présence d'un chauffage par de l'énergie non radiative se manifestant dans le "manteau."

On voit également, pour une partie du gaz du "manteau," des vitesses très grandes dirigées vers l'extérieur. La Table 4-5 montre les vitesses maximum d'éjection observées; elles vont de 200 km s^{-1} environ pour le type A0 jusqu'à 2000 km s^{-1} pour le type B0. On trouve empiriquement la relation $u_\infty \sim T_{\text{eff}}^{2.30}$. Pour le type A0 ce vent stellaire ne se voit que dans des ions à faible potentiel d'ionisation comme Mg II, Al II, et C II. Pour le type B0 le vent se voit le mieux à des niveaux d'ionisation plus élevés comme Si IV, C IV, N V, et O VI.

D'après les théories des atmosphères stellaires en expansion exposées dans la quatrième section du chapitre 6, l'énergie contenue dans la composante en émission devrait compenser sensiblement celle qui est soustraite dans la composante en absorption déplacée du côté des courtes longueurs d'onde. Ce n'est pas ce que l'on observe: les composantes en émission, si même elles existent, sont toujours faibles. Dans le cas du doublet de Si IV dont les raies en absorption sont fortes mais bien séparées dans les supergéantes B2 et B3, on peut voir une faible émission pour la raie à 1402 Å, mais l'émission est pratiquement toujours absente pour la raie à 1393 Å qui est deux fois plus intense. Ces résultats peuvent être dus à la présence de raies d'absorption photosphériques dans le rayonnement diffusé par les ions situés dans le "manteau"' La faible intensité de l'émission dans les raies de résonance ultraviolettes provenant d'ions à fort potentiel d'ionisation suggère que ces ions sont localisés dans une région voisine de la photosphère ou dans un disque équatorial. Cette dernière possibilité a l'avantage d'expliquer la polarisation intrinsèque des supergéantes B. Par ailleurs, si les ions de haut potentiel d'ionisation présentent les vitesses d'éjection les plus grandes, on voit également dans leur cas des vitesses dont la composante sur la ligne de visée est voisine de zero.

Il est clair que si l'on admet que les ions de haut niveau d'ionisation sont produits par les collisions avec les électrons, il faut envisager la coexistence de régions à des températures différentes dans le "manteau" des supergéantes B. En effet des vitesses d'éjection de l'ordre de -100 ± 50 km s^{-1} sont observées aussi bien dans les raies fortes de H I et He I que dans les raies de résonance des ions de haut niveau d'excitation, correspondant à des énergies supérieures à 25 eV. De plus, pour les supergéantes B0, on voit dans les raies de résonance de Si IV une absorption intense, aussi forte que dans les raies de résonance de C IV, alors que les potentiels d'ionisation de Si^{+3} et C^{+2} sont respectivement 45,1 et 47,9 eV. S'il y avait une seule température et si l'équilibre d'ionisation (du aux collisions avec les électrons) favorisait la formation de C^{+3} par suite de l'ionisation presque complète de C^{+2}, il ne devrait rester que très peu d'ion Si^{+3} et le silicium serait presque entièrement à l'état d'ions Si^{+4} inobservables. Il est clair que ce n'est pas le cas. On admet donc que les ions C^{+3} sont formés par un mécanisme particulier (peut-être l'ionisation Auger) alors que les ions Si^{+3} résultent de l'équilibre d'ionisation du aux collisions avec les électrons.

Des modèles détaillés du "manteau" seraient nécessaires pour expliquer comment les mêmes vitesses peuvent s'observer à la fois pour des atomes neutres (H, He) et pour des ions de fort potentiel d'ionisation (Si^{+3}, C^{+3}) dans les supergéantes des premiers types B. Il n'y a que peu d'indices que les atomes neutres puissent présenter des vitesses voisines du maximum observé, mais on voit fréquemment des vitesses importantes.

Les Figures 4-15 et 4-16 montrent l'existence de plusieurs composantes d'une raie d'absorption correspondant à des vitesses radiales différentes. Les déplacements et les intensités de ces composantes sont variables. Ce phénomène a été signalé pour la première fois par Underhill (1975a, 1975b) sur les spectres de η CMa (B5 Ia) obtenus grâce à Copernicus. Il

semble qu'il soit présent dans toutes les supergéantes et c'est dans les raies non saturées qu'on le décèle le plus facilement. La présence de ces diverses composantes des raies de résonance ultraviolettes et leur variabilité indiquent que le "manteau" des supergéantes B n'est pas homogène et que sa structure varie avec le temps. On observe aussi parfois une composante déplacée dans l'une ou l'autre des raies fortes du spectre visible. L'interprétation que nous donnons ici semble préférable à celle que donne Gutman (1967) pour le spectre visible de ρ Leo (B1 Ib) en faisant intervenir une abondance très anormale de ^{3}He.

La cinquième section traite du spectre infrarouge et radio des supergéantes B. On montre que les supergéantes Ia présentent souvent un excès de radiation vers 10 microns. Cet excès n'existe pas pour les supergéantes Ib. Les Figures 4-17 et 4-18 montrent comment cet excès de radiation varie avec la longueur d'onde pour P Cyg (B1 Iap), β Ori (B8 Ia) et α Cyg (A2 Ia). On voit sur les Figures 4-2 et 4-28 que l'excès d'infrarouge peut s'étendre jusque dans le domaine visible pour les étoiles B avancées et pour P Cyg Des considérations théoriques simples (Cohen et al., 1975) permettent d'obtenir la température électronique T_e du gaz produisant l'excès d'infrarouge à partir de la longueur d'onde λ_p (en microns) du maximum de l'émission: $\lambda_p \times T_e = 14.400$. On obtient ainsi des valeurs de Te voisines de 22.000 K, température très supérieure à la température effective de la plupart des supergéantes B.

Pour les longueurs supérieures à 1 micron, l'excès d'infrarouge S_ν varie sensiblement comme ν^α. Dans le cas de P Cygni la valeur $\alpha = 0{,}77$ permet de relier les flux radio aux flux infrarouge. Pour les supergéantes moins avancées que B2, $\alpha = 0{,}77$ est encore une valeur acceptable (voir les données de la Table 4-6 et les notes), mais dans le cas de β Ori et α Cyg, les observations indiquent des valeurs de α nettement plus grandes (1,2 et 1,1, respectivement, voir Figure 4-18). Il semble que pour les supergéantes des derniers types B et des premiers types A, le gaz émettant un spectre "free-free" devienne optiquement épais aux grandes longueurs d'onde. Ceci expliquerait pourquoi ces étoiles ont un flux radio aussi faible malgré leur grand excès d'infrarouge (voir Abbott et al., 1980).

La Figure 4-19 montre que les supergéantes Ia ont des excès d'infrarouge plus élevés que les supergéantes Ib. On voit aussi que l'étoile α Cyg (A2 Ia) a un excès d'infrarouge beaucoup plus important que celui que l'on observe en moyenne dans les autres supergéantes Ia. Ceci indique que la quantité de matière responsable de l'émission "free-free" contenue dans le "manteau" est plus importante pour les supergéantes Ia que pour les Ib; cette quantité de matière serait particulièrement grande pour α Cyg. Ainsi, la quantité de gaz contenue dans le "manteau" semble augmenter avec la luminosité, mais ceci n'est pas une règle absolue puisque α Cyg a une une luminosité tout à fait comparable à celle des autres supergéantes Ia et que par ailleurs, P Cyg qui possède un "manteau" particulièrement important n'est pas une étoile particulièrement lumineuse. La Figure 4-19 montre également que l'excès d'infrarouge, donc la quantité de gaz du "manteau," dépend peu de la température effective.

Des spectres à grande résolution entre 0,48 et 1,03 microns ont été publiés par Johnson et al. (1978) et Johnson (1978) pour huit supergéantes des premiers types B. Après analyse, ces spectres devraient fournir des informations sur le "manteau."

La sixième section concerne les supergéantes les plus lumineuses et également la supergéante très particulière P Cyg. Dans cette section le cas de P Cyg est examiné. Après correction de l'extinction interstellaire et de l'excès d'infrarouge (qui se manifeste jusque dans le domaine visible) le rayonnement observé correspond à une température effective de 12 à 13.000 K et un diamètre angulaire de 4,1 10^{-4} arcsec. De la distance de P Cyg, estimée à 1,7 kpc, on déduit le rayon de la photosphère: $R = 75\ R_\odot$. La luminosité peut alors être

calculée et on trouve pour $\log L/L_\odot$ la valeur 5,05 qui correspond aux supergéantes Ia des derniers types B. On discute les évaluations de la perte de masse de P Cyg et on montre que $\dot{M} = (1{,}5 \pm 0{,}5) .10^{-5}\ M_\odot$ par an.

Dans le domaine visible, le spectre de P Cyg présente des caractères tout à fait particuliers; il comporte presque exclusivement des raies d'émission, accompagnées d'une composante en absorption déplacée vers les courtes longueurs d'onde. Les déplacements vont de -50 à -220 km s^{-1}. Quelques composantes en absorption sont doubles, ou même triples (dans les dernières raies de Balmer, par exemple). L'émission à Hα culmine à un niveau qui est 17 fois celui du continu adjacent; au point le plus bas de la composante en absorption, le flux est 40 pour cent de celui du continu. Une émission aussi forte par rapport à l'absorption n'existe jamais dans les raies de type P-Cygni des supergéantes B normales et on ne peut pas l'expliquer par les modèles existants d'atmosphères sphériques en expansion (Oergle, 1977; Lee, 1979).

Les déplacements des raies d'absorption du spectre visible sont plus ou moins corrélés avec l'énergie nécessaire pour mettre l'atome ou l'ion au niveau inférieur correspondant à la raie, les vitesses d'éjection les plus grandes étant observées pour les niveaux correspondant aux énergies les plus faibles. Cette relation, représentée schématiquement par la Figure 4-21, est en réalité très floue. Les raies ultraviolettes montrent la même tendance, les vitesses d'éjection observées allant de -90 à -215 km s^{-1}.

Les profils des raies de résonance ultraviolette de P Cyg sont comparés à ceux de κ Cas (B1 Ia) et η CMa (B5 Ia) dans les Figures 4-22 à 4-25 qui montrent que P Cyg ressemble beaucoup plus à la B5 Ia, η CMa qu'à la B1 Ia, κ Cas. Les composantes en émission sont faibles dans l'ultraviolet et elles apparaissent surtout du côté des grandes longueurs d'onde des raies de résonance dans le spectre des éléments légers et des métaux une seule fois ionisés. Les émissions les plus fortes dans le spectre ultraviolet de P Cyg sont dues au multiplet UV 13.04 de Si II (raies 1305,59, 1309,46, et 1309,77 Å, produites par le processus de recombinaison diélectronique. $Si^{++}\ (3s3p) + e \rightarrow Si^{+}\ (3s3p(^3P^o)3d) \rightarrow Si^{+}\ (3s3p^2) + h\nu$).

On trouve, enfin, des renseignements sur les supergéantes les plus lumineuses, celles de classe de luminosité Ia^+ ou Ia − 0. Dans la Table 4-9 on donne une liste de 18 d'entre elles, 8 dans la Galaxie et 10 dans le Grand Nuage de Magellan. Ces étoiles ont des magnitudes absolues dans la fourchette $-8{,}3 \pm 0{,}5$ mag. Etant donné que la correction bolométrique va de $-1{,}7$ pour le type B1 à $-0{,}3$ pour le type A0, la luminosité de ces supergéantes extrêmes va de $\log L/L_\odot = 5{,}9$ pour le type B1 à $\log L/L_\odot = 5{,}3$ pour le type A0.

Des renseignements sont donnés sur les propriétés des étoiles B1 Ia^+, et en particulier sur celles de ζ^1 Sco qui est la mieux étudiée. Les températures effectives sont voisines de 18.000 K. L'extension vers les courtes longueurs d'onde des raies de résonance fortes dans ζ^1 Sco suggère des vitesses d'éjection de 500 km s^{-1} au maximum. Les émissions dans ces étoiles B1 Ia^+ sont beaucoup moins intenses que dans P Cyg, mais cependant plus fortes que dans les B1 Ia. Le spectre ultraviolet de ζ^1 Sco ressemble à celui d'une B2 ou d'une B3 Ia. Le taux de perte de masse est de quelques $10^{-6}\ M_\odot$ par an.

Les binaires à rayons X comportant une supergéante B sont discutées dans la septième section. La Table 4-10 fournit une liste de 5 systèmes. Le spectre ultraviolet de HD 77581 (B0,5 Ib) suggère une perte de masse voisine de $10^{-6}\ M_\odot$ par an. La vitesse d'éjection maximum observée est environ 860 km s^{-1}, deux fois plus faible que ce que l'on voit dans les étoiles simples B1 Ia ou B1 Ib.

Une discussion des propriétés des supergéantes B est faite dans la dernier section. On montre que la meilleure structure pour interpréter les propriétés de ces étoiles est celle qui comporte une photosphère et un "manteau."

La photosphère peut être représentée par un modèle classique qui permet d'interpréter la plus grande partie du spectre continu, ainsi que les raies d'absorption faibles et non déplacées d'ions peu abondants.

La présence d'un excès de rayonnement dans le continu de Balmer, dans les domaines infrarouge et radio et dans celui des rayons X pour les supergéantes B indique que pour représenter le spectre de ces étoiles il faut ajouter à la photosphère classique un "manteau" dont le modèle est à faire. L'intensité observée pour les raies intrinsèquement fortes des éléments abondants, la présence de raies d'émission, celle de composantes distinctes et parfois variables d'une même raie, l'indication de très fortes vitesses d'éjection et l'importance des absorptions produites par des ions de très haut potentiel d'ionisation sont également des phénomènes qui ne peuvent être interprétés que par la présence d'un "manteau" dont les propriétés diffèrent de celles de la photosphère classique sous-jacente. Les déplacements et les asymétries variables des raies spectrales et leur élargissement par macroturbulence montrent que le "manteau" n'est ni homogène ni statique. La polarisation intrinsèque de beaucoup de supergéantes indique que leur "manteau" n'a pas de symétrie sphérique.

Les principales propriétés du "manteau" sont la transparence dans la plus grande partie du spectre continu, la présence d'un chauffage, l'éjection de matière, l'inhomogénéité et la variabilité. L'énergie non radiative apparaissant dans le "manteau" serait d'origine magnétique. L'éjection de matière pourrait avoir son origine à la base du "manteau," non loin de la limite extérieure de la photosphère et l'impulsion initiale pourrait être fournie par des effets magnétiques. Une fois cette impulsion initiale donnée, le gas est accéléré par la pression de radiation.

On rappelle que les propriétés de la photosphère sont déterminées principalement par la valeur de la température effective, le second paramètre étant $\log g$. Les observations indiquent que pour les supergéantes B, les propriétés du "manteau" ne sont pas définies de façon unique par les paramètres caractérisant la photosphère. Elles dépendent d'autres paramètres qui pourraient être la densité d'énergie de la source d'énergie non radiative et l'efficacité du mécanisme de couplage entre cette énergie non radiative et le gaz présent dans le "manteau." Les intensités relatives des émissions dans les raies de l'hydrogène d'une part et dans les continus "bound-free" et "free-free" de l'hydrogène d'autre part seraient des paramètres importants dans une tentative de modélisation du "manteau" des supergéantes B. Des problèmes analogues se posent pour les étoiles Be/shell, mais les conditions physiques sont très différentes.

Le chapitre 5 traite de quelques types particuliers d'étoiles B. La première section est consacrée aux étoiles de type Beta Cephei. Ces étoiles présentent des variations en magnitude et en vitesse radiale avec des périodes de 3 à 6 heures, trop courtes pour correspondre à un mouvement orbital. Leurs types spectraux sont peu avancés et compris dans un intervalle restreint (B0, 5 II – III à B2 IV). La courbe de lumière est en général en retard d'un quart de période sur la courbe de vitesse radiale. Les périodes sont constantes et leurs valeurs correspondent aux oscillations de modèles stellaires de 10 à 15 masses solaires.

Les spectres des étoiles Beta Cephei qui ont été classées dans le système MK sont absolument normaux et quelques étoiles Beta Cephei ont même été prises comme standards pour la classification MK. Beaucoup, mais pas toutes, ont des raies très fines. Leur composition chimique semble analogue à celle du Soleil. Leur température effective et leur gravité sont normales pour le type MK qu'elles présentent. Leur luminosité semble également bien correspondre à leur type MK.

L'existence d'une ou plusieurs périodes secondaires se manifeste dans les courbes de lumière et de vitesse radiale de la plupart des étoiles Beta Cephei. Les amplitudes et les

périodes sont données dans la Table 5-1 pour 21 étoiles Beta Cephei particulièrement bien étudiées. La variation de lumière est toujours plus grande dans l'ultraviolet que dans le domaine visible.

Les spectres à grande résolution du domaine visible montrent que les raies sont généralement étroites et profondes sur la branche ascendante de la courbe de vitesse radiale. Sur la branche descendante, elles sont plus larges et moins profondes; des asymétries apparaissent quelquefois, et même une division en deux composantes. Pendant les phases qui correspondent au maximum du rayon, les raies de l'hydrogène apparaissent comblées en partie, comme par de l'émission provenant d'une atmosphère étendue. Les observations de β Cep faites à haute résolution dans l'ultraviolet ont montré que le blend constitué par les raies de résonance de C IV à 1550 Å apparaissait et disparaissait avec une période de 6 jours. Des effets analogues ont été observés pour N V. Mais ce type de variations n'a été détecté jusqu'ici que pour β Cep et l'on effectue actuellement des observations avec IUE pour préciser leur importance en ce qui concerne la nature du phénomène Beta Cephei.

Sur le diagramme HR, les étoiles Beta Cephei se placent dans une bande sensiblement parallèle à la séquence principale d'age zéro (ZAMS) entre B0 et B3, et à environ 1,5 magnitude au dessus de celle-ci. Les limites exactes de la zone des étoiles Beta Cephei n'ont pas été déterminées de façon très précise. Les travaux théoriques sur l'évolution des étoiles massives montrent que cette zone peut correspondre ou bien à des étoiles en train de bruler l'hydrogène dans le noyau, ou bien à des étoiles dans une phase de contraction ou bien à des étoiles brulant l'hydrogène dans une enveloppe autour du noyau. On ignore lequel de ces états d'évolution permettrait la meilleure description du phénomène Beta Cephei.

Dans la deuxième section du chapitre 5 on décrit quelques catégories d'étoiles B particulières. Les Tables 5-2 à 5-5 donnent les propriétés caractéristiques de chacune de ces catégories. Les anomalies discutées sont uniquement celles qui sont décelables sur les spectres servant à la classification spectrale MK; par conséquent, les étoiles B dites particulières sont celles qui ne s'intégrant pas normalement dans cette classification.

Bien que la plupart des étoiles chaudes sous-lumineuses soient de type O plutôt que B, ces étoiles ont été incluses dans la discussion parce que quelques unes de leurs anomalies se retrouvent pour les types plus avancés. La Table 5-2 donne les propriétés de quelques exemplaires typiques de cette catégorie.

La Table 5-3 donne une liste d'étoiles à raies d'hélium fortes avec leurs principales propriétés. Les spectres sont de type B. Dans le diagramme HR, ces étoiles se situent près de la séquence principale correspondant à la combustion de l'hydrogène. L'exemple le plus étudié de ce type d'étoile est σ Ori E. Malgré l'intensité apparente des raies de l'hélium, la quantité d'hydrogène dans l'atmosphère est encore importante, du même ordre de grandeur que celle de l'hélium en nombres d'atomes.

Ce n'est plus le cas pour les 9 étoiles à hélium extrême présentées dans la Table 5-4, où l'hydrogène est pratiquement absent. Ces étoiles présentent d'autres anomalies de composition chimique, en particulier pour le carbone (surabondant) et l'oxygène (sousabondant). Leur haute latitude galactique et leurs vitesses élevées les distinguent des étoiles à raies d'hélium fortes discutées plus haut et les apparentent aux étoiles de la popluation II.

La Table 5-5 donne une liste d'étoiles où les raies de l'hélium sont plus faibles que dans les étoiles normales, ou même absentes. Les autres raies ont des intensités normales. Aucune de ces étoiles ne parait avoir un champ magnétique important.

Enfin, il existe une catégorie d'étoiles où l'intensité des raies de l'hélium oscille périodiquement, entre des valeurs plus fortes et des valeurs plus faibles que la normale. Le proto-

type est *a* Cen, avec une période de 8,81 jour. Le spectre de l'hydrogène est sensiblement constant.

Les étoiles à mercure et à manganèse ont des températures effectives et des gravités correspondant aux type B avancés de la série principale. Elles ont des rotations faibles et leur champ magnétique est trop petit pour être observable. La photométrie ultraviolette montre que leur flux ultraviolet extrême est trop faible pour leurs couleurs UBV.

Les étoiles Bp vraies sont les étoiles à raies de silicium fortes. On les trouve parmi les types B8 et B9 et elles semblent constituer une extension vers les hautes températures des étoiles à strontium, europium et chrome qui forment le gros des étoiles Ap. Les étoiles Bp ont des champs magnétiques intenses, et parfois variables. Elles présentent très souvent des variations dans le spectre ou dans la magnitude.

Le chapitre 6 est consacré aux modèles d'atmosphère. Dans la première section, on indique les principes appliqués pour construire des modèles d'atmosphère dans le cas des étoiles B. Les spectres calculés à partir de ces modèles, dont la physique est bien définie, sont alors comparés aux spectres observés; l'accord ou le désaccord entre le spectre calculé et le spectre réel donne des indications sur les conditions physiques qui règnent dans l'atmosphère de l'étoile observée.

Les modèles classiques d'atmosphère sont constitués par des couches planes et parallèles de gaz en équilibre radiatif et hydrostatique. Les deux paramètres qui définissent une atmosphère classique, une fois la composition chimique fixée, sont la température effective et l'accélération de la pesanteur due à la masse de l'étoile. La physique utilisée est celle d'un gaz de faible densité et partiellement ionisé en contact avec un champ de rayonnement. L'ensemble de ces données théoriques et expérimentales permet de déterminer les interactions entre le rayonnement et la matière dans l'atmosphère de l'étoile.

Bien que la condition de l'équilibre hydrostatique ne soit rigoureusement remplie que dans très peu d'étoiles B réelles, les grilles de modèles existantes sont des outils très efficaces pour l'interprétation des spectres d'étoiles B.

Il faut cependant garder à l'esprit qu'il est très difficile, sinon complètement impossible, de prouver que le modèle adopté est l'unique manière de représenter le spectre observé.

L'hypothèse de l'équilibre thermodynamique local (ETL) n'est pas entièrement justifiée pour une atmosphère stellaire dont le rayonnement s'échappe dans l'espace. Elle permet cependant d'obtenir des modèles d'atmosphère et des spectres calculés très utiles dans la pratique. C'est seulement lorsque l'on veut représenter des raies fortes d'ions abondants ou bien certaines raies particulières, qu'il est nécessaire d'utiliser des concepts plus élaborés (dits hors-ETL) et de calculer la distribution des atomes et des ions sur les différents niveaux d'énergie suivant les principes de l'équilibre statistique. Dans le cas des raies fortes, la physique hors-ETL elle-même est encore insuffisante pour éliminer tous les désaccords entre les spectres prédits et observés.

Dans la deuxième section la procédure utilisée pour construire les modèles d'étoiles B est décrite rapidement. On souligne la valeur de la grille de modèles (dans l'hypothèse de l'ETL et compte tenu de l'effet des raies) publiés par Kurucz en 1979. Cet ensemble de modèles est le plus complet de ceux qui existent actuellement pour interpréter les spectres des étoiles B. Le spectre continu fourni par les modèles de Kurucz est donné de façon suffisamment détaillée pour que la comparaison avec les spectres observés puisse se faire facilement. Un autre ensemble de modèles, utilisant la physique hors-ETL, a été publié par Mihalas (1972a). Ces derniers modèles sont utiles principalement pour les étoiles B des premiers types. Mihalas ne donne le flux émergent que pour un petit nombre de longueurs d'onde, par contre il donne des profils détaillés pour $H\alpha$, $H\beta$, et $H\gamma$. Les distributions

d'énergie des modèles de Kurucz et des modèles de Mihalas ont à très peu de chose près la même forme de 1200 Å à 1 micron. L'utilisation de la physique hor-ETL produit une légère augmentation (de 15 à 20 pour cent) de la température électronique dans les couches extérieures des modèles de Mihalas, à partir d'un minimum atteint pour une faible profondeur optique. Dans les modèles de Kurucz (en ETL), la température décroit constamment de l'intérieur vers l'extérieur de l'atmosphère.

Dans la troisième section on compare les spectres prédits par des modèles constitués de couches planes et parallèles avec les spectres observés Des indications sont données sur la manière de choisir un modèle d'atmosphère pour une étoile réelle L'utilisation de la forme de la distribution d'énergie et, pour les étoiles de la série principale, celle de la grandeur de la discontinuité de Balmer, donnent des résultats satisfaisants L'utilisation de la largeur équivalente de Hγ ou celle du nombre quantique de la dernière raie de Balmer observée constituent également des méthodes efficaces (Fischel et Klinglesmith, 1973). On signale enfin que Kurucz et ses collaborateurs ont pu prédire de façon précise la plupart des relations entre couleurs observées pour les étoiles B dans les photométries à bandes passantes larges et intermédiaries.

En principe la distribution de l'énergie d'une étoil en rotation doit différer de celle de la même étoile sans rotation. Le travail de Collins et Sonneborn (1977) sur ce sujet est signalé. Seules des rotations très rapides peuvent produire des modifications observables dans les couleurs et, dans la plupart des cas, un modèle stationnaire est suffisant pour représenter une étoile B normale.

Lorsque l'on possède des observations complètes dans un grand domaine spectral s'étendant de l'ultraviolet à l'infrarouge, la meilleure façon de procéder pour choisir un modèle consiste à déterminer la température effective et le rayon par la méthode directe décrite dans le chapitre 3. Si de plus l'étoile fait partie d'un système binaire et que sa masse est donnée par le calcul de l'orbite, on peut obtenir la gravité superficielle de façon directe. Sinon, on peut obtenir une valeur relativement sûre de la gravité en ajustant les profils des ailes des raies de Balmer du modèle à ceux de l'étoile.

Dans la troisième section on examine comment les abondances peuvent être déduites des largeurs équivalentes et des profils des raies. Pour les étoiles de la série principale on trouve en gros des compositions voisines de celle du Soleil L'application des techniques dites "fine analysis" aux supergéantes est examinée aussi dans la section. On note que dans le cas des supergéantes, il peut exister un "manteau" non homogène, avec des parties plus froides et d'autres plus chaudes Cette possibilité jette un doute sur la réalité des abondances anormales trouvées pour l'azote et éventuellement pour d'autres éléments, en utilisant un modèle classique.

Dans cette même section, on signale que la technique dite "fine analysis" utilisée dans le cadre de la physique hor-ETL pour déterminer l'abondance à partir de raies faibles et de raies fortes d'un même élément conduit à des résultats plus cohérents que lorsque l'hypothèse de l'équilibre thermodynamique local est faite. L'introduction de la physique hors-ETL permet donc de réduire le rôle de la microturbulence, utlisée comme facteur d'adjustement. Cependant, aussi bien pour les naines que pour les supergéantes, on trouve que les parties centrales des raies fortes (par exemple, He I 5876, 6678, 7065, 7281, et 10830 Å) ne sont bien représentées ni par les modèles ETL ni par les modèles hors-ETL. Dans ce cas, ce sont les effets du "manteau" que l'on observe et cette partie de l'atmosphère n'est pas incluse dans les modèles, qui représentent seulement la photosphère.

Les principales différences qui résultent de l'utilisation de la physique ETL et hors-ETL sont signalées dans la troisième section En gros, la physique hors-ETL produit des effets sur

le continu qui résultent des excès ou des défauts d'ionisation par rapport à ce qui se passe dans le cas ETL, et des effets sur les raies qui résultent des changements dans les populations des niveaux.

En résumé, les modèles donnant une bonne représentation de la photosphère, les méthodes classiques permettent en général d'interpréter correctement le spectre continu des étoiles B. Cependant, beaucoup d'aspects du spectre en ce qui concerne les raies et même, dans le cas des supergéantes, en ce qui concerne le continu, ne peuvent s'interpréter par les modèles classiques. Dans la même section on indique quels sont ces aspects du spectre non-prévisibles et on les discute.

Dans la quatrième section on passe en revue les théories permettant la modélisation des atmosphères en mouvement. Les types d'atmosphère en mouvement qui ont été étudiés constituent des modèles simples pour les couches extérieures de l'atmosphère, que l'on a appelées par commodité "manteau." La valeur de ces modèles pour obtenir les conditions physiques réelles qui règnent dans le "manteau" ne pourra être reconnue que par une comparaison détaillée avec les observations. Beaucoup des problèmes rencontrés dans ces travaux théoriques ont un aspect mathématique difficile.

Dans les premiers travaux sur les atmosphères en mouvement les équations de transfert du rayonnement étaient résolues analytiquement. Les travaux plus récents font grand usage de solutions numériques obtenues au prix de quelques hypothèses simplificatrices en ce qui concerne les conditions physiques régnant dans le "manteau." Dès l'origine, l'étude du transfert du rayonnement dans les atmosphères en mouvement a donné un résultat très important en montrant le rôle joué par l'expansion de l'atmosphère et par son étendue dans la forme des raies d'absorption et d'émission que l'on observe dans les étoiles ayant un spectre anormal

Une simplification importante de la théorie du transfert dans les atmosphères en mouvement a été introduite par Sobolev (1947). Sobolev a utilisé la notion de "probabilité d'échappement" et montre que dans le processus de formation d'une raie en présence de gradients de vitesse élevés, seule la matière contenue dans une ou éventuellement, un petit nombre de très petite(s) portion(s) de l'atmosphère le long de chaque ligne de visée intervient dans l'intensité observée en un point donné du profil de la raie. Cette simplification due aux gradients de vitesse est intéressante surtout dans le cas où une seule portion de l'atmosphère intervient le long de chaque ligne de visée; cela se produit lorsque la vitesse projetée sur la ligne de visée varie de façon monotonique le long de cette ligne. Les positions géométriques dans l'atmosphère des différentes régions correspondant à chaque point du profil de la raie sont déterminées par la loi de distribution des vitesses adoptée.

Depuis 1960 des méthodes élégantes ont été développées pour traiter le problème mathématique du transfert du rayonnement dans les atmosphères en mouvement. Dans tous les cas traités, la loi de vitesse et la variation de la température en fonction de la distance à la photosphère ont été représentéespar des fonctions choisies arbitrairement. La densité est ensuite calculée en admettant que le flux de masse est le même à travers toutes les couches successives de l'atmosphère. L'état physique du modèle de "manteau" ainsi constitué est alors entièrement défini et l'on résout le problème du transfert du rayonnement. Les profils des raies et leurs largeurs équivalentes sont calculés pour différentes valeurs caractéristiques des paramètres qui définissent le modèle.

Pour résoudre les équations de transfert du rayonnement dans une atmosphère en mouvement à trois dimensions et dans laquelle la vitesse augmente vers l'extérieur, on peut procéder de deux façons. Ou bien l'on admet que la raie est produite par diffusion et l'on fait l'approximation de Sobolev (Lucy, 1971; Olson, 1978; Surdej, 1979; Castor et Lamers,

1979), ou bien l'on résout les équations dans un système de référence lié en chaque point à l'atmosphère en mouvement (Mihalas et Kunasz, 1978). Dans ce dernier cas, aucune hypothèse simplificatrice n'est faite en ce qui concerne les effets des gradients de vitesse sur les interactions entre la matière et le rayonnement provenant des différents points de l'atmosphère. Des profils typiques obtenus par ces calculs théoriques sont donnés dans les Figures 6-5 et 6-6.

La théorie de la formation des raies dans les atmosphères en mouvement a permis de mettre en évidence un résultat très important (voir Hummer, 1976) · la relation d'Eddington-Barbier (indiquant que le flux émergent monochromatique en un point d'une raie est égal à la valeur de la fonction source à l'endroit où la profondeur optique monochromatique correspondante est égale à 1) n'est plus valable lorsque les couches atmosphériques ne sont plus statiques. Ceci signifie que l'on ne peut déterminer les conditions physiques régnant dans l'atmosphère aux endroits d'où provient le rayonnement reçu en un point particulier du profil d'une raie.

Martı et Noerdlinger (1977), puis Rybicki et Hummer (1978) ont étudié la théorie de la formation des raies dans une atmosphère en mouvement à trois dimensions dans laquelle la projection de la vitesse sur la ligne de visée ne varie pas de façon monotonique. Dans ce cas, les surfaces d'égale vitesse sont coupées en plus d'un point par la ligne de visée et le rayonnement ne s'échappe plus librement.

Tous ces travaux montrent qu'il est très difficile d'interpréter la forme d'un profil de type "P-Cygni" sans ambiguité, au moyen d'un flux de masse dont tous les paramètres seraient bien définis. Par exemple, Rybicki et Hummer (1978) ont montré qu'une raie formée d'une absorption déplacée vers les courtes longueurs d'ondes et d'une composante en émission située du côté des grandes longueurs d'onde peut être produite par une atmosphère dans laquelle une brusque accélération au voisinage de la photosphère est suivie par une décélération. Le profil prédit dans ce cas ne diffère que par des détails minimes du profil donné par une atmosphère accélérée vers l'extérieur à tous les niveaux au dessus de la photosphère. Des profils typiques pour ce dernier cas ont été donnés par Olson (1978), Surdej (1979) et Castor et Lamers (1979).

On donne les résultats obtenus en interprétant les profils observés pour Hα, Hβ et Hγ dans P Cyg à la lumière des idées théoriques exposées plus haut. Les profils calculés ressemblent à ceux que l'on observe réellement mais on n'obtient jamais un accord excellent, même lorsque l'on utilise l'analyse statistique pour déterminer la distribution des atomes d'hydrogène sur les différents niveaux d'énergie possibles (Oergle, 1977; Lee, 1979)

Le travail de Oergle et van Blerkom (1976) et celui de Karp (1978) sur la formation des raies de He I dans les atmosphères en mouvement donnent l'espoir que les déplacements relatifs observés pour une raie forte et une raie faible de He I permettront d'obtenir des informations sur les gradients de vitesse.

Les théories existantes sur le "manteau" des étoiles B ont surtout la valeur d'expériences numériques montrant quelle sorte de spectre peut apparaîte lorsque certaines conditions de champs de vitesses et de distributions de températures règnent dans le "manteau." Ces théories manquent de cohérence par le fait qu'aucune tentative n'est faite pour traiter de façon globale le problème du transfert radiatif et la résolution des équations de conservation, dans le but d'obtenir un modèle de "manteau" ayant une signification physique réelle. Ce dernier problème est très difficile et son étude n'a pas encore été abordée.

Le chapitre 7 traite de l'évolution des étoiles massives. On donne les principaux résultats de la théorie de l'évolution des modèles d'étoiles massives Les trajets évolutifs suivis

par ces modèles dans un diagramme HR sont comparés avec les distributions observées pour les étoiles B réelles dans le même diagramme. Le diagramme HR utilisé dans ce chapitre est celui qui donne $\log L/L_{\odot}$ en fonction de $\log T_{\text{eff}}$.

Dans la deuxième section on examine le problème de l'évolution sans perte de masse Quelques aperçus sont donnés sur le choix de la composition chimique des modèles (X, Y, Z), sur celui des tables d'opacité et sur la représentation du transport de l'énergie lorsque les méchanismes radiatifs et convectifs sont présents à la fois

La Figure 7-1 montre des trajets évolutifs théoriques obtenus en utilisant les tables de Cox-Stewart pour obtenir les opacités et le critère Schwarzschild pour traiter le problème du transport de l'énergie lorsque de la convection se produit dans l'enveloppe. Quelques positions représentatives d'étoiles réelles ont été ajoutées à la Figure 7-1 pour les situer par rapport aux trajets évolutifs théoriques. On montre également que les trajets évolutifs des modèles utilisant le critère de Ledoux pour la convection traversent la région occupée par les supergéantes B à des luminosités plus faibles que lorsque le critère de Schwartzschild est utilisé.

La Figure 7-2 montre les trajets évolutifs de deux modèles, de 15 et 25 masses solaires, calculés avec les opacités du Cox-Stewart et le critère de Schwarzschild. Le modèle de 15 masses solaires est encore en train de bruler de l'hélium dans le noyau après avoir traversé la région des supergéantes bleues alors que le modèle de 25 masses solaires a terminé cette combustion en quittant le domaine des supergéantes B.

La Figure 7-3 montre des trajets évolutifs d'étoiles massives calculés avec les opacités de Carson et le critère de Schwarzschild. Dans ce cas, les modèles ayant des masses supérieures à 15 $M_{\odot}$ brulent encore de l'hydrogène dans le noyau lorsqu'ils quittent la région des supergéantes bleues

Les différences observées entre les trajets évolutifs des Figures 7-1 et 7-3 donnent une idée de ce qui se passe lorsque l'on change la composition chimique, le choix des tables d'opacité et la manière de traiter le problème de la convection. Enfin, on signale les raisons de penser que les tables d'opacité de Cox-Stewart conduisent à la meilleure représentation des diagrammes HR observés que l'on puisse obtenir actuellement.

Les propriétés des modèles ayant des masses inférieures à 10 $M_{\odot}$ sont pratiquement insensibles au choix de la composition chimique, à celui des tables d'opacité et au traitement de la convection. Pour les masses supérieures à 10 $M_{\odot}$, les positions des trajets évolutifs sont sensibles à la manière dont le modèle est construit. Ceci est particulièrement vrai pour les parties du trajet évolutif qui se trouvent dans la région du diagramme HR occupée par les supergéantes bleues. Le temps passé par le modèle dans la phase de combustion de l'hydrogène dans le noyau dépend principalement de la masse et très peu des autres choix faits dans la construction du modèle. La Table 7-1 donne quelques valeurs typiques de ce temps. Les modèles d'étoile parcourent ensuite rapidement les phases de contraction et de combusion de l'hydrogène dans une couche extérieure au noyau. La combustion de l'hélium dans le noyau commence et sa durée est environ dix fois plus courte que celle de la combustion de l'hydrogène

La troisième section traite de l'évolution des modèles avec perte de masse. Les premiers travaux sur l'évolution de modèles nonhomogènes avec perte de masse ont été faits par Tanaka (1966) Les résultats de Tanaka ont été confirmés et développés par toutes les études ultérieures. Par comparaison avec une étoile évoluant sans perte de masse, une étoile massive qui perd de la matière a une luminosité et une température effective plus basses pour une même diminution de la proportion d'hydrogène dans la partie centrale. Elle a de plus une stabilité accrue vis à vis de la convection dans l'enveloppe et une plus grande frac-

tion de sa masse se trouve dans le noyau convectif. La durée de la phase de combustion de l'hydrogène est également plus grande que pour une étoile évoluant sans perte de masse. Trois algorithmes, et une variante du premier d'entre eux, ont été utilisés pour représenter le taux de perte de masse en fonction de la luminosité, du rayon et de la masse de l'étoile. Ces algorithmes sont: (1) $\dot{M} = -kLR/M$, (2) $\dot{M} = -NL/c^2$, et (3) une fonction compliquée déduite de la théorie des vents stellaires de Castor et al. Dans (1), k est une constante dont la valeur doit être voisine de 1.0×10^{-11} pour que le taux de perte de masse obtenu pour une étoile B0 soit celui que l'on admet généralement, L, M, et R étant exprimés en unités solaires. Dans (2), N est une constante également et sa valeur est voisine de 100. La fonction qui représente la perte de masse dans le cas (3) d'un vent stellaire entraîné par la pression de radiation contient deux paramètres, α et K auxquels on attribue des valeurs numériques; elle contient aussi le rapport Γ entre la luminosité instantanée de l'étoile et sa luminosité Eddington, rapport qui varie comme L/M. On a également examiné les effets de la rotation sur la perte de masse.

Quelques tracés évolutifs typiques obenus dans le cas où il y a perte de masse sont reproduits dans la Figure 7-4. La Table 7-2 donne les valeurs calculées du taux de perte de masse pour différents stades de l'évolution d'un modèle d'étoile massive. Les calculs faits montrent que l'inclusion dans le modèle d'un taux de perte de masse de l'ordre des taux observés produit des changements dans la position des trajets évolutifs du même ordre de grandeur que ceux qui résultent des divers choix possibles pour la composition chimique, les tables d'opacité et le mode de traitement de la convection. C'est dans la région du diagramme HR occupée par les supergéantes B que l'influence de la perte de masse sur les trajets évolutifs est la plus sensible.

A cause des incertitudes sur la position exacte des trajets évolutifs, il n'est pas possible d'obtenir de façon précise la masse d'une supergéante à partir de sa position observée dans le diagramme HR. On ne pourrait le faire que si l'on possédait par ailleurs des informations supplémentaires permettant de faire des choix corrects pour la composition chimique, les opacités, le traitement de la convection et la perte de masse.

Dans la quatrième section les diagrammes HR observés sont comparés aux diagrammes HR calculés pour des étoiles massives évoluant sans perte de masse.

Les résultats sont discutés dans la cinquième section La Figure 7-5 montre les positions observées de 160 étoiles des premiers types dans le diagramme HR. Sur la même figure on a placé les deux bandes correspondant aux deux séquences principales calculées par Stothers (1976), la première avec les opacités de Cox-Stewart, la deuxième avec celles de Carson. La plupart des étoiles O et B de la Figure 7-5 sont des étoiles voisines du Soleil et beaucoup sont des standards MK

L'examen de la Figure 7-5 permet de tirer deux conclusions importantes. (1) La formation d'étoiles au voisinage du Soleil s'est produite à deux époques différentes. Les étoiles de types B3 et plus avancés, y compris α Lyr, sont quelque peu évoluées et ont des âges situés approximativement entre 2,2 et 24.10^7 ans. Les étoiles B les moins avancées et les supergéantes sont un peu plus jeunes, avec des âges compris entre 0,6 et 2.10^7 ans. Toutes ces étoiles sont donc plus jeunes que le Soleil par un facteur 10 ou 100. Elles ont été choisies d'après leur magnitude apparente car seules les étoiles brillantes ont été observées photométriquement à la fois dans l'ultraviolet, le visible et l'infrarouge. (2) En différents endroits du diagramme HR on trouve juxtaposées des étoiles dont les types spectraux sont différents. Par exemple les étoiles de Wolf-Rayet occupent la même place que les étoiles B0 de classes de luminosité III et Ia, les étoiles Beta Cephei sont dans une région occupée également par des étoiles normales et par des étoiles dont les profils de raies sont variables; les étoiles Be

occupent une région située en grande partie sur la région la plus à droite dans la séquence principale, région qui est peuplée aussi d'étoiles B normales; la même chose est vraie pour les étoiles Bp, qui coexistent avec les étoiles B normales de type avancé

Il paraît clair que pour les étoiles B le type spectral par lui-même n'est pas un critère indiquant l'exclusivité de la position occupée dans le diagramme HR. Ceci est particulièrement vrai lorsque les critères que définissent le type spectral sont basés sur des raies formées principalement dans le "manteau" de l'étoile.

D'une façon générale, la théorie de l'évolution des étoiles massives donne une interprétation cohérente de la position de la plupart des étoiles B de la séquence principale. Les masses obtenues à partir des orbites d'étoiles doubles sont en accord avec celles que l'on déduit de la théorie de l'évolution. L'interprétation des positions observées pour les étoiles qui ont quitté la séquence principale et se dirigent vers la région des supergéantes n'est pas encore satisfaisante et des modèles meilleurs et plus détaillés seraient nécessaires pour les phases où il y a combustion de l'hydrogène dans une couche extérieure au noyau et combustion de l'hélium dans le noyau

Le diagramme HR observé de Humphreys (1978) qui correspond à des étoiles O et B lumineuses est très semblable à celui de la Figure 7-5. Les échelles de températures effectives et de corrections bolométriques adoptées par Humphreys sont différentes de celles utilisées ici. Le choix de Humphreys n'est pas recommandé car de meilleures données existent actuellement Les luminosités trouvées par Humphreys et Davidson (1979) pour P Cyg et quelques étoiles de très grande luminosité sont beaucoup trop grandes.

Les positions de la séquence principale d'âge zéro (ZAMS) pour les étoiles B déterminées par Eggen (1974a) et par Crawford (1978) à partir d'une photométrie à bandes intermédiaires sont comparées dans la Figure 7-6 à la position théorique de la ZAMS. On observe de petits écarts systématiques dus probablement à l'utilisation par Eggen et par Crawford de quelques étoiles un peu évoluées.

La position d'une étoile dans le diagramme HR est déterminée par sa masse et son âge, ou, ce qui est équivalent, par sa source d'énergie. Mais plus d'une apparence spectroscopique peut être associée à un point donné ($\log L/L_{\odot}$, $\log T_{\rm eff}$) du diagramme HR. Ceci se produit parce que dans le cas des étoiles B, et plus particulièrement dans celui des supergéantes B, les critères spectroscopiques choisis empiriquement pour définir le type spectral dépendent non seulement de $\log g$ et de $T_{\rm eff}$ mais aussi de l'état du "manteau." Le lien éventuel entre l'état physique du "manteau" et l'âge de l'étoile n'est pas clair dans l'état actuel des choses. Peut-être les conditions physiques régnant dans le "manteau" pourraient-elles avoir un lien avec ce qui se passe dans l'enveloppe et avec la façon dont l'énergie s'y propage.

Les modèles d'étoiles massives pulsantes sont analysés dans le fins du chapitre 7.

Dans le chapitre 8 on passe en revue les problèmes non résolus. Les données de l'observation et les théories présentées dans cette première partie du livre sur les étoiles B sont passées en revue dans le but de (1) déterminer jusqu'à quel point nous comprenons réellement la physique d'une étoile B dans le cas le plus simple où elle est isolée dans l'espace, (2) recenser et discuter les problèmes qui sont encore sans solution satisfaisante, et (3) suggérer quelques voies dans lesquelles on pourrait s'engager pour améliorer la modélisation des étoiles B

Les principaux résultats concernant les températures effectives, les rayons, les masses et la composition chimique des étoiles B sont résumés dans la deuxième section de ce chapitre. Si l'on veut expliquer toutes les observations faites sur les spectres des différentes catégories d'étoiles B, il est nécessaire de tenir compte des régions les plus extérieures de l'atmosphère de l'étoile, régions situées au-delà de la photosphère et où l'on observe les effets de la dis-

sipation d'énergie non radiative. L'ensemble de ces régions a été désigné par le terme de "manteau."

Les propriétés du "manteau" sont décrites dans la deuxième section. Dans un "manteau," les concepts d'équilibre radiatif et d'équilibre hydrostatique ne sont plus valables pour décrire l'état du gaz, et il est nécessaire d'utiliser une géométrie à trois dimensions.

Le "manteau" d'une étoile chaude est en général transparent dans la plus grande partie du spectre continu, il est par contre opaque pour les raies fortes des ions abondants. Le plasma contenu dans le "manteau" est porté à des températures électroniques supérieures à celles que pourrait lui communiquer l'énergie radiative correspondant à la température effective de l'étoile et transmise en équilibre radiatif.

L'inhomogénéité est une caractère très fréquemment observé dans un "manteau," particulièrement dans celui des supergéantes. Cette inhomogénéité se manifeste par la présence de régions chaudes et de régions froides qui n'ont pas en général de symétrie sphérique et ne recouvrent pas forcément toute la surface de l'étoile. De la matière s'échappe du "manteau" avec des vitesses supérieures à la vitesse d'échappement à partir de la photosphère.

Le "manteau" se manifeste à des degrés très différents pour les étoiles de la série principale et pour les supergéantes. Il peut donner un spectre continu dû aux transitions "bound-free" de l'hydrogène et à des transitions "free-free," des raies d'émission (ou parfois d'absorption) de l'hydrogène, et des raies d'absorption correspondant à des ions de haut degré d'ionisation, situées dans l'ultraviolet. La détection de rayon X en provenance d'une étoile B indique de façon certaine la présence d'un "manteau." Le "manteau" est particulièrement visible dans le cas des supergéantes ou dans celui des étoiles Be/shell, il est très difficile à détecter pour les étoiles de la série principale Des pertes de masse avec des taux d'environ 2×10^{-6} $M_{\odot}$ par an peuvent s'observer dans les supergéantes B0 Ia. Pour les supergéantes Ia de type avancé le taux de perte de masse est de l'ordre de 10^{-7} $M_{\odot}$ par an. Pour les supergéantes Ib, les taux de perte de masse semblent plus faibles. Mais même pour les étoiles de la série principale, on observe des caractères spectroscopiques suggérant l'existence d'un flux de matière dirigé vers l'extérieur. Les taux de perte de masse correspondants sont probablement inférieurs au millième de ceux que l'on observe pour les supergéantes ayant le même sous-type spectral. Il y a de faibles indices en faveur de températures électroniques plus élevées dans le "manteau" lorsque la densité est faible que lorsqu'elle est relativement forte.

Dans la troisième section les résultats de la théorie de l'évolution sont confrontés avec les luminosités et les températures effectives observées pour les étoiles B. L'interprétation des positions observées semble avoir une base solide pour les étoiles de la série principale. Mais dans tous les cas où la source d'énergie n'est plus constituée par la combustion de l'hydrogène dans le noyau, des améliorations dans le calcul du transport de l'énergie à travers les enveloppes et dans celui de leur opacité seront nécessaires avant de pouvoir interpréter de façon sûre la position des étoiles B dans la partie correspondante du diagramme HR.

Dans la quatrième section on compare les résultats de la théorie des spectres stellaires avec les spectres observés et l'on développe le schéma d'un modèle de "manteau." La conclusion est que la théorie existante des atmosphères stellaires permet d'interpréter correctement la partie du spectre d'une étoile B qui se forme dans la photosphère Cette partie du spectre comprend presque tout le continu et les raies des ions peu abondants. Lorsque les raies sont suffisamment fortes pour être formées, au moins en partie, dans le "manteau" la théorie existante est en défaut car elle repose sur des hypothèses valables pour la photosphère mais qui ne permettent pas de déterminer les températures et les densités dans le "manteau." L'utilisation de la physique hors-ETL améliore un peu les résultats mais les dif-

ficultés liées au fait que beaucoup de raies importantes sont formées partiellement ou totalement dans le "manteau" subsistent.

Six catégories de phénomènes spectroscopiques, totalement inexpliqués par la théorie classique sont recencés dans la section Leur existence conduit à développer des modèles de "manteau" en utilisant d'autres relations et d'autres paramètres que ceux qui ont permis de donner une bonne représentation du spectre issu de la photosphère. On examine quels sont les caractères que doit présenter le "manteau" et quelle est la signature spectroscopique de chacun d'eux. Pour les étoiles B on est conduit à considérer que le "manteau" est formé de trois parties: (1) une région de type pseudo-coronal où les températures électroniques sont élevées mais cependant inférieures à 10^6 K, (2) des régions coronales, probablement de petites dimensions et imbriquées dans la zone pseudo-coronale, avec des températures atteignant 10^7 K, et (3) une région post-coronale où se produit le refroidissement et où l'on atteint progressivement les conditions règnant dans le milieu interstellaire local. Les accélérations et les décélérations de la matière dans la région post-coronale sont probablement peu importantes

Des descriptions schématiques des atmosphères des étoiles B sont données de manière à rendre le concept de "manteau" plus concret En ce qui concerne le degré d'activité de leur "manteau," les étoiles B peuvent être classées en (1) étoiles B normales de la série principale montrant peu ou pas de variations, (2) supergéantes, montrant constamment des variations de faible amplitude, (3) Be/shell qui peuvent présenter des changements très importants à des intervalles de quelques mois ou quelques années

Si la source d'énergie non radiative qui est à l'origine de la formation du "manteau" reste encore à identifier, on peut déjà franchir une première étape en évaluant la quantité d'énergie et la quantité de mouvement qu'elle doit fournir. Ceci est fait dans la quatrième section pour des étoiles B0 et B9 typiques de la série principale et de la région des supergéantes. On trouve que la quantité d'énergie nécessaire pour maintenir le "manteau" des étoiles naines et des supergéantes est seulement une petite fraction de l'énergie radiative provenant de la photosphère. Cependant, dans le cas d'une supergéante B9 ayant un "manteau" très important qui émet le spectre de l'hydrogène, la quantité d'énergie nécessaire n'est plus très petite vis-à-vis de celle que transmet la photosphère.

La quantité d'énergie perdue par le "manteau" par conduction, par rayonnement et sous la forme d'énergie cinétique emportée par les particules qui s'échappent, a été estimée. On montre qu'elle est faible sauf dans le cas où une partie importante du "manteau" est à température relativement basse et rayonne fortement dans le spectre de l'hydrogène, et que les quantités d'énergie les plus importantes émises par le "manteau" d'une étoile B sont celles que l'on détecte dans le spectre continu de l'hydrogène et dans les émissions de type "free-free" observées dans l'infrarouge et aux longueurs d'onde radio. Dans les étoiles qui présentent un grand excès d'infrarouge, la source qui produit le chauffage du "manteau" doit avoir un débit d'énergie comparable à celui de l'étoile elle-même. Lorsque l'on ne détecte aucune émission dans le spectre de l'hydrogène, l'énergie qui apparaît dans le "manteau" ne dépasse pas le dix-millième de l'énergie produite par l'étoile.

Dans la quatrième section du chapitre 8, on examine aussi le problème de la modélisation du "manteau." On part de l'idée que toutes les étoiles B ont un "manteau" et que ce "manteau" est plus ou moins bien détecté suivant nos possibilités d'observer l'étoile dans tous les domaines spectraux et à tous les moments de son existence car les conditions favorisant ou freinant le développement d'un "manteau" peuvent varier.

On propose ensuite, un modèle schématique de "manteau" dans lequel l'énergie non radiative provient de champs magnétiques dont la présence dans les couches extérieures de

l'étoile est admise L'énergie contenue dans ces champs magnétiques serait dissipée par suite des mouvements de turbulence qui existent dans les couches extérieures des étoiles B.

Ces idées ont pour origine une suggestion faite par Rosner et al. (1978) pour expliquer les hautes températures et les inhomogénéités rencontrées dans la couronne solaire. Les hautes températures seraient dues à la dissipation d'énergie électrique dans des structures géométriques constituées par des sortes d'arches chauffées par des courants qui sont sensiblement parallèles aux lignes de force du champ magnétique et n'occupent qu'une faible partie du volume enfermé dans l'arche.

Il est facile d'admettre la présence de champs magnétiques trop faibles pour être directement observables dans les couches extérieures des étoiles B. Ces champs magnétiques pourraient provenir des champs magnétiques enfermés dans l'étoile au moment de sa formation, ils pourraient également avoir été créés par effet dynamo à la suite des convections qui se produisent dans l'enveloppe de l'étoile à différents stades de son évolution, en particulier pendant la phase de contraction qui suit la fin de la combustion de l'hydrogène dans le noyau. La turbulence qui existe dans les atmosphères d'étoiles B produit des mouvements différentiels qui ont pour résultat de libérer l'énergie contenue dans les champs magnétiques présents; cette turbulence peut être favorisée par une rotation différentielle de l'étoile. On montre que l'énergie nécessaire à la formation d'un "manteau" tel que ceux que l'on observe couramment dans les étoiles B peut être fournie par des champs magnétiques assez faibles pour être indétectables, et que de tels champs magnétiques peuvent réellement exister dans les étoiles B

On propose comme paramètre pour caractériser un modèle de "manteau" un nombre qui représenterait la densité moyenne de l'énergie magnétique dans le "manteau." Un second paramètre devrait caractériser l'efficacité avec laquelle l'énergie magnétique est transférée au gaz, ce pourrait être l'amplitude moyenne des mouvements différentiels.

Le "manteau" de l'étoile B se manifesterait au moment où les lignes de force du champ magnétique créé par effet dynamo dans l'enveloppe sortent de la photosphère en produisant, comme dans le cas du Soleil, des structures en forme d'arche. Ces structures sont certainement très complexes. Leur aspect dépend de la densité du gaz et de la turbulence dans les couches extérieures de l'étoile, il dépend aussi de la rotation de létoile. La rotation des structures avec la photosphère, la croissance et la décroissance des arches peuvent expliquer une grande partie des variations spectrales observées dans les supergéantes.

Une rotation rapide de l'étoile peut produire une torsion des structures en arche et les entremêler jusqu'à la formation d'un disque Il peut arriver que l'apparition d'énergie dans le disque soit ralentie, dans ce cas le disque se refroidit et un spectre de type "shell" apparait. Après un certain laps de temps, les effets dynamo dans l'enveloppe peuvent diminuer d'intensité, les structures en arche pourront alors disparaitre. Le disque disparaitra également. Le comportement du Soleil pendant le minimum de Maunder des taches solaires aide à comprendre comment la structure magnétique d'une étoile peut changer de façon notable avec une échelle de temps de plusieurs années.

Les structures en arche, qui sont considérées comme les structures fondamentales dans le modèle de "manteau" considéré ici, peuvent servir de canal pour la transmission d'énergie mécanique/acoustique produite dans les zones de convection qui apparaissent, d'après la théorie, dans l'enveloppe des étoiles massives, en particulier vers la fin de la combustion de l'hydrogène dans le noyau

Un flux de matière le long de lignes de force magnétiques ouvertes sur l'espace interstellaire peut être à l'origine des composantes déplacées par effet Doppler que l'on observe

souvent dans les raies ultraviolettes des supergéantes, et même parfois dans les raies du spectre visible. La matière peut recevoir son impulsion initiale des forces magnétiques. Une fois qu'elle a atteint une vitesse sonique, elle peut continuer à être accélérée par la pression de radiation. Ce type d'accélération est particulièrement efficace aux hautes températures

La cinquième section du chapitre 8 donne un résumé des principaux problèmes non encore résolus pour les étoiles B. Ils concernent le développement de modèles détaillés de structure interne pour les étoiles massives lorsqu'elles commencent à évoluer rapidement après la fin de la combustion de l'hydrogène dans le noyau, le développement de modèles détaillés pour le "manteau" et l'étude du transfert du rayonnement dans des masses gazeuses en mouvement, inhomogènes et à température élevée. Les théories existantes sur le transfert du rayonnement dans les atmosphères étendues en mouvement exposées dans le chapitre 6 ne sont pas d'un grand secours pour interpréter le spectre d'un "manteau" réel. En effet, ces théories (1) supposent dans presque tous les cas que la température des couches extérieures à la photosphère est du même ordre de grandeur que la température effective de l'étoile, (2) admettent une loi de vitesse ad hoc au lieu de déterminer une loi de vitesse compatible avec les forces qui s'exercent sur le plasma, et (3) ignorent l'inhomogénéité caractéristique du "manteau."

Avant que l'on puisse comprendre complètement les étoiles B, il sera nécessaire de rechercher tout ce que l'on peut tirer à l'heure actuelle, par l'observation et par la théorie, de l'étude détaillée du "manteau" du Soleil et de voir dans quelle mesure les résultats obtenus pourront être utilisés dans le cas des étoiles chaudes.

Résumé de la deuxième partie: les étoiles Be

La deuxième partie de ce volume, consacrée aux étoiles Be, comporte quatre chapitres. Le chapitre 10 présente une vue d'ensemble de ces étoiles. Le chapitre 11 est consacré aux données d'observation terrestre et aux modèles ad hoc construits d'après ces données pour représenter leur atmosphère. Dans le chapitre 12 sont décrites les données d'observation spatiale faites dans l'ultraviolet lointain et dans le domaine des rayons X. Dans le chapitre 13, sont présentées, en collaboration avec R. N. Thomas, les grandes lignes d'un modèle empirique, physiquement cohérent, et qui permet de décrire l'atmosphère des étoiles Be en tenant compte des données d'observations faites dans toutes les longueurs d'ondes, depuis le domaine des rayons X jusqu'au domaine des ondes radio.

Le chapitre 10 constitue un exposé introductif aux problèmes posés par les étoiles Be. On définit leur anomalie la présence de raies d'émission dans les raies de Balmer au lieu des raies d'absorption observées dans la majorité des étoiles, et prévues par la théorie classique des atmosphères stellaires. On les situe par rapport aux étoiles de type B de toutes les classes de luminosité et par rapport à l'ensemble des étoiles du diagramme HR. On décrit les grandes lignes du modèle rotationnel, proposé il y a un demi-siècle par Struve, basé sur les observations du spectre visible et qui postulait, pour ces étoiles, l'existence d'une atmosphère étendue Les observations spatiales, faites dans le domaine de l'ultraviolet lointain et des rayons X, placent les problèmes posés par la présence de raies d'émission dans un contexte différent puisque les étoiles normales et anormales possèdent, désormais, une atmosphère étendue, ce qui constitue une anomalie par rapport aux modèles thermiques

Dans le chapitre 11, la première section donne une description du spectre de raies des étoiles Be dans le visible et l'infrarouge. De la masse considérable des observations se dégagent trois propriétés du phénomène Be: il est fortement individualisé pour un même type

spectral, il est progressif—on n'observe pas de coupure franche entre étoiles Be et étoiles B normales, il est, enfin, variable.

Les raies d'émission des étoiles Be présentent une grande variété de profils; on observe souvent un renversement central plus ou moins profond, ou encore des structures plus ou moins irrégulières sur le contour de la raie d'émission, ou encore trois pics d'émission. Le spectre dénommé *shell* se définit par des centres d'absorption, fine et très profonde, bordés ou non d'ailes d'émission dans les raies d'hydrogène et dans les raies des métaux une fois ionisés (principalement Fe II). Les composantes d'émission ou de "shell" perturbent souvent les raies d'absorption photosphériques rendant la classification spectrale des étoiles Be difficile et imprécise.

Les études statistiques montrent que les étoiles Be sont, en moyenne, plus lumineuses que les étoiles B normales de même type spectral. Leur position dans le diagramme HR, qui correspondrait à la phase de contraction secondaire faisant suite à l'exhaustion de l' hydrogène dans le noyau, a souvent été interprétée en termes d'évolution. Cette interprétation se heurte à des difficultés sérieuses dont la plus importante est le changement du position qu' occupe une étoile Be individuelle dans ce diagramme en fonction de sa phase de variation. Ces changements de position se produisent en des temps très courts comparés aux temps évolutifs.

L'origine des raies d'émission dans le spectre des étoiles Be a été attribuée par Struve, en 1931, à une enveloppe étendue où le gaz est ionisé par le rayonnement ultraviolet de l'étoile. On n'observe cependant pas de grandes vitesses d'éjection dans le spectre visible permettant de justifier la présence d'une enveloppe étendue. En montrant que les raies d'absorption des étoiles Be sont plus larges que celles des étoiles B normales et que la largeur des raies d'émission est proportionnelle à la longueur d'onde, Struve établissait les bases du modèle rotationnel Cette grande largeur des raies d'absorption, attribuée à la rotation, conduisait Struve à définir les étoiles Be comme les rotateurs rapides de la classe B. Il postulait ensuite que la vitesse de rotation était critique pour expliquer l'éjection équatoriale de matière par instabilité rotationnelle. Le modèle rotationnel proposé par Struve pour représenter les étoiles Be est donc celui d'une étoile en rotation critique, entourée d'une enveloppe gazeuse également en rotation, modérément dense, étendue et aplatie à l'équateur. C'est l'image d'une petite nébuleuse planétaire. Son état d'excitation est plus faible que celui de la photosphère ainsi que l'indique la présence de raies d'émission ou de "shell" de Fe II, raies que l'on n'observe avec une aussi grande intensité que dans les spectres de type A. Dans ce modèle, la diversité du spectre de raies d'émission des étoiles Be est expliquée par des effets géométriques.

Le modèle rotationnel se heurte à deux difficultés d'une part, il n'existe aucune évidence de la rotation critique des étoiles Be; d'autre part, la variabilité des étoiles Be ne trouve aucune explication dans ce modèle. Avec l'ère spatiale, le problème de l'origine de l'atmosphère étendue des étoiles Be se pose en des termes différents. On sait, en effet, maintenant, que les étoiles normales peuvent aussi posséder une atmosphère extérieure à la photosphère. La question qu'on se posait du temps de Struve "Pourquoi les étoiles Be ont-elles une atmosphère extérieure à la photosphère alors que les étoiles B normales n'en ont pas"? est maintenant remplacée par la question suivante. "Pourquoi deux étoiles B de même type spectral, possédant toutes deux un flux de masse et un flux d'énergie non radiative, ne possèdent-elles pas toutes les deux, dans leur atmosphère extérieure, les régions froides où se forment les raies d'émission des étoiles Be observées dans le visible"?

La deuxième section du chapitre 11 décrit les observations du spectre continu des étoiles Be, du proche ultraviolet au domaine radio. Barbier et Chalonge obtenaient, dès 1941,

les conclusions les plus détaillées et les plus précises, et l'essentiel des résultats concernant la répartition de l'énergie des étoiles Be entre 3200 et 6000 Å. Ils montraient que la présence de raies d'émission dans le spectre visible des étoiles B s'accompagnait statistiquement de deux effets (1) un rougissement dans le continu de Paschen et de Balmer, c'est-à-dire une température de couleur plus faible que celle d'une étoile B normale de même type spectral, (2) une modification de la discontinuité de Balmer, celle-ci pouvant présenter des aspects différents pour les spectres Be et les spectres "shell", et subir des variations lorsque le spectre de raies d'émission varie Du fait de l'existence d'un rougissement intrinsèque, il n'est pas possible d'appliquer aux étoiles Be les méthodes usuelles de correction de l'extinction interstellaire que l'on applique aux étoiles normales Il n'existe, à l'heure actuelle, aucune méthode véritablement satisfaisante permettant d'évaluer le rougissement interstellaire des étoiles Be, de sorte que la comparaison de leur flux à celui des étoiles B normales est entachée d'une erreur difficile à chiffrer

Les déviations du spectre continu des étoiles Be par rapport aux étoiles B normales, observées dans le visible, se poursuivent en s'amplifiant dans l'infrarouge. Dans ce domaine spectral, une grande gamme d'excès de flux est observée, depuis les plus faibles, en majorité parmi les étoiles Be "ordinaires," aux plus forts, parmi les étoiles B[e] ou Bep présentant des raies interdites dans leur spectre, et parmi les étoiles associées à des nébulosités (dont les étoiles Ae et Be de Herbig). Toutes les étoiles à raies d'émission présentent dans l'infrarouge des écarts par rapport à la normale, et, si l'on voit se dessiner une certaine progression des excès, des étoiles Of aux supergéantes M, le caractère le plus frappant de ces excès est leur diversité à l'intérieur d'une même classe spectrale. Les excès les plus faibles—quelques dixièmes de magnitude vers 2 μ—sont interprétés en terme d'émission libre-libre (ou free-free) dans une enveloppe étendue de gaz ionisé ayant une température d'environ 10^4 K, tandis que les excès les plus forts sont expliqués par une réémission thermique due à des poussières circumstellaires. Ces poussières ont été identifiées dans un certain nombre d'étoiles, mais pas encore dans les étoiles Be et Bep, par la présence des deux bosses d'émission (vers 10 μ et 20 μ) caractéristiques des silicates.

Une émission continue dans le domaine radio, attribuable à un rayonnement thermique libre-libre, a été détectée dans quelques étoiles Bep et, plus généralement, parmi les étoiles ayant des enveloppes denses et très étendues. L'intérêt essentiel de l'étude du spectre radio est de permettre une détermination de la distribution des densités dans l'enveloppe circumstellaire, et de la perte de masse, si l'on connaît, par ailleurs, la vitesse d'expansion dans les régions où ce spectre est émis.

La troisième section du chapitre 11 est consacrée à la variabilité des étoiles Be dans le visible et le proche infrarouge. En règle générale, toutes les étoiles Be sont variables aussi bien dans leur spectre de raies que dans leur spectre continu. Cette variabilité a d'abord été observée dans le visible, mais en étendant les observations à d'autres domaines spectraux, comme l'infrarouge ou l'ultraviolet, on constate que ce caractère est général, de sorte que toute interprétation du phénomène Be doit en tenir compte. La masse des données concernant les étoiles Be est parmi les plus riches qui soient, si l'on considère la durée des observations (près d'un siècle) et la diversité des caractères spectraux qui ont été observés. Malgré cela, il n'est pas possible de fournir un schéma général de la variation de ces étoiles ni de prédire le comportement individuel d'une étoile Be particulière. Cela est dû, essentiellement, au caractère irrégulier des variations et à l'individualité du comportement de ces étoiles. Cela résulte, également, du fait que presque toute notre connaissance de la variabilité des étoiles Be provient de l'observation d'une seule région spectrale, le visible, et que nous ne possédons pas encore une vision globale du comportement de toute l'atmosphère extérieure

de ces étoiles, depuis les régions chromosphériques et coronales proches de l'étoile, observées dans les domaines ultraviolet et X, jusqu'aux régions les plus éloignées, observées dans le domaine radio. Le lieu où se forment les raies d'émission dans le visible ne constitue qu'une région intermédiaire qui ne permet pas, à elle seule, d'extrapoler le comportement des autres régions. Néanmoins, le comportement de cette région, dont l'existence définit à elle seule l'anomalie des étoiles Be, doit constituer une base fondamentale dans l'interprétation de ces étoiles.

La variabilité des étoiles Be se manifeste sous des formes très diverses. On observe: (1) la transformation d'un spectre normal en un spectre anormal et réciproquement. Des spectres Be ou "shell" peuvent perdre tous leurs caractères émissifs ou "shell", et présenter un spectre d'étoile B normale. Pour certaines étoiles, on a observé un retour à la phase Be ou "shell" au bout de quelques mois ou années; pour d'autres, après plusieurs décennies le spectre est toujours celui d'une étoile B normale. Il n'existe aucun moyen de distinguer le spectre d'une ex-étoile Be de celui d'une étoile B normale. La situation inverse est aussi observée: une étoile B connue pour avoir un spectre B normal peut présenter brusquement un spectre Be ou "shell". (2) La transformation d'un spectre ayant un type d'anomalie en un spectre ayant un autre type d'anomalie: un spectre Be peut se transformer en spectre "shell" et réciproquement. (3) Des changements non associés à une transformation de spectre. A l'intérieur d'une même phase, Be ou "shell", la variabilité affecte, plus ou moins fortement suivant les étoiles, et, pour une étoile donnée, suivant l'époque d'observation, l'intensité, le profil et le déplacment des raies d'émission ou de "shell". Les deux premiers types de variations suggèrent fortement que le spectre Be, le spectre "shell", et le spectre B normal ne représentent que différentes phases de variation d'un même objet et non différents types d'objets ou différentes phases d'évolution d'un objet. Le fait que des étoiles B normales puissent devenir pour un certain temps des étoiles B à raies d'émission, et réciproquement, pose la question—que Struve soulevait déjà en 1942—de savoir si n'importe quelle étoile B normale n'est pas susceptible de développer, de façon temporaire, cette anomalie. Si cela était le cas, la présence de raies d'émission et l'existence de variations devraient être considérées comme des phénomènes exhibés par des étoiles normales, violant ainsi les conditions d'équilibre postulées par la théorie classique des atmosphères stellaires.

De même que l'observation d'un échantillon d'étoiles Be, à un moment donné, montre la diversité de leurs caractères spectraux, l'observation des étoiles Be pendant une durée assez longue—plusieurs décennies—montre qu'elles exhibent, au cours du temps, des caractères spectraux et des comportements très divers. Dans certains cas, on observe de longues périodes (décennies) relativement calmes auxquelles succèdent de brèves périodes (années) de grande activité. Dans d'autres cas, on observe une oscillation, plus ou moins régulière, des variations, avec un amortissement plus ou moins rapide Cependant, les observations récentes de 59 Cyg faites dans l'ultraviolet lointain montrent que le spectre visible ne permet pas à lui seul de définir les périodes de "calme" et d'"activité" des étoiles Be.

Les différents types de variations qui ont été étudiées sont: (1) les variations de phase, au cours desquelles un spectre Be se transforme en spectre "shell" et/ou en spectre B normal. (2) Les variations E/C, qui traduisent les variations de l'émission dans les raies rapportées au continu adjacent. (3) Les variations de profil, que l'on décrit souvent par le rapport V/R, rapport d'intensité des pics rouges et violets des raies d'émission. Des variations rapides de profil, de l'ordre de quelques minutes, ont été également observées. Celles-ci affectent, essentiellement, la structure fine du profil plutôt que l'intensité totale de la raie. Un nouveau type de variation rapide a récemment été mis en évidence. Ces variations à courte période, de l'ordre de 0,7 jour, sont à rapprocher de celles des étoiles de type β

Cephei (4) Les variations de vitesses radiales, qui fournissent des indications importantes sur le mouvement de l'enveloppe. A certaines phases de variation, on observe une progression des vitesses avec le numéro de la raie d'hydrogène dans la série de Balmer; cette progression Balmer peut changer de sens avec le temps. Les échelles de temps sont différentes d'une étoile à une autre et, pour une même étoile, d'une époque à une autre. En règle générale, les vitesses observées dans le visible sont faibles, beaucoup plus faibles que la vitesse de libération à la surface de l'étoile. Le mouvement indiqué est, le plus souvent, une expansion, mais un mouvement de retombée de matière est aussi observé.

Le comportement des étoiles Be est illustré par la description des variations de γ Cas, 59 Cyg, Pleione, 88 Her, et EW Lac. γ Cas et 59 Cyg ont été choisies pour avoir exhibé dans le visible, pendant près de 70 ans, une grande similitude de comportement. Toutes deux ont présenté une longue phase Be de plusieurs décennies à la fin de laquelle un épisode de variations spectaculaires—deux brèves phases "shell" succédant à des phases Be de très forte émission—précède la dispersion complète de l'enveloppe et le retour à la phase B normale. Pour ces deux étoiles, cette phase B normale, ou quasi-normale, de courte durée, se poursuit par une nouvelle phase Be d'émission croissante. On observe donc, tour à tour, l'ensemble des caractères que peut présenter un échantillon quelconque d'étoiles Be: spectre Be, spectre "shell," spectre B normal, démontrant que ces trois types de spectres ne représentent pas différents types d'objets mais différentes phases de variations d'un même objet. L'exemple de ces deux étoiles montre que la description du comportement des étoiles Be à partir d'observations faites sur une ou deux décennies constitue une très pauvre représentation du phénomène Be et qu'il devrait être analysé, plutôt, sur une échelle de temps de l'ordre du siècle.

Les observations de γ Cas, par leur régularité, la diversité des caractères étudiés, l'ampleur des variations exhibées, ont permis de dégager des corrélations. Celles-ci montrent que l'augmentation de l'émission dans les raies de Balmer pendant la phase Be s'accompagne d'une augmentation de la luminosité dans le visible, et d'une diminution de la température de couleur dans le continu de Paschen et de Balmer. Le développement de la phase "shell" correspond à une bien plus faible luminosité, d'environ une magnitude et demie, et à une bien plus grande température de couleur

Les variations à long terme de Pleione mettent en évidence les différences de luminosité entre la phase "shell" et la phase Be, tandis que pour 88 Her une grande différence de luminosité est observée entre la phase "shell d'hydrogène" et la phase "shell d'hydrogène plus métaux".

Les variations de EW Lac montrent que des variations de lumière à court terme, environ 0,7 jours, se produisent à une époque où le spectre de raies subit peu de variations. L'étude du comportement à long terme de l'étoile met en évidence une modulation des variations de lumière dues à la courte période. Ces variations rapides suggèrent, une fois de plus, des liens étroits entre certains aspects du phénomène Be et le phénomène β Cephei.

Les variations du spectre de raies, comme celles du spectre continu, dans les étoiles Be montrent que toute tentative d'interprétation de la position de ces étoiles dans un diagramme HR en terme d'évolution devrait d'abord se débarrasser de tous les effets atmosphériques qui déplacent dans ce diagramme, en des temps courts comparés aux temps évolutifs, les étoiles anormales par rapport aux étoiles normales de même type spectral. Pour pouvoir chiffrer tous les effets, il faudrait d'abord construire un modèle d'atmosphère qui tienne compte de toutes les propriétés de ces étoiles, dans toutes les longueurs d'ondes.

Dans la quatrième section du chapitre 11, on décrit les propriétés de la polarisation du

rayonnement des étoiles Be dans le visible et l'infrarouge. Le rayonnement de la majorité des étoiles Be présente une polarisation linéaire dans le continu, de faible valeur, elle ne dépasse pas 2 pour cent. La polarisation intrinsèque des étoiles Be possède deux propriétés caractéristiques: (1) sa variation en fonction de la longueur d'onde, qui diffère de la polarisation interstellaire; (2) sa variation en passant du continu aux raies de Balmer en émission. L'existence d'une polarisation intrinsèque fournit, à l'heure actuelle, l'argument le plus fort pour conclure à la non sphéricité de l'atmosphère extérieure des étoiles Be. Il est généralement admis que la polarisation intrinsèque des étoiles Be est due à la diffusion du rayonnement stellaire par les électrons contenus dans une enveloppe de géométrie non sphérique par rapport à l'observateur, où la dépendance de la polarisation en fonction de la longueur d'onde est due, principalement, à l'absorption continue de l'hydrogène. Les changements de polarisation en traversant une raie d'émission peuvent s'expliquer, en première approximation, par l'addition d'un rayonnement non polarisé, ou de faible polarisation, émis dans la raie Une telle interprétation suppose que le rayonnement est polarisé, en majeure partie, dans les régions proches de l'étoile et que les raies d'émission se forment plus loin dans l'atmosphère.

La distribution des taux de polarisation des étoiles Be montre que la majorité d'entre elles ont une très faible polarisation, alors que la majorité des étoiles Be ont de grandes valeurs de $v \sin i$ Ceci montre que la majorité des étoiles Be ont des atmosphères quasi-sphériques et non des enveloppes fortement aplaties. On ne peut donc pas représenter toutes les étoiles Be par des enveloppes ayant le même degré d'aplatissement, comme on le suppose assez souvent.

C'est grâce à son caractère variable que la polarisation intrinsèque des étoiles Be a été découverte, mais elle n'a pas encore été mise en relation systématique avec d'autres quantités observables du spectre, sauf pour certaines binaires spectroscopiques. Dans le cas de ζ Tau et φ Per, aucune corrélation entre les variations de la polarisation et la phase du mouvement orbital n'a été établie, alors que pour la binaire β Lyr on a observé une corrélation très nette.

La dernière section du chapitre 11 décrit les modèles ad hoc d'étoiles Be, fondés sur les observations faites dans le visible. Il n'existe pas de théorie du phénomène Be, et on ne connaît pas encore les causes physiques qui sont à l'origine de sa manifestation. Il existe seulement un ensemble d'interprétations des différents caractères observés dans le spectre visible de ces étoiles. Les grandes lignes de cette représentation ont été proposées, il y a un demi-siècle, par Struve qui, établissant les bases du modèle rotationnel, attribue, d'une part, l'origine des raies d'émission observées dans le spectre visible à une enveloppe étendue, c'est-à-dire à un effet de volume, et, d'autre part, la formation de l'enveloppe étendue à une éjection équatoriale de matière due aux instabilités engendrées par la rotation critique de l'étoile. A la même époque, Gerasimovic suggérait que l'éjection équatoriale de matière était due à la pression de radiation aidée par la diminution de la gravité effective due à la rotation rapide de l'étoile, tandis que McLaughlin invoquait un mouvement d'expansion ou de contraction, combiné à la rotation, pour expliquer les variations V/R observées. Les modèles ad hoc d'étoiles Be ont retenu l'ensemble de ces hypothèses bâties autour du même postulat: les étoiles Be sont des étoiles B qui tournent à la rotation critique. Ce postulat (auquel, comme le remarque Collins (1970), ne correspond aucune évidence observationnelle) est à l'origine de la géométrie généralement adoptée pour représenter les atmosphères étendues de ces étoiles. disque ou même anneau équatorial. Le modèle rotationnel a résisté à près d'un demi-siècle d'observations nouvelles tant que celles-ci étaient limitées au domaine visible ou infrarouge. Cette relative harmonie entre le modèle et les observations vient de ce

que les anomalies qui se manifestent dans le spectre visible et infrarouge des étoiles Be trouvent, pour une grande part, leur origine dans la même région atmosphérique: l'enveloppe étendue froide, de faible excitation, où se forment les raies de Balmer en émission, celles des métaux une fois ionisés, le rayonnement libre-libre et libre-lié, et la diffusion du rayonnement stellaire par les électrons dans l'enveloppe. Cependant, il était facile de reconnaître sa grande faiblesse face à l'individualité et à la variabilité des étoiles Be. On ne peut, en effet, éviter la conclusion que la présence des raies d'émission et la variabilité sont deux phénomènes associés, de sorte que l'on ne peut décrire le premier si l'on ne comprend pas le second. Mais la véritable contradiction entre le modèle et l'observation vient de l'ultraviolet lointain où est mise en évidence une nouvelle région dans l'atmosphère extérieure des étoiles Be. Au lieu d'une région froide et de faible excitation, on observe une région chaude et superionisée, c'est-à-dire une région chromosphérique et coronale. Au lieu des grandes vitesses de rotation, on observe de grandes vitesses d'expansion, supérieures à la vitesse de libération à la surface de l'étoile. Au lieu des éjections de matière qu'on supposait limitées aux seules régions équatoriales, on observe de grandes vitesses d'expansion dans les étoiles classées "pole-on", c'est-à-dire, dans celles que l'on observe dans la direction postulée de l'axe de rotation. A l'image du disque équatorial froid, sous-ionisé et en rotation, s'oppose l'image d'une atmosphère chaude et superionisée, animée de violents mouvements d'expansion. Aucun modèle existant d'étoiles Be n'est capable d'assimiler ces faits nouveaux.

Les modèles d'étoiles Be ont presque tous adopté les grandes lignes du modèle rotationnel. A ce titre, ils devraient, logiquement, comporter deux parties interconnectées. (1) le traitement du problème hydrodynamique de la formation de l'enveloppe à partir des instabilités engendrées par la rotation critique de l'étoile—sa solution devrait définir, en chaque point, la distribution des densités, des températures, et, si l'on suppose que le flux de masse est conservé radialement, celle des vitesses, (2) la résolution de l'équation de transfert du rayonnement pour effectuer la comparaison entre le spectre calculé et le spectre observé. Les travaux de Limber, qui se proposait de fournir une solution hydrodynamique au problème de l'éjection forcée par la rotation, sont exposés en détail. On constate qu'ils n'aboutissent, en fait, qu'à une solution d'équilibre où le flux de masse est nul partout et où l'enveloppe est infinie, homogène et statique. Si l'on veut décrire une enveloppe réelle non homogène, le flux de masse doit constituter, nécessairement, un paramètre physique supplémentaire et indépendant des paramètres définissant la photosphère de l'étoile, et qui doit être imposé. Limber attribue l'origine de ce flux de masse aux propriétés de la sous-atmosphère des étoiles B en rotation rapide.

Du fait que le problème hydrodynamique de la formation de l'enveloppe n'a pas trouvé de solution, jusqu'à présent, tous les modèles d'étoiles Be sont ad hoc, et, en tant que tels, ils ne peuvent prétendre, et ils ne prétendent pas être physiquement cohérents. A ce titre, il faut garder à l'esprit le caractère arbitraire de certaines hypothèses qui sont à la base de leur construction, et ne pas s'attendre à ce que cette représentation corresponde à une description de l'étoile réelle. Les modèles existants d'étoiles Be diffèrent entre eux par les conditions ad hoc adoptées, par les méthodes utilisées pour déterminer l'état d'excitation de l'enveloppe et les profils des raies d'émission. L'accord entre le modèle et l'observation est dû, en grande partie, au nombre élevé de paramètres libres que l'on fixe de façon plus ou moins arbitraire Ils sont tous caractérisés par la non unicité de la solution. Parmi les modèles existants, celui de Marlborough et Poeckert, construit d'après les idées de Limber pour représenter le spectre de γ Cas, a été capable de reproduire le plus grand nombre de caractères observables. On décrit ici les méthodes utilisées pour construire leur modèle, son appli-

cation à γ Cas et l'influence des différents paramètres définissant le modèle sur le spectre calculé. On constate que le paramètre v sin i et la géométrie adoptée pour représenter l'enveloppe ont une influence déterminante sur le spectre calculé.

Le chapitre 12 présente les données spatiales obtenues pour les étoiles Be dans le domaine de l'ultraviolet lointain et des rayons X. On rappelle que les observations faites dans l'ultraviolet ont mis en évidence dans le spectre des étoiles chaudes, normales et anormales, quatre faits dont les implications sont fondamentales pour la théorie des atmosphères stellaires. (1) La présence de raies de résonance provenant d'états d'ionisation aussi élevés que O VI et N V, bien plus élevés que ceux prévus, dans les conditions d'équilibre radiatif, aux températures effectives de ces étoiles. Ceci implique l'existence d'une source d'énergie non radiative pour expliquer leur formation. Cette source de chauffage non thermique entraîne nécessairement l'existence d'une region chromosphérique et coronale, ainsi qu'il est d'usage d'appeler ces régions. (2) Le grand déplacement ou l'asymétrie des raies superionisées montre l'existence d'un flux de masse. (3) L'intensité, le profil et le déplacement des raies superionisées peuvent être différents pour des étoiles de même type spectral et de même classe de luminosité. Ceci montre que les paramètres T_{eff} et g_{eff} retenus pour décrire la photosphère des étoiles ne suffisent plus pour décrire leurs couches extérieures. (4) La variabilité des déplacements, des intensités et des profils des raies superionisées est un phénomène qui s'observe dans les étoiles normales aussi bien que dans les étoiles anormales.

La première section du chapitre 12 donne une description du spectre de raies des étoiles Be dans l'ultraviolet lointain. Alors que le spectre de raies des étoiles Be présente des différences frappantes par rapport à celui des étoiles B normales dans le visible, il ne s'en distingue pas de façon spécifique dans l'ultraviolet. Dans ce domaine spectral, l'anomalie—l'existence d'un flux de masse et d'un flux d'énergie non radiative observés parmi ces deux classes d'étoiles—se définit par rapport aux modèles thermiques et non par rapport aux étoiles normales. Les observations suggèrent que ces deux flux sont observés jusqu'à des types spectraux B plus tardifs parmi les étoiles à raies d'émission que parmi les étoiles normales. Mais les différences observées parmi les étoiles Be et les étoiles B normales ne reflètent pas l'existence de phénomènes distincts, elles reflètent seulement une différence d'amplitude d'une meme anomalie: l'écart par rapport aux modeles thermiques.

Contrairement aux observations faites dans le visible où les déplacements des raies d'émission sont généralement faibles, les raies superionisées indiquent souvent des vitesses d'expansion plus grandes que la vitesse de libération à la surface de l'étoile. Ces grandes vitesses sont observées pour les étoiles ayant de grandes ou de faibles valeurs de v sin i. Il n'existe aucune tendance de grandes vitesses d'expansion avec v sin i; il y en a plutôt avec la phase de variation de l'étoile. Ceci implique que l'éjection de matière n'est pas limitée aux régions équatoriales mais qu'elle se produit également dans les régions polaires de l'étoile—si l'on suppose que toutes les étoiles Be tournent à la rotation critique et que la valeur de v sin i fournit une mesure de i.

La deuxième section du chapitre 12 est consacrée à l'étude du spectre continu des étoiles Be. Il s'agit de savoir si la plus grande luminosité des étoiles Be par rapport aux étoiles normales, observée statistiquement dans le visible et l'infrarouge, se poursuit dans l'ultraviolet lointain, domaine où le maximum de l'énergie est émis pour ces étoiles. Si cela était, les étoiles Be auraient une magnitude bolométrique plus brillante que les étoiles B normales, un tel résultat aurait des implications importantes tant du point de vue de la structure interne que du point de vue de l'évolution. En particulier, il faudrait expliquer comment la luminosité totale de l'étoile peut changer aussi rapidement, étant donné la variabilité des étoiles Be. Bien que plusieurs études aient été faites pour comparer le flux

ultraviolet des étoiles B et Be, il n'est pas possible de répondre à la question posée car les conclusions auxquelles elles aboutissent sont contradictoires. C'est la raison pour laquelle on a insisté sur les différents problèmes qu'il faut résoudre avant d'effectuer une telle comparaison. On montre que les conclusions de ces études reflètent ultraviolet essentiellement l'effet des approximations utilisées.

Pour comparer les flux ultravıolets des étoiles B et Be, il faut d'abord calculer la correction de l'extinction interstellaire à appliquer au flux ultraviolet observé des étoiles Be. Il faut ensuite comparer les flux ultraviolets des étoiles B et Be en plaçant les étoiles à la même distance. Or, normaliser les flux à la même magnitude V n'est pas équivalent à placer les étoiles B et Be à la même distance, à cause de leur différence de luminosité intrinsèque dans le visible. En effectuant une telle normalisation, on *sousestime* le flux ultraviolet des étoiles Be. La correction de l'extinction interstellaire a été effectuée de deux façons différentes. (1) en se servant de l'excès E (B − V) que l'on utilise habituellement pour les étoiles normales, ce qui néglige le rougissement intrinsèque des étoiles Be dans le visible et *surestime* leur flux ultraviolet, (2) à l'aide de la bosse d'absorption interstellaire à λ 2200 Å—il faut dans ce cas s'assurer que la mesure de cette absorption n'est pas perturbée par les raies d'enveloppe, variables suivant les étoiles, ou modifiée par une absorption circumstellaire. Toutes les études faites ont normalisé les flux ultraviolets des étoiles B et Be à la même magnitude V, de sorte que dans la méthode (1) les erreurs sont de signes contraires et peuvent se compenser tandis que dans la méthode (2) on sousestime certainement le flux ultraviolet des étoiles Be. On note un point important *dans tous ces travaux, les conclusions font état de "déficiences" ou "d'excès" de flux ultraviolet des étoiles Be par rapport aux étoiles B normales, alors que les méthodes utilisées peuvent seulement fournir des conclusions sur le rougissement ou le bleuissement d'un indice quelconque* (λ_{uv} − *V) des étoiles Be par rapport aux étoiles B normales* On rappelle que, dans le visible, les étoiles Be ont un rougissement intrinsèque et, malgré celà, présentent un excès de flux par rapport aux étoiles B normales Tant que des méthodes sûres pour évaluer les deux corrections mentionnées ci-dessus ne sont pas trouvées, et étant donné les difficultés inhérentes au traitement statistique des étoiles Be—puisque chaque étoile individuelle introduit une erreur qui lui est propre, et qu'on ne sait pas chiffrer—il vaut mieux étudier dans le détail et dans le plus grand intervalle de longueur d'onde possible, le comportement de quelques étoiles individuelles dans des phases de variation différentes, car les effets différentiels peuvent être reliés sans ambiguité à d'autres caractères du spectre. C'est ainsi que l'observation de 59 Cyg et de Pleione dans les phases Be et "shell" montre que la phase "shell" correspond à une baisse de luminosité d'environ une magnitude dans l'ultraviolet par rapport à la phase Be. La phase "shell" correspond donc bien, alors, depuis le visible jusqu'à l'ultraviolet lointain, à une phase de moindre luminosité.

Dans la troisième section du chapitre 12, on décrit le comportement des étoiles Be dans l'ultraviolet lointain. Malgré la faible base de temps des observations dans l'ultraviolet spatial, il a été rapidement établi que les étoiles Be sont également variables dans cette région du spectre. Des variations sensibles peuvent se produire en des temps de l'ordre de l'heure, du jour, du mois ou de l'année, suivant l'époque des variations. Ces variations sont beaucoup plus grandes que celles que l'on observe dans le visible (pour 59 Cyg, les déplacements des raies de résonance de N V et de C IV ont varié de −200 à −1000 km s^{-1} environ). Avant les observations dans l'ultraviolet, l'atmosphère extérieure des étoiles Be aurait pu être assimilée à une atmosphère statique, étant donné les faibles vitesses et les faibles variations généralement observées dans le visible. Ce calme relatif de l'enveloppe froide, éloignée de l'étoiles, contrast de façon frappante avec la violence et l'ampleur des variations des régions super-

ionisées, proches de l'étoile, que l'on découvre dans l'ultraviolet. Indépendamment de la richesse des observations faites dans le visible, le choix de γ Cas et de 59 Cyg s'imposait pour illuster les variations des étoiles Be dans l'ultraviolet car, parmi les étoiles chaudes, ce sont celles pour lesquelles les plus grandes variations ont été observées dans ce nouveau domaine spectral. Les variations affectent, principalement, les déplacements et les profils des raies superionisées, celles précisément qui sont utilisées pour déterminer, dans l'ultraviolet, la perte de masse des étoiles, impliquant par la même que le flux de masse est fortement variable. Toute interprétation physique du phénomène Be et de l'origine du flux de masse dans ces étoiles devra nécessairement tenir compte de cette conclusion.

Pour γ Cas, les observations dans l'ultraviolet se situent pendant la longue phase Be d'émission croissante. On observe, à certaines époques, pour les raies de résonance de NV, C IV et Si IV, en plus des absorptions larges et asymétriques de faible déplacement (≈ -100 km s^{-1}), la présence de composantes d'absorption fine, fortement déplacées de -1200 à -1500 km s^{-1} et de profondeur variable. Ces absorptions secondaires semblent se former en quelques jours et disparaître en 2 mois environ. Ce comportement a été interprété en terme de vent stellaire, plus ou moins stationnaire, auquel se superposent des "bouffées" de perte de masse, des "puffs". Une deuxième interprétation consiste à attribuer à la région de transition chromosphère-couronne, de température croissante, l'origine de la composante à faible vitesse, et à la région post-coronale, de température décroissante, celle de la composante à grande vitesse.

Contrairement à γ Cas, les observations de 59 Cyg se situent pendant et après l'épisode de variations spectaculaires dans le visible, caractérisées par une succession rapide de phases différentes, qui se termine par une phase B quasi-normale et se poursuit par une nouvelle phase Be d'émission croissante de faible intensité. Cette phase de faible émission à Hα dans le visible serait considérée comme une phase de faible activité. Or c'est précisément pendant cette phase que la plus grande activité d'éjection de masse a été observée dans l'ultraviolet pour cette étoile. La période de plus grande activité dans l'ultraviolet correspond à une période que l'on considère comme inintéressante dans le spectre visible, une période calme et quiescente. Ceci montre que toute description de l'activité du flux de masse dans les étoiles Be doit combiner les observations dans l'ultraviolet et dans le visible, et que toute interprétation du phénomène Be fondée sur les seules données du spectre visible peut être entièrement trompeuse.

La plupart des spectres ultraviolets de 59 Cyg montre deux composantes pour les raies de résonance superionisées de N V et de C IV l'une, de faible vitesse d'expansion, plus faible que 100 km s^{-1}, qui est, généralement, la composante la plus faible; l'autre, de forte vitesse d'expansion, de l'ordre de 600 à 1000 km s^{-1}, qui est, généralement, la composante la plus forte. En contraste frappant avec le comportement des raies de C IV et N V, les raies de résonance de Si IV ne présentent pratiquement pas de variations.

La longue base de temps des observations de 59 Cyg, dans le visible et dans l'ultraviolet (72 ans dans le visible, 10 ans dans l'ultraviolet), permet de dégager des conclusions importantes pour la compréhension du phénomène Be: (1) Les vitesses d'éjection observées, variant de plus d'un facteur 10, suggèrent fortement l'existence d'un flux de masse variable. (2) Les observations faites de 1978 à 1981 suggèrent que le début d'une nouvelle phase Be correspond aux plus fortes valeurs du flux de masse. (3) L'activité d'une étoile Be consiste en un véritable cycle, depuis le début de la formation de l'enveloppe étendue jusqu'à sa dispersion complète. On ne peut pas décrire, à partir des seules observations faites dans le visible, l'activité d'éjection de masse de l'étoile. La vieille description de l'activité de l'étoile que l'on reliait seulement aux phases de forte émission de Hα, négligeant les phases de faible

émission, considérées comme minteressantes, peut conduire à une description complètement fausse du phénomène Be. (4) Il n'est pas possible de construire un modèle d'étoile Be à partir des observations faites seulement dans le visible. Celles-ci conduiraient à la représenter par une atmosphère extérieure "froide" où peuvent seulement se former les raies de Balmer en émission et celles de Fe II sous-ionisées De même, il n'est pas possible de construire un modèle d'étoile Be à partir des seules observations ultraviolettes puisqu' elles conduiraient à la représenter par une atmosphère extérieure superionisée, dans un grand nombre de cas Le modèle doit nécessairement être fondé sur les phénomènes se produisant dans ces deux régions. De plus, étant donné l'importance du cycle d'activité tout entier, une interprétation du phénomène Be doit, nécessairement, tenir compte de "l'histoire" de ce cycle, c'est-à-dire, en définitive, tout modèle d'étoile Be doit dépendre du temps.

Dans la quatrième section du chapitre 12, on décrit les observations des étoiles Be dans le domaine des rayons X. Alors que les observations dans l'ultraviolet lointain mettent en évidence une remontée de la température dans les régions chromosphériques et coronales, elles ne permettent pas, à elles seules, de connaître la température maximum de l'atmosphère extérieure, puisque les raies de résonance des ions abondants de plus forte ionisation se trouvent dans des régions de plus courte longueur d'onde que le domaine spectral étudié dans l'ultraviolet. Ainsi, les observations dans l'ultraviolet et dans le domaine des rayons X sont-elles, toutes deux, nécessaires pour connaître la distribution de la température dans les régions superionisées de l'atmosphère extérieure. On rappelle, tout d'abord, les résultats récents obtenus avec le satellite Einstein, résultats qui ont modifié notre vision de la structure des atmosphères stellaires, en général, en détectant une émission X de faible luminosité ($\lesssim 10^{35}$ ergs s^{-1}), dans le domaine des rayons X mous (0.2 à 3 keV), provenant d'étoiles appartenant à tous les types spectraux du diagramme HR. Ainsi, l'existence de couronnes stellaires, loin d'apparaître comme une anomalie, constitue un caractère normal de la structure des atmosphères stellaires. Le caractère individuel des étoiles par rapport aux paramètres classiques T_{eff} et g_{eff}, qui émergeait des observations faites dans l'ultraviolet, est nettement accusé dans le domaine des rayons X.

Si les observations dans le domaine des rayons X mous ont pu montrer le caractère général de l'existence des couronnes stellaires, celles du domaine des rayons X durs ont généralement été interprétées comme résultant d'une interaction dynamique dans un système double comprenant un objet compact. L'accrétion par le compagnon compact de la matière transférée par la primaire constitue, selon cette interprétation, le mécanisme de chauffage nécessaire à la production de rayons X. Parmi les étoiles Be identifiées à des sources X, γ Cas et X Per ont été observées sur une base de temps assez longue dans ce nouveau domaine spectral. On montre qu'il n'existe, à l'heure actuelle, aucune observation permettant de justifier l'hypothèse que γ Cas est une binaire spectroscopique. On décrit le modèle proposé par Marlborough (1977), qui rend compte de l'émission X de γ Cas par la présence d'une couronne d'une température de plus de 2×10^7 K; une telle région prolonge de façon cohérente les régions superionisées détectées dans le domaine de l'ultraviolet lointain. On décrit ensuite les caractères de l'émission X de la source 3U0352 + 30 identifiée à X Per et où une période de 13,9 minutes a été mise en évidence On montre que les conclusions de l'analyse des vitesses, mesurées dans le domaine visible, sont quelque peu confuses; la période et l'amplitude des vitesses radiales, suggérées par les mesures faites à une époque de forte émission dans les raies de Balmer, présentent un caractère de plus en plus vague avec la décroissance de l'émission Tous les modèles de X Per proposés supposent l'existence d'un système binaire où l'émission X est produite par accrétion par une étoile

magnétique à neutrons. Ils diffèrent essentiellement par la valeur de la période orbitale adoptée pour définir le système; ils sont, cependant, loin de pouvoir interpréter tous les faits observés

Le chapitre 13, écrit en collaboration avec R. N. Thomas, présente les grandes lignes d'un modèle empirique pour les étoiles Be qui repose sur les observations faites dans tous les domaines spectraux et pas seulement dans le visible. L'objectif de ce chapitre, dans l'esprit de la présente série de monographies, est de répondre aux questions suivantes (1) Peut-on établir, à partir des observations et pour chaque type d'étoiles étudié, un schéma général de sa structure atmosphérique qui soit physiquement cohérent? (2) Peut-on déterminer les paramètres thermodynamiques nécessaires et suffisants pour décrire une telle structure? (3) Les observations existantes d'une étoile donnée sont-elles suffisantes pour construire un modèle propre à cette étoile? (4) Quelles sont les conditions qui fixent la valeur particulière de ces paramètres pour une étoile donnée?

Dans la première section, on résume les propriétés des étoiles Be. On note que la variabilité, l'individualité, le caractère graduel de la transition entre la phase d'étoile normale et d'étoile anormale, ainsi que l'apparente nécessité de caractériser chaque étoile Be particulière par l'histoire de ses variations, sont des propriétés communes à une bien plus grande classe d'objets à raies d'émission, englobant les Wolf-Rayet, les étoiles symbiotiques, etc. Cette similitude conduit à rechercher, pour l'ensemble de ces étoiles, ainsi que l'avait proposé Struve en 1942, un schéma commun pour représenter leur atmosphère. L'existence des propriétés énumérées, ci-dessus, montre que les deux paramètres thermodynamiques, le flux radiatif et la gravité, ne permettent pas de décrire un tel modèle. Les observations actuelles suggèrent fortement qu'on doit y ajouter un flux de masse et un flux d'énergie non radiative. La question posée, à l'heure actuelle, est de savoir si ces deux flux sont des paramètres indépendants ou si l'un d'eux, ou tous les deux, peuvent être prédits à partir des deux paramètres classiques.

Dans la deuxième section, on présente une synthèse des observations des étoiles Be décrites dans les trois chapitres précédents, et, en les ordonnant, on dégage un schéma empirique de la structure de leur atmosphère. L'analyse des observations montre que les régions sous-ionisées, animées de faibles vitesses, et où les raies d'émission de l'hydrogène et de Fe II trouvent leur origine, sont les plus éloignées de l'étoile, tandis que les régions superionisées, en forte expansion, prolongent la photosphère. L'absence de corrélation entre la température ou la vitesse d'expansion avec v sin i est en faveur d'une distribution radiale de ces deux régions; il n'existe aucune observation qui rende nécessaire une distribution de ces régions chaudes et froides dans des secteurs différents. Le faible taux de polarisation des étoiles Be montre qu'une telle distribution doit présenter une certaine asymétrie par rapport à l'observateur mais que celle-ci doit être faible.

Les conditions imposées par l'existence des régions superionisées et sous-ionisées montrent, qu'à partir de la photosphère, on doit rencontrer successivement les régions suivantes. (1) la chromosphère, définie par l'augmentation de la température due au chauffage non radiatif et par la condition que la distribution des densités est celle de l'équilibre hydrostatique. (2) La couronne, caractérisée encore par une augmentation de la température, mais avec une distribution dynamique des densités, suivant l'inverse carré du rayon. La région de transition chromosphère-couronne correspond, d'après cette définition, au point thermique où la vitesse du vent stellaire est égale à la vitesse thermique uni-dimensionnelle. Ce point définit aussi la basse couronne; dans la haute couronne, la vitesse du vent stellaire dépasse la vitesse de libération. (3) Une région de transition entre la couronne chaude, en forte expansion, et les régions sous-ionisées quasi-statiques, qui, pour les étoiles Be, doit se trouver à cinq rayons stellaires, environ. (4) L'enveloppe froide étendue, ayant une température de

1×10^4 à 2×10^4 K, où se forment les raies d'émission de Balmer. Dans cette région, le vent stellaire a déjà été décéléré jusqu'à une valeur ≤ 100 km s^{-1}. Les modèles ad hoc montrent qu'une telle région peut s'étendre jusqu'à environ 50 rayons stellaires. (5) Une enveloppe froide, encore plus étendue, où se forment les raies d'absorption du spectre de "shell". (6) Dans le cas d'étoiles Bep, d'étoiles symbiotiques etc., l'extension de l'enveloppe est encore plus grande, avec des densités très faibles, de l'ordre de 10^{-5} cm^{-3}, pour permettre la formation de raies interdites. Elle est encore plus étendue lorsqu'elle est le siège d'une émission radio—de l'ordre de milliers de rayons stellaires. Elle doit être aussi beaucoup plus froide dans ses régions les plus éloignées, avec des températures de l'ordre de 1000 à 2000 K, lorsqu'elle émet un flux infrarouge très important dû à une réémission thermique par les poussières circumstellaires. Cette séquence de régions, fondée sur l'ensemble des observations existantes, constitue le modèle "solaire-planétaire" proposé dans ce chapitre pour décrire la structure de l'atmosphère extérieure des étoiles Be et autres objets similaires. On indique, ensuite, la méthode qui permet de définir quantitativement ces régions. Une discussion plus détaillée de ce modèle est donnée dans le volume édité par R. N. Thomas dans cette série de monographies.

Part I
B Stars

1

UNDERSTANDING B-TYPE STARS

BACKGROUND

When observations of B stars made from space are added to observations made from the ground and the total body of observational information is confronted with our theoretical expectations about B stars, it is clear that nonthermal phenomena occur in the atmospheres of B stars What are these phenomena and what do they imply about the physical state of a B star and how a B star evolves? These are the questions which we shall examine in this book. In particular we shall use knowledge of the spectrum of a B star as a key to obtaining an understanding of what a B star is like.

This volume, *B Stars with and without Emission Lines*, together with the book *O, Of, and Wolf-Rayet Stars* (Underhill and Divan, to be published) provide a sequel to *The Early Type Stars* (Underhill, 1966a). In *The Early Type Stars*, the properties of early type stars and the methods for finding information about B, O, and Wolf-Rayet stars are summarized. In 1965, when the manuscript for *The Early Type Stars* was completed, the explosion of knowledge which has led to the revision of our thinking about how to model the atmospheres of early type stars outlined in the next two sections was just beginning A few sounding rocket observations of the ultraviolet spectra of O and B stars had been made, and infrared astronomy was in its infancy. The techniques of analyzing stellar spectra by means of model atmospheres were just being adapted to large computers. The development, in the ensuing fifteen years, of our observational capabilities and of our theoretical understanding of stellar spectra has laid the foundation for the present book

Most of the literature on B stars and on the theory and observation of their spectra which has appeared since 1965 has been referenced. The search for new material was closed about October 1980. In addition, some original work is presented here. The overall view of B stars which is outlined in Part I has not been published in its entirety elsewhere.

These nine chapters, which compose Part I, summarize the spectroscopic observations of stars which have been given the spectral type B and describe what B stars are like--determining from spectroscopic and photometric observations the sizes, masses, and composition of the B stars as well as how B stars generate energy and produce a spectrum Because some of the characteristic properties of the B-type supergiants are similar to those of some O and Wolf-Rayet stars, the interested reader will find it advantageous to read also the book *O, Of, and Wolf-Rayet Stars* (Underhill and Divan, to be published). The sections of that book which deal with mass loss and with the interpretation of features formed in the mantle of the star are particularly relevant

Most of Part I was written by Anne B. Underhill. She was assisted by Janet Rountree Lesh who wrote Chapter 5 on the Beta Cephei variables and the peculiar B stars, by Lucienne Divan who contributed to the discussion of interstellar extinction and gradients (Chapter 3) as well as to the

discussion of the Balmer continuum in emission (Chapter 4), and by Morris L. Aizenman who contributed the summary of the pulsational properties of massive model stars which appears at the end of Chapter 7. Contributions to Chapter 2 were made by Janet Rountree Lesh and by Vera Doazan, Lucienne Divan prepared the French summary.

The line of thought which leads to the introduction of the word "mantle" as a name for the outer part of the atmosphere of a star is presented in Chapter 1. Here the groundwork is laid for the method of analysis which is followed in Part I. In Chapter 2, the B stars are introduced to the inexperienced reader and knowledge existing in 1977 about the properties of B stars and about the types of observation which have been made is summarized.

In Chapter 3, the spectroscopic observations of B stars which lie in the main-sequence band, that is those in luminosity classes II, III, IV, and V, are summarized and some inferences about the physical state of B-type atmospheres are drawn. The results concerning the effective temperatures and bolometric corrections of main-sequence B stars are given in this chapter. Chapter 3 presents a basis of comparison for the results on the special types of B stars which are discussed in Chapters 4 and 5

The characteristic properties of the B-type supergiants are described in Chapter 4, and those of the Beta Cephei variables and of some of the peculiar B stars are summarized in Chapter 5. The need for a two-part model of the atmosphere is emphasized for the supergiants. Use of such a model may ease the understanding of the many detailed spectrum and light changes which are observed for the Beta Cephei variables and for some of the peculiar B stars. However, this topic is not developed here.

The existing theory of stellar atmospheres and the interpretation of stellar line profiles, which is relevant for B stars, is reviewed in Chapter 6. A brief review is given also of the existing theories for extended, moving atmospheres. A more extensive review may be found in *O, Of, and Wolf-Rayet Stars* (Underhill and Divan, to be published).

In Chapter 7, the theory of the evolution of massive stars both with and without mass loss is summarized, and the observed positions of B stars in the Hertzsprung-Russell (HR) diagram are compared with the predicted positions One of the interesting facts confirmed by this comparison is that stars having different spectral types, such as B1 IV and B1 IVe, or different temporal behavior, such as the normal B1 III stars and the Beta Cephei variables, occupy the same area in the HR diagram. Quite obviously, showing the spectroscopic criteria which result in classification of the star as being different from a normal, constant light B star does not imply necessarily a different position in the HR diagram.

In Chapter 8, the results attained from the studies given in the preceding chapters are brought together, and an attempt is made to deduce the physical character of the processes leading to the generation of the specific spectroscopic phenomena which are used to differentiate between B stars of all subclasses, and to draw a coherent picture of the physical state of the atmospheres of B-type stars of all varieties

In Chapter 9, a summary is given of each chapter in Part I. This text serves as the base for the French summary of Part I.

THE GENERAL PROBLEM OF THE B STARS

The B-type stars, those stars whose visible spectra are dominated by lines of He I and the Balmer series of hydrogen, are rather hot, massive stars with effective temperatures in the range from 1.0×10^4 to 3.0×10^4 K and masses in the range from 2 to 20 solar masses. They are believed to be young and moving relatively rapidly through the first stages of evolution of a star. They are typically found in the spiral arms of galaxies. Their numbers are relatively few in comparison to the large numbers of stars known which have masses of the order of one solar mass or less

It is of great interest to understand the physical state of B stars in order to study the behavior of objects in the solar neighborhood which the theory of stellar evolution tells us are young. We expect to show how spectral types can be inter-

preted consistently to yield the physical state of the atmosphere of the star, and we shall investigate whether the spectral type is an unambiguous indicator of the stage of evolution of a star We would like to know whether each point in the theoretical HR diagram is related in a one-to-one manner with a single spectral type or whether more than one spectral type may be seen at some locations in the HR diagram.

The physical state of a stellar atmosphere is inferred from a study of the detailed distribution of light in the line and continuous spectrum of the star and the state of the atmosphere is related to the rate of energy generation and stage of evolution of the star through the theory of stellar structure and evolution. Consequently, a valid theory of spectroscopic diagnosis is a necessary tool for the study of stellar evolution. One purpose of this book is to review the methods of spectroscopic analysis applied to B stars and to evaluate the results.

Two classical ideas which are basic to the goal of reaching an understanding of the physical state of the universe through obtaining an understanding of the physical states of stars of the various spectral classes are (1) that each spectral type defines a unique set of physical conditions which can be determined by means of the theory of stellar spectra, and (2) that each set of physical conditions is determined uniquely by the composition, mass, and stage of evolution of the star, the Vogt-Russell theorem.

Since the spectral types have been defined empirically in terms of the relative intensities and apparent shapes of spectral lines in the blue-violet spectral range, confidence in proceeding to considerations of stellar and galactic evolution is only as secure as the capability we have for monotonically relating the empirically selected criteria for spectral type to unique physical states that can be unambiguously related to stages in the evolution of a star. One major purpose of this book is to review what is known about the spectra and physical state of B stars and to find out where simple theory and expectations can be supported and where a more complex approach must be taken to understanding what B stars are like.

NOTES ABOUT MODELING

The method followed in Part I is to compare observational results determined from the spectrum with the predictions from models. Attention is directed chiefly toward isolated, single stars because we wish to minimize the complexities which may ensue from having to disentangle the blended radiation from two or more sources. If agreement is obtained between the selected observed spectroscopic details and the selected predicted spectroscopic details, it is concluded that the physical state of the model is representative for the part of the star giving rise to the spectroscopic features under analysis.

It should always be kept in mind, however, that most B stars, whether they are in a stage of showing emission lines in their spectra or whether they are not in such a stage, are massive stars of essentially solar composition. Their spectra result from the interactions between gas and radiation which occur in the environment provided by the outer layers of the stellar atmosphere. Since the physics of gas and radiation is unchanged by the evolutionary state of a star, it is clear that when we are attempting to interpret stellar spectra, we are determining the properties of the environment from which the radiation has come. The forces acting on the gas of the stellar atmosphere are relatively long range ones, such as (1) the attraction of gravity due to the mass of the star, (2) the force exerted by radiation on atoms, ions, and electrons as a result of interactions between the radiation field and the constituents of the stellar atmosphere, (3) Coulomb forces between the charged particles present in the atmosphere, and (4) electromagnetic forces generated by the motion of charged particles in any magnetic fields which may be present in the stellar atmosphere.

We attempt to understand stellar spectra and the structure of stars by making models of the star, and in each model taking account of the action of only those forces which appear to be most important for determining the particular details of the stellar spectrum which we are interpreting The basic method for finding out what a star is like makes use of the same princi-

ples of physics, no matter what particular subclass the B star belongs to. What differs in the several applications of the modeling method reported in this book are the decisions which are made in each case about which are the important forces and interactions to consider for the problem in hand, and what is an appropriate geometrical description to use for the problem under study.

The simplest approach to modeling a star is to divide the star into two parts. (1) the interior, which is all of the star deeper than the layers from which radiation escapes to space, and (2) the atmosphere, which is the boundary layer of the star from which radiation escapes to space.

Studies of stellar structure have shown that, when developing models for the interior of a star, it is useful to divide the interior into two parts the core, where energy is generated, and the envelope, which transmits the energy stream from the core to the boundary layer, or atmosphere, of the star. The radiation escapes into space from the atmosphere. Modern observations have shown also that some mass escapes from the star in the form of a wind.

To achieve the goal of deducing the physical state of a B star, it is convenient and effective to divide the atmosphere of the star into two parts, each of which is modeled using different concepts. Underhill (1980b, 1981a) has suggested that the two parts of the stellar atmosphere be named the *photosphere* and the *mantle*. A justification for the choice of the word "mantle" is given below. The photosphere is the inner part of the atmosphere where most of the continuous spectrum is formed and where lines from ions of low abundance are formed. The mantle lies outside the photosphere. It comprises the outer part of the atmosphere where the state of the gas is significantly affected by the deposition of nonradiative energy and momentum.

The photosphere can be modeled successfully using the classical constraints of (1) no incident radiation except that which comes from the envelope of the star, (2) radiative equilibrium, and (3) hydrostatic equilibrium. A model photosphere, given the composition, can be specified by means of two parameters: effective temperature and the value of the acceleration of gravity in the atmosphere of the star due to the mass of the star.

A model mantle should be described by means of appropriate equations derived from the conservation laws for energy, mass, and momentum. The amounts of nonradiative energy and momentum which are put into the model must be specified as well as the radiation field which is incident from the photosphere. The first need may be met by giving the value of a parameter which specifies the energy density of the source which provides the nonradiative energy and momentum and a parameter which specifies the efficiency of the process which transfers energy and momentum from the storage mode to the gas in the mantle. The radiation field incident from the photosphere can be found from observed and predicted photospheric spectra.

The modeling of mantles is still in a very tentative form. Several opinions exist about what is the appropriate storage model for the nonradiative energy and momentum, and about how the stored energy and momentum is transferred to the gas in the mantle It is proposed in Chapter 4, with further development of the idea and justification of it in Chapter 8, that the ambient magnetic field in the mantle may be an appropriate source of nonradiative energy and momentum for B stars, and that the process which transfers energy and momentum to the gas may involve interactions between local differential motion in the gas and the local value for the magnetic field. It is suggested that the average magnetic field in the mantle and the average amplitude of the differential motion may be appropriate parameters for specifying a model mantle

The ideas which are introduced in Chapter 4 in connection with understanding the mantles of B-type supergiants, and which are developed further in Chapter 8, may be applied also to understanding the spectra of Be stars. The simple model of magnetic loops which are twisted and matted to form a disk as a result of the rapid rotation of a Be star offers many interesting possibilities for understanding what is seen. If this

suggestion has some basis in fact, then the irregular generation of conditions giving Be-type spectra followed by the disappearance of these conditions may be linked to the generation and destruction of magnetic loops in the outer atmospheres of B stars.

In Part I, the first steps are taken toward recognizing the systematic effects which enable one to detect a mantle, and it is shown that the factors proposed here for controlling the physical state of a mantle are plausible. It is believed that the assembled observational results will be useful for discriminating between the present proposal for generating a mantle and others which may be published later. To discriminate between such proposals, it will be necessary to work out the details of how the physical state of a mantle arises and how the mantle modifies the radiation field of a star from its form as it leaves the photosphere of the star.

The First Approximation to Modeling

The simplest way to model a stellar atmosphere, a first approximation, is to represent the atmosphere by a single uniform layer of gas at one temperature and one density and to find the distribution of the atoms in their various stages of ionization and excitation by means of the laws of Saha and Boltzmann. These laws are valid for radiation and gas in a state of thermodynamic equilibrium.

Development of this pattern of thought led to the realization that the B stars are hot stars and to the first interpretations of the place of B stars in the evolution of the universe. However, a detailed study of that part of the line spectrum of B stars which can be observed from the surface of the Earth soon revealed significant discrepancies between theory and observation.

The relative strengths of the He I lines, and particularly the lines of the diffuse series, could not be represented well by curve-of-growth theory. The first members of each series required greater abundances of helium for their interpretation than did the later members, while in some "shell" stars, the lines from the 2^3S and 2^1S levels of He I were found to be unexpectedly strong. The latter observation was called a "dilution" effect (Struve and Wurm, 1938), and it was specifically noted to be the result of the departure from thermodynamic equilibrium of the physical state in the outer atmospheres of stars with "shell" spectra. Also the relative strengths of lines of Si II, Si III, and Si IV could not all be accurately represented by simple curve-of-growth analysis at the same time. The simplest theory was too simple

The Second Approach to Modeling

The second approach was to modify the theory so that numerical models of stellar atmospheres could be constructed in which the density decreased outward and was constrained so as to maintain hydrostatic equilibrium under the attraction of gravity in the atmosphere, and the temperature decreased outward so that radiative equilibrium was enforced. With the advent of large computers, it became possible to replace the rather unrealistic assumption of local thermodynamic equilibrium for determining the populations of the energy levels of the atoms and ions in the model atmosphere by the more realistic assumption that the distribution of the atoms and ions among their various states of ionization and excitation is determined by the condition that statistical equilibrium exists for the level populations. The calculation of theoretical line and continuous spectra using well-determined cross sections for the interactions between particles and radiation resulted in good agreement with many of the observed details of B-type spectra, and it was shown that the composition of B stars is essentially solar. However, even in the visible spectral range, a few nagging discrepancies between the appearance of the theoretical and the observed spectra continued to remain.

The relative strengths and shapes of the He I lines are represented far better by detailed models and line-formation theory that uses the condition of statistical equilibrium to determine level populations than is the case with models and theory

based on the assumption of local thermodynamic equilibrium, but still the leading members of the several series of He I, such as the lines at 5876, 6678, and 7065 Å, are observed to have larger equivalent widths and to be deeper than the calculations suggest, even for main-sequence stars. For B supergiants the discrepancy is marked and in addition stronger emission is seen at Hα, and sometimes at He I 5876, than the theory predicts. Also, attempts to determine the effective temperatures of B stars from fitting the shape of the continuous spectrum and from fitting the relative intensities of lines in two or more stages of ionization of one element, such as Si II, Si III, and Si IV, do not yield results as internally consistent as the degree of sophistication of the theory suggests should be the case

When spectra extending to 1000 Å became available from observations made from sounding rockets and from satellites, and spectra extending well into the infrared were in hand, it became evident that the model of a B-type stellar atmosphere as a series of layers in hydrostatic and radiative equilibrium was inadequate to explain all that was seen

A Third Approach to Modeling

The presence in B-type spectra of the resonance lines of ions such as C^{+3}, N^{+4}, and O^{+5} indicates the presence in the atmospheres of B stars of gas heated to higher electron temperatures than the effective temperatures of the B stars In addition the shapes and displacements of the profiles of the resonance lines of these ions, and others, indicate that outflow of matter occurs at speeds exceeding the velocity of escape from the photospheres of main-sequence and of supergiant B stars. These conditions, superheating and rapid flow, violate the constraints of radiative and hydrostatic equilibrium, respectively. Furthermore, soft X-rays have been observed from a few B stars. The production of X-rays cannot take place in a classical model atmosphere, that is in a second-approach model

A structure like that of the outer atmosphere of the Sun appears to be more appropriate for modeling the outer atmospheres of B stars than is the classical model of static layers in radiative equilibrium. We postulate that there is a photosphere, which may be represented reasonably accurately by means of a classical model atmosphere consisting of plane parallel layers in hydrostatic, radiative, and statistical equilibrium, outside of which there is an outer atmosphere, or mantle. In the mantle, the effects of the deposition of nonradiative energy and momentum become apparent.

The part of the stellar atmosphere we are calling a mantle is the outer part of the atmosphere. It must be distinguished from the inner part of the atmosphere, called the photosphere, because, when developing a model for the mantle, it is essential to take account of the effects of the deposition of nonradiative energy and momentum in addition to the effects due to the energy and momentum injected by means of the radiation field coming from the center of the star. When making a model of the photosphere, one needs to take account of only one source of energy and momentum, and to enforce the condition of hydrostatic equilibrium. In the photosphere, the prime source of energy and momentum is the radiation field which is transmitted to the photosphere by the envelope of the star.

It is more effective to refer to the outer and inner parts of the atmosphere by separate names, *mantle* and *photosphere*, respectively, than to use for both one noun, "atmosphere" and to modify it by a different adjective, "outer" and "inner," respectively. Concepts which are not necessary for making successful models of the photosphere must be employed when making models of the mantle.

CHARACTERISTIC PROPERTIES OF A MANTLE

The word *mantle* (something that covers, envelopes, and conceals) is introduced here as a collective noun to represent all parts of the atmosphere outside the photosphere. A new word is required because we wish to place new emphasis on the properties of the outer layers where the effects of the deposition of nonradiative energy and momentum are readily apparent,

as distinct from the properties of the photosphere where radiative and hydrostatic equilibrium are good approximations. The mantle is modeled differently from the photosphere.

It is very probable that all stars have layers of gas outside their classical photospheres These layers can be detected only when observations are made of spectral features which are formed particularly in these outer layers. Observations of X-rays from B stars confirm the presence in the mantles of B stars of regions as hot as the solar corona These very hot, truly coronal regions may be of small extent. Large regions at lower temperatures than those seen in normal B-type photospheres are known to be present around some B stars, the so-called "shell" stars

The mantle can be conveniently divided into two parts: an inner part which corresponds to the chromosphere, transition layer, and inner corona of the Sun, and a post-coronal region. The first part might be called a corona-like region, outward flow is seen here and the electron temperatures are inferred to be high, perhaps of the order of 10^5 K over most of the volume. The observations of X-rays from some B-type stars indicate that parts of the mantles of B stars have temperatures in the range 10^6 to 10^7 K, as is found for the solar corona. Regions radiating X-rays truly are similar to parts of the solar corona.

The post-coronal region can be differentiated from the truly coronal regions (which may be of small extent), and from the corona-like region, as being a region where little or no net input of energy and outward directed momentum occurs Because energy continues to be lost by the escape of radiation to space, the temperature will decrease as distance from the star increases, eventually reaching the temperatures of the surrounding interstellar medium. The interesting question is how rapidly does the temperature decrease. The degree of ionization and the temperature at each place in the post-coronal region and of the corona-like region will be determined by the balance between the rates of the ionization, recombination, and charge-exchange processes that can take place at the ambient particle and radiation densities, and the rates at which energy is injected into and radiated from the mantle. The outward velocity of the wind as it traverses the post-coronal region may be expected to change little because only weak forces are thought to exist in the post-coronal region to cause a change of velocity The stellar wind is expected to coalesce with the interstellar medium under shock conditions.

The mantle is transparent in most continuum frequencies longward of the Lyman limit of hydrogen, but opaque in many line frequencies. One goal of the discussion of B-type spectra given in the following chapters is to describe which spectral features enable us to see the mantle and which the photosphere. Another goal is to determine the physical properties of the mantle. Very little modeling has yet been done of structures like that sketched for the mantle.

Several words are in common use for referring to the parts of the outer atmosphere of a star which we are calling a mantle. In the case of B stars, use of the word "chromosphere" when referring to the transition layer between the photosphere and the observed hot ($T \lesssim 10^5$ K) region lying further out is not entirely desirable because this word is the name of a part of the Sun, and it brings with it connotations of the temperature and density ranges encountered in the Sun Observations indicate that the transition layers of B stars are often hotter than the most conspicuous parts of the solar chromosphere. Likewise, it is preferable to speak of corona-like layers rather than of a "corona" when we mean the volume of gas around a B star where the electron temperature is of the order of 10^5 K The temperatures in the solar corona are greater than 10^6 K. The temperatures in the regions of the mantles of B stars where X-rays are formed appear to be similar to the temperatures in the parts of the solar corona where X-rays are generated.

Use of words "envelope" and "shell" for referring to the layers of the atmospheres of B stars which we are calling a mantle is unwise because the envelope of a star is a term used in the theory of stellar structure to describe the layers immediately outside the energy generating

core of the star and the word "shell" has at least two different uses (1) to denote a thin spherical region around the core of a star where a particular energy-generation process occurs, and (2) to denote a cool part of the region we are calling a mantle, this part being an extended region contiguous with the photosphere in some discussions but a thin detached layer in others

GOALS OF PART I

Important goals of Part I are (1) to review the information presently available about B-type stars, in particular that about their spectra, and (2) to deduce preliminary characteristics for each part of the two-part structure, photosphere and mantle, that seems to be needed to understand the spectra of B stars. A third important goal is (3) to find the positions of the B stars in the HR diagram and to compare these with the predictions from the theory of stellar evolution. Finally, an attempt will be made (4) to specify the character of the mechanisms by which the physical state of the mantles of B stars is generated and to determine what parameters are important for determining the efficiency of these mechanisms.

In connection with the third goal, it is important to determine whether or not the instantaneous state of a mantle can be related unambiguously to the evolutionary phase of a star The physical state of a mantle is generated as the result of the deposition of nonradiative energy and momentum in the outer parts of a stellar atmosphere. At this time, it is not clear whether or not the availability of the nonradiative energy and momentum of an appropriate kind is a single-valued function of the phase of stellar evolution. The phase of evolution of a massive star is a measure of how energy is being generated in the core of the star at each instant of the life of the star. The instantaneous effective temperature and radius of the star are criteria which allow us to determine the evolutionary state of a star. They may be found by studying the part of the stellar spectrum that is formed in the photosphere of the star. The question which we are raising now is whether the physical state of the mantle of the star, and thus the values of the parameters which determine that state, can be used as a criterion of the phase of evolution of a star

So long as the outer atmospheres of B stars were considered to be in a state of equilibrium, hydrostatic, radiative, and local thermodynamic (LTE) or statistical equilibrium (non-LTE), the mechanisms by which the atmosphere attained its state were of little concern. However, since modern observations show that a state of activity is common to many B stars, the question of determining the character of the mechanisms causing change becomes urgent. The relationship of these mechanisms to the progress of stellar evolution also becomes a pressing question.

NOTES ON THE METHOD TO BE FOLLOWED

The only star which can be observed in minute detail spatially, temporally, and over a large range of wavelengths from X-ray to radio is the Sun. This nondescript star (from the viewpoint of a lover of the massive, luminous early type stars) has a corona which is hotter and at lower densities than the corona-like regions observed for B stars, and it has a lower rate of mass loss than B stars. Importantly, the Sun tells us that magnetic fields and the flow motion of particles in the outer atmosphere have much to do with causing varied spectroscopic phenomena like those which we see in B stars. Although full understanding of the mechanisms causing the observed solar phenomena is not yet at hand (see Jordan, 1981), it is imperative for understanding the B stars to adopt the same point of view, so far as possible, as has been done for the Sun. This means, among other things, that one recognizes that certain types of spectroscopic lines or continua reveal information about certain temperature and density regimes while other phenomena speak of other conditions.

If we wish to study the photosphere, we must study only spectroscopic details that are characteristic of the conditions we believe to exist in the photosphere. Likewise for studying the superheated parts of the mantle and the post-

coronal flow, we should confine ourselves to the analysis of spectroscopic details which are formed in these regions. Furthermore, since the Sun tells us that the outer, low density parts of a stellar atmosphere may not be uniform in their geometric and physical state (jets, prominences, coronal holes, and so forth being seen for the Sun), we must be prepared to recognize that the spectroscopic phenomena of B stars which we are studying may be giving information about volumes of gas which are not spherically symmetrical about the star and which are not homogeneous

Natural reluctance to create a more involved model than necessary will influence us to attempt to interpet the observed stellar spectra with as simple models as possible. Still it must be recognized that the resonance and other lines of abundant ions and the emission lines, in particular those of hydrogen, tend to tell us about the state of parts of the outer atmosphere which are not observed by means of intrinsically weak features from atoms and ions of moderate to low abundance. It is our problem to deduce the likely geometric distribution and physical state of the material we are seeing and to infer what causes stellar material to appear in such a state

In most stars, particularly the Be stars, the shapes and intensities of the spectroscopic lines and continua which most easily reveal the presence and physical state of material in the mantle sometimes change in relatively short intervals of time. It is interesting to ask what is the cause of these temporal changes and in what manner, if at all, this cause may be related to the progress of stellar evolution, so far as it is known. Recognizing that at least part of the mantle of a B star is heated to electron temperatures higher than the effective temperature of the star means that one must conclude that additional energy is being deposited in the mantle by some nonradiative means. If the radiation stream from the core of the star were the only source of energy, the electron temperatures in the mantle would be lower than the effective temperature of the star. The occurrence of outflow at modest densities means that one is seeing the effects of the deposition of nonradiative momentum. The momentum accelerates the material through the sonic velocity and puts it into such a state of motion that it may be further accelerated by radiation pressure

B STARS AND EVOLUTION

Let us return to the expectations of those whose interest is chiefly in interpreting the evolution of our galaxy and of other galaxies in terms of a global world picture In order to proceed with such a global synthesis of knowledge, one attempts to deal with only the predominant characteristic properties of stars so far as the evolution of the elementary units (groups of stars) of the universe is concerned. Up to now, it has been assumed that the empirically assigned spectral types are appropriate factors by which to characterize the position of stars in the HR diagram in a monotonic, unambiguous way. We shall see that for the B stars this is not entirely possible, and that many of the details which are enshrined in the luminosity classification process and in assigning such descriptors as "peculiar," "Be," or "shell star" refer to the unusual visibility of parts of the mantle. It is not yet known whether or not the state of the mantle can be used as a criterion for the stage of evolution of a massive star.

A major goal of this book is to clarify the meaning of the observations and to define more clearly than is presently done the types of physical processes which are occurring in B-type stellar atmospheres. Until the largely unknown mechanisms causing various sorts of mantles to appear around B stars, which seem to occupy the same position in the HR diagram, can be related reasonably rigorously to the processes which occur during stellar evolution and their importance can be assessed, caution seems appropriate in developing scenarios for the evolution of galaxies.

To understand the B stars and their significance for theories of the evolution of the universe, we must understand how conditions in the photosphere are generated as well as how conditions in the mantle arise The remainder of Part I summarizes the state of our knowledge of this subject at the end of 1980

2

INTRODUCING THE B STARS

THE CLASSIFICATION OF B STARS: THE VISIBLE REGION

The fundamental spectral range for spectral classification is the visible range. It was to describe spectra obtained in this range that spectral types were first devised.

From Low Resolution Spectra

The various schemes for classifying B-type spectra in the visible range using low dispersion spectra (about 100 Å mm^{-1}) have been summarized by Underhill (1966a) The most widely used system is the MK system developed by W. W Morgan and P C Keenan. Within the MK system, the spectral types are assigned by visual inspection of widened, low dispersion spectra, covering the range from 3900 to 5000 Å, and by interpolation between the appearance of the spectra of certain standard stars. Therefore, the MK system is defined in terms of standard stars. Astronomers have acknowledged that when the stars in any one spectral class–luminosity class box are looked at with high dispersion, differences may be seen. The MK system brings together stars having about the same spectral properties. Because the overall character of the spectrum is a result of the stream of radiation which is generated in the center of the star passing through the layers of the atmosphere, the words *similar spectrum*, by and large, are taken to imply similar energy generation and similar size.

The most recent list of standard stars for defining the B spectral types has been published by Morgan and Keenan (1973). The adopted spectral types range from B0, B0.5, B1 to B9. The B0 spectra show the highest level of excitation, while the B9 stars show the lowest level of excitation in the group. In general B-type spectra are defined as those containing lines of He I and lines of H I in absorption. When lines of He II are also visible on low dispersion spectra, the type becomes O; when the He I lines are very weak or absent but the H I lines are strong the type is A. Weak lines of O II, N II, Si II, Si IV, and Mg II are used to define the subclasses. The precise criteria for the main-sequence stars and those just a little brighter than the main sequence have been listed by Lesh (1968). In addition she has determined spectral types on the MK system for 464 stars with type B5 or earlier in the *Henry Draper Catalogue*, with visual magnitudes brighter than about 6.5 and lying north of declination $-20°$ The bright B-type stars south of declination $-20°$ have been classified on the MK system by Hiltner, et al. (1969). The spectral types and other kinematic characteristics of these stars are tabulated by Lesh (1972). MK spectral types for southern OB stars brighter than B = 10 are listed by Garrison, Hiltner, and Schild (1977).

On the MK system the stars are put into five luminosity classes

V, which is a dwarf or main-sequence star,
IV, which is a subgiant star,
III, which is a giant star,
II, which is a bright giant star,

Ib, which is a faint supergiant, and

Ia, which is a bright supergiant.

The luminosity class Iab is sometimes interpolated between Ia and Ib.

Occasionally the letters *n* or *nn* are added to indicate that the absorption lines are diffuse and shallow. In some cases the letters *e* and *p* are added to the spectral type; the letter *e* means that at least the first member of the Balmer series of hydrogen Hα is in emission, and the letter *p* means that the relative strengths of the weak absorption lines are peculiar for the assigned spectral type. Although Hα is in emission in many supergiants of type B, generally the supergiants are not known as Be stars. This classification is reserved for those B stars in luminosity classes V, IV, and III that sometimes show emission in the Balmer series, frequently to Hγ and sometimes to later members of the Balmer series. Usually with the supergiants, the emission in the Balmer series of hydrogen is seen only at Hα Not all Ib supergiants show Hα in emission, although all the Ia supergiants generally do at one time or another. Emission in the Balmer lines of hydrogen and occasionally in other lines is not a permanent property of a star. Most supergiants and Be stars that have been observed frequently show changes in the strength of the emission in intervals of weeks or months. A few cases of more rapid change are known. This topic will be discussed in detail in later chapters.

On spectra having a dispersion of 63 Å mm^{-1}, the stars of types B2.5 and earlier show many lines from spectra of the ions of C, N, O, and Si. Walborn (1971) has developed a detailed classification system for early B stars which uses ratios of lines of Si II, Si III, and Si IV as well as lines of He I to determine the spectral types and to assign luminosity classes. He has introduced the type B0.7 between B1 and B0.5 and the type B0 2 between B0.5 and B0 in order to resolve some ambiguities between luminosity class and spectral type which exist in the MK system. Spectral types for several stars in the range B2.5 to O9 are given in Walborn (1971). In addition, Walborn has drawn attention to the fact that the lines of N II, C II, and C III sometimes have anomalous intensities in B stars. He has introduced the designation BN for those B stars which have anomalously strong lines of N II and BC for those B stars which have anomalously strong lines of C II or C III, and weak lines of N II. This type of variation in spectra, which are normal so far as the standard spectral classification criteria are concerned, extends into type O The stars known to have anomalous N and C lines are listed in Walborn (1976). Walborn's system of spectral classification for the OB stars is described in detail in the volume in this monograph series entitled *O, Of, and Wolf-Rayet Stars* (Underhill and Divan, to be published).

From Broadband Colors

The UBV broadband system of colors and magnitudes was introduced by Johnson and Morgan (1953). The width of each pass band is of the order of 1000 Å and the zero point for color is established by setting

$$B - V = U - B = 0 \qquad (2\text{-}1)$$

for the six A0 stars, α Lyrae, γ Ursae Majoris, 109 Virginis. α Coronae Borealis, γ Ophiuchi, and HR 3314. For B stars, the effective wavelengths of the U, B, and V magnitudes are 3460, 4370, and 5460 Å, respectively. Johnson and Morgan introduced the quantity

$$Q = (U - B) - \left(\frac{E(U-B)}{E(B-V)}\right)(B-V), \qquad (2\text{-}2)$$

which is independent of reddening so long as the actual ratio of the color excesses, $E(U - B)$ and $E(B - V)$, of the observed star is equal to the average value for the interstellar reddening law A definitive description of the interstellar reddening law may be found in Savage and Mathis (1979). Johnson and Morgan showed that Q can be monotonically related to the spectral type throughout classes O and B. A revised spectral type–Q relation is given by Johnson (1958). This relation is valid for main-sequence stars only.

In principle the ratio of the color excesses obtained with the UBV magnitudes and the recommended intrinsic colors for each spectral

type should be constant because they are a function of the reddening law and of energy generation of the stars. However, since the pass bands of the UBV system are wide, there is some dependence of the ratio of color excesses on spectral type and on the amount of interstellar reddening. FitzGerald (1970) has analyzed the data given in the *Photoelectric Catalogue* (Blanco et al., 1968) and has derived a more consistent set of intrinsic colors than that recommended by Johnson (1958), but he does not develop another spectral type–Q relation. The Q method for determining spectral types of early type stars has been reviewed by Gutiérrez-Moreno (1975). He lists consistent values of intrinsic colors $(B-V)_0$, $(U-B)_0$, and Q as a function of spectral type for the B-type stars depending upon what is assumed about the ratio of the color excesses $E(U-B)/E(B-V)$. This method of spectral classification from broadband photometric data alone is useful for the many faint stars for which spectra are not available, but it does not yield the quantity of information that may be found from spectra of moderate or high dispersion.

The question of the best intrinsic colors for the B stars has also been studied by Schmidt-Kaler (1965) who presents a slightly different set of $(U-B)_0$ and $(B-V)_0$ for the B stars. This problem has also been discussed by Heintze (1973) who considers the problem of allowing for the interstellar reddening in detail and presents a table of MK spectral types and what he considers the best values of $(U-B)_0$, $(B-V)_0$, and Q to be associated with each type from O9 to B9.5.

The intrinsic UBV colors for B-type stars and suggestions for Q are given in Table 2-1 for main-sequence B stars. The referenced authors give slightly different values for the more luminous B stars. Intrinsic colors for the supergiants in the Large Magellanic Cloud have been derived by Brunet (1975). They differ slightly from the values of FitzGerald for the supergiants of our galaxy. With these broadband colors there is no way of differentiating photometrically Be stars from B stars without emission lines or supergiants from main-sequence stars. In order to make a luminosity separation and to recognize Be stars one must look at spectra. With intermediate-band photometry, which includes an index measuring the strength of one of the first three Balmer lines, Be stars and supergiants can

Table 2-1
The Intrinsic Colors and Q Values for Luminosity Class V B Stars

MK Spectral Type	Johnson (1963) $(B-V)_0$ (mag)	Johnson (1963) $(U-B)_0$ (mag)	Schmidt-Kaler (1965) $(B-V)_0$ (mag)	Schmidt-Kaler (1965) $(U-B)_0$ (mag)	FitzGerald (1970) $(B-V)_0$ (mag)	FitzGerald (1970) $(U-B)_0$ (mag)	Heintze (1973) $(B-V)_0$ (mag)	Heintze (1973) $(U-B)_0$ (mag)	Johnson (1958) Q (mag)	Heintze (1973) Q (mag)
O9	−0 31	−1 12	−0 31	−1 12	−0 31	−1 13	−0 29	−1 09	−0 90	−0 90
O9 5	−0 30	−1 10	−0 31	−1 10	−0 30	−1 10	−0 29	−1 07	−0 88	−0 87
B0	−0 30	−1 08	−0 30	−1 08	−0 30	−1 08	−0 28	−1 03	−0 86	−0 85
B0 5	−0 28	−1 01	−0 29	−1 03	−0 28	−1 00	−0 27	−0 98	−0 81	−0 81
B1	−0 26	−0 93	−0 28	−0 95	−0 26	−0 95	−0 26	−0 94	−0 74	−0 77
B2	−0 24	−0 86	−0 26	−0 87	−0 24	−0 81	−0 24	−0 86	−0 69	−0 70
B3	−0 20	−0 71	−0 22	−0 73	−0 20	−0 68	−0 22	−0 76	−0 57	−0 62
B4	–	–	–	–	−0 18	−0 63	−0 19	−0 67	–	−0 54
B5	−0 16	−0 56	−0 18	−0 58	−0 16	−0 58	−0 17	−0 58	−0 44	−0 46
B6	−0 14	−0 49	−0 16	−0 51	−0 14	−0 49	−0 15	−0 49	−0 39	−0 39
B7	−0 12	−0 42	−0 14	−0 43	−0 13	−0 43	−0 13	−0 39	−0 33	−0 31
B8	−0 09	−0 30	−0 12	−0 34	−0 11	−0 36	−0 11	−0 30	−0 24	−0 23
B9	−0 06	−0 19	−0 08	−0 21	−0 07	−0 18	−0 09	−0 22	−0 15	−0 16
B9 5	−0 03	−0 10	–	–	−0 04	−0 10	−0 08	−0 18	−0 08	−0 12

Dashes (–) represent data not defined

be separated from main-sequence, absorption-line B stars fairly well, as described below.

From Intermediate-Band Colors and Hβ

Because of the inconsistencies with the UBV photometric system caused by its wide bands, Strömgren introduced a system of photometry using bands of intermediate width, 180 to 300 Å. This system has proved to be very effective and it is known as the uvby, β system. A description of the system and its general properties and the types of problems that can be solved with it has been given by Strömgren (1966). It makes use of four bands, u, v, b, y, and an index, β, which measures the strength of the Hβ line by comparing the light transmitted through a narrow (about 30 Å wide) band at Hβ and a band about 150 Å wide. The mean wavelengths of u, v, b, and y are 3500, 4110, 4670, and 5470 Å, they are not dependent on the spectral type. The y magnitude is effectively the same as the V magnitude. Crawford and his colleagues at the Kitt Peak National Observatory have developed the system and have calibrated it in terms of spectral type and absolute magnitude (see Crawford, 1973, 1975a, 1975b, 1978). The quantities used are the following.

- y, which is an apparent magnitude on the same system as the V of the UBV system;
- (b − y), which is a color index freer of line blanketing effects than (B − V) of the UBV system;
- (u − b), which is a color index which relates well with the subclasses of type B;
- $m_1 = (v - b) - (b - y)$, which is a color difference which gives a measurement of the line blanketing in the 4100 Å region;
- $c_1 = (u - v) - (v - b)$, which is a color difference which gives a measurement of the Balmer discontinuity; and
- β, which is a hydrogen line-strength parameter.

Strömgren (1966) defined the quantities $[c_1]$, $[m_1]$, and $[u - b]$ as c_1, m_1, and u − b corrected for interstellar reddening. He gives

$$[c_1] = c_1 - 0.20(b - y), \qquad (2\text{-}3)$$

$$[m_1] = m_1 + 0.18(b - y), \qquad (2\text{-}4)$$

$$[u - b] = (u - b) - 1.84(b - y) = [c_1] + 2[m_1]. \qquad (2\text{-}5)$$

Further study, particularly by Crawford, indicates that the numerical constant in the relation for $[m_1]$ should be +0.30, and this is generally used in later work. The numerical factors suggested by Strömgren take account of interstellar reddening according to the theoretical curve Van De Hulst No. 15. Empirical reddening corrections have been derived by Crawford (1973, 1975a), he recommends use of the quantities

$$(b - y)_0 = (b - y) - E(b - y), \qquad (2\text{-}6)$$

$$(u - b)_0 = (u - b) - E(u - b), \qquad (2\text{-}7)$$

$$c_0 = c_1 - E(c_1), \qquad (2\text{-}8)$$

$$m_0 = m_1 - E(m_1), \qquad (2\text{-}9)$$

where

$$E(u - b) = 1.61E(b - y), \qquad (2\text{-}10)$$

$$E(c_1) = 0.25E(b - y), \qquad (2\text{-}11)$$

$$E(m_1) = -0.32E(b - y). \qquad (2\text{-}12)$$

The quantity $E(b - y)$ can be found by an iterative process starting from the approximate relation (Crawford and Barnes, 1974)

$$(b - y)_0^1 = -0.116 + 0.097c_1, \qquad (2\text{-}13)$$

or by the method outlined by Crawford (1978). These empirical corrections for interstellar reddening are preferable to adopting corrections based on a theoretical expression for the interstellar reddening law.

For the B stars, both $[c_1]$ and c_0 correlate well with MK spectral type while β is a good parameter for luminosity. The average uvby, β parameters for luminosity classes III and V, types B0 to A0, have been evaluated by Crawford

(1978); they are given in Table 2-2. Warren (1976), from a study of stars in the Orion Association, has derived average values of the uvby, β parameters for stars of luminosity class V, types O9 to A0; these are given in Table 2-3. They agree well with the values of Crawford, with small differences because of the different sets of stars collected in each spectral type–luminosity class box Study of high dispersion spectra shows that the stars of a given MK or photometrically defined box are rather diverse in their properties; thus, empirical relations between average photometric quantities and MK spectral type will always differ slightly, depending upon which stars are used to derive the relation. Warren has noted slight deviations from his tabulated data for stars which are rotating rapidly, v sin i > 250 km s^{-1}.

A calibration of the intermediate-band system colors in terms of visual absolute magnitude for the B stars was first provided by Eggen (1974a). He used the published observations of Crawford and colleagues on stars in open clusters or in wide binary systems and his own intermediate-band observations to derive a relationship between [u − b], as defined by Strömgren in 1966, and M_V, using the method of cluster fitting. Eggen set the zero point using stars from the Pleiades, NGC 2287, the α Persei cluster, and NGC 2602. He derived the formula

$$M_V = M - A(\beta_c - \beta_{obs}), \qquad (2\text{-}14)$$

where

$$\beta_c = 0.255\,[u-b] + 2.610. \qquad (2\text{-}15)$$

Table 2-2
Average Parameters for MK Types

Spectral Type	Luminosity Class V			Luminosity Class III		
	β (mag)	m_0 (mag)	c_0 (mag)	β (mag)	m_0 (mag)	c_0 (mag)
B0	2.606	0.055	−0.06	2.577	0.058	−0.10
B0.5	2.604	0.074	−0.04	2.583	0.069	−0.07
B1	2.609	0.082	0.02	2.596	0.074	0.00
B1.5	2.633	0.092	0.12	2.604	0.084	0.04
B2	2.646	0.096	0.22	2.605	0 080	0.10
B2.5	2.650	0.097	0.25	–	–	–
B3	2.681	0.104	0.32	2.644	0.084	0.32
B4	2.672	0.100	0 38	–	–	–
B5	2.701	0.106	0.42	2.686	0.102	0.45
B6	2.716	0.110	0.50	2.705	0.102	0.57
B7	2.723	0.107	0.55	2.707	0.105	0.55
B8	2.748	0.118	0.66	2.718	0.110	0.61
B9	2.795	0.126	0.83	2.740	0.110	0.80
B9.5	2.827	0.134	0.97	2.796	0.120	0.96
A0	2.861	0.154	1.01	2.822	0.133	1.03

Source Crawford (1978).
Dashes (–) represent no existing data.

Table 2-3
uvby, β–MK Spectral Type Calibration for B-Type Stars

MK Type	β (mag)	$(b-y)_0$ (mag)	m_0 (mag)	c_0 (mag)	$(u-b)_0$ (mag)
O9 V	2.586	−0.128	0.074	−0.122	−0.288
O9 5 V	2.594	−0.125	0 059	−0.098	−0.231
B0 V	2.602	−0 121	0.058	−0.056	−0 183
B0.5 V	2.605	−0.120	0.075	−0.038	−0.128
B1 V	2.616	−0.114	0.082	0.022	−0 041
B1.5 V	2.630	−0 108	0.091	0.086	0.053
B2 V	2.651	−0.096	0.095	0.205	0.203
B2.5 V	2.660	−0.091	0.100	0.255	0.272
B3 V	2.683	−0.085	0.105	0.319	0.358
B4 V	2.681	−0.081	0 105	0.364	0.412
B5 V	2.705	−0.075	0 110	0.424	0.494
B6 V	2 716	−0.068	0.114	0.493	0 584
B7 V	2.724	−0.061	0.111	0 565	0 664
B8 V	2.752	−0.049	0 118	0 690	0 829
B8.5 V	2.771	−0.043	0.126	0 752	0.918
B9 V	2.797	−0 035	0.127	0 830	1.013
B9.5 V	2.836	−0.026	0.138	0.927	1.151
A0 V	2.862	−0.019	0.154	1.002	1.272

Source: Warren (1976)

The constants M and A are empirically determined functions of [u − b]; they are given in Table 2-4. The results from this calibration agree well with those that may be determined from the calibration of Crawford (1978), with slight systematic differences appearing only for the evolved stars which were handled differently by Eggen and by Crawford.

The calibration of Crawford (1978) was found by the usual method of fitting cluster sequences. Crawford sets the zero point by means of an adopted distance for the Pleiades cluster and from the trigonometric parallaxes of the nearby stars Sirius and Vega as well as from a visual absolute magnitude for α Vir based on interferometric work. His final calibration of β for B stars in terms of M_V is given in Table 2-5. A correction

$$\Delta M_V(\beta) = -10(\beta_{ZAMS} - \beta_{obs}), \qquad (2\text{-}16)$$

must be added to $M_V(\beta)$ for those stars with c_0 in the range 0.20 to 0.90 to allow for evolution from the main sequence. Values of β_{ZAMS} as a function of c_0 are given in Table 2-5. The symbol β_{ZAMS} is the value of β for an unevolved star lying on the zero-age main sequence (ZAMS).

A calibration of β in terms of M_V has been provided by Neckel and Klare (1976). They adopt the M_V − MK spectral-type calibration of Schmidt-Kaler (1965) and via the known MK spectral types for 678 stars they derive a relation

Table 2-4

Parameters of Eggen's (1974a) Calibration of the uvby, β Photometry in Terms of M_V

[u − b]	M	A	[u − b]	M	A	[u − b]	M	A
−0 050	−4 25[a]	42 5	0 450	0 0	33 0	0 950	1 35	19 0
0.000	−3 5[a]	41 0	0 500	0 2	32 0	1 000	1 4	18 2
0 050	−2 75	40 0	0 550	0.4	31.0	1.050	1.45	17 4
0 100	−2 2	39 1	0 600	0.55	30 0	1 100	1 5	16 6
0 150	−1 75	38 3	0 650	0 7	28 0	1 150	1.55	15 7
0 200	−1 4	37 5	0 700	0 85	25.8	1 200	1.6	15.0
0 250	−1 1	36.7	0 750	0 95	23.5	1 250	1.65	14.5
0 300	−0 8	35 8	0 800	1.05	21.3	1.300	1.75	14 0
0 350	−0 5	35 0	0 850	1 15	20 5	–	–	–
0 400	−0 2	34 0	0 900	1 25	19 8	–	–	–

Dashes (–) represent data not obtained
[a]Uncertain value

Table 2-5

Crawford's (1978) Calibration of β in Terms of M_V for B Stars

β (mag)	$M_V(\beta)$ (mag)	β (mag)	$M_V(\beta)$ (mag)	Parameters of the ZAMS	
				c_0	β_{ZAMS}
2 560	−6 51	2 740	0 04	−0 20	2.593[a]
2 570	−5 84	2.750	0 18	−0.15	2 596
2 580	−5 22	2 760	0 30	−0 10	2 605
2 590	−4 65	2 770	0 41	−0 05	2 615
2 600	−4 12	2 780	0 51	0 00	2 625
2 610	−3 62	2 790	0.60	0 10	2 648
2 620	−3 17	2 800	0.68	0.20	2 672
2 630	−2 75	2 810	0 76	0 30	2 695
2 640	−2 36	2 820	0.83	0 40	2 719
2 650	−2 01	2 830	0 90	0 50	2 742
2 660	−1 69	2 840	0 97	0 60	2 765
2 670	−1 39	2 850	1.03	0 70	2 792
2 680	−1 12	2 860	1 10	0 80	2 825
2 690	−0 87	2 870	1 17	0 90	2 870
2 700	−0 65	2 880	1 24	1 00	2 910
2 710	−0 45	2 890	1 31	1 10	2 910[b]
2 720	−0 27	2 900	1 39	–	–
2 730	−0 10	–	–	–	–

Dashes (–) represent no existing data
[a]Uncertain value
[b]Very uncertain value

between M_V and β which they claim will give the visual absolute magnitude of a B-type star with an accuracy better than 0.5 mag. The use of the calibrations by Eggen and by Crawford is more accurate than this, but none of these calibrations can be used for stars which have Hβ in emission.

Intermediate-band data for more than 2900 stars with MK spectral types in the range B, A, and F have been studied by Oblak et al. (1976). They derive mean values of the usual color indices and color differences as functions of spectral type. The results for main-sequence and near main-sequence stars support those derived by Crawford and by Warren. The color indices and color differences which they find for the supergiants differ somewhat from those for main-sequence stars but they conclude that an insufficient number of supergiants have been observed with the intermediate-band photometric system to derive precise intrinsic colors for the supergiants. The index β varies very little with spectral type among the B-type supergiants, as is expected from spectroscopic studies of the strengths of the hydrogen lines in B-type stars of all luminosities and spectral types. Standard stars for uvby photometry are listed by Crawford and Barnes (1970), those for Hβ photometry are given by Crawford and Mander (1966).

Shobbrook (1976) has paid particular attention to finding an empirical relation between c_0 and $(b-y)_0$ for B-type supergiants, making use of published uvby and UBV photometry for 60 O9.5 and B field supergiants without known emission. He has been able to show that $(b-y)_0$ *is distinctly redder for B-type supergiants having* a selected value of c_0 than it is for main-sequence stars with the same value of c_0. His intrinsic intermediate-band colors for B-type supergiants are given as a function of MK spectral type in Table 2-6. They support the findings from broad-

Table 2-6
Intrinsic Intermediate-Band Colors for B-Type Supergiants

Spectral Type	$(b-y)_0$		c_0	
	Ia	Ib	Ia	Ib
O9 5	−0 14	−0.12	−0 15	−0 16
B0	−0 10	−0 09[a]	−0 12	–
B0 5	−0 10	−0 09	−0 13	−0 10
B1	−0 07	−0 06	−0 09	−0 05
B1 5	−0 05	–	−0 09[a]	–
B2	−0 05	−0 05	−0 10	+0 02
B2 5	(−0 05)*	–	−0 11[a]	+0 05[a]
B3	−0 04	–	+0 09	–
B4	−0.01[a]	–	+0 08[a]	–
B5	+0 00	+0 00	+0 2[a]	–
B6	–	+0.00	–	+0 4[a]
B8	+0 05	+0 05	+0 25[a]	+0 5[a]
B9	(+0 04)*	–	+0.4[a]	+0.8[a]
A0	(+0 06)*	–	–	–

*From Shobbrook's table it is not clear whether the values put in parentheses here refer to luminosity class Ia or Ib
Source Shobbrook (1976)
Dashes (–) represent no existing data
[a]Uncertain value

band photometry that, for a given MK spectral type, the colors of B supergiants are redder than the colors of main-sequence stars. This may readily be verified by comparing the data in Tables 2-2, 2-3, and 2-6.

In many B-type stars, the Balmer lines of hydrogen appear in emission, and although the emission at Hα can be detected on objective prism spectra, the separation of Be stars from supergiants requires spectra of moderate dispersion. A sensitive photometric criterion would facilitate the investigation of many faint stars and aid in the study of galactic structure, because supergiants are good indicators of distant spiral arms. Abt and Golson (1966) investigated the photometric separation of Be stars and Ia supergiants by means of an α index derived by comparing the signals obtained through a filter about 35 Å wide and through one about 150 Å wide They showed that the α index was much reduced for Be stars relative to its value for normal main-sequence B stars. However, use of the α index alone did not permit the certain separation of supergiants from Be stars. They found that plotting α–β against α separated Be stars from supergiants most of the time, although a few Be stars fall in the part of the diagram occupied by supergiants. The α index is usually small for Be stars. According to Abt and Golson, by means of their α and β indices one can isolate two-thirds of the Be stars from the supergiants in a mixed sample of early type stars having Hα in emission. Abt and Golson concluded that all B and early A Ia supergiants have some emission in Hα and Hβ and that the A-type supergiants tend to have weaker Hα emission and smaller Balmer decrements than do the B-type supergiants.

A comprehensive survey of the strength of Hα in stars of types O, B, and A has been carried out by Andrews (1968), using a filter 36 Å wide centered on Hα itself and filters 20 Å wide on either side of Hα Andrews noted that some stars have a variable Hα index, Rα, and that the work of Abt and Golson appears to contain some large random errors. He also found that Be stars can be separated pretty well from absorption-line B stars and from supergiants by means of an $R\alpha$–β or $R\alpha$–γ diagram. He derived a relationship between his $R\alpha$ parameter and M_V, valid for B stars, using cluster membership as a means of establishing the luminosity of the star.

Similar photometric work on a variety of early type stars and some stars of types A and F has been done by Tebbe (1969), Peton et al. (1972), Feinstein (1974), Baliunas et al. (1975), Dachs and Schmidt-Kaler (1975), and by Cester et al. (1977). It is shown that in a $(U - B)_0$ vs. α, [u − b] vs. α, or $[c_1]$ vs. α diagram the Be stars may be separated fairly well from the normal B stars without emission lines. If the filter centered at Hα is very narrow—for instance, it is only 13 Å wide in the case of Dachs and Schmidt-Kaler—the separation of Be stars from supergiants is good when the α index is plotted against the β index. All these photometric observations show that the α indices for the Be stars and for the OB supergiants tend to vary by a small amount, whereas the α index is constant for the normal absorption-line B stars. Narrow-band photometric observations made at Hα are useful for differentiating Be stars and shell stars from normal B stars. However, the photometry at Hα tends to have larger intrinsic errors than the photometry in the normal blue-violet spectral region, because B stars are less bright at Hα than they are shortward of 5500 Å unless they suffer very heavy interstellar extinction.

Absolute Magnitude as a Function of Hβ and Hγ Strength and of Luminosity Class

The Stark broadening of the Balmer lines of hydrogen has been recognized to be a good indicator of the luminosity of the star since the first studies of the shapes and equivalent widths of the hydrogen lines in B-type spectra. In the atmospheres of main-sequence stars where the acceleration caused by gravity is large and the electron pressure is large, the Balmer lines are greatly broadened by Stark effect and have extensive wings. This leads to a large equivalent width. In the atmospheres of supergiants, where the acceleration of gravity is 10 to 50 times smaller and the electron pressure is smaller, the Stark effect is less intense, and the hydrogen lines have small wings. The equivalent width of a

typical line such as Hβ or Hγ is then small. In the supergiants the equivalent width of Hγ varies only a little with spectral type; for main-sequence stars there is a significant dependence of the equivalent width of Hγ on spectral type as well as on luminosity.

The attempts completed by 1965 to calibrate the strength of Hγ in terms of visual absolute magnitude and attempts to calibrate the MK spectral types and luminosity classes for the B-type stars have been summarized by Underhill (1966a). Because B stars are few in number and are intrinsically bright, most of the stars observed are at distances so large that the fundamental method of trigonometric parallaxes cannot be used to establish their true distances, hence luminosities. The calibration of the luminosity criterion must be carried out using B stars which are members of clusters or multiple systems whose distance can be determined by means of the later type members of the cluster or system. The luminosities of these stars (types A and later) are well related to the geometrical scale of distance. One assumes that all members of the group are at the same distance and that any necessary correction of the apparent magnitudes of the B stars for interstellar extinction can be deduced from the correction for the stars of later type belonging to the cluster or system. The results of Eggen (1974a) and of Crawford (1978) on the calibration of the β index for main-sequence B stars have been referred to in the section on Intermediate-Band Colors and Hβ. They used the customary method of fitting the sequences formed by plotting the value of the criterion (β index) for all stars of a cluster against V_0, the apparent magnitude corrected for interstellar extinction, and they fitted each cluster sequence piecewise to form a curve valid over a wide range of spectral types. The individual sequences given by the data for individual clusters are not sharp. There is a significant spread introduced by the facts that some stars have evolved off the main sequence, some have companions for which no correction is made in the photometric work, and some nonmembers (foreground or background stars) also may be present. It is postulated that there is a lower limit to the display of points and that this limit corresponds to the luminosities of stars which are on the zero-age main sequence. The art of this method of calibrating a luminosity criterion is to fit the individual cluster sequences so that a precise and accurate ZAMS is derived. The shifts of the clusters relative to the sequence for a standard cluster produce cluster distance moduli relative to that for the nearby cluster, usually the Pleiades or the Hyades, which is adopted as an anchor. Alternatively, one may adopt distance moduli for the clusters used from some other source of information. The luminosity calibrations of Blaauw (1963) and of Schmidt-Kaler (1965) for MK luminosity classes use this concept of a unique ZAMS also.

Petrie (1952, 1965) developed a quantitative relationship valid for B stars between the equivalent width of Hγ, W(Hγ), measured on moderate dispersion spectra and visual absolute magnitude. He provided a correction table to take account of the small dependence of the result on the spectral type of the star. This calibration gives M_V for stars of types B3 and later in good accord with the results of Blaauw (1963) and of Schmidt-Kaler (1965) but for the range B2 to O9 Petrie gives fainter absolute magnitudes, by about 0.4 mag on the average, than the calibrations of the MK spectral types suggest. The set of stars of known absolute magnitude (from cluster membership and membership in eclipsing binary systems) used by Petrie gives poor overlap between the position of his $W(\mathrm{H}\gamma) - M_V$ relation determined for stars of types B2 and earlier and the relation valid for B stars of types B3 and later; this poor overlap may be the reason why Petrie's system of absolute magnitudes does not give the same result that Blaauw and Schmidt-Kaler have found.

To investigate this question, Balona and Crampton (1974) assembled equivalent widths of Hγ for B stars in eight clusters or associations in both the northern and the southern hemispheres and developed a new calibration of W(Hγ) in terms of M_V. When measuring the equivalent width of Hγ they made no allowance for the blending effects of He II in the O stars but they did correct for the blends caused by O II in the

early B stars. The apparent visual magnitude V was corrected to allow for known spectroscopic companions and for interstellar extinction using the relation

$$A_V = 3E(B-V). \qquad (2\text{-}17)$$

The MK spectral types were taken from the literature. The calibration procedure of Balona and Crampton assumes (1) that M_V is a function of $W(H\gamma)$ and spectral type alone and (2) that this function is the same for all clusters. To establish the zero point of their system of absolute magnitudes they adopt Blaauw's (1963) distance modulus for the Pleiades of 5 55 mag. The results give M_V as a function of $(B-V)_0$ and $\log_{10} W(H\gamma)$ with coefficients determined by the method of least squares or M_V as a function of $\log_{10} W(H\gamma)$ alone with the coefficients depending weakly on spectral type. These explicit dependences on $(B-V)_0$ or of the adopted coefficients on the spectral type, which needs to be known only roughly, do away with the need for the spectral-type corrections introduced by Petrie.

Compared to the results of Petrie (1965), this new calibration of $W(H\gamma)$ in terms of absolute magnitude gives M_V up to one magnitude brighter for the O stars; at other spectral types it gives essentially the same results as Petrie found. Thus, the discrepancy with the Blaauw (1963) calibration of the MK spectral classes for types O9 to B2 remains. Balona and Crampton have collected $W(H\gamma)$ measurements for 1932 OB stars with MK spectral types, and from this material they have derived the calibration of the MK spectral types in terms of M_V which is given in Table 2-7. The main differences with the calibration of Blaauw (1963) are as follows.

Table 2-7
MK Absolute Magnitude Calibration

Spectral Type	Balona and Crampton (1974)							Lesh (1979)		
	V	IV	III	II	Ib	Iab	Ia	V	IV	III
O9	−4 5	−4 8	−5 0	−5 1	−5 7	–	−6 8	−4 3	−5 0	−5 6
O9 5	–	–	–	–	–	–	–	−4 1	−4 7	−5 3
B0	−3 8	−4.3	−4 6	−5 0	−5 6	−6 0	−7 0	−3 9	−4 4	−5 0
B0 2	–	–	–	–	–	–	–	−3 8	−4 2	−4 9
B0 5	–	–	–	–	–	–	–	−3 7	−4 1	−4 8
B0 7	–	–	–	–	–	–	–	−3 6	−4 0	−4 4
B1	−3 2	−3 7	−4 1	−4.7	−5.5	−6 2	−7 0	−3 5	−3 8	−4 0
B1.5	–	–	–	–	–	–	–	−2 8	−3 5	−3 7
B2	−2 5	−3 1	−3 7	−4 5	−5 4	−6 2	−7 0	−2 2	−3 0	−3 3
B2.5	–	–	–	–	–	–	–	−1 9	−2 1	−2 5
B3	−2.0	−2 6	−3 1	−4.2	−5 3	−6 1	−7 0	−1 3	−1 7	−2 2
B4	−1 6	−2 2	−2 6	−3 9	−5 2	−6 0	−7 0	−1 1	−1 6	−1 9
B5	−1.3	−1 8	−2 0	−3 6	−5 0	−5 9	−7 0	−0 9	−1 0	−1 6
B6	−0.9	−1 4	−1 7	−3 3	−4 9	−5 7	−7.0	–	–	–
B7	−0.5	−1 0	−1 4	−3 0	−4 7	−5 6	−7.0	–	–	–
B8	−0 1	−0.6	−1 1	−2 6	−4 5	−5 4	−7 0	–	–	–
B9	+0 4	−0 2	−0 7	−2 3	−4 2	−5 2	−7 0	–	–	–

Dashes (–) represent no existing data

1. For types earlier than B2 and in luminosity classes III to V, the Balona–Crampton calibration is 0.4 mag fainter;
2. For B3 to B6 V stars, the Balona–Crampton calibration is 0.3 mag brighter;
3. For types later than B3, luminosity classes Iab and Ib, the Balona–Crampton calibration gives fainter M_V;
4. For luminosity class Ia, types earlier than B2, the Balona–Crampton calibration gives brighter M_V.

A revised absolute magnitude calibration for the B0 to B5 stars of luminosity classes III, IV, and V has been derived by Lesh (1979) from consideration of her earlier data (Lesh, 1968, 1972) and the revised spectral types and absolute magnitudes given by Walborn (1971) for some early B-type stars. This calibration is also given in Table 2-7. It gives values of M_V for the fractional subclasses which Walborn has interpolated between B0 and B1 as well as for the subtypes which were originally recognized. The differences between this calibration and that of Balona and Crampton are typical of the uncertainties in determining absolute magnitude at certain places in the HR diagram because of the need to interpolate between scanty data no matter what criterion is used for luminosity.

The BCD System and its Relation to the MK System

A spectral classification system for stars of types O, B, A, and F making use of low dispersion, prismatic spectrograms extending to 3100 Å has been developed by Barbier, Chalonge, and Divan. In the definitive paper by Chalonge and Divan (1952), the parameters used to classify the B stars are D, a measure of the size of the Balmer jump ($D = \log F_R - \log F_V$, where F_R is the flux on the longward side of the Balmer jump and F_V is the flux on the shortward side of the Balmer jump), and λ_1 which gives the effective wavelength of the Balmer jump as seen on the low dispersion spectra used by Barbier, Chalonge, and Divan. This system of spectral classification has been described by Underhill (1966a). It is calibrated in terms of MK spectral types and luminosity classes. For the B stars the value of D is a good criterion for spectral type, and λ_1 (Figure 2-1) is a useful parameter for luminosity. However, D has a small but definite dependence on luminosity class for dwarfs and giants (V to III) and a very strong one for supergiants (Ia, Ib, II) (Figure 2-2). The parameter λ_1 as well does not depend only on luminosity class.

Since the above work was begun, the tech-

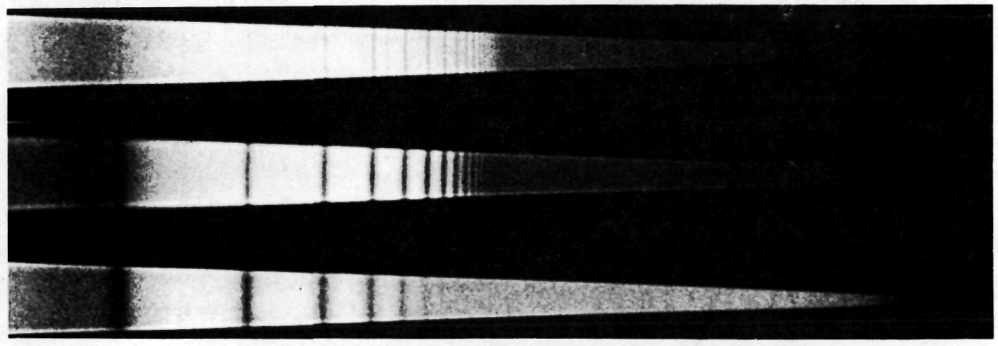

Figure 2-1. Spectra of three stars with the same effective temperature but very different gravities: (1) a supergiant in the Small Magellanic Cloud (R 21), (2) a normal dwarf (α Lyr), and (3) a white dwarf (40 Eri B). The shift of the position of the Balmer jump is clearly visible. The corresponding values of the λ_1 parameter are −02 and +65 in Å units, for R 21 and αLyr, respectively. Since this parameter is measurable with an accuracy of about 2 Å one can distinguish more than 30 different levels of luminosity between the supergiants and the normal dwarfs (from D. Chalonge and L. Divan, unpublished).

niques used have improved in quality and a large number of stars have been measured. It is now possible to derive more information about stars from the BCD spectra than was first possible. The improved calibration of the parameters λ_1 and D in terms of MK spectral type and a calibration in terms of intrinsic color (Figure 2-2) have been given by Chalonge and Divan (1973). They have introduced two new continuous parameters, s which depends only on spectral type, and l which depends only on luminosity class. Like D which it replaces, the parameter s can have the same value for early B stars and for F stars. In a later paper, Chalonge and Divan (1977) introduced a spectral type parameter, $\mathscr{S}$, which changes monotonically with spectral type. They demonstrated that this spectral type parameter correlates monotonically with the empirical effective temperatures for O-, B-, A-, and F-type stars derived from Hanbury Brown's angular diameters and from ultraviolet and ground-based spectrophotometry by Code et al (1976).

A calibration of the λ_1 D plane in absolute magnitudes has been made by Chalonge and Divan (1973). It is based on five clusters or associations for which distance moduli have been given by Johnson et al. (1961). The absolute magnitude M_V is calculated for each star from the V magnitude after a careful determination of the interstellar absorption, using the color excess of the continuum. In this way M_V was found for 76 points in the λ_1 D plane. From this information curves of equal absolute magnitude can be traced without much ambiguity These curves are reproduced in Figure 2-2. The uncertainty in M_V caused by the uncertainty in λ_1 and D is ±0.1 or ±0.2 mag for spectral types later than B2, a little larger for earlier types. Although the uncertainty in the positions of the curves of equal absolute magnitude can increase these numbers, the precision obtained is quite satisfactory and probably better than when M_V is deduced from a spectral type alone.

Chalonge and Divan have accurate spectrophotometric observations which measure the shape of the continuous spectrum both above and below the Balmer jump of all the bright O, B, A, and F stars The correction for interstellar

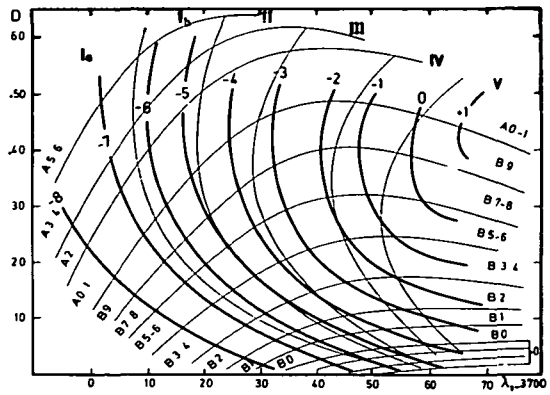

Figure 2-2. Calibration of the λ_1 D plane in terms of MK spectral type and absolute magnitude (Chalonge and Divan, 1973). The thin continuous lines indicate the limits of MK spectral types and luminosity classes. The curves of equal intrinsic color temperature in the spectral range 4600 to 4000 Å coincide with the curves of equal spectral type for luminosity classes V to III. They probably differ by a small and still uncertain amount for the supergiants Values of constant visual absolute magnitude are indicated on each heavy line. Note the large range in absolute magnitude for a given spectral type–luminosity class box For instance, M_V can have values between −1.4 and −3.5 for the spectral type B9 III.

reddening is important for the O and B stars and it has been carefully determined. These monochromatic energy distributions contain more information than photometric indices; they are also more easily compared to model atmospheres. For example, both empirical results and model atmosphere calculations demonstrate that the shape of the continuous spectrum and the size of the Balmer jump relate monotonically to the effective temperatures for normal, absorption-line, main-sequence, and near main-sequence B stars. Underhill et al. (1979) have used this result to assign effective temperatures to stars with known Balmer jumps. Inversely, in the case of supergiant stars there is a marked discrepancy between the observed and model Balmer jumps in the sense that the observed Balmer jumps are much smaller than those calculated from either local thermodynamic equilibrium (LTE) or non-LTE models in radiative and hydrostatic equilibrium.

Stars which show emission lines possibly caused by a hot mantle and/or an extended atmosphere in which the electron temperature is lower than in the photosphere may show a Balmer jump, D, and blue or ultraviolet gradients, ϕ_b or ϕ_{uv}, which differ from those of normal stars. Sometimes two Balmer jumps are seen, one at the normal position for a main-sequence star, and one at a shorter wavelength, λ_1. The latter Balmer discontinuity may be in emission or in absorption and in the case of a few stars it has been observed to change as the intensity of the emission lines changes, as discussed in Part II: The Be Stars.

CLASSIFICATION OF B STARS: THE ULTRAVIOLET REGION

As soon as ultraviolet spectra became available, astronomers began to create classification systems based solely on the appearance of the stellar spectrum in the ultraviolet wavelength range. We shall review now the chief results attained for B stars.

OAO-2 Spectrophotometry

With the spectrum scanners of the Second Orbiting Astronomical Observatory (OAO-2) satellite launched by the National Aeronautics and Space Administration (NASA) in 1968 (see Code et al., 1970 and Savage and Jenkins, 1972 for a description of these instruments), the spectrum is scanned by rotating a grating in discrete wavelength steps and allowing the light to fall through a fixed exit slot onto a photomultiplier The spectral region from 1150 to 1850 Å is covered in steps of about 10 Å, the full width at half maximum (FWHM) of the instrumental profile being about 12 Å; the spectral region from 1850 to 3600 Å is covered in steps of about 20 Å, the FWHM of the instrumental profile being about 22 Å. Code and Meade (1979) have published *An Atlas of Ultraviolet Spectra* with an extension by Meade and Code (1980). They present tabulations of the observed fluxes from bright stars in ergs cm^{-2} s^{-1} $Å^{-1}$ and give small-scale tracings of the spectrum from 1150 to 3600 Å. For stars of type B3 and earlier the spectral region from 1850 to 3600 Å, when observed at the low spectral resolution of the OAO-2 long wavelength scanner, is featureless; at types B5 and later, some characteristic line blends begin to appear. Underhill (1973b) has measured the apparent line blocking for late B-type and early A-type stars in the region 1900 to 3600 Å which averages 10 to 15 percent. Higher resolution than is afforded by OAO-2 long wavelength spectrum scanner is required to study the details of the near ultraviolet spectrum of B stars. In the spectral region from 1150 to 1850 Å, some characteristic absorption features are seen, particularly for types B3 and earlier

Panek and Savage (1976) have studied this spectral region in detail. Figures 2-3 and 2-4, reproduced from their paper, show the major changes due to the resonance lines of Si II, Si III, Si IV, and C IV. At the low resolution of the OAO-2 spectrum scanner, every feature is a blend of several components and the composition of these blends changes with spectral type. Lists of prominent features and their possible contributors are given by Underhill et al. (1972) and by Panek and Savage. The LTE model atmosphere calculations by Peytremann (1975) of the blend at 1550 Å suggest that the blend is chiefly caused by Fe III in the case of main-sequence stars with effective temperatures less than about 3.0×10^4 K. The observations of Swings et al. (1976) confirm this theoretical result.

For main-sequence stars of types earlier than B3, the strengths of the blends caused by the Si IV resonance lines at 1393 and 1403 Å and the Fe III blend with the C IV resonance lines at 1548 and 1550 Å correlate well with spectral type. The Si IV blend has peak intensity at B1 while the Fe III and C IV blend increases from B2, through B0 to O9. Both blends increase significantly, by a factor 2 or 3, in equivalent width as the luminosity increases for a given spectral type. In the O stars, these lines tend to have a P-Cygni profile At types B5 and later, high resolution scans obtained with the Copernicus (OAO-3) satellite show that the Si IV resonance lines have effectively disappeared from the spectra of main-sequence stars (see,

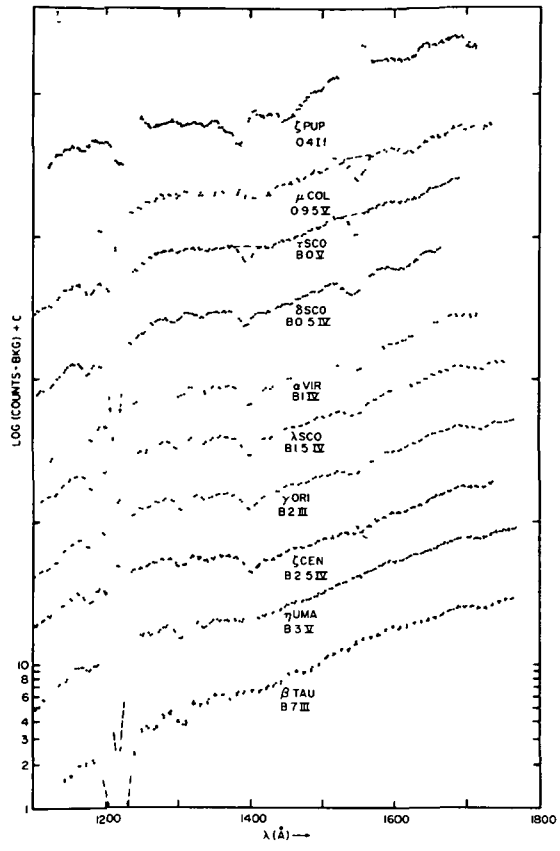

Figure 2-3. Composite OAO-2 spectrometer scans. Each spectrum was produced by combining two or more individual scans obtained with the nominal sample interval of 10 Å. The overall shape of the spectra is primarily determined by the instrumental response. The strongest features are Lyman alpha of hydrogen, mostly interstellar in origin, the C II 1334, 1335 blend, the Si IV 1393, 1402 blend, and the blend due to C IV 1548 and 1550 The dashed lines at the Si IV and C IV features represent the manner of determining the continuum level (from Panek and Savage, 1976)

for example, Underhill and Adelman, 1977)

A feature at 1720 Å was noted by Underhill et al. (1972) to be prominent in supergiants of all subclasses of type B and in the shell star ζ Tauri. The composition of this blend probably changes with spectral type High resolution spectra of ζ Tauri obtained by Heap (1975) from a sounding rocket show that a major contribution to this blend is made by multiplet

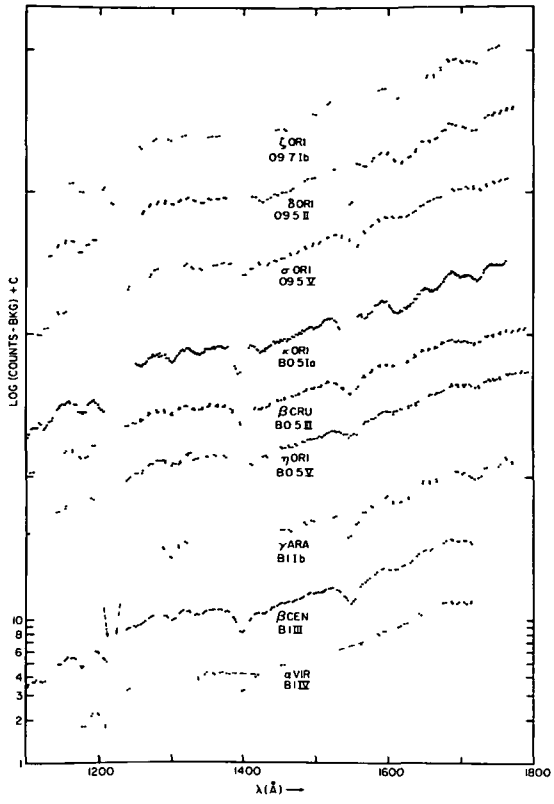

Figure 2-4. Composite OAO-2 spectra for stars of spectral classes O9 5, B0.5, and B1 (from Panek and Savage, 1976).

UV6 of A1 II. This multiplet arises from metastable levels and it may be expected to be enhanced in strength in low density extended atmospheres where the electron temperature is near 1.5×10^4 K

Objective Prism and Objective Grating Spectra

Low resolution spectral scans covering the region longward of 2000 Å obtained from objective prism and objective grating spectra have shown that the relative energy distribution of B stars longward of 2000 Å is similar to that predicted by model atmospheres (see Chapter 6, Model Atmospheres, Predicted Spectra, and Colors) Near ultraviolet relative energy distributions for 48 bright stars, many of them B stars, obtained from a balloon-borne Schmidt camera and objective prism have been published by Navach et al. (1973). These energy distributions,

when corrected for interstellar reddening, have been shown by Navach (1973) to continue the trends of color with spectral type indicated by ground-based work using intermediate and broad-band photometry.

Objective grating spectra of nine bright OB stars in Orion covering the region 2500 to 4400 Å at a nominal dispersion of 183 Å mm^{-1} were obtained by the astronauts Conrad and Gordon during the Gemini 11 mission in 1966. A small camera with an ultraviolet transmitting lens of aperture 22 mm and a reflection grating ruled at 600 lines mm^{-1} was used. The field diameter was 30 degrees. Relative energy distributions for these hot, luminous OB stars have been derived by Morgan et al. (1975). The results, when corrected for interstellar reddening, are in agreement with the predictions from model atmospheres and they confirm the results of Navach et al. (1973). The energy distribution of the star κ Orionis, B0.5 Ia according to Lesh (1968), is mildly deficient shortward of 2800 Å with respect to the energy distributions of supergiants of comparable spectral type. This observation, when joined to the comment of Underhill (1966a) that the spectrum of κ Orionis looks like that of a shell star on some spectra obtained at the Dominion Astrophysical Observatory, indicates that a high resolution study of κ Orionis is desirable to show whether κ Orionis is truly a supergiant.

In December 1973, observations of the near ultraviolet spectra of many faint stars were obtained with the space observatory Orion-2 on board the spaceship Soyuz 13. A wide-angle meniscus telescope, aperture 24 cm, was used with a 4°-quartz prism to obtain spectra from about 2000 to 5000 Å. The spectral resolution is about 8 Å at 2000 Å and 28 Å at 3000 Å. The first results were reported by Gurzadyan et al. (1974), a comprehensive summary of what has been done with these spectra is given by Gurzadyan (1975). Many of the stars are of spectral types A to K5 and most stars range in brightness from mag 10 to 13. Gurzadyan (1974) has noted that the extent of the spectrum shortward of 3500 Å for stars of a restricted magnitude range is a good indication of their spectral type, particularly for stars later than B9 or A0. For 10 B-type stars, Gurzadyan and his colleagues have shown that the relative energy distribution between 3800 Å and about 2200 Å, when corrected for interstellar reddening, agrees with the predictions from model atmospheres.

In the summer of 1973, objective prism spectra were obtained from Skylab for several fields containing O and B stars. The instrument is an objective prism spectrograph with a 15-cm aperture and a 4° prism of CaF_2. It gives a resolution of 2 Å at 1400 Å and 12 Å at 2000 Å. The first results have been discussed by Henize et al. (1975). A quantitative evaluation of the use for the classification of B stars of eye estimates of the strengths of the Si IV and C IV resonance lines as seen on these spectra is given by Henize et al. (1976) Here Henize and his colleagues give eye estimates from well-exposed spectra of the relative strengths of Si IV 1393 and the C IV blend at 1550 Å for 34 stars of types B0 to B2. No supergiants are included in this group. For 22 non-emission-line stars, the Si IV/C IV ratio decreases from 8 or 10 at B2 to 1/5 at B0. The 12 emission-line stars generally show smaller ratios, which is the result of the C IV blend being enhanced in strength, probably caused by increased Fe III absorption. Because the feature at 1550 Å has quite a sharp core on their spectra, Henize et al. believe that it is primarily caused by C IV in stars of type B2 and earlier. High resolution spectra will be necessary to resolve this question; C IV is a rather high level of ionization to be seen in the photospheres of B2 stars, as Peytremann (1975) has pointed out.

The material studied by Henize et al. (1975) and by Parsons et al. (1977) shows that the feature at 1550 Å attributed to C IV strengthens very rapidly between B2 and B0 and then remains more or less constant through the O stars. At B1 this feature strengthens significantly with increasing luminosity. In luminosity class V stars, Si IV peaks sharply at B1 and has virtually disappeared at O9.5. In luminosity class I stars, Si IV remains strong through the O stars. In class V stars the blend of C II resonance lines at 1335 Å varies little between types A0 and O9 5; it reaches peak intensity between B5 and B2. Between B3

and B1 the C II/Si IV ratio is an excellent spectral type (temperature) criterion. In the hottest and most luminous stars, P-Cygni profiles are seen for the Si IV and C IV resonance lines. On the Skylab spectra, a borderline for the definite occurrence of the P-Cygni phenomenon runs diagonally across the HR diagram from O7 V to O9 5 III to B3 Ia. The strength of the 1720 Å feature in B-type supergiants is confirmed and the 1720 Å feature is found to be present also in O stars, attaining maximum strength near O8 I. In the O stars, N IV 1718 is probably the dominant contributor to the observed blend.

Observations Made from the TD1 Satellite

Experiment S2/68 Spectral Scans. The TD1 satellite was launched by the European Space Research Organization (ESRO) in 1972, and it carried two experiments for observing stellar spectra, S2/68 and S59. The satellite was three-axis stabilized and in such an orbit that the full sky was scanned in 6 months. The low resolution scanning spectrometer S2/68 is described by Boksenberg et al. (1973); it gives data from a photometric channel centered at 2740 Å, for which the FWHM of the pass band is 310 Å, and from three scanning spectrometers which cover the region 1350 to 2550 Å with an effective pass band in the range 35 to 40 Å, the width depending on the channel The instrument has been calibrated to give absolute energies (Humphries et al , 1976) A catalogue giving the observed energy distribution in ergs cm^{-2} s^{-1} $Å^{-1}$ for 1356 bright stars, most of spectral types O and B, has been published by Jamar et al (1976). A catalogue of ultraviolet energies for 31215 stars has been published by Thompson et al (1978) A supplement has been published by Macau et al (1978)

From a study of the observations for more than 200 stars of types O to A5, Nandy et al. (1974) have found that a parameter

$$\phi = (U_1 - V) - X(U_3 - U_2), \qquad (2\text{-}18)$$

where U_1, U_2, and U_3 are the magnitudes at wavelengths 2740, 2500, and 2190 Å, respectively, V is the visual magnitude, and X is a ratio of color excesses,

$$X = \frac{E(U_1 - V)}{E(U_3 - U_2)}, \qquad (2\text{-}19)$$

correlates well with MK spectral type and with the Q parameter of Johnson and Morgan (1953). Humphries et al (1973) have shown that X = 1 0 ± 0.2. The pass band for U_1 is 310 Å FWHM; that of U_2 and U_3 is effectively 75 Å. The parameter ϕ permits a rough classification of early type stars from their near ultraviolet spectrum. The color index $(U_1 - V)$ is not significantly affected by luminosity, but the color $(U_3 - U_2)$ for luminous stars may be more positive by 0.2 mag than its value for main-sequence stars of similar spectral type. This difference between the near ultraviolet colors of main-sequence stars and supergiants is in the same direction as the differences at shorter wavelengths that are shown by the wide-band photometric work of Smith (1967), Carruthers (1969), and Weber et al. (1971), and by the analysis of OAO-2 spectrum scans by Laget (1972)

The possibility of assigning spectral types on the MK system from only the information contained in S2/68 scans has been investigated by Cucchiaro et al (1976, 1977). They find that using ratios of the apparent flux at the bottom of depressions near 1410, 1550, and 1620 Å permits one to classify within ±1 subtype on the MK system and that the stars can be separated into groups corresponding to dwarf, giant, and supergiant stars. The ratio of the flux at 1410 Å to that at 1550 Å is the criterion which relates best to spectral type and temperature. The ratio of the flux near 1620 Å to that near 1550 Å acts as a discriminant for luminosity. Among the stars of type B6 and later, stars classified as Bp in the visible spectral range may be readily recognized from abnormalities visible in their S2/68 spectra

The shape of the interstellar extinction curve through the ultraviolet has been deduced by Nandy et al (1975, 1976) from S2/68 spectral scans of several hundred O- and B-type stars distributed throughout the galactic plane. Particular attention was paid to comparing heavily

reddened and lightly reddened stars of the same spectral type and luminosity class. Lightly reddened supergiants were compared with more heavily reddened supergiants in order to avoid carrying luminosity-dependent intrinsic spectral differences into the deductions about the shape of the interstellar extinction curve. Nandy et al. have combined their results, which show no dependence on galactic longitude greater than can be accounted for by observational error, with photometric results in the visible range to derive the reddening law given in Table 2-8. This table contains data from Nandy et al. (1975) for the range λ^{-1} equal to 1.00 to 2 20μm^{-1} and from Nandy et al. (1976) for the remainder of the table. In Table 2-8, $A(\lambda)$ is the absorption in mag at wavelength λ and $E(B - V)$ is the $(B - V)$ color excess. This law for the wavelength dependence of interstellar extinction will serve as a first correction for the effects of interstellar extinction. Once the major correction has been applied, observational data may be studied in detail to see if any real differences of interstellar extinction exist in different areas of the galaxy.

A broad region of absorption centered at 1920 Å which becomes pronounced in stars of high luminosity has been noted by Thompson et al. (1974). They show that this feature is probably caused by Fe III, a view which is confirmed by the observations of ζ Tauri by Heap (1975) and by the observations of Swings et al. (1976). This feature strengthens in stars of high luminosity and in shell stars.

Experiment S59 Spectral Scans. The S59 spectrum scanner records three bands in the near ultraviolet, each about 100 Å long, namely from 2064 to 2158 Å, 2497 to 2591 Å, and 2777 to 2868 Å. The spectral resolution changes a little from band to band, but it averages 1.8 Å. The instrument has been described by de Jager et al. (1974); three moving exit slots scan the spectrum in the three bands simultaneously taking steps of about 0.46 Å and letting the light fall on three solar-blind photomultipliers As the TD1 satellite scanned the sky, spectra were recorded every time a star bright enough to trigger the S59 experiment was encountered. In all about 3500 spectra of about 200 stars ranging in spectral type from O4 If to F0 Ia were obtained. Review of this material (de Jager et al , 1975) shows that many stars which have the same spectral type

Table 2-8
Scale of Interstellar Extinction $A(\lambda)/E(B - V)$

λ^{-1} $(\mu m)^{-1}$	$\frac{A(\lambda)}{E(B-V)}$	λ^{-1} $(\mu m)^{-1}$	$\frac{A(\lambda)}{E(B-V)}$	λ^{-1} $(\mu m)^{-1}$	$\frac{A(\lambda)}{E(B-V)}$
1 00	1 20	2.00	3.40	4.76	9.23
1.10	1.28	2.10	3.61	5.00	8.52
1 20	1.68	2 20	3.80	5.26	7 90
1.30	1.88	2.30	4.02	5.56	7 65
1.40	2.08	2 91	4.80	5.88	7 77
1.50	2.28	3 65	6.10	6.25	8.02
1 60	2.50	4.00	7.19	6.71	8.05
1.70	2.72	4.17	7.90	7 18	8 39
1.80	2.98	4 35	8.77	–	–
1.90	3.20	4.57	9.57	–	–

Source Nandy et al. (1975, 1976).
Dashes (–) represent no existing data.

according to classification based on the visible spectrum show important differences in the near ultraviolet part of the spectrum. Peculiar stars of types B and A (Bp, Ap spectra) are readily recognized The Mn II lines at 2576 and 2557 Å and the Mg II lines at 2795 and 2803 Å are sensitive indicators of peculiar spectral type and the Fe II/ Fe III ratio is found to be a useful classification criterion in the near ultraviolet. Lamers and Snijders (1975) have found that the Mg II lines near 2800 Å afford a sensitive criterion for spectral type among the late B and early A stars However, since in some emission-line B stars the Mg II lines are weakened, presumably because of the occurrence of sharp emission components which are not resolved at the resolution of the S59 experiment, while in others they are strengthened and because the Mg II lines may be strengthened or weakened in peculiar spectra, use of the strength of the four Mg II lines near 2800 Å alone will not enable one to relate unambiguously to MK spectral type.

The line blocking in the S59 spectral bands for 35 stars of types B6 to A0 has been measured by Underhill and van der Hucht (1977) On the average, the line blocking per 10 Å is about 10 to 15 percent. This percentage increases toward later spectral types; a steep increase in the strength of the Mg II lines is seen at the later spectral types. Additional information is given by Lamers et al. (1978a).

INFRARED OBSERVATIONS OF B STARS

The infrared range comprises wavelengths between about 7000 Å and 100 μm. A few B stars have been observed in this range, and the major results will be summarized.

Broadband Colors

Early type stars are faint in the infrared, the spectrum of normal absorption-line stars consisting of a continuum and a few shallow absorption lines. Model atmosphere computations indicate that the spectral distribution should be well represented by that of a blackbody at the nominal effective temperature for the spectral type Because the infrared wavelengths from 1 to 20 μm or so lie far in the Rayleigh-Jeans tail of the blackbody curve, the slope of the stellar energy distribution here is not very sensitive to the effective temperature of the star. Photometric observations of a number of O, B, and Be stars have been made (Johnson et al., 1966; Allen, 1973, Gehrz et al., 1974; Barlow and Cohen, 1977) using the broadband filters listed in Table 2-9. The response curves of the Johnson filters, which take into account reflection from two aluminized mirrors, are given by Johnson (1965a). These curves are not symmetrical about the characteristic wavelengths, λ_0, the shortward side usually being fairly steep, the longward side tailing off rather slowly. The effective wavelengths and band passes listed by Gehrz et al. (1974) give no information about the shape of the transmission functions used by them. This group also lists an absolute calibration of the transmission of these filters based on the absolute calibration by Johnson (1965b) of his broadband filters. Details concerning the effective wavelengths, band passes, and absolute calibration of the filters used by Barlow and Cohen are given by Cohen (1973a). Observations from 3371 Å through the near infrared to 1.10 μm of 1380 bright stars including many B stars, using a 13-color intermediate-band system have been published by Johnson and Mitchell (1975) These observations are calibrated in terms of absolute energy and they provide a very homogeneous body of data free from systematic errors.

Review of the available broadband observations shows that the B-type supergiants have an infrared excess detectable at 10 μm, but not always at shorter wavelengths, which can be attributed to free-free emission (Barlow and Cohen, 1977). The Be stars of all sorts show quite a strong infrared excess but normal B-type main-sequence stars appear to radiate in the range 2 3 to 19.5 μm like blackbodies (Gehrz et al., 1974). These authors have shown that the infrared excess of Be stars can be interpreted as free-free emission coming from a shell having, on the average, a radius 4.1 times the stellar radius. The infrared excess increases as the spectral type becomes earlier. The infrared data for Be stars

Table 2-9
Broadband Filter Photometry

Johnson (1966)			Gehrz et al. (1974)			Barlow and Cohen (1977)[a]		
Filter Designation	λ_0 (μm)	FWHM (μm)	Filter Designation	λ_{eff} (μm)	Band Pass (μm)	Filter Designation	λ_{eff} (μm)	Band Pass (μm)
U	0.36	0 07	[2 3]	2 3	0.7	[2.2]	2.2	0.5
B	0 44	0.10	[3.6]	3.6	1 2	[3.6]	3 65	1.2
V	0.55	0.09	[4.9]	4.9	0.7	[4.8]	4.8	0.3
R	0.70	0.21	[8.7]	8 7	1.0	[8 6]	8.6	0.9
I	0.90	0.22	[10 0]	10.0	5.8	[10.0]	10.8	0.8
J	1.25	0 36	[11.4]	11 4	2.0	[11.3]	11 3	2.2
K	2 2	0 6	[12.6]	12.6	0.8	[18.0]	18.0	4.0
L	3.4	0 7	[19.5]	19.0	5.8	–	–	–
M	5.0	1 2	–	–	–	–	–	–
N	10.4	5.7	–	–	–	–	–	–

Dashes (–) represent no existing data

[a]Source is Cohen (1973a)

are discussed in more detail in Part II The Be Stars. Schultz and Wiener (1975) have studied the published broadband colors of 350 O and B stars with normal spectra with a view to determining the shape of the interstellar extinction law and they note that a few of these stars appear to have small infrared excesses.

Infrared Spectra of B Stars

The general characteristics of the near infrared spectra of B stars with and without emission lines have been demonstrated by Andrillat and Houziaux (1967, 1972) and by Andrillat and Swings (1976) who published pictures of some representative spectra. There are few absorption lines–chiefly the lines of the Paschen series of hydrogen and the He I lines at 7065 and 10830 Å. These lines are shallow. The O I blend at 7772 Å due to multiplet 1 may appear strongly marked in absorption, especially in shell stars, and it sometimes appears in emission; on the other hand, the O I lines from multiplet 4 at 8446 Å frequently appear in emission, sometimes with a central absorption. In the Be stars and the peculiar Be stars which show emission lines of [Fe II], lines of Ca II, multiplet 2, at 8498, 8542, and 8662 Å frequently appear in emission. On the low resolution infrared spectrograms, the lines at 8542 and 8662 Å are blended with Paschen lines of hydrogen at 8545 and 8665 Å. Lines of N I, multiplet 1, at 8680 Å, and He I, multiplet 1, at 10830 Å as well as most of the Paschen lines of hydrogen appear in emission in many stars. In addition, lines of Fe II, [Fe II], [S II], and [S III] often appear in emission. Emission lines of [N I], multiplet 3F, at 10395 and 10404 Å are present in a few objects. The forbidden lines are not prominent in normal Be stars, their intensity correlates with the size of the infrared excess measured by broadband photometry.

The continuous spectrum of B stars in the near infrared is not strong and its shape in the region between 7000 and 10000 Å is relatively insensitive to the precise effective temperature of the star, as might be expected from the fact that these wavelengths lie in the Rayleigh-Jeans

tail of blackbody curves at the effective temperatures of B stars. Because the continuous spectrum of B stars is not intense in the near infrared, both permitted and forbidden lines become visible in emission when the energy radiated in the infrared wavelengths is rather small.

B Stars Enveloped in Nebulosity

Many early type stars are known to be obscured by dust and some are seen surrounded by nebulosity which they illuminate. Herbig (1960) observed the spectra of 26 stars which were selected because they lay in obscured regions and were known to illuminate nearby nebulosity. He was looking for stars that had masses in the range 3 to 20 $M_{\odot}$ and which could be proved to be contracting to the main sequence. The stars which he observed are faint and most are known to be photometric variables. Their spectra fall into two groups: (1) a group which shows emission lines of hydrogen plus absorption lines attributable to a cool overlying shell or those which appear like a conventional Be star, and (2) a group which has emission lines with a P-Cygni character indicative of outflow velocities of the order of 150 to 200 km s^{-1}. One star, V380 Ori, has an A-type spectrum with a superimposed emission spectrum that marginally meets T Tauri criteria. Herbig concluded that the spectral peculiarities found were not unique to stars enmeshed in nebulosity and that the details seen on low resolution spectra cannot be used to prove that these stars are still contracting.

High resolution profiles of Hα (resolution unit equal 0.2 Å or 9.3 km s^{-1}) have been obtained by Garrison and Anderson (1977) for 14 of the Herbig Ae/Be stars. Very diverse profiles are found. For example in one star, at the epoch of observation, the emission is barely detectable as a very weak bump in the middle of a broad absorption trough; in four stars, there is a moderately broad, single-peaked emission with no prominent absorption feature; while in four other stars, the Hα profile has a classical P-Cygni structure consisting of a strong emission which is essentially undisplaced and a shortward displaced absorption trough which dips below the continuum. In these four stars, a weak emission tail is seen shortward of the absorption trough. In the remaining five stars, the Hα profiles are quite varied. In each case there is a central absorption dip which is rather narrow and which at the spectral resolution that is used does not dip below the local continuum. In three of these stars, the shortward emission peak is stronger than the longward peak; in the other two the situation is reversed. One of the latter two stars shows, in addition to the central absorption feature, a fairly sharp, shortward displaced absorption dip. The spectra of all are known to vary. The emission-line B stars enmeshed in nebulosity have Hα emission profiles that differ strongly from the Hα profiles of normal B-type Ia supergiants but which are somewhat similar to those of the normal Be stars.

The BQ[ ] stars (Ciatti et al , 1974; Ciatti and Mammano, 1975) also have spectroscopic characteristics like those of the B stars enveloped in nebulosity. Some BQ[ ] stars from their spectra seem to be associated with a late type supergiant. The designation BQ[ ] means that the stars have forbidden emission lines in their spectra and that some lines show shortward displaced absorption cores accomplished by a nearly undisplaced emission peak as does P Cyg.

RADIO OBSERVATIONS OF B STARS

Announcement of the detection at radio wavelengths of a star was made by Wade and Hjellming (1971) and by Hjellming and Wade (1971) who showed that the binary system Alpha Scorpii, M1 Ib + B3 V, emitted radiation at 3.7 and 11.7 cm and that the origin of the radiation was closely linked with the position of the B-type star. Since that time, many stars and stellar systems have been observed at radio wavelengths and a few objects have been detected.

The sources known by 1973 have been listed by Braes (1974). The results of comprehensive search programs have been published by the following by Sistla and Hong (1975) who observed at 3 7 and 11.1 cm, by Altenhoff et al. (1976) who observed at 10.69, 5.0, and 1 4 GHz, by Marsh et al. (1976) who observed at 22.2,

10.6, 8.1, and 2.7 GHz, and by Woodsworth and Hughes (1977) who observed at 10 6 GHz

Types of Objects Detected

The early type objects detected all have an infrared excess that can be attributed to free-free emission and/or emission from cool dust in the immediate neighborhood of the object The following binaries with at least one B-type component are known to emit radiation at radio wavelengths, the intensity of the radiation usually being variable Cygnus X-1 (= HD 226868), B0 Ib + ?, Beta Lyrae (Bpe + B7 V), Beta Persei, B8 V + G8 III, Alpha Scorpii, M1 Ib + B3 V; RY Scuti (B0ep + late) In addition the unusual B1 Ia supergiant P Cyg has been detected and several BQ[ ] objects and symbiotic stars such as HD 167362, HBV 475, MWC 137, MWC 349, and V 1016 Cyg

Many of the apparently bright Be and shell stars, some B-type supergiants, and some Of and Wolf-Rayet stars have been observed, but only ζ Pup, γ^2 Vel, and P Cyg are known to radiate sufficiently strongly at radio wavelengths to be detected easily. Abbott et al. (1980) have detected more stars using the very large array (VLA). The early type stars which are usually detected are hot objects enveloped in an extended atmosphere or small nebula Some early type stars have spectral characteristics which place them among the heterogeneous group of objects known as symbiotic stars. Usual O and B stars do not seem to be surrounded by sufficient low density gas at a low electron temperature to generate detectable radio emission. A theory relating the intensity of radio and infrared emission from a star to the rate of mass loss has been developed by Wright and Barlow (1975). An early review of the implications of infrared and radio emission from early type stars has been given by Pecker (1972). He noted that an infrared excess and radio emission might indicate the presence of a remnant of the cloud from which the star had formed However, he noted that a continuous stellar wind would destroy such a remnant cloud rapidly. The dust grains inferred to surround some radio stars are believed to have been formed when hot gas that has been ejected cools suddenly Marsh (1976) has shown that the viscous force of dust grains driven by radiation pressure is likely to provide an effective acceleration mechanism for the gaseous envelopes of early type emission-line stars such as V 1016 Cyg, provided that the dust grains are mixed uniformly with the gas.

MASSES AND RADII OF B STARS

The masses and radii of stars are fundamental physical quantities. Here we shall review what information is available for B stars concerning these quantities.

Masses

The most direct way to obtain the masses of B-type stars is by combining data from solutions of the radial-velocity orbits of double-lined spectroscopic binaries with data from solutions of the light curves of eclipsing binaries. When the stars to be handled in this way have been carefully selected from the point of view that the light curves and the spectra are not seriously distorted by the presence of gas in the system surrounding or streaming from one or both components, precise masses and radii can be obtained. Popper (1974, 1978) has paid particular attention to selecting stars for study which will yield reliable masses and radii. A similarly precise study of the system CV Vel has been performed by Andersen (1975). The accurate masses and radii for B stars resulting from these studies are given in Table 2-10.

It is difficult to assign spectral types to double-lined spectroscopic binaries solely on the MK classification system because of the confusion caused by the presence of the spectra of two stars and because the spectrograms obtained for radial-velocity studies usually are narrower and at considerably higher dispersion than the spectrograms typically used for spectral classification. The spectral types listed in column 2 of Table 2-10 are from the *7th Catalogue of the Orbital Elements of Spectroscopic Binary Systems* (Batten et al., 1978). We feel that the spectral

types given in the *7th Catalogue* probably form as consistent as possible a set of spectral classifications on the MK system as is presently available. However, it must be remembered that in each MK spectral-type box, the properties of the stars are divergent and that this natural spread in character is enhanced when double-lined spectra must be classified.

The spectral type of the secondary star is often very uncertain, particularly when the secondary is significantly fainter than the primary star. Another estimate of the spectral type of the secondary is given in parentheses in column 4 of Table 2-10 These types were found by using the information given in the notes to the *7th Catalogue* to find the magnitude difference between the two stars Then, assuming that both stars are on the main sequence, the primary being at its stated spectral type, the spectral type of the secondary can be found. We used the main-sequence of Balona and Crampton (see Table 2-7). In a few cases where this method was applied by us, the magnitude difference was sufficiently great that one might consider the possibility that the secondary star was in a different luminosity class than the primary. However, usually at a given spectral type for the primary star, the separation between the luminosity of stars in different luminosity classes is greater than the difference in magnitude estimated for the two stars. Thus, one is constrained to move along the line defined by the results of Balona and Crampton for luminosity classes V and IV

In the *7th Catalogue*, there are 45 systems containing 71 main-sequence (luminosity classes IV and V) B stars for which an estimate of the

Table 2-10
Precise Masses for B-Type Stars

HD No. Name	Spectral Type	$M/M_{\odot}$	Source (type secondary)	$R/R_{\odot}$
198846 A	B0 IV	16 7 ± 0.4	[a]	6.0 ± 0.10
Y Cyg B	B0 IV	16 7 ± 0 4	(B0 IV)	6.0 ± 0.10
218066 A	B0.5 IV-V	11 5 ± 0 15	[a]	5.25 ± 0.25
CW Cep B	B0 5 IV-V	11.5 ± 0 15	(B2 IV)	5.25 ± 0.25
116658 A	B1 V	10.9 ± 1.3	[a]	8.10 ± 0.50
α Vir B	–	–	(B3 V)	–
77464 A	B2 5 V	6.05 ± 0 04	[b]	4.05
CV Vel B	B2 5 V	6.05 ± 0 04	(B2 V)	4.05
156247 A	B5 V*	5.16 ± 0 10	[a]	3.36 ± 0.07
U Oph B	B5 V*	4.60 ± 0 06	(B6 V)	3.17 ± 0.07
25833 A	B5p (V)*	4.53 ± 0.07	[a]	2.87 ± 0.10
AG Per B	–	4.12 ± 0.06	(B6 V)	2.60 ± 0.10
6882 A	B8 V	3.85 ± 0.20	[a]	2.96 ± 0.05
ζ Phe	–	–	–	–

[a] Popper (1974)
[b] Andersen (1975)
*Popper (private communication) has stressed that spectral type B5 V for this star is as late as can be considered, the spectral type may well be earlier
Dashes (–) represent no existing data

inclination is given. For these systems we adopted the listed value for i and calculated the mass of each component from the listed minimum mass. For the primary star we adopted the spectral type given in the *7th Catalogue*, but for the secondary we proceeded as outlined above. Following advice from Popper (private communication), we omitted the system HD 34333 = EO Aur from our statistics because his new spectra suggest that the published results are quite uncertain. We have found average masses for each main-sequence spectral type and the results are given in Table 2-11 and displayed in Figure 2-5. Notes to Table 2-11 indicate mean values containing results which Popper tells us are uncertain because even at greatest separation the two sets of spectral lines overlap in part Some examples of what occurs are shown in Popper (1978)

The formal dispersion about the mean value is a result of not only the uncertainties in the orbital elements and inclinations tabulated in the *7th Catalogue* but also the uncertainties of spectral classification. The precise masses given in Table 2-10 are plotted in Figure 2-5 as crosses. It is clear that the mass range for main-sequence B stars is fairly well defined. At type B0, the mass is typically 16 $M_{\odot}$, while at B9 it is near 2.5 $M_{\odot}$

Masses for 5 luminosity class III stars can be estimated from the data given in the *7th Cata-*

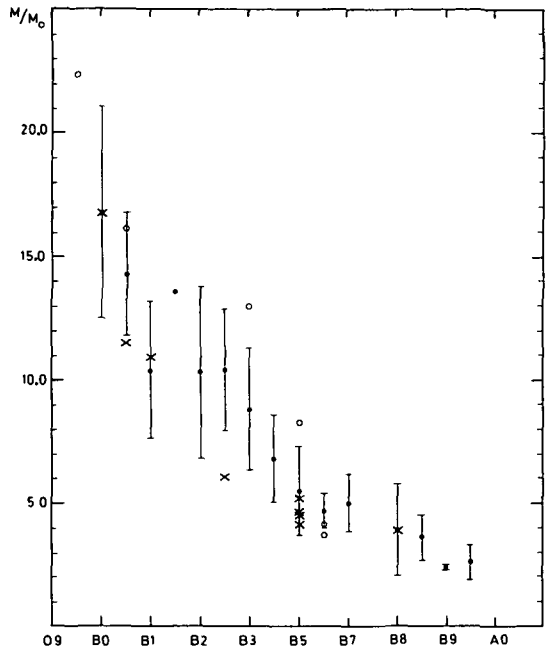

Figure 2-5. Average mass of main-sequence (luminosity classes IV and V) B stars as a function of spectral type. The precise values of Popper are shown by crosses. The individual results for 5 luminosity class III stars are shown by open circles.

Table 2-11
Average Masses of B-Type Main-Sequence Stars

Spectral Type	$M/M_{\odot}$	Standard Deviation	No.	Spectral Type	$M/M_{\odot}$	Standard Deviation	No.
B0	16.8*	4.3	8	B5	5.5*	1.8	9
B0.5	14.3	2.5	2	B6	4.7*	0.7	5
B1	10.4*	2.8	3	B7	5 0	1.2	3
B1.5	13.6	–	1	B8	3 9	1.9	7
B2	10.3*	3.5	8	B8 5	3.6	0.9	2
B2 5	10.4	2.5	2	B9	2.4	0.1	3
B3	8.8*	2.5	7	B9.5	2.6	0.7	5
B4	6.8	1.8	6	–	–	–	–

*The mean value contains some results derived from spectra in which the lines of the two stars are never fully separated.

logue. The results are shown as open circles in Figure 2-5. The secondary star of HD 190967 = V448 Cyg may be classified by means of Δm as B1 II, B0 V, or O9.5 IV. Because of its relatively large mass, 22.4 $M_\odot$, we suspect that V448 Cyg B is an O star; it is plotted in Figure 2-5 at type O9.5.

Estimates of the masses for O- and B-type supergiants obtained from orbital motion are very few. In his discussion of the masses of X-ray stars, Bahcall (1978) has given some limits on the masses of two B-type supergiants. He finds that the mass of HD 77581, B0.5 Iab, lies in the range 19 to 32 $M_\odot$ while that of SK 160, B0 I, lies in the range 13 to 22 $M_\odot$. The primary component of V448 Cyg has been classified (Batten et al., 1978) as B1 Ib-II; its mass is 17.5 $M_\odot$. The mass of the primary star of HD 163181 = V453 Sco, B0.5 Iae, is 14.2 $M_\odot$. The secondary star of V453 Sco may be classified as B1 II or O8 V from its Δm; its mass is 24.8 $M_\odot$. Thus, the information available on the masses of the OB supergiants from orbital motion suggests that the masses are of the order of 20 ± 5 $M_\odot$. There is no direct evidence for the masses of the luminous B-type stars exceeding 30 $M_\odot$. In fact, the weight of the evidence points toward masses lying between 10 and 20 $M_\odot$ for the supergiants. The masses of the luminosity class III B-type stars seem to be at most 50 percent larger than those of main-sequence B stars.

Radii

The precise radii for main-sequence B stars available from the eclipsing, double-lined spectroscopic binaries are given in Table 2-10. These values may be supplemented by the linear radii estimated by Underhill et al. (1979) from the angular diameters and distances of 142 B stars. Underhill et al. were able to show that because their angular diameters are accurately on the system of angular diameters measured by Hanbury Brown et al. (1974) and because the available estimates of distance for these stars are internally consistent, the error in their radii should not exceed ±20 percent.

The average radii for each spectral type and luminosity range are given in Table 2-12. The dispersion about the mean values is caused as

Table 2-12
Average Linear Radii for B Stars

Spectral Type	IV, V			II, III			Ib			Ia		
	$R/R_\odot$	Standard Deviation	No	$R/R_\odot$	Standard Deviation	No	$R/R_\odot$	Standard Deviation	No	$R/R_\odot$	Standard Deviation	No
B0*	–	–	–	12 5	–	1	–	–	–	35 8	–	1
B0 5	8 2	0 6	2	10 2	–	1	–	–	–	–	–	–
B1	6 8	0 8	2	8 6	0 4	4	26 6	0 6	2	–	–	–
B1 5	6 3	0 1	3	7 7	0 5	2	–	–	–	–	–	–
B2	6 0	0 2	14	8 8	0 7	7	26 6	4 6	2	59 4	–	1
B2 5	5 2	0 7	8	9 0	–	1	–	–	–	–	–	–
B3	5 1	0 1	11	–	–	–	–	–	–	57 2	2 8	2
B4	4 7	0 4	8	–	–	–	24 9	–	1	–	–	–
B5	4 7	0 3	9	5 2	0 4	4	–	–	–	56 3	–	1
B6	4 5	0 2	3	5 5	0 4	5	–	–	–	–	–	–
B7	3 9	0 2	4	8 2	–	1	–	–	–	–	–	–
B8	3 6	0 3	4	4 7	0 1	5	–	–	–	74 3	6 4	2
B9	3 1	0 1	10	3 9	0 6	4	30 0	–	1	–	–	–
B9 5	2 7	–	1	–	–	–	–	–	–	–	–	–

*BCD spectrophotometry for κ Aql obtained since the work of Underhill et al (1979) indicates that this star should be placed in the box for giants rather than in that for main-sequence stars as was done by Underhill et al (1979)
Dashes (–) only 1 measurement

Table 2-13
Typical Escape Velocities and Values of Log g for Main-Sequence B Stars

Spectral Type	log g	u_{esc} (km s^{-1})	Spectral Type	log g	u_{esc} (km s^{-1})
B1	3.71	779	B6	3.79	618
B2	3.85	769	B7	3.84	610
B3	3.92	764	B8	3.83	583
B4	3.90	721	B9	3.89	577
B5	3.82	656	—	—	—

Dashes (—) represent no existing data.

much by the differing character of the stars grouped in each spectral type–luminosity class box as by the uncertainty of the data. The average radii found for the main-sequence stars are a little larger than the few values found from eclipsing binaries. The luminosity class III stars are about 30 percent larger than main-sequence stars: while the B-type supergiants are quite large, the radius of the Ia stars increasing from 36 $R_\odot$ at B0 to about 75 $R_\odot$ at type B8.

Velocity of Escape

From the average masses for main-sequence stars which may be read from Figure 2-3 and from the average radii listed in Table 2-12, one may estimate typical values of log g and the velocity of escape from the photosphere for B stars on or near the main-sequence. These values are given in Table 2-13. The velocity of escape (u_{esc}) has been calculated from the formula

$$u_{esc} = 618\left(\frac{M}{R}\right)^{1/2} \text{ km s}^{-1}, \qquad (2\text{-}20)$$

where the mass and the radius are given in solar units. Because the average radii given in Table 2-12 are a little larger than those estimated from eclipsing variables, the values of log g and u_{esc} for giant and supergiant stars can be obtained by scaling according to the differences in mass and radius at each spectral type which are suggested by the data reviewed above.

3

OBSERVATIONS OF NORMAL MAIN-SEQUENCE AND GIANT B STARS

THE CONTINUOUS SPECTRUM: LOW RESOLUTION SPECTRA

In the spectral range accessible from the surface of the Earth the spectra of B stars present a nearly continuous distribution of energy which is crossed by a few strong absorption lines and a modest number of weak absorption lines. In some B stars a few emission lines are also seen. It is advantageous from the point of view of interpreting B-type spectra by means of theory (see Chapter 6) to consider B-type spectra as being composed of a strictly continuous spectrum, which can be modeled in terms of absorbers and scatterers, interacting with the radiation only by cross sections which are continuous functions of wavelength, and to consider the formation of lines as secondary events that may be introduced into the theory later. The lines may be in absorption, in which case they take energy away from the continuum in a given short wavelength interval, or in emission, in which case they add energy to a restricted wavelength interval over that normally encountered

Stellar spectra which contain only absorption features (lines and absorption edges) in the spectral range accessible from ground are called normal. Those which also contain emission lines are considered to be abnormal To model emission-line stars some additional features must be added to the model used to interpret spectra from normal stars The terminology which is used to give a quantitative description of stellar spectra has been developed to facilitate the modeling of normal stellar spectra.

Because one cannot study absolute photometry over a wide wavelength range (a range of at least several hundred angstroms) using a slit spectrograph on a ground-based telescope, much attention has been directed toward interpreting the relative change of intensity across single absorption lines or absorption edges which are confined to a short wavelength range. One prime reason why one cannot do absolute photometry over a wide wavelength range with narrow-slit spectrographs is that the star image is already a spectrum owing to the effects of atmospheric dispersion and one cannot ensure that the same fraction of light at each wavelength enters the narrow slit of the spectrograph during the sometimes long exposure which is required to obtain a high dispersion spectrogram. This condition can be met easily for wavelength intervals less than about 50 Å. Also the star light has been attenuated differently at different wavelengths during its passage through the Earth's atmosphere and the interstellar medium.

The first step in the analysis of the absorption lines of normal stellar spectra is to draw on an intensity tracing of the spectrum a pseudocontinuum in order to define the apparent level of the light at wavelengths where no lines are believed to be present. The level of this continuum above zero intensity varies slowly with wavelength as a result of the actual variation of the continuous energy that passes the narrow slit of the spectrograph and of the wavelength dependence of the sensitivity of the dispersing and detecting equipment The energy removed by the line under study is measured relative to this continuum. This ener-

gy is expressed in terms of an equivalent width—that width which an absorption line having a rectangular shape and going to zero intensity would have if the line removed the same amount of energy. Thus, the equivalent width in wavelength units is

$$W_\lambda = \int_a^b \left(\frac{I_c - I_\lambda}{I_c}\right) d\lambda . \qquad (3\text{-}1)$$

Here a and b are the effective wavelength limits to which the wings of the line extend, I_c is the intensity of the pseudocontinuum in the center of the line, and I_λ is the intensity of light at wavelength λ within the line These intensities are measured on an arbitrary linear scale A line profile is described by giving I_λ/I_c as a function of wavelength.

Some astronomers measure the intensity of emission lines relative to the same pseudocontinuum as is used for absorption lines. In this case the equivalent width has a negative sign since I_λ is greater than I_c. The interpretation of such a measure of the intensity of an emission line is model-dependent. One way of looking at the question is to approximate the physical situation by an equivalent normal star which produces only absorption lines, a superposed emitting region which produces line emission, and perhaps some continuous absorption and emission. The line emission is seen superposed on or added to the "normal" absorption-line spectrum.

It may be appropriate to quantify the strength of the line emission in terms of the energy radiated from within the absorption line rather than relative to a pseudocontinuum that crosses an absorption line. Such a pseudocontinuum never really exists. Stars never transmit as much energy within an absorption line as they do in nearby wavelength regions where there are no absorption lines. The pseudocontinuum is a reference level, useful in the analysis of absorption line spectra. When an analysis of abnormal spectra containing emission lines is attempted, attention must be directed to the method to be used in order to obtain an exact quantitative measurement of the energy in the emission line. No simple recommendation can be given as to the best procedure. The observational approach should be matched to the modeling approach.

Physical information can be obtained from the shape of the actual continuum of a star, when one considers the change in amount of the measured energy over several hundred to several thousand angstroms Information on this shape and on the absolute amount of energy can only be found by photometric procedures which permit correction of the observed energies for the wavelength-dependent transmission of the Earth's atmosphere and of interstellar space and for the wavelength-dependent sensitivity of the light gathering and detecting instrumentation Usually one uses results from photometric observations made using intermediate-band filters or from spectrum scanners which have effective pass bands of 10 to 50 Å width. One considers only data from pass bands that exclude major absorption and emission lines. If such data are plotted against wavelength, a slowly varying curve is usually found which can be interpreted in terms of the continuous spectrum predicted using a model atmosphere. A significant discontinuity often is seen close to 3,750 Å, due to the confluence of the Balmer lines and the onset of absorption in the Balmer continuum of hydrogen. The interpretation of photometric observations of the "continuous" spectrum of B stars is discussed in Chapter 6.

Because B-type stars are intrinsically bright, they may be observed readily at large distances from the Sun, because most of them lie in the plane of the galaxy, the light from most of them suffers a wavelength-dependent extinction due to interstellar dust. The method for correcting for this deformation of the true continuous spectrum of a B star has been described in the section Observations Made from the TD1 Satellite in Chapter 2, and the shape of a representative interstellar extinction curve is given in Table 2-8. Further information about correcting for the effects of interstellar extinction is presented in the section on Radii of B stars in this chapter.

It is conceivable that the shape of the continuous spectrum from a star and the amount of

light reaching us may be modified by the presence of "circumstellar matter" in the immediate neighborhood of the star. The possible effects of dust and gas remaining from the original cloud from which the star condensed have been considered by Pecker (1963, 1972). In the second paper Pecker puts particular emphasis on the interpretation of infrared excess radiation in terms of a "circumstellar cloud." The normal B stars, which are the stars discussed in this chapter, do not show infrared excesses. Consequently, one must conclude that any possible "circumstellar cloud" which is enveloping them contains too little material to be visible to us. We shall see in the section on Effective Temperatures for B Stars in the Main-Sequence Band that the energy distributions of normal main-sequence B stars are very similar to what is predicted by means of detailed model atmospheres. Consequently, the possibility of "circumstellar gas and dust" enveloping normal B stars is not discussed in this chapter; there are no observations of normal B stars in the main-sequence band which require us to consider such a possibility.

The case concerning the B-type supergiants (Chapter 4) and the Be stars (Part II) is different. Infrared excess radiation has been detected for many of these two types of B stars. Some of these stars also show excess emission in the hydrogen bound-free continua. In Part I of this book, we take the point of view that such excess radiation comes from the mantle, and that it tells us about the properties of the mantle (Chapter 4, Discussion).

A discussion is given in Chapter 8 of how one may use the amount of excess radiation which is observed to obtain an estimate of the amount of nonradiative energy that is released in the mantles of supergiants and Be/shell stars. The shape of the infrared excess radiation from B-type supergiants and from many Be stars suggests that this radiation is free-free (bremsstrahlung) radiation. For some peculiar Be stars there is a hump in the infrared excess near 10 μm that raises the possibility that some of the infrared excess may be caused by radiation from cool dust grains in a cloud close to the star.

In his discussion of possible circumstellar material, Pecker (1963, 1972) worked from the hypothesis that the energy released at long wavelengths had been absorbed from the stellar spectrum at visible and ultraviolet wavelengths. Thus, Pecker took the point of view that the total amount of energy that leaves each cm^2 of surface of the star should include the observed normal radiation field plus the excess infrared and radio radiation. The point of view taken in this part is that the observed amount of radiation received from a B star in the wavelength range from about 1200 Å to 10 μm after correction for any infrared excess and of course for interstellar extinction is due to the energy sources in the center of the star. In addition the radiation stream which emerges defines T_{eff}. The infrared excess radiation and emission in the hydrogen spectrum is thought to come from another source, a nonradiative one, which heats the mantle (Chapter 8).

How one approaches the question of understanding B stars which show unusual excess radiation in some wavelength ranges is a matter of choice. For reasons that will become clear as we review the observational material which is now available about the radiation from B stars, and which was not available when Pecker made his suggestions, the point of view is taken here that the spectra of B stars can best be understood in terms of a traditional photosphere and a mantle which is heated from a source of nonradiative energy, rather than the point of view that all of the observations are to be interpreted in terms of an extensive atmosphere and circumstellar cloud heated only by radiation from the center of the star.

In the visible and infrared parts of the spectrum, B stars have relatively few lines, and it is rather easy to define a pseudocontinuum except near the confluence of the Balmer and of the Paschen series of hydrogen. In the ultraviolet spectral region shortward of 2000 Å, many absorption lines occur. Consequently, although one can define a reference level relative to which equivalent widths may be measured, how to relate this pseudocontinuum to the continuum of a given model atmosphere becomes a subtle question. A mismatch may systematically displace the relation of observed equivalent widths

to theoretical equivalent widths from a 1 1 ratio and the displacement factor may be dependent on wavelength in an unknown manner.

In Chapter 1 we noted that it is useful to think of the atmospheres of stars as being composed of a photosphere and an outer atmosphere or mantle. The classical methods of analyzing spectra have been developed to determine the properties of the photosphere, with the photosphere being considered to be homogeneous in layers and its properties being functions only of the geometrical depth in the atmosphere The presence of emission lines and of some types of absorption lines in the ultraviolet and visible spectral ranges of the spectra of B stars reveals the presence of the mantle Analysis of these features should tell the properties of the mantle. That the mantle may contain some very hot regions can be deduced from the fact that X-rays have been observed from the normal B7 IV star π Cet (Cash et al , 1979) and from the direction of the active Be star γ Cas (see Cowley et al , 1976, Marlborough, 1977b)

It is very likely that the mantle is not homogeneous in its properties, it may have a three-dimensional structure In a review of the properties of the solar corona and of the theories for understanding that corona, Vaiana and Rosner (1978) have emphasized the value of an approach that considers the inhomogeneity of the solar mantle (the chromosphere, transition zone, corona, and post-coronal region) to be a significant property of the mantle A successful theory should attempt to model the observed inhomogeneities Vaiana and Rosner indicate that the structure of the corona appears to be closely related to the topology of the solar magnetic field. Therefore, in reviewing what B-type spectra tell us about the atmospheres of B stars, we should keep in mind the possibility that the mantle is not homogeneous in spherical layers and that its structure may be intimately related to the structure and amount of the magnetic fields present in the outer layers of B stars. Rather small fields, less than 100 gauss, could easily go undetected with the present state of our observing techniques for measuring the magnetic fields of B stars. Such small fields may be sufficient to control the structure and physical state of an inhomogeneous mantle. Local differential motions, originating in the differential rotation of B stars or in nonradial pulsation, might play a role in B Stars that is equivalent to that played in the Sun by convective motions.

Observations Concerning the Shape of the Visible Continuous Spectrum

Chalonge and Divan (1952, 1973) have carried through a comprehensive program of work to determine by means of photographic photometry the apparent shape of the continuous spectrum of B stars in the spectral region accessible from the ground Their procedure is to obtain 20 to 30 low dispersion spectra of program stars and standard stars on one photographic plate using a quartz-prism spectrograph and from these to find $\log i(\lambda,*) - \log i(\lambda,std)$ for three ranges of wavelength, namely 3150 to 3700 Å (their uv range), 4000 to 4600 Å (their b range) and from 4000 to 6200 (their rb range) The median wavelengths for the uv and rb ranges are 3500 and 5000 Å. These are the ranges which have proved to be most informative for B stars The Chalonge and Divan photometry is corrected for extinction by the Earth's atmosphere by means of special observations of extinction stars and the work is done only at observing sites where the transparency of the sky is good

Since it turns out that logarithmic relative energy distributions of B stars are linear in λ^{-1} over regions of several hundred angstroms, these energy distributions can be succinctly described in terms of gradients. By definition, the relative gradient between the energy distributions of two sources, * and *std*, is

$$G_{\bar{\lambda}} = -2.30 \frac{d}{\left(d \frac{1}{\lambda}\right)} \log\left(\frac{i(\lambda,*)}{i(\lambda, std)}\right) . \qquad (3\text{-}2)$$

Here $\bar{\lambda}$ is the median wavelength for the range λ_1 to λ_2 over which the gradient is valid The true gradient of any star is

$$\phi_{\lambda_1\lambda_2}(*) = G_{\bar{\lambda}} + \phi_{\lambda_1\lambda_2}(std), \qquad (3\text{-}3)$$

where $\phi_{\lambda_1\lambda_2}$ (*std*) is the absolue gradient for the wavelength range λ_1 to λ_2 of the true energy distribution of the standard star. The zero-point corrections to the measured relative gradients of Chalonge and Divan, that is the values of $\phi_{\lambda_1\lambda_2}$ (*std*), have been found for each standard star by comparing its energy distribution to that of a standard light source These values have been published in Divan (1966) Consequently, a set of absolute gradients for many B stars, ϕ_{uv}, ϕ_b and ϕ_{rb}, have been determined, the values can be found in Chalonge and Divan (1952, 1973) and in the appendix to Underhill et al., (1979). The data in Chalonge and Divan (1973) is given in graphical form only

The absolute gradients, when corrected for interstellar extinction, may be designated as ϕ^0_{uv}, ϕ^0_b, and ϕ^0_{rb}; they contain information on the true shape of the continuous spectra of B stars

For preliminary studies it is useful to compare the true gradients to the gradients of blackbodies For a blackbody, we have

$$\frac{d \log B(\lambda T)}{d\left(\frac{1}{\lambda}\right)} = 2\,172\lambda - 0.4343\Phi, \qquad (3\text{-}4)$$

where

$$\Phi = \frac{c_2}{T\left[1 - \exp\left(\frac{-c_2}{\lambda T}\right)\right]} \qquad (3\text{-}5)$$

Here c_2 equals $14320\,\mu m\ deg^{-1}$. One can compare the absolute gradient of a star for a particular wavelength region with that for a blackbody and deduce a color temperature Early work of this sort suggested lower color temperatures for some B stars than seemed likely in view of the level of ionization and excitation seen in their line spectra Resolution of this contradiction was one of the clues leading to the recognition of wavelength-dependent interstellar extinction. If one wishes to classify B-type stars according to the shape of their continuous spectrum, selection of stars having the same values of ϕ^0_{uv}, ϕ^0_b or ϕ^0_{rb} is a good way to proceed Chalonge and Divan (1952, table V) have demonstrated the dependence along the main sequence of ϕ^0_{uv} and ϕ^0_b on spectral type.

We have discussed in Chapter 2 the use of broadband and intermediate-band filter photometry for classifying stars. In Chapter 6 we show how photometric colors in the UBV and the uvby systems, when corrected for interstellar extinction, can be used to select a model atmosphere which produces a continuum having a shape similar to that of the star. The calibration of the photometric responses of the broadband filters UBVRIKLMN in terms of absolute energy has been studied by H.L. Johnson. Johnson (1966) has given the calibration factors for converting a measured magnitude in any of the broadbands into absolute energy. The calibration by Gehrz et al. (1974) of their infrared broadband photometry in terms of absolute energy is based on that of Johnson, the calibration of other similar broadbands in the infrared in terms of energy has been given by Cohen (1973a). These calibration factors have been revised slightly by Hayes (1979).

Since B-type spectra do contain a certain number of rather strong lines of hydrogen and helium, the use of broadband photometry is not an ideal way by which to determine the shape of the continuous spectrum. The use of spectrum scanners provides information that is more satisfactory because the pass bands can be selected to avoid the strongest absorption (emission) lines. The choice of pass bands, usually of widths near 50 Å, and the photometric techniques to be followed so as to achieve reliable spectrophotometry have been reviewed by Oke (1965). In the photoelectric spectrophotometry done with spectrum scanners as with the photographic spectrophotometry of Chalonge and Divan, the observations are made relative to a set of standard stars The energy distributions of the standard stars are then measured relative to standard sources of light and by this means the whole body of relative photometric results can be transformed into absolute energy units.

The prime standard star for calibrating energy distributions is α Lyr Its energy distribution has been measured many times since the first attempts were made to obtain absolute measure-

ments of the radiation received from stars. The earliest results have been discussed critically by Code (1960), a recent study of the data for α Lyr is that by Hayes and Latham (1975) On the whole, it is believed that the energy distribution of α Lyr is well known throughout the energy range accessible from the surface of the Earth, but some small uncertainties, of the order of a few hundredths of a magnitude, still exist particularly for those wavelength ranges where the transmission of the Earth's atmosphere is most variable. Evidence concerning this problem has been discussed carefully by Johnson and Mitchell (1975) in their determination of the absolute calibration of their 13-color, intermediate-band photometry. The 13-color photometry gives an internally consistent set of absolute energies for many stars brighter than the fifth magnitude. One great advantage of this set of observations is that it extends from 3371 to 11084 Å.

In recent years many spectrophotometric scans of B stars and of other stars have been published Much of this material has been assembled in a catalogue by Breger (1976a, 1976b) and put on a self-consistent basis relative to the standard star α Lyr Consequently, this material may be used to find absolute energy distributions Usually in this catalogue one can find results in the range 3300 to 8800 Å. Additional data for 16 relatively bright B stars have been published by Adelman (1978). When the data for the B stars are corrected for interstellar extinction, they may be used to help in the selection of a representative model atmosphere (see Chapter 6) and to find the effective temperatures of the stars by permitting one to evaluate the part of the integrated flux radiated by the star which can be measured from the surface of the Earth. Observations from sounding rockets and from satellites have provided us with quantitative data on the absolute energies radiated by B stars in the wavelength range shortward of 3150 Å, where the Earth's atmosphere becomes opaque

Many of the magnetic Bp and Ap stars, particularly those with unusually strong Si II lines, have spectra which in other respects, that is their B − V color and the strength of their hydrogen and He I lines, place them with the late B-type stars. Spectrophotometric scans of Ap stars often show shallow broad depressions near 4200, 5300, and 6300 Å which are typically 0.03 to 0.08 mag deep. The observational data on this point has been summarized by Adelman (1975, 1977a). The dips are most certainly real, but efforts to find a cause for them as either an unusual collection of absorption lines or as a bound-free ionization discontinuity (Adelman and Wolken, 1976) have ended inconclusively.

Leckrone (1973) has demonstrated by means of OAO-2 photometry that the flux distributions from the ultraviolet through the visible spectra of Ap stars do not resemble those of normal stars. The Ap stars which Leckrone studied are flux deficient in the ultraviolet in comparison to what would be expected from the energy distributions of normal stars having the same B − V colors. Leckrone, Fowler, and Adelman (1974) carried out numerical experiments with model atmospheres showing that energy distributions like those observed would result if the continuous and line opacity in the ultraviolet were enhanced by a factor of 10 or more.

The shape of the ultraviolet spectra of Ap stars, in particular of Si stars, has been examined by Jamar et al. (1978) using the spectrophotometric scans obtained with the S2/68 experiment on the TD1 satellite. They note that the Si stars are often deficient near 1400 Å and they attribute this deficiency to unusual strength of the Si II autoionization lines which may appear near 1400 Å. In addition Jamar et al. (1978) suggest that the broad, shallow dips near 4200 and 5300 Å are caused by other Si II autoionization lines. The properties of Ap stars are discussed in more detail in Wolff (*A Stars*, to be published); some types of Bp stars are described in Chapter 5

Observations Concerning the Shape and Absolute Value of the Ultraviolet Continuous Spectrum

The absolute energy received at the Earth from many B stars has been measured by means of spectrophotometric instruments carried on satellites. These spectrophotometric instruments were calibrated, in terms of absolute energy

response, before the satellite was launched and the sensitivity of the response at different wavelengths was checked by means of observations from sounding rockets. Here we shall review the major sources of information for the ultraviolet energies from B stars as well as the conclusions about the validity of each calibration reached by those who have intercompared the results from the several sets of data.

It turns out that reliable, moderately detailed energy distributions have been derived longward of about 1500 Å but that more effort still is required to determine with certainty the energies radiated by B stars shortward of 1500 Å. When the observed energy distributions of B stars are corrected for the wavelength-dependent extinction due to the interstellar medium, they are found to be very similar to those predicted by means of model atmospheres (see Chapter 6)

Two major sources of information about the absolute energies received from stars in the ultraviolet are the observations made with the spectrum scanners of the OAO-2 satellite and the spectral scans obtained with the S2/68 experiment on the TD1 satellite. (See Chapter 2 for a description of these instruments and for the details of their spectral resolution.) Energy profiles for 91 B stars have been published by Code and Meade (1979) and for an additional 166 B stars by Meade and Code (1980). More data can be obtained from the National Space Science Data Center (NSSDC) at the Goddard Space Flight Center. Detailed energy curves measured with the S2/68 experiment have been published by Jamar et al. (1976) for 1021 bright B stars, while the catalogue of Thompson et al. (1978) contains the energies observed in four bands of intermediate width for 9485 B stars. The supplement by Macau-Hercot et al. (1978) to the Bright-Star Catalogue of Jamar et al. contains detailed ultraviolet fluxes for 292 B stars.

The procedure to correct the ultraviolet fluxes for interstellar extinction has been described in Chapter 2. Recently Sapar and Kuusik (1978) and Savage and Mathis (1979) have rediscussed all the information available on the shape of the interstellar extinction curve and have provided useful tables of $A_\lambda/E(B-V)$ valid from 1000 Å to 10 μm. The energy curves noted above have been obtained at resolutions of from 10 to 40 Å. Consequently, they give results that have been smoothed over the many absorption and few emission lines that occur in the ultraviolet. They do not represent the level of a true continuum as is known in the visible part of B-type spectra.

At the time of writing, observations are being made with the International Ultraviolet Explorer (IUE) satellite. Although the detectors, SEC vidicon tubes, used with the spectrographs of IUE are not ideal for spectrophotometric work, the energy distribution in the ultraviolet can be determined for point sources measured in the large aperture by means of the low resolution modes of the spectrographs The photometric calibration of the IUE low resolution spectrographs has been studied by Bohlin et al. (1980) and sensitivity curves have been published for converting the observed relative intensities into true fluxes. So far no catalogues of stellar energies have been published; IUE has the capacity to observe much fainter objects than were studied by OAO-2 or by the S2/68 experiment on the TD1 satellite.

Intermediate-band absolute photometry in the ultraviolet has been done by the Astronomical Netherlands Satellite (ANS) for many stars, some quite faint. The central wavelengths of the six photometric bands, their FWHM, and their absolute calibration are given by Van Duinen et al. (1975) and by Wesselius et al. (1980a). A catalogue containing results for about 4000 stars has been complied by Wesselius et al. (1980b) The ANS photometric bands are defined by exit slots along the focal plane of a spherical grating The entrance aperture to the instrument is a 2.5 by 2.5 arcmin slot The ANS photometric system was calibrated in terms of absolute energy response, and ANS observations provide one of the several sets of reliable observations of absolute ultraviolet energies for numerous astronomical objects. The central wavelengths of ANS bands and their FWHM are given in Table 3-1

The OAO-2 satellite carried stellar photometers which have been described by Code et al. (1970). They consist of four 8-inch telescopes each of

which is equipped with interference filters defining three pass bands. Photomultipliers are used as detectors. In practice 11 of the photometer/filter combinations have proved useful for absolute photometry. The absolute response of these photometer/filter combinations has been studied by Code et al. (1980) who also summarized the reduction procedures to be followed for obtaining absolute fluxes from the OAO-2 photometers. The final OAO-2 magnitude system has been placed on such a basis that the absolute flux, in ergs cm^{-2} s^{-1} $Å^{-1}$, at the constant energy wavelength of each filter is given by

$$\log f_\lambda = -0.4 m_\lambda - 8.440. \qquad (3\text{-}6)$$

In their paper Code et al. tabulate the monochromatic magnitudes for 485 stars, 250 of which are B stars Most are brighter than sixth magnitude.

The constant energy wavelengths of the OAO-2 photometers/filters and their FWHM are listed in Table 3-1. Not every star has data at all the wavelengths; some of the filters have red leaks or are nonuniform. The factors which affect the accuracy of the OAO-2 photometric data are discussed by Code et al. (1980). The absolute calibration which they use is based on that of the OAO-2 spectrum scanners which is itself based on the results of observations made with filter photometers during a sounding rocket flight (Bless et al., 1976).

The Energy Distribution of η UMa, B4 V

A good way to maintain the calibration of the intensity response of satellite instruments while they are in orbit is to observe standard stars which are known to be constant in light and for which the energy distribution is known. The star with the best known ultraviolet intensity distribution is η UMa. It is a B4 V star with $v \sin i = 150$ km s^{-1}, according to Slettebak et al. (1975). Here the spectral types of Underhill et al. (1979) are used whenever possible because these spectral types result from an evaluation of all information on this point available in 1978. That η UMa rotates rapidly is an advantage because this means that its absorption lines are broad and shallow with the result that the energy distribution should be rather smooth.

The star η UMa has been observed from OAO-2, both by filter photometry and by scans (Code and Meade, 1979, Code et al., 1980), by the S2/68 experiment (Jamar et al., 1976; Thompson et al., 1978), from Apollo 17 (Henry et al., 1975),

Table 3-1
The Wavelengths and FWHM of Ultraviolet Filters Used From Satellites

ANS Photometry[a]			OAO-2 Photometry[b]					
Filter Name	λ (Å)	FWHM (Å)	Photometer/ Filter	λ (Å)	FWHM (Å)	Photometer/ Filter	λ (Å)	FWHM (Å)
15N	1545	50	S1 F3	4250	856	S3 F1	1910	268
15W	1549	149	S1 F1	3320	527	S2 F3	1680	270
18	1799	149	S1 F4	2980	405	S4 F1	1550	272
22	2200	200	S3 F2	2460	367	S4 F3	1430	233
25	2493	150	S2 F5	2380	332	S4 F4	1330	192
33	3294	101	S2 F1	2035	181	–	–	–

[a]Van Duinen et al. (1975)
[b]Code et al (1980).
Dashes (–) represent no information exists for these values

and from sounding rockets (Stecher, 1968, Bless et al., 1976; and Strongylis and Bohlin, 1979). Ground-based observations which may be put on an absolute energy scale also exist (see the catalogue of scans, Breger, 1976b and the 13-color photometry of Johnson and Mitchell, 1975). The absolute energy distribution of η UMa is given in Table 3-2. The fluxes in the range 1200 to 3300 Å have been taken from the listing of Bohlin et al. (1980); those from 3300 to 11084 Å are from the 13-color photometry and the absolute fluxes which may be derived from the scans listed by Breger when these are put on the absolute scale established by the calibration of α Lyr by Hayes and Lathan (1975). In addition absolute fluxes in the infrared are given from the broadband photometry of Johnson et al. (1966) and Gehrz et al. (1974). All the ground-based data were plotted and a smooth curve was drawn through the results to yield the values given in Table 3-2. The star η UMa is at a distance of 39 pc and it is unreddened (Underhill et al., 1979). A plot of the individual photometric results is shown in Figure 3-1.

Beeckmans (1977a) has intercompared absolute energies from the S2/68 experiment with those from OAO-2, Apollo 17, and a rocket experiment, while Strongylis and Bohlin (1979) as well as Bohlin et al. (1980) have intercompared the OAO-2, S2/68, ANS, Apollo 17, and sounding rocket measurements of absolute energy. It turns out that all of the measurements of the spectrum of η UMa give about the same result longward of 1750 Å but that shortward of this the OAO-2 results are higher than the other observations. Bohlin et al. (1980) conclude that the energy distribution which they give for η UMa is accurate to within ± 10 percent longward of 1200 Å.

The observed relative energy distribution of η UMa (Table 3-2) is shown by the points in Figure 3-2. It has been normalized to the flux at 8000 Å. Also shown (by a line) is the relative energy distribution, normalized to the flux at 8000 Å, from a Kurucz (1979) model atmosphere with $T_{\text{eff}} = 1.7 \times 10^4$ K, log $g = 4.0$ and normal abundances. This theoretical relative energy distribution is very like the observed energy distribution for η UMa. Underhill et al. (1979) have shown that the flux effective temperature of η UMa is 1.682×10^4 K.

The agreement shown in Figure 3-2 between the shape of the observed and theoretical relative energy curves for η UMa gives strong circumstantial evidence for believing that the absolute calibrations of flux measurements in the ultraviolet and in the visible are essentially correct and for concluding that the energy distributions from LTE line-blanketed model atmospheres represent well the energy distributions of main-sequence B stars. The data presented in Figure 3-2 are normalized to the flux at 8000 Å because the theoretical results in this range are insensitive to the precise details of how the models are constructed and there are few strong stellar absorption or emission lines here to distort the observed "continuum" energy.

The observed normalized energy curve of η UMa falls a little below the theoretical curve for an effective temperature of 1.7×10^4 K. Figure 3-3 shows a plot on an enlarged scale of the observed relative ultraviolet fluxes compared to those from model atmospheres with effective temperatures of 1.6×10^4 K and 1.7×10^4 K. The agreement between theory and observation is satisfactory, but since η UMa is rotating at a projected speed of 150 km s^{-1} while the models are for stationary stars, one has some hesitation in inferring from the shape of the spectrum a precise effective temperature between 1.6×10^4 and 1.7×10^4.

Collins and Sonneborn (1977) have studied theoretically the changes in the shape of the continuous spectra of rotating stars of types B0 to F0 as the speed of rotation and the angle of viewing are changed. They assume a mass, radius, luminosity, and equivalent effective temperature for a stationary, spherical star of each spectral type and find how the energy distribution changes as the star changes its speed of rotation with consequent changes of shape and surface temperature distribution. They use model atmospheres constructed with the Kurucz (1970) ATLAS program, thus, their models use opacity

Table 3-2
Observed Flux f_λ from η UMa

λ (Å)	f_λ (ergs cm^{-2} s^{-1} Å^{-1})		λ (Å)	f_λ (ergs cm^{-2} s^{-1} Å^{-1})		λ (μm)	f_λ (ergs cm^{-2} s^{-1} μm^{-1})	
1200	1.00	−8[a]	4500	1.31	−9[a]	1.11	5 80	−7[a]
1300	1.32	−8	4600	1 20	−9	1 25	4.20	−7
1400	1.14	−8	4700	1.12	−9	2.2	4 28	−8
1500	1 05	−8	4800	1.04	−9	2 3	4 00	−8
1600	8.60	−9	4900	9.60	−10	3 4	9.39	−9
1700	7.85	−9	5000	9 10	−10	3.6	7.42	−9
1800	7.05	−9	5100	8 40	−10	4 9	2.26	−9
1900	5.95	−9	5200	7.86	−10	8.7	2.39	−10
2000	5 50	−9	5300	7 35	−10	10.0	1.22	−10
2100	4.93	−9	5400	6.90	−10	11 4	9.14	−11
2200	4 46	−9	5500	6 55	−10	12.6	5 24	−11
2300	4.04	−9	5600	6.10	−10			
2400	3.63	−9	5700	5 70	−10			
2500	3.40	−9	5800	5 35	−10			
2600	3 17	−9	5900	5 00	−10			
2700	2.90	−9	6000	4 65	−10			
2800	2.61	−9	6200	4.20	−10			
2900	2 45	−9	6400	3 80	−10			
3000	2 28	−9	6600	3 55	−10			
3100	2.13	−9	6800	3 20	−10			
3200	2.00	−9	7000	3.00	−10			
3300	1.89	−9	7200	2.76	−10			
3400	1.77	−9	7400	2.35	−10			
3500	1 65	−9	7600	2 20	−10			
3600	1.54	−9	7800	2.03	−10			
3700	1 44	−9	8000	1 86	−10			
4000	1.86	−9	8500	1 44	−10			
4100	1 74	−9	9000	1 15	−10			
4200	1 64	−9	9500	1 00	−10			
4300	1 52	−9	10000	8 80	−11			
4400	1 41	−9						

[a]Power of 10 by which to multiply the first number

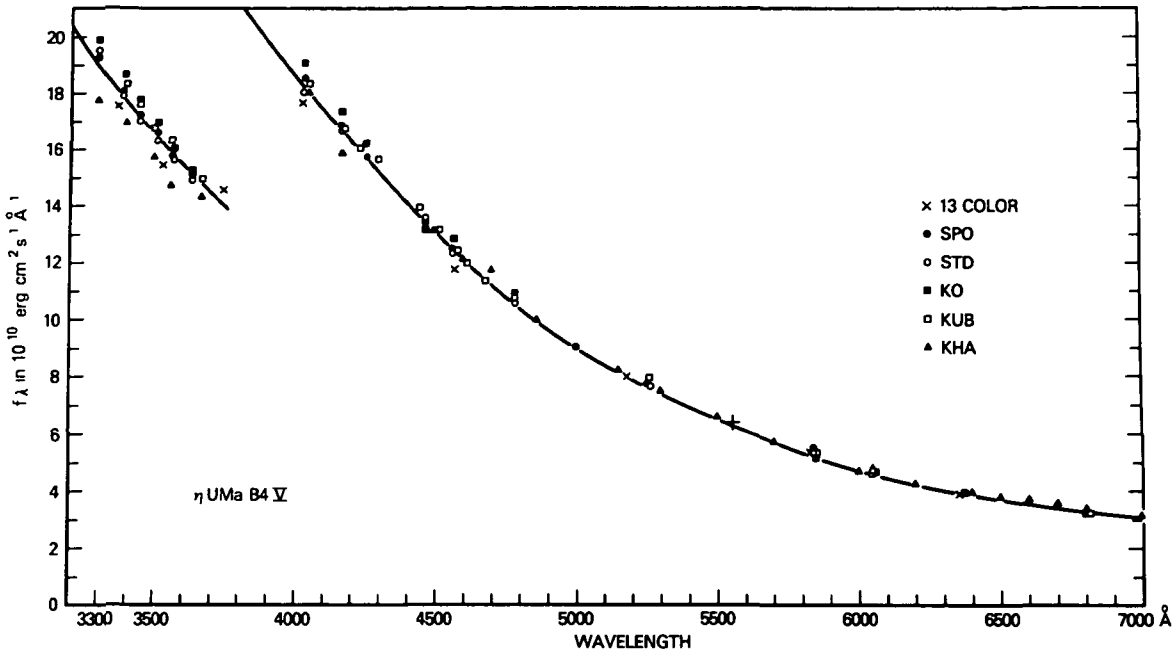

Figure 3-1. The observed visible energy distribution of η UMa, B4 V. The points show the measured fluxes The data of Johnson and Mitchell (1975) are shown by crosses; those of Schild et al. (1971) by filled circles, those of Breger (1976a) for η UMa as a secondary standard by open circles, those of Kodaira (1970) by filled squares; those of Kubiak (1973) by open squares, and those of Kharnitov (1963) by filled triangles. All of the data except that of Johnson and Mitchell were taken from Breger (1976b).

caused by the continua of hydrogen, helium, and the light elements, by the hydrogen lines, and by electron and Rayleigh scattering. A survey of their results shows that the relative energy distributions, normalized to the flux at 8000 Å, change very little for constant speed of rotation as the inclination changes from 0 to 90 degrees. However, as the speed of rotation increase from low values to break-up speed, the spectrum becomes fainter in the ultraviolet and brighter in the infrared. The flux at 8000 Å increases as the speed of rotation increases. The changes are not significant until the speed of rotation exceeds 80 percent of the break-up speed. For middle B stars, this means exceeding about 300 km s^{-1}. Consequently, the observed relative energy distribution of η UMa is probably not modified by the rotation of the star unless it happens that η UMa is being viewed nearly pole-on.

EFFECTIVE TEMPERATURES FOR B STARS IN THE MAIN-SEQUENCE BAND

By definition, the effective temperature of a star is a measure of the total flux in ergs s^{-1} in all wavelengths radiated from each cm^2 of the surface of the star. We have

$$\sigma_R T_{eff}^4 = \int_0^\infty F_\lambda d\lambda \qquad (3\text{-}7)$$

where σ_R is the Stefan-Boltzmann constant. The monochromatic flux radiated by a star is related to that measured and corrected for interstellar extinction, f_λ, by means of the angular diameter θ_λ. A subscript λ is attached to the symbol for angular diameter in order to emphasize that always the angular diameter is measured by means of radiation in a restricted wavelength band.

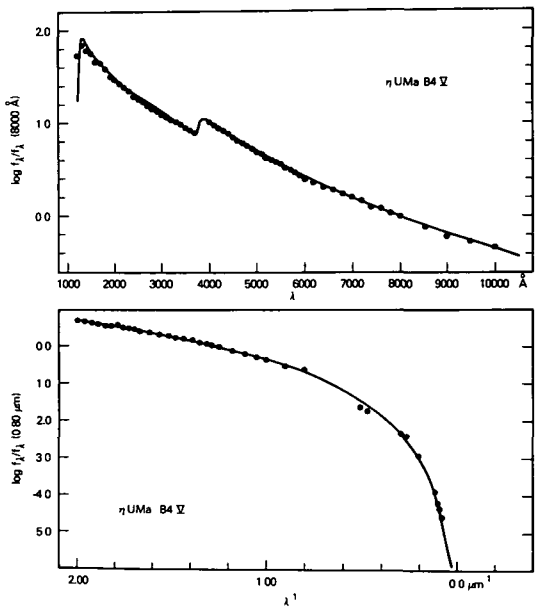

Figure 3-2 The observed relative energy distribution of η UMa The data are from Table 3-2 and their values are normalized to the observed flux at 8000 Å. The line gives the normalized energy distribution of the Kurucz (1979) model atmosphere having normal composition, T_{eff} = 1.7 X 10^4 K and log g = 4 0.

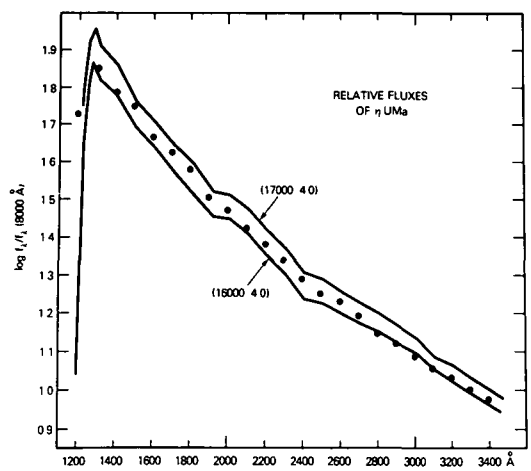

Figure 3-3 The observed relative ultraviolet flux of η UMa on an enlarged scale The lines show the energy distributions from two Kurucz (1979) model atmospheres having normal composition.

Simple geometry gives

$$\theta_\lambda = 2\left(\frac{f_\lambda}{F_\lambda}\right)^{1/2}, \qquad (3\text{-}8)$$

where F_λ is the flux measured at the star. If one assumes that the angular diameter has the same value, θ, at all wavelengths then one can write

$$\sigma_R T_{eff}^4 = 4\theta^{-2} \int_0^\infty f\lambda d\lambda. \qquad (3\text{-}9)$$

If one can measure f_λ over a wide range of wavelengths for a set of stars for which one has angular diameters and if one estimates from theory $\int f_\lambda d_\lambda$ for the extreme wavelength ranges that are not accessible to observation, one can find the effective temperatures of these stars.

This was done for 16 stars of types B0 to B8 (12 in luminosity classes V to II and 4 supergiants) by Code et al. (1976). This group used the angular diameters measured at 4430 Å by Hanbury Brown et al. (1974) by means of the intensity interferometer. They made use of observed fluxes from OAO-2 and from the ground. Additional results for 142 B stars have been provided by Underhill et al. (1979). They used angular diameters found by replacing F_λ in Equation (3-8) by the monochromatic fluxes from a model atmosphere in the wavelength range from 6000 to 11000 Å, ultraviolet fluxes from the S2/68 experiment on the TD1 satellite, and the 13-color absolute photometry of Johnson and Mitchell (1975).

The results for the stars in the main-sequence band (luminosity classes V to II) will be discussed here. They are compared with indirect estimates of effective temperature obtained by comparing the observed shape of the visible and ultraviolet spectrum of B stars with the shapes predicted by means of model atmospheres and from results of the analysis of line strengths using model atmospheres. The effective temperatures of B stars in the main-sequence band range from 3.08 X 10^4 K at type B0 to 1.02 X 10^4 K at type B9.5.

The Determination of Angular Diameters

Angular diameters of 16 bright B stars have been measured directly by Hanbury Brown et al. (1974) using the intensity interferometer These results, together with those for α Lyr, A0 V, are given in Table 3-3, they are fundamental. The angular diameter θ_{LD} of Hanbury Brown et al is listed, this value allows for the effects of limb darkening. Also listed are the results of Underhill et al. (1979). Typically the angular diameters of B stars are a few times 10^{-4} arcsec. Consequently, other methods for determining angular diameter such as occultations or speckle interferometry, give little help for B stars

Another way of finding angular diameter in addition to using the intensity interferometer is to make use of Equation (3-8) To do so, one must have observed absolute monochromatic fluxes corrected for interstellar extinction and secure estimates of the fluxes emitted at the star. The latter estimates can be found by noting that at wavelengths which are well into the tail of the blackbody function for a temperature like the effective temperature of the star, model atmospheres predict fluxes which are only slightly dependent on the procedures used to construct the model atmosphere (see Chapter 6). The predicted fluxes are essentially determined by the adopted effective temperature of the model. Blackwell and Shallis (1977) tested these assertions using observed infrared fluxes from stars observed by Hanbury Brown et al. and showed that one could set up an iterative method to obtain angular diameters and effective temperatures for stars for which one

Table 3-3
Angular Diameters of B Stars and of α Lyr

			Angular Diameter (10^{-4} arsec)		
HR	HD	Name	HB+[a]	UDPD[b]	Spectral Type
472	10144	α Eri	19.2	15.91	B3 Vpe
1713	34085	β Ori	25.5	26 67	B8 Ia
1790	35468	γ Ori	7.2	7.43	B2 III
1903	37128	ϵ Ori	6.9	7.08	B0 Ia
2004	38771	κ Ori	4.5	–	B0 5 Ia
2294	44743	β CMa	5.2	5.55	B1 II-III
2618	52089	ϵ CMa	8 0	7 75	B2 II
2827	58350	η CMa	7.5	8 62	B5 Ia
3982	87901	α Leo	13.7	13 65	B7 V
4662	106625	γ Crv	7.5	–	B8 III
4853	111123	β Cru	7.22	–	B0 5 III
5056	116658	α Vir	8.7	–	B1 IV
5132	118716	ϵ Cen	4.8	–	B1 III
5953	143275	δ Sco	4.6	4.84	B0.5 IV
7001	172167	α Lyr	32.4	32 67	A0 V
7790	193924	α Pav	8 0	7 11	B2.5 V
8425	209952	α Gru	10.2	10.74	B7 IV

[a] Hanbury Brown et al (1974).
[b] Underhill et al (1979)
Dashes (–) represent no information exists for these values.

had predictions of the continuum fluxes from representative model atmospheres and for which one had observations of the absolute flux over a wide wavelength interval.

This idea was applied by Underhill et al. (1979) to find the angular diameters of 142 B stars; their results for 12 of the stars measured by Hanbury Brown et al. (1974) are given in Table 3-3. The model atmosphere continuum fluxes from LTE, line-blanketed models by Kurucz (1979) were used. A starting model for each star was adopted using one of the methods explained in Chapter 6 for identifying a particular star with a model from measurements of the continuous energy distribution only. Underhill et al. found that they could quickly converge on a value for the angular diameter of each star. They made use of the 13-color absolute photometry of Johnson and Mitchell (1975) for wavelengths from 6356 to 11084 Å. It is a basic assumption that the shape of the observed continuous spectrum between 6000 and 11000 Å will be represented by the fluxes from one of the Kurucz model atmospheres. That the Kurucz model fluxes have the shape of the observed spectra from B stars over a wide wavelength range has been illustrated in the section on Observations Concerning the Shape and Absolute Value of the Ultraviolet Continuous Spectrum. It is necessary to correct the observed fluxes accurately for interstellar extinction. This procedure is described in the section on Correction for Interstellar Extinction.

The angular diameters found by Underhill et al. fit accurately onto the scale and zero point of the angular diameters measured by the intensity interferometer. This may be seen by comparing the data in Table 3-3. A least-squares solution shows that

$$\theta = -(0.124 \pm 0.214) + (1.012 \pm 0.017)\,\theta_{LD}, \qquad (3\text{-}10)$$

where θ is in units of 10^{-4} arcsec. The solution was calculated excluding the supergiants and α Eri, which is a Be star for which the spectral classification and the photometric data are not internally consistent, and adding the O star, ζ Pup. The excellence of the fit of θ derived from Equation (3-8) to the measured values of θ_{LD} demonstrates that the absolute values of the continuum fluxes from the Kurucz model atmospheres as well as the shape of the visible and near infrared spectrum are representative for B stars in general. The assumption that the angular diameter is independent of wavelength seems to be valid from 6000 to 11000 Å. In Chapter 4 it is noted that adequate agreement is also found for supergiants.

In the case of Be stars, one hesitates to assume that the angular diameter is independent of the wavelength, and one suspects that in some cases the observed flux contains a significant contribution from the mantle of ionized gas surrounding the star in addition to the photospheric flux. The Be stars are discussed in Part II.

Radii of B Stars

If the distance of a star is known, an angular diameter can be transformed into a linear radius. This has been done by Code et al. (1976) using distances which they assigned and the angular diameters of Hanbury Brown et al. (1974) as well as by Underhill et al. (1979) who assigned distances to their 142 B stars after considering several estimates of distance for each star. Radii can also be found from the combined solutions for the radial-velocity orbits and the light curves of eclipsing binaries. The available information for B stars is discussed in the section on Radii in Chapter 2, and the results of Underhill et al. for each spectral class can be found in Table 2-12. On the main sequence, the radius increases from about 3 $R_\odot$ at type B9 to 12 $R_\odot$ at type B0. The giant stars, on the average, are about 30 percent larger than the dwarfs.

Correction for Interstellar Extinction

The monochromatic fluxes corrected for interstellar extinction can be found from a set of observed monochromatic fluxes, f_λ^{obs}, by

evaluating the equation

$$f_\lambda = f_\lambda^{obs}\, 10^{[0.4 A_\lambda/E\,(B-V)]\; E\,(B-V)} \quad (3\text{-}11)$$

Here A_λ/E (B − V) is a tabulated function giving the amount of extinction due to the interstellar medium at each wavelength in terms of the value of the color excess E(B − V). The shape of the interstellar extinction curve has been studied by several groups. It is usually found by intercomparing the absolute energies of lightly reddened and heavily reddened B and O stars having the same intrinsic energy distribution. Usually it is assumed that the same spectral type means the same intrinsic energy distribution Tables of A_λ/E(B − V) have been given by Nandy et al. (1975, 1976) and by Code et al. (1976) for the ultraviolet, visible, and near infrared. Recently Sapar and Kuusik (1978) and Savage and Mathis (1979) have rediscussed all available material and have provided detailed listings of A_λ/E(B − V) valid from 1100 Å to 10 μm. The values of A_λ/E(B − V) are fairly well known longward of 1400 Å, but shortward of this, present knowledge is still insecure. Some typical values are given in Table 2-8.

The value of E(B − V) for a star may be estimated by comparing the star's measured UBV colors to the intrinsic colors for its spectral type, by measuring the depth of the 2200 Å broad absorption feature, and from BCD spectrophotometry (see Chapter 2) The solutions of Underhill et al. (1979) for angular diameter give a check on the adopted value of E(B − V). If the adopted value is wrong, the values of θ_λ found at several wavelengths will have a systematic trend with wavelength However, as has long been known, a change in effective temperature of the adopted model will produce a small change in shape of the visible spectrum which is similar to that produced by a small change in the adopted amount of interstellar extinction. More interstellar extinction and lower effective temperature for the model both result in reddened energy distributions. Thus, to increase the certainty of the angular diameters found by using Equation (3-8), one should use, if possible, a criterion for selecting the representative model atmosphere that is not dependent on the shape of the spectrum over a wide wavelength range. The size of the Balmer jump provides a useful criterion for B stars in the main-sequence band.

Effective Temperatures of B Stars

The definition of effective temperature is given in Equation (3-7), the direct way to find T_{eff} is to evaluate Equation (3-9). This has been done for 16 bright B stars by Code et al. (1976) and for 142 by Underhill et al. (1979). Indirect ways of estimating effective temperatures exist, the methods use some properties of the spectrum such as the shape of the spectrum over a limited wavelength interval, the size of the Balmer jump, and the relative strengths of absorption lines from elements present in two or more stages of ionization to identify a star with a model atmosphere. The effective temperature of the model atmosphere which gives the best representation of the observed data is said to be equivalent to the effective temperature of the star. The same observations lead to somewhat different effective temperatures when models which have been constructed according to different prescriptions are used. The models may be constructed using LTE or non-LTE physics and they may have different compositions and take different sources of opacity into account. The methods for identifying a particular star with a particular model atmosphere are outlined in Chapter 6. The types of difficulty and inconsistency that occur have been thoroughly discussed by many authors. The review by Aller and Jugaku (1969) is based on much experience and on a large body of data.

The effective temperatures and log g values for 37 B stars in the main-sequence band which have two or more determinations of effective temperature are given in Table 3-4. These results are typical of what is known about B stars. The source for each piece of information is listed and an indication is given of the method followed to find T_{eff} and log g. The values of log g found from model atmospheres determine the electron density needed to reproduce the selected criteria. They are not necessarily precisely equal to GM_*/R_*^2.

Table 3-4
Effective Temperatures and Log g for B Stars in the Main-Sequence Band

HR	Name	Spectral Type*	T_{eff} (10^4K)	log g	Method	Source
1855	υ Ori	09 V	3 100	4 3	5	Leckrone (1971)
			3.435	4.5	11	Underhill et al (1979)
6165	τ Sco	B0 V	3.280	4.45	1	Traving (1955)
			3 500	4 3	2	Aller et al (1957)
			3 280	4 2	1	Scholz (1967)
			3 200	4 1	1	Hardorp and Scholz (1970)
			2 860	4 2	4	Norris (1971)
			3 102	4 0	3	Underhill (1972)
			3 150	4 15	8	Auer and Mihalas (1972)
			3 320	4 50	9	Kamp (1978)
			3 005	4 2	11	Underhill (1979a)
1756	λ Lep	B0 5 IV	3 090	4 05	1	Hardorp and Scholz (1970)
			2 961	4 0	11	Underhill et al (1979)
2387	ξ^1 CMa	B0 5 IV	3 130	4 2	1	Aller and Jugaku (1969)
			3 030	4 25	9	Kamp (1978)
5953	δ Sco	B0 5 IV	3 146	–	10	Code et al (1976)
			2 893	4 0	11	Underhill et al (1979)
5056	α Vir	B1 IV	2 230	4 0	12	Henry et al (1975)
			2 393	–	10	Code et al (1976)
			2 450	–	10	Brune et al (1979)
6084	σ Sco	B1 III	2 860	4 0	12	Schild et al. (1971)
			2 904	3 5	11	Underhill et al (1979)
8238	β Cep	B1 III	2 420	4 0	12	Schild et al (1971)
			2 578	4 0	11	Underhill et al (1979)
2294	β CMa	B1 II-III	2 518	–	10	Code et al (1976)
			2 582	3 5	11	Underhill et al (1979)
3468	α Pyx	B1 5 III	2 200	3 65	4	Norris (1971)
			2 372	3 5	11	Underhill et al (1979)
5285	χ Cen	B2 V	1 940	4 05	4	Norris (1971)
			2 120	3 0	9	Kamp (1978)

*as determined by Underhill et al (1979)
Dashes (–) represent no information exists for these values

Table 3-4 (cont.)

HR	Name	Spectral Type*	T_{eff} (10^4K)	log g	Method	Source
39	γ Peg	B2 IV	2.400	3 8	3	Aller and Jugaku (1959)
			2.190	4 1	5	Leckrone (1971)
			2.080	3 9	4	Norris (1971)
			2.170	4 0	12	Schild et al (1971)
			2 567	4 0	3	Underhill (1972)
			2 150	3 7	7	Peters (1976a)
			2 550	3 9	9	Kamp (1978)
			2 199	4 0	11	Underhill et al. (1979)
779	δ Cet	B2 IV	2 190	4 0	12	Schild et al (1971)
			2 357	4 0	11	Underhill et al. (1979)
6453	θ Oph	B2 IV	2 070	3 9	4	Norris (1971)
			2 286	4 0	11	Underhill et al (1979)
1790	γ Ori	B2 III	2 230	4 0	12	Schild et al (1971)
			2 158	–	10	Code et al (1976)
			2 194	3 5	11	Underhill et al (1979)
1910	ζ Tau	B2 IIIe	1 750	4 0	12	Schild et al (1971)
			1 850	4 0	12	Henry et al. (1975)
			2 124	3 5	11	Underhill et al (1979)
2618	ϵ CMa	B2 II	2 200	3 0	12	Schild et al (1971)
			2 099	–	10	Code et al (1976)
			2 267	3 5	11	Underhill et al (1979)
7790	α Pav	B2 5 V	1 788	–	10	Code et al (1976)
			1 959	4 0	11	Underhill et al (1979)
3454	η Hya	B3 V	1 890	4 0	12	Schild et al. (1971)
			1 879	4 0	11	Underhill et al (1979)
472	α Eri	B3 Vp	1 580	4 0	12	Henry et al (1975)
			1 451	–	10	Code et al (1976)
			1 400	–	10	Brune et al (1979)
			1 756	4 0	11	Underhill et al (1979)

*as determined by Underhill et al (1979)
Dashes (–) represent no information exists for these values

Table 3-4 (cont.)

HR	Name	Spectral Type*	T_{eff} (10^4K)	log g	Method	Source
6588	ι Her	B3 IV	1 540	4.0	12	Wolff et al (1968)
			2 020	3 75	1	Kodaira and Scholz (1970)
			1 800	4 0	3	Peters and Aller (1970)
			1 750	4 0	5	Leckrone (1971)
			1 920	4 0	3	Underhill (1972)
			1 950	3 18	9	Kamp (1978)
			1 781	4 0	11	Underhill et al (1979)
6897	α Tel	B3 IV	1 690	4 0	4	Norris (1971)
			1 902	4 0	11	Underhill et al (1979)
5191	η UMa	B4 V	1 500	4 0	12	Wolff et al (1968)
			1 740	4 0	12	Schild et al (1971)
			1 710	4 0	12	Henry et al (1975)
			1 700	4 0	12	Strongylis and Bohlin (1979)
			1 682	4 0	11	Underhill et al (1979)
542	ϵ Cas	B4 IV	1 590	4 0	12	Schild et al (1971)
			1 535	4 0	11	Underhill et al (1979)
8858	ψ^2 Aqr	B5 V	1 510	4 0	12	Wolff et al (1968)
			1 521	4 0	11	Underhill et al (1979)
6092	τ Her	B5 IV	1 500	4 0	7	Adelman (1977b)
			1 640	3 3	9	Kamp (1978)
			1 501	4 0	11	Underhill et al (1979)
1122	δ Per	B5 III	1 430	4 0	12	Schild et al. (1971)
			1 404	4 0	11	Underhill et al (1979)
1791	β Tau	B6 IV	1 400	4 0	12	Schild et al (1971)
			1 382	4 0	11	Underhill et al. (1979)
6396	ζ Dra	B6 III	1 340	4 0	12	Schild et al (1971)
			1 360	3 6	6	Underhill (1973)
			1 296	3 5	11	Underhill et al (1979)
3982	α Leo	B7 V	1 330	4 0	12	Wolff et al (1968)
			1 290	4 0	12	Schild et al (1971)
			1 221	–	10	Code et al. (1976)
			1 239	4 0	11	Underhill et al (1979)

*as determined by Underhill et al (1979)
Dashes (–) represent no information exists for these values

Table 3-4 (cont.)

HR	Name	Spectral Type*	T_{eff} (10^4K)	log g	Method	Source
811	π Cet	B7 IV	1 330	4 0	12	Wolff et al (1968)
			1 350	3 8	5	Leckrone (1971)
			1 270	3 65	4	Norris (1971)
			1 326	4 0	11	Underhill et al (1979)
8425	α Gru	B7 IV	1 335	4 0	12	Henry et al. (1975)
			1 405	–	10	Code et al (1976)
			1.326	4 0	11	Underhill et al (1979)
2845	β CMi	B8 IVe	1.200	4 0	12	Schild et al (1971)
			1.151	4 0	11	Underhill et al (1979)
8965	ι And	B8 IV	1 190	4 0	12	Wolff et al (1968)
			1 186	4 0	11	Underhill et al (1979)
7236	λ Aql	B9 V	1 170	4 0	12	Schild et al (1971)
			1 141	4 0	11	Underhill et al (1979)
8597	η Aqr	B9 V	1 180	4 0	12	Wolff et al (1968)
			1 122	4.0	11	Underhill et al (1979)
7906	α Del	B9 IV	1 090	4 0	12	Wolff et al (1968)
			1 068	4 0	11	Underhill et al (1979)

*as determined by Underhill et al (1979)
Dashes (–) represent no information exists for these values

Method 1 was developed by Traving (1955), it uses LTE model atmospheres to calculate representative values of the Balmer jump, the strength of Hγ and Hδ, and the ionization balance from several absorption lines of elements present in two stages of ionization. Method 2, developed by Aller et al. (1957), is similar but it does not make use of the Balmer jump. Method 3 uses LTE model atmospheres and fits only the strengths of the hydrogen lines and the relative strengths of lines in several stages of ionization. Method 4, developed by Norris (1971), uses LTE model atmospheres to fit the shape of the visible continuous spectrum and the shape of Hγ Method 5 of Leckrone (1971) is similar. Leckrone places much weight on predicting the size of the Balmer jump correctly. He publishes best-fit values of T_{eff} and log g for three different relative absolute calibrations of the photometric measurements, but eventually concludes that the values given in Table 3-4 provide the best systematic accuracy for predicting the strengths of the He I lines. With this choice there is no systematic change in the derived helium abundance along the spectral sequence.

Method 6, used by Underhill (1973), relies on fitting the strength of Hγ and the break-off of the Balmer series Method 7, used by Peters (1976a) and by Adelman (1977b), is like method 2, but use is made of spectrophotometric scans extending into the rocket ultraviolet as well as scans in the visible spectral range. Method 8 uses non-LTE model atmo-

spheres and the criteria for selecting a representative model take into account the effects of non-LTE physics on the strengths of the He I and He II lines. The criteria of method 9 are based on representing the observed relative intensities of lines of Si II, III, and IV accurately. Non-LTE model atmospheres and a non-LTE theory of line formation are used. The values of $T_{\rm eff}$ and log g found by this method and listed in Table 3-4 correspond to the positions of the points representing the individual stars in Figure 2 (Kamp, 1978).

Method 10, used by Code et al. (1976) and by Brune et al (1979), uses observed flux integrals and observed angular diameters The dependence on model atmospheres is slight, for models are used only as a guide for estimating the unobserved part of the flux integral. No value for log g is found Method 11, used by Underhill et al. (1979), has been explained and evaluated above. Monochromatic fluxes from LTE model atmospheres are used to find angular diameters and to estimate the unobserved part of the flux integral, but the dependence of the results on the character of the model atmospheres is small. The value of log g is that of the model atmosphere used, the derived angular diameters and effective temperatures are not sensitive to the choice of log g

Method 12 consists of fitting observed normalized energy distributions to the normalized energy distributions from model atmospheres It requires good relative absolute energy calibration of the spectrophotometric instruments. The deduced effective temperatures will be too low if the correction for interstellar extinction has been underestimated. The shape of model–atmosphere energy distributions over the range 2000 to 8000 Å, when normalized to a flux near 6000 Å, is insensitive to the detailed procedures used to construct the model atmosphere. The sensitive parameter is effective temperature The inclusion of line blanketing in B-type models makes little change in the shape of the energy distribution except near the hydrogen discontinuities, but it does result in a change in the absolute amount of the energy in each frequency interval. Wolff et al. (1968) used energy scans covering the range from 3200 to 7530 Å and line-blanketed model atmospheres, and they showed that their estimates for effective temperature from the shape of the continuous spectrum yielded about the same value as their fits to the Balmer jump did. In Table 3-4 we have listed the average of their two results for each star for which we have other determinations of $T_{\rm eff}$. Schild et al. (1971) used scans from 3300 Å to 6050 Å with hydrogen line-blanketed model atmospheres and showed that they could fit the shape of the Paschen continuum and the Balmer jump with the same model. Strongylis and Bohlin (1979) fitted their observed energy distribution over the range 1100 to 3200 Å. Henry et al. (1975) fitted to the fluxes from model atmospheres by Kurucz et al. (1974) over the range 1180 to 1680 Å. In all these cases, the value of log g listed in Table 3-4 is that of the model used.

The estimates of effective temperature given in Table 3-4 can be placed in three groups. Group A contains values found by methods 1, 2, 3, 8, and 9 Here the emphasis is on finding the effective temperature and log g value of a model atmosphere that represents well the electron temperatures and densities in layers important for forming the prominent absorption lines in the spectrum Group B contains values found by methods 4, 5, 6, 7, and 12 Here the emphasis is on finding the effective temperature of a model atmosphere that represents well the layers where the visible continuous spectrum and the wings of the Balmer lines are formed These layers may be called the photosphere of the star Group C contains values found from the integrated flux These values are effective temperatures in the true meaning of the words. Log g is not a well-determined parameter Some thought-provoking trends are seen when, for each star, one forms mean effective temperatures from all values in groups A, B, and C and considers the differences between these mean values

If the line forming regions of a stellar atmosphere and the continuum forming regions were both well represented by a classical model atmosphere (see Chapter 6 for a description of the classical model atmosphere and its modifica-

tions), the $\langle T_{eff} \rangle_A$, $\langle T_{eff} \rangle_B$ and $\langle T_{eff} \rangle_C$ should be the same within a few hundred degrees. The actual trends are that $\langle T_{eff} \rangle_A$ is larger than $\langle T_{eff} \rangle_B$ or $\langle T_{eff} \rangle_C$ by 1.2×10^3 to 3.1×10^3 K. The trends can be seen by examining the results for τ Sco, λ Lep, γ Peg, ι Her, and τ Her. The larger value means that the electron temperatures in the line-forming layers of these main-sequence B stars correspond to higher effective temperatures than are suggested by the value of the integrated flux from these stars and by the shape of the continuous spectrum.

On the whole, if one does not consider differences less than $\pm 1.0 \times 10^3$ K, the $\langle T_{eff} \rangle_B$ are about equal to the $\langle T_{eff} \rangle_C$ for stars of type B4 and later. For stars of earlier type, $\langle T_{eff} \rangle_B$ tends to be smaller than $\langle T_{eff} \rangle_C$. This difference may be due to the fact that the studies put into Group B have sometimes adopted a smaller interstellar extinction than is the case for the studies of Group C. The results from methods 4, 5, 7, and 12 are particularly sensitive to the correction for interstellar extinction. The results from methods 10 and 11 are also sensitive to the choice of E (B − V), but the choice has usually been checked more thoroughly than has been done in the studies which used methods 4, 5, and 12. The large difference in the case of υ Ori between $\langle T_{eff} \rangle_B$ and $\langle T_{eff} \rangle_C$ is largely due to the fact that Underhill et al. (1979) classified this star as type O9 V. If Leckrone had done so, he would have applied a reddening correction and would have found a larger effective temperature. The general agreement between $\langle T_{eff} \rangle_B$ and $\langle T_{eff} \rangle_C$ demonstrates that the absolute energy calibrations of the various spectrum scanners are systematically reliable.

This study of the effective temperature of B stars in the main-sequence band can be summarized by saying that if one corrects for interstellar extinction carefully, methods based on interpreting the shape of the continuous spectrum and the wings of the hydrogen lines by means of classical model atmospheres lead to effective temperatures in good agreement with those that may be found by evaluating the flux integral and finding the angular diameter of the star. Methods based on the effective temperatures of classical model atmospheres that represent well the relative intensities of prominent lines in the spectrum tend to result in effective temperatures that are too high. Using non-LTE physics does not remove the discrepancies, although it may make the results from different stages of ionization of different elements more compatible with each other. What is seen here seems to be a beginning of the type of behavior which is striking for B-type supergiants (see Chapter 4) and for O and Wolf-Rayet stars (see Underhill and Divan, *O, Of, and Wolf-Rayet Stars*, to be published). The parts of the atmosphere where the prominent lines are formed correspond to higher electron temperatures than can be maintained by the application of the constraint of radiative equilibrium to the radiation field of the star as it traverses the atmosphere. Heating/cooling occurs in addition to that resulting from the interaction of radiation with the atoms and ions of the atmosphere.

The results for the Be stars are somewhat uncertain because of the distortions of the shape of their continua owing to overlying emission. Underhill et al. (1979) in their survey of effective temperatures of the B stars found no evidence to suggest that the effective temperatures of β Cephei stars or of Bp stars are substantially different from those of normal B stars of the same spectral type. These two classes of B stars are discussed in Chapter 5.

Bolometric Corrections

The bolometric correction for a B star can be found from the tabulation of Buser and Kurucz (1978) of the bolometric correction as a function of effective temperature. The values are insensitive to the value of log g adopted for the star. The appropriate value is their

$$B.C.' = (B.C.)_{calc} + 0.100 \qquad (3\text{-}12)$$

These values of the bolometric correction are recommended since T_{eff} and the $B.C.$ should come from the same set of model atmospheres (Underhill, 1966c). We have shown above that the energy distributions of the Kurucz (1979)

model atmospheres match well the shapes of the observed energy curves of main-sequence B stars and the observed absolute values of the flux in the range 6000 to 11000 Å, given an angular diameter.

Effective Temperature in Terms of Spectral Type and $(B - V)_0$

Although each star in a spectral type–luminosity class box is not identical with the other stars in that box, it is useful for orientation purposes to form average effective temperatures for spectral type–luminosity class boxes from the data for 142 B stars given by Underhill et al (1979). The resulting average effective temperatures are given in Table 3-5 together with the intrinsic colors from FitzGerald (1970) Most of the stars in the center part of the table are in luminosity class III. The standard deviation, s.d., of each mean value is given and the number of results included in each mean value The size of the standard deviation represents as much the disparity of the stars in each box as the uncertainties of the individual effective temperatures. The effective temperatures for luminosity classes II and III do not differ significantly from those for luminosity classes IV and V

Lesh (1977) used the flux effective temperatures of Code et al. (1976) with the color index $(1910 - V)_0$ for each star, obtained from OAO-2 photometry, to show that a linear relation

$$\theta_{eff} = (0.111 \pm 0.001) \times (1910 - V)_0 + (0.565 \pm 0.002) \qquad (3\text{-}13)$$

exists for B stars. Here θ_{eff} is $5040.4/T_{eff}$ and probable errors are indicated Using the body of OAO-2 photometry that exists and applying corrections for interstellar extinction, Lesh then found a mean value of $(1910 - V)_0$ for stars of MK spectral types between B0 and B9.5, luminosity classes IV and V, and derived the

Table 3-5
Average Effective Temperatures as a Function of Spectral Type and Intrinsic Color

	Luminosity Classes IV, V				Luminosity Classes II, III				IV, V (Lesh)
Spectral Type	$(B-V)_0$ (mag)	T_{eff} (10^4 K)	s.d. (10^2 K)	No.	$(B-V)_0$ (mag)	T_{eff} (10^4 K)	s.d. (10^2 K)	No	T_{eff} (10^4 K)
B0	−0.30	3 078	–	1	−0.30	–	–	–	3 11
B0.5	−0 28	2.927	2.4	2	−0.28	2.747	–	1	2.87
B1	−0.26	2.690	8 3	2	−0.26	2.632	7 3	4	2.60
B1.5	−0.25	2 572	4.4	3	−0.25	2.475	7.3	2	2.33
B2	−0.24	2.282	1 7	14	−0.25	2.227	3.8	7	2.18
B2.5	−0.22	2.038	5.6	8	−0 22	2.032	–	1	2.02
B3	−0.20	1.853	1.9	11	−0.20	–	–	–	1 81
B4	−0.18	1.634	1.9	8	−0 18	–	–	–	1.72
B5	−0 16	1.517	1.8	9	−0.16	1.485	5.0	4	1.54
B6	−0.14	1.374	1.6	3	−0.14	1 366	2.0	5	1.47
B7	−0 13	1.298	1.8	4	−0.12	1.275	–	1	1.35
B8	−0.10	1.190	1.3	4	−0.10	1.193	2.8	5	1.24
B9	−0.07	1.092	4.8	10	−0.08	1.078	1.2	4	1.08
B9 5	−0.04	1.020	–	1	−0.05	–	–	–	1.07

Sources Underhill et al (1979) and Lesh (1977) for T_{eff}, FitzGerald (1970) for $(B - V)_0$
Dashes (–) represent no information available for these places

temperature law given in the final column of Table 3-5

The effective temperatures from Table 3-5 for luminosity classes IV and V are plotted as a function of $(B - V)_0$ in Figure 3-4 together with earlier information proposed by Morton and Adams (1968), Wolff et al (1968), Schild et al (1971), and Code et al (1976) The points listed by these authors as representing their final relation have been plotted

The relation between $(B - V)_0$ and spectral class is not exact, it does depend on how well the correction for interstellar extinction has been determined. Also the relation between T_{eff} and spectral type or $(B - V)_0$ has some width Therefore, one should not expect to be able to derive a precise relationship between $(B - V)_0$ and T_{eff} using the data presently available Since the body of data used by Underhill et al (1979) is the largest independent set of data shown in Figure 3-4, a line has been drawn joining these points This line should afford a reasonable estimate of the effective temperature for a star for which only $(B - V)_0$ is known. The effective temperatures for the early B types due to Schild et al (1971) and some of those of Morton and Adams (1968) are lower than later work suggests. This difference occurs probably because the interstellar extinction for the few stars of early type in the first studies was underestimated.

Extensive intermediate-band filter photometry of stars in open clusters and in the field has been performed at the Geneva Observatory using 7 filters designated as U, B, V, B_1, B_2, V_1, and G. These bands have effective wavelengths and effective widths (in parentheses) of 3456(170), 4245(283), 5500(296), 4024(196), 4480(163), 5405(201), and 5805(204) Å, respectively. A catalogue of observations in these filters for about 10,000 stars has been published by Rufener (1976) Cramer and Maeder (1979) have shown that the color combination,

$$X = 0.3788 + 1.3764U - 1.2162B_1 - 0.8498B_2 - 0.1554V_1 + 0.8450G, \quad (3\text{-}14)$$

correlates well with spectral type for B stars.

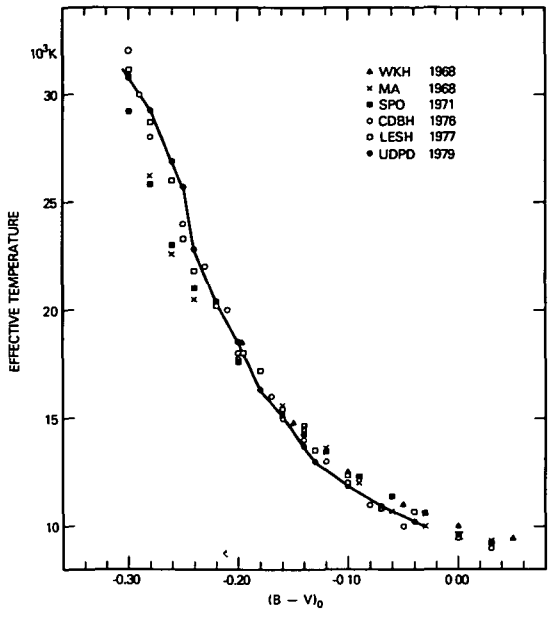

Figure 3-4 Effective temperature as a function of $(B - V)_0$ for B stars in the main-sequence band. The values recommended by Wolff et al. (1968) are shown by filled triangles, those of Morton and Adams (1968) by crosses, those of Schild et al. (1971) by filled squares, those of Code et al (1976) by open circles, and those from Table 3-5 by filled circles which are joined by a line, those of Lesh (1977) by open squares.

Using the observations of effective temperature by Code et al (1976), Cramer and Maeder have calibrated the parameter X in terms of effective temperature giving one relation for stars of luminosity classes III, IV, and V and another for the Ia supergiants. The set of Geneva photometric observations gives information about many faint O and B stars in open clusters as well as about stars of other spectral types The relation derived by Cramer and Maeder between the color combination X and effective temperature is useful for deriving a first estimate of the effective temperature of a star for which only Geneva photometric information exists Another color combination,

$$Y = -0.8288 + 0.3235U - 2.3228B_2 + 2.3363B_2 + 0.7495V_2 - 1.0865G, \quad (3\text{-}15)$$

has been calibrated by Cramer and Maeder in combination with X in terms of M_V for the early type stars while a third,

$$Z = -0.4572 + 0.0255U - 0.1740B_1 + 0.469B_2 - 1.1205V_1 + 0.7994G, \quad (3\text{-}16)$$

serves in combination with X to separate Bp and Ap stars from normal stars.

THE LINE SPECTRUM

When one begins to study the line spectra of B stars, the first step is to identify the absorption lines which are present.

Identifications: Major Constituents of B-Type Spectra

In the photographic blue-violet range, the spectra of main-sequence B stars contain strong broad-winged lines from the Balmer series of hydrogen converging to the Balmer limit, and a number of strong lines of He I, the lines from the $2^1P^o - n^1D$ and $2^3P^o - n^3D$ series showing well-developed Stark-broadened wings and the presence of forbidden lines from the $2^1P^o - n\ ^1F^o$ and $2^3P^o - n^3F^o$ series. Also a few moderately strong lines from C II, N II, O II, Mg II, Si II, Si III, and Si IV appear. Weak lines from Ne II, C III, N III, S III, and Fe III may be detected in early B-type spectra while lines of Fe II are seen in the late B-type spectra. Lines of Ne I, S II, P II, Al II, Al III, etc. occur in the middle B stars.

The process of measuring spectral lines for wavelength and identifying lines has been described by Underhill (1966a). She has given the sources for line identifications in the visible spectral range. At low resolution, B-type spectra seem to contain few lines, but at high resolution, the spectra of sharp-lined B stars are found to be full of weak absorption lines.

In the ultraviolet spectral range, the absorption lines are more conspicuous than in the visible range. Lines from the second and third spectra of the light elements and the metals fill the spectrum, see the atlas of Copernicus (OAO-3) spectra by Snow and Jenkins (1977) for some typical intensity tracings covering the range 1000 to 1400 Å. The resonance lines of C II, C IV, N V, Mg II, Al III, Si III, and Si IV are strong, the lines from C IV, N V, and Si IV dominating in stars of type B1 and earlier, those of Mg II, C II, Al III, and Si III in stars of later type. Ultraviolet line identification lists have been published for τ Her, B5 IV, and ζ Dra, B6 III, by Underhill and Adelman (1977), for γ Peg, B2 IV, by Hill and Adelman (1978) and for ι Her, B3 IV, by Upson and Rogerson (1980). Most B-type stars have normal solar composition (see Chapter 6), and their spectra contain lines from the most abundant elements; the resonance and other strong lines from some rare elements may also be detected in the ultraviolet. In general, few lines from neutral atoms are seen in B-type spectra except for hydrogen, helium, and neon.

Good pictures of high resolution spectra of typical B stars and linear intensity tracings of the blue-violet spectral range have been published by Wright et al. (1964), pictures of high resolution spectra of a few sharp-lined stars are also given, together with line identifications, by Adams and Dunham (1938), Struve (1931a, 1939), and Underhill (1948b, 1948d).

Variation of the Strength of the Lines Along the Main-Sequence Band

The equivalent widths of many lines in the visible region of the spectra of B stars have been measured in attempts to determine abundances. Most of the relevant papers are listed in Table 3-4 as sources for effective temperatures determined from studies of the line spectrum. Figures 3-5 and 3-6 show the variation with spectral type of the equivalent widths of some of the prominent lines in B-type spectra. To prepare these figures, measured equivalent widths were extracted from Unsöld (1942), Underhill (1948c), Wright et al. (1964), Peterson and Shipman

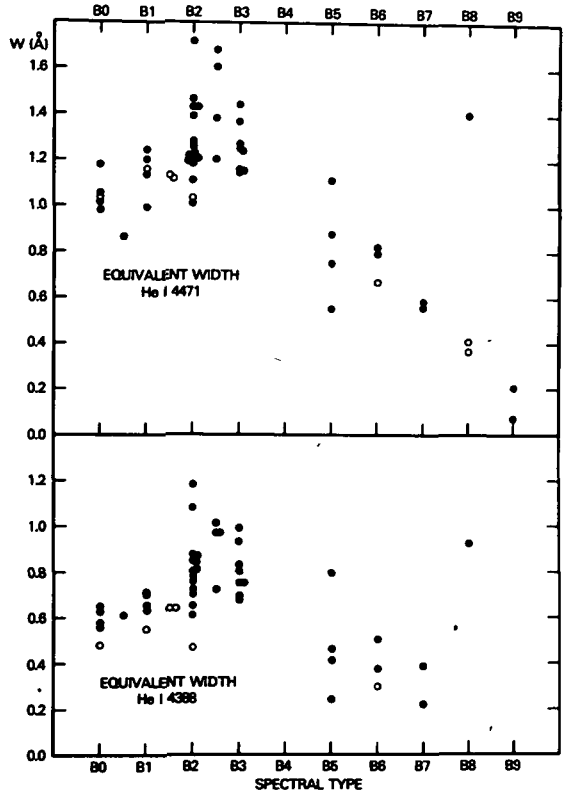

Figure 3-5. The variation of He I line strengths with spectral type. Luminosity class V and class IV stars are represented by filled circles, class III by open circles

(1973), and Adelman (1973) as well as from the sources given in Table 3-4.

Although the measured values of the equivalent widths of lines depend upon the accuracy of the intensity calibration of the spectra used, the amount of scattered light in the spectrograph (which may be non-negligible in the case of grating spectrographs), the spectral resolution of the spectrograph, and the way in which the investigators resolve blends, all published values of equivalent width of the selected lines are combined uncritically in Figures 3-5 and 3-6. In the case of Mg II 4481 and C II 4267 the combined strength of two close lines is used. Some of the scatter in the diagrams is due to observational error in determining equivalent widths and some is due to inconsistencies in the spectral classifications assigned to the various stars For instance, in Figure 3-5 one star is assigned spectral type B8, whereas the measured strength of its He I lines suggests an earlier type.

The He I lines increase in strength from spectral type B9 where they are first recognized on low dispersion spectra, to about type B2. After that they decline in strength, the singlet He I lines declining more rapidly as one moves into the O types than do the triplet He I lines. Among the B stars of the main-sequence band there is a small luminosity effect for the He I lines of the diffuse series owing to Stark effect. Lines such as He I 4471 ($2^3P^o - 4^3$ D) and He I 4388 ($2^1P^o - 5^1$ D) are stronger in luminosity class V than they are in luminosity class III owing to the development of Stark-broadened wings and the appearance of forbidden lines

Typical He I line profiles for a B1 V star are shown in Figure 3-7 which is from Leckrone (1971). These profiles show the difficulties which

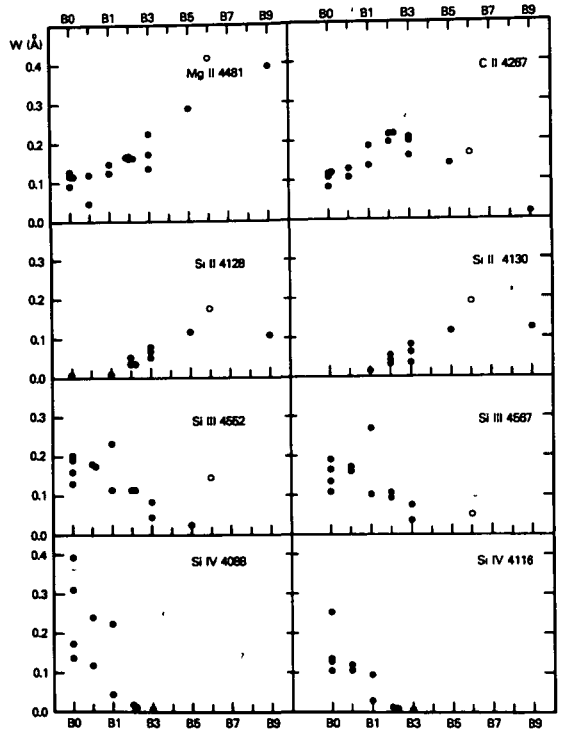

Figure 3-6. The variation of the strengths of lines of Mg II, C II, Si II, Si III, and Si IV with spectral class. Luminosity class V and class IV stars are represented by filled circles; class III by open circles.

exist in obtaining a fit between observation and theory. The theory of the line spectra of B stars is reviewed in Chapter 6 The He I lines from the diffuse series have broad shallow wings which merge slowly with the continuum. The measured equivalent widths can vary by a significant amount depending upon the level at which the investigator drew the continuum and what he did about attempting to exclude the distortions caused by blending lines

The theoretical line profiles shown in Figure 3-7 were calculated using LTE theory of line formation and the best available theory of the Stark broadening of He I The fact that the predicted cores of the strong lines of He I are much shallower than the observed values can be largely corrected by using non-LTE theory

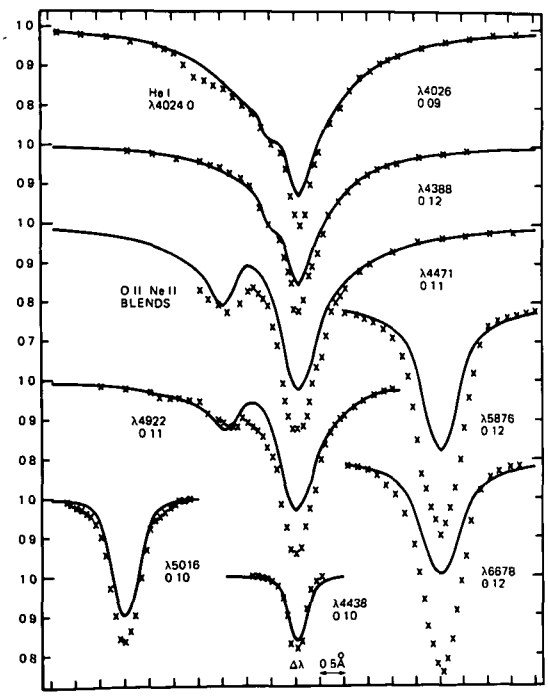

Figure 3-7 Profiles of He I lines in the B1 V star HR 1861 from Leckrone (1971) Observed profiles are shown by crosses, calculated profiles, using LTE theory, by a line The positions of some blending lines are indicated The number lying under the wavelength gives the value of N(He)/N(H) required to obtain a fit between theory and observation in the wings of the line.

(see Auer and Mihalas, 1973a, and Mihalas et al., 1974, where theoretical profiles are given for He I 4471 using the most recent Stark-broadening theory)

In main-sequence stars of types B3 and earlier and in the O stars, the cores of He I 6678, 5876, 4922, and 4471 as well as He I 5015 and 3889, from the 2^1S and 2^3S levels, are observed to be a little stronger than the non-LTE calculations suggest Great strengthening is seen in the spectra of some stars having shells (see Part II) Great strength of the cores of the lines from 2^3P^o can be used as a diagnostic criterion for the presence of a hot, low density plasma with electron temperatures in the range 2.0×10^4 to 5.0×10^4 K and electron density of the order of 10^{13} cm^{-3} occurring in the outer parts of the star. Such conditions lead to a weakening of lines from 2^3S, such as He I 3187 (Dufton and McKeith, 1980) The line at 3187 Å is strongest at electron temperatures near 2.0×10^4 K and it weakens at higher and lower temperatures Since Dufton and McKeith have observed that the line He I 3187 in main-sequence B stars is about twice as strong as computations using non-LTE physics suggest it should be, one infers that the B stars of all subtypes are surrounded by much gas in addition to the usual atmospheric layers, and that the electron temperatures in the gas are near 2.0×10^4.

The variation of the equivalent widths of eight prominent lines in the blue-violet spectral range of B stars is shown in Figure 3-6 A slight luminosity effect is seen in these lines in the sense that these lines tend to be stronger in luminosity class III than in luminosity class V. The blended doublet of Mg II at 4481 Å is strongest at type B9 and declines in strength toward the O stars. Its persistence into the O spectral types is a non-LTE effect (Mihalas, 1972c) The blended doublet of C II at 4267 Å has peak intensity at type B3. At earlier spectral types lines of C III begin to appear The lines of Si II are strongest in the late B-type stars while those of Si III peak near B0. The lines of Si IV appear at about type B2 and increase in strength into the O types where in some luminous stars they appear in emission. The relative

strengths of the silicon lines of all three stages of ionization cannot be represented correctly by LTE theory (Underhill, 1963), use of non-LTE theory (Kamp, 1978) greatly improves the agreement between observation and theory but it does not resolve all the difficulties, much as in the case of He I.

Walborn (1971) has used the relative strengths of lines of Si II, Si III, and Si IV with strengths of the He I lines to devise a detailed spectral classification scheme for stars of types B2.5 through O9. He found that there was a certain ambiguity between the definition of spectral type and luminosity class for this group of stars, particularly for the most luminous stars. He resolved the problem by defining intermediate types between those usually recognized Part of his difficulty is due to the sensitivity to non-LTE effects of the lines of Si III and Si IV which he uses (they are shown in Figure 3-6). Care must be taken to separate the effects due to true high luminosity from those resulting from the presence of hot or cold, low density plasma in a mantle around stars of moderate luminosity.

The strength of the Balmer lines of hydrogen decreases from type B9 through type B0. In the main sequence these lines develop strong broad wings because of the Stark effect. The amount of the Stark effect, measured by the equivalent width of Hγ, by the shape of the wings of Hγ or Hδ, or by the point at which the Balmer series breaks off is used as a criterion of luminosity for the B stars. For the early B stars, the lines of hydrogen, although still strong, have profiles in which the effects of Stark broadening and of rotation combine in such a way as to make it difficult to differentiate from visual inspection of low resolution spectra between spectral type changes and those due to small differences in luminosity. For this reason Walborn attempted to define other luminosity criteria involving the Si II, III, IV, and the He I lines.

The Ultraviolet Spectrum

Much interest attaches to the variation in strength and shape of the resonance lines of the ions of abundant elements as one traverses the spectral sequence from B9 to B0 in the main-sequence band (luminosity classes II, III, IV, and V) In this section, illustrations compiled from observations made by Leckrone and by Underhill with the IUE are presented for spectral types B9 5, B7, B5, B3, and B1. Also the information available in the literature about the behavior of the Mg II lines near 2800 Å in B stars is reviewed The implications concerning the mantles of B stars are noted. Leckrone has graciously made his material available before publication of his research.

Net monochromatic fluxes, corrected for the echelle ripple and for the interorder background obtained using the short wavelength, high resolution echelle spectrograph of IUE are used here to demonstrate how the ultraviolet spectrum changes from type B9.5 to type B1. The resolution element is about 0 12 Å in these spectral tracings. The standard IUE photometric processing has been accepted as valid. It must be recognized, however, that the correction for the interorder background is difficult to determine at wavelengths shortward of 1400 Å because of crowding of the orders. Consequently, the true level of zero intensity in the stellar spectrum is uncertain at the shortest wavelengths. The nominal level of zero intensity is marked on the figures. The intensity tracings are interrupted at the places where reseau marks fall on the spectrum.

The wavelength calibration has been checked for the spectral regions illustrated here by identifying many lines, and the calibration is believed to be accurate The several spectral tracings shown in each figure are aligned to within ±0.1Å The apparent centers of the resonance lines were not used to establish the zero point in wavelength for each section of tracing because we wished to find out whether any displacements in wavelength attributable to outflow exist. No significant displacements of the resonance lines relative to other sharp lines are apparent in the observations used here.

Information about the sharp-lined stars selected as typical for the main-sequence band and for showing changes across the main sequence

at type B5 as the luminosity of the star increases is given in Table 3-6. The spectral types and effective temperatures have been taken from Underhill et al. (1979), when available there. The selected stars are apparently bright and some have been studied many times. The spectral types assigned by Underhill et al. are used here because these types result from an evaluation of all information available in 1978 In other references slightly different spectral types may be found.

The spectral intensities displayed here have been corrected for the wavelength variation introduced by the echelle ripple but not for the wavelength-dependent variation of interstellar extinction. Since each wavelength region used is short, the local continuum may be thought of as a line parallel to the line of zero intensity A reasonable estimate for the level of the continuum is through the highest region shown in each spectral range. The uncertainty in the photometry is of the order of ± 5 percent.

The region near the C II resonance lines at 1334.53, 1335.66, and 1335.71 Å is shown in Figure 3-8 The C II lines are strong in spectral types B3 to B9 5 and they show typical radiation-damping wings. At type B1, only a relatively narrow Doppler core remains. The P III resonance line at 1334 87 Å can be seen easily in the spectrum of HR 1861; it may also be detected for ι Her and perhaps τ Her. The C II resonance lines are not displaced in the stars selected here as representative for sharp-lined, main-sequence stars. If these stars possess a wind this wind does not contain C^+ ions in abundance. The star HR 1861 is sufficiently distant that interstellar absorption may be contributing to the cores seen at the positions of the C II lines.

The region of the C IV resonance lines at 1548.18 and 1550.77 Å is shown in Figure 3-9. The C IV resonance lines are moderately strong at type B1 and they show a slightly extended shortward wing suggestive of a wind containing C^{+3} ions. Weak sharp C IV lines appear to be present at B3 and B5, lines of Fe III in this region dominate in the middle and late B stars.

The region of the A1 III resonance lines at 1854.72 and 1862.79 Å is shown in Figure 3-10. These lines are strong, undisplaced, and essentially symmetrical from type B1 to B9 5, giving no evidence for a wind. Multiplet UV 4 of A1 II, with lines at 1855 93, 1858.03, and 1862.31 Å, also falls in this region. The A1 II lines are moderately strong in types B3 to B9.5 but they have effectively vanished by B1

Table 3-6
Stars Used to Illustrate the Ultraviolet Spectra of B Stars

HD	HR	Name	Spectral Type	T_{eff} (10^4 K)	SWP Image No	Observer
17081	811	π Cet	B7 IV	1 326	1944	DSL
36591	1861	–	B1 V	2 690[a]	4694	DSL
58350	2827	η CMa	B5 Ia	1 298	4304	ABU
147394	6092	τ Her	B5 IV	1 501	3246	DSL
155763	6396	ζ Dra	B6 III	1 296	1827	ABU
160762	6588	ι Her	B3 IV	1 781	3244	DSL
164353	6714	67 Oph	B5 Ib	1.322[b]	1857	ABU
193432	7773	ν Cap	B9 5 V	1.088[b]	1942	DSL

[a]Mean effective temperature for this spectral type
[b]Unpublished result by Underhill
Dashes (–) represents no name for this star

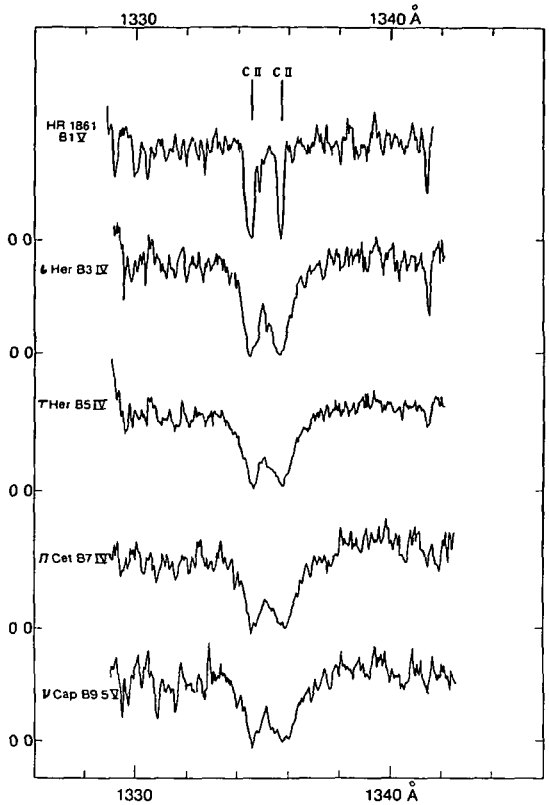

Figure 3-8 The C II resonance lines near 1335 Å. The spectra have been lined up in wavelength using the position of the Si III line at 1341.46 Å as a zero point. The intensity scale is linear, the nominal level of zero intensity being indicated for each spectral tracing. Leader lines show the laboratory wavelengths for the two strong lines of multiplet UV 1 of C II

Several lines of Fe III persist throughout this wavelength region and Fe II becomes strong in stars of types B7 and later. Any winds possessed by these stars are not visible in Al III.

The region of the Si II resonance lines at 1526.71 and 1533 43 Å is shown in Figure 3-11 These lines are strongest at type B9.5, showing damping wings there, and they weaken toward earlier types. At B1 the line at 1526 Å is essentially interstellar, as usual, no interstellar line is seen at 1533 Å because this line arises from the excited level of the ground configuration Lines of Fe III blend in the longward wing of Si II 1526. Since the Si II resonance lines are not displaced and since they do not show shortward extended wings, we may conclude that any winds possessed by these stars contain few Si^+ ions.

The region of the Si IV resonance lines at 1393.76 and 1402.77 Å is shown in Figure 3-12. Both lines are visible at types B5 and earlier, but only the line at 1393 Å, the line with the larger *f*-value, can be surely detected at types B7 and B9 5. Damping wings are beginning to develop at type B3, and by type B1 they are well developed. It will take a detailed, careful study of the shapes of the profiles at type B1 and of the possible blending lines as well as the apparent wavelengths of the lines to deter-

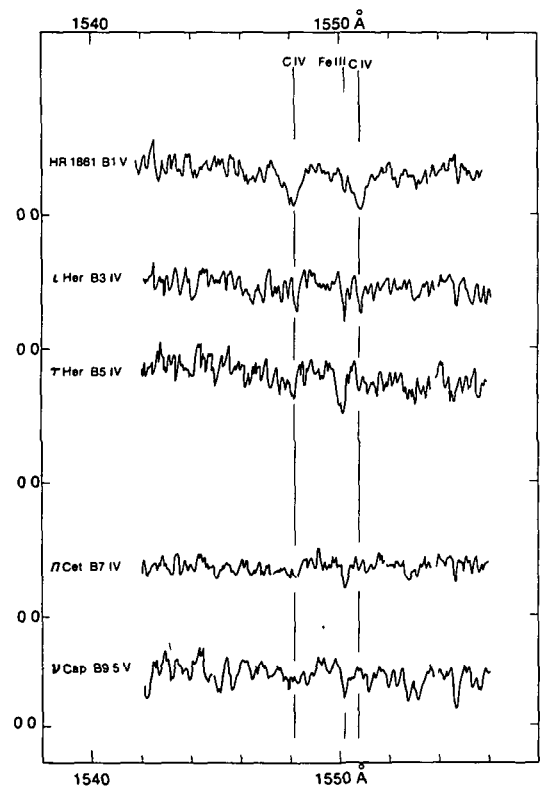

Figure 3-9. The C IV resonance lines near 1550 Å. The spectra have been lined up in wavelength using the position of the Fe III line at 1550 20 Å as a zero point. The intensity scale is linear, the nominal level of zero intensity being indicated for each spectral tracing. Leader lines show the laboratory wavelengths for the two lines of multiplet UV 1 of C IV.

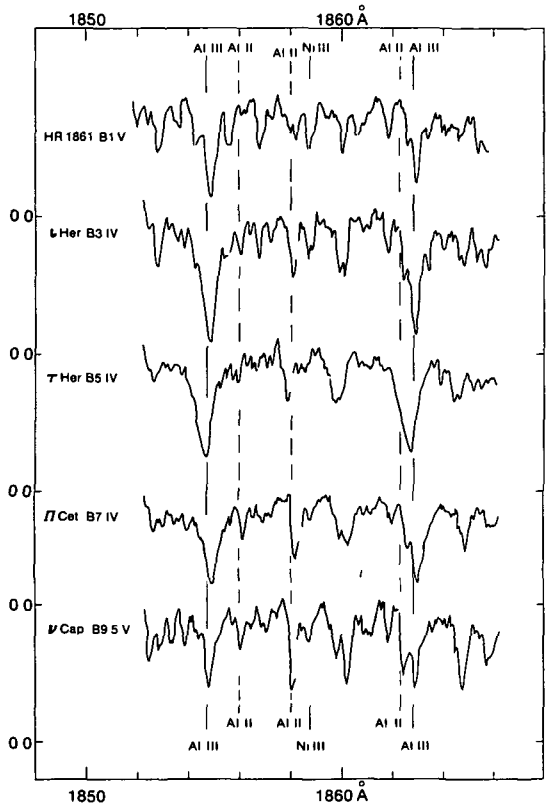

Figure 3-10. The Al III resonance lines near 1860 Å. The spectra have been lined up in wavelength using the position of the Ni III line at 1858 75 Å as a zero point. The intensity scale is linear, the nominal level of zero intensity being indicated for each spectral tracing Solid leader lines show the laboratory wavelengths for the two lines of multiplet UV 1 of Al III, broken leader lines indicate the laboratory wavelengths of lines of multiplet UV 4 of Al II.

mine whether a wind can be seen in the Si IV lines. Any wind possessed by the stars studied here is not conspicuous in Si IV.

The variation of the equivalent widths of the Mg II lines along the main-sequence band through the B types has been studied using observations from the S59 experiment on the TD1 satellite by Snijders and Lamers (1975) and Lamers and Snijders (1975). These authors find that, on the whole, the observed strengths vary about as expected from theory However, in shell stars and in Bp stars, the observed strengths may be greater than normal for the spectral type, presumably owing to extra absorption in the mantle, or weaker than normal, owing to emission from the mantle. Kondo et al. (1976) have used high resolution ultraviolet spectra obtained with Copernicus OAO-3, to look for emission in the Mg II lines from four B stars. Such emission might indicate the presence of gas in the mantles having a temperature near 2.0×10^4 K Possible weak emission features were seen in the spectra of α Gru (B7 III) and β Cen (B1 III), a β Cephei star Observations of other B stars from a balloon (Morgan et al., 1977) and from Copernicus (Kondo et al ,

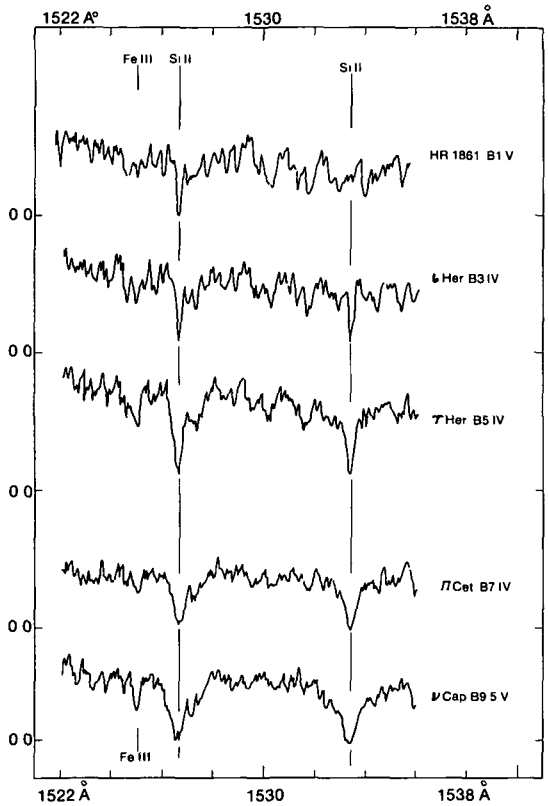

Figure 3-11. The Si II resonance lines near 1530 Å. The spectra have been lined up in wavelength using the position of the Fe III line at 1525 04 Å as a zero point. The intensity scale is linear, the nominal level of zero intensity being indicated for each spectral tracing Leader lines show the laboratory wavelengths of the two lines of multiplet UV 2 of Si II.

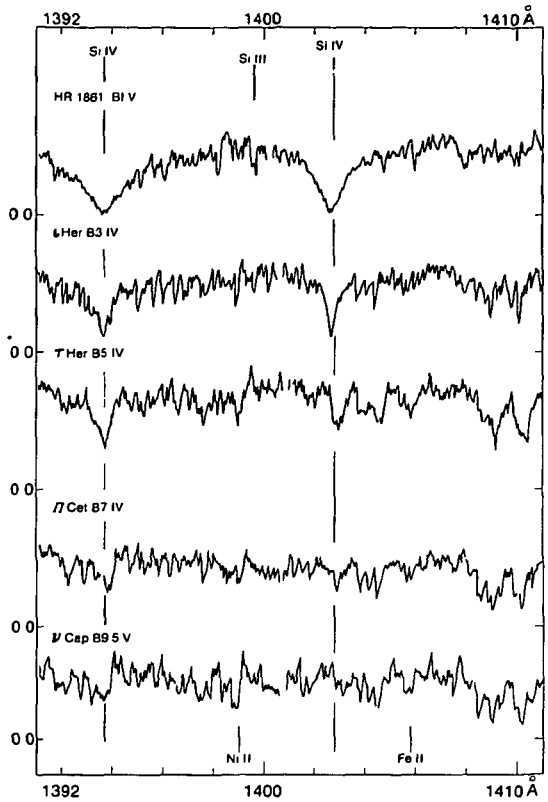

Figure 3-12 The Si IV resonance lines near 1400 Å. The spectra of HR 1861 and ι Her have been lined up in wavelength using the position of the Si III line at 1399 62 Å as a zero point; for τ Her, π Cet and ν Cap, the position of the Ni II line at 1399 03 Å was used. The intensity scale is linear, the nominal level of zero intensity being indicated for each spectral tracing. Leader lines show the laboratory wavelengths of the lines of multiplet UV 1 of Si IV.

1975) provide results similar to those of Lamers and Snijders although with better spectral resolution

A section of the ultraviolet spectrum near 1300 Å is shown in Figure 3-13. Here one may see how lines of Si III, multiplet UV 4, Si II, multiplets UV 3 and 13.04, and of O I, multiplet UV 2 vary along the main sequence. The Si III lines are strong in all the B stars, reaching maximum strength at about type B3 The line of O I 1302 17 Å may have a contribution from the interstellar gas. If the other lines of multiplet UV 2 at 1304.86 and 1306.03 Å are present, as may be the case for the late B stars, a stellar component also exists for O I 1302.17. A remarkable illustration of the increase in radiation damping which results when the lifetime of an upper level is made very short may be seen by comparing the strengths and profiles of lines of multiplets UV 3 and UV 13 04 of Si II. Multiplet UV 3 at 1304.37 and 1309.28 Å is due to transitions from the ground levels of Si II, $3s^2 3p\ ^2P^o$, to the $3s3p^2\ ^2S$ level. A strong interstellar component may contribute to the absorption seen at 1304.37 Å. Multiplet UV 13.04 is caused by transitions between the $3p^2\ ^2D$ and $3p(^3P^o)\ 3d\ ^2F^o$ levels The latter levels straddle the laboratory value for the prime ionization limit of Si II in energy The energy of the prime ionization limit depends upon the electron density in the plasma; in B star atmospheres both of the 3s 3p 3d $^2F^o$ levels can autoionize (Underhill, 1981b). The effect of this is to shorten the lifetime of ions in the 3p 3d $^2F^o$ levels and to result in a large damping constant for the dominant lines of multiplet UV 13.04. Consequently, the lines at 1305.59 and 1309.46 Å, shown by broken leader lines in Figure 3-13, are strong with broad wings. This is obvious at all spectral types in the main-sequence band where Si II is a prominent spectrum

The behavior of the lines of multiplet UV 13.04 of Si II at type B5 as the stars increase in luminosity is shown in Figure 3-14. The radiation damping wings are less striking in the supergiants than in the main-sequence stars. However, some autoionization appears to be occurring still in the supergiants This demonstration that autoionization is significant for the Si II spectrum makes it wise to include autoionization and dielectronic recombination when solving the equations of statistical equilibrium for the Si^+ ions Multiplet UV 13.04 of Si II is anomalously strong also in IUE spectra obtained by Leckrone of the Si stars 108 Aqr and 21 Per.

Through type B along the main sequence, the resonance lines of the light elements behave about as expected according to the theory of stellar spectra (see Chapter 6). Of the stars used here as examples of typical main-sequence stars, only HR 1861 shows slight evidence for

the presence of a wind. If there is outflow from these stars, the density of the flow and the level of ionization is such as to leave very few signatures on the part of the ultraviolet spectrum accessible to IUE. The B0 V star τ Sco is known to show outflow (Rogerson and Lamers, 1975; Lamers and Rogerson, 1978; see the section on Sharp-Lined Constant B Stars) and the star ι Her is a profile variable (Smith, 1978b; see the section on Line-Profile Variables).

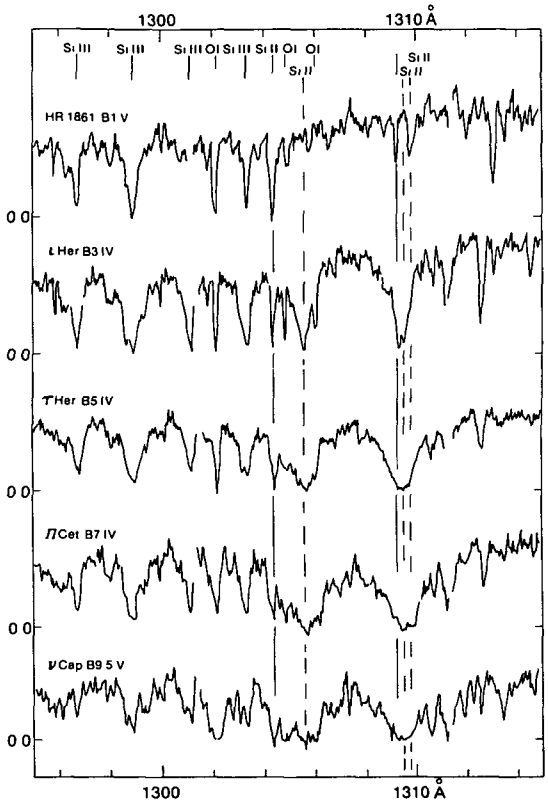

Figure 3-13 The behavior of multiplets UV 3 and 13 04 of Si II along the main sequence, illustrating the effects of autoionization on the damping constant for multiplet UV 13.04 The spectra was lined up in wavelength using the position of the Si III line at 1296 73 Å as a zero point. The intensity scale is linear, the nominal level of zero intensity being indicated for each spectral tracing Solid leader lines show the laboratory wavelengths of the lines of multiplet UV 3; broken leader lines show the laboratory wavelengths of the lines of multiplet UV 13.04.

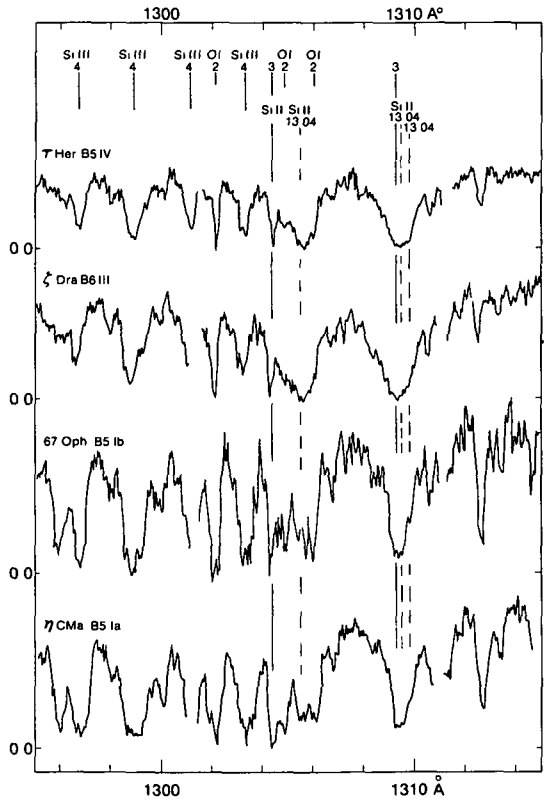

Figure 3-14. The variation with luminosity of multiplets UV 3 and UV 13.04 of Si II at type B5. The spectral tracings have been aligned as described for Figure 3-13.

X-rays have been detected from the star π Cet (Cash et al., 1979). One cannot say that these stars do not have mantles in which outflow is generated and where some parcels of gas are heated to high temperatures. It seems likely that such mantles do exist but that in most cases they have a sufficiently tenuous structure as to be undetectable with IUE.

The ultraviolet spectra of a number of the B stars in the main-sequence band, some of them being emission-line stars, have been surveyed by Snow and Morton (1976) and by Lamers and Snow (1978) using Copernicus. These authors find what is demonstrated above, namely that there is little evidence for outflow from the atmospheres of most normal B stars. Line asymmetries and displacements suggestive of outflow are sometimes seen for stars known to show hy-

drogen lines in emission and/or shell spectra. This topic is discussed further in Part II.

Ultraviolet Line Blocking and Intrinsic Colors

The amount of line blocking in the near ultraviolet spectra of B stars has been measured for 10-Å wide bands in the regions observed by the S59 experiment of the TD1 satellite, that is from 2070 to 2150 Å (the 2100 channel), 2500 to 2590 Å (the 2500 channel), and 2790 to 2860 Å (the 2800 channel). Results for 35 stars of spectral types from B6 to A0 have been presented by Underhill and van der Hucht (1977), while results for 132 stars have been published by Lamers et al. (1978a). The results of Underhill and van der Hucht are based on a preliminary determination of the sensitivity function of the instrument, those of Lamers et al. on the definitive sensitivity function. Although small systematic differences exist between the two sets of results the general trend with spectral type of the line blocking is clear. For main-sequence stars of type B, on the average about 5 to 10 percent of the light observed in the 2100 and 2500 channels is removed in each 10-Å wide band from a smooth continuum The actual amount of light removed depends on the precise wavelength of the band considered and the spectral type of the star. In the 2800 channel, the amount of blocking increases to 15 percent in the late B stars with the Mg II lines becoming prominent in spectra of type B8 and later. The line blocking is larger in the spectra of supergiants than it is in main-sequence stars of the same subtype. This is particularly true in the regions where lines of Fe III and Cr III are abundant.

Lamers et al (1978a) have listed intrinsic magnitude differences (colors), $m^c_{\lambda_i} - m^c_{\lambda_{i+1}}$, for each star using photometry in four wavelength bands having nominal wavelengths such that λ_i = 2100, 2500, 2800, and 5480 Å. These colors represent the shape of the continuum which Lamers et al. have adopted after consideration of the detailed shape of the continuum from model atmospheres. It is found that intrinsic magnitude difference ($m^c_{2500} - V_0$) is a sensitive function of spectral type, changing from −3.0 at type B0 to +0.5 at type A4.

The intrinsic ultraviolet colors of main-sequence B stars have been determined by Wesselius et al. (1980a) from a study of ANS intermediate-band photometry (see the section on Observations Concerning the Shape and Absolute Value of the Ultraviolet Continuous Spectrum). Wesselius et al. compared the observed colors with those predicted by means of the Kurucz line-blanketed model atmospheres. For the B stars, the observed shape of the spectrum agrees well with that which is predicted over the wavelength range from 1550 to 5500 Å.

VARIATIONS IN LIGHT AND SPECTRUM

When the sharp-lined B stars lying in the main-sequence band are observed with ground-based, high precision (error $\lesssim$ 1 percent) spectroscopic and photometric equipment, many of these stars are found to vary in light and to show changes in the profiles of some of their absorption lines. The occurrence of spectral changes had been suspected for some of these stars for a long time (see Underhill, 1966a), but photographic techniques did not permit a definitive answer to be found In the visible wavelength range, the amplitude of the light changes is usually small; in the ultraviolet it may be larger. However, far fewer ultraviolet observations are available for analysis than visible observations, so our knowledge of the variations in light and spectrum of the sharp-lined B stars is based primarily on the visible range.

As two stars revolve around one another, the amount of light received from the binary system may change in a periodic manner and some spectroscopic changes may be seen. These effects are due to the different geometric aspect presented to the observer at different phases of the binary system and they are not what will be discussed in this section Rather, we shall try to summarize the information which is available about the intrinsic changes that occur in the amount of light and the line spectrum emitted

by single main-sequence B stars. It has been known for a long time that Be stars often vary irregularly in light by a small amount and that their spectrum may change. These stars are described in Part II. The light and spectrum changes of B-type supergiants are described in Chapter 4.

Intrinsic changes that are periodic may be caused by the pulsation of the star in either radial or nonradial modes or in both. The nonradial modes considered for interpreting B-type spectra are traveling surface waves that are generated by some internal intrinsic instability of the star just as the radial pulsations of the star are. Radial pulsation is believed to be the dominant source of the spectrum and light variations of classical Cepheids and of long period variables. The effects of waves of various types in the solar atmosphere are reviewed in Jordan (1981).

It has been known since the beginning of the twentieth century that a few early type B stars show light and radial-velocity changes of small amplitude in periods of the order of 4 to 6 hours. These are the Beta Cephei or Beta Canis Majoris stars and they are described in Chapter 5. These stars are intrinsic variables which have much in common with the other pulsating variables seen at later spectral types. However, in the case of the B stars, we shall see that the pulsating variables do not seem to be the sole occupants of an area in the HR diagram, in contrast to the situation for pulsating stars of later spectral type. Beardsley et al. (1980) have shown that three of the bright, sharp-lined late B-type stars in the Pleiades show radial-velocity changes suggestive of pulsation with short periods, 0.10 to 0.27 day. Changes in the shapes of the line profiles also are seen to occur.

Careful observation has shown that many of the apparently bright B stars vary in light periodically and that some show changes of their line shapes which repeat periodically. The amplitude of the light changes in the visible range is usually less than 0.03 mag, while the line-shape changes can only be detected with the most precise spectrophotometry at high spectral resolution. This type of intrinsic variable, the 53 Persei variable, is the subject of this section Most of the work on these stars has been done by M.A. Smith and his colleagues at the University of Texas working in the visible spectral range with solid state detectors and high resolution spectrographs.

Changes in the amount of light received from a star in a restricted passband and in the shape of the line profiles imply that the physical conditions change in the photosphere of the star and/or in the mantle or outer atmosphere. An interpretation made by fitting predicted line profiles and energy distributions from classical model atmospheres to the observed data allows one to infer the changes in effective temperature and log g, or radius, which may have occurred. Changes in these two parameters imply changes in the energy generation cycle in the interior of the star and/or of the mechanisms which control how effectively the energy travels through the envelope of the star. On the other hand, the spectroscopic changes which are seen in some lines may be, at least in part, due to changes in the character and efficiency of the physical processes controlling the state of the mantle. In this case, the observed variations would be giving information chiefly about conditions at the surface of the star This possibility is attractive because it makes it easier to understand the observed fact (see below, Chapter 5, and Chapter 7), that radially and nonradially pulsating stars as well as stars not known to pulsate seem to lie in about the same place in the HR diagram.

Line-Profile Variables (53 Persei Variables)

Intensive observation at a resolution of 0.1 Å with solid state detectors of the Si II lines at 4128 and 4130 Å and of the Si III lines at 4552, 4567, and 4574 Å of sharp-lined B stars by M. A. Smith and his colleagues (see Smith, 1978a, 1980c, for reviews) have shown that almost all of the stars observed show periodic changes in the shapes of their line profiles. At the same time, detailed photometric work (see, for instance, Percy and Lane, 1977, Buta and Smith, 1979, Smith and Buta, 1979, and Percy,

1980), has shown that most of these stars show periodic, small amplitude changes in brightness. Small changes in equivalent width can be detected for lines not on the flat part of the curve of growth, and the radial velocity of the star may vary by a small amount.

The line-profile variable stars have been designated as "53 Persei" variables after their prototype. These stars lie in the main-sequence band in the same general region as the β Cephei stars do. This is shown by Figure 3-15 which has been taken from Smith (1980c) It may be shown by extracting data from published photometric catalogues that other B stars also fall in this general area. Detailed descriptions have been published of the spectral changes of the following stars: 53 Per (Smith and McCall, 1978; Buta and Smith, 1979), ι Her and 10 Lac (Smith, 1978b); 22 Ori (Smith, 1980a); υ Ori (Smith, 1981a). Sometimes the change in line strength is such that very weak lines—"phantom lines"—can be detected at some epochs but not at others (Smith, 1981b).

The observed changes in line profile are varied, a weak wing sometimes appearing on the longward side of the line and sometimes on the shortward side. Smith and Stern (1978) have shown that the observed changes can best be interpreted as being caused by nonradial pulsation and that the determination of the period and mode of the pulsation by the methods described by Smith (1978b) and by Buta and Smith (1979) are reliable. A study of the β Cephei star 12 Lac (Smith, 1980b) has shown how the method of profile fitting can be used to verify four modes of pulsation, one radial and three nonradial.

With nonradial pulsation, there are distinct

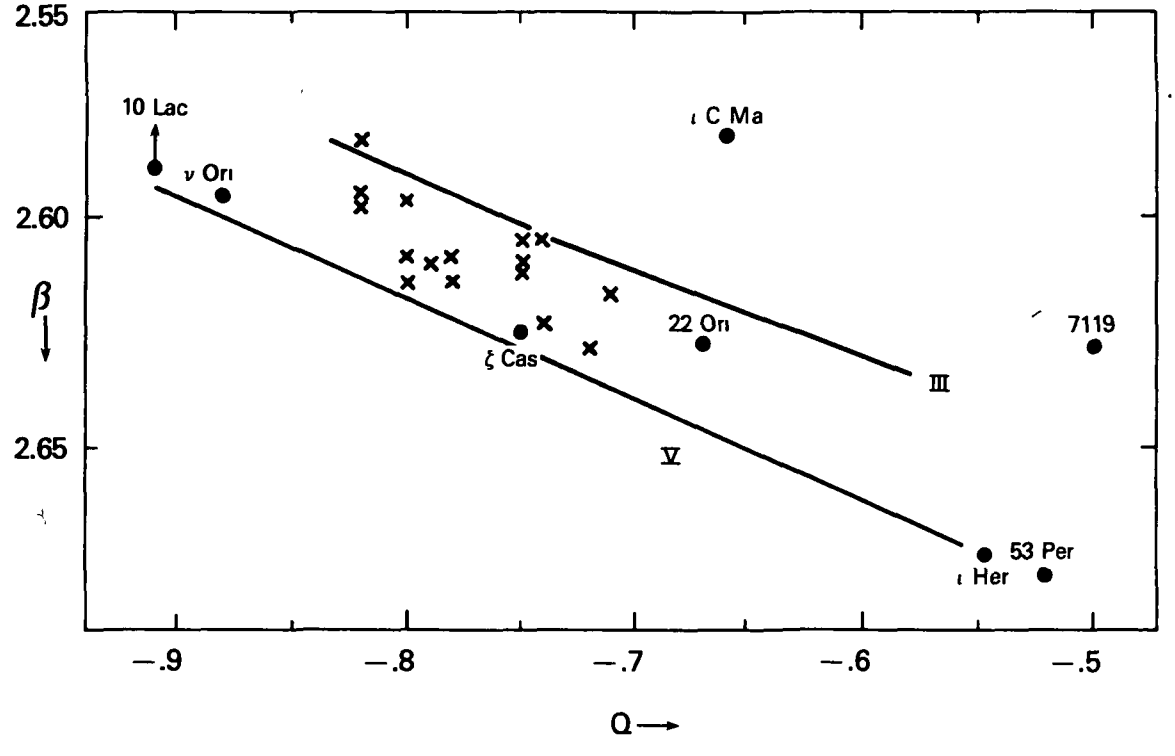

Figure 3-15. A photometric HR diagram for B stars in the main-sequence band. The Q index is a quantitative measure of the spectral type of the star (see Chapter 2) while the β index measures the luminosity of the star. The line-profile variables are shown by points and are named; the positions of β Cephei stars are shown by crosses (from Smith, 1980c). The star near 10 Lac is Upsilon Ori.

periodic changes in the shape of the line wings, but the displacements of the lines change by only a small amount Also with nonradial pulsation there is a small periodic change in magnitude (for instance, in the v band of the uvby photometric system), but very little change in the v − b or b − y color For radial pulsation, the changes in color and radial velocity are quite significant Large profile variations and small radial-velocity changes usually mean that the active mode is a sectorial wave traveling around the equator.

The periods of the line-profile (53 Per) variables lie in the range between 3.6 hours (Smith and McCall, 1978b) and 2 days (Buta and Smith, 1979), typically they are near 12 hours. However, the periods are highly unstable, each having a typical lifetime of 1 month or so. The same period will often recur. Frequently, the periods found are nearly in the ratio of 2 1, but noninteger values of the ratio of new to old period are observed. It is possible to consider that several modes having different periods are present all the time and that the amount of energy in each mode changes in a matter of months, one mode being the most visible one for 1 month or so, another at a later time. This behavior is called "mode switching." The periods are too long to arise from radial pulsation or from p-mode nonradial pulsation.

The rapid time scale for mode changes (they occur in a few days) suggests that the nonradial oscillations are excited in the stellar envelope rather than in the core. Smith (1980b) has considered the necessary conditions for the transfer of energy between modes and he believes that the fact that the lifetime of any one mode of a 53 Per star is short means that the driving mechanism in the stellar envelope, for any particular mode, has a variable efficiency It seems unlikely that the mode changes are caused by events in the core of the star

Sharp-Lined Constant B Stars

Most sharp-lined B stars, when they are observed intensively, turn out to show low amplitude, line-profile and magnitude changes. However, Smith and Stern (1978) were able to show that any changes exhibited by the peculiar B star 3 Cen A were below a low detection limit. This star is discussed in Chapter 5; it is believed to be rich in ^{3}He.

The star τ Sco, B0 V, also shows no line-profile changes. However, the lines are asymmetric (Smith and Karp, 1978, 1979) with an extended wing shortward. Smith and Karp have shown that the line profiles in the visible spectrum can be described in terms of a rotational velocity of 5 km s^{-1}, radial-tangential macroturbulence of 6 km s^{-1}, and microturbulence of 3 km s^{-1}. The slightly depressed shortward wing can be described as the result of a systematic outflow occurring deep in the photosphere. This outflow does not necessarily imply a large mass flux through the atmosphere. Similar line widths and slightly depressed shortward wings were found also for lines in the 1000 to 1100 Å region and they can be described by similar parameters as are required to describe the visible spectrum In the ultraviolet, the strong, relatively sharp lines are shortward displaced by about 6 km s^{-1} with respect to the weak, sharp lines Smith and Karp (1979) conclude that an outward flow of matter is present even in the deep photospheric layers of τ Sco. The methods used to interpret the line profiles do not permit Smith and Karp to specify exactly the geometry of the flow, that is whether it is a cellular or a unidirectional flow

The ultraviolet spectrum of τ Sco has been studied in detail by Lamers and Rogerson (1978) who followed up the discovery by Rogerson and Lamers (1975) of the outflow from τ Sco of highly ionized material. Figure 3-16 displays spectral tracings (from Lamers and Rogerson, 1978) in the neighborhood of the resonance lines of O VI, N V, Si IV, and C IV. The profiles of these resonance lines are formed in the mantle and they have the typical shape of lines formed in a rapidly flowing wind (see Chapter 6, Extended Moving Atmospheres). In the mantle the degree of ionization is high and one sees evidence for an expansion velocity which increases to about 2000 km s^{-1} The resonance lines of O VI and N V extend in absorption longward for a short distance. This is interpreted by Lamers and Rogerson as evidence for "turbulent" velocities

of the order of 150 km s^{-1} in the mantle because no significant absorption in the O VI and N V lines is to be expected from the photosphere of τ Sco. The photosphere can be represented by a classical model atmosphere having T_{eff} near 3 1 X 10^4 K and log g near 4 2 (see Table 3-4). According to Lamers and Rogerson, heating to a temperature near 2 X 10^5 K occurs in the mantle before the velocity outward has reached a value greatly different from 0 km s^{-1}. This result is obtained by assuming that the ionization of oxygen is caused by collisions with electrons.

The intrinsic sharpness of most of the absorption lines in the spectrum of τ Sco is shown well in Figure 3-16. It is for lines like these that Smith and Karp (1979) found a small depressed shortward wing.

The strong symmetrical absorption line at about − 1900 km s^{-1} in the top panel of Figure 3-16 is Lβ, which is mostly due to interstellar absorption. The moderately strong, fairly sharp line at +2100 km s^{-1} in the second panel is due to C III 1247..

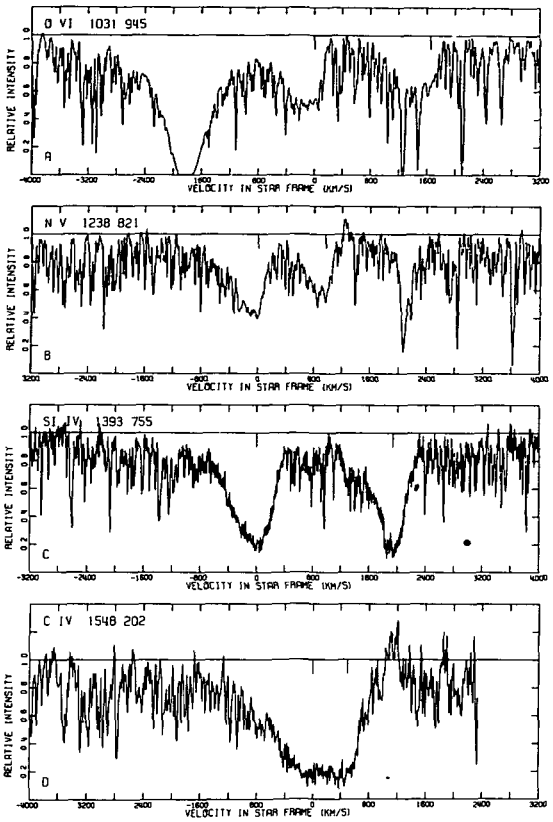

Figure 3-16. Parts of the ultraviolet spectrum of τ Sco near the resonance lines of O VI, N V, Si IV, and C IV as observed by Corpernicus. The laboratory wavelength of each line in these doublets is marked at the top of each panel The adopted continuum was determined from an inspection of a wavelength region of 50 to 100 Å in the vicinity of the lines (from Lamers and Rogerson, 1978).

DISCUSSION

We have noted that when interpreting the continuous and line spectra of B stars, it is helpful to think in terms of a model consisting of a photosphere and a mantle, the mantle being the outer part of the atmosphere where the effects of nonradiative heating are seen. The results of our survey of the spectra of B stars shows that conditions in the photosphere determine most of what is seen, and in the case of most B stars the presence of mantles can be detected only by subtle effects.

It turns out that the shape of the continuous spectrum and the total amount of light radiated per unit surface area by the B stars of the main-sequence band can be well represented by means of classical, line-blanketed model atmospheres calculated using the constraints of radiative, hydrostatic and local thermodynamic equilibrium. This conclusion is demonstrated in Figure 3-2, where the shape of the spectrum of η UMa, B4 V, from the ultraviolet to the infrared, is compared to that from a classical model atmosphere. The star η UMa has one of the most accurately determined energy distributions of any astronomical object and its energy is known from 1200 Å to 12 6 μm (see Table 3-2).

We see that the shape of the predicted spectrum from a model atmosphere in which account is taken of line blanketing as well as of the dominant sources of continuous opacity (see Kurucz, 1979) is very closely similar to what is observed for η UMa. This comparison and work on other stars has shown that assuming plane-parallel layers of gas and using LTE physics provides

adequate modeling for predicting the continuous spectrum from the ultraviolet through the infrared for normal stars in the main-sequence band.

In the case of Bp and Ap stars, shallow broad dips appear in the continuous spectrum at 4200, 5300 and 6300 Å which are not present for normal stars. Jamar et al. (1978) have suggested that these dips may be due to autoionization in the spectrum of Si II. Evidence for a related effect in the Si II spectrum has been noted in the section on Variation of the Strength of the Lines Along the Main-Sequence Band. It is demonstrated that exceptionally strong radiation damping wings are present for the absorption lines of multiplet UV 13.04 of Si II in the spectra of normal B stars. This exceptional broadening of the lines of multiplet UV 13.04 is also seen in the spectra of Si stars Clearly autoionization and the inverse process, dielectronic recombination, should be taken into consideration when determining the fraction of Si present as Si^0, Si^+, and Si^{++} in the atmospheres of B stars.

The effective temperatures of the B stars in the main-sequence band, determined from integrated flux and angular diameters, range from about 1.0×10^4 K at type B9 to about 3.1×10^4 K at type B0 (see Table 3-5). There is no significant dependence, at any B type, on luminosity class over the range V to II. Effective temperatures determined from the relative strengths of lines from elements present in two stages of ionization tend to be higher by 1.0×10^3 to 3.0×10^3 K than the effective temperatures determined from measurements of the continuous spectrum. This suggests that the relative strengths of the absorption lines are giving us information about elevated electron temperatures in a superheated mantle. Except for this small but systematic effect, the mantles of stars in the main-sequence band have little influence on the spectrum in the visible range.

Often the mantles of stars are revealed by spectroscopic details seen in the ultraviolet. However, in the case of the normal B stars of the main-sequence band, the major resonance lines in the ultraviolet part of the spectrum give very little evidence for either outflow or the presence of gas at high temperature. This is the reverse of what is found for the B-type supergiants (see Chapter 4).

It is possible, as Figure 3-9 shows, that the lines of C IV of the B1 V star HR 1861 are slightly asymmetric, but the deepest parts of these lines are not displaced by a significant amount. The profiles and wavelengths of the Si IV lines in the stars studied here are equally definite in providing very little evidence for the presence of superheated gas and outflow along the main sequence Although Snow and Morton (1976) and Lamers and Snow (1978) have indicated that evidence for outflow from a few B stars of the main-sequence band can be seen on Corpernicus spectral tracings, we must conclude that detectable outflow is not a common state of affairs and that the amount of gas in winds originating from normal B stars is small. Furenlid and Young (1980) have observed distortions in the shapes of the Hα profiles from rotating B stars which they suggest are the result of outflow from these stars.

Small parcels of very hot gas could be present in the mantles of the normal B stars and not be detected using IUE. The observation of X-rays from π Cet, B7 IV, by Cash et al. (1979), proves this point, for the ultraviolet spectrum of this star gives no obvious evidence for the presence of hot gas or outflow, as Figures 3-8 to 3-13 show

The star τ Sco, B0 V is quite atypical of B stars in the main-sequence band in that its ultraviolet spectrum gives clear evidence for outflow and the presence of high temperature gas (see Figure 3-16). Rogerson and Lamers (1975) first recognized the significance of the ultraviolet spectrum of τ Sco. Smith and Karp (1978, 1979) have shown that many of the weak lines formed in the photosphere of τ Sco have an extended shortward wing which suggest the presence of flow deep in the photosphere. This type of behavior has not been seen for other apparently bright, sharp-lined B stars possibly because of the distortion of the line profiles in these stars by nonradial pulsation. However, most of the apparently bright, sharp-lined B stars (see the

section on Variations in Light and Spectrum) do give evidence for the occurrence of nonradial pulsation in their photospheres with small periodic line-profile changes and changes in light. Because the nonradial pulsation is observed to change rather rapidly from one mode to another, Smith (1980b) considers that the cause of the nonradial pulsation is likely to be found in the upper part of the stellar envelope. It seems unlikely that the mode changes are caused by events in the core of the star Probably more than a coincidence is that the line-profile variables, the β Cephei stars, and stars for which no periodic variation of the spectrum is known occur in the same area of the HR diagram.

A suspected infrared excess and emission in the Balmer and Paschen continua of hydrogen can be detected and evaluated quantitatively for B stars of the main-sequence band by comparing the observed energy distributions of stars showing emission lines with the energy distributions of model atmospheres having effective temperatures similar to those estimated, perhaps from the assigned spectral type. Such theoretical energy distributions provide a reasonable first approximation for the energy distribution coming from the photospheres of emission-line stars. Care must be taken to evaluate the correction for interstellar extinction accurately before carrying out such a comparison

Any estimate made in this way of the amount of excess radiation emitted as continuous radiation by an abnormal star will be, of course, only a crude first estimate. This is because proceeding in the manner indicated implicitly assumes (1) that the photosphere of an abnormal star can be represented, to a first approximation, by the photosphere of an equivalent normal star, and (2) that the features leading to the classification as an abnormal star arise from a surrounding, abnormal mantle It is implicit in the second assumption that the surrounding mantle has no significant influence on the physical state of the photosphere of the underlying star. Although the last hypothesis is unlikely to result in a wholly valid representation of the actual situation, it is a useful hypothesis because the energy stream coming from the core of the star appears to be the dominating influence determining the physical state of the photospheres of most stars. If the spectrum of a star contains enough nearly normal absorption lines to result in classification as a B spectral type, modified by the addition of the letters *e* or *p*, it is likely that the photosphere is nearly normal. This statement is based on the general experience that the two factors which determine the physical state of the outer boundary layers of stars, that is, of the photospheres, are the total radiation stream, specified by the effective temperature, and the radius of the star, or $\log g$. Here we are carefully distinguishing the outermost parts of the star, or mantle from the photosphere. In the mantle, the physical state is largely determined by the deposition of non-radiative energy and momentum. A discussion of this question together with a suggestion concerning the source of the non-radiative energy and momentum is given in Chapter 8.

If conditions in the mantle have a strong effect on conditions in the photosphere, then it will be impossible to assign a spectral type suggestive of a normal type, one will have to model the entire structure of photosphere and mantle ab initio in order to obtain an understanding of the physical situation implied by the spectrum of the abnormal star. When the results summarized in this chapter are compared with those predicted by the theory of stellar atmospheres (see Chapter 6) it is clear that most of the details in the spectra of normal B stars can be understood quite well. There are discrepancies that point to the existence of mantles around the normal B stars, but the mantles are not a necessary part of the models required for understanding most of the spectrum. What causes mantles to exist is an interesting question which has not yet been solved.

4

OBSERVATIONS OF B-TYPE SUPERGIANTS

INTRODUCTION

The B-type supergiants are luminous stars with M_V near − 7.0 for the Ia stars and near − 6.0 for the Ib stars. Because their absorption lines have a typical "chunky" look, supergiants are easily recognized by means of spectra of moderate dispersion covering the blue-violet spectral region The cores of the lines are rather broad, the sides are steep, and the wings are small or nonexistent The lines of the Balmer series of hydrogen show little Stark effect and the Balmer series in the B Ia supergiants extends to about n = 22 (see Underhill, 1970) A weak, variable emission line is often seen at Hα for the Ia supergiants, but rarely for the Ib supergiants. The spectral classification of B supergiants and the general properties of B supergiants have been presented in Chapter 2

Careful photometry of the B supergiants using intermediate-band filters, such as that reported by Sterken (1977) and by Rufener et al. (1978), has shown that often B-type supergiants vary in light with a peak-to-peak amplitude between 0 035 and 0.065 mag in the visual range The semi-period of the variations in light, although not well defined, tends to increase as the spectral type becomes later, being of the order of 16 days for middle B supergiants and 36 days for middle A supergiants (Sterken, 1977, Burki et al., 1978) The shapes and strengths of some lines in the spectra of supergiants also have been observed to change irregularly. In this chapter we will discuss the spectra of the B-type supergiants and attempt to develop a descriptive model for the atmospheres of these rather rare stars.

The use of a two-part model atmosphere consisting of a photosphere and a mantle, as introduced in Chapter 1, is particularly helpful for understanding the spectra of B-type supergiants. We shall see that the photosphere, which is the place of origin of the continuous spectrum in most spectral regions, can usually be represented well by a classical model atmosphere consisting of plane-parallel layers of gas in hydrostatic, radiative, and statistical equilibrium. However, the conspicuous lines in the spectrum are formed in a part of the atmosphere lying outside the photosphere, that is in the mantle In the mantle the effects of the deposition of nonradiative energy are seen and large-scale motions, including outflow, occur Consequently, model atmospheres based on the classical constraints of radiative and hydrostatic equilibrium have little validity for representing the mantle. The observation of short-lived changes in the profiles of strong lines and of the sporadic appearance of sharp displaced absorption lines makes it seem probable that the structure of the mantle is inhomogeneous

In the case of the Sun, which is a low luminosity star, the mantle (chromosphere and corona) is known to be inhomogeneous. In fact, in a review article Vaiana and Rosner (1978) have emphasized that inhomogeneity is an essential property of the mantle of the Sun. We shall see that inhomogeneity probably is an important characteristic of the mantles of the B-type supergiants.

It is not certain, a priori, that the mantles of B-type supergiants are spherical. Hot stars which have a nonspherical shape usually show intrinsic polarization. In the case of some Be stars, intrinsic polarization is known to occur In some cases, the polarization has been found to vary (see Part II)

Polarization measurements for 12 B-type supergiants have been listed by Serkowski (1968, 1970). Four of the supergiants in Serkowski's lists show variable polarization They are HD 41117 χ^2 Ori (B2 Ia), HD 79186 (B5 Ia), HD 148379 (B2 Iap), and HD 169454 (B1 Ia+) The fact that the degree of polarization is variable suggests that the shape of the supergiant is not spherically symmetrical and that changes in shape occur Since the polarization measurements have been made using broadband filters, the observations imply an intrinsic polarization of the continuous spectrum This intrinsic polarization is believed to result from electron scattering in the outer parts of the atmosphere of the supergiant

The effective temperature and diameter of a B-type supergiant give a quantitative measurement of the total amount of energy emerging from the core of the star. Our present knowledge concerning the important parameters, T_{eff}, and radius, $R/R_{\odot}$, of B-type supergiants is reviewed in the section on Effective Temperatures, Radii, and Bolometric Corrections for Supergiants. Such data are fundamental for placing the B-type supergiants in an observational HR diagram so that the stage of evolution of the supergiants may be inferred and the internal consistency of the present theories of the evolution of massive stars may be evaluated. This subject is discussed further in Chapter 7.

In the mantle, the physical conditions are a result of the nonradiative energy deposited there and of the passage of radiation from the underlying photosphere. Analysis of spectral features formed in the mantle should lead to a determination of the physical state of the mantle. However, the art of diagnosis is presently in a preliminary stage, and we are still discovering which spectroscopic features to analyze in order to determine information about the photosphere and which to determine the physical state of the mantle.

In the case of the early B-type supergiants the mantle is most easily seen by means of the ultraviolet resonance lines. What the ultraviolet spectra reveal is reported in the section on Ultraviolet Spectrum of Supergiants at High Resolution. Evidence is found suggesting electron temperatures greater than the effective temperature of the star, outflow, and inhomogeneity. In the case of the late type B supergiants, it is difficult to find spectroscopic features which can be analyzed to give information about the mantle. Consequently, little information exists about the mantles of late B supergiants

Observations of the visible spectrum are summarized in The Visible Spectrum of Supergiants. These observations give information about the photosphere as well as about the mantle.

Estimates of the electron temperature in the outer regions of the mantle can be obtained if one is able to detect excess free-free emission in the near infrared Let F_{λ} represent the free-free excess energy at wavelength λ per unit wavelength interval It is found that when one plots log λF_{λ} vs. log λ, a curve results which rises sharply as wavelength increases, reaching a maximum at a wavelength λ_p, and then declines. Simple considerations (see, for instance, Cohen et al., 1975) suggest that λ_p should be related to the electron temperature, T_e (assumed constant), by the condition that

$$\lambda_p T_e = 1.44 \times 10^4 \text{ K} \qquad (4\text{-}1)$$

Here λ_p is in μm and T_e is in degrees Kelvin Use of Equation (4-1) for a few late B-type supergiants for which the necessary observations exist (see the section on The Infrared and Radio Spectrum of Supergiants) has shown that the electron temperature in the outer mantle is near 2 2 $\times$ 10^4 K. Thus, for the supergiants studied by this method, T_e, in the part of the mantle from which the free-free radiation is radiated, is about two times the effective temperature of the star.

The spectrum of the peculiar supergiant P Cyg shows many of the special features of supergiant spectra to an enhanced degree. The obser-

vations of this star are discussed in The Peculiar Supergiant P Cyg and the Superluminous Supergiants.

The masses of stars are most directly determined from the motion of the stars in binary orbits. A few B-type supergiants are known to be the most luminous components of X-ray binaries. What our observation of X-ray binaries implies about the properties of B-type supergiants is briefly summarized in X-Ray Binaries. In the final section of this chapter, a discussion is given of the implications concerning the physical state of supergiants resulting from the observations summarized in this chapter, and a comparison is made with what is known about B stars in the main-sequence band.

EFFECTIVE TEMPERATURES, RADII, AND BOLOMETRIC CORRECTIONS FOR SUPERGIANTS

How to determine the effective temperatures of B stars has been described in Chapter 3. The direct method is described in the second section of Chapter 3 along with three indirect methods. These methods have been applied to supergiants and the results will be summarized here.

On the average, supergiants are more distant than stars of similar apparent magnitude in the main-sequence band, with the result that most B-type supergiants suffer significant wavelength-dependent interstellar extinction. Therefore, an important preliminary step when determining the effective temperatures of supergiants by the direct method, which makes use of the integrated flux from the star, or by indirect methods based on comparing the shape of the observed spectrum with that from a model atmosphere is to determine the interstellar extinction along the line of sight to each supergiant. Some B-type supergiants are known to show Hα as a weak emission line Consequently, one must be alert to the possibility that the apparent energy distribution of the star may be modified by continuous emission in the Balmer and Paschen continua of hydrogen and by emission of a free-free continuum. It may be necessary to correct the observed continuum fluxes for the presence of this excess radiation.

Two ways of estimating the color excess $E(B - V)$, which is used to scale the interstellar extinction law, are (1) by comparing the observed $(B - V)$ color of a supergiant with the empirical intrinsic color $(B - V)_0$ for its spectral type, and (2) by finding that value of $E(B - V)$ needed to compensate for the depth of the absorption band near 2200 Å caused by interstellar material A similar procedure to method (2) is to make use of an empirical correlation between the depth of the diffuse interstellar band at 4430 Å and $E(B - V)$. However, since the 4430 Å band is much weaker than the 2200 Å band and the correlation is not tight, the uncertainty in the resulting $E(B - V)$ determined in this way may be greater than when the 2200 Å band is used. A third way is to use correlations between the intensity of the interstellar Lα line and $E(B - V)$.

When using photometric measurements to establish $E(B - V)$ for a star, it is important to use an empirical relationship between intrinsic color and spectral type, such as that by FitzGerald (1970), rather than to make use of intrinsic colors calculated from model atmospheres. This is because continuous excess emission extending into the visible spectral range is present for some B supergiants, particularly those of late B types (see below), this excess emission reddens the intrinsic color from what a model atmosphere predicts. The empirically determined $(B - V)_0$ for each spectral type takes account of the intrinsic reddening due to the presence of an infrared excess extending into the visible range in a statistical manner

The question of whether the infrared excesses of B-type supergiants and other types of B stars may originate from a circumstellar cloud of dust and gas left over from the formation of the star has been considered by Pecker (1963, 1972) He has adopted the point of view that residual circumstellar matter may absorb some of the energy emitted by the star in the visible and ultraviolet wavelength ranges causing an apparent reddening of the star; in addition, he believes that this absorbed radiation is emitted as an infrared excess.

The point of view adopted here is that the observed energy distribution from a B-type star, after correction for wavelength-dependent interstellar extinction, can be interpreted as being caused by the radiation emerging from the photosphere plus any contribution which may arise from the mantle. Furthermore, it is assumed that the effective temperature of the star is determined by the angular diameter of the star and the integral over all wavelengths of the monochromatic flux received at the Earth from the photosphere alone after this flux has been corrected for interstellar extinction (Equation 3-9).

The fact that the intrinsic colors of B-type supergiants are redder than those of main-sequence stars of the same spectral type (see Chapter 2) can be understood by noting that the effective temperatures of B-type supergiants are lower than those of main-sequence B stars of the same subtype, and by noting that in the case of supergiants of types B5 Ia to B9 Ia, an infrared excess which extends to about 5000 Å is present

An additional reason for believing that the infrared excess radiation of B-type supergiants is principally caused by free-free emission rather than by radiation from dust, is the fact that Hα is seen in emission in those supergiants with the most prominent infrared excesses If Hα is in emission, we must expect to see emission in the other parts of the hydrogen spectrum including the bound-free and the free-free continua.

One of the puzzling results of the first ultraviolet photometry of B-type supergiants was the observation that the amount of energy in the ultraviolet relative to that in the V band was less than was found for main-sequence B stars of the same subtype (Chapter 2). Because of the difficulty of determining accurately the interstellar extinction suffered by supergiants, it was not clear whether the deficiency of ultraviolet light of supergiants was evidence for an intrinsic difference between supergiant and main-sequence stars of the same subtype or merely evidence of an imprecise determination of the interstellar extinction (see, for instance, the discussions by Carruthers, 1969, and Mihalas, 1970a). Humphries et al. (1975) showed from ultraviolet spectrophotometry done with the S2/68 experiment on the TD1 satellite conclusive evidence for intrinsic differences between B-type supergiants and main-sequence stars of the same subtype. Humphries et al compared the energy distributions of supergiants and main-sequence stars having similar small amounts of interstellar extinction and the same spectral type and derived differences in color temperature using a baseline of some 4000 Å. They found that the color temperature of a B1 supergiant is about 3.0×10^3 K lower than that of a main-sequence B1 star. At B5 the difference is about $1\ 7 \times 10^3$ K, while at B8 it is about $1\ 0 \times 10^3$ K If one equates color temperature to effective temperature then these differences indicate that the effective temperatures of B-type supergiants should be significantly lower than effective temperatures of main-sequence B stars Barlow and Cohen (1977) used the temperature differences of Humphries et al to derive an approximate effective temperature scale for early type supergiants, working from the effective temperature scale for main-sequence B stars of Schild et al (1971). Flower (1977) has interpolated a temperature law for supergiants using the temperatures found by Code et al (1976) as a base

An effective temperature scale for supergiants in the range O4 to B3 has been given by Panagia (1973). He assumed that the effective temperatures for supergiants in the range O9.5 to B3 were $0\ 9 T_{\rm eff}$(Lum. C1 V), and adopted the effective temperature scale of Morton and Adams (1968) for B stars in luminosity class V. Modern work supersedes his ad hoc results

In the case of B stars in the main-sequence band, matching the observed size of the Balmer jump to that computed from a model atmosphere and saying that the effective temperature of the selected model atmosphere is the effective temperature of the star gives results consistent with those from direct determinations of $T_{\rm eff}$ (see Chapter 3) This important indirect method for determining effective temperature has the advantage that it is insensitive to the amount of interstellar extinction However, it cannot be used for supergiants because the observed Balmer jumps are much smaller than the theoretical values resulting from model atmospheres which,

on general grounds, should be representative for the photospheres of the supergiants It will be shown that the discrepancy occurs because the supergiants all show continuous emission in the Balmer continuum This emission is not seen separately on the low dispersion BCD spectra in the way that Balmer jumps in emission are seen for some Be stars (see Part II), because the emission begins at about the same wavelength as does the absorption discontinuity due to the confluence of the Balmer lines formed in the photosphere This near coincidence of wavelength between the Balmer jump formed in the photosphere of the supergiant and that (in emission) formed in the mantle of the supergiant indicates that the electron densities are comparable in parts of the photospheres and mantles of B-type supergiants. In the case of Be/shell stars, there is a clear separation on BCD spectra between the absorption discontinuity due to the photosphere and the discontinuity (in emission or in absorption) due to the mantle. This means that there is a significant difference in density between the photosphere and the mantle of a Be/shell star. Inglis and Teller (1939) showed that in a stellar atmosphere the observed wavelength of the Balmer discontinuity is a function of the electron density in the stellar atmosphere.

Many years ago Chalonge and Divan (1952, 1973) remarked on the small values found for D in the spectra of B-type supergiants. However, they could not discuss the meaning of their observations owing to the absence of appropriate predicted spectra for supergiants with which to compare More recently Schild and Chaffee (1975) have obtained spectrophotometric scans, 50-Å wide pass bands, for 17 luminous stars having spectral types in the range O9.5 to B2. They found that the apparent size of the Balmer jump correlated neither with spectral type (effective temperature) nor with luminosity, and that it was smaller for these stars than for main-sequence stars of similar spectral types, as was first demonstrated by Barbier and Chalonge (1939a) They gave no explanation for the observed state of affairs, which is contrary to the known behavior for main-sequence stars. Use of the concept of a photosphere and a mantle allows us to understand the observations in the way sketched above.

Use of the third important indirect method for determining effective temperature, namely representing by means of model atmosphere calculations the relative intensities of lines in two stages of ionization seen in the visible spectrum of the star, results in effective temperatures for B supergiants that are higher than those found by the direct method These results will be discussed in Indirect Determinations of Effective Temperatures. In the remainder of this section, the quantity determined by the direct method is called the *effective temperature of the supergiant*. This number is believed to be a measure of the amount of radiation crossing each square centimeter of surface per second. Ultimately the radiation stream originates in the core of the star and is a result of nuclear burning taking place there.

Direct Determinations of Effective Temperature and Radius

The first direct determinations of effective temperature and radius for B-type supergiants were made by Code et al (1976), who used monochromatic fluxes obtained with the OAO-2 satellite and ground-based photometric observations to find the integrated flux from each star. They adopted the angular diameters measured by Hanbury Brown et al (1974) by means of an intensity interferometer The list of stars studied by Code et al. contains four supergiants, ζ Ori A_1 (O9 5 I), ϵ Ori (B0 Ia), η CMa (B5 Ia), and β Ori (B8 Ia) The results for these four stars have been confirmed by Beeckmans (1977a), who made use of ultraviolet fluxes from the S2/68 experiment on the TD1 satellite (Jamar et al., 1976) and the same ground-based photometry and angular diameters as used by Code et al., these stars also appear in the study by Underhill et al. (1979).

Effective temperatures for 16 supergiants in the spectral type range O9.5 to B9 have been determined by Underhill et al (1979) using the S2/68 bright star ultraviolet photometry (Jamar et al , 1976) and the 13-color photometry in the visible and near infrared of Johnson and Mitchell

(1975). The method of Underhill et al is described in Chapter 3, and tests of the accuracy of the results are reported there. This method has been used by Underhill (1979b, 1980c, 1981a) to determine the effective temperatures of 14 more supergiants with spectral types in the range B0 to A2. In these studies Underhill makes use of the S2/68 faint star photometry (Thompson et al., 1978), photometry with the ANS satellite (Wesselius et al., 1980b), and other ground-based photometry as well as the 13-color photometry. She has found that the work of Underhill et al. (1979) can be made more consistent for stars of type B5 and later by correcting for the infrared excess which extends into the visible spectral range.

Directly determined values of the effective temperature are collected in Table 4-1 for 30 supergiants of types O9.5 to A2. Information on the interstellar extinction suffered by these stars and on the angular diameters and linear radii which result from the adopted distances is given. The adopted values of $E(B - V)$ were selected after considering all available information on this subject The uncertainty in $E(B - V)$ is of the order of ± 0.02 mag, an amount which is too small to bias the determinations of effective temperature by a significant amount. The notes to the table give alternative results found in studies other than those selected for entry in Table 4-1.

The effective temperatures of the supergiants are shown plotted against spectral type in Figure 4-1. A line (long dashes) has been sketched to show a possible effective temperature–spectral type law for the supergiants. The average effective temperature law for stars of luminosity classes IV and V (from Table 3-5) is shown as a dotted line. It is clear that throughout type B, the effective temperatures of supergiants are lower than those of main sequence stars of the same subtype.

The uncertainty in the effective temperatures given in Table 4-1 is less than ± 5.0×10^2 K in the best cases. It is unlikely to exceed ± 1.0×10^3 K Consequently, the effective temperature law for B-type supergiants is well defined; the same law is found for the Ia and the Ib supergiants.

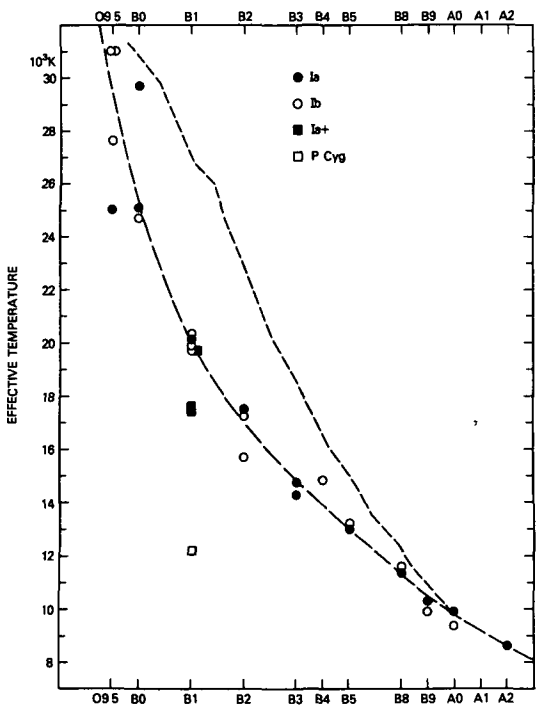

Figure 4-1. The effective temperature–spectral type relation for B-type supergiants. The dotted line represents the average effective temperature–spectral type relation for B stars of luminosity classes IV and V. The star P Cyg has an effective temperature typical of B7 rather than B1, which is its spectral type.

However, in two cases out of three, the stars which are classified as B1 Ia+ have lower effective temperatures than the B1 Ia or B1 Ib stars; the peculiar supergiant P Cyg, B1 Iap, is a B7 star according to its effective temperature.

Two of the hottest supergiants have effective temperatures and spectral types that do not agree well with the average effective temperature law for O9/B0 supergiants. They are 15 Sgr which is classified as B0 Ia (O9.7 Iab according to Walborn, 1973), but has an effective temperature typical of a star of type O9.5, and α Cam which is classified as O9.5 Ia but has an effective temperature typical of a B0 Ia star. Among the luminous stars having effective temperatures near 2.6×10^4 K, one also finds the WN7 stars (see Underhill, 1981a). Quite clearly, in the case of luminous stars having effective temperatures in

Table 4-1
The Effective Temperatures and Radii of B-Type Supergiants

HR No	Name	Spectral Type	$E(B-V)$ (mag)	θ (10^{-4} arcsec)	T_{eff} (10^4 K)	d (pc)	$\frac{R}{R_\odot}$	Notes
1542	α Cam	O9 5 Ia	0 30	2 92	2 5000	1175	37	1
1852	δ Ori	O9 5 I	0 05	4 26	3 1080	345	16	1
1948	ζ Ori	O9 5 I	0.06	5 27	2 7580	350	20	1,2
7589	188209	O9 5 Ib	0 20	1 09	3 1080	1652	19	1
1903	ϵ Ori	B0 Ia	0 09	7 08	2 5090	470	36	1,3
6822	15 Sgr	B0 Ia[a]	0 31	1 55	2 9700	1940	32	4
8209	69 Cyg	B0 Ib	0 17	1 19	2 4700	1930	25	4
130	κ Cas	B1 Ia	0 34	3 90	2 0100	960	40	5
1203	ζ Per	B1 Ib	0 31	7 02	1 9870	363	27	1
4133	ρ Leo	B1 Ib	0 07	3 18	2 0300	630	22	5
6262	ζ^1 Sco	B1 Ia+[b]	0 65	5 39	1 7600	1970	114	6,7
6462	γ Ara	B1 Ib	0 06	4 10	1 9710	583	26	1
—	169454	B1 Ia+	0 95	3 18	1 7400	2560	87	6,8
7678	190603	B1 Ia+[c]	0 78	3 72	1 9700	2030	81	5,8
7763	P Cyg	B1 Iap	0 35	4 12	1 2200	1200	53	5
2135	χ^2 Ori	B2 Ia	0 45	4 25	1 7460	1300	59	1
6743	θ Ara	B2 Ib	0 08	4 05	1 7230	461	20	1
8279	9 Cep	B2 Ib	0 46	4 35	1 5730	708	33	1
2653	o^2 CMa	B3 Ia	0 05	5 87	1 4760	843	53	1
7977	55 Cyg	B3 Ia	0 55	5 31	1 4270	1072	61	1
2596	ι CMa	B4 Ib	0 10	3 38	1 4860	685	25	1
2827	η CMa	B5 Ia	0 00	7 69	1 3020	608	50	9,10,11
6714	67 Oph	B5 Ib	0 11	4 40	1 3220	540	25	10,11,12
589	53 Cas	B8 Ib	0 41	3 62	1 1600	930	36	10
1713	β Ori	B8 Ia	0 00	25 10	1 1380	228	62	10,11,13
1035	21291	B9 Ia	0 41	7 27	1 0310	1030	80	10,11,14
8541	4 Lac	B9 Ib	0 11	4 59	0 9930	608	30	1
1040	21389	A0 Ia	0 54	8 05	0 9890	1000	87	10,11,14
3975	η Leo	A0 Ib	0 02	6 90	0 9400	540	40	10,11,15
7924	α Cyg	A2 Ia	0 03	21 07	0 8640	450	102	10,11,14

[a] O9 7 Iab (Walborn, 1973)
[b] This star is classified as B1 5 Ia+p by Lesh (1972)
[c] This star is classified as B1 5 Ia by Lesh (1968)

Notes to Table 4-1

1 Data from Underhill et al (1979)
2 Hanbury Brown et al (1974) give $\theta = (4\ 8 \pm 0\ 4) \times 10^{-4}$ arcsec, Code et al (1976) give $T_{eff} = 2\ 991 \times 10^4$ K, Beeckmans (1977a) gives $T_{eff} = 3\ 063 \times 10^4$ K
3 Hanbury Brown et al (1974) give $\theta = (6\ 9 \pm 0\ 4) \times 10^{-4}$ arcsec, Code et al (1976) give $T_{eff} = 2\ 482 \times 10^4$ K, Beeckmans (1977a) gives $T_{eff} = 2\ 408 \times 10^4$ K
4 Data from Underhill (1981a)
5 Data from Underhill (1979b)
6 Data from Underhill (1981a)
7 The distance comes from assuming $M_V = -8\ 7$
8 The distance comes from assuming $M_V = -8\ 3$
9 Hanbury Brown et al (1974) give $\theta = (7.5 \pm 0\ 6) \times 10^{-4}$ arcsec, Code et al (1976) give $T_{eff} = 1\ 331 \times 10^4$ K, Beeckmans (1977a) gives $T_{eff} = 1\ 330 \times 10^4$ K, Underhill et al (1979) give $T_{eff} = 1\ 298 \times 10^4$ K
10 Data from Underhill (1980c)
11 The fluxes longward of 4030 Å have been corrected for an infrared excess which extends into the visible
12 The distance comes from assuming $M_V = -5\ 0$
13 Hanbury Brown et al (1974) give $\theta = (25\ 5 \pm 0\ 5) \times 10^{-4}$ arcsec, Code et al (1976) give $T_{eff} = 1\ 155 \times 10^4$ K, Beeckmans (1977a) gives $T_{eff} = 1\ 141 \times 10^4$ K, Underhill et al (1979) give $T_{eff} = 1\ 178 \times 10^4$ K
14 The distance comes from assuming $M_V = -7\ 1$
15 The distance comes from assuming $M_V = -6\ 0$

the range 2.5×10^4 to $3\,1 \times 10^4$ K, more than one spectral type may be associated with a given effective temperature. We have noted above that all of the stars classified as supergiants of type B1 do not have effective temperatures near the value 2.0×10^4 K, which is typical for normal B1 supergiants. It is apparent that the criteria which have been empirically selected to determine spectral subtype among the B supergiants do not ensure a single-valued relationship between effective temperature and spectral type.

A typical scale of effective temperature as a function of spectral type, valid for B supergiants, is given in Table 4-2. It has been found by reading the effective temperature law shown in Figure 4-1 to the nearest 5.0×10^2 K. The temperature law for supergiants proposed by Barlow and Cohen (1977) is also given in Table 4-2 These two temperature laws agree remarkably well considering the difference in the methods used to obtain each set of results.

A temperature law for supergiants as a function of B − V has been deduced by Flower (1977). For the B-type supergiants he has used the effective temperatures of Code et al (1976) and the B − V colors of FitzGerald (1970). Flower tends to assign a somewhat higher effective temperature for each spectral class than we adopt here The temperature scale for B-type supergiants of Table 4-2 and Figure 4-1 is preferable to that of Flower because it is based on more material than was available to Flower. Flower has also interpolated effective temperature scales for main-sequence and giant B stars from the results of Code et al., using the intrinsic colors of FitzGerald. These scales differ a little from those presented in Table 3-5, Flower's effective temperatures for a given value of B − V tending to be higher than those given in Table 3-5.

The data given in Table 4-2 confirm the conclusion reached in Chapter 3 for the B stars of the main-sequence band, namely that color temperatures derived on a baseline which extends from the visible spectral range to the ultraviolet usually agree well with effective temperatures determined by the direct method from angular diameters and integrated fluxes

In order to use both the direct method and the indirect method based on the shape of the spectrum, it is essential to determine the wavelength-dependent correction for interstellar extinction in a reliable manner. This means finding accurately a value of $E(B-V)$ with which to scale the adopted interstellar extinction law, which is given by a table of values of $A_\lambda/E(B-V)$ as a function of λ. One way of checking that the correction for interstellar extinction is adequate is to compare the shape of the corrected energy distribution for the star with that of an energy distribution from a model atmosphere If the

Table 4-2
Typical Effective Temperatures for Supergiants

Spectral Type	T_{eff} $(10^4$ K)[b]	T_{eff} $(10^4$ K)[a]	Spectral Type	T_{eff} $(10^4$ K)[b]	T_{eff} $(10^4$ K)[a]
O9.5	2.95	3 00	B5	1.30	1 350
B0	2.50	2.50	B6	1.25	1.290
B0.5	2.25	2 20	B7	1.20	1 240
B1	2.00	2 00	B8	1.15	1.150
B1.5	1.85	1 90	B9	1.05	1.080
B2	1.70	1 80	A0	0.95	0 960
B3	1.50	1.50	A1	0.90	0.933
B4	1.40	1 43	A2	0.85	0 904

[a] Barlow and Cohen (1977)
[b] Based on Figure 4-1

differences between the two energy distributions reflect the shape of the interstellar-extinction law, it is likely that the adopted value of $E(B-V)$ is in error A sensitive wavelength range in which to make the comparison is in the neighborhood of the interstellar absorption band at 2175 Å. If the differences, when plotted as a function of wavelength have another form, then additional information must be used to determine whether the adopted interstellar extinction law has an incorrect shape, or whether the star really does not produce a spectrum shaped like that from the adopted model atmosphere The effective temperatures presented here and those of Barlow and Cohen (1977) were obtained using the interstellar extinction law of Nandy et al (1975, 1976)

If light from a strong infrared excess extends to 5000 or 6000 Å and no correction is made to the observed fluxes for the presence of this light, then an angular diameter found by means of Equation (3-8) will be too large The error is subtle, for it may seem in a first trial that θ_λ depends on λ because of an incorrect estimate of $E(B-V)$ and the true dependence of θ_λ on λ may be nullified by taking a larger value of $E(B-V)$ than is really required. When an infrared excess is known to exist at wavelengths longer than 1 μm, it is wise to use the method described in Underhill (1979b) to correct the observed fluxes in the 5000 Å to 1 μm range for the infrared excess before proceeding with a determination of θ and T_{eff}. When this correction procedure is used, one cannot determine the dispersion about the mean value of θ arising from the errors of observation and the lack of fit between the shape of the model fluxes and the observed fluxes This situation arises because all deviations are thrown into the value deduced for the infrared excess and the shape of the corrected flux distribution is forced to be that of a model atmosphere.

The following results show the effect of neglecting to correct for an infrared excess

Star	η CMa	B5 Ia	β Ori	B8 Ia
Item	$E(B-V)$	θ	$E(B-V)$	θ
Units	mag	10^{-4} arcsec	mag	10^{-4} arcsec
Hanbury Brown et al. (1974)[a]	0.00	7.5 ± 0.6	0 00	25.5 ± 0.5
Underhill et al. (1979)[b]	0.04	8.62 ± 0.09	0.04	26.67 ± 0.35
Underhill (1980c)[c]	0.00	7 7	0 00	25.1

[a] Measured with the intensity interferometer.
[b] No correction made for an infrared excess
[c] After correcting for an infrared excess.

When an infrared excess is allowed for, the angular diameters found by means of Equation (3-8) agree well with the measured values. When the presence of an infrared excess is not recognized (Underhill et al., 1979), a small value of $E(B-V)$ is deduced and, although the dispersion of the individual values about the mean is made acceptably small, the value of the angular diameter is systematically too large by about 10 percent. However, as shown by the notes to Table 4-1, the error in effective temperature is insignificant. Both η CMa and β Ori are apparently bright stars at small distances (see Table 4-1), so it is reasonable to expect that they should suffer little or no interstellar extinction.

Indirect Determinations of Effective Temperature

When the observed shape of the spectrum from a B-type supergiant, corrected for interstellar extinction, is found to match well the

shape of the spectrum from a model atmosphere, the effective temperature of the model atmosphere may be taken to be equivalent to the effective temperature of the supergiant Effective temperatures determined in this indirect way usually agree fairly well with those determined from the integrated flux. The temperature scale of Barlow and Cohen (1977) is typical of the results that may be attained. It is essential to know the correction for interstellar extinction accurately and to work over a wide wavelength range.

A second indirect way of determining the effective temperatures of stars is by matching the observed size of the Balmer jump to that predicted by means of a model atmosphere and equating the effective temperature of the star to that of the model which gives a best fit. If the comparison is carried out over a restricted wavelength range near 3750 Å, it is not necessary to know the correction for interstellar extinction accurately. This method works well for B stars in the main-sequence band, but it does not work for supergiants because the Balmer continuum is in emission in most B supergiants

Figure 4-2 shows the observed energy distribution, corrected for interstellar extinction, of five B-type supergiants compared with the energy distributions from model atmospheres having effective temperatures like those of the stars. The directly determined effective temperatures for these stars are given in Table 4-1. The model atmospheres are fully line-blanketed and their spectra have been computed by Kurucz (1979) using LTE physics. The shape of the spectrum over the wavelength range shown is not sensitive to the value of log g which is used to make the model atmosphere. Usually the lowest value of log g given by Kurucz has been selected. The theoretical energy curves have been fitted to the observed energy curves between 4000 and 4100 Å. The fitting is done here because in this spectral range the stellar continuum is minimally disturbed by infrared free-free emission and by absorption lines.

The various sources of photometry used for Figure 4-2 and the width of the pass bands have been described in Chapter 2. The plotted points

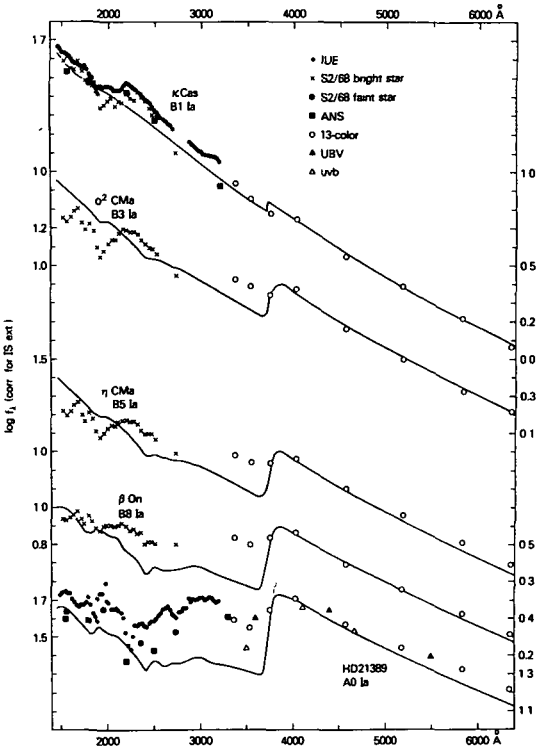

Figure 4-2. Observed energy distributions for B supergiants corrected for interstellar extinction compared to the observed energy distributions from Kurucz (1979) model atmospheres. For κ Cas, E (B − V) = 0 34, and the model has T_{eff} = 2 0 × 10^4 K, log g = 2.5; for o^2 CMa, E(B − V) = 0.05, and the model has T_{eff} = 1 5 × 10^4 K, log g = 3.0, for η CMa, E(B − V) = 0.00, and the model has T_{eff} = 1.3 × 10^4 K, log g = 3.0; for β Ori, E(B − V) = 0.00, and the model has T_{eff} = 1 1 × 10^4 K, log g = 2.5; for HD 21389, E(B − V) = 0.54, and the model has T_{eff} = 1.0 × 10^4 K, log g = 2.5. The units of flux are 10^{-10} ergs cm^{-2} s^{-1} Å^{-1} for κ Cas, o^2 CMa, and ηCMa, 10^{-9} ergs cm^{-2} s^{-1} Å^{-1} for β Ori, and 10^{-11} ergs cm^{-2} s^{-1} Å^{-1} for HD 21389.

(crosses) from the S2/68 *Bright Star Catalogue* (Jamar et al., 1976) have been smoothed by forming a running mean of 3 points. As one goes from spectral type A0 Ia to B1 Ia, the spectrum becomes steeper, much as the model atmosphere spectra do. The IUE absolute fluxes have been determined from low dispersion spectra taken with the star in the large aperture. In deriving Figure 4-2, the energy calibration regularly used

by the IUE project has not been corrected in the way recommended by Bohlin and Holm (1980). The resolution element for the low dispersion IUE spectra is between 6 and 7 Å. A continuum was drawn through the high points of each spectral range and the intensity of this reference level was measured every 25 Å. The IUE fluxes should give an upper limit corresponding to the classical continuum of the star. The fluxes from the S2/68 experiment, from the ANS satellite, and from the filter photometers which are used with ground-based telescopes include the blanketing caused by the absorption lines which fall in each pass band. They present lower limits to the continuum flux. The stars β Ori, η CMa, and o^2 CMa are too bright for observation by IUE.

Although the supergiants are known to be variable stars of small range and although the observations shown in Figure 4-2 were obtained at different epochs, the observed energies trace out spectrum envelopes which are reasonably well defined Typically, the error in the energy plotted at each point is 10 percent This error is caused by the variability of the star, by the inhomogeneities in the absolute calibrations which have been used, and by the inherent difficulties of measuring energy accurately in many pass bands. Thus, typically, deviations of the order of or less than 0.04 dex should be ignored.

Three significant types of departure occur from the spectral shapes predicted by means of model atmospheres.

1 Absorption dips due to blended Fe III, Cr III, and similar lines are present. The dip near 1900 Å is chiefly due to lines of Fe III, that near 2250 Å, visible best in the A0 Ia star, is due to Cr III.
2 An emission continuum starting near 3700 Å is apparent for all of the stars. It is probably due to the Balmer continuum of hydrogen. This continuum increases in intensity relative to the nearby continuum as the spectral type becomes later.
3. An infrared excess extending to approximately 5000 Å is visible for η CMa, β Ori, and HD 21389 At type B3 and earlier the infrared excess is detected only longward of 2 μm

From the observations shown in Figure 4-2, it is clear why a color based on the fluxes at about 1600 and 4000 Å is a good measure of the effective temperatures of B stars. At these wavelengths the observed fluxes fit the model flux distributions rather well and there is little likelihood that the observed fluxes will be seriously contaminated by emission continua or by exceptionally strong absorption lines formed in the mantle. It is obvious that the apparent size of the Balmer jump is not a good criterion for determining the effective temperatures of B-type supergiants because emission from the mantle reduces the Balmer jump in absorption formed in the photosphere to a small value.

A third, indirect way of finding the effective temperature of a star is by adopting the effective temperature of the model atmosphere which reproduces well the relative strengths of lines from elements which are present in two stages of ionization. This value may be called T_{eff}(line). This method selects that model atmosphere which has electron temperatures in the layers important for forming the prominent lines which are like those in the line forming layers of the star These layers compose the deepest part of the mantle. Invariably, the effective temperature determined in this way is higher than the effective temperature found directly from the angular diameter and integrated flux

Generally, the use of non-LTE physics for analyzing stellar spectra improves the accuracy of the representation of the equivalent widths of lines of different strengths with one adopted abundance and without the assumption of microturbulence, but it does not remove the systematic trend that T_{eff}(line) is larger than the value of T_{eff} which is found directly. The most probable explanation for this result is that the lines which have been analyzed are formed chiefly in parts of the mantle where heating has occurred owing to the deposition of nonradiative energy This subject is discussed in greater depth in Chapter 6

Discussion

The effective temperatures of B-type super-

giants are significantly lower than those of main-sequence stars of the same subtype. This is because the subtype is determined by the relative strengths of empirically selected lines which are visible on low dispersion spectra and for the supergiants the classification lines are formed mostly in the mantle where superheating has occurred as a result of the deposition of non-radiative energy In the case of the main-sequence stars (see Chapter 3) the superheating of the low layers of the mantle is smaller in amount and T_{eff}(line) is close to, although higher than, T_{eff} determined directly Because the effective temperatures of supergiants are significantly lower than the effective temperatures of main-sequence stars, the supergiants radiate less ultraviolet light relative to what the main-sequence stars radiate for equal brightness in the visible region

The fact that the intrinsic visible colors of early B supergiants are red relative to the intrinsic visible colors of B main-sequence stars of the same subtype can be understood in terms of the difference in effective temperature In the case of the late B supergiants, additional reddening may be caused by light contributed by a free-free infrared excess which extends into the visible spectral region This excess radiation can be seen in Figure 4-2 for η CMa, β Ori, and HD 21389 The electron temperature in the region which is radiating the free-free emission seems to be of the order of 2.2×10^4 K. Since the effective temperatures of the supergiants which show a strong infrared excess are less than or equal to 1.3×10^4 K, we deduce that the emitting region is superheated by nonradiative energy.

The radii of the B Ia supergiants increase from about 35 solar radii at type B0 to about 87 solar radii at type A0; the B Ib stars are smaller. Since the effective temperatures of Ia and Ib supergiants of the same subtype are about the same, the radii differ by an amount sufficient to account for the difference in visual absolute magnitude

Bolometric Corrections

The bolometric corrections, BC, for B-type supergiants can be estimated from the calculations of Buser and Kurucz (1978). The value is insensitive to the choice of log g. Results valid for stars having log g in the range 2.5 to 3.0 are given in Table 4-3. Thus, if the spectral type of a B supergiant is known, one may obtain an estimate of the star's effective temperature by entering Table 4-2 or using Figure 4-1, and of its BC by entering Table 4-3 The appropriate factor to use is BC' of Buser and Kurucz which is equal to BC. (calc.) + 0 100

Proceeding in this way assumes that the B supergiants radiate over the full spectral range like model atmospheres do for an assigned effective temperature. The effective temperatures used to develop Figure 4-1 and Table 4-2 are probably upper limits because no correction has has been made for the flux contributed by the emission in the Balmer continuum and in the infrared excess This energy is generated by the nonradiative energy sources which heat the mantle. The amount of radiative energy from the mantle is small in comparison to that generated in the interior of the star and radiated from the photosphere as the continuous spectrum of the star. Consequently, the error in the effective temperature is probably negligibly small.

A scale of bolometric corrections for B-type stars as a function of B − V has been presented by Flower (1977). Flower's bolometric corrections are not quite as large as those of Table 4-3 for a given value of the effective temperature of a supergiant.

THE VISIBLE SPECTRUM OF SUPERGIANTS

The most striking factor which differentiates the visible spectra of supergiants from those of stars of similar subtype but having luminosities such that they lie in the main-sequence band is the shape of the absorption lines This is best seen by comparing high dispersion, high resolution spectra of such a quality that the instrumental profile is narrower than the intrinsic width of the spectral lines.

Table 4-3
Bolometric Corrections for B-Type Supergiants

T_{eff} (10^4 K)	B.C. (mag)	T_{eff} (10^4 K)	B.C. (mag)	T_{eff} (10^4 K)	B.C. (mag)
0 950	−0.28	1 4	−1.05	2 00	−1.90
1.000	−0.29	1 5	−1 21	2 25	−2.18
1 100	−0.49	1.6	−1 38	2.50	−2.42
1 200	−0.68	1 7	−1.52	3 00	−2.84
1.300	−0.87	1 8	−1 66	—	—

Dashes (—) represent nonexisting data at these values.

It should be recalled that spectral types are assigned from a visual evaluation of the apparent relative strengths of selected absorption lines of neutral atoms and ions using low dispersion, low resolution spectra Each spectral type is defined by well-specified ratios of apparent strength. Each luminosity class for the B stars is primarily determined by the amount of Stark broadening shown by the lines of H I and He I. In the case of the supergiants, the Stark-broadened line wings of H I and He I are minimal and the Balmer series of hydrogen is found to extend to about $n = 22$. In the case of stars in luminosity classes IV and V, the Stark broadened wings are strong, and forbidden lines of He I are seen, the Balmer series breaks off near $n = 14$. In the case of stars in luminosity classes II and III, the wings of the H I and He I lines have moderate extent and the Balmer series breaks off near $n = 18$ or 19.

When the spectra of B stars in the main-sequence band are observed at high dispersion, a few stars are found to have sharp lines, while the rest show broadened absorption lines. The shapes of the broadened lines can be understood in terms of rotation of the star. The basic theory of the broadening of stellar absorption lines by rotation of the star has been summarized by Huang and Struve (1960), recent developments in this theory are reviewed in Chapter 6. Rotational broadening is a geometrical form of line broadening and it is important for understanding the shapes of the lines of most main-sequence B stars The shapes of the lines of B-type supergiants also seem to be dominated by rotational broadening, although the amount is less than for the average main-sequence star

In the case of the supergiants, the line shape can also be interpreted as the result of a statistical distribution of line-of-sight velocities of the parcels of atmosphere which contribute to the formation of the line This type of broadening is called macroturbulence (see Huang and Struve, 1960, p 350 ff). Typically the line shape is Gaussian and the FWHM, when interpreted in terms of a most probable velocity, results in supersonic velocities That is, the most probable "turbulent velocity" is larger than the velocity of sound in a plasma of hydrogen at a temperature equal to the effective temperature of the star. Macroturbulence is a concept introduced to provide a geometric explanation for the widths and shapes of the strong absorption lines in the visible spectra of supergiants. It may provide a rough idea of the range of velocity which occurs along the line of sight in the line forming region of the stellar atmosphere.

When curve-of-growth analysis is applied to the spectra of supergiants in order to deduce the physical state of the atmosphere, a rather large value is frequently deduced for the quantity which is termed microturbulent velocity. The microturbulent velocity is a fudge factor which permits one to represent reasonably well the relative strengths of intrinsically weak and intrinsically strong absorption lines from the same multiplet in terms of the temperature and density of a single layer of gas. Long ago it was noted (Struve and Elvey, 1934) that for supergiants the

strongest lines in multiplets were considerably stronger relative to the weak lines than was the case for main-sequence stars. This observational fact, which describes one of the characteristic features of supergiant spectra, received an interpretation by postulating an extra large small-scale motion, microturbulent motion, which has a similar effect on the theory of line formation to that of the thermal Doppler motion of the atoms and ions. That is, microturbulence broadens the shape of the line absorption coefficient. However, it is postulated that microturbulence does not affect the level of ionization or excitation in the stellar atmosphere.

A summary of the observational facts basic to this approach to understanding the shapes and strengths of the absorption lines of the visible spectra of supergiants can be found in the review article by Underhill (1961); the review article by Pecker and Thomas (1961) summarizes the relevant theory of spectral line formation. The final statement of Pecker and Thomas is still true If one is to obtain true information from the discussion of microturbulence and macroturbulence, as used in astrophysics and summarized here, a detailed discussion of the form and the behavior of the source function S_ν, in the column of gas where the absorption line is presumed to be formed, is a necessary part of the study.

Absorption Lines from Elements Other Than Hydrogen

The interpretation of the equivalent widths of the absorption lines of the visible part of the spectra of 11 B-type supergiants is discussed in Chapter 6. On the whole, the evidence is that the composition of the B-type supergiants is similar to that of the Sun. There is weak evidence that nitrogen is deficient in three supergiants, that oxygen is deficient in one, and neon is overabundant in two. However, since on the one hand each analysis has been carried out by modeling the line forming parts of the atmosphere as homogeneous plane-parallel layers of gas in which radiative and hydrostatic equilibrium exist while on the other hand there is quite a bit of evidence that the line forming parts of the atmospheres of supergiants are inhomogeneous both in temperature structure and density structure, the interpretation of the unusual observed line intensities as evidence for abundance anomalies is insecure.

It has been noted earlier that the effective temperatures deduced for B-type supergiants from model atmsospheres which represent well the relative strengths of absorption lines from two or more stages of ionization are significantly higher than the effective temperatures deduced from angular diameters and integrated fluxes. This result indicates that the use of classical model atmospheres for representing the regions where the most easily measured absorption lines in the visible spectrum of B-type supergiants are formed is a precarious procedure.

In the early B-type supergiants weak emission components, usually accompanied by a strong shortward displaced absorption core, are sometimes seen for the He I lines at 5876 and 6678 Å (see Hutchings, 1970a, Rosendhal, 1973c, Sterken and Wolf, 1978). The shape of these line profiles suggests that one is seeing regions of gas in outflow. The theory of line formation in a moving atmosphere is reviewed in Chapter 6. There the justification may be found for interpreting "P-Cygni" type line profiles as evidence for outflow. It is noted in Chapter 6 that classical modeling even with non-LTE physics does not account for the observed strengths of the intrinsically strong He I lines in supergiants (see also the comments of Rosendhal, 1973b).

The radial velocities of B supergiants, found from absorption lines in the visible spectral range, vary irregularly with a small amplitude, and the profiles of some of the strong lines are known to change in shape irregularly by a small amount. Typical changes in the radial velocity and in the profile of Hα have been discussed by Underhill (1966a). Continuing observation of B-type supergiants (see, for instance, the work reported by Sterken, 1976) has confirmed that irregular small-range variability is a normal characteristic of B-type supergiants. It seems that the more luminous the star, the more obvious it is that the

radial velocity and the line strengths and profiles vary The variations are not strictly periodic. They may be interpreted most simply as the result of changes in the velocity, temperature, and density pattern of the mantle of the star. In none of the apparently bright, thus, frequently observed, B-type supergiants have the spectrum variations been suspected to be the result of the regular passage of a companion bound to the supergiant in a binary orbit.

Some unexpected shifts in the apparent wavelengths of the strongest He I lines were observed on several spectrograms of the supergiant ρ Leo (B1 Ib or B1 Iab) by Gutman (1967) who concluded that these displacements indicated the presence of an anomalously large amount of the helium isotope ^{3}He in the atmosphere of ρ Leo However, Wallerstein (1971) was not able to confirm these shifts. Wallerstein did note some interesting changes in the shape of the profile of Hα from time to time Recently Smith and Ebbets (1981), using a high dispersion spectrograph and solid state detector such that precise spectrophotometery could be carried out with excellent spectral resolution, have detected changes which occur on a time scale of hours in the profiles of the Si III lines at 4552, 4568, and 4574 Å and in the profile of Hα. It seems probable that Gutman's observations of the He I lines were the result of changes in the velocity field in the atmosphere of ρ Leo which were of moderately long duration They could be changes such as those which may be postulated to provide the doubling in some ultraviolet resonance lines which has been noted by Fahey and Underhill (1980, The Visible Spectrum of Supergiants, this chapter) It is significant that Gutman found the biggest shifts for the lines with the greatest intrinsic strength. It is very improbable that the isotope ^{3}He is overabundant by a large factor in the atmosphere of ρ Leo It is likewise improbable that Gutman's results are due to faulty equipment or faulty measuring procedures

The Lines of Hydrogen

It has been known for a long time that the line Hα may appear weakly in emission in the spectra of B-type supergiants and that the shape of the profile changes from time to time as does the displacement of the deepest point of the absorption core. In most B-type supergiants emission is not seen at the positions of the remainder of the Balmer series, although the deepest points of the absorption cores often show variable displacements In some supergiants a Balmer progression—the systematic increase or decrease of the velocity displacement of the absorption cores of the Balmer lines as one proceeds from the head of the series at Hα to lines of high upper quantum number—is seen (see, for instance, the observation by Hutchings, 1968a, 1970a, and those by Sterken, 1976). We shall first review the results of the systematic study of the Hα line profile by Rosendhal (1973a, 1973c), and then look at typical information on the Balmer progression in B-type supergiants The results which we shall discuss are typical of what is found every time a B-type supergiant is observed intensively.

Hα in B-Type Supergiants. Some typical Hα profiles in B0 and B1 supergiants are shown in Figure 4-3 which has been taken from Rosendhal (1973c) These profiles were obtained by photographic spectrophotometry. Very precisely determined Hα line profiles in the spectrum of ρ Leo are shown in Figure 4-4, which is from Smith and Ebbets (1981) Many more profiles of Hα in these and other stars can be found in the literature which has been quoted above Some interesting line-profile changes are shown by Underhill (1960) and Rosendhal (1973a). A typical series of changes of the Hα profile in the O9.5 Ia supergiant α Cam is shown by the observations of Ebbets (1980) In this star the emission is unusually strong and it obliterates completely the underlying photospheric absorption line. This star has an unusually strong infrared excess. One sees almost every conceivable combination of absorption and weak emission. Only in the superluminous supergiants, such as HD 152236 ζ^1 Sco, does the emission at Hα rise more than a few percent above the continuum in the neighborhood of Hα In α Cam it rises to about 20 percent, which is a large amount for a B-type supergiant

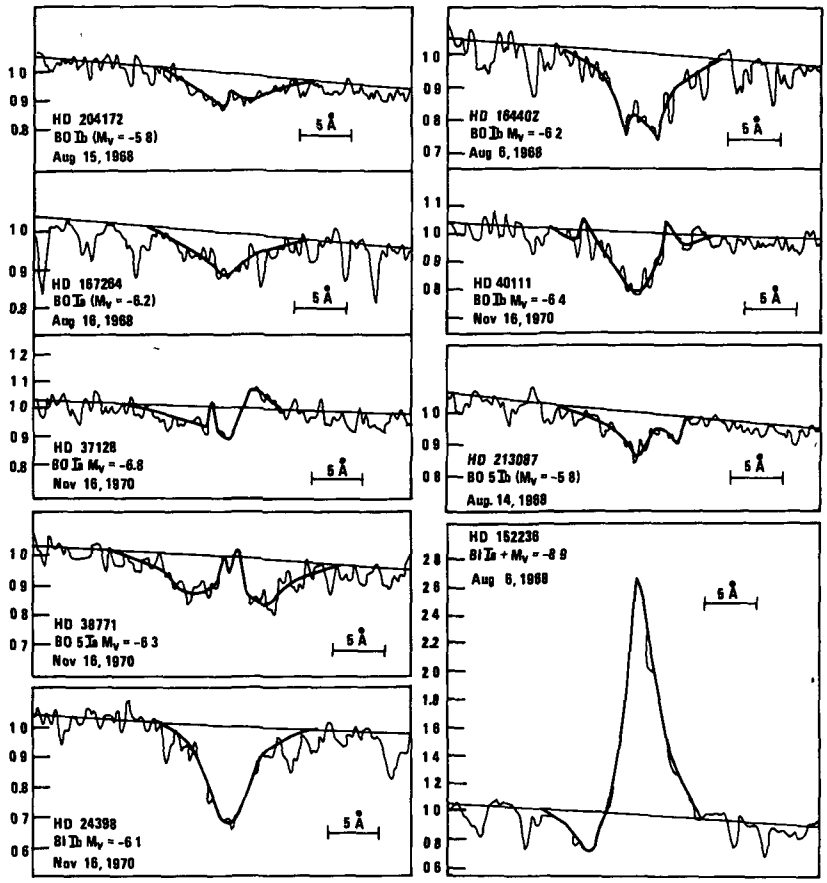

Figure 4-3. Representative profiles of Hα in B0 to B1 supergiants taken from Rosendhal (1973c). The thin line shows the observed intensity distribution in the neighborhood of Hα, the heavy line shows a smoothed line profile. The date of each observation is given. Typically the projected slit width is of the order of 0.3 Å. No zero point is shown for the wavelength scale, but the length of 5 Å is noted. Insecure estimates of M_V are placed in parentheses

One can easily ascertain that the Hα profiles of the B supergiants vary from time to time and that the type of change which is seen is related to luminosity rather than to spectral class. The Hα profiles of stars of type B0 Ia vary in the same way as do those of stars of type A2 Ia. The Ib supergiants seem to show less prominent variation than do the Ia or Ia+ supergiants. The observations of Ebbets (1980) and of Smith and Ebbets (1981) show the types of change which may occur on time scales of the order of a few days.

When the observed profiles of Figures 4-3 and 4-4 are compared with the predicted line profiles from the best model atmospheres available at this time, the amount of the discordance between observation and theory is apparent. Typical theoretical profiles are shown in Chapter 6 presenting the results from LTE and non-LTE model atmospheres which represent well the shape and amount of the continuous spectrum of B1 supergiants. These are the models with $\log g = 2.5$.

According to the theory which represents well the behavior of the continuous spectrum of B1 supergiants in all spectral regions except just shortward of the Balmer jump, the Hα profile should be in absorption with a core having a FWHM of about 0.54 Å and a central intensity of about 37 percent. The theoretical profile has shallow extended wings, due to the Stark effect,

which begin at about ±0.3 Å. Although the continuous spectrum of ρ Leo is well represented by the model having $T_{eff} = 2.0 \times 10^4$ K, $\log g = 2.5$, the shape of Hα is not well represented. In ρ Leo, which is a B1 Ib or Iab star, the amount of emission in the profile is minimal, the FWHM varies from about 4.4 Å to 5.3 Å, and the central intensity varies from about 76 percent to about 84 percent. The shallow part of the wings seems to begin at about ± 4 Å from the line center.

The equivalent width of the theoretical Hα profile from the non-LTE model atmosphere with $T_{eff} = 2.0 \times 10^4$ K, $\log g = 2.5$ is 1.38 Å (Mihalas, 1972b), that of the observed Hα profiles of Smith and Ebbets varies from about 0.94 Å to 1.6 Å with an average value of 1.3 Å. Thus, the observed line has about the predicted equivalent width in spite of the difference in shape between the observed profiles and the theoretical profile. The differences in shape might be interpreted as being due to rotation of ρ Leo with additional small changes produced by the presence of variable weak emission.

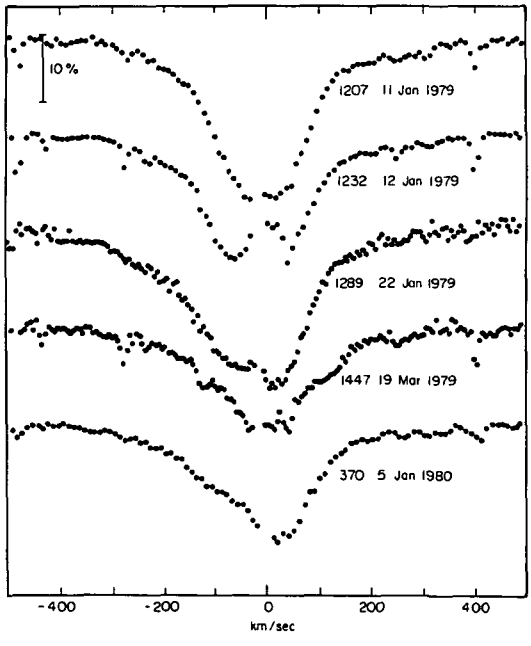

Figure 4-4. Profiles of Hα in the spectrum of ρ Leo taken from Smith and Ebbets (1981). At Hα, 200 km s^{-1} is equivalent to 4.38 Å. The photometric uncertainty of each point is of the order of ± 1.5 percent of the continuum level. The sharp absorption lines are from the Earth's atmosphere.

When one looks at the observed profiles presented by Rosendhal, especially those for the Ia supergiants, it is clear that the shape of the Hα line may be greatly modified by the presence of emission. According to Mihalas (1972b), the equivalent width of the absorption line at Hα provided by a model atmosphere with $T_{eff} = 2.5 \times 10^4$ K, $\log g = 3.0$ is 1.89 Å. Such a model will represent well the shape of the continuous spectra of B0 supergiants and the observed amount of radiation, it does not provide Hα profiles like those which are observed.

The emission in Hα must be formed in the mantle of the B-type supergiants. No emission of the sort which is observed can be provided by a classical model atmosphere composed of plane parallel layers of gas. Hutchings (1968b) has performed numerical experiments to see if he can produce Hα and other line profiles like what are seen. Using a simple ad hoc theory, Hutchings models the mantle as an extended sphere in which lines are formed by coherent scattering, the continuum by electron scattering. He introduces arbitrary velocity, temperature, and density fields which have properties like those which can be deduced for supergiants, using simple ideas. He attempts to determine the free parameters in his models by fitting the observed profiles of two or more lines per star but finds that it is difficult to represent several lines at a a time equally accurately Hutchings concludes that in early B supergiants the Hα emission is formed chiefly at about 1.5 R_*.

One of the major findings by Rosendhal (1973c) was that the net equivalent width of Hα, defined as the area in Å units of the part of the profile of Hα below the adopted continuum minus the area of the part of the profile which rises above the adopted continuum, decreases, and eventually may become negative as the luminosity of the star increases. The rate of decrease of the net equivalent width of Hα with increasing luminosity is found to be steeper for supergiants of types B0 to B1.5 than for supergiants in the spectral class range B8 to A3. The significance of

this is that the emission makes a greater fractional contribution to the "net equivalent width of Hα" at early B spectral types than for late B spectral types. At all subtypes, the luminous supergiants have stronger Hα emission, on the average, than do the less luminous supergiants.

When the question is approached of how best to evaluate the observed line profiles in a quantitative way, so that information about the physical state of the photosphere and mantle of a supergiant may be inferred, use of the net equivalent width of Hα as defined by Rosendhal is not a very productive procedure. The extra energy (emission) seen in Hα originates in the mantle. It can be measured best by comparing the observed energy distribution with well-defined theoretical reference spectra which portray what a photosphere would radiate.

The predicted Hα profiles from the non-LTE model atmospheres of Mihalas (1972a, 1972b) provide suitable reference energy distributions giving what a typical photosphere would produce if it were not overlaid by a mantle. These theoretical Hα profiles may be broadened by rotation and by macroturbulence, if so desired, and the result compared with the observed profiles The differences in equivalent width and in line shape between the theoretical energy curves and the observed ones give reasonable first estimates of the amount of energy originating in the mantle The shape of the net energy profile as a function of wavelength, in principle, contains information about the field of motion in the mantle. The amount of energy contains information about the source function for the Hα line. The appropriate model atmosphere to select is that one which will reproduce well over a wide wavelength range the continuous energy distribution from the supergiant. Of course, a correction for wavelength-dependent interstellar extinction must be applied.

The net Hα equivalent width defined by Rosendhal has no theoretical significance because the adopted reference line is entirely fictional No B-type supergiant, even though its entire outer atmosphere behaved in the manner of a classical model atmosphere, will emit a continuous spectrum in the close neighborhood of the Hα line. The best approximation to what such a (fictional) supergiant will radiate is given by one of the predicted Hα profiles from the set of non-LTE model atmospheres of Mihalas. The profiles are given relative to the continuum in the neighborhood of Hα. The theoretical Hα profiles may be put on an absolute energy scale by multiplying them by the monochromatic brightness in the continuum near Hα.

Rosendhal concluded that the net emission vanishes at approximately the same bolometric luminosity for all the early B supergiants, i.e , near $M_V = -5.8$. Among the late B supergiants, a net emission is seen only for stars with M_V brighter than -6.8 This result is chiefly due to the fact that the normal photospheric absorption in Hα is stronger for B8 to A3 supergiants than for B0 to B1.5 supergiants.

Rosendhal also considered the radial-velocity displacements shown by Hα and the strong lines of He I, C II, and Si II which fall in the yellow-red part of the spectrum. He found that in most supergiants, the lines of He I, C II, and Si II give the same radial velocity, so far as can be determined. In the case of the very luminous early B-type supergiants, the lines of He I sometimes are displaced shortward by a few km s^{-1}, the displacement reaching the largest negative values in the most luminous stars The radial-velocity displacement of the Hα core reaches large negative values (more than -50 km s^{-1}) for the superluminous stars. The peak of the Hα emission component is generally longward displaced relative to the radial velocities indicated by the C II and Si II lines, by up to $+100$ km s^{-1} for the most luminous stars Rosendhal concludes that the differences in radial velocity shown by the absorption and emission components of Hα are predominantly a measure of the gradient in the flow velocity in the mantle He concludes that this data indicate that the flows [in the mantle] have a distinct temperature dependence with there being a transition in the general flow properties at spectral type B5. He suggests that the simplest explanation for the existence of such a transition seems to be in the nature of the mechanism driving the flow. These remarks, which imply that the region of the atmosphere we are calling a

mantle is rather different in stars of spectral type later than B5 than it is in the early B supergiants, are borne out by observations made later of the ultraviolet spectra of the B-type supergiants (as described in the next section).

The Balmer Progression. The Balmer progression for three B-type supergiants is shown in Figure 4-5. The radial velocities for the lines Hβ to H19 have been taken from Hutchings (1968a, 1970a), those for Hα from Rosendhal (1973b). The radial velocity shown by the Hα core of χ^2 Ori was obtained on November 16, 1970, that of the other hydrogen absorption lines on October 16, 1968. For HD 190603, the dates are August 11, 1968 and June 5, 1968, while for ζ^1 Sco, they are August 8, 1968 and July 27, 1966. The dates of the observations are noted here because all three stars are known to have slightly variable radial velocities and their velocities may be different by ± 10 km s^{-1} or so at other times. One main fact is clear. In each case the radial velocity of the gas responsible for forming the absorption core of Hα is more than 140 km s^{-1} more negative than that shown by the gas responsible for forming the cores of lines with upper quantum numbers greater than about seven. The high members of the Balmer series show radial velocities which are about the same, within the uncertainties of measurement, with those shown by other lines which are considered to be formed in the same deep layers of the mantle. This may be ascertained by looking at the detailed information on radial velocities of these stars given by Hutchings (1970a) and at the information to be found in radial-velocity catalogues. The lines Hα, Hβ, and Hγ tend to show more negative radial velocities than do the high members of the Balmer series. This sytematic trend is shown by most B-type supergiants that have been investigated in detail (see also Hutchings, 1976a, 1980). The direction of the Balmer progression is never reversed for B supergiants. That is, the absorption cores of Hα and Hβ never show more positive radial velocities than the high Balmer lines do This is not the case for Be and shell stars, for Balmer progressions going in both directions are seen (see Part II).

Hutchings (1976a, 1980) believes that he has detected velocity gradients in the atmospheres of B-type supergiants by means of lines in the spectrum that come from ions of the elements N, O, Mg, and Si. However, this result is precarious, the suspected systematic displacements are of the order of the uncertainty of a radial-velocity determination from a single absorption line. Hutchings suggests that the lines coming from ions which require much energy for their formation show little outflow while the lines from ions which require little energy for their formation show a larger velocity of outflow. The data (see particularly Hutchings, 1976b) can also be interpreted to show a radial velocity that is the same for all absorption lines not from He I and H I. The detection of velocity gradients in a stellar atmosphere is discussed in more detail later in this chapter where the observations of P Cyg are presented.

Evidence for Outflow from the Visible Spectrum

The chief indication in the visible spectrum that outflow may be occurring in the mantles of B-type supergiants is the fact that a Balmer progression, as shown in Figure 4-5, is observed for the Ia supergiants. Usually the outflow velocity

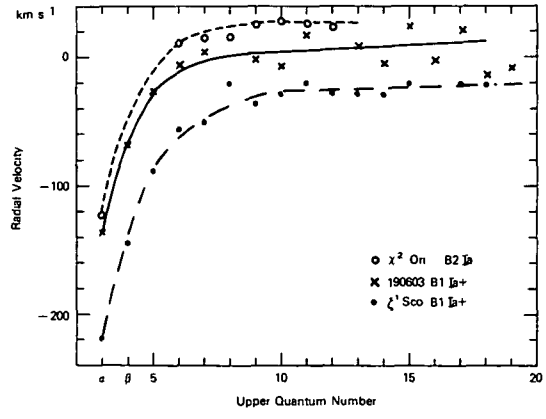

Figure 4-5. Balmer progressions from three B-type supergiants. The plotted radial velocities have been taken from Hutchings (1968a, 1970a) and from Rosendhal (1973c) See the text for the dates when the observations were made.

indicated by the displacement of the absorption core is not more than about 140 km s^{-1} In the star ζ^1 Sco a displacement of about − 200 km s^{-1} is seen.

We have seen in Chapter 2 that at a distance R solar radii from the center of a star which has a mass equal to M solar masses, the escape velocity is

$$u_{esc}(R_\odot) = 618\left(\frac{M_\odot}{R_\odot}\right)^{1/2} \text{km s}^{-1}. \qquad (4\text{-}2)$$

Values of the outward directed velocity necessary for particles to escape from the photospheres of main-sequence stars are given in Table 2-13 These may be scaled to give estimates for the escape velocity from supergiants using typical values for the radii of supergiants (see Table 4-1) and typical values for the masses of supergiants. The typical values for the masses and radii of main-sequence B stars are given in Tables 2-11 and 2-12, respectively. At the present time, there is little secure knowledge about the masses of the B-type supergiants (see Chapter 2).

Estimated escape velocities from the level of the photosphere ($R = R_*$) and from a distance of $2R_*$ are given in Table 4-4 for two cases (1) that when the mass of the B-type supergiant is 30 solar masses, and (2) that when it is 10 solar masses.

We see that the outflow velocities indicated by the displacement of the deepest point of the Hα absorption feature in the B-type supergiants are usually of the order of or smaller than the escape velocity at $2R_*$, if the mass of the supergiant equals or exceeds 10 solar masses. Very likely in the Hα line we are seeing mass that is leaving the star from a level near $2R_*$ because calculations of profiles of moderately opaque lines formed in expanding atmospheres (see Chapter 6) indicate that with the moderately opaque lines displacement of the deepest part of the profile usually corresponds to about 0 5 times the terminal velocity. The deepest point moves close to the undisplaced position of the line when the opacity in the line is small. When the opacity is very large (resonance lines), the deepest point moves close to the terminal outflow velocity

The calculations of Mihalas and Kunasz (1978) show the types of line profile which result for subordinate lines of a He^+-like ion when line formation takes place in a differentially expanding atmosphere. Since the hydrogen atom has a similar energy level structure to the He^+-like ion studied by Mihalas and Kunasz, the profile which Mihalas and Kunasz show for λ 1640 may be typical of what might be expected for Hα from a cooler model atmosphere than the one which they investigated.

In the normal Ia supergiants, not nearly so much emission relative to the size of the absorption component is seen as is given by the calculations of Mihalas and Kunasz. A model with a velocity and density distribution like that investigated by Mihalas and Kunasz but having cooler

Table 4-4
Estimated Escape Velocities from B-Type Supergiants (km s^{-1})

Spectral Type	B1	B2	B3	B5	B8
(1) Case $M/M_\odot$= 30					
$u_{esc}(R=R_*)$	545	418	422	470	389
$u_{esc}(R=2R_*)$	385	296	298	332	275
(2) Case $M/M_\odot$= 10					
$u_{esc}(R=R_*)$	315	242	243	271	225
$u_{esc}(R=2R_*)$	223	171	211	192	159

electron temperatures is unlikely to produce Hα profiles like those seen in the normal Ia or Ib B-type supergiants Calculations done with a cool model atmosphere using the procedures of Mihalas and Kunasz might have relevance for understanding the meaning of the Hα profile from the superluminous supergiant ζ^1 Sco This method has been used to calculate theoretical profiles for P Cyg (see The Peculiar Supergiant P Cyg) The observed emission features in the H I and He I spectra of B-type supergiants are generally less intense than those suggested by the published calculations made with three-dimensional differentially expanding atmospheres. Therefore, it may be appropriate to modify the models by considering the expanding shells to be only partially filled with gas at the appropriate stage of ionization for forming He I and H I lines.

THE ULTRAVIOLET SPECTRUM OF SUPERGIANTS AT HIGH RESOLUTION

The first observations of the ultraviolet spectra of B-type supergiants from sounding rockets and spacecraft carrying spectrographic equipment giving moderate dispersion spectra have been described in Chapter 2 Three major conclusions were reached as a result of these observations They are (1) that the B-type supergiants are deficient in ultraviolet light relative to main-sequence stars of the same subtype, (2) that the profiles of the resonance lines of Si IV, C IV, N V, and O VI have a "P-Cygni" character, and (3) that unexpectedly strong absorption is seen in the resonance lines of high ions. These are ions that require higher electron temperatures for their formation in abundance than seem likely to be present if the temperatures in the mantles of B-type supergiants are determined by the constraint of radiative equilibrium applied to the radiation stream from the core of the star

The first conclusion can be understood when one compares the effective temperatures of supergiant and main-sequence stars of the same subtype: the second implies that rapidly flowing winds (outflow velocities of 500 to 2000 km s^{-1}) emanate from the B-type supergiants, the third indicates that extra energy is deposited in the mantle beyond that contributed by the radiation field from the core of the star.

In this section, we shall present typical spectrum profiles in the neighborhood of the conspicuous absorption and emission lines of the ultraviolet spectra of B-type supergiants. Since the conspicuous ultraviolet absorption lines are strong, their greatest depth often approaching 100 percent absorption, we deduce that these lines are formed high in the atmosphere of the star, far outside the photosphere where the continuous spectrum and weak subordinate lines are formed. The strong ultraviolet lines carry information about the physical state in the part of the star which we are calling a mantle.

The ultraviolet spectra of the B-type supergiants also contain many weak, somewhat broad absorption lines like many of the lines seen in the visible spectral range These lines may be interpreted by means of the standard theory of stellar spectra. Analysis of these lines gives information about conditions in the photosphere and the inner parts of the mantle We shall not focus attention on the weak lines Modeling done by Underhill and Silversmith (1976) indicates that the relative strengths of most of these lines can be represented rather well by means of the standard theory of radiative transfer in stellar atmospheres using model atmospheres which represent well the formation of the continuous spectrum of the supergiants

Luminosity Effects in the Ultraviolet

In the visible spectral range, three effects make the spectra of B-type supergiants different from the spectra of main-sequence stars of the same subtype. The first is Stark broadening of the H I and He I lines Stark broadening due to increased electron density causes the wings of H I and He I lines to increase in prominence relative to the core of the line as the luminosity of the star decreases The second is macroturbulence. It causes the cores of the lines of supergiants to become broadened and to take on a "chunky" look Third, increased microturbulence in supergiants causes the strong lines of multiplets to

become even stronger relative to the weak lines than they are in main-sequence stars.

No lines which are strongly susceptible to the Stark effect fall in the most easily observed part of the ultraviolet spectral range. Therefore, the Stark effect does not produce useful luminosity criteria in the ultraviolet. Macroturbulence and microturbulence, however, do act in the same way in which they act in the visible range. Thus, the strengths of the strong lines of multiplets relative to the weak lines are enhanced in supergiants in comparison to what is seen for main-sequence stars. Also the strong absorption lines have a broad, "chunky" look. These effects produce in the ultraviolet a luminosity effect like that which is used in the visible range for F and G stars. The result is that the strengths of resonance lines are enhanced in luminous stars in comparison to their strengths in main-sequence stars.

Underhill (1975a) and Underhill and Silversmith (1976) showed that the strengths of the resonance lines from ions of moderate abundance such as P^{+2} are enhanced in the spectrum of the B5 Ia supergiant η CMa over what their strength is in the B6 III giant ζ Dra Furthermore, they noted that in the spectrum of η CMa, the resonance lines from the abundant low ion C^{+} are very much enhanced in strength and that the line profile is displaced and changed in shape in such a way as to suggest the outflow of material. Thus, a new effect that seems to be related to luminosity appears in the ultraviolet. It is that the mantle is readily visible by means of the resonance lines of abundant ions and that there is evidence for outflow from the mantle. These phenomena are seen for some main-sequence and some subluminous stars, but the amount of the effect is different than for supergiants

A survey of the ultraviolet spectrum of 31 stars of type O9.5 to A2 in all luminosity classes has been made by Snow and Morton (1976). They used Copernicus spectra covering the spectral range from 1150 to 1250 Å for all the stars and extending to 1000 Å and 1440 Å for a few stars. They have published spectral tracings of the region from 1150 to 1250 Å for most stars and short regions around the O VI and the Si IV resonance lines for a few stars. Short sections of the spectrum of ζ Ori A, in the regions of the resonance lines of C III, O VI, S IV, P V, and Si IV are also given. Snow and Morton tabulate values for the maximum outflow velocity from each star and their best choices for M_V and T_{eff}. They derive the quantities $R/R_\odot$, $M/M_\odot$ and $\log g$ from the values of M_V and T_{eff} which they adopt For most of the supergiants, the values of Snow and Morton for T_{eff} are higher than what we have shown here to be correct. This is because Snow and Morton put considerable weight on temperature scales appropriate for main-sequence stars Additional information on B stars in the main-sequence band has been derived from Copernicus spectra and tabulated by Lamers and Snow (1978)

Here we present information derived from IUE spectra covering the range from 1200 to 3200 Å. The results are summarized in Table 4-5. In those cases where a value of the maximum outflow velocity, u_∞, is available from Snow and Morton (1976), this value is given in column 4 in parentheses.

In the case of stars of types B1 and earlier, outflow from the mantle is visible in the resonance lines of ions such as Si^{+3}, C^{+3}, N^{+4}, and O^{+5}. In middle and late B-type stars the outflow is best seen in the resonance lines of ions such as Mg^{+}, C^{+}, Al^{+2}, and Si^{+3}. In the case of supergiants (luminosity classes Ia and Ib), outflow can usually be detected easily. In the case of giant stars (luminosity classes II and III), the mantle with its associated outflow is barely visible, in the case of main-sequence stars (luminosity classes IV and V), the presence of a mantle and outflow can only sometimes be detected (see Snow and Morton, 1976, Lamers and Snow, 1978, and Chapter 3).

Some typical profiles of resonance lines in the spectra of B-type supergiants are shown in Figures 4-6 to 4-10. In each of these figures the undisplaced positions of the resonance lines are indicated as well as the positions of some blending lines of interest. It is to be noted that lines of Fe III can be seen in all the spectra studied here. At type B0 lines of Fe IV, Ni IV, Cr IV, etc. become significant, while at type B8 and later

Table 4-5
Maximum Outflow Velocities for B Supergiants and Properties of the Wind Spectrum

HD	Name	Spectral Type	v_∞ km s^{-1}	Wind Seen in*	Wind Not Seen in*	Notes
87737	η Leo	A0 Ib	200	Al II Mg II C II	Al III Si IV CIV N V	1 2
21389	HR 1040	A0 Ia	230	Al II Mg II C II	Al III Si IV C IV N V	2 3
21291	HR 1035	B9 Ia	260	Al II Mg II C II Al III	Si IV C IV N V	3
12301	53 Cas	B8 Ib	400	C II Al III Si IV C IV	Al II Mg II N V	4 5 7
34085	β Ori	B8 Ia	270 (530)	Al II Mg II CII Al III Si IV	C IV N V	6 7
164353	67 Oph	B5 Ib	440 (500)	C II Si IV C IV	Al II Mg II Al III N V	3 7 8
58350	η CMa	B5 Ia	410 (590)	C II Al III Si IV C IV?	Al II Mg II N V	7 9 26
198478	55 Cyg	B3 Ia	570	C II Al III Si IV C IV	Al II Mg II N V	1 7 8 10 11 12
53138	σ^2 CMa	B3 Ia	530 (580)	C II Al III Si IV C IV	Al II Mg II N V	7 8 10 11 12 13
206165	δ Cep	B2 Ib	950	Mg II C II Al III Si IV C IV	Al II N V	1 8 9 10 12 14 15 16 17
41117	χ^2 Ori	B2 Ia	660	Mg II C II Al III Si IV C IV	Al II N V	1 4 7 8 10 12 14 15
190603	HR 7678	B1 Ia+	640	Al II Mg II C II Al III Si IV C IV	N V	1 6 7 8 10 12 18 19 20
91316	ρ Leo	B1 Ib	1420 (1580)	Si IV C IV N V	Al II Mg II C II Al III	7 8 9 12 18 21
2905	κ Cas	B1 Ia	1220	Mg II C II Al III Si IV C IV N V	Al II	1 4 7 8 10 12 15 16 18 22 23
38771	κ Ori	B0.5 Ia	1950 (3450)	Si IV C IV N V	Al II Mg II C II Al III	7 8 9 12 18 21
167264	15 Sgr	B0 Ia	2040	Mg II Si IV C IV N V	Al II C II Al III	7 8 9 21 24
30614	α Cam	O9.5 Ia	1920 (1890)	Si IV C IV N V	Al II Mg II C II Al III	8 9 17 21 25

*These results are from IUE spectra only

Notes to Table 4-5

1 Emission occurs longward of C II 1335
2 There is slight, ambiguous evidence for the presence of C IV 1548 and Si IV 1393 in absorption
3 There is no emission at any wind line
4 There is possibly weak emission at Si IV 1393, definite emission at Si IV 1402
5 There is emission for C IV 1548 which is separated from C IV 1550, but there is no emission at C IV 1550
6 There is emission longward of Al II 1670
7 The absorption troughs due to Si IV 1393 and Si IV 1402 are separated
8 The absorption troughs due to C IV 1548 and C IV 1550 are blended
9 There is no emission for Si IV 1393 but weak emission for Si IV 1402
10 Emission occurs for both Al III 1854 and Al III 1862
11 Emission occurs for both Si IV 1393 and Si IV 1402, the latter component being the stronger one
12 There is emission longward of C IV 1550
13 Shortward displaced absorption components are seen in Mg II at -178 km s^{-1}
14 The Mg II lines show a weak tail shortward and possible weak displaced components
15 Displaced absorption components are seen in C II
16 Displaced absorption components are seen in Al III
17 The absorption troughs of Si IV 1393 and Si IV 1402 overlap
18 Displaced absorption components are seen in Si IV
19 There is emission at Mg II 2795 and Mg II 2802
20 Displaced components of Mg II occur at -324 km s^{-1}
21 The absorption troughs of N V 1238 and N V 1242 are blended emission occurs longward of 1242 Å
22 Displaced components of Mg II occur at -368 km s^{-1} but an absorption trough due to a spherical expanding wind is not seen
23 The N V resonance lines are weak in absorption, if present at all
24 Sharp components are seen at -54.6 km s^{-1} in Mg II and at -56.0 km s^{-1} in Mg I 2852
25 Little or no emission exists for C IV
26 Sharp displaced components of Mg II are seen at -180 and -228 km s^{-1}

lines of Fe II become comparable in strength to the lines of Fe III.

Figures 4-6 to 4-10 have been made from intensity tracing prepared from high resolution IUE spectra In each case, the zero point of wavelength has been adjusted so that, on the average, the interstellar lines from the first and second spectra of the light elements and metals have no displacement. The wavelength scale is believed to be accurate to better than ± 0.1 Å and to represent the wavelength scale at the star unless it happens that the radial velocity of the star falls outside the range ± 20 km s^{-1}. At wavelengths shortward of 1400 Å, it is difficult to determine accurately the correction for the background between the orders of the echelle spectrogram. The

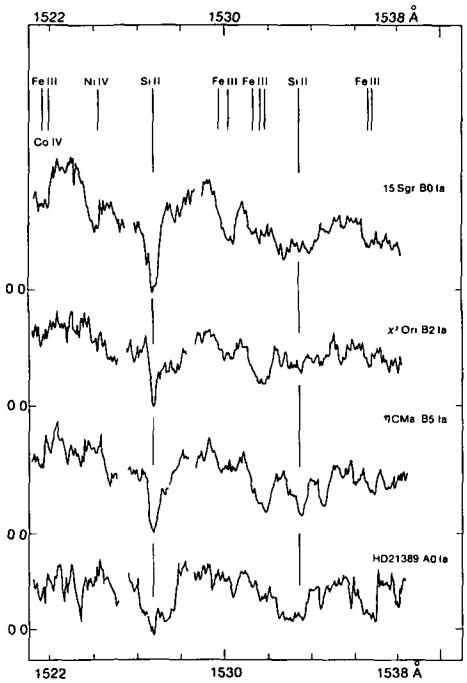

Figure 4-6 Profiles of the Si II resonance lines at 1526 and 1533 Å in B-type supergiants. The intensity scale is linear on an arbitrary scale for each tracing and the level of zero intensity is indicated for each spectral tracing. The local continuum can be considered to be a line parallel to the bottom of the diagram through the highest point in each diagram which is not obviously an emission component. The right part of this diagram overlaps with Figure 4-10.

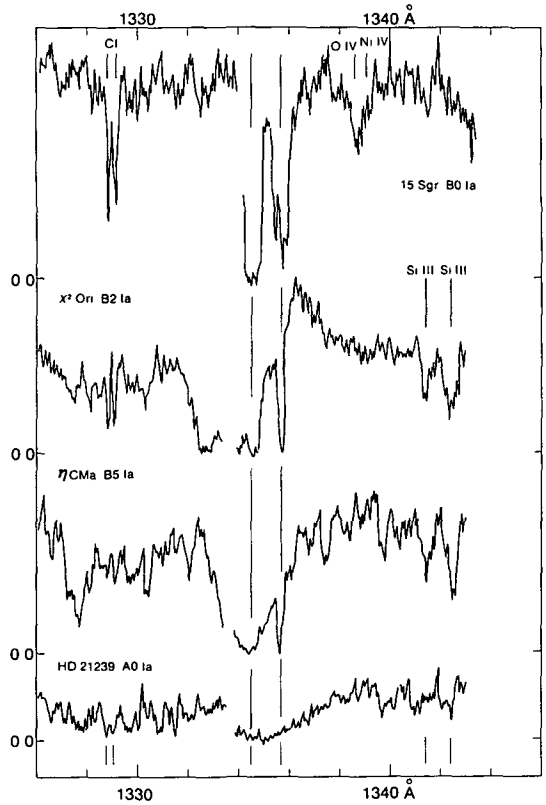

Figure 4-7. Profiles of the C II resonance lines at 1334 and 1335 Å in B-type supergiants. The arrangement is as in Figure 4-6. Sharp interstellar lines due to C I and C II are present. Emission occurs for χ^2 Ori longward of the line at 1335 Å.

indicated level of zero intensity is, in each case, the nominal value determined by the IUE project The intensity tracings used here were reduced with the corrected intensity transfer function; the photometric uncertainty of each point is expected to be of the order of ± 5 percent of the local continuum. The spectrum profiles have been interrupted at the positions of the reseau marks.

In Figure 4-6, which shows a part of the spectrum near multiplet UV 2 of Si II, an interstellar contribution may be expected for Si II 1526 but not for Si II 1533. There are many blending lines in this part of the spectrum and for the B1 and B0 supergiants, the "wind" profile caused by C IV resonance lines may suppress the spectrum longward of about 1530 Å. In

none of the normal B supergiants do the Si II resonance lines show displacements or shortward absorption troughs suggestive of outflow. Conditions in the mantles of B supergiants do not favor absorption in the resonance lines of Si II

In Figure 4-7, which shows a part of the spectrum near multiplet UV 1 of C II, strong interstellar components contribute to the absorption seen at 1334 and 1335 Å for 15 Sgr, χ^2 Ori, and η CMa. Although HD 21389 is distant, about 1 kpc, and it is heavily reddened, it does not show obvious interstellar C II absorption lines. This may be because the level of intensity is low here due to the presence of strong photospheric absorption in C II, also the photometric errors obscure the interstellar lines. However, it is surprising that there is no evidence for C II 1335 which is very strong in the relatively nearby B5 Ia star η CMa. The C II resonance lines give little evidence for outflow in the case of HD 21389, A0 Ia. In the case of η CMa, however, and of χ^2 Ori, B2 Ia, outflow is clearly visible. A classical "P-Cygni" type profile with an absorption trough and an emission component is seen for χ^2 Ori. This profile is typical for spectral types near B2 At type B0, the level of ionization in the mantle is sufficiently high that the C II lines have disappeared. Lines of O IV are quite strong in the spectrum of 15 Sgr, a feature that is in keeping with the relatively high effective temperature of 2.97×10^4 K found for this star (see Table 4-1)

A section of the spectrum near multiplet UV 1 of Al III is shown in Figure 4-8. Here blending lines of interest are shown including the lines of multiplet UV 4 of Al II which arise for the metastable 3^3P^o levels These lines (they are shown by broken leader lines) are quite strong at type A0 Ia. The Al III resonance lines are strong in all the stars, showing typical "wind" profiles for χ^2 Ori and η CMa. For some stars, sharp,

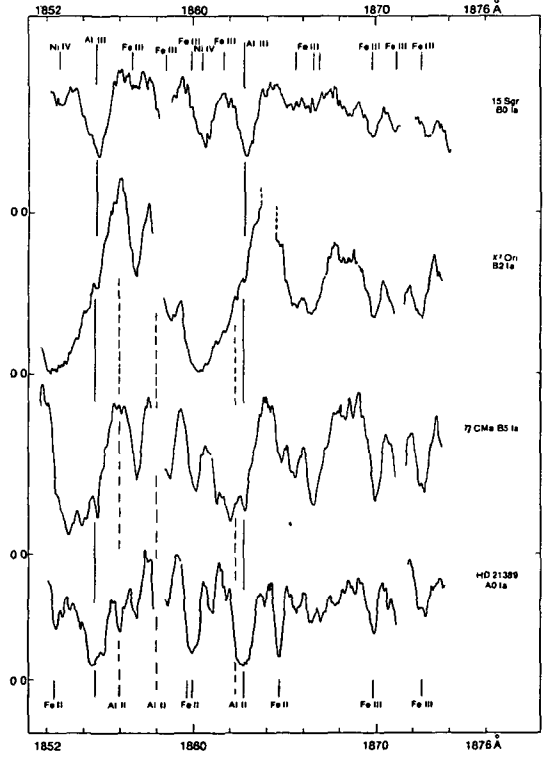

Figure 4-8. Profiles of the Al III resonance lines at 1854 and 1862 Å in B-type supergiants. The arrangement is as in Figure 4-6. Emission occurs for χ^2 Ori on the longward edge of both Al III resonance lines.

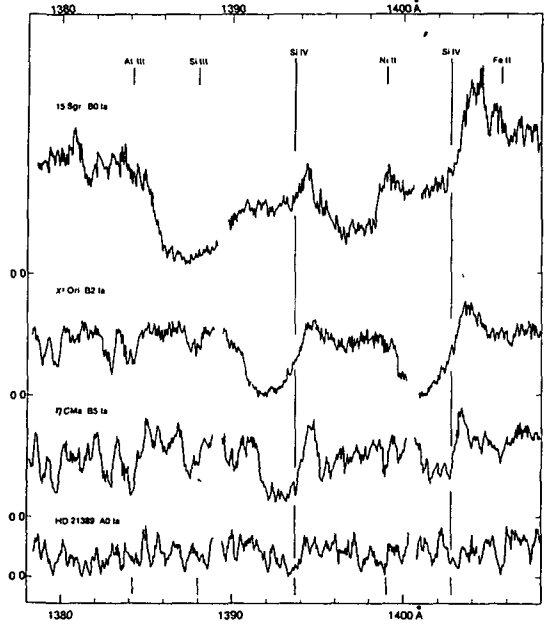

Figure 4-9. Profiles of the Si IV resonance lines at 1393 and 1402 Å in B-type supergiants. The arrangement is as in Figure 4-6. Emission occurs for χ^2 Ori and 15 Sgr longward of the Si IV line at 1402 Å.

relatively undisplaced, components are also seen. These may be formed in a more or less stationary circumstellar halo. It is only for the B2 Ia star that the emission component is strong. Many Fe III lines of considerable strength occur in this spectral region and Fe II is prominent at type A0 Ia

The spectral region in the vicinity of multiplet UV 1 of Si IV is shown in Figure 4-9. A few blending lines are identified. At type A0 Ia the Si IV lines are very weakly present in absorption, if at all. They do not suggest the presence of an outflowing wind which contains Si^{+3} ions. At type B5 Ia and earlier, the Si IV lines show conspicuous "wind" profiles, the two lines tending to overlap in the case of 15 Sgr, B0 Ia. An emission component is visible for Si IV 1402 at types B0 Ia, B2 Ia, and B5 Ia but not for Si IV 1393. The latter line has an intrinsic strength which is twice that of Si IV 1402. The greater emission intensity of Si IV 1402 must result from the blending caused by the superposition of the spectrum from the mantle on that from the photosphere.

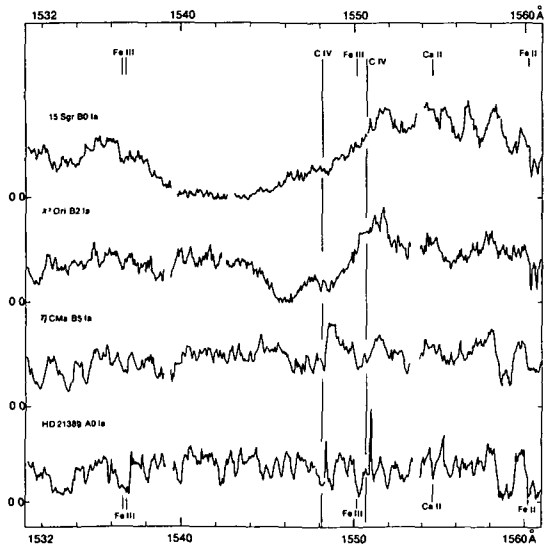

Figure 4-10. Profiles of the C IV resonance lines at 1548 and 1550 Å in B-type supergiants. The arrangement is as in Figure 4-6. See the text for a discussion of the emission components which occur. The left part of this diagram overlaps with Figure 4-6.

The observations can be understood qualitatively by recalling that classical "P-Cygni" type profiles arise from resonance scattering of an incident continuum flux by ions in expanding spherical shells (see Chapter 6) If the incident radiation from the photosphere is depleted at wavelengths near the line center, owing to the presence of a photospheric absorption line, then one may expect that the "P-Cygni" emission component will be weakened. The strong shortward displaced absorption trough is largely formed by resonant scattering from ions in the volume along the line of sight projected against the disk of the star. Deep absorption at high velocity displacements means that many Si^{+3} ions occur in the regions which have large outflow line-of-sight velocities. For early B stars, one would expect that the "quasi-continuum" in the neighborhood of 1402 Å would be stronger than that in the neighborhood of 1393 Å because the photospheric absorption Si IV line at 1402 Å would be weaker than that at 1393 Å Consequently, the emission component of Si IV 1402 may be expected to be stronger than that of Si IV 1393 Numerical calculations demonstrating the effect of photospheric absorption lines have been made by Castor and Lamers (1979).

The Si IV lines appear to be saturated at type B2 Ia but not at types B0 Ia and B5 Ia. In addition to rather weak, broad displaced absorption troughs, the star η CMa shows fairly strong, sharp, essentially undisplaced components of the Si IV resonance lines. These components may be formed in a hot region (possibly caused by shocks in the interstellar gas) between the Earth and this nearby star

The spectral region in the vicinity of multiplet UV 1 of C IV is shown in Figure 4-10. Since the two C IV resonance lines are separated by only 2.59 Å, the C IV lines become inextricably blended when conditions are such that strong absorption lines are formed in the photosphere and/or in the mantle. Consequently, although the resulting blended profiles are unmistakable, their interpretation is not simple. Many lines of Fe III occur in the spectral region (shown in Figure 4-10) and a few of the strongest have been identified. Also some lines of Ca II and Fe II,

strong chiefly in late B supergiants, occur.

In the case of HD 21389, A0 Ia, there is no evidence for the presence of photospheric absorption lines of C IV, nor for typical "wind" profiles formed in a highly ionized, outflowing mantle. However, from time to time, sharp, essentially undisplaced C IV emission lines sporadically occur (Underhill, 1979c). They look much like the C IV emission lines seen in the ultraviolet spectra of late type supergiants. The occurrence of these sharp emission lines suggests the temporary presence of a small amount of stationary hot gas in the mantle of HD 21389. This gas may be similar to that giving the C IV emission lines of late type stars.

In the case of η CMa, there is fragmentary evidence for the presence of weak "wind" profiles formed by scattering from a small number of C^{+3} ions in the outflowing mantle. In this case, it appears that the P-Cygni type emission component is strongest for C IV 1548. The line at 1548 Å is the line with the greater intrinsic strength. At spectral type B5 Ia, the ionization conditions in the mantle do not favor the production of C^{+3} ions.

At type B2 Ia (χ^2 Ori), however, a typical "wind" profile due to C IV is evident The line at 1548 Å is clearly saturated. By type B0 Ia (15 Sgr), the "wind" profile due to both C IV lines is strongly saturated. This blend retains a shape like this throughout spectral class O. The resonance lines due to N V and O VI can be seen in the spectra of some early B supergiants shown in the Atlas prepared by Snow and Jenkins (1977) from Copernicus spectra

In summary, the shapes and strengths of the "wind" profiles seen for the resonance lines in the ultraviolet spectra of B supergiants give an indication of the level of ionization in the gas which is seen flowing from the mantles of the B-type supergiants. At type B0, the level of ionization is high with many C^{+3} and Si^{+3} ions being seen at high outflow velocities as well as N^{+4} and some O^{+5} ions. No ions of a moderate level of ionization such as Al^{+2}, C^{+}, Si^{+}, or Mg^{+} are seen in the flowing gas from B0 supergiants. At type B2, many C^{+3} and Si^{+3} ions are seen in the flow; there are also many ions of a moderate level of ionization such as Al^{+2} and C^{+}. At B5 and later, few ions having a high level of ionization such as C^{+3} can be detected in the flow. The flow contains an abundance of ions of more moderate energy such as Si^{+3}, Al^{+2}, C^{+}, and Mg^{+}. At types B8 and later, the evidence for the presence of C^{+3} or Si^{+3} in the flow is weak. The most prominent ions are those of moderate to low energy such as C^{+}, Mg^{+}, and, in some cases, Fe^{+}. For the stars of all types, flow is also detected by means of the Balmer series of hydrogen (see the section on the Visible Spectrum of Supergiants). There is a large change in the level of ionization seen in the outflow from the mantles of B supergiants as one goes from spectral type B0 to A0. Table 4-1 shows that the effective temperatures of the supergiants decrease by a factor of about 2.6 over this spectral class range

Very probably the mantles of the B-type supergiants contain plasma in at least two temperature regimes because not only atoms of neutral hydrogen are seen in outflow, but also high ions which require different energies for their formation are seen. Here "temperature" is used as an indicator of the level of ionization. If the level of ionization of the plasma in the mantle were the result of electron impact, then the fractional abundance of a given ion would vary in proportion to the value of the ratio $I.P./T$ (cf., Saha's Law in Allen, 1973). Here $I.P$ denotes the ionization potential of the ion. We note that in 15 Sgr the "wind" profiles due to C IV and to Si IV are strong, thus, we infer that the relative abundance of C^{+3} is large and that, similarly, Si^{+3} is the dominant ion of silicon. However, the ionization potential of C^{+2} is 47.9 eV while that of Si^{+3} is only 45.1 eV. Thus, if conditions are such as to predominantly ionize carbon to the state C^{+3}, then silicon should be largely in the unobservable state of Si^{+4}. However, we are seeing many Si^{+3} ions and they have outflow velocities similar to those seen for C^{+3} ions. The necessary conditions to account for the observations could be present if the C^{+3} ions were predominantly in different parcels of plasma from those containing many Si^{+3} ions. Clearly the neutral hydrogen atoms which

produce the observed displaced absorption cores of the strong Balmer lines may lie in other cooler parcels of plasma

Considerations such as those sketched in the preceding paragraph are too simple to form a basis for developing a model for the mantle of a supergiant. Nevertheless, they do suggest that it may be appropriate to consider the possibility that the mantle of a B-type supergiant is inhomogeneous The observation of sporadic, undisplaced, sharp C IV emission lines in the spectrum of HD 21389, A0 Ia, at the same time as strong wind profiles are seen for Mg^+ also points toward a model for the mantle in which inhomogeneity is an important property The subject of inhomogeneity is treated further in the section, Discussion, when all of the observations of B supergiants are considered

The change in the profiles of the resonance lines of C II, Si IV, and C IV as one goes from luminosity class B2 IV to B2 Ia is illustrated in Figures 4-11, 4-12, and 4-13. These figures have been made from tracings of IUE high dispersion spectra, the spectra of γ Peg and ζ Cas having been kindly made available by Janet R Lesh, and the profiles for ϵ CMa by L W Kamp. The spectrum tracings presented for ϵ CMa have a slightly different wavelength scale than is used for the other four stars In each case, the zero point of the wavelength scale has been adjusted so that the interstellar lines from atoms and first ions have zero displacement on the average. For each spectrum tracing the intensity scale is linear on an arbitrary scale, the nominal level of zero intensity is indicated and a line has been drawn to represent the level of the continuum in each section of spectrum. The spectrum tracings are interrupted at the positions of reseau marks. The resolution of the IUE short wavelength, high dispersion spectrograph is shown by the apparent shapes of the C I interstellar lines near 1329 Å and by the many sharp photospheric lines of γ Peg Although both γ Peg and ζ Cas are given the spectral type B2 IV, it is clear that the Si IV and C IV resonance lines differ for these stars The photospheric spectral lines of ζ Cas are a little

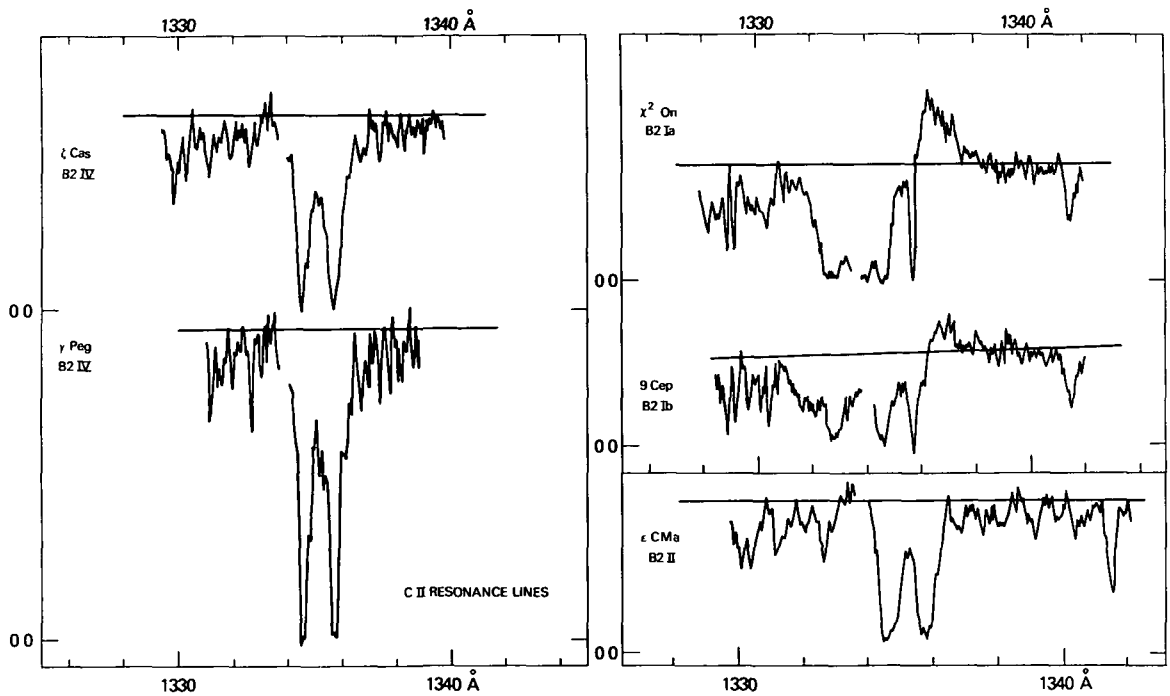

Figure 4-11. The C II resonance lines in spectral types B2 IV to B2 Ia. The intensity scale is linear; the wavelength scale for ϵ CMa is different from that for the other stars

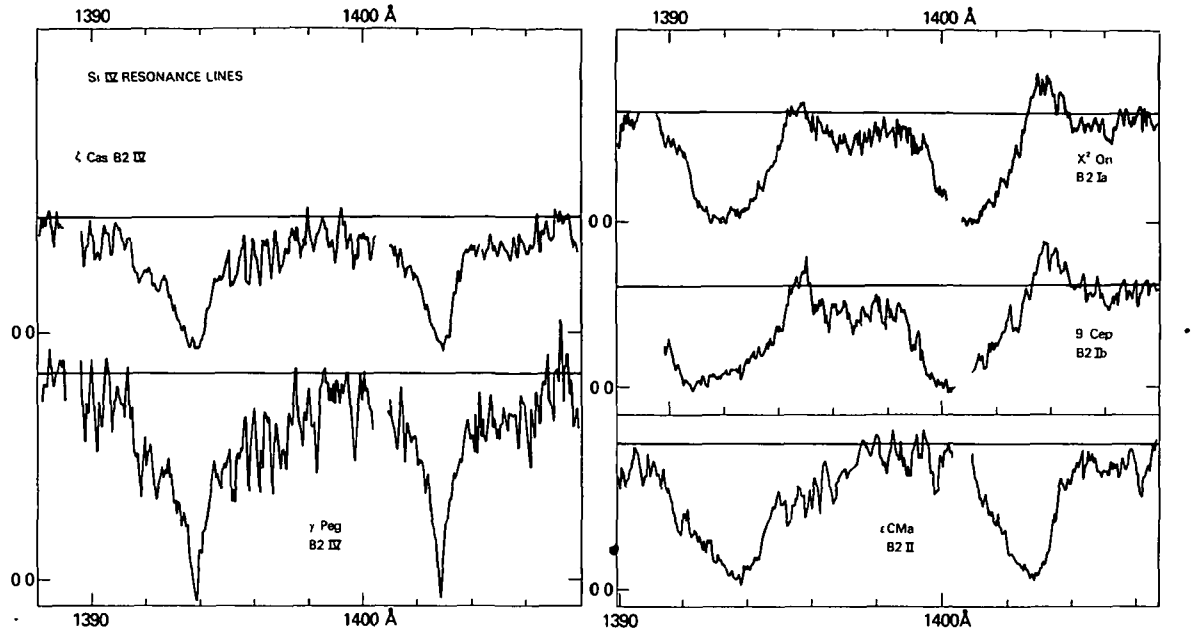

Figure 4-12. The Si IV resonance lines in spectral types B2 IV to B2 Ia. The intensity scale is linear; the wavelength scale for ε CMa is different from that for the other stars.

broader than those of γ Peg The star γ Peg is a β Cephei variable and it is discussed in Chapter 5

The C II resonance lines of γ Peg and ζ Cas (see Figure 4-11) are strong and they probably originate mostly in the photosphere. There is no detectable asymmetry due to wind. The character of the C II resonance lines at type B2 IV fits in with the appearance of the series of C II line profiles for main-sequence stars (shown in Figure 3-8). It should be noted that C II 1335.71 has a larger *gf* value than C II 1334 53 has and that, as expected, for spectral types B9.5 to B2 on the main-sequence, it is the stronger line of the pair When, however, the lines are caused by absorption by the interstellar medium, as for HR 1861 (see Figure 3-8), the line C II 1334.53 is the stronger line This is because the line at 1335.71 Å arises from a level which has an excitation energy of 63.42 cm^{-1}, whereas the excitation energy of C II 1334.53 is 0 00 cm^{-1}.

At type B2 II, ε CMa, the profiles of the C II resonance lines are broader than at luminosity class IV and they are symmetrical. The stars γ Peg, ζ Cas, and ε CMa are at 134, 179, and 153 pc, respectively (Underhill et al., 1979). Weak interstellar C II lines may possibly be present, but they cannot be resolved from the stellar lines

The supergiants 9 Cep, B2 Ib, and χ^2 Ori, B2 Ia are at 708 and 1300 pc, respectively (Underhill et al , 1979). A strong sharp line is seen at the position of C II 1335.71 and a broader line appears at the undisplaced position of C II 1334.53. Both are due to the interstellar medium. There is no evidence for the presence of photospheric C II lines The photospheric radiation at these wavelengths has been entirely modified by the overlying mantle. In both supergiants there is a complex, shortward displaced structure which may be interpreted as a composite feature formed by the blending of some moderately sharp, shortward displaced components of C II and a typical absorption trough due to a spherically symmetrical expanding wind. The number density of the C^+ ions in the wind of χ^2 Ori is greater than that in the wind of 9 Cep because the emission component is stronger for χ^2 Ori than it is for 9 Cep and the absorption trough is deeper. The shortward edge of the wind profile occurs at about 1331 5 Å for both supergiants, indicating a maximum outflow velocity of about

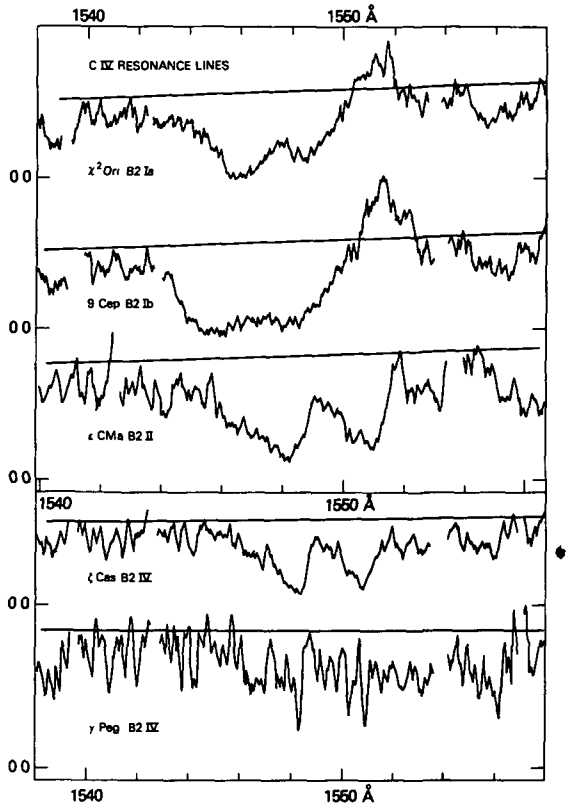

Figure 4-13. The C IV resonance lines in spectral types B2 IV to B2 Ia. The intensity scale is linear; the wavelength scale for ε CMa is different from that for the other stars.

670 km s^{-1} The profile of the C II resonance lines of 9 Cep is variable. The moderately sharp component seen at about 1332.7 Å in the spectrum of χ^2 Ori is probably a displaced component of C II 1334.53. The companion component due to C II 1335.71 would lie at 1333.9 Å. Although most of this region is obscured by a reseau mark, it seems that an absorption core may lie here Sharp, discrete components of C II have been noted for η CMa, B5 Ia by Underhill (1975b).

The change in appearance of the profiles of the Si IV resonance lines at 1393 76 and 1402.77 Å as one goes from spectral type B2 IV to B2 Ia is shown in Figure 4-12. The Si IV lines appear to be entirely photospheric in γ Peg, they fit into the series for main-sequence stars (Figure 3-12). However, the cores of the Si IV lines for ζ Cas have an asymmetry which is suggestive of outflow. This asymmetry is enhanced in the spectrum of ϵ CMa, B2 II. Both 9 Cep and χ^2 Ori show typical "wind" profiles. It is clear that the emission component for Si IV 1393 is very weak, if present at all. The absence of this expected P-Cygni emission component cannot be explained as a result of the overlapping of the two resonance lines of Si IV because, quite obviously, the Si IV lines do not overlap. A series of blended absorption lines chiefly due to lines of Cr III and Fe III intervenes. An explanation for the weakness of the emission component due to Si IV 1393 has been proffered above.

The change in appearance of the profiles of the C IV resonance lines at 1548.18 and 1550.77 Å as one goes from spectral type B2 IV to B2 Ia is shown in Figure 4-13. In the spectrum of γ Peg, the C IV lines appear only as sharp cores, most of the structure seen is due to Fe III. In the spectra of ζ Cas and ϵ CMa, the C IV resonance lines are well developed in absorption and the line profiles show asymmetries suggestive of outflow. In the spectra of the supergiants 9 Cep and χ^2 Ori, the line profile is typical of a wind. It is interesting that the C IV line in the spectrum of 9 Cep is stronger in absorption and emission than is that of χ^2 Ori. This suggests that the wind of 9 Cep contains a greater density of C^{+3} ions than does that of χ^2 Ori. The maximum detectable outflow velocity is about the same for the two stars. No moderately sharp displaced components, as seen for C^+, are detectable in the spectra of 9 Cep and χ^2 Ori by means of Si^{+3} or C^{+3} ions.

The profiles of ultraviolet resonance lines in the spectra of B-type supergiants shown in Figures 4-6 to 4-13 demonstrate that the presence of emission components is not common. When emission is seen, it is usually rather weak in comparison to the strength of the absorption trough. The energy contained in the emission component is never equal to that removed by the absorption trough, as would be the case were the lines formed according to the theories of the formation of resonance lines in expanding spherical atmospheres (reviewed in Chapter 6).

Outflow Velocities

Theoretical considerations (see Chapter 6) show that the shortward end of the absorption trough formed by resonance scattering in an expanding spherical atmosphere occurs at a distance from the undisplaced position of the line such that the $\Delta\lambda$ corresponds to the maximum outflow velocity experienced by the ions in the expanding atmosphere. Therefore, determining the positions of the end points of absorption troughs will provide estimates of the maximum outflow velocities which occur in the part of the expanding atmsophere where the ions in question are abundant Although it is conceivable that the ions may continue to be accelerated when they are in an unobservable state, this value of the outflow velocity is called the terminal velocity and it is denoted as u_∞. The maximum outflow velocity is large for O stars and it decreases as the spectral type becomes later.

Some typical values of u_∞ found from IUE spectra are given in Table 4-5 for 17 B supergiants. These numbers are the mean values from several lines. To determine them, the profiles of the resonance lines of Fe II, Al II, Mg II, C II, Al III, Si IV, C IV, and N V were measured In none of the stars was the wind visible in Fe II No information about the O VI resonance lines can be found out from IUE spectra.

It is difficult to say how uncertain the listed values of u_∞ are because the accuracy of finding the position of the shortward edge of the absorption trough depends upon how strong the absorption trough is (saturated lines having steep shortward edges, unsaturated lines rather slowly sloping edges),upon how many photospheric lines due to other ions may blend near the edge of the line, upon how strongly developed the underlying photospheric resonance lines are, and upon the value of c/λ for the line The factor c/λ varies from 107 km s^{-1} $Å^{-1}$ for the Mg II lines at 2800 Å to 242 km s^{-1} for N V 1238 It may be realistic to adopt $\pm$ 50 km s^{-1} as the typical uncertainty in the listed values of u_∞

Notes about the spectrum of the wind, in particular the occurrence of P-Cygni type emission components and of rather sharp, displaced absorption components, are given at the end of Table 4-5. Strong interstellar lines of C II, Mg II, Al II, and Fe II occur in all the spectra. Weak, sharp, essentially undisplaced absorption in the resonance lines of C IV and Si IV, and sometimes Al III, is seen for some of the stars.

The character of the wind spectrum is not uniquely related to the spectral type of the star, although the level of ionization seen in the wind is lower near type A0 than it is near type B0 The strengths of the wind lines in the spectra of the Ib supergiants, on the whole, suggest that the density of the wind is less for the Ib supergiants than it is for the Ia supergiants. Stars which are considered to be exceptionally luminous for their spectral class, such as χ^2 Ori and HD 190603, show more and stronger emission components than do the less luminous stars The level of ionization in their winds appears to be lower than for stars of similar T_{eff} but lower luminosity.

The maximum outflow velocity which is observed increases as the effective temperature of the star increases This is shown in Figure 4-14 where log u_∞ is plotted against log T_{eff} taken from Table 4-1. A linear relationship seems to exist, although the scatter of the points is moderate. The straight line which is shown corresponds to

$$u_\infty \sim T_{eff}^{2.30}. \qquad (4\text{-}3)$$

The maximum outflow velocities which are detected for supergiants seem to be about the same as those seen for main-sequence stars having about the same effective temperature. It is difficult to detect outflow from main-sequence stars because the density in the winds of these stars is very low and little information exists on this point

A correlation of u_∞ with T_{eff} is not unexpected because it is reasonable to think that the terminal velocity will be a function of the accelerating force. In the case of the B-type supergiants, this force is believed to be radiation pressure. In the case of a blackbody radiation field, the radiation pressure is equal to $aT^4/3$. Here a is the radiation-density constant A search could be made for correlations between the ter-

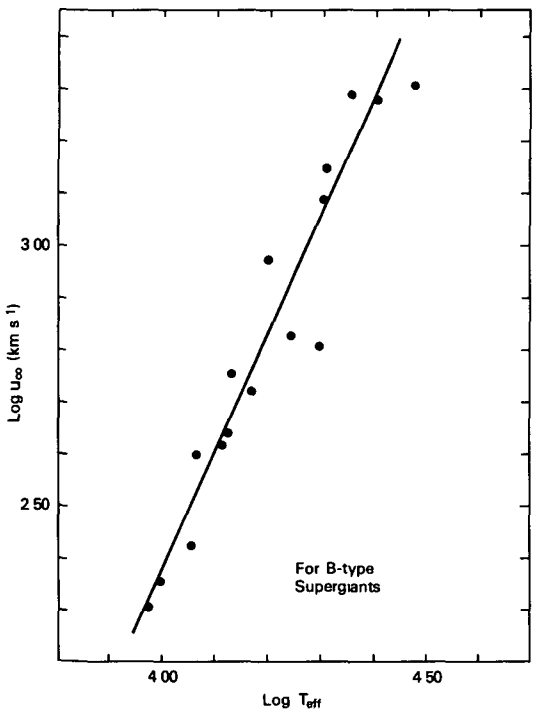

Figure 4-14. The variation of u_∞ with T_{eff} for B-type supergiants.

minal velocity, u_∞, and the mass, radius, or luminosity of a supergiant, but the results would be indecisive because the masses of single B-type supergiants are only very poorly known, and there is an uncertainty of the order of 10 percent in the radii and 20 percent in $L/L_\odot$owing to the lack of precision of our knowledge of the distances of the supergiants. The radii and effective temperatures of the supergiants in Table 4-5 are given in Table 4-1 The uncertainty in the values of T_{eff} is less than about 5 percent.

Shortward displaced, rather sharp absorption components are seen for some of the supergiants in some resonance lines. A few notes about this are given in Table 4-5 This subject is discussed in the next section. Similar components are seen in the spectra of some Be stars (see Part II).

Variability in the Ultraviolet Spectrum

The presence of rather sharp displaced absorption components of the resonance lines of ions has been known ever since it has been possible to study high resolution ultraviolet spectra of the B-type supergiants (see, for instance, Underhill, 1975a, 1975b; Lamers et al., 1978b) Continued observation of a star often shows that the displacements and intensities of the sharp components vary

The notes to Table 4-5 indicate that the occurrence of discrete, moderately sharp, displaced absorption lines formed by the winds from supergiants is fairly common. The displaced components are best seen in the resonance lines of an ion that is only moderately abundant in the wind. (If the ion is very abundant, the absorption trough formed by the wind may be optically thick. Then intensity variations caused by changing densities in some parts of the wind cannot be detected.) Lamers et al. picture the discrete components as being caused by "puffs" which occur in the wind. Much evidence for the occurrence of discrete shortwards displaced components of resonance lines in the spectra of O stars has been compiled by Lamers (1981a) from Copernicus spectra.

Examples of the appearance of rather strong discrete components of Si IV in the spectrum of ρ Leo, B1 Ib, are shown in Figure 4-15. The displacements and intensities of the displaced components vary in a matter of days. The variation of components like these is the chief cause of variation in the ultraviolet spectra of B-type supergiants. The occurrence of fine structure, like that shown at the bottom of the displaced components of ρ Leo, appears to be real; the pattern is constantly changing

Quite clearly, the mantles of the B stars are not homogeneous. The fact that the discrete components are moderately sharp (the ones shown in Figure 4-15 being unusually wide) means that moderate densities of plasma are confined to restricted line-of-sight velocity ranges as seen by a distant observer.

When three observations of the B1 Ib star ρ Leo made on different days using IUE are compared with three observations of the B1 Ia star κ Cas, it is notable that changes in the spectrum are more obvious for ρ Leo than for κ Cas. The same is true when three spectra of 9 Cep, B2 Ib, are compared with three spectra of χ^2 Ori, B2 Ia.

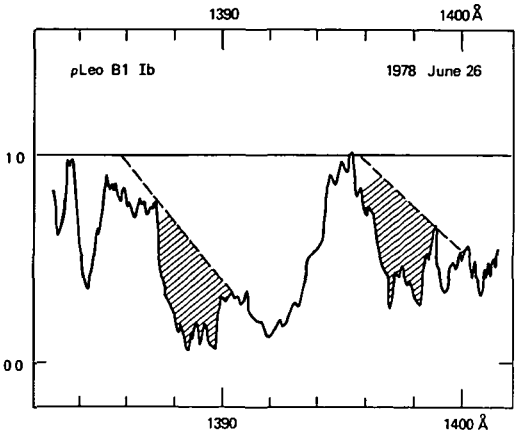

Figure 4-15. Discrete shortward displaced absorption components of Si IV in the spectrum of ρ Leo. The absorption which is attributed to the displaced components is cross-hatched It is seen against the absorption trough formed by an expanding spherical wind, the separation between the two types of absorption being shown approximately by a broken line.

The fluctuations in the density and flow pattern of the mantles of the Ib supergiants are probably seen more easily than are those of the Ia supergiants because the wind profiles observed for Ib supergiants, on the whole, appear to be less saturated than are those for Ia supergiants

Some changes in the profile of the C II resonance lines in the spectrum of 9 Cep are shown in Figure 4-16. The reproducibility of IUE spectra can be gauged by noting the appearance of the interstellar C I lines near 1329 Å and the profiles of the interstellar components of C II. Changes larger than those seen for these features do occur in the detailed structure of the wind component due to C II. These changes indicate that the part of the wind projected against the disk of the star changes its velocity pattern and its density pattern in times of the order of days.

THE INFRARED AND RADIO SPECTRUM OF SUPERGIANTS

Broadband photometric measurements of many B-type supergiants have been made by Johnson et al. (1966), Gehrz et al. (1974), and Barlow and Cohen (1977), intermediate-band results to 11084 Å are given by Johnson and Mitchell (1975). The published magnitudes of Johnson et al. can be converted to absolute energy by means of the broadband photometric calibration factors of Hayes (1979); those of Gehrz et al by the calibration given in their paper, those of Barlow and Cohen by means of the calibration factors given by Cohen (1973a); and those of Johnson and Mitchell by means of the calibration factors which they give in their paper. Infrared observations can be found for 23 of the supergiants listed in Table 4-1. When the observed gross fluxes are corrected for interstellar extinction and plotted against wavelength, comparison with the model flux distributions, found from a study of the angular diameters and effective temperatures to be representative for these stars, shows that many of the supergiants have an infrared excess This infrared excess is believed to be due to free-free emission by electrons in the vicinity of hydrogen ions around the star.

The infrared excess, F_λ (IR) at a wavelength λ is defined here as the difference between the

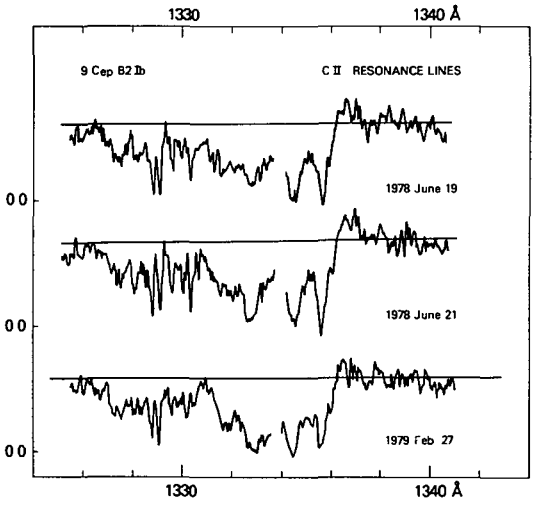

Figure 4-16. Changes in the profiles of the C II lines of 9 Cep, B2 Ib. The intensity scale is linear and the nominal level of zero intensity is marked for each spectrum. A reference line has been drawn to represent the level of the stellar continuum on each spectrum tracing.

observed gross flux at λ, corrected for interstellar extinction, and the quantity $(\theta^2/4)\pi F_\lambda$ (model) which represents the stellar flux. Here θ is the angular diameter of the star listed in Table 4-1 In the present work, F_λ (model) is the monochromatic flux at wavelength λ predicted by Kurucz (1979) for the selected representative model atmosphere To obtain the interstellar extinction at wavelengths longer than 1 μm, the extinction curve of Nandy et al (1975) is extrapolated keeping in mind the estimates of Barlow and Cohen (1977) for the extinction at a few infrared wavelengths. The values of $E(B-V)$ of Table 4-1 are adopted as the factors by which to scale the resulting extinction law. All available excess fluxes for each star were plotted as a function of wavelength and the best value at 10 μm was interpolated graphically.

The infrared excesses at 10 μm for 23 bright B-type supergiants are given in Table 4-6 together with some notes In column 6 an estimate is given of the radio flux at 6 cm that may be expected *if* it is valid to extrapolate the excess spectrum from 10 μm to 6 cm using a power law with slope $\alpha = 0.77$.

Plots of $\log S_\nu$ (IR) vs. $\log \lambda$ for those stars for which measurements of the infrared excess exist to more than 10 μm show that $\log S_\nu$ (IR) can be represented as a linear function of $\log \lambda$ when λ is longer than about 1 μm. Some typical results are represented in Figures 4-17 and 4-18; the curve for P Cyg is from Underhill (1979b). Observations at radio wavelengths exist for P Cyg as well as many observations in the infrared. The justification of selecting $E(B-V) = 0.35$ for P Cyg is given in the next section. A power law with a slope $\alpha = 0.77$ relates accurately the excess flux of P Cyg at 10 μm to the fluxes observed at radio wavelengths.

If the emitting region were optically thin and isothermal, one would expect α to be about 0 6 (Barlow, 1979). Should the emitting region become optically thick at long wavelengths, the value of α will increase because the shape of the spectrum will tend toward that of a blackbody at a low temperature This means that one would expect S_ν (IR) to vary as $T\lambda^{-2}$ as λ increases Predicted radio fluxes at 6 cm, calculated for the case $\alpha = 0.77$, are given in Table 4-6 for those supergiants which have a detectable 10 μm excess They may be compared with the radio fluxes observed at 6 cm.

Six of the stars in Table 4-6 have been observed at 6 cm by Abbott et al. (1980) using the VLA, and the results are given in the notes to Table 4-6. The extrapolated 6-cm fluxes are comparable to the observed 6-cm fluxes for the four stars of spectral type B1 and earlier which are in common with Abbott et al. In the case of β Ori, B8 Ia, and α Cyg, A2 Ia, the observed radio fluxes are much smaller than what is predicted with $\alpha = 0.77$ This result strongly suggests that for the late B and early A supergiants, the infrared excess becomes optically thick and that the effective value of α is significantly greater than 0.77.

The infrared excess fluxes of β Ori and α Cyg are shown plotted as a function of wavelength in Figure 4-18. The infrared excess of both stars extends into the visible spectral range (discussed earlier in this chapter). In fact it seems probable that this happens for all late B and early A supergiants. Barlow and Cohen (1977) noted that the excess in the color difference (K − L) was less for late B stars than for early B stars. This

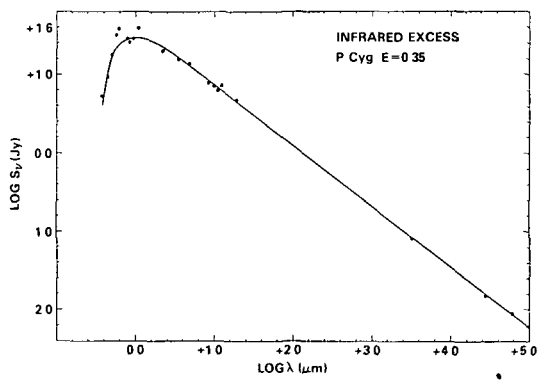

Figure 4-17. The infrared excess of P Cyg and its radio flux plotted as a function of log λ. The observations have been corrected for interstellar extinction using $E(B-V) = 0.35$ The excess is relative to the flux from a model atmosphere with $T_{eff} = 1\,2 \times 10^4$ K, log g = 3.0 (from Underhill, 1979b).

Table 4-6
Excess Radiation at 10 μm and 6 cm for B-Type Supergiants

HR	Name HD	Spectral Type	Sources for Broad-band Photometry[a]	S_ν (10 μm) (Jy)	S_ν (6 cm)[b] (mJy)	Notes
130	κ Ca.	B1 Ia	J66, GHJ, BC	0.44	0.54	
1035	21291	B9 Ia	J66, BC	0.52	0.64	
1040	21389	A0 Ia	J66, BC	0.78	0.96	
1203	ζ Per	B1 Ib	J66, BC	0.0	–	1
1542	α Cam	O9.5 Ia	J66, GHJ	0.01	0.02	
1713	β Ori	B8 Ia	J66, GHJ, BC	12.8	15.8	2
1852	δ Ori	O9.5 I	J66, BC	0.65	0.80	
1903	ε Ori	B0 Ia	J66, GHJ, BC	0.90	1.1	3
1948	ζ Ori A_1	O9.5 I	J66, GHJ, BC	0.90	1.1	4,5
2135	χ^2 Ori	B2 Ia	J66, GHJ, BC	0.46	0 57	
2596	ι CMa	B4 Ib	J66	–	–	6
2653	o^2 CMa	B3 Ia	J66, BC	0.81	1.0	
2827	η CMa	B5 Ia	J66, BC	0.39	0.48	
3975	η Leo	A0 Ib	J66, GHJ, BC	0.0	–	7
4133	ρ Leo	B1 Ib	J66, GHJ, BC	0.13	0.16	
6714	67 Oph	B5 Ib	J66, BC	0.09	0.11	
7589	188209	O9.5 I	J66	–	–	6
7678	190603	B1 Ia+	J66, BC	0.30	0.37	8
7763	P Cyg	B1 Iap	J66, GHJ	7.3	9 0	9
7924	α Cyg	A2 Ia	J66, BC	13.8	17.0	10
7977	55 Cyg	B3 Ia	J66, BC	0.07	0.09	
8279	9 Cep	B2 Ib	J66	–	–	11
8541	4 Lac	B9 Ib	J66, BC	0.27	0 33	

[a] All of the stars have 13-color photometry to 11084 Å.
J66 = Johnson et al (1966)
GHJ = Gehrz et al (1974).
BC = Barlow and Cohen (1977)
[b] An extrapolation has been made from S_ν (10 μm) with $\alpha = 0.77$.

Notes to Table 4-6

1. No excess apparent to 10 μm.
2. Abbott et al. (1980) find S_ν (6 cm) < 1.5 mJy.
3. Abbott et al. (1980) find S_ν (6 cm) = 1.6 mJy.
4. Photometry has been corrected for the presence of companions.
5. Abbott et al. (1980) find S_ν (6 cm) = 0.7 mJy.
6. No excess apparent to 0.9 μm.
7. No excess apparent to 11.4 μm.
8. Abbott et al. (1980) give S_ν (6 cm) $\leq$ 0 5 mJy.
9. Abbott et al. (1980) give S_ν (6 cm) = 10.8 mJy.
10. Abbott et al. (1980) give S_ν (6 cm) < 0.4 mJy
11. No excess apparent at 3.6 μm

quantity measures the slope of the excess spectrum between 3.6 and 10.0 μm. That a flattening of the spectrum occurs is confirmed by the observations shown in Figure 4-18. These data give $\alpha = 1.22$ for β Ori and $\alpha = 1.11$ for α Cyg. These values of α are significantly larger than the values near 0.77 which are found for P Cyg and for early B-type supergiants.

As the wavelength decreases, the infrared excess will become optically thin, a turnover occurs at a wavelength shortward of 1 μm when

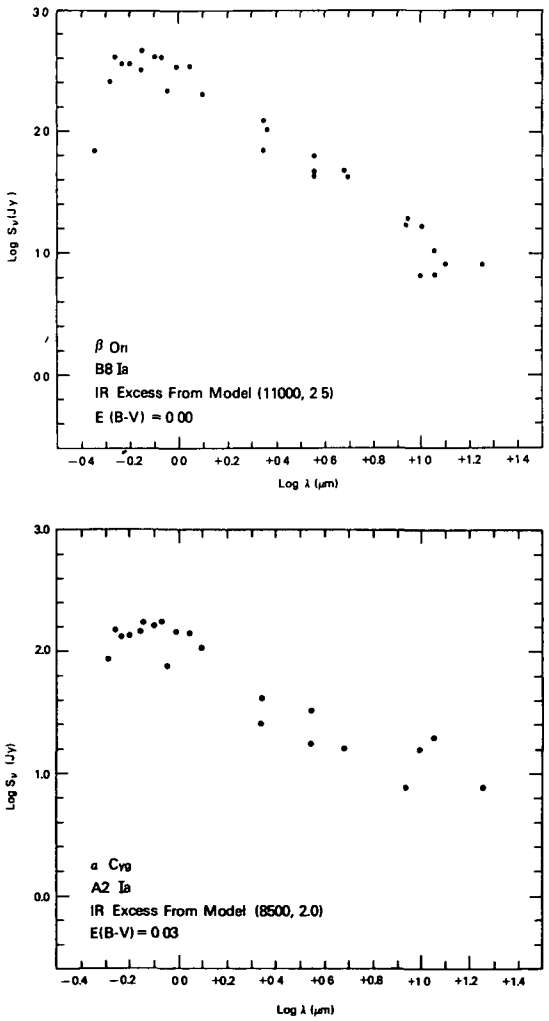

Figure 4-18. The infrared excesses of the supergiants β Ori and α Cyg plotted as functions of log λ. The observations have been corrected for interstellar extinction using the noted values of $E(B-V)$.

log S_ν (IR) is plotted against log λ. Simple considerations (see, for instance, Cohen et al., 1975) show that if λ_p is the wavelength of the peak of the curve in a plot of log λF_λ (or log νS_ν) against log λ, then the electron temperature in the emitting region can be estimated from the relation given in Equation (4-1). The emitting region is assumed to be an isothermal sphere of hydrogenic gas. Typically λ_p occurs at about 0.65 μm in the case of the B-type supergiants which have an infrared excess; thus, the electron temperature in the emitting regions around the B-type supergiants is about $2\,2 \times 10^4$ K. Since the effective temperatures of the late B-type supergiants are of the order of $1\,1 \times 10^4$ K or smaller, it is clear that the infrared excess from these stars is coming from a region that is superheated relative to the photospheres of the late B-type supergiants. Since the effective temperatures of the early B supergiants fall in the range 2.5×10^4 K to 1.8×10^4 K, the electron temperatures in the region which is emitting the infrared excess are of the order of the effective temperature of the star or a little higher.

The amount of infrared excess energy which is measured for a star varies inversely as the square of the distance to the star, other factors being equal Thus, before comparing the strengths of the infrared excess in a group of stars, it is desirable to scale the measured excesses so that they correspond to stars all at the same distance Figure 4-19 shows the infrared fluxes at 10 μm normalized for a distance of 1 kpc and plotted as a function of spectral type. It is clear that the Ib supergiants have small infrared excesses in comparison to what is seen for the Ia supergiants, the superluminous supergiant HD 190603, and for P Cyg

The star P Cyg, in keeping with its well-known, strong hydrogen emission spectrum, has an unusually strong infrared excess. The Ia supergiant α Cyg (A2 Ia) also has an unusually strong infrared excess The strength of the infrared excess of HD 190603 is larger than that of most Ia supergiants, but it is not outstanding There seems to be no monotonic trend of the strength of the infrared excess with either luminosity or spectral type (effective temperature).

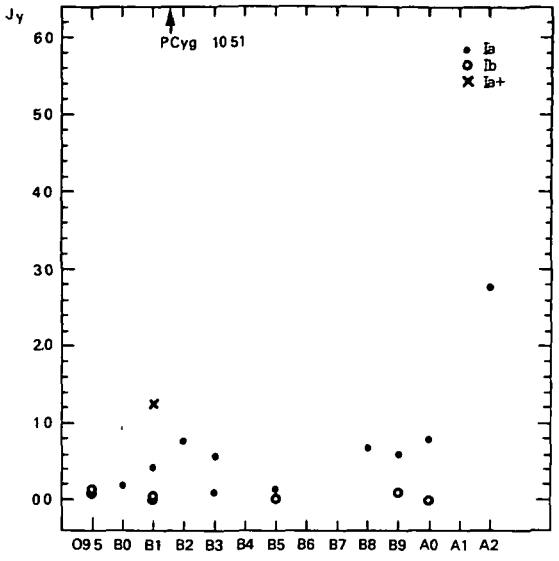

Figure 4-19. Infrared excesses of supergiants at 10 μm, normalized to a distance of 1 kpc, and plotted against spectral type.

The infrared excess of a supergiant is believed to result from free-free emission in a volume of gas surrounding the supergiant. The density and extent of a region emitting free-free radiation will surely be intimately connected with the physical state of the mantle. We have seen from a survey of the ultraviolet spectra of the B supergiants that the state of the mantle is not uniquely determined by the effective temperature of the star nor by the luminosity, although the mantles around Ib supergiants appear to be less dense than those around Ia supergiants. The intrinsic strengths of the infrared excesses also are in accord with this picture It is important to note that so far as can be determined, the electron temperature in the part of the mantle which radiates the infrared excess is near $2\,2 \times 10^4$ K for B supergiants of all effective temperatures. This probably means that the occurrence of a detectable amount of free-free emission depends more on the properties of the mantle and on the physics of the hydrogen atom than on the properties of the underlying star For all Ia supergiants, a large enough volume at appropriate density to give a detectable amount of free-free emission does occur around the star. It is uncertain at this time whether or not the volume that gives the free-free infrared excess emission is the same as that which gives the Paschen and Balmer lines and continua in emission. Possibly a study of the relative amounts of energy in these several parts of the hydrogen emission spectrum would provide an answer to this question.

Few high dispersion observations of the line spectra of B-type supergiants in the infrared have been published because the faintness of B stars at long wavelengths coupled with the lack of sensitivity of photographic emulsions has made it very difficult to obtain useful observations. The development of electronic detectors and methods of obtaining spectral dispersion other than by the use of a grating or prism have lead to new advances.

Spectra of the supergiants ζ Ori (O9.5 I), ϵ Ori (B0 Ia), P Cyg (B1 Iap), 55 Cyg (B3 Ia), χ Aur (B5 Iab), HD 183143 (B7 Ia), β Ori (B8 Ia), and α Cyg (A2 Ia) have been published by Johnson (1978) and by Johnson et al. (1978). The published spectral intensity tracings were made with a Michelson spectrophotometer, the spectral range is from 4800 to 10300 Å and the element of resolution is 3.85 cm^{-1}.

Lines of H and He I are seen clearly in absorption as well as quite a few lines from the second and third spectra of the light elements and of iron. A few emission lines occur The published spectra confirm that a luminosity effect in the strength of O I 7774 occurs, particularly in the spectra of stars of types B5 to G0, as was discussed earlier by Keenan and Hynek (1950). The O I lines at 8446 and 7774 Å sometimes appear in emission in supergiants and in Be stars. The occurrence of emission in O I 8446 is believed to be related to the intensity of emission in Lβ of hydrogen at 1025 Å (see Bowen, 1947; Kitchin and Meadows, 1970). Because the continuous absorption coefficient in the atmospheres of B stars is strong at near infrared wavelengths, chiefly because of free-free absorption, the infrared absorption lines reveal information about conditions high in the photosphere or low in the mantle of B stars No analyses have been published at the time of writing of the infrared spectra of B supergiants or main-sequence stars

presented by Johnson (1978) and by Johnson et al. (1978). The spectral intensity tracings obtained with the Michelson spectrophotometer have a photometric accuracy of the order of or better than 2 percent, and the wavelength scale is very stable since it is determined by the properties of the interferometer which is used and the stability of the HeNe reference laser.

THE PECULIAR SUPERGIANT P CYG AND THE SUPERLUMINOUS SUPERGIANTS

The star P Cyg is a unique object, and it is the archetype for understanding a particular combination of emission and absorption in spectral lines The properties of this famous star and those of the superluminous supergiants will be discussed in this section.

P Cyg

The star P Cyg is unique among the relatively bright stars in that it is the only one which, in the visible spectral range, shows a spectrum almost exclusively composed of emission lines each accompanied by a shortward displaced absorption core. This type of line profile—the "P-Cygni" profile—can be understood in terms of an outflowing spherical atmosphere (see Chapter 6).

A brief summary of the history of the light variations of P Cyg and of the types of spectroscopic features that occur in the spectral range accessible from the Earth can be found in Underhill (1966a). More extensive summaries of early observations are given by de Groot (1969) and by Ambartzumian et al. (1979). In this section, spectroscopic observations made since 1965 will be reviewed and an attempt will be made to interpret what is seen by means of a qualitative model like that which is useful for understanding the spectra of B-type supergiants. Fernie (1969) has shown that P Cyg now is rather constant in light.

A detailed study of the radial-velocity variations, aswell as some line-profile information has been presented by de Groot (1969); he also determined the equivalent widths of the most conspicuous lines and applied simple diagnostic techniques to find out the physical characteristics of P Cyg. De Groot made use of high dispersion spectra spanning the range from 3150 to 8800 Å. Very extensive measurements of radial-velocity displacements made on high dispersion spectra have been published by Özemre (1978); these data have been discussed by Avcioğlu (1979, 1980) Long lists of identifications have been given by de Groot (1969), by Özemre (1978), and by Johnson et al. (1978) who published intensity tracings of the spectrum of P Cyg from 4800 to 10300 Å obtained with a Michelson spectrophotometer. Some identifications and measurements of equivalent widths from moderate dispersion spectra have been given by Luud (1967). Luud interpreted his measurements by means of the curve of growth and found that the ionization temperature in the atmosphere of P Cyg is near 2.1×10^4 K and that the composition is like that of B-type supergiants. Hutchings (1969) has interpreted the earlier observations of Beals (1950) and of Struve and Roach (1939) to find a model for the expanding atmosphere and to estimate the rate of mass loss.

Profiles of Hα, Hβ, and Hγ, determined from 16 Å mm^{-1} spectra, are shown in Kuan and Kuhi (1975) while profiles of the lines He I 7065, He I 5876, and Hα, determined with high accuracy using electronic detectors, are presented by Bernat and Lambert (1978). The intensity of the Pα line of hydrogen has been measured by Jones and Wolff (1980). Frank et al. (1980) have observed a classical "P-Cygni" profile for He I 10830 with the emission reaching five times the height of the continuum.

High resolution observations of the spectrum of P Cyg have also been made in the ultraviolet. Short spectral regions have been studied by Hutchings (1976c) and by Ambartzumian et al. (1979) using Copernicus. The full range from 1170 to 3200 Å has been observed using the high resolution spectrographs of IUE (see Cassatella et al., 1979; Hutchings, 1979; Underhill, 1979b, 1980c; Luud and Sapar, 1980).

The chief results found from all these observations will be discussed here and an attempt will be made to coordinate what is seen with the

characteristics of a model which will represent the photosphere and mantle of P Cyg. It must be emphasized that although it is frequently noted that the spectra of the normal B-type supergiants contain a few lines which have a typical "P-Cygni" profile, the spectrum of P Cyg is very unlike that of a normal early type supergiant. In the spectrum of P Cyg, all of the absorption lines are displaced shortward by a significant amount (different types of lines being displaced by different amounts), and most of the lines in the visible spectral range appear in emission as well as in absorption One sees very few, if any, absorption lines that may be associated with the presence of a more or less normal, stationary photosphere. The spectrum of P Cyg is composed entirely of features which may be associated with line formation in a superheated, outflowing mantle.

Visible Observations. The study of high dispersion spectra of P Cyg has resulted in an abundance of information about the displacements of the absorption cores of lines in the spectrum of P Cyg and information about the shapes of the line profiles. De Groot showed that, at the very highest dispersion, one could see three absorption components for the Balmer lines. This is illustrated in Figure 4-20 which is taken from de Groot (1969). Here a first attempt is made to separate the blended profile due to three absorption components and an emission feature into its component parts The longward side of the emission feature was reflected and subtracted from the observed profile to obtain the blended profile due to the absorption components (thin line) The "unblended" profile of the least displaced component is found by rectifying the observed absorption dip relative to the continuum represented by the longward wing of the central absorption component. Van Blerkom (1970) has warned that the procedure followed by de Groot can lead to spurious results in the case of strong emission components

De Groot found that absorption component 1, the component nearest the undisplaced position of the line, usually has a displacement near -95 km s^{-1}, that absorption component 2 has a displacement near -140 km s^{-1}, and that absorption component 3 has a displacement in the range -180 to -240 km s^{-1}. The radial velocities shown by the third component appear to vary with a period of 114 days. The positions which De Groot deduces for the centers of the three absorption components and the emission component after applying his correction for blending below the measured positions are shown in Figure 4-20. Blending does modify the position of each extremity of the profile a little, but it does not seriously affect the apparent position of absorption component 3. Consequently, de Groot's conclusion that absorption component 3 shows a variable radial velocity is secure. Absorption components 2 and 1 as well as the emission component do not appear to change in wavelength. The Balmer lines do not usually show a Balmer progression.

Most of the spectra studied by de Groot have a dispersion of 10 Å mm^{-1} or better Therefore

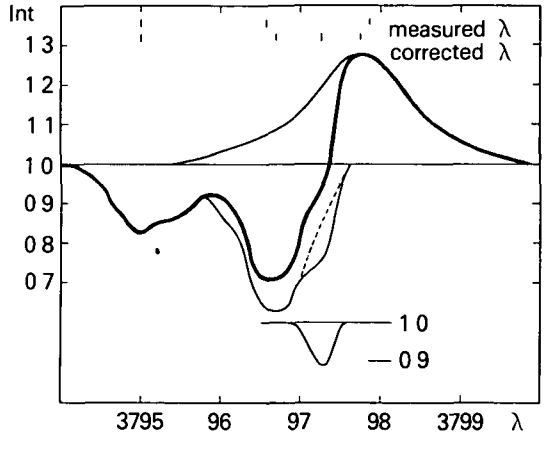

Figure 4-20. The profile of H10 at 3897.900 Å in P Cyg. The observed profile is shown by a heavy line and the measured wavelengths for the emission component and two absorption cores are indicated at the top of the diagram. A thin line shows the reconstructed full emission component and the resulting absorption profile corrected for blending with the emission. The weak least displaced absorption component, reconstructed by adopting the dotted line as its continuum, is shown below the main profile (from de Groot, 1969)

de Groot was able to resolve the several components seen in the strong lines of the spectrum of P Cyg. This is important for understanding what is occurring. The profiles presented by Kuan and Kuhi (1975) for Hα, Hβ, and Hγ are from lower dispersion spectra; they do not show the full complex structure which is present. This is partly a result of the very strong emission seen for the first few members of the Balmer series. Luud (1967) has presented data showing that sometimes the pattern of absorption components changes and only one component can be seen where two were present on another date. Ozemre (1978) used high dispersion spectra and she was able to resolve most of the structure seen by de Groot.

The profiles of He I 7065, He I 5876, and Hα shown by Bernat and Lambert (1978) have broad, extensive, weak emission wings which Bernat and Lambert conclude are due to electron scattering. A double absorption structure is not visible for the lines observed by Bernat and Lambert chiefly because the emission component is very strong and it extends to about 100 km s^{-1} shortward of the undisplaced position of the line. The great strength of the emission component of these lines means that the emission comes from an extended region around the star.

Beals (1950) noted that the lines coming from the ions which need the most energy for their formation generally have the smallest shortward displacement, whereas lines from abundant neutral atoms, such as hydrogen and helium, show larger displacements. In general the shortward displacement of the deepest point of the absorption core decreases as the total excitation energy of the line increases. The total excitation energy is defined to be the sum of the excitation energy of the lower level of the ion plus the ionization energy of all preceding stages of ionization.

The measurements of de Groot and particularly of Özemre have done much to define what occurs. The relationship between the total excitation energy of the lower level of the line and the displacement is not sharply defined, nor is it unique, since some lines have two or more components. A schematic representation of the observed relationship, developed from the data of Avcioğlu (1980), is shown in Figure 4-21. Quite definitely the material seen by means of absorption lines in the visible spectrum of P Cyg shows a wide range of outwardly directed line-of-sight velocities. Not all velocities are represented equally frequently. Lines having a total excitation energy in the range 60 to 100 eV usually show radial velocities in the range − 10 to − 60 km s^{-1}. Most of the lines having a total excitation energy in the range 30 to 60 eV show a radial velocity in the range − 40 to − 150 km s^{-1} Lines having total excitation energies in the range 0 to 30 eV show a radial velocity in the range − 140 to − 240 km s^{-1}. Many of the lines from H and He I and some of the strongest lines of N II and Fe III show two components clearly, a third component is seen for hydrogen lines for which the emission is not strong.

A schematic representation shown in Figure 4-21 represents the most frequently observed relationship between radial-velocity displacement and total excitation energy. Typically the scatter about each branch of the relation is ± 20 km s^{-1} Those lines with a total excitation

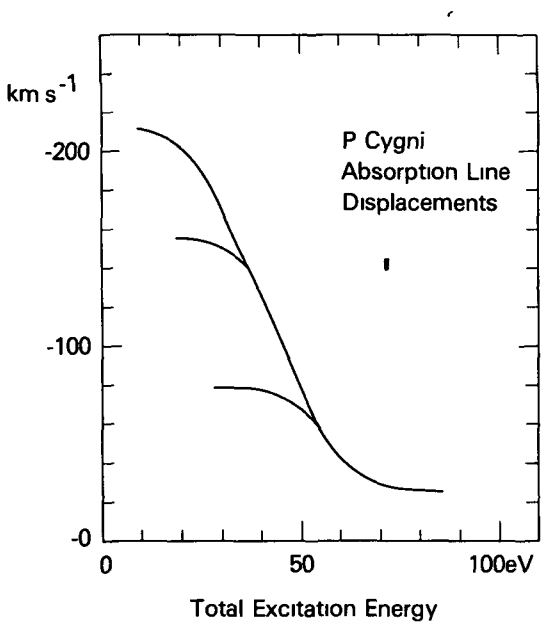

Figure 4-21. A schematic representation of the relation between line displacement and the total excitation energy of the line (from Avcioğlu, 1980).

energy less than about 20 eV (chiefly lines of H and He I) show predominantly displacements in the range − 120 to − 240 km s^{-1} De Groot was able to measure some hydrogen components (total excitation energy of 10.15 eV) having displacements near −95 km s^{-1}.

Beals (1950) concluded that the Na I resonance lines (total excitation energy of 0.00 eV) showed displacements of about −185 km s^{-1}, and he attributed the weak emission features which he saw near the positions of the interstellar Na D lines to Na I De Groot and Özemre interpreted the spectrum near 5890 Å in the same way, although they noted that lines of C II and Fe III could be blending with the Na I lines. The spectrum profile shown by Bernat and Lambert (1978) for the region from 5830 to 5930 Å suggests that the emission attributed by Beals to Na I is really part of the extended emission wings of He I 5876. This conclusion is supported by the facts that Beals, de Groot, and Özemre do not find a strongly displaced absorption component that they can attribute to the resonance line of Ca I at 4227 Å and that IUE spectra covering the region of the Mg I resonance line at 2852 Å reveal only an interstellar line. Absorption lines from neutral atoms with ionization potentials less than 10 eV do not seem to be present in the spectrum of P Cyg except as interstellar lines, and there is no secure evidence for emission from these neutral atoms

The profiles of the resonance lines formed in absorption in the wind of P Cyg reveal the presence of outflow velocities far exceeding what is seen from the visible spectrum (see the next section).

Both Luud (1967) and de Groot (1969) analyzed the equivalent widths of lines in the visible spectrum by simple techniques which represent the line-forming layers as a stationary layer of constant temperature and pressure. The ionization temperature and densities which result are comparable to the values found for normal B1 supergiants. The true meaning of the numbers is doubtful, considering that the radial-velocity displacements indicate that regions where the general level of ionization and excitation is high show a smaller outflow velocity than do those regions where the level of ionization and excitation is low. De Groot compared all measurements of equivalent width which were available to him and concluded that real changes in the intensities of the absorption lines occur over a range of about 30 percent

The interpretation of the profiles of Hα, Hβ, and Hγ in terms of an atmosphere which is accelerating outward or one which is decelerating outward is discussed in Chapter 6.

Ultraviolet Observations What is presented here has mostly been developed from studies of high resolution IUE spectra of P Cyg which cover the range 1200 to 3200 Å. Unfortunately all of the information published by Cassatella et al (1979), Hutchings (1979), and Underhill (1979) having to do with the shapes and intensities of lines in the spectrum of P Cyg is inaccurate because the spectra were reduced with an erroneous photometric transfer function The results concerning velocity displacements are reliable because the wavelength scale was not affected by the photometric error. The work of Underhill (1980c) is based on new spectrum tracings which have been made using the correct photometric transfer function Thus, the line profiles presented here, as illustrative of what is seen in the ultraviolet spectrum of P Cyg, are photometrically correct. The results of Hutchings (1976c) and of Ambartzumian et al. (1979), which are based on the analysis of short sections of spectral tracings obtained with the Copernicus satellite, are in agreement with what is presented here

Presently available information on the displacements of the ultraviolet lines is summarized in Table 4-7 The ranges of uncertainty given by each author probably represent the dispersion about each mean value These numbers represent the uncertainty of any one wavelength measurement of an absorption line in the spectrum of P Cyg The ultraviolet spectrum of P Cyg is full of lines, a fact which can be seen from the short sections of spectrum shown in Figures 4-22 to 4-27 Because of the crowding of lines, the accuracy with which the apparent center of the line can be determined ranges from about 0.05 to 0.10 Å The wavelength of the lines measured lie

Table 4-7

Outflow Velocities (km s^{-1}) for P Cyg deduced from the Positions of the Centers of Displaced Absorption Lines from the Second and Third Spectra of the Elements Mg to Y

Spectrum	LS[a]	Hu[a]	C+[a]	Spectrum	LS[a]	Hu[a]	C+[a]
Mg II	−158 ± 9	−200 ± 5	−200	Cr II	−170 ± 62	—	−213 ± 2
Al II	−178 ± 18	—	—	Cr III	− 123 ± 25	[b]	− 93 ± 20
Al III	−188 ± 25	−183 ± 5	—	Mn II	−153	—	−246 ± 20
Si II	−180 ± 19	−227 ± 16	—	Mn III	− 89 ± 18	[b]	—
Si III	−110 ± 29	−140 ± 10	−71 ± 14	Fe II	−202 ± 14	−230 ± 5	−215 ± 15[c]
P II	−163 ± 54	—	—	Fe III	−133 ± 26	−157 ± 5	−103 ± 37
P III	−213 ± 32	—	—	Co III	−181	—	—
S II	−178 ± 14	—	—	Ni II	−182 ± 17	—	−205 ± 10[c]
Ca II	−128 ± 21	—	—	Ni III	−131 ± 22	[b]	− 79 ± 6
Sc III	−136 ± 28	—	—	Sr II	−183	—	—
Ti III	−137 ± 33	[b]	−112 ± 15	Y III	−182 ± 37	—	—

[a] LS is Luud and Sapar (1980), Hu is Hutchings (1979), C+ is Cassatella et al (1979)

[b] Hutchings (1979) gives a mean outflow velocity of − 155 ± 10 km s^{-1} from 100 lines of Ni III, Mn III, Cr III, Ti III, and V III taken together

[c] A second component is measured by Cassatella et al , (1979) for Mn II at − 197 ± 6 km s^{-1}, for Fe II at − 171 ± 8 km s^{-1}, and for Ni II at − 158 ± 4 km s^{-1}

Dashes (—) represent no information available from this source.

in the range 1200 to 3000 Å Thus, the velocity factors, c/λ, vary from 250 km s^{-1} $Å^{-1}$ to 100 km s^{-1} $Å^{-1}$ This indicates that typically the center of a line may be determined to within a displacement of 10 to 25 km s^{-1}.

Most of the ultraviolet lines in the third spectra of the light elements and metals have excitation potentials less than 15 eV. Consequently, the "total excitation energy" of the lines measured in the ultraviolet usually lies in the range 6 to 35 eV. This means that the lines are expected to have displacements in the range −90 to −220 km s^{-1} (see Figure 4-21). The results in Table 4-7 show that the displacements of the ultraviolet lines are compatible with what is shown by the visible spectrum. Very few of the ultraviolet lines appear to show two components This result is chiefly due to the limited resolution of IUE, $\Delta\lambda$ = 0.10 to 0 12 Å, and to the size of the ultraviolet velocity factors. In most cases the lines of the second spectra of the light elements and the metals show greater displacements than do the lines of the third spectra

In Figures 4-22 to 4-25, the profiles of the resonance lines from abundant ions are compared with profiles of resonance lines in the spectra of κ Cas, B1 Ia, and η CMa, B5 Ia In the figures some neighboring lines are identified and their displaced positions in P Cyg are indicated. It is evident that the ultraviolet spectrum of P Cyg is more similar to that of η CMa than to that of κ Cas. This is particularly true for the resonance lines of N V, not shown. These lines are strong at type B1 Ia but absent at B5 Ia, they are not seen for P Cyg

The profile of the blended resonance lines of C II (Figure 4-22) in P Cyg shows sharp components due to the interstellar gas and a strong absorption trough composed of displaced, discrete absorption components and a typical "wind" absorption profile. The emission component is strong. It has been partially obliterated by the interstellar line at 1335.71 Å. The star P Cyg resembles κ Cas in showing emission in the C II resonance lines

The Mg II resonance lines as well as the lines of multiplet UV 3 of Mg II (which have an excitation potential of 4 4 eV) are shown in Figure 4-23. All three stars show strong interstellar lines due to Mg II. Neither κ Cas nor η CMa show

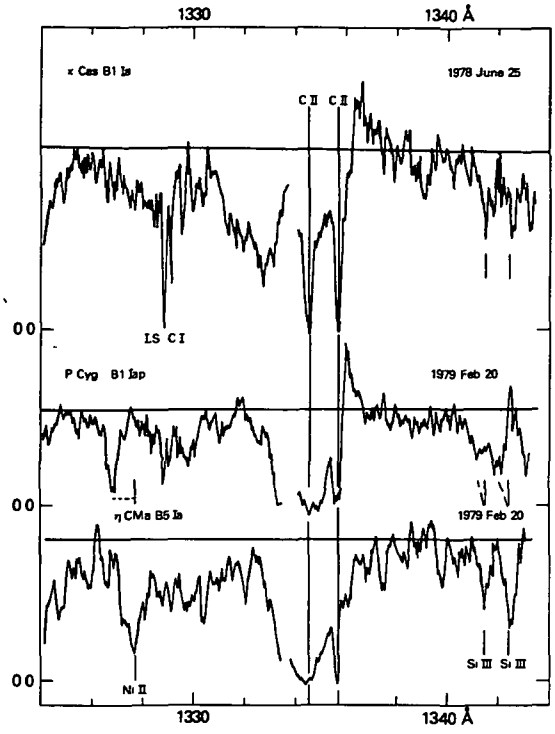

Figure 4-22. The spectrum of P Cyg in the neighborhood of the C II resonance lines compared with those of κ Cas and η CMa. The intensity scale in each section is linear and the nominal level of zero intensity has been marked for each section. A continuum has been drawn for each section after consideration of long stretches of spectrum. A few neighboring lines from excited levels are identified and their displacement is shown for P Cyg. The zero point of the wavelength scale is such that the interstellar lines have zero displacement on the average.

wind profiles from Mg II. However, η CMa shows photospheric lines of moderate strength. The Mg II lines of P Cyg show "wind" profiles with strong emission components and conspicuous flat-bottomed absorption troughs indicating saturation in the resonance lines of Mg II. The energy removed by the absorption troughs is much greater than that which appears in the emission peaks. This result may be due in part to the strength of the interstellar absorption lines It may also be a result of the presence of Mg II absorption lines in the photospheric spectrum which is scattered by the mantle The strength of the lines of multiplet UV 3 of Mg II in the spectrum of P Cyg suggests that P Cyg has a later spectral type than B1.

The profiles of the resonance lines of Si IV of κ Cas, P Cyg, and η CMa are compared in Figure 4-24. The Si IV lines are very strong in the spectra of normal B1 supergiants but only moderately strong at type B5 Ia. The Si IV lines of P Cyg are comparable to those of η CMa but no emission is seen. Rather strong, sharp, undisplaced lines of Si IV occur in the spectra of P Cyg and η CMa. They are probably formed in a distant circumstellar region which lies between the observer and the star. Similar components cannot be clearly distinguished for κ Cas The spectrum of displaced lines from excited levels in P Cyg is similar to the normal photospheric spectrum of η CMa.

The profiles of the C IV resonance lines of κ Cas, P Cyg, and η CMa are compared in Figure 4-25. The broad absorption trough and emission

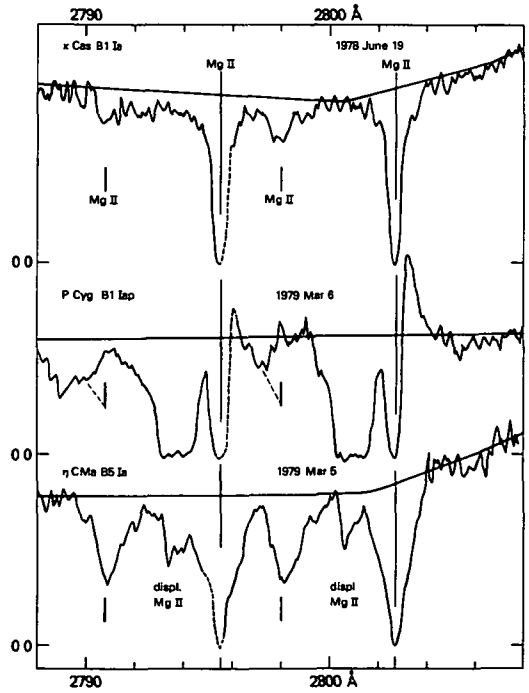

Figure 4-23. The spectrum of P Cyg in the neighborhood of the Mg II resonance lines compared with those of κ Cas and η CMa.

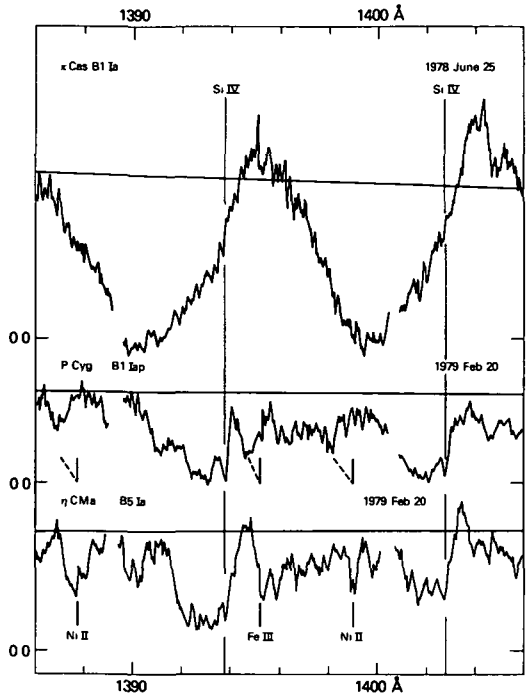

Figure 4-24. The spectrum of P Cyg in the neighborhood of the Si IV resonance lines compared with those of κ Cas and η CMa.

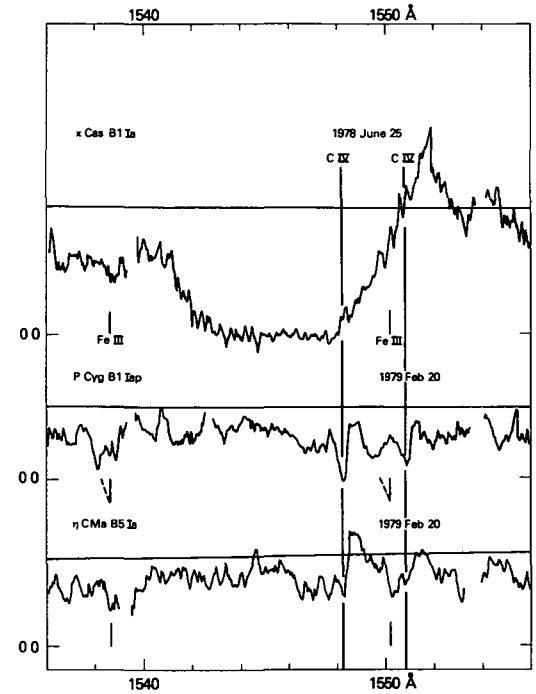

Figure 4-25. The spectrum of P Cyg in the neighborhood of the C IV resonance lines compared with those of κ Cas and η CMa.

component that is typical at type B1 Ia and at earlier types is conspicuous for κ Cas. Weak C IV resonance lines with wind profiles appear to be present for η CMa and probably for P Cyg. This special region is difficult to interpret because it is a complex blend for both P Cyg and η CMa Many lines of Fe III, some quite strong, fall in this region. The positions of two of the strongest lines of Fe III are indicated. Rather sharp undisplaced components due to C IV are very strong in P Cyg, they are present, but weaker, in the spectrum of η CMa and present also, possibly, for κ Cas

The presence of strong, rather sharp circumstellar absorption components for the Si IV and C IV resonance lines as well as the presence of many moderately strong displaced lines due to Cr III (mostly near Si IV) and Fe III (mostly near C IV) make it difficult to decide on the true shape of the profiles of the resonance lines of Si IV and C IV in P Cyg. It seems unlikely that strong photospheric lines with central emissions are present as Cassatella et al. (1979) have suggested.

This review of the profiles and strengths of the strong resonance lines which are formed in the mantle of the star shows that the mantle of P Cyg is similar to that of η CMa, so far as these lines are concerned. It is not similar to that of a B1 supergiant The width of these profiles in the spectrum of P Cyg is similar to that of the lines of η CMa. The profiles of the strong resonance lines in the spectrum of κ Cas are much wider.

Profiles of resonance lines from the metals are shown in Figure 4-26. Here a leader line is drawn to the displaced resonance line and the identification of nearby lines is indicated The interstellar components of Mn II, Fe II, and Ni II are also indicated There is no interstellar component for Si II 1533 because the excitation energy of the lower level of this line is 287 32 cm^{-1} This line has no emission component Review of these profiles and the profiles of other resonance lines of Fe II, Ni II, and Si II as well as of strong lines

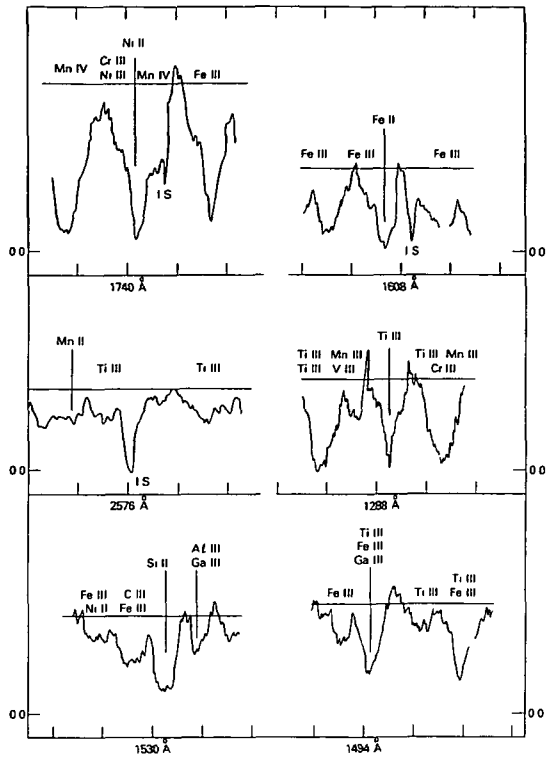

Figure 4-26 The spectrum of P Cyg in the neighborhood of resonance lines of the metals. The intensity scale is linear in each section and a continuum has been drawn after considering long sections of spectrum. The zero point of the wavelength scale is such that the interstellar lines have zero displacement on the average The major components of each absorption line are indicated (see the text).

from excited levels shows that the lines of the second spectra are generally narrower than the lines from the third spectra of the elements having moderate abundances Information about the outflow velocities implied by the position of the shortward edge of each resonance line is given in Table 4-8 together with information about the presence of emission. The strongest resonance lines of moderately abundant ions are flat bottomed.

The lines of Mn II are not strong in the spectrum of P Cyg, although the interstellar lines due to Mn II are very strong The second components measured by Cassatella et al. for Mn II, Fe II, and Ni II correspond to the inflections seen on the longward side of the Ni II and Fe II profiles displayed here. The resonance lines of Ti III look like the Ti III lines coming from excited levels. Emission accompanies some of these lines.

The resonance lines of Ga III may be contributing to the lines shown in the bottom sections of Figure 4-26. These lines have weak emission components in contrast to what is seen for most lines in their neighborhood Comparison with the spectrum of η CMa suggests that the absorption components are a little stronger in P Cyg relative to absorption features due to other lines in the appropriate multiplets of Ti III, Fe III, and Al III than in η CMa. The presence of distinct emission components next to the absorption lines at 1494.25 and 1533.80 Å is unusual. It can be understood if resonance lines are contributing to the blends which are seen The cosmic abundance of gallium is less than 10^{-5} that of iron

The values given in Table 4-8 for the maximum outflow velocities seen by means of the ultraviolet lines arising from ground states of various ions are average values The number of results used to form each average value is indicated as well as whether or not emission can be detected on the longward side of the profile. For the lines having an excitation potential of exactly 0 00 cm^{-1}, a strong interstellar line lies at the undisplaced position of the line, it tends to obliterate the emission. Typical cases are shown by the profiles of Ni II 1741 and Fe II 1608 When no interstellar lines are present, as for Ti III and Ga III, the emission, if present, is seen easily. The maximum outflow velocities in parentheses are particularly uncertain values owing to difficulty in defining the shortward wing of the line profile because of blending by overlapping lines.

The outflow velocities seen by means of the Si III and Si IV lines are a little larger than those seen by means of the Fe II and Ni II lines In the ultraviolet, weak emission is usually seen near lines from the second spectrum but not often from lines of the third spectrum This may occur because the photospheric radiation which is resonantly scattered to form the emission peak has been depleted to a greater extent by the presence of photospheric absorption lines in the case of third spectra than for second spectra

Table 4-8
Maximum Outflow Velocities and Emission Seen by Means of Resonance Lines in the Ultraviolet Spectrum of P Cyg

Spectrum	u_∞ km s^{-1}	No. Lines	Emission	Spectrum	u_∞ km s^{-1}	No. Lines	Emission
C II	−410	1	yes	Si IV	(−430)	2	no
C III[a]	−280	1	no	S II	−260	2	yes
Mg II	−430	2	yes	Ti III	−310	2	yes
Al II	(−150)	1	yes	Fe II	−300	6	?
Al III	(−404)	2	no	Ni II	−260	6	yes
Si II	(−350)	10	yes	Zn II	−280	1	no
Si III	−420	1	no	Ga III[b]	−270	2	yes

[a] Lines from the metastable 2^3P^o levels, blended multiplet UV 4
[b] Ga III is only one contributor to these lines (see text).
? means that the presence or absence of emission is uncertain

When one compares the maximum outflow velocities in Table 4-8 with those for normal B-type supergiants given in Table 4-5, one sees that the outflow velocities for P Cyg are similar to those for late B-type supergiants. They are about 0.25 times those seen for B1 supergiants. In this respect the nominal spectral type of P Cyg, B1 Iap, does not give a good guide to what is actually seen.

The largest outflow velocities, about − 400 km s^{-1}, are seen for the most abundant ions Maximum outflow velocities in the range − 260 to − 300 km s^{-1} are seen for less abundant ions These values are close to the values indicated by the positions of the shortward edges of the Ti III, Cr III, and Fe III lines from excited levels and to the value suggested by the width of the blended C III feature at 1176 Å.

Interpretation of the relation between total excitation energy and outflow velocity established from studies of the visible spectrum (see Figure 4-21) is not straightforward. From Figure 4-21 one would expect lines having total excitation energies near 55 eV to show evidence for outflow velocities from about − 15 to about − 80 km s^{-1} The resonance lines of Si IV have just this total excitation energy. Figure 4-24 and Table 4-8 illustrate that Si^{+3} ions are seen with velocities in the range from 0 to − 400 km s^{-1} or so. The wavelengths of the centers of the cores of the wind profiles of Si IV correspond to an outflow velocity of about − 220 km s^{-1}. Quite clearly the true relationship between excitation energy and velocity is not to be deduced simply by correlating the displacements of the deepest points in the absorption profiles with the total excitation energies Correlation of the position of the shortward edge of the wing with the total excitation energy of the level from which the observed line arises is equally difficult to interpret.

The transfer of photons through the moving atmosphere determines what type of line profile we see. The observed profiles are the result of a complicated line-formation process which cannot be inverted readily to yield velocity, electron temperature (or level of excitation), and density as a function of the distance from the photosphere of the star. Almost as high velocities are seen by means of the Si II spectrum as are seen by means of Si III and Si IV The velocities seen by means of the silicon ions are a little higher than what are seen by means of Fe II or Ni II.

The strongest emission lines in the ultraviolet spectrum of P Cyg are shown in Figure 4-27. They are broad lines due to transitions in the lines of multiplet UV 13.04 of Si II. The emission is cut up by strong absorption cores due

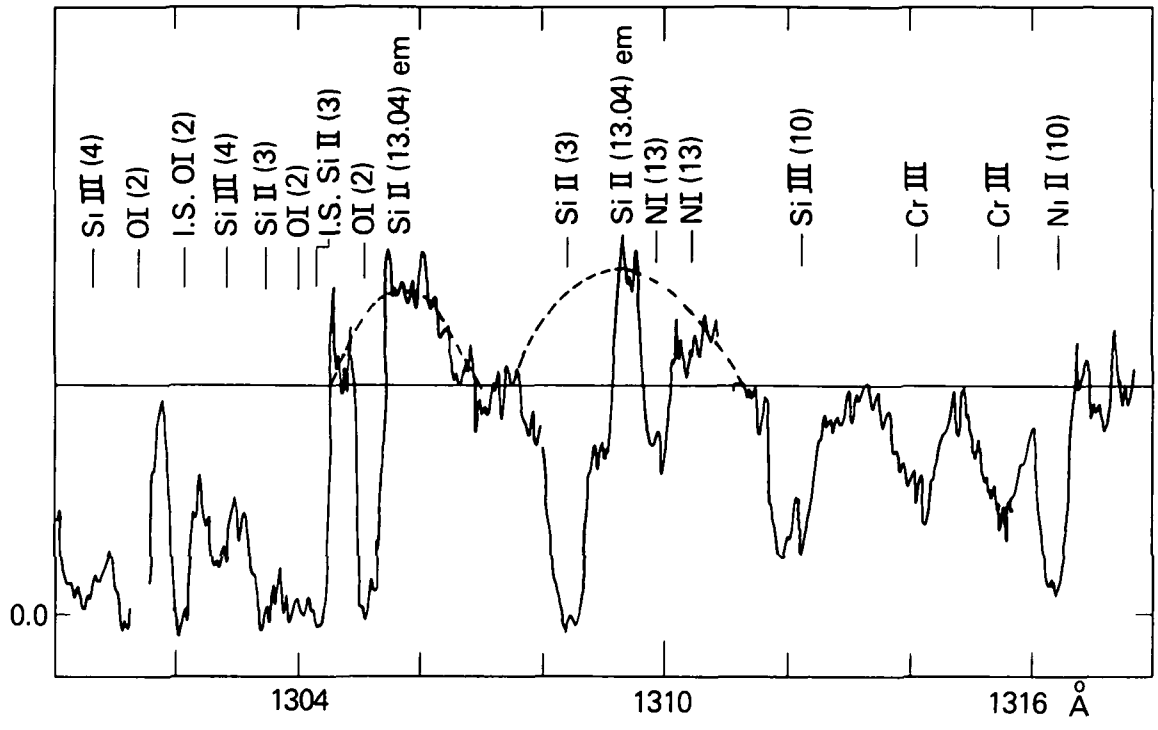

Figure 4-27. Emission lines in the spectrum of P Cyg due to dielectronic recombination and cascade through multiplet UV 13.04 of Si II Broken lines have been drawn to guide the eye toward the minimum and the maximum width of emission that might be considered The intensity scale is linear and the nominal level of zero intensity is indicated. The positions of two interstellar absorption lines are shown and the positions are noted of displaced absorption components due to lines of multiplet UV 2 of O I, multiplets UV 4 and UV 10 of Si III, multiplet UV 3 of Si II, multiplet UV 13 of N II, multiplet UV 10 of Ni II, and of two lines of Cr III which are in unnumbered multiplets. Displaced absorption lines due to multiplet UV 13.04 of Si II occur about 0.85 Å shortward of the undisplaced positions for these lines. This diagram was made from IUE image SWP 4307 Similar detail is seen on SWP 4308 and SWP 4504.

to the several lines noted in Figure 4-27 These broad emission features are the end result of the following dielectronic recombination process

$$Si^{++}\,(3s3p) + e \rightarrow Si^{+}\,(3s3p(^3P^o)\,3d) \rightarrow$$

$$Si^{+}(3s3p^2) + h\nu \qquad (4\text{-}4)$$

In Chapter 3 it was noted that the lines of multiplet UV 13.04 of Si II, which is the transition $3p^2\ ^2D - 3s3p3d\ ^2F^o$, are exceptionally strong in the spectra of main-sequence B stars and, it was proposed that this is caused by the very short lifetime of the upper levels The 3s3p3d $^2F^o$ levels may undergo autoionization (Underhill, 1981b). The observation of broad emission lines at 1305 6 and 1309 6 Å in the spectrum of P Cyg is evidence that the reverse process to autoionization, dielectronic recombination, takes place It appears that the balance between autoionization and dielectronic recombination is an important factor governing the distribution of ions between the states Si^+ and Si^{++}

Two factors have to be considered when evaluating the assertion that the line emission which is seen in the spectrum of P Cyg near 1305.6 and 1309 6 Å arises from a stabilizing cascade following dielectronic recombination. First it is necessary to confirm the placement of the adopted continuum, and, second, it is necessary to show that the proposed identification is

the dominant one for the emission features in question.

The adopted continuum in Figure 4-27 passes through flat regions of the spectrum near 1307.5 Å and 1317.5 Å and just above the high region near 1313.2 Å. A review of IUE spectra of supergiants in the range B2 to B8 confirms that the selected intervals are regions where the continuum is observed. Further confirmation can be found by looking at Figures 3-13 and 3-14. It should be noted that the absorption lines of P Cyg are displaced shortward by about 0.9 Å with respect to the interstellar lines and the spectra of normal B stars. Thus, the flat spectral region near 1307.3 Å in the spectrum of P Cyg corresponds to what is seen near 1308.2 Å for normal B stars. The adopted level of the continuum in Figure 4-27 is reasonable. This means that emission equivalent to an intensity of 1.25 to 1.30 times the level of the continuum is truly present and centered on 1305.6 and 1309.6 Å. Broken lines have been drawn to guide the eye toward seeing the maximum and the minimum amount of emission that might be considered.

In Figure 4-27, the positions of the displaced absorption troughs for the three lines of multiplet UV 2 of O I have been indicated Since the undisplaced positions of these lines are at 1302.17, 1304.86, and 1306.03 Å, one would expect to see emission features just longward of the undisplaced positions for each line if these lines were formed by resonance scattering of a continuum. The emission features might be expected to have relative intensities like the relative *gf* values for the lines, namely 0 16, 0.096, and 0.032, respectively However, if strong photospheric lines due to O I, multiplet UV 2, are present, the emission features will be weakened for the strongest lines. This point has been discussed in connection with the Si IV resonance multiplet.

The fact is that the only emission seen that may conceivably be attributed to O I is the feature centered at 1305.6 Å. Because the displaced absorption component of the line of multiplet UV 4 of Si III, having a wavelength of 1303.32 Å, is weaker than that of the Si III line, multiplet UV 4, having a wavelength of 1301 15 Å (although their *gf* values are 0.70 and 0.56, respectively), one may infer that some emission occurs for the O I line at 1302.17 Å If an emission component was present for the O I line at 1304.86 Å, the emission would not be obliterated by the Si II interstellar line at 1304.47 Å because the interstellar line is expected to have a FWHM like that of the interstellar line due to O I, λ 1302.17, thus, about 0 3 Å. The steep longward flank of the interstellar Si II line is seen at 1304.5 Å. This interstellar line will not obliterate emission on the longward side of the O I line beginning at 1304.86 Å. Only a very weak emission feature is seen between the longward flank of the Si II interstellar line and the shortward flank of the displaced absorption trough due to the O I line λ 1306.03 Because the evidence for emission components from the two strongest lines of the O I resonance multiplet is weak, it seems improbable that O I makes a significant contribution to the emission feature centered at 1305.6 Å

One can argue, in a similar way, that the displaced absorption troughs of the lines of multiplet UV 3 of Si II should be accompanied by emission features starting at 1304.37 and 1309.27 Å and extending longward, and that these emission features contribute to what is observed. We see that the evidence for significant emission due to resonance scattering in an expanding body of gas by the line Si II 1304.37 Å is as weak as it is for O I 1304.86 Å. A strong displaced absorption trough is seen for Si II 1309.27 Å The emission seen centered at 1309 3 Å could be due, at least in part, to this line. However, the similar resonance line of Si II, multiplet UV 2, at 1533.43 Å shows no emission (see Figure 4-26), even though its *gf* value is 0.52, a value more than 1.5 times the value for the line at 1309 27 Å. One must conclude that the contribution of emission from lines of multiplet UV 3 of Si II to the observed features at 1305.6 Å and 1309 6 Å is small

This leaves multiplet UV 13.04 of Si II as the chief source for the observed emission features. Emission resulting from the stabilizing cascade following dielectronic recombination taking place in a large spherical body of gas which is expand-

ing with a maximum velocity of about 400 km s^{-1} would be expected to form broad emission lines about as sketched in Figure 4-27 The broken lines show the maximum width and minimum width that might be considered. The portion of the expanding gas which was projected against the disk of the star would form a displaced absorption trough. Inflections are indeed seen in the observed spectrum at about 1304.75 and 1308.95 Å, which are the expected positions for the lines of multiplet UV 13.04 of Si II. Similar displaced absorption components have been noted by de Groot (1969) for the lines of multiplet UV 1 of Si II which arise from the same lower levels as do the lines of multiplet UV 13 04. It is to be noted that although the lines of multiplet UV 1 of Si II have quite large *gf* values (0.22, 0 13, and 0.024), these lines do not have emission components. This observation adds weight to the conclusion, evident from the present analysis of the 1300-Å region of the spectrum of P Cyg, that the emission features seen at 1305.6 and 1309.6 Å are primarily due to cascades in a stabilizing transition following dielectronic recombination and not to a general recombination spectrum

Since all published analyses of the strengths of Si II and Si III lines to obtain the abundance of silicon have not taken autoionization and dielectronic recombination into account, it is possible that the estimates of the abundance of silicon are more uncertain than was previously thought. If these processes act particularly strongly under certain conditions, throwing the ionization balance of silicon toward a large abundance of Si^{+}, the great strength of the Si II lines in "silicon" stars may, perhaps, be understood without invoking an unusually large abundance of silicon. This subject has not yet been studied in detail.

Energy Distribution, Effective Temperature, and Luminosity. The apparent energy distribution of P Cyg can be determined from 1200 to 11000 Å by means of ultraviolet observations obtained using the low resolution mode of IUE (Underhill, 1980c), from the S2/68 faint-star observations (Thompson et al., 1978), from ANS observations (Wesselius et al., 1980b), and from the 13-color photometry (Johnson and Mitchell, 1975). The results, corrected for interstellar extinction by assuming that $E(B - V) = 0.35$, are shown in Figure 4-28. The units of f_{λ}, corrected for interstellar extinction, are 10^{-11} ergs $cm^{-2}s^{-1}$ $Å^{-1}$. The observed energy distribution is compared with the energy distributions from two Kurucz (1979) line-blanketed, LTE model atmospheres The theoretical energy distributions have been fitted to the observed energy distribution at 4030 Å. At this wavelength the observed fluxes are not expected to be seriously affected by the presence of the infrared excess nor by the presence of strong emission lines from the mantle. The theoretical energy distributions have different shapes shortward of 3650 Å, but they have essentially the same shape in the region from 3650 to 8000 Å The adopted choice of $E(B - V)$ was made following Ambartzumian et al. (1979) who showed that the strength of the interstellar $L\alpha$ absorption feature is compatible with an extinction factor of about this amount. Because P Cyg has a strong infrared excess which extends into the visible region, the value of $E(B - V)$ may not be estimated by subtracting the intrinsic color of a B1 Ia star from the observed $B - V$ color Doing that will result in a value that is sure to be too large. Moreover, since the ultraviolet line spectrum of P Cyg is like that of a B5 supergiant rather than like that of a B1 supergiant (as discussed in the preceding section) there is little reason to expect that the intrinsic color of P Cyg is similar to that of a B1 Ia star.

The IUE energies shown in Figure 4-28 correspond to continuum energies which ignore the presence of the strong absorption lines formed in the mantle. They, therefore, give an upper limit to the ultraviolet energy radiated by P Cyg. Since both the S2/68 experiment and the ANS satellite measured energies in bands of intermediate width (each band about 200 to 300 Å wide), the results from these instruments will give lower limits to the true continuum energy from P Cyg. This is because the dimming effect of all the absorption lines formed in the mantle is included in the measured energies. When one compares with a model atmosphere, one should use measured

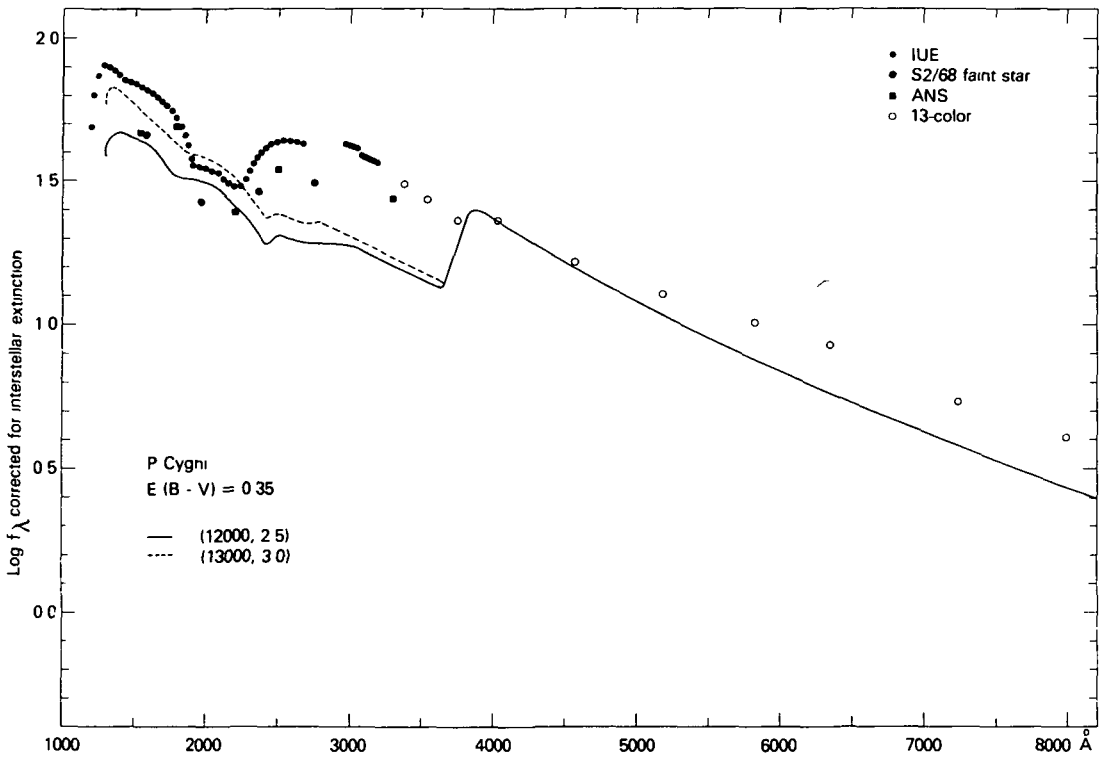

Figure 4-28. The energy distribution of P Cyg corrected for interstellar extinction compared to the energy distributions from two Kurucz (1979) model atmospheres. The observed and theoretical energy distributions have been fitted together at 4030 Å. The unit for the observed flux corrected for interstellar extinction is 10^{-11} ergs cm^{-2} s^{-1} $Å^{-1}$.

values of the continuum emitted by the photosphere as it is modified by normal line blanketing in the photosphere.

The relative positions of all the points shown in Figure 4-28 are established by the absolute calibrations which turn the measured signals into absolute energy. These calibrations probably contain errors and inconsistencies of the order of ± 10 percent. Consequently, deviations of the order of ± 0.04 dex in the ordinate are of little meaning.

Three conclusions can be drawn from Figure 4-28. First the Balmer continuum is strongly in emission in P Cyg. Second there is an infrared excess which can be detected to about 4500 Å. And finally the shape of the energy curve is suggestive of an effective temperature near 1.3 × 10^4 K.

The third conclusion is in accord with the fact that the ultraviolet line spectrum of P Cyg looks like that of a B5 Ia supergiant. Underhill (1979b) using S2/68 and 13-color photometric data, derived an effective temperature of 1.22 × 10^4 K from the angular diameter and integrated flux of P Cyg. She corrected for the presence of the infrared excess, but not for the presence of Balmer continuum emission. Her result has a probable error of ± 5.0 × 10^2 to ± 1.0 × 10^3 K. Hutchings (1979) compared the shape of the ultraviolet spectrum of P Cyg over the wavelength range from 1200 to 3000 Å with those of other O and B stars and with the continuous spectra from LTE line-blanketed model atmospheres of Kurucz et al. (1974). He came to the conclusion that the effective temperature of P Cyg lies in the range 1.7 × 10^4 ± 3.0 × 10^3 K. Hutchings did not recognize explicitly that the Balmer continuum is strongly in emission in P Cyg and that there is a strong infrared excess extending into the visible region. It seems that the best estimate

available at this time for the effective temperature of P Cyg is that of Underhill, namely 1.22×10^4 K. Very likely her neglect of a correction for the emission in the Balmer continuum compensates for the fact that the S2/68 ultraviolet fluxes include the subtraction of light by the strong absorption lines formed in the mantle of P Cyg Underhill's estimate of the angular diameter of P Cyg, 4.12×10^{-4} arcsec, is reliable and it probably does not have an uncertainty greater than ± 5 percent.

In order to find the radius of the photosphere of P Cyg, one must know the distance to P Cyg. Because the spectrum of P Cyg is not that of a normal B-type supergiant, it is not appropriate to use the apparent strengths of the normal luminosity criteria in the visible range to deduce a visual absolute magnitude, M_V, as Kopylov (1958) and Hutchings (1976a) have done. The best way is to use the information that P Cyg appears to be a member of the open cluster IC 4996. The distance modulus to this cluster, determined from normal B stars, and the V magnitude of P Cyg, corrected for interstellar extinction, will determine M_V. Beals (1950) estimated that P Cyg was at a distance of 1.2 ± 0.6 kpc from his study of IC 4996. Since that time several studies of IC 4996 and the OB association, of which it is a part, have been carried out.

The subject of the distance to P Cyg has been reviewed by Van Schewick (1968) who has used proper motions to determine that P Cyg is indeed a member of IC 4996. He has concluded that the distance modulus of IC 4996 is 11.14 mag. If V = 4.83 for P Cyg and $E(B-V) = 0.35$, then M_V for P Cyg is − 7.4. This value is typical for late B-type Ia supergiants. According to Van Schewick, the uncertainty in the distance modulus lies in the range − 0.4 to + 0.6 mag. The suggestion of Isserstedt (1970) that P Cyg lies at a distance corresponding to that of his star ring, no. 274, and thus, has a modulus of 12.24 mag, is poorly founded.

If P Cyg has a distance modulus of 11.14 mag, its distance is 1.69 kpc and its radius is 75 $R_\odot$, with the permissible range being from 61 to 79 $R_\odot$. If P Cyg is at 1.2 kpc, as Beals proposed, its radius is 53 $R_\odot$ (see Table 4-1). The radius of the photosphere is comparable with that of a late B-type Ia supergiant (see Table 4-1). The size of the mantle is not securely determined. De Groot (1969) has argued that it may be of the order of 160 $R_\odot$.

The infrared excess of P Cyg is shown in Figure 4-17 plotted as a function of wavelength. The wavelength of the turnover point indicates that the electron temperature in the emitting region is near 2.2×10^4 K. The slope of the straight line portion of the curve corresponds to a power law dependence of S_ν on ν with $\alpha = 0.77$.

Wright and Barlow (1975) have shown that the rate of mass loss from a homogeneous sphere of hydrogen gas expanding at a constant velocity u_∞ can be written as

$$-\dot{M} = 0\,095\,\mu Z^{-1}\,(\gamma g_\nu)^{-1/2} u_\infty S_\nu^{3/4} D^{3/2} \nu^{-1/2} \quad M_\odot \mathrm{yr}^{-1}. \tag{4-5}$$

Here u_∞ is in km s^{-1}, S_ν is the flux at radio frequency ν in janskys, D is the distance of the star in kpc, and μ, Z, γ and g_ν are, respectively, the mean atomic weight of the gas, the average charge on each ion, the average number of electrons per ion, and the value of the gaunt factor at frequency ν. This formula may be used to estimate the rate of mass loss from P Cyg from its observed radio flux once a value for u_∞ and the distance are known. The following results have been obtained:

Authors	Distance (kpc)	u_∞ (km s^{-1})	T of plasma (10^4 K)	$\dot{M}$ ($M_\odot \mathrm{yr}^{-1}$)
Barlow and Cohen (1977)	1.8	300	2.0	1.5×10^{-5}
Underhill (1979b)	1.2	400	2.2	$4\,3 \times 10^{-6}$
Underhill (1979b)	1.8	400	2 2	8.0×10^{-6}
Abbott et al (1980)	1.8	400	2.0	2.1×10^{-5}

The results of Barlow and Cohen and of Underhill for a distance of 1.8 kpc differ because different values for u_∞ and different values for μ, Z, γ and g_ν have been adopted The ultraviolet spectrum of P Cyg shows that u_∞ is at least 400 km s^{-1}, thus, leaving all other factors unchanged, Barlow and Cohen's result should be increased by four-thirds. However, their result does depend upon knowing the true values for μ, Z, γ, and g_ν as well as the correct distance to P Cyg The best estimate of the rate of mass loss from P Cyg appears to be $(1\,5 \pm 0\,5) \times 10^{-5}\ M_\odot\ yr^{-1}$.

This estimate made from the radio flux is more secure than are the estimates of de Groot (1969) of $2 \times 10^{-4}\ M_\odot yr^{-1}$ and of Hutchings (1969) of $5 \times 10^{-4}\ M_\odot yr^{-1}$, because both these latter estimates are based on less satisfactory hypotheses about the formation of the visible spectrum than the hypotheses used for interpeting the radio spectrum of P Cyg.

Summary. Spectroscopic and photometric observations of P Cyg show that P Cyg is an unusual luminous star. It has an energy distribution in its continuum and in its ultraviolet absoprtion lines that is like that of a late B-type supergiant. The line spectrum in the visible range resembles the spectrum of an early B-type supergiant sufficiently well to lead to a spectral type of B1 Iap. In the visible range many lines are present in emission as well as in absorption. In the ultraviolet, the emission lines are much less conspicuous.

There is strong emission in the Balmer continuum and there is a strong free-free infrared excess which can be detected from long wavelengths to about 4500 Å. The deepest observable levels of the photosphere show outflow with velocities of the order of − 20 to − 50 km s^{-1}. Lines coming from higher levels (levels which form the mantle) show outflow velocities over the full range from − 50 to − 400 km s^{-1} or so. Thus all of the observable part of the atmosphere, that is both the photosphere and the mantle, appear to be in outflow

Although the spectral type of P Cyg is B1 Iap, P Cyg shows outflow velocities that are only about one-fourth as large as those of normal B1 supergiants. P Cyg radiates only sufficient ultraviolet light to correspond to a late B-type spectral class. The ultraviolet spectrum does not show strong resonance lines of C IV or N V, both of which are strong in the spectra of normal early B-type supergiants but weak or absent in the ultraviolet spectra of late B-type supergiants.

The radiation field of P Cyg is compatible with an effective temperature near 1.22×10^4 K. The lines used for spectral classification seem to be formed in a superheated part of the mantle and their strengths do not give information about the amount of energy coming from the core of the star as a stream of radiation.

If the distance of P Cyg is 1.2 kpc, its linear radius is 53 $R_\odot$; if the distance is 1.69 kpc, the linear radius is 75 $R_\odot$. These values are appropriate for a late B supergiant The part of the mantle which shows outflow velocities near − 220 km s^{-1} has a radius of the order of 3 times that of the photosphere according to de Groot (1969). The part which shows outflow velocities near 400 km s^{-1} must be larger than this by an undetermined amount

The largest outflow velocities are seen in the resonance lines of Si IV. This indicates that high electron temperatures exist in at least part of the outer mantle and that high outflow velocities occur there. On the other hand, the shape of the infrared excess indicates that an outer part of the mantle has cooled to about 2.2×10^4 K This plasma will also emit radiation in the hydrogen-line spectrum and it may contribute to the strong emission seen in Hα, Hβ, and Hγ. Only outflow velocities less than about 300 km s^{-1} are seen by means of the hydrogen-line spectrum.

The rate of mass loss from P Cyg is best found from the intensity of the radio spectrum. The value deduced depends upon the three-halves power of the distance which is assumed for P Cyg as well as upon the parameters describing the state of the plasma. It is probable that the true value lies in the range $(1.5 \pm 0.5) \times 10^{-5}\ M_\odot yr^{-1}$. The theoretical interpretations of the shapes of the H I and He I lines in the spectrum of P Cyg (reviewed in Chapter 6) suggest that the rate of mass loss lies in the range from a few times $10^{-6}\ M_\odot yr^{-1}$ to $3 \times 10^{-5}\ M_\odot yr^{-1}$.

Like the normal B-type supergiants, P Cyg

possesses a superheated mantle that is in outflow and is inhomogeneous This latter property can be deduced from the facts that two or more components are seen for many of the strong absorption lines and that the relative intensities of the absorption lines do seem to change irregularly. The most displaced absorption components of the Balmer lines show a variable radial velocity. The changes seem to occur in a period of about 114 days.

Hutchings (1979) has suggested that spectra like that of P Cyg may occur when a massive star is evolving rapidly across the HR diagram toward the area of the red giants. Certainly it seems clear that the photosphere and mantle of P Cyg are being ejected No material has been seen to be falling into the star The initial propulsion of the photosphere outward is probably caused by a force which is not radiation pressure Otherwise all late B supergiants should show a similar spectrum. The expulsion has been continuing at about the same strength for the entire period during which P Cyg has been observed spectroscopically, some 80 years This is different from what occurs for recurrent novae and slow novae In those cases, the ejection rate decreases rather rapidly after the first explosion with the result that after a short time a large expanding photosphere is no longer seen A rather permanent large photosphere is seen for P Cyg in spite of its continuing mass loss

The Superluminous Supergiants

When viewing slit spectra having a reciprocal dispersion of 60 to 100 Å mm^{-1}, it is fairly straightforward to pick out B-type supergiants from the general appearance of the spectrum To determine whether the luminosity class is Ib, Ia, or Ia+ (sometimes denoted as Ia-0) it is necessary to compare the relative strengths of lines of He I, He II, Si II, Si III, and Si IV Walborn (1973) has listed criteria valid for supergiants of types B2.5 to O9 The MK spectral classification scheme is defined by means of standard stars.

The superluminous supergiants are those supergiants for which the luminosity criteria reach extreme values, the change being in the direction of going from luminosity class Ib to luminosity class Ia Empirically it has been found that stars selected by this rule are, indeed, usually more luminous than normal Ia supergiants The superluminous supergiants vary in light with amplitudes of up to about 0.1 mag in the visible range, and their radial velocities vary with a range of about 30 km s^{-1} (see, for instance, Hutchings, 1968a; Sterken, 1977; and Sterken and Wolf, 1978). The variations in light and radial velocity are like those found for the normal B-type supergiants of luminosity classes Ib and Ia, but the time scales on which the changes occur are longer. The superluminous supergiants having spectral types near B1 are known to show Balmer progressions indicating a range of about − 200 km s^{-1} between the radial velocity shown by Hα and that shown by members of the Balmer series having an upper quantum number $n \geq 9$ (see Figure 4-5, and Sterken and Wolf, 1978). These stars show "P-Cygni" type emission accompanied by a shortward displaced absorption core at He I 5876 and He I 6678 as well as at Hα and often at Hβ (Hutchings, 1968a, 1970a, Sterken and Wolf, 1978) The shapes of the P-Cygni type lines change from time to time. These stars differ from P Cyg in that they show emission only for the strongest H I and He I lines

Typical Superluminous B-Type Supergiants. Some typical superluminous supergiants in our galaxy and in the Large Magellanic Cloud are listed in Table 4-9. Most of the spectral types and visual absolute magnitudes are those listed by Humphreys (1978, 1979). Humphreys has used membership in clusters and associations to determine the distances to the stars and the extinction by interstellar dust. The star HD 190603 is not listed by Humphreys, it does not appear to be in a cluster. Slightly different spectral types and absolute magnitudes may be found in other sources. The star HD 152236, ζ^1 Sco, has been observed in most detail because it is apparently bright, V = 4.77; it is the prototype of superluminous supergiants having spectral types near B1. Here we shall discuss only data about galactic superluminous supergiants.

Table 4-9

Typical Superluminous Supergiants of Types B1 to A0

Stars in our Galaxy				Stars in the LMC			
HD BD	Spectral Type	M_V (mag)	Notes	HD HDE	Spectral Type	M_V (mag)	Notes
169454	B1 Ia+	−8.0		269700	B1 Iae	−8.7	5
190603	B1.5 Ia+	(−8.3)	1	269859	B1 Ia	−8.5	
152236	B1.5 Ia+	−8.7	2	269546	B5 Ia	−9.0	
−14°5037	B1.5 Ia+	−6.9	3	269647	B8 Ia	−9.2	
134959	B2 Ia+	−8.5		32034	B9 Iae	−9.2	
168625	B8 Ia+	−7.8		268654	B9 Ia	−8.7	
168607	B9 Ia+	−8.2	4	268946	A0 Ia	−8.6	
223960	A0 Ia+	−7.1		269661	A0 Ia+	−8.6	
				269781	A0 Iae	−8.9	
				269832	A0 Ia	−8.5	

Notes to Table 4-9

1. This star is not in a cluster or association; the listed M_V is a typical value for superluminous B-type supergiants.
2. ζ^1 Sco; Sterken (1977) gives $M_V = -7.15$.
3. The data is from Sterken and Wolf (1978); Sterken (1977) gives $M_V = -7.15$.
4. Sterken (1977) gives $M_V = -9\,01$.

Effective Temperatures, Luminosities, and Radii. The effective temperatures of three superluminous supergiants having spectral types near B1 have been found from integrated fluxes and angular diameters. These results are listed in Table 4-1. The average effective temperature of ζ^1 Sco, HD 169454, and HD 190603 is 1.82×10^4 K which is significantly lower than the value of $2\,0 \times 10^4$ K which is appropriate for type B1 Ib or Ia and about equal to what is expected for a normal B1.5 supergiant (see Table 4-2). Hutchings (1979) has estimated from the shape of the ultraviolet spectrum that the effective temperature of ζ^1 Sco is $1.9 \times 10^4 \pm 3.0 \times 10^3$ K. Appenzeller and Wolf (1979) compared the shape of the ultraviolet and visible spectrum, corrected for interstellar extinction, to that from a blackbody and concluded that T_{eff} is near 1.9×10^4 K. It seems that the amount of ultraviolet light received from ζ^1 Sco is sufficient for it to have an effective temperature like that for a normal B1.5 supergiant. This is in contrast to the case for P Cyg which has an effective temperature and an ultraviolet spectrum like that of a late B supergiant.

The visual absolute magnitudes of the galactic superluminous supergiants lie in the range $M_V = -8.3 \pm 0.5$ except for BD −14°5037 and HD 223960 which have luminosities like those of normal Ia supergiants. From Table 4-3 we see that we can expect the bolometric correction to be about −1.7 mag at type B1 and about −0.3 mag at type A0. Thus, the luminosities of the superluminous supergiants appear to run from $\log L/L_\odot = 5.90$ at type B1 to 5.34 at type A0. This is brighter than normal Ia B-type supergiants by about 1 2 mag or 0.48 dex. The bolometric luminosities of B1 Ia+ stars given by Sterken and Wolf (1978) are too high because Sterken and Wolf adopted effective temperatures appropriate

for main-sequence B1 5 stars.

The radii of the photospheres of the superluminous supergiants included in Table 4-1 are 114, 87, and 81 $R_{\odot}$, respectively for ζ^1 Sco, HD 169454, and HD 190603. This is about 2 5 times as large as for normal B1 Ia supergiants. The radius of the photosphere of P Cyg is only one-half to two-thirds times that of a typical B1 Ia+ star. The photospheric radii given by Sterken and Wolf for B1 Ia+ stars are too small because these values have been calculated from adopted bolometric magnitudes using effective temperatures which are too high.

Spectroscopic Characteristics of B1 Superluminous Supergiants Only the spectrum of ζ^1 Sco, B1.5 Ia+, has been described in detail in the visible range (Hutchings, 1968a) and in the ultraviolet (Appenzeller and Wolf, 1979, Hutchings, 1979) The observations in the visible range of Sterken and Wolf (1978) show that the spectra of the stars HD 169454, BD − 14°5037, and HDE 269700 look very much like that of ζ^1 Sco and that all four stars show similar radial-velocity changes and line-profile changes. Outflow is seen by means of the leading members of the Balmer series and the leading members of the He I series. The visible spectrum of these stars differs from that of P Cyg by showing emission only in the strongest lines of H I and He I We can conclude that the photosphere is not moving outward because the moderately weak absorption lines appear to give radial velocities compatible with the expected radial velocities for these stars due to galactic rotation.

The ultraviolet observations of Appenzeller and Wolf and of Hutchings were made by means of IUE. Because the spectral tracings which they use for the region shortward of 2100 Å (the range covered by the SWP camera) were prepared using an erroneous photometric transfer function, the line profiles presented by these authors for the ultraviolet region shortward of 2100 Å are inaccurate. Nevertheless, these spectral tracings allow one to determine the general characteristics of the ultraviolet spectrum of ζ^1 Sco.

It is found that the strong resonance lines and the strong lines of the third spectra of the metals as well as lines in the Si III spectrum are displaced shortward The positions of the centers of the strong lines from third spectra indicate outflow velocities of the order of − 150 to − 300 km s^{-1} The centers of the strong resonance lines due to Mg II, Si IV, and C IV indicate velocities in the range − 300 to − 350 km s^{-1} The shortward edges of the strong resonance lines suggest maximum outflow velocities of the order of − 500 km s^{-1} Appenzeller and Wolf state that the weak lines from the third spectra of the metals show a radial velocity of only − 30 km s^{-1} which is about what is found from photospheric lines in the visible spectral range. Hutchings gives no information on this point All of the investigators note that the resonance and other lines of Fe II are weak, if present at all, in the spectrum of ζ^1 Sco. This is a difference from the case of P Cyg where the Fe II and Ni II lines are strong and the resonance lines of the second spectra of the metals show wind profiles.

In the case of ζ^1 Sco, as for P Cyg, the resonance lines of C II, Al II, and Mg II show wind profiles with a definite emission peak The resonance lines of Si IV and C IV show strong absorption troughs due to a wind, but no emission. The ultraviolet spectrum of ζ^1 Sco thus shows a lower level of ionization than that of ρ Leo, B1 Ib, or κ Cas, B1 Ia It is more like that of χ^2 Ori, B2 Ia or o^2 CMa, B3 Ia, than like that of an early B-type supergiant Similarly, the maximum outflow velocity seen for ζ^1 Sco is more like that for a B3 Ia supergiant than it is like that of a B1 Ia supergiant (see Table 4-5) The ultraviolet spectrum of ζ^1 Sco is more like the ultraviolet spectra of normal B supergiants of types near B2 or B3 than of types near B1 5 or B1.

The presence of strong lines of Si IV and C IV in the spectrum of ζ^1 Sco indicates that a superheated mantle is present Inhomogeneity also seems to be present, for some lines in the visible spectrum are sometimes seen to be double (see, for instance, Hutchings, 1968a). Not as much material is in the mantle as is the case for P Cyg, for fewer emission lines are seen.

Rate of Mass Loss from B1 Ia+ Stars. Sterken and Wolf (1978), from fitting the Hα profile,

have estimated that the rate of mass loss of ζ^1 Sco is $1.8 \times 10^{-6}\ M_\odot yr^{-1}$, Barlow and Cohen (1977) have suggested a rate of $1.5 \times 10^{-5}\ M_\odot$ yr^{-1}. They obtained this value by adopting a velocity law similar to that which they deduce is valid for P Cyg and fitting the infrared spectrum. The suggestion of Barlow and Cohen is uncertain because there are many reasons for doubting that the velocity law deduced by them for P Cyg is valid for ζ^1 Sco (see Wolf and Appenzeller, 1979), and there is some reason to doubt that the procedure followed by Barlow and Cohen is reliable (see Discussion). Sterken and Wolf have estimated the rate of mass loss from HD 169454, BD−14°5037, and HDE 269700 using the Hα profiles. They find that $\dot{M}$ is a few times $10^{-6}\ M_\odot$ yr^{-1}. Definitely the rate of mass loss from the B1 Ia+ stars is 4 to 8 times less than that believed to be occurring for P Cyg.

X-RAY BINARIES

Five X-ray binaries contain optical components which are classified as having B-type supergiant spectra. These systems are listed in Table 4-10. The data for this table have been taken from Henrichs (1980). The designations in the first column indicate the constellation name of the X-ray source or its position name (RA in hours and minutes of time, DEC in degrees). The second column gives the number of the optical star in the catalogue indicated by the first letters. The optical companion of the X-ray source 1538-52 is very faint and it is not listed in any of the usual catalogues which have been developed from studies of objective-prism spectra.

As well as yielding information on the masses of stars which show B-type supergiant spectra (see Chapter 2) the X-ray binaries allow one to deduce information about the winds from massive stars An order of magnitude estimate of the mass loss rate can be obtained for unevolved stars which do not fill their Roche lobes (see Henrichs, 1980). Such a star is WRA 977, the first star in Table 4-10. Henrichs shows that if the pulsar in the binary system is to maintain its observed period, the rate of mass loss should be less than about $10^{-9}\ M_\odot yr^{-1}$.

In the case of the binary systems where the optical star is believed to be filling its Roche lobe, the last four stars of Table 4-10, the rate of mass loss can be estimated by means of detailed modeling of the wind

The star HD 77581 is moderately bright and it has been observed spectroscopically and photometrically from the ground as well as from space using IUE, Copernicus, and the Ariel 5 satellite. Many simultaneous observations made in all spectral regions have been analyzed by Dupree et al. (1980) They have shown from IUE spectra that the P-Cygni type profiles of the resonance lines of Si IV and C IV change with phase in the manner which Hatchett and McCray (1977) suggested should occur as the state of ionization in the wind from the supergiant was changed by the passage of the orbiting X-ray source. Dupree et al. find that the rate of mass loss from HD 77581 is about $1 \times 10^{-6}\ M_\odot yr^{-1}$, and that the

Table 4-10
X-Ray Binaries Having a B-Type Supergiant as One Component

X-ray Source	Optical Star	Spectral Type	m_V (mag)	L_x / L_{opt}	Binary Period	Pulse Period
1223-62	WRA 997	B1 Ia	10.8	0.003	$22^d.6$?	669^s
SMC X-1	Sk 160	B0 I	13.3	1.2	3.9	3 6
Vel X-1	HD 77581	B0.5 Ib	6.9	0.003	9.0	283
1538-52	–	B0 I	14.5	0 01	3.7	529
Cyg X-1	HDE 226868	O9.7 Iab	8 9	0.02	5.6	–

Dash (–) represents no existing data at this value.

maximum outflow velocity is about 860 km s^{-1} This latter value is about half the outflow velocity expected from a normal, single supergiant of spectral type B0.5, (see Table 4-5). The fact that the optical star of the binary system Vela X-1 is believed to have evolved to the stage of filling its Roche lobe appears to have reduced the amount of acceleration the material in the wind undergoes. The observed velocity is well below that which is observed for a single star of the same spectral type.

Dupree et al follow Conti (1978) and adopt $T_{eff} = 2.6 \times 10^4$ K for the optical component of HD 77581 Such a value is too high for type B0 5 Ib. A value near 2.25×10^4 K might be more appropriate (see Table 4-2). If Figure 4-14 has real significance, the observed value of the maximum outflow velocity leads to a value for T_{eff} that is in the neighborhood of 1.8×10^4 K. Dupree et al did not use the absolute energies radiated in the ultraviolet spectrum of HD 77581, which could be determined from their exposures at low resolution in the large aperture of IUE, to estimate T_{eff} either from the shape of the spectrum or from the integrated flux. The angular diameter of HD 77581 could be estimated from its visual brightness.

DISCUSSION

This discussion of the meaning of the observations of the B-type supergiants summarized in the preceding sections of Chapter 4 will be carried out within the framework of the hypothesis that the atmosphere of a star may be considered to be composed of two parts (1) a photosphere which can be modeled successully by means of the classical assumptions of plane-parallel layers, radiative equilibrium, and hydrostatic equilibrium, and (2) a mantle which is inhomogeneous and in which the deposition of nonradiative energy and the transfer of outward directed momentum to the constituent gas occurs.

The photosphere is best seen by means of the continuous spectrum and weak lines from excited levels. It is believed to have a normal solar composition. The mantle is seen most easily by means of the resonance lines from abundant elements and by means of the strong lines from excited levels Emission in the Hα line, in the Balmer continuum, and in the free-free continuum also gives information about the mantle

Parts of the mantle are superheated as a result of the deposition of nonradiative energy, and an outward flow, started by some presently unspecified forces, possibly those connected with the twisting, matting, and breaking of magnetic lines of force, is seen. This outward flow appears to be initiated close to or in the photosphere and it may be accelerated in the mantle by the force due to radiation pressure.

In the case of the B-type supergiants, the outermost parts of the mantle are seen best by means of the infrared excess and the radio radiation coming from free-free interactions between electrons and ionized hydrogen atoms. These outermost parts are not believed to contribute significantly to the emission seen in the Hα line. If they did so, that line should show a broad profile rather as do some of the emission lines seen in the Wolf-Rayet stars.

The electron temperature in each part of the mantle is established as a result of the local balance between the deposition of energy from magnetic, mechanical, and radiative sources and the losses of energy due to the emission of radiation and the transport of excited material out of the region. If magnetic fields play a role in the mantle, the local density will be constrained by the interplay of magnetic forces as well as by the streaming motion which occurs under the influences of gravitational attraction, radiation pressure, and whatever centrifugal or Coriolis forces may result from the rotation of the star.

If the forces initiating the flow in or below the photosphere cause small irregularities in the flow there, these irregularities may develop into shocks because the density decreases outward in supergiant atmospheres. Under appropriate circumstances, the resulting shocks may produce heating in the mantle (see Lucy and White, 1980).

Properties of the Photospheres of B-Type Supergiants

The effective temperatures of B-type super-

giants range from about 2.5×10^4 K at type B0 to about 1.0×10^4 K at type B9 (see Table 4-2) The radii of the Ib supergiants range from about 20 $R_\odot$ at type O9.5 Ib to 30 $R_\odot$ at type B9 Ib, the radii of the Ia supergiants range from about 35 $R_\odot$ at type B0 Ia to about 80 $R_\odot$ at type B9 Ia, (see Table 4-1). The superluminous supergiants having types near B1 have radii of the order of 80 to 90 $R_\odot$ The particle density in the photosphere, estimated from the break off of the Balmer series, is about 10^{12} cm^{-3}

The masses of single B-type supergiants are unknown. The data from X-ray binaries (see Chapter 2) suggest that for early B supergiants the masses may be in the range $20 \pm 5\ M_\odot$. Masses deduced from placing B-type supergiants in an HR diagram are discussed in Chapter 7. Confidence in the theory that is used must exist before these values can be taken seriously.

The spectral lines of B-type supergiants are rather broad and steep-sided. Their shape suggests the presence of differential motion which can be interpreted as macroturbulence and/or rotation. The range encountered suggests the presence of differential motions from about 20 to 50 km s^{-1}. Analysis of the spectra of supergiants by standard fine analysis methods (Table 6-1) lead to estimates of from 10 to 22.5 km s^{-1} for the microturbulent velocity. Thus, it appears that differential velocities exist in the photospheres of B-type supergiants The typical velocity is least for the late B-type supergiants, about 10 to 15 km s^{-1}, and largest for the early B-type supergiants, 20 to 30 km s^{-1}.

Properties of the Mantles of B-Type Supergiants

The mantles of all B-type supergiants appear to be inhomogeneous. This can be deduced from the frequent occurrence of discrete displaced components of the resonance lines of moderately abundant ions in the ultraviolet and the occasional doubling of strong lines from excited levels seen in the visible spectrum. Inhomogeneity is an important property of the mantles of all types of stars.

At least part of the gas in the mantles of B-type supergiants is superheated. This may be deduced from the fact that strong absorption lines are seen from ions that should not be present in abundance were the electron temperatures only of the order of 1.0 ± 0.1 times the effective temperature of the star, and from the fact that X-rays are detected from some early type supergiants (Cassinelli et al , 1981). If the radiation field generated in the core of the star were the only source of heating in the mantle, one should not see evidence for the presence of electron temperatures exceeding the effective temperature of the star by a significant amount. Both the occurrence of strong resonance lines from high ions in the ultraviolet spectra of B-type supergiants and the wavelength of the "turnover point" of the infrared free-free excess indicate the presence of electron temperatures which are higher than can be expected according to the hypothesis of radiative equilibrium at the effective temperatures of these stars. The detailed energy distribution of the radiation received from the mantle suggests in the case of all supergiants that the mantle is being heated as a result of the deposition of nonradiative energy. Until appropriate diagnostic techniques are developed, it is impossible to deduce from line profiles and equivalent widths the run of electron temperature with distance from the star. The theory summarized in Chapter 6 gives no assistance with this problem.

The resonance lines which give evidence for the presence of a high level of ionization in the mantle come from "persistent" ions, that is, from ions which persist in relatively great abundance over a wide range of temperatures and densities owing to the energy structure of the outer shells of electrons forming the ion. This fact, together with the fact that rapid line-of-sight motion tends to make a gas transparent in line frequencies, makes it difficult, if not impossible, to analyze the ultraviolet spectra of B-type supergiants and find a temperature-radius relation.

The density of the mantle is expected to decrease outward. As the density becomes low, the mantle will lose much energy owing to the escape of photons and to the outflow of heated gas Thus, the electron temperature is expected

to reach a maximum at some distance from the star and then to decrease. Eventually, at great distances from the star, the gas in the mantle is expected to coalesce with the surrounding interstellar gas, under shock conditions. If density inhomogeneities persist over large distances, temperature inhomogeneities may also be present

Forbidden emission lines, such as those of [Fe II], are not observed in the spectra of normal B-type supergiants although they are seen in the spectra of BQ [ ] stars. This indicates that a large volume having a particle density of the order of 10^7 to 10^9 cm^{-3} does not form around supergiants in contrast to what is seen for the less luminous BQ [ ] stars

The electron temperatures in the mantles of O9/B0 Ia supergiants are such that absorption is seen in the resonance lines of O VI and N V, while in the mantles of supergiants of type B9/A0, it is doubtful if a level of ionization higher than that necessary to make the resonance lines of Si IV and Al III marginally visible is present. Although the effective temperature changes by only a factor 2.5 in going from type O9/B0 to type B9/A0, the level of ionization changes from the presence in moderate abundance of ions that require 113.9 eV for their formation from the next lower stage of ionization (ionization of O^{+4} to form O^{+5}), to 33.5 eV for their formation (ionization of Si^{+2} to Si^{+3}) Additional energy beyond that present in the radiation field is required to achieve the observed level of ionization in the mantles of B-type supergiants.

By comparing the Stark broadening of the hydrogen lines in the spectra of B-type supergiants in luminosity classes Ib, Ia, and Ia+, one can show that the densities in the photospheres of Ib supergiants are greater than those in the photospheres of Ia supergiants and of Ia+ supergiants. However, in the mantle the densities behave differently The particle density in the mantle at a given spectral type appears to increase as one goes from luminosity class Ib to Ia to Ia+ This can be seen by comparing the strengths of the resonance lines of moderately abundant elements such as Si, the strengths of the Hα emission feature and the intensity of the infrared free-free emission of stars such as ρ Leo, B1 Ib, κ Cas, B1 Ia, HD 190603, B1 Ia+, and ζ^1 Sco, B1.5 Ia+. One must compare infrared excesses normalized to a constant distance as in Figure 4-19. The first three stars have effective temperatures near 20×10^4 K, while the effective temperature of ζ^1 Sco appears to be near 1.8×10^4 K.

The level of ionization in the mantle seems to be highest for ρ Leo, lowest for ζ^1 Sco. The level of ionization is a result of the balance between the input of radiative and nonradiative energy per unit volume and the loss of energy chiefly by radiation. It appears that low density in the mantle, shown by weak Hα emission and a weak infrared excess, leads to high ionization and vice versa.

The normal supergiants ρ Leo and κ Cas show greater outflow velocities than are seen for superluminous supergiants of about the same spectral type such as HD 190603 and ζ^1 Sco. On the whole, the maximum outflow velocity that is seen increases as $T_{eff}^{2.30}$ (see Figure 4-14) but there does appear to be some dependence on luminosity, the maximum observed outflow velocity, for stars having a given effective temperature, being small for the most luminous stars and large for the least luminous stars.

Whether or not one can detect radio emission from a star depends upon the distance to the star and the amount of material around the star that is at an appropriate density and temperature for emitting much free-free radiation. If it is assumed that material is flowing through the emitting region in such a way that the material is conserved in homogeneous spherical shells at one temperature, one obtains Equation (4-4) between the rate of mass loss, $\dot{M}$, and the radio flux at a frequency ν. Among the B-type supergiants, the first star detected (Wendker et al., 1973) was the peculiar supergiant P Cyg. Spectroscopic observations have shown that this star is buried in an unusually dense and extensive mantle. Abbott et al. (1980) have observed 15 early type supergiants with the VLA of the National Radio Astronomy Observatory; they detected ϵ Ori, B0 Ia, surely, and possibly HD 190603 and β Ori.

The failure to detect radio emission from

late B-type supergiants which have a strong infrared excess at 10 μm can be interpreted to mean that the mantles of the late B-type supergiants have cooled to relatively low temperatures, and that they are, as a consequence, opaque at long wavelengths. The monochromatic free-free radio flux, S_ν, per unit volume is expected to vary as $T\lambda^{-2}$ in a cool plasma. In the case of a mantle that is opaque at radio wavelengths, radio radiation will come to the observer only from the transparent outer skin of the mantle.

Radio radiation has been detected from several BQ [ ] stars. This is in contrast to the case for late B-type supergiants and it confirms our inference from the lack of observable [Fe II] lines in supergiant spectra that the mantles of B-type supergiants do not contain large volumes having particle densities in the range 10^7 to 10^9 cm^{-3}. The density seems to be larger for a B-type supergiant in the region where the ultraviolet resonance lines are formed than it is for Be stars. This may be deduced from the difference in the strengths of ultraviolet resonance lines observed for the two types of stars. The density seems to decrease outward more steeply for supergiants than is the case for BQ [ ] stars.

The relative intensities in the spectra of B-type supergiants of the emission in the hydrogen lines and in the hydrogen bound-free and free-free continua should, in principle, tell us about conditions in the mantles of B-type supergiants. Similar emission features are observed for some Be/shell stars and their analysis should yield information about the state of the mantles of Be/shell stars. When one compares the relative amount of energy in the emission feature at Hα, at the head of the emission in the Balmer continuum, and at 10μm, say, in the free-free emission continuum, one finds different results for the Ia supergiants than for the Be/shell stars With the Be/shell stars, sometimes there is a second Balmer continuum in absorption rather than a second Balmer continuum in emission. This state of affairs indicates that a large fraction of the hydrogen in the part of the mantle which is seen by a distant observer to be projected against the disk of the star, is neutral. There is always a net emission in the free-free continuum for Be/shell stars and a net emission feature at Hα.

Let us define an emission index for the Balmer continuum as

$$D_{em}(\mathrm{Ba}) = \log (F_{em} + F_{uv}) - \log F_{uv}, \quad (4\text{-}6)$$

where F_{em} is the measured flux per angstrom at the head of the Balmer emission continuum after correction for interstellar extinction, and F_{uv} is the flux expected per angstrom in the continuum at the shortward side of the Balmer discontinuity if there were no emission from the mantle. The quantity F_{uv} can be estimated from observed continuum fluxes at wavelengths free of emission features (after correction for interstellar extinction) by using the shape of the continuous spectrum from a model atmosphere as an interpolation formula. One of the energy distributions predicted by Kurucz (1979) will do for this. When the Balmer jump is in absorption, one may define D_{abs} (Ba) in a similar manner. The quantity is negative. The observation of a second Balmer jump in absorption means that much of the hydrogen in the mantle is not ionized.

An Hα index, $D(\alpha)$ may be defined as the logarithm of the ratio of the energy in the emission line at Hα to the energy per angstrom in the continuum at 6562 Å. It follows that

$$D(\alpha) = \log W(\alpha\ \mathrm{em}), \quad (4\text{-}7)$$

where W (α em) is the equivalent width in angstroms of the emission in Hα including the energy required to fill up the underlying photospheric absorption line.

Finally, one may define a free-free index at 10 μm as

$$D_{ff}(10\mu\mathrm{m}) = \log (F_\lambda(ff) + F_\lambda(*)) - \log F_\lambda(*) \quad (4\text{-}8)$$

Here $F_\lambda(ff)$ is the energy per angstrom radiated at a wavelength of 10 μm by the mantle, and F_λ (*) is the energy per angstrom radiated by the star. The quantity F_λ (*) may be estimated from the angular diameter of the star and the flux emergent from a representative model atmo-

sphere for the photosphere, say from one of the models given by Kurucz (1979) The sum of the radiation from the photosphere and the mantle at 10 μm is what is measured.

A comparison of D_{em} (Ba), D (α), and D_{ff} (10 μm) for a given star should yield information about conditions in the mantle, while intercomparison of these quantities for several Ia supergiants and Be/shell stars should tell about the differences between the mantles for these stars. The wavelength, λ_p, at which the quantity log λF_λ turns over when log λF_λ is plotted against log λ will indicate the temperature in the plasma which is emitting a free-free continuum. In the case of the Ia supergiants of type B the temperature is near 2.2×10^4; in the case of the shell stars ζ Tau and 48 Lib, it is near 1.5×10^4 K.

It is well known that D (α) is smaller for Ia supergiants of type B than for Be/shell stars. The data presented in Figure 4-2 show that for a late B-type supergiant, D_{em} (Ba) may be of the order of 0.3 (see β Ori, in particular). From the information given by Chalonge and Divan (1952) and from unpublished work of Divan, we find for Be stars with the Balmer continuum in emission, that D_{em} (Ba) lies in the range 0.02 to 0.10. A typical value is near 0.05. Thus, the difference D (α) $- D_{em}$(Ba) is algebraically smaller for Ia supergiants than for Be/shell stars which show an emission Balmer continuum.

Significant infrared excesses at 10 μm have been noted above for 16 early type Ia supergiants (see Table 4-6). The equivalent free-free indices, D_{ff} (10 μm), are given in Table 4-11 for 13 Ia supergiants and P Cyg. In addition, similar free-free indices, determined from the infrared photometry of Gehrz et al. (1974) and the angular diameters and effective temperatures found by Underhill et al. (1979) are given for 13 Be/shell stars.

The D_{ff} (10 μm) given in Table 4-11 for the Be/shell stars are lower limits because the angular diameters of Underhill et al. were determined without correcting for a possible extension of the free-free emission into the spectral region between 6000 and 11000 Å. Consequently, these angular diameters may be too large by a few percent. It is quite clear that D_{ff} (10 μm) is considerably

Table 4-11
Infrared Excess Indices at 10 μm

B-Type Ia Supergiants			Be/Shell Stars			
Star	Spectral Type	D_{ff} (10 μm)	Star	Spectral Type	S_ν (10μm) Jy	D_{ff} (10 μm)
δ Ori	09.5 I	0 13	φ Per	B0 IVe	1.60	0.23
ζ Ori A_1	09.5 I	0.11	π Aqr	B1 Ve	3.17	0 92
ϵ Ori	B0 Ia	0 10	ζ Tau	B2 IIIe	6.37	0.80
κ Cas	B1 Ia	0.14	48 Lib	B3 Ve	1.92	0.92
190603	B1 Ia+	0.12	ψ Per	B4 IVe	2.40	0.67
P Cyg	B1 Iap	1.03	48 Per	B4 IVe	2.69	0.64
χ^2 Ori	B2 Ia	0.17	κ Dra	B5 IVe	2.09	0 56
o^2 CMa	B3 Ia	0.16	23 Tau	B6 IVe	2.56	1.8
55 Cyg	B3 Ia	0.02	ν Gem	B6 IIIe	0.32	0.20
η CMa	B5 Ia	0.06	θ CrB	B6 Ve	0.10	0 07
β Ori	B8 Ia	0.16	η Tau	B7 IIIe	1.75	0.24
21291	B9 Ia	0.10	o Aqr	B7 IVe	1.20	0.59
21389	A0 Ia	0.12	α Col	B8 Ve	4.97	0 47
α Cyg	A2 Ia	0.33				

larger for the Be/shell stars than it is for the Ia supergiants. Since D_{em} (Ba) is smaller for the Be/shell stars than it is for the Ia supergiants, the difference $D_{ff} - D_{em}$(Ba) is systematically larger for the Be/shell stars than it is for the Ia supergiants of type B.

The data of Table 4-11 show that typically D_{ff}(10 μm) is 0.12 for a B-type Ia star, while for a Be/shell star it is near 0.53. This means that typically the excess radiation at 10 μm for a B-type Ia supergiant is 0.32 times the expected continuum radiation at 10 μm, while for a typical Be/shell star it is 2.39 times the expected continuum radiation from the star. In the case of the Ia supergiants, the shape of the infrared excess suggests free-free emission from a plasma with an electron temperature near 2.2×10^4 K. In the case of ζ Tau and 48 Lib, both of which are stars with a strong shell spectrum and a second Balmer jump in absorption, the turnover of the infrared excess toward short wavelengths indicates that the electron temperature is near 1.5×10^4 K in the plasma which radiates the infrared excess.

The differences between the strength of the emission in the hydrogen spectrum from the mantles of B-type Ia supergiants and of Be/shell stars can be understood primarily in terms of differing degrees of ionization of hydrogen in the mantle, and different volumes of emitting gas. In the mantles of B-type Ia supergiants, the hydrogen seems to be predominantly ionized, which results in a relatively weak emission feature at Hα and moderately strong Balmer continuum and free-free emission. In the case of the Be/shell stars, a considerable fraction of the gas is neutral hydrogen. This neutral hydrogen gas makes its presence known by producing sharp absorption cores for the Balmer lines of hydrogen, and by reducing the intensity of the emission in the hydrogen Balmer continuum. The presence of neutral hydrogen sometimes results in a second Balmer continuum in absorption.

Since a second Balmer continuum in absorption has never been observed for a B-type supergiant, one must infer that the quantity of neutral hydrogen at moderately low densities (densities like those in the shells around some Be stars) around a normal B-type supergiant is small. Because the emission continuum from the mantle of a B-type supergiant begins at about the same wavelength as the absorption Balmer jump formed in the photosphere occurs (see Figure 4-2 and the work of Chalonge and Divan), we may infer that the particle density in the mantle of a B-type supergiant is of the same order of magnitude as that in the outer parts of the photosphere of the star.

Mass Loss from B-Type Supergiants

Two comprehensive lists of estimated rates of mass loss have been published for O and B stars. They are that of Hutchings (1976a) and that of Barlow and Cohen (1977). Hutchings adopted published rates of mass loss, $\dot{M}$, for seven supergiants having spectral types of B1 and earlier, and he used these values to "calibrate" empirically spectroscopic criteria in the visible spectrum which he concluded are sensitive indicators of mass loss. The rates of mass loss used for the calibration process include three found by Morton (1968) from modeling resonance lines in the ultraviolet spectrum and three found by himself (Hutchings, 1968b) by modeling lines in the visible spectrum as well as his result for P Cyg (Hutchings, 1970a) and that of de Groot (1969) Hutchings' results will not be discussed further here because they are seriously biased toward high values of $\dot{M}$. He adopted $\dot{M} = 3.5 \times 10^{-4}\ M_\odot\ \mathrm{yr}^{-1}$ for P Cyg, which is a value that more recent work does not support, in addition, most of his standard objects are unusual stars.

Barlow and Cohen (1977) found their values of $\dot{M}$ by modeling the infrared excesses which they determined for 33 O-, B-, and A-type supergiants. Their procedure was to assume that the velocity law which they derived for P Cyg (by modeling the observed infrared excess of P Cyg using the theory which is acceptable for interpreting radio free-free emission from an expanding sphere of gas around a star) was valid for all O, B, and A supergiants and then to find, by means of Equation (4-5), that value of $\dot{M}/u_\infty$

for each star which made the infrared measurements most consistent. Then they adopted a value of u_∞ for each star and found the rate of mass loss for each star. The procedure of Barlow and Cohen can be criticized on the grounds (1) that P Cyg is a very unusual star and it is unlikely that the velocity law deduced for it is typical of the state of affairs in the mantles of normal O, B, and A supergiants, and (2) that the assumptions that the gas is expanding at a constant speed u_∞ and that it is optically thin at all wavelengths, which underlie Equation (4-5), are not appropriate for modeling the formation of an infrared excess.

A third way of estimating the rate of mass loss from a B-type supergiant is to model the formation of the emission component at Hα Hearn (1975a) has interpreted the Hα emission in the spectrum of ζ Ori A_1, O9.5 Ib, in terms of a hot, thin corona lying above the photosphere, and he finds that a rate of mass loss of the order of $1.8 \times 10^{-6}\ M_\odot \mathrm{yr}^{-1}$ is required to account for the observed emission intensity He concluded that a hot coronal wind driven by a corona with an electron temperature not less than 2.6×10^6 K was present. In a following study (Hearn, 1975b) he considered the energy balance of the hot coronae of luminous early type stars and concluded that the main energy loss for OB supergiants is by mass loss.

The profile of the Hα line in four B1 Ia+ supergiants has been interpreted by Sterken and Wolf (1978) by the same method. They found that $\dot{M} = 2.1 \times 10^{-6}$, 1.8×10^{-6}, 4.3×10^{-7}, and $2.3 \times 10^{-6}\ M_\odot\ \mathrm{yr}^{-1}$ for HD 169454, ζ^1 Sco, BD − 14°5037, and HDE 269700, respectively. At the other end of the B-type supergiant sequence, Lamers et al. (1978b) have modeled a cool mantle for α Cyg They interpret the profiles of the Fe II resonance lines and suggest that the rate of mass loss from α Cyg is about $1 \times 10^{-8}\ M_\odot \mathrm{yr}^{-1}$.

Another way to model the part of the mantle contributing to the Hα emission line is to consider that the stellar wind has a temperature about equal to the effective temperature of the star and to model the consequences of acceleration by radiation pressure in lines on those parts of the mantle where the outflow velocity exceeds about 30 km s^{-1}. This type of theory was developed for O stars by Castor et al. (1975) It was applied by Klein and Castor (1978) to interpret the strengths of the emission lines in the He II spectrum and at Hα in Of stars. Klein and Castor have derived an empirical correlation between the intensity of the emission at Hα and the rate of mass loss. They give results for four O9.5 I stars, the average result being a rate of mass loss of $3.2 \times 10^{-6}\ M_\odot \mathrm{yr}^{-1}$.

Lamers and Snow (1978) have studied the ionization conditions in the mantles of B-type supergiants, basing their results on a study of the Si IV, N V, and O VI resonance lines observed by mean of Copernicus spectra They found that a cool model mantle, such as that postulated by Castor et al. (1975), could not account for the observed relative strengths of the resonance lines of Si IV, N V, and O VI. They concluded that a model was required in which some heating occurred in the mantle, as postulated by Hearn (1975a), or that a model of the type proposed by Cannon and Thomas (1977) was needed This latter type they call the imperfect flow model. In this model the wind is produced by an imposed outward velocity in the subatmospheric regions, and the heating is caused by shocks in the trans-sonic region.

The consequences for O stars of the presence of a small very hot corona just above the photosphere have been studied by Olson (1978) and by Cassinelli and Olson (1979). They showed that the presence of such a structure could account for the high stages of ionization seen in the ultraviolet spectra of O stars, but at that time too little information was available for them to postulate an origin for the very hot corona. Cassinelli and Hartmann (1977) showed that such a structure could account for the infrared excess of an O star The theory is also applicable to B-type supergiants and Cassinelli et al. (1978) have applied it to interpreting the Hα emission and the infrared excess of ζ Ori A_1. They find that $\dot{M} = 3 \times 10^{-6}\ M_\odot \mathrm{yr}^{-1}$. The theory of stellar winds and the data supporting this theory have been reviewed by Cassinelli (1979).

Neither the theory of a radiatively driven

wind nor that of outflow resulting from the presence of thin, very hot coronal regions takes account of the possibility that material may be ejected outward impulsively as a result of the twisting and breaking of magnetic field lines. This type of process is seen to occur sometimes on the Sun. It is possible that from time to time the outflow from B-type supergiants may be guided in particular directions by the presence of magnetic lines of force which are open to the interstellar medium, as in the case of the Sun. Such a process would serve to explain the temporary presence of discrete, displaced absorption components which are sometimes seen in the ultraviolet spectra of B-type supergiants

A fourth way of estimating the rate of mass loss from a B-type supergiant is by means of the radio spectrum. This method makes use of Equation (4-5). It seems probable that the assumption of a uniformly expanding sphere of homogeneous gas at one temperature which underlies Equation (4-5) is more likely to be valid for the part of the mantle which radiates the radio spectrum than it is for any other part of the mantle. Rates of mass loss estimated by means of Equation (4-5) for 12 supergiants are given in Table 4-12. These are probably the most reliable rates of mass loss available for these stars. Typically they are uncertain by at least ±50 percent.

The distances used have been taken from Table 4-1 with three distances being used for P Cyg in order to explore the effect of changing the distance to this star. The adopted values of u_∞ are from Table 4-5, or failing that source,

Table 4-12
Rates of Mass Loss for B-Type Supergiants from Radio Fluxes

HR	Name	Spectral Type	$\dot{M}$ ($M_\odot yr^{-1}$)		log T_{eff}	log $L/L_\odot$	Notes
130	κ Cas	B1 Ia	2.4	−6	4.303	5.37	
1713	β Ori	B8 Ia	≤1.3	−7	4.071	4.87	1
1852	δ Ori	O9.5 I	1.4	−6	4.492	5.33	
1903	ϵ Ori	B0 Ia	2.3	−6	4.400	5.67	2
1948	ζ Ori A_1	O9.5 Ib	1.7	−6	4.441	5.38	3
2135	χ^2 Ori	B2 Ia	2.1	−6	4.242	5.46	
2653	o^2 CMa	B3 Ia	1 4	−6	4.169	5.09	
4133	ρ Leo	B1 Ib	5.9	−7	4.307	4.87	
7678	190603	B1 Ia+	2.9	−6	4.294	5.40	4
7768	P Cyg	B1 Iap	1.5	−5	4.086	5.05	5
7977	55 Cyg	B3 Ia	3.4	−7	4.154	5.12	
7924	α Cyg	A2 Ia	≤1.4	−7	3.967	4 72	6

Notes to Table 4-12

1. Abbot et al. (1980) give $\dot{M} \leq 9.1 \times 10^{-7}\ M_\odot yr^{-1}$.
2. Abbott et al. (1980) give $\dot{M} = 3.1 \times 10^{-6}\ M_\odot yr^{-1}$.
3. Abbott et al. (1980) give $\dot{M} = 2.3 \times 10^{-6}\ M_\odot yr^{-1}$.
4. Abbott et al. (1980) give $\dot{M} \leq 4.1 \times 10^{-6}\ M_\odot yr^{-1}$.
5. Abbott et al. (1980) give $\dot{M} = 2.10 \times 10^{-5}\ M_\odot yr^{-1}$; the adopted S_ν (6 cm) gives $\dot{M} = 9.0 \times 10^{-6}\ M_\odot yr^{-1}$, if $D = 1.2$ kpc; $1.7 \times 10^{-5}\ M_\odot yr^{-1}$, if $D = 1.8$ kpc.
6. Abbott et al. (1980) give $\dot{M} \leq 2\ 5 \times 10^{-7}\ M_\odot yr^{-1}$.

from Abbott (1978); the values of S_ν (6 cm) are the estimated values determined for stars of types B3 and earlier from the measured infrared excesses at 10 μm, they are listed in Table 4-6. The justification for the extrapolation process which has been used to find S_ν (6 cm) is the generally good agreement with the measured values by Abbott et al. (1980; see also the notes to Table 4-6). By proceeding in this way, we obtain results for more stars than have been observed directly at 6 cm. The fluxes at 6 cm listed for β Ori, B8 Ia, and for α Cyg, A2 Ia, are the upper limits measured by Abbott et al. The rates of mass loss given in Table 4-12 differ somewhat from the values given by Abbott et al. because the distances adopted here are different from those adopted by Abbott et al. The rates of mass loss derived by Abbott et al. for six of the stars are given in the notes to Table 4-12

The value of log $T_{\rm eff}$ (from Table 4-1) and of log $L/L_\odot$, determined from the relation

$$\log L/L_\odot = 4\log T_{\rm eff} + 2\log R/R_\odot - 15.045, \quad (4\text{-}9)$$

is listed for each star The constant term in Equation (4-6) is determined by assuming that $T_{\rm eff} = 5.77 \times 10^3$ K for the Sun.

In all the work on the rate of mass loss from early type supergiants reported here, it is assumed that u_∞ is, indeed, the maximum outflow velocity that is seen by means of the ultraviolet spectrum. The temperature in the radio-emitting region is assumed here to be 2.2×10^4 K, which is a value consistent with the observed turnover point in the infrared excesses of supergiants. The rates of mass loss derived from radio fluxes are slightly sensitive to the adopted value of T because, according to Spitzer (1962), the value of the Gaunt factor at 6 cm depends on the temperature as

$$g_\nu = 1.9042 \log T - 2.5958. \quad (4\text{-}10)$$

It is assumed that the emitting plasma has cosmic composition with an atomic weight of 1.2, an average charge per ion of 1.1, and an average number of electrons per ion of 1 1.

Except for P Cyg, the rates of mass loss given in Table 4-12 for early B-type supergiants are a few times 10^{-6} $M_\odot$yr^{-1}. The values for stars of types O9.5 to B1 are commensurable with those estimated from analysis of the Hα emission profile. The B1 Ib star ρ Leo has a lower rate of mass loss than is found for the luminous B1 supergiants. The rate of mass loss for late B-type supergiants decreases to a few times 10^{-7} $M_\odot$yr^{-1}.

One cannot conclude that $\dot{M}$ is proportional to luminosity alone because the rate of mass loss from P Cyg is about 10 times larger than it is from most of the other supergiants, even though the luminosity of this star is like the luminosities of the other early type supergiants. Quite clearly, some mechanism in addition to those considered for normal mantles causes an unusually strong Hα and infrared excess emission for the unusual emission-line star, P Cyg.

Both Oegerle (1977) and Lee (1979) have attempted to model the outflowing atmosphere of P Cyg using the Sobolev theory and solving the equations of statistical equilibrium to find the distribution of hydrogen over its possible energy states. Both have noted that it is impossible to model accurately the strong emission at Hα and the deep absorption core, which is observed, within the normal framework of expanding homogeneous shells of gas. To obtain the observed deep absorption cores, one must have the source function in Hα decrease more rapidly with radius than the adopted model suggests. Lee is able to show that the velocity laws in the mantles of HD 190603, ζ^1 Sco, and χ^2 Ori are much steeper than the law which appears to be valid for P Cyg.

A General Model for the Mantles of B-Type Stars

In the preceding section, we have seen that models for the mantles of B-type supergiants which consist of a plasma having a temperature like the effective temperature of the star, and which are accelerated by radiation pressure in lines, as well as models in which the outflow follows from the presence of a thin, hot corona can be used to deduce rates of mass loss from the profiles of resonance lines and from the intensity of the emission of Hα. The rates of mass loss

found in these ways are about the same as the rate of mass loss which can be deduced from a simple model for radio emission from a uniformly expanding, constant temperature sphere of gas around the star. This means that with each type of model one requires about the same amount of material to interpret the chosen criterion (the absorption troughs and emission peaks of ultraviolet resonance lines, the Hα emission strength, or the flux of energy emitted at 6 cm). However, in each type of model the relation between distance, outflow velocity, electron temperature, and local density may be rather different. The referenced studies give very little real information about the physical conditions in mantles and how these conditions are generated. They merely postulate certain conditions and trace out the consequences

In order for a mantle to exist, one must inject additional energy beyond that normally transferred by the passage of the radiation stream from the core of the star and one must inject additional outward momentum into the outermost levels of the star. The need for additional nonradiative energy arises from the fact that more ions requiring much energy for their generation are seen than can be expected according to the constraint of radiative equilibrium, given the effective temperature of the star. The need for additional outward momentum comes from the fact that we see material escaping from the star at velocities that differ by a significant amount from zero. These two needs cause one to ask what is the origin of the additional energy and momentum, and to inquire by what physical processes the energy and momentum are transferred from a storage mode to the modes in which we detect them.

It is hoped that one will be able to develop models for mantles that are characterized by two parameters. These are new parameters, in addition to those, T_{eff} and $\log g$, which are used to characterize classical models of the photosphere. The value of the parameter T_{eff} together with the constraint of radiative equilibrium permits one to model the distribution of temperature in a photosphere. The value of the parameter $\log g$ together with the constraint of hydrostatic equilibrium and the condition that matter be conserved permits one to model the distribution of density and outflow in the photosphere. To develop models of the mantle, one would use two additional parameters, one to define the energy density of the source which provides the nonradiative energy in the mantle and the other to define the efficiency of the process by which outward momentum is transferred to the material forming the mantle. These parameters would be used with the conservation laws and representations of the appropriate interactions between matter and radiation to build a self-consistent theoretical model Then one would predict a few observable quantities and use the agreement between the predictions and observation to determine appropriate values for the additional parameters.

Papers describing such models have not yet been published nor is there at present any consensus about what source of energy and momentum in a star is to be tapped, or about what the appropriate parameters might be. However, it is sufficiently urgent that these questions be studied, that a few remarks will be presented here on what may possibly prove to be viable directions to explore.

The stars are natural systems just as the Sun is. Therefore, in considering possible models for the mantles of the stars, it seems appropriate to start by considering the Sun. The Sun is a nearby astronomical body and many observational data are known in a wealth of detail. In a review of the observations and theory concerning the solar corona, Vaiana and Rosner (1978) have made two related points (1) that inhomogeneity is an essential property of the solar corona, and (2) that the topology of the structure of the ambient coronal magnetic fields largely determines the physical state of the coronal plasma. Many of the spectroscopic observations of the mantle of the Sun, which is the solar corona plus the transition layers leading to the photosphere, can be interpreted in terms of material constrained to lie in coronal loops and material lying in coronal holes and moving outward along open lines of force.

Therefore, by analogy, it seems that it might

be profitable to consider the possibility that the presence of weak magnetic fields may be fundamental for establishing the properties of stellar mantles. The question to study is how energy and momentum may be moved from storage in the magnetic field to the gas of the mantle. Interactions resulting from differential motion in, or just above, the photosphere appear to be important. The transfer of energy and momentum from the magnetic field of the Sun to the gas of the corona as a result of differential motion in the low layers of the solar mantle is important for determining the physical state of the solar corona and the spectroscopic observations which we obtain of the solar corona.

It is not suggested here that the origin of the magnetic field in the Sun is the same as for B-type stars. Nor is it necessary that the origin of differential motion in the upper part of the photosphere of the Sun be the same as for B stars. It is, however, important to realize that given the presence of a magnetic field of suitable density and the presence of differential motion of an appropriate amount, that similar structures to those which we see for the Sun might be generated in the mantles of stars of all spectral types. Such structures could explain many of our observations of what occurs in the mantles of B stars.

Underhill (1980b) has shown that if a small magnetic field were occluded as an early type star formed, the field would not have had time to decay by the time the star was becoming a supergiant. She then showed that given the presence of differential motion of an amount that seems to be present in the photospheres of B-type supergiants, one might expect sufficient heat to be transferred to the mantle by quiescent magneto/dynamic processes that the observed amount of heating would occur. It is possible in this way to account for the difference in level of ionization seen between the mantles of O9/B0 supergiants and B9/A0 supergiants. Although this suggestion about a possible source for the heating of the mantles of B-type supergiants is plausible, no detailed theoretical model has been worked out at this time In particular, no specific suggestion has been given for the origin of the differential motions inferred to be present in the photospheres of B-type supergiants.

It is sometimes suggested that macroturbulence originates from the differential rotation that is suspected to be present in the outer layers of main-sequence B stars. Perhaps as the rotation of the star is braked (possibly by magnetic interaction with the surrounding interstellar medium), the differential motion which is called macroturbulence is generated and becomes visible by means of the spectra of supergiants.

It seems unlikely that satisfactory models of the mantles of B stars of any luminosity class can be developed until the effects of the presence of magnetic fields and of differential motion are included in the theoretical framework which is used. It would be very satisfactory if the same set of hypotheses could be used for modeling the mantles of main-sequence B stars, including Be/shell stars, as for modeling the mantles of supergiants. Appropriate parameters governing the type of model which would result, seem to be, at this time, a number establishing the density of the magnetic energy per unit volume in the upper photosphere and a number specifying the typical size of the differential motions which twist, mat, and break the magnetic field lines. The theory of stellar evolution should be widened to relate the sizes of these parameters to the chronological age of a star and to its speed of evolution. The subject of modeling mantles is discussed further in Chapter 8.

Comparison with Properties of B-Stars in the Main-Sequence Band

The effective temperatures of B supergiants of a given spectral type are lower than those of main-sequence stars. This may be seen from Figure 4-1 where the two temperature laws are compared. At type B1, the difference is about 7.0×10^3 K. The radii of main-sequence B stars are about 3 times smaller than those of Ia supergiants at type B1 and about 30 times smaller at type A0. The masses of B supergiants are larger than the masses of B main-sequence stars of the same subtype, but the factor is not well known. It seems to be something between

about 1.5 and 4.0.

So far as the photosphere is concerned, the density in the case of main-sequence stars is about 100 times that for supergiant stars. This may be deduced from the fact that the Balmer series breaks off at about $n = 14$ for main-sequence stars but at about $n = 22$ for supergiants. The microturbulent velocity in the photospheres of supergiants is about 3 times its value for main-sequence stars. The spectral lines of many B-type main-sequence stars are strongly broadened by rotation with $v \sin i$ in the range 100 to 250 km s^{-1}, being a quite common occurrence. In the case of supergiants, $v \sin i$ is usually less than about 50 km s^{-1}. Macroturbulence seems to be present for supergiants but not for main-sequence stars. Smith and Ebbets (1981) suggest that it might be due to noncoherent electron scattering in supergiants

The mantles of B supergiants are much more conspicuous than those of main-sequence stars. They give clear evidence for mass loss at a rate in the range from a few times $10^{-7}\ M_{\odot}\mathrm{yr}^{-1}$ for late B supergiants, to a few times $10^{-6}\ M_{\odot}\mathrm{yr}^{-1}$ for early B supergiants. In the case of the main-sequence stars, outflow is suggested for a few stars by the asymmetries of the profiles of some ultraviolet resonance lines. However, little information is available on what the rate of mass loss might be because models of the mantles of main-sequence stars are of an even more tenuous character than are those of supergiants. Consequently, the profiles of the ultraviolet resonance lines cannot be interpreted reliably. Since main-sequence B stars do not normally show Hα emission or radio emission, these alternative indicators of mass flow cannot be used to estimate the value of $\dot{M}$ from normal main-sequence stars. It seems unlikely that $\dot{M}$ exceeds $10^{-9}\ M_{\odot}\ \mathrm{yr}^{-1}$ for most normal main-sequence B stars.

From the fact that the same ultraviolet resonance lines are seen in the spectra of main-sequence B stars of a given type, as in the spectra of B supergiants, if such lines are seen at all, it seems that the high electron temperatures in the mantles of main-sequence B stars are about the same as in the mantles of B-type supergiants. This means that nonradiative energy is being deposited in the mantles of main-sequence B stars just as it is in the mantles of supergiant B stars. The amount of gas that is heated, however, seems to be much smaller for main-sequence stars than for supergiants.

The visible spectra of Be/shell stars indicate that a greater amount of cool plasma may lie outside the photospheres of these stars than is the case for supergiants of the same spectral type. This is a major difference between the mantles of main-sequence stars and of supergiants. In the case of the supergiants, the evidence is that, at most, small pockets of plasma having electron temperatures lower than are normal for the photosphere exist. In the case of shell stars, the spectroscopic evidence for the presence of cool plasma in moderate abundance is strong. However, this cool plasma is not a permanent part of the star. It comes and goes in a matter of a few months to a few years.

The mantles of main-sequence B stars are like those of the supergiants in that they indicate (1) the presence of heating by nonradiative energy and (2) inhomogeneity by the occasional presence of relatively sharp components that come and go (see Part II). They differ from those of supergiants in that they seem to contain material at a lower density (the Balmer series may extend to $n = 35$, or so) yet, at the same time, they may show evidence for the presence of abnormally cool plasma.

The maximum velocity of outflow seen for τ Sco, B0 V, is 1200 km s^{-1} (Snow and Morton, 1976). This value is a little smaller than the value observed for B0 Ia stars (see Table 4-5). This would seem to be evidence that radiative acceleration, the amount depending on T_{eff}, is active in the mantles of main-sequence stars and in those of supergiants of type B. Because the lines showing outflow for τ Sco are not saturated (see Figure 3-16), it is probable that the value 1200 km s^{-1} is a lower limit to the true value for u_{∞} which occurs for this star.

5

SPECIAL TYPES OF B STARS

Janet Rountree Lesh

THE BETA CEPHEI STARS

The Beta Cephei stars are a group of early B stars which have long been recognized as variable in light and spectrum.

Properties of the Group

The β Cephei variables are a small group of early B stars that exhibit light and radial-velocity variations having the same short period (generally 3 to 6 hours), which is too short to be ascribed to stellar rotation or binary interaction. The light curve generally lags one quarter period behind the radial-velocity curve, unlike the situation in classical Cepheids The periods are stable over observing intervals of up to 50 years, and are typical vibration periods for 10 to 15 $M_\odot$ stellar models—the mass range believed to be appropriate for β Cephei stars (cf., Chapter 7). Therefore, these stars are usually considered to be a class of pulsating variables. Their observational properties have recently been reviewed by Lesh and Aizenman (1978). The cause of their pulsational instability remains unknown.

Spectral Types and Luminosities. The "classical" β Cephei stars—those stars discovered between 1902 and about 1960, and extensively studied in the 1920's and 1950's—fall in the narrow spectral type range between B0.5 II to III and B2 IV on the MK system. The question of whether stars whose spectral types fall well outside this range can be β Cephei stars is still being debated. However, it is generally agreed that the following groups of stars are not β Cephei stars. (1) Be stars, which frequently show irregular light and spectrum variations (although a few β Cephei stars do exhibit transient emission features, especially at Hα), (2) supergiants with irregular light, velocity or profile variations (but one or two supergiants have been proposed for membership in the β Cephei class on the basis of apparently periodic variations); (3) ellipsoidal variables, where the radial-velocity period is usually twice the light period, and other geometric variables, (4) long-period (8 to 12 hours and more) profile variable B stars like the ones studied by Smith and his coworkers (Smith and Karp, 1976; cf., Chapter 3), which usually do not exhibit light and radial-velocity variations with the same period as the profile variations, and whose periods are most often unstable. The relationship between the "ultrashort-period variables" ($P < 1$ hour) recently observed by Jakate (1979) and the β Cephei stars can be specified only when more data become available for the new variables.

In any case, the spectral types of those β Cephei variables that have been classified on the MK system are completely normal—indeed, many of them are MK standards. Although the classical β Cephei stars were all sharp-lined and therefore were thought to be slow rotators, many broad-lined candidates have recently been put forward (This is due to the fact that early studies of these stars were mainly spectroscopic, and small radial-velocity variations are more easily detected in sharp-lined stars than in broad-lined

stars. On the other hand, most present-day searches for new variables are conducted photometrically, and therefore are not affected by line width.) It seems clear that sharp lines are not a necessary condition for membership in the β Cephei class. What this implies about the role of rotation in the β Cephei phenomenon is unclear, since a star can be a rapid rotator with narrow lines (pole-on rotation) or a slow rotator with broad lines (if the line broadening is produced by atmospheric effects rather than by rotation).

High resolution spectra of a few β Cephei stars have not shown any abundance anomalies large enough to have a significant effect on the stellar structure, such as by causing the buildup of a substantial partial-ionization zone, making a major change in the opacity; or by creating an inversion in the mean molecular weight—all of which have been suggested from time to time as possible driving mechanisms for the pulsation. Peters (1976a) found that all abundances she derived for γ Peg were within 0.2 dex of the currently accepted solar values (except for Ne, Cl, and A, where the discrepancy may be due to a combination of non-LTE effects and uncertainties in the solar abundances). The overabundance of carbon, by a factor of 2 with respect to average B stars, which was found by Grabowski (1969) for 12 Lac, does not appear to be typical of this class of variable. Except for an underabundance of nitrogen, Grabowski found the abundances of the remaining elements in 12 Lac to be comparable with those in other B stars. Using a curve-of-growth analysis, Watson (1971a) studied a sample of 12 β Cephei stars and found the mean relative abundances of 10 different metals to be virtually identical with the average values for nonvarying B stars All investigators agree that the helium abundance, an important parameter for stellar structure, is normal in β Cephei stars.

The temperatures and luminosities of β Cephei variables—as derived from the calibration of MK spectral types, broadband photometry, narrow-band photometry, equivalent widths of the Balmer lines, or by other methods—are usually found to be typical for early B stars. Temperature scales based on UBV photometry have been established by Lesh and Aizenman (1973) and by Balona and Feast (1975), while Shaw (1975) used uvby photometry. Ultraviolet temperature criteria are discussed by Lesh (1976), Beeckmans and Burger (1977), and Lesh and Wesselius (1979). Generally speaking, all these temperature scales agree to within a few percent.

Luminosities of the β Cephei stars have been determined by Lesh and Aizenman (1973) and Shaw (1975), using the Hβ index, and by Balona and Feast (1975), using the Hγ index. The systematic difference among these three luminosity scales is about 0.2 mag. Jones and Shobbrook (1974) added 0.5 mag to the absolute magnitude they derived from the Balmer-line indices in order to make the luminosities correspond to their astrometric distance scale. Thus, their luminosity calibration is fainter than any of the others In all these investigations, the β Cephei stars are found not to differ systematically in luminosity from nonvariable B stars.

There are, however, one or two cases of β Cephei variables that show signs of unusually high luminosity For example, ξ^1 CMa has an anomalously small Hβ index for its spectral type (Lesh and Aizenman, 1973) and exceptionally strong ultraviolet C IV and Si IV lines (Panek and Savage, 1976, Beeckmans and Burger, 1977). There is a similar but less pronounced effect in the ultraviolet spectrum of β Cep The mass determined for α Vir by means of the intensity interferometer (Herbison-Evans et al , 1971) does not equal the mass corresponding to the luminosity derived from total flux measurements; so this star is sometimes considered to be "overluminous" for its mass. (Alternatively, the standard error of the mass determination may have been underestimated.) Whether any of these points is connected with the nature of the variability remains to be seen.

No β Cephei star has yet been observed at radio wavelengths Woodsworth and Hughes (1977) included α Vir in their 10.6 GHz survey, but did not detect it. Several β Cephei variables are on the list of stars to be surveyed in the X-ray region with the Einstein Observatory (HEAO-B satellite), but the results have not been reported as of this writing.

Variable intrinsic polarization could, on theo-

retical grounds, be expected in the light from β Cephei stars if they are nonradial pulsators (see, e g , Odell, 1979). Schafgans and Tinbergen (1979) searched for such time variations in linear polarization from β Cep, but did not detect them (at the 4×10^{-4} rms level) However, Odell (1981) observed a variation having the predicted order of magnitude in BW Vul. Rudy and Kemp (1978) used measurements of circular polarization in the wings of the Balmer lines to survey nine β Cephei stars for magnetic fields Only 1 of their 80 measurements—an observation of β Cep itself—was above the 3 σ level, but a χ^2 analysis suggested that fields as large as 1 kG might be present in β Cep and γ Peg, and possibly in this class of stars as a whole

Periods A pervasive phenomenon among β Cephei stars is multiperiodicity—the existence of one or more secondary periods in addition to the principal 3 to 6 hour period. In the earliest studies of the radial-velocity variations of the "classical" β Cephei stars, the amplitude of the velocity curve often appeared to be modulated with a "long" period, of the order of days. This was interpreted as an interference between two nearly equal short periods, and the long period was known as the "beat period." The second short period was derived from the frequency difference between the principal period and the beat period. The observational aspects of the phenomenon of multiperiodicity have been reviewed by Lesh and Aizenman (1976).

Modern techniques of examining data for periodicities, such as periodogram analysis, make it possible to determine a number of short periods without going through the intermediate step of looking for long-period modulation. The largest number of persistent frequencies discovered so far is for 12 Lac, where six periods between 2 and 6 hours have been computed from several data sets by Jerzykiewicz (1978) and Jarzebowski et al. (1979). First and higher overtones of the principal frequency sometimes also appear in a periodogram analysis, but this means only that the light curve or velocity curve is slightly nonsinusoidal.

On the other hand, some investigators have put forward the idea that the "long" period in β Cephei stars is a physically meaningful quantity. Again referring to 12 Lac, Opolski and Ciurla (1961) considered the 8.9-day "beat" period to be the real physical period "related to small pulsations in the star," while the average of the short periods would be a disturbance resulting from "shock waves." Along a similar line, Fitch (1967, 1969) suggested that the long period in many of the β Cephei stars (not all of them known double systems) is a binary period. According to him, the principal oscillation in these stars is perturbed by the variation in tide raising potential as the companion moves in its orbit Linear combinations of the orbital and pulsation frequency are preferentially excited if they have a natural resonance with another pulsation overtone, thus accounting for the other short periods observed in multiperiodic stars

Although these theories have an attractive simplicity, they probably do not apply to the majority of multiperiodic β Cephei stars. Counterexamples readily come to mind in β CMa, for example, the two short periods cannot be artifacts because one of them carries most of the light variation while the other carries most of the radial-velocity variation; this star shows no evidence of being a binary system But in some well-known binary variables such as α Vir, only a single short pulsation period is observed. Although this oscillation is slightly perturbed by the binary motion, no secondary frequencies are excited.

There is much current interest in the question of whether or not the β Cephei stars obey a single period–luminosity relation, like the classical Cepheids A simple plot of the logarithm of the period versus the absolute visual magnitude for the best-known β Cephei stars shows a general linear trend, with considerable scatter. The scatter is partly due to the finite width of the β Cephei "instability strip" in the HR diagram, it can be reduced by introducing a color term into the period–luminosity relation. The question is whether the remaining scatter is greater than the observational errors; if so, this might indicate that the β Cephei stars are not all pulsating in the same mode. Theoretical period–luminosity relations for various radial and nonradial pulsa-

tion modes have been presented by Lesh and Aizenman (1974), who concluded that most of the well-known variables are in the first or second harmonic radial mode, or a nonradial p-mode (cf., Chapter 7).

When recently detected β Cephei candidates are included in the sample used to compute the period–luminosity relation, widely differing results are obtained by different investigators. For instance, Shobbrook (1979a) finds that a period–luminosity–color relation can be so well defined using the Strömgren photometry, that the scatter about this relation is less than the observational errors. However, Jerzykiewicz and Sterken (1979) conclude that there is no unique period–luminosity relation for β Cephei variables, implying that a variety of nonradial modes is present. Jakate (1980) also finds that the scatter in the period–luminosity–color relation exceeds the observational error, but attributes this to the presence of stars with different evolutionary states, rather than different pulsation modes This problem is intimately connected with that of the β Cephei instability strip, to be discussed in the section on Position in the HR Diagram.

Although the individual oscillations in most β Cephei stars appear to be stable on time scales of the order of 50 years, slightly different values of the period are often obtained from data sets with different mean epochs of observation. If these period differences are considered to be continuous secular changes, the rates of change sometimes amount to several seconds per century. Both increasing and decreasing periods have been detected in this fashion. It is tempting to interpret these period changes as secular effects due to the star's evolution across the instability region. As the stellar model evolves to the right in the HR diagram, its period increases, and as it moves to the left, the period decreases, at a rate that is proportional to the rate of stellar evolution. (This effect is governed mainly by changes in the stellar radius as the model evolves.) Thus, the observed period changes could, in principle, be used to determine the evolutionary state of an individual star. Eggleton and Percy (1973) have computed the rates of secular period change expected for stars in the range of masses and ages relevant for β Cephei stars.

However, there are many problems with such an interpretation. First, there is the difficulty of the measurement itself. To detect a period change of 1 second per century, one must measure the period to one part in 10^6. This requires a long time baseline. But in trying to use older data sets in conjunction with recent observations, one often encounters an ambiguity in the number of full cycles that have elapsed between the mean epochs of observation. Second, the period changes may not be truly secular, but rather discontinuous. This is to be suspected especially in cases where very different values of the period change (even with opposite signs!) have been found by combining different pairs of data sets. Finally, some investigators believe that the period changes may not really be connected with the interior structure of the star, as they would have to be if they reflected evolutionary trends. Rather, they may be determined by fairly superficial effects in the stellar envelope.

Light Variations. The light curves of β Cephei stars are nearly sinusoidal, and nearly in phase at all wavelengths. (Small, nonsystematic departures from these conditions are seen in some stars.) The amplitude at visual wavelengths (the passband of a V or y filter) is very small, rarely more than 0.1 mag and often only a few thousandths of a magnitude. Even from early, ground-based observations it was apparent that the amplitude is greater at shorter wavelengths (B and U filter passbands) than in the visual region. Since the light curves are more or less in phase, this means that the stars are "bluest" (and hottest, assuming the color index to be a temperature indicator) at maximum light. Because the light curve lags the radial-velocity curve by about one-quarter period, the phase of maximum light and temperature coincides with minimum radius, as would be the case if the compression were adiabatic.

Since the effective temperatures of the β Cephei stars are such that much of their energy is radiated in the far ultraviolet (peaking at around 1200 Å), it was to be expected that small temperature changes would produce the

greatest effect in this wavelength region, causing the light amplitude there to be even greater than in the near ultraviolet. This prediction was borne out when satellite observations became available; it was shown that the light amplitude increases steadily with decreasing wavelength. The large ultraviolet amplitude of the prototype star β Cep was first observed by Fischel and Sparks (1972), using the OAO-2 scanner, and by Lesh and Bohlin (1975), using the spectrometer on board Mariner 9. Lesh (1976, 1978, 1981) studied photometric data from OAO-2 at a maximum of 8 wavelengths between 4250 Å and 1330 Å for 10 β Cephei stars, including both singly and multiply periodic variables, objects with secularly changing periods and amplitudes, and stars having nonsinusoidal light curves All of these variables exhibited the trend of increasing amplitude with decreasing wavelength, see Figure 5-1 for a typical example. Beeckmans and Burger (1977) obtained similar data for 15 stars using the TD1A satellite, while Hutchings and Hill (1977) used the scanners on board the Copernicus satellite to observe the

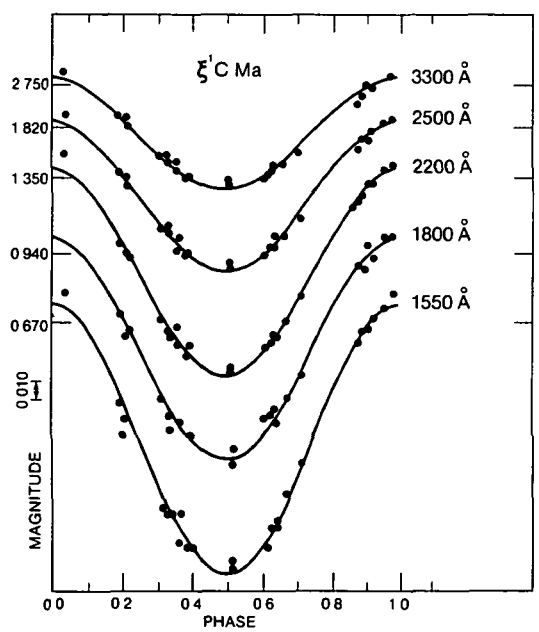

Figure 5-1. Ultraviolet light curves for ξ^1 CMa, obtained with the ANS satellite (from Lesh and Wesselius, 1979)

light variations of β Cep all the way down to 970 Å, showing that the amplitude is still increasing at this short wavelength. Lesh and Wesselius (1979) derived five-color light curves for three stars from ANS data One of these, HD 61068, was the first β Cephei star to be discovered by satellite

Because of the larger amplitudes at short wavelengths, ultraviolet observations are well suited to the confirmation of suspected variables whose light variation is marginal at visible wavelengths, and to the detection of new variables. A photometric survey with satellite instrumentation would do much to settle the question of the incidence of β Cephei variables among the nearby stars. Moreover, the long baseline in wavelength afforded by the combination of ultraviolet and visual observations is very useful for the measurement of small temperature differences Lesh (1976) showed that temperature variations as small as about 2.0×10^2 K could be measured by a comparison of the amplitude at 1900 Å (observed by means of OAO-2) with the visual amplitude Similar temperature parameters for the TD1A and ANS satellites, respectively, were derived by Beeckmans and Burger (1977) and by Lesh and Wesselius (1979) Taken as a whole, these investigations show that the temperature variations in β Cephei stars are rarely greater than 1.5×10^3 K

It was once thought that the small visual light amplitudes of the β Cephei stars, in comparison with their radial-velocity amplitudes, were evidence for the presence of nonradial pulsation in these stars However, Watson (1971b) showed that when the variation of the bolometric magnitude is taken into account, the β Cephei stars are similar to other classes of variables that are believed to be radial pulsators But Stamford and Watson (1977) showed that the color-to-light ratio, $\Delta(U - B)/\Delta V$, could be used as a discriminator between radial and nonradial pulsation, and later (Stamford and Watson, 1979) they extended their work to the far ultraviolet, deriving curves of $\Delta m(\lambda)/\Delta m(1550)$ for a long wavelength baseline. Their conclusion was that the existing data for most known β Cephei stars are consistent with the radial-pulsation hypothesis.

Velocity Variations. The radial-velocity amplitudes of the β Cephei stars generally lie between 10 and 100 km s^{-1}. Most of the velocity curves are sinusoidal, but some of them exhibit a plateau or "stillstand" on the descending branch, and in a few extreme cases the curve appears to be discontinuous. This phenomenon is now attributed to variations in the absorption-line profiles. These variations were first perceived as changes in line width; with higher resolution, it was shown that the line profiles in some β Cephei stars exhibit continuous changes in asymmetry, which can include the splitting of the line into two or more components As one component becomes weaker and another becomes stronger, on the descending branch of the velocity curve, a "stillstand" results if the components are not resolved; if they are resolved, the velocity curve appears discontinuous.

A number of spectrographic and spectrophotometric studies, with high resolution in time and wavelength, have recently been made from ground-based observations; they concern the β Cephei stars ν Eri (Laskarides et al , 1971, Laskarides, 1973), β Cep (Goldberg et al , 1974), 12 Lac (Heard et al., 1976, Allison et al , 1977), BW Vul (Kubiak, 1972; Goldberg et al , 1976), γ Peg (Smith and McCall, 1978a), and γ Peg, β Cep, δ Cet, and σ Sco (Campos and Smith, 1980) The profiles most often monitored are those of the Si III lines around 4550 to 4575 Å, but other absorption lines, including some from hydrogen and helium, are also observed in some cases.

The spectral lines are generally narrow and have steep sides on the ascending branch of the radial-velocity curve, and are broad and shallow on the descending branch, where the most pronounced effects of asymmetry (or line splitting) are observed. The O I and He I lines, as well as the Si III lines, follow this pattern, in which the equivalent width is approximately conserved. The hydrogen lines show "filling in," presumably by emission from the extended atmosphere, at phases around maximum radius

Some initial efforts have been made to observe similar phenomena in the far ultraviolet with satellite-borne spectrometers. Although the resolution of the OAO-2 scanner was not sufficient to detect subtle profile variations, Fischel and Sparks (1972) observed a far more striking effect in β Cep· the "disappearance" and reappearance, on a 6-day cycle, of the C IV line at 1550 Å. This effect, whose connection with the short-period pulsation is problematical, was not confirmed by Lesh and Bohlin (1975), who found no statistical evidence for equivalent width variations in any of the lines of γ Peg or β Cep, which they observed with the Mariner 9 spectrometer. However, Hutchings and Hill (1977) observed large variations in the strength of the C IV lines in β Cep, using the Copernicus U2 scanner. Fischel and Sparks (1981) confirmed their initial findings by means of high resolution spectra from IUE. They detected similar variations in other resonance lines, notably those of N V. The only star to exhibit such an effect seems to be β Cep itself.

High resolution ($\Delta\lambda$ = 0.05 Å) Copernicus scans were used by Lesh and Karp (1977) and Lesh (1978b) to follow the profile variations in a number of ultraviolet absorption lines, especially Si III 1294.5 Å, over one or more pulsation cycles in five β Cephei stars. The most notable feature of these observations was that the profiles in σ Sco and ν Eri were dominated by a shortward asymmetry ("depressed blue wing") over the entire pulsation cycle, rather than exhibiting alternate shortward and longward asymmetry, as is the case in the visible wavelength region. Moreover, in σ Sco the phase of maximum asymmetry occurred on the rising, rather than the descending, branch of the radial-velocity curve New studies of ultraviolet spectral variations making use of the IUE satellite, now being undertaken by Fischel and Sparks and by Lesh, should shed new light on the phenomenology of β Cephei behavior in this area.

The profile variations in β Cephei stars are generally interpreted in terms of a velocity field in the stellar atmosphere, induced by radial or nonradial pulsation At present, the observations (and the theory[1]) are not sufficiently precise to distinguish between these two hypotheses. Lesh and Karp attempted to explain the persistent shortward asymmetry they observed as a stellar wind

superimposed on the pulsational velocity field. However, they were not able to find a self-consistent model for these phenomena For an overview of the theory of line formation in an oscillating atmosphere, on which the interpretation of β Cephei line profiles is based, see Chapter 3 and the paper by Mihalas (1980).

Typical Members of the Group

A list of the most generally accepted members of the β Cephei group, together with their essential observational properties, is given in Table 5-1. Only those stars are included for which both light and radial-velocity curves have been obtained. Many other probable β Cephei stars have recently been discovered photometrically, but their radial-velocity variations have not been studied. Most of the data in Table 5-1 are taken from Lesh and Aizenman (1978), where references to the original observations may be found. New observations have been added in a few cases. the authors are Shobbrook (1979b), β Cru, τ^1 Lup, and α Lup; Jarzebowski et al. (1979), 12 Lac and 16 Lac; Lomb (1978), α Vir; Lane and Percy (1979), KP Per, and Smith and McCall (1978a), γ Peg. We have also added a column giving the ultraviolet amplitude at a wavelength near 1900 Å, when observed. We choose this wavelength because it is most often used as a temperature indicator. The sources are Lesh (1976, 1978a, 1981) for observations at 1910 Å, Beeckmans and Burger (1977), 1950 Å, and Lesh and Wesselius (1979), 1800 Å.

Position in the HR Diagram

It is well known that the classical Cepheids and related variable stars occupy a well-defined "instability strip" in the HR diagram. Virtually all the stars within this strip are variable, and no Cepheids are to be found outside it. Since the β Cephei stars also occur in a small area of the HR diagram (lying well outside the Cepheid region), it is natural to ask whether they define an instability strip in the same sense—namely, a strict segregation of variables from nonvariables. The answer to this question may have significant implications for the evolutionary state of the β Cephei stars.

Table 5-1
Basic Observational Data for Representative β Cephei Stars

HD	Name	Spectral Type	V (mag)	B–V (mag)	Period (day)	2K (km s^{-1})	Δm(V) (mag)	Δm(UV) (mag)	v sin i (km s^{-1})
886	γ Peg	B2 IV	2 84	−0 23	0 1517502	6 8	0 017	0 035[a]	5
16582	δ Cet	B2 IV	4 06	−0 21	0 1611380	12 6	0 025	0 073[a]	25
21803	KP Per	B2 IV	6 40	+0 03	0 201778	50	0 072	–	–
					0 1982	5	0 036	–	–
29248	ν Eri	B2 III	3 96	−0 22	0 1735089	49 0	0 114	–	31
					0 1779	16	0 067	–	–
44743	β CMa	B1 II-III	1 97	−0 24	0 2512985	6 6	0 0210	0 037[b]	38
					0 25003	10 6	0 0044	0 016[b]	–
					0 23904	2 2	0 003	–	–
46328	ξ^1 CMa	B1 III	4 34	−0 25	0 2095755	36 0	0 034	0 130[c]	33
50707	15 CMa	B1 III	4 82	−0 22	0 184557	6 5	0 005 to 0 02	0 033[c]	69
111123	β Cru	B0 5 III	1 25	−0 24	0 19120	4 4	0 04	–	32
116658	α Vir	B1 IV	0 97	−0 23	0 173787	8	0 to 0 029	–	172
122451	β Cen	B1 III	0 62	−0 24	0 157	14 4	0 to 0 04	–	128
126341	τ^1 Lup	B2 IV	4 55	−0 16	0 17738884	10 62	0 027	–	0
129056	α Lup	B1 5 III	2 30	−0 20	0 2598462	14 20	0 021	0 061[a]	0

[a] At 1910 Å
[b] At 1950 Å
[c] At 1800 Å
Dashes (–) represent no existing data at these values

Table 5-1 (cont.)

HD	Name	Spectral Type	V (mag)	B–V (mag)	Period (day)	2K (km s^{-1})	Δm(V) (mag)	Δm(UV) (mag)	v sin i (km s^{-1})
147165	σ Sco	B1 III	2 88	+0 14	0 2468429	100	0 040	–	53
					0 23945	15	0 021	–	–
157056	θ Oph	B2 IV	3 28	−0 21	0 140531	12	0 02	0 04[a]	51
158926	λ Sco	B1 5 IV	1 63	−0 22	0 2137015	17 2	0 0231	0 053[b]	300
160578	κ Sco	B1 5 III	2 42	−0 22	0 1998303	5 8	0 0087	0 03[a]	99
					0 205430	–	0 0038	–	–
163472	HR6684	B2 IV-V	5 84	+0 09	0 1398903	22 6	0 028	0 10[b]	–
199140	BW Vul	B2 III	6 52	−0 15	0 2010298	160	0 16 to 0 21	0 59[a]	–
205021	β Cep	B1 III	3 19	−0 23	0 1904881	45	0 0365	0 127[b]	43
214993	12 Lac	B1 5 III	5 26	−0 14	0 193096	37 5	0 077	0 235[a]	79
					0 197382	17 5	0 034	–	–
					0 182127	–	0 025	–	–
					0 18746	–	0 014	–	–
216916	16 Lac	B2 IV	5 61	−0 15	0 169170	29 6	0 040	0 116[a]	37
					0 170793	9 0	0 020	–	–
					0 18172	–	0 022	–	–

[a] At 1910 Å
[b] At 1950 Å
[c] At 1800 Å
Dashes (–) represent no existing data at these values

The Observational HR Diagram. The actual locus of the hypothetical instability strip in the observational HR diagram is well defined by the "classical" β Cephei stars. They lie in a region about 1.5 mag above the zero-age main sequence for early B stars, from about B0 to B3, and approximately parallel to the ZAMS. The "strip" appears to be of finite length, but its upper and lower boundaries have not been precisely determined. Percy (1971) and Percy and Madore (1972) proposed a low luminosity cutoff of $M_V = -3$ and a high luminosity cutoff of $M_V = -5$, respectively, but Eggen suggested, on the basis of a sample of candidate stars, that the strip must extend at least from $M_V \approx -6$ to $M_V = -2$

Recent work has focused on the width of the β Cephei instability strip. Jerzykiewicz and Sterken (1979) defined a strip in the (c_0, β) plane with a width of 0.025 mag in the β coordinate (see Figure 5-2), while Shobbrook (1978a) found a width of only 0.003 mag in β, and concluded that the strip is so narrow that it is not even resolved by the observations. Both of these studies were based on large (but different) samples of known β Cephei stars and candidate variables. On the other hand, some workers (e.g., Hill, 1967; Sareyan, 1979) include a large variety of early type variables in the β Cephei class, reaching the conclusion that the instability strip is so broad as to be essentially nonexistent, since it covers a substantial area of the HR diagram

Obviously, the observed width of the "instability strip" depends not only on the accuracy of the measurements, but more importantly on the stars considered to lie within the region of interest Defining the strip too narrowly leaves one open to the charge of neglecting some of the variables (and to changes when new ones are discovered), while enlarging it too much may generalize the concept of a β Cephei variable to the point where it is no longer useful

A related question is whether the β Cephei region in the HR diagram contains only variable stars, or whether it is populated by a mixture of variable and nonvariable stars–in other words, whether it is really an "instability strip" in the same sense as the classical Cepheid region is Opposite conclusions were reached by Watson (1972), who believed that he had isolated the variables in the ($\log g - T_{eff}$) plane, and by Lesh

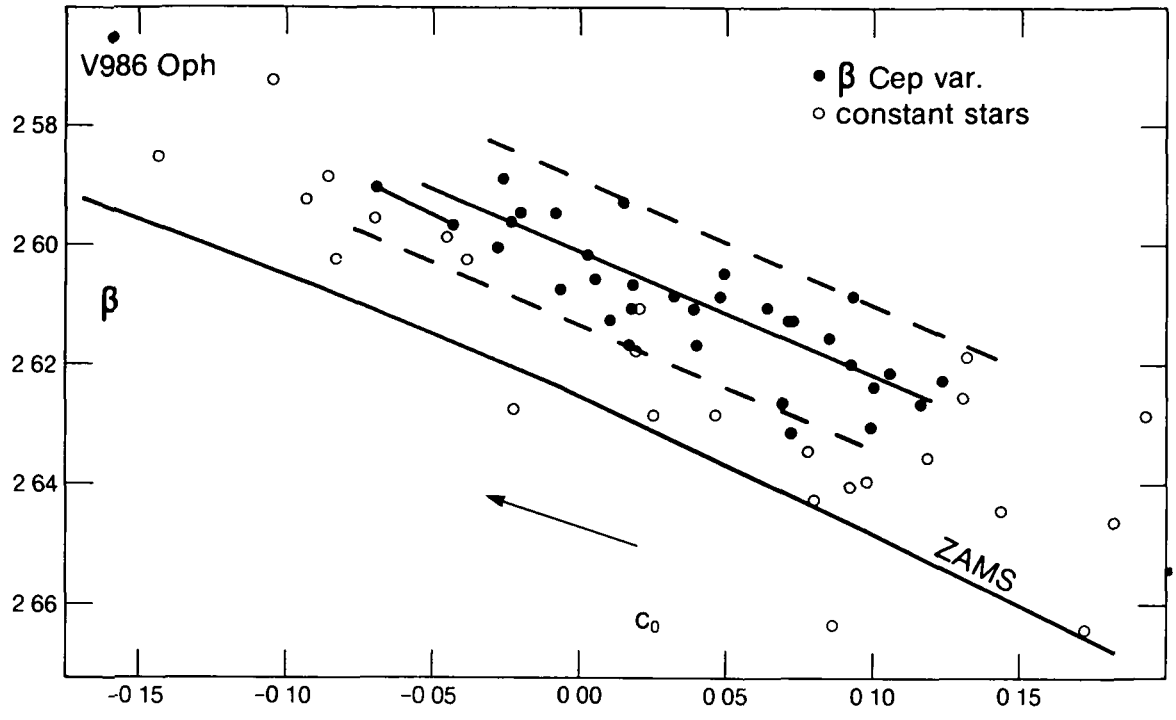

Figure 5-2. The β Cephei variables (filled circles) and constant early B stars (open circles) in the $c_0 - \beta$ plane (from Jerzykiewicz and Sterken, 1979).

and Aizenman (1973), who maintained that variables and nonvariables coexisted within the instability region. More recent studies still disagree on this point: Jerzykiewicz and Sterken (1979) state that their relatively broad instability strip is free of nonvariable stars, while Shobbrook (1978b) still finds nonvariables in his extremely narrow strip (see also Figure 3-14)

The Theoretical HR Diagram Assuming that the β Cephei variables occupy a relatively restricted region in the observational HR diagram, one may ask where the corresponding region lies in the theoretical HR diagram—that is, in the ($\log T_{\rm eff}$, $M_{\rm bol}$) plane. The mapping from observational to theoretical coordinates requires the calibration of the observational parameters one must assume a temperature scale, a luminosity scale, and a bolometric correction. As a by-product of the calibration, approximate values of the radii and masses of the stars are obtained (see Lesh and Aizenman, 1978 for some typical values of these quantities) Finally, the position of the variable stars in the theoretical diagram is compared with that of stellar models of various masses, compositions, and ages

Despite the uncertainties involved in the temperature and luminosity calibrations, there is general agreement on the location of the β Cephei "instability strip" with respect to the evolutionary tracks of massive stars The β Cephei stars tend to occupy a region variously known as the "core collapse zone," "S bend," or "hydrogen exhaustion phase" (see Figure 5-3). This is the region in which the stellar model briefly evolves toward higher temperatures and luminosities as its core contracts, following depletion of hydrogen in the core and preceding the ignition of hydrogen in a thick shell In the theoretical HR diagram, this region can be occupied by stars with three quite different internal structures stars that are still burning hydrogen in the core, those with contracting cores ("secondary contraction"), and those with a hydrogen shell source. It is not yet clear which of these evolutionary models best describes the β Cephei stars

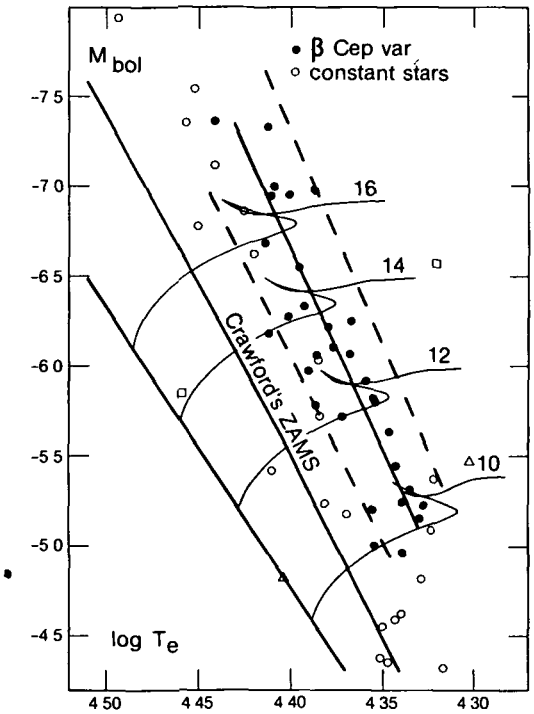

Figure 5-3 The β Cephei variables (filled circles) and constant early B stars (open circles) in the theoretical HR diagram (from Jerzykiewicz and Sterken, 1979).

Among investigators who have found the "instability strip" to be wide enough to take in most of the "S bend" region, and who have also found nonvariable stars in the strip, opinion is divided (on statistical grounds) between core burning and secondary contraction as the most likely evolutionary stage for β Cephei stars. Shobbrook (1978b), having found a very narrow strip containing a few nonvariable stars, favored the end of core hydrogen burning for the onset of instability, from the point of view of pulsation theory (see Chapter 7), the stage of shell ignition would also be a plausible locus for a very narrow strip. On the other hand, if the β Cephei phenomenon occurs over a large area of the HR diagram, it may not be associated with any particular evolutionary phase. Jerzykiewicz and Sterken (1979) make the same argument for an instability strip containing no nonvariable stars—the stage of evolution may be less important for instability than the actual values of the temperature and luminosity of the stars.

The size of the β Cephei instability strip also has implications for the location of the zone driving the pulsation in the stellar interior. If there is a fairly narrow instability strip, the driving zone is likely to be associated with the stellar core (the site of nuclear energy generation), while a broader instability region would point to an envelope instability mechanism, possibly an opacity effect (cf , Osaki, 1979; Cox and Stellingwerf, 1979)

THE PECULIAR B STARS

Even at classification dispersion, it is apparent that certain B-type stars exhibit anomalous line strengths. The anomalies are most easily detected in the lines of neutral helium, which reach their peak at spectral type B2. Both abnormally strong and abnormally weak helium lines are observed to occur The use of higher dispersion spectrograms and a comparison between broadband photometry and spectral classification has shown that peculiar stars—"peculiar" in the sense that they cannot be classified in the ordinary two-dimensional system—exist throughout the entire temperature range covered by the B stars, and overlap with the late O stars ("hot subdwarfs") and the early A stars ("magnetic" and "metallic-line" stars) The spectral anomalies involve not only the helium and hydrogen lines, but certain metallic lines as well.

These B stars with anomalous spectra are sometimes called "chemically peculiar B stars," or "CP stars" for short We prefer to avoid this nomenclature, because it implies that the spectrum anomalies reflect anomalies in the overall chemical abundances, which is not necessarily the case In fact, there is growing support for the idea that seemingly contradictory phenomena—such as abnormal helium-line strength and weakness—may be produced by the same mechanism, and that several of the classes of peculiar B stars may form a nearly continuous temperature sequence, connecting the O subdwarfs with the Ap and Am stars.

In this section, we shall describe the various types of peculiar B stars, in order of decreasing effective temperature—that is, from the earliest to the latest spectral type. We shall not try to

make an exhaustive list of the stars of each type, but shall name some typical examples and describe a few of them in detail Finally, we shall indicate the possible arrangement of these stars into families or sequences and briefly describe some of the theoretical schemes that have been put forward to explain their existence. Review articles dealing with peculiar B stars include those by Hack (1967), Dinger (1970), Preston (1974), Hunger (1975), Baschek (1975), and Wolff and Wolff (1976). For a discussion of the "CNO stars" (early B supergiants with atypical line ratios of carbon, nitrogen, and oxygen), which are not dealt with here, the reader is particularly referred to Jaschek and Jaschek (1974a).

Hot Subdwarfs

Although most hot subdwarfs are O stars rather than B stars, we discuss them briefly here because of the similarity between some of their spectral anomalies and those that occur at later spectral types, and because of possible generic connections between the O subdwarfs and some classes of peculiar B stars (for a more extensive discussion, see Underhill and Divan, *O, Of, and Wolf-Rayet Stars*, to be published)

Lying several magnitudes below the ordinary (hydrogen burning) main sequence in the HR diagram, the O-type subdwarfs have spectra dominated by absorption lines of hydrogen and neutral and ionized helium, high excitation lines of nitrogen are also sometimes present At least two groups of subdwarfs can be recognized the "N" or "intermediate" subgroup (Richter, 1971) in which the helium lines are stronger than normal with respect to the hydrogen lines, implying approximately equal abundances of hydrogen and helium by number, and carbon and oxygen appear to be deficient, and the "extreme" subgroup, in which hydrogen does not appear at all If He II 4686 is absent in an underluminous star, the star may be classified as a B subdwarf. Hot subdwarfs without an apparent overabundance of helium have exceptionally strong and broad hydrogen lines compared to helium lines, because of their high surface gravities (Sargent and Searle, 1968). In fact, many of the B subdwarfs actually appear to be helium-deficient

Table 5-2 lists several of the brightest hot subdwarfs in each group, with some relevant observational and theoretically derived parameters. Most of the data are from Hunger (1975) and Richter (1971). Other references are given in the last column Several dozen other hot subdwarfs are known, but they are too faint to have been identified with a particular subgroup as yet.

The exact location of the hot subdwarfs in the HR diagram is very poorly determined Goy (1980) recently obtained model-independent estimates of $M_V = 3.5$ and $M_V = 4.0$ for the subdwarf components of HD 113001 and HD 128220, respectively, from a consideration of the spectra of their F-type companions The stars of the extreme subgroup appear to be located on or near the helium main sequence, which may imply that they are the descendants of massive main-sequence stars which have undergone extensive mass loss It is not yet clear to which of the helium-rich B stars they are related, if any

Helium-Strong Stars

The helium-strong stars or "intermediate helium stars," unlike the hot subdwarfs, lie on or near the hydrogen burning main sequence in the HR diagram, with spectral types centered on B2 V Abnormally strong lines of He I are readily apparent on MK-dispersion spectrograms, causing a "p" to be appended to the classification, but quantitative analyses show that the helium content is enriched to only a moderate degree (helium approximately equal to hydrogen by number) The temperatures and gravities of these stars, as deduced from model atmospheres, are comparable to those of "normal" stars of similar spectral type (T_{eff} = 1 8 X 10^4 to 2.7 X 10^4 K, log $g \simeq 4$) Except for helium, the abundances are not strikingly abnormal, although Osmer and Peterson (1974) point to overabundances of oxygen and nitrogen Although helium-strong stars are typically slow rotators, a number of rapid rotators also belong to this class Many of these stars show variability in their helium spectra (Pedersen and Thomsen, 1977, Pedersen, 1979) and also in Hα,

Table 5-2
Hot Subdwarfs

Star	Spectral Type	V (mag)	B − V (mag)	U − B (mag)	M_V (mag)	T_{eff} (10^4 K)	$\frac{M}{M_\odot}$	log g	Ref
N Subgroup									
HD 49798	O6	8 3	−0 24	−0.18	+1.0	4 5	1.0	5 0	1,2
BD +75°325	sdO	8.9	–	–	>+5	5 0	–	5.3	3
HD 113001B	sdO	9.6	−0 25	−1.25	+3.5	4.1	0.7	5 7	4
HZ 44	Op	11.7	−0.29	−1.19	+3 5	4 0	0.9	5.7	
HD 127493	sdO8p	9.5	−0.24	−1 17	+3 5	4 3	0.8	5.7	5
HD 128220B	sdO9	8.5	+0.21	−0 85	+4.0	4.1	2	4.7	6
BD +25°4655	sdO6	9.8	−0.27	−1.20	+5.5	4 3	1.2	6 7	
Extreme Subgroup									
CPD −31°1701	–	10.5	−0.31	−1.17	–	4.5	–	6	7,8
BD +48°1777	–	10 7	−0.34	−1.15	–	–	–	–	9
BD +39°3226	sdOp	9.6	–	–	–	–	–	–	10
BD +37°1977	–	–	–	–	–	5 5	–	4	11
BD +37°442	–	–	–	–	–	5 5	–	4	11
SB 21	–	13.9	–	–	–	3.5	–	5.5	8
Other									
BD +13°3224	–	10.5	−0.19	−0 97	–	–	–	–	12
BD +28°4211	–	9.5	−0.34	−1.26	–	–	–	–	
AGK2 +81°266	sdO	11 8	–	–	–	–	–	–	10
BD +34°1543B	sdB	10 6	–	–	–	–	–	–	10

Dashes (–) represent no existing data at these values

References

1 Richter (1971)
2 Kudritzki and Simon (1978)
3 Kudritzki et al (1980)
4 Goy (1980)
5 Simon (1979)
6 Goy (1977)
7 Garrison and Hiltner (1973)
8 Hunger and Kudritzki (1980)
9 Berger et al (1974).
10 Berger and Fringant (1978)
11. Darius et al (1979)
12 Landolt (1975)

while light and radial-velocity variations are less common. Borra and Landstreet (1979) detected strong magnetic fields in five of the eight helium-strong stars they observed, pointing to a possible connection between these stars and the cooler Bp and Ap stars. A variable infrared excess at 4.9 μm has also been observed (Groote et al., 1980).

Table 5-3 lists a number of the better known helium-strong stars. The spectroscopy and photometry, as well as model-derived parameters such as luminosity, temperature, mass, gravity, and composition, are drawn from Hunger (1975) or from the individual papers indicated in the last column. The masses must be regarded as very uncertain. Data concerning variability come from Pedersen and Thomsen (1977) and Pedersen (1979), while the magnetic fields are those observed by Borra and Landstreet (1979).

The most extensively observed of the helium-strong stars is undoubtedly σ Ori E, which has

Table 5-3
Helium-Strong Stars

Star	Spectral Type	V (mag)	B − V (mag)	U − B (mag)	$\log \frac{L}{L_\odot}$	T_{eff} (10^4 K)	$\frac{M}{M_\odot}$	$\frac{n_{He}}{n_H}$	Period (day)	Mag Field (gauss)	log g	Ref
HD 37017	B1 5 V	–	–	–	–	–	–	–	0 90	−2300/−400	–	
HD 37479[a]	B2 Vp	6 7	−0 16	−0 89	–	2 350	6 2	0 59	1 19	−2800/−2200	3 85	
HD 37776	B2 V	7 0	–	–	–	–	–	–	1 54	+250/−2000	–	
HD 60344	B2 V	7.8	−0 18	−0 85	3 49	2 500	1 3	0 62	–	–	3 6	1
HD 64740	B1 5 Vp	4 6	−0 23	−0 92	3 62	2 240	4 5	0 29	1 33	+400/−800	4 15	2,3
HD 93030[b]	B0 5 Vp	2.8	−0 22	−1 04	–	–	–	–	0 70	–	–	
HD 96446	B2 V	6 7	−0 15	−0 84	3 70	2 525	7 6	0 90	23 0	−1400/?	4 20	4
HD 120640	B2 Vp	5.8	−0 16	–	–	2 130	–	0 18	–	–	4 02	
HD 133518	B3 V	6 4	−0 098	−0 724	–	2 140	–	1 20	–	–	4 36	
HD 144941	–	10 1	+0 05	−0 71	3 48	2 150	2 0	14 6	–	–	3 5	5
HD 168785	–	8 49	−0 04	−0 74	3 82	2 400	1 0	0 76	–	–	3 3	6
CPD −69°2698	–	9 3	−0 11	−0 88	3 60	2 900	4 5	0 38	–	–	4 1	5
HD 184927	B2 Vp	7 7	−0 16	−0 80	4 1	2 250	12 4	0 50	9 48	–	3 80	7,8, 9,10
CPD −46°4639	–	10 0	+0 08	−0 67	–	2 970	–	0 41	–	–	4 37	
HD 186205	B2 Vp	–	–	–	4 0	2 350	12 3	0 72	–	–	3 97	9,11
CPD −69°1618	–	–	–	–	–	2 730	–	0 59	–	–	4 12	

[a] σ Ori E
[b] θ Car
Dashes (–) represent no existing data at these values in references cited

References

1 Kaufmann and Hunger (1975)
2 Lester (1976)
3 Groote et al (1978)
4 Wolf (1973)
5 Hunger and Kaufmann (1973)
6 Kaufmann et al (1974)
7 Higgenbotham and Lee (1974)
8 Bond and Levato (1976)
9 Walborn (1975)
10 Higginbotham et al (1974)
11 Lee and O Brien (1977)

been studied in detail by Greenstein and Wallerstein (1958), Klinglesmith et al. (1970), and Osmer and Peterson (1974). These analyses led to values of T_{eff} between 2.35×10^4 and 2.45×10^4 K, log g from 4.05 to 4.3, and n_H from 0.5 to 0 6. The quantity n_H is the fraction of hydrogen by number. On classification dispersion spectrograms, σ Ori E looks like a normal B2 V star, except for the exceptionally strong helium lines. It is a member of the multiple system σ Ori, of which components A and B form a well-known spectroscopic binary. The σ Ori system is, in turn, a member of the Belt subgroup of the Orion association (Ori OB 1b), with a well-established distance modulus of 8.3 (Lesh, 1968). Like most Orion stars, σ Ori E is a rapid rotator, with v sin i = 150 km s^{-1}

In addition to its global properties, however, σ Ori E exhibits a variety of short-term phenomena that vary with a period of about 1.19 days there is an Hα emission feature 1800 km s^{-1} wide, which changes in intensity by nearly an order of magnitude on a time scale of minutes (Walborn, 1974, Walborn and Hesser, 1976); the equivalent widths of the He I lines vary with an amplitude of around 50 percent, while the Si III lines vary in antiphase (Hunger, 1974, Thomsen, 1974); the number of the last resolved Balmer line changes periodically, indicating the presence of an additional variable absorber (Groote and Hunger, 1976), but the equivalent widths of Hγ and Hδ are nearly constant; and the light curve has two maxima, resembling the light curve of an eclipsing binary system (Hesser et al., 1976). The radial velocity appears constant except during the two minima (Groote and Hunger, 1977), while the period of the other phenomena is apparently stable, at least on a time scale of years (Hesser et al., 1977).

Attempts to model σ Ori E have involved mass transfer binary systems and oblique rotators. The possible formation of the σ Ori system by fragmentation is discussed by Odell (1974). The question remains as to whether σ Ori E is unique

among the helium-strong stars, or whether its array of phenomena would be found in all or most of these objects if they were observed in sufficient detail.

Extreme Helium Stars

In the extreme helium stars, the hydrogen lines are either absent or very weak (implying $n_H/n_{He} \lesssim 10^{-3}$). Oxygen is often absent, with carbon, nitrogen, and neon strong The extreme helium stars are, on the average, cooler than the "intermediate" or "helium-strong" stars discussed in the preceding section they have a typical effective temperature of around $1\,5 \times 10^4$ K, and lie somewhat above the hydrogen burning main sequence in the HR diagram Their average distance from the galactic plane is high (1600 pc according to Hunger, 1975) as is their mean radial velocity, which may imply that they belong to Population II. Because of their high apparent carbon abundances, the extreme helium stars are sometimes linked with the cooler carbon stars, like R CrB Among the early type stars, they resemble the helium-rich hot subdwarfs more than the other classes of helium-strong or helium-weak stars.

Table 5-4 lists the eight extreme helium stars described by Hunger (1975), with one additional star discovered by Drilling (1978). Detailed analyses are referenced in the last column. The initial analysis of BD + 10° 2179, which may be considered the prototype star of this group, by Hunger and Klinglesmith (1969) indicated a surprisingly high carbon abundance, almost equal to the helium abundance (with a negligible amount of hydrogen). Although the carbon abundance of BD + 10° 2179 has since been revised downward in more sophisticated analyses, it remains the case that the extreme helium stars are typically rich in carbon and poor in oxygen. An exception is LS II +33° 5 (Drilling, 1978), which has strong O II lines in its spectrum. Because of the low opacity resulting from the absence of hydrogen and the transparency of He I, the line absorption in extreme helium stars is enhanced The numerous sharp, strong metallic lines make the spectrum resemble somewhat that of a supergiant. Several of the extreme helium stars exhibit short-term light variations (Landolt, 1975; Walker and Kilkenny, 1980).

Table 5-4
Extreme Helium Stars

Star	V (mag)	B − V (mag)	U − B (mag)	Spectral Type	M_V (mag)	T_{eff} (10^4 K)	log g	n_{He}	n_C	$\frac{M}{M_\odot}$	Ref
BD +37°442	10 0	−0 28	−1 17	–	–	–	–	–	–	–	
BD +37°1977	9 2	–	–	–	–	–	–	–	–	–	
BD +10°2179	10 0	−0 18	−0 90	B3	<−1 6	1 60	2 3	0 97	0 03	≥0 4	1,2
HD 124448	10 0	−0 07	−0 76	B3	−3 9	1 60	2 2	0 99	0 008	1	3
BD −9°4395	10 6	+0 07	−0 84	–	−3 5	2 50	2 6	0 99	0 006	0 8	4
HD 160641	9 8	+0 18	−0 85	O	–	3 50	–	–	–	–	4
BD −1°3438	10 4	+0 43	−0 29	–	–	–	–	–	–	–	
HD 168476	9 3	−0 01	−0 67	B5	–	1 35	1 3	–	–	–	1
LS II+33°5	10 4	+0 13	−0 75	B2 3	–	–	–	–	–	–	5

Dashes (–) represent no existing data at these values

References

1 Schönberner and Wolf (1974)
2 Hunger and Klinglesmith (1969)
3 Schonberner and Wolf (1974)
4 Kaufmann and Schönberner (1977)
5 Drilling (1978)

Helium Variables

Many of the helium-strong stars have variable helium spectra, as described in the preceding sections; the sections to follow illustrate that the helium-weak stars are frequently variable as well. It may therefore seem both difficult and unnecessary to attempt to isolate a group of B stars to be identified as helium variables However, there is an important distinction. the helium-strong and helium-weak stars that are spectrum variables, remain helium strong or helium weak, respectively, throughout their cycles But the stars that are here referred to as "helium variables" change in appearance from helium strong to helium weak in the course of a single cycle, and thus form a link between the hot and cool peculiar B stars. In fact, the helium variables occupy a position in the HR diagram that lies between the helium-strong and helium-weak stars.

The prototype helium variable is α Cen, which has a period of 8.81 days. At maximum strength of the helium lines, it resembles a helium-strong star of spectral type around B2, while at helium minimum it looks like a B8 helium-weak star (Jaschek et al , 1968) The hydrogen spectrum is relatively constant, except for possible radial-velocity variations (Norris, 1971), while the metallic lines have radial-velocity variations with the same period as the helium lines, and a total amplitude of about 3 km s^{-1}. Broad, shallow absorption features sometimes appear at the positions of the Fe I lines (Underhill et al., 1975). The star varies by about 0 05 mag throughout the ultraviolet and visual wavelength regions, with maximum brightness at helium minimum (Molnar, 1974). There is also a magnetic field varying between +1000 and −1000 gauss, whose maximum coincides with helium minimum (Wolff and Morrison, 1974)

The temperature and gravity of α Cen are generally assumed to be those of an early B star ($T_{\rm eff} \simeq 2.0 \times 10^4$ K, $\log g \simeq 4$). Mihalas (1973b) proposed an oblique rotator model to account for the variability, while Molnar (1974) suggested a distorted stellar disk in the shape of a prolate spheroid. Although slightly cooler than α Cen, HR 7129 (= HD 175362) apparently shares many of the properties of the prototype helium variable (Balona, 1975, Wolff and Wolff, 1976).

Helium-Weak Stars

In contrast to the early type peculiar B stars, those of later type are characterized by abnormal weakness of the lines of neutral helium. The hottest group of such stars, called the helium-weak stars, is defined by the fact that although the helium lines are too weak for the broadband colors, no enhanced or peculiar metallic lines are observed at classification dispersion. Attention was first drawn to these stars by Sargent and Strittmatter (1966), Garrison (1967), and Bernacca (1968) Their properties were codified by Molnar (1972) and Jaschek and Jaschek (1974b). If classified from their helium spectra alone, these stars would be given spectral types around B8 III, but their broadband colors are more representative of early main-sequence stars (around B3 V) The profiles of the hydrogen lines tend to support the earlier spectral types, while the true effective temperatures are between $1\,4 \times 10^4$ and 2.0×10^4 K. The weak helium lines therefore represent apparent helium deficiencies by factors of 2 to 15. In the ultraviolet, about half of the helium-weak stars have normal fluxes when compared with standard stars of the same UBV colors, while others appear to be flux-deficient in the ultraviolet for their color types (Bernacca and Molnar, 1972; Ciatti et al., 1978).

The helium-weak stars occur both in the field and in open clusters and associations, in general, they are slow rotators None of the stars in this group has been observed to have a significant magnetic field. Both spectrum and photometric variability are common among the helium-weak stars (Winzer, 1974; Pedersen, 1976; Pedersen and Thomsen, 1977; Pedersen, 1979) Typical periods are of the order of a day However, α Scl has a period of about 20 days superimposed on a longer period variation. Vilhu (1978) attributes the long-term variation in the radial velocities to spectroscopic binary motion No ultrashort period (6 to 500 s) oscillations have been detected (Haefner et al., 1978)

Although the helium-weak stars do not ex-

hibit abnormal metallic lines at classification dispersion, certain enhancements are visible on higher dispersion spectrograms. Baschek (1975) distinguished three subgroups of helium-weak stars: (1) the Si subgroup (or "blue helium-weak stars") in which Si II lines are stronger than normal, for example, 3 Sco (Norris and Strittmatter, 1975) and HD 144334, (2) the P-Ga subgroup ("phosphorus stars"), characterized by strongly enhanced lines of phosphorus, krypton, and gallium, for example, 3 Cen A (Hack and Stalio, 1976), ι Ori B, HD 82984, and HD 144844; (3) the Ti-Sr subgroup ("α Scl stars"), whose prototype is α Scl and which have enhanced lines of metallic ions such as Ti II, Fe II, Fe III, and Sr II. In some of the helium-weak stars, a substantial fraction of the helium present is in the form of ^{3}He (Hartoog and Cowley, 1979) The ^{3}He stars are not confined to any one of the above subgroups, however. In general, the helium-weak stars tend to be strongly deficient in oxygen, while carbon is moderately deficient to normal. Magnesium and neon are normal, while silicon may be either over- or underabundant. Table 5-5 lists a number of bright, helium-weak stars. Data are taken from Molnar (1972), Eggen (1974b), Baschek (1975), and Vilhu et al. (1976). When these stars are discussed, the term *underabundance* is used as a synonym for lines which are unusually weak relative to other lines in normal B-type spectra.

Mercury-Manganese Stars

The Hg-Mn stars fall within the temperature limits 1.1×10^4 K $< T_{\rm eff} < 1.6 \times 10^4$ K, and comprise a significant fraction of all the main-sequence stars in this range (Wolff and Wolff, 1976) They are slow rotators (v sin $i < 100$ km s^{-1}) and have no observable magnetic fields

Table 5-5
Helium-Weak Stars

HD	Name	Spectral Type	V (mag)	B − V (mag)	U − B (mag)	$T_{\rm eff}$ (10^4 K)	log g	Group	Ref
5737	α Scl	B8 IIIp	4 27	−0 18	−0 57	1 530	3 4	Ti-Sr	1,2
21699	HR 1063	B9 III	5 46	−0 10	−0 57	1 660	3 9	–	3
23408	20 Tau	B7 III	3 86	−0 07	−0 40	1 400	3 4	Ti-Sr	2,3
37043B	ι Ori B	Bp	7 3	–	–	–	–	P,Ga,^{3}He	
37058	–	B3 Vp	7 3	–	–	2 100	4 4	Ti-Sr	
49606	33 Gem	B8 III	5 69	−0 14	−0 53	1 480	4 2	Ti-Sr	3
79158	36 Lyn	B0 5 II	5 19	−0 14	−0 48	1 400	3 8	Ti-Sr	
82984	HR 8317	B4 Vn	5 10	−0 13	–	–	–	P-Ga	
120709	3 Cen A	B5 IIIp	4 72	−0 14	−0 59	1 815	3 7	P,Ga,^{3}He	1
142301	3 Sco	B7-8 IVp	5 89	−0 06	−0 60	–	–	Si	
144334	HR 5988	B8-9 IIIp	5 90	−0 08	−0 56	–	–	Si	1
144844	HR 6003	B9 IVp	5 89	+0 01	−0 32	–	–	P-Ga	
183339	HR 7401	B8	6 62	−0 14	−0 54	1 530	4 2	Ti-Sr	1,2
217833	HR 8770	B9 III	6 38	−0 08	−0 56	1 630	4 2	Ti-Sr	3

Dashes (–) represent no existing data at these values

References

1 Eggen (1974b)
2 Vilhu et al (1976)
3 Molnar (1972)

Although the percentage of spectroscopic binaries is high among Hg-Mn stars, no conspicuous light or spectrum variations are found.

The brighter stars in the Hg-Mn class include κ Cnc, 112 Her A, ϕ Her, ι Cr B, π^1 Boo, 53 Tau, 46 Dra (A + B), μ Lep, and χ Lup The spectra of these stars are characterized by abnormally strong lines of Mn II (especially λ 3474) and Hg II (λ 3984). A study of the isotopic structure of the latter line permits the deduction of an overabundance of mercury by a factor of up to 4×10^5 over the solar value (Cowley and Aikman, 1975). Other elements which tend to be overabundant include P, Ga, Sr, Y, and Zr (Adelman and Pyper, 1979), but the anomalous yttrium abundance pattern once believed to be present has not been confirmed by more recent work (Allen, 1977).

Ultraviolet photometry shows that the Hg-Mn stars are flux-deficient in the extreme ultraviolet, for their UBV colors, but less so than the Ap stars (Leckrone, 1973). High dispersion ultraviolet spectra confirm the mercury and gallium anomalies derived from ground-based observations (Leckrone, 1980), while making the resonance lines of Mn II available for observation (Faraggiana and van der Hucht, 1975). Since even a moderate degree of rotation can mask the Mn II lines in the visible region, it may prove more reliable to search for new Hg-Mn stars in the ultraviolet. Lines of Hg III are absent in the ultraviolet spectra, but Au III appears to be present in κ Cnc, implying an abundance of gold about 10^6 times the solar value (Leckrone and Heacox, 1978).

Magnetic B Stars

The true Bp stars, or silicon stars, are found around spectral types B8 and B9 and are clearly the extension to higher temperatures of the Sr-Eu-Cr stars, the main body of Ap stars. Like the latter, the Bp stars have strong, sometimes variable magnetic fields, and frequently are spectrum and/or photometric variables. Their silicon abundances range from nearly normal to a hundred times overabundant. Like the Hg-Mn stars, their extreme ultraviolet fluxes are fainter than those of normal stars of similar UBV colors. Well-studied silicon stars include 56 Ari, CU Vir, HD 215441, HD 34452, and α^2 CVn. These stars are briefly reviewed by Preston (1974) and Baschek (1975). But because of their similarity to the Ap stars, we shall not discuss them in detail here, but rather refer the reader to Wolff (*A Stars*, to be published)

Discussion

Despite their differences, the peculiar B stars described in this chapter have many similarities, and because they occupy more or less discrete but contiguous regions in the HR diagram, it is tempting to consider them as one or more sequences of related stars, produced by a common physical mechanism. Wolff and Wolff (1976) propose a distinction based on the presence or absence of magnetic fields. Thus, the Ap stars, Bp (silicon) stars, and helium-strong stars would form one sequence, while the Am stars, Hg-Mn stars, and helium-weak stars would be members of a second This grouping, however, does not explain the presence of the helium variables, which seem to imply a connection between the helium-strong and helium-weak stars The hot subdwarfs and extreme helium stars may or may not be related to each other, but they probably have a different origin from the rest of the stars discussed here.

The principal theory advanced to explain the anomalous spectra of early type stars, without resorting to ad hoc assumptions or complicated evolutionary histories, is the diffusion theory (Michaud, 1970). Although it has been successful in explaining many of the gross features, this theory still runs into difficulty with some of the detailed abundance patterns (cf., Leckrone, 1980) For a full discussion, the reader is again referred to Wolff (*A Stars*, to be published)

6

MODEL ATMOSPHERES, PREDICTED SPECTRA, AND COLORS

PHILOSOPHY OF MODEL MAKING

Theoretical models of stellar atmospheres and of the process of forming a spectrum are important tools for interpreting stellar spectra. In this chapter we shall review those parts of the theory of stellar spectra that are needed for interpreting the spectra of B stars

Definition of a Model

Predicted or synthetic spectra are found by numerical procedures from model atmospheres in order to provide a well-understood norm to which observed stellar spectra may be compared. If the observed spectrum is the same as the predicted spectrum in significant characteristics, the model is said to be representative of the star and it is concluded that the parameters and physical processes used to construct the model are similar to what actually occurs in the stellar atmosphere Models always provide a simplified representation of the physical processes occurring in a real stellar atmosphere They can rarely be proved to give a unique representation of the stellar atmosphere. It is hoped that by a judicious selection of the spectroscopic detail by means of which a model is identified with a real star, the chief characteristics of the star will be described accurately

Much of the modeling that has been done for B-type stars since the mid 1940's has been based on interpreting the part of the spectrum between 3000 and 7000 Å and finding sensitive criteria in this spectral range for demonstrating the validity of models Model spectra have been calculated also covering the ultraviolet and infrared parts of the spectrum; some of these have enabled the presence of new parts of the stars such as a hot corona and/or an expanding mantle to be inferred.

A model consists of a set of particle densities, degrees of ionization and excitation of the various constituents present, and electron temperatures as a function of the geometric depth in the model atmosphere It is assumed that the atmosphere is a perfect gas through which a flux of radiation is flowing The radiation is allowed to interact with the gas according to the physical laws valid in the laboratory and to theoretically established principles for an ionized gas in contact with radiation.

In the case of classical models of B stars, the gas is considered to have temperatures in the range 8.0×10^3 to 1.0×10^5 K, and the radiation field treated extends from wavelengths of a few hundred angstroms to, perhaps, 10^5 angstroms It is assumed that radiative equilibrium exists. Thus, an amount of energy, prescribed by the effective temperature of the model or by the requirement that the electron temperature have a selected value at the depths in the photosphere where the continuous spectrum at say, 5000 Å, is formed, is injected into the model atmosphere at its deepest layer and this energy is followed as it works its way out through the model No radiative energy is lost or gained in the model atmosphere, but the detailed shape of the spectrum is changed as a result of the interactions with the ionized gas. The predicted spectrum which will

be compared with observed spectra in order to find what type of star the model represents is that spectrum which is present in the model at a geometric level where the optical depth in continuum frequencies is essentially zero. Models which have been defined by means of constraints on the continuous spectrum are not always defined in sufficient detail at high layers that the centers of very strong lines may be calculated accurately. In the deepest layers of the model, the radiation field is assumed to have the shape of a blackbody spectrum.

In normal model atmospheres for B-type stars, there is no change of state in the material at any layer in the gas. If it is desired to model the formation of dust in the outermost layers of the model, then an appropriate change in the energy content of the radiation field and of the gas would have to be introduced in order to take account of the energy tied up as heat of condensation. No detailed model atmospheres have been made for B stars taking into account outflow, although the problem of radiative transfer has been studied for the case when there is outflow.

The Constraints Defining the Run of Physical Variables in a Model

In classical model atmospheres, the variation of gas pressure (density) with geometric height in a model is defined by means of the equation of hydrostatic equilibrium. Use of this equation, which comes from consideration of the conservation of momentum, implies that there are no flow velocities in the gas which exceed about 0.3 times the local thermal velocity. Since observations of B stars of many sorts (see Chapters 3, 4, and 5) suggest that the gas in the outer layers of the atmosphere often moves with velocities in excess of 5 km s^{-1}, strictly speaking classical model atmospheres are not valid for representing the layers of B stars in which the prominent spectral lines are formed. However, comprehensive classical model atmospheres exist and they are the only models presently available in sufficient numbers to act as useful tools for interpreting B-type spectra, so they are used even though the condition of hydrostatic equilibrium is met exactly in few real stellar atmospheres.

The condition that radiative equilibrium occurs is used to define the variation of temperature with depth in the model. In the case of planar model atmospheres, this condition may be expressed in terms of the gradient with height of the integrated net flux being zero,

$$\int_0^\infty \frac{dF_\nu}{dz}\, d\nu = 0, \qquad (6\text{-}1)$$

or by requiring that the net monochromatic flux F_ν (the outward directed flux minus the inward directed flux) integrated over all frequencies be constant and equal to a value given by the relation

$$\sigma_R T_{eff}^{\ 4} = \pi \int_0^\infty [F_\nu\,(\text{outward}) - F_\nu\,(\text{inward})]\, d\nu, \qquad (6\text{-}2)$$

where T_{eff} is the desired effective temperature for the model. In the above equations σ_R is the Stefan-Boltzmann constant, and z is the distance along the line of sight measured outward from the center of the star

Methods for constructing model atmospheres for O and B stars are given in many review articles and textbooks on the theory of stellar atmospheres (see, for instance, Gingerich, 1969; Mihalas, 1970b, and Gray, 1976) The question of how accurately Equations (6-1) or (6-2) must be enforced in order to be sure that radiative equilibrium truly occurs in the model atmosphere has been thoroughly studied (see, for example, Avrett, 1964, and other contributions reported there). A unique variation of temperature with depth in the atmosphere is found only when the condition of radiative equilibrium is strictly enforced. It is unfortunately true that when one considers a relatively short wavelength range in the visible, of length, say, 1000 to 1500 Å, and one considers the photometric uncertainty of most observations, that the same spectrum in relative flux units can be matched with models that differ considerably as to composition, type

of opacity that occurs in various wavelength intervals, and actual temperature-density structure. Usually observations present only relative flux distributions with wavelength, thus, the discrimination between models of somewhat different characteristics is not always easy or even possible.

When absolute fluxes are available from observation, and the distance and radius of the star are known, a better discrimination can be made. In Chapters 3 and 4 the determination of flux effective temperatures was discussed for main-sequence stars and supergiants. Here it was shown how the absolute values of the angular diameters measured by Hanbury Brown et al. (1974) could be used to demonstrate that the LTE classical model atmospheres of Kurucz (1979) give a reliable representation of the layers forming the continuous spectrum of B stars.

At each level in the model atmosphere one needs to know the relative population of each stage of ionization of each element and the populations of the different energy levels from which lines and continua of interest are absorbed. Philosophically, the most satisfying method of finding these populations and the density of electrons is to set up the equations of statistical equilibrium for the populations of all states of each element; when doing so, one must take account of the relative probabilities for transition between the different states by spontaneous emission, as a result of the absorption of radiation and as a result of collisions with electrons and other particles. One constrains the total particle density to be in accord with that required by the equation of hydrostatic equilibrium in the case that matter is conserved (no mass loss). This is the method followed when non-LTE model atmospheres are constructed. It requires use of a fast and large computer. The first step is usually to assume that at each level in the model, the atoms and ions are distributed over their possible energy states as though they were in thermodynamic equilibrium (TE) at the local temperature. This is called local thermodynamic equilibrium. Since the laws of Saha and of Boltzmann are then valid, it is a relatively simple matter to calculate the distribution of all atoms and ions over their various possible energy states.

The simplifications in the physical representation of what occurs in a stellar atmosphere which are made in order to obtain a set of equations that are tractable are discussed by Thomas (*The Stellar Atmosphere*, to be published). In the case of the predictions of the continuous spectrum of B stars and the shapes and strengths of many weak absorption lines in the optical spectral range, the simplifying assumption of LTE leads to results indistinguishable from those obtained by the more correct assumption of statistical equilibrium. Consequently, most model atmosphere analysis of B-type spectra is performed by means of LTE model atmospheres, for in practice LTE models are the only type of model that can be easily constructed.

Composition of Model Atmospheres and Geometries Used

The composition of model atmospheres is usually taken to be about 10 to 1 in number of hydrogen and helium with a small admixture of the other elements in which one is interested. A few helium-rich model atmospheres have been made. The geometry is usually taken to be plane parallel layers, the density gradients are established by specifying a value of log g. Classical, static model atmospheres require two parameters for their specification, log g and $T_{\rm eff}$, in addition to their composition and geometry. A few model atmospheres have been constructed in which spherical geometry is used and a few attempts have been made to predict the spectrum from flowing plane parallel layer and spherical model atmospheres. These more complex modelings of the formation of the spectra of O and B stars are described in the section on Extended and Moving Atmospheres.

Interactions Between Radiation and Matter

Specifying log g and $T_{\rm eff}$ for model atmospheres defines the particle and radiation densities in the models. Specifying the composition of the gas comprising the model and use of known

expressions for photon emission and absorption, photon scattering and of the collision cross sections of the atoms/ions with electrons determines the distribution of the particle ensemble over its possible set of energy states and the detailed shape of the spectrum. The appropriate physics and theory of radiative transfer is described in all textbooks on the theory of stellar atmospheres (see, for instance, Unsöld, 1955; Jefferies, 1968, Mihalas, 1970b; Athay, 1972; Gray, 1976; Mihalas, 1978).

Three types of interaction occur between an atom/ion and radiation: namely bound-bound transitions in which the atom/ion goes from one bound energy state to another bound state of a different energy with the absorption or release of a photon; bound-free transitions in which the atom/ion goes from a bound energy state to one in which it has lost an electron, the electron being able to move off with a wide range of energies and a photon being absorbed, or vice versa; and free-free transitions in which photons are exchanged during the time an electron is close to an ion. The bound-bound transitions result in the absorption or emission of spectral lines, the bound-free and free-free transitions result in the absorption and emission of continua.

The spectral lines are not precisely monochromatic, as they should be if the energy states of atoms and ions were sharply defined, but they are broadened, the probability of absorption (emission) being greatest at the center of the line and decreasing but remaining finite over a range of energies (frequencies) greater and lesser than the nominal energy corresponding to the transition. One has line broadening due to natural damping, to Stark effect and collisional broadening, to Zeeman effect, and as a result of the spread in thermal velocities of the atoms/ions at each point in the stellar atmosphere (Doppler broadening). One may have additional broadening if the star rotates or if its atmosphere is turbulent, and if a screen of rapidly moving electrons exists around the star, as is thought to happen for some hot stars with extended atmospheres. All these causes of line broadening and how they are represented by expressions for the shape of the line-absorption coefficient are described in most textbooks on the theory of stellar spectra. We take the point of view here that these phenomena are known and can be described in terms of local electron temperature, local particle densities, and the intrinsic radiative and collision cross sections for atoms and ions known experimentally or theoretically from the physics of radiation and gases at moderate to low densities.

CLASSICAL MODEL ATMOSPHERES

Classical model atmospheres are models composed of plane parallel layers of gas in which the temperature and density structures are such that radiative and hydrostatic equilibrium occur.

Models of H and He

The idea of making model atmospheres consisting of plane parallel layers of gas in hydrostatic and radiative equilibrium to represent the atmospheres of hot stars and of predicting theoretical spectra for use in interpreting observed spectra has roots which go back to the time when the first quantitative studies of stellar spectra were begun. In his comprehensive review article, Pecker (1965) summarizes the history of the subject from its first beginnings with the work by Pannekoek (1935) in Amsterdam and by Mustel (1940, 1941, 1944) in Moscow. Pecker also gives a detailed presentation of the equations which are needed to find the temperature and pressure at each level in the model atmosphere and to calculate the spectrum. Practical methods (based on the procedures developed by Strömgren, 1940, 1944, for modeling the atmospheres of F- and G-type stars) of making model atmospheres for hot stars were developed by Pecker (1950) and independently by Underhill (1950, 1951) for the case that the model atmosphere is composed of hydrogen and helium. Related methods were developed by Rudkjøbing (1947).

Later, solutions of the model atmosphere problem for hot stars, still following rather closely the techniques initiated by Strömgren, were devised for large computers (see, for instance, Underhill, 1962, Mihalas, 1965, 1966; and Strom and Avrett, 1965). Particular atten-

tion was paid in the work of Mihalas, and that of Strom and Avrett, to programming the computer so that *that* temperature law could be found which ensured that radiative equilibrium was enforced in such a way that the integrated flux from the model corresponded precisely to a preassigned value for the effective temperature. A trial and error method for satisfying the constraint of radiative equilibrium was developed by Underhill. In her model atmosphere procedures, the aim is to find that model atmosphere in radiative and hydrostatic equilibrium in which the electron temperature has a specified value in a layer of the model near the level where the continuum optical depth is 0.1. The specified value is estimated from the excitation temperatures of B and O stars found by means of curve-of-growth analyses of the equivalent widths of lines in the visible part of the spectrum. Such temperature estimates were available when she began her work, but little was known then about the effective temperatures of O and B stars. Both approaches to finding representative model atmospheres for O and B stars are valid In the first, the starting point is knowledge of T_{eff}; in the second, the starting point is knowledge of T_{ex} in the layers most important for forming the lines of the visible spectrum.

The mathematics of the model atmosphere problem is described by Pecker (1965), in chapter 6 of Mihalas (1970b), and in chapter 7 of Mihalas (1978). Sets of model atmospheres making use of continuous sources of opacity only are given by Mihalas (1965, 1966), by Strom and Avrett (1965), and by Underhill (1968, 1972). The modeling procedures based on the work of Strömgren require significant computing power for their execution.

Great economy of effort becomes possible when a different numerical analysis technique, that developed by Feautrier (1967, 1968), is employed. In Feautrier's method, the equations for hydrostatic and radiative equilibrium are linearized and solved simultaneously. Methods based on Strömgren's procedures (which were designed for hand calculation) solve the equations iteratively, first solving the equation for hydrostatic equilibrium with an approximate temperature law and then solving the equations for radiative equilibrium to find improvements to the temperature law. The powerful techniques introduced by Feautrier have been applied in most model atmosphere work on hot stars done since 1970.

LTE Models with Line Blanketing

The availability of large computers makes it feasible to incorporate line opacity into the algorithms for computing the opacity in model atmospheres. Inclusion of line blanketing, particularly at wavelengths where the flux from unblanketed model atmospheres is large, has a significant effect on the temperature-pressure structure of a model atmosphere; the temperature in the outermost layers usually goes to lower values for a given value of pressure and the general level of the continuous spectrum changes in the visible spectral range from what it was for models which did not include the opacity due to lines. Some early experiments to determine what is the effect of line blanketing have been described by Underhill (1966b), who summarizes what happens when the opacity due to lines is taken into account in an approximate manner.

Line blanketing due to the hydrogen lines has been systematically taken into account by Klinglesmith (1971) who has provided a useful grid of hydrogen line-blanketed model atmospheres. Detailed procedures for deriving and using distribution functions to take account of the blanketing due to many lines in a statistical manner have been described by Kurucz et al. (1974) and by Kurucz (1979); a comprehensive set of classical model atmospheres which include the effects of line blanketing is given in Kurucz (1979). The state of LTE is assumed to exist throughout these model atmospheres. Here the emergent flux is also presented in great detail for the range 229 to 2.0×10^5 Å. The relative balance of the two effects of line blanketing, namely backwarming and depression of the temperature in the outermost layers of an LTE model atmosphere, has been critically discussed by Phillips (1977).

In making model atmospheres, a pragmatic approach must be taken between balancing the

reality of the representation of the details of line formation and the shape of the line and continuum absorption coefficients against the amount of costly computer time required to construct a grid of models. For the purpose of representing the shape and intensity of the continuous spectrum of O and B stars longward of 1400 Å, the model atmosphere emergent fluxes of Kurucz (1979) are quite acceptable, as the work of Underhill et al. (1979) has shown (see also, Chapter 3).

Models Using the Concept of Statistical Equilibrium

In the outermost layers of model atmospheres, the approximation that the distribution of the atoms and ions over their various possible energy states can be described using the Saha and Boltzmann laws at the local temperature and density cannot be logically sustained. The fact that radiation escapes from the outer layers makes the hypothesis of LTE untenable. To find the actual populations of the possible energy states, one must solve simultaneously in a self-consistent manner the sets of equations which describe statistical equilibrium, radiative equilibrium, and hydrostatic equilibrium. The development of successful and economical numerical techniques to solve this problem is described in chapter 7 of Mihalas (1978). Many of the ingenious numerical procedures used by Mihalas were derived by L. H. Auer.

A set of model atmospheres for O and B stars, their emergent energy distributions and hydrogen line spectrum (Hα, Hβ, Hγ), have been published by Mihalas (1972a). The computer program that was used is described by Mihalas et al. (1975). In this program the powerful numerical techniques of Feautrier are used. The composition of the non-LTE model atmospheres consists of hydrogen and helium in a ratio by number of 10 to 1 with a small admixture of a "representative, fictitious light element" which has abundance and ionization stages so adjusted as to represent approximately the effect of the continuous absorption due to the ions of C, N, and O.

The effect of taking account of the non-LTE populations of H and He is to introduce a small rise in temperature in the outermost layers of the models over what would be the case were LTE strictly valid in all layers of the model. It is important to take into account the line transitions between the lowest levels of H, He I, and He II as well as the departures of the ionization fractions from the values they would have if LTE were valid. The temperatures in the outer layers of a non-LTE model are about 15 to 20 percent greater than they are for a comparable LTE model. At depths such that the opacity in the visible continuum is of the order of unity, the two temperature distributions become essentially identical.

PREDICTED SPECTRA VS. OBSERVED SPECTRA: PLANE-PARALLEL LAYERS

In this section we shall review how the spectra predicted from planar model atmospheres compare with the observed spectra of B stars.

Main-Sequence Stars: LTE Assumed

Most model atmosphere studies of B-type spectra have been executed making use of the assumption that a state of local thermodynamic equilibrium exists. We shall review here the results of these studies. The first step in analyzing a stellar spectrum is to select an appropriate model atmosphere to represent the atmosphere of the star under study.

Criteria for Selecting a Model. The energy distribution in the continuous spectrum is the major spectroscopic output from the calculations made to construct B-type model atmospheres. Usually insufficient detail is computed to define any of the line profiles in detail. Therefore, it is desirable to begin the process of identifying a star with a particular model by means of a fit to the continuous spectrum. This process is an iterative procedure one starts with a preliminary estimate of a likely composition, effective temperature, and a log g for the model and then proceeds to calculate the spectrum. In later stages additional models may be developed with changed values

of the input parameters. Usually a grid of models is used, all having the same composition but different values of T_{eff} and log g. One interpolates between the spectra from the separate models to find a representative value of T_{eff} and of log g.

Since the continuous spectrum in the wavelength range which is observed from the surface of the Earth is usually formed at moderate depths in the model where the particle density is 10^{13} or greater, the approximation of LTE is tenable. Mihalas (1972b) has shown that the shape of the continuous spectrum predicted by LTE and by non-LTE models representing stars of type B0 and later is the same in all essentials. Consequently, LTE models are adequate for representing the continuous spectrum of B stars.

Because most B stars are reddened by interstellar extinction, the available relative-absolute spectrophotometry of these stars does not give the true energy distribution in the continuous spectrum. A correction for interstellar extinction must be applied before the observed shape of the continuous spectrum is compared to the shape of predicted energy distributions. However, often the amount of the interstellar extinction is poorly known. Therefore one of the best ways to identify a model atmosphere with a B star is to compare observed and predicted values of the Balmer jump. The BCD spectrophotometry (see Chapter 2) has provided measured values of D, the size of the Balmer jump for many B stars. Calculated values of D as a function of T_{eff} and log g have been found by Underhill et al. (1979) for the sets of LTE models published by Kurucz et al. (1974) and Kurucz (1979), using a method entirely parallel to the method used to find an observed $D = \log (F_R/F_V)$, where F_R is the true continuum flux on the longward side of the Balmer jump and F_V is the continuum flux shortward of the Balmer jump. The theoretical diagram is shown in Figure 6-1. For stars having log g in the range 3.5 to 4.5, that is all main-sequence and giant B stars, D does not depend strongly on log g. Thus, in order to find a preliminary value of T_{eff} for a B star, all one has to do is to adopt a value for log g and measure D. From Figure 6-1 one may read the appropriate T_{eff}. For stars for which no measurement of D exists, one may make

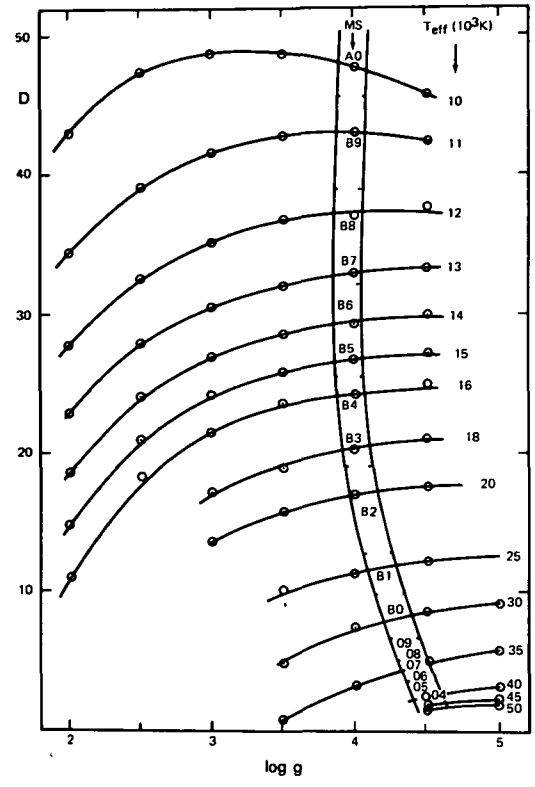

Figure 6-1. The theoretical relationship between D, as measured by Chalonge and Divan, and log g and T_{eff} for the model atmospheres of Kurucz et al. (1974) and of Kurucz (1979). The position of the empirical main-sequence band is shown in this diagram (from Underhill et al., 1979).

use of the measured colors to estimate T_{eff} for a model (see the next section).

Often one wishes to select a model atmosphere in order to analyze the strengths of the absorption lines in the blue-violet spectral region. The purpose is to find T_{eff}, log g, and the relative abundances of the elements for the star. High resolution spectra are available, but often little or no photometric information exists about the relative shape of the unreddened continuous spectrum in the spectral region accessible from the Earth. The method to be described permits one to select a representative model atmosphere using a fit between the theoretical absorption-line spectrum from the model atmosphere and the observed absorption-line spectrum. This method

may, however, lead to misleading results for T_{eff} if, in the atmospheric layers where the key lines to be analyzed are formed, the basic constraints upon which classical model atmospheres are built, namely radiative equilibrium, hydrostatic equilibrium, and local thermodynamic equilibrium, are not valid. The method is performed iteratively to converge on precise values of T_{eff} and $\log g$.

It has long been known that the Stark broadening of Hγ and Hδ is a good index to the electron pressure in the photosphere of a B star (cf. Chapter 2), hence of $\log g$. This value of $\log g$ is not necessarily precisely equal to GM_*/R_*^2. Matching the shape of the observed wings of Hγ or Hδ to the computed wings of a theoretical profile for Hγ or Hδ is a good way of determining the value of $\log g$ to be used in constructing a model atmosphere. For best results one should have a moderately close estimate of the appropriate effective temperature before fitting the observed and predicted line profiles. A first estimate of T_{eff} can be obtained from a measured value of the size of the Balmer jump, or from the intrinsic B − V or b − y color of the star, or from an approximate spectral type–effective temperature relation. The relative abundance of hydrogen is not a significant factor unless the fractional abundance by number of hydrogen is less than 10 percent (see the subsection on Profiles and Abundances).

In order to sharpen the estimate of effective temperature, the relative strengths of lines from elements which appear in two or more stages of ionization are studied. These relative strengths are insensitive to the choice of $\log g$. Trial values of model effective temperature are varied until the observed strengths of several absorption lines formed in two stages of ionization of a single element are reproduced satisfactorily for a fixed value of the relative abundance of the element. One uses only spectral lines for which the equivalent width can be measured reliably and for which the oscillator strength and damping constant are known accurately.

There are two underlying hypotheses. (1) that the relative strengths of lines in two stages of ionization of the same element are insensitive to the adopted abundance of the element, and (2) that the distribution of the element among its available stages of ionization and energy levels in each stage of ionization may be calculated sufficiently accurately by using the Saha and Boltzmann laws. The end result is that in the model atmosphere which is accepted as representative, the electron temperatures in the line forming layers give level populations which reproduce the observed equivalent widths. These electron temperatures are specified in terms of the parameter T_{eff} by invoking the constraint of radiative equilibrium when constructing the model atmospheres.

Experience shows that (1) ratios of line strengths in three different stages of ionization for the same element or for two stages of ionization for several different elements do not closely lead the same effective temperature and (2) the effective temperatures deduced in this manner from relative line strengths are higher than the values that may be deduced from the size of the Balmer jump or from the shape (color) of the visible spectrum (see, for instance, the analyses of two B0 main-sequence stars by Hardorp and Scholz, 1979; and of six O-type stars by Peterson and Scholz, 1971; or the analyses of supergiant spectra by Dufton, 1979). In stars where lines in the visible spectrum from three stages of ionization of an element are present, for instance Si II, Si III, and Si IV, predictions using classical, LTE model atmospheres rarely reproduce the observed relative strengths of all the lines (Underhill, 1963) even when microturbulence is taken into account. This subject has been carefully investigated by Kamp (1978) using non-LTE methods of analysis, and he finds that use of non-LTE physics does not entirely remove this problem.

Observed and Computed Intrinsic Colors. The empirical intrinsic broadband colors of the UBV photometric system and the intermediate-band intrinsic colors of the Strömgren uvby photometric system for B stars have been presented as functions of spectral type in Chapter 2. If one has knowledge of the correction necessary to remove the effects of interstellar reddening from observed colors, one can, in principle, use the intrinsic colors of a star to select a model atmo-

sphere. Several sets of computed intrinsic colors of model atmospheres exist in the literature (see, for instance, Morton and Adams, 1968; Mihalas, 1972b; Relyea and Kurucz, 1978; Buser and Kurucz, 1978). We shall discuss here only the comprehensive results of Kurucz and his coworkers as these results take the place of previous results based on fewer and less internally consistent sets of model atmospheres for B stars.

The empirical intrinsic colors for B stars may be affected by the rotation of the star because the shape and surface temperature distribution of a rapidly rotating star are believed to be different from those of a nonrotating star The theoretical spectra from normal model atmospheres should represent accurately the spectral distributions from nonrotating or slowly rotating stars. We shall first discuss how the empirical intrinsic colors of nonrotating stars may be used to select the parameters for a representative model atmosphere. Following that we shall review the changes which rapid rotation may bring to our theoretical relationships between intrinsic color and effective temperature or spectral type. The empirical relations between intrinsic color and spectral type have been established from observations of a group of stars having a mixture of speeds of rotation.

Nonrotating Stars and Models. To compute theoretical colors, all one requires are the shapes and relative transmissions of the response functions for the filters and detectors used and theoretical energy distributions from model atmospheres. The response functions of the Strömgren filters are well known, and it has been evident from the first attempts to calculate the theoretical equivalents of the color indices used in the uvby photometric system that the observed trends with spectral type of the uvby photometry could be reproduced satisfactorily. Comprehensive theoretical diagrams of the various color indices defined by Strömgren as functions of $(b-y)_0$ and $(u-b)_0$ have been prepared by Relyea and Kurucz (1978). One may enter these diagrams with observed values of the intrinsic color indices and read off the appropriate values of $\log g$ and $T_{\rm eff}$ by which to select a representative model atmosphere from among the many models presented by Kurucz (1979).

The response functions in the UBV photometric system are broad, and it has become clear from many studies that in practice the results observed in the U filter may be affected by the transmission of the Earth's atmosphere as well as by the spectral type of the star The question of what are the most accurate representations for the response functions of the U, B, and V filters has been studied once again by Buser (1978), and Buser and Kurucz (1978) have presented the results of the calculation of the equivalent B − V and U − B colors of the Kurucz (1979) model atmospheres. Excellent agreement with Johnson's (1966) mean intrinsic U − B and B − V colors for main-sequence stars is obtained. In addition Buser and Kurucz have derived a practical relation between the bolometric correction, as defined observationally, and the effective temperatures of the Kurucz model atmospheres.

For main-sequence stars one may use the intrinsic broadband color $(B-V)_0$ and the results of Buser and Kurucz to find a first estimate of the effective temperature of a representative model atmosphere. It is preferable to use the theoretical colors of the Kurucz model atmospheres given by Buser and Kurucz rather than to use the arbitrary zero-point correction for the calculated intrinsic B − V colors of the Kurucz et al. (1974) model atmospheres adopted by Peytremann and Davis (1974).

The zero-point corrections to the published theoretical intrinsic B − V colors of the Kurucz et al. model atmospheres derived by Underhill et al. (1979) lead to the same result as Buser and Kurucz (1978) find. The intrinsic B − V colors of the LTE model atmospheres by Kurucz et al. (1974) and by Kurucz (1979) are essentially the same.

Rotating Models. Prediction of the intrinsic colors and line shapes for rotating stars is a problem that has been studied by several groups. A comprehensive set of internally consistent results has been published by Collins and Sonneborn (1977) who have summarized in their paper the developments in the theoretical approach that

have taken place as it became possible to model the emergent spectrum from rotating stars in more and more realistic detail.

The procedure that Collins and Sonneborn follow is to assign typical values of mass, luminosity, radius, and effective temperature to stars on the main sequence at spectral types from B0 to F8 and then to calculate the spectrum and note the changes that occur as the shape of the star is distorted owing to rapid rotation. The amount of radiation and its spectral distribution crossing each unit of area is changed as a function of the latitude on the stellar surface and of the speed of rotation of the model star. Finally, various photometric indices are calculated as the star is viewed at several angles of inclination of the rotation axis to the line of sight between 0° and 90°, and the speed of rotation takes several values. A different model atmosphere is used at different places on the stellar surface, the choice of model atmosphere being linked to the predictions of surface temperatures from the theory of the stellar interior for the case of stars which rotate rigidly or nearly so.

The results of Collins and Sonneborn are useful for demonstrating how large the differential effects may be which result from differing speeds of rotation and differing angles of inclination of the axis of rotation to the line of sight. If conclusions are to be drawn concerning the effects of stellar rotation from comparing the absolute values of the Strömgren photometric indices that have been calculated by Collins and Sonneborn with the empirical knowledge about these indices as functions of spectral type, then first one should show that the results of Collins and Sonneborn for nonrotating stars reproduce what is known for nonrotating stars.

The empirical relations which exist between the Strömgren photometric indices have been developed from observation of a group of stars having a variety of speeds of rotation and angles of view. The values of the two parameters, i and v, which occur cannot be separately identified. Thus, it is, perhaps, fruitless to emphasize trying to derive theoretical agreement with observational relations valid for strictly nonrotating stars. The theoretical results of Collins and Sonneborn for nonrotating main-sequence model stars of a given effective temperature do not agree very closely in all aspects with those of others, for instance, Relyea and Kurucz (1978). The latter authors have shown that their theoretical indices do reproduce the empirically known relationships between the Strömgren indices for B-type stars in general.

The theoretical results of Collins and Sonneborn (1977) are very useful for illustrating what amount of spread in the empirical relations between the Strömgren photometric indices may be expected owing to the set of values of inclination and speed of rotation that stars in general exhibit. Typically for B-star models, as the angle of inclination varies from 0° to 90°, the index b − y varies through a range of ±0.003 mag and the change in c_1 falls in the range ±0.010 mag. At a fixed angle of inclination, increasing the rotational velocity to a greater fraction of the breakup rotational velocity (greater value of the parameter w) will make both b − y and c_1 become more positive. Typical increases are less than +0.03 and less than +0.25 mag for b − y and for c_1, respectively, as w increases from 0.2 to 0.9. The change in c_1, as calculated by Collins and Sonneborn, is large in some of the cases which they calculate. However, the algorithm used to calculate c_1 seems to be sensitive to the way in which the detailed model fluxes are calculated, for although in the case of b − y the results of Collins and Sonneborn agree fairly well with those of Relyea and Kurucz for the same T_{eff}, the agreement in the case of c_1 is poor.

The general result of these numerical experiments is that rapid rotation tends to make a model star slightly redder than what it would have been if it rotated slowly. Using model calculations which are based on model atmospheres for nonrotating stars for interpreting observed photometric indices connected with the shape of the continuous spectrum will not cause serious error, no matter what the speed of rotation or angle of inclination of the axis of rotation of the real stars. Caution is advisable in interpreting c_1, however.

Equivalent Widths and Abundances. With classical

model atmospheres it is straightforward to compute the equivalent width of an absorption line, for once a model atmosphere has been selected, it is just a question of calculating a line profile, given by the ratio F_λ/F_{cont}, and finding the area in angstrom units of the flux which has been absorbed. A suitable algorithm must be defined by means of which the practical extent of the wings of the line are determined, and one must have a suitable expression for the line-absorption coefficient in terms of the number of atoms/ions in the level from which the line is formed, the *gf* value for the line, and the damping constant.

The usual procedure for determining abundances, once a representative model atmosphere has been selected, is to measure the equivalent widths, of as many as possible, lines of different atoms and ions for which one has *gf* values and damping constants and then find that abundance which results in a computed equivalent width which is the same as the observed value. This is done for all the available lines of each element, and an abundance for the star is determined by taking a weighted mean of the results for the individual lines. The weights are arbitrary, depending on the accuracy of the measurements as well as on the reliability of the *gf* values and the damping constants. Some weight should also be assigned to represent the probability that the distribution of the atom or the ion over its several possible energy states has been computed accurately by the adopted algorithm for doing this, that is by LTE or non-LTE.

Most lines studied in B-type spectra fall on the flat part of the curve of growth or just around the knee toward the weak line part of the curve of growth. Consequently, the choice of the value of the parameter ξ_t, which gives the microturbulent velocity, is important. The appropriate value of ξ_t is found by trial using the condition that the abundances derived from weak lines and from strong lines of a given stage of ionization of any element should be independent of the intrinsic strength of the line.

The method for determining abundances described in this section is called "fine analysis." A survey of the results obtained for normal O and B stars to 1971 has been given by Scholz (1972). By and large, B stars have a composition similar to that of the Sun. The work reported by Scholz can be criticized on the grounds that the selection of the representative model atmosphere may be insecure because the choice of T_{eff}, and log g is usually made only from analysis of line strengths. Two recent analyses of the spectra of main-sequence B stars (Peters, 1976a, γ Peg B2 IV; and Adelman, 1977b, τ Her B5 IV) confirm that the normal B stars have solar abundances. These two studies make use of observations covering the ultraviolet and the visible spectrum and they use spectrophotometric scans as well as high resolution spectra. Thus, their choices of representative model atmospheres are secure. On the other hand Dufton has concluded that his analysis of high resolution spectra of B-type supergiants points toward some abundance anomalies (see next subsection).

Although the lines of He I have Stark broadened wings that lend themselves to the determination of abundances by the method of profile fitting, it is also informative to analyze the equivalent widths of those He I lines which are not strongly affected by departures from LTE using model atmosphere methods Such a study has been carried out by Norris (1971) who used the He I lines normally seen in stellar spectra except He I 4009, 5047, 5876, and 6678, the latter two of which are strongly sensitive to non-LTE effects. Norris selected his model atmospheres by fitting the shape of the continuous spectrum in the range 3400 to 5600 Å and the wings of Hγ. From fourteen sharp-lined B stars in the main-sequence band he finds that N(He)/N(H) = 0.09 ± 0.015.

The analysis of equivalent widths only takes no account of the information which may be present in the shapes of the line profiles regarding the validity of the representative model atmosphere. It is assumed that rotation of the star does not affect the equivalent width of the line. Actually, all analyses that have been carried out are for rather sharp-lined B-type spectra because rapid rotation so shallows and broadens the weak lines that enough lines from a variety of elements cannot be measured reliably in the

case of rapidly rotating B stars. It is assumed that the required spectroscopic data such as *gf* values, damping constants, and functional form for the line-absorption coefficient are free from gross error. Determining such data by means of laboratory and theoretical physics has been a major part of the work which has led to our present knowledge of the abundances of the elements in B stars.

Profiles and Abundances Comparing line profiles from high resolution spectrograms with computed profiles gives additional information about the validity of the representation of the process of line formation which is used and the abundances of the elements. If the observed lines are narrow, having FWHM of the order of the width of the projected slit image, it is advisable to broaden the computed line profiles by the instrumental profile of the spectrograph before comparing them with observed profiles. In addition trials of the effect of a small amount of rotational broadening may be made.

Calculating the broadening of spectral lines by rotation when allowance is made for limb darkening and for the different line-of-sight velocities of the various elements of the stellar disk resulting from rotation is straightforward. A simple formula, valid for rapid rotation, has been given by Unsöld (1955). When the speed of rotation is small, being of the order of the average velocity due to thermal motion in the atmosphere or due to thermal motion plus "microturbulent velocity" (a parameter that may not describe a real velocity field) more complex integration schemes than that of Unsöld must be used to obtain accurate rotationally broadened line profiles from model atmospheres This problem has been treated by Underhill (1968) and by Stoeckley and Mihalas (1973) for the case in which one model atmosphere is used for the full stellar disk and by Collins and Sonneborn (1977) for the case when different model atmospheres are fitted at different parts of the disk. Line profiles for rotationally broadened He I lines and for Mg II 4481 in the model atmospheres of Mihalas are tabulated by Stoeckley and Mihalas while Collins and Sonneborn present the profiles of several He I lines as well as Mg II 4481 resulting from their analysis If it is assumed that rotation of the star does not require use of different model atmospheres at different parts of the disk, as in the treatments by Unsold, Underhill, and Stoeckley and Mihalas, the equivalent width of the line is unaffected as the speed of rotation increases or the angle of inclination varies. However, Collins and Sonneborn find that changes, which may be as large as 30 percent, may occur as the inclination and the speed of rotation change. These changes may be positive or negative; they are indicated in the diagrams published by Collins and Sonneborn. For B star models, increasing the inclination and the speed of rotation usually results in a smaller equivalent width. The shape of the wings of the Balmer lines of hydrogen is not affected by rotational velocities up to 300 km s^{-1}, although rapid rotation of a star will make the cores of the Balmer lines disappear, the center of the line assuming a shallow, rounded shape.

Fitting the shapes of the wings of the Balmer lines of hydrogen, in particular Hγ and Hδ, gives a good control on the choice of $\log g$. Unless the relative abundance of hydrogen is less than 10 percent, the depth of the wings of Hγ and Hδ is insensitive to the abundance of hydrogen. This is so because in B star models at these wavelengths both the continuous absorption coefficient and the line-absorption coefficient are proportional to the number of neutral hydrogen atoms and the depth of the wings is approximately proportional to the ratio $\ell_\nu/(\kappa_\nu + \ell_\nu)$, where ℓ_ν is the monochromatic line-absorption coefficient and κ_ν is the monochromatic continuous absorption coefficient.

The lines of He I accessible in stellar spectra are sensitive to Stark effect and many of these lines have quite extensive wings which may be measured on high resolution spectra. Also "forbidden lines" (lines having a quadrupole transition probability such that *gf* increases as the electron density increases) appear at moderate strength in the spectra of main-sequence stars. Fitting calculated line profiles of the He I lines to the observed profiles confirms $\log g$ for a model atmosphere and determines the abundance

of helium. A comprehensive comparison of the observed He I profiles in normal B stars with He I profiles computed by LTE physics using B-type model atmospheres has been made by Leckrone (1971). He selected his model atmospheres by means of the shape of the continuous spectrum in the range 3300 to 7500 Å and by fitting the wings of the profiles of Hγ and Hδ. From six stars using 46 lines, Leckrone finds that N(He)/N(H) = 0.106 in Population I B stars, a value in accord with the results of Norris (1971).

The comparisons by Leckrone and by others of the shapes of Hγ and Hδ as well as of the He I lines reveals two things: (1) the wings of these lines in main-sequence stars can be fitted reasonably well using LTE theory and the existing sets of model atmospheres, although there are some problems with fitting accurately the forbidden components near He I 4471 and He I 4026 (cf., Snijders and Underhill, 1971; and Leckrone, 1971), and (2) the cores of the strong lines are deeper than the modeling predicts. The latter deficiency of the calculations may be corrected when the equations of statistical equilibrium are used to model the distribution of hydrogen and helium atoms over their possible energy states.

The Last Balmer Line. The sensitivity of the Balmer lines of hydrogen to Stark effect is a phenomenon that permits one to classify stars according to the typical electron density in their atmospheres. If one assumes that hydrostatic equilibrium occurs, the typical value of the electron density in the layers where the wings of the Balmer lines are formed is monotonically related to the value of log g, provided that the effective temperature is kept constant or nearly so. These practical facts are the basis for determining an appropriate value of log g for a model atmosphere by means of the shape of the wings of Hγ.

Another result of the sensitivity to Stark effect of hydrogen is that the uppermost levels of hydrogen are destroyed with the result that the Balmer series (and other series) contains a limited number of lines. Consequently, noting the upper quantum number, n_m, of the last Balmer line can give a luminosity classification of B stars. The break-off occurs at about H14 in main-sequence stars, H18 in giants and H22 in supergiants. This behavior provides the physical basis for the success of the (D, λ_1) classification system of Chalonge and Divan (1952, 1973; see Chapter 2).

The confluence of the Balmer series in some typical B-type supergiants is shown in Figure 6-2. It is clear that the break-off of the Balmer series is abrupt and that the central intensities of the Balmer lines remain about constant as one goes up the series. One reason that the electron density is believed to be low in the shells of Be stars (see Part II) is that frequently the Balmer series of these stars is seen to extend in absorption to H35 or higher.

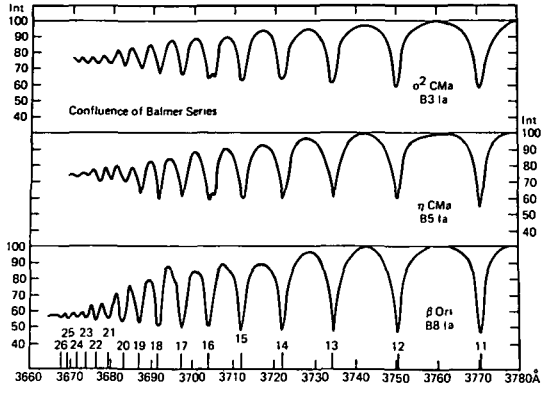

Figure 6-2. The confluence of the Balmer series at types B3 Ia, B5 Ia, and B8 Ia. The blend of H16 at 3703.86 Å and the He I line at 3705.00 Å is resolved except in the case of β Orionis where the He I line is very weak (from Underhill, 1970)

The observed break-off point of the Balmer series may be used with the model atmosphere calculations of Fischel and Klinglesmith (1973) to find a preliminary estimate of log g. By entering table 1 of Fischel and Klinglesmith with an observed value of n_m and a rough estimate of T_{eff}, one can find log g using the results given in the column for X = 2/3 which approximates normal composition. If the equivalent width of Hγ is available as well as an estimate of n_m, figure 4 of Fischel and Klinglesmith, reproduced here as Figure 6-3, will provide reliable starting estimates for both T_{eff} and log g. Although the

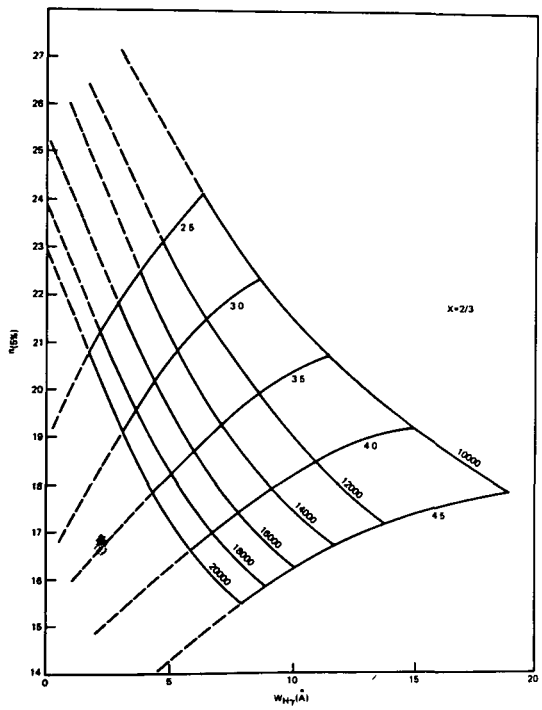

Figure 6-3. The relationship between n (5%) and the equivalent width of Hγ in model atmospheres where the fractional abundance of hydrogen by weight is two-thirds. The grid lines are identified according to the value of log g and of T_{eff}. The theoretical quantity n (5%) is equivalent to the observed quantity n_m (data from Fischel and Klinglesmith, 1973).

results of Fischel and Klinglesmith were obtained for a set of hydrogen line-blanketed model atmospheres, they are valid for determining starting values of T_{eff} and log g for use with any hydrogen-rich model atmospheres. According to Fischel and Klinglesmith, reducing the abundance of hydrogen relative to helium reduces n_m slightly and increases the equivalent width of Hγ in the temperature range 1.0×10^4 K to 2.0×10^4 K.

Application to Supergiant Stars

The methods of fine analysis described above for analyzing the shape of the continuous spectrum and the strengths of the lines in B-type spectra have been applied to 11 supergiants ranging in spectral type from B8 to O9.5. Also a few B-type supergiants have been analyzed by the methods of coarse analysis (see Underhill, 1966a). The results obtained by fine analysis are summarized in Table 6-1, where reference to the original studies is given. In the cases where the authors have selected particular values of T_{eff} and log g from the various values which they have found to be compatible with some of the observations, these values are listed. In the cases where the authors have left it to the reader to decide which results are most significant among those obtained by means of LTE or non-LTE theory, by fitting the shape of the continuous spectrum or by reproducing the apparent ionization equilibrium, the range of values found to give a reasonable solution is indicated. The value of the microturbulent velocity which was used in each abundance analysis is listed as well as a brief summary of the major abundance anomalies noted by the several authors.

From the discussion of the preceding sections and from the qualitative understanding of the physical conditions in supergiant atmospheres reviewed in Chapter 4, it is clear that the set of physical conditions envisaged by the presently available atmosphere modeling procedures are unlikely to be representative for B-type supergiants. Nevertheless, the results summarized in Table 6-1 are interesting.

The effective temperature found from the analysis of the line spectrum is always systematically higher by several thousand degrees than that which may be inferred from the total flux of radiation received from the star (see Chapter 4). The high effective temperatures which are deduced by the methods of fine analysis mean that the electron temperatures in the line forming regions of the supergiants are higher than the electron temperatures which can be maintained by the radiative flux flowing through the atmosphere under the constraint of radiative equilibrium. This result suggests that the lines in the visible part of the spectrum are giving information about a hot transition layer between the relatively cool photosphere, where the continuous spectrum is formed, and the hot mantle, known from ultraviolet spectra to exist for all B supergiants.

Table 6-1
Analyses of B-Type Supergiants

HD	Name	Spectral Type	Reference	T_{eff} (10^4 K)	log g	ξ_t (km s^{-1})	Abundance Anomaly*
34085	β Ori	B8 Ia	Stalio et al (1977)	1 21-1 50	1 8-2 0	–	–
58350	η CMa	B5 Ia	Underhill and Fahey (1973)	1 75-2 00	2 0-2.5	15	N ?
53138	o^2 CMa	B3 Ia	Van Helden (1972)	2 00	2 5	24	O d
165024	θ Ara	B2 Ib	Dufton (1979)	2 35-2 80	3 4-4 0	15	None
96159	–	B1 Ib	Dufton (1979)	2 10-2 45	3 1-3 5	15	N d
96261	–	B1 Ib	Dufton (1979)	2 45-2 85	3 3-3 7	15	N d
96248	–	B1 Iab	Dufton (1972, 1979)	2 60-2 65	3 1-3 3	10	N d
164402	–	B0 Ib	Dufton (1972)	3 30	4 1	10	None
37128	ϵ Ori	B0 Ia	Lamers (1974)	2 88	3 0	–	–
209975	19 Cep	O9 5 Ib	Takada (1977)	3 00-3 50	3 3	22 5	Ne e
30614	α Cam	O9 5 Ia	Takada (1977)	2 90-3 25	3 0-3 2	20	Ne e

*d means that the element is deficient relative to solar composition
e means that the element is in excess relative to solar composition
Dashes (–) represent no existing data at these values

The B supergiants are known to have rapidly flowing winds and their radial velocities, found from lines formed in the transition layer just above the continuum forming layers, vary irregularly with a small amplitude. Therefore, it is somewhat improbable that the condition of hydrostatic equilibrium is met in the atmospheres of B supergiants The values of log g listed are those values of that parameter which give model atmospheres having densities like those needed to predict the observed spectra with existing theory. The true values of log g, where $g = GM_*/R_*^2$, probably are larger than these values because the motions of the line forming layers probably cause the densities in the line forming layers to be lower than they would be if an equation representing the hydrodynamics of the situation was used to determine the density with the true value of gravity entering as a parameter

The microturbulent velocities listed are factors introduced in order to obtain consistency between abundances determined from weak and from strong lines of a given species. It is probable that they do not represent real velocities because they are of the order or exceed the average thermal velocity at the electron temperatures believed to exist in the line forming layers. This may be readily noted by recalling that the thermal velocity of hydrogen is 9.1, 12.8, 15.7, and 20.3 km s^{-1} at 1.0×10^4, 2.0×10^4, 3.0×10^4 and 5.0×10^4 K. In addition, the factor, microturbulent velocity, serves as a convenient "fudge factor" to allow for the increased equivalent widths sometimes resulting from non-LTE calculations (see the next section)

It is clear that on the whole the composition of the atmospheres of the B-type supergiants is normal. The discussion of the next section shows how sensitive the relative strengths of some lines are to the details of the physics of the process of line formation. One cannot determine the abundances accurately until one is certain that the theoretical modeling process takes adequate account of all relevant factors in the line forming

process. It is appropriate to note that nitrogen appears to be underabundant in some supergiants and neon overabundant (Takada, 1977; Dufton, 1979). However, recollection of the problems still remaining with modeling accurately the line formation process for the lines of He I at 5876, 6678, 7065, and 7281 Å (Auer and Mihalas, 1973a) as well as of the Si IV lines at 4088 and 4116 Å (Kamp, 1978) and the spectroscopically equivalent lines of C IV at 5801 and 5812 Å makes one hesitate to conclude that real abundance anomalies occur in B-type supergiants Underhill and Fahey (1972) were not able to reproduce well the relative strengths of lines of N II and of Si II by LTE calculations for cool B supergiants

The spectra of two B-type supergiants in the Small Magellanic Cloud (SMC) and one in the Large Magellanic Cloud have been compared by Osmer (1973) with those of B-type supergiants in our galaxy. Osmer argues qualitatively that the weakness of some of the lines of the light metals in the SMC stars indicates a true deficiency of metals in the material from which these stars were formed. In view of the complexities revealed by the abundance analyses based on high resolution spectra of galactic supergiants and of the practical fact that these are exceptionally luminous stars, Osmer's conclusion based on 39 Å mm^{-1} spectra should be regarded with caution. The stars which he studies have types in the range B3 Ia to B1 Ia, a range where the inconsistencies in the methods of fine analysis are particularly evident. Similarly, Dufton's evidence for real abundance anomalies in galactic stars is weak, for it is by no means certain that his model atmospheres represent accurately the regions where the N II lines are formed (Dufton, 1979).

Predicted Line Spectra Using Statistical Equilibrium

It may be argued that the most realistic models representing the atmospheres of B stars are those constructed by applying the constraints of hydrostatic equilibrium, radiative equilibrium, and statistical equilibrium to hydrogen, helium, and a representative light ion. Experience shows that use of such models rather than LTE models which are fully line blanketed (Kurucz, 1979) results in the shape of the continuous spectrum and its absolute value throughout the observed range longward of 1100 Å having little difference from the LTE values. On the other hand, when one compares in detail the predicted line spectrum obtained using the constraint of statistical equilibrium for finding the level populations in place of assuming validity of the Saha and Boltzmann laws, significant differences may occur in the line profiles and in the equivalent widths of lines. In this section the method used to find non-LTE predicted spectra and the results obtained will be summarized.

Most applications of non-LTE methods have been made using the non-LTE model atmospheres of Mihalas (1972a). Use of other model atmospheres probably would result in only minor differences except for lines formed almost entirely in the outermost layers of the model where there is a small temperature rise in the non-LTE models relative to what occurs in LTE models. Lines which might be sensitive to the temperature rise are those for which the line-absorption coefficient has a very large value at low densities. For most lines, at wavelengths a few Doppler widths from the line center, however, the absorption coefficient is small and the model properties in deep layers where the difference between non-LTE and LTE models is negligible are what determine the line profile. Thus, use of non-LTE models may cause significant differences only in the centers of strong lines. The results which have been obtained for most line profiles are the same for LTE and for non-LTE models.

Method for Predicting Line Profiles Using Non-LTE Physics. The first step is to select a model atmosphere for the star by the methods described earlier. If the lines of H, He I, or He II are to be interpreted, the model must be determined by non-LTE methods. The number of H and He atoms and ions found at each level in the model are retained for use in predicting the detailed line spectrum. If lines of a trace element are to be interpreted, it is sufficient to adopt any model atmosphere and to add the desired element, treat-

ing it as an impurity which does not alter the temperature and density (pressure) structure of the model.

The second step is to adopt a model atom and to assemble information on all required radiative and collision cross sections which affect the populations of the levels involved in the lines for which profiles and equivalent widths are to be found. Considerations concerning the speed of the computer available and of its memory capacity generally limit model atoms to one or two stages of ionization containing 10 to 15 levels explicitly described by their excitation energies and statistical weights, a few high levels linked to the population of the ground level of the next highest level of ionization by the Saha-Boltzmann relations and finally a highest ion consisting of a one-level atom. Typical model atoms are described in the papers listed in Table 6-2 In this table the spectra are listed for which non-LTE studies relevant to interpreting B-type spectra have been carried out. Sources for the required radiative and collision cross sections are given in these papers and many atomic spectroscopic data are summarized together with the relevant formulas for calculating the dependence of the cross sections on frequency, ν, temperature, and electron density.

The third step is to solve the coupled equations of statistical equilibrium and radiative transfer using the method of complete linearization developed by Auer and Mihalas to find the distribution of the element of interest over its several states of ionization and excitation. The methods used are described in the papers listed in Table 6-2 Some variations on the original method, which are particularly effective when a very extensive model atom is required, have been described by Kamp (1973, 1976).

The final step is to use the level populations with a detailed expression for the depth-dependent, line-absorption coefficient to solve the equation of radiative transfer and predict line profiles and equivalent widths. The parameter, ξ_t, microturbulent velocity, may be given arbitrary values as desired and the abundance of the trace element may be varied. Attention must be paid to calculating accurately the background opacity upon which the line of interest is seen projected. Line blends may be evaluated.

Differences Between LTE and Non-LTE Line Profiles. Comparison of the profiles of lines formed in a model atmosphere using LTE and non-LTE physics shows that the changes which occur are complex One cannot easily generalize to a simple pattern of behavior. Departures from LTE results can occur in lines of all strengths from weak to strong For instance, the lines of Ne I studied by Auer and Mihalas (1973b) are weak (small equivalent width), yet use of non-LTE physics results in an increase in equivalent width by as much as a factor of 3 in some cases. In most spectra, lines in the visible spectral region are strengthened by non-LTE effects, but occasionally the equivalent width becomes smaller.

In general, the cores of lines which have well-developed wings in the visible spectral region become deeper when non-LTE physics is used. The wings of the lines may be changed very little. This point is illustrated by the profiles of Hα and Hγ, taken from Mihalas (1972a) (Figure 6-4). The changes due to non-LTE are much more striking at Hα than at Hγ. The equivalent widths of lines like Hγ are not much changed from their LTE values because the core contributes little to the equivalent width. It is particularly reassuring to note that the wings of Hγ are little changed because fitting the wings of Hγ is an important way of estimating log g and it is easier to do this using LTE models and physics then non-LTE models and physics The present results indicate that essentially the same value of log g will be obtained by either LTE or non-LTE analysis.

The non-LTE effects on the leading members of the series of hydrogen and helium lines seen longward of 5000 Å are stronger than for later members of the series. This may be seen by comparing the profiles of Hα shown in Figure 6-4 with those of Hγ. For Hα, use of non-LTE physics results in a strong deep core and somewhat shallower wings. Similar effects occur for the He I leading members at 5876, 6678, 7065, 7281, and 10803 Å. A strong deep core is formed which greatly increases the equivalent width of the line. If lines that are affected by non-LTE in this way

Table 6-2
Spectra Studied Using Non-LTE Physics

Spectrum	Reference	Equiv. Widths	Line Profiles	Discontinuities
H I	Peterson and Strom (1969)		*	*
	Auer and Mihalas (1972)	*	*	*
	Mihalas (1972a)	*	*	*
He I	Auer and Mihalas (1972)	*	*	*
	Auer and Mihalas (1973a)	*	*	*
He II	Auer and Mihalas (1972)	*	*	*
C I	Snijders (1977)			*
N II	Dufton (1979)	*		
N III	Mihalas and Hummer (1973)	*		
Ne I	Auer and Mihalas (1973b)	*		
Mg II	Mihalas (1972c)	*		
	Snijders and Lamers (1975)	*		
Si I	Leckrone and Snijders (1979)			*
Si II	Kamp (1976)	*	*	
	Kamp (1978)	*		
Si III	Kamp (1973)	*		
	Kamp (1976)	*	*	
	Kamp (1978)	*		
Si IV	Kamp (1973)	*		
	Kamp (1976)	*	*	
	Kamp (1978)	*		
Ca II	Mihalas (1973a)	*		
	Snijders (1975)	*		

are analyzed by standard LTE fine analysis techniques, a large overabundance of the element may be deduced. In the case of hydrogen in the supergiants, the detailed modeling of Auer and Mihalas provides hydrogen-line profiles with wings approximately as observed. The concern of Underhill (1970) that supergiants might be deficient in hydrogen seems to be unfounded. The

predicted cores of the Balmer lines are deeper than what is observed. A small amount of rotation or macroturbulence would make the calculated profiles look very much like the observed profiles; some emission may also occur in the observed profiles. The non-LTE calculations do not provide emission components at Hα as strong as are observed in the B Ia supergiants (see Chapter 4).

Kamp (1978) showed that the equivalent widths of the strong ultraviolet lines of Si II, Si III, and Si IV are almost unchanged when non-LTE physics is used in place of LTE physics. Lines from high levels sometimes show a significant change. The behavior of lines when going from LTE physics to non-LTE physics differs depending upon whether the line intensities under consideration are before or after their maximum in a plot of line strength against spectral type or effective temperature. The changes which occur in the line strengths are a result of the changed populations of various levels in the model atom at different layers in the model atmosphere. One can roughly speak of two types of effects: (1) continuum effects, which result in an over or under ionization of the atom or ion relative to what would occur in LTE and (2) line effects, which result from changes in the relative populations of the upper and lower levels of the line under study. The first type of effect is produced as a result of differences in the shape of the continuous spectrum of the model due to non-LTE physics at wavelengths important for ionizing the atom or ion under consideration. Typical examples have been described by Snijders (1977) and by Leckrone and Snijders (1979) in connection with understanding why strong discontinuities due to C I and Si I are not seen in Ap stars. The second type affects the value of the source function chiefly, making the source function much smaller than the local value of the Planck function at the depth in the atmosphere where the core of the line is formed. This results in deep absorption lines with prominent cores.

Several authors have noted that large ficti-

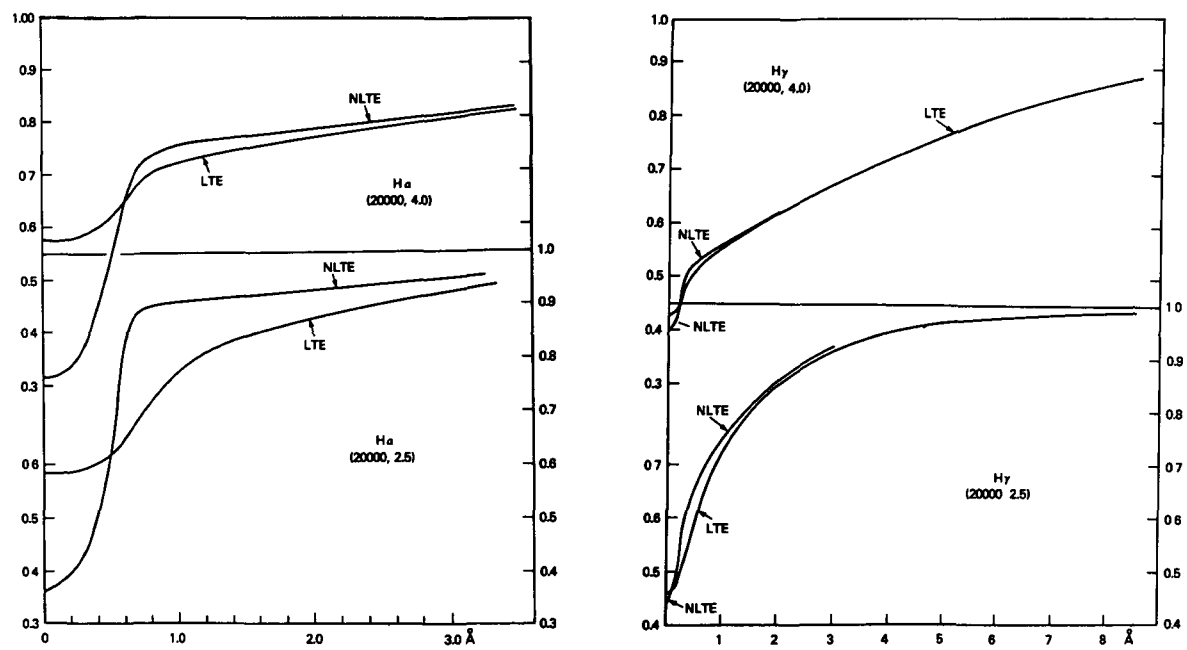

Figure 6-4a. Profiles of Hα in non-LTE model atmospheres calculated using LTE and non-LTE theory for the process of line formation (data from Mihalas, 1972a). Figure 6-4b. Profiles of Hγ for the same models as are displayed in Figure 6-4a.

tious values of microturbulence may be deduced if microturbulence is used in an LTE analysis to remove, so far as possible, a trend toward large abundances from strong lines when the increase is really due to an increase in equivalent width resulting from non-LTE effects. The few applications that have been made of non-LTE physics to find abundances show that normal, solar abundances used with a small microturbulence will reproduce the observed equivalent widths of B star lines.

Abundances. The choice of a representative model atmosphere is a sensitive first step in analyzing stellar spectra to obtain abundances. This choice should be based on fitting criteria sensitive to the fact that the cores of lines are formed in parts of the outer atmosphere or mantle. In the case of main-sequence B stars, fitting the shape of the Balmer and Paschen continua, including the Balmer jump, and fitting the wings of Hγ seem to provide reliable values of $T_{\rm eff}$ and $\log g$. In the case of the B-type supergiants, fitting the Balmer jump may result in an erroneous conclusion (see Chapter 4). In none of the stars is fitting ionization balances a reliable procedure for selecting a model because always one has to use the equivalent widths of lines which are susceptible to non-LTE effects.

How to recognize lines which may be strongly susceptible to non-LTE effects has been discussed by Underhill (1969). The most susceptible lines are those formed between isolated levels, the lower of which is relatively high above the ground level and the higher of which is not far below a set of levels which is connected to the ground state of the next highest ion by collisional processes. Unfortunately, many of the strong lines in the visible part of the spectra of B stars have this character. These lines are easily measured accurately and most have reliable gf values and damping constants. Consequently, they are frequently used to determine effective temperature by means of matching the apparent strengths of lines in two stages of ionization of a single element. This procedure always leads to an effective temperature which is higher than that which is found from the total amount of radiation emitted by the star (see Chapters 3 and 4).

Caution is required concerning the degree of faith one should place in abundances derived by non-LTE analysis in place of LTE analysis. The careful analysis both by LTE and by standard non-LTE methods of N II lines in the spectra of B1 Ib supergiants by Dufton (1979) shows that about the same underabundance of nitrogen is found in each case. In addition, Dufton presents three significant pieces of information. They are as follows: (1) his comment that the dominant stage of ionization of nitrogen is N^{++}, thus that the spectrum being analyzed (N II) is past its maximum, (2) that increasing the effective temperature by an arbitrary amount, thus increasing the electron temperature in the outer layers of the model, reduces the abundance of nitrogen necessary to reproduce the observed equivalent widths of N II lines, and (3) that arbitrarily reducing $\log g$, thus reducing the particle densities in the outer layers of the model, also reduces the abundance of nitrogen required to reproduce the observed equivalent widths If one is satisfied that the selected model atmospheres represent accurately the line forming regions of the atmospheres of B1 Ib stars, there is no escape from the conclusion that the abundance of nitrogen is low in the stars studied. However, if one permits a doubt that the selected model atmospheres are correct, the possibility that the nitrogen abundance is normal cannot be excluded. If the outermost layers of the anomalous B1 Ib supergiants were at a lower temperature and had a higher density than for the normal B1 Ib supergiants, the observed weak N II lines could be interpreted with a normal abundance.

It has been emphasized in Chapter 4 (and above) that the spectra of B-type supergiants present evidence for the presence of a hot mantle and extensive superheated transition layer which can be seen in the ultraviolet spectrum and in some of the lines used for spectral classification. The presence of the superheated transition layer means that the electron temperatures are higher in the layers where lines from spectra past their maximum are formed than LTE or the available non-LTE radiative-equilibrium models suggest and that the densities are probably lower. Both types

of changes cannot be detected by the usual methods used to select a model atmosphere. However, they will act together in such a manner as to result in an anomalously low abundance for an element such as N when the abundance is determined from lines of N II Thus, until abundance determinations have been performed with model atmospheres that can be proved to model accurately the conditions in the superheated transition layer lying between the photosphere and the hot mantle, one should be cautious about concluding that real abundance anomalies exist in B-type supergiants.

The determination of abundances is a very demanding activity. Not only must the physics of line formation be represented by reasonably accurate formulas, but also the adopted model atmosphere must represent accurately the conditions in the line forming layers as well as in the layers of the star where the continuous spectrum is formed. It is not simple to devise tests of one's method to assure that the formulas used and the model selected are indeed truly representative of conditions in all relevant parts of the star

What Is Not Predicted by Classical Modeling

The classical methods of interpreting stellar spectra described above have been successful in interpreting the continuous spectrum of B stars and in modeling the photospheric layers of many stars. For main-sequence stars determinations of the effective temperature from fitting the shape of the continuous spectrum agree with the results obtained from the integrated flux and estimates of $\log g$ from the shape of the wings of the Balmer lines are in line with what is suggested by knowledge of masses and radii. For supergiants the agreements are less satisfactory, fitting the size of the Balmer jump will lead to effective temperatures that are higher than those suggested by the integrated flux although fitting the shape of the continuous spectrum over a long wavelength range gives more accordant results. No check on the values of $\log g$ can be obtained because the masses of B-type supergiants are poorly known.

The classical methods are based on applying the constraints of radiative equilibrium and hydrostatic equilibrium. Attention to the use of realistic physics for representing the distribution of the atoms and ions over their possible energy levels has cleared up some outstanding questions in abundance determinations, but we have become aware that our determinations of abundance are no more secure than are our models of the line forming layers.

Interpreting B-type spectra is not yet a subject with no surprises. Ultraviolet spectra reveal resonance lines from high ions (C IV, N V, and O VI) suggesting the presence of a hot coronal region, possibly of small extent, in the outer parts of many B stars, as well as a wind. The classical modeling methods will not allow the electron temperatures to rise to temperatures of the order of 10^5 K, as are required to produce the high ions which are seen by electron collision, and they do not permit flow at speeds significantly exceeding the local thermal velocity in the medium. When flow motions exceeding the local thermal velocity occur, hydrostatic equilibrium is not a valid concept and one must use the full equations of hydrodynamic flow in order to obtain the pressure-density structure of the atmosphere. To attain high electron temperatures in the outer levels of a model, one must allow for the input of energy from mechanical and/or magnetic sources.

No modeling techniques incorporating these improvements have yet been developed for B stars. Thus, classical model atmospheres and the classical techniques of spectrum analysis suffice only for interpreting the parts of the spectrum formed in the photospheric layers of quiescent stars. They certainly are inadequate for analyzing the line spectra of B-type supergiants because there is ample spectroscopic evidence indicating the presence of significant rates of mass flow and the presence of superheated outer layers in supergiants. Similarly, the available methods are inadequate for modeling the changeable outer atmospheres around main-sequence B stars which have been classified as Be or B with a shell

It is straightforward to conclude that the cause of the different types of the outer atmosphere which are required in order to model in a simple way the parts of B stars which give rise to the

dominant spectroscopic characteristics of Be stars and of B supergiants comes from below the photosphere. It is another question, presently unsolved, to describe in physical terms the relevant process which is occurring and to model it in an adequate manner.

Some models have been developed to demonstrate what motions in the outer layers of a star will do to the spectrum and to explore the effects of using geometries different from plane parallel layers (see the next section). The models are conceptually simple, but they have led to some difficult problems of numerical analysis, some of which have received elegant solutions in recent years It is by comparing the shapes and intensities of observed line profiles with those predicted by these sometimes very simple models that we have been able to conclude that many B stars have winds and some may have infalling atmospheres. By noting that certain lines appear in stellar spectra that require electron temperatures which cannot be provided by the underlying radiation field of the stars, we know that we must consider that heating occurs as a result of the deposit of mechanical/magnetic energy. These conclusions, which become inescapable once ultraviolet spectra of B stars are studied, have revitalized the study of B-type spectra A new picture is required in which B stars have outer structures of a similar character to those of the Sun and most late-type stars, namely a mantle and a wind. This is an area where much work remains to be done, first to obtain insight about the physical processes which drive the nonclassical outer atmospheres, and second to model the outer atmospheres in order to obtain quantitative knowledge about what is occurring.

EXTENDED AND MOVING ATMOSPHERES

One may postulate that the material in a model atmosphere has a systematic motion in the line of sight, set up the appropriate, modified equations of transfer for computing the emergent spectrum, and find out how the spectrum from a moving atmosphere may differ from that of a stationary model atmosphere All of the work to be reviewed in this section falls into this category. Here only a brief summary of the theoretical results obtained will be given. A more detailed review of this subject can be found in *O, Of, and Wolf-Rayet Stars* by Underhill and Divan (to be published).

The studies aimed at evaluating the effects of line-of-sight motion in the atmosphere on the profiles of stellar absorption and emission lines make use of ad hoc models. Typically, the velocity field is specified as a simple functional relation involving the distance of each element of volume in the atmosphere from the photosphere of the star, the density is obtained by conserving matter as it flows from one level in the atmosphere to the next, and a simple assumption is made about the distribution of electron temperature with distance from the photosphere.

Three general types of velocity fields have been considered (1) those in which the outward directed motion is negligible at the photosphere and it increases outward to a terminal velocity, (2) those which start with a suddenly acquired large outward directed velocity near the photosphere after which the material slows down owing to deceleration by the force of gravity, and (3) extended atmospheres where the velocity field results from the infall of material. Some studies postulate a constant velocity field, others postulate that large velocity gradients occur along the line of sight

The existence of an acceleration or a deceleration of the material in a stellar atmosphere implies the action of a propulsion force or of a retarding force. The early work of Milne (1926) indicated that the outward propulsion of atoms and ions by means of the radiation field flowing in line frequencies would be important only in the outermost layers of an atmosphere. Later work by Castor et al. (1975) showed that if the formula adopted by them for the force exerted by radiation on atoms and ions is valid, a significant outward acceleration may ensue for an atmosphere in which large velocity gradients exist Kurucz and Schild (1976) have demonstrated that in the outer layers of static model atmospheres for B stars, the size of the net outward acceleration due to radiation is finite and small compared to the acceleration inward due to gravity.

The effects of magnetic fields on the flow of ions in a B-type model atmosphere may provide outward acceleration, but this topic has not yet been studied in depth. In the case of a rotating star it has been postulated that rotationally forced ejection may occur. This latter problem has been studied by Limber (1967) who concluded that it may be important for causing the mass outflow observed to occur for Wolf-Rayet and some Be stars. In a later study Limber and Marlborough (1968) emphasized the need for viscosity (magnetic or turbulent) in order to maintain extended atmospheres of the types believed to exist for Be stars.

Since changes in the mass flow from stars are inferred to occur sometimes in intervals as short as a few weeks (see Chapters 3 and 4 and Part II), it is clear that the propulsion forces cannot arise only from interactions between global forces such as gravity, rotation, and radiation pressure. Magnetic forces are an interesting possibility for causing the short time scale changes. Limber (1974, 1976) has drawn attention to the effects caused by magnetic lines of force being twisted and broken. If one invokes the twisting and breaking of magnetic lines of force to account for changes in mass flow, one must fasten attention on a stage further back, namely on the problem of the generation and maintenance of magnetic fields in the early type stars. It would be an exciting result if the study of the spectrum produced by moving atmospheres could yield information on the magnetic fields in B-type stars, but this goal has, at present, not been attained.

When one postulates that moving atmospheres exist for early type stars, one should consider the aerodynamics of these atmospheres. The topic of aerodynamics in stellar atmospheres has not been taken into consideration in most of the work to be reviewed here.

The occurrence of directed flow in an atmosphere at velocities in excess of about one-third the local thermal velocity requires one to consider the effect of these motions on the structure of the atmosphere and their origin The possible answers will not be reported here in detail. Thomas (1973) and Cannon and Thomas (1977) have analyzed the problems which are involved. We agree with their conclusion that the ultimate source of the outward directed motions which are inferred to exist in the atmospheres of stars may be sought in mass flow from the subphotospheric layers Very small velocity fields there may become spectacular velocity fields in the low density, extended outer atmospheres of some early type stars. Other propulsion forces may also be active One is still faced, however, with finding a reason for the first small systematic outflow which occurs at depths below the photosphere in the picture due to Thomas.

It has been noted in Chapters 3, 4, and in Part II that the ultraviolet spectra of B stars contain spectral lines which come from highly ionized ions. The presence of these high ions in relative abundance forces us to conclude that high electron temperatures exist somewhere in the outer layers of B stars Studies have been made to find a source of the energy needed to produce the high ions, particularly for the O stars The effectiveness of radiative amplification of sound waves has been investigated by Hearn (1972, 1973), by Nelson and Hearn (1978), and by MacGregor et al. (1979); Cassinelli and Hartmann (1977) have studied the effects of a hot corona on the radiation field from an early type star although they have not explicitly suggested a physical cause for the postulated heating of a corona, similarly, Olson (1978) has explored the effects on the outer atmosphere of an early type star of the presence of a very hot, thin corona lying just above the photosphere. He shows that it is possible in this way to account for the population of high ions which is seen However, he does not say what physical process produces the thin, hot corona. Underhill (1980b) has suggested that interactions between small intrinsic magnetic fields and differential motion may cause the nonradiative heating

The dissipation of energy in the layers just above the photosphere by sources other than radiation has an important bearing on the temperature and velocity laws which are inferred to exist in the outer moving layers of a star. The constraint of radiative equilibrium is no longer adequate for determining the temperature law. No fully consistent study of the possibly signifi-

cant processes has been made for B stars. The temperature laws which are assumed are completely ad hoc in character and the velocity laws are tenuously related to the postulated effects of radiation pressure as an accelerating force.

Early Work on Extended and Moving Atmospheres

Early in the study of stellar spectra it was realized that the atmosphere of a star might have a systematic motion in the line of sight relative to the motion of the star perceived by the observer, and that spherical geometry might be required to model the atmosphere rather than the geometry of plane parallel layers Spherical geometry is required when the linear extent of the atmospheric region, which is important for the transfer of radiation in line frequencies (for line formation), is comparable to the radius of the star. Normally, the linear depth of the photosphere of a star, the region where the continuous spectrum in the visible spectral range is formed, is less than one-tenth of the radius of the star. Then one is justified in modeling the atmosphere by means of plane parallel layers Such a model may also be used for studying lines which are formed in layers of comparable extension. Introducing motions into the model atmosphere and going to spherical geometry both greatly complicate the mathematics of the theory of radiative transfer in a stellar atmosphere. The early results on how motion and/or extension of the atmosphere would modify the predicted spectrum from an atmosphere were attained at the cost of severely simplifying the mathematics and by adopting simple functional forms for the physics of the interactions between the radiation field and the material of the stellar atmosphere.

Among the first to consider the effects of motion of the atmosphere on the shape of a line profile were Shapley and Nicholson (1919) who considered the problem of a pulsating star with a thin atmosphere. Their theoretical line profiles show the major characteristics that all later, more sophisticated studies have shown. Expansion of a thin atmosphere results in an absorption line profile with a steep gradient of intensity on the shortward side, the deepest point is displaced by about 75 percent of the expansion velocity, and the longward side reaches the continuum level with a slow slope, its end point being at the undisplaced position of the line. Infall of an atmosphere produces a reversed profile shape to expansion. Rotation of a star is shown to result in a rounded, shallow profile with the wings extending to $\pm v \sin i$. An elegant mathematical treatment of these problems, valid for small velocities, was developed by Carroll (1928). Carroll confirmed the general results of Shapley and Nicholson and he indicated how specific information about details of the motion of the stellar surface might be obtained from a careful study of the shapes of absorption lines. Additional work on the effects of an expanding atmosphere on the line profile was presented by O. C. Wilson (1935), who was interested in understanding the line shapes to be expected from novae as well as those from pulsating stars.

It was early realized that if there was a velocity gradient along the line of sight, radiation which is seen at frequency ν by a stationary external observer will be seen at different frequencies ν' and ν'' by hypothetical observers who are comoving with the material at positions along the line of sight where the line-of-sight velocity seen by the external observer is u' and u'' This happens because of the Doppler effect, it greatly complicates the equation of transfer for monochromatic radiation. The modern attack on solving the equations of transfer in a moving atmosphere was initiated with the appearance of the landmark paper of Chandrasekhar (1945). Here Chandrasekhar shows explicitly how one might efficiently handle the problem of the interlocking frequencies which results from a velocity gradient along the line of sight; he derives detailed profiles (still schematic to some extent) for lines formed in plane parallel layers which are expanding.

The problems of radiative transfer in spherical atmospheres were first attacked in a significant manner by McCrea (1928). This work was soon followed by other studies, notably by that of Kosirev (1934) which was concerned with the question of whether the relatively red colors of the Wolf-Rayet stars could be due to these stars

possessing greatly extended atmospheres, and by Chandrasekhar (1935) who was interested in how the shapes of absorption lines formed in a spherical atmosphere differed from those formed in a plane parallel atmosphere This phase of the study of the effects of spherical atmospheres closed with the work of Underhill (1948a), who applied the numerical methods developed by Chandrasekhar for hand-computing techniques (see Chandrasekhar, 1950, for a summary of this theory) to find that in a spherical atmosphere the wings of a strong line might be deepened in comparison to what would be found for a plane-parallel layer atmosphere and that the core would become less deep

The question of accounting for the shapes of the rather broad emission lines of Wolf-Rayet stars was attacked by Menzel (1929) and by Beals (1929, 1931) within the simple framework of ideas which existed in the 1920's for interpreting the shapes of absorption lines formed in moving atmospheres Both Beals and Menzel postulated an expanding spherical atmosphere in which the emissivity in line frequencies was much greater than that in continuum frequencies The expanding atmosphere was transparent in continuum frequencies No chain of reasoning was developed to support the hypothesis that the line emissivity per unit volume in the expanding spherical shell is larger than that in continuum frequencies, but one infers that this hypothesis was not considered to be unreasonable because it was known at that time that the emission-line spectra of Wolf-Rayet stars contain lines from high ions which are not generally seen in the absorption-line spectra of the hottest stars known at that time and that the continuous absorption was small In the first studies, the expanding shell of gas was assumed to be transparent to its own radiation.

The simple modeling of this early work shows that flat-topped emission lines would arise from an optically thin emitting sphere and that parabolically shaped emission lines would arise from an optically thick sphere The work of Bappu and Menzel (1954) brought this type of analysis to its maximum development. When the opacity of the material in line frequencies is taken into account a shortward displaced absorption core, formed in the column of atmosphere projected against the stellar disk, may appear next to some emission lines Theoretical profiles for P-Cygni stars were calculated by Rottenberg (1952) using a simple method which, nevertheless, recognizes the features which were later handled explicitly using powerful methods of numerical analysis. His approximations are tenable when the optical thickness in line frequencies is not large.

In isolation from work that was occurring elsewhere on understanding the formation of emission lines in an extended moving atmosphere, Sobolev (1947) developed a method for modeling the process of emission-line formation in the case of optically thick lines of Be, Wolf-Rayet, and P-Cygni stars He introduced the concept of "escape probability" and made the explicit approximation that because of velocity gradients along the line of sight, only material in very short sections along each line of sight would interact with the radiation field to contribute to the line profile under study The local line-of-sight velocity, u, of the effective interacting volume for radiation of a frequency ν (as seen by a stationary external observer), which is different by an amount $(\nu - \nu_0)$ from the line center, is given by the relation $(\nu - \nu_0)/\nu_0 = u/c$ Here ν_0 is the central frequency of the line as determined by the stationary external observer The geometric positions of the interacting regions within the stellar atmosphere are determined by the postulated velocity law which gives the dependence of the line-of-sight velocity on distance from the stellar photosphere. Castor (1970) used the escape probability method to confirm the earlier results of Beals and Menzel and to deepen the understanding of Wolf-Rayet atmospheres.

The main conclusions to be drawn from this early work on moving and/or extended atmospheres are that expansion of the atmosphere and extension of the atmosphere do play a role in interpreting the shapes of the absorption and emission lines seen in stars with abnormal spectra, but that to solve in a self-consistent manner the problems of radiative transfer that are encountered in trying to develop a physically consistent model for the atmosphere will require very powerful techniques of mathematical analysis.

Modern Work on Extended, Moving Atmospheres

By the late 1960's it was becoming evident that many of the characteristic features of the spectra of early type stars, particularly of those having a high luminosity, were due to line formation in an extended moving atmosphere, and attention was directed to developing methods for handling the mathematics of radiative transfer in moving atmospheres. It was realized by some that the presence of strong absorption lines from the resonance lines of C^{+3}, N^{+4}, and O^{+5} implied the presence of regions in the outer atmospheres of O and B stars where the electron temperature was higher than could be attained using the constraint of radiative equilibrium with the flux determined by the effective temperatures of these stars and that energy was being deposited from sources in addition to the radiation flowing through the atmosphere, but at the time of writing no model atmospheres fully consistent with the physical processes that appear to occur have been developed and used for predicting spectra. Consequently, all theoretical spectra that have been predicted are for ad hoc representations of the stellar atmosphere. Some elegant methods for handling the mathematics of radiative transfer in moving atmospheres have been developed and applied. In what follows, a few of the key results of the past decade will be reviewed.

Moving Plane-Parallel Layers. The definitive paper on this subject is by Noerdlinger and Rybicki (1974) who solve the radiative transfer problem for a two-level atom in plane-parallel layer geometry in an expanding atmosphere. They adopt Schuster-type boundary conditions, namely that an underlying continuum is emergent from the photosphere over which the moving atmosphere lies and that there is no inwardly directed radiation incident on the outer boundary of the atmosphere The cases for which they calculate the line profiles are for a uniform velocity gradient but their method allows generalization to other types of velocity gradient When the temperature decreases outward or is constant, the computed profiles have the characteristics first recognized by Shapley and Nicholson (1919) to be due to expansion (contraction). When the temperature increases outward, an emission hump appears in the longward wing of a line formed in an expanding atmosphere The radiative pressure is evaluated and it is found to compress the inner part of the atmosphere and to expand the outer part. The mathematical stability of the method of Noerdlinger and Rybicki arises from their choice of working in the fluid or comoving frame and adapting this formulation to the Feautrier method for solving the equations of transfer.

The question of how to represent mathematically the transfer of radiation in extended spherical or plane-parallel layer moving atmospheres has been formulated in modern terminology by Rybicki (1970). Here Rybicki also discusses the meaning of making the "Sobolev" approximation, namely of assuming that in a moving atmosphere only material in a narrow zone interacts with the radiation of a given frequency as seen by an external stationary observer. Use of the Sobolev approximation greatly simplifies the theory of radiative transfer in a moving medium. It implies the presence of large velocity gradients If the acceleration to a large velocity takes place within a distance that is of the order of or smaller than one stellar radius and if the final velocity is large in comparison to the local thermal velocity, the Sobolev approximation may be made. In its original form, Sobolev's theory envisaged only one "resonance region" along each line of sight, thus a velocity law that increased along a radius.

The effects of velocity gradients in a model atmosphere on such quantities as the apparent value of the microturbulence parameter, the broadband colors, and the line profiles have been investigated by Karp (1973, 1975a, 1975b, 1975c), with particular reference to Cepheid variables. Karp used his own hydrodynamic model atmospheres, which did not include line blanketing, non-LTE effects, or non-gray radiative transfer. He assumed that the source function was unperturbed by the motion, thus neglecting the possible interlocking effects of radiation of different frequencies, resulting from the relative

motion of different parts of the model atmosphere. He did, however, allow for the displacement of the line at each layer in the model as seen by a stationary external observer. Karp showed that the observed asymmetry in strong lines of Cepheids could be due to velocity gradients in the line forming region; however, his method is justified only for the case of small velocity gradients and for lines where LTE is a good approximation. Lesh and Karp (1977) applied this technique to B-type model atmospheres, assuming both a uniform expansion (contraction) term and a velocity gradient, their purpose was to predict line profiles in pulsating B stars (β Cephei stars, see Chapter 5).

All the studies mentioned so far concerning the shapes of line profiles in model atmospheres of pulsating stars have implicitly assumed that the pulsation is radial – that is, alternate expansion and contraction (uniform or differential) of a spherically symmetric model. However, there is some evidence that certain types of stars – including some B stars – undergo nonradial pulsation. A pioneering study on the shapes of line profiles affected by a nonradial velocity field was published by Osaki (1971). Osaki did not construct a model atmosphere at all, but merely convolved a rotationally broadened profile with the pattern of Doppler shifts produced by line-of-sight motion of elements of the stellar surface due to the nonradial pulsation. He showed that very large changes in line width and asymmetry occur at various phases of the pulsation cycle. Following Osaki, similar investigations for various nonradial modes were performed by Smith (1977), Stamford and Watson (1977), and Kubiak (1978). A preliminary attempt at using Karp's method to combine the effects of a depth-dependent velocity field and nonradial pulsation was reported by Lesh (1978b) However, hydrodynamic effects and radiative transfer have not yet been correctly taken into account in any nonradial pulsation model. No study of either radial or nonradial pulsation has considered the interaction between the velocity field and the thermodynamic structure of the atmosphere.

Other problems to which Karp's method has been applied include the interpretation of asymmetries in some line profiles of τ Sco (B0 V) in terms of outflow (Smith and Karp, 1978), and the combined effect of expansion and rotation in producing asymmetric line profiles (Duval and Karp, 1978). Duval and Karp convolved the line shape from a stationary model atmosphere with a function representing the displacement of the line profile at various points on the stellar disk, as seen by an external stationary observer. This is akin to the early methods used to determine rotationally broadened profiles, its sidesteps having to evaluate the effects of differential motion in the atmosphere on the source function.

Karp (1978) has studied in detail the more complex inverse problem of using the observed absorption-line asymmetries to determine velocity gradients in a stellar atmosphere. He assumed that the atmosphere could be represented by moving plane-parallel layers, and that the source function was a slowly varying function of wavelength. For several simple, ad hoc relations between velocity and depth in the atmosphere, Karp found only small differences in asymmetry between strong and weak lines; but there were significant differences in the displacement of the line centers. Thus, a careful comparison of observed differential displacements between lines of different intrinsic strength might be used, with Karp's predictions, to deduce the size of the velocity gradients occurring in stellar atmospheres. But one must be alert to the fact that the physical characteristics of the models are ad hoc in nature, and may not accurately represent the real physical situation.

Three-Dimensional Model Atmospheres. Although it has been observed that whenever stellar atmospheres seem to be extended and to require three-dimensional geometry for their representation, outflow or other large-scale motion seems to occur, it is a useful exercise to investigate how the properties, in particular those of the emergent continuous spectrum of static extended model atmospheres differ from those of static plane-parallel layer models. A few such models have been constructed using spherically symmetrical geometry. The constraint of radiative equi-

librium is used with a prescribed luminosity and effective radius to determine the variation of temperature throughout the model and the equation of hydrostatic equilibrium is used with an assumed surface gravity due to the mass of the star to obtain the density structure The effects of gravity are diminished by means of the force of radiation pressure which acts as a force to extend the atmosphere

Several model atmospheres for hot stars with extended atmospheres have been constructed by Mihalas and Hummer (1974) and by Kunasz et al. (1975) using a generalization of the techniques of Auer and Mihalas for solving the radiative transfer problem without assuming LTE. The force due to radiation pressure is represented by a simple ad hoc formula which contains exponentials in terms of the optical depth and two free parameters

The problem of developing static spherical model atmospheres has been considered by Hundt et al (1975) and by Schmid-Burgk and Scholz (1975) They studied the case of gray and nongray absorption coefficients and they included radiative support of the atmosphere against gravity. They used the techniques for solving the equations of radiative transfer in the case of LTE in spherical atmospheres which had been developed by Schmid-Burgk (1975) This group was interested in finding out whether stars with extended, static atmospheres could exist and where such stars might be located in the HR diagram. They determined that very massive stars and Wolf-Rayet stars probably do not have extended static atmospheres but that such atmospheres might occur for low mass stars of high luminosity

None of the models developed by Mihalas et al have parameters like those expected to be relevant for interpreting the spectra of B-type supergiants or Be stars The properties of their model atmospheres are discussed further in *O, Of, and Wolf-Rayet Stars* (Underhill and Divan, to be published) It is found that the shape of the spectrum from models which might represent the continuum forming layers of a star like ζ Pup, O4 f, differs little over the observable spectrum range from that predicted using a plane-parallel layer model of appropriate $T_{\rm eff}$ and $\log g$.

Moving Three-Dimensional Atmospheres Few model atmospheres of this type have been constructed but the question of solving the radiative transfer problem in models where the temperature, velocity, and density structures are described by analytical expressions has been studied from several points of view. Some extensive sets of predicted line profiles are now available for the case of resonance lines and for some types of subordinate lines.

The model moving atmospheres in which the lines are formed are entirely ad hoc in nature; the temperature structure is arbitrary, the velocity field is assumed to follow a power law or other simple dependence on distance from the center of the star, and the density structure is related to the velocity structure by requiring that the material be conserved in spherical shells

The theoretical profiles obtained from such models indicate how the line profile may be changed when a line is formed in a moving spherical atmosphere rather than in a stationary one, but they give little basis for deducing a detailed, internally consistent physical model of the outer layers of a star from a quantitative study of the profiles of lines formed in the outer layers of a star In order to perform this last task, one should solve, simultaneously, the combined equations for conservation of mass, momentum, and energy as well as the equations of radiative transfer in a plane-parallel layer or spherical atmosphere taking into account all the ways in which gas, radiation, and magnetic fields can interact and exchange energy. The boundary conditions are that the atmosphere is irradiated on the inner side by a flux of radiation and of mechanical or magnetic energy, both generated in the interior of the star, and that it is open on the other side to interstellar space A wind may flow from the star

The full problem is too difficult for solution at this time, but insight may be gained by comparing the results of calculations based on less realistic models to the observed line profiles One is

still at the stage of trying to establish what are the critical factors which must be kept in a realistic model.

The theory of line formation in a moving atmosphere has been reviewed by Hummer (1976). He gives examples of the type of problem encountered and how each may be handled mathematically as well as typical results. An important conclusion is reached, namely that the Eddington-Barbier relation (the statement that the emergent monochromatic flux in a line can be approximated by the value of the source function at the depth where the monochromatic optical depth is unity) can no longer be used in diagnostic analysis when the atmospheric layers are moving.

Here we shall mention only a few of the papers in which the theory of radiative transfer in moving atmospheres has been applied, selecting those results that are possibly relevant for understanding the meaning of the line profiles which are observed for B stars with moving atmospheres. The reader is referred to Hummer (1976) and the papers he references there for the mathematical foundations of the subject.

The mathematical approach has been either to make the Sobolev approximation for the case of a flow which varies monotonically with radius (see Olson, 1978, Surdej, 1979; Castor and Lamers, 1979), or to work in the comoving frame without making this approximation (see Lucy, 1971, Mihalas and Kunasz, 1978). How to handle radiative transfer in a moving atmosphere in which the line-of-sight component of the flow velocity is not monotonic by means of the Sobolev or escape probability method has been studied by Martı and Noerdlinger (1977) and by Rybicki and Hummer (1978). In such cases, radiative coupling between distant parts of the atmosphere must be taken into account.

The calculations of Olson, of Surdej, and of Castor and Lamers have provided grids of "P-Cygni" type line profiles consisting of a shortward displaced absorption component and an emission feature on the longward side of the absorption. Sample results are displayed in Figure 6-5. The theory used may be appropriate for resonance lines; each author assumed that the lines are formed by scattering. In the cases of Surdej and of Olson the scattering is coherent and isotropic, in the case of Castor and Lamers, isotropic scattering takes place with complete frequency redistribution Because the Sobolev approximation breaks down for small line-of-sight velocities, the profiles are expected to be unreliable in the range $|w| < 0.25$. Here $w = u/u_\infty$, where u_∞ is the terminal velocity reached by the moving material and u is the component of velocity along a radius at each point in the atmosphere.

In the work of Castor and Lamers, the essential physical conditions in the moving, spherical atmosphere are represented by simple analytical expressions. The velocity law has the form

$$w = 0.01 + 0.99\,(1 - \frac{1}{x})^{\beta}, \qquad (6\text{-}3)$$

where $x = r/R_*$. Here R_* is the radius of the photosphere of the star. The quantity $x > 1.0$. The strength of the line depends on the number of ions along the line of sight capable of absorbing the line, thus on the total optical depth in the

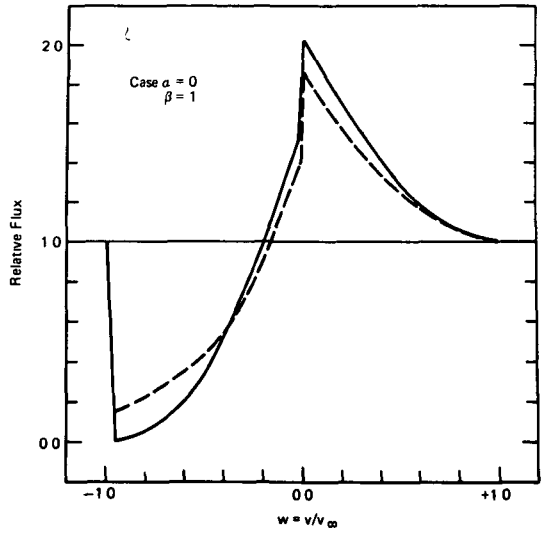

Figure 6-5 Calculated profiles for a model atmosphere that is accelerating outward (data taken from Castor and Lamers, 1979). The solid line is for $T = 10^3$, the broken line for $T = 2$. For the meaning of the parameters α, β, and T see the text.

line center. Castor and Lamers postulate that

$$\tau(w) = \text{const.}\ w^{\alpha}, \qquad (6\text{-}4)$$

and they characterize the optical depth by a parameter T. The profiles displayed in Figure 6-5 are for the cases $\alpha = 0, \beta = 1$, and $T = 2$ and 10^3.

To infer information about the physical state of the expanding atmosphere, one fits the extreme parts of a normalized observed line profile to one of the calculated profiles and notes the appropriate values of α, β, and T. The fit should be carried out at $|w| > 0.25$ Cautions are given by Castor and Lamers on how to use their grid of theoretical profiles

The results of these several studies of line formation in accelerating atmospheres show that the profile of the absorption component depends sensitively on the value of the parameter T, but little on the shape of the velocity law. On the other hand, the calculated intensity of the emission component at small positive w is sensitive both to the assumed optical depth and to the shape of the velocity law. Consequently, the ratio of the equivalent width in the emission component to that in the absorption component, W_E/W_A, is sensitively dependent on the choice of the parameter α However, in view of the unsatisfactory character of the Sobolev approximation when w is small, the true meaning of W_E/W_A is obscure.

When one fits observed profiles to calculated profiles in order to infer the physical state of the expanding atmosphere, one must consider carefully how exact the fit should be in order to obtain meaningful results and how one is to invert the parameters describing the schematic model atmosphere into true physical quantities. This problem is touched upon in further detail in the next section. Suffice it to note here that if one is to decide between $T = 10^3$ and $T = 2$ for the case $\alpha = 0, \beta = 1$ displayed in Figure 6-5, one must have accurate photometry of the line profile in the region $w = -0.7$ to -0.9.

The calculations of Mihalas and Kunasz (1978) are aimed at solving the problem of line formation in a moving atmosphere while taking into account explicitly the distribution of the atoms and ions over their several energy states. They solve the equations of statistical equilibrium together with the equations of radiative transfer and they do not make the Sobolev approximation. They have published results for a simplified He^+-like model atom in a parameterized isothermal wind. Some of their calculated profiles for subordinate lines are shown in Figure 6-6.

In this example, the model wind has a constant temperature of 4.0×10^4 K and its inner and outer radii are 10^{12} and 10^{13} cm, respectively. The expansion velocity starts from near sonic velocity at the photosphere and reaches 1000 km s^{-1} at 5×10^{12} cm, 1360 km s^{-1} at 10^{13} cm. The density distribution is found by conserving matter in spherical shells as it flows and postulating a rate of mass loss of $5.6 \times 10^{-6}\ M_{\odot}\ yr^{-1}$

Comparison of the line profiles in Figures 6-5 and 6-6 shows that in Mihalas and Kunasz's calculations the subordinate lines have much shallower absorption components than do the resonance lines of Castor and Lamers and that the height of the emission peak may exceed that found by any of the calculations done using the Sobolev approximation and pure scattering as the mode of line formation. Mihalas and Kunasz do not portray the profile of the resonance line from their model atom. Their computational method does not break down when the component of flow velocity in the line of sight is small. Typically the lower level of their model atom is overpopulated relative to LTE conditions by a factor of several thousand while the upper levels are depopulated It is noteworthy that their calculations show the emission component extending significantly shortward of the undisplaced line position while the peak of the emission feature occurs near the position of the undisplaced line.

Line Formation in Decelerating Atmospheres

Marti and Noerdlinger (1977) and Rybicki and Hummer (1978) explored the results of line transfer in a moving three-dimensional atmosphere in which the projection of the flow velocity on the line of sight is not necessarily monotonic; such expansion has the result that some constant velocity surfaces are intersected more than once by some lines of sight. This work demonstrates how

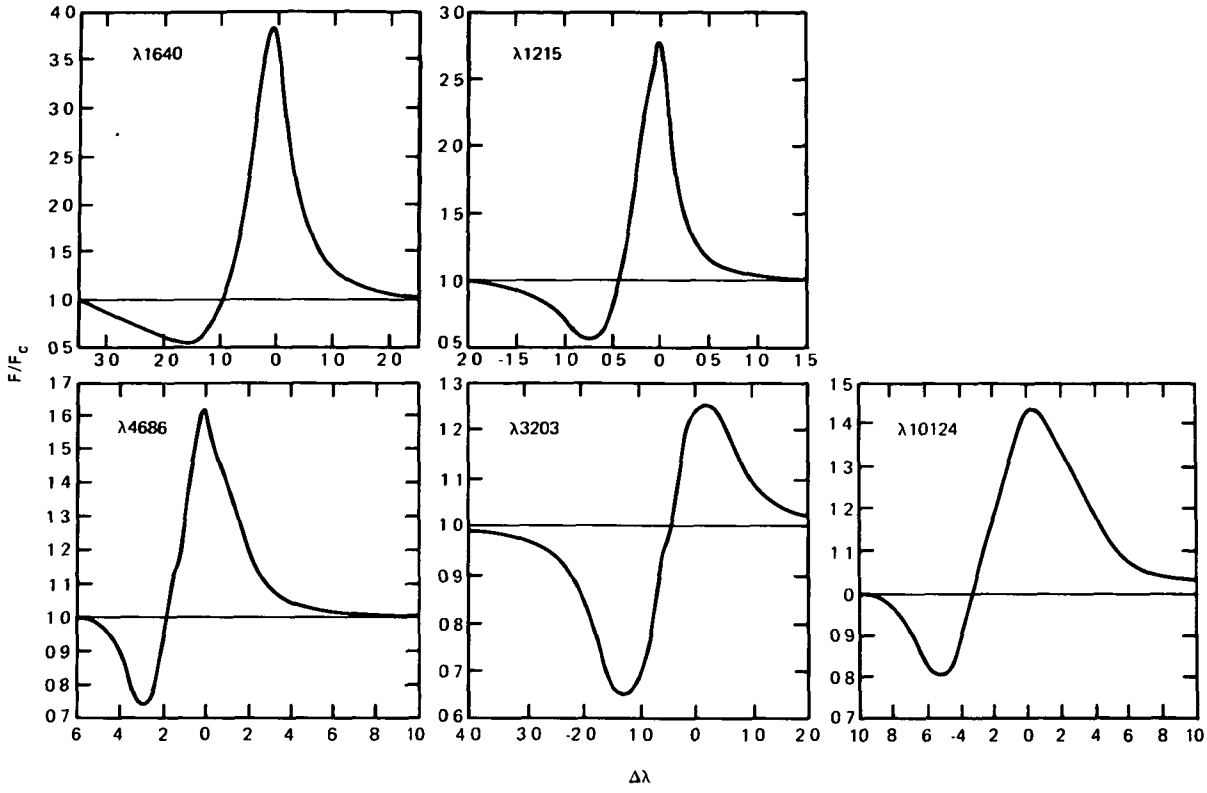

Figure 6-6. Calculated line profiles from a He^+-like ion in a moving model atmosphere (from the work of Mihalas and Kunasz, 1978)

difficult it is to interpret the shape of a "P-Cygni" type line profile in terms of one type of flow. Rybicki and Hummer studied the case of radiative transfer for a two-level atom in a moving three-dimensional atmosphere The source function is the result of scattering with complete redistribution and of collisional de-excitation of the upper level The theory is developed in its most general terms and then numerical examples are computed for spherical atmospheres with specified velocity laws, sizes of atmosphere, and line optical depths

A prototype velocity law which gives rise to constant velocity surfaces which cross some lines of sight twice is the inverse power law This can be written as

$$u(r) = u_0 (r_0/r)^{\alpha}, \qquad (6\text{-}5)$$

where r_0 is the radius of the photosphere. At the photosphere, the outflow velocity has a large value u_0. Rybicki and Hummer give results for $\alpha = 0.5$ and $\alpha = 1.0$ and for cases where $r_{max} = 10, 10^2$, and 10^3 times r_0. The density pattern is established by conserving mass in shells as the material flows outward, and the temperature pattern is modeled by specifying the dependence of the integrated Planck function, B, on radius. In addition the atmosphere is described by specifying τ_0, the tangential (along the line $\mu = 0$) optical thickness of the velocity surface at the inner radius r_0, and the value (which remains constant) of ϵ, the ratio of collisional to total de-excitation rates from the upper level. Here μ is the cosine of the angle between the line of sight and the beam of radiation being considered.

The profiles which Rybicki and Hummer present, although they come from an atmosphere in which the velocity is decreasing outward, show a shortward displaced absorption core and an emission component centered, more or less, on the undisplaced position of the line. The profiles have similar characteristics to those calculated by

Surdej, by Olson, and by Castor and Lamers for atmospheres which are accelerating outward.

Profiles with different ratios of emission to absorption intensity and different shapes can be obtained as one varies the parameters to concentrate the emissivity by a greater or lesser amount in the outer regions of the atmosphere. In the outer regions the outflow velocity is small; in the inner part of the atmosphere, the outflow velocity is large. In addition Rybicki and Hummer show that in some cases neglecting the interlocking of radiation from different parts of the atmosphere (which is caused by the double crossings of the constant velocity surfaces) changes the value of the source function very little. Quite clearly, the appearance of a shortward displaced absorption trough with an emission component on its longward side is not a unique signature for an envelope that is accelerating outward It is a signature for an envelope in which there is a large outward velocity in a region where the density of atoms/ions forming the line is large. Velocity laws of the type considered by Rybicki and Hummer can also produce very strong absorption features with little or no accompanying emission. None of the examples presented show a line profile that has a negligible absorption component. Marti and Noerdlinger (1977) reached similar conclusions.

Interpretation of the Hydrogen Line Profiles of P Cyg. Three attempts to interpret the strengths and shapes of Hα, Hβ, and Hγ in the spectrum of P Cyg have been made using modern theories of line formation in a moving atmosphere. The first is by Kuan and Kuhi (1975) who postulated an outflow velocity of -270 km s^{-1} near the photosphere and deceleration by gravity They neglected the interlocking with radiation from distant parts of the envelope when solving the radiative transfer problem. The second is by Van Blerkom (1978) who used the Sobolev approximation and a velocity law in which the velocity increased as r to a terminal velocity of 300 km s^{-1} and solved the equations of statistical equilibrium for a constant temperature atmosphere. The third is by Kunasz and Van Blerkom (1978) who solved the same problem by working in the comoving frame. All three studies result in profiles that look rather like the observed profiles of Hα, Hβ, and Hγ in P Cyg. The real question is how does one select between these possible representations for the atmosphere of P Cyg. (The observations for P Cyg are discussed in Chapter 4.)

A selection between the possible models might be made by attempting to represent simultaneously the profiles of several lines from more than one atom or ion However, this would not be a very practical undertaking unless one could establish from independent arguments based on physical reasoning a likely shape for the electron temperature and velocity distributions as a function of radius and a formula for calculating the local ionization and excitation balance.

One of the reasons why it is difficult to invert the observed profiles of lines formed in the winds from stars into a physical representation for the wind is that the only lines for which we have observations come from persistent and abundant atoms/ions Such atoms/ions are present in detectable abundance for a wide range of densities and electron temperatures and we have no sensitive way of telling from the line profile whether the material is concentrated close to the photosphere or whether it is at some distance. All methods of inverting observed line profiles to find the physical character of the atmosphere depend on the ability to localize the "effective place of formation" of a line. In the case of moving atmospheres this ability is greatly diminished because of the failure of the Eddington-Barbier relation.

Marti and Noerdlinger have pointed out that lines formed in a decelerating envelope show a very steep descent from the emission peak to the deepest point of the absorption component while the shortward edge of the absorption component rises somewhat slowly to the continuum. Since the reverse is true for resonance lines formed in an accelerating atmosphere (see Figure 6-5), attention to the exact shape of a P-Cygni profile may give information about the type of velocity gradient existing in an expanding spherical atmosphere. However, subordinate lines may behave differently (see Figure 6-6). In addition, one might study the relative displacements of lines of different

strengths as Karp (1978) has suggested.

Models to account for the profiles and displacements of the He I lines in P Cyg have been developed by Oergle and Van Blerkom (1976). Their conclusion is that acceleration outward is the only type of motion which will account for the fact that the weaker He I lines in the spectrum of P Cyg show lesser shortward displacements. Although the effective temperature and radius of P Cyg which Oergle and Van Blerkom adopt cannot be accepted now (see Chapter 4), the computations of Oergle and Van Blerkom do show that the relative displacements of He I lines of different strengths give important information about the velocity gradients in the spherical flowing atmosphere of P Cyg.

7

THE EVOLUTION OF MASSIVE STARS

INTRODUCTION

The observations of B stars summarized in Chapters 2, 3, 4, 5, and in Part II allow us to place the B stars in an observational HR diagram. In this chapter the intention is to summarize the results leading to predictions of theoretical HR diagrams and to compare theory and observation. By relating the observed B stars to the theory, one can tie the properties of these stars to those of other stars in a different mass range and obtain information on the overall pattern of stellar evolution.

The theory of the evolution of massive stars predicts how stars may change as their sources of internal energy change. We do not intend to review this theory critically. Rather we shall point out the chief assumptions underlying the relevant theoretical work and we shall intercompare theoretical results which are relevant to interpreting the significance of B stars in the scheme of stellar evolution Then we shall see how well the properties of the observed B stars agree with those of the model stars.

We are interested in models having masses in the range of 2 to 30 solar masses. Generally speaking, the mass of a model star determines the luminosity range in which the model star will lie. There are small changes of detail in the predicted HR diagrams when the underlying assumptions of the theory are modified, but these changes are not large. Model stars having masses of 30 $M_{\odot}$ reach luminosities in the range $\log L/L_{\odot} = 5.0$ to 5.5 as they move through the early stages of evolution, those having masses of the order of 2.25 $M_{\odot}$go through a range from $\log L/L_{\odot} = 1.5$ to 1.8 during the time in which they have effective temperatures in the range of the B stars. These two luminosity ranges for effective temperatures lying in the range 3.0×10^4 to 1.0×10^4 K, which is that spanned by the B stars, cover the luminosity range which is observed for normal B stars.

Here we are interested only in single stars and their evolution. We shall say nothing about evolution in binary systems with or without mass loss and exchange of mass. We are deliberately excluding this large topic from discussion since almost all of our data have been derived by analyzing the light from single stars. Likewise we are saying nothing about the evolution of model stars at late stages when, under certain circumstances, the model stars may traverse again the effective temperature range of the B stars. We note that theory indicates that some stars may have luminosities in the range of the luminosities of normal B stars as a result of moving along a "blue loop" in the HR diagram or of crossing on their way to the main sequence appropriate for helium stars. Nevertheless, we shall not explore this extensive field of investigation. Some stars with Bp spectra are suspected to belong to this latter group of hot stars. Model stars in such late stages of evolution may show changes in composition in their surface layers.

The goals of this chapter are three: (1) to summarize the hypotheses underlying theoretical studies of the evolution of massive model stars,

with and without mass loss; (2) to give the major results of studies of the evolution of massive model stars; and (3) to compare observed HR diagrams containing B stars with the predictions of theory and derive conclusions about the evolutionary state of real massive stars in the solar neighborhood.

The theoretical results concerning the evolution of massive stars without mass loss are summarized in the next section; those concerning evolution with mass loss are given in the section following the next, Evolution With Mass Loss. Finally, the results of theory and the observations are discussed and evaluated in the section, Discussion. In the section, Observed HR Diagrams for B Stars, observed HR diagrams are compared with the predictions, and some conclusions are drawn. The pulsational properties of massive model stars are reviewed briefly in the final section by Morris L. Aizenman.

EVOLUTION WITHOUT MASS LOSS

The evolution at constant mass of model stars having masses greater than $2\,M_{\odot}$ has been studied by several groups (see, for instance, Paczynski, 1970a, 1970b, 1971; Chiosi and Summa, 1970; and Robertson, 1972). We choose to review the work of Iben (1965, 1966a, 1966b, 1966c, 1967a), and Lamb et al. (1976), and of Stothers (1974) and Stothers and Chin (1975, 1976, 1977) because these groups work from similar assumptions, and by using their results we can span the mass range which is of interest for B stars. From the selected studies we shall extract information about the properties of the model stars while the model stars have effective temperatures in the range from about 3.0×10^4 to 1.0×10^4 K. The original papers should be consulted for detailed information on the numerical methods used and on the changing internal structure of the model stars as the models cross the HR diagram. We are not reporting information about the properties of the models when the models cross the B star region of the HR diagram while on a blue loop or during their descent to the region of the hot subluminous stars. This information can be found by reference to those papers which explore the evolution of massive stars during and after the phase of burning helium in the core. Helpful reviews of the theory of stellar structure as it applies to massive stellar models have been presented by Iben (1967b, 1974).

Hypotheses Underlying the Theory of Stellar Evolution

Model stars are assumed to be spherically symmetrical volumes of gas which initially have a uniform composition. This composition is described by giving the mass fraction, X, of hydrogen, Y, of helium, and, Z, of all other elements. The composition is altered as a function of radius as the nuclear reactions in the center of the star generate energy by burning first hydrogen and then helium to form heavier elements. The pressure structure is obtained by assuming hydrostatic equilibrium under the attraction of gravity. To find the temperature structure, the transfer of radiation through the model is handled in the diffusion approximation. However, under certain circumstances transfer of energy by convection can be as important as or more important than the transport of energy by radiation. Then to find the temperature structure of the model, the transport of energy must be formulated in such a way that a major part or all of the energy is transported by convection.

Just how to represent theoretically the transport of energy through a model star when conditions are such that convection may occur is a subject which is still under active study. Straightforward considerations (see Chandrasekhar, 1939; or Schwarzschild, 1958) show that the exact condition for stability against convection in a star is

$$-\frac{1}{\gamma}\,\frac{1}{P}\,\frac{dP}{dr} < -\frac{1}{\rho}\,\frac{d\rho}{dr}\,. \qquad (7\text{-}1)$$

Here γ is the ratio of specific heats c_p/c_v, P is the total pressure, and ρ is the density. The radial coordinate is r. Temperature, pressure, and density are related through the perfect gas law. For a layer to be stable against convection, the actual temperature gradient must be lower in absolute

amount than the adiabatic temperature gradient.

In early studies of convection in astronomical bodies, by K. Schwarzschild (1906), for instance, the gas was considered to have a constant mean molecular weight throughout the body. Then, if $\gamma = 5/3$, which is appropriate for a monatomic gas, the condition that the gas will be stable against convection is such that the actual temperature gradient must be less than or equal to the adiabatic gradient:

$$\frac{d \log T}{d \log P} \leq \left(\frac{d \log T}{d \log P}\right)_{ad} = \frac{2}{5} . \qquad (7\text{-}2)$$

This is the Schwarzschild criterion.

However, in a model star where the composition in the core is changing as the result of nuclear reactions, convection will mix the unprocessed material of the envelope with the processed material of the core. A gradient in mean molecular weight develops for model stars with $M \geq 10\, M_{\odot}$. Ledoux (1947) considered this question and pointed out that then an appropriate relationship for a monatomic gas having $\gamma = 5/3$ would be

$$\frac{d \log T}{d \log P} \leq \frac{2}{5} + \frac{d \log \mu}{d \log P} . \qquad (7\text{-}3)$$

Here μ is the mean molecular weight of the gas. This is the Ledoux criterion for stability against convection.

More recent studies of the problem are concerned with how to represent the gradients explicitly in terms of the gas and radiation present in each layer of the model and how to handle the transport of energy when energy is transported both by convection and by radiation (see Ledoux, 1965 for a review of basic theory).

For those regions of the model star where radiative transfer is important for transporting energy, the efficiency of the transport depends on the opacity of the stellar material to radiation. Thus, knowing the opacity of mixtures of gas having stellar composition as a function of temperature and pressure is a necessary first step to model making. Two sets of stellar opacity tables have been used for massive model stars and they are described in the next subsection.

Opacity Tables

The most frequently used opacity tables are those developed by Cox and Stewart (1965, 1970) and Magee et al. (1974). In these tables, the opacity is calculated on the basis of a "hydrogenic" model of the atom. Although the "hydrogenic" model is satisfactory for the abundant elements H and He, it is not particularly satisfactory for the next most abundant elements C, N, and O. Therefore Carson and Hollingsworth (1968) and Carson et al. (1968) began studies to improve the physics behind the opacity tables. Carson et al. explored the use of a "Thomas-Fermi" model for the atom. The various approaches to developing opacity tables suitable for making models of stars have been described by Carson (1976). Carson has prepared opacity tables using revised theory and he has made these new tables available to Stothers and others.

The physics used by Carson has been reexamined by the Los Alamos group and according to Cox (private communication), the principles that were used by Carson and his colleagues have been confirmed. However, the Los Alamos group has not been able to reproduce the values of the Carson opacity coefficients in the density regions where the Carson and the Cox-Stewart opacities differ most widely. The Los Alamos group obtains results which are closely similar to the Cox-Stewart opacities throughout the density and temperature range which is relevant for making models of early type stars.

Stothers (1974) has noted that the Carson opacities are similar to the Cox-Stewart opacities except at the extremes of high and low density. At densities such as are relevant for making models of the envelopes of stars with masses greater than about $15\, M_{\odot}$, the Carson opacities are larger than the Cox-Stewart opacities. Here we shall report the results of using the Carson opacities because this work forms a valuable numerical experiment showing how sensitive the results of stellar evolution are to underlying

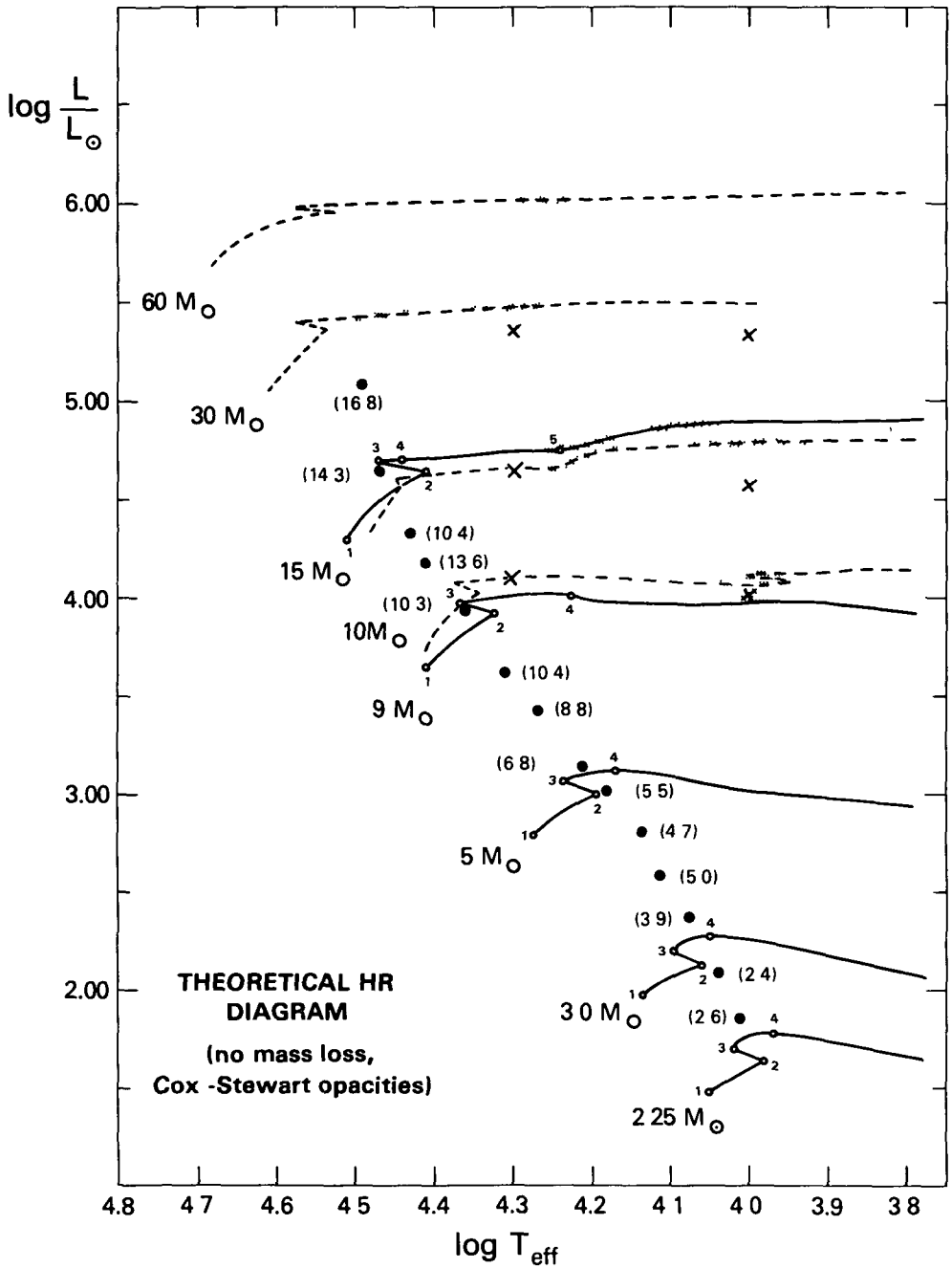

Figure 7-1. Theoretical evolutionary tracks for model stars having masses in the range 2.25 to 60 $M_\odot$. Cox-Stewart opacities are used. The Schwarzschild criterion is used for handling convection. Tracks due to Stothers and Chin (1976) are shown by broken lines, those due to Iben (1965, 1966a, 1966b, 1966c, 1967a) are shown by full lines. Crosses (X) mark where tracks computed by Stothers and Chin (1975) using the Ledoux criterion cross the supergiant range. Gray shaded areas show where the B-type supergiants are found. Typical average main-sequence stars are represented by filled circles, typical masses being given in parentheses near the point. The models of Stothers and Chin have a composition (0.739, 0.021); those of Iben have (0.708, 0.020).

assumptions such as the value of the stellar opacity.

Theoretical HR Diagrams for Massive Model Stars

The precise position of an evolutionary track for a model star in a theoretical HR diagram is a function of the choice which is made concerning opacity tables. We shall report the results from two different choices for opacity tables

Models Made with Cox-Stewart Opacities. Evolutionary tracks for model stars having masses of 2.25, 3, 5, 7, 9, and 15 $M_{\odot}$ have been published by Iben (1965, 1966a, 1966b, 1966c, 1967a) Lamb et al. (1976) have published tracks for models having masses of 15 and 25 $M_{\odot}$ Stothers and Chin (1976) have published comparable models for M = 10, 15, 30, and 60 $M_{\odot}$. In all these models the Schwarzschild criterion is used for determining when instability against convection occurs.

The evolutionary tracks for Iben's models with an initial composition (X, Z) of (0.708, 0.020) and Stothers and Chin's with an initial composition of (0.739, 0.021) are shown in Figure 7-1 for the range $4.8 < \log T_{\rm eff} < 3.8$. In the case of a few of the models, a blue loop enters the part of the HR diagram displayed here, but we have suppressed such loops. Blue loops may occur at later stages of evolution than we are emphasizing, but they are not important for understanding stars in their early stages of evolution. The position of a blue loop in the HR diagram is sensitive to the precise manner in which the model is constructed. Reference should be made to the original papers for information on this point.

The position of the nearly horizontal part of the evolutionary track is sensitive to the formulation which is used to handle convection in the model star. Stothers and Chin (1975) have studied stellar evolution at constant mass using the Ledoux criterion. A cross indicates, for the models with M = 10, 15, and 30 $M_{\odot}$, where the track lies at the moments that $\log T_{\rm eff} = 4.0$ and 4.3. Typically, use of the Ledoux criterion causes the track to move across the HR diagram at somewhat lower luminosities than what are found when the Schwarzschild criterion is used.

Numbers have been placed at several places on the tracks computed by Iben, the solid lines in Figure 7-1. They indicate where key changes occur in the energy generation scheme of the models. Between points 1 and 2, the energy is generated by burning hydrogen in the core of the star. Between points 2 and 3, overall contraction of the star and the last stages of core hydrogen burning occur, while between points 3 and 4, burning of hydrogen in a thick shell becomes established. In the models with $M \leq 9\ M_{\odot}$ helium burning in the core of the star does not begin until later phases than those shown here. Reference to Iben's papers gives much information on what is occurring. In Iben's model with M = 15 $M_{\odot}$, hydrogen burning in a shell source begins at about point 4. Helium burning in the core begins at about point 5.

Improved models for M = 15 $M_{\odot}$ and M = 25 $M_{\odot}$ have been calculated by Lamb et al. (1976). The evolution has been followed until carbon burning is established. The first stages of evolution of these massive models are shown in Figure 7-2. Here the area in the HR diagram observed to be occupied by B-type supergiants is shown by gray shading. Points A indicate the end of core hydrogen burning, while points B and C mark the beginning and ending of core

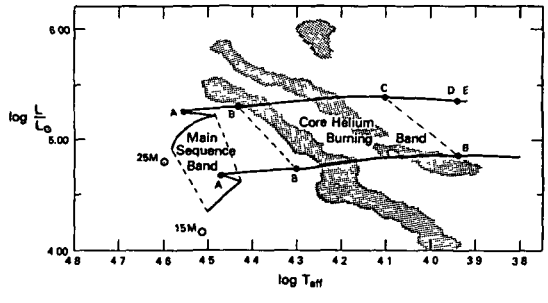

Figure 7-2. Evolutionary tracks for massive stars from Lamb et al. (1976). The observed area occupied by B-type supergiants is shown by gray shading. For an explanation of the significance of the letters A through E, see the text. The composition of the models is (0.70, 0.02).

helium burning. Points D and E mark the beginning and ending of core carbon burning. In the case of the 15 $M_\odot$ model star, carbon ignition takes place as the model becomes a red supergiant. The blue supergiants are expected to lie in the area marked out by the points BBCB'. The position of the main-sequence band is the area included between the starting points of the tracks and the first sharp inflection point when overall contraction begins as the model moves toward point A where the end of core hydrogen burning occurs.

Some observational data are shown in Figures 7-1 and 7-2 in order to give a quick impression of where B stars are observed to lie in the HR diagram. The filled points are representative for a typical luminosity class IV or V star. They have been found by using the average effective temperature given for each spectral class in Table 3-5 and the typical average radii given in Table 2-12. The typical mass for each spectral type, from Table 2-11 is noted in parentheses. The average effective temperatures and radii are found from data from single stars; the typical masses are from spectroscopic binaries.

The luminosity for each point has been calculated from the relation

$$\log L/L_\odot = 4 \log T_{\text{eff}} + 2 \log R/R_\odot - 15.045. \qquad (7\text{-}4)$$

This assumes that T_{eff} for the Sun is 5.77×10^3 K.

The areas occupied by the supergiants of Table 4-1 are shown by gray shading. A clear separation of the areas for Ib, Ia and Ia+ stars occurs because the distances given in Table 4-1, and hence the linear radii of the stars, have been found by adopting the absolute magnitude calibration for B-type supergiants given in Table 2-7. The B1 Ia+ stars are assumed to have M_V in the range 8.3 ± 0.5 mag.

The uncertainty in $\log L/L_\odot$ which arises from uncertainties in M_V and in T_{eff} is

$$\Delta \log L/L_\odot = 0.4\, \Delta M_V - 0.4 \frac{\partial B.C.}{\partial T_{\text{eff}}} \Delta T_{\text{eff}}. \qquad (7\text{-}5)$$

The second term on the right-hand side of Equation (7-5) is negligible in comparison to the first term. This can be seen from the work of Buser and Kurucz (1978). Since ΔM_V is typically ± 0.5 mag for B-type supergiants, one may expect an uncertainty of the order of ± 0.20 associated with the value of $\log L/L_\odot$ for each supergiant. The uncertainty in $\log L/L_\odot$ for the points representing the average observed main sequence is probably about half this value. The uncertainty in T_{eff} is typically of the order of 5 percent; thus, typically $\Delta \log T_{\text{eff}}$ is about ± 0.02.

Models Made With Carson Opacities. Evolutionary tracks for massive model stars have been prepared by Carson and Stothers (1976) and by Stothers and Chin (1977) using the Carson opacities and the Schwarzschild criterion for convection. Some are displayed in Figure 7-3; they have a composition of (0.71, 0.03). The same observational data are displayed here, for orientation purposes, as are shown in Figure 7-1. Full evolutionary tracks for model stars with masses less than 5 $M_\odot$ have not been published. Stothers (1974) has published the initial points (ZAMS) for some low mass models made with Carson opacities. Some of these points are shown by plus signs in Figure 7-3.

The evolutionary tracks selected for display in Figures 7-1, 7-2, and 7-3 have been chosen because they have nearly the same initial composition and because they all use the same criterion, the Schwarzschild criterion, for convection. Somewhat different numerical methods and representations of the nuclear reactions in the core of the star are used in the various studies which have produced these tracks. What has been used can be found out by reference to the original papers. Since we know that the mean molecular weight of the various layers of the star must change as the evolution of the star proceeds and convection mixes the unprocessed envelope with the core in the case of stellar masses $\geq 10\, M_\odot$, it might seem more logical to display evolutionary

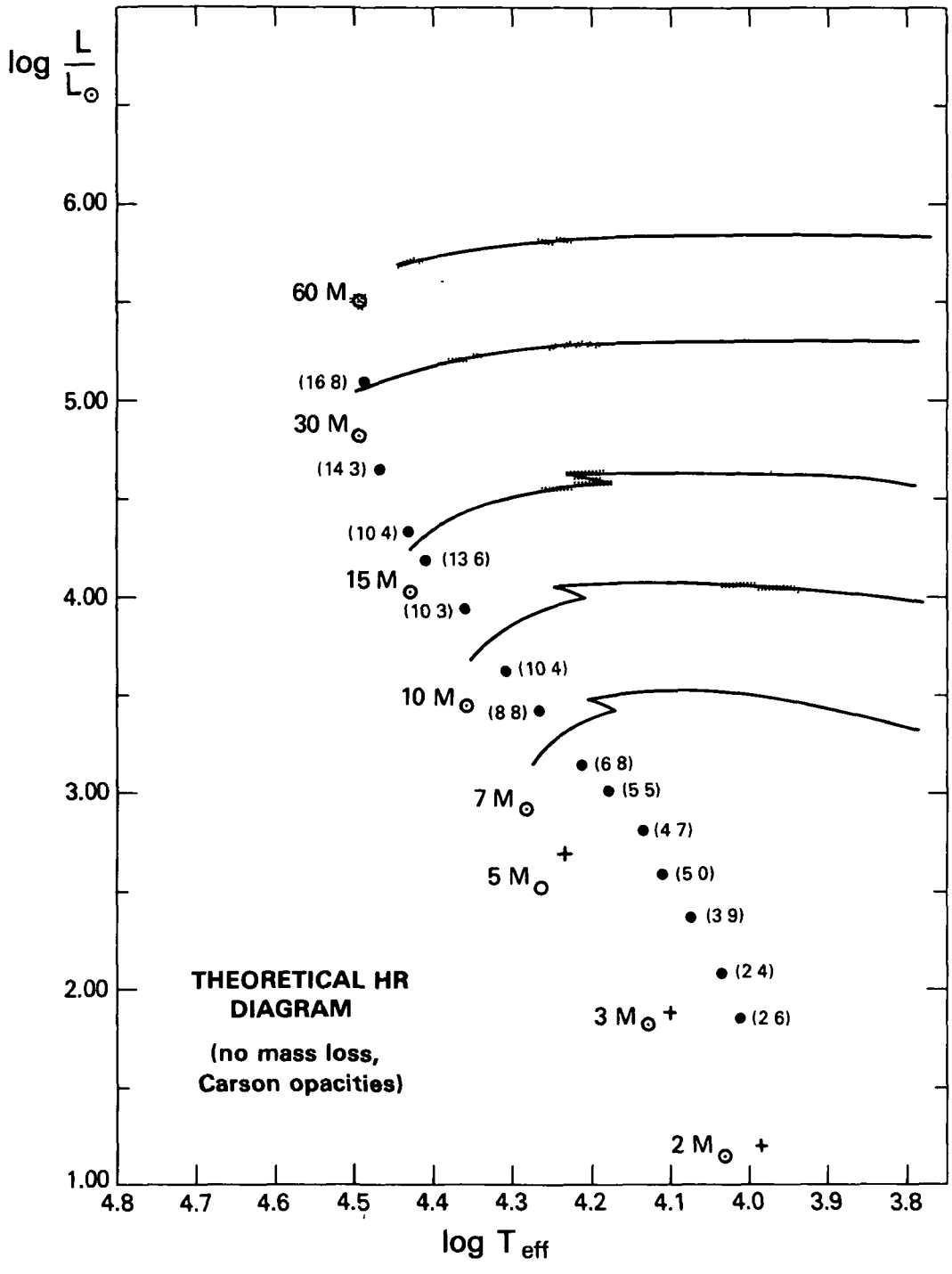

Figure 7-3. Theoretical evolutionary tracks computed by Stothers and Chin (1977) for model stars having masses in the range 7 to 60 $M_\odot$. Carson opacities and the Schwarzschild criterion for convection are used. The composition of the models is (0.71, 0.04). The initial positions (Stothers, 1974) of comparable models having masses of 2, 3, and 5 $M_\odot$ are shown by plus signs; these models have a composition which is (0.739, 0.021) The observational data are the same as that shown in Figure 7-1.

tracks made using the Ledoux criterion than those we have shown. However, the Schwarzschild criterion is more generally used. In the case of models with $M < 10\ M_{\odot}$, the tracks are the same whichever criterion is used for convection.

Helium Stars. A theoretical HR diagram for helium star models during the main phase of core helium depletion has been presented by Stothers (1976). Here Stothers gives the helium zero-age main sequence and the terminal-age main sequence (TAMS) for both Cox-Stewart and Carson opacities. These calculations are not of interest for interpreting the positions of B stars in the HR diagram because even for a mass as low as $1\ M_{\odot}$, the effective temperature of the model star is greater than 4.0×10^4 K. This puts the models into class O.

Schönberner (1977) has discussed the positions in the HR diagram of hydrogen-deficient stars having effective temperatures in the B-star range. These stars are believed to be remnants of stars which have evolved past the stage of being red giants. They evolve rapidly through the effective temperature range of B stars, in a matter of 2000 to 2500 years. Their masses appear to be less than $1\ M_{\odot}$.

Discussion

We have noted above that when Cox-Stewart opacities are adopted, use of the Ledoux criterion for handling convection will cause a change in where the evolutionary tracks of stars with masses greater than $10\ M_{\odot}$ cross the HR diagram during the stages of hydrogen burning in a shell and helium burning in the core. These tracks cross at lower luminosities than are predicted by use of the Schwarzschild criterion for convection. This crossing is shown in Figure 7-1. Similar results are found for models constructed using the Carson opacities (see Stothers and Chin, 1977).

Comparison of the tracks presented in Figures 7-1 and 7-3 makes clear the main effects of changing the composition and the opacity tables. Stothers (1976) has discussed this subject. To begin with, in the cases we show, the starting point for each mass occurs at a less luminous point and for lower $T_{\rm eff}$ in Figure 7-3 (Carson opacities and composition, 0.71, 0.04) than in Figure 7-1 (Cox-Stewart opacities and composition, 0.739, 0.021). The difference in luminosity, $\Delta \log L/L_{\odot}$ ranges from about 0.1 at $M = 3\ M_{\odot}$ to about 0.0 at $M = 60\ M_{\odot}$. The greatest difference is in $\log T_{\rm eff}$, the Carson-opacity models beginning at lower $T_{\rm eff}$ than do the Cox-Stewart opacity models. At $3\ M_{\odot}$ the difference is about 0.03, but by $M = 15\ M_{\odot}$ the difference has increased to 0.05. By $M = 60\ M_{\odot}$ the difference is 0.20. These are about the largest differences that can be expected. When models of the same composition are rigorously compared (see Stothers, 1974), the differences are smaller.

The most important difference between models constructed with the Cox-Stewart opacities and those with the Carson opacities is in the energy generation processes which occur in the core for a model of a selected mass. For a given mass, the inflection points on the tracks which mark the beginning of overall contraction, points 2 on the tracks due to Iben, are found at lower effective temperatures and slightly fainter luminosities when the Carson opacities are used than when the Cox-Stewart opacities are used. For the Carson opacity models with $M = 30$ and $60\ M_{\odot}$, no inflection point is reached over the range in $\log T_{\rm eff}$ shown here. Throughout the O and B star range of effective temperature, massive models (those with $M \geq 20\ M_{\odot}$) constructed with the Carson opacities are burning hydrogen in their cores. Figures 7-1 and 7-2 show that when Cox-Stewart opacities are used, core hydrogen burning stops for models with $M \geq 20\ M_{\odot}$ when $\log T_{\rm eff}$ is still high. The burning of helium in the core has been completed by the time a $25\ M_{\odot}$ model star has crossed the region of the B-type supergiants (see Lamb et al., 1976).

The relatively large values for stellar opacity given by the Carson tables for the densities and temperatures which occur in the envelopes of model stars with $M \geq 15\ M_{\odot}$ cause the radii of these models to expand rapidly. This has the result that massive model stars made with the Carson opacities do not reach the stage of helium burning in their cores until they have reached

low effective temperatures. With use of the Carson opacities, there is an upper limit to the effective temperature which a massive model may attain on the zero-age main sequence (see Figure 7-3) This corresponds to about $\log T_{eff} = 4.5$ or $T_{eff} = 3.2 \times 10^4$ K The value of the maximum T_{eff} is very sensitive to the choice of chemical composition and of convective mixing length in the CNO convection zone which is present for these massive model stars. With the Cox-Stewart opacities, the effective temperature when the model is on the ZAMS continues to increase as the mass of the model increases (see Figure 7-1).

In Figure 7-1, the points representing "average" main-sequence stars tend to fall to the right of the main-sequence band, particularly for stars having masses less than 10 $M_\odot$. In the case of the Carson opacities (Figure 7-3), the observed "average" points fall near the theoretical ZAMS, particularly when $M \geq 10\ M_\odot$. The observations are compared in detail with the predictions in the section on Observed HR Diagrams for B Stars. One aim of that discussion will be to decide whether or not the observations of B-type stars give any guidance on the question of which theoretical representation of the evolution of massive stars is the most satisfactory one. Before discussing the observations further, however, we wish to summarize the theoretical results on evolution with mass loss.

Stothers (1976) has compared the properties of the model stars constructed with Carson opacities with those of models constructed with Cox-Stewart opacities. The models made with Carson opacities, in particular those having $L/M > 10^3$ solar units, show a very large central condensation and a high radiation pressure in the envelope. Convective instability occurs in the CNO ionization zone and pulsational instability is generated via the κ-mechanism. Stothers has warned that the problem of convection and its interaction with pulsation has so far been solved only in a crude way and that the results obtained are quite sensitive to the adopted choice of metals abundance and the convective mixing length. This means that the positions of the evolutionary tracks for massive stars in the area to the right of the main-sequence band of the Cox-Stewart opacity models (the region to the right of the line joining the points numbered 2 in Figure 7-1) are quite model dependent. This makes it precarious to derive masses for B-type supergiants by relating their positions in the HR diagram to particular evolutionary tracks.

The calculations of Stothers and Chin (1976, 1977) show that models of massive stars passing through the same part of the HR diagram may differ greatly in their internal structure and in the energy generation process which is active. The internal state of the model depends upon what is adopted for the stellar opacity. For instance, when the mass is about 30 $M_\odot$ and Cox-Stewart opacities are used, a model passing near the point $\log L/L_\odot = 5.5$, $\log T_{eff} = 4.4$ is burning helium in its core. The track passing through the same point in an HR diagram which has been calculated with Carson opacities would require a mass equal to about 50 $M_\odot$ and the model star would be burning hydrogen in its core. One has to be sure from other information than the position of the star in the HR diagram what is the correct representation for the stellar opacity as a function of temperature and pressure before one can make reliable deductions about the source of energy in the center of a massive star and the internal structure of such a star. The problem is less acute for stars having masses less than 10 $M_\odot$.

The length of time spent burning hydrogen in the core by massive model stars is a fairly consistent result of the theory. Some results for the case that the Schwarzschild criterion is used for convection are given in Table 7-1. The composition of the models by Iben (1965, 1966a, 1966b, 1966c, 1967a) is (0.708, 0.20). For the selected models of Stothers and Chin (1976) the composition is (0.739, 0.021) while for those of Stothers and Chin (1977) the composition is (0.730, 0.20). For the models of Lamb et al. (1976), the composition is (0.700, 0.20). The composition has a small effect on the result attained.

The evolution goes much faster once the models begin overall contraction and proceed to burning hydrogen in a shell and then to burning helium in the core. Stothers and Chin (1975,

Table 7-1
Lifetimes During Hydrogen Burning in the Core

$M/M_\odot$	Cox-Stewart Opacities[a] (τ_H in years)		$M/M_\odot$	Cox-Stewart Opacities[b] (τ_H in years)		Carson Opacities[c] (τ_H in years)	
2.25	4.97	+8	7	–	–	4.37	+7
3.0	2.31	+8	10	2.13	+7	2.27	+7
5.0	6.77	+7	15	1.20	+7	1.27	+7
9.0	2.20	+7	20	–	–	8.90	+6
15.0	1.03	+7	30	6.10	+6	5.99	+6
25.0	5.99	+6	60	3.83	+6	>3.10	+6

[a]Iben (1965, 1966a, 1966b, 1966c, 1967a); Lamb et al. (1976).
[b]Stothers and Chin (1976).
[c]Stothers and Chin (1977).
Dash (–) represents no existing data at these values; the lifetimes are given in floating point notation.

1976, 1977) have shown that the lifetime for burning helium is of the order of 0.1 to 0.15 times the hydrogen burning lifetime, the precise result depending on the composition of the model and the procedures adopted for handling convection.

The numbers given in Table 7-1 indicate that the hydrogen burning lifetimes of B stars may range from about 10^7 years for stars with masses near 16 $M_\odot$ to about 5×10^8 years for stars with masses near 2.25 $M_\odot$. What the choice for opacity coefficients is makes little difference to this result. The calculations of Stothers and Chin (1975) for the case of Cox-Stewart opacities and the Ledoux criterion for convection give τ_H = 2.11×10^7, 1.19×10^7, and 5.76×10^6 years for model stars having masses of 10, 15, and 30 $M_\odot$, respectively. These results are similar to those obtained with the Schwarzschild criterion.

EVOLUTION WITH MASS LOSS

The question of how mass loss changes the evolutionary track of a massive model star which has an inhomogeneous internal structure was first investigated by Tanaka (1966). He investigated the effects of mass loss at a constant rate. Tanaka's purpose was to try to understand the meaning of the observed distribution in the HR diagram of the luminous stars of the open clusters h and χ Persei. This distribution is not what is expected from the information available to Tanaka about the evolution of massive model stars at constant mass. Tanaka was able to demonstrate the major effects of mass loss on the evolution of massive model stars. These effects have been recovered by all later, more specialized, studies of this subject.

Tanaka's basic conclusions were that compared with a star which evolves without mass loss, a massive mass losing star at the same stage of central hydrogen depletion has a lower luminosity and a lower effective temperature. In the mass losing star there is increased stability against convection in the envelope, and a larger fraction of the mass is in the convective core than is the case for a star evolving without mass loss. The hydrogen burning lifetime of the model mass losing star is increased over that of a model star evolving without mass loss. Subsequent work on mass loss has verified and expanded all of Tanaka's conclusions.

Here we shall review the most recently published results of the major groups which have

studied the evolution with mass loss of massive, single stars. A compact summary of the historical development of the subject can be found in Stothers and Chin (1979). The chief difference among the published papers concerns the manner in which the rate of mass loss is related to the instantaneous luminosity, radius, and mass of the evolving star. All but one study use the Cox-Stewart opacities; convection is usually handled by means of the Schwarzschild criterion.

The evolution of stars of 20 and 40 $M_\odot$ was followed by Chiosi and Nasi (1974) for the case that the rate of mass loss follows the relation suggested by McCrea (1962), namely

$$\dot{M} = -kLR/M. \tag{7-6}$$

Here L, R, and M are the instantaneous values for the luminosity, radius, and mass of the star. Chiosi and Nasi chose the scaling constant, k, so that $\dot{M}$ on the main sequence is about $10^{-6}\ M_\odot$ yr^{-1}. The composition of their models is (0.602, 0.044).

A group led by de Loore has concentrated on what occurs if the rate of mass loss varies as

$$\dot{M} = -NL/c^2. \tag{7-7}$$

Here N is a scaling factor which is constant for any evolutionary sequence. From a study of the observed rates of mass loss from B-type supergiants de Loore et al. (1977) suggest that N = 100 may be appropriate for B-type supergiants. They investigate evolutionary tracks for models having masses of 20, 25, 30, 40, and 50 $M_\odot$. The composition is (0.70, 0.03). This type of study has been continued by de Loore et al. (1978) for models having masses of 50, 60, 80, and 100 $M_\odot$. Such model stars have higher effective temperatures than are observed for B stars.

Sreenivasan and Wilson (1978a, 1978b) have investigated the evolution of a rotating model star having a mass of 15 $M_\odot$. They paid attention to the effects of losing angular momentum as well as mass and to what occurs when allowance is made for semiconvection. Sreenivasan and Wilson studied the case when the rate of mass loss is given by

$$\dot{M} = -\epsilon L/u_{esc}c. \tag{7-8}$$

Here ϵ is an efficiency factor which depends on the instantaneous effective temperature of the star and on the luminosity through the relations

$$\log \epsilon = -a + 8.0 \log (T_{eff}/10^4), \tag{7-9}$$

and

$$a = 5.7 - 6.0 \log (L/L_\odot). \tag{7-10}$$

Sreenivasan and Wilson also explored the effect of mass loss according to a formulation developed by Castor et al (1975) for a radiatively driven wind. In this case

$$\dot{M} = -\left(\frac{L}{cu_{th}}\right)\left(\frac{\alpha}{\Gamma}\right)\left(\frac{1-\alpha}{1-\Gamma}\right)^{(1-\alpha)/\alpha} (K\Gamma)^{1/\alpha}. \tag{7-11}$$

Here c is the speed of light, u_{th} is the thermal velocity in the photosphere of the star, and Γ is the ratio of the instantaneous luminosity of the star to the Eddington luminosity. Thus,

$$\Gamma = \sigma_e L/4\pi GMc, \tag{7-12}$$

where σ_e is the value of the electron scattering coefficient in the photosphere, G is the gravitational constant, and M is the mass of the star. In Equation (7-11), α and K are assigned constants. Sreenivasan and Wilson published cases with K = 0.076, a choice which they justify by reference to the work of Castor et al. (1975), and α having values of 0.88 and 0.99. Their models have a composition of (0.70, 0.03). It is assumed that the rate of mass loss during the red giant stages of evolution is proportional to the amount of acoustic energy generated in the convective zone. Sreenivasan and Wilson found that low to moderate rates of mass loss in the early evolutionary phases do not radically alter the evolution of a 15 $M_\odot$ star. Rotation, at most, increases $\dot{M}$ by about 20 percent in the early stages of evolution.

Chiosi et al. (1978) have explored the evolution of models having masses of 20, 30, 40, 60,

80, and 100 $M_\odot$, an initial composition of (0.70, 0.02) and rate of mass loss given by Equation (7-11). They adopt the value 0.04 for K and present results for α = 0.76, 0.83, and 0.90. During the red giant stage of their models, the rate of mass loss is proportional to the acoustic energy generated in the convection zone. According to Paerels et al. (1980), a numerical error occurred in the work of Chiosi et al. (1978) so that in effect they used K = 0.014.

Dearborn et al. (1978) and Dearborn and Blake (1979) have investigated stellar evolution for the case that

$$\dot{M} = \zeta\phi(T)LR/M. \qquad (7\text{-}13)$$

Here ζ is a scaling factor, and $\phi(T)$ is a function designed to make the mass losing process more efficient for hot stars than for cool stars. Dearborn and associates put

$$\phi(T) = (\pi/\sigma_R T_{eff}^4)\int_0^{2200\text{Å}} B(\lambda,T_{eff})d\lambda. \qquad (7\text{-}14)$$

Here $B(\lambda,T_{eff})$ is the Planck function and σ_R is the Stefan-Boltzmann constant.

Dearborn and his associates have investigated models of 15, 30, and 60 $M_\odot$ having the composition (0.732, 0.02). They explore values of ζ such that the rate of mass loss is larger than is observed for early type main-sequence stars. They are particularly interested in the effects of an initially large rate of mass loss.

Stothers and Chin (1978, 1979) have investigated the evolution of stars of masses 15, 30, and 60 $M_\odot$ for the case that the mass loss starts on the main sequence and is given by Equation (7-6). In the first paper they use Carson's opacities and a composition of (0.71, 0.04); they explore cases with $k = 1 \times 10^{-11}$. In the second paper they use the Cox-Stewart opacities and a composition of (0.739, 0.021). They present results for $k = 1 \times 10^{-11}$ and 3×10^{-11}. These values of k are for L, R, and M in solar units. Stothers and Chin also explore what happens when mass loss takes place only when log T_{eff} < 3.85, that is only when the model is representative for a late type supergiant.

The Effects of Mass Loss on the Evolution of Massive Stars

Evolutionary tracks with mass loss calculated by Stothers and Chin (1979) are shown in Figure 7-4 for model stars having initial masses of 15 and 30 $M_\odot$. Each track is labeled with the value of the scaling constant, k, which is used. Gray shading shows the area occupied by the evolutionary tracks with mass loss calculated by de Loore et al. (1977) and by Chiosi et al. (1978) for models of 30 $M_\odot$. All of the tracks have been computed using the Cox-Stewart opacities. Broken lines outline the areas in the HR diagram observed to be occupied by the B-type supergiants of Table 4-1.

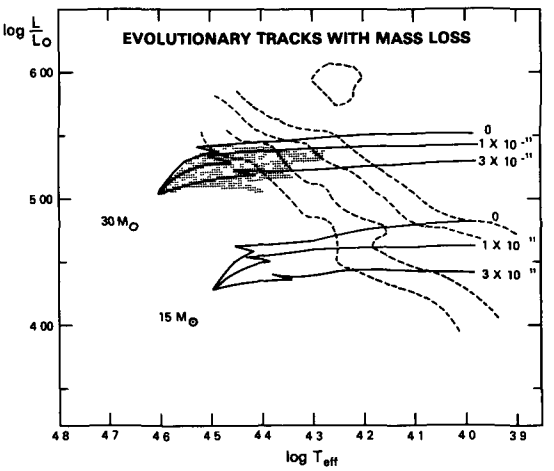

Figure 7-4. Evolutionary tracks computed by Stothers and Chin (1979) for the case of mass loss varying as LR/M. Cox-Stewart opacities and the Schwarzschild criterion for convection are used. The composition is (0.739, 0.021). Each track is labeled with the scaling factor, k, used to find the instantaneous rate of mass loss. The gray shading indicates the area occupied by the evolutionary tracks of Chiosi et al. (1978) and of de Loore et al. (1978) for the evolution of a 30 $M_\odot$ star which is losing mass. See the text for the expressions these authors use to evaluate the instantaneous rate of mass loss.

Table 7-2
Rate of Mass Loss, $\dot{M}$, in Units of $10^{-6}\ M_{\odot}\mathrm{yr}^{-1}$ at Various Stages of Evolution of the Models

	SC(1979)[a]		
$M/M_{\odot}$	Point on Track	$\dot{M}$	$\dot{M}$
15	ZAMS	0.0619	0.186
	1st inflection	0.220	0.483
	2nd inflection	0.198	0.464
	log T_{eff} = 4.3	0.444	0.667
	log T_{eff} = 4.1	1.15	1.92
30	ZAMS	0.258	0.773
	1st inflection	1.16	3.01
	2nd inflection	1.11	2.84
	log T_{eff} = 4.3	3.45	5.86
	log T_{eff} = 4.1	9.46	15.8

	dL + (1977)[b]		CNS (1978)[c]	
$M/M_{\odot}$	N	$\langle\dot{M}_{\mathrm{MS}}\rangle$	Stage	$\dot{M}$
20	100	0.3	ZAMS	0.20
	300	0.8	B	0.45
	500	1.8	C	0.52
30	100	0.8	ZAMS	0.63
	300	2.0	B	1.4
	500	2.7	C	1.5

[a] Stothers and Chin (1979); first column is for $k = 1 \times 10^{-11}$, second column for $k = 3 \times 10^{-11}$.
[b] de Loore et al. (1977). The value of N indicates the case reported. An average $\dot{M}$ is given for the time the model star is in the main-sequence band
[c] Chiosi et al. (1978). Results are given for the case $\alpha = 0.83$, $K = 0.04$. Stage B is at the lowest effective temperature (1st inflection point); Stage C is when central hydrogen has been exhausted.

Two conclusions can be reached immediately (1) During the early stages of evolution, that is during the phase in which hydrogen is burned in the core as well as a little later, the same area in the HR diagram is traversed by the models no matter which formulation is used for finding the instantaneous rate of mass loss, and (2) unless one know the appropriate formulation for the

rate of mass loss as a function of the evolutionary stage of the star, one cannot accurately deduce the mass of a B-type supergiant from the observed position of the supergiant in the HR diagram. The same position can be traversed by models having different masses and different formulations for $\dot{M}$ as a function of L, R (or T_{eff}), and M.

The formulation for $\dot{M}$ used by Stothers and Chin (Equation 7-6) implies the rates of mass loss which are given in Table 7-2 for several points on the tracks calculated by Stothers and Chin. Representative values of the rates of mass loss found by de Loore et al. (1977) and by Chiosi et al. (1978) are also given in Table 7-2. Over the area in the HR diagram covered by all the studies, that for the case $M = 30\ M_{\odot}$ and $4.3 < \log T_{\text{eff}} < 4.6$, the theoretical rates of mass loss are of the same order of magnitude from all the studies. Typically with a $30\ M_{\odot}$ model star, $\dot{M}$ is about $5 \times 10^{-7}\ M_{\odot}\ \text{yr}^{-1}$ on the ZAMS and it increases as the star evolves. For less massive model stars, $\dot{M}$ is smaller. The values of $\dot{M}$ given in Table 7-2 are compared with the observed rates of mass loss later. Stothers and Chin (1980) have explored the effects of composition, of the method of handling convection, and of mass loss on the evolution of a model star of $30\ M_{\odot}$. The effects of mass loss are insignificant when compared with the effects of the uncertainties in the evolutionary track introduced by lack of knowledge of the mass, composition of a real star, and treatment of convection.

OBSERVED HR DIAGRAMS FOR B STARS

To obtain an observed HR diagram for B stars, one must find $\log L/L_{\odot}$ and $\log T_{\text{eff}}$ for each star from observations.

An HR Diagram from Effective Temperatures and Radii

When theoretical evolutionary tracks in the HR diagram are to be compared with observation, we must use an observational HR diagram that is based on effective temperatures that represent the total energy stream which is generated in the star by nuclear reactions and by contraction. Such an observational HR diagram is presented in Figure 7-5. Here the positions of 164 apparently bright O and B stars, the mean position of 5 Wolf-Rayet stars, the position of P Cyg, and the position of α Lyr are shown. This figure is from Underhill (1980a). To prepare it, luminosities were found using Equation (7-4); use was made of the effective temperatures and radii of the 160 stars studied by Underhill et al. (1979) as well as the effective temperatures and radii of κ Cas, ρ Leo, HD 190603, and P Cyg given by Underhill (1979b). The data for the Wolf-Rayet stars HR 50896, HD 165763, HD 191765, HD 192103, and HD 192163, and for α Lyr are from Underhill (1980a). In each of these cases, the effective temperature has been determined from an integrated flux and an angular diameter.

The significance of the observed positions in the HR diagram of O and Wolf-Rayet stars is discussed in *O, Of, and Wolf-Rayet Stars* by Underhill and Divan (to be published). We merely note here that Wolf-Rayet stars of types WN5, WN6, WC6, and WC8 lie in the area occupied by the B0 III stars. Underhill (1981a) has shown that three WN7 stars and one WN8 star lie in the area occupied by the B0 Ia stars.

The stars which appear in Figure 7-5 are apparently bright, thus they lie relatively close to the Sun and their distances are well known in most cases. The adopted distance to each star is an important factor in determining the accuracy of $\log L/L_{\odot}$ (see Equation 7-5). The evidence regarding the distance of each star was reviewed carefully by Underhill et al. (1979). Typically for the 140 main-sequence stars studied by Underhill et al. (1979) the uncertainty in M_V is about ±0.3 mag. In the case of the 20 supergiants studied by Underhill et al. (1979), the uncertainty may be larger, but probably it is not more than ±0.4 mag. Thus, typically, the uncertainty in $\log L/L_{\odot}$ of each point in the main-sequence band is ±0.12; for supergiants the uncertainty in $\log L/L_{\odot}$ may lie in the range ±0.16 to ±0.20. The uncertainty in $\log T_{\text{eff}}$ is much smaller. Typically it is ±0.02.

Information concerning $\log T_{\text{eff}}$ and $R/R_{\odot}$ is given for additional B-type supergiants in Table

4-1. This information allows us to delineate the gray shaded areas in Figures 7-1, 7-2, and 7-3. These are the areas observed to be occupied by B-type supergiants. Roughly speaking, the Ib and Ia supergiants occupy zones which run diagonally across the HR diagram to the right of and above the main-sequence band. The apparent separation of the zones is artificial. It is due to the assumption that the Ib supergiants are about 1 mag fainter than the Ia supergiants. Probably it would be wise to consider that the B-type supergiants occupy a diagonal zone having a center line which runs from a point (log $L/L_\odot$, log T_{eff}) which is close to the point (5.65, 4.45) and extends to the point (4.25, 3.95). The supergiants occupy an area which spreads about this line by ±0.40 to ±0.60 in log $L/L_\odot$. The cut off in log T_{eff} at each end is artificial and due to our restriction to spectral class B. A few supergiants are known at higher effective temperatures but not much higher luminosities; the A-type supergiants occur at lower effective temperatures. The Ia supergiants of type A have luminosities of the order of log $L/L_\odot = 4.5$.

The peculiar supergiant P Cyg falls inside the zone for the normal Ia and Ib supergiants. The Ia+ supergiants lie at significantly higher log $L/L_\odot$ than is found for the normal Ia and Ib supergiants. However, their position is very uncertain because of the weakness of our information about the distances to the Ia+ supergiants.

One can see that very few of the apparently bright stars lie to the right of and above a line in the HR diagram running from the point (5.80, 4.40) to the point (4.80, 3.90). The upper edge of the band delineated by the B stars in luminosity classes II, III, IV, and V runs diagonally from the point (5.00, 4.43) to the point (2.15, 4.00). When log $T_{\text{eff}} < 4.25$, a real separation is seen between the stars of luminosity classes II to V and those in luminosity classes Ib and Ia.

The main-sequence band observed by means of the apparently bright B stars of types B3 and later definitely lies to the right of the theoretical position of the ZAMS, whatever assumptions are used to determine the theoretical position of the ZAMS. Both the theoretical results and the observational results are based on absolute data

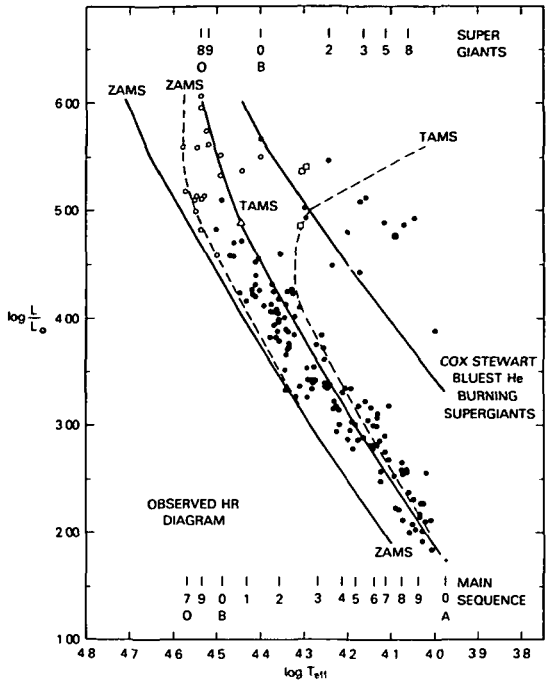

Figure 7-5. An observed HR diagram for O, B, and Wolf-Rayet stars from Underhill (1980a). The positions of the B stars are shown by filled circles, those of O stars by open circles. An open triangle marks the mean position for five Wolf-Rayet stars, open squares show the positions of κ Cas, ρ Leo, and HD 190603 (assuming M_V = −7.0); a filled square marks the position of P Cyg for the case that it is at 1.2 kpc. The position of α Lyr, A0 V, is shown by a plus sign. The theoretical boundaries of the main-sequence band as presented by Stothers (1976) are shown by a continuous line for the case of the Cox-Stewart opacities and by a broken line for the case of the Carson opacities. In both cases, a composition of (0.73, 0.02) has been used

and no shift can be introduced to bring the observed lower edge of the main sequence for stars in the neighborhood of the Sun into agreement with the theoretical position of the ZAMS. Since the theoretical position of the ZAMS for log $T_{\text{eff}} < 4.3$ is insensitive to the composition of the models, to the choice for the opacity tables, and to the numerical methods used for making the model stars, it must be concluded that the late B-type stars in the solar neighborhood have

all evolved away from the ZAMS. Typically the mass of a B5 main-sequence star is 5.5 $M_{\odot}$. From Table 7-1, we see that such a star may be expected to burn hydrogen in its core for about 6.9×10^7 years. Less massive stars, those corresponding to B8, for instance, may take 1.5×10^8 years to burn their core hydrogen. The observed positions of the late B-type stars in the HR diagram suggest that these stars are younger than the Sun by a factor between 10 and 100. They all lie in the immediate neighborhood of the Sun.

There are 10 Beta Cephei stars, 4 Bp stars, and 31 Be stars in the group of B stars studied by Underhill et al. (1979). For two-thirds of the Be stars in this sample and for all of the Beta Cephei and Bp stars, no significant difference was found by Underhill et al. (1979) between the derived T_{eff} and radius of these stars and the results for normal stars of the same spectral type. In the case of the Be stars which show intense activity, the effective temperatures and radii are of dubious value because the assumptions that the angular diameter is the same at all wavelengths and that the star is spherical in shape may not be valid. Also the observations which were used by Underhill et al. (1979) were not obtained at the same epoch and these stars are known to vary in light. However, even if the uncertainty in log $L/L_{\odot}$ and in log T_{eff} for the active Be stars in the list of Underhill et al. (1979) is double that for normal stars, the general trend of the points in Figure 7-5 will not be changed. The points shown in Figure 7-5 are believed to delineate accurately the position of the main-sequence band for B stars in the solar neighborhood. They also show the area occupied by B-type supergiants.

One of the uses to which we may put Figure 7-5 is to try to answer the question of whether or not the observations give support for the use of the Carson opacities in place of the Cox-Stewart opacities. First of all we note from Table 7-1 that the time which a model star spends burning hydrogen in its core is about the same no matter which set of opacity tables and what composition are used. However, where the star moves in the HR diagram during this time does depend on the choice of opacity tables. In the case of the Cox-Stewart opacity tables, a massive star (one with $M \geq 15\, M_{\odot}$, thus roughly one of spectral type B0 in the main sequence or a middle B-type supergiant) spends the full time of core hydrogen burning in the zone of the HR diagram where log $T_{\text{eff}} \geq 4.425$. In the case of the Carson opacity tables, a model star of 15 $M_{\odot}$ may reach log T_{eff} as low as 4.2 by the time overall stellar contraction begins. One having a mass of 20 $M_{\odot}$ may reach log $T_{\text{eff}} = 4.0$ by the time overall contraction begins. In both cases, the luminosity remains high.

If we knew when the field stars of the study by Underhill et al. (1979) were formed, and whether this was an event that occurred at one time or continuously, we might hope to make a decision regarding the use of the Cox-Stewart or the Carson opacities by noting how many stars occupy each zone of the HR diagram. For instance, if we had a population of stars having an age of about 10^7 years, the stars having masses of the order of 15 $M_{\odot}$ should be confined to the region of the HR diagram where log $T_{\text{eff}} \geq 4.425$ in the case that the Cox-Stewart opacities are appropriate. They should be stretched over the range in log T_{eff} from 4.45 to 4.1, or so, if the Carson opacities are appropriate. The calculations of Stothers and Chin (1977) show that a 15 $M_{\odot}$ model star begins to move quickly to the right in the HR diagram once the fraction of hydrogen in the core drops below $X = 0.2$. For model stars having masses in the range 15 to 20 $M_{\odot}$, this means once log $T_{\text{eff}} < 4.3$. Thus, if the Carson opacities are appropriate and the population age is of the order of 10^7 years, we should expect to find some stars with log T_{eff} in the range 4 45 to 4.3 and a few in the range 4.3 to 4.1 The stars with masses near 15 $M_{\odot}$ should have log $L/L_{\odot} > 4.5$ during most of the 10^7 years; those with M near 20 $M_{\odot}$ will have log $L/L_{\odot} > 4.8$ during this period. If the age of the group is greater than 10^7 years, the most massive stars will have evolved to log $T_{\text{eff}} < 3.9$ and be out of the part of the HR diagram which we are considering. The distribution of luminous stars in the HR diagram can only be used to direct the choice between the Cox-Stewart and the Carson opacity tables if one can show that the population being considered has an age of

10^6 to 10^7 years. This conclusion is not modified by referring the observations to theoretical HR diagrams calculated to represent evolution with mass loss.

We have seen that all the nearby B stars, that is those within about 500 pc of the Sun, seem to have evolved away from the theoretical ZAMS. In fact quite a few are found in the region of the HR diagram where hydrogen burning in a shell is beginning. This suggests that the age of this group is approximately 10^8 years. Any massive stars ($M \geq 15\ M_\odot$) which may have been associated with this group of B stars near the Sun would by now have evolved to $\log T_{\text{eff}} < 3.9$ and they would not be shown in Figure 7-5. The supergiants shown in Figure 7-5 probably all must have masses greater than $10\ M_\odot$ in order to achieve their observed luminosities. Most may have masses greater than $15\ M_\odot$. The calculations of Lamb et al. (1976) show that a model star with $M = 15\ M_\odot$ takes 1.30×10^6 years to go from points B to B′ in Figure 7-2. After passing point B′ the model star moves very quickly to a region near $\log T_{\text{eff}} \approx 3.55$. Since the duration of the core hydrogen burning stage is 1.03×10^7 years, the time spent in the blue supergiant range relative to that spent in the main-sequence band is about $1.3/10.3 = 0.13$. In a coeval population having an age of about 10^8 years, none of the stars with masses near $15\ M_\odot$ should appear as luminous blue stars. We must conclude that the early type B stars and the B supergiants belong to a younger population than most of the apparently bright stars of type B3 and later near the Sun. The gap between the main-sequence band and the supergiants which is clear for $\log T_{\text{eff}} < 4.25$ is due chiefly to the rapidity with which model stars having moderate masses evolve once they get well into the phase of burning hydrogen in a shell.

The fact that no stars in Figure 7-5 lie by a significant amount to the left of the ZAMS found with the Carson opacities might be construed as evidence in support of the Carson opacities. However, this evidence is very weak because only two stars in Figure 7-5 have spectral types earlier than O7. They are ζ Pup, O4ef, and λ Cep, O6ef. Information about the effective temperatures of four O4 stars derived from integrated fluxes and angular diameters has been presented by Underhill (1981a). This material indicates that some O stars may have effective temperatures higher by a significant amount than what is suggested by the calculations of the evolution of massive stars done with the Carson opacities. The case for using the Carson opacities in preference to the Cox-Stewart opacities is not strong. At this time, we may conclude that the observed HR diagram for B stars is in agreement with the predictions made using the Cox-Stewart opacities and it is not in serious disagreement with the HR diagram predicted using the Carson opacities. We cannot rule out use of the Carson opacities until better statistical information is available about the ages of the apparently bright luminous B stars.

The results of the calculations of evolution with mass loss do not seriously change this discussion of the meaning of the observed HR diagram for B stars. Lamers (1981b) has collected estimates of the rates of mass loss from 53 early type stars. There are 5 main-sequence stars in his list having a spectral type in the range from B0.5 to O9.5. The average rate of mass loss from these stars is $1.3 \times 10^{-7}\ M_\odot \text{yr}^{-1}$. Let us take this as a typical value for a B0 star which is halfway between the ZAMS and the first inflection point in its evolutionary track.

Such a star may be expected to have a mass near $15\ M_\odot$ (see Table 2-10). From the data given in Table 7-2, we see that the calculations of Stothers and Chin (1979) for the case with $k = 1 \times 10^{-11}$ may be representative. The calculations of de Loore et al (1977) for the case $N = 100$ and those of Chiosi et al. (1978) suggest slightly larger rates of mass loss than are observed while a real star is in the main-sequence band. The rates of mass loss from B-type supergiants (see Table 4-12) are consistent with $k = 1 \times 10^{-11}$ when a plausible estimate is made for the mass of the star However, because the rate of mass loss for α Cyg (A2 Ia) is observed to be less than $1.4 \times 10^{-7}\ M_\odot\ \text{yr}^{-1}$ (see Table 4-12), whereas the calculated value of $\dot{M}$ for model stars (see Table 7-2) having a mass of $15\ M_\odot$ is of the order of $10^{-6}\ M_\odot\ \text{yr}^{-1}$ when T_{eff} is about 1.25×10^4 K, we must infer that the masses of the

late B and early A-type supergiants are less than 15 $M_{\odot}$, or that the theoretical estimates of the rate of mass loss are unacceptedly high.

Figure 7-4 for the case of $M = 15\ M_{\odot}$, $k = 1 \times 10^{-11}$ shows that the evolutionary track with mass loss is not moved sufficiently far from the evolutionary track for evolution at constant mass that any of the conclusions noted above would be changed. At most, $\log L/L_{\odot}$ is reduced by 0.10 over the range of $\log T_{\text{eff}}$ which is of interest for interpreting the evolution of massive B stars. Changes of this order in the track may arise from handling the transport of energy by convection differently and by changing the composition of the model star

In the case of middle and late B-type stars mass loss while the star is in the main-sequence band is difficult to detect. However, Furenlid and Young (1980) have found asymmetries in the Hα profiles of main-sequence B stars that suggest mass is flowing from some of these stars at a low rate. There is little reason to expect that loss of mass at the rate which is seen will make the evolutionary tracks for B stars having masses in the range 2 to 10 $M_{\odot}$ seriously different from the tracks shown in Figures 7-1 and 7-3. Therefore, the interpretation of the HR diagram given above is as secure as the uncertainties in the observations and the uncertainties in the theory of stellar evolution allow it to be.

Observational HR Diagrams for B Stars from Spectral Types and UBV Photometry

An observational HR diagram in the form of M_V plotted against spectral type has been presented by Humphreys (1978) for O stars, B0 to B1 main-sequence stars, and supergiants from type B to type M. She uses stars which are found in associations and clusters in our galaxy. In a companion paper (Humphreys, 1979) she has presented information about the M-type supergiants in the Large Magellanic Cloud and she has collected from the literature the information about spectral types and M_V for the early type supergiants in the LMC. These two papers give the most extensive information that is presently available about the positions in the HR diagram of luminous early type stars. The meaning of these HR diagrams has been discussed by Humphreys and Davidson (1979). The results of Humphreys will be compared here with those of Underhill discussed above.

In her study of the luminous stars of our galaxy, Humphreys assigned membership in associations and clusters on the basis of the apparent position of the star in galactic coordinates, the photometric distance, and the radial velocity when that was available. In her extensive catalogue of luminous stars in the galaxy, Humphreys included only those stars for which published MK spectral types and UBV photometry could be found. She corrected the apparent V magnitudes for interstellar extinction, using the value $A_V/E(B-V) = 3.0$ and the intrinsic colors of Johnson (1963) for all stars but the M supergiants, and estimated distances. She adopted the luminosity calibration of Walborn (1972, 1973) to find M_V for the O and early B stars and the calibration of MK types in terms of M_V of Blaauw (1963) for the supergiants of later type.

To obtain an HR diagram in the coordinates used in theoretical studies, Humphreys (1978) derived an effective temperature scale for luminous stars, and she adopted a scale of bolometric corrections. Her temperature and bolometric correction scales for the O and B stars are based on those of Conti (1973) for the O stars and those of Code et al. (1976) for the B stars. Humphreys used M_{bol} as the coordinate for luminosity. It may readily be shown that

$$\log L/L_{\odot} = -0.4(M_V + B.C.) + 1.90, \quad (7\text{-}15)$$

where the constant factor reflects the assumption that $M_{\text{bol}} = +4.75$ for the Sun.

The distribution of the luminous B stars in the M_V-Spectral Type plane found by Humphreys is the same as that given in this book because essentially the same definitions of spectral type and the relation of spectral type to M_V have been used. Humphreys (1979) shows that the distribution of luminous early type stars in the M_V-Spectral Type plane is essentially the same in

our galaxy and in the LMC

Comparison of the results of Underhill with those of Humphreys in the $\log L/L_{\odot}$ (or M_{bol}) – $\log T_{eff}$ plane is, however, not straightforward because Humphreys has adopted an effective temperature scale that is different from that shown in Chapter 4 to be valid for the luminous B stars and she has adopted a different scale of bolometric corrections as a function of effective temperature than is shown to be valid in Chapter 4. Thus, Humphreys' diagram of M_{bol} vs. $\log T_{eff}$ is stretched in an irregular manner with respect to the equivalent diagram in $\log L/L_{\odot}$ vs. $\log T_{eff}$ given by Underhill (1980a) and discussed above. For the reasons given in Chapter 4, we believe that the effective temperature scale for B-type supergiants given in Table 4-2 and the bolometric correction scale given in Table 4-3 are superior to those adopted by Humphreys (1978). Underhill and Divan (*O, Of, and Wolf-Rayet Stars*, to be published) discuss this question for the O and Wolf-Rayet stars and present there a superior calibration to that adopted by Humphreys.

The types of distortion that exist between Humphreys' diagrams of M_{bol} vs. $\log T_{eff}$ and the data shown in Figure 7-5 for the luminous B-type stars can be found by considering the scales of effective temperature and bolometric correction given in Table 7-3. Since both Humphreys and Underhill adopt about the same scale of M_V as a function of spectral type, no difference exists between their results in that area except the differences due to accidental errors. The accidental error in M_V is of the order of ±0.5 mag at all spectral types.

From Equation (7-15) one sees that the difference in $\log L/L_{\odot}$ between Humphreys and Underhill is

$$\log L/L_{\odot}(\mathrm{H}) - \log L/L_{\odot}(\mathrm{U}) =$$

$$-0.4\,(B.C.(\mathrm{H}) - B.C.(\mathrm{U})), \qquad (7\text{-}16)$$

when it is acknowledged that, on the average, ΔM_V is zero. Table 7-3 shows that for supergiants of types O9.5 to B3, typically $\Delta B.C.$ is −0.3 mag. Thus, the value of $\log L/L_{\odot}$ assigned by Humphreys is systematically +0.12 larger than that assigned by Underhill to stars of type B3 and earlier. In the case of stars of type B5 and later, the $\log L/L_{\odot}$ values of Humphreys are larger than those of Underhill by about +0.03.

The effective temperatures assigned by Humphreys to stars of type B2 and earlier are systematically higher than those assigned by Underhill. Typically the $\log T_{eff}$ of Humphreys for these stars is larger than the value of Underhill by 0.04. Humphreys assigns lower effective temperatures than Underhill does to stars of types B3 and later. Typically Humphreys' values of $\log T_{eff}$ for those stars are smaller than those of Underhill by 0.06. These differences should be kept in mind when comparing the distribution of the B-type supergiants found by Humphreys in the theoretical HR diagram with the distribution found by Underhill.

If one does not regard the few points in Humphreys' diagram for the superluminous (Ia+) supergiants, on the grounds that M_V for these stars is poorly known, and if one ignores the point for P Cyg on the grounds that Humphreys assigns the value $T_{eff} = 2.1 \times 10^4$ K to this star because of its spectral type and that she adopts the erroneous M_V value of Kopylov (1958) and Hutchings (1976a) (Chapter 4), and if one applies mentally the stretchings indicated in the preceding paragraphs, one can see that Humphreys finds that the B-type supergiants lie in about the same area of the HR diagram as Underhill finds. Therefore, we can take the shaded areas shown in Figures 7-1, 7-2, and 7-3 to have substance. Normal Ib and Ia supergiants in our galaxy and in the LMC generally do fall in the area enclosed by the uppermost and the lowest edges of these gray-shaded areas. The discussion of 30 B supergiants is true in general for B-type supergiants.

Humphreys has given no information about the distribution in the HR diagram of main-sequence B stars of types later than B1 Her data for main-sequence B stars of types B0 and B1 are in accord with that of Underhill.

Humphreys and Davidson (1979) have discussed the interpretation of the most luminous part of their HR diagram relative to the theory of stellar evolution with mass loss. We believe that

Table 7-3
A Comparison of Adopted Effective Temperatures and Bolometric Corrections for B-Type Supergiants

Spectral Type	Table 4-2 T_{eff} (10^4 K)	Table 4-3 *B.C.* (mag)	Humphreys (1978) T_{eff} (10^4 K)	Humphreys (1978) *B.C.* (mag)
O9.5	2.95	−2.80	3.10	−3.0
B0	2.50	−2.42	2.80	−2.75
B0.5	2.25	−2.18	2.40	−2.5[a]
B1	2.00	−1.90	2.10	−2.3[a]
B1.5	1.85	−1.72	1.90	−2 1[a]
B2	1.70	−1.52	1.70	−1.9[a]
B3	1.50	−1.21	1.40	−1.5[a]
B5	1.30	−0.87	1.20	−1.05[a]
B6	1.25	−0.78	1.10	−0.85[a]
B7	1.20	−0.68	1.05	−0.75
B8	1.15	−0.58	1.00	−0.64
B9	1.05	−0.39	0.98	−0.52
A0	0.95	−0.28	0.94	−0.38

[a]Uncertain value.

the part of their diagram which concerns O stars, particularly early O stars, is biased to high luminosity and high effective temperature as a result of the effective temperature and bolometric correction scales adopted by Humphreys (1978). This point is discussed by Underhill and Divan (*O, Of, and Wolf-Rayet Stars*, to be published). The conclusions of Humphreys and Davidson about evolution at very high mass are marred by this bias and by the bias which they have introduced by adopting an effective temperature and luminosity for P Cyg that are higher than can be supported by recent studies (see Chapter 4). It seems that only a very few supergiants, the Ia+ stars, may have M_{bol} brighter than −9. The upper limit to luminosity discussed by Humphreys and Davidson for stars in our galaxy and in the LMC should be reduced by approximately 0 5 mag throughout their diagram. Underhill finds their arguments in favor of the existence of main-sequence stars having masses greater than 60 $M_\odot$ unconvincing and she doubts that stars more massive than 60 $M_\odot$ are the progenitors of the B-type supergiants.

Observational HR Diagrams for B Stars from Photometry Only

The intermediate-band photometry of the uvby, β, system reviewed in Chapter 2 allows one to place B stars in an observational HR diagram made with the coordinates M_V and [u − b] or M_V and c_0. For this purpose the calibration of Eggen (1974a) or that of Crawford (1978) of the luminosity parameter β in terms of M_V is used These calibrations and the related empirical ZAMS are given, respectively, in Tables 2-4 and 2-5.

The observational coordinates of the ZAMS may be transformed to the theoretical coordi-

nates log $L/L_{\odot}$ and log $T_{\rm eff}$ by making use of theoretical relations between [u − b] or c_0 and $T_{\rm eff}$ and between $T_{\rm eff}$ and the bolometric correction. We have seen in Chapter 3 that the observed, unreddened intensity distributions of main-sequence B stars are well represented by the energy distributions predicted from line-blanketed LTE model atmospheres by Kurucz (1979). The calculations of Relyea and Kurucz (1978) give theoretical values of [u − b], the u − b color corrected for interstellar extinction, and c_0, the color difference measuring the size of the Balmer jump corrected for interstellar extinction, for each model atmosphere. By using this material we can find an equivalent log $T_{\rm eff}$ for each observed value of [u − b] or c_0. It is necessary to adopt a value of log g for each point, we adopt the value log g = 4.0 as representative for the ZAMS

Reference to the tables of Buser and Kurucz (1978) allows us to find the bolometric correction corresponding to each set of values of $T_{\rm eff}$ and log g. We note that the appropriate value to use is the quantity denoted by Buser and Kurucz as *B.C.'*. We have

$$B.C.' = B.C. + 0.100, \qquad (7\text{-}17)$$

where *B.C.* is the calculated bolometric correction given in table 2 of Buser and Kurucz. The constant factor places the calculated bolometric corrections on the empirical scale which is used for bolometric magnitude In what follows, we adopt the quantity *B.C.'* found from Equation (7-17) as the bolometric correction corresponding to each observed value of [u − b] or c_0. Values of $T_{\rm eff}$ are found for each [u − b] or c_0 of the empirical ZAMS by interpolating in table 1 of Relyea and Kurucz for models with log g = 4.0. In this way the values of M_V as a function of [u − b] or of c_0 given in Tables 2-4 and 2-5 may be transformed into the theoretical coordinates log $L/L_{\odot}$ and log $T_{\rm eff}$.

This has been done for the empirical zero-age main sequences of Eggen (1974a) and Crawford (1978), and the results are shown in Figure 7-6. In this figure, the ZAMS of Eggen is shown by filled points and that of Crawford by crosses. A line indicates the position of the theoretical ZAMS obtained by joining the starting points of the evolutionary tracks shown in Figure 7-1. The open circles give the observed positions of "average" main-sequence B stars at each spectral type.

Three points are of interest in evaluating Figure 7-6. (1) The relationship between [u − b] or of c_0 and $T_{\rm eff}$ is rather secure, the uncertainty in log $T_{\rm eff}$ being less than about ±0 02 for a given value of [u − b] or c_0, (2) The uncertainty in the positions of the points defining the empirical ZAMS is small until log $T_{\rm eff}$ exceeds 4.3, and (3) The positions of the points defining the top of the empirical ZAMS, in each case, are somewhat uncertain, chiefly because of uncertainties concerning the question of whether or not the observational data which are available for analysis really include data for unevolved early B-type stars.

We note that the empirical positions for the ZAMS lie above the theoretical position for the ZAMS. If the correction factor +0 100 had not been introduced by means of Equation (7-17), the empirical positions for the ZAMS would have fallen above the theoretical ZAMS determined by the theory of stellar evolution, by a further amount of +0 04. The ZAMS recommended by Eggen does fall close to the theoretical ZAMS for main-sequence stars with log $T_{\rm eff}$ in the range 4.2 to 4.05. This corresponds to spectral types from about B2.5 to about B8 The ZAMS recommended by Crawford for B stars lies above the theoretical ZAMS at all effective temperatures (spectral types) The position of the highest point on each empirical ZAMS is quite uncertain

The empirical positions for the ZAMS are found by fitting together cluster sequences in the (V, [u − b]) or (V, c_0) planes and determining a lower envelope. It has been known for some time (see, for instance, the material presented by Eggen, 1974a), that the upper parts of the sequences followed by early type cluster members in a color-magnitude diagram tend to turn off from the main sequence toward high luminosities. In fact the amount of the turn off from that ZAMS which is determined by means of stellar evolution calculations has been used to

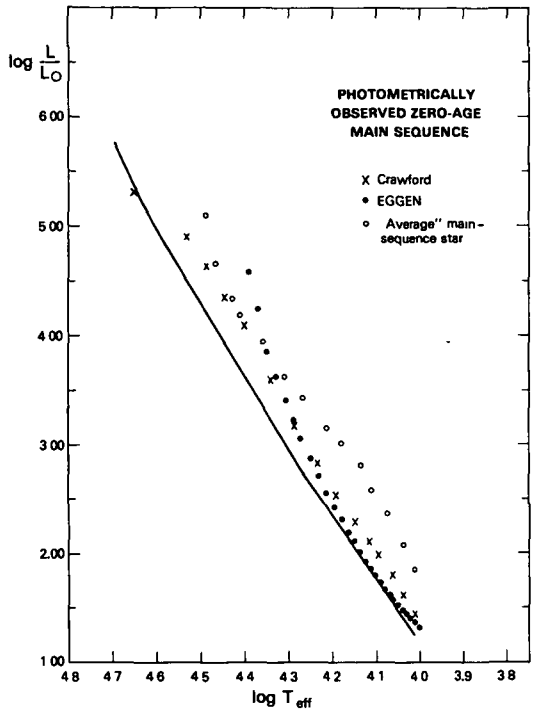

Figure 7-6. The positions of the empirical ZAMS of Eggen (1974a) and that of Crawford (1978) in the theoretical HR diagram. The line gives the position of the ZAMS found by joining the starting points of the evolutionary tracks shown in Figure 7-1. The observed positions of "average" main-sequence stars at each B spectral type are shown by open circles. The points defining Eggen's ZAMS are shown by filled circles, those defining Crawford's ZAMS by crosses.

estimate ages for clusters containing O and B stars (see, for instance, the summary by Stothers, 1972 and that by Eggen, 1974a). The theory underlying age determinations has been reviewed by Sears and Brownlee (1965). To make an estimate of the age of a cluster one must assume that all of the stars are formed at the same time. Eggen (1976) has considered this question and has noted that the observations give support to the idea that two epochs of star formation may have occurred in many clusters, low mass stars having been formed predominantly at a different time from when the massive members of the cluster were formed. A list of cluster ages is given by C W. Allen (1973).

The difference between the position of the theoretical ZAMS in Figure 7-6 and the position of each empirical ZAMS could be due to the fact that the position of each empirical ZAMS is determined from apparently bright B stars, on the whole. We have seen that the apparently bright B stars in the solar neighborhood seem to be evolved somewhat. It appears that many of the cluster O and B stars used by Eggen and by Crawford also are evolved. Determining ages for open clusters which contain O and B stars by fitting to an empirical ZAMS near type B8 to A0 may lead to a systematically young age if the ZAMS of Crawford is used.

The age of the cluster is determined from where a steep rise occurs in the track of the cluster in the color-magnitude diagram (see, for instance, the discussion by Stothers, 1972). The positions of the theoretical tracks for massive model stars which are in the stage of burning hydrogen in a shell and of beginning to burn core helium are what determine the cluster ages. These positions are uncertain, as we have seen, and they do depend on the methods used to construct the model stars. The theoretical positions may also be changed by mass loss. Paerels et al. (1980) have considered this question. They show that mass loss in the amount that is observed for O and early B stars in the main-sequence band does not substantially change the inferred ages for young clusters. Thus, the problem still exists that evolutionary ages estimated from the position in the HR diagram of the brightest early type stars in open clusters are longer than the ages that may be estimated by considering the apparent expansion of the cluster (see Blaauw, 1964, Stothers, 1972). The proper motions and radial velocities which permit one to estimate a kinematic age for an open cluster containing O and B stars are not certain. Because this is so, and because it is uncertain that all the stars of an open cluster were formed at one epoch, it seems advisable at this time not to stress the apparent discrepancy between evolutionary ages and kinematic ages for massive stars.

DISCUSSION

The distribution of stars in an HR diagram is

believed to give strong evidence concerning the stage of evolution of the stars Here we discuss what theory and observation allow us to find out in the case of B stars.

Uncertainties

When comparing the tracks of massive model stars in theoretical HR diagrams with the distribution of real stars in an observational HR diagram, one must pay attention to the uncertainties in the theoretical results as well as to the uncertainties of the observations. The uncertainties are not the same in each part of the diagram. The basic coordinates for an HR diagram are $\log L/L_{\odot}$ and $\log T_{\text{eff}}$, where T_{eff} represents the integrated flux of radiation emerging from a model star and from a real star. The most important free parameter for determining where a model star will lie in the HR diagram is the mass of the model star.

Uncertainties in the Theory. Uncertainties in the theoretical results may arise from incompleteness in the theoretical representation of the physics of how a model star is constructed and how energy is transported through the star from the place where it is generated by nuclear burning or by contraction to the place where it is emitted as radiation, the photosphere. The major uncertainties related to the transport of energy from one level in the model to the next arise in the formulation of the expression for the opacity as a function of composition, temperature, and density, and in how the transport of energy by means of convection is represented.

In Figure 7-1, we have shown that the evolutionary tracks for massive model stars tend to cross the part of the HR diagram where the B-type supergiants are found at lower luminosities when the Ledoux criterion for convection is used than when the Schwarzschild criterion is used. This is illustrated by the position of the crosses (X) relative to the evolutionary tracks shown by broken lines. We show only the positions for instants when the model star has $\log T_{\text{eff}} = 4.3$ and 4.1. These calculations are for the case of Cox-Stewart opacities.

By comparing Figure 7-1 with Figure 7-3, one can see what change in the opacity tables does to the evolutionary track of a star of a given mass. Use of the Carson opacities leads to a lower luminosity for a fixed mass and effective temperature than is found when Cox-Stewart opacities are used. This is particularly evident for the tracks of massive model stars which go through the region occupied by the B-type supergiants.

Use of the Cox-Stewart opacities leads to the inference of a major change in the energy generation process which is active for a star when the star is crossing the part of the HR diagram occupied by the B-type supergiants. When the Carson opacities are used, most of the energy generation while massive models are in the region of the B supergiants is from burning hydrogen in the core. In the case of the Cox-Stewart opacities, the energy generation is from burning hydrogen in a shell and burning helium in the core. Until one can decide on independent grounds what is the correct representation for the stellar opacity, any deductions about the energy sources for B-type supergiants will be very uncertain. It is disturbing that changes in the opacity tables over a limited range of temperature and density can have such a large effect on the inferences that may be made concerning the energy generation of B-type supergiants. Over much of the range of temperature and density of interest for making massive model stars, the Carson opacity tables do not differ much from the Cox-Stewart tables. It is only at low densities that large differences occur.

Mass loss also causes the position for a given initial mass and a given effective temperature to lie lower in the HR diagram than when a model star evolves without mass loss. Where the track goes depends to some extent on the formulation which is used for finding the rate of mass loss as a function of the instantaneous luminosity, mass, and radius of the model star.

The pulsation properties of the model star, while it is changing its source of energy from burning hydrogen in the core to contraction and to burning hydrogen in a shell, also depend sensitively on the physical structure of the model and how the transport of energy by convection is represented.

Consequently, although the theoretical posi-

tion of the zero-age main sequence is not very sensitive to the initial composition assumed for the model star, at least for initial masses less than 10 $M_{\odot}$, the inferred physical state of a star at all other times in its lifetime as a B star is sensitively dependent on how the physics of the star is represented in the model. Factors presently under study include taking accurate account of the rotation of the star, the effects of magnetic fields, and of convective overshooting. Only very rough conclusions can be drawn about the mass of a star by comparing its observed luminosity for a selected value of the effective temperature with the theoretical evolutionary tracks for model stars of different masses and physical representations. Thus, one can conclude that the masses of the B-type supergiants are most likely greater than 10 $M_{\odot}$ and that the early B supergiants are more massive than the late B supergiants; but one cannot surely determine masses within an uncertainty of 1 or 2 solar masses.

Uncertainties in the Observed Log $L/L_{\odot}$ and Log T_{eff}. The data reviewed in Chapters 3 and 4 show that usually the uncertainty in log T_{eff} is less than ±0.02 when the effective temperature is determined from integrated fluxes and angular diameters. The uncertainty in log $L/L_{\odot}$ is essentially equal to 0.4 ΔM_V, where ΔM_V is the uncertainty in visual absolute magnitude. Typically, for main-sequence stars that are well studied with much photometric and spectroscopic data available, ΔM_V may be as small as ±0.3 mag. In the case of the B-type supergiants, ΔM_V is usually of the order of ±0.5 mag. Thus, for a real star, the uncertainty in log $L/L_{\odot}$ arising from the uncertainty in the distance of the star, or its M_V, is in the range from ±0.12 to ±0.20. The uncertainty in effective temperature introduces an uncertainty in the bolometric correction. If the theoretical relationship between effective temperature and bolometric correction derived by Buser and Kurucz (1978) is used for B stars, typically the uncertainty in the bolometric correction may be of the order of ±0.03 mag. This leads to an additional uncertainty in log $L/L_{\odot}$ of ±0.012, which is negligible.

It is important to use effective temperatures found from integrated fluxes and angular diameters when placing B stars in the HR diagram. Effective temperatures deduced from the relative strengths of lines from several stages of ionization in the spectrum invariably are too high. In the case of main-sequence stars, this systematic error is not large (see Chapter 3) but for supergiants, the systematic error is large (see Chapter 4). Effective temperatures deduced from the size of the Balmer jump may be useful for main-sequence stars, but not for supergiants or Be stars because of emission in the Balmer continuum. Effective temperatures deduced from color temperatures based on a wide range of wavelengths can be used if the correction for interstellar extinction can be determined accurately and if correction can be made for the presence of an infrared excess that may extend into the visible range.

Uncertainties in the Deduced Ages of B Stars. The information summarized in Table 7-1 shows that the ages of model B stars while the models are in the main-sequence band, that is in the phase of burning hydrogen in the core, are almost independent of the details of how the models are constructed and what the initial composition is assumed to be. The hydrogen-burning ages are dependent chiefly on the mass of the model star. Additional theoretical results, mostly by Stothers and Chin, show that the duration of the phase of helium burning is approximately one-tenth that of the phase of hydrogen burning. Thus, if the masses of B stars are known moderately well and their positions in the HR diagram can be established, the lifetimes of the early stages of evolution of B stars can be found to within about 10 percent.

The lifetimes of open clusters which contain O and B stars depend upon whether or not one is justified in assuming that the stars are all coeval. Since stars of 9 $M_{\odot}$, thus stars of about type B2.5 in luminosity classes IV or V, have hydrogen burning ages which are only one-tenth the length of the ages of stars of 3 $M_{\odot}$, that is stars of type about B8 in the main sequence, any group of stars which is observed to contain B8 and B2.5 and earlier stars in the main-sequence

band cannot be considered to have been formed all at one time. If the stars are coeval, either the B8 stars will be on or close to the zero-age main sequence and the B2.5 and earlier stars will be somewhat evolved, or the B8 and later stars will not yet have arrived at the ZAMS and the B2.5 and earlier stars will be on or near the main sequence. This effect is what is used to estimate the ages of open clusters containing O and B stars. We have shown that the empirical ZAMS of Eggen (1974a) lies closer to the theoretical ZAMS than does that of Crawford (1978) (see Figure 7-6). Crawford's ZAMS represents the position of stars which have evolved by a measurable amount. Its use for determining cluster ages will lead to minimum ages. The assumption that all of the stars are coeval is crucial. It must be justified by arguments not based on where the stars of the cluster lie in the HR diagram, if reliable results are to be obtained.

Major Conclusions

Here we gather together the information which has resulted from comparing theoretical and observational HR diagrams.

Theory of Stellar Evolution. The luminosity range through which a model star evolves is primarily determined by the mass of the model star. The numerical methods used to represent the transport of energy through the star and the choice which is made for the opacity tables have small effects. In the part of the track which passes through the part of the HR diagram occupied by B-type supergiants, use of the Carson opacities or use of the Ledoux criterion for convection, or consideration of mass loss will place an evolutionary track for a star of a given initial mass through a point of lower $\log L/L_{\odot}$ for a selected value of $\log T_{\text{eff}}$ than use of Cox-Stewart opacities, the Schwarzschild criterion or consideration of evolution at constant mass will do. Increasing the abundance of the metals, Z, increases the opacity while using a larger helium abundance, Y, increases the mean molecular weight and thus the luminosity of the star. Rotation and magnetic fields generally lower the luminosity (Stothers, private communication).

The lifetime of a model star while it is burning hydrogen in the core is dependent chiefly on the mass of the model star. The lifetime for burning helium in the core is roughly one-tenth as long as the hydrogen-burning lifetime. The precise relative length is dependent on the details of the modeling procedures used. The lifetime in the phase of burning hydrogen in the core is usually lengthened when mass loss is taken into consideration. It may also be shortened. A model is said to be in the main-sequence band when it is burning hydrogen in its core.

When a model star that loses mass is compared with one which evolves without mass loss, it is found that at the same stage of central hydrogen depletion the mass losing model star has a lower luminosity and a lower effective temperature than does the model evolving at constant mass. There is an increased stability against convection in the mass losing star relative to the star which evolves at constant mass.

Knowledge of the luminosity and effective temperature of a star is not enough information to allow one to deduce securely that the internal structure and source of energy of the star are similar to these of a model. One must be able to specify the stellar mass within close limits and one must be sure of the correct representation for the transport of energy through the envelope of the star and of the effects of convection on the pressure structure in the envelope. If these factors can be determined, within small ranges, to be what is assumed for the model, one can be reasonably sure that one has an adequate model.

The fact that only some of the B stars (the Beta Cephei stars and the line-profile variables, see Chapter 3) on the evolved side of the main-sequence band change their surface conditions periodically shows that the conditions which control the opacity and convection in the envelope and core of a B star can be different for stars of apparently very similar luminosity and effective temperature. The period switching of the line-profile variables indicates that conditions in the envelopes of B stars may be in a state of unstable equilibrium.

In Chapter 4, we have noted that interactions

between small surface magnetic fields and differential motion in the outer layers of a supergiant may create the conditions which generate emission lines, superheated plasma, and outflow, both general and sporadic. This is probably true also for main-sequence stars, but only in the case of Be/shell stars are emission lines and outflow or inflow often detectable. Probably the ultimate cause of the changes of the spectra of supergiants and Be stars has its origin in an unstable equilibrium in the envelope of the star.

The observations reported in Chapters 3 and 4 and in Part II show that rather different characteristic times may be associated with the spectroscopic changes seen for Beta Cephei variables, line-profile variables, Be/shell stars, and supergiants. Thus, one may infer that the unstable equilibrium which occurs in the envelopes of these several types of stars has a different fundamental scale in each type of object. Obviously, the geometric length scale of any unstable equilibrium situation in a model star may be a function of the rotational velocity of the star and of how rotation couples inward through a star. This subject has not been studied in detail, and, indeed, it is very difficult, for one must consider at least six independent variables, three for the geometric dimensions and three for the independent components of angular momentum.

Interpretation of the HR Diagram. In Figure 7-1 and Figure 7-3, we have indicated the typical mass of an "average" star of each B subtype near to each observed point. The typical masses are taken from Table 2-11. On the whole, the typical masses agree reasonably well with the predicted tracks obtained using Cox-Stewart opacities (see Figure 7-1). It must be recalled that the spectral types of components in binary systems are more uncertain than the spectral types of single stars and that the typical masses have been found from an extended set of data that does not obey all the rules for determining precise masses. The predicted tracks for masses greater than $15\,M_{\odot}$ obtained using the Carson opacities for the case (0.71, 0.04) (see Figure 7-3), lie lower in log $L/L_{\odot}$ than do the tracks for the same masses predicted using Cox-Stewart opacities and the case (0.739, 0.021). The predictions for massive model stars obtained using the Carson opacities and large Z do not match the observations well so far as mass is concerned. Stothers (1976) finds that when a small value for Z and a large mixing length are used, the two sets of opacities give rather similar model stars on the ZAMS. The discrepancies noted here provide reason for giving theoretical results obtained using the Carson opacities low weight when inferring the internal structure of massive stars.

Precise masses for several B stars in the main-sequence band are given in Table 2-10. Positions in the HR diagram may be deduced for these stars by assigning each the typical effective temperature for its spectral type, using Table 3-5. When this is done, the positions of these stars are found to be in good agreement with the predictions shown in Figure 7-1 except for the star ζ Phe A. It would fit better if it had a type of B6 or B7. Such a change in the spectral type is not excluded, given the difficulty of classifying the spectra of double-lined spectroscopic binaries.

Thus, we may conclude that the predictions for the evolutionary tracks of stars having masses in the range 2.25 to $15\,M_{\odot}$ and lying in the main-sequence band agree well with the observations when the Cox-Stewart opacities are used to make the model stars. The agreement when the Carson opacities are used is satisfactory for stars having spectral types of B1 and later, but the points for Y Cyg and CW Cep, which have spectral types of B0 IV and B0.5 IV to V, respectively, lie to the left of the ZAMS predicted by means of the Carson opacities for the case of (0.71, 0.04) and small mixing length.

The observational HR diagram for apparently bright O and B stars in the solar neighborhood shown in Figure 7-5 indicates that all of the apparently bright B stars having types of B3 or later have evolved by a significant amount. None of them are close to the theoretical ZAMS. These stars are surely younger than the Sun which has an age of about 5×10^9 years. Typically such stars have masses between 2.5 and 8 solar masses. According to the information in Table 7-1, they may be expected to remain in the main-sequence band for 3×10^7 to 5×10^8 years. After that

they will evolve rather rapidly through the phases of overall contraction and hydrogen burning in a shell. Iben's (1965) calculations for a model star with $M = 3\ M_{\odot}$ indicate that the model will be beginning its rapid traverse of the area to the right of the main-sequence band after 2.44×10^8 years. His calculations (Iben, 1966b) for a model star with $M = 9\ M_{\odot}$ show that that model takes 2.19×10^7 years to reach the same stage. There seems little doubt that there is a range of about a factor of 10 in the ages of the B stars of types B3 and later plotted in Figure 7-5, and that the ages of even the least massive of these stars are only about one-tenth the age of the Sun. The B stars having masses of the order of $15\ M_{\odot}$ and lying in the main-sequence band have ages of the order of or less than 10^7 years. There seem to be very few, if any, very young low mass B stars near the Sun.

The effective temperatures of the supergiants of types B3 and earlier are greater than or equal to 1.5×10^4 K (see Table 4-2). Thus, the apparently bright early B supergiants lie to the left of a line in Figure 7-5 corresponding to $\log T_{eff} = 4.175$. If the evolutionary tracks of Figure 7-1 are indicative, most of the early B supergiants have masses in the range 12 to $30\ M_{\odot}$. The information in Table 7-1 suggests that their ages are of the order of 2×10^7 to 6×10^6 years. These ages are comparable with the ages of the main-sequence stars having masses of the order of $15\ M_{\odot}$ or more. This population of apparently bright stars (the main-sequence stars of types B0 and earlier and the supergiants of types B3 and earlier) are significantly younger than the apparently bright stars of types B3 and later. Two populations of B stars appear to be present within about 1.2 kpc of the Sun, one with ages in the range 0.6 to 2×10^7 years, and one with ages in the range from 2.2 to 24×10^7 years. The young group is composed chiefly of stars in the Orion-Canis Major region. Low mass B stars in this direction are too faint to be included in this survey. Frogel and Stothers (1977) from a study of the kinematics of the O to B5 stars in the solar neighborhood have suggested that star formation may have taken place at two times in the past, namely 2×10^7 years ago and 6×10^7 years ago.

From their luminosities, the B9/A0 Ia supergiants appear to have masses as low as $10\ M_{\odot}$. These stars must all be younger than about 2.2×10^7 years. Thus, they are part of the young population of massive stars in the solar neighborhood. It seems that the formation of stars with masses greater than $2.5\ M_{\odot}$ within 1.2 kpc of the Sun did not occur at only one moment.

The massive stars which were formed with the group of stars of type B3 and later, shown in Figure 7-5 to lie on the right-hand side of the main-sequence band, would by this time have evolved out of the part of the HR diagram displayed here. The low mass stars formed with the young bright massive stars and the B-type supergiants would be too faint for inclusion in the present survey which is limited by apparent magnitude. They should lie close to the ZAMS. Their visual absolute magnitudes should be approximately +0.75 mag fainter than those of the luminosity class IV and V standard stars included in the study of Underhill et al. (1979) and shown in Figure 7-5. It appears that some of the standard stars for luminosity class V, type B, are evolved stars. Note particularly the position of Vega in Figure 7-5.

When the positions of the Beta Cephei stars, the Bp stars, and the Be/shell stars in the list of Underhill et al. (1979) are reviewed, it is found that these stars are mixed in the main-sequence band with normal B stars, and that there is a tendency for them to be found on the right-hand side of the band. This suggests that these stars, typically, are more evolved than other stars of their effective temperatures. It does not seem to be so that Beta Cephei stars, Bp stars, and Be/shell stars occupy well-defined regions in the HR diagram where all stars have the selected unusual spectroscopic behavior. In the case of the Beta Cephei stars, this topic is discussed in Chapter 5. There it is noted that opinion diverges on whether or not Beta Cephei stars occupy a region in the HR diagram which is not occupied by other types of B stars.

It can be seen from Figure 7-5, and from data given by Underhill (1981a), that the Wolf-Rayet stars occupy the same general region of the HR

diagram as do B0 stars of luminosity classes III and Ia. Having a spectrum that is conspicuous because it contains emission lines is no more a condition for occupying exclusively one region in the HR diagram than is varying in light and radial velocity in a period of 4 to 6 hours (the Beta Cephei stars), or showing unusual strengths of some absorption lines (Bp stars). Whatever is the cause of the peculiarities which we recognize by means of the spectrum of the star, this cause is not linked to the mass of the star and to the star's instantaneous position in the HR diagram in a one-to-one manner.

Not all stars passing through the region in the HR diagram where Wolf-Rayet stars are found show a Wolf-Rayet spectrum anymore than is so with Beta Cephei stars or Be stars. The data of Figures 3-15, 5-2, and 5-3 show that the parts of the HR diagram occupied by Beta Cephei stars also contain line-profile variables and stars whose spectrum has not been noted to change. This part lies to the right of the theoretical ZAMS for stars with masses greater than about 2 $M_{\odot}$. Clearly, position in the HR diagram is not an unambiguous indicator of the type of spectrum that will be seen. More than one spectral type and one type of temporal behavior may be associated with one area in the HR diagram.

Position in the HR diagram, on the whole, is determined by the mass of a star and its age or, equivalently, its source of energy. At many positions in the HR diagram, more than one spectroscopic signature may occur. Our observations have clearly shown that the spectroscopic signature may change in some details within intervals of time from hours to tens of years. Such changes must be connected with the possible instabilities that may occur in the envelope of the star where convection and radiation together transport energy outward. Definitely, among the stars shown in Figure 7-5, changing absorption-line spectra and changing emission-line spectra are more frequently found among stars which are approaching or have passed the right-hand edge of the main-sequence band than among stars close to the ZAMS In this discussion we have deliberately excluded changes in spectrum resulting from the revolution of a companion about the star under study.

PULSATION PROPERTIES OF MASSIVE MODEL STARS*

The fundamental theory of stellar pulsation has been the subject of numerous review articles. Several books have appeared recently dealing with this subject. The reader is referred to J. P. Cox (1980) and Unno et al. (1979). In addition to these texts one must also mention the classic monographs of Ledoux and Walraven (1958) and Ledoux (1958). Almost all of the theory that has been developed has been based on a linear analysis of infinitely small perturbations. Primary emphasis has been placed on the theory of radial oscillations, but in recent years there has been an extensive series of theoretical developments in the area of nonradial oscillations. In almost all cases the underlying equilibrium configuration is assumed to be spherical. The effects of rotation have been considered, with most analyses assuming that the rotation is small. Such an assumption means that distortions of the underlying equilibrium configuration and its associated physical parameters (temperature, pressure, density, etc.) from spherical symmetry can be neglected.

Of particular interest in any calculation are the pulsation periods of the star and the growth rates for the pulsations. The pulsation period of low order modes is of the order of the time for the propagation of a sound wave across the diameter of a star, while the growth rate of an infinitesimal oscillation is related to the time required for a star to adjust to departures from thermal equilibrium. This time is usually orders of magnitude longer than the pulsation time.

It is readily shown from a consideration of the equation of hydrostatic equilibrium that, to a very close approximation, the product of the pulsation period and the square root of the mean density is a constant. This period-mean density relation is usually written in the form

$$P(\text{days})\,(\bar{\rho}/\rho_{\odot})^{1/2} = Q(\text{days}), \qquad (7\text{-}18)$$

*This section was written by Morris L. Aizenman.

where Q is known as the pulsation constant. Strictly speaking, Q depends on the structure of the star and the value of the generalized adiabatic exponent Γ_1 (Chandrasekhar, 1939). It is possible to calculate Q for a given model and a given mode of oscillation. Such calculations have been made, and they relate Q to the physical parameters of the star. It is found that Q depends only weakly on such parameters. In fact, nonlinearity and nonadiabaticity change Q by only a few percent. For a 10 $M_\odot$ star it is found that $Q \approx 0.037$ days for the radial fundamental mode, and $Q \approx 0.027$ days for the first radial overtone (Lesh and Aizenman, 1974). Comparisons of observed and calculated values of Q serve as an important diagnostic tool in determining the mode of oscillation of a star. Unfortunately, Q values for radial oscillations and nonradial oscillations are sufficiently similar to preclude using this parameter as an unambiguous criterion as to whether the star is undergoing radial or nonradial oscillation.

The massive stars near the main sequence do not lie in any apparent theoretical region of instability and there is little that would lead one to believe that any unusual phenomena should be expected. Calculations of the pulsation properties (both radial and nonradial) of massive stars have been made (see Lesh and Aizenman, 1974 or the references referred to by J. P. Cox (1980) and these cover the main sequence, the core hydrogen burning phase, the overall contraction phase, and the shell burning phase. The radial modes are well behaved, but the nonradial modes show a number of unusual characteristics which take place as the star evolves away from the main sequence Most prominent among them is the phenomenon of "avoided crossings." As the star evolves the low order gravity modes take on higher frequencies (i.e., shorter periods) than the nonradial pressure modes (Osaki, 1975; Aizenman et al., 1977)

The effects of rotation on the vibrational frequencies of a star are of two types: (1) If the perturbations are such that the configuration maintains axial symmetry, the effects of rotation are always proportional to the square of the angular rotation frequency; (2) In the case of more general perturbations the effects are linear in the angular rotation frequency. It is this latter type of perturbation that is of greatest interest. For slow rotation we have the result that rotation splits the degeneracies that exist for nonradial oscillations in the nonrotating star. Hansen et al. (1977) have shown that the oscillation frequency of a rotating star (in the inertial frame) is

$$\sigma = \sigma_0 - m(1 - C - C_1)\,\Omega, \qquad (7\text{-}19)$$

where σ_0 is the frequency of the nonrotating star, m is the azimuthal "quantum" number, Ω is the angular frequency of rotation, C is an integral which takes into account the oscillation properties of the nonrotating star, and C_1 is a term which accounts for small effects arising from differential rotation.

In addition to splitting the usual nonradial modes, rotation introduces a new set of modes known as toroidal modes. These modes have frequencies of the order of the rotation frequency (Papaloizou and Pringle, 1978) and are given by

$$\sigma = -m\Omega + \frac{2m\Omega}{\ell(\ell+1)} + O(\Omega^3). \qquad (7\text{-}20)$$

To order Ω^2 these frequencies are independent of the actual structure of the star.

The existence of a group of variable stars in the B star region of the HR diagram (the Beta Cephei variables, Chapter 5) is a mystery. There are no known instabilities that give rise to such a phenomenon. The pulsation periods for these stars (Lesh and Aizenman, 1974) are those expected from elementary adiabatic radial or nonradial calculations. A comparison of the observed Q values and the theoretical Q values shows that the observed periods are those to be expected of first or higher overtone radial oscillators, or low order nonradial acoustic modes.

Most theoretical work on the pulsation properties of massive stars has concentrated on masses of 10 $M_\odot$ or greater. This is the region where the Beta Cephei phenomenon is observed. In Tables 7-4, 7-5, and 7-6 we present some results of

Table 7-4
Some Model Parameters

$M/M_\odot$	$\log L/L_\odot$	$\log T_e$ (K)	$\log T_c$ (K)	$\rho_c/\bar{\rho}$	$R/R_\odot$	β_c	$M_c/M_\odot$
10	3.757	4.422	7.473	23.36	3.65	0.94	0.314
20	4.637	4.552	7.525	23.35	5.52	0.85	0.463
30	5.073	4.611	7.550	22.70	6.96	0.77	0.562
40	5.352	4.645	7.565	22.58	8.18	0.72	0.636
50	5.552	4.668	7.576	22.71	9.26	0.67	0.686

Table 7-5
Pulsation Period for Radial and Quadrupole ($\ell = 2$) Oscillations[a]

$M/M_\odot$	F	$1H$	$2H$	p_3	p_2	p_1	f	g_1^+	g_2^+	g_3^+
10	2.246	1.562	1.184	0.967	1.207	1.608	2.390	5.000	7.572	10.135
20	3.440	2.144	1.600	1.297	1.624	2.176	3.338	8.469	13.056	17.642
30	4.406	2.540	1.882	1.520	1.905	2.559	3.963	11.679	18.176	24.661
40	5.226	2 844	2.099	1.691	2.121	2.854	4.435	14.755	23.084	31.360
50	5.945	3.099	2.281	1.834	2.302	3.098	4.820	17.747	27.857	37.848

[a]Here F is the fundamental radial period, $1H$ and $2H$ its first and second overtones. The letters p_3 through g_3^+ denote the modes of the quadrupole nonradial oscillations The pulsation period, Π, is in hours.

Table 7-6
Pulsation Period for $\ell = 1$ Oscillations[a]

$M/M_\odot$	p_3	p_2	p_1	g_1^+
10	1.050	1.335	1.825	7.867
20	1.417	1.814	2.510	13.515
30	1.666	2.143	2.995	18.804
40	1.857	2.398	3.378	23.916
50	2.016	2.611	3.701	28.919

[a]The letters p_3 through g_1^+ denote the modes of the $\ell = 1$ nonradial oscillations. The pulsation period, Π, is in hours.

Aizenman et al. (1975) on the pulsation characteristics (both radial and nonradial) for main-sequence stars with masses of $10 - 50\ M_{\odot}$. The chemical composition is $X = 0.72$, $Y = 0\ 25$, and $Z = 0.03$. The pulsation properties of stars which have evolved away from the main sequence have been considered by many authors. Shibahashi and Osaki (1976) have examined the stability of gravity modes for 5, 11, 20, and $40\ M_{\odot}$. Lesh and Aizenman (1974) have computed the pulsation properties of stars of 10 and $15\ M_{\odot}$ at several stages in their evolution away from the main sequence. Two abundances have been considered: $X = 0.72$, $Z = 0.03$ and $X = 0.69$, $Z = 0.06$. A comprehensive study of the nonradial modes of oscillations of stars of 5, 10, and $16\ M_{\odot}$ has been made by Roth and Weigert (1979) with an initial chemical composition of $X = 0.602$, $Z = 0.044$. Unfortunately, no tables are provided of the oscillation frequencies or the damping times. Their results are presented in graphical form. Nevertheless, these graphs provide an excellent example of the phenomenon of "avoided crossings."

While there have been indications of instabilities in some nonradial modes, these results are all based on a quasi-adiabatic calculation. All such work needs to be confirmed by a full non-adiabatic analysis. Very few calculations of this latter type have been made.

Page intentionally left blank

Page intentionally left blank

8
UNSOLVED PROBLEMS

INTRODUCTION

In the preceding chapters observational and theoretical information about B stars has been reviewed and evaluated. Now we shall attempt to find out how far we have come in studying B stars

Some important goals of this chapter are (1) to assess the level of understanding we have of the physics of single, isolated B stars; (2) to discuss the problems which still face us; and (3) to suggest some ways in which the modeling of B stars might be improved. An important step is to compare observed details in the spectra of B stars, with the expectations we have from the existing models for B-type atmospheres and the process of spectrum formation, and to note the agreements and inconsistencies that exist taking into account all the energy regimes for which we have information. We shall compare the fundamental properties of B stars such as mass, effective temperature, and radius, with the results of the theory of the evolution of massive stars, and take note of the agreement that exists.

Emphasis is placed on the analysis of the light from single stars because in these cases the interpretation of the spectrum is reasonably straightforward. Stars which have companions are expected to behave in much the same way as single stars do, but the interpretation of their spectra may be complicated by the presence of light from both of the stars as well as of light from gas in the system, and the physical state in the atmosphere of one star may be influenced by the presence of the companion star. Reference is made to double and multiple stars only when observations of such systems can be used to determine some geometrical or dynamical factors.

General information about the B stars has been given in Chapter 2, while the character of the spectra of B stars of different sorts has been reviewed in Chapters 3, 4, and 5. The significant results are summarized in the next section. The theory of stellar spectra has been summarized in Chapter 6 and that of stellar evolution in Chapter 7. In the third section of this chapter the confrontation between the theory of stellar evolution and the observations is examined. In the fourth section several lines of thought concerning modeling stellar atmospheres are considered and some new ideas are advanced. In the final section we draw conclusions and make recommendations concerning directions in which further work would be valuable.

SIGNIFICANT OBSERVATIONAL RESULTS

Here we summarize what is known about B stars.

Masses

Studies of eclipsing double-lined spectroscopic binaries have shown that the B stars of the main-sequence band have masses in the range from about 2.5 to 16.5 $M_{\odot}$ (see Table 2-11), and that

the B-type supergiants may have masses in the range 20 ± 5 $M_\odot$. However, the masses of the supergiants are rather poorly known from direct information. The theory of evolution has shown that the luminosity of a model star when the star has a specified effective temperature is determined chiefly by the mass of the star. This result is rather insensitive to the details of the modeling process. Reliance on this fact lets us conclude that the masses of the B-type supergiants fall in the range from 10 to 30 $M_\odot$ (see Chapter 7).

Radii

From studies of eclipsing binaries, we find that B stars in luminosity classes IV and V have radii in the range from 2.6 to 8.1 $R_\odot$ (see Table 2-10). Use of angular diameters and distances estimated from the various calibrations of luminosity criteria in terms of M_V (see Chapter 2) leads to radii in the range 2.7 to 8.2 $R_\odot$ for stars of luminosity classes IV and V and to radii in the range 3.9 to 12.5 $R_\odot$ for stars in luminosity classes II and III (see Table 2-12) The supergiants are larger, the Ib supergiants having radii in the range 20 to 30 $R_\odot$, and the Ia supergiants radii in the range 35 to 80 $R_\odot$ (see Tables 2-12 and 4-1). The linear radii of supergiants are more uncertain than those of main-sequence stars because the distances to the supergiants are uncertain. If precise absolute photometry is available, angular diameters can be determined with an uncertainty of only 2 percent. Among the B stars of the main-sequence band, that is stars in luminosity classes II to V, those with high effective temperatures are larger than those with low effective temperatures. Among the supergiants the situation is reversed; the late B supergiants, particularly those of luminosity class Ia, are larger than the early B supergiants.

Effective Temperatures

The effective temperatures of B stars in the main-sequence band range from about 1.1×10^4 K at type B9 to about 3.1×10^4 K at type B0 (see Tables 3-4 and 3-5). The effective temperatures of the B-type supergiants are lower than those of B stars in the main-sequence band having the same subtype (see Figure 4-1). Their effective temperatures range from $1\ 05 \times 10^4$ K at type B9 to 2.5×10^4 K at type B0. The effective temperature is the same, so far as can be determined, for Ib and Ia supergiants of the same subtype. The superluminous supergiants of type B1 Ia+ are about $2\ 0 \times 10^3$ K cooler than the Ib/Ia supergiants of type B1. Any luminous star which has a spectral type with the letter p attached tends to be cooler than normal Ib/Ia supergiants of the same subtype.

So far as can be determined, Beta Cephei stars and the Bp stars of the main-sequence band have about the same effective temperatures as normal B stars with the same nominal spectral type. This is also true for Be stars when the emission in the hydrogen lines is not strong. In the cases when the photometry of Be stars which is used to determine angular diameters and effective temperatures has been obtained while the star was in an active phase of emission-line activity or showing conspicuous shell lines, the interpretation of the photometric data in terms of an angular diameter and effective temperature is somewhat insecure. Nevertheless, the photometry does give a global measurement of the energy received from the star. This quantity is what determines the effective temperature of the star. Probably the effective temperatures listed for such active stars by Underhill et al. (1979) are more uncertain than the values for normal stars, but they are not without meaning since the effective temperature varies as the one-fourth power of the integrated flux (see Chapter 3). One can tolerate an error of 25 percent in the estimated integrated flux.

In each case studied, the total amount of radiation which is received from an active Be star is confirmed by the general appearance of the light from the star, that is the spectral type. Thus, it is unlikely that the uncertainty of the derived effective temperature is greater than $\pm 2.0 \times 10^3$ K. The uncertainty may well be smaller than this. Similarly, the angular diameters which are derived for active Be/shell stars are not completely meaningless, particularly when flux radiated in bands of intermediate width and not containing

strong shell absorption or emission lines are used. The angular diameter is proportional to the one-half power of the monochromatic flux. Typically, the uncertainty in the angular diameter should not exceed ± 10 percent. Thus, although the positions of active Be/shell stars in the HR diagram are more uncertain than are the positions of inactive Be stars, they are not unknown

The effective temperature found from an integrated flux and from an angular diameter of a B-type star may be confirmed by comparing the shape of the spectrum over a wide range of wavelengths with that predicted from a model atmosphere. Theory shows that the shape of the continuous spectrum from a model over the range from 1500 to 8000 Å is sensitive chiefly to T_{eff} and very little to the methods used to construct the model atmosphere (see Chapter 6). When using the shape of the spectrum to confirm an effective temperature, one must first make a reliable correction for interstellar extinction and one must make the comparison over ranges of spectrum that are free from emission in the hydrogen bound-free continua formed in the mantle and from free-free emission which is most often seen as an infrared excess. A color index evaluated between 1600 and 4000 Å and corrected for interstellar extinction is a useful and sensitive indicator of effective temperature.

The size of the Balmer jump is a good indicator of effective temperature for B stars which do not show Hα in emission. It has the advantage that a secure correction for interstellar extinction is not needed. However, stars which show unusual strength of Hα in emission or in absorption, usually show the Balmer continuum in emission or as an extra strong absorption as in some shell stars. Then, unless one can be sure that the measurement of the size of the Balmer jump refers only to the energy radiated from the photosphere and that it is not contaminated by the energy absorbed or radiated by the mantle, the size of the Balmer jump is an unsatisfactory indicator of effective temperature.

The relative intensities of lines from elements present in the spectrum of the star in two or more stages of ionization is usually an unreliable indicator of effective temperature. In Chapter 3, we have shown that this criterion leads to values for the effective temperatures of main-sequence stars that are slightly high In the case of supergiants, the bias is very significantly toward high temperatures (see the discussion in Chapter 6 and in Chapter 4). This method of estimating effective temperatures for B stars is unsatisfactory because it yields results that are biased toward high values. Now that the continuous spectrum of B stars can be observed over a long wavelength range, it is desirable to find the effective temperatures of B stars from absolute spectrophotometry of the continuous spectrum. Assumption of a universal law of interstellar extinction is a necessary and acceptable first step. Only in the case of very heavily reddened stars may the results of an effective temperature determination be sensitive to the precise form adopted for the interstellar extinction law Then confirmation of one's choice of extinction law must be sought by seeking support from the analysis of the relative strengths of lines formed in the photosphere of the star to determine the effective temperature

Composition

The relative abundances of the elements in B stars are determined by analyzing the relative strengths of lines by means of model atmospheres (see Chapter 6) Since the presently available model atmospheres are suitable for representing only the photospheres of B stars and not the mantles, the most reliable results are obtained when the analysis is confined to lines which can be shown to be formed predominantly in the photosphere. Practically all analyses that have been done indicate that the composition of the atmospheres of B-type stars is solar.

In a few cases, some lines having anomalous strengths have been analyzed and anomalous abundances, usually by a factor 3 to 5 at most, are suggested to be present This type of conclusion may be questioned on the grounds that the absorption lines which are found to suggest anomalous abundances are formed in the mantle of the star. Until appropriate models for the mantles of stars have been developed, caution is advised in concluding that abundance anomalies

are present in B stars.

We have presented data showing that autoionization and dielectronic recombination may be important for determining the ionization balance between Si II and Si III. This may be deduced on the one hand from the observation that the lines of multiplet UV 13.04 of Si II at 1305.59, 1309.46 and 1309.77 Å are unusually strong and broad in main-sequence and supergiant stars (see Chapter 3) and on the other hand from the observation of these Si II lines in emission in the spectrum of P Cyg (see Chapter 4). It appears that the lifetime of the $3s3p3d\ ^2F^o$ levels of Si II is shortened by autoionization with the result that the damping constants of the lines of multiplet UV 13.04 are unusually large, while in the low density gas of the outer part of the atmosphere of P Cyg dielectronic recombination drives the lines of multiplet UV 13.04 into emission. No calculations of the ionization balance between Si^+ and Si^{++} have been made taking these processes into account. Because of this, the Si abundance in B stars is uncertain.

In the second and third spectra of the rare earths and other elements with many electrons, several series of energy levels having doubly excited electrons are known to exist. It seems very likely that the ionization balance which is established in stellar atmospheres between the various ions of this sort may be a result of autoionization and dielectronic recombination as well as of radiative and collisional transitions between levels in which only one electron is excited. Some of the differences in line strengths which are attributed in the existing analyses of B-type spectra to differing abundances may be due to inaccurate evaluations of the degree of ionization and excitation in the stellar atmosphere. The new observations of multiplet UV 13 04 of Si II reported here provide a warning that calculations of abundances based on LTE, or even on the more complex premises of non-LTE, can be in error when processes such as autoionization and dielectronic recombination are incompletely evaluated, or not evaluated at all.

One significant abundance anomaly is seen in the spectra of a few B stars, which appear in other respects to have spectra very like normal B stars. This is that the hydrogen lines may be very weak or absent and the He I lines strong. There is no doubt that a few B stars have lost all, or nearly all, of their outer hydrogen-rich envelope and that they are now showing to us layers that are enriched in helium. These stars are reviewed in Chapter 5. The conclusion that they are old stars on their way to becoming subluminous hot stars seems justified.

The interpretation of the spectra of the stars which show variations in the intensity of their He I lines is not yet fully satisfactory. Plausible arguments can be made that the observed changes in line strength occur because the star has a spotted disk and at different times it presents areas having different compositions, particularly as regards the relative abundance of hydrogen to helium However, it is not clear what causes the spots to appear and how they obtain a different composition from the rest of the star and maintain this separate composition.

Since so many of the conspicuous lines in the visible spectra of B-type supergiants are formed in the mantle or high in the photosphere where conditions in the mantle are affecting conditions in the photosphere, claims that some of the B-type supergiants show anomalous compositions must be treated with caution. A better understanding of the observations should result once appropriate models have been made for the mantles of B-type supergiants.

Properties of the Mantle

In Chapter 3 we have reviewed the information given by the ultraviolet spectrum of B stars in the main-sequence band and in Chapter 4 we have made a similar review for B-type supergiants. From these studies and after review of what was known from the part of the spectrum observed from the surface of the Earth, it became apparent that the atmosphere of a star should be modeled in two parts. (1) a photosphere where the classical conditions of radiative and hydrostatic equilibrium in plane-parallel layers give a firm basis for developing useful models, and (2) a mantle where radiative and hydrostatic equilibrium are no longer adequate concepts and where considera-

tion of three-dimensional geometry is essential

We have seen that mantles all possess the following properties·

1 Mantles contain plasma that is heated to electron temperatures above what can be supported by the amount of radiative energy provided by the effective temperature of the star and distributed under the constraint of radiative equilibrium.
2 Mantles are inhomogeneous; evidence can be seen, especially in the supergiants, for the presence of hot and of cold plasma in regions which do not necessarily cover the whole disk of the star or remain confined to spherical shells.
3. Matter flows out of mantles at speeds which exceed the velocity necessary for gas to travel from the photosphere to an infinite distance and arrive there with zero velocity.

The spectroscopic evidence is incontrovertible that energy is being deposited in the outer parts of the atmosphere in excess of the amount carried there by the radiation field, and that outward directed momentum is being transferred to the plasma in the outer part of the atmosphere. In Chapter 4, we noted that a plausible source for this nonradiative energy and the extra momentum was interaction between the small ambient magnetic fields, which may be expected to be present in the photosphere, and differential motion, possibly generated by the rotation of the star We suggested that a number establishing the density of magnetic energy per unit volume in the upper photosphere and a number specifying the typical size of the differential motions might be useful parameters to govern the conditions in a model of a mantle The temperature distribution and the density and velocity distributions in a mantle must be found from solutions of the equations for conservation of energy, mass, and momentum.

The visibility of the mantle of a B star differs for stars in the main-sequence band from its value for supergiants. The mantles of the B-type supergiants are readily visible by means of the ultraviolet spectrum, and especially for late B-type supergiants, by means of the infrared excess In the case of the main-sequence stars, the mantles are much more difficult to see and only occasionally does the presence in the spectrum of a wing on Hα, wind profiles from high ions, or the detection of X-rays indicate that a mantle is present

The detection of emission at Hα in the spectra of main-sequence and supergiant B stars is always an indication of the presence of a mantle, as is the observation of emission in the Balmer continuum or a free-free infrared excess. The possibility that the subluminous B stars also have mantles has not been excluded, although observations demonstrating this are not known to us.

The rate of mass loss from the mantles of B-type supergiants has been reviewed in Chapter 4; some results are given in Table 4-11. For the B0 Ia supergiants, $\dot{M}$ is of the order of $2 \times 10^{-6}\ M_{\odot}$ yr^{-1}; for late B supergiants $\dot{M}$ is of the order of $10^{-7}\ M_{\odot}\ yr^{-1}$. The rate of mass loss from the atmospheres of main-sequence B stars is suspected to be of the order of 1 percent of these values, but few estimates have been made of $\dot{M}$ from main-sequence stars because of the paucity of features to analyze. When the Hα observations of Furenlid and Young (1980) have been analyzed by means of models of the part of the mantle which is in outflow, some information may become available on the rate of mass loss from main-sequence B stars.

CONFRONTATION WITH THE THEORY OF THE EVOLUTION OF MASSIVE STARS

Here we summarize what we have found out in this field of study.

Choices in the Methods for Making Model Stars

Four areas in which choices are made in the methods used to construct massive model stars have been examined in Chapter 7. They are (1) the choice concerning the opacity tables used to calculate the transport of energy by radiation, (2) the way in which the transport of energy by convection is handled, (3) the choice of composition, and (4) the choice whether to include mass loss or not.

Chapter 7 shows that in the case of model

stars with masses less than 10 $M_{\odot}$, there is not much difference in the theoretical HR diagram and other results obtained from the theory of the evolution of stars when the Carson opacities are used from when Cox-Stewart opacities are used. However, when the mass of the model star is greater than 10 $M_{\odot}$, significant differences do occur in the theoretical HR diagram, in the internal structure of the model stars, and in the energy sources which the model stars tap as they traverse the various areas in the HR diagram. The Carson opacities are found by using a "Fermi-Thomas" model atom when calculating the opacity of stellar material at temperatures and densities relevant for constructing massive model stars; the Cox-Stewart opacities use a simpler "hydrogenic" model for atoms. (See Carson, 1976 for a review of the theory used for evaluating the opacity to radiation of stellar material.)

Massive model stars having $L/M > 10^3$ in solar units and made using the Carson opacities show a large central condensation and a high radiation pressure in their envelopes. The time spent by these model stars in the phase of burning hydrogen in the core is about the same as that spent by massive model stars made with the Cox-Stewart opacities (see Table 7-1). The time spent in the core-hydrogen burning phase is dependent chiefly on the mass of the star However, the luminosity and the source of energy are different when model stars of the same mass but different opacities have the same effective temperature Model stars having masses of 30 $M_{\odot}$ and made using the Carson opacities are burning hydrogen in the core as they traverse the region occupied by the B-type supergiants while similar model burning helium in their cores. The observed masses and radii of the B0 stars and the observed effective temperatures of some O4 stars (Underhill, 1981a) indicate that real massive stars do not behave quite as do the massive model stars calculated by Stothers and Chin (1977) using the Carson opacities. Therefore, in what follows, we shall refer to the results obtained using the Cox-Stewart opacities to make model stars even though use of a "hydrogenic" model atom for the relatively abundant elements C, N, and O is not truly satisfying

If the Schwarzschild criterion is used to decide whether convection may be important for carrying energy and to find the appropriate temperature law in the envelope when convection occurs, changes in the mean molecular weight brought about by mixing the processed material of the core with the unprocessed material of the envelope are ignored. When the Ledoux criterion is used, the changes in mean molecular weight are taken into consideration. At present the problems of how best to handle the transport of energy when both convection and radiation transport energy, and how to determine the pressure and temperature structure of the envelope of a model star are under study. The situation in the envelopes of massive model stars is made even more difficult by the instabilities to pulsation which may develop. The results which we have selected for display in Figures 7-1, 7-2, and 7-3 make use of the Schwarzschild criterion. The position of the evolutionary track of a massive star as it crosses the region of the B-type supergiants is quite sensitive to the choice which is made in the modeling method as regards convection and composition. Therefore, it is not possible to deduce accurately the mass of a supergiant from knowledge of its position in the HR diagram.

The initial composition of the model star, so long as the model is in the main-sequence band and it has a more or less Population I composition, makes very little difference to the predicted luminosity and effective temperature of the model. When, however, the model star begins its rapid traverse of the HR diagram toward the position of the red supergiants, the composition may have a significant effect on the position of the deduced track in the HR diagram. We have selected for display models with X in the range 0.70 to 0.74 and Z in the range 0.02 to 0.04. At present we cannot choose between the available models. All are adequate for helping us to interpret the observed HR diagram.

The effects of mass loss on massive model stars have been investigated for three formulations of the rate of mass loss in terms of the instantaneous mass, luminosity, and radius (or effective temperature) of the model star. This is reviewed in Chapter 7. When the adjustable parameters

are selected so that the models give rates of mass loss like those observed for B stars in the main-sequence band, it makes very little difference which formulation for $\dot{M}$ is used. Appropriate results for B0 stars are obtained with $\dot{M} = -kLM/R$, where L, M, and R are in the solar units and k has a value near 1×10^{-11}. They are also obtained by using the formulation $\dot{M} = -NL/c^2$ with the constant N having a value near 100. The third formulation which is used is a complicated one which has been deduced from the theory for radiatively driven winds of Castor et al. (1975). This formulation contains two free parameters, K and α which are given appropriate values (see Chapter 7). The quantity Γ in the formulation varies as L/M.

If the model star is constrained to lose mass at the rate seen for a real star in the middle of the main-sequence band, the evolutionary track for the model star is found to cross the region of the B-type supergiants in about the same area as is found for evolution without mass loss The change in $\log L/L_{\odot}$ when the model has a selected value of $\log T_{\text{eff}}$ is comparable to what may occur by changing the composition of the model or the representation of how convection is handled.

Tanaka (1966) showed that the major effects of mass loss on the evolution of a massive star were the following. (1) At the same stage of central hydrogen depletion, a massive mass-losing model star will have a lower luminosity and a lower effective temperature than a model star of the same initial mass but which evolves at constant mass; (2) in the mass-losing model star, there is increased stability against convection in the envelope; (3) in the mass-losing model star there is a larger fraction of the mass in the convective core than is the case for a model star evolving without mass loss. Subsequent work on mass loss has verified and expanded these conclusions. Frequently, the hydrogen burning lifetime of a model star is increased when the model star loses mass, but in some published results, the lifetime is shortened slightly.

For interpreting the positions of main-sequence and supergiant B stars in the HR diagram, consideration of mass loss leads to uncertainties of the same order as those introduced by the choices which are made concerning the representation of the opacity as a function of temperature and density, the transport of energy by convection in the envelope, and the composition of the star. These uncertainties are not large while the model stars are in the main-sequence band, but they do become significant when the massive model stars move to the right of the main-sequence band in a plot of $\log L/L_{\odot}$ against $\log T_{\text{eff}}$. The time spent burning helium in the core is of the order of one-tenth that spent by the model star in the main-sequence band burning hydrogen in the core. Model stars with masses of the order of $10\,M_{\odot}$ or less do not commence to burn helium in their cores until they enter the region of the red supergiants. A model star of $25\,M_{\odot}$ has completed its helium burning in the core by the time it leaves the region of the B-type supergiants.

In the adopted models for massive stars, it is assumed here that the representations of the processes which generate energy in the core of a star used by the several investigators are satisfactory. We make no attempt here to offer a critique of what is presented for the rates of burning hydrogen and helium in the cores of massive stars and for the generation of energy by contraction.

Comparison of Observed HR Diagrams with Theory

Main-Sequence B Stars. A comparison of the positions of nearby B stars in the HR diagram with the theoretical position of the main-sequence band is shown in Figure 7-5. All the stars of type B3 and later are observed to be evolved and to lie on the right-hand side of the main-sequence band or past the point where burning hydrogen in a shell has begun. Their age is estimated to lie in the range 2.2 to 24×10^7 years. The early B-type stars close to the Sun do occupy the full main-sequence band and their ages are estimated to lie in the range 0.6 to 2×10^7 years. It seems that the star formation within about 500 pc of the Sun has occurred at two times.

The empirical position for the ZAMS for stars of type B2.5 and later recommended by

Eggen (1974a) is found to lie close to the theoretical ZAMS, but for early B stars it deviates into positions occupied by evolved stars (see Figure 7-6). The empirical ZAMS of Crawford (1978) parallels the shape of the theoretical ZAMS for spectral types from B0 to B9, but it is displaced toward brighter luminosities by about 0.2 in $\log L/L_{\odot}$.

Supergiant B Stars. The B-type supergiants are found to lie in a diagonal area of the HR diagram to the right of and above the main-sequence band Only the O9/B0 supergiants of luminosity class Ia and the B1 Ia+ supergiants are found to have luminosities, $\log L/L_{\odot}$, in the range from 5.5 to 6.0. All the others are fainter than this. The peculiar supergiant P Cyg is found to lie in the band occupied by the normal Ia supergiants. It has $\log L/L_{\odot} = 5.05$ or $M_{bol} = -8.1$. The supergiants within about 1.5 kpc of the Sun appear to belong to the young population of B stars. Most seem to have ages less than about 10^7 years. The uncertainty in $\log L/L_{\odot}$ for the supergiants is due chiefly to uncertainties in their distances. It is about ± 0.2.

The observations of Humphreys (1978, 1979) show that the B-type supergiants of our galaxy occupy about the same region in the HR diagram as do the B-type supergiants of the Large Magellanic Cloud. Since Humphreys adopts different effective temperature and bolometric correction scales for supergiants than are found to be valid here, her diagram of M_{bol} vs $\log T_{eff}$ must be stretched in an irregular manner before it can be compared with the results shown in Figure 7-5 (see Chapter 7 for details). When such a mental stretching is done, it is found that Humphreys' results for the supergiants are about the same as those presented here. Humphreys' luminosity for P Cyg of $M_{bol} = -10.7$ (see Humphreys and Davidson, 1979) is much too high. Her result is obtained chiefly by adopting an effective temperature of 2.1×10^4 K for P Cyg, the high visual absolute magnitude recommended by Kopylov (1958), and a bolometric correction of −2.3 mag. Humphreys and Davidson do not say what extinction they assumed for P Cyg The information reviewed in Chapter 4 shows that more appropriate values for P Cyg are $T_{eff} = 1.22 \times 10^4$ K, and $B.C. = -0.72$. The interstellar extinction is characterized by $E(B - V) = 0.35$ and the visual absolute magnitude is about −7.4.

CONFRONTATION WITH THE THEORY OF STELLAR ATMOSPHERES

Classically each star may be considered to be a sphere of gas in which a stream of energy is generated in the central core. The energy percolates outward and the net flow of energy appears as the light which is radiated from the layers on the surface of the star. The amount of energy leaving each cm^2 of the surface of the star as radiation is represented by the parameter called effective temperature. The radius and mass of the star are combined in the parameter g which gives the acceleration due to gravity in the photosphere of the star.

Classically the boundary layers of a model star form the photosphere. Here the pressure is very small in comparison to its value in the center of the star and the electron temperatures in the boundary layers have values close to the effective temperature of the star At great distances from the star, the temperatures are expected to reach the low values of the interstellar medium and the density will become equivalent to that of the interstellar medium.

We have seen in our review of B-type spectra that for the purpose of understanding stellar spectra, it is helpful to divide the atmosphere into two parts, the photosphere and the mantle. We have found that spectral features formed in the photospheres of the B stars may be interpreted by means of classical models constructed of plane-parallel layers in hydrostatic and radiative equilibrium. It has turned out that for most B stars nearly all of the continuous spectrum can be interpreted consistently by means of the classical picture. However, several discrepancies are evident when the strong absorption lines in the range of wavelength accessible from the ground are analyzed in detail, and when the continuous spectrum from 3100 Å to 10 μm is studied. When the observations made from space are added to the observations obtained from the surface of

the Earth, it becomes obvious that the classical picture of the stellar atmosphere is inadequate. Features which are formed in the part of the atmosphere which we have called the mantle cannot be described satisfactorily by means of classical models of the stellar atmosphere.

Briefly, observations from space and from the surface of the Earth of B stars reveal six types of spectroscopic phenomena which are completely unexpected and unexplained by means of the classical theoretical framework. They are as follows:

1. the presence of emission lines whose intensities are often seen to vary,
2. the presence of absorption lines from higher ions than may be expected to be present in the atmosphere according to the principle of radiative equilibrium and the value of the effective temperature of the star;
3. the existence of the outflow of matter at velocities exceeding the velocity of escape from the photosphere of the star,
4. the presence of discrete components for some of the resonance lines, these components often being seen to vary in intensity and velocity displacement,
5. the presence of X-rays;
6. the presence of an infrared excess and of radio emission from some Be stars and some B-type supergiants.

The occurrence of these spectroscopic phenomena has required us to revise our picture of the physical state of the atmospheres of B stars. Two-part models as described in the next section are required to enable us to make order among the multitude of observational facts. When the abundance of observational detail which has appeared in the last fifteen years has been reduced to some semblance of order, it will become possible to estimate the physical conditions in each part of the two-part model atmospheres and to pose questions such as how did these conditions arise, what are the mechanisms causing the phenomena which we see, and do these mechanisms have any significance for the evolution of B stars. We are particularly interested in understanding the factors that cause the particular types of B stars reviewed in Chapters 3, 4, and 5, and in Part II to show variable and anomalous spectra.

A Two-Part Atmospheric Model

In Chapter 1 we noted that it is helpful to think of the atmospheres of B stars as being divided into two parts: a photosphere where chiefly the continuous spectrum is formed and a mantle, or outer covering, where the dominant lines are formed. This model has been used in the discussion of the observations presented in Chapters 3 and 4. The mantle is postulated to be transparent or nearly so in most continuum wavelengths but opaque in the central wavelengths of the prominent spectroscopic lines The deposition of nonradiative energy in the mantle is an important factor which establishes the physical state of the mantle.

The mantle may be divided into three parts. (1) an inner corona-like region where the electron temperatures are high relative to the effective temperature of the star, but they do not exceed 10^6 K, (2) truly coronal regions which have temperatures of the order of or greater than 10^6 K and which may be small, and (3) a post-coronal region where cooling to the state of the surrounding interstellar medium takes place. For many stars, outward flow of material seems to start in or just above the photosphere, possibly in the same region where the deposition of nonradiative energy begins to become apparent.

The analyses of the spectra of supergiant B stars suggest that usually the acceleration of particles to trans-sonic velocities takes place within a short geometric distance of the outer edge of the photosphere and that the rise to high temperatures takes place also within a short geometric distance of the photosphere. It seems that the corona-like region of the mantle may contain truly coronal regions, perhaps small, in which X-rays are generated. The corona-like region is followed by a post-coronal region in which accelerations and decelerations may be small and in which cooling occurs. The material of the post-coronal region will eventually reach a state which matches the conditions of the surrounding interstellar medium.

Since the photosphere of a B star and the

three parts of the mantle have rather different temperatures, densities, and states of motion, each of these parts of the atmosphere of a B star is best observed by means of different spectroscopic features. Possible spectroscopic signatures for the photosphere, the corona-like region, the truly coronal regions, and the post-coronal flow are described in the next section. They have been selected after considering the implications of the theory of stellar spectra as applied to B stars (see Chapter 6), and the detailed appearance of B-type spectra over a wide wavelength range (see Chapters 3, 4, 5, and Part II).

There is no reason to believe that the mantles of all B stars are spherically symmetrical and uniform in their properties. However, the mantles of B-type supergiants and of normal main-sequence B stars are usually considered in a first approximation to be spherically symmetrical. The occurrence of relatively sharp, displaced absorption components for some ultraviolet resonance lines indicates that the mantles can be inhomogeneous. The changes in the displacement and the strength of the components show that the pattern of the inhomogeneity changes as time progresses. Rapid rotation may alter the shape of a star from being truly spherical to being flattened at the poles and rotation may modify the temperature distribution over the face of the star (see, for instance, the work of Collins and Sonneborn, 1977). In the discussion which follows, distortions from a purely spherical shape of the photosphere will be neglected because their effects on the observed spectra are of secondary importance to those caused by the mantle.

Spectroscopic Signatures

Photospheres. The shape of the continuous spectrum, after correction for wavelength-dependent interstellar extinction, is the best spectroscopic criterion by which to observe the photosphere of a B star. The rather dense layers of the photosphere have only a small geometric extent relative to the radius of the star and they can be modeled satisfactorily by means of classical plane-parallel layer models which are in radiative and hydrostatic equilibrium. Only the densest and most extensive mantles of B stars have enough opacity in wavelengths near the heads of the continua of hydrogen and in infrared wavelengths, where free-free opacity is large, to be visible in continuum wavelengths.

Mantles: The Corona-Like Regions. An extensive mantle containing much material may be observed by means of continuous emission or absorption near the heads of the Balmer and Paschen continua and by means of free-free emission or absorption. Observations of this sort have been made for some B-type supergiants and for some Be stars. In these cases, the mantle modifies the continuous spectrum radiated by the photosphere, adding and subtracting radiation by a detectable amount at continuum wavelengths where the absorption coefficient is large Whether the mantle is seen as causing extra emission or as causing extra absorption at wavelengths in the continuum depends upon the orientation of the mantle relative to the photosphere and on the aspect at which the mantle is viewed by a distant observer. It also depends on the distribution of temperature and density in the mantle. The geometrical shape of the mantle and its temperature and pressure structure determine the values for the source function along each line of sight to the star. The energy that is observed at the Earth in a stellar spectrum is the integrated energy received from all lines of sight coming from the extended face presented to the observer by the star and its mantle and collected by the observer's telescope.

The corona-like parts of the mantles of B stars are revealed readily by absorption and emission in lines from ions which are particularly abundant when electron temperatures are high and densities are low. Useful lines are those from the ground levels of C^{+3}, N^{+4}, O^{+5}, and Si^{+3}. Cool regions of the mantle may be seen in lines of He I, particularly lines from the 2^1S, 2^3S, 2^1P^o and 2^3P^o levels, and the resonance lines and lines from metastable levels of the once and twice ionized metals. The coolest regions of the mantle are most easily observed by means of lines from low lying levels of neutral atoms.

The designations "hot" and "cool" are relative to the electron temperatures in the photo-

sphere. In the photosphere, where radiative equilibrium is dominant, the electron temperatures lie in the range from about 0.8 T_{eff} to about 1.2 T_{eff}. This is the range of temperature in the photosphere most important for forming the continuum in visible wavelengths and for forming weak absorption lines from ions which are not abundant.

Mantles: The Truly Coronal Regions. The temperatures in the corona of the Sun are greater than 10^6 K. X-rays as well as lines from very high ions such as Si XII, Fe XV, and Mg X are emitted from localized regions of the solar corona. Although X-rays have been observed from a few main-sequence and a few supergiant B stars, generally the part of the spectrum of B stars at wavelengths shortward of 912 Å is not accessible to observation from the vicinity of the Earth owing to the extinction caused by the interstellar gas which lies between us and the B stars. Thus, we have very little information that can be used to place limits on the physical conditions in the hottest parts of the mantles of B stars

In the corona-like regions which we do see by means of ultraviolet spectra, the electron temperature may be of the order of 10^5 K. However, it is not excluded that for all stars, the electron temperatures in some limited parts of the mantle may be as high as or higher than 10^6 K. Such regions are expected to be the places where X-rays are generated. If the X-rays are to emerge from the star, the very hot regions must be in the outer part of the mantle. Lucy and White (1980) have proposed that appropriate regions could be generated by means of shocks resulting from conditions in a turbulent, flowing gas driven by radiation pressure. X-rays are observed from cool B stars, such as π Cet, B7 IV, as well as from the luminous OB stars. The origin for the X-rays may be different for stars occurring in different areas of the HR diagram.

Mantles: The Post-Coronal Region. This region is best observed by means of radio emission and an infrared excess. It has been detected for some Be stars and some supergiants (see Chapters 2, 4, and Part II)

Conditions That Appear to Exist in a Mantle

Let us consider some very simple schematic representations of the dependence of the physical state of a mantle upon position in the mantle. In this first approximation we shall ignore the indications that mantles are inhomogeneous

Let the position of any point in the mantle of a star be defined by giving its polar coordinates ϕ, ϑ, and r, where ϕ is an azimuthal angle about the axis of rotation of the star, ϑ is a latitude measured from the equator, and r is the distance from the center of the star to the point in question. We shall usually consider descriptions that show a dependence only upon r, the properties of the mantle supposedly being spherically symmetrical. The patterns which are sketched below have been developed from the observations presented in previous chapters and summarized in the section Significant Observational Results of this chapter. These patterns are mnemonic rather than factual.

Figure 8-1 shows how the electron temperature in a star might vary as distance from the center of the star increases. No scale is marked on the axes for temperature, T, and distance, r, and the scale along each coordinate is neither linear nor uniform. The purpose of Figure 8-1 is to show the major types of change in the temperature law that seem to occur rather than to present an accurate graph of what is known for any one star. The values for the effective temperature of the star and the radius of the photosphere are marked on the axes.

The temperature of the star decreases outward from the high values which occur in the core, where energy is generated, the rate of decrease in the photospheric layers is that appropriate for radiative equilibrium. At a short distance beyond the level where the temperature equals the effective temperature of the star, an input of nonradiative energy becomes significant and the temperature rises rapidly to temperatures of the order of 10^5 K, the maximum temperature reached and the thickness of the region in which this temperature is maintained being determined by a balance between the efficiency of the heating processes and the rate of cooling which results from the expansion of the gas in these layers, the conduc-

tion of heat to denser layers, and the radiation of the gas to interstellar space.

The true spatial relationships between the photosphere, the transition layer, the hot corona-like layer and the truly coronal regions can be determined only by making a hydrodynamical model of these layers, which model should include the effects of the yet unspecified heating mechanism. The appropriate model can be selected from several trial models by calculating theoretical line profiles and comparing them with the observed profiles of lines believed to be formed in the mantle. A preliminary estimate of the extent of the corona-like layer can be made by noting that the emission components of most resonance lines of high ions seen in the spectra of B-type supergiants are not prominent (see Chapter 4) and emission components are not detected at all for normal B-type main-sequence stars (see Chapter 3). In analogy with the results deduced from the analysis of the profiles of resonance lines of high ions in the spectra of O stars and a few B-type supergiants (see, for instance, Hearn, 1975a, Lamers and Morton, 1976; Lamers and Snow, 1978; Cassinelli et al., 1978; Olson, 1978, and Cassinelli and Olson, 1979), one is led to conclude that the corona-like region lies close to the photosphere and that it is not extensive Most probably $R < 2R_*$. In a study which compares mass flow in an atmosphere to that of gas through a nozzle, Thomas (1973) has suggested that an outward flow of material starts in the photosphere at very small velocities and that for the OB supergiants the outward directed velocities attain trans-sonic values at a distance of about 1.001 stellar radii. By this distance the transition layer leading to a corona-like region is believed to be well established. The discussion of Hearn (1975a) indicates that as the temperature in the corona-like region increases, the critical point where the trans-sonic velocities are attained may be expected to move closer to the photosphere. Thus, the size of the region where outward velocities significantly higher than the local thermal velocity occur is linked to the efficiency of the heating process which produces the corona-like region. Small, truly coronal regions giving rise to X-rays are believed to be imbedded in the corona-like region.

At distances where the major input of energy has ceased, a cooling of the mantle will take place. Slow cooling with increasing distance is expected for mantles having low densities (represented by curve A in Figure 8-1), for these will not radiate strongly and conduction to the denser transition layer leading to the photosphere will be small, rapid cooling with increasing distance will occur when the densities and temperatures are such that the gas in the mantle radiates a strong line spectrum and losses by conduction are large. This situation is represented by curve B. The schematic boundaries of the three regions, photosphere, corona-like layers, and post-coronal region are shown in Figure 8-1. The stellar envelope, which has its properties determined by the theory of stellar structure and evolution, lies below the photosphere

The rate of flow of the material in a mantle may vary with the distance from the photosphere. The proper way to model the directed velocity field, which observations indicate exists, is to use the equations for hydrodynamic flow. Several ad

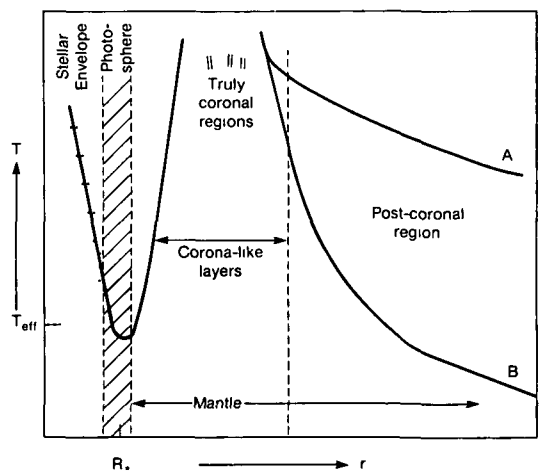

Figure 8-1. The suggested behavior of temperature as a function of distance in the photosphere and mantle of a B star. The thickness of the photosphere is less than about 0.1 R_*. Curve A suggests the temperature law for a low density mantle, curve B that for a high density mantle. The truly coronal regions are imbedded in the corona-like layers.

hoc velocity laws have been suggested for B stars, (see Chapters 4 and 6), and typical ones are illustrated in Figure 8-2. Here the radial-flow velocity is given in units of the outward directed velocity needed for material to escape from the photosphere and arrive at infinity with zero kinetic energy. Our knowledge about the escape velocities of B stars has been summarized in Chapter 2 and a reasonable extension of this has been presented in Chapter 4. The scale in the distance coordinate of Figures 8-2 and 8-3 is neither linear nor uniform.

Curves A and B of Figure 8-2 are the types of velocity laws that have been suggested for supergiants, while curve C may be valid for main-sequence stars. The terminal velocities observed by means of the winds from supergiants are greater than those observed for main-sequence stars of the same subtype. In fact, winds have been detected for only a few main-sequence B-type stars (see, for instance, Lamers and Snow, 1978, Furenlid and Young, 1980).

In all the models suggested so far for the mantle, the density distribution is determined from the adopted velocity distribution by assuming a constant rate of mass loss and conservation of matter in spherical shells. Thus, the parameter which governs the density distribution in these models is the estimated rate of mass loss.

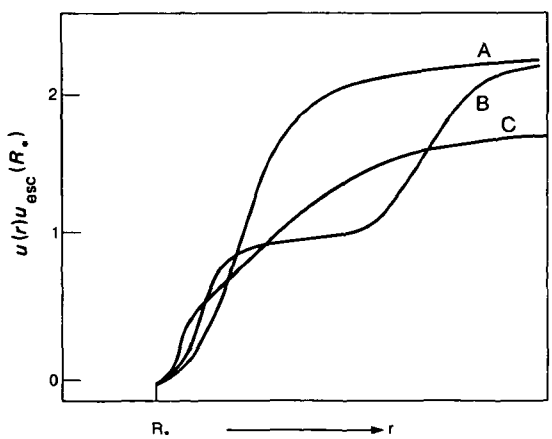

Figure 8-2. The behavior that has been suggested for the outward directed flow velocity as a function of distance in the atmospheres of B-type supergiants, curves A and B, and in the atmospheres of B-type, main-sequence stars, curve C.

No attempt has been made to solve for values of T, ρ, and u which are internally consistent with the set of equations which can be derived from the conditions that matter and momentum be conserved throughout the mantle and that the temperature results from the balance between all relevant gains and losses of energy.

In Figure 8-3 sketches are given of the cross sections presented to a distant observer by the several types of models that have been discussed in the literature for understanding the spectra of different types of B stars. Figure 8-3a shows the usual spherically symmetrical model; Figure 8-3b shows that which may be relevant for the interpretation of the line-intensity anomalies seen for some Bp stars and which may account

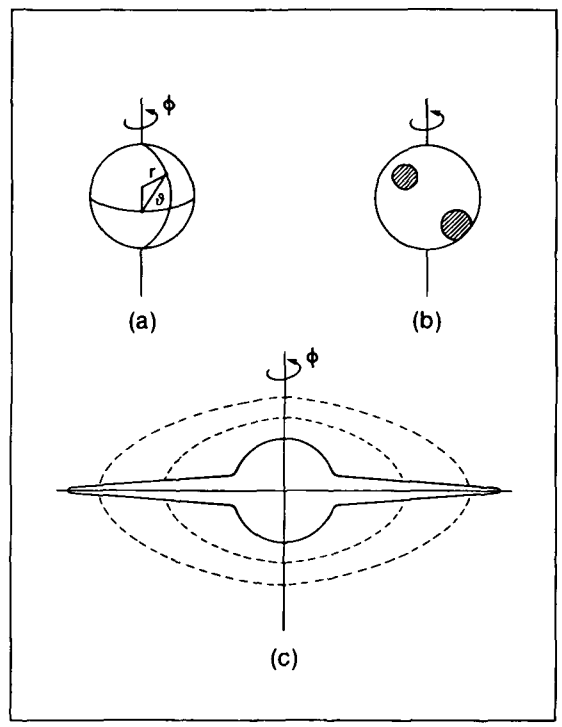

Figure 8-3. Cross sections perpendicular to the line of sight of three types of mantles. (a) the spherically symmetrical case, (b) a mantle that is composed of two or more streams (spots) of material having different temperature, density and flow patterns, each with a different dependence on the coordinates ϕ, ϑ, and r; (c) a mantle in which the symmetry about the equatorial plane differs from that about the axis of rotation.

for the short-term spectral variations of some supergiants; Figure 8-3c shows the classical model for a star which has cylindrical symmetry.

In Figure 8-3b, the emphasis is on nonuniformity of the cross section of the star as regards temperature, density, and possibly, rate of flow. This figure can be used to represent the oblique-rotator model, first introduced by Stibbs (1950) and later developed by others to explain the spectral variations of the Bp stars (see, for instance, the summary by Deutsch, 1970 and the application to B stars by Mihalas, 1973b). A spotted-rotator model may also be used for understanding the spectra of supergiants in terms of hot and cold streams, somewhat as for the Sun with its coronal holes and coronal streamers. The spots may be irregularly spaced and their distribution may change with time.

The temporal behavior of mantles is frequently irregular. Examples of the typical changes that are seen in the spectra of supergiants have been reviewed in Chapter 4. These spectral changes imply changes in the physical state of the mantle and of its geometric form. Strictly periodic change is not seen for supergiants. The visibility of the mantle generally has remained much the same for supergiants over the interval in which the supergiants have been observed.

Changes in the Hα profile do occur at irregular intervals, but the spectra of supergiants always maintain supergiant characteristics. On the other hand, the spectra of Be/shell stars sometimes look almost identical with those of normal B stars, the emission lines and the shell absorption lines having disappeared, at least on spectra of moderate resolution. The disappearance or great weakening of spectral features that are the signature for the presence of a mantle implies that the amount of material in the mantle has been greatly reduced. The physical state (temperature, density, and flow pattern) of the mantle also may have changed greatly.

The B stars can be roughly arranged in the following sequence as regards the activity seen in their mantles (1) normal B stars in the main-sequence band which show little or no variation, (2) supergiants which show constantly a small range of change, and (3) Be/shell stars which may show a striking range of changes over intervals of a few months to a few years.

Energy and Momentum Budget

Here we wish to find out how much energy and momentum must be supplied to the outer layers of a B star if a mantle containing a hot corona-like region and cool regions is to be represented by a model We postulate that material flows through the model mantle at such a rate that the observed rate of mass loss for a B star occurs. Energy must be added to the mantle from some source which is in addition to the net radiation field which has emerged from the photosphere and which passes through the mantle. The rate at which energy is added to the mantle must be sufficient to maintain the high electron temperatures of the corona-like layers and the even higher electron temperatures of the small, truly coronal regions imbedded in the corona-like region, in spite of losses due to the escape of photons and gas from the mantle and due to the conduction of heat to cooler parts of the atmosphere. In the photosphere where the radiation field is the dominant source of energy, the electron temperatures are of the order of the effective temperature of the star. Is the amount of energy required to generate and maintain a mantle, like the mantles which are observed for B stars, large or small relative to the amount of energy which is known to be radiated by a B star each second? How does this requirement change as one goes from type B0 to type B9 in the main-sequence band and for supergiants?

In a model for a mantle, the constraint of hydrostatic equilibrium may not be used to determine the pressure structure. The pressure and the velocity structure should be determined from the hydrodynamic equations which result from the conditions that mass and momentum be conserved. The gas forming the mantle is assumed to be a perfect gas in contact with radiation. The momentum which is removed from the model star by the wind must come from the radiation field, which passes through the mantle, and from whatever source of energy is postulated to provide the additional energy needed to create the

high electron temperatures observed to be present in some parts of the mantle.

A comparison of the internal energy of the gas forming the photosphere with that of the hot corona-like region will give an idea of how much energy has to be deposited per unit volume to achieve the high electron temperatures of the corona-like layer. An estimate of the amount of light radiated by the mantle will indicate the size of the energy losses that occur. An estimate of the amount of energy carried away by the wind in the form of kinetic energy will indicate the net amount of outward directed momentum that must be imparted to the mantle. This budget can be compared with estimates of what may be available from mechanical sources such as the passage of pressure waves of some sort or from magnetic sources such as plasma in current sheets. If a magnetic field pervades the mantle, it may provide a store of energy having a density of $B^2/8\pi$ ergs cm^{-3}, where B is the average magnetic field in gauss. The energy radiated as X-rays is only about 1.4×10^{-7} times the normal optical luminosity of the star (Pallavacini et al., 1981; Vaiana et al., 1981).

Internal Energy of the Photosphere and the Mantle. Consider the photosphere to be a homogeneous spherical layer of radius R_1 cm and thickness ΔR_1 cm in which the density is N_1 particles cm^{-3}. The electron temperature is T_1. Then since the internal energy per particle is 3/2 kT plus the energy required to maintain atoms and ions in excited states, a lower limit to the total internal energy of the photosphere, E_1, will be $6\pi kT_1N_1R_1^2\Delta R_1$. A lower limit, E_2, for the internal energy in a part of the mantle having a temperature T_2, density N_2, and occupying a volume equivalent to a spherical shell of radius $R_1 + \Delta R_1$ and thickness ΔR_2, can be estimated in a similar manner. The ratio of the lower limit to the internal energy in a part of the mantle to that of the photosphere is then

$$\frac{E_2}{E_1} = \frac{N_2}{N_1} \cdot \frac{T_2}{T_1} \left(\frac{R_1 + \Delta R_1}{R_1} \right)^2 \frac{\Delta R_2}{\Delta R_1} \qquad (8\text{-}1)$$

Typically, conditions in the photospheres and in the mantles of main-sequence stars of types B0 and B9 may be represented by the numbers given in Table 8-1. Here we have postulated that the

Table 8-1
Typical Conditions Defining Representative Simple Models for the Photospheres and Mantles of Main-Sequence B Stars

Item	B0 Star			B9 Star		
		Mantle			Mantle	
	Photosphere	Hot Part	Cool Part	Photosphere	Hot Part	Cool Part
Temperature (10^4 K)	3 0	10 0	2 0	1 1	5 0	0 9
Inner Radius ($R_\odot$)	10	10 50	10 50	3	3 15	3 15
Mass of Star ($M_\odot$)	15	–	–	3	–	–
Thickness (R_*)	0 05	0 2	20	0 05	0 2	20
Particle Density (cm^{-3})	10^{14}	10^{10}	10^{10}	10^{14}	10^{10}	10^{10}
Internal Energy (ergs)	$> 1\ 32 \times 10^{38}$	$> 1\ 93 \times 10^{35}$	$> 3\ 88 \times 10^{36}$	$> 1\ 30 \times 10^{36}$	$> 2\ 61 \times 10^{33}$	$> 4\ 70 \times 10^{34}$
Luminosity (ergs s^{-1})	$2\ 79 \times 10^{38}$	–	–	$4\ 55 \times 10^{35}$	–	–

Dashes (–) represent irrelevant quantities at these places in the table

hot part of the mantle is equivalent to a spherical corona-like layer of geometrical thickness $0.2\,R_*$. The cool part of the mantle is postulated to be equivalent to a spherical layer having a geometrical thickness of $20\,R_*$. The model stellar atmospheres of this example correspond to what might be found for B0 and B9 shell stars. A B0 or a B9 star which did not show a shell spectrum would have an equivalent cool layer in its mantle which contained very little material. In such cases, the internal energy given in the fourth and seventh columns of Table 8-1 should be neglected. At this level of approximation, the hot part of the mantle is assumed to be the same in a star without a shell as in the one with a shell The "volume" of the cool part of the mantle is estimated by the formula appropriate for a shell of infinitesimal thickness.

The lower limits for the internal energy of the photosphere, the hot part of the mantle, and the cool part of the mantle have been estimated by ignoring the energy which may be bound up in keeping atoms and ions in excited states. Such energy is larger in the photosphere than in the mantle because more atoms and ions are in excited states in the photosphere than in the mantle. The internal energy which must be supplied to keep the mantles of B0 and B9 shell stars in their observed states is, respectively, 0.015 and 0.11 times the amount of energy that is radiated per second by the star. If only the hot part of the mantle is present, the fractions of the radiated energy per second required are 0.007 and 0.006.

A similar analysis is shown in Table 8-2 for simple models of the atmospheres of B0 and B9 supergiants. The model for the cool part of the mantle is supposed to be representative for the body of gas that gives the infrared excess and the radio emission observed for B-type supergiants. In the case of the model B0 supergiant, the internal energy of the mantle is about one-sixth that of the photosphere. In the case of the B9 supergiant, it is about one-third that of the photosphere. The internal energy of the model mantle for the B0 supergiant is only about 0.005 times the amount of energy radiated by the star per second. In the case of the model B9 supergiant, the internal energy of the mantle is a little more than one-fourth of the energy radiated by the star per second.

Although the temperatures in the photosphere and hot part of the mantle are lower for the B9 model atmosphere than for the B0 model atmosphere, the amount of energy stored as internal energy in the mantle is larger for the B9 supergiant than for the B0 supergiant. This is because the B9 supergiant is more than twice as big as the B0 supergiant and it has a much more exten-

Table 8-2
Typical Conditions Defining Representative Simple Models for the Photospheres and Mantles of Supergiant B Stars

	B0 Star			B9 Star		
		Mantle			Mantle	
Item	Photosphere	Hot Part	Cool Part	Photosphere	Hot Part	Cool Part
Temperature (10^4 K)	2 5	10 0	2 0	1 05	5 0	2 0
Inner Radius ($R_\odot$)	35	36 75	36 75	80	84	84
Mass of Star ($M_\odot$)	25	–	–	10	–	–
Thickness (R_*)	0 05	0 2	20	0 05	0 2	20
Particle Density (cm^{-3})	10^{12}	10^{10}	10^8	10^{12}	10^{10}	10^8
Internal Energy (ergs)	$>4\,70 \times 10^{37}$	$>6\,93 \times 10^{36}$	$>1\,38 \times 10^{36}$	$>2\,36 \times 10^{38}$	$>4\,95 \times 10^{37}$	$>1\,98 \times 10^{37}$
Luminosity (ergs s^{-1})	$1\,65 \times 10^{39}$	–	–	$2\,68 \times 10^{38}$	–	–

Dashes (–) represent irrelevant quantities at these places in the table

sive mantle than does the B0 supergiant

These simple calculations show that the amount of internal energy that must be supplied to maintain the mantles of main-sequence B stars in their observed state is only a small fraction of the energy that is radiated per second by the star. The presence of a cool region which gives a shell spectrum increases the need for internal energy. In the case of the model B0 supergiant atmosphere, the process heating the mantle must supply only a small fraction of the energy that is radiated per second, but in the case of a B9 supergiant, the energy requirement to maintain a mantle of the type which is observed is a significant fraction of the amount of energy which is radiated per second by the star When the energy radiated by the mantles and the energy carried away by conduction and by a wind is added, the energy required to maintain the mantle is increased.

Energy Loss from the Mantle by Conduction. Energy can be transferred by conduction from the hot, relatively low density layers of the corona-like region in a mantle to the denser and cooler layers of the transition layer between the photosphere and the corona-like region. In order to estimate this loss, one must know the temperature gradient between the corona-like region and the photosphere as well as the density of the gas in the transition layer. We have estimated this loss in the framework discussed by Hearn (1975b), and the results are given in Table 8-3 as a fraction F_c/F_* of the luminosities of the model stars.

Hearn (1975b) has determined the rate at which energy may be transferred from a hot corona by conduction, by a wind, and by radiation. The corona is postulated to be optically thin and to be hot with electron temperatures like those seen for the Sun. The density in the model corona is determined by outflow at a constant rate with matter conserved in spherical shells. The factor determining the density or pressure, p_0, at the base of the corona is the adopted rate of mass loss, which is a free parameter.

From Hearn's equations (13), (14), and (19), we find that the flux of energy per cm^2 carried away by conduction, F_c, by the wind, F_w, and by radiation from the hot corona, F_R, can be written as

$$F_c = 6.94 \times 10^6 (M/R)^{3/4} p_0 y^{-3/4}, \qquad (8\text{-}2)$$

$$F_w = 6.18 \times 10^7 (M/R)^{1/2} p_0 \times$$

$$[y^{1/2} \exp(1.3261 - 1.1559y - 0\ 03636y^2)], \qquad (8\text{-}3)$$

and

$$F_R = 2.84 \times 10^5 (M/R)^{-3} R p_0^2 \times$$

$$(0.2080y^2 + 1.0321y - 1.268). \qquad (8\text{-}4)$$

Here the unit for flux is ergs cm^{-2} s^{-1} and y is r_c/R, where r_c is the radius to the level at which the critical point occurs, and R is the radius of the photosphere. The mass and radius of the star are in solar units. The critical point is where the flow velocity equals the thermal velocity. In our case, we assume that y is close to unity.

Values of F_c, F_w, and F_R are given in Table 8-3 for our model stars using the dimensions given in Tables 8-1 and 8-2, and the values of p_0 which follow from the noted rates of mass loss (see Hearn's equation 37). Each flux of outgoing energy is expressed as a fraction of the luminosity of the star

The loss of energy by radiation has been calculated for $y = 1.05$ because Equation (8-4) becomes negative if this approximate formulation is evaluated at $y = 1.0$. The F_c and F_w have been evaluated for $y = 1.0$. It is straightforward to find the appropriate values at other values of y if this is desired.

It is immediately obvious from the numbers in Table 8-3 that the energy losses from our model mantles, when these losses are calculated by Hearn's formulation, are negligible in comparison to the energy which is radiated by the photosphere. If a mantle behaves as Hearn postulates, then the source of energy required to maintain the mantle in the form we have adopted is small. The loss by conduction is less than about 4×10^{-5} of the luminosity of the star in the worst case shown here.

Hearn considered only the light which is radi-

Table 8-3
Relative Rates of Energy Loss from a Mantle[a]

Item	B0 Main-Sequence With Shell	B9 Main-Sequence With Shell	B0 Supergiant	B9 Supergiant
Mass of Star ($M_\odot$)	15	3	25	10
$\dot{M}$ ($10^{-6}\ M_\odot yr^{-1}$)	1.0×10^{-2}	1.1×10^{-3}	1.8	5.7×10^{-1}
p_0 (dyne cm^{-2})	4	4	40	1
F_w/F_* ($v = 1.0$)	7.5×10^{-6}	3.4×10^{-4}	1.1×10^{-4}	3.6×10^{-5}
F_c/F_* ($v = 1.0$)	8.2×10^{-7}	3.4×10^{-5}	9.8×10^{-6}	2.1×10^{-6}
F_R/F_* ($v = 1.05$)	1.3×10^{-8}	7.4×10^{-7}	8.8×10^{-5}	7.6×10^{-4}

[a] These rates are based on the formulation of Hearn (1975b).

ated by a hot, optically thin plasma like the solar corona. However, observations have shown that B-type supergiants and B stars with extensive mantles produce radiation in the hydrogen spectrum at a detectable rate. This radiation is seen as an emission line at Hα, and sometimes at other Balmer lines and the Paschen lines, as an infrared excess and as radio emission. The amount of energy radiated is estimated in the next subsection. This radiation is generated in the mantle and it is in excess of the radiation field which comes from the interior of the star.

Energy Loss from the Mantle Resulting from Outflow. Hearn (1975b) has given an estimate for the rate at which energy is being taken from a star by a wind, F_w. The values for our model mantles are given in Table 8-3. The values of these estimates of F_w may be checked by the following simple argument.

If a star is losing mass at a rate of $\dot{M}\ g\ s^{-1}$ and the material is moving at a terminal velocity of u_∞, then the kinetic energy being carried away per second is $\frac{1}{2}\dot{M}u_\infty^2$. This corresponds to $3.15 \times 10^{35}\ nm^2$ ergs s^{-1} when the rate of mass loss is expressed in units of $10^{-6}\ M_\odot\ yr^{-1}$ (designated by n) and the terminal velocity is expressed in units of 10^3 km s^{-1} (designated by m).

The rates of loss of kinetic energy by our typical model mantles for B0 and B9 shell stars and supergiants estimated by this simple argument are given in Table 8-4. Here the adopted values for $\dot{M}$ and u_∞ have been estimated from the information given in Chapters 3, 4, and 7. There is no observational information about mass loss from a B9 main-sequence star. The values given in parentheses are rough guesses of what may be true. The rate at which a B star loses kinetic energy in its wind is small in comparison to the rate at which it loses energy by radiation from the photosphere.

Energy Loss from the Mantle by Radiation. Energy is lost from the mantles of B stars through the emission of radiation chiefly in the hydrogen spectrum. One may obtain a crude estimate of the rate of energy loss by radiation by interpreting the intensity of the emission feature at Hα as being due to a recombination spectrum. The mantle interacts with the persistent ions of the abundant elements by resonance scattering in lines which originate from the ground levels of these ions. This interaction does not provide a means for the mantle to lose energy by radiation.

Table 8-4
The Rate of Loss of Kinetic Energy from a Typical Mantle

Type of Star	$\dot{M}$ ($10^{-6}\ M_\odot\ yr^{-1}$)	u_∞ (10^3 km s^{-1})	Rate of Loss of Kinetic Energy (ergs s^{-1})	$\frac{L_w}{L_*}$
B0 main sequence	0.1	1.0	3.15×10^{34}	1.13×10^{-4}
B9 main sequence	(0.001)	(0.1)	(3.15×10^{30})	(6.92×10^{-6})
B0 supergiant	2.3	2.0	2.90×10^{35}	1.76×10^{-4}
B9 supergiant	0.1	0.3	2.84×10^{33}	1.06×10^{-5}

When collisional processes are important in the mantle, they add to the value of the internal energy estimated to be in the mantle. The energy used in maintaining a population of excited hydrogen atoms may be important for the cool parts of the mantles, the energy needed to maintain a population of excited neutral helium atoms may be important for somewhat warmer parts of mantles. However, when the population of the mantle consists chiefly of H^+, He^+, He^{++}, and the second and higher ions of the abundant elements, the amount of energy that can be bound as excitation energy becomes small since collisions with electrons having energies typical of the temperatures we are considering for the corona-like region are inefficient for populating the low levels of the ions which are present In the mantle, as in nebulae, the ionization may be controlled by a process that can provide the large amount of energy per particle needed to form the ions which are seen, while the degree of excitation to the energy levels from which radiation is observed to come may result from another process. The observed level of excitation reflects a balance between collisional excitation and de-excitation and spontaneous radiative processes following recombination.

Let us consider the case of a hydrogen recombination spectrum as shown, for instance, by gaseous nebulae We shall make use of results for the case in which the Lyman lines and Lyman continuum are in detailed balance. The data given by Brocklehurst (1971) and by Osterbrock (1974) show that for hydrogen gas at 1.0×10^4 K, the energy radiated in all lines and continua is about 300 times that radiated in Hα; when the temperature is 2.0×10^4 K, the factor is about 500 times. This is true so long as the gas is optically thin in all wavelengths longward of 912 Å except the wavelengths of the Lyman lines These results are insensitive to the value of the electron density in the gas. We shall assume that the energy radiated by the mantle in all hydrogen lines and continua is 400 times that radiated in Hα This estimate should be correct to within a factor of ± 25 percent.

The amount of energy radiated at Hα is equal to the equivalent width of the emission feature at Hα times the monochromatic energy radiated by the star in the continuum near Hα. We use the model fluxes of Kurucz (1979) to estimate the continuum energy for our model stars. It follows that the ratio of the energy radiated by the mantle in the hydrogen spectrum to the total energy radiated by the star is $400W$ (Hα) πF_λ (model)/ $\sigma_R T_{eff}^4$ Here σ_R is the Stefan-Boltzmann constant.

The energy losses by radiation from the model mantles of Tables 8-1 and 8-2 are given in Table 8-5. Here we indicate the Kurucz (1979) model atmosphere adopted as representative of the photosphere of each model star and we assign a

Table 8-5
Rates of Loss of Energy by Radiation from the Mantles of Typical B Stars

Type of Star	Model Photosphere		W (Hα) (Å)	L_R (ergs s^{-1})	$\frac{L_R}{L_*}$
	T_{eff} (10^4 K)	log g			
B0 main sequence with shell	3.00	4.0	20	1.06×10^{38}	0.38
B9 main sequence with shell	1.10	4.0	20	$1\ 59 \times 10^{36}$	3.5
B0 supergiant	2.50	3.0	2	1.03×10^{38}	0.062
B9 supergiant	1.05	2.0	2	1.16×10^{38}	0.43

typical value for the equivalent width of the Hα emission from each model mantle.

If the equivalent width of the Hα emission from a B0 shell star is 20 Å, the energy being lost from the mantle by radiation in the hydrogen spectrum will be about 0 38 times that being radiated by the star. In the case of a B9 shell star showing an equivalent width in emission of 20 Å for Hα, the mantle is losing 3.5 times as much energy per second in the hydrogen spectrum as is lost from the photosphere in the form of radiation.

In the case of the model B0 supergiant, the radiation is being lost from the mantle in the hydrogen spectrum at only 0 06 times the rate of loss of energy by radiation from the photosphere. Such a mantle probably would generate a recombination spectrum of He I and perhaps it would show recombination lines from a few other abundant ions such as C^{++}. It is, however, unlikely that the mantle of a B0 supergiant would lose energy by radiation at a rate of more than 0.1 times the rate of loss of energy by radiation from the photosphere

In the case of the model B9 supergiant, the mantle loses energy by radiation in the hydrogen spectrum at about 0.43 times the rate of loss by radiation from the photosphere. A cool, peculiar supergiant like P Cyg with many emission lines in its spectrum and a strong hydrogen emission spectrum might be radiating energy from its mantle at 10 times the rate it is losing energy by radiation from its photosphere.

These estimates of the rate of loss of energy from mantles by radiation show us that the late B shell stars and supergiants lose energy from their mantles at a considerably greater rate, relative to the rate they lose energy by radiation from the photosphere, than do early B shell stars and supergiants. In the case of the model B9 shell star, the estimated rate of loss of energy from the mantle by radiation is surely an underestimate. This is because no account has been taken of the emission that is observed to be present in other spectra such as Fe II. Also the equivalent width in emission of Hα may be greater than 20 Å. In any case, even with the present estimate, the mantle of the model B9 shell star is losing energy by radiation more rapidly than the star is losing energy by radiation from the photosphere. We conclude that the source of energy for the mantles of supergiants and B stars with extensive mantles must provide energy at a rate of the order of or greater than the rate of energy loss which is seen to flow from the photosphere as radiation. The source must support a relatively greater rate of energy loss in the case of shell stars than it does in the case of supergiants.

Normal main-sequence B stars do not show emission at Hα. Therefore, one may conclude that they lose little energy from their mantles by radiation. The estimates made by means of Hearn's formulation of the problem (see Table 8-3) may be appropriate. The spectrum of a normal B star may show absorption profiles

from the ultraviolet resonance lines of abundant ions These lines are believed to be formed by resonance scattering and they do not take energy from the mantle.

The most important loss of energy from the mantle of a B star is that which is seen by means of the hydrogen continua and the free-free emission detected in the infrared and at radio wavelengths. In the stars which show an infrared excess, the source of energy which is heating the mantle must provide energy at a rate which is comparable to the luminosity of the star. When emission in the hydrogen spectrum is not seen from a B star, the rate of loss of energy from the mantle is of the order of or less than 10^{-4} times the luminosity of the star The amount of momentum seen in the wind is relatively small in comparison to what is in the radiation field

Discussion

The character of the spectroscopic features which reveal the presence of a mantle is intimately connected with the physical state of each part of the mantle Thus, many of the differences between the spectra of supergiants, Be/shell stars, and normal B stars indicate differences in the mantles of these stars. The occurrence of mantles with different properties means that the efficiency of the heating and propulsion processes that are active in the mantles of these different sorts of B stars differ. At this time we cannot say whether there is only one type of process which operates at different efficiencies to produce the different kinds of mantles which we see, or whether more than one process is active in producing the mantles and winds of B stars. We would, however, like to emphasize the point that all stars have mantles The visibility of the mantle is a function of our capability to observe the star in all energy regimes and of the varying circumstances in the star which promote or hinder the processes which generate a mantle.

A Model for the Mantle. In a review of the physics of the solar corona, Vaiana and Rosner (1978) have stressed that the inhomogeneity of the solar corona is one of the most important properties of the solar corona. This inhomogeneity and the physical state of each local volume of the solar corona is intimately connected with the changing state of the magnetic fields which pervade the solar corona.

The typical dimensions of the elements of structure, the densities, temperatures, and rates of flow of matter in the mantles of the B stars are not expected to be the same as those of the mantle of the Sun (The mantle of the Sun includes all parts of the extended solar atmosphere lying above the photosphere. It extends far into interplanetary space.) It does seem likely, however, that the Sun is a useful and practical model of what sorts of heating and propulsion process may occur in nature. In Jordan (1981), valuable information is given about what is observed in the Sun and about the theory which has been developed to provide an understanding of what is seen in the mantle of the Sun.

According to Rosner et al (1978), the observed high temperature of the plasma of the solar corona, the inhomogeneous structure of the solar corona, and the long-term spatial and temporal evolution of coronal features can be explained by in situ heating of the coronal plasma by means of anomalous current dissipation. The basic geometrical structure is a loop configuration heated by nearly field-aligned currents occupying a small fraction of the total loop volume.

This picture may be relevant for understanding the conditions which we observe to be present in the mantles of the B stars. We should like to suggest that the mantles of B stars have a loop structure much like that of the mantle of the Sun. Undetectably small magnetic fields must be assumed to be present. The necessary velocity field to cause the generation of currents, which in the solar case is provided by convection of the subphotospheric layers of the Sun, may be provided, in the case of B stars, by the turbulence which is inferred to occur as a result of differential rotation of the star.

The shapes of the absorption lines of B-type supergiants show that there is much turbulence in the outer atmospheres of the B supergiants. The spectrum of a B-type supergiant changes by a small amount in intervals of time which are com-

parable to the expected periods of rotation for the supergiants. On the whole, however, the spectrum remains constant in time. It is plausible to postulate that the mantles of the B-type supergiants are created by energy released from the small magnetic fields which must be present. In analogy with the Sun, we postulate that the release of energy results from interactions with the small amplitude, differential motions which are present in the atmospheres of the supergiants. So far as magnetic fields are concerned, it is straightforward to show that any magnetic field occluded as a massive star formed from the interstellar medium would not have decayed by a significant amount by the time the star had evolved to the region in the HR diagram occupied by the B-type supergiants (Underhill, 1980b). Such seed fields could cause irregular magnetic fields to be generated in the envelopes of B supergiants as convective motions developed in the envelope just below the photosphere. In any case, whether the magnetic fields are primordial or secondary, it is a reasonable supposition that small magnetic fields exist in the outer atmospheres of B-type supergiants. Such fields will heat the outer atmosphere and cause it to show the characteristics of a mantle. Magnetic forces may cause the initial propulsion of gas from the mantle to occur. The aspect of the fields and the structure of the mantle will change as the star rotates. The material that starts to move outward may be accelerated by radiation pressure.

The evidence for turbulence in the atmospheres of main-sequence B stars is less striking than it is for supergiants A little small-scale turbulence seems to be present, but the amplitude of the motions is smaller than for the supergiants. Outflow visible in Hα has been observed by Furenlid and Young (1980) from many main-sequence stars that have v sin i values of 200 km s^{-1} or greater. There seems to be a correlation between the strength of the asymmetrical absorption in the Hα profile and the v sin i in the sense that the more rapid the rotation is, the stronger the absorption is on the shortward side of the Hα absorption-line profile. No significant asymmetry suggesting outflow is seen for B stars which appear to be observed pole-on, or to be rotating slowly. More than half of the rapidly rotating main-sequence B stars of type B0 to B3 observed by Furenlid and Young show an asymmetrical shortward wing on the Hα profile. If the ultraviolet spectra of the rather sharp-lined B stars shown in Chapters 3 and 4 are typical for main-sequence B stars, one may conclude that there is evidence for the presence of superheating in the mantle and outflow in some main-sequence B stars. It is, perhaps, significant that the evidence for superheating and outflow is more obvious for ζ Cas, B2 IV, than it is for γ Peg, B2 IV (see Figures 4-12 and 4-13). The normal absorption lines of ζ Cas, although sharp, are not quite so sharp as those of γ Peg. Thus, ζ Cas appears to be rotating a little faster than γ Peg

Underhill (1980b) has shown that heating by quiescent magnetodynamic processes may deposit enough energy to account for the differences in level of ionization observed between the corona-like layers of O9/B0 supergiants and those of B9/A0 supergiants (see Chapter 4).

To have a mantle, a star must tap a source of energy that is in addition to the energy coming from the center of the star as radiation. From our energy and momentum budget, we have seen that in the case of supergiants and shell stars this source must be able to provide energy at a rate which is about equivalent to the luminosity of the B star. In many normal B stars the rate of energy supplied may be much less than this because many normal B stars do not show conspicuous mantles.

Let us suppose that the energy radiated by the mantle and that needed to maintain the observed internal energy of the mantle comes from the energy stored in a magnetic field which pervades the mantle. How large a magnetic field would be required? Could we detect such a field?

Let us assume that the process which transfers energy from the magnetic field to the mantle works with an efficiency of 1 percent, and that a constant, average magnetic field of B gauss fills the volume occupied by the mantle. Then the total energy in ergs s^{-1} which is postulated to be transferred to the mantle is $0.01B^2/8\pi$ times the volume of the mantle An estimate of the necessary field strength can be found by equating

this rate of energy transfer to the rate at which energy is lost by radiation from the mantle (see Table 8-4). The volume of the part of the mantle which is the place of origin of the hydrogen emission can be estimated from the typical dimensions given in Tables 8-1 and 8-2.

We find for the model BO star with an extended, cool mantle that one requires an average magnetic field of 5.3 gauss For the model BO supergiant one requires an average magnetic field of 0.80 gauss For the model B9 star with an extended, cool mantle the average magnetic field required is 0.28 gauss, and for the model B9 supergiant the average magnetic field is 0.25 gauss Average magnetic fields of these magnitudes could easily be present in the mantles of B stars and remain undetected We conclude that the energy stored in a small average magnetic field which pervades the cool part of the mantle of a B star is a sufficient source for providing the energy that is lost by the mantle as radiation and bound in the mantle as internal energy. If the efficiency at which energy was transferred to the plasma from the magnetic field were greater than 1 percent, the average field would be even smaller.

Study of the Sun reveals that magnetic fields are found in constrained structures and that one can speak of an average magnetic field only in the loosest way. The same is probably true for B stars Unfortunately, there is no simple way of observing the detailed structure of the mantles of B stars and confirming the presence of magnetic structures like the loops and coronal holes seen on the Sun. The observations which we do have of the presence of discrete displaced absorption components for some resonance lines, and of the change in strength and displacement of these components, strongly suggest that the mantles of B stars are inhomogeneous. The same conclusion can be reached from changes seen in the profile of the emission component at Hα.

The required small magnetic fields may be primordial initially. The development of convection layers in the envelope of the star as the star crosses the HR diagram from the right-hand side of the main-sequence band into the domain of the supergiants may generate some dynamo action in the envelopes of B stars. The locally distributed magnetic field that can be expected to emerge from the photosphere as a result of such dynamo action might be enough to generate the superheated mantles which are observed for B-type supergiants and to a lesser degree for some main-sequence stars.

The theory of stellar evolution shows that stars having masses in the range 5 to 15 $M_{\odot}$ will very quickly move from being blue supergiants to being red supergiants (see, for instance, Iben, 1966a, 1966b; and Lamb et al , 1976). The luminous red stars are known from IUE observations to show an emission-line spectrum having many of the characteristics of the solar ultraviolet spectrum. Presumably, their mantles are generated in much the same way that the mantle of the Sun is This requires the presence of magnetic fields. Any magnetic fields which are present now in the mantles of the luminous red stars would also have been present in the mantles of their progenitors, the blue luminous stars. This is because the time which elapses between the appearance of a massive model star as a blue supergiant and as a red supergiant is short.

There is no obvious reason for excluding the hypothesis that weak magnetic fields are present in the mantles of B stars which show hydrogen in emission and that they provide the energy which heats the mantle. It is possible that the magnetic loops act as conduits for mechanical energy generated in the envelope of the star This is believed to happen in the Sun (Jordan, 1981).

According to the picture developed here, the energy bound as internal energy in a mantle and that radiated from a mantle as well as that lost by the outflow of a wind comes from the energy stored in the local magnetic fields which are present in the mantle. An appropriate parameter for characterizing a model mantle is, therefore, a number which gives the typical energy density of the magnetic field.

A second parameter is required to complete the definition of the model mantle. It is one which characterizes the efficiency of the process which transfers energy from the magnetic field to the mantle. Observation of the Sun suggests that the amplitude of the differential motion which is

present might be an appropriate parameter. It appears that energy is transferred from the magnetic field to the gas as a result of the shearing and twisting of magnetic lines of force by the differential motions of the gas. Therefore, the amplitude of these motions would seem to be an important parameter for characterizing a model mantle.

Propulsion of a Wind. In the Sun, high velocity streams of gas are observed to be emanating from coronal holes. According to Hearn (1977), the most likely explanation of the high velocity streams from the Sun may be that put forward by Durney and Hundhausen (1974) who have pointed out that a reduction in the density at the bottom of a conductively maintained solar wind gives an increased expansion speed throughout interplanetary space. A similar action may occur for B stars. However, in the case of the hottest B stars, acceleration of the wind by radiation pressure will modify the flow from a pattern like that believed to be valid for the Sun. The Sun is a star for which radiative acceleration is small. Before radiative acceleration can become effective, the gas must have received a significant propulsion outward. This is necessary because the absorption lines in the moving material must be displaced shortward of the absorption lines of the photosphere before the moving ions are bathed in much radiation from the photosphere. The necessary initial propulsion may come from magnetic forces.

Flow along magnetic field lines that have become open to interstellar space may be the cause of the displaced discrete absorption components seen often in the ultraviolet spectra of the B-type supergiants (see Chapter 4). Similar discrete components are seen in the ultraviolet spectra of some Be/shell stars (see Part II)

UNSOLVED PROBLEMS

Comparison of the predictions of the theory of the evolution of massive stars with the observed distribution of B-type stars in the HR diagram, as a function of the observed masses of B stars, shows that theory and observation are in reasonably good agreement for B stars which are in the main-sequence band. During the phase of burning hydrogen in the core, the predicted results are not very sensitive to the details of the theoretical treatment, so the comparison is limited chiefly by the inaccuracies of the observations. When, however, a model star begins to generate its energy by contraction and by burning hydrogen in a shell, the properties of the model star become sensitive to the details of the representations used to take account of the transfer of energy through the envelope of the star. At this stage in its evolution the model star is near the S bend in the evolutionary tracks, close to the right-hand side of the main-sequence band in the HR diagram. Many of the B stars observed to lie in this region of the HR diagram show variable line profiles and variable radial velocities. Some show small variations in light suggesting pulsation. Others sometimes show emission lines of hydrogen.

More work is required to make improved interior models for stars at these stages of evolution and to determine what effect the interior structure has on the photosphere and on the mantle of the star. Some of the observed spectroscopic changes of stars on the right-hand side of the main-sequence band appear to be related chiefly to changes in the physical state of the mantle. For instance, the prominent changes seen in the spectra of Be stars seem to indicate larger changes in the mantle than in the photosphere. On the other hand, other changes such as the growth of asymmetrical wings on weak lines, as is seen for the line-profile variables, may have their origin in the photosphere. This latter point is not really clear. Displaced weak asymmetrical absorption lines originating in a mantle could combine with normal weak photospheric lines to give some of the observations which are seen for the line-profile variables and attributed to nonradial pulsation of the photosphere.

Unfortunately, here we run into the problem of demonstrating whether any model, made according to reasonable hypotheses, is unique. This can rarely be done. With the present crude models for mantles, the situation cannot be resolved decisively.

When one comes to interpreting the position

of B-type supergiants in the HR diagram in terms of the existing interior models for massive stars, sharp conclusions cannot be drawn because the predicted results are quite sensitive to the adopted representations for the composition and opacity of stellar material, for how convection in the envelopes of the models is handled, and for mass loss More work needs to be done in this area, including the introduction of a realistic physical mechanism for mass loss in place of one or other of the ad hoc expressions which have been used.

We have found that most of the continuous spectrum of B stars and the absorption lines from ions which are not abundant can be interpreted satisfactorily by means of the classical LTE, line-blanketed model atmospheres of Kurucz (1979). The composition of most B stars seems to be solar, although a few have a deficiency of hydrogen. We conclude that the theoretical interpretation is satisfactory because the predicted continuum fluxes, when they are combined with observed angular diameters, reproduce the absolute values for the monochromatic fluxes observed for B stars in the main-sequence band and for supergiants. In the case of supergiants and Be stars, care must be taken, in some cases, to correct the photometry for the presence of infrared excess emission and for emission in the Balmer and Paschen continua. This test which makes use of measured angular diameters is powerful. Since it has been carried out for nearby B stars, the corrections for interstellar extinction are secure. We have presented observations in Chapters 3 and 4 to show that the shape of the predicted continua from the LTE line-blanketed model atmospheres of Kurucz (1979) are closely similar to what is observed for B stars from 1200 Å to 10 μm. The observations must be corrected for wavelength-dependent interstellar extinction before making the comparison.

The theory of the parts of the spectra of B stars which are formed in the photosphere seems to be satisfactory. Use of the condition that statistical equilibrium exists to determine the ionization balance and the level of excitation in the photosphere is preferable to assuming LTE, but it is not always practical. In the case of intrinsically weak lines and continua, LTE often, but not always, is an adequate approximation.

When, however, the spectral features are intrinsically strong, as for the Balmer lines of hydrogen and the leading members of the He I series, as well as for some of the prominent lines of the ions of C, N, O, and Si, the features may be partly formed in the mantle. This is often true for supergiants. Then, model atmospheres which are adequate for analyzing weak features formed in the photosphere are not suitable tools for analyzing the strong lines of the spectra. A model which represents conditions in the mantle must be used in addition to the model of the photosphere.

At present no detailed models for mantles having the observed properties of high electron temperature, outflow, and inhomogeneity exist. Much work is required in this direction. The ad hoc models of expanding and contracting atmospheres, and of radiative transfer in such models, reviewed in Chapter 6 are inadequate to serve as a basis for interpreting prominent spectral features which are formed in a mantle.

The greatest drawbacks of the existing models for moving atmospheres are (1) that in almost all cases the mantles are assumed to be at a temperature like the effective temperature of the star, (2) that an ad hoc velocity law has been adopted in place of solving for a velocity law that is appropriate for the forces which act on the plasma in the mantle, and (3) that the inhomogeneity of mantles is ignored.

Improved models require introducing a plausible representation for the release of nonradiative energy in the model mantle in an amount to account for the estimated losses of energy from the mantle, and deducing a temperature law, and making use of the appropriate equations of hydrodynamic flow when plausible representations are introduced for the forces which act on the plasma. A geometrical representation that takes account of the apparent inhomogeneity of mantles is desirable.

All of these requirements are difficult It may be some time before appropriate models for the mantle can be developed. In the meantime, it is wise to be very cautious about deducing quantities such as abundances from the apparent strengths of absorption lines in the spectra of B-

type supergiants. Until the line formation process and the medium in which the line is formed can be modeled securely, any derived abundance is nothing more than a fitting factor.

In this chapter, we have presented a heuristic model for the mantles of B-type stars of all sorts. This model emphasizes the importance of weak magnetic fields and of differential motion for accounting for what we see. A major area of new work is that of evaluating what is known at this time from the detailed observational and theoretical studies of the mantle of the Sun and seeing how much of this body of knowledge is truly relevant for understanding the mantles of hot stars. The arguments presented in this chapter are based on the hypothesis that a study of this type will further our understanding of the spectra of B stars with and without emission lines.

9

SUMMARY

INTRODUCTION

In the years since 1965, tremendous increases have occurred in our ability to observe B stars and to interpret their light in terms of the physics of gas and radiation. During this time observations of B stars have been obtained in all energy regimes from X-rays to radio wavelengths, and detailed numerical models have been made of the stellar interior and of the stellar atmosphere. Together the observational and theoretical results have led to a revolution in our understanding of B stars. Many observations have been obtained from space. The development of electronic detectors and powerful computing equipment have revolutionized the observational capabilities and the possibilities for developing theory.

Part I has been written by three authors (Underhill, Doazan, and Lesh) with the assistance of L. Divan in preparing the survey of observational information presented in Chapter 2 and of M. Aizenman in preparing the summary of the pulsational properties of the models of massive stars given in Chapter 7. All three authors collaborated in Chapter 2. Chapters 1, 3, 4, 6, 7, and 8 were prepared by Anne B. Underhill; Chapter 5 was prepared by Janet Rountree Lesh.

In Chapter 1, the general problem of understanding the B stars is introduced, and it is argued that the wealth of new information from space makes it desirable to think of the atmospheres of B stars as being composed of two parts: a photosphere and a mantle.

The atmosphere of a star is the outer part of the star from which radiation escapes into space. Its transparency is a function of wavelength. The photosphere is equivalent to the classical boundary layer of a star, and in the case of B stars, the photosphere can be modeled successfully in terms of plane-parallel layers in which energy is transported under the constraint of radiative equilibrium. For B stars the density (pressure) structure in the photosphere is such that hydrostatic equilibrium exists. The composition of the atmospheres of most B stars is solar. Two parameters, the effective temperature and the acceleration of gravity at the surface of the star, serve to define the properties of a photosphere when they are used with the constraints of radiative and hydrostatic equilibrium. A model B star consists of gas in contact with radiation throughout its volume.

Observations from space show that in the atmosphere of a B star there are also regions where the electron temperatures are much higher than can be generated by the radiation stream flowing from the core of the star. Outflow at high velocity is often seen, and the gas appears to be inhomogeneous. Such regions are generated by the deposition of nonradiative energy in addition to the heating which occurs from the passage of the radiation stream from the center of the star, and by the supply of outward directed momentum to at least parts of the gas. Because additional energy and momentum are deposited in the outer part of the atmosphere beyond what comes from the radiation field, this part of the atmosphere is different from the photosphere. This entity in itself is called a *mantle*.

The chromosphere, corona, and wind from the Sun together are equivalent to the part of the atmosphere of a B-type star which is called a mantle. Retrospect shows that the mantles of stars are visible by means of observations made from the surface of the Earth, for instance, by the presence of emission lines of hydrogen as well as by means of observations made from space. However, a compelling need to recognize the mantle of a star as a separate entity did not arise until the observation of X-rays from B stars and until the recognition of the presence of lines from highly ionized ions in the ultraviolet spectra of B stars forced it upon us.

In Chapter 8 a schematic model for a mantle was presented. Appropriate parameters for a mantle are the energy density in the source of energy which is tapped to generate the mantle and the efficiency of the factor which couples the energy source to the gas in the mantle. Specifically, the value of the average magnetic field in the mantle and the amplitude of the differential motion there may be appropriate parameters for the mantles of B stars.

Throughout Part I a model star is thought of as being composed of four parts. (1) the convective core where energy is generated by nuclear burning, (2) the envelope which lies between the core and the boundary layer of the star and which transmits energy from the core to the boundary layer; (3) the photosphere which is the classical boundary layer of a star and from which the continuous spectrum of the star is seen to come, and (4) the mantle where the effects of the deposition of nonradiative energy are seen and where a wind arises.

The signature for the core of a star is the total energy stream observed as radiation from the star. This quantity is indicated by the parameter, effective temperature. The properties of the envelope can be recognized chiefly through the radius of the star and the variations in light from the star which may be due to pulsation. The properties of the photosphere can be determined chiefly from the energy distribution in the continuous spectrum and from the strengths of weak absorption lines and the wings of the Balmer lines of hydrogen. The properties of the mantle are revealed by the presence of emission lines in the spectrum and the profiles and intensities of resonance lines in the ultraviolet. Only the most conspicuous mantles can be detected by means of subordinate lines in the spectra of elements other than hydrogen and helium There is a wide range in the visibility of the mantles of B stars as one considers main-sequence stars and supergiants.

INTRODUCING THE B STARS

Chapter 2 describes the general properties of B stars for the orientation of the newcomer to the study of B stars. The spectral classification scheme for B stars, and the calibrations of the various spectroscopic criteria for luminosity in terms of visual absolute magnitude, M_V, are presented. Particular care is taken to relate the broadband and intermediate-band photometric indices to the scheme of spectral types: tables of data on this point are supplied. The correction of continuum fluxes for wavelength-dependent interstellar extinction is reviewed and information on the shape of the interstellar extinction law is given. The relationship of the classification scheme of Barbier, Chalonge, and Divan, the BCD system, to the better known MK spectral classification system is presented. The BCD system is based on the shape of the continuous energy spectrum of B stars in the range observable from the surface of the Earth and it is well suited to classifying B stars according to the properties of their photospheres.

The first ultraviolet observations of B stars are reviewed in the second section of Chapter 2 and the spectral classification schemes based on the energy received from the star in ultraviolet wavelengths are noted. The B-type supergiants are found to be deficient in ultraviolet light relative to main-sequence B stars of the same subtype and visual magnitude.

The observations of B stars in the infrared and at radio wavelengths are summarized in the third and fourth sections. Broadband photometry to about 10 μm is available for quite a few B stars, and high resolution spectra in the infrared are available for a small number of stars Only a

very few B stars have been detected at radio wavelengths. The most easily detected objects are those with large low density regions of gas around them such as the BQ [ ] stars and a few B-type supergiants. The implications of the infrared and radio observations of B-type supergiants are discussed in Chapter 4

Information about the masses and radii of B stars is assembled in the fifth section. Studies of eclipsing binaries which show double-lined spectra have revealed that the masses of B stars of luminosity classes IV and V range from about 2.5 $M_\odot$ at type B9 to about 17 $M_\odot$ at B0. The masses of giant B stars in luminosity class III are less well known. They appear to be a little larger than those of stars in luminosity classes IV and V. Direct information on the masses of B-type supergiants can be inferred from the orbital motion of X-ray sources in which the optical star is a B-type supergiant. It appears that the masses of B-type supergiants lie in the range $20 \pm 5\ M_\odot$

The radii of B stars can be determined from the solutions for the light curves of double-lined spectroscopic binaries which are eclipsing and from angular diameters and distances The latter method is discussed in Chapter 3. The radii of B stars of luminosity classes IV and V range from about 3 $R_\odot$ at type B9 to about 9 $R_\odot$ at type B0; the radii of giant stars of luminosity classes II and III range from about 4 $R_\odot$ at type B9 to about 12.5 $R_\odot$ at type B0. Table 4-1 shows that the radii for Ib supergiants range from about 30 $R_\odot$ at type B9 to about 25 $R_\odot$ at type B0. The radii for the Ia supergiants range from about 80 $R_\odot$ at type B9 to about 35 $R_\odot$ at type B0 The B stars in the main-sequence band become larger as the type becomes earlier, but among the supergiants this trend is reversed, the late B-type Ia supergiants being more than twice as large as the early B-type Ia supergiants.

The velocity of escape from the photospheres of main-sequence B stars is shown to range from about 580 km s^{-1} at type B9 to about 880 km s^{-1} at type B1. The velocity of escape from the photospheres of supergiants is less than these values, the amount depending upon the poorly known values for the masses of supergiants.

OBSERVATIONS OF NORMAL MAIN-SEQUENCE AND GIANT B STARS

In Chapter 3 observations of normal main-sequence and giant B stars made in the visible and the ultraviolet spectral regions are reviewed. Most of what is seen can be accounted for by a classical photosphere using the existing theory of stellar spectra However, there are some observations in the visible range and a few in the ultraviolet range which require the presence of a mantle for their interpretation. The fact that X-rays are observed from some nearby main-sequence B stars (see, for instance, Cash et al., 1979) is a result that unequivocally demands the presence of a mantle around normal B stars

The mantles of the B stars in the main-sequence band are tenuous and difficult to detect However, mantles appear definitely to be present for stars in luminosity classes II to V. The density in the winds from these main-sequence stars appears to be very low. The giant stars, those in luminosity classes II and III, appear to possess denser mantles than do the normal stars of luminosity classes IV and V. The observational data from normal B stars reviewed in Chapter 3 form a basis for comparison with the data from stars with conspicuous mantles such as the supergiants and the Be/shell stars.

The shape of the energy distributions from the LTE, line-blanketed model atmospheres of Kurucz (1979) represent well the shape of the energy distributions observed for main-sequence B stars. The absolute energy spectrum of the star η UMa is well determined. This star may be used as a standard energy source, its energy distribution in absolute units, from 1200 Å to 12.6 μm is given in Table 3-2. The good agreement between the data plotted in Figure 3-1 shows that the absolute calibrations for photometry done from the surface of the Earth are now internally consistent.

The methods for determining the effective temperatures of B stars are presented. The direct method makes use of angular diameters and integrated fluxes. Indirect methods determine the effective temperature by comparing selected, observed spectroscopic criteria with predicted

values for these criteria obtained by means of classical model atmospheres. It is shown that methods which make use of the shape of the continuous spectrum and/or the size of the Balmer jump result in estimates for the effective temperature of a star which are about the same as the effective temperature found directly from integrated fluxes and angular diameters. Estimates obtained indirectly by selecting the relative strengths of lines observed in two or more stages of ionization of an element tend to be higher than the true effective temperature of the star. The difference is 1.5×10^3 to 3.1×10^3 K in the case of B stars of luminosity classes IV and V, the differences being largest for the early B stars.

The effective temperatures of 37 B stars for which two or more determinations of effective temperature exist are given in Table 3-4. Values of log g are also given, estimated by means of the adopted model atmospheres. The available material on the effective temperatures of B stars as a function of spectral type and intrinsic color, $(B - V)_0$, is assembled in Table 3-5 and shown in Figure 3-4. The temperature law delineated by these data is adequate for determing the effective temperature of a B star in the main-sequence band within an uncertainty of about $\pm 5.0 \times 10^2$ K, given either a spectral type or the intrinsic $B - V$ color of the star. Stars of type B9 have effective temperatures near 1.09×10^4 K, those of type B0 near 3.09×10^4 K.

The angular diameters of main-sequence B stars determined by comparing observed absolute monochromatic fluxes from B stars in the range $\lambda > 6000$ Å with the predictions from LTE, line-blanketed model atmospheres are on the same scale and zero-point as the angular diameters measured directly by Hanbury Brown et al. (1974). This result demonstrates that the continuum fluxes from the model atmospheres of Kurucz (1979) have the correct absolute values. The comparison mentioned above with the observed shape of the spectrum from η UMa, B4 V, shows that the continuous spectra of the model atmospheres of Kurucz are correct from 1200 Å to 12.6 μm. Therefore we conclude that the LTE, line-blanketed model atmospheres of Kurucz (1979) represent well the photospheres of main-sequence B stars.

The absorption-line spectrum of B-type stars in the main-sequence band is surveyed. The general change in strength with spectral type of dominant lines in the visible spectral range is shown in Figures 3-5 and 3-6. When the profiles and equivalent widths of lines in sharp-lined stars are compared with the detailed predictions from model atmospheres, most of the visible spectrum of a B star can be understood using a solar composition and a classical model atmosphere. The use of non-LTE physics improves the representation of the relative strengths of lines of He I, Si II, Si III, Si IV, Ne I, and Mg II. However, some clear anomalies remain which indicate that the contribution of the mantle of the star to the strongest lines in the visible range is not totally insignificant. For instance, the observed strengths of the cores of the leading members of the He I series are not correctly represented by non-LTE models of the photosphere coupled with a non-LTE theory of line formation. A similar result is the interesting observation of Dufton and McKeith (1980) that the He I line at 3187 Å, which arises from the metastable 2^3S level, is about twice as strong as computations using non-LTE physics suggest it should be. Main-sequence stars are surrounded by mantles in which the electron temperatures are near 2.0×10^4 K in at least part of the volume.

Anomalies still exist in representing the relative strengths of the Si II, Si III, and Si IV lines, in spite of the detailed non-LTE analysis by Kamp (1978). These problems might be resolved if a mantle were added to the model for the atmosphere of a B star.

Because the observed relative strengths of the strong lines of He I, Si II, Si III, and Si IV even in the spectra of main-sequence B stars are anomalous and require the addition of a model mantle to the normal model of a photosphere if they are to be interpreted consistently, it must be concluded that the spectral type and luminosity criteria for stars of types B2.5 and earlier which have been selected by Walborn (1971) classify stars not only according to the properties of their photospheres, but also according to the

properties of their mantles.

A review of the prominent lines in the ultraviolet spectra of main-sequence B stars is presented and typical profiles for the resonance lines of C II, C IV, Al III, Si II, and Si IV are shown in Figures 3-8 to 3-12. Profiles are shown for HR 1861 (B1 V), ι Her (B3 IV), τ Her (B5 IV), π Cet (B7 IV), and ν Cap (B9.5 V). The variation of the line profiles through luminosity classes IV to Ia at type B5 is shown in Figure 3-14 for the spectral region near 1300 Å. The cores of the ultraviolet resonance lines are not usually displaced shortward; in only a very few main-sequence B stars is there an asymmetry in the shortward wing of the resonance lines suggesting outflow in a low density wind of high electron temperature.

The lines of multiplet UV 13.04 of Si II at 1305.59, 1309.46, and 1309.77 Å are unexpectedly strong and broad. This observation implies that the radiation damping for these lines is exceptionally strong. Probably the cause of this is autoionization from the $3s3p3d\ ^2F^\circ$ levels. This observation indicates that autoionization and dielectronic recombination may be important factors for establishing the ionization balance between Si^+ and Si^{++}.

The variations in light and line shape from sharp-lined B stars which have been observed with precise spectrophotometry are reviewed. It seems that most sharp-lined B stars undergo periodic, small amplitude changes in brightness, radial velocity, and line shape. These changes may be caused by nonradial pulsation in the envelope of the star. Radial pulsation is believed to be active for the Beta Cephei stars. The sharp-lined star, τ Sco, has been shown to have asymmetrical lines with wings suggesting outflow. This star does not appear to be variable. It is not a typical main-sequence B star, for its mantle seems to be more easily visible than is usual for stars in luminosity class V.

The whole body of observational material is discussed and the evidence pointing toward the presence of tenuous mantles around B stars in the main-sequence band is drawn together. The fact that X-rays have been observed from the otherwise inconspicuous B7 IV star, π Cet, is sure evidence that parcels of very hot gas, $T \approx 10^7$ K, exist in the outer atmosphere of this main-sequence star. Having a photosphere that is normal is no guarantee that a star will not have a mantle that is observable.

OBSERVATIONS OF B-TYPE SUPERGIANTS

The observations of B-type supergiants are reviewed in Chapter 4. A model mantle must be added to a classical model photosphere if the observations are to be fully understood. The shape of most of the continuous spectrum of a B-type supergiant and the absolute intensity of the light received from the star over the range from ultraviolet to infrared can be interpreted using a classical model atmosphere to represent the photosphere of the star. However, the observations of the Balmer continuum in emission, the presence of an infrared excess and radio emission, as well as many details of the line spectrum in the visible and the ultraviolet require one to postulate the presence of a mantle. The mantle is superheated as a result of the deposition of nonradiative energy, it is in outflow, and it is inhomogeneous. All three properties are required in order to account for the observed line spectrum of B-type supergiants

Twelve B-type supergiants are known to show intrinsic polarization This indicates that their atmospheres are not spherically symmetrical and that electron scattering is important. In the case of four of these B-type supergiants, the degree of polarization has been observed to change with time. All B-type supergiants are slightly variable in magnitude and in radial velocity. The changes do not seem to be strictly periodic, but usually a semiperiod of several days, which increases as the spectral type becomes later, can be defined

In the second section of Chapter 4 the determination of the effective temperatures, radii, and bolometric corrections for B-type supergiants is reviewed The directly determined effective temperatures of B-type supergiants run from about 1.05×10^4 K at type B9 to about 2.5×10^4 K at type B0.

Effective temperatures determined from the shape of the continuous spectrum are in accord

with those determined from angular diameters and integrated fluxes. A color index over the range from 1600 to 4000 Å is a useful criterion for effective temperature. Color indices which include the region of the head of the Balmer continuum should not be used because the Balmer continuum is found to be in emission in B-type supergiants. Similarly, for late B-type supergiants, color indices based on the visual and red region of the spectrum are not good indicators of effective temperature because the late B-type supergiants, particularly those in luminosity class Ia, are found to have a significant infrared excess which may be detectable to about 5000 Å.

Effective temperatures determined from model atmosphere analysis of the strengths of absorption lines in the visible spectrum are always too high for B-type supergiants. Typically at type B1, T_{eff} (lines) $-$ T_{eff} (integrated flux) $\approx +$ 5.0 $\times$ 10^3 K

The uncertainty of the effective temperatures given in Table 4-1 is of the order of $\pm$ 5.0 $\times$ 10^2 K Use of the temperature law given in Table 4-2 should determine the effective temperature of a B star in luminosity classes Ib or Ia within $\pm$ 10^3 K if a reliable spectral classification is available.

In the spectral range O9.5 to B0.5, the spectral type is not necessarily an unambiguous indicator of effective temperature, the effective temperatures of α Cam (O9.5 Ia), 15 Sgr (O9.7 Iab or B0 Ia), and ϵ Ori (B0 Ia) being, respectively, 2.5 $\times$ 10^4, 2.97 $\times$ 10^4, and 2 509 $\times$ 10^4 K. Underhill (1981a) has shown that 3 WN7 stars and 1 WN8 star also have effective temperatures near 2.5 $\times$ 10^4 K

The accuracy of the linear radii of the B-type sugergiants determined from angular diameters depends chiefly upon the accuracy with which the distance to the star can be determined. The percentage uncertainty in the radius is equal to 0.2 ΔMod, where ΔMod is the uncertainty in the distance modulus to the star. Typically ΔMod $<$ 0.5 mag. The random errors in the angular diameters are believed to be less than about 2 percent.

The visible spectrum of B-type supergiants is reviewed in the third section. The absorption lines, typically, have a "boxy" look which is attributed to geometrical broadening by macroturbulence. Rotational broadening is present also, but it is small in comparison to what is frequently seen for B-type main-sequence stars. The total broadening due to macroturbulence and rotation is usually less than 50 km s^{-1}. The composition of B-type supergiants appears to be solar. The evidence for true carbon or nitrogen over or under abundances is weak. It is true, however, that the pattern of relative line strengths for some lines of C, N, and O is not always precisely the same for all early B supergiants. This can be explained in other ways than by assuming an abundance difference.

Weak emission components with a shortward displaced absorption core are often seen at Hα and sometimes at He I 5876 and He I 6678 in the early B Ia supergiants. Emission is not often obvious for the Ib supergiants. The profiles of the strong lines vary and so do the radial velocities indicated by the position of the deepest point in the line profile. Information about the Hα profiles in B-type supergiants is reviewed and it is noted that the most luminous stars tend to show a Balmer progression with Hα and Hβ showing significant velocities of outflow relative to the radial velocity indicated by the high members of the Balmer series and by lines of He I and ions of the light elements. The star α Cam, O9 5 Ia, is noted to have an unusually intense, variable Hα emission feature. Weak, variable Hα emission is shown for the B1 Ib supergiant, ρ Leo. Usually the intensity of the emission at Hα does not rise 20 percent above the continuum

The ultraviolet spectrum of B-type supergiants is the topic of the fourth section. Typical profiles observed from high resolution IUE spectra of the resonance lines of Si II, C II, Al III, Si IV, and C IV are shown for 15 Sgr (B0 Ia), χ^2 Ori (B2 Ia), η CMa (B5 Ia), and HD 21389 (A0 Ia). The changes in the spectrum at type B2 as the luminosity increases from luminosity class IV (γ Peg, ζ Cas), to class II (ϵ CMa) to Class Ib (9 Cep), to class Ia (χ^2 Ori) are also shown. The profiles of the resonance lines of C II, Al III, Si IV, C IV, N V, and O VI are found to have a "P-Cygni" shape with a shortward displaced absorption

trough and sometimes a weak emission component on the longward side of the line. The presence of strong absorption in the resonance lines of higher ions than can be maintained by the passage of the radiation field from the photosphere of the star implies heating by nonradiative energy which is deposited in the mantle.

Some of the gas in the mantle is seen to be accelerated to high outflow velocities The data in Table 5-5 show that the maximum velocity of outflow is about 200 km s^{-1} at type A0 and about 2000 km s^{-1} at type B0. Empirically, it is noted that $u_\infty \sim T_{\rm eff}^{2.30}$. At type A0, the wind is seen only in low ions like Mg II, Al II, and C II. At type B0 the wind is seen best in high ions like Si IV, C IV, N V, and O VI.

According to the theory for expanding spherical model atmospheres reviewed in Chapter 6, the energy contained in the emission component should be about equivalent to that removed by the shortward displaced absorption trough This is never observed to be the case, the emission components, if present at all, are always weak In the case of the Si IV doublet, the lines of which are strong in absorption but well separated in the spectra of B2 and B3 supergiants, weak emission may be present for the line at 1402 Å but it is rarely, if ever, present for the line 1393 Å. The intrinsic strength of λ 1393 is twice that of λ 1402 The observed result may be caused by the presence of photospheric absorption lines in the radiation which is scattered by ions in the mantle. The general weakness of the emission components for the ultraviolet resonance lines from high ions in the spectra of B-type supergiants suggests that the high ions are confined to a region near the photosphere or to an equatorial disk. The latter possibility gains credence from the fact that B-type supergiants show intrinsic polarization. Maximum outflow velocities are seen for these high ions, but high ions are also seen to have low components of line-of-sight velocity near 0 km s^{-1}.

It is clear that if one thinks of high ions as resulting from collisions with electrons, one needs to consider at least two regimes of temperature in the mantles of B-type supergiants. This is because outflow velocities of the order of -100 ± 50 km s^{-1} are seen in the strong lines of H I and He I, as well as in the resonance lines of high ions which require energies greater than 25 eV for their formation Furthermore, in the B0 supergiants, strong absorption is seen in the resonance lines of Si IV as well as in those of C IV. However, the ionization potential of Si^{+3} is 45 1 eV while that of C^{+2} is 47.9 eV. Thus, if there were only one temperature regime and the ionization balance (due to collisions with electrons) was such as to favor the presence of C^{+3} ions, that is nearly complete ionization of C^{+2}, then little or no Si^{+3} should remain and most of the silicon ions should be in the unobservable Si^{+4} state. Clearly, this is not the case. Thus, either one infers that the C^{+3} ions are formed by some special process (perhaps Auger ionization) while the Si^{+3} ions result from an ionization balance caused by collisions with electrons, or one assumes that at least two temperature regimes exist, in each of which the ionization is primarily due to collisions with electrons.

Detailed models are required showing how in the mantles of early B supergiants one can have neutral atoms (H, He) and high ions (Si^{+3}, C^{+3}) showing similar velocity ranges. There is little or no evidence for the neutral atoms moving with flow velocities near the maximum observed velocity of outflow, but there is evidence of their moving with substantial outflow velocities.

In Figures 4-15 and 4-16, evidence is presented for the presence of discrete, displaced absorption components in the ultraviolet spectra of B-type supergiants. The displacements and intensities of these components vary. The presence of discrete components was first noted by Underhill (1975a, 1975b) on Copernicus spectra of η CMa, B5 Ia. Such components seem to occur in all supergiants and are most easily seen in lines which are not saturated. The presence of discrete components of the ultraviolet resonance lines and their variation suggests strongly that the mantles of B-type supergiants are inhomogeneous and that the structure varies from time to time Occasionally, extra displaced components have been reported for some strong lines in the visible spectrum. This interpretation seems preferable for the observations of Gutman (1967) in the spectrum

of ρ Leo, B1 Ib, rather than an explanation in terms of a very unusual abundance of ^{3}He.

The infrared and radio spectrum of B-type supergiants is reviewed in the fifth section. The Ia supergiants frequently show excess radiation at 10 μm. The excess is not detectable in many Ib supergiants. The dependence of the excess energy on wavelength is shown in Figures 4-17 and 4-18 for P Cyg (B1 Iap), β Ori (B8 Ia), and α Cyg (A2 Ia). That an infrared excess extending into the visible spectral range is present for late B stars and for P Cyg can be seen from Figures 4-2 and 4-28. A turnover point occurs between 6000 and 7000 Å. Simple theoretical considerations (Cohen et al., 1975) indicate that the electron temperature in the emitting gas is near 2.2×10^4 K, a value well in excess of the effective temperatures of most of the B supergiants.

Throughout the observed range longward of 1 μm, the infrared excess energy, S_ν, from B-type supergiants appears to vary as ν^α. In the case of P Cyg a value $\alpha = 0.77$ serves to relate the observed radio fluxes to the infrared excess fluxes. In the case of supergiants of type B1 and earlier, it is also true that $\alpha = 0.77$ is a reasonable value. In the case of β Ori and α Cyg, the observations indicate that $\alpha = 1.2$ and 1.1, respectively. It seems that for the late B and early A supergiants, the gas emitting a free-free spectrum becomes optically thick at long wavelengths. This explains why these stars, although they show prominent infrared excesses, show very weak radio fluxes, (Abbott et al., 1980).

The star α Cyg (A2 Ia) is found to have an unusually strong infrared excess in comparison to what is observed for other Ia supergiants. The fact that the infrared excesses are much stronger for Ia supergiants than for the Ib supergiants indicates that the column density is much higher in the outer part of the mantles of Ia supergiants than it is for Ib supergiants. The column density must be particularly high for α Cyg. Showing an infrared excess seems to be more a function of the amount of material in the mantle than of the effective temperature of the star. Stars which show prominent infrared excesses also show prominent emission at Hα. The amount of gas in the mantle seems to be largest for the most luminous stars. This rule is not absolute, however, for, although P Cyg has an unusually conspicuous mantle, it is not an unusually luminous star.

High resolution spectra of eight early type supergiants over the spectral range from 0.48 to 1.03 μm have been published by Johnson et al. (1978) and Johnson (1978). These spectra, when they are analyzed, should yield information about the properties of the mantle.

In the sixth section, the information about the peculiar supergiant P Cyg and about the superluminous supergiants is reviewed. In the case of P Cyg, the amount of the ultraviolet and visible light, after correction for interstellar extinction and for the presence of an infrared excess which extends into the visible region, corresponds to an effective temperature of 1.22×10^4 K. It is noted that the distance to P Cyg is close to 1.69 kpc. This distance, with the observed angular diameter, leads to a linear diameter of 75 $R_\odot$ for the photosphere of P Cyg. The luminosity, $\log L/L_\odot$, is then 5.05, a value typical for late B supergiants of luminosity class Ia. The information about the rate of mass loss from P Cyg is reviewed and it is shown that $\dot{M} = (1.5 \pm 0.5) \times 10^{-5} M_\odot \mathrm{yr}^{-1}$.

The spectrum of P Cyg is unusual in the visible range in that it contains many strong emission lines, each of which is accompanied by a shortward displaced absorption core. There are also absorption lines without emission components. Every absorption line in the visible spectrum is displaced shortward by an amount between -50 and -220 km s^{-1}. Some absorption components are double; three components can be seen in absorption for the upper members of the Balmer series The emission at Hα rises to about 17 times the height of the continuum while the central intensity of the deepest point of the Hα absorption component is about 0.4 (Bernat and Lambert, 1978). Such a large intensity of the emission relative to the strength of the absorption trough is not seen for the "P-Cygni" type lines in normal B-type supergiants. It cannot be explained by the existing theory of expanding, spherical model atmospheres (Oegerle, 1977; Lee, 1979).

The displacements of absorption lines in the visible spectrum correlate roughly with the energy required to put an ion in the lower level from

which the line arises. Larger velocities of outflow are seen by means of lines from levels of low excitation potential in atoms and ions requiring little energy for their formation than from lines which arise from levels requiring much energy for their excitation. The relationship is neither exact nor single valued. This trend is confirmed by absorption lines visible in the ultraviolet region. The ultraviolet lines show outflow velocities in the range −90 to −215 km s^{-1}.

Line profiles are presented for the ultraviolet resonance lines visible on IUE spectra. The ultraviolet spectrum of P Cyg is much more like that of the B5 Ia supergiant, η CMa, than it is like that of the B1 Ia supergiant, κ Cas. Emission components are weak in the ultraviolet and they appear chiefly on the longward edges of the resonance lines from the second spectra of the light elements and the metals. The strongest emission lines in the ultraviolet spectrum of P Cyg are those due to multiplet UV 13.04 of Si II with lines at 1305.59, 1309.46, and 1309.77 Å. These lines arise from the dielectronic recombination process

$$Si^{++}\,(3s3p) + e \rightarrow Si^{+}\,(3s3p\,(^3P^o)\,3d)$$

$$\rightarrow Si^{+}\,(3s3p^2) + h\nu. \qquad (9\text{-}1)$$

Information about the superluminous supergiants, luminosity class Ia+ or Ia−0, is given. A list of 8 superluminous supergiants in our galaxy and 10 in the Large Magellanic Cloud is presented in Table 4-9. Typically, the superluminous supergiants have M_V in the range −8.3 ± 0.5 mag. Since the bolometric correction runs from about −1 7 mag at type B1 to about −0.3 mag at type A0, the luminosity of the superluminous supergiants runs from $\log L/L_\odot$ = 5.9 at type B1 to about $\log L/L_\odot$ = 5.3 at type A0.

The star ζ^1 Sco is the best studied superluminous star of type B1 Ia+. Information on this star and on other B1 Ia+ stars is summarized. The effective temperatures of the B1 Ia+ stars are found to be near 1.8×10^4 K. The shortward edges of the strong ultraviolet resonance lines of ζ^1 Sco suggest maximum outflow velocities of the order of 500 km s^{-1}. The emission lines in the spectra of the B1 Ia+ stars are much less intense than those of P Cyg, although they are stronger than those of the B1 Ia supergiants. The ultraviolet spectrum of ζ^1 Sco is like that of a B2 or B3 Ia supergiant. The rate of mass loss from the B1 Ia+ stars appears to be of the order of a few times $10^{-6}\ M_\odot\ yr^{-1}$.

The X-ray binaries containing B-type supergiants are discussed. A list of five systems is given in Table 4-10. The ultraviolet spectrum of HD 77581, B0.5 Ib, suggests a rate of mass loss near $1 \times 10^{-6}\ M_\odot\ yr^{-1}$. The maximum rate of outflow seen for HD 77581 is about 860 km s^{-1} which is about half what is seen for single B1 Ia or B1 Ib stars.

The properties of the B-type supergiants are discussed in the eighth section. The spectra of the supergiants can best be interpreted in terms of a model photosphere and a model mantle. The photosphere can be modeled well by a classical model atmosphere. This procedure serves to interpret most of the continuous spectrum and undisplaced weak absorption lines from ions which are not abundant.

The observations of the Balmer continuum in emission, of an infrared excess and radio emission, and of X-rays from B-type supergiants require that a model mantle be added to a model photosphere if the atmosphere of a B-type supergiant is to be accurately represented. Additionally, the observed strengths of the intrinsically strong lines of abundant elements, the presence of emission lines, the presence of discrete components and their variation, the indications of outflow at high speed, as well as the presence of strong absorption in the resonance lines of high ions demand that a mantle having properties different from those of the photosphere be postulated to be present. The varying line asymmetries and line shifts and the broadening by macroturbulence of spectral lines all show that the mantle is neither homogeneous nor static. The fact that the light from many supergiants is polarized indicates that the mantles are not necessarily spherically symmetrical.

The principle properties of a mantle are transparency in most continuum frequencies, superheating, outflow, inhomogeneity, and variability.

A schematic model for a mantle of a supergiant is outlined. It is suggested that the energy required to heat the mantle is released as a result of local differential motions in the atmosphere The nonradiative energy which is tapped is that stored in the ambient magnetic field.

Mass loss is probably initiated by magnetic effects low in the mantle. After the gas receives an initial impulse outward, it is accelerated by radiation pressure.

It should be recalled that the properties of the photosphere of a supergiant are primarily determined by the value of the effective temperature of the star. The value of log g is a second parameter. The properties of the mantle, however, depend on other parameters. These may be the energy density of the source from which the material in the mantle receives its energy, and the efficiency of the mechanism which couples the nonradiative source of energy to the gas of the mantle. The observations of the spectra of B-type supergiants indicate that mantles having widely different properties may be associated with photospheres which are characterized by very similar effective temperatures and values of log g

SPECIAL TYPES OF B STARS

The characteristic properties of the Beta Cephei stars are reviewed in the first section of Chapter 5. The Beta Cephei variables are a group of B stars having spectral types in the range B0.5 II to III to B2 IV on the MK system. They exhibit light and radial-velocity variations in periods of 3 to 6 hours. The light curve generally lags behind the radial-velocity curve by one-quarter period. The periods are stable and they are typical of vibration periods for stellar models of 10 to 15 solar masses.

The spectral types of those Beta Cephei variables which have been classified on the MK system are completely normal. Indeed some Beta Cephei stars are MK standards and many have very sharp lines. However, having sharp lines is not a necessary condition for inclusion in the Beta Cephei class. The composition of the Beta Cephei stars appears to be solar. Their effective temperatures and log g values are normal for stars of their assigned spectral types The Beta Cephei stars do not differ systematically in luminosity from nonvariable B stars of the same MK spectral type.

In the case of most Beta Cephei stars, the light and radial-velocity variations give evidence for the existence of one or more secondary periods in addition to the principal 3- to 6-hour period. Information on the periods and light and radial-velocity amplitudes of 21 well-studied Beta Cephei stars is given in Table 5-1. The light amplitude is always larger at ultraviolet wavelengths than it is in the visual range

High resolution studies of the visible spectrum of sharp-lined Beta Cephei stars show that the spectral lines are generally narrow and have steep sides on the ascending branch of the radial-velocity curve. On the descending branch the lines are broad and shallow Here asymmetrical lines sometimes are seen and the line may split into two components. At phases around maximum radius, the hydrogen lines appear to be filled in by emission from an extended atmosphere. Observations of the ultraviolet spectrum of β Cep at high resolution show that the blend of the C IV resonance lines at 1550 Å disappears and reappears on a 6-day cycle. Similar effects have been observed in N V. Observations are presently being made with IUE to clarify how the ultraviolet spectra of Beta Cephei stars vary and to find out whether the short periods characteristic for the visible spectrum are dominant or whether periods of several days are relevant for understanding the changes in the ultraviolet spectrum

At present there is no agreement on whether or not the Beta Cephei variables obey a single period-luminosity relation similar to that followed by the classical cepheids. The search for a cause of the Beta Cephei phenomenon has so far been unsuccessful. At present it appears that nonvariable B stars and line-profile variables also may be found in the area of the HR diagram which is occupied by Beta Cephei stars.

The observed positions of the Beta Cephei stars in the HR diagram fall in a region about 1 5 mag above the zero-age main sequence for early B stars from about B0 to B3 and approximately parallel

to the ZAMS. The "Beta Cephei" strip appears to be of finite length; its upper and lower boundaries have not been precisely determined. Theoretical studies of the evolution of massive model stars show that the observed zone occupied by the Beta Cephei stars can be occupied by stars that are still burning hydrogen in the core, by those with contracting cores, and by those with a hydrogen shell source It is not clear yet which of these evolutionary models best describes the Beta Cephei stars.

In the second section of Chapter 5, information is summarized about the peculiar B stars The anomalies being discussed are those which are visible on classification spectra The spectra of these stars do not fit into the MK classification scheme exactly. Typical stars of each group are listed in Tables 5-2 to 5-5.

Although most hot subdwarfs are O stars rather than B stars, these stars are discussed briefly because some of their spectral anomalies are similar to those that occur at later spectral types The helium-strong stars do have spectral types in the B range. They lie in the HR diagram on or near the hydrogen-burning main sequence. One of the best studied members is σ Ori E.

The extreme helium stars have spectra in which the hydrogen lines are very weak or absent. This implies that the fractional abundance by number of hydrogen to helium is of the order of or less than 0.001. The helium-weak stars are characterized by abnormal weakness of the lines of neutral helium. At classification dispersion no enhanced or peculiar metallic lines are observed, but at high dispersion certain enhancements are visible. None of these stars have been observed to have a significant magnetic field.

The helium-strong and helium-weak stars which are spectrum variables maintain He I lines of the same strength throughout their cycle. On the other hand, the helium variables are B stars in which the strengths of the He I lines vary periodically; they are B stars which change their appearance from helium-strong to helium-weak in the course of a single cycle. The hydrogen lines change little, if at all, during the cycle. The prototype star is α Cen (HD 125823).

The mercury-manganese (Hg-Mn) stars fall in the effective temperature range of the B stars They are slow rotators with no observable magnetic fields. They comprise a significant fraction of the late B-type stars in the main-sequence band. Ultraviolet photometry shows that the Hg-Mn stars are flux deficient in the extreme ultraviolet for their UBV colors.

The true Bp stars, or silicon stars, are found around types B8 and B9. They appear to be an extension to higher temperatures of the Sr-Eu-Cr stars which form the main body of Ap stars. The Bp stars have strong, sometimes variable magnetic fields, and they are frequently spectrum and/or photometric variables.

MODEL ATMOSPHERES, PREDICTED SPECTRA, AND COLORS

In Chapter 6 the philosophy of model making is described as it is applied to making models of the atmospheres of B stars. Predicted spectra found by numerical procedures from model atmospheres provide a well-understood norm to which observed stellar spectra may be compared. Deductions may be made about the physical state of the stellar atmosphere after considering the agreements and differences between predicted and observed spectra.

Classical model atmospheres are composed of plane-parallel layers of gas in radiative and hydrostatic equilibrium. The two parameters which define the properties of a classical model atmosphere, after its composition has been specified, are the effective temperature and the acceleration of gravity in the atmosphere due to the mass of the star. The physics of a low density, partially ionized gas in contact with radiation is used. This body of theoretical and experimental results is used for representing the interactions which occur between the radiation field and the stellar material in the atmosphere of the star

It should be noted that the condition of hydrostatic equilibrium is met exactly in very few real B-type stars. In spite of this, the existing grids of classical model atmospheres serve as useful tools for interpreting the spectra of B stars. However, it should be borne in mind that it is difficult, if not impossible, to prove that any adopted

model atmosphere and an adopted representation for the process of forming a spectrum is unique.

The concept of local thermodynamic equilibrium cannot be fully justified in stellar atmospheres where radiation is escaping into space. Nevertheless, LTE proves to be a very useful and economical concept when calculating model atmospheres and model spectra. It is essential to use the more elaborate concept of non-LTE, which makes use of the principle of statistical equilibrium to determine the distribution of atoms and ions over their several possible energy states, if the strong lines from abundant ions and certain other lines are to be interpreted correctly. However, use of this principle does not relieve all inconsistencies encountered when the predicted and observed line spectra of B stars are compared.

Chapter 6 also reviews briefly the process of making model atmospheres for B stars. The value of the set of LTE, line-blanketed model atmospheres of Kurucz (1979) is noted. This set of model atmospheres is the most comprehensive set presently available for interpreting the continuous spectra of B stars. Information about the continuous spectrum produced by Kurucz's model atmospheres is presented in sufficient detail that comparisons can easily be made with observations. A set of model atmospheres based on use of non-LTE physics has been provided by Mihalas (1972a). These models are useful chiefly for early B-stars. Mihalas gives the emergent energy distributions from these models at only a few wavelengths, but he does give detailed profiles for Hα, Hβ, and Hγ. The energy distributions of the models of Kurucz and those of Mihalas have closely the same shape over the observable spectral range, from 1200 Å to 1 μm. Use of non-LTE physics produces a slight rise (15 to 20 percent) in the electron temperatures in the outer layers of Mihalas' models from the minimum temperature which is reached at a small optical depth. In the case of the LTE, line-blanketed models of Kurucz, the temperature decreases steadily outward.

The spectra predicted from models composed of plane-parallel layers are compared with observed spectra in the third section of Chapter 6. Some comments are made about how to select a model atmosphere that is representative of the atmosphere of a real star. Use of the shape of the continuous spectrum, and, in the main-sequence stars, the size of the Balmer jump are satisfactory methods. Use of the equivalent width of Hγ and the break-off point of the Balmer series also is an effective procedure (Fischel and Klinglesmith, 1973). It is noted that Kurucz and his colleagues have been able to predict accurately most of the color relationships observed for B stars using broadband and intermediate-band photometry.

In principle, rotation of the model star should modify the predicted color relationships from those obtained using nonrotating models. The work of Collins and Sonneborn (1977) on this subject is reviewed, and it is shown that the modifications are small unless the star is rotating very rapidly. It is usually satisfactory to select a model atmosphere for a normal B-type main-sequence star by comparing the observed continuous spectrum with that from a stationary model star. The best way to proceed for stars having much observational data covering the spectral range from the ultraviolet to the infrared is to find effective temperatures and radii by the direct method described in Chapter 3. If the mass of the star is known from solution of a binary orbit, one can obtain $\log g$ directly. In most cases, fitting the shapes of the wings of the Balmer lines results in a secure estimate of $\log g$.

How to determine abundances from observed equivalent widths and line profiles is reviewed for B stars By and large, main-sequence B stars are found to have solar composition. Application of the techniques of "fine analysis" to supergiants is reviewed. An inhomogeneous mantle around a supergiant, part of which may be hot and part of which may be cool, may be present Such a possibility makes it unclear that the deduced abundances of nitrogen and possibly other elements, found using normal model atmospheres, are truly anomalous.

Fine analysis carried out using the condition for statistical equilibrium (non-LTE) for determining the distribution of atoms and ions over their several possible energy states makes the problem of determining abundances from weak and strong lines of the same element more self-

consistent than it is when LTE is assumed to be valid. The role of microturbulence as a "fudge" factor then decreases. Nevertheless, in both main-sequence and supergiant stars, the cores of strong lines from abundant elements, for instance the He I lines at 5876, 6678, 7065, 7281, and 10830 Å are not well represented by non-LTE physics and non-LTE model atmospheres. Here we are observing the effects of the mantle. This part of the atmosphere is not included in any model atmospheres made to represent the photosphere

The major differences which result between LTE and non-LTE analysis are noted. Roughly, with non-LTE one has "continuum effects," which result in an over- or underionization of an atom or ion relative to what occurs in LTE, and "line effects" which result from changes in the relative populations of the upper and lower levels of the line under study.

The classical methods of interpreting stellar spectra provide successful interpretations for the continuous spectra of B stars of all luminosity classes. Classical model atmospheres are appropriate for modeling the photospheric layers of B stars. For main-sequence stars, most of the visible spectrum can be interpreted well. However, for the supergiants, many striking features in the spectrum cannot be properly represented by means of classical model atmospheres. These features are those which we have noted to give evidence for the presence of a mantle. What is not predicted by classical modeling is also discussed.

The existing theory for modeling extended, moving atmospheres is reviewed. The types of moving atmospheres which are considered provide simple models for mantles. Their relevance for describing the conditions in actual mantles can only be decided after the key assumptions for developing these model atmospheres have been compared with the observed dominant characteristic properties of real mantles Many of the problems that are encountered in this theoretical work are of a difficult mathematical nature.

The early work on moving atmospheres was characterized by analytical solutions for the equations of radiative transfer which were set up. Recent work makes great use of numerical solutions obtained at the expense of some simplifying assumptions about the physical state of mantles. A major conclusion that can be drawn from the early work on the transfer of radiation through moving and extended atmospheres is that expansion of the atmosphere and extension of the atmosphere do play a role in determining the shapes of the absorption and emission lines which are observed in the spectra of stars with abnormal spectral types.

An important simplification in the theory of radiative transfer in moving atmospheres was introduced by Sobolev (1947). Sobolev made use of the concept of "escape probability" and he argued that in the presence of large monotonic velocity gradients only material in very short sections of atmosphere along each line of sight would interact with the radiation field to contribute to the line profile under study. The geometric positions of the interacting regions within the stellar atmosphere are determined by the postulated velocity law. This law gives the dependence of the line-of-sight velocity on the distance of the parcel of atmosphere from the stellar photosphere.

Since 1960, some elegant methods for handling the mathematics of radiative transfer in moving atmospheres have been developed and applied. In all of the cases which have been worked out, the dependence of temperature on distance from the photosphere is specified by an ad hoc function, a dependence of line-of-sight velocity on the distance from the photosphere is assumed, and the density is found by requiring that matter be conserved in spherical shells so that there is a constant rate of loss of mass from the atmosphere. In this way the physical state of the model mantle is specified. The problem of radiative transfer in the model mantle is solved and line profiles are calculated for typical values of the parameters which define the model mantle and the intrinsic strength of the lines.

In order to solve the equations of radiative transfer in moving three-dimensional atmospheres where the velocity increases outward, one of two procedures is followed Either the line is assumed to be formed by scattering and the Sobolev

approximation is made (Olson, 1978; Surdej, 1979; Castor and Lamers, 1979), or the equations are solved in the comoving frame without making the Sobolev approximation (Lucy, 1971; Mihalas and Kunasz, 1978). In the latter case, no simplifying assumptions are made concerning the effects of velocity gradients on the interlocking of radiation from different geometrical parts of the atmosphere. Some typical line profiles resulting from these theoretical studies are shown in Figures 6-5 and 6-6.

One very important general conclusion has emerged from the theory of line formation in moving atmospheres (see Hummer, 1976). It is that the Eddington-Barbier relation (the statement that the emergent monochromatic flux in a line can be approximated by the value of the source function at the depth where the monochromatic optical depth is unity) can no longer be used in diagnostic analysis when the atmospheric layers are moving. This means that one cannot determine a geometric place of origin for the radiation seen at a particular place in a line profile.

Marti and Noerdlinger (1977) and Rybicki and Hummer (1978) have explored the theory of line formation in a moving three-dimensional atmosphere in which the projection of the flow velocity on the line of sight is not monotonic. This condition has the result that some constant velocity surfaces are intersected more than once by some lines of sight. Interlocking of radiation then occurs.

These studies show that it is very difficult to interpret the shape of a "P-Cygni" type line profile unambiguously in terms of one type of flow pattern. For instance, Rybicki and Hummer (1978) show that a line profile with a shortward displaced absorption trough and an emission component on its longward edge can result from an atmosphere in which there is a sudden acceleration near the photosphere followed by deceleration. The predicted profile differs only in small details from that which will result from an atmosphere which is accelerating outward at all levels above the photosphere. Typical profiles for the latter case have been given by Olson (1978), Surdej (1979), and Castor and Lamers (1979).

Also in Chapter 6, the results of applying these theoretical ideas to interpreting the observed profiles for Hα, Hβ, and Hγ in P Cyg are reviewed. All treatments produce line profiles rather like what is seen, but none give a truly good fit. Even when the problem of the hydrogen lines is treated by using the theory of statistical equilibrium to determine the distribution of the hydrogen atoms among the several possible energy states (Oegerle, 1977; Lee, 1979), the fit is not really satisfactory.

Work by Oegerle and Van Blerkom (1976) and by Karp (1978) on the formation of the He I lines in moving atmospheres gives some promise that the observed relative displacements of strong and weak He I lines will reveal information on the velocity gradients in moving stellar atmospheres.

The existing theories for the mantles of B stars are valuable chiefly as numerical experiments which show what sort of spectrum will result if certain conditions of flow and temperature are present in a mantle. They are inconsistent in that they make no attempt to join the theory of radiative transfer to simultaneous solutions of the conservation equations for the purpose of obtaining a physically real model of the mantle at the same time as the predicted spectrum is found. This full problem is very difficult and it awaits study.

THE EVOLUTION OF MASSIVE STARS

In Chapter 7 the results of the theory of the evolution of massive model stars are summarized; in addition, the tracks followed by the models across theoretical Hertzsprung-Russell diagrams are compared with the observed distribution of B stars in an HR diagram. In Chapter 7 use is made of HR diagrams in the form of plots of $\log L/L_{\odot}$ against $\log T_{\mathrm{eff}}$.

The evolution of massive model stars without mass loss is reviewed. Background is presented for understanding the choices which are made regarding the composition of the model stars (X, Y, Z), the selection of opacity tables, and the representation of the transport of energy when both radiation and convection are effective.

Theoretical evolutionary tracks for massive

model stars are shown in Figure 7-1 for the case that the Cox-Stewart opacity tables are used, and the Schwarzschild criterion is used to describe the transport of energy when convection occurs in the envelope. Some representative observational data are presented for orientation purposes. The tracks for models in which the Ledoux criterion for convection is used cross the region of the HR diagram occupied by B-type supergiants at lower luminosities than are followed when the Schwarzschild criterion is used.

Evolutionary tracks for 15- and 25-solar mass models prepared using Cox-Stewart opacities and the Schwarzschild criterion are shown in Figure 7-2. The 15-solar mass model is still burning helium by the time it has crossed the region occupied by the blue supergiants, but the 25-solar mass model has completed burning helium in its core by the time it leaves the area of the HR diagram occupied by B-type supergiants.

Theoretical evolutionary tracks for massive stellar models made using the Carson opacities and the Schwarzschild criterion are displayed in Figure 7-3 Models with masses greater than 15 $M_{\odot}$ made in this way are still burning hydrogen in their cores when they leave the region of the blue supergiants. The differences between Figures 7-1 and 7-3 are typical of what happens as the composition, the choice of opacity tables, and method for handling convection are varied Evidence is presented that choice of the Cox-Stewart opacity tables gives the best representation of the observed HR diagram that can be achieved at this time.

The properties of model stars with $M \leq 10\ M_{\odot}$ are insensitive to the choices made for composition, opacity tables, and method for handling convection. When the mass of the model star exceeds 10 $M_{\odot}$, the positions of the tracks are sensitive to how the models are constructed. This is particularly true for the parts of the tracks which cross the region of the HR diagram occupied by the blue supergiants. The time spent by a model star in the phase of burning hydrogen in its core is sensitive chiefly to the mass of the model There is very little sensitivity to the other choices made in constructing the models. Some typical hydrogen burning lifetimes are given in Table 7-1. The model stars pass quickly through the stages of overall contraction of the core and burning hydrogen in a shell. Their lifetimes for burning helium in the core are roughly one-tenth as long as their lifetimes for burning hydrogen.

The evolution of massive model stars which are losing mass is reviewed. The first study of the evolution of inhomogeneous model stars undergoing mass loss was done by Tanaka (1966). His results have been confirmed and expanded by all subsequent studies Tanaka found that compared with a star which evolves without mass loss, a massive, mass-losing star at the same stage of central hydrogen depletion has a lower luminosity and a lower effective temperature. In the mass-losing star there is increased stability against convection in the envelope, and a larger fraction of the mass is in the convective core than is the case for a star evolving without mass loss. The hydrogen burning lifetime of the model mass-losing star is increased over that of a model star evolving without mass loss.

Three algorithms, and a modification of the first of them, have been used for representing the rate of mass loss as a function of the instantaneous luminosity, radius, and mass of the star We have (1) $\dot{M} = -kLR/M$, (2) $\dot{M} = -NL/c^2$, and (3) a complicated function that has been derived from the theory of radiatively driven winds of Castor et al (1975) In (1) k is a constant which has a value near 1×10^{-11} if the rate of mass loss is to be typical for a B0 star, and L, R, and M are given in solar units Similarly, in (2), N is a different constant which is of the order of 100 The function representing mass loss by a radiatively driven wind contains two parameters, α and K, which are given typical values; this function depends on the ratio Γ of the instantaneous luminosity of the star to the Eddington luminosity The parameter Γ varies as L/M. The effects of rotation on mass loss have been explored also.

Some typical evolutionary tracks obtained with mass loss are shown in Figure 7-4 and some typical calculated rates of mass loss at various stages in the evolution of a massive model star are given in Table 7-2 It is found that the inclusion

of mass loss at a rate which is equivalent to the observed rates of mass loss introduces changes in the position of the evolutionary track which are of the same order of magnitude as those that result from changes in the choice for composition, opacity tables, and method for handling convection. The changes are most evident in the parts of the tracks crossing the region of the HR diagram occupied by B-type supergiants.

Because of the uncertainties concerning where the evolutionary track lies (uncertainties which depend on the choice made concerning composition, opacity tables, treatment of convection, and treatment of mass loss), it is not possible to determine the mass of a supergiant accurately from its position in the HR diagram. To do so, one must have external information as to which are the correct choices to make in the four areas in which a model must be specified.

Observed HR diagrams are compared with the predicted HR diagram for massive model stars which evolve without mass loss. The observational and theoretical results are discussed in the fifth section of Chapter 7.

The positions of 160 early type stars are shown in Figure 7-5 with the positions of the main-sequence band calculated by Stothers (1976) for Cox-Stewart and for Carson opacities. Most of the O and B stars shown in Figure 7-5 are field stars near the Sun and many are MK standards of spectral type.

Two major conclusions result from Figure 7-5. (1) Star formation in the neighborhood of the Sun has occurred at two epochs. The stars of type B3 and later in the diagrams, including α Lyr, are somewhat evolved. They may have been formed some 2.2 to 24.0 $\times 10^7$ years ago. The early B stars in the diagram and the B-type supergiants are younger than this. They may have been formed some 0.6 to 2.0 $\times 10^7$ years ago. The observed stars have been selected according to apparent magnitude because only the apparently bright stars have been observed photometrically in the ultraviolet and in the visible to infrared range. (2) At several places in the HR diagram, stars with different spectral types are found side by side. Thus, the Wolf-Rayet stars occupy the same area as do B0 stars of luminosity classes III and Ia; the Beta Cephei stars occupy a region filled also with the line-profile variables and with normal nonvarying stars; the Be stars occupy a region, mostly on the right-hand side of the main-sequence band, where normal B stars also occur; the same is true for Bp stars and normal late B-type stars.

It seems clear that among the B stars spectral type, per se, is not a criterion denoting exclusive position in the HR diagram. This is particularly true when the criteria which define the spectral type are based on lines which are chiefly formed in the mantle of the star.

On the whole, the theory of the evolution of massive stars provides a consistent interpretation for the positions of most B stars in the main-sequence band. The masses deduced from binary star orbits are in accord with those required by the theory of stellar evolution. The interpretation of the observed positions of stars as they leave the main-sequence band and transit the supergiant region requires improved detailed models of stellar evolution through the phases of hydrogen burning in a shell and helium burning if good agreement is to be obtained between theory and observation.

The observational HR diagram of Humphreys (1978) for luminous O and B stars is similar to that shown in Figure 7-5. Humphreys' choice of effective temperature and bolometric correction scales is different from those used in Chapter 7. Use of the temperature and bolometric correction scales of Humphreys is not recommended now that better data are available. The luminosities deduced by Humphreys and Davidson (1979) for P Cyg and some superluminous supergiants are unacceptably high.

The positions of the zero-age main sequence for B stars deduced by Eggen (1974a) and by Crawford (1978) from intermediate-band photometry are compared in Figure 7-6 with the position of the theoretical ZAMS. Small systematic displacements, attributable to the use of some evolved stars by Eggen and by Crawford in defining their positions for the ZAMS, exist.

Position in the HR diagram, on the whole, is determined by the mass of a star and its age, or equivalently, its source of energy. More than one

spectroscopic signature may be associated with each pair of points ($\log L/L_{\odot}$, $T_{\rm eff}$). This happens because among the B stars, particularly among the luminous B stars, the empirically selected criteria for spectral type depend not only on $\log g$ and $T_{\rm eff}$ but also on the state of the mantle. It is not yet clear how the physical state of a mantle may be related to the stage of evolution of a massive star. Tentatively, conditions in the mantle appear to be related to the physical state of the envelope of the star and to how energy is transported outward there. The pulsational properties of models of massive stars are described in the last section of Chapter 7.

UNSOLVED PROBLEMS

In Chapter 8 the material presented in Part I is reviewed with the purpose of (1) assessing the level of understanding we have of the physics of single, isolated B stars, (2) discussing the problems which still face us, and (3) suggesting some ways in which the modeling of B stars may be improved.

The significant observational results concerning the effective temperatures, radii, masses, and composition of B-type stars are summarized in the second section of Chapter 8. The convenience and value of introducing the word *mantle* to describe the outer parts of the atmospheres of B stars, parts where the effects of the deposition of nonradiative energy is observed, is evident by the time all the observations of the spectra of all sorts of B-type stars have been reviewed.

The properties of a mantle are reviewed. In a mantle, the concepts of radiative equilibrium and hydrostatic equilibrium are no longer adequate for finding the state of the gas, and it is necessary to consider three-dimensional geometry.

All mantles of hot stars are transparent in most continuum frequencies but opaque in intrinsically strong lines from abundant ions. Mantles contain plasma that is heated to electron temperatures above those which can be supported by the amount of radiative energy provided by the effective temperature of the star and distributed under the constraint of radiative equilibrium Mantles are inhomogeneous, evidence can be seen, especially in the supergiants, of the presence of hot and cold plasma in regions which do not necessarily cover the whole disk of the star or remain confined to spherical shells. Matter flows out of the mantles at speeds which exceed the velocity necessary for gas to travel from the photosphere to an infinite distance and arrive there with zero velocity.

The visibility of the mantle of a B star is very different for stars in the main-sequence band from what it is for supergiants. Mantles may be seen by means of emission in the bound-free continua of hydrogen and by free-free emission. They are seen by means of emission, and sometimes absorption, in the hydrogen lines as well as by means of absorption in the resonance lines of high ions in the ultraviolet. The detection of X-rays from a B star is sure evidence of the presence of a mantle.

Mantles are conspicuous for supergiants and for Be/shell stars, but they are very difficult to detect for normal main-sequence B stars. Mass loss at a rate of the order of $2 \times 10^{-6}\ M_{\odot}\,{\rm yr}^{-1}$ appears to occur for B0 Ia supergiants The rate of mass loss is of the order of $10^{-7}\ M_{\odot}\ {\rm yr}^{-1}$ for late B Ia supergiants. The rate of mass loss from Ib supergiants appears to be smaller than these values; the rate of mass loss has been estimated for very few B stars in the main-sequence band. However, there is spectroscopic evidence suggesting that outflow from some stars in the main-sequence band does occur. The rates of mass loss from main-sequence stars probably are less than 10^{-3} times those from supergiants of the same subtype. There is tenuous evidence that the electron temperatures are higher in mantles of low density than they are in mantles where the density is relatively high

The results of the theory of the evolution of massive stars are confronted with the observed luminosities and effective temperatures of B stars The interpretation of the observed positions of stars in the main-sequence band seems to be firmly based. However, improvements in the treatment of the transport of energy through the envelopes of stars as well as of the value of the opacity in the envelopes are required before one can surely interpret the meaning of the observed

positions of B stars in the part of the HR diagram where massive model stars are changing their energy generation from burning hydrogen in the core to other sources of energy.

The results of the theory of stellar spectra are confronted with observed B-type spectra and a heuristic model for a mantle is developed. The existing theory of stellar atmospheres is adequate for interpreting the part of the spectrum of a B star that is formed in the photosphere. This includes most of the continuous spectrum and the lines from ions which are not abundant When, however, the lines are strong enough that they are formed in the mantle, the existing theory fails This is because the temperatures and densities in the mantle are not primarily determined by the parameters T_{eff} and $\log g$ which, together with the constraints of radiative and hydrostatic equilibrium, specify conditions in the photosphere. Introducing the concept of statistical equilibrium to determine the distribution of the atoms and ions over the several possible energy states improves the classical theory somewhat, but it does not relieve difficulties associated with the fact that many conspicuous lines in the visible spectral region are formed partly, or wholly, in the mantle.

Six types of spectroscopic phenomena are completely unexpected and unexplained by means of the classical framework. These phenomena force us to develop models for mantles using other constraints and parameters than proven successful for modeling photospheres and the process of spectrum formation in the photosphere.

The required properties for a model of the mantle are reviewed, and the spectroscopic signatures for each part of the mantle are noted. Mantles of B stars can be considered to consist of three parts. (1) a corona-like region where the electron temperatures are high but less than about 10^6 K; (2) truly coronal regions, probably small and imbedded in the corona-like region, where $T \approx 10^7$ K; and (3) a post-coronal region where cooling to the state of the surrounding interstellar medium takes place Accelerations and decelerations may be small in the post-coronal region.

Schematic descriptions of the atmospheres of B stars are presented in order to make our concept of mantles for B stars concrete The B stars can be arranged in the following sequence as regards the activity seen in their mantles. (1) normal B stars in the main-sequence band which show little or no variation, (2) supergiants which show constantly a small range of change, and (3) Be/shell stars which may show a striking range of changes over intervals of a few months to a few years

If the source of the nonradiative energy which causes a mantle to exist is to be identified, a necessary first step is to make an estimate of how much energy and momentum is needed. This is done for typical B0 and B9 stars from the main-sequence band and for supergiants. The amount of internal energy that must be supplied to maintain the mantles of main-sequence and supergiant stars in their observed state is only a small fraction of the amount of energy which is radiated per second from the photosphere However, in the case of a B9 supergiant with a large mantle emitting the hydrogen spectrum, the required amount of energy becomes significant relative to the luminosity of the star.

The amount of energy lost from the mantle by conduction, by radiation, and as kinetic energy of the escaping particles is also estimated and shown to be small except for those cases where a large cool part of the mantle which radiates strongly in the hydrogen spectrum is present. The most important loss of energy from the mantle of a B star is that which is seen by means of the hydrogen continuum and the free-free emission detected in the infrared and at radio wavelengths. In the stars which show an infrared excess, the source of energy which is heating the mantle must provide energy at a rate which is comparable to the luminosity of the star. When emission in the hydrogen spectrum is not seen from a B star, the rate of loss of energy from the mantle is of the order of or less than 10^{-4} times the luminosity of the star.

The question of modeling mantles for B stars is also discussed in Chapter 8. The point of view is taken that all stars have mantles, and that the visibility of the mantle is a function of our

capability to observe the star in all energy regimes and of the varying circumstances in the star which promote or hinder the processes which generate a mantle.

A heuristic model for a mantle is developed in which the energy source is postulated to be the magnetic field which pervades the mantle. It is suggested that the energy in the magnetic field is released as a result of the differential motions which are present in the outer atmospheres of B stars. These ideas are based on the suggestion of Rosner et al (1978) concerning the source of the high temperature and inhomogeneous structure of the solar corona. In the Sun, the high temperatures are believed to be the result of in situ heating by means of anomalous current dissipation. The basic geometrical structure is a loop configuration heated by nearly field-aligned currents which occupy a small fraction of the loop volume.

We note that it is reasonable to suppose that undetectably small magnetic fields are present in the outer layers of B stars. The active fields may be the original seed fields occluded when the star was formed, or they may be secondary fields generated in dynamos which are created as convection occurs in the envelope of the star as the star changes its energy generation from burning hydrogen in the core to overall contraction of the core, to burning hydrogen in a shell, to burning helium in the core. Turbulence in the atmospheres of B stars provides the differential motions which act to release the energy stored in the magnetic field This turbulence may be generated by differential rotation.

To have a mantle, a star must tap a source of energy that is in addition to the energy coming from the center of the star as radiation. We show that although one can speak of an average magnetic field in only the loosest of ways, the required magnetic fields to provide the energy needed to form mantles of the types seen are undetectably small and quite possibly present in B stars.

We suggest that an appropriate parameter for characterizing a model mantle is a number which gives the typical energy density of the magnetic field in the mantle. A second parameter is required to specify the efficiency with which the stored energy is transferred to the gas in the mantle. We suggest that the amplitude of the differential motion which is present may be an appropriate parameter.

The mantle of a B star will develop as magnetic lines of force, which are created by the dynamos which result from convection in the envelope, erupt from the photosphere. The loop pattern is sure to be a complex structure which depends on the density of the gas into which the magnetic loops erupt, the rate of rotation of the star, and the amount of turbulence present. Rotation of the loop pattern (which is attached to the photosphere), as well as the growth and decay of the magnetic loops may account for many of the spectral changes seen for supergiants. Rapid rotation of a star may cause the magnetic loops erupting from the photosphere to twist and mat together, forming a disk. This may have the result that the deposition of energy in the disk is inhibited. If so, the disk will cool and a shell spectrum will be seen. After a while, the dynamos in the envelope may decay with the result that the loops weaken and disappear. The disk will also disappear. The known behavior of the Sun during the Maunder Minimum of sunspots gives support to the idea that the general magnetic structure of a star may change by a significant amount for intervals of quite a few years.

The magnetic loops which are considered in this model to be the basic structural unit for a mantle may act as conduits for mechanical/acoustical energy which is generated in the areas of convection which the theory of stellar evolution tells us occur in the envelope of a massive star, particularly as the star nears the end of its lifetime for burning hydrogen in its core.

Flow along magnetic field lines which have become open to interstellar space may be the cause of the discrete displaced components often seen in the ultraviolet spectra of supergiants, and occasionally seen in the visible spectrum. Material may be initially propelled outward by magnetic forces Once it has attained trans-sonic velocity, the material may be accelerated by radiation pressure. This type of acceleration is particularly

effective for high temperature stars.

The chief unsolved problems for B stars are summarized in the final section of Chapter 8. They concern developing appropriate detailed models for the internal structure of massive stars which are beginning to evolve rapidly as they complete burning hydrogen in their cores, and developing detailed models for mantles, and for the transfer of radiation in high temperature, inhomogeneous, moving bodies of gas. The existing theories of radiative transfer in moving, extended atmospheres, reviewed in Chapter 6, are not much help for interpreting the spectrum formed in a real mantle. Three reasons why the existing theory of radiative transfer in mantles is limited are the following (1) in almost all cases the mantles are assumed to be at temperatures like the effective temperature of the star, (2) an ad hoc velocity law is adopted in place of solving for a velocity law that is appropriate for the forces which act on the plasma in a mantle, and (3) the inhomogeneity of mantles is ignored.

A major area of new work that is necessary before B stars can be fully understood is evaluating what is known at this time from the detailed observational and theoretical studies of the mantle of the Sun, and finding out how much of this body of knowledge is truly relevant for understanding the mantles of hot stars.

Part II
Be Stars

"In one sense, every star is more or less peculiar, which features and phenomena are to be considered as normal, and which are to be singled out as peculiar, must depend on the state of our knowledge and on the taste of the individual investigator."

Otto Struve, 1951

Page intentionally left blank

Page intentionally left blank

10

INTRODUCTION TO Be STARS

Among the B stars, from the main sequence to the giant region, we observe stars that exhibit hydrogen emission lines in the visible wavelength range, often accompanied by emission lines of singly ionized metals. In order to distinguish them from the more numerous absorption-line B stars of the same spectral type, we add the suffix *e* to the spectral type determined by MK classification methods. The presence of emission lines in stars occupying this area of the HR diagram is therefore an anomaly in the system used to classify stellar spectra at visible wavelengths. It is also an anomaly in the classical theory of stellar atmospheres, which predicts only absorption lines

Emission lines in the visible wavelength region are observed not only in B stars of luminosity classes V, IV, and III, but are also found in the most luminous B stars, of classes I and II. However, it is customary to distinguish between the Be stars, on the one hand, and the supergiants, on the other. This distinction rests primarily on the great difference in absolute magnitude exhibited by these two groups of stars Then, we note that the intensity of the emission lines is statistically much greater for the Be stars than for the supergiants. Finally, only Hα is observed generally in emission among the supergiants, while the emission generally extends to higher members of the Balmer series for the Be stars. Thus, in contrast to the Be stars, the supergiants generally do not exhibit emission lines in the photographic spectral region, which is used for classification purposes.

As a general rule, the Hα line is in emission in the most luminous supergiants, those of class Ia Far from being an anomaly, the presence of emission in these stars is thus a normal characteristic. This is not the case for the Ib supergiants, where Hα is very rarely observed in emission.

Thus, the classification system used in the visible wavelength region does not take into account the strongest line of the most abundant element, which forms the best criterion to detect the most striking anomaly with respect to classical model atmospheres. the presence of an emission line instead of an absorption line. Classical taxonomy considers the Ia supergiants, in which Hα is in emission, and the Ib supergiants, where this line may be either in emission or in absorption, to be equally normal. As for the Be stars, the only ones detected as peculiar objects will be those whose emission or shell characteristics are strong enough to extend to Balmer lines higher than Hα.

The Be stars make up a large subset of the B stars, they represent about 20 percent of these stars, with a maximum frequency at type B2-B3. Therefore, theoretical studies cannot pass over their existence. Moreover, far from being exceptional, their anomaly—the presence of emission lines—is pervasive throughout the HR diagram. Alongside the normal stars of every spectral type (X) in the HR diagram, one can find emission-line stars of the same spectral type (Xe).

Among the emission-line stars, the Be stars have been observed most frequently and in the greatest detail, over a long baseline in time. Discovered in 1866 by A Secchi, only five of them were known in 1886 The catalogues of Merrill and Burwell (1933, 1943, 1949, 1950) contain

1088 Be stars, while Wackerling (1970) compiled a list containing nearly 3000. However, the census is far from complete; new Be stars are still being discovered among the bright B stars, listed as normal stars.

Among the Be stars, one distinguishes two types of spectra. The term *Be/shell* is used here to designate that set of stars showing spectra of either of these two types the Be spectrum and the Be shell spectrum. In the Be spectrum, emission lines show either no reversal or a more or less central reversal In the Be shell spectrum, Balmer lines and singly ionized metal lines exhibit narrow and deep absorption cores, which may or may not be bordered by emission wings. Based on all the Be/shell observations in the visual spectral region, and we shall see that this is also becoming characteristic of other spectral regions, three properties stand out (1) in general, all Be/shell stars are variable, with this variability pertaining to all the spectral features which accompany the Be phenomenon, (2) there is a gradual transition from B to Be/shell stars, there is no clean break between these two types of stars; (3) Be/shell stars exhibit many individual differences at the same spectral type These three properties are important, for they are not peculiar to Be stars alone. They are observed in other emission-line stars, for example, the T Tauri stars The variability of Be stars can manifest itself in various ways depending on the star in question. In some cases, the Be/shell star loses its emission or shell features completely and becomes a normal B star, or vice versa. In other cases, a Be spectrum becomes a shell spectrum, or vice versa. This strongly suggests that B stars and Be/shell stars are not different kinds of objects but merely represent different phases in the variation of the same object.

Struve (1931b) attributed the origin of the emission lines in the spectra of Be stars to an extended envelope, where the gas is ionized by the ultraviolet radiation of the star; thus, the emission spectrum is a recombination spectrum. This interpretation requires envelopes whose radii are of the order of 5 to 15 R_*, and whose densities are around 10^{11} to 10^{12} cm^{-3}. The frequent presence of Fe II indicates an electron temperature of the order of 10^4 K so that the matter of the envelope is subionized relative to the photosphere.

In contrast to the Wolf-Rayet stars and the novae, no large expansion velocities, which would provide observational evidence for the formation of the hypothetical extended atmosphere, are observed in the visible spectra of Be stars. By showing that the absorption lines in Be stars are broader than those in normal B stars, Struve laid the foundation for the rotation model. The great width of the lines, which Struve attributed to rotation, led him to define the Be stars as rapidly rotating B stars. He then assumed that the rotational velocity had reached its critical value—although such a high rotational velocity has never been measured in these stars—so that matter could be ejected at the equator by rotational instability, forming an equatorial disk or ring. Thus, the presence of emission lines in the visible spectra of Be stars was evidence for the existence of an extended atmosphere, whose origin was attributed to the ejection of matter from these stars. In Struve's model, the Be phenomenon is limited to stars that rotate at the critical velocity. We shall see that, in order to be physically self-consistent, such a hypothesis must also require the existence of a mass flux in the subatmospheric regions of the star.

Our knowledge of the relatively cool outer atmospheres of the Be stars has been improved in the last 15 years by observations made at infrared wavelengths where it has been shown that there is an excess flux in this spectral region for Be stars as well as for all classes of emission-line stars. This excess is attributed to free-free radiation, emitted in the ionized gas of the outer atmosphere. For a large number of Bep or B[e] stars, so called because they also exhibit forbidden emission lines in their visible spectra, the infrared excess seems to be too large to be interpreted in terms of free-free radiation alone. The presence of circumstellar dust in the most distant and coolest regions of the atmosphere is invoked; the dust particles absorb visible stellar radiation and re-emit it at longer wavelengths. The temperature in these regions is of the order of 10^3 K. When radio emission is detected, as is the case for some

Bep stars, the envelope of ionized gas must have very large dimensions, of the order of several hundreds or thousands of stellar radii.

Thus, the observations in the visible, infrared, and radio regions show that there is a great diversity in the dimensions of the outer atmospheres of Be stars, from the small envelopes, some stellar radii in size, which are necessary to form a weak Hα emission line, to the very extended envelopes, where the density must still be significant at hundreds or thousands of stellar radii, in order for radio emission to be detectable This diversity is also observable for a single spectral type, implying that any attempt to interpret the formation of these atmospheres in terms of the parameters T_{eff} and g_{eff} alone, as in classical methods of describing stellar photospheres, is inevitably doomed to defeat. One can, in fact, observe much greater resemblances among the outer atmospheres of objects belonging to different classes of emission-line stars, than among stars of the same spectral type and the same luminosity class.

The picture of Be star envelopes resulting from visible, infrared, and radio observations is strikingly different from that discovered in the last 10 years by means of observations in the ultraviolet spectrum observed from space The ultraviolet observations show evidence for highly superionized regions with temperatures of the order of 10^5 K, far from being quiet, they are the site of violent ejections of matter and highly variable. Like the cool, quiet regions previously detected, this hot, tumultuous atmosphere exhibits variable characteristics with respect to the parameters T_{eff} and g_{eff} that describe the photosphere. Thus, we see, once more, that the classification set up in the visible wavelength region—which consists, in the end, of classifying stellar photospheres—is not uniquely correlated with the properties of the outer atmospheres

Struve's interpretation of the Be phenomenon provided the basic hypothesis for ad hoc models of Be stars. In these models the Be star, rotating at the critical velocity, has a cool, extended envelope that is confined to the equatorial regions, where the dominant motion is that of rotation. The framework of these models turned out to be too limited, for it was unable to entail the observations made in the ultraviolet spectrum observed from space. It is, in fact, necessary (1) to add superionized regions, with temperatures from 10^5 to 10^6 K which imply the existence of a nonradiative flux, (2) to assume ejection velocities that often exceed the escape velocity at the surface of the star, so that the dominant motion in these regions is no longer rotation but expansion implying the existence of a mass flux, (3) to explain such ejection velocities in the polar regions as well as at the equator, thus contradicting the basic hypothesis of the model in which the ejection of matter must be confined to the equatorial regions, on account of the postulated critical rotational velocity. Not only was the possible existence of these three facts ignored in the construction of the models, but the ad hoc models were actually constructed on the assumption that such a possibility was *a priori* excluded.

Not only do the ultraviolet spectra observed from space overturn the models of Be star atmospheres, but they pose similar problems for the normal stars. Among the normal B stars, a nonradiative energy flux and a mass flux have also been detected, in addition to the radiative energy flux. Moreover, the conclusion of the Einstein Observatory survey that X-ray emission, far from being an anomaly, constitutes a normal character of stars across the whole HR diagram strengthens the nonthermal properties of stellar atmospheres, in general. These properties have been observed among main-sequence stars or more evolved ones, with a high or low value of $v \sin i$. In other words, normal stars also have extended atmospheres. The Be stars are distinguished from these other stars essentially by the existence of cool regions, which make it possible to detect the extended atmosphere even in the visible wavelength region.

The existence of these three kinds of flux—the radiative flux, nonradiative energy flux, and mass flux—shows that a normal star has an atmospheric structure in which (1) the radiative flux is emitted in the photosphere under the conditions of radiative equilibrium and hydrostatic equilibrium; (2) the nonradiative energy flux provides additional heating and governs the temperature distribution in the outer atmosphere; and (3) the mass flux, which governs the density dis-

tribution, produces a wind that accelerates outward, passing through regions where the velocities are, in turn, subthermal, transthermal, and superthermal. The temperature increases outward and then decreases on account of radiative losses. The temperature and density distributions define the following successive regions in the outward direction the photosphere, the chromosphere, the corona, and the post-corona. The velocity distribution corresponds to a density distribution that decreases as $(r^2\ T^{1/2})^{-1}$ as far as the corona, that is, much more slowly than the exponential decrease in the photosphere, and as $(r^2\ u)^{-1}$ in the post-coronal regions, which undergo an additional acceleration (see Chapter 13).

In a Be star, additional conditions are imposed by the observations in the visible concerning the Be phenomenon· the small velocities of the hydrogen emission lines and the presence of low excitation lines like Fe II. In order to account for the intensity of these emission lines, the envelope in which they are formed must be very extensive. Therefore, they cannot be entirely produced in the small fraction of a stellar radius between the photosphere and the chromosphere. They must be formed far from the star, in the post-coronal regions, which are cool enough. These regions, located at distances of several stellar radii (5 to 15 R_*), must also have been decelerated, since the velocity of these ions, as observed in the visible, is small. Such a deceleration could be produced by an interaction between the stellar wind and the interstellar medium; but this interaction must take place at much smaller distances than the "bubbles" which are observed at several parsecs around some stars.

Thus, the atmospheres of Be stars are distinguished from normal B stars by the existence in the post-corona of a cool, decelerated region that we shall call the *envelope*, a region which is not observed in normal B stars. The question that arises in the present context is this. Why do only certain B stars have cool post-coronal regions of low velocity, and dense enough for fairly strong emission lines to be observed in the visible? Part of the answer to this question can be provided by the space ultraviolet observations. In spite of their small time baseline, these observations show that Be stars are distinguished from normal stars of the same spectral type by statistically greater values of the mass loss and by greater variability in the stellar wind, at least at certain epochs of the variations. The amplitude of the variations is such that they cannot be interpreted as perturbations, and the conclusion is unavoidable that the mass flux is highly variable in these stars. The strong variability of the mass flux could create a favorable condition for the formation of their cool envelope

The ultraviolet observations suggest that the anomalies observed among the stars of a single spectral type, like those that define the group of Be stars among the class of B-type stars, essentially reflect differences in the values and the behavior of certain physical parameters—such as the mass flux and the nonradiative energy flux—whose very existence is forbidden by the equilibrium conditions imposed by the classical theory of stellar atmospheres. From this point of view, the study of peculiar stars makes it possible to analyze an amplified mode of phenomena occurring on a much smaller scale in normal stars. Among the peculiar B stars, the large amplitude of the variations in the Be stars affords the possibility of studying the correlations between the variations of the mass flux and the nonradiative energy flux, and the variations that take place in the cool extended envelope where the visible emission lines are formed—that is, the phenomena that take place in the entire outer atmosphere of the star.

This second part of the volume will be organized in the following manner. In Chapter 11, we shall describe the observations in the visible, the infrared, and the radio region, and the ad hoc models that have been proposed to interpret them. We shall see that these observations refer essentially to the photosphere and to the regions of the outer atmosphere where the gas is already cooled and at low velocity—that is, the cool envelope of the star. The nonradiatively heated chromospheric and coronal regions are known to us only through the ultraviolet and X-ray spectra observed from space, which are given in Chapter 12 These are the data that Struve was lacking when he proposed the rotation model, a model

that served as a guide for nearly half a century in studies of the outer atmospheres of hot stars. In Chapter 13, in collaboration with R N. Thomas, we shall outline the construction of an empirical model for Be stars, a model which will attempt to account for the observational data concerning these stars, from X-rays to the radio region.

I am most indebted to Janet Rountree Lesh for a superb translation from French into English of Chapters 10 through 12. She has preserved the content, spirit, and style of what I have tried to express. I am equally indebted to R.N Thomas for collaboration in the synthesis of the observational material on the stars discussed here into a preliminary, tentative atmospheric pattern

11

GROUND-BASED OBSERVATIONS AND AD HOC MODELS

THE VISIBLE AND INFRARED LINE SPECTRUM

The Be stars have been extensively observed ever since their discovery It would be impossible to cite all of the countless articles that have been devoted to them. Nevertheless, we cannot fail to mention the names of McLaughlin, Swings, Merrill, and especially Struve, whose work enabled him to propose, as early as 1931, the extended envelope model that is still adopted today. Struve's review article (1942) explains very clearly the properties of these hot, emission-line stars and their interpretation in terms of an extended atmosphere The books by Underhill (1966a) and Hack and Struve (1970), and IAU Symposia Nos. 70 and 98 contain an extensive bibliography concerning these stars.

The Visible Spectrum

The most striking manifestation of the Be phenomenon in the visible spectral region is the existence of emission lines in the Balmer series, in a spectrum which would be classified as type B from its absorption lines The hydrogen emission lines are often accompanied by emission lines of singly ionized metals, mainly Fe II The large body of observations that have been made shows that the character of the emission is different from one star to another, and that it undergoes perceptible variations with time in a single star. If one observes a set of Be stars at a given time, one notes that the emission can be of greatly varying intensity and extent in the Balmer series, though it always decreases from Hα toward the higher members. The emission may be rather weak and confined to the Hα line In that case, the commonly used MK classification system does not take the Be anomaly into account, since the blue region of the spectrum is analogous to that of a normal B star Moreover, even if the red region of the spectrum is observed, the emission intensity at Hα may be too weak to be detected at low dispersion—for it then appears as a weak emission reversal within an absorption line—so that the Be star can be recognized only on high-dispersion spectra The transition between Be stars and normal B stars is gradual in nature; there is no sharp division between these two groups of objects.

Statistically speaking, the Hα emission decreases from the earliest B-type stars to the A stars, but there is a very large scatter about this trend. One can find early B stars with very weak emission and late B stars with strong emission. This scatter results from the variability and the individuality of the Be stars.

In addition, a certain number of Be stars exhibit forbidden emission lines; they are called peculiar Be stars, Bep, or, more logically, B[e]. The B[e] stars are generally fainter than the Be stars, and have been much less well observed. Descriptions of their spectra have been given mainly by Swings and Struve (1941, 1945), Ciatti et al. (1974), Ciatti and Mammano (1975), and Allen and Swings (1976). Emission in the forbidden lines of elements like O I, Fe II, N II,

S II, and Fe III is observed in various stars, with varying intensity.

The emission lines in Be stars exhibit a great variety of profiles. Figure 11-1 illustrates a few of the most typical Hα profiles. They most often exhibit a shallow, more or less central reversal. The intensity and width vary with time, but the emission intensity generally exhibits much greater variations than the line width. Emission profiles without a central reversal are also observed, as well as profiles with three emission peaks

The use of high resolution spectra shows that the profile is often complex, exhibiting details or structures that are not detectable on moderate resolution spectra. A profile that appears simple at low resolution may exhibit a weak central reversal at high resolution, and/or structure in its contours. It is these structural components that show the greatest variability, when a single Be star is observed at very short time intervals, of the order of a few minutes (see the section on Variability of the Line Spectrum and the Continuous Spectrum in the Visible and the Near Infrared Regions). The profiles of the metallic lines are similar to the hydrogen-line profiles, but they are always weaker and narrower.

Struve had originally introduced the term *shell* as an abbreviation for stars with extended atmospheres. Since then, this term has been applied to spectra having the following characteristics: (1) the hydrogen lines exhibit sharp, very deep absorption cores, generally bordered by emission wings for the lowest Balmer lines; (2) the lines of ionized metals, mainly Fe II, Ti II, Cr II, etc., appear as sharp absorption lines, with or without emission wings. A shell spectrum simulates a later spectral type than it would be given from the appearance of the photospheric lines. When the shell spectrum is most highly developed, it is similar to that of the A2 Ia supergiant, α Cyg. The absorption spectrum can also include lines of Si II, Mg II, He I, Ca II, Na I, Mg I, etc. In some cases, Fe III lines or even Fe I lines are also observed. When the shell spectrum is highly developed and the photospheric lines exhibit narrow shell components, the spectral type is very difficult to determine.

Like Be spectra, the shell spectrum may be more or less pronounced from star to star, or depending on the epoch in the variation of a given star. For some stars, like 48 Lib or EW Lac, sharp absorption cores have been observed in the Balmer lines out to H42, accompanied by a complete metallic spectrum. For other stars, the sharp absorption core is observed only for the lowest Balmer lines, while the metallic spectrum is absent. In still other cases, a very poorly developed shell spectrum can be recognized only at high resolution and sometimes only at Hα. The recognition of a shell spectrum depends on this kind of degree of development, and on the resolution used. The transition between a shell spectrum and a Be spectrum or a normal B spectrum is a gradual one. As an example, Figure 11-42 shows the gradual nature of the transition of the Be spectrum to the shell spectrum for Pleione as observed by Gulliver (1977)

The intrinsic variability of the Be stars is such that a star can lose and recover its shell characteristics in the course of time. It is customary to use the term *shell star* for a star that exhibits a shell spectrum. This designation implies that the shell characteristics are permanent, and that Be and shell stars are two different kinds of objects, or else it implies that a given star can show only one of these two types of spectra, Be or shell But the observations show that in many cases, the same star can exhibit both types of spectra alternately, over a period of time. Although many stars have always been observed with a single type of spectrum, Be or shell, so that it could be tempting to use the term Be or shell star to designate them, it seems better to consider these different spectra as defining a Be "phase" or a shell "phase" of the star, taking into account the different appearances that the same object may present. This comment is reinforced by the observation of transitions from a Be spectrum to a shell spectrum and to a normal B spectrum, and so forth, this transition may be made in any direction. Thus, the same object may exhibit the three types of spectra, in turn, corresponding to the Be phase, the Be shell phase, and the normal B phase. This observational fact has been known for nearly a century, but it seems not to have received the attention it deserves.

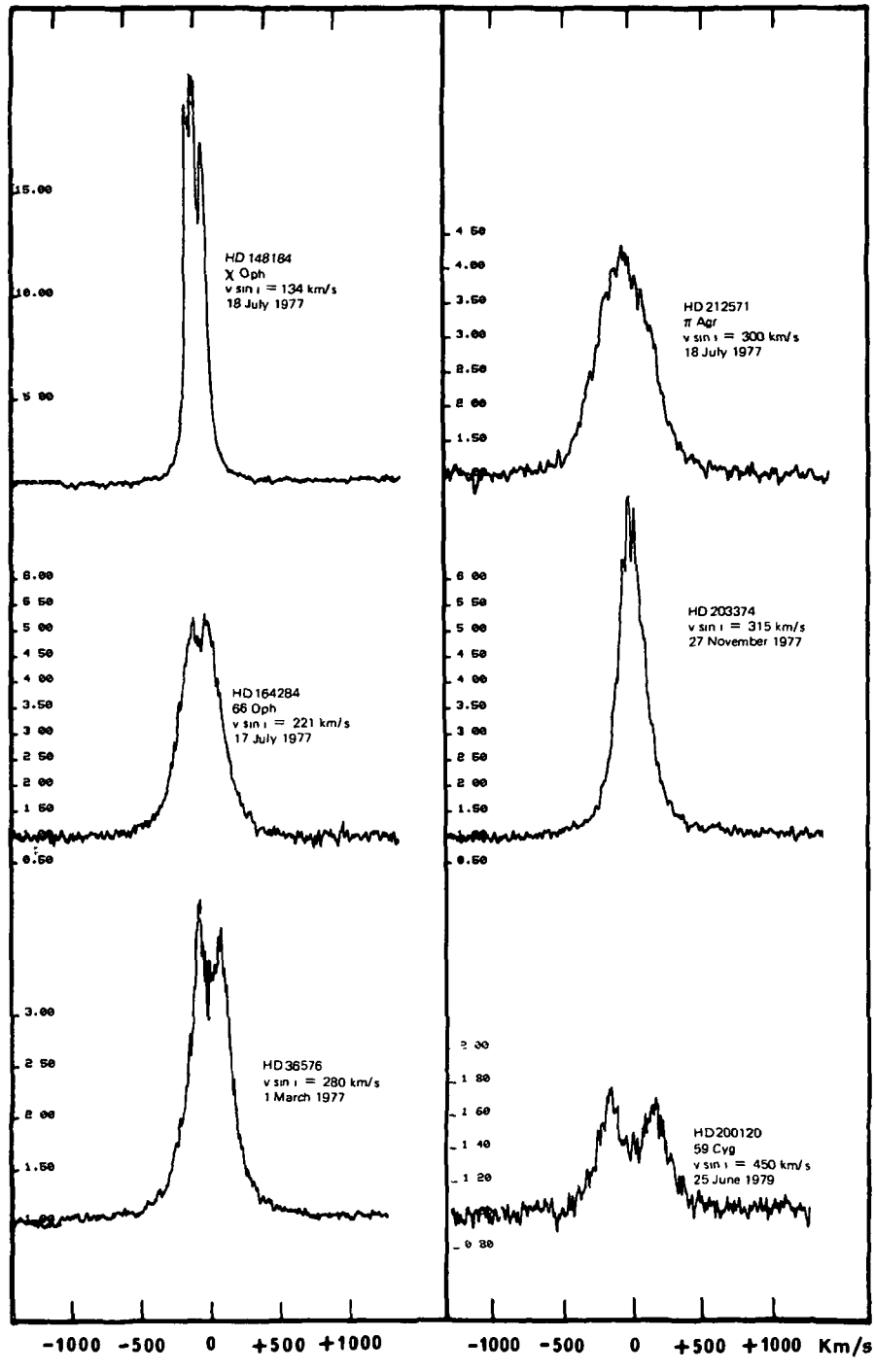

Figure 11-1. Hα line profiles of Be spectra, original dispersion 12.2 Å mm^{-1} (Haute-Provence Observatory). The most common aspect is the self-reversal. The structures on the contour of the line are seen on high dispersion profiles. Three peaks are also observed for both low and high v sin i. *As a general character the width at the base of the Hα emission line is very large, much higher than the* v sin i *value inferred from the photospheric absorption lines (He I).*

Typical profiles of Hα shell lines are given in Figure 11-2. Their basic feature is the sharp absorption core. This absorption is more or less central and more or less deep, depending on the star, and for the same star, depending on the epoch of variation P Cygni-type profiles are rarely observed in shell spectra, and it often happens that an improved signal-to-noise ratio reveals a violet emission wing, as was the case for P Cyg itself The emission wings may be stronger or weaker, or even absent, as for Maia at certain epochs of its variations. As in the profiles in Be spectra, structure is generally observed in the profiles of the shell lines. This structure is apparent only on high-resolution spectra and only with a good signal-to-noise ratio Figure 11-3 shows the Hα line in EW Lac observed at low dispersion by Slettebak and Reynolds (1978), where the shell characteristics are not even perceptible, and at high dispersion on fine-grain IIIa-J plates by Poeckert (1980) where they are clearly seen. The metallic lines have profiles similar to those for hydrogen, but their absorption core is shallower

The Infrared Spectrum

Relatively few observations have been made of the Be stars in the near infrared. References earlier than 1947 can be found in Hiltner (1947). The first systematic observations covering a large number of stars in the near infrared region were made by Andrillat and Houziaux (1967, 1972, 1975), Polidan and Peters (1976), and Polidan (1976). The most frequently observed wavelength region extends out to around 8800 Å, where the end of the Paschen series is observable beginning with P11. Not all the Be stars are distinct from normal B stars in this spectral region; only some of them exhibit emission, mainly in the Paschen series, the O I lines (λ 7774 Å, λ 8446 Å), the Ca II triplet (λ 8498 Å, λ 8542 Å, λ 8662 Å), and the Fe II line (λ 7712 Å). As for the Balmer lines, the emission in the Paschen lines decreases, statistically speaking, from the early B stars to the A stars. A statistical study covering 68 Be stars shows that the lower Balmer lines have stronger emission in stars where the Paschen lines are in emission than in stars where the Paschen lines are

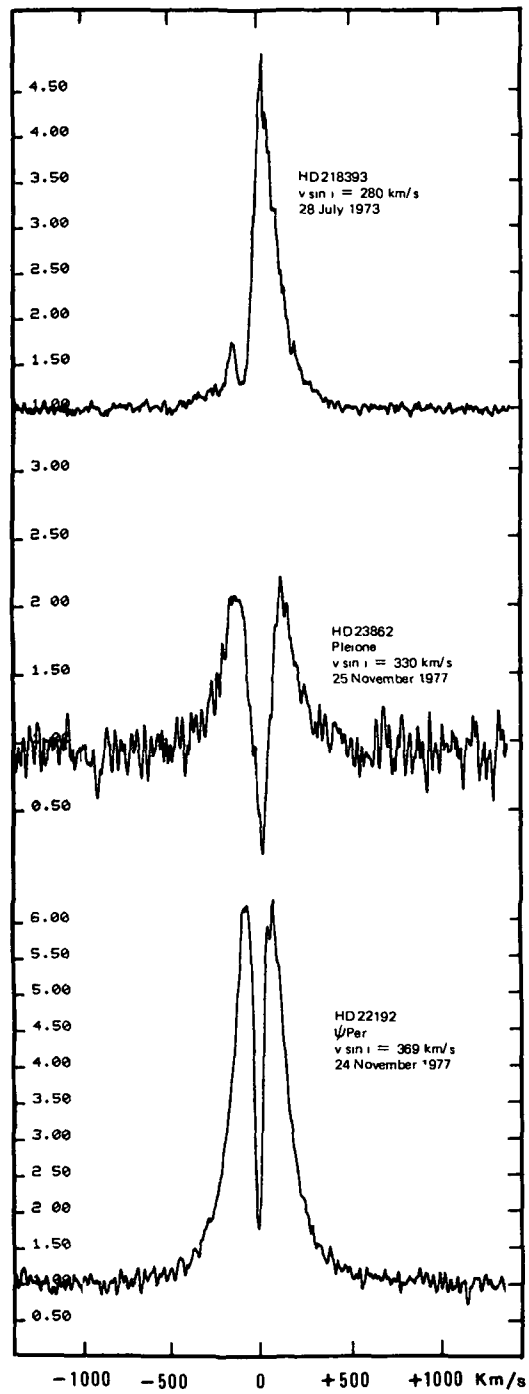

Figure 11-2. Hα line profiles of shell spectra; original dispersion 12.2 Å mm^{-1} (Haute-Provence Observatory) The characteristic feature is the narrowness of the self-reversal. Note the diversity of depth of this feature The width at the base of the line is again much larger than the value of v *sin i.*

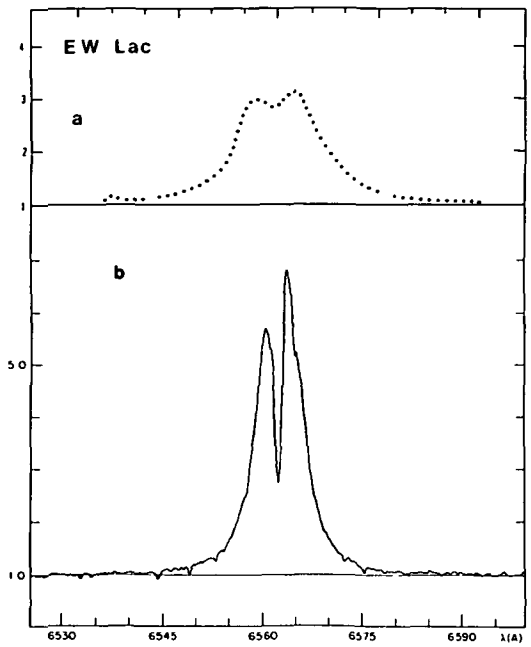

Figure 11-3. Hα line profile of EW Lac whose spectrum shows pronounced shell characteristics: (a) at low resolution (Slettebak and Reynolds, 1978), (b) at high resolution (Poeckert, 1980). Note that the shell characteristic, i.e., the narrow and deep self-reversal, is completely wiped out at low resolution and is similar to a self-reversal of a Be spectrum. At high resolution, a structure on the red peak is also clearly seen.

in absorption (Briot, 1977). But this is only a statistical result, and it is possible to find two stars of the same spectral type which have similar emission strengths in the Balmer lines and different behavior in the Paschen lines Moreover, the Paschen lines sometimes exhibit strong emission when there is no trace of emission in the analogous lines of the Balmer series (Andrillat and Houziaux, 1967).

The first observations made in the infrared attest to anomalies in the behavior of the O I lines (λ 7774 Å, λ 8446 Å). Bowen (1947) explained the greater tendency to emission in λ 8466 Å by the fluorescence mechanism due to the fortuitous coincidence of the levels of L β (λ 1025 717 Å) and O I (λ 1025.766 Å). The predicted correlation between the intensity of Hα and of λ 8446 Å of O I was observed by Kitchin and Meadows (1970) and Polidan and Peters (1976), however, the latter authors note that there are exceptions to this correlation

All the stars that exhibit λ 7774 Å of O I in emission seem to exhibit also the Fe II lines in emission. But the inverse relation is not always observed. A certain correlation exists between the intensity of the emission at λ 7774 Å of O I and that at λ 7712 Å of Fe II, suggesting that these lines are formed in the same region (Polidan and Peters, 1976).

Polidan and Peters have studied the behavior of the infrared triplet of Ca II in a sample of 120 Be stars. They find no correlation between the presence or the intensity of the emission in these lines and any other characteristic of the star, they note that the triplet emission is not accompanied by significant emission in the H and K lines, which arise from a transition having the same upper level. Moreover, the intensity ratio of the observed lines (1 1:1) is very different from the predicted theoretical ratio (1:9.5). This indicates that the emission in the Ca infrared triplet is produced in an optically thick, low temperature region with $T = 5 \times 10^3$ K (Polidan, 1976). Polidan notes the lack of correlation between the presence of the Ca triplet in emission and any other feature in the spectrum, he discusses a possible relationship between the presence of emission in the triplet and the binary nature of the star.

The spectra of γ Cas and φ Per between λ 4700 and 10300 Å were observed by Johnson et al. (1978), using a Michelson interferometer In addition to the previously known lines, they identified the Mg II doublet (λ 9217 Å, λ 9243 Å) strongly in emission. Meisel (1971) observed the spectra of γ Cas and ζ Tau from λ 10300 to 12000 Å with an image tube, the He I line (λ 10830 Å), which is in emission in γ Cas, has a P Cygni profile in ζ Tau. Maillard (1973) obtained a spectrum of γ Cas in the range of 1 to 2.5 μ by Fourier spectrometry He observed the Paschen lines Pβ and Pγ, the Brackett lines from Bγ to B18, and the Pfund line Pf20, as well as the λ 10830 Å line of He I All these lines are in emission, with a central reversal.

Infrared observations of B[e] stars are less

common than observations of ordinary Be stars Ciatti et al. (1974), Ciatti and Mammano (1975), and Andrillat and Swings (1976) give a description of their spectra and a list of the lines that have been identified. The strongest lines observed are those of the Paschen series, the Ca II triplet, λ 8446 Å of O I, λ 10830 Å of He I, λλ 9069 Å and 9532 Å of [S III], and λ 10504 Å of [Fe III], then come the lines of [S II] and [Fe II].

Few infrared emission-line profiles have been published. According to the descriptions given of them, they have the same characteristics as those in the visible region a reversal of varying depth in the Be spectra, and sharp absorption components in the shell spectra

Spectral Classification

The classification of Be stars is generally difficult. The difficulty is essentially the result of (1) the width and the diffuseness of the absorption lines and (2) the perturbation of the absorption-line spectrum by the emission-line or shell spectrum. Keenan and Morgan (1951) considered the Be stars to be among the groups of stars "which do not fit the two-dimensional classification" Nevertheless, spectral types have been assigned to them according to the criteria adopted for normal B stars, based on the ratios of selected absorption lines. The accuracy of these spectral types is not very high. This is reflected in the differences between the spectral types assigned to the same star observed at the same epoch by different authors On the average, there is a difference of two to three spectral subtypes, and one to two luminosity classes The MK classification of the Be stars has been performed by Morgan et al (1955) (in spite of the remark quoted above), Mendoza (1958), Lesh (1968), Hiltner et al (1969), and Garrison et al (1977) The Be stars have also been classified in the BCD system, based on the properties of their continuous spectra A long list of the Be stars classified in this system is given in Underhill et al. (1979)

The Absolute Visual Magnitude and the Evolutionary State of the Be Stars

The absolute magnitude of the Be stars has been determined mainly on the basis of their membership in clusters. In an HR diagram, the class III to V Be stars are located, on the average, around one magnitude above the main sequence (Schmidt-Kaler, 1964; Schild, 1965) A similar result is found by studying the class V Be stars that belong to physical double systems (Meisel, 1968) That does not mean that all the Be stars are located above the main sequence, this result is only a statistical effect. Be stars can be found throughout the entire band from the main sequence to the giant branch (Bond, 1973; Schild and Romanishin, 1976; Abt and Levato, 1977).

The location of the Be stars in the HR diagram has been interpreted in terms of the effects of gravity darkening, resulting from their rapid rotation (Collins, 1966, Collins and Sonneborn, 1977) It has also been interpreted as an evolutionary effect by Crampin and Hoyle (1960), based on the position of Pleione in the HR diagram of the Pleiades This position corresponds to the secondary contraction phase, following the exhaustion of hydrogen in the core. In this view, evolutionary effects play a decisive role in the manifestation of the Be phenomenon In the course of its evolution, the rapidly rotating Be star contracts and, through conservation of angular momentum, turns faster and faster, until it reaches the critical rotational velocity. The equatorial regions, which receive more and more high velocity material, form an envelope "by rotationally forced ejection" However, Sackmann and Anand (1970) computed the evolutionary track of a rapidly rotating B star and showed that the Be stage could be reached before the secondary contraction phase.

The evolutionary hypothesis encounters three serious difficulties: (1) the study of individual Be stars shows that their position in the HR diagram changes on very short time scales (months, years, decades), and these variations can take them along tracks that cross several spectral subtypes and several luminosity classes, in any direction whatsoever. In particular, Pleione, which Crampin and Hoyle took as an example, underwent a drop of 0.6 mag in luminosity within less than one year in 1973, producing a large displacement toward the main sequence of the point representing it in

the HR diagram (see the section on Variability of the Line Spectrum and the Continuous Spectrum in the Visible and the Near Infrared Regions) (2) The Be phenomenon is fundamentally variable a Be star can lose all of its emission features on time scales (years, decades) that are very short in comparison with evolutionary time scales then recover its Be characteristics and so on. This observation, rather, suggests that the location of a Be star in the HR diagram results largely, if not completely, from the particular amplitude of the atmospheric effects due to nonthermal phenomena, which are responsible for the star's peculiarity (3) The percentage of Be stars in luminosity class V is high, of the order of 25 percent, among the Be stars classified in the BCD system (Divan, 1979). This contradicts the suggestion that the Be phenomenon is connected with a post-main-sequence phase of evolution Moreover, it has been shown that the ratio of Be stars to normal B stars is too high for the former to be in the short secondary contraction phase (Hardorp and Strittmatter, 1970)

Interpretation of the Be Phenomenon Based on the Visible Spectrum

Struve's Rotation Model Struve (1931b) attributed the emission lines in Be stars to a gaseous outer envelope, or nebula, by analogy with the interpretation of the novae and the Wolf-Rayet stars given by Menzel (1929) and Beals (1930). However, the Be stars have very different characteristics from the novae and the Wolf-Rayet stars, if one considers only their visible spectra. High expansion velocities, which provide direct evidence for the mass flux responsible for the formation of the extended envelope, are observed in Wolf-Rayet stars and novae, in Be stars, the line shifts are too small to be directly interpreted in terms of the ejection of matter (cf , the section on Variability of the Line Spectrum and the Continuous Spectrum in the Visible and the Near Infrared Regions). It is only recently, with observations in the ultraviolet region, that the existence of a mass flux in the Be stars has been finally proven (cf., Chapter 12).

Struve based the outline of his interpretation of the Be stars essentially on two observational facts· (1) the width of the emission lines is markedly proportional to λ, as shown by Curtis (1923) for 11 Be stars—this is the relation to be expected if the line width is due to the Doppler effect; (2) there is a correlation between the width of the emission lines and the width of the absorption lines Struve established this correlation by visually estimating the widths of the emission and absorption lines in around 50 Be stars He noted, moreover, that the absorption-line profiles in the majority of the stars were "dish-shaped," which was a criterion for axial rotation. This correlation was interpreted as an effect of the inclination of the rotation axis with respect to the line of sight On the basis of these correlations, Struve put forward the hypothesis that the presence of emission lines in the spectrum and the rapid rotation of the star were two connected phenomena. Assuming that rapid rotation produces instabilities, and, according to the Jeans hypothesis, matter is ejected at the equator of the flattened body of the star Thus, the rapidly rotating Be star forms a gaseous equatorial ring. In addition to the above two correlations, it was observed that the majority of the Bn stars (where the suffix *n* refers to the nebulous, or diffuse character of the lines) are Be stars.

Rapid rotation made it possible to justify the formation of an extended atmosphere in the Be stars So it was natural to assume that the emission lines were formed by the same mechanism as in the gaseous envelopes of planetary nebulae where the radiation density is reduced by the dilution factor

$$W = \frac{1}{4}\left(\frac{R_*}{R_{\text{env}}}\right)^2 , \qquad (11\text{-}1)$$

where R_* is the radius of the star and R_{env} is the radius of the envelope Atoms are ionized in the envelope by absorption of the ultraviolet quanta produced by the central star Recombinations to higher levels and cascading to lower levels produce the observed emission in the Balmer lines This conversion of high-energy radiation to low-energy radiation is due to the dilution of the radiation field, which, according to the classical theorem of Rosseland (1926), favors cyclic transitions of

the type 1→3→2 over transitions of the type 1→2→3, where 1, 2, and 3 are three states of increasing energy.

In the case of the planetary nebulae, the dilution factors are of the order of 10^{-14} so that ionization takes place entirely from the ground level, this is what makes the case of the planetary nebulae easier to deal with, in the first approximation, than the case of the Be stars The dilution factor for the Be stars is much greater than that for the planetary nebulae; it is of the order of 10^{-1} to 10^{-2} Under these conditions, ionization from excited levels is no longer negligible, and the envelope may be opaque in the lines of the subordinate series

The model proposed by Struve in 1931 to represent the Be stars is that of a B star in rapid rotation, surrounded by a gaseous envelope which is also in rotation, the envelope is moderately dense, extended, and flattened at the equator. Its state of excitation is lower than that of the photosphere (Struve and Swings, 1932) This low excitation is indicated by the presence of emission or shell lines of Fe II, which are observed with equal strength in type A spectra

Figure 11-4 is an outline of Struve's model. This model explains the diversity of the emission lines in Be star spectra by geometric effects alone; moreover, all the lines formed in the envelope are symmetrical and invariant. If the star is viewed equator-on, the rapid rotation produces the broad, photospheric absorption lines, while the broad emission lines are formed in the two lobes of the rotating envelope, one moving toward the observer and the other moving away. The part of the envelope that is projected onto the stellar disk produces a sharp central absorption component, that is, the shell characteristic. The equator-on Be stars are thus, those that exhibit a shell spectrum. If the star is viewed pole-on, the photospheric absorption lines are, on the contrary, narrow, as are the emission lines which have no central reversal If the star is viewed at an intermediate angle, the emission line exhibits a weak central reversal, and a Be spectrum is observed.

Struve's model attributes the broadening of the emission lines to the rotation of the envelope. Assuming that the envelope rotates while conserving angular momentum, the width of the emission lines makes it possible to compute the size of the envelope. Typical values for the envelope radius, found under this hypothesis, are of the order of 3 to 5 R_* Different rotation speeds are often observed for different elements; this is attributed to a distance effect. The stratification found in this way generally corresponds to an outward decrease in ionization.

Confrontation of the Rotation Model with the Observations. Here, we shall consider to what point Struve's hypotheses are in agreement with the observations.

The Rotational Velocities of the Be Stars. Struve's model has inspired a great deal of work on the rotation of the B and Be stars. A documented description, including most of the references on this subject, can be found in Slettebak (1976, 1979); the catalogue of Uesugi and Fukuda (1970) gives an annotated compilation of all the published values of v sin i.

Most of the values of v sin i have been determined from moderate dispersion spectra (≈ 40 Å mm^{-1}) using the method of Shajn and Struve (1929). The observed profile is compared with a grid of profiles that have been computed by applying rotational broadening to the spectrum of a sharp-lined star, assumed to have a zero rotation In most cases, corrections have been made

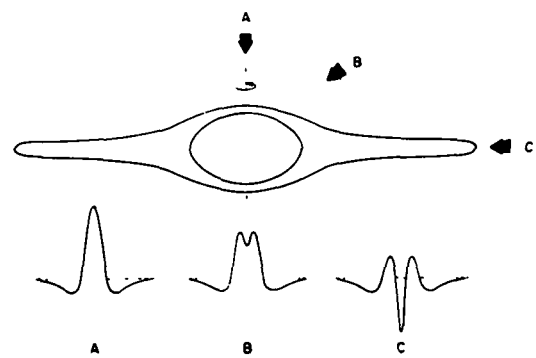

Figure 11-4. A schematic representation of Struve's rotation model The different types of profiles, A, B, and C, are interpreted in terms of different angles of inclination of the line of sight on the rotation axis (from Slettebak, 1979).

to take into account the distortion of the stellar disk and the change in the limb-darkening law due to the rapid rotation of the star. Slettebak (1949, 1966) and Slettebak and Howard (1955) have determined values of v sin i for B and Be stars by this method. A more elaborate method is to use the line profiles from rotating atmosphere models, which have been computed by Collins (1974) and which also take into account the above-mentioned corrections. These calculations show that the values of v sin i obtained by the preceding method are overestimated by about 15 percent (Slettebak et al., 1975).

The refinement of methods for determining v sin i represents only the technical side of the problem. The application of these methods to Be stars encounters much more serious difficulties, which are connected with the presence of the envelope and its effects on the absorption lines. The following paragraphs describe the effects which must be estimated for each star individually.

1. Contamination of the lines by blends. The lines generally used for the determination of v sin i are those of He I, λ 4471 Å and λ 4026 Å. Figure 11-5 shows these two regions in the shell spectrum of EW Lac, as observed by Poeckert (1980) at two different epochs. Poeckert gives an identification list of 350 shell lines between λ 3600 Å and λ 6600 Å. We note in particular that λ 4026 Å

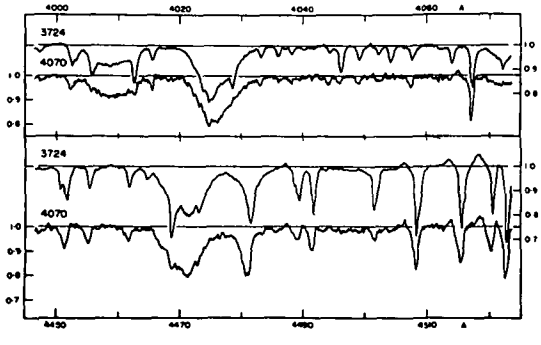

Figure 11-5. The region of λ 4471 and λ 4026 of He I in the shell spectrum of EW Lac at 2 different epochs (JD 2440000 + 3724 and + 4070) observed by Poeckert (1980) Note the blends due to metallic shell lines and their changes from one epoch to another.

of He I is blended with λ 4024 Å of Fe II and with λλ 4025 Å and 4028 Å of Ti II, and that λ 4471 Å of He I is blended with λλ 4464 Å, 4468 Å, and 4470 Å of Ti II, and with λ 4473 Å of Fe II. The profiles are seriously perturbed. There are also intensity variations in these shell lines, which affect the He I profiles in a different way from one epoch to another The shell lines that produce these blends do not exist in the spectra of normal B stars of the same spectral type. But the values of v sin i have generally been determined from moderate-dispersion spectra ($\simeq$40 Å mm^{-1}), on which these blends are hard to detect and therefore impossible to eliminate The He I profile in the shell spectrum experiences a perturbation due to the presence of the envelope, which does not exist in the theoretical profile of a normal B spectrum, to which the shell spectrum is compared

2. Contamination of the photospheric lines by the envelope In addition to blends, the He I lines can be contaminated by absorption and/or emission in the same lines, produced in the envelope. The components are observed unambiguously at certain shell or Be phases (cf., the variations of γ Cas and 59 Cyg). High-resolution spectra are necessary to show them when they are only weakly present

3. Contamination of the lines by veiling. The continuous spectra of Be stars generally exhibit a flux excess and an intrinsic reddening due to free-free and free-bound emission in the outer atmosphere of the star (cf., the section on Variability of the Line Spectrum and the Continuous Spectrum in the Visible and the Near Infrared Regions) This effect is clearly observed at some phases of the variation in the form of a veil, in which the absorption lines may be completely swamped.

Effects (1), (2), and (3) cannot be calculated once and for all, for they are generally variable from one star to another and, in the same star, from one epoch to another They have never been taken into account in determining v sin i for Be stars; it has always been assumed that the photospheric lines and the continua of Be stars are not perturbed by the presence of the envelope. This hypothesis might be justified if one wanted only to estimate the order of magnitude of a physical

parameter It is not obvious that it is justified if the analysis of these spectral features is to be used to determine small differences in comparison with normal B stars The influence of the envelope on these lines must be analyzed very carefully, in order to determine the extent to which the results reflect perturbations of the photospheric lines in Be stars as a result of the presence of the envelope When the importance of these effects is estimated, the interpretation of the values of v sin i for Be stars will be less ambiguous. We can only agree with Slettebak's (1976) remark "All v sin i's derived from line profiles for Be stars must be considered rather uncertain."

The measurements made by Slettebak (1949) and Slettebak and Howard (1955) show that, statistically speaking, the Be stars exhibit larger values of v sin i than the B stars More exactly, the same range of values of v sin i is observed for the B stars and the Be stars, but the mean value of v sin i is higher for the Be stars.

According to Struve's model, all the Be stars are rotating at the critical velocity. Figure 11-6 from Slettebak (1976) shows the theoretical curve of the critical equatorial velocity computed by Collins (1974), and the points representing the highest values of v sin i observed for Be stars. According to this figure, there is no observational evidence to show that the Be stars are rotating at the critical velocity. The largest measured value of v sin i is 400 km s^{-1}, while the critical rotational velocities are much higher And we can only agree with Collins' (1970b) remark, "There is not a single piece of observational evidence that Be stars rotate at the critical velocity."

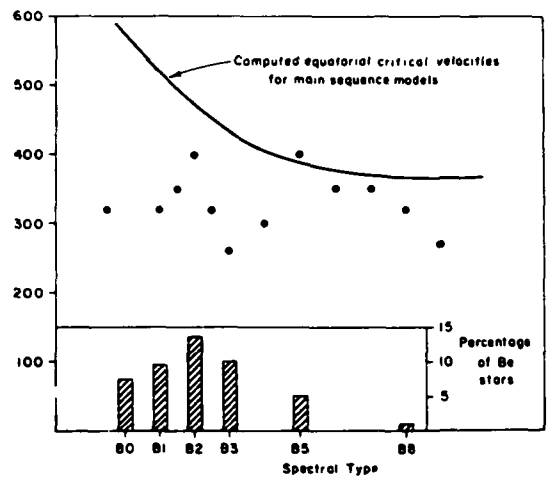

Figure 11-6. The computed equatorial critical velocities for main-sequence B stars and the largest observed rotational velocities for Be stars (from Slettebak, 1979). The relative frequency of Be stars is also shown (Slettebak, 1976).

Finally, we note an important point critical rotation alone cannot be the source of an ejection of matter. It does not allow the displacement of matter from the surface of the star out to large distances. It can only balance the gravitational force with the centrifugal force. No model in which the only effect of rapid rotation is to reduce g_{eff} can explain the production of a mass flux. According to Limber and Marlborough (1968), if the atmosphere of a star rotating at the critical velocity exhibits viscous or magnetic forces, it may have a mass flux. But we note that if the rotation of the star is differential, without having to invoke critical rotation, it will produce systematic motions in the subatmosphere; these nonthermal storage modes will produce a mass flux and a flux of nonradiative energy (Thomas, 1973; Cannon and Thomas, 1977).

The Widths of the Emission Lines. The proportionality between the widths of the emission lines and their wavelengths has been reanalyzed by Doazan (1970), using high resolution and including the Hα line, her sample was larger than that of Curtis (1923). One of the most striking features of the emission-line profiles in Be stars is the great extent of their wings, which often exceeds 1000 km s^{-1} at Hα for both Be and shell spectra. Doazan's work is therefore based on this maximum width With the exception of Hα, the correlation between emission width and wavelength is fairly well confirmed. It is observed, however, that for all the stars studied, the velocity of the emission edge at Hα is greater than the rotational velocity of the absorption lines; in a large number of cases, it is two to three times greater than v sin i. This leads to the absurd conclusion that the envelope rotates faster than the star, and that its rotational velocity is two to three times

greater than the critical value. This contradiction implies that the width of the emission lines is not due to rotation alone. Underhill (1953) was the first to notice the excess width of the Hα emission line in two stars, one Be and one shell. She suggested that large, high velocity currents of matter at great distances from the star broadened the line. Marlborough (1969) and Poeckert and Marlborough (1979) tried to account for the excess width of the Hα wings by means of their model in which the envelope undergoes rotation and expansion (see the section Be Star Models Based on Observations at Visible Wavelengths). They showed that scattering of the photons in the line by electrons can produce considerable broadening in the wings, that is, a large number of photons can be scattered from the center of the emission lines into the wings. This effect is less important for the higher Balmer lines. Figure 11-7 shows their computed and observed profiles of Hα in φ Per. Note that the width of the profile computed in this way is greater than that of a profile broadened only by the rotation of the star, but that it is still significantly narrower than the observed profile.

When one uses the maximum extent of the emission wings of the lowest lines one observes little or no correlation with the widths of the absorption lines (v sin i); the correlation coefficients are 0.3 and 0.4 (Doazan, 1970). On the other hand, if one uses the widths at half-maximum, the correlation is better (Slettebak, 1976, 1979). Such a result should actually be considered as a "trend," because the scatter of the emission-line widths can be quite large for a given value of v sin i Moreover, at certain epochs, a given star can exhibit large variations in the width of the emission lines as their intensity varies (see the section on Variability of the Line Spectrum and the Continuous Spectrum in the Visible and Near Infrared Regions).

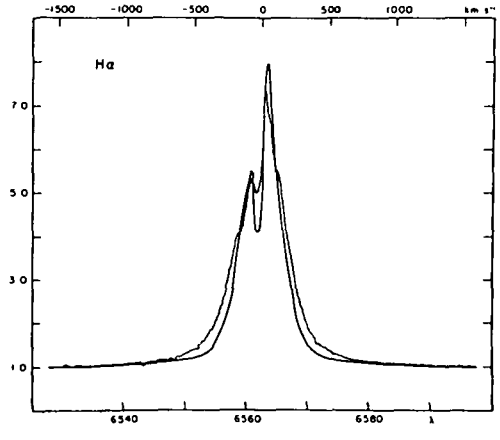

Figure 11-7. The observed Hα line profile of φ Per (at JD 244357), and the calculated Hα profile (smoothed curve) (from Poeckert and Marlborough, 1979).

The Rotation Model and the Variability of Be Stars. Interpreting the Be phenomenon amounts to explaining two observational facts: (1) the presence of emission lines in the visible spectrum, while the theory predicts the presence of absorption lines only; and (2) the variability of the emission lines and of the continuous spectrum. This second fact was well known at the time that Struve proposed his model. Thus, Struve and Swings (1932) noted the following: "The frequent variation of the bright lines constitutes the most vulnerable point of the rotational hypothesis." Subsequent observations have only increased the evidence for the variability of the Be stars. It could be said that almost all the articles devoted to observations of Be stars consider their variations. Observations from space in the ultraviolet spectral region (cf., Chapter 12) only accentuate this characteristic by demonstrating much larger variations than those observed in the visible region.

The rotation model encounters difficulties with the following three observations which will be described in the section on Variability of the Line Spectrum and the Continuous Spectrum in the Visible and Near Infrared Regions: (1) the intensity and the profile of the emission or shell lines are variable; (2) the same star may exhibit a Be spectrum or a shell spectrum at different times; and (3) a star may lose all the Be or shell features from its spectrum and become a normal B star. In many cases, the Be or shell spectrum reappears after a certain time. Clearly, geometrical-orientation effects cannot explain observations (1) to (3) in a given star

In order to interpret the V/R variations, which essentially refer to the relative intensity of the red and violet peaks of the emission lines, McLaughlin (1931) proposed, in the same year as Struve, a model in which the envelope undergoes both rotational and pulsational motion. Gerasimovic (1934, 1935) invoked the effect of radiation pressure to account for the formation of the envelopes in rapidly rotating stars where effective gravity is reduced by rapid rotation. In this model, time variations were explained by varying optical thickness of the outer atmosphere. Since then, most of the ad hoc models that have been developed to interpret the visible spectra of Be stars in the visible have retained the rotation and the expansion motions (see the section on Be Star Models Based on Observations at Visible Wavelengths).

The Rotation Model and the Ultraviolet Observations from Space. In order to understand the origin of the Be phenomenon, Struve and Swings (1932) tried to answer the following two questions. (1) Are the absorption-line profiles in Be stars broadened by rotation? and (2) Are the emission lines broadened by the rotation of the outer envelope? These two questions were of a fundamental nature in Struve's day; it was necessary to find a mechanism that would produce an extended atmosphere in some B stars and not in others, because only some of them exhibited emission lines in their spectra. The observations made at that time suggested that only the emission-line stars had an extended atmosphere, that is, a mass flux that could be responsible for the formation of such an atmosphere. But for more than 10 years, ultraviolet observations from space have shown that there exists a mass flux and a nonradiative energy flux in normal B stars as well as in Be stars. The question to be answered at present is no longer the one that was asked 50 years ago Why do the Be stars have a mass flux while the normal B stars do not? Rather, it is If two B stars of the same spectral type both have a mass flux and a nonradiative energy flux, why do they not both have cool and low velocity regions in their outer atmospheres, where the emission lines observed in the visible are formed? There is no longer any need to invoke a special mechanism to produce a mass flux in the Be stars alone, since a mass flux is also observed in some normal B stars of the same spectral type. It must be explained why the mass flux and the nonradiative energy flux produce chromospheric, coronal, and post-coronal regions where the velocities undergo increasing expansion in the outer atmospheres of certain normal B stars, while in the Be stars, the post-coronal region is much denser and experiences a deceleration in the cool parts where the Balmer lines and the Fe II emission lines are formed.

In the following discussion, in order to avoid confusion, we shall keep the term *envelope* to denote the region of the outer atmosphere where the visible emission lines of the Be stars are formed. In Struve's time, the envelope made up the entire outer atmosphere of the Be star. Since the ultraviolet observations from space have been made, this envelope refers only to a limited, well-defined region of the outer atmosphere—the region where the emission in the Balmer lines is formed, and whose existence defines the anomaly of the Be stars in the visible. The term *extended atmosphere*, traditionally used to denote the outer atmosphere of the Be stars, can now refer to the atmosphere of normal B stars as well as of Be stars.

THE CONTINUOUS SPECTRUM FROM THE NEAR ULTRAVIOLET TO THE RADIO REGION

Just like the line spectrum, the continuous spectrum of Be stars is different from that of normal B stars. Since the turn of the century, Gerasimovic (1929) has pointed out that some of the "yellow" B-type stars recognized by Hertzsprung (1923) were characterized by enhanced emission on the ultraviolet part of the Balmer series limit. In 1934, Williams found that Be stars show an intrinsic color excess which seemed to be related to the intensity of the hydrogen emission, the stars with stronger emission being, on the average, lower in color temperature. But it was through observations of γ Cas, whose visible gradient, visual magnitude, and line spectrum were under-

going large variations in 1936 (see section on Variability of the Line Spectrum and the Continuous Spectrum in the Visible and the Near Infrared Regions), that the intrinsic nature of the visible reddening was definitively established (Chalonge and Safir, 1936, Greaves and Martin, 1938). Observations of this star also made it possible to show that when the emission was strongest in the Balmer lines, the star was brightest, although its color temperature was lowest; this implied that the reddening was caused by an excess of radiation at long wavelengths in the Paschen continuum. This is the behavior to be expected from free-free and free-bound emission, arising in an envelope of ionized gas that is optically thin in the continuum.

The differences between the continuous spectrum of Be stars and that of normal B stars, as observed in the visible spectral region, are even greater in the infrared. There is a large range of excesses in this spectral region, from the weakest—found mostly among the "ordinary" Be stars—to the strongest—observed among the B[e] or Bep stars, which have forbidden lines in their spectrum, and among the stars associated with nebulosities, including the Herbig Ae and Be stars. All the emission-line stars exhibit anomalies in the infrared; and although there is a certain progression from the Of stars to the M supergiants, the most striking characteristic of these excesses is their diversity within a single spectral type The weakest excesses—a few tenths of a magnitude at 2 μ—are interpreted as a free-free emission spectrum in an extended, ionized envelope, with a temperature of around 10^4 K, the stronger excesses, on the other hand, are explained by thermal re-emission by dust particles in the circumstellar envelope. In some stars (but not in the Be and Bep stars until now), these dust particles have been identified as silicates, from the presence of two emission bumps in the neighborhood of 10 and 20 μ.

Continuous emission in the radio region, which can be attributed to thermal free-free radiation, has been detected in a certain number of Bep stars and, more generally, among the stars that have extended, dense circumstellar envelopes. One of the advantages of studying the radio spectrum is that it allows a determination of the density distribution in the circumstellar envelope, and of the mass flux if the expansion velocity is known in the regions where this spectrum is emitted.

The Energy Distribution in the Be Stars, from the Near Ultraviolet to the Visible Region (3200 Å < λ < 6000 Å)

The Balmer Discontinuity in the Be Stars. The most accurate and detailed conclusions concerning the energy distribution of the Be stars from 3200 Å to 6000 Å have been obtained by photographic spectrophotometry. Barbier and Chalonge (1941) applied their method, which was developed for the study of stellar continuous spectra and which led to the BCD classification system, to the Be stars. They showed that the presence of emission lines in the visible spectrum of B stars was usually accompanied by two effects. (1) a reddening of the continuous spectrum in the visible (4600 to 3700 Å) and in the ultraviolet (3150 to 3600 Å) ranges, that is, a color temperature lower than that of a normal B star of the same spectral type, (2) a change in the Balmer jump, which may have a different appearance for Be spectra and for shell spectra, and may exhibit variations when the intensity of the emission or shell lines varies.

Figure 11-8 shows the Balmer jump of ζ Tau, whose spectrum has pronounced shell characteristics, and that of two normal stars, η UMa (a main-sequence star) and η CMa (a B supergiant), as observed by Barbier and Chalonge (1939b). These authors brought to light the existence of two discontinuities in the spectrum of ζ Tau. The first jump, A, corresponds to the position of the discontinuity in a dwarf star, at around H14, the second one, B, is located at shorter wavelengths, around H22, as in a supergiant. They concluded that the two discontinuities are produced in two different regions of the stellar atmosphere the photosphere and the extended envelope where the pressure is much lower.

The observations of γ Cas show that the second discontinuity can also be in emission (Barbier and Chalonge, 1941). The "emission"

characteristic of the second jump is defined with respect to the Balmer continuum of a normal star of the same spectral type. A second Balmer jump in emission can simulate a Balmer jump smaller than that of a normal star of the same spectral type; it can make the jump disappear altogether, or it can be in emission with respect to the Paschen continuum. Figure 11-9 shows the different appearances that can be taken on by the Balmer jump in the Be stars (Divan, 1979). Note in the spectrum of α Ara, which exhibits a second discontinuity, *d*, in emission with respect to the Balmer continuum of a normal B star, that the continuous emission begins at a longer wavelength than the theoretical value of 3647 Å; the same is true for the continuous absorption that begins at the second absorption discontinuity in 48 Lib. However, not all the Be stars exhibit two Balmer jumps; many of them have only one discontinuity, which is normal for their spectral type, even though their spectrum exhibits emission in the Balmer lines, with or without shell features.

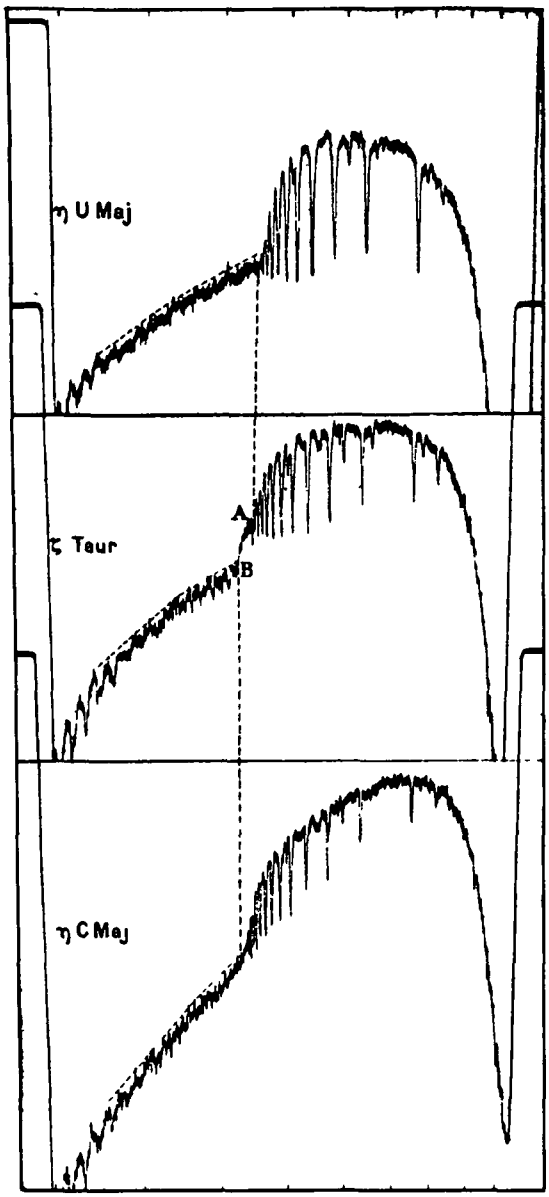

Figure 11-8. The 2 Balmer jumps in the shell spectrum of ζ Tau (from Barbier and Chalonge, 1939b). The first jump corresponds to the position of the discontinuity in a B dwarf star (here η UMa). The second one is located at a shorter wavelength, as in a supergiant (here η CMa)

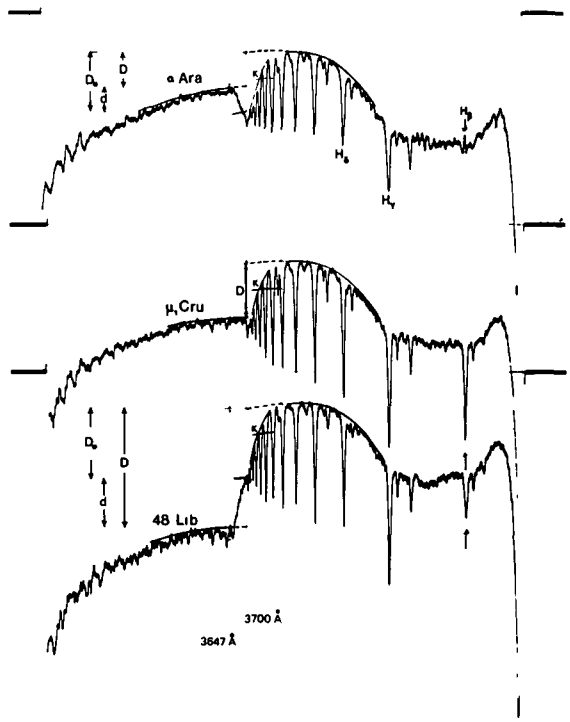

Figure 11-9. The different aspects of the region of the Balmer discontinuity in Be and shell spectra. For comparison, the Balmer discontinuity of the normal B star μ_1 Cru is also represented (from Divan, 1979) In the Be spectrum of α Ara the second Balmer discontinuity is in emission relative to the level of the Balmer continuum of a normal B star; in 48 Lib it is in absorption.

Divan (1979) has shown that when the emission lines undergo variations in the visible, only the second discontinuity, d, varies (Figures 11-10 and 11-11); thus, the position, λ_1, and the magnitude of the first discontinuity, D_*, which are constant, define the spectral type of the star. Thus, in the BCD system, the Be stars can be classified just like normal stars. Divan's observations suggest that the second discontinuity, d, is more often in emission in the early Be stars, while it is more often in absorption in the later Be stars. But this result reflects only a trend; one can find stars of all types having either kind of discontinuity.

This set of observations raises the question of whether there is a correlation between the intensity of the Balmer-line emission and the magnitude of the second discontinuity. Schild (1978) made simultaneous photoelectric measurements of the Hα emission and the Balmer jump for Be stars in 14 clusters. His low resolution (≈ 50 Å) enabled him to measure only the overall discontinuity, that is, the difference in intensity between the two sides of the Balmer limit. He calculated the "Balmer jump discrepancy," which is the difference between the Balmer jump of the Be star and the Balmer jump of a normal star of the same luminosity. The Be stars with the strongest emission at Hα also have the most pronounced "filling in" of the Balmer jump, but the correlation is very poor and does not enable one to predict the magnitude of the Balmer jump from the measurement of Hα (Figure 11-12).

Divan et al. (1982) have measured the Balmer jump in around 30 Be stars on BCD classification spectra, and the Hα emission on high-resolution spectra that were obtained simultaneously. In spite of the obvious improvement in the measurements, they find essentially the same results as Schild, confirming the absence of a correlation between the Balmer jump and the Hα emission. Like him, they observe that the Balmer jump is more often in emission when the emission at Hα is strong; but there is a very large

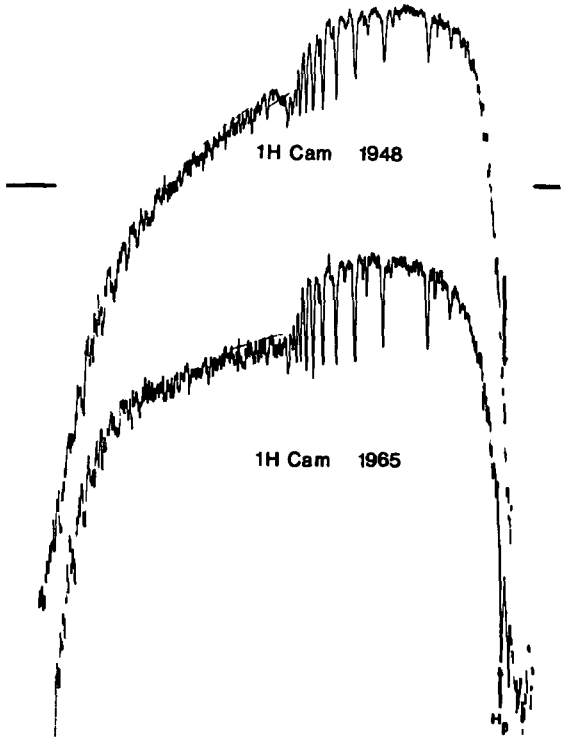

Figure 11-10. The variation of the second Balmer discontinuity in 1 H Cam (from Divan, 1979)

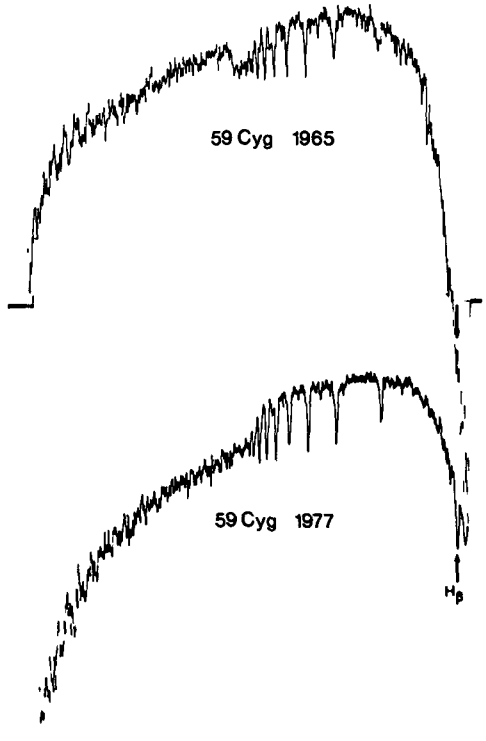

Figure 11-11. The variation of the second Balmer discontinuity in 59 Cyg (from Divan, 1979).

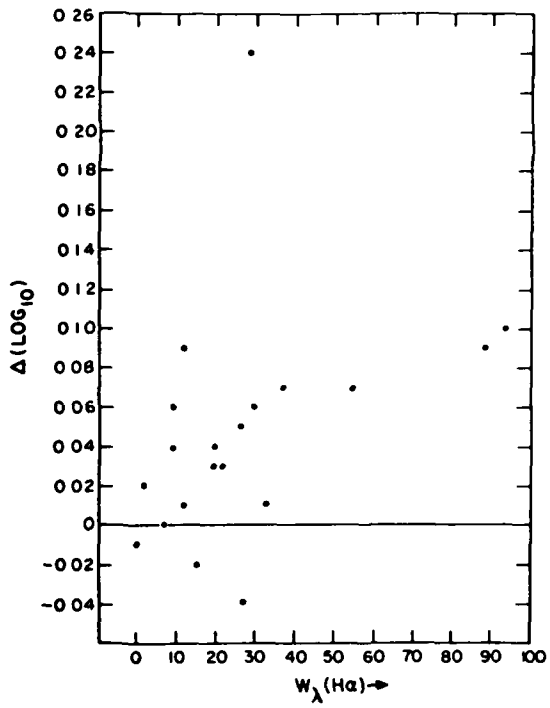

Figure 11-12. The correlation between the equivalent width of the emission at Hα, $W_\lambda(H\alpha)$, and the Balmer jump discrepancy, Δ, as defined in the text (from Schild, 1978).

scatter in the values of Hα found for a given value of the Balmer jump. These two studies show that it is impossible to give a representative value of the Balmer jump in the Be stars. A list of the values of the Balmer jump in the Be stars measured by Divan is given in Underhill et al (1979).

The Color Gradients. Observations of γ Cas during its episode of spectacular variations from 1932 to 1942 made it possible to prove the existence of an intrinsic reddening in the Be stars from the variability of this reddening with the epoch of variation (as discussed in the next section). Thus, the colors of the Be stars are affected, on the one hand, by the reddening caused by interstellar absorption, and on the other hand, by the reddening caused by the envelope. Observations of the energy distribution in these stars do not, in and of themselves, make it possible to separate these two effects. Divan et al. (1981) have measured the gradients ϕ_{rb} (6200 to 4000 Å) and ϕ_{uv} (3700 to 3130 Å) at different epochs of the variation of X Per, when the emission in the Balmer lines was very strong and when it was very weak. Figure 11-13 shows that the gradients ϕ_{rb} and ϕ_{uv} vary in a quasi-linear fashion with d, the second Balmer jump. The points for 1977 correspond to an epoch when the emission in the Balmer lines was very weak, and visible only at Hα. If one assumes that at this epoch when the Hα emission is weak, the reddening due to the envelope is negligible, then the observed color excess is due to interstellar absorption only. Divan (1979) has suggested that if these relations were the same for all Be stars, or if the appropriate relation could be determined from their spectrum, it would be possible to determine the interstellar reddening. This determination could be made even if the Be star is observed at an epoch when the line emission is strong, by extrapolating the values of ϕ_{rb} and ϕ_{uv}, to the point

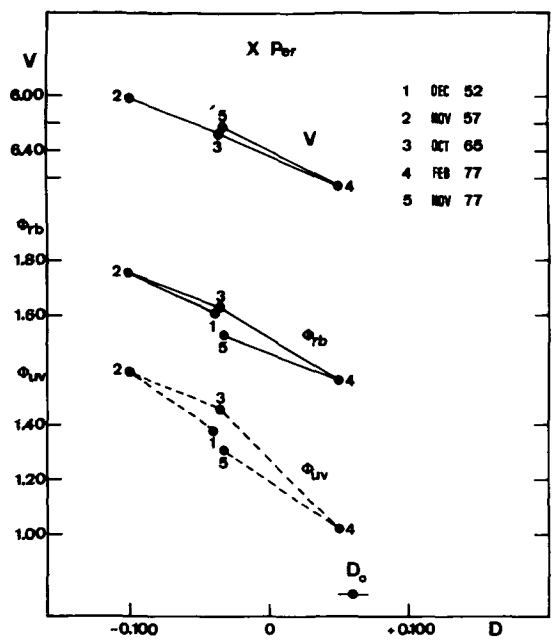

Figure 11-13. The variation of the V magnitude, the red and ultraviolet gradients, φ_{rb} and φ_{uv}, of X Per as a function of the Balmer jump, D, from 1952 to 1977 (from Divan et al., 1981). The luminosity of the star is the greatest when the color temperature is the lowest on both sides of the Balmer limit

where $d = 0$. This method does not seem appropriate to us, for there are a great many Be stars with a single discontinuity ($d = 0$) whose Balmer-line emission is not weak, and whose colors suggest the existence of a non-negligible intrinsic reddening. We shall see, in the case of 88 Her, that large color variations can take place even when the Balmer-line emission is weak and even if only a single discontinuity is observed.

The magnitude measurements made by Divan et al (1981) for X Per show that the star is most luminous in the V band when the Balmer discontinuity is in emission, that is, when the emission is strongest in the Balmer lines (Figure 11-13). This is also the epoch at which the intrinsic reddening of the Paschen and Balmer continua is greatest. Thus, the luminosity of the star is greatest when the color temperature is lowest in the visible.

The Flux of the Be Stars in the Visible Several studies have been made by means of a scanner ($R \approx 50$ Å) to compare the energy distribution of the Be stars to that of normal B stars, from the near ultraviolet to the near infrared spectral regions. These studies recover essentially the same results as obtained by photographic spectrophotometry, and summarized above, namely: (1) in most cases, the Balmer jump of the Be stars is smaller than the normal jump in B stars, but the jump of Be stars can also be normal, or in emission, or deeper in absorption than the normal jump; (2) the majority of the Be stars exhibit an intrinsic reddening in the Paschen continuum. The energy distributions of a large number of cluster and field Be stars, Bep stars, pole-on Be stars, and "extreme" Be stars (which Schild defines as those that have pronounced and permanent emission features) are to be found in Schild et al. (1974) and Schild (1976, 1978).

The main problem involved in the determination of the flux distribution in Be stars is the correction for interstellar extinction. Different methods have been used in the articles cited above (1) the use of the color excess $E(B-V)$; in this case, the intrinsic reddening is not taken into account, and this method is, therefore, not justified for the majority of the Be stars; (2) the fitting of the observed continuum to that of atmospheric models in the 4000 to 5000 Å region, after trying different values of $E(B-V)$; this method assumes a priori that the envelope is transparent in the fitting region, a hypothesis that is certainly not justified in many cases, because the flux variations observed in different spectral regions show that the contribution of the envelope can be large at all wavelengths (as discussed in the next section); (3) the determination of the interstellar extinction for cluster Be stars from that of the neighboring stars; it is assumed a priori that the interstellar absorption is constant in the region of the cluster, which is generally not the case. These three methods entail errors that are difficult to evaluate, since the energy distribution of the Be stars is variable from one star to another and is also variable for the same star, depending on its epoch of variation. It is obvious that the observation of the continuous spectrum of a Be star during its normal B phase leads to the most reliable determination of the interstellar absorption. A second method may be provided by the observation of Be stars that belong to binary systems with a large enough separation. The observation of the companion, if it is a normal star, makes it possible to compute the interstellar absorption correction to be applied to the Be star.

A study of the energy distribution, from 3200 to 8500 Å, of the Be stars in 14 clusters (Schild, 1978) shows that once the interstellar extinction correction has been applied, the intrinsic reddening of the Be stars in the visible more or less follows the interstellar reddening law in λ^{-1}, but this is not the case in the near ultraviolet and infrared spectral regions. Figure 11-14 shows that after correction for the intrinsic reddening in the visible, an infrared flux excess and an excess in the Balmer continuum are still clearly observed. The energy distribution obtained in this way differs considerably from any model atmosphere for a normal star in the near infrared and ultraviolet spectral regions. Schild shows that the intrinsic reddening $E(B-V)$ of the Be stars is often around 0.10 mag, it can be as great as 0.15 mag, corresponding to a difference of several spectral subtypes.

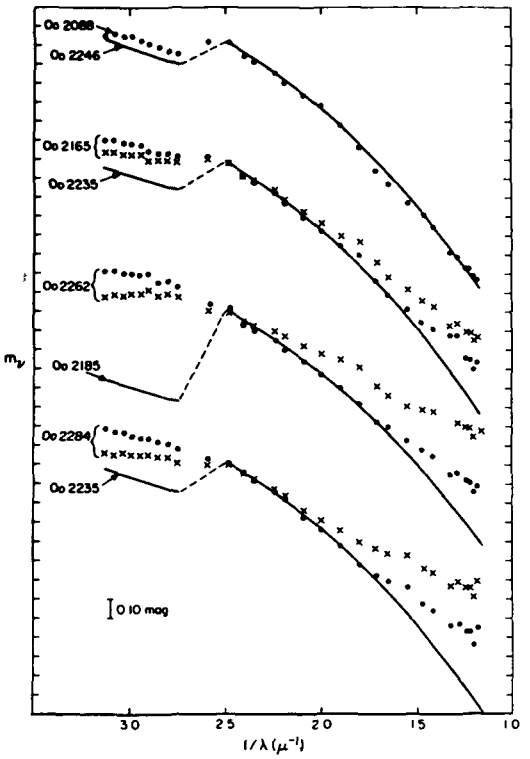

Figure 11-14. The dereddened energy distributions of cluster Be stars in χ Per, normal B stars are represented by solid curves. The energy distributions of Be stars are shown for two choices of color excess, the best fit to the normal B stars in the 4 – 5500 Å region is shown as dots, crosses show the energy distributions dereddened by using the cluster mean reddening (from Schild, 1978).

The Be stars have also been observed using broadband photometry. The advantage of this method is that a large number of objects can be measured quickly But the UBV system has been used generally to observe the Be stars, with the result that the gain in observing time has been largely offset by the loss of information concerning the Balmer jump, on account of the spread of the U band on both sides of the jump

Mendoza (1958) made a statistical study of 175 Be stars of spectral types B0 to B5, luminosity classes III to V. These are the Be stars brighter than magnitude 8.6 and north declination −20° from the catalogues of Merrill and Burwell (1933, 1943, 1949). He classified the stars on the MK system using the appropriate type of spectra, and observed them on the UBV photometric system. His diagram representing the B2e stars (Figure 11-15) shows the large scatter of the points around the reddening line for normal stars. Mendoza corrected the (U − B) color index for the effects of interstellar reddening by means of the relation used for normal stars. He concluded that the B0 to B2 stars exhibit a mean ultraviolet excess of the order of 0.3 mag, while the excess decreases from B2 to B5. He gave no interpretation of the points lying below the reddening line. But the use of the usual dereddening relation does not take into account the intrinsic reddening of the Be stars, which affects the (B − V) color index; thus, the computed (U − B) color index overestimates the ultraviolet excess. It is obvious that the use of the UBV bands does not enable one to separate the intrinsic reddening from the interstellar reddening in the Be stars. This was already clear from the results of Barbier and Chalonge (1941). Feinstein's (1968) observations led to the same conclusion.

Schild (1966) distinguishes two groups of Be stars in the region of h and χ Per; the ordinary Be stars, having spectra of various kinds, and the

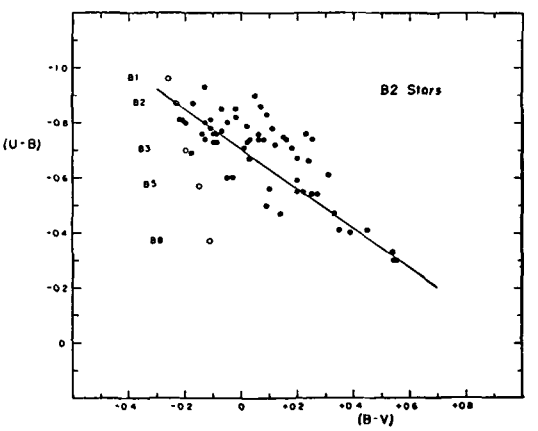

Figure 11-15. Color-color diagram of the B2e stars (filled circles). The main-sequence intrinsic color indices values are indicated by open circles. The reddening path is shown by a heavy line. The large scatter reflects the large range of intrinsic reddening of the Be stars (figure from Mendoza, 1958).

"extreme" Be stars, all of which seem to have pronounced and permanent emission features In the HR diagram, the "extreme" Be stars are located 1.5 mag above the main sequence. Their E (B − V) color excesses are of the order of 0.15 mag, while there is no comparable excess at (U − B) Schild suggests that the faint "extreme" Be stars are rapidly rotating B stars, undergoing rapid core contraction subsequent to hydrogen exhaustion in their cores. However, it must be noted that the nine faint "extreme" Be stars have been very infrequently observed The permanance of the emission in eight of these stars has been deduced from the comparison of spectra taken at only two or three different epochs. The interstellar reddening of the Be stars is removed by using the corrections found for the nearby normal stars.

The Energy Distribution in the Be Stars in the Infrared Region ($0.6\ \mu < \lambda < 20\ \mu$)

The Infrared Excess of the Be and B[e] Stars. In seeking a relation between the (K − L) color index and the spectral type for hot stars, Johnson (1967) discovered an excess in this index for emission-line stars (Of, Be), with respect to normal stars. Subsequently, the observation of emission-line stars and related objects showed that the infrared excess was a common feature among all these objects; like the presence of emission lines in the visible spectrum, the infrared excess became an indicator of an extended atmosphere, suggesting the existence of a mass flux as its source.

The infrared spectrum of the Be stars has mainly been observed by means of broadband or intermediate-band photometry, usually out to 3.5 μ but sometimes out to 20 μ. Most of the observations were not coordinated with observations of the visible spectrum, this is a definite handicap for the establishment of correlations between the infrared excess and the spectral features, given the variable behavior of these stars. With the first infrared surveys of emission-line stars, it was quickly recognized that the Be stars exhibited different degrees of excess. The observation of 248 early-type emission-line stars and related objects (Allen, 1973) in the H (1.6 μ), K (2.2 μ), and L (3.5 μ) bands showed that most of the Be and shell stars exhibited an infrared excess in the (K − L) color index of the order of a few tenths of a magnitude, while most of the B[e] stars, which have forbidden lines in their spectrum, exhibited much larger excesses, greater than 1 magnitude. Although the infrared excesses of the Be stars were satisfactorily explained by free-free transitions emitted in an envelope of ionized gas (Woolf et al., 1970), the large excesses found for the B[e] stars generally led to the rejection of this interpretation in favor of thermal radiation re-emitted by circumstellar dust particles (Gillet and Stein, 1971; Allen and Swings, 1972; Allen, 1973; Allen and Swings, 1976). Pecker (1972) gives a very complete discussion of the various interpretations of these excesses Thus, there developed a certain dichotomy between the Be and shell stars without forbidden lines, often called "conventional" or "classical" or even "ordinary" Be stars and the B[e] stars, which are also called peculiar Be stars or Bep stars. Nevertheless, there is an overlap in the excesses of these two groups which cannot be separated completely. Note, also, that the distinction between an infrared excess due to free-free emission and an excess due to thermal re-emission by dust is not always unambiguous, even when the observations extend out to 20 μ. Finally, none of the models put forward to interpret the infrared excess takes into account the existence of chromospheric and coronal regions, which have been observed in the ultraviolet and X-ray ranges for these stars and where free-free radiation is also emitted (see Chapter 12).

The Infrared Excess in the Conventional Be Stars. Johnson's (1967) observations, which revealed the infrared excess of the Be stars, were fully confirmed by subsequent observations, including those of Feinstein (1968), Erro (1969), Woolf et al. (1970), Allen (1973), Gehrz et al. (1974), Schild et al. (1974), and Schild (1976, 1978). Taken as a whole, the observations show that the majority of the Be stars exhibit an extra-photospheric component in their infrared radiation, which varies in magnitude from star to star. The

infrared excesses have generally been measured by assuming that the observed spectrum can be matched with the photospheric continuum in the visible spectral region, thus ignoring the intrinsic reddening observed in the visible region. This procedure tends to underestimate the infrared excess, but the general conclusions are unchanged, for the excesses are, on the average, much larger in the infrared than in the visible region.

The correlation between the presence of emission lines in the spectrum and the observed infrared excess suggested that all of these extra-photospheric features might originate in the same plasma surrounding the star (Johnson, 1967). Following this suggestion, Woolf et al. (1970) showed that the energy distribution in the Be stars out to 10 μ was compatible with free-free radiation emitted by a plasma with a temperature of 1 5 X 10^4 K, superimposed on the stellar continuum. The observations of Be stars in the 2.3 to 19 5 μ range by Gehrz et al. (1974) showed the diversity of the infrared spectra in these stars. Among the 33 Be stars they observed, 28 exhibited an infrared excess. The infrared excesses seemed to be larger for the earlier spectral types, but no correlation was found between the excesses and v sin i

The great diversity of the observed infrared excesses led to a search for correlations with features in the visible and infrared line spectrum. The Be stars that exhibit emission until the end of the Paschen series tend to exhibit the largest infrared excesses. At 10 μ, the flux of these stars being 7 times greater than the flux of a normal B star, while for the Be stars that have the end of the Paschen series in absorption, it is only 2.5 times greater (Briot, 1977).

The wavelength, λ_c, at which the free-free emission becomes optically thick can be determined from the shape of the infrared spectrum by extrapolating the optically thin and optically thick regions of the continuum (as shown in Figure 11-16, from Gehrz et al., 1974) These authors distinguish two types of infrared spectra (1) those for which the energy distribution is compatible with a hot stellar continuum to which is added free-free emission in a plasma at 10^4 K becoming optically thick around 7 μ, the spectrum of φ Per is typical of this group (Figure 11-16), (2) those for which the free-free emission remains optically thin out to at least 12.6 μ, like that of β CMi (Figure 11-17). They note that none of the Be stars shows the emission features at around 10 and 20 μ that are attributed to silicates, and reject any interpretation of the infrared excess in the Be stars they observed (which are all "conventional" Be stars) in terms of thermal re-emission from circumstellar dust. Gehrz et al. compute the electron density, n_e, and the radius of the envelope, R_{env}, in the case of a homogeneous medium, when the value of λ_c can be determined. Writing that $\tau_c = 1$ for λ_c,

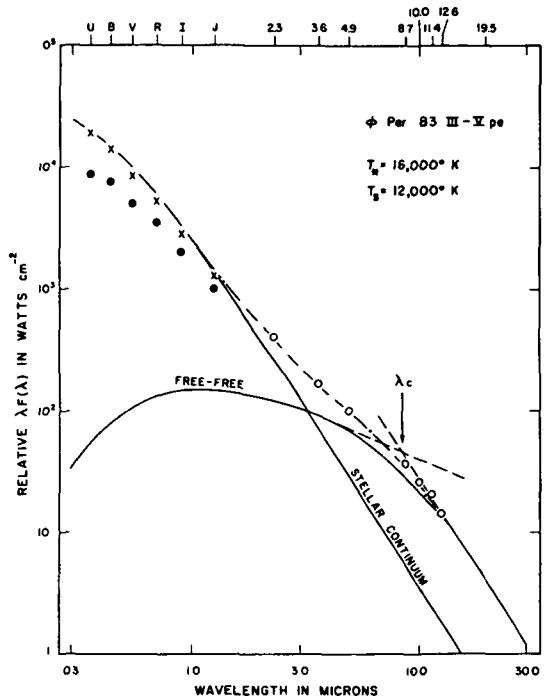

Figure 11-16. The infrared excess of φ Per fitted by a free-free model. The wavelength λ_c at which $\tau = 1$ is defined by the intersections of the extrapolation of the optically thick and optically thin parts of the observed spectrum (dashed lines). The UBVRIJ data (filled circles) are from Johnson et al. (1966) and reddening corrections are denoted by crosses. The open circles are the infrared data of Gehrz et al. (1974) (diagram from Gehrz et al., 1974).

$$R_{env} n_e n_p = 5.1 \times 10^{22} T_{env}^{3/2} \lambda_c^{-2} f_p(i) A, \quad (11\text{-}2)$$

where A is the ratio of the radius R_{env} to the thickness of the envelope, and $f_p(i)$ is a factor that takes into account the inclination of the axis of rotation to the line of sight. It is assumed that the Gaunt factor $g = Z = 1$.

The ratio F of the flux of the envelope, extrapolated from the optically thick regions, to the flux of the star at λ_c provides an expression for the radius of the envelope, R_{env}:

$$R_{env} = \left(\frac{R_*^2 \quad T_* F}{f_p(i) \quad T_{env}} \right)^{1/2} . \qquad (11\text{-}3)$$

These two expressions make it possible to compute n_e in a homogeneous, completely ionized envelope.

$$n_e = 2.3 \times 10^{11} \frac{T_{env}}{\lambda_c} \left(\frac{f_p^3(i) A^2}{F T_* R_*^2} \right)^{1/4} . \qquad (11\text{-}4)$$

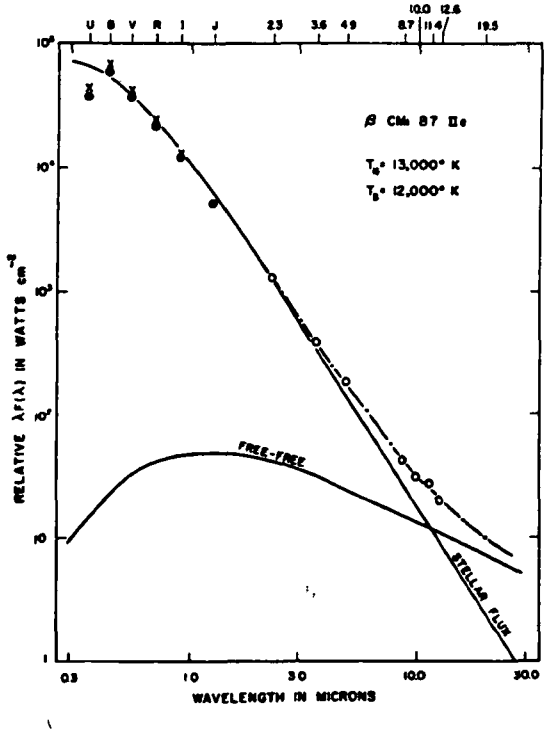

Figure 11-17. The infrared excess of β CMi fitted by an optically thin free-free emission arising in the envelope. Symbols are the same as in Figure 11-16 (figure from Gehrz et al., 1974).

Assuming that $A = 5$ and $T_{env} = 10^4$ K, Gehrz et al. find that a typical envelope is characterized by $n_e = 3 \times 10^{11}$ cm^{-3} and by a radius of 2.5×10^{12} cm ($\approx 4\ R_*$). Note that in these calculations, it is assumed that the envelopes are homogeneous and have the same flattening factor, which is certainly not the case.

Gehrz et al. discuss the possibility of interpreting the infrared excess by the addition of a cool blackbody to the hot stellar continuum, as an alternative to the hypothesis of free-free emission This second possibility is compatible with the energy distribution of 48 Lib, ξ Per, φ Per, β Psc, and ζ Tau Figure 11-18 shows the infrared spectrum of ζ Tau and the two proposed interpretations. free-free emission from a plasma at 10^4 K and the presence of a cool companion at 1.2×10^3 K. However, the properties of the visible spectrum of this star, often interpreted as a binary system, imply that the companion has a temperature of at least 2.1×10^3 K, which would not fit satisfactorily the observed infrared flux. The infrared observations provide an advantageous method of testing the binary interpretations that are often advanced to explain the variations in the visible spectrum of Be stars. The major objection of Gehrz et al. to explaining the infrared excess of the Be stars by the presence of a cool companion is that this explanation could apply to a few Be stars only, while the observed excess is so general that it must be connected with the "Be phenomenon" itself, a mechanism common to all these stars should therefore be sought.

γ Cas has been observed in the 1 to 4 μ region with a resolution of 2 percent, by means of a Cassegrain telescope mounted in an aircraft flying at an altitude of 12,500 m (Scargle et al., 1978). These observations, together with the broadband observations, are given in Figure 11-19 The most striking feature in the spectrum is the Brackett discontinuity, at 1.46 μ, in emission. Scargle et al interpret the infrared excess by means of isothermal, LTE models that take into account the free-free and free-bound hydrogen emission and the attenuation of the stellar radiation by the extended envelope; they do not assume, a priori, that the contribution of the enve-

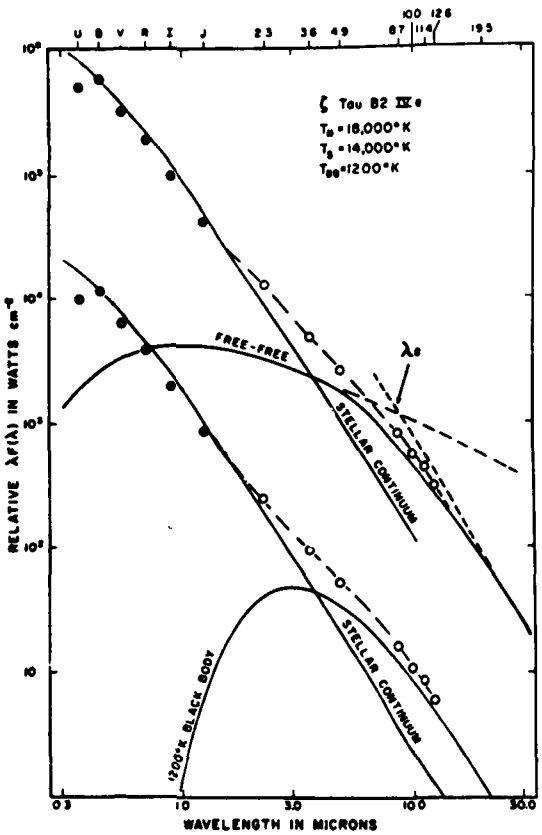

Figure 11-18. The 2 interpretations of the infrared spectrum of ζ Tau; at the top, a 1.4 × 10^4 K free-free spectrum is added to the stellar continuum; at the bottom, a 1.2 × 10^3 K blackbody spectrum is fitted to the observations (from Gehrz et al., 1974).

lope is negligible in any spectral region. The shape of the photospheric contribution, depending on the spectral type, is known from the models of Mihalas (1965). The interstellar reddening correction is a fitting parameter for the model over the entire observed spectrum. The flux is not normalized at any wavelength, in contrast to previous studies in which the B band was chosen to fit the observed continuum to the photospheric continuum. The normalization factor is a free parameter, determined by the condition that the model must agree with the data across the Balmer jump, which was observed in emission in γ Cas. It can be seen in Figure 11-19 that the observed flux longward of 5 μ is much smaller than the best of the computed optically thin models, which indicates that the long-wavelength radiation is self-absorbed. Scargle et al. determine 21 models, with two geometric configurations (sphere or disk), all of which lead to the conclusion that the infrared excess of γ Cas can be almost entirely explained by free-free emission (28 percent) and free-bound emission (72 percent). Two models are shown in Figure 11-20: the disk model, with T_{env} = 17, 540 K, τ (1 μ) = 0.5, $n_e = 10^{12}$, $R_{env} = 2 \times 10^{12}$ cm ($\approx 4\ R_*$), and the two-disk model, with an inhomogeneous source function which better represents the observations beyond 5 μ. The envelope contribution amounts to 33 percent of the total flux in the 0.36 to 20 μ region.

Schild et al. (1974) studied the energy distribution of 10 "extreme" Be stars in the χ Per region, with a resolution of 50 Å from 3200 Å to 3.5 μ. The fluxes were dereddened by using a map of the color excesses of the nearby OB stars in the h and χ Per cluster, and compared with the dereddened flux of HD 13900, a B1 III star of similar temperature, luminosity, and age.

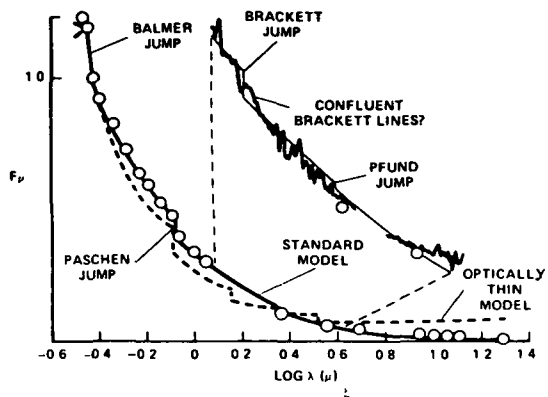

Figure 11-19. The observed energy distribution of the continuum in γ Cas. The points (⊙) are broadband data (Johnson and Mitchell, 1975; Gehrz et al., 1974) corrected for an interstellar reddening E(B − V) = 0.1. The most important feature is that all discontinuities–Balmer, Paschen, Brackett–are in emission. The smooth solid line is the standard model (slab) and the dashed line is an optically thin model which deviates considerably from the observations (from Scargle et al., 1978).

Schild et al. note that all the "extreme" Be stars have a similar infrared excess beginning at 0.5 μ, with a maximum around 1 μ and a decrease at longer wavelengths (Figure 11-21). They suggest that the peak around 1 μ is analogous to that of the free-bound H^- continuum from an isothermal envelope at $T_e = 3 \times 10^3$ K, as computed by Milkey and Dyck (1973) However, the wavelength of the observed peak is displaced by about 3000 Å toward the blue, with respect to the theoretical wavelength. This infrared peak exhibits little or no correlation with the intensity of the Hα emission (Schild, 1978). According to the interpretation of Schild et al., the infrared excess of the "extreme" Be stars is produced by a cool ($T_e = 3 \times 10^3$ K), very extended envelope, in which hydrogen is predominantly neutral

Snow (1975) tried unsuccessfully to identify the absorption feature of H^- at 1129 Å, which is due to a resonance photoabsorption, in the ultraviolet spectrum of χ Oph, a star classified as "extreme" Be by Schild et al. (1974). A comparison of the synthetic ultraviolet spectrum of H^- with that of χ Oph, and the ratio of the infrared flux to the stellar flux, lead to a disagreement between the values of $N(H^-)$ computed by these two methods; this disagreement could result

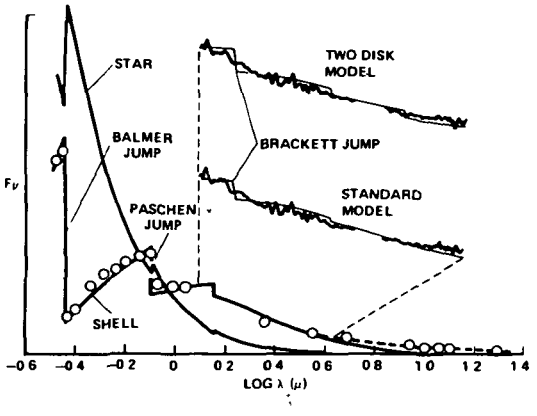

Figure 11-20. Energy distribution of the continuum in γ Cas decomposed into star and shell contributions according to the standard model (a slab) and the two-disk model. The shell contributes 33 percent of the total energy in the wavelength range shown in this figure (from Scargle et al., 1978).

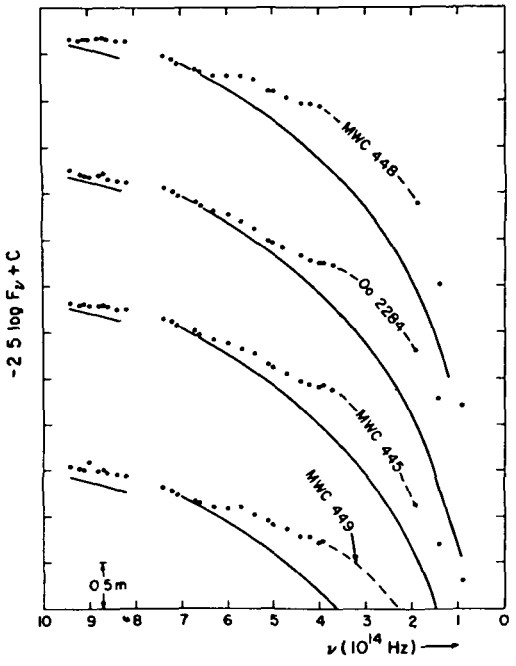

Figure 11-21. Energy distribution of "extreme" Be stars in the region of χ Per. The dereddened continuum of the normal B1 III star, HD 13900, is shown as solid curves (from Schild et al., 1974).

either from an incorrect theoretical prediction of the H^- absorption in the ultraviolet region, or from an incorrect identification of the 1 μ feature or an incorrect interpretation of the infrared excess in terms of free-bound transitions of H^-.

The Infrared Excess in the B[e] Stars. The majority of the Be stars that have a large infrared excess, greater than 1 magnitude at 2 to 3 μ, are those that exhibit forbidden emission lines in their spectrum, that is, the B[e] stars, also called peculiar Be stars (Bep). This correlation between the "peculiar" features and the large infrared excesses, among stars which are already peculiar because of the presence of emission lines in the visible, is clear from the infrared observations of 248 early-type emission-line stars and related objects made by Allen (1973). The tendency for emission-line stars to have strong infrared excesses when low excitation and forbidden emission lines are present in their spectrum is not limited to Be stars alone. It is observed among stars belonging

to various categories—Ae, Be, T Tau, symbiotic stars, novae, planetary nebulae, cool giants, etc. (Geisel, 1970, Allen and Swings, 1972). Geisel suggested that these objects, which are characterized by high rates of mass loss, have circumstellar envelopes in which dust grains form rapidly. Thus, there is a common feature—a strong infrared excess—in various types of objects that are considered distinct from one another, and that are found in completely different evolutionary states. An analysis by Allen and Swings (1976) of the Be stars having strong infrared excesses at 2 μ shows that these Be stars exhibit quite varied spectral characteristics, from those found in the conventional Be stars to those of the planetary nebulae, by way of the B[e] stars, so that there is no clean break in the infrared excesses between the conventional Be stars and the Bep stars These authors show that the Be stars with large infrared excesses can exhibit a rather weak emission spectrum in the Balmer and Fe II lines, occasionally with [OI] lines present; or a rich emission spectrum in which the low ionization elements, [Fe II], [S II], [O II], [O I], predominate; or even a spectrum in which higher stages of ionization are observed, like [O III] and [Ne III]. In this last case, the spectrum resembles that of a planetary nebula, and a number of these objects have been catalogued as such. Thus, a progression of spectral features, as well as of infrared excesses, is observed, from the conventional Be stars through the Bep stars to the planetary nebulae; but there is a large scatter within this tendency, so that it is impossible to define a precise boundary among these groups of objects.

We have seen that, in the case of the conventional Be stars, the weak infrared excesses were interpreted in terms of free-free hydrogen emission produced by the ionized circumstellar envelope. All the calculations of the free-free spectrum implicitly assume that: (1) the ionization of the gas in the envelope is radiative, and due to the Lyman continuum emitted by the photosphere; (2) the T_e of the envelope, of the order of 10^4 K, is lower than the T_{eff} of the star; (3) the free-free emission is produced in the star's H II region, a classical Stromgren sphere. Under these conditions, the total energy emitted by the free-free radiation cannot be greater than the ionizing radiation of the star in the Lyman continuum. For a B star, this free-free emission cannot give an infrared excess greater than a few tenths of a magnitude at 3 μ Up to this amount, and under these hypotheses, the infrared excess of the Be stars can be interpreted in terms of free-free radiation. For larger excesses, another explanation must be sought.

Dyck and Milkey (1972) tried to avoid the latter two conditions. On the one hand, they assume the existence of a cooler gas envelope, with a temperature of around 3×10^3 K, under these conditions, the free-free emission increases rapidly toward longer wavelengths, so long as the atmosphere is optically thin. On the other hand, surrounding the H II region where all the photons with wavelengths shorter than 912 Å have been used to ionize the hydrogen, there are zones in which the hydrogen is neutral but the ionized metals are a source of free electrons. Milkey and Dyck (1973) show that the free-free and free-bound emission from H^- in these regions, where the circumstellar envelope is composed of neutral hydrogen at a T_e of around 3×10^3 K, can be a considerable source of infrared radiation. But although this mechanism can provide a significant contribution to the observed infrared excesses, it has not been adopted for two reasons first, the predicted infrared excesses are still much weaker than those that are observed; second, the predicted emission peak at around 1 μ, due to free-bound H^- emission, is not observed The only observations that show any sign of this peak are those of Schild (1976), but the observed feature is shifted toward the blue by about 3000 Å with respect to the theoretical position, making its identification doubtful.

The generally proposed interpretation of the large infrared excesses is one which invokes the presence of solid particles in the circumstellar envelope, these particles absorb the visible radiation and re-emit it, degrading it into the infrared wavelength range. This interpretation was first suggested by Pecker (1962, 1963) to explain the infrared excess of young objects. It is now known that strong infrared excesses are ob-

served from objects in very diverse stages of evolution, and that the existence of these excesses does not characterize only the pre-main-sequence objects. Dust particles have been identified in the spectrum of some cool supergiants on the basis of their spectral features, such as the two emission peaks at around 10 and 20 μ, which are considered to be the signature of the silicates. The equilibrium temperature of the dust grains is reached when the energy absorbed is equal to the energy emitted. The temperatures found for dust grains in circumstellar envelopes vary from a few K to around 10^3 K; the latter value is most often advanced for the dust envelopes of hot stars Note that at temperatures higher than around 2×10^3 K, the grains evaporate, so that the hot stars form a hostile environment for dust Nevertheless, the silicate features have been observed in the Herbig Ae and Be stars (Cohen, 1980). They have not yet been detected in the Be or Bep stars. The interpretation of the infrared excesses by thermal emission from circumstellar dust in the Bep stars is invoked essentially because the infrared excess due to free-free emission—under the restrictive conditions that photoionization is produced by the Lyman continuum and the free-free radiation originates only in the region of the envelope where the T_e is around 10^4 K—is much smaller than the observed excesses.

Figure 11-22 gives the infrared spectra of two Bep stars with strong excesses, out to 20 μ, observed by Allen (1973). In most cases, the spectrum can be represented, for these stars, by the photospheric continuum, upon which is superimposed a blackbody continuum with a temperature of around 10^3 K. The agreement between this two-component model and the observations is generally good between 1 and 5 μ, but at longer wavelengths the observed continuum tends to be higher than in this simple model. An energy distribution that is broader than a single Planck function is generally attributed to circumstellar dust particles at different temperatures.

In the free-free emission model, which neglects free-bound emission, all the reddening in the visible region is of interstellar origin; but in the circumstellar dust envelope model, the visible

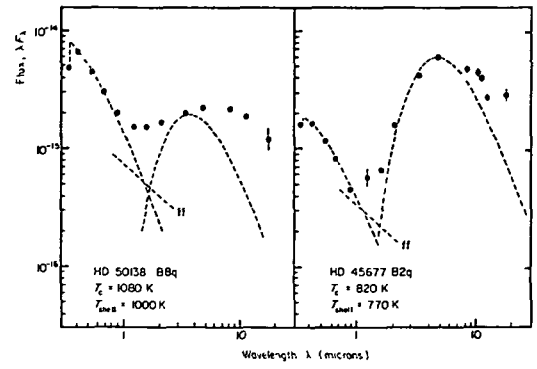

Figure 11-22. Energy distributions of 2 Bep stars from the visible to 20 μ. The infrared excess may be fitted from 1 to 5 μ by a single blackbody, but the extension of this blackbody to longer wavelengths tends to fall below the measured fluxes. T shell is the temperature of this blackbody. T_c is the color temperature of the envelope derived from the position of the star in a H − K/K − L diagram (from Allen, 1973).

and ultraviolet reddening must be large, and the energy emitted in the infrared must be equal to the energy absorbed at shorter wavelengths. The way in which the stellar flux is modified by the circumstellar dust depends on the optical properties of the grains, their distribution in the envelope, and the geometry of the envelope. Savage et al. (1978) have computed the flux emitted by a normal B2 star surrounded by a spherical envelope of dust particles that have the same wavelength-dependent optical properties as the interstellar dust. Figure 11-23 shows how the flux distribution of γ Ori (B2 III), from the ultraviolet to 1 μ, is modified because of (1) interstellar extinction and (2) circumstellar extinction, each producing an E (B − V) of 0.25 mag These authors show that the two distributions differ because in the interstellar case, both the absorbed and the scattered photons are destroyed, while in the circumstellar case only the absorbed photons are suppressed. The energy absorbed by the dust particles is represented by the difference between the flux of the normal star and the flux of the star that has been reddened by circumstellar dust. This energy, which heats the dust, reappears in the infrared in the

form of an excess. The extrapolation, longward of 1 μ, of the flux of the star surrounded by a dust envelope is shown in Figure 11-23, assuming that all the energy absorbed between 0.2 and 1 μ is re-emitted between 1.4 and 20 μ.

Among the peculiar stars, the B2ep star HD 45677 is the one whose continuous spectrum has been most thoroughly studied, over the greatest spectral range. In order to interpret the observations in the visible, Swings (1973) proposed a model in which three regions could be distinguished in the envelope. The first region, in which the Balmer-emission lines are formed, extends out to around 10 R_*. A continuous outflow of matter—detected by means of the P Cygni profiles of the hydrogen lines—takes place there, as well as rapid motions, pulsations, or disorganized motions—inferred by means of the variable structure of the hydrogen lines. The second region, much farther from the star, in which the forbidden lines of [O I], [S II], [Fe II], [Ni II], and [Cr II] are formed, has a density of the order of 10^8 cm^{-3} and a temperature of the order of 4.5×10^3 K. The third region, or "dust shell," which is responsible for the strong infrared excess, has a radius of about 30 a.u. and a temperature of 640 K. Low et al. (1970), who discovered the large infrared excess of HD 45677, interpreted it by the presence of a cold companion at 580 K. However, Swings and Allen (1971) showed that the lack of periodicity in the radial velocities of the photospheric and shell lines, over 48 years of observation, as well as the evidence for a mass flux given by the P Cygni profiles of the hydrogen lines, militated in favor of interpreting the infrared excess in terms of thermal re-emission by dust particles.

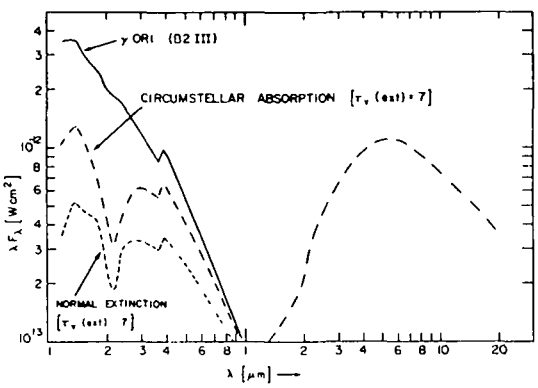

Figure 11-23. The distinction between interstellar and circumstellar absorption. The solid line shows the OAO–2 energy distribution of the normal B2 III star, slightly reddened, γ Ori. The dashed line represents the energy distribution of γ Ori for an interstellar extinction with τ(ext) = 0.7. The dot-dashed line shows the emergent spectrum if γ Ori is surrounded by a circumstellar dust shell with τ(ext) = 0.7. Energy conservation between the ultraviolet and the infrared regions has been assumed in order to derive the infrared part of the spectrum (from Savage et al., 1978).

The spectrum of the B2ep star HD 45677 has been observed almost simultaneously over a great spectral range, from 0.12 to 12.6 μ (Sitko and Savage, 1980). Figure 11-24 shows the energy distribution, λF_λ vs. λ, of the Bep star and of a normal star of the same spectral type, whose flux has been normalized to that of HD 45677 at 1 μ, where the absorption and thermal emission should be small. Note that the flux of the Bep star is greatly reduced in the ultraviolet and optical region with respect to that of the normal star. According to the estimate of Savage et al. (1978), the interstellar reddening of the Bep star is small, with E (B − V) of the order of 0.04; this corresponds to a deficiency of no more than 0.3 mag at 1500 Å, so that the remaining 2.1 mag of deficiency should be due to absorption by circumstellar dust particles. If the optical and ultraviolet flux is compared to the infrared flux, the flux deficiency in the visible and ultraviolet spectral regions is equal to around 75 percent of the integrated infrared flux. Assuming that the stellar flux below 1200 Å is given by classical stellar atmospheres, the infrared excess is equal to the flux deficiency observed in the ultraviolet and the visible spectral regions Sitko and Savage note that the infrared emission, which is broad and featureless, is similar to that observed in some carbon stars and WC 9 stars. If that were the case, the infrared emission would be produced by radiation from carbon-rich particles, the same particles would be responsible for the

deep absorption bump at 2200 Å, which is probably of circumstellar origin if these authors are correct in saying that the interstellar absorption for this star is small.

In Figure 11-24, the earlier photometric observations are also shown which indicate a significant decrease in the ultraviolet and visible flux in around a decade, while the infrared flux does not seem to exhibit large changes Sitko and Savage suggest that the dust distribution in the envelope is not uniform, so that the infrared flux remains constant while the ultraviolet and visible flux, which depends on the dust distribution along the line of sight, may vary.

The energy distribution of HD 45677 is a choice subject for study, for the observations have been made almost simultaneously over the entire observable wavelength range (from 0 12 to 20 μ), thus avoiding the incalculable error due to possible variations in the star itself. Savage et al. and Sitko and Savage propose a self-consistent interpretation of the observed flux distribution over a large wavelength range, using the circumstellar dust envelope model. But it must be noted

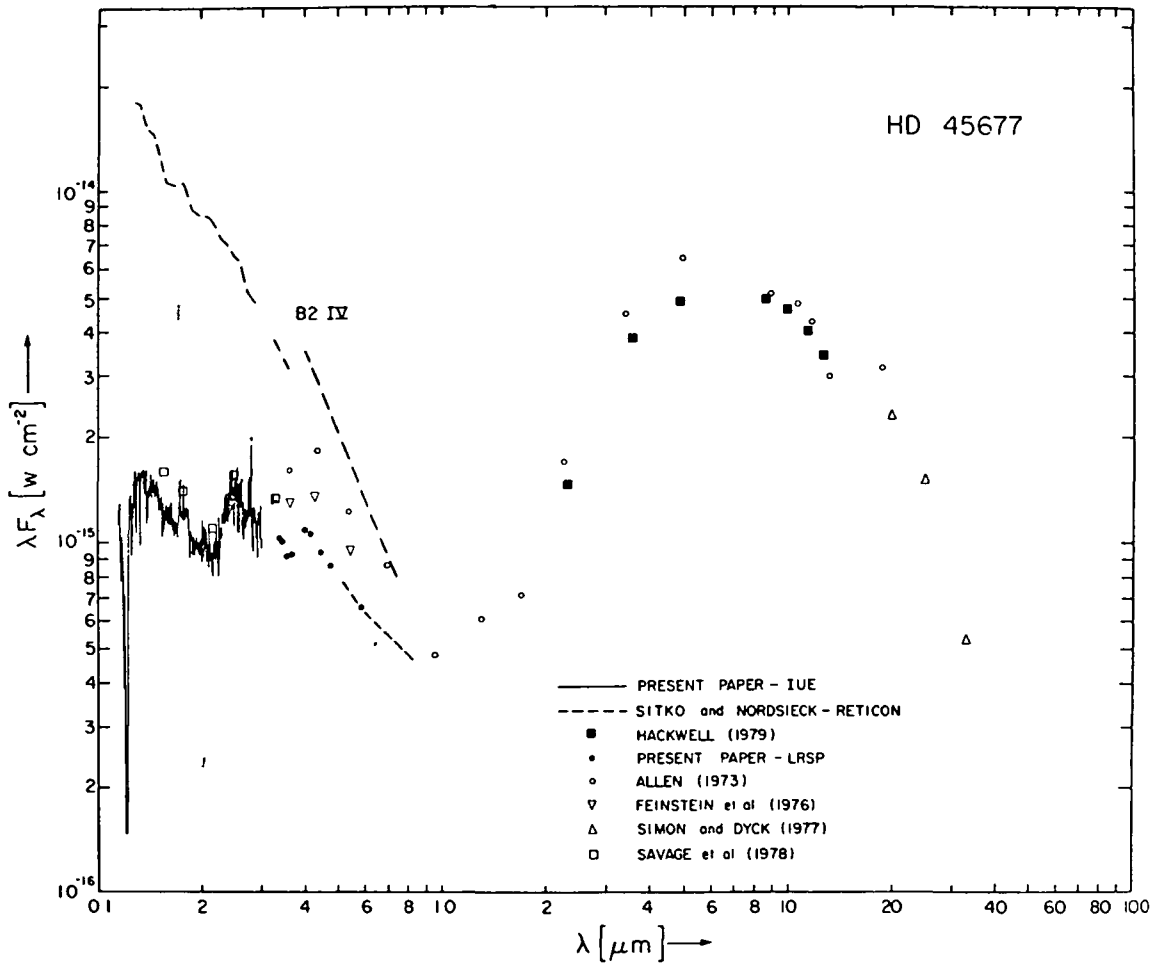

Figure 11-24 Energy distribution of the Bep star HD 45677 from the ultraviolet to the infrared region, assuming E(B − V) = 0.04. Open symbols refer to observations made at different epochs, as indicated in the figure (from Sitko and Savage, 1980). Note the large ultraviolet deficiency of HD 45677 relative to the normal B2 III star, γ Ori, when this interstellar correction is applied

this interpretation depends almost entirely on the estimate of the interstellar extinction correction.

It is well known that for emission-line stars the determination of the interstellar extinction correction from the E (B − V) excess is not very accurate, on account of their intrinsic reddening in the visible For objects having strong infrared excesses, interpreted in terms of circumstellar dust, the use of the standard ultraviolet extinction curve to choose the value of E (B − V) that cancels the absorption bump at 2200 Å is uncertain (Smyth and Nandy, 1978; Savage et al., 1978). But oddly enough, these two methods yield the same value of E (B − V) for HD 45677, 0.2 mag If this value is used to deredden the flux, reasonable agreement is obtained between the distribution of the B2ep star and the B2 normal star for $\lambda > 0.2\ \mu$, as can be seen in Figure 11-25 For $\lambda < 0.2\ \mu$, the flux of HD 45677 is slightly lower than that of the normal star, but this difference is infinitely smaller than the observed infrared excess. Savage et al. (1978) do not use either of these two methods, but choose to base their analysis on the interstellar lines of Ca II and Na I in HD 45677 These lines are weak in the optical region and could imply a very low value of the interstellar extinction. From the mean values of the absorption in these lines and the corresponding mean values of E (B − V), they conclude that the value of E (B − V) for HD 45677 is around 0 04, the value finally adopted to obtain the energy distribution emitted by the star. However, the correlation between the strength of the interstellar Ca II and Na I lines and the interstellar extinction has only a statistical meaning, and is difficult to apply to the case of an individual star. It is obvious that their entire interpretation of the infrared excess and all their conclusions depend on the choice of this value.

Although the interpretation of the infrared excesses in Be stars by the presence of a cool companion can be excluded in the general case, it is much more difficult to decide in many cases whether the infrared excess is due to free-free emission from an ionized envelope or to thermal re-emission by circumstellar dust But note first of all that the presence of emission in the Balmer lines requires the existence of a plasma at around 1.0 to 2.0 × 10^4 K, and that this plasma will emit free-free radiation whose spectrum will depend on n_e and T_e. Moreover, the ultraviolet and X-ray observations have amply demonstrated the existence of chromospheric and coronal regions in stars in general, and in the Be stars in particular, thus, this hot plasma, whose ionization is due to the nonradiative energy of the star, will also be a source of free-free emission which will produce an additional infrared excess.

In order to explain the observed infrared and radio excesses of hot stars, Cassinelli and Hartmann (1977) have studied the effects of a corona on the flux emitted in the long wavelength region of the spectrum. They analyze the source of the two kinds of excesses to be expected in the presence of a mass flux and a nonradiative energy

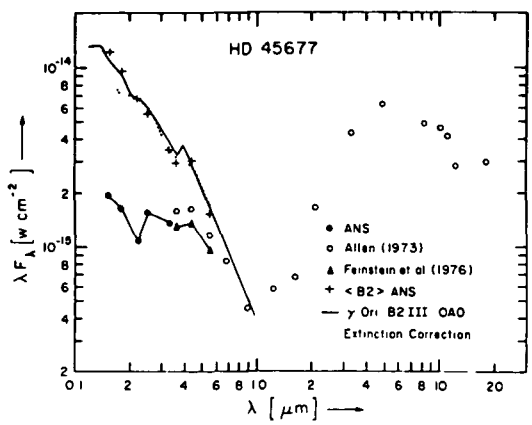

Figure 11-25. Energy distribution of the Bep star, HD 45677, from the ultraviolet to the infrared region. The continuum of the normal B2 III star, slightly reddened, γ Ori, is indicated by the solid line. The dotted curve has been obtained by applying the standard interstellar extinction correction of E(B − V) = 0.20 (from Savage et al., 1978) By means of this procedure, the ultraviolet flux of the Bep star is quite similar to that of the normal B star. For a comparison see Figure 11-24, where the Bep star shows strong ultraviolet deficiency relative to the normal B star when an interstellar extinction correction of E(B − V) = 0.04 is applied.

flux. They show that the first excess results from the existence of an extended atmosphere—the consequence of the mass flux—and the second results from the existence of nonradiatively heated regions. The effect of the extended atmosphere is to increase the effective radius R_λ in proportion to λ^2, since the absorption coefficient $k_\lambda \propto \rho^2 T^{-3/2} \lambda^2$ This will produce an excess of radiation with respect to the Rayleigh-Jeans value for long wavelengths, since $\lambda F_\lambda \propto R_\lambda^2 T_e \lambda^{-3}$, for an optically thick atmosphere. There is an additional effect due to the high temperatures of the superionized regions where λF_λ increases with T_e if the atmosphere is optically thick

For the hot star, ζ Pup, O4f, Cassinelli and Hartmann (1977) study three coronal models with $T_e = 2 \times 10^5$ and 2×10^6 K, small dimensions (0.15 and 0 25 R_*), and mass loss rates of 7.2×10^{-6} and 1.44×10^{-6} $M_\odot$ yr^{-1} They assume that the density in the stellar wind is large enough for recombination cooling to be rapid in the regions where nonradiative heating has stopped They adopt a velocity law that increases linearly with radius out to 1 5 R_* and which then approaches 2800 km s^{-1} asymptotically at large distances. Under these conditions, the coronal region produces a large bump in the infrared continuum between 20 and 100 μ, with a maximum excess of 2 mag. These calculations show that the effect of the coronal regions cannot be neglected in the interpretation of the infrared excesses, and that their contribution must be evaluated in the case of the Be stars This would make it possible to count all the sources of free-free emission in the outer atmospheres of these stars. Up to now, the distinction between the excesses due to free-free emission and those due to thermal re-emission by dust particles have been based solely on an estimate of the effects of the cold envelope, in which the visible emission lines arise. Cassinelli and Hartmann clearly show that this estimate is incomplete.

Radio Emission from Be Stars

The common characteristic of the stars for which radio emission has been detected is the presence of dense, extended circumstellar regions. From this point of view, the Be stars are high on the list of stars to be observed in this spectral region. But up to now, the number of undetected Be stars is much larger than the number detected. The review article by Purton (1976a) gives an excellent summary of this question and contains many references.

The only Be stars for which radio emission has been detected, until now, are the Bep stars, that is, those which exhibit forbidden emission lines in their optical spectrum and which have large infrared excesses which are generally attributed to thermal re-emission by circumstellar dust. The B[e] stars are also the ones that have the most extended and densest atmospheres. No conventional Be star seems to have been detected in the radio range as yet, and only upper limits on the flux are available for them. In spite of this apparent correlation between strong infrared excesses and radio emission, the surveys that have been made show that it is not possible to predict the behavior of a star in the radio region from its infrared properties (Altenhoff et al., 1976)

The observed radio spectra are of two kinds. those in which the flux, S_ν, increases with ν, and those in which the flux is approximately constant with frequency These two kinds of spectra are compatible with free-free emission that arises in an optically thick region, in the former case, and in an optically thin region, in the latter case. When the electron density of the medium is uniform, the flux emitted in the optically thick case is proportional to ν^2 for $\nu < \nu_c$, while in the optically thin case the flux is proportional to $\nu^{-0.1}$, for $\nu > \nu_c$. When the electron density distribution is not uniform, the flux depends on ν in a different way, thus, the observation of the radio spectrum provides information on the density structure of the outer atmosphere. If the outer atmosphere originates in the mass flux of the star, the density distribution follows an inverse square law in the regions in which the expansion velocity is constant In the case of a completely ionized gaseous envelope, spherically symmetric and with constant T_e, the radio flux of an optically thick source can be written

(Panagia and Felli, 1975)·

$$S_\nu = 32.7 \left(\frac{n_0 r_0^2}{10^{36}\text{cm}^{-1}}\right)^{4/3} \left(\frac{\nu}{10\text{ GHz}}\right)^{0.6}$$

$$\times \left(\frac{T_e}{10^4\text{ K}}\right)^{0.1} \left(\frac{d}{\text{Kpc}}\right)^{-2} \text{ m.f.u}, \quad (11\text{-}5)$$

where n_0 is the electron density at the photosphere, whose radius is r_0; then the radius of the region that emits half of the observed flux is

$$R_\nu = 1.57 \times 10^{15} \left(\frac{n_0 r_0^2}{10^{36}\text{ cm}^{-1}}\right)^{2/3}$$

$$\times \left(\frac{\nu}{10\text{ GHz}}\right)^{-0.7} \left(\frac{T_e}{10^4\text{ K}}\right)^{-0.45} \text{ cm}, \quad (11\text{-}6)$$

from which it can be seen that the radius $R(\nu)$ is a decreasing function of ν. In the case considered, the mass loss rate $\dot{M}$ can be determined from the radio spectrum, as long as the expansion velocity u_{exp} in the relevant regions and the distance of the star are known. Panagia and Felli derive the following expressions:

$$\dot{M} = 4\pi r^2 n_e(r) u_{exp} \mu m_H, \quad (11\text{-}7)$$

where μ is the mean atomic weight per electron, and

$$S(\nu) = 5.12 \times \bar{Z}^{-2/3} \left(\frac{\nu}{10\text{ GHz}}\right)^{0.6} \left(\frac{T_e}{10^4\text{K}}\right)^{0.1} \quad (11\text{-}8)$$

$$\times \left(\frac{\dot{M}}{10^{-5} M_\odot \text{yr}^{-1}}\right)^{4/3} \left(\frac{\mu}{1.2}\right)^{-4.3} \left(\frac{u_{exp}}{10^3\text{ km s}^{-1}}\right)^{-4/3} \left(\frac{d}{\text{kpc}}\right)^{-2} \text{m.f.u},$$

where $\bar{Z}$ is an average ionic charge taking into account the composition of the gas. If the density decreases more rapidly than r^{-2}, the velocities are accelerated outward and the radio spectrum has a steeper slope. Details of the calculations leading to formulae for the flux in the general case, and in many particular cases, can be found in Panagia and Felli (1975), Wright and Barlow (1975), and Olnon (1975).

One of the best-observed Be stars in the radio range is MWC 349, which is classified Bep Its spectrum, which is shown in Figure 11-26 (Purton, 1976a), is that of an optically thick gas at all observed frequencies. The flux varies as $\nu^{0.7}$, that is, it corresponds approximately to an r^{-2} density distribution. The radio data, combined with a measurement of the emission volume at Hβ, imply a density between 10^6 and 10^8 cm^{-3} for the regions near the star, in which Hβ is formed (Olnon, 1975). The uncertainty in this value is largely due to the uncertainty in the circumstellar extinction correction, which is estimated at around 9 mag in the visible and which is needed to determine the flux emitted at Hβ. Note that the derived value of n_e is much lower than the value (10^{12} to 10^{11} cm^{-3}) adopted in the models that are used to compute the Hα profiles (see the section on Be Star Models Based on Observations at Visible Wavelengths).

For a certain number of objects, the radio spectrum is of the form $S_\nu \propto \nu^{+1}$. Such a fre-

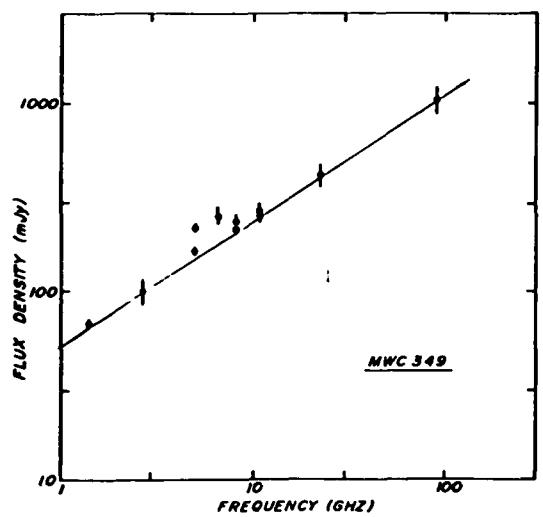

Figure 11-26. The radio spectrum of MWC 349 is that of an optically thick gas at all observed frequencies (from Purton, 1976a).

quency dependence can be explained by a density distribution that falls off more rapidly than r^{-2}; it corresponds to the case in which the expansion velocity in the medium is accelerated. Marsh (1976) has suggested that when the star is surrounded by an envelope of circumstellar dust, the viscous force of the dust particles pushed by the radiation pressure could provide an effective mechanism, provided that the gas and the dust are uniformly mixed. Another explanation rests on the assumption that the density, in fact, follows an inverse square law, but that it is truncated for a certain value of the outer radius (Marsh, 1975). In this case, the mass flux is not continuous; the cut-off corresponds to the finite size of the envelope, which was ejected during a limited time.

The second kind of radio spectrum observed among the Be stars is one in which the flux remains approximately constant with ν, it corresponds to free-free emission in an optically thin gas. Figure 11-27 shows the spectrum of MWC 957. This star exhibits an infrared excess that is interpreted as free-free radiation (Allen, 1973), but if one tries to predict the infrared spectrum by extrapolating the observed radio spectrum, one obtains an infrared flux only half as large as the observed value. This could result from the fact that part of the infrared excess is produced by thermal emission from dust particles (Marsh et al , 1976). This behavior of the radio and infrared spectra is not unusual, it is also observed in other emission-line stars and in symbiotic stars.

The characteristics of the radio spectrum of the Bep stars are not peculiar to these stars alone, they are found among objects that belong to different classes, both according to their spectral type and from the point of view of their evolutionary state, like the Wolf-Rayet stars, the symbiotic stars, the planetary nebulae, for example This same remark has already been made concerning the infrared spectrum. In other words, the radiation arising in the outer regions of the atmospheres of emission-line stars, taken as a whole, can exhibit great similarities for objects of different classes. And much greater differences can be observed within a single class of objects than among certain objects that belong to different classes.

As the nature of the stellar emission becomes more complicated by the presence of new peculiarities—such as, the forbidden lines—the classification of emission-line stars into different groups becomes more and more ambiguous, and it is not unusual to see the same star appear in catalogues of different types of objects. This ambiguity clearly results from the fact that the "emission" phenomenon, which is a consequence of the existence of a mass flux, can exhibit very diverse characteristics for a single spectral type, depending on the value of the mass flux; the latter parameter determines the density distribution in the outer atmosphere of the stars The classification sequence set up in the visible, which amounts to a classification of the stellar photospheres, does not correspond to the classification that could be defined from the characteristics of the infrared and radio spectra of the same stars. This shows that the properties of the atmospheric regions outside the photosphere do not depend only on the parameters T_{eff} and g_{eff} which describe the photosphere.

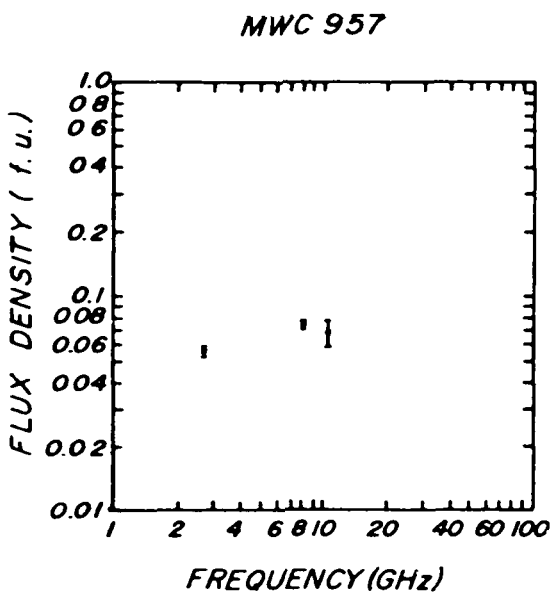

Figure 11-27. The radio spectrum of MWC 957 is that of an optically thin gas (from Marsh et al , 1976).

VARIABILITY OF THE LINE SPECTRUM AND THE CONTINUOUS SPECTRUM IN THE VISIBLE AND THE NEAR INFRARED REGIONS

As a general rule, all the Be stars are variable in their line spectrum as well as in their continuous spectrum. This variability has been observed mainly in the visible region, but when the observations are extended to other spectral regions, such as the infrared and the ultraviolet, it becomes apparent that this is a general characteristic. In order words, this aspect of the problem cannot be considered to be secondary; any interpretation of the Be phenomenon must account for it. But variability is not a characteristic peculiar to the Be stars; it is observed in all the classes of emission-line stars that are found throughout the HR diagram. The body of observations pertaining to the Be stars is among the richest data sets in existence, because the baseline extends over nearly a century in time, and because many different spectral features have been studied. Nevertheless, it is impossible to provide a general outline of the behavior of these stars. After a century of observations, it is impossible to predict the long-term behavior of any Be star. This is essentially due to the irregular nature of the variations and to the individual characteristics of the stars. It is also a result of the fact that almost all our knowledge of the variability of the Be stars comes, until now, from observations of a single spectral region, the visible. We do not yet have an overall view of the behavior of the entire outer atmosphere of the star, from the chromospheric and coronal regions—which are observed at ultraviolet and X-ray wavelengths—to the most distant regions—which are observed at the radio wavelengths The region in which the visible emission lines are formed is only an intermediate one, which does not, in itself, enable us to extrapolate to the behavior of the other regions However, the behavior of this region—whose very existence defines the Be star anomaly—must form the basis for the interpretation of these stars

General Characteristics of the Variability of the Line Spectrum

The variability of the Be stars presents itself in a variety of forms. We observe the following (1) the transformation of a normal spectrum into a peculiar spectrum, and vice versa, (2) the transformation of a spectrum having one kind of peculiarity into a spectrum that has another kind of peculiarity—a Be spectrum can change into a shell spectrum, and vice versa, and (3) changes that are not associated with a change in the type of spectrum. Within a single phase (Be or shell), the intensities, the profiles, and the wavelength shifts of the lines are more or less variable, depending on the star. Be or shell stars can lose all their emission or shell features and become normal stars. Some stars have been observed to go back to the Be or shell phase after a few months or years, while others still have a normal B spectrum after several decades A non-negligible number of the stars that appear in Be star catalogues exhibit a normal B spectrum at the present time, and there is no way to distinguish the spectrum of an ex-Be star from that of a normal B star The reverse situation has also been observed a B star that has been known for decades to have a normal spectrum can suddenly exhibit a Be or shell spectrum Variations (1) and (2) can take place several times for the same star, with the transition between the Be, shell, and normal B phases occurring in any order These phenomena have been observed in so many Be stars that they cannot be considered exceptional This type of observation strongly suggests that the Be spectrum, the shell spectrum, and the normal B spectrum are only phases in the variation of a single object, and do not represent different kinds of objects or different stages of evolution.

The fact that normal B stars can become emission-line B stars for a certain time, and vice versa, raises the question of whether any normal B star is capable of temporarily developing this peculiarity If this were the case, the presence of emission lines and the existence of variations would have to be considered as phenomena exhibited by normal stars, thus violating the equilibrium conditions postulated by the classical

theory of stellar atmospheres. This is not a new question, Struve raised it as early as 1942 in a review article. The more recent observations in the ultraviolet spectrum show the problem in a more universal light, for in this spectral range, variability is observed in normal stars as well as in peculiar stars, and there are often greater differences among normal B stars of the same spectral type than between B and Be stars (Costero et al., 1981).

Just as the observation of a sample of Be stars at a given time shows the diversity of their spectral characteristics, so the observation of particular Be stars over a fairly long period—several decades—shows that they exhibit different spectral features and behaviors at different times There is a large body of data concerning the variations of the Be stars, which is impossible to review completely here. The reader is referred to the catalogues and bibliographies of Merrill and Burwell (1933, 1943, 1949, 1950) for observations made earlier than 1950, to the bibliography of Jaschek et al. (1971), and to the Be star atlas of Hubert-Delplace and Hubert (1979), which is made up of the low-dispersion spectra obtained by R. Herman and her group between 1953 and 1976, at the Haute-Provence Observatory A great deal of information can be found in the IAU Symposia No. 70 and No. 98 devoted to Be stars.

If one tries to group some of the Be stars according to the spectral features they have exhibited at a given time, one observes that there are also large differences in their behavior; this is the very hallmark of the individuality of these stars. Jaschek et al (1980) tried to distinguish different groups of Be stars according to their spectral features and their behavior over 20 years of observations. However, earlier observations show that the stars from one group migrate into another group in the course of time, making this classification meaningless.

The degree and pattern of variability differ from star to star, and for a given Be star, they may differ from epoch to epoch. In certain cases, long, relatively quiet periods (of the order of decades) are observed, followed by short, highly active periods (of the order of years), and so on. In other cases, there is a more or less regular oscillation of the variations which are damped out at varying time scales, and that pattern may repeat. These oscillations can take place over months, years, or decades. Be stars behave in a highly individual manner, up to now, there is no way of predicting their behavior. Moreover, recent ultraviolet observations show that the visible spectrum is not sufficient to define the "quiet" and "active" periods of Be stars. For example, observations of 59 Cyg reveal the existence of spectacular variations in the ultraviolet spectral region, while the visible spectrum exhibits relatively weak Balmer emission (Doazan et al, 1981a, see also Chapter 12)

Because of the generally irregular nature of the variations, the study of long-term behavior allows us to determine time scales only and not, strictly speaking, periods. These time scales are generally not the same for all the variable features in the spectrum. In some stars, some of these features are correlated with each other, while other features may vary on a completely different time scale. Thus, there is great confusion when the "period" of the variation is mentioned, without specifying which phenomenon is being considered and especially without taking into account the fact that the phenomenon is generally not periodic. We shall review the various features of the line spectrum whose variations have been studied.

Phase Variations. Phase variations—that is, the transformation of a Be spectrum into a shell spectrum and/or a normal B spectrum—are the most striking feature of the variability of Be stars. In the subsection on Variability Patterns in Individual Stars, a series of profiles of γ Cas, 59 Cyg, and Pleione illustrates these changes. The total duration of each of the phases (months, years, decades) depends on the star and on the epoch at which the variations take place These changes can occur in any direction and can take place several times for the same star The time interval between two Be phases, two shell phases, or two normal B phases can be very different from one epoch to another, for the same star. For example, in more than a century γ Cas has

exhibited only two shell phases, separated by four years; and in spite of the fact that this star has been observed with exceptional regularity, the epoch of the next shell phase (if there is one) cannot be predicted. The time intervals can also differ greatly from star to star, for 59 Cyg, the time interval between the last two shell phases was 1 year while for Pleione it was 35 years. No one time scale represents this phenomenon better than another. Of all observations in the visible spectral region, the phase variations and the E/C variations, which are described below, give the most direct indication that the mass flux in Be stars is variable.

E/C Variations. E/C is the ratio of the emission in the lines to the adjacent continuum. The variation of this quantity simply represents the variation in the strength of the Be phenomenon. E/C variations have been traced over half a century or more for a few Be stars (see, for example, Lacoarret, 1965; Kitchin, 1970a).

The time interval between two successive maxima of the line emission is variable from one star to another; for a given star, it also varies with the epoch of observation. The observed time scales are of the order of months, years, or decades. HD 174237 seems to be the Be star that has exhibited the shortest time scales, seven days, for the variation of emission (Lacoarret, 1965). Figure 11-28 shows the variation of the Hα line in μ Cen, as observed by Peters (1979) at an epoch when the E/C variations were the dominant feature of the line variability. Note that also in this figure the emission line becomes broader as the emission grows stronger. This observation shows that there cannot be a very close correlation between the width of the emission lines and v sin *i*. For a given Be star, there is no unique value of the width of the emission line; it can vary with time. Moreover, if it is assumed that the envelope is only rotating, then the hypothesis of the conservation of angular momentum, which is generally adopted, implies that the emission line should be broadest when the emission is weakest. This conclusion is completely contradicted by the observed variations in μ Cen and in some other stars. Throughout this

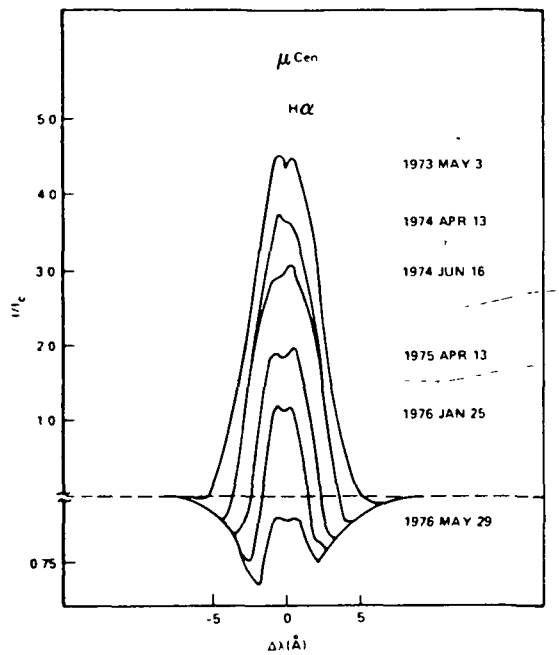

Figure 11-28. The decreasing intensity of the Hα emission line in μ Cen from 1973 to 1976 (from Peters, 1979). Note the large variation of the emission line width. This demonstrates that a given value of v *sin i is not tightly correlated to the width of the emission line.*

section, we shall encounter other data that create difficulties for the rotation model.

Profile Variations. One of the most striking features of the profile variations in the emission lines is the variation of V/R, the ratio of the violet to red emission peaks. In a certain number of stars, such a variation takes place although the total emission in the line does not vary greatly. This type of variation has been especially studied by McLaughlin (1937), who discovered a quasi-periodic oscillation of this ratio for certain Be stars, which he called V/R variables. The time scales of these oscillations are of the order of years. This quasi-periodic behavior can last for some time, and then disappear. It is not a permanent feature that makes it possible to distinguish a particular category of Be stars, at any epoch. This is the case with the V/R variations of the Hβ line in β^1 Mon, which were observed by Cowley and Gugula (1973) over a long baseline. It

can be seen in Figure 11-29 that these variations are repeated three times in a row, with a quasi-period of 12.5 years; before and after this series of three oscillations the variations fade away. The radial velocity of the central absorption and the emission edges undergo changes that generally follow the V/R variations. It can be seen in this figure that the emission line as a whole is shifted, so that the V/R variations cannot be interpreted as a shift of the absorption line within a fixed emission line. In several stars, the whole emission line, as well as the central absorption, is shifted toward long wavelengths when $V/R > 1$; there is a shortward shift when $V/R < 1$. This is the case with β^1 Mon, in which the observed shifts are of the order of 50 km s^{-1}. For the shell spectrum, the shifts of the emission line seem to be much smaller than those of the central absorption.

If we examine the V/R variations of the various Balmer lines, we often observe that the behavior of these lines differs from one to another; the V/R ratio may be much greater than one for Hγ, for example, and much smaller than one for

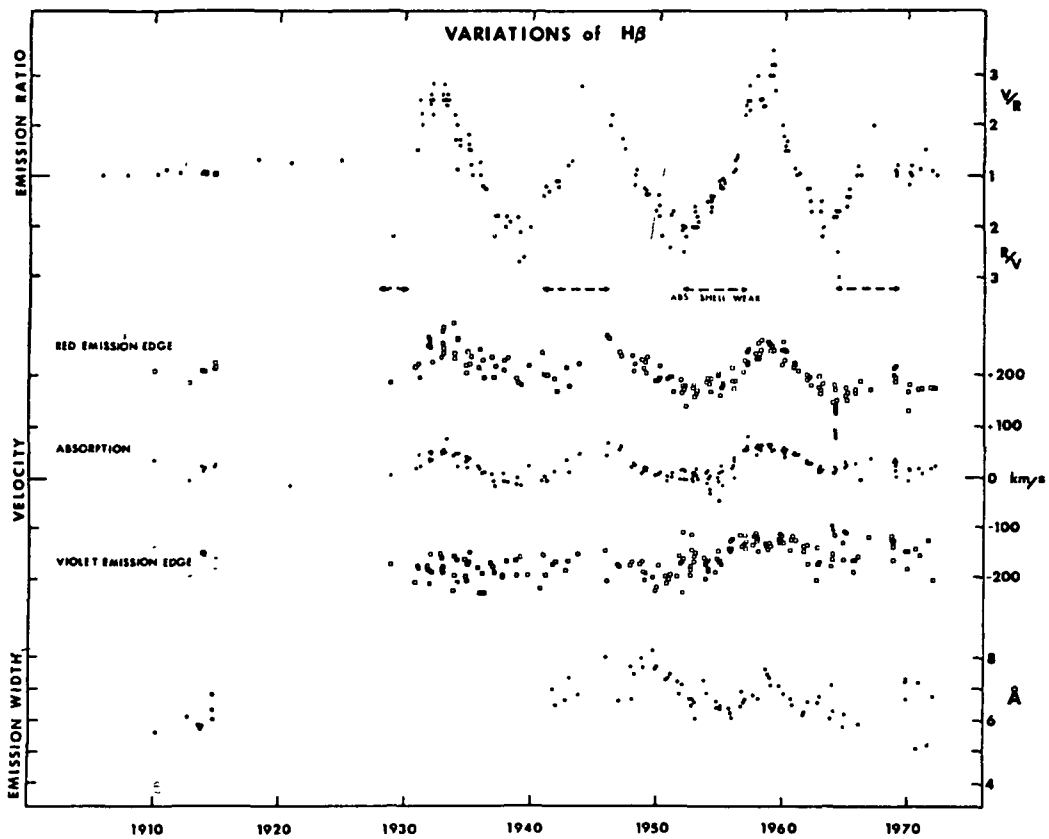

Figure 11-29. Variation of Hβ in β^1 Mon. The V/R ratio of the red and violet emission peaks, shown at the top of the figure, are eye estimates. The dashed line under this curve indicates when the central absorption component in the hydrogen lines was weak or even absent. In the central part of the figure the filled circles represent the velocity of the central absorption and the open circles the velocity of the red and violet outer emission edges. Note that the whole emission line is displaced, so that V/R variations cannot be interpreted as resulting from the displacement of an absorption feature across an undisplaced emission line At the bottom is shown the change in the total width of the Hβ emission, demonstrating that a given value of v sin i cannot be tightly correlated to the width of the emission line Here the width of the line varies from about 300 km s^{-1} to 450 km s^{-1} (from Cowley and Gugula, 1973)

the higher members of the series. A similar but much more recent observation was made by Krautter and Bastian (1980) for DR Tau, a T Tau star. In this star, the lower members of the Balmer series have a P Cygni profile, while on the same spectrogram, the higher members are observed to have an inverse P Cygni profile. This comparison strongly suggests that the observed phenomenon is widespread in the outer atmospheres of emission-line stars, and there must be a single explanation for it. This also shows that one cannot construct a model to represent the envelope of a Be star on the basis of a single Balmer line.

In Struve's picture, the broad, underlying absorption lines are formed in the photosphere of the rapidly rotating star, while the Balmer-line emission is formed in a rotating envelope or gaseous ring. Such a model cannot account for the asymmetries or for the profile variations. Just as Struve was proposing the rotating model, McLaughlin (1931, 1933) suggested a model which combined Struve's rotating envelope model with the expanding envelope model proposed by Beals (1930) to explain the P Cygni type profiles. In this model, which implicitly assumes that the atmosphere is optically thin, an emission line with $V/R < 1$ is produced in a rotating, expanding atmosphere, while a line with $V/R > 1$ is produced in a rotating, contracting atmosphere. McLaughlin himself later rejected this model because it did not account for the shift of the entire emission line. Note, however, that most of the present ad hoc models have completely resumed the model of a rotating, expanding atmosphere, as initially proposed by McLaughlin.

Struve (1931a), M. Johnson (1958), and later McLaughlin (1961) suggested that the V/R variations, and especially the shifts in the emission lines, could be explained by the rotation of the line of apsides of an equatorial, elliptical ring of gas, in which the atoms follow Keplerian orbits. This model, which was developed by Huang (1972, 1973) and Albert and Huang (1974), makes it possible to obtain good agreement with the observations by adjusting the geometric parameters of the model. But it cannot explain the case in which V/R is less than 1 for the lower Balmer lines and greater than 1 for the higher ones.

The V/R variations are only an outline of the profile variations of an emission or shell line. When E/C varies, as it does for most Be stars, the V/R variations are not enough to characterize the variations of the line. A gradual change in the profile with time is generally observed, combining the E/C and V/R variations. In some stars, like ζ Tau, the V/R variations dominate the E/C variations, a change from a P Cygni profile to an inverse P Cygni profile has been observed in a matter of years (Delplace, 1970). In other stars, the V/R variations are much smaller than the E/C variations (for example, Pleione and γ Cas, discussed later).

When observed at high resolution, the profile of an emission or shell line is generally not smooth, but shows a certain amount of structure. When the same star is observed at short time intervals—minutes, hours, or days—small, rapid, irregular variations can be detected. These variations have been reported for the lower Balmer lines. Rapid variations in the total emission strength have been observed (Bahng, 1971, 1976; Slettebak and Snow, 1978), as well as profile variations (Hutchings et al, 1971; Hutchings, 1967, 1969b, 1976, Doazan, 1976). Bijaoui and Doazan (1979) developed a method of cross-correlation analysis which they applied to high-resolution (0.15 Å) observations of α Col. They observed a slow, weak variation extending over several nights, on which were superimposed rapid, irregular variations; according to the statistical tests applied, these variations were real

The reality of these rapid variations has been questioned by Lacy (1977), whose analysis of observations at a resolution of 4 to 5 Å shows that fewer than 5 percent of the Be stars undergo detectable variations. Slettebak and Reynolds (1978) reach a similar conclusion from observations at a resolution of 5.5 Å, although, on the other hand, Slettebak and Snow (1978) also indicate the presence of rapid variations in γ Cas. Note that the various authors cited above have generally used different detectors with different spectral and temporal resolutions, so that the relative amplitude of a detectable variation is

different for each of them Most of the reported variations are concerned with rapid changes in the structure of the profile, they can obviously be detected only at high resolution, whereas the absence of variations has been concluded from low resolution spectra. Moreover, the irregular nature of the variations requires the same star to be observed continuously for several successive nights, in order to detect the changes

A new type of rapid variation has recently been discovered by Baade (1980, 1981) in the bright Be star 28 CMa. The novel aspects of this variation are, first, its periodicity (1 36 days), and second, the fact that it has been observed mainly in the absorption lines. The previously reported variations generally involved the emission lines and, in most cases, it was impossible to determine a true period for them.

The profiles of all the absorption lines are affected by the variability of 28 CMa, there are changes in the asymmetry of the line as a whole. Figure 11-30 shows the He I lines at 4026 and 4009 Å. These profile variations are strikingly similar to those observed in the β Cephei stars. They seem to be accompanied by small V/R variations in the H I and Fe II lines. An interesting feature of these variations is their short period, which has apparently not changed over an interval of more than 9 years. For completeness, we point out that Harmanec (private communication) has offered a binary interpretation of these rapid variations

Note, finally, that the detection of the variations in 28 CMa was possible for three reasons (1) the star was observed at high dispersion, which has only rarely been the case in the search for rapid variations in the Be stars; (2) the star was bright enough to allow a good time resolution (5 minutes) with a medium-sized telescope; (3) the He I lines in this star were relatively sharp for a Be star (v sin i = 80 km s^{-1}) If the lines had been broad, it would have been impossible to detect the variations, considering their small amplitude.

A great deal of evidence has now accumulated for the existence of rapid variations in the line spectrum of the Be stars. The small amplitude of these variations makes them difficult to detect. If they were of the same type as those observed in pulsating variables, they would provide a new approach to the study of the variability of Be stars

Radial Velocity Variations. Measurement of the radial velocities of the shell or emission lines indicates whether the envelope is expanding, contracting, or stationary, if the radial velocity of the star is also known. The latter can be determined from the photospheric lines if they are not perturbed by absorption or emission lines from the envelope. But these lines, for example, the He I lines, are generally broad and weak, so that measurements of their position are often inaccurate.

Expansion is often observed, but in some cases there is also a sequence of expanding and contracting motions. The radial velocities measured in the visible range are generally low, of the order of 50 km s^{-1}; they may reach or exceed 100 km s^{-1} at certain rare epochs of high activity.

Because of the accuracy of position measurements for sharp absorption lines, the behavior of the radial velocities of the envelope lines has been studied in great detail from shell spectra. In many stars, the radial velocities of the sharp

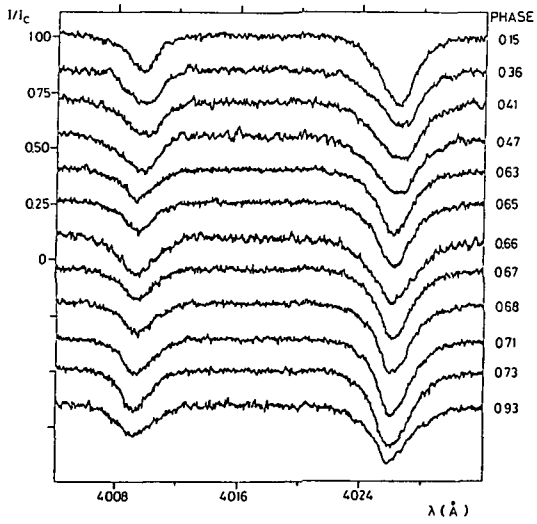

Figure 11-30. Short-term variability of the He I lines λ 4026 and λ 4009 Å of 28 CMa during the period of 1.36 days (from Baade, 1981)

absorption cores have different values for the different lines in the Balmer series; the variation of the velocity as a function of the number of the line in the series defines the Balmer progression Merrill, who introduced this term, studied the variation of the Balmer progression with time in a large number of Be stars. If the point at which the various lines in the series are formed can be localized, then the sign of the progression indicates whether the expansion or contraction is accelerated or decelerated Thus, the behavior of the Balmer progression can provide important information concerning the velocity field in the envelope. It has generally been assumed that the higher members of the series are formed in deeper layers than the lower members.

It has been shown that for HD 50138 (Doazan, 1965) and HD 218393 (Doazan and Peton, 1970), there are successive periods of accelerated expansion and decelerated expansion in the envelope For these two stars, the largest velocity variations occur for the higher members of the Balmer series—that is, in the deepest layers of the envelope—while the smallest variations take place in the surface layers

The behavior of the velocities of ζ Tau and 48 Lib has been studied in detail on a long time scale. A documented description of the variations of these two stars can be found in Underhill (1966a), Delplace and Chambon (1976), and Aydin and Faraggiana (1978). An analysis similar to that made for the preceding two stars, under the same hypotheses, shows that the largest motions take place in the deepest layers However, instead of an expansion that is alternately accelerated and decelerated, a sequence of expanding and contracting motions is observed in the envelope, that is, a series of ejections and falling back of material

When a star changes from one phase to another, for example, from a shell phase to a Be phase, the radial velocities often undergo a large variation. In the case of Pleione, the disappearance of the shell was accompanied by a large increase in the expansion velocity for the higher members of the Balmer series. For 59 Cyg, the behavior was different. the maximum expansion velocity was observed at the time of maximum strength of the shell phase, the expansion subsequently decreased, and returned to its initial value when the shell spectrum completely disappeared (Barker, 1979). For 88 Her, on the other hand, no change was observed in the behavior of the radial velocities during the transition from a shell spectrum with hydrogen and metals to a shell hydrogen spectrum alone, and vice versa. These three examples show that the behavior of a single Be star cannot be considered as typical of the behavior of Be stars in general, such an assumption neglects one of the fundamental properties of the Be stars, their individuality

The variations of the radial velocities, like those of the other spectral characteristics, are generally not periodic. The time scales of these variations are very different from one star to another. The velocities have been observed to oscillate on time scales ranging from a few days to years or decades.

In some stars, however, like 88 Her and 4 Her, the radial velocities of the shell lines exhibit low-amplitude, strictly periodic variations This periodicity has been interpreted by Harmanec et al. (1973, 1974) in terms of orbital motion, although, on account of the inaccuracy of the measurements of the photospheric lines, it was only possible to show that these lines followed the radial-velocity curve, in a statistical sense For these two stars, the radial-velocity periods are not correlated with the observed long-term variations of the spectrum. In these two cases, for which very detailed information is available, the signs of the Be phenomenon are completely independent of the period of the proposed binary system. Given the inherent ambiguity of representing the radial motion of a star by the velocities of lines formed in an envelope which is itself in motion, a question arises as to whether the periodic variation of the radial velocities represents a periodic variation of the envelope or the binary nature of the star If it is a variation of the envelope, the total absence of correlation with the long-term behavior of the spectrum is difficult to understand. If it is a binary system, this lack of correlation would indicate that the Be phenomenon in the primary is completely indepen-

dent of the presence of the companion.

The study of radial velocities in the visible region provides information only on the motion of the cool envelope with respect to the photosphere. In order to study the motion of the entire outer atmosphere of the star, one must know the velocities of the various regions from the photosphere to the intersection with the interstellar medium, including the chromosphere, the corona, and the post-coronal regions. An empirical model of the outer atmosphere of a Be star should account for the behavior of the radial velocities in the visible and the ultraviolet regions.

The most important result of the analyses of radial velocities in the visible region is that the shifts of the emission or shell lines are usually small, of the order of 50 km s^{-1}, and are rarely greater than 100 km s^{-1}. Expanding motions have most often been emphasized, but alternating sequences of expansion and contraction are also observed. The velocities in the envelope are much smaller than the escape velocity at the photosphere for the star with the highest observed value of v sin i, so that the conclusion that a mass flux exists, from observations in the visible region, depends entirely on the model. In the extended envelope model developed from Struve's hypothesis, the degree of excitation decreases outward, and the regions in which the emission and shell lines are formed are located at a distance of several stellar radii The escape velocity in these distant, low-excitation regions is reduced by the distance factor, thus, a low expansion velocity can indicate the existence of a mass flux if the envelope is sufficiently extended

The observations made in the ultraviolet spectral region have had a profound effect on the model constructed to explain the observations in the visible. As we shall see in Chapter 12, these observations have brought to light (1) large expansion velocities, which exceed the escape velocity at the surface of the star, at certain phases of the variations, thus demonstrating the existence of a mass flux, (2) chromospheric regions, detected by the presence of lines of superionized elements. Struve's extended envelope model is completely incapable of assimilating these new data without considerable modification. This model, based on the existence of regions cooler than the photosphere, is characterized by low velocities. Regions hotter than the photosphere, characterized by high expansion velocities, must be added. The Balmer lines in emission and the shell lines cannot be formed in the chromospheric or coronal regions close to the star, they must be produced in regions where the outer atmosphere has been sufficiently cooled, that is, in distant regions of the atmosphere. Moreover, the low observed values of the radial velocities require that the high velocities of the stellar wind observed in the chromospheric and coronal regions must have been decelerated in the cool regions. Thus, an overall radial structure of the velocities in the outer atmosphere is suggested by the observations in the ultraviolet and the visible regions. If the chromosphere and the corona lie close to the star these high velocity regions must give way to a low velocity and more distant cool region. This empirical overall velocity structure is required for stars with small values of v sin i (pole-on) as well as for stars with large values of v sin i (equator-on).

General Characteristics of the Variability of the Continuous Spectrum

Like the line spectrum, the continuous spectrum of the Be stars undergoes variations They have most often been observed in the visible region, by means of broadband photometry. The luminosity and color variations exhibit a great diversity from star to star, and highly individual characteristics. As for the line spectrum, these variations are generally irregular, their time scales may run from a fraction of a day to several decades.

A statistical study by Feinstein (1968) shows that nearly half of the 72 stars he observed over a period of 3 years vary by more than 0.06 mag in V, around one-third of them vary by more than 0.06 mag in (U − B), and one-fifth of them vary by more than 0.06 mag in (B − V). The variations can apparently be either smooth or irregular; in this sense, they exhibit the same characteristics as the visible spectrum. Variations

of the order of 0.3 mag have been observed. This photometric variability of the Be stars has been amply confirmed by further studies (Feinstein, 1970, 1975; Jaschek and Ferrer, 1971, Haupt and Schroll, 1974, Nordh and Olofsson, 1977, Harmanec et al., 1980). A few rare stars have been observed quite regularly, both photometrically and spectroscopically, for example, γ Cas, Pleione, and 88 Her. The study of individual stars shows that the amplitudes of the variations can be large during relatively short time intervals, of the order of months. These variations generally take place when the line spectrum exhibits high-amplitude variation within a single phase, or when the star changes phase. At these particular times, certain correlations clearly stand out.

First, when there is increasing emission in the Balmer lines during a single Be phase, the luminosity of the star increases in the V band, the (B − V) color index reddens, the reddening in the Paschen continuum increases, and vice versa. This correlation was very clearly observed in γ Cas during its spectacular variation of 1936 to 1942. It has also been demonstrated in the long-term variations of other Be stars, such as π Aqr (Nordh and Olofsson, 1977) and X Per (Divan et al., 1981). But an analysis of the variations of γ Cas, Pleione, and 88 Her also shows that there is no one-to-one correspondence between the visual magnitude and the color or the Balmer-line emission, that is, the star can have the same visual magnitude while its line spectrum is completely different (see the next subsection). This means that if one considers two corresponding epochs, either in two different Be phases separated by a shell phase, or in two Be phases of which one has increasing emission and the other decreasing emission, an increase in the line emission between these two epochs will not necessarily correspond to a greater visual luminosity or to a redder (B − V) color index. In the case of π Aqr, Nordh and Oloffson show that the (U − B) index becomes bluer when the Hβ emission increases, indicating flux excess in the Balmer continuum with respect to the Paschen continuum For X Per, Divan's (1979) measurements show, in addition, that the reddening in the Balmer and Paschen continua increases when the Hα emission increases.

Second, both a transition from a Be phase to a shell phase, and one from a hydrogen shell phase to a hydrogen-plus-metals shell phase are preceded by a large, abrupt decrease in the luminosity of the star from the near ultraviolet to the red spectral region. This phenomenon, which has been observed for Pleione, γ Cas, 59 Cyg, and 88 Her, is hard to catch in the process, for it takes place rapidly (in less than a year) and is unpredictable. Very regular spectroscopic and photometric observations covering years or decades are generally necessary to show it. If this correlation were of a general nature, it would be of basic importance to study it in order to understand the shell phase phenomenon. In order to do so, it would be necessary to organize regular, simultaneous photometric and spectroscopic observations of a certain number of Be stars, over the greatest possible wavelength range. The variations of Pleione and 88 Her, which we shall describe in the next subsection, clearly show the sharp, abrupt nature of this transition.

In contrast to these examples, in which the continuous spectrum and the line spectrum exhibit some correlation, there are stars in which large, quasi-periodic variations in the continuum (of the order of 0.1 mag in the U band) are observed on very short time scales (hours or days). At the same time, the line spectrum undergoes little variation. Attempts have often been made to reduce the rapid variations of the continuum to a single period, but without success until now However, the order of magnitude of the time scale remains remarkably constant over decades— 0 7 day, for example, for EW Lac (Lester, 1975). This quasi-periodicity of the rapid variations is strikingly similar to β Cephei-type behavior. These observations led Percy (1979) to conclude that "the major light variations of Be stars occur on a time scale of hours, rather than a time scale of days or weeks as previously believed " However, as Harmanec et al. (1979) point out, the long-term variations in light and color are always most pronounced in the well-observed cases. These relatively large rapid variations in the continuum contrast with the small rapid variations in

the emission lines that have been detected up to now.

This double aspect (long-term and short-period) of the variability strongly suggests that a superposition of two different phenomena is being observed. the long-term variations may result essentially from variations in the opacity of the envelope and mainly reflect variations in the mass flux, while the rapid variations may be connected with the phenomena observed in short period variables. For periods shorter than 0 3 day, there could be radial pulsation, while for longer periods the variations could be due to nonradial pulsations, like those that Smith (1977) has observed in a certain number of B stars. Note, finally, that it has also been suggested that this phenomenon may be related to the rotation of the star The stars in which rapid light variations have been observed are also known to have undergone long-term variations in their spectra, with or without one or more transitions from a Be phase to a shell phase and/or to a normal B phase. Their spectral features and their behavior in the visible region do not distinguish them from the other Be stars.

Variability Patterns in Individual Stars

To illustrate the behavior of the Be stars, five of them will be described in this section. γ Cas, 59 Cyg, Pleione, 88 Her, and EW Lac. γ Cas and 59 Cyg were chosen because they have exhibited very similar variations in the visible spectrum over a long period of time (nearly 70 years). They are also the Be stars for which the largest variations have been observed in the ultraviolet region. The second pair, Pleione and 88 Her, have exhibited spectacular variations in the visible, in both line and continuous spectra. These are the stars for which we have the most complete observations concerning long-term behavior in the lines and the continuum during a phase transition. At different epochs, these two pairs of stars have exhibited different phases from those in which we see them today Striking similarities emerge from their long-term behavior, but there are also profound differences in the amplitude and duration of their variations, thus demonstrating the individuality of the Be stars The history of their variations shows that a particular phase cannot be studied in isolation from the sequence of phases that preceded or followed it. A phase of variation does not constitute an isolated phenomenon, but is the result of a series of phenomena This remark explains why any attempt to form groups of Be stars, based on the similarity of certain spectral features exhibited during a relatively short time interval (one or two decades), is meaningless It is actually quite rare for a similarity observed at a certain epoch to continue for long, as shown by observations made at different epochs. The remarkable similarity in the behavior of the long-term variations of γ Cas and 59 Cyg is, up to now, an exception, and has not yet been observed in any other stars Finally, we shall illustrate the double aspect of variability of the continuum in some Be stars by taking EW Lac as an example.

General Characteristics of γ Cas (B0.5 IVe) and 59 Cyg (B1.5 Ve) Secchi discovered the first Be star in 1866 by observing the Hβ line in emission in the spectrum of γ Cas Since then, γ Cas has been observed regularly enough for the history of its behavior to be traced over more than a century, with a reasonable hope that no interesting phase of its variation has escaped the observers. The example of γ Cas is particularly instructive, for the visible spectrum of this star has exhibited, in turn, all the features that are observed in a random sample of Be stars a Be spectrum, a shell spectrum, and a quasi-normal B spectrum; this immediately proves that these different types of spectra do not represent different objects but different phases in the variation of a single object.

γ Cas is particularly interesting because its behavior was long considered unique on account of the spectacular variations in light, color, and line spectra that were observed from 1932 to 1942. However, after the recent period of activity in 59 Cyg, striking similarities have emerged from a comparison of the behavior of these two stars in the visible, over the entire period during which they have been observed Both of them have exhibited (1) a long Be phase, lasting 60 or 70

years, followed by spectacular variations of a few years' duration. During this spectacular episode, ending with a quasi-normal B phase, in which the star exhibited very weak emission in the Hα line alone, two strong, brief shell phases, following two very intense emission phases, were observed, (2) a new slowly and irregularly increasing Be phase, following the quasi-normal B phase.

Thus, a remarkable sequence of events has been observed for both stars for nearly a century, with the Be, Be shell, normal B, and Be phases following each other at a comparable rate. Note also that similar long-term behavior has not yet been detected, to our knowledge, in other Be stars. The example of these two stars shows that a description of a Be star based on observations made on a time scale of 1 or 2 decades gives a very poor representation of the star's behavior. Instead, the Be phenomenon should be analyzed on a time scale of the order of a century. This means that in describing this phenomenon, it is much better to use all the existing observations of a few selected Be stars over the longest possible baseline in time rather than a larger sample of stars observed over too short a time interval.

γ Cas (B0.5 IVe). The spectrum of γ Cas and its variations have been fully described The bibliography of this star is extremely large, and cannot be completely cited in this chapter. We shall indicate only the articles of Baldwin (1940), Edwards (1956), Cowley and Marlborough (1968), Kitchin (1970a), Cowley et al. (1976), Doazan et al. (1980c), and the references therein which provide the essential data on the long-term variations of this star

The long-term variations of γ Cas can be divided into two periods (1) from 1866 to 1942, there was a long, relatively calm Be phase, with moderate to strong emission undergoing small variations from 1866 to 1932. This calm phase ended in an episode of spectacular variations from 1932 to 1942, at the end of which the star fell back into a quasi-normal B phase, (2) from 1942 to 1981, the star went from the quasi-normal B phase to a second, slowly and irregularly increasing Be phase, undergoing small fluctuations and V/R variations.

From 1866 to 1942–A Long Be Phase Ending with the Complete Dispersion of the Envelope. The first observations of γ Cas were made visually, and entailed uncertainties that are difficult to estimate. However, we know that Hα, Hβ, and the D3 line of He I were in emission. Starting in 1888, the many, regularly-spaced photographic observations enable us to trace the history of γ Cas with confidence. For the period 1888 to 1915, there is no evidence for variations in the intensity of the hydrogen emission lines up to H8, nor in the emission lines of singly ionized metals, nor in the He I absorption lines Starting in 1915, a small variation in V/R for Hγ was detected From 1925 to 1932 these variations were stronger, and the visual magnitude varied slightly about its mean value of 2 2 This period can be summarized by saying that for more than 25 years γ Cas did not appear to exhibit variations in its spectrum, while during the next 17 years it became a variable star although the observed variations were small.

In 1932, McLaughlin stated "The brighter Be stars deserve continuous close attention for some years to come. Unusual developments may occur at any time in the spectrum of any one of them." In 1936, he added· "At the time that was written, the star which appeared least likely to serve as an example was γ Cas. Its history up to that time gave no hint whatever that it was about to embark upon a sequence of spectral changes which has been unique " It is striking to note that a half-century of additional observations have only reinforced McLaughlin's first remark, while the example cited in his second remark shows that it is impossible to predict the behavior of a Be star even after 50 years of unusually regular observations, such as were available for γ Cas

The large variations in the ratio V/R of the two emission peaks in the hydrogen lines were the precursor of the episode of spectacular variations that concluded with the complete dispersion of the envelope. In 1932, there was a strong, rapid, irregular increase in the Balmer-line emission. The V/R ratio increased rapidly, each of the two emission peaks became narrower while the emission increased. They came closer together

until they apparently formed only a simple line whose total width decreased At the maximum of this phase, in 1934, emission was visible out to H18; the lines of Fe II, He I, Mg II, Si II, and Ca II were also in emission. In this phase, in contrast to the preceding period, the widths of the Balmer emission lines exhibited velocities that differed significantly from one line to another; the highest velocities were observed for the lower members of the series At the same time, the photospheric absorption lines were weakened, indicating the presence of considerable veiling from the continuum.

This period of intense emission was followed by a period of decreasing intensity, in which only the lowest Balmer lines were seen in emission The structure and the width of the lines then changed: the V/R ratio decreased greatly, the two emission peaks separated, and the veiling decreased

In October 1935, a new phase of variations was observed with the appearance of a shell spectrum that lasted only 11 months. During this entire phase, only the lowest Balmer lines exhibited emission. The beginning of this shell phase was proclaimed by the appearance of a sharp absorption core in the He I line at 3889 Å, which arises from a metastable state Sharp absorption cores developed in the hydrogen lines and the helium emission lines were replaced by strong, sharp absorption lines, while the veiling gradually disappeared, vanishing completely in December 1935. The maximum development of the shell spectrum occurred between April and June 1936. The intensity of the shell spectrum then decreased rapidly, and it disappeared completely in September 1936.

The same scenario as in 1933 was then repeated, but with much greater intensity in both the Be phase and the shell phase The emission increased and reached a maximum in September 1937 It was observed in the hydrogen lines out to H32; the lines of Fe II, Ca II, Ti II, Cr II, Al II, Mg II, Si II, Ca II, and He II were also in emission. The visual luminosity of the star increased greatly, to a visual magnitude of 1.7, while the color temperature in the Paschen continuum reached its lowest value of about 8 5 X 10^3 K. After a rapid decrease of the line emission and the luminosity, a second maximum developed in June 1938, followed by a second decrease.

Another shell phase followed this emission phase, it was even stronger than the previous one, and exhibited its maximum development in January 1940. At that time, the emission was visible only in the lowest Balmer lines, the visual luminosity of the star was lowest ($m_v \approx 3$), and the color temperature was highest ($\simeq 3 \times 10^4$ K). This second shell phase, whose beginning was again indicated by the presence of a sharp absorption core in the He I line at 3889 Å, differed from the preceding one in the presence of strong absorptions lines of Fe III, while the lines of Fe II, Mg II, and Si II were absent. The dissipation of this shell was slower and more irregular than in 1936. After a period of variations with brief, weak reappearances of the shell lines, the last sign of the shell disappeared with the sharp absorption line of He I at 3889 Å

By 1942, γ Cas had lost almost all its emission, leaving only a very weak emission component at Hα, in the blue region, its spectrum was that of a normal B star, with broad, diffuse photospheric absorption lines.

The observations of γ Cas made during the episode of spectacular variations are among the most complete and regular in existence The amplitude of the variations is large enough to demonstrate correlations among the various physical parameters while, at the same time, bringing to light the difficulties with the interpretation of the origin of the extended atmospheres of Be stars in terms of the equatorial ejection of material owing to the rapid rotation of the star

Figure 11-31 shows the Hδ profiles published by Baldwin (1941), where the changes in this line can be followed during the most typical phases of the period from 1927 to 1940 There is no equivalent series for Hα Note the huge variations in the emission and in V/R Similar intensity variations are observed in the He I lines, except for their V/R ratio, which remains equal to 1 throughout this period Another striking feature is the large variation of the Hδ absorption wings, whose depth reaches a maximum at the

a

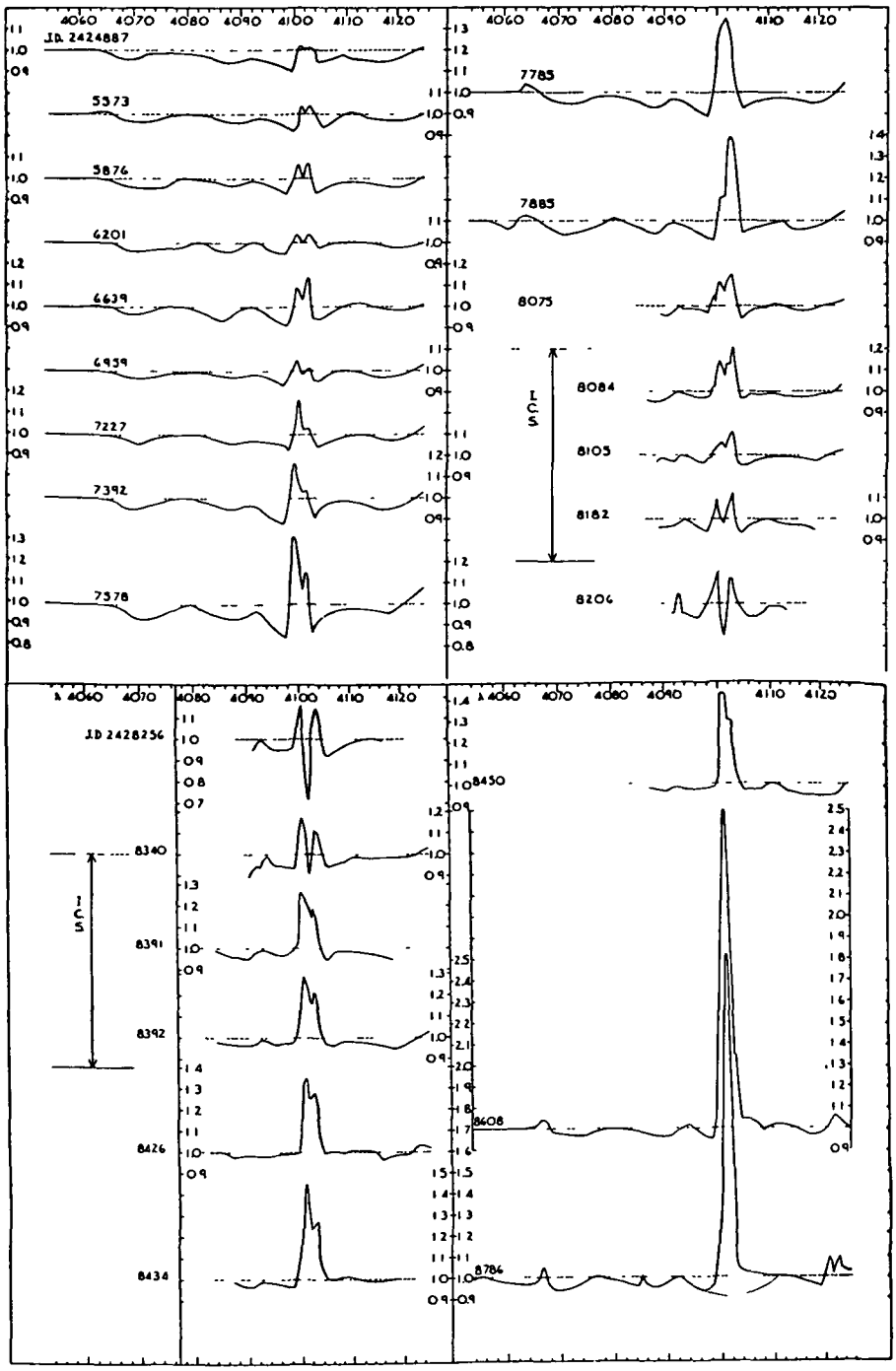
ID 2424887
5373
5876
6201
6639
6959
7227
7392
7578
7785
7885
8075
8084
8105
8182
8206
ID 2428256
8340
8391
8392
8426
8434
8450
8608
8784

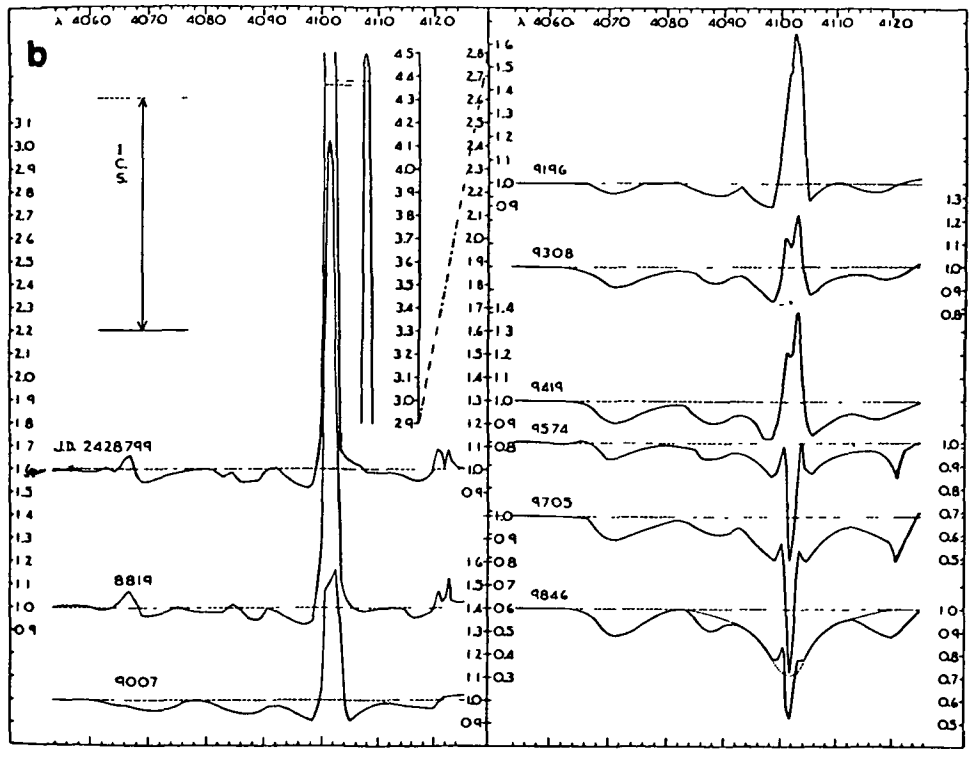

Figure 11-31a and b. The Hδ line in γ Cas, from 1927 to 1940, during the epoch of spectacular variations. The first strong Be and shell phases are seen at JD 2427785, and 2428256, respectively. The second strong Be and shell phases are seen at JD 2428819 and 2429705, respectively. Note the narrowness of the emission line when the emission is very strong during the "single line stage," and the large variations of the Hδ absorption wings whose depth reaches a maximum at the end of the second shell phase (from Baldwin, 1941).

end of the second shell phase. The same phenomenon is observed in other photospheric lines, such as O II and Si II. Variations in the width of the He I absorption wings have also been noted.

The observations clearly show that the photospheric absorption lines undergo intensity and profile variations when the star changes from one phase to another—Be, Be shell, normal B No systematic study of these variations has been made up to now, although they could have an important effect on the interpretation of the Be phenomenon. They essentially affect the determination of the spectral type from the weak photospheric absorption lines, that of g_{eff} from the absorption wings of the hydrogen lines, and that of v sin i from the profiles of the He I lines. In all these calculations, it is assumed that the photospheric lines are not modified by the presence of the envelope; classical methods and model atmospheres of normal B stars are therefore applied to Be stars. Considering the basic importance of the parameter v sin i in the usual interpretation of the Be stars, it would be interesting to compute it for the same Be star in its various phases—Be, Be shell, normal B.

Figure 11-32 presents the essential data on the lines and the continuum. The curves in Figure 11-32a, obtained by Baldwin (1939), rep-

resent the position of the red and violet edges of the Hδ emission line, those of the red and violet emission peaks, and that of the central absorption core. They make it possible to visualize the shifts and changing structure of the line. The emission lines of He I, Mg II, Fe II, and Si II exhibit changes of the same kind. The "narrow-line stage" observed at the time of strongest line emission seems to be characteristic of this particular phase of very intense emission, it has also been observed in 59 Cyg (see the next subsection). It is clear from this figure that there is no one emission-line width that is characteristic of a given Be star, it can only be characteristic of a phase of that star. This is very important for the construction of empirical models of Be stars, for one of the most important quantities that fixes the width of the emission line is the value of v sin i, it cannot be changed if it is assumed that this quantity reflects the rotation velocity of the star.

Figures 11-32c and 11-32d represent the light curve of γ Cas, the star undergoes a variation of 1.5 mag between the very strong emission phase and the end of the episode of spectacular variations, at which time the star returns to a normal, or quasi-normal, B phase It is immediately obvious that the emission phases are the ones in which the star is most luminous, while the shell phase is much less luminous. This correlation between phases and luminosity has also been observed in other stars, like Pleione.

Figure 11-32b shows the variations in the emission at Hδ, as measured by Baldwin It immediately appears that the increase in line emission is accompanied by an increase in the visual luminosity of the star. However, a more detailed examination shows that there is a phase lag between these two variations. The emission line continues to increase after the light maximum has passed and while the star undergoes a large decrease in luminosity for two or three months. This can be explained if one notes that the variations described are those of the equivalent widths of the Hδ emission; they represent the flux variations of the line with respect to the continuum flux. These measurements should therefore be corrected for the continuum flux variations in order to represent the line flux correctly Note that the observed effect is exactly in the right sense, the sudden drop in the luminosity is probably sufficient to explain the observed phase lag.

Figure 11-32e shows the variations in the Balmer discontinuity measured by Barbier and Chalonge (1941) at various epochs Although these measurements are not as accurate as present measurements in the BCD system, the variation of the discontinuity is definitely significant It seems to follow the variations in the line emission and the luminosity.

Figures 11-32f and 11-32g show the variations in the blue and ultraviolet gradients, the color temperature is lowest when the emission in the Be phase is strongest and the luminosity is greatest, it is highest in the quasi-normal B phase. Although it is difficult to measure the gradients, and although the observational errors were very large at that time, the trend shown in this figure is real, for it has been confirmed by a large number of other measurements made by other observers, especially at Greenwich (see the references in Baldwin, 1941) The amplitude of the observed variations is definitely greater than the errors of measurement if a series of homogeneous observations is analyzed using the same standard stars.

The variations observed in γ Cas, in both the emission-line and continuous spectra, are of such high amplitude that over a period of time they represent a large fraction of the range of characteristics that can be seen in a given sample of Be stars observed at a given epoch. In other words, these characteristics do not define objects of distinct classes. Moreover, since these different characteristics are observed in the same star, they must be interpreted independently of the geometric effect so often invoked to explain the great variety of spectra observed among the Be stars—that is, the effect of the inclination of the star's axis of rotation to the line of sight.

From 1942 to 1980—The New Slowly and Irregularly Increasing Be Phase. During this period, γ Cas went from a normal B phase to a new Be phase, with irregularly increasing emission and small fluctuations. From 1942 to 1948, the spec-

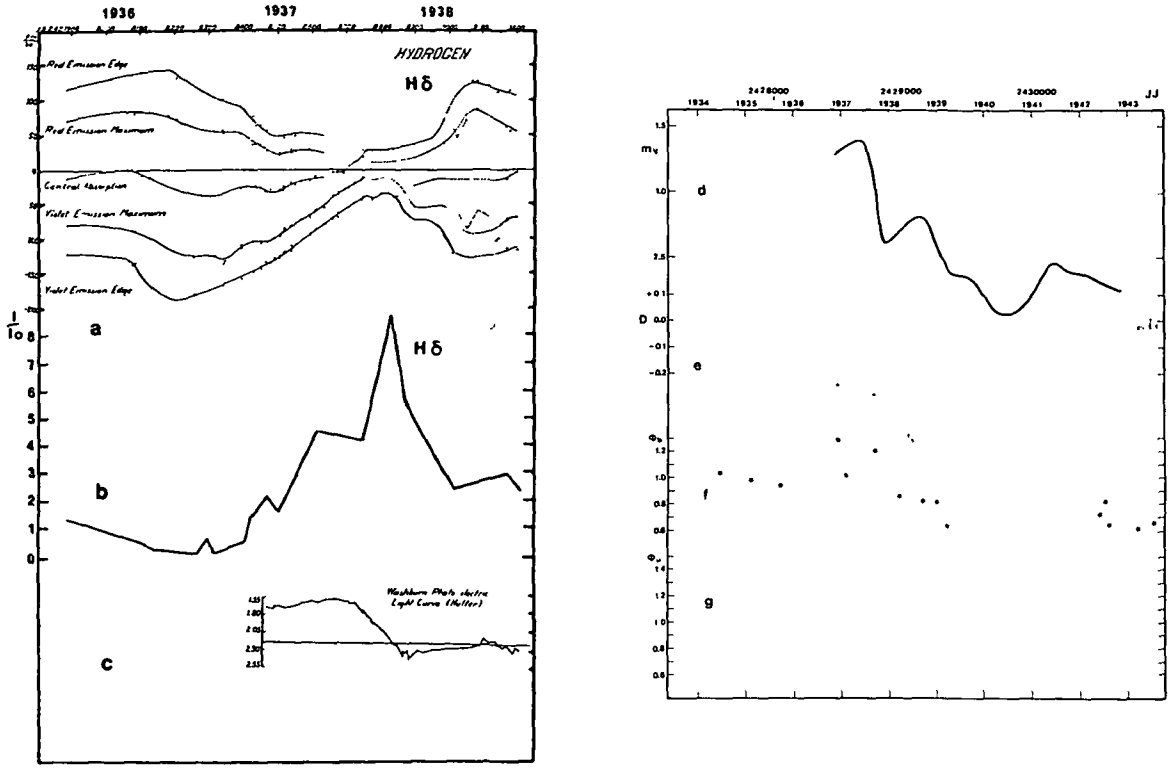

Figure 11-32 The behavior of different spectral features and light variations of γ Cas during the second strong Be phase of the spectacular episode, culminating in September 1937. Figure 11-32 (a) represents the variation of the position of the red and violet edges of the Hδ emission line, that of the red and violet emission peaks, and that of the absorption core (from Baldwin, 1939). The line is the narrowest when the emission is the strongest during the "single line stage." Such a narrow emission line is usually considered as a characteristic of "pole-on" stars. This figure shows that the width of an emission line is clearly a characteristic of the phase of variation of the star. The curve in (b) shows the variation in the equivalent width of the emission at Hδ as measured by Baldwin (1939) The photo-electric light curve of γ Cas, as measured by Huffer (1939) is given in (c) The light curve from AAVSO smoothed observations is given in (d). In (e), (f), and (g) are plotted the Balmer Jump, and the blue and ultraviolet gradients measured by Barbier and Chalonge (1941) The star undergoes a variation of about 1.5 mag between the very strong emission phase and the end of the spectacular variation in 1942, at which time the star returns to a normal, or quasi-normal B phase. At maximum emission in 1937, the star is the brightest and the reddest in the visual. During the strong shell phase, in 1940, the star is the faintest and the bluest.

trum of γ Cas was similar to that of a normal B star in the visible spectral region, which is classically used to define the spectral type of a star. The emission began to grow in 1948 and exhibited a low-level maximum in 1953, followed by a slow decline until 1962. A return to a moderate level was then observed up to 1969, when a period of strong V/R observations began, these variations were observed up to 1981, and were accompanied by small variations in the emission intensity. During this phase of growing emission, the visual luminosity of the star increased: m_v went from 3.0 to 2.35, approaching the value it had had before the spectacular episode 1932–1940.

To conclude this description of the variations of γ Cas in the visible region, we point out that it has not been possible to determine a period for the variation of any measurable quantity in its

spectrum. In particular, the analysis of the radial velocities gives no indication of a periodic variation, as we shall see in Chapter 12. Many authors have searched for a period in the V/R variations, and there is some indication that this ratio varies on a time scale of 3 to 4 years. However, it has not yet been possible to represent these variations by a unique period. Moreover, no other phenomenon in the visible region (Balmer-line emission, visual magnitude, radial velocities, etc.) exhibits any correlation with this time scale.

At the end of this description, we shall give in Figure 11-33 an outline of the variations of the Balmer-line emission in γ Cas since it was first observed. This is a convenient way of following the various phases in the evolution of its spectrum. For the periods 1915–1932, 1942–1975, and 1975–1980, during which the emission in the higher members of the Balmer series varied little, we have used, respectively, the visual estimates of the Hβ emission made by Kitchin (1970a), Cowley et al. (1976), and by ourselves, using spectrograms taken regularly at the Haute-Provence Observatory. For the period 1932 to 1942, we used the descriptions and measurements made by Baldwin (1939, 1941), Edwards (1956), and Cowley and Marlborough (1968) to illustrate the emission in the whole Balmer series, and not only in Hβ. The intensity scale is arbitrary, and has been matched with the visual estimates cited above. This figure should not be considered a quantitative representation of the emission, it serves only to pick out rapidly the two periods we have described, and it demonstrates the following three important points.

1. The variations of γ Cas in the visible region and its transition through three phases–Be, Be shell, and normal B–clearly show that the density structure of the envelope is variable. This structure is determined, in the first approximation, by the value of the mass flux (see Chapter 13 and Thomas, 1983). Thus, observations of the Be stars in the visible have made it possible for decades to conclude that the mass flux cannot be connected only with the values of T_{eff} and g_{eff}, and that the mass flux is variable. Moreover, the observed variations are so large–a transition from Hα in emission many times brighter than the continuum to Hα in absorption–that they cannot be compared with simple fluctuations about a mean value, which in turn may be connected with T_{eff} and g_{eff}.

2. After nearly a century of observing γ Cas, it is not possible to determine any period for the variation of the phenomena exhibited in the visible region; nor is it possible, in spite of the huge body of data we possess, to predict the behavior of γ Cas. The ultimate reason for this unpredictability of γ Cas, and of the Be stars in general, rests on the fact that the phenomena observed in the visible spectra are the result of a mass flux that does not depend only on T_{eff} and g_{eff}, and whose law of variation we do not yet know.

3. For nearly a century, the dominant phase of the star was a relatively quiet Be phase, during which the variations did not exhibit any characteristic that could be called exceptional. The spectacular episode was relatively short with respect to the Be phase. Nevertheless, it is obvious that this phase cannot be considered negligible. In other words, one cannot study one phase of the star independently of the one that preceded it and the one that followed it. A real physical model must take into account its history. The majority of the Be stars have been observed in a single phase, Be or shell, much less frequently than γ Cas, and over a much shorter time span. The example of γ Cas shows that it can be very dangerous to attempt to classify the Be stars into homogeneous groups, based on common characteristics observed during a time period which does not represent the whole range of characteristics exhibited by a single star. These attempts at classification do not represent

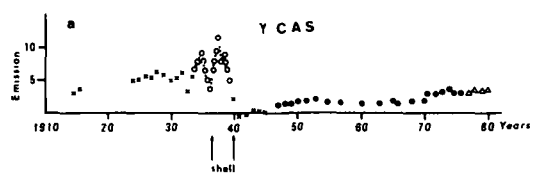

Figure 11-33. A schematic representation of the variation of Balmer line emission in γ Cas (from Doazan et al., 1980b) The intensity scale is arbitrary (see text).

groupings of identical objects, but rather groupings of objects that exhibit similar phases of variation, during a limited period of observation. When the length of the observation period is increased, the stars of a given group are classified in a different group, because of their unpredictable variations. For example, from 1880 to 1932, γ Cas would have been included in the group of Be stars with strong Balmer and Fe II lines in emission. From 1932 to 1948, it would have been placed among the stars exhibiting Be, Be shell, and normal B phases. And from 1948 to 1980, it would have been in the group of Be stars with moderate Balmer emission lines but without Fe II in emission.

The example of γ Cas, like that of a large number of Be stars observed over a long baseline in time, shows that the description of the Be phenomenon requires the analysis of observations made on time scales of the order of a century, rather than 1 or 2 decades. The importance of the development of the "Be cycle," from the beginning of the formation of the envelope up to its complete dissipation in the interstellar medium, is clearly shown by the observations made in the ultraviolet region, where apparently uninteresting phases in the visible spectra correspond to episodes of spectacular variations (see Chapter 12). It clearly appears that the spectral features of a Be star observed on a time scale that is short with respect to the length of the cycle do not in any way characterize a particular class of Be stars, but only the particular phase in which the star is found.

Rapid Variations of γ Cas in the Visible Region. Small, rapid profile variations, on a time scale of a few minutes, have been detected for Hβ by Hutchings (1976d) and Doazan (1976), and for Hα by Slettebak and Snow (1978). These variations are weak, irregular, and difficult to demonstrate. They essentially affect the structure of the line rather than the total emission intensity. It is impossible to observe them without very good spectral and time resolution. No period has been established for these weak variations, and for the moment they are considered to be erratic.

Variability in the Infrared Region. There has been no systematic search, on a sufficiently long time scale, for variations of γ Cas in the infrared region. However, Ferrari-Toniolo et al. (1978) compared their measurements in the BVRIKMN bands to those of Johnson et al (1966) and Gehrz et al. (1974) and concluded that the flux of γ Cas in the K band was 75 percent higher from 1972 to 1973 than in 1976. This shows that the infrared flux is also variable.

59 Cyg (B1.5 Ve). McLaughlin noted in 1948 that the spectrum of 59 Cyg seems to be "characterized by long periods of quiescence and short periods of activity." However, it was not until 1972 that 59 Cyg entered a period of spectacular variations in the visible region which had never been observed before The rapid succession, within 5 years, of a double sequence of strong Be phases and strong shell phases, ending in a normal or quasi-normal B phase, marked the end of a Be cycle that had, apparently, begun in 1917. This quasi-normal B phase was followed by a weak, slowly and irregularly increasing Be phase during which the largest mass ejection activity, ever observed in this star, was detected in the ultraviolet range. A comparison of the long-term variations of 59 Cyg and γ Cas brought to light striking similarities in their long-term, general pattern of behavior (Doazan et al., 1980b, 1980c). These are, moreover, the only stars for which such great similarities have been noted over a period as long as nearly 70 years. Nevertheless, a certain number of differences can be noted; they reflect what we have called the individuality of the Be stars. In Chapter 12, we shall present the ultraviolet observations of 59 Cyg made from 1972 to 1980. Taken together, these visible and ultraviolet observations constitute a unique body of information, for 59 Cyg is still the only star to have been observed systematically and simultaneously in the ultraviolet and the visible regions at different phases of its variation. An analysis of these observations leads to the conclusion that the mass flux is highly variable, and that its value depends on the phase of variation of the star, implying that it cannot depend only on the parameters T_{eff} and g_{eff}. This analysis also sug-

gests that the mass flux is highest when the star is entering a new phase of growing emission.

Most of the bibliography of 59 Cyg is given by Merrill and Burwell (1933, 1949), Jaschek et al. (1971), Snow and Marlborough (1980), Doazan et al. (1980a, 1980b), and Barker (1979) The observations made before 1972, unlike those of γ Cas, generally provide only qualitative descriptions of the spectrum. It must be pointed out that these descriptions are often ambiguous, and that they are interpreted differently by different authors. One must, in practice, take into account the dispersion of the spectra used, the number of the Balmer lines observed, and especially the great confusion produced by the use of the word *shell*, which can mean either a kind of spectrum or simply a line which is not photospheric but which originates in the extended atmosphere–the "shell" Finally, we note that 59 Cyg has been much less well observed than γ Cas and that, unlike the latter case, one cannot be sure that an important phase of variation has not escaped the observers. Nonetheless, we have tried to trace the "history" of 59 Cyg, for an analysis of the long-term activity cycle of this star is essential for an understanding of the Be phenomenon.

Three periods of variation can be distinguished in 59 Cyg, since it was first observed in 1904. (1) from 1904 to 1916–a Be phase decreasing to a normal B phase, (2) from 1917 to 1977–the star went through a complete variation cycle, going from the normal B phase into a new, long Be phase, in which it underwent strong variations culminating with a spectacular sequence of phase changes over a period of 5 years, at the end of which it returned to a normal or quasi-normal B phase; (3) from 1978 to the present–the star has begun another Be cycle by entering another phase of growing emission. This new Be phase, with weak emission in the Balmer lines, corresponds to a phase of great activity in the ultraviolet region (see Chapter 12).

From 1904 to 1916. In 1904, 59 Cyg exhibited strong Balmer-line emission which was visible out to Hζ. In 1909, the emission was weak; it fluctuated while decreasing in intensity, and then disappeared entirely, even at Hα, in 1916 Although the observations were not very frequent at that time, descriptions of the spectrum were published at least once a year from 1909 to 1916, thus, it is reasonable to believe that this normal B phase was not the end of a spectacular episode, which might have escaped observation.

From 1917 to 1977. Another Be phase, in which the Balmer-line emission intensity increased slowly and irregularly, began in 1917. It reached its first maximum in 1927 From 1926 to 1929, strong V/R variations were observed. The emission was much weaker, barely perceptible at Hβ, by 1932. It began to increase once again in 1936, and in 1942 the Fe II lines were seen in emission. A very strong emission phase, the strongest reported up to that time, was observed from 1946 to 1948. Paschen-line emission was also observed in 1946. The emission was weaker from 1953 to 1956, but still quite visible at Hα and Hβ. In 1965, Hα was strong and the Paschen lines were observed in emission. From 1967 to 1971, the emission fluctuated, while remaining at a moderate level According to the low dispersion observations made by R. Herman's group and recorded in the Atlas of Be Stars (Hubert-Delplace and Hubert, 1979), small variations took place from 1953 to 1971. Although this description is very brief, it shows that throughout this period, the variations in the emission of 59 Cyg were much greater and much more irregular than those observed in γ Cas, except for the spectacular episode of 1932–1942.

The long Be phase which began in 1917, and which exhibited a period of very strong emission from 1946 to 1948, underwent a second increase in emission in 1972. This increase was apparently the first sign of the beginning of an episode of spectacular variations, which continued up to 1977 and concluded with a return to a normal or quasi-normal B phase.

The strengthening of the emission in 1972 was followed by a first shell phase, of which only two observations exist (Doazan et al., 1975). The shell spectrum exhibited a completely developed set of lines of singly ionized metals and sharp absorption cores visible out to H30. In December

1973, the shell phase had completely disappeared, giving way to a Be phase with very strong emission visible out to H19 on low-dispersion spectra (Duval et al., 1975) A second shell phase was observed in November 1974; its development was monitored very regularly by Barker (1979). It lasted until June 1975. Figure 11-34 shows the spectrum of 59 Cyg in July 1974, at the end of the second Be phase, when the emission in the hydrogen lines had already decreased. However, this emission was still very strong and visible out to H17; the He I line at 4471 Å and the Mg II line at 4481 Å were also in emission, as well as the Balmer discontinuity. Two months later, in September 1974, the emission disappeared in the higher Balmer lines (Figure 11-35), and the shell absorption began to develop in the center of Hβ Note, however, that the Balmer discontinuity was still in emission. This observation clearly shows that one cannot associate a standard value of the Balmer jump with a given value of the Hα emission. This is also indicated by the lack of correlation between these two quantities as noted by Schild (1978) and Divan et al (1982; see also the previous subsection) In December 1974 (Figure 11-36), the shell spectrum was completely developed and observed out to H25 in the Balmer lines. The singly ionized metal lines were also strong in absorption. All the photospheric lines were strongly affected by a shell absorption component. It is impossible, of course, to say whether the second shell was stronger than the first one, since the first shell was observed on only two spectra taken a few days apart, and its maximum degree of development is completely unknown. During the second shell phase, the Balmer discontinuity was in absorption and larger than the discontinuity in a normal B star of the same spectral type. In October 1975, the shell had disappeared and the spectrum looked like that of a normal B star in the photographic region, but Hα was still strong in emission (Figure 11-37). The Balmer discontinuity was still in absorption, but much weaker; it was probably close to the value for a normal B star, but no value of the discontinuity was published for this epoch

Figure 11-38 shows the profiles of Hα observed from July 1974 to October 1975 by Barker (1979). The resolution is not high enough to analyze the details of the profiles. Nevertheless, it can be clearly seen that during the strong emission phase—as during the strong emission phase of γ Cas—the width of the emission line decreases very markedly, and its profile looks simple while the emission increases During the shell phase, the shell feature is not very distinct at Hα, but it is clearly observed for the higher Balmer lines, beginning with Hβ. This often happens when the emission is strong and when moderate dispersion spectra are used. Figure 11-39 illustrates the variations of Hγ obtained by Barker, from 1974 to January 1976. Note, on these profiles, that the sharp absorption component is displaced toward the violet at the beginning of the shell phase, simulating a P Cygni profile in November and December 1974. Figure 11-40 shows the behavior of the radial velocities of the shell lines, as measured by Barker during the second shell phase. Note that the greatest expansion velocity (≈ -100 km s^{-1}) accompanies the appearance of the shell spectrum. The velocity then gradually decreases during the development of this spectrum, and reaches its smallest value at the time of the maximum of the second shell phase. This figure is to be compared with the one for Pleione (Figure 11-43, discussed later) in which the expansion velocity is a maximum at the time the shell spectrum disappears. This shows that a single phenomenon—the appearance or disappearance of a shell phase—can show quite a different behavior in different stars. This is the very hallmark of what we have called the individuality of the Be stars.

The dissipation of the second shell phase was followed by a Be phase, in which the emission decreased rapidly. In 1976, the emission was very weak, it decreased, with fluctuations, until it reached a very low level at Hα in November 1977.

From 1978 to 1981 Another Be phase followed the quasi-normal B phase. In August 1978, a weak emission was visible in Hα alone. It increased slowly and irregularly, exhibiting V/R variations up to 1981, when the emission was moderately strong at Hα and began to appear at Hβ. It was during this phase that the ultraviolet

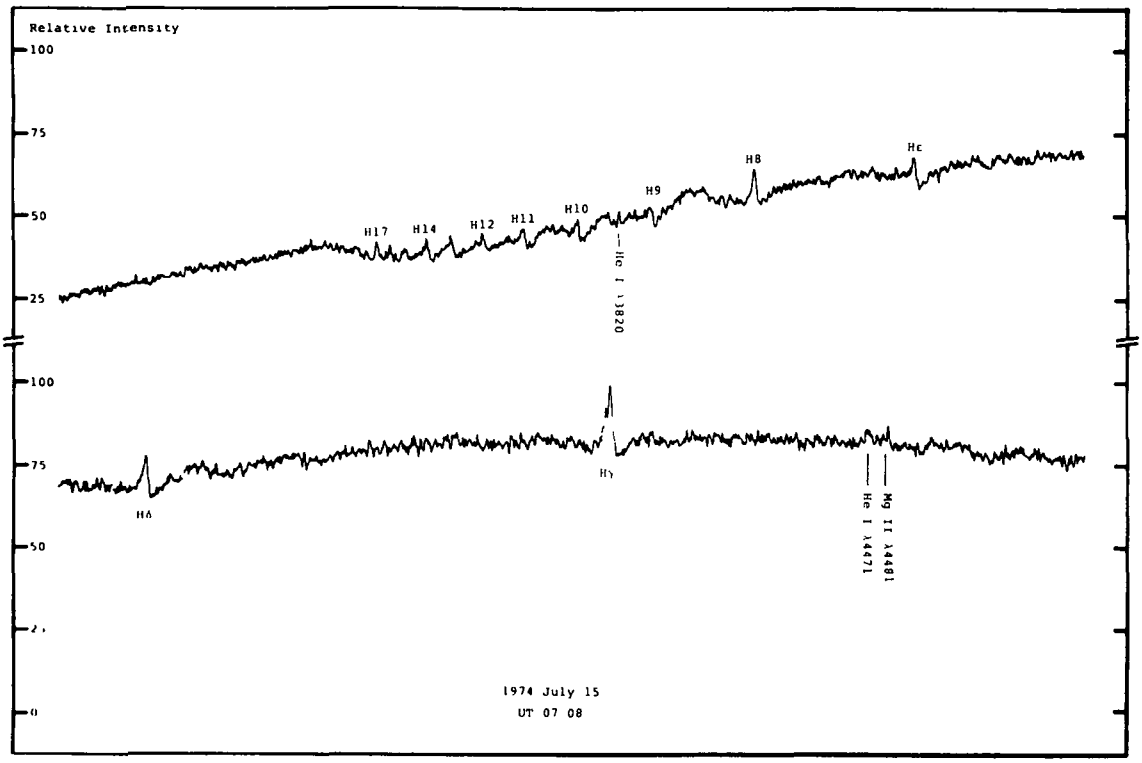

Figure 11-34. The spectrum of 59 Cyg in July 1974 during the strong second Be phase (from Barker, 1979) The Balmer-line emission is seen until H17, He I, λ 4471, and Mg II, λ 4481, are both in emission; the Balmer discontinuity is in emission.

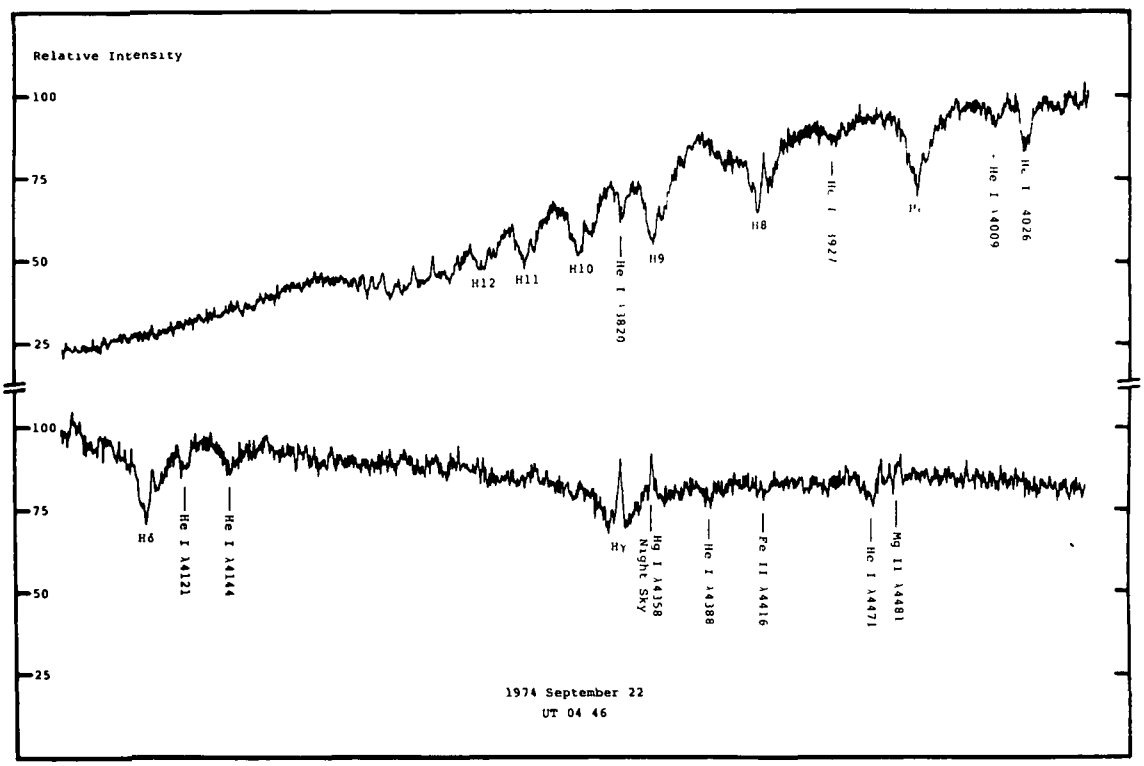

Figure 11-35. The spectrum of 59 Cyg in September 1974 at the end of the second Be phase (from Barker, 1979) The Balmer-line emission has strongly decreased and has disappeared in the higher Balmer lines. Note, however, that the Balmer discontinuity is still in emission and that some emission is still present in He I, λ 4471, and Mg II, λ 4481.

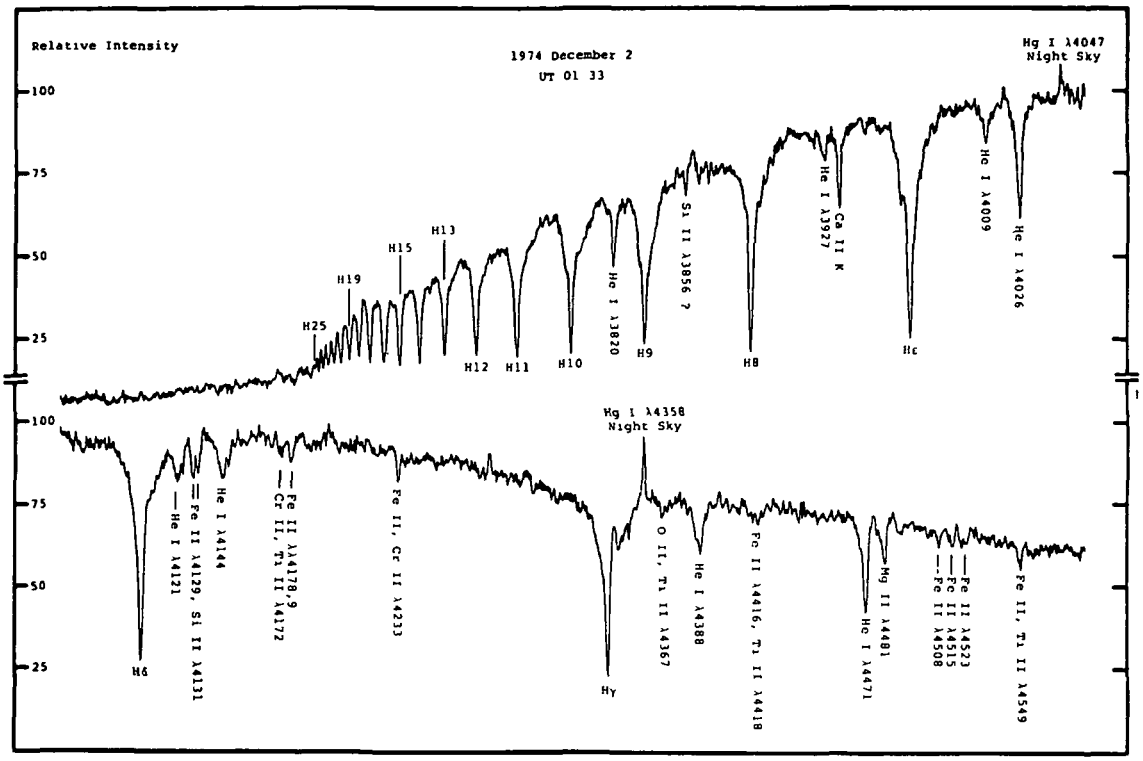

Figure 11-36. The spectrum of 59 Cyg in December 1974 (from Barker, 1979). The shell spectrum is completely developed; shell absorption in the Balmer lines is observed until H25 and singly ionized metals are strong in absorption. All the photospheric lines are enhanced and strongly affected by the shell component, as is seen in the He I lines, for example. Note the large Balmer discontinuity in absorption.

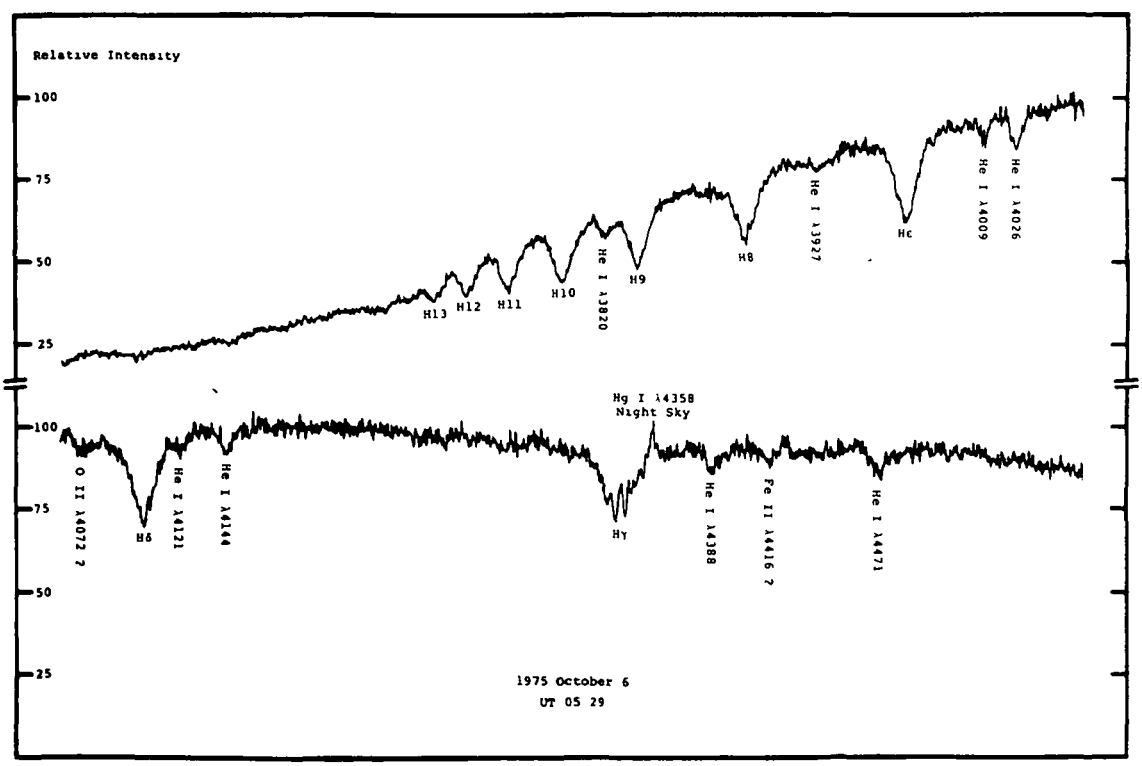

Figure 11-37. The spectrum of 59 Cyg in October 1975 looks like that of a normal B star in the photographic region although Hα is still fairly strong in emission (figure from Barker, 1979).

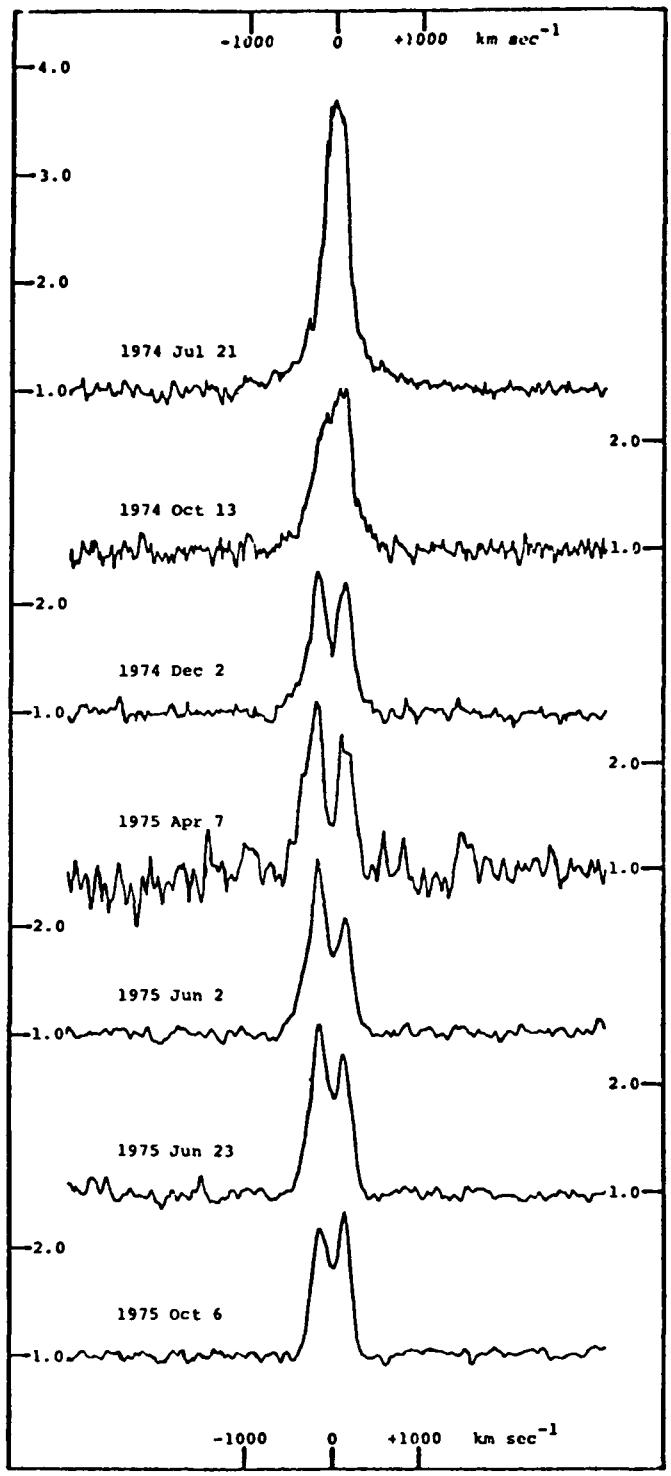

Figure 11-38. Hα profile of 59 Cyg from July 1974 to October 1975 (from Barker, 1979). Note the narrowness of the emission line in July 1974 during the strong Be phase The behavior of the variation of the line width is very similar to that of γ Cas (see Figures 11-31 and 11-32a).

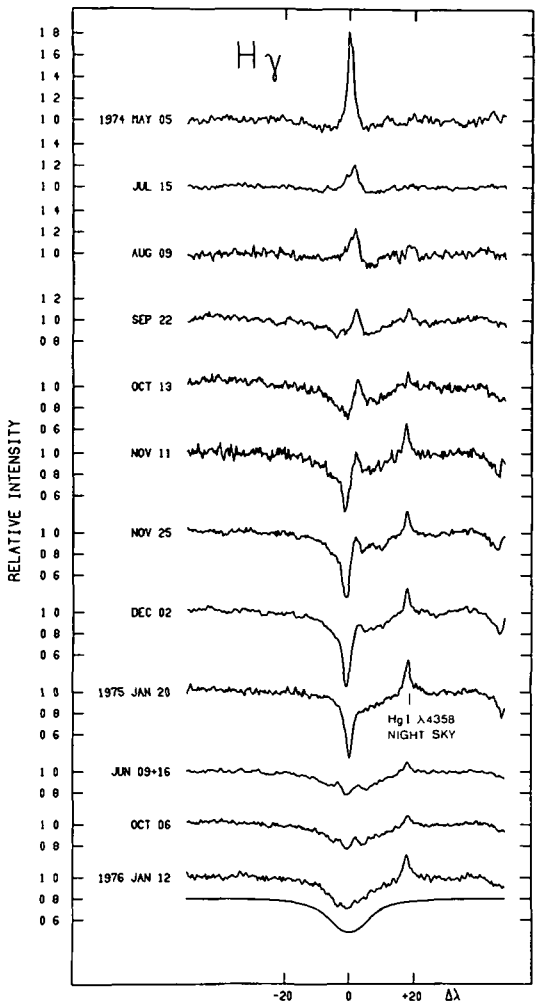

Figure 11-39 Hγ profile of 59 Cyg, from May 1974 to January 1976 (from Barker, 1979) The beginning of the shell phase is accompanied by a violet displacement of the narrow absorption component simulating a P Cygni profile The smooth profile shows the Hγ profile for a standard model.

observations showed the greatest shifts and the strongest variations of the superionized lines formed in the chromospheric and coronal regions In the visible region, the phase of spectacular variations consists of a double sequence of phase changes from strong Be to strong shell, passing through another Be phase before ending in a quasi-normal or normal B phase. In the ultraviolet region, on the other hand, the phase of spectacular variations takes place during the new Be phase, with weak, increasing emission The

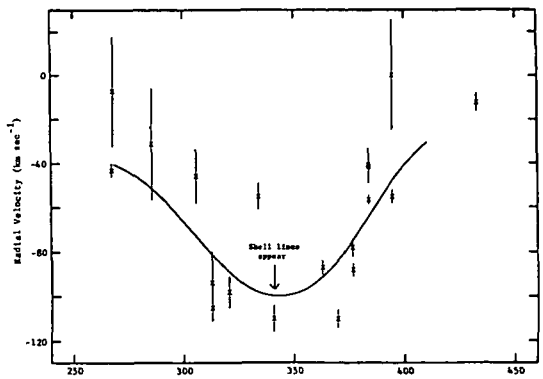

Figure 11-40. Radial-velocity variation of the shell lines in 59 Cyg (from Barker, 1979). Note that the greatest expansion velocity accompanies the appearance of the shell spectrum. The solid curve is a least-squares fit to the data; the dotted line indicates the system velocity. Error bars mark the probable error.

spectacular variations in the ultraviolet region during this Be phase are given in Chapter 12.

We have drawn in Figure 11-41 the long-term variations of the Hα emission—often extrapolated from the behavior of Hβ—on an arbitrary scale, using the qualitative descriptions from the referenced articles. As for γ Cas, this figure is only an outline of the Balmer-line emission in 59 Cyg; it should not be considered a quantitative estimate of the emission. A comparison of this figure with Figure 11-33 for γ Cas shows the striking similarity of their long-term pattern of general behavior. We note that for both stars, the dominant phase is a long Be phase, and that the episode of spectacular variations in the visible range is relatively

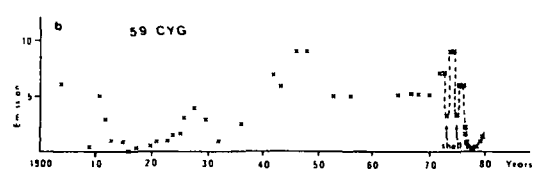

Figure 11-41. Long-term variation of the Hα emission in 59 Cyg often extrapolated from the behavior of Hβ, on an arbitrary scale (from Doazan et al, 1980b). From the comparison of this figure to Figure 11-33 emerges the striking similarity of the long-term pattern of variability of 59 Cyg and γ Cas

short in comparison with the baseline of the observations. The remarkable sequence of events, which takes place on the same time scale for both stars, shows the close connection among the three phases—Be, Be shell, and quasi-normal B. This connection requires a dynamic, time-dependent treatment of the Be phenomenon. The ultraviolet observations show that after the end of this rapid succession of phases, marked by the quasi-normal B phase, the development of a new Be phase with increasing emission is characterized by a very high mass flux. This elucidates the important points on which any Be-star model should be based, and suggests that it is precisely during this unspectacular period in the visible range—the beginning of a Be phase with weak, increasing emission—that the mass flux and the energy storage determine the formation and structure of the outer atmosphere.

It must be emphasized that 59 Cyg and γ Cas are the only Be stars for which similarities have been noted over such a long time span. But these similarities refer only to the general aspect of their behavior. If the variations are examined more closely, the two stars maintain their individuality which can be recognized in the amplitude and duration of each of the events, as well as in the details of the spectra Note also that one currently reads in the articles devoted to Be stars that the time scales of the variations are of the order of 10 years. The examples of 59 Cyg and γ Cas show that, depending on the spectral feature under consideration, several time scales can be defined. For 59 Cyg, it is actually possible to define a complete cycle of the Be phenomenon, from the "filling" of the envelope in 1917 to its complete dispersion in 1977. After the dissipation of this envelope, the star rapidly enters a new Be phase. The similarity between 59 Cyg and γ Cas extends to the whole of this series of phases, it does not apply only to a particular short episode of variations. It is in this respect that the similarity between these two stars constitutes, for the present, an exceptional case.

Pleione (B8 Ve). The history of Pleione is of special interest, for the spectacular variations of its line spectrum and luminosity have been regularly observed, giving a striking demonstration of the luminosity differences between the Be phase and the shell phase. The long time baseline of the observations allows a comparison between its variations and those of 59 Cyg and γ Cas, from which the individual nature of the variability of these stars can be deduced Pleione was discovered as a Be star in 1888. Since then, it has exhibited a normal B phase about 33 years long and two shell phases separated by 35 years. In 1905, it lost all traces of emission and looked like a normal B8 V star until 1936. Emission lines were observed once again in 1938 with a completely developed spectrum of singly ionized metals. This shell phase lasted for several years; then, in 1948, the shell absorption lines decreased rapidly up to 1951. They disappeared completely in 1954, leaving the star in a Be phase.

The emission in the Balmer lines and the Fe II lines then increased more or less regularly and exhibited an intensity maximum around 1963. A large, rapid decrease in the emission was observed in 1972, preceding the appearance of another shell phase in December 1972. This phase developed gradually, accompanied by an increase in emission. In 1980, Pleione once more exhibited a completely developed shell spectrum of the α Cygni type. The variations of the spectrum of Pleione, from 1938 to 1975, have been described in detail by Gulliver (1977) who gives a well-documented bibliography of this star. Figures 11-42a and 11-42b, taken from Gulliver, show the Hβ profiles at various phases, particularly the transition from the shell phase to the Be phase, and vice versa. This figure clearly illustrates the gradual nature of the transition between these two phases.

The behavior of the radial velocities, as studied by Merrill (1952), is shown in Figure 11-43. Note that the expansion velocity of the higher members of the Balmer series is greatest at the time of the disappearance of the shell, and that the velocities of the lower members undergo a much smaller variation. This is very different from the behavior of 59 Cyg, in which the maximum expansion velocity is observed at the beginning of the shell phase

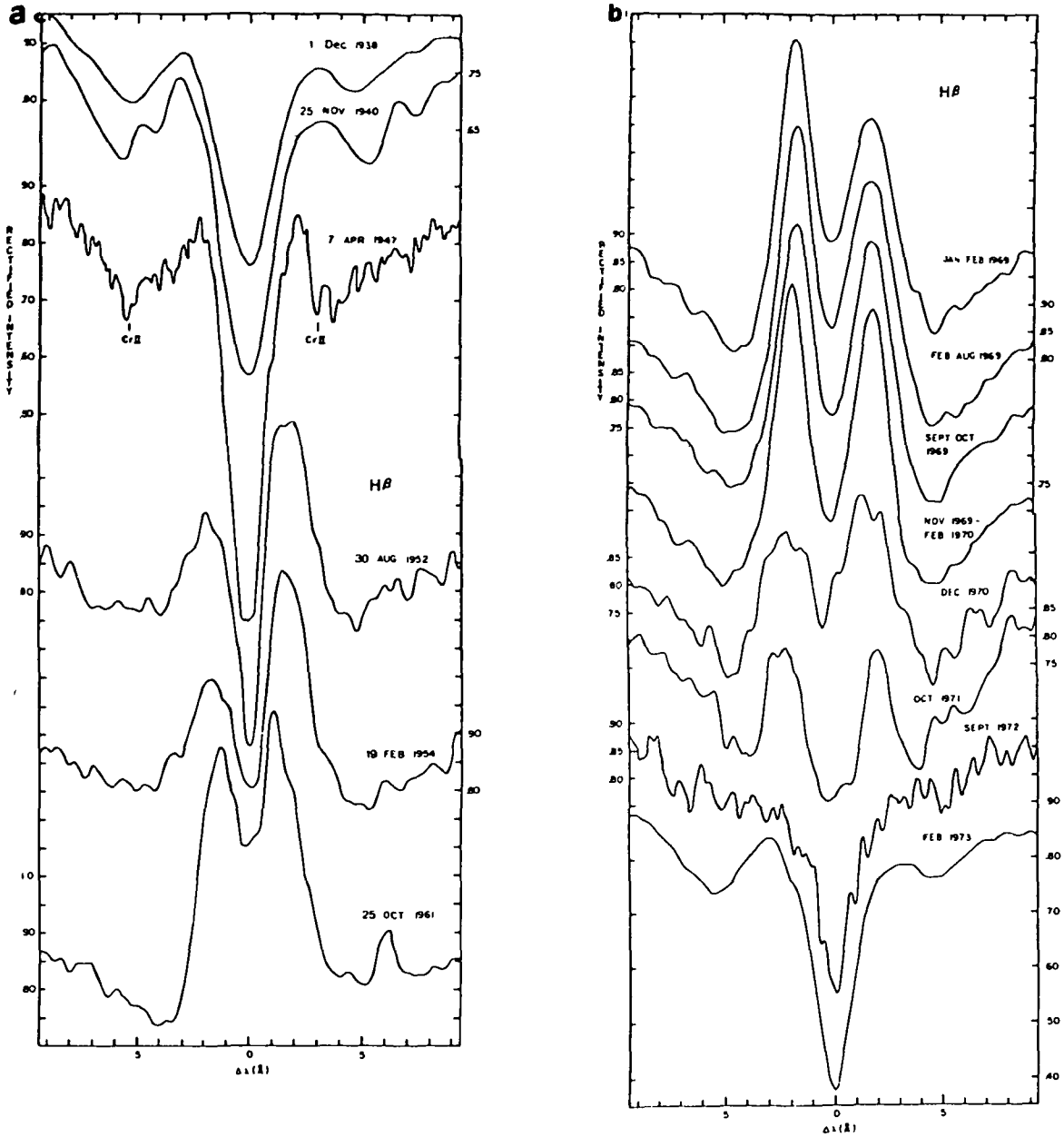

Figure 11-42 Hβ profiles of Pleione from 1938 to 1973 (from Gulliver, 1977) The transition from the shell phase to the Be phase is seen in (a). The transition from the Be phase to the shell phase is seen in (b) Note the progressiveness of these transitions.

Hirata and Kogure (1976, 1977) discovered a very unusual change in the K line of Ca II in Pleione, at the time when the second shell phase developed. A broad and shallow feature, which extended to about ±430 km s^{-1} from the center of the narrow Ca II shell line, was observed during the development of the second shell phase. This same feature was also noted on the spectra of the first shell phase, which were studied by Gulliver. Hirata and Kogure suggested that this line originates in a rapidly rotating layer surrounding the equator of the star, and that the

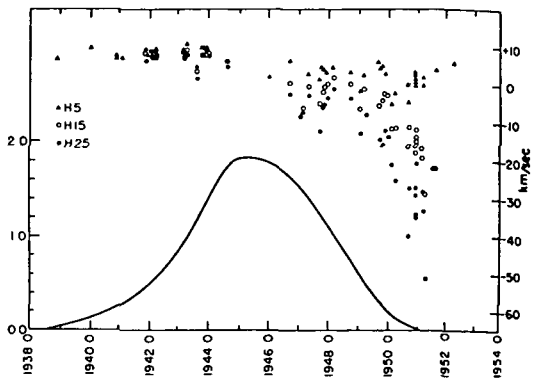

Figure 11-43. The behavior of the radial velocities in Pleione during the development and the disappearance of the shell during the transition shell phase → Be phase, as measured by Merrill (1952) (figure from Limber, 1969) The solid curve represents the depth variation of the shell lines. Note that the expansion velocity of the higher members of Pleione is greatest at the time of the disappearance of the shell This behavior is very different from that of 59 Cyg (see Figure 11-40).

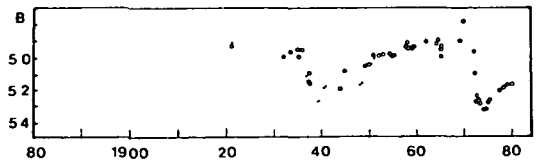

Figure 11-44 The light variations of Pleione since 1880 (from Sharov and Lyuty, 1976; Hopp and Witzigmann, 1980). Filled circles are visual measurements, open circles are photoelectric measurements. Note the abrupt decline in light during the transition Be → shell which was particularly well observed in 1973 by Sharov and Lyuty.

rotational instability of this layer produces the ejection of material They gave no physical justification for this interpretation.

The light variations of Pleione since 1880 have been traced by Sharov and Lyuty (1976), who closely observed the transition from the Be phase to the shell phase from 1971 to 1975, Hopp and Witzigmann (1980) brought the observations down to 1980 These variations are illustrated in Figure 11-44. Note that: (1) although there is a certain pattern in the behavior of the visual magnitude of the star, no period can be determined, one can only suggest time scales for the duration of each phase, or for the interval between two phases; (2) the appearance of each of the shell phases in 1938 and 1973 was *preceded* by an abrupt decrease in the stellar luminosity, amounting to 0.6 mag in the B band, this decrease was not restricted to the visible region, but showed up between 2000 and 6000 Å (Golay and Mauron, 1977); (3) the brightest of the three phases (Be, Be shell, and normal B) in the visible range was the Be phase (1955 to 1971), and the faintest were the shell phases (1938 to 1955 and 1972 to 1981); the normal B phase was a little fainter than the Be phase, but the difference was only about 0 1 mag, (4) on the light curve of Pleione, a single value of the visual magnitude can be found which corresponds, at different epochs, to each of the three phases of the star, Be, Be shell, and normal B. This means that at a single point in the HR diagram (characterized by the visual magnitude and spectral type), the same star would, at different times, be described as normal or peculiar (with two different types of peculiarity, emission and shell spectra). Figure 11-45 shows the path followed by Pleione in the (U − B), (B − V) diagram from 1962 to 1973, that is, from the Be to the shell phase; we see that the location of the star in this diagram depends on its epoch of variation. This shows that any attempt to interpret the location of the Be stars in an HR diagram–the M_V, (B − V) diagram, for example–in terms of stellar evolution, must first remove all the atmospheric effects that displace the peculiar stars from the location of the normal stars of the same spectral type, on time scales that are short with respect to the evolutionary time scale. But in order to compute all these atmospheric effects, one must first construct a model atmosphere that takes into account all the properties of these stars at all wavelengths.

88 Her (B7 Ve). The variations of another Be star, 88 Her, exhibit striking similarities to those of Pleione; nevertheless, there are important differences. 88 Her has been observed since 1912, and was first classified as an Ap star Balmer-line

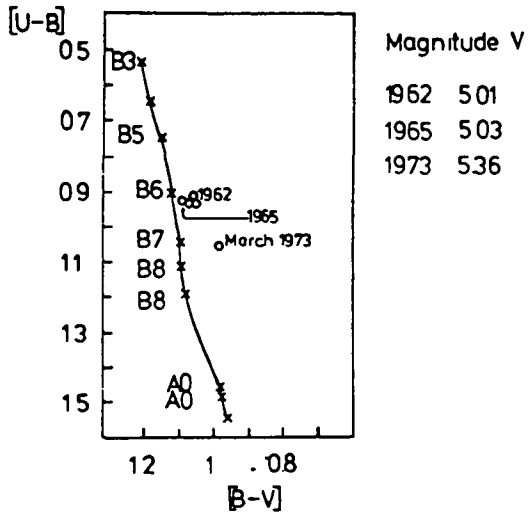

Figure 11-45 The path followed by Pleione in the (U−B), (B − V) diagram, from 1962 to 1973, that is, from the Be to the shell phase (from Golay and Mauron, 1977) The location of the star in this diagram clearly depends on its phase of variation.

emission was first observed in 1955 and a shell spectrum was present in 1959, with all of the singly ionized metallic lines in absorption. The metallic absorption lines disappeared in 1970, while the Balmer-line emission began to decrease. This change in the spectrum was accompanied by a luminosity increase in the UBV bands and by a shift in the star's colors toward the blue, the maximum of these effects seems to have coincided with the complete disappearance of the metallic lines and the minimum emission at Hα After 88 Her had exhibited a nearly constant luminosity and spectrum for around 7 years, in a phase of very weak Hα emission with weak shell absorption cores in the hydrogen lines alone—undetectable at low dispersion—its luminosity suddenly dropped by 0.33 mag in the U band in a space of around 7 months This sudden drop *preceded* the reappearance of the metallic shell lines. These lines developed gradually, while the emission in the Balmer lines increased and the star became brighter This behavior strikingly resembles that of Pleione (Hirata, 1978).

One of the peculiarities of 88 Her is the strict periodicity in the radial-velocity variation of the shell lines (86.7 days), ever since the star was first observed in 1912, the behavior of the radial velocity variations did not change at all during the variations of the spectrum. Harmanec et al. (1972, 1974) have interpreted this periodicity in terms of an interacting spectroscopic binary. Note, however, that none of the other long-term light or spectrum variations of this star can be interpreted in terms of the proposed orbital period. A detailed description of the light, color, and line-spectrum variations of 88 Her is given in Harmanec et al. (1978), Doazan (1973), and Doazan et al (1982), where most of the references on this star are also to be found

Figure 11-46 illustrates the long-term variation of 88 Her in the UBV bands, from 1968 to 1980, it is apparent that the U magnitude undergoes the largest variations. This curve can be divided into three sections (1) a section of increasing luminosity, at the end of which the metallic shell lines disappear while the Hα emission decreases, (2) a section of constant luminosity, during which the spectrum varies little, (3) a section in which the luminosity drops abruptly while the spectrum undergoes few variations, but *at the middle* of which the metallic shell spectrum begins to appear. Following these three sections, there is a period during which the luminosity again increases rapidly while the shell spectrum develops and the emission in the Balmer lines increases

The similarities between the light curve of 88 Her and that of Pleione are striking. (1) an abrupt drop in luminosity before the appearance of the shell spectrum, (2) a gradual luminosity increase with the development of the shell lines and the Balmer-line emission. However, there are important differences in the behavior of these two stars First, Pleione goes through a transition (Be shell) → (Be) → (Be shell), while 88 Her goes through a transition [Be shell (hydrogen + metals)] → [Be shell (hydrogen)] → [Be shell (hydrogen + metals)]. The sharp absorption cores in the Balmer lines have never disappeared in 88 Her on high-dispersion spectra, one observes only large variations in the depth of these cores and in the number of hydrogen lines having a shell feature Second, while the disappearance of the

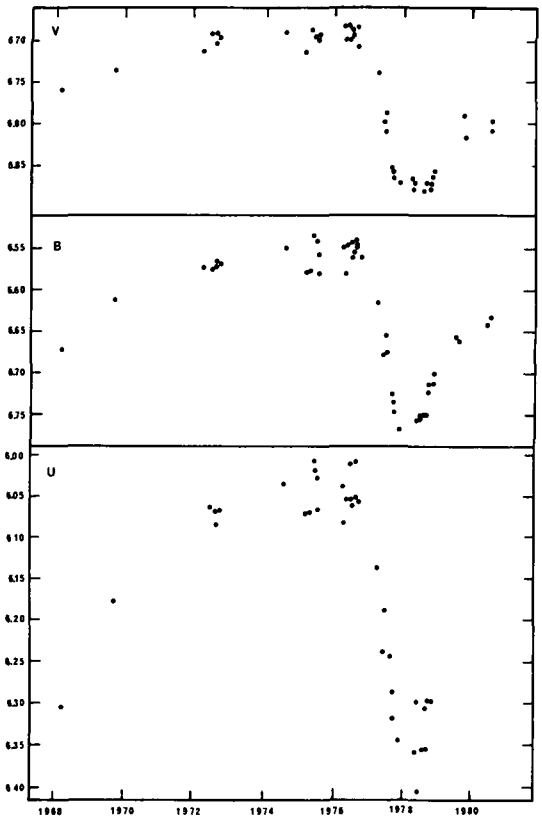

Figure 11-46. The long-term light variation of 88 Her in the UBV bands from 1968 to 1980 Note the rapid drop of the luminosity in the 3 bands before the development of the metallic shell spectrum, the largest drop occurs in the U band. (For 1968 to 1977, this figure is from Harmanec et al., 1978, and the data for 1977 to 1980 are from Harmanec et al., 1980, Nakagiri and Hirata, 1979, Baldinelli and Ghedini, private communication, and Magalashvili and Kumsishvili, 1980.)

shell in Pleione was accompanied by a strong expansion in the Balmer-line radial velocities, mainly for the higher members of the Balmer series, the radial velocities of the shell lines in 88 Her have maintained the same periodic behavior since 1912

In Figure 11-47, we see the path followed by the star in a (U − B), (B − V) diagram from 1968 to 1977, the colors correspond to a spectral type of B8 at the time when the shell spectrum is most highly developed, and to a spectral type of B6 when the metallic lines and the emission have almost disappeared. Once more, we note that the spectrum can look very different for the same value of the magnitude in the UBV bands and for the same color indices

EW Lac (B2 Ve). In EW Lac, the continuous spectrum exhibits short-term and long-term variations at an epoch when the line spectrum is undergoing few variations. This star, which has been observed for nearly a century, exhibited strong variations until 1920, characterized by several disappearances and reappearances of the shell spectrum. This period of high activity was followed by a remarkably quiet period, from 1926 to 1977, during which the shell spectrum, which was well developed in the hydrogen lines out to H42 and in the metallic lines, underwent few variations. Only very small profile and radial-velocity variations were observed.

It was, however, during this quiet period in the visible line spectrum that strong photometric variations were detected. Walker (1953) observed rapid variations in the V magnitude with a quasi-periodicity of 0.8 day. Twenty years later,

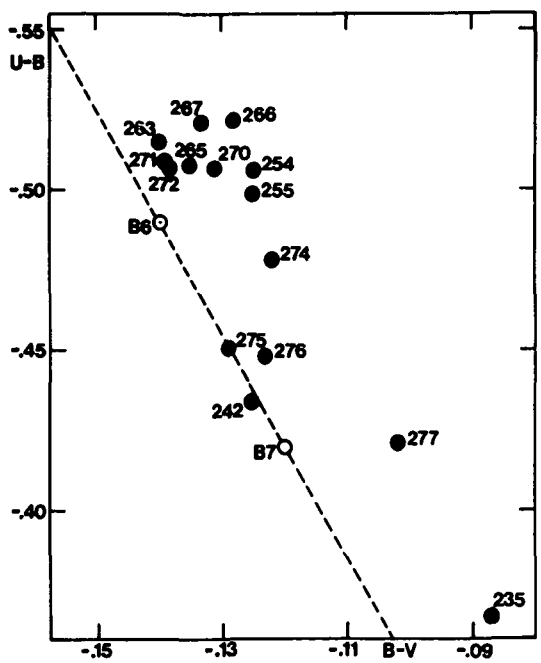

Figure 11-47. The path followed by 88 Her in the (U − B), (B − V) diagram from cycle 235 to 277, i.e. 1968 to 1977 (from Harmanec et al., 1978).

Lester (1975) detected similar light oscillations, with a quasi-period of 0.7 day. Figure 11-48 shows the variations in the Hα index—which is a narrow-band photometric measurement of the intensity at Hα—and in the uvby magnitudes The variations are very similar to those that have been observed in other Be stars by Lynds (1959, 1960), Olsen (1972), Guerrero and Mantegazza (1979).

The most striking characteristic of the rapid variations of EW Lac is the large variation in the Balmer jump, which is well represented by the difference between the u and v magnitudes and which is accompanied only by very small, barely detectable variations in the Hα index. These measurements are related only to the total Balmer jump; they can give no information concerning the two Balmer jumps that appear on BCD classification spectra (see the previous section) Lester compared the observed variations with those that could be predicted from various models The wavelength dependence of the variations seems to exclude an interpretation in terms of variations in the absorption, emission, or scattering in the envelope Rather, it suggests a temperature variation in the atmosphere of the star.

In 1978, the star entered a new phase of activity, characterized by a strong variation in the Balmer progression (Hadrava et al , 1978). By analyzing the behavior of the continuous spectrum from 1968 to 1978, one clearly sees that the amplitude of the long-term variations is much

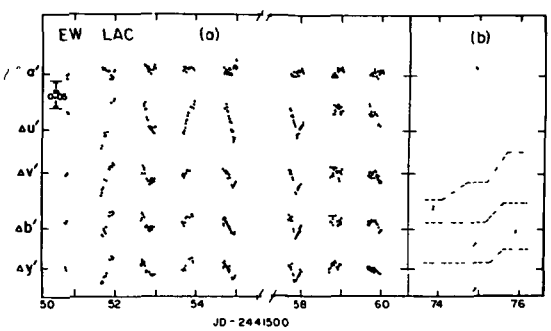

Figure 11-48. Rapid light variations of EW Lac as observed in the u, v, b, y, and Hα narrow bands. (a) Observations of EW Lac during the time of periodic activity; (b) Observations during a sudden fading (from Lester, 1975).

greater than that of the rapid variations (Harmanec et al., 1979) Figure 11-49 traced by these authors, shows the path followed by the star in a (U − B), (B − V) diagram, in the course of its long-term variations, the large scatter of the points corresponding to a single epoch of observation represents the short-term variations. Such a diagram shows the two aspects of the light variations in EW Lac first, the long-term variations, in which we see the point representing the star move slowly across the diagram in one direction or another, second, the short-term variations, which cause a scatter of the points along the locus of the long-term variations. These rapid variations, whose period has, apparently, remained remarkably stable in order of magnitude for more than 20 years, suggest a close

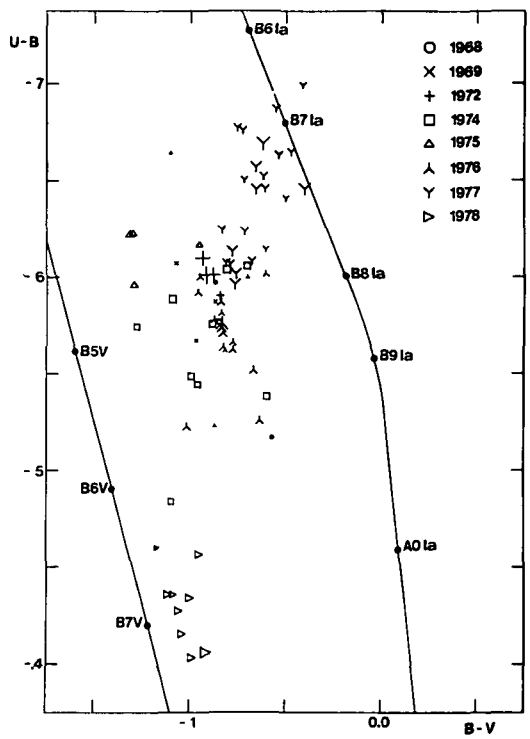

Figure 11-49. The path followed by EW Lac in the (U − B), (B − V) diagram from 1968 to 1978 (from Harmanec et al., 1979) The two aspects of the light variations in EW Lac are seen first, the long-term variations, in which the star moves slowly across the diagram from the top to the bottom, second, the short-term variation which causes a scatter of the points along the locus of the long-term variations

connection between the Be phenomenon and the β Cephei phenomenon (See Chapter 5) We note that from 1972 to 1977, the photometric variations of EW Lac were very large, while the line spectrum varied little, in 1978, when a change in the Balmer progression was observed, the photometric variations were not much greater than before. The correlation between the variations of the continuum and those of the line spectrum does not seem to be very close, contrary to the preceding examples in which variations in the continuous spectrum accompanied those in the line spectrum

LINEAR POLARIZATION IN THE Be STARS

The linear polarization of radiation is not a peculiar feature of Be stars; it is observed in many other emission-line stars, like Herbig's Ae and Be stars, the Of and Wolf-Rayet stars, and the supergiants. Its existence has been proven by the observation of its variations with time, as was the case for the intrinsic reddening of Be stars in the visible. It was, in fact, by observing the variation of the polarization in γ Cas that Behr (1959) discovered the intrinsic linear polarization in Be stars. Shakhovskoi (1962) then detected a variable polarization in χ Oph, a Be star considered to be pole-on. Subsequent observations have produced evidence for polarized radiation in the majority of the Be stars observed. The degree of polarization in the continuum is not high; it is of the order of 1 percent, and does not exceed 2 percent.

The intrinsic polarization of the Be stars has two characteristic properties. (1) The polarization decreases rapidly with wavelength in the ultraviolet spectrum across the Balmer limit, this wavelength dependence differs from that of the interstellar polarization, as was first noted by Serkowski (1968) Like most of the properties of the Be stars, this wavelength dependence exhibits a certain individuality and variability, while maintaining this peculiar characteristic. (2) The polarization decreases from the continuum across the spectral features, such as the Balmer emission lines.

The existence of an intrinsic polarization currently provides the strongest evidence for the asphericity of the outer atmosphere of the Be stars. Indeed, theoretical work seems to show that it is difficult to obtain the observed degree of polarization, by electron scattering, from purely photospheric effects The work of Nagirner (1962), Collins (1970a), and Rucinski (1970) on rotationally deformed atmospheres in the non-gray case shows that the computed polarization in the visible region is very small, of the order of 0.1 percent. Moreover, Serkowski noted that among the stars having large values of v sin i, only the emission-line stars exhibit a measurable polarization, thus, suggesting that the polarization originates in an extended atmosphere of these latter stars. If we adopt the rotation model, in which the star is surrounded by a cool envelope, flattened at the equator, then the pole-on Be stars, whose configuration is symmetrical with respect to the line of sight, should have nearly zero polarization, while the equator-on Be stars should have the strongest polarization.

The simplest method of producing linear polarization is to have the stellar radiation scattered by the particles contained in a volume that is not spherically symmetrical with respect to the observer. This was the interpretation proposed by Shakhovskoi (1964) and Rucinski (1966, 1967) to explain the polarization of the eclipsing binary β Lyr. Then, a qualitative interpretation of the wavelength dependence of the polarization in β Lyr was given by Appenzeller and Hiltner (1967). They showed that the drop in polarization in the ultraviolet spectral region could be understood by means of the greater absorption on the shortward side of the Balmer jump, owing to the hydrogen contained in the envelope. Far from being peculiar to β Lyr, this wavelength dependence of polarization, p (λ), turned out to be common for the hot stars with extended atmospheres (Serkowski, 1968). This led Coyne and Kruczewski (1969) to propose a model in which the intrinsic polarization of the Be stars is caused by electron scattering in the envelope, whose geometry is aspherical with respect to the observer, and where the wavelength dependence of the polarization is mainly due to continuous

absorption by hydrogen The deciding factors in the computation of models are the geometry of the envelope and the ratio between the opacities for hydrogen absorption and electron scattering, and, of course, the electron temperature The changes in polarization from the continuum across an emission line can be explained, in the first approximation, by the addition of unpolarized line emission, or emission whose degree of polarization is much less than that of the continuum. Such an interpretation implies that most of the radiation is polarized in the regions near the star, and that the emission lines are formed farther out in the atmosphere. Very well-documented review articles on the polarization in Be stars have been published by Coyne (1976a), McLean and Clarke (1976), and Coyne and McLean (1981), the polarization in various types of emission-line objects has been reviewed by Zellner and Serkowski (1972) and Kruszewski (1974).

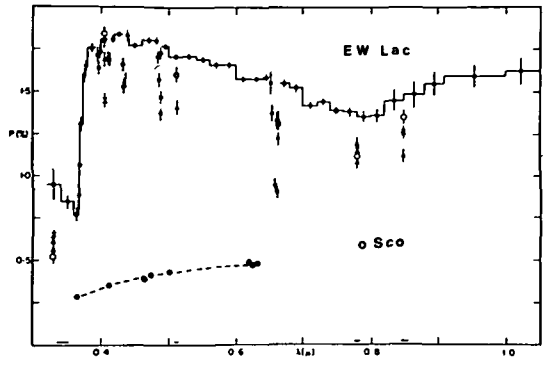

Figure 11-50 The wavelength dependence of the polarization in the Be shell star, EW Lac (from Poeckert et al , 1979) and in the normal star, o Sco, representing the interstellar polarization (from Coyne, 1976b) The striking feature of the polarization of the Be star is the rapid decrease in crossing the Balmer limit toward shorter wavelengths

The Wavelength Dependence of the Continuum Polarization

The principal characteristic of the wavelength dependence of the polarization in Be stars was discovered by Serkowski (1968), who showed that the polarization in these stars decreases more rapidly toward the ultraviolet region than does the interstellar polarization. Curves showing the wavelength dependence of the polarization in the Be stars can be found in Coyne and Kruszewski (1969), Coyne (1971), Kruszewski (1974), and Poeckert et al (1979). Figure 11-50 shows the polarization curve of σ Sco, a bright standard star whose radiation is highly polarized by the interstellar medium and whose wavelength dependence is that of the normal interstellar polarization (Coyne, 1976b), and EW Lac, a Be shell star which was observed at higher resolution (20 Å in the blue and visual regions and 40 Å in the near infrared region) by Poeckert et al. (1979). The striking feature of the polarization curve of the Be star is the rapid decrease in crossing the Balmer limit toward shorter wavelengths, while the normal interstellar polarization decreases gradually toward shorter wavelengths in the Paschen continuum. This peculiar feature emerges in a striking fashion from all the observations. Except for this feature, which is common to all the Be stars, we can see from Figure 11-51 that there is a great variety of forms for the wavelength dependence of polarization in Be stars. This figure is not typical of a random sample of Be stars; it is made up of the stars that exhibit high intrinsic polarization at the present epoch of observation.

The rapid decrease of the polarization in crossing the Balmer limit toward shorter wavelengths is an inverse function of the variation of the bound-free hydrogen opacity in this spectral region (Coyne and Kruszewski, 1969) Such a polarization curve can be constructed by combining the effects of electron scattering, which is independent of wavelength, with those of continuous hydrogen absorption in a plasma whose electron density and temperature are adjusted to reproduce the observed polarization law. In Coyne and Kruszewski's model, the star is a point source; by varying n_e and T_e in the envelope (Coyne, 1971, 1976a) and the degree of flattening (Brown and McLean, 1977), one can obtain good agreement with the observations.

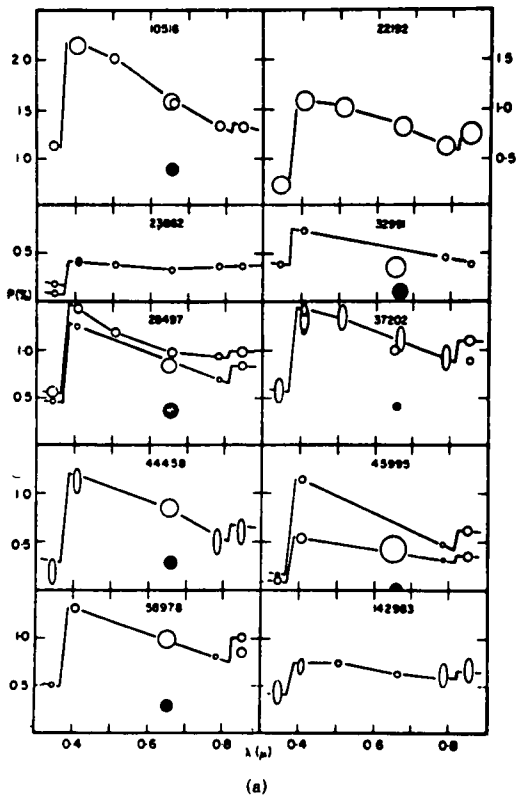

Figure 11-51. Intrinsic polarization in Be stars (from Poeckert et al., 1979). The sizes of the circles represent the observational error. The ellipses indicate time variations in polarization whose range is represented by the major axis. Filled circles represent Hα line polarization.

Cassinelli and Haisch (1974) showed that polarization by electron scattering in rotationally deformed stars could reach 2 percent for a Roche model; it could be as high as 6 percent for a disk-shaped envelope. They used the results of the equations of transfer from Cassinelli and Hummer (1971), which were obtained for extended atmospheres in which the density decreases as r^{-n} instead of decreasing according to the exponential law for normal atmospheres. The increased polarization in these atmospheres is essentially caused by the forward peaking of the radiation field.

Haisch and Cassinelli (1976) studied the wavelength dependence of polarization, using the equations of transfer, when the bound-free and free-free opacities in the extended atmospheres are taken in account. They showed that only very flattened, disk-shaped envelopes could provide degrees of polarization greater than 1 percent, such as are sometimes observed. However, the form of the wavelength dependence is far from exhibiting as strong a decrease on the short wavelength side of the Balmer jump as is seen in the observed curves.

Poeckert and Marlborough (1977, 1978a, 1978b) used the model developed by Marlborough (1969) to account for the profile of the Hα emission line and for the continuous polarization in γ Cas (see the next section). They showed that 75 percent of the polarized flux originates in regions near the star, within $2\,R_*$ of the surface. This is in contrast to the much more extended region, of the order of $15\,R_*$, in which the Hα emission is formed. They took into account the bound-free and free-free processes and showed that the wavelength dependence of the continuous polarization is dominated by absorption effects in the envelope, as Coyne and Kruczewski had suggested. The degree of polarization depends, in the first instance, on the inclination of the equatorial, disk-shaped envelope, and then on the density; but the decrease in polarization at the Balmer and Paschen limits depends essentially on the density.

The wavelength dependence of polarization out to 2.2 μ has been studied by Capps et al. (1973), Coyne and McLean (1975), Coyne and Vrba (1976), and Jones (1979). For ζ Tau, φ Per, γ Cas, and EW Lac there is a more or less rapid decrease of polarization at wavelengths greater than 1 μ. Figure 11-52 shows the wavelength dependence of polarization for EW Lac. The stars 48 Lib, ε Cap, and σ Aqr maintain a high level of polarization out to 2.2 μ, as can be seen in Figure 11-53 for 48 Lib. These different types of wavelength dependences in the infrared cannot be explained by a single envelope structure (Jones, 1979). Note that these different polarization curves do not depend on the shell or Be nature of the spectrum, nor on the value of v sin *i*. In Jones' first group, illustrated by the polarization curve of EW Lac, the values of v sin *i* range from 230 to 450 km s^{-1}, in the second group, they range from 280 to 400 km s^{-1}.

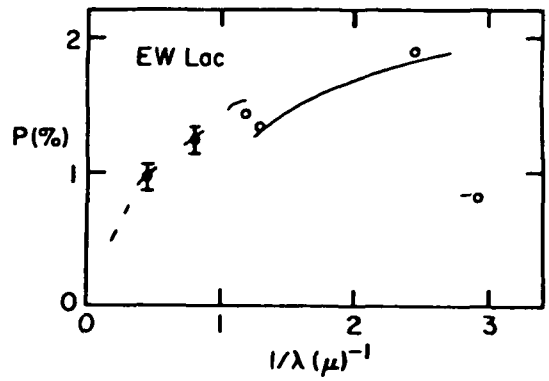

Figure 11-52. Wavelength dependence of the polarization of EW Lac out to 2.2 μ. Note the high degree of polarization in the Paschen continuum and longward. The best fit model of Jones is indicated as solid and dashed lines (from Jones, 1979).

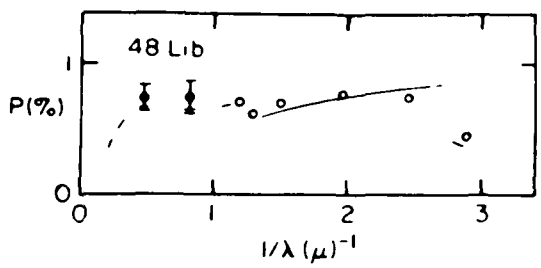

Figure 11-53. Wavelength dependence of the polarization of 48 Lib The best fit model of Jones is indicated by solid and dashed lines. The polarization is nearly constant in the Paschen continuum and at longer wavelengths (from Jones, 1979)

In order to explain the wavelength dependence of the polarization in ζ Tau, Capps et al. (1973) suggested a model in which the star is surrounded by a homogeneous, optically thin hydrogen envelope, shaped like a flat, detached disk and viewed equator-on. The disk is illuminated by the central star which is assumed to be a point source. The radiation emitted in the disk is assumed to be unpolarized. These authors showed that the electron scattering produced in the disk, modified by the bound-free absorption and by the addition of the unpolarized free-bound continuous emission from the disk, does not account for the rapid decrease in polarization with wavelength between 0.9 and 2.2 μ. In order to obtain agreement with the observations, unpolarized free-free emission from the disk must be added. In this model, the variation of the polarization in the infrared region is determined mainly by the relative magnitude of the free-bound emission and the free-free emission, which, in turn, depends on the values of n_e and T_e in the disk. The models were computed for values in the range $T_e = 8 \times 10^3$ to 2×10^4 K and $n_e = 10^{11}$ to 10^{12} cm^{-3} in the disk. There is reasonable agreement with the observations for models from $T_e = 10^4$ K, $n_e = 2.0 \times 10^{11}$ cm^{-3}, to $T_e = 2.0 \times 10^4$ K, $n_e = 3.5 \times 10^{11}$ cm^{-3}. However, it can be seen from Figure 11-54 that there is a significant difference between the computed and observed polarization toward shorter wavelengths. Models similar to those of Capps et al. have been studied by McLean (1979)

Jones (1979) developed a disk model in which the polarization is caused by electron scattering of the radiation from the star and from the disk.

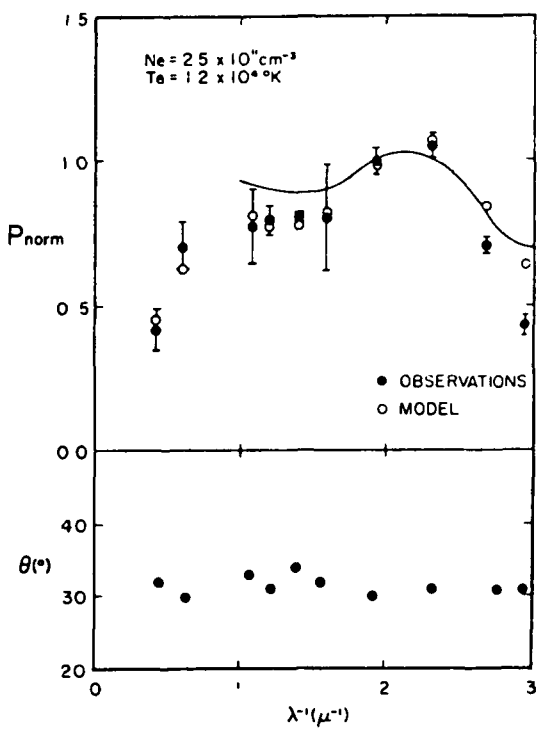

Figure 11-54. Comparison of observed and calculated normalized polarization for ζ Tau (from Capps et al., 1973)

The stellar radiation is scattered twice, and the disk radiation only once. He showed that the electrons that scatter the stellar and disk radiation are the same as those that produce the infrared excess These four stars–ζ Tau, φ Per, γ Cas, and EW Lac–which exhibit a decrease in polarization for wavelengths greater than 1 μ cannot be modeled with uniform density; the density must decrease as r^{-2} above the photosphere. In this case, the disk becomes optically thick in the infrared at wavelengths shorter than those suggested by Gehrz et al. (1974), who considered the case of a homogeneous envelope; this was also shown by Hartmann (1978). 48 Lib and σ Aqr cannot be modeled with the same geometry and density structure as the preceding stars.

At some epochs of variation, the B2ep star, HD 45677, which was observed from about 0.33 μ to 1 μ by Coyne and Vrba (1976), shows a very different wavelength dependence of polarization from that of the two Be shell stars, ζ Tau and φ Per In the previous section, we have described the features of its visible, ultraviolet, and infrared spectrum, and the interpretation of its strong infrared excess in terms of thermal reemission by dust particles. Figure 11-55 shows the polarization curve of this star at four different epochs. The duration of each epoch of observation is from 3 to 6 months, with an interval of around 7 months between the epochs. It can be seen that at epoch II, the polarization exhibits a pronounced maximum near 6500 Å,

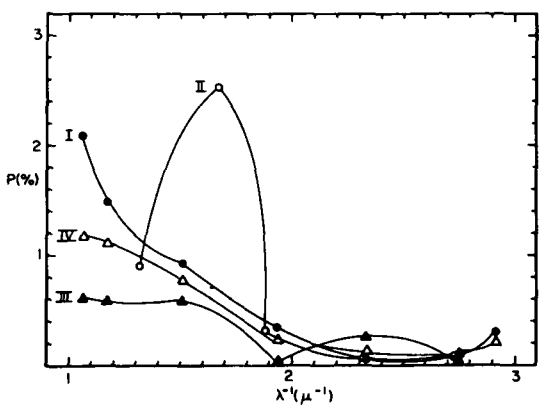

Figure 11-55. Intrinsic polarization for the B2ep star, HD 45677, at four different epochs (from Coyne and Vrba, 1976).

which, according to the analysis given by the authors, is real. We see that the variability of the polarization of HD 45677 in the infrared is characterized by a more or less steep increase toward long wavelengths. Such a dependence was reported by Vrba (1975) for several Herbig Ae and Be stars.

The increase in polarization with wavelength for $\lambda > 0.5$ μ shows that the polarization cannot be due to electron scattering only, modified by bound-free absorption and unpolarized free-bound emission as is usually assumed. In this case, scattering by larger particles–on the order of the wavelength–in an atmosphere that is asymmetric with respect to the observer, must be invoked, as has been noted by Coyne and Vrba (1976). These authors explain the observed polarization by the light scattered from individual clouds of dust in the envelope. They attributed the variability of the polarization to the variable position of the clouds with respect to the observer. The same interpretation was also given by Sitko and Savage (1980) to explain the variations in the ultraviolet flux of this star (see the previous section, The Continuous Spectrum, from the Near Ultraviolet to the Radio Region).

Changes in Polarization Across the Balmer Emission Lines

The first observation of the change in polarization across an emission line was made by Serkowski, and mentioned in Zellner and Serkowski (1972). This feature of the polarization in the Be stars has since been amply confirmed by subsequent observations (Clarke and McLean, 1974, 1975, 1976; Hayes and Illing, 1974; Hayes, 1975; Coyne, 1974, 1976b; Coyne and McLean, 1975; Poeckert, 1975; Poeckert and Marlborough, 1976, 1977, 1978a; McLean et al., 1979; and McLean and Clarke, 1979). These measurements have shown that among the observed stars, those that preferentially exhibit a change in polarization across the emission lines are the Be shell stars and that pole-on stars tend to have little or no change.

The first observations in the lower Balmer lines indicated that the reduction in polarization is, at

first approximation, an inverse function of the emission intensity (Clarke and McLean, 1974, 1976; Poeckert, 1975), which could be explained by the addition of the unpolarized flux from the emission line. In this interpretation, the emission line is formed in more distant regions than those that produce the electron scattering polarization observed in the continuum. This implies that the region in which the emission lines are formed is optically thin for electron scattering. If this hypothesis is verified, the observation of the change in polarization across the emission lines in Be stars provides an indication of the depth at which the emission lines are formed, and also a method of separating the intrinsic polarization from the interstellar polarization. However, a more detailed study shows that the real situation is not so simple (McLean and Clarke, 1979). The changes in polarization and in position angle across the emission lines cannot, in many cases, be explained by the simple addition of unpolarized flux in the line, as was assumed by Coyne and McLean (1975), Poeckert (1975), and Poeckert and Marlborough (1976). The decrease of polarization in the emission line is also due to absorption in the line, which attenuates the polarized flux.

The high-resolution observations (0.30 Å) made by McLean et al. (1979), using a 106-element Digicon, have brought new details to light. Figure 11-56 shows the variation of the polarization across the Hβ line in γ Cas, φ Per, ψ Per, and ζ Tau. We see that the polarization decreases in going from the emission line wing toward the center. At the center of the line, the polarization increases; it then exhibits a secondary maximum and minimum in the wings, at about ± 10 Å from the center. There are also complex variations in the position angle. Thus, in the entire envelope, as Coyne and McLean (1981) point out, the polarized flux can be absorbed in the line, and the flux emitted in the line can be polarized or unpolarized. Finally, considering the large mass motions in the envelope, the flux emitted at a given frequency in the line arises from different depths in the envelope. This complicated situation requires the construction of a very complete model to interpret the observed polarization profile.

Determination of the Intrinsic Polarization

The polarization values deduced from the observations are the sum of the effects of the interstellar medium and the circumstellar medium. McLean and Clarke (1979) have made a critical analysis of the various methods used to separate the interstellar polarization from the intrinsic polarization. The problem is similar to that of separating the effects of the interstellar extinction from those of the intrinsic reddening which affects the continuous spectrum of the Be stars (see the previous section, The Continuous Spectrum, from the Near Ultraviolet to the Radio Region). The problem is made more difficult by the fact that the degree of intrinsic polarization is small, and often comparable to

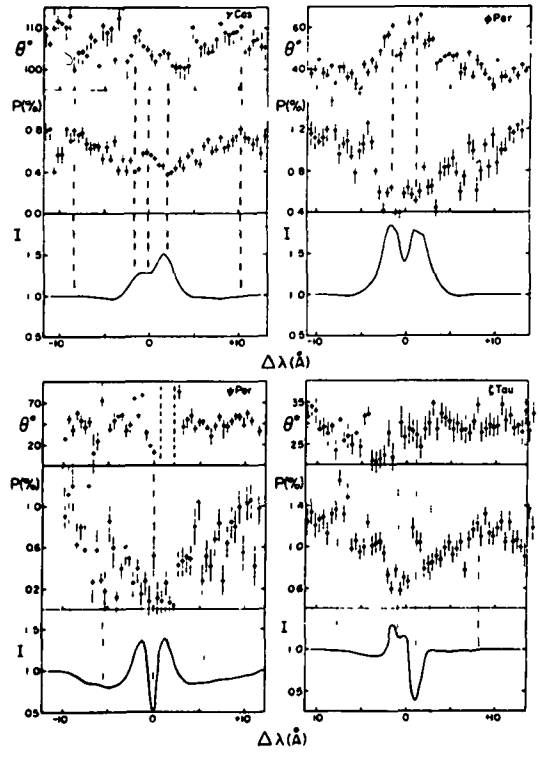

Figure 11-56. High resolution polarization structure across Hβ, and polarization angles for γ Cas, φ Per, ψ Per, and ζ Tau (from McLean et al., 1979). At the center of the line the polarization increases, a secondary maximum and minimum is exhibited in the wings

the degree of interstellar polarization.

All the methods assume that the interstellar polarization does not vary with time. The first method consists in determining the mean polarization properties of the stars located in the neighborhood of the star under consideration. One can also use the properties of the polarization vectors when one observes its variations. Finally, one can assume that the emission flux is not polarized in the line; then the interstellar polarization is determined, in magnitude and direction, from the change in polarization across the line. In the latter case, the underlying hypothesis is that the radiation is polarized near the star, but unpolarized in the emission line. As has been said above, the application of this last method to all the Be/shell stars, without distinction, is of doubtful value, in certain cases it leads to differences in the values of the interstellar parameters which are barely within the allowable errors (McLean and Clarke, 1979). One method of verification consists of taking the mean of the values obtained for two lines, and comparing it to the results obtained by other methods. At the moment, there is no one good method; there are several methods, each of which has its limitations.

Statistical Properties of the Linear Polarization in Be Stars

The interpretation of the observed polarization in the Be stars in terms of scattering of the stellar radiation by the electrons in a circumstellar envelope, whose configuration is asymmetric with respect to the observer, leads to the possibility of a correlation between the intrinsic polarization and v sin i. In the rotation model, it is assumed that the Be star rotates at the critical velocity and that its outer atmosphere is confined to the equatorial plane. This implies that stars observed at the pole, whose configuration is symmetric with respect to the observer, should have zero polarization, while stars observed at the equator should have high polarization. From the time of the very first observations of polarization in the Be stars, it was recognized that the real situation was much less simple. In fact, χ Oph, which is classified as a pole-on star, was one of the first Be stars for which intrinsic polarization was detected, on account of the variability of its polarization. The mean value of the polarization in the visible is 0.52 percent and the amplitude of the variation is 0.39 percent (Coyne, 1976a).

Hayes (1980) studied the polarization of five pole-on Be stars and monitored their behavior over a period of 5 to 17 months. For these five stars, a very low mean level of intrinsic polarization was detected. Variations in the polarization of ω Ori were clearly demonstrated. Analysis shows that the equatorial Stokes parameters, Q and U, vary in such a way that they describe a nearly straight line in the (Q, U) plane. This colinear variation of the polarization can be obtained if the scattering particles are distributed axisymmetrically (Shakhovskoi, 1965; McLean, 1979). The variable polarization of ω Ori shows that if this star is rotating at the critical velocity and the envelope is confined to the equatorial plane, then the star is not viewed pole-on, in spite of its low value of v sin i (160 km s^{-1}). Assuming that the polarization variations are due to changes in the optical depth—that is, changes in the density of the envelope—Hayes concluded that the mass flux of ω Ori must be variable. The existence of a mass flux in this star was demonstrated by Peters (1981), who observed shifts of -750 km s^{-1} in the C IV resonance lines on ultraviolet spectrograms (see Chapter 12). This direct evidence for the ejection of material, as well as the existence of polarization and its variations, in a star which has been classified as pole-on, leads one to believe that the asymmetry of the outer atmosphere in a Be star is better defined by its polarization than by its value of v sin i (Hartmann, 1978).

Brown and McLean (1977) showed that the polarization, P, observed in the continuous radiation of the Be stars, after scattering by the electrons in an axisymmetric, circumstellar envelope, is given by $P = 2\,\overline{\tau}\,(1 - 3\,\gamma)\sin^2 i$. It depends on three parameters: $\overline{\tau}$, the optical depth of the electron scattering averaged over the solid angle, as seen from the central star; i, the angle between the axis of symmetry of the envelope and the line of sight; and γ, the flattening factor of the

envelope. Thus, the measurement of the polarization alone does not permit a separation of the effects of the parameters $\overline{\tau}$, i, and γ. The statistical distribution of $p = 2\,\overline{\tau}\,(1 - 3\,\gamma)$ can be determined from the distribution of the observed polarization, P, if the axes of rotation are assumed to be randomly distributed, since the probability distribution of $\sin^2 i$ is known. McLean and Brown (1978) studied the statistical properties of the polarization in a sample of 67 Be stars; their distributions of observed polarization and v sin i are given in Figure 11-57. Most of the Be stars are seen to have large values of v sin i, as is well known. On the other hand, the polarization distribution shows that *most of the Be stars have very small polarizations*. This implies that the majority of the Be stars have quasi-spherical atmospheres and not highly flattened, disk-shaped envelopes. Note also that no polarization higher than 2 percent is observed; McLean and Brown conclude that very flattened envelopes do not exist. These trends show that one cannot represent all the Be stars by the same degree of flattening, as is often assumed.

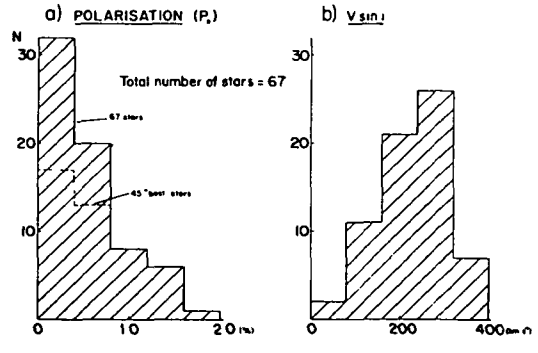

Figure 11-57. Diagram from McLean and Brown (1978). (a) The observed distribution of the intrinsic linear polarization for the blue spectral region for 67 Be stars. The dashed histogram applies to those 45 stars for which the removal of interstellar polarization has introduced the least uncertainty. The most uncertain polarization values are for Be stars exhibiting a low, or very low, degree of polarization. (b) The v sin i distribution of the 67 Be stars of (a). These two histograms show that, even though most Be stars exhibit high values of v sin i, *most Be stars exhibit a low degree of polarization.*

Figure 11-58 shows the polarization as a function of v sin i. We note that for the smallest values of v sin i, the polarization is generally small, while the polarization can take on any value from 0 to 2 percent for large values of v sin i. Putting $k = P/v^2 \sin^2 i$, the figure shows that a large range of k values is observed in the Be stars. But there is also an upper limit on k, which reflects the fact that few Be stars have both a small value of v sin i and a large polarization Poeckert and Marlborough (1976) constructed a similar diagram for 48 Be stars. They compared the observations with their model, in which all the stars are rotating at the critical velocity and all the envelopes are in the form of an equatorial disk. Under these conditions, the polarization depends only on the density. They showed that the disk model is in agreement with the observations, and that a density of $n_e = 5 \times 10^{11}$ cm^{-3} can account for the polarization in all of the observed stars.

The variation of the polarization with Hα emission intensity has also been studied by Poeckert and Marlborough (1976) and McLean (1979). There is a very weak tendency for large values of the polarization to accompany large

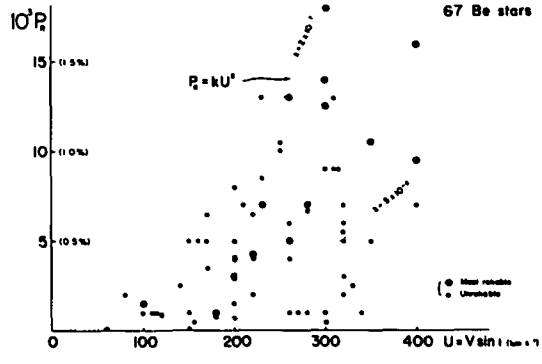

Figure 11-58. The polarization of Be stars versus v sin i *for the stars of Figure 11-57. Solid dots are for the "best" stars (the largest dots are for data of the best quality) and open circles for the less reliable data which are also for stars showing the lowest degree of polarization. Few Be stars have both a small value of* v sin i *and a large polarization. On the other hand, stars having high values of* v sin i *exhibit all kinds of degrees of polarization (from McLean and Brown, 1978).*

values of Hα, and the scatter of the points in the diagram is large. Since, to a certain extent, the intensity of the Hα emission represents the electron density in the envelope if it is optically thin, then if all the envelopes are of the same size and shape, this diagram reflects the variation of the polarization with n_e.

Variability of the Intrinsic Linear Polarization

The intrinsic polarization of the Be stars was discovered by means of its variability. Serkowski (1970) estimated that 40 percent of the Be stars observed more than once exhibited variable polarization. As with the other characteristics of the spectrum, statistical studies do not adequately reflect the amplitude and the generality of the polarization variability. This variability seems to be irregular in nature, with slow variations extending over several months, interspersed with short periods (of the order of days) of stronger variations (Coyne, 1976a).

Up to now, there have not been any systematic studies made simultaneously with other observable quantities in the spectrum, except for certain Be stars that are considered to be spectroscopic binaries. In the case of ζ Tau and φ Per, no correlation was established between the polarization variations and the orbital motion (Coyne, 1975), while for the binary β Lyr, there is a very clear correlation between the polarization variations and phase (Appenzeller and Hiltner, 1967). The infrared observations made for this purpose likewise have given no positive results. In most cases, it seems that the intrinsic position angle, θ_i, does not undergo significant variations. Figure 11-59 shows the variations of the polarization in p Car. The ratios of the polarization in the UBV bands, p_*^U/p_*^B and p_*^V/p_*^B, are much less variable than the polarization itself. The fact that the position angle does not depend on time or wavelength strongly suggests that the envelope is axisymmetric. However, the recent measurements of McLean and Clarke (1979) show that in some stars, the intrinsic position angles also vary with time. This effect is important, for it clearly indicates, in this case, that the region responsible for

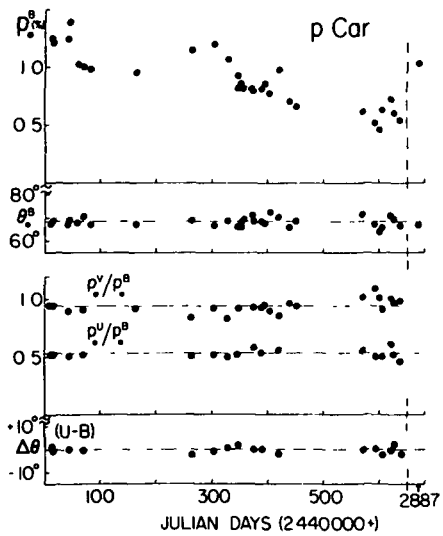

Figure 11-59 Variations of the intrinsic polarization of p Car At the bottom of the figure are shown the variations of the wavelength dependence of polarization as indicated by the ratios p_*^u/p_*^B and p_*^v/p_*^B, and the position angle (from McLean, 1979)

the polarization does not exhibit axisymmetric geometry with respect to the observer. This effect could be attributed to the binary nature of the object, which has yet to be proven. Finally, we note that it is not yet known how the position angle varies when the star goes from a Be phase to a shell phase, or from one Be phase to another Be phase separated by a normal B phase, that is, after the complete disappearance of one envelope and the formation of a new envelope.

Finally, we point out that rapid polarization variations, of the order of days or fractions of a day, have been reported by Serkowski (1970), Poeckert (1975), Clarke and McLean (1976), Poeckert and Marlborough (1978a), and Poeckert et al. (1979). These variations are irregular in nature; they are superimposed on a general, long-term variation.

Be STAR MODELS BASED ON OBSERVATIONS AT VISIBLE WAVELENGTHS

There is no theory of the Be phenomenon,

and the physical causes of its appearance are not yet known. Nevertheless, there is a set of interpretations of the various features observed in the visible spectrum of these stars, which has resulted in an ad hoc representation of their atmosphere. The outline of this picture was suggested half a century ago by Struve (1931b), who laid the foundation for the rotation model. This model attempted to answer two questions (i) In what region of the atmosphere are the emission lines observed at visible wavelengths formed? (ii) What is the mechanism responsible for the formation of this region? The answers to these two questions are the two sides of the rotation model

The origin of the emission lines observed at visible wavelengths. The origin of these lines is attributed to the existence of an extended envelope—that is, a volume effect This interpretation is a logical extension of the one already given to explain the spectrum of the Wolf-Rayet and P Cygni stars. It is essentially based on the Zanstra theory and the Rosseland theorem, which were developed for planetary nebulae (see the section on The Visible and Infrared Spectrum). The essential difference between these three types of stars and the planetary nebulae arises from the very different orders of magnitude of the dilution factor—much smaller in the case of the nebulae—while the Be stars are distinguished from the Wolf-Rayet and P Cygni stars by the large difference in the opacity of their outer atmosphere. The envelope opacity is relatively small in the Be stars, but is large enough in the Wolf-Rayet and P Cygni stars to modify the photospheric radiation considerably. Struve's (1942) article presents most clearly this overall view of the emission-line stars, in which the various types of stars are integrated into a general framework, and where the observed differences in their spectrum essentially reflect the difference in the relative size of the envelope with respect to the photosphere We shall return to this very general interpretation of the emission-line stars, as given by Struve (see Chapter 13).

There is no direct evidence in the visible region to support the assumed existence of an extended envelope for the Be stars. For the planetary nebulae, the extended atmosphere is directly observable, for the Wolf-Rayet and P Cygni stars, the high expansion velocities observed provide a reasonable justification for the formation of an envelope by the ejection of material. This is not the case for the Be stars, where the velocities observed in the visible region are generally too low, as we have seen in the previous sections. As long as the observations were limited to the visible region, the best observational justification for the existence of an extended envelope was found indirectly in the model-dependent explanation of the hydrogen emission lines, and in the dilution effect that is seen in the He I lines. In the extended envelope, where the photospheric radiation is diluted, the predicted accumulation of He I atoms in the metastable levels is observed, as well as a reinforcement of the triplets (2^3S) with respect to the singlets (2^1S) (Struve and Wurm, 1938; Wellman, 1952, Mattis, 1957).

The origin of the extended envelope. Earlier in this chapter we described the observational data that led Struve to attribute the formation of a Be-star envelope to an equatorial ejection of material due to instabilities produced by the critical rotation of the star. Such an interpretation necessarily implies that all the Be stars are rotating at the critical velocity Gerasimovic (1934) suggested that the equatorial mass ejection was due to radiation pressure, whose effectiveness was increased by the decrease in effective gravity due to rapid rotation The observation of V/R variations and the shifts in the edges of the emission line and of the central absorption led McLaughlin (1933) to propose a model in which an expansion and/or contraction was combined with the rotational motion Be-star models have retained this set of hypotheses, which were constructed around a single postulate· the Be stars are B stars rotating at the critical velocity. This postulate is the basis for the geometry generally adopted to represent the extended atmospheres in these stars an equatorial disk or even a ring, also in rotation and subject to expansion or contraction. Because of the small radial velocities observed in the visible region, the dominant motion in the envelope is one of rotation. The reader is

referred to the first section in this chapter for a discussion of the observational data, and the problems raised by the determination of v sin i values for the Be stars. We recall only that it has often been shown that rotation alone is not a sufficient mechanism to form an extended envelope. Its only effect is to reduce the effective gravity at the equator, thus moving the critical point nearer the photosphere (Marlborough and Zamir, 1975). As for radiation pressure, it can only accelerate a motion that has already begun. The second side of the model, thus, has much greater weaknesses than the first side, from both the observational and theoretical points of view. A review of the Be-star models can be found in Marlborough (1976) and Poeckert (1981); Hummer (1976) reviews the problem of line formation in expanding atmospheres.

Nevertheless, the rotation model has stood up to nearly half a century of new observations, as long as the observations were restricted to the visible or infrared regions, it provided a convenient picture into which a large amount of new data could be fitted. This relative agreement between the model and the observations is a result of the fact that the anomalies that appear in the visible and infrared spectrum of the Be stars originate, for the most part, in the same atmospheric region—the cool, low-excitation extended envelope; here are formed the Balmer emission lines, the emission lines of singly ionized metals, the free-free and bound-free radiation, and the electron scattering However, even in the visible region, it should have been possible to guess that the suggested picture was too narrow for the richness and diversity of the properties of the Be stars, and that one could not reasonably hope to describe them while using only the parameters T_{eff}, g, and v sin i, on the one hand, and while remaining within the general framework of the classical theory of stellar atmospheres, on the other hand.

One year after the model had been proposed, Struve and Swings (1932) noted its great vulnerability and weakness when confronted with the variations observed in the Be stars. Half a century later, we are forced to admit that emission lines and variability are two associated phenomena, and that we cannot describe the first without understanding the second. Nevertheless, we shall see in Chapter 12 that the real contradiction between the model and the observations comes from the far ultraviolet, where there is evidence for a new region in the outer atmosphere of a Be star, which no theory or model has predicted. Instead of a cold, low-excitation region, one observes a hot, superionized region—that is, a chromosphere-corona. Instead of high rotation velocities, one observes expansion velocities higher than the escape velocity at the surface of the star. Instead of the mass ejections which were assumed to be restricted to the equatorial regions, one observes high expansion velocities in the stars classified as pole-on—that is, in the presumed direction of the axis of rotation (Peters, 1981) The picture of a cool, rotating equatorial disk is confronted with the picture of a hot, superionized atmosphere in violent expansion. The rotation model appears to be shaken by the observation of these new features. It is clear that any Be-star model must represent all these observations within a coherent, physically self-consistent framework

In Chapter 13, written in collaboration with R. N. Thomas, we shall use the whole range of observations in an attempt to determine the guidelines to be followed in constructing an empirical model. Here, we shall describe the existing models, confining ourselves to those that consider the Be phenomenon as an occurrence in a single star. We refer to the review articles of Harmanec (1981) and Plavec (1976) for the interpretation of the Be phenomenon in terms of mass transfer in close binary systems. The phenomenon of "emission-line stars," being widespread in the HR diagram, undoubtedly exists for single stars; only this case will be treated here.

Almost all the Be-star models have adopted the general features of Struve's rotation model. As such, they should logically include two interconnected parts (a) the treatment of the hydrodynamic problem of the formation of the envelope, starting from the rotational instabilities produced by the critical rotation of the star; the solution of this problem should define the density, the temperature, and, assuming the mass flux to

be constant, the velocity distribution at each point in the envelope, (b) the solution of the equation of transfer, in order to compare the computed spectrum with the observed spectrum. If one wants to represent a real star, the parameters defining the model should take into account the variable nature of the Be stars and the different types of spectra that can be exhibited by the same object—the Be, Be shell, and normal B phases. Moreover, the study of the variations of individual stars strongly suggests that the sequence of events is of physical significance, and that these events are irreversible. Therefore the parameters defining the model should also vary with time. Needless to say, the construction of Be-star models is far from having furnished a complete solution to these two problems, especially the first one; instead of treating the hydrodynamic problem, one guesses at its solution in order to obtain the density distribution in the envelope. It is essentially this first part that constitutes the ad hoc aspect of the models. As for the second part, although it has received considerable refinement in the area of radiation transfer theory, these improvements have not been fully used to construct a model of a real Be star, on account of the great complexity of the problem. But although the progress made in the treatment of the equation of transfer, and in the use of the escape probability method introduced by Sobolev, does not contribute to a better understanding of the Be phenomenon itself, they certainly refine the mathematical tools that enable us to investigate it. The utility of the ad hoc models has often been discussed. Their greatest weakness arises from the fact that new observations have always resulted in genuine surprises for the models, and the modifications necessary to take such observations into account generally give the models an even more arbitrary nature. Nevertheless, if one keeps in mind the ad hoc considerations on which they are based, these models can form a convenient framework for further research.

We shall first describe the conclusions derived from the analysis of the Balmer-line emission spectrum for the construction of empirical Be star models. Then we shall describe the ad hoc models constructed to represent the atmospheres of these stars. We shall begin by outlining the only model, that of Limber, which intended to provide a hydrodynamic solution to the problem of "rotationally forced ejection." We shall see that, in fact, it results only in an equilibrium solution in which the mass flux is zero everywhere, and in which the envelope is infinite, static, and homogeneous. Thus, the mass flux necessarily constitutes an additional physical parameter, independent of the parameters that define the photosphere of the star. It must be imposed if one wants to describe the case of a real envelope. Limber attributes its origin to the properties of the subatmosphere. For Limber, these properties of the Be stars are mainly derived from their critical rotation. Next, we shall describe the model of Marlborough and Poeckert, which is based on Limber's envelope model and which is currently the most complete Be-star model in the number of observable features it is capable of representing.

Inferences from the Balmer Emission Spectrum

The classical theory of atmospheres predicts only absorption lines in stellar spectra; even by taking non-LTE conditions into account, one can produce only weak emission cores in the lines. The presence of emission lines with the intensities observed in Be stars, or even in hot supergiants, shows that the conditions of hydrostatic equilibrium and/or radiative equilibrium do not hold. The interpretation of the emission lines in terms of an extended envelope implies, at the least, that hydrostatic equilibrium is not realized in these atmospheres.

The various mechanisms capable of producing emission lines in the spectra of hot stars have been fully studied; they are very clearly described in the review article by Pagel (1960). The first problem that arises in the interpretation of emission-line spectra is that of the excitation of the atoms. Most works assume that the emission lines are caused by the recombination that follows the photoionization of the gas in the envelope by the radiation of the star. However, it was quickly realized that the results obtained in studies of planetary nebulae cannot be applied to Be stars,

because the radii of their envelopes are much smaller than those of the nebulae, thus making the Rosseland cycles ineffective. The first determinations of the radii, made principally by Struve from the observed widths of the emission lines, assuming that angular momentum is conserved in the envelope, led to values of the order of 3 to 5 R_*. Burbidge and Burbidge (1953) proposed a simple method to determine the radius and the electron density in the envelope from the observed Balmer-line emission, assuming a low optical depth in the lines. Writing that the line emission is proportional to the total number of atoms in the upper energy level of the transition, they obtained a relation among the equivalent width of the emission line, the volume of the emitting region, and the density of atoms in the appropriate level. They used the Inglis-Teller relation to estimate the electron density of the emitting envelope, and computed the neutral hydrogen density by means of the Saha equation. Assuming that the emission in all the Balmer lines other than Hα, represents 1 percent of the emission in Hα, they found that the radius of a disk-shaped envelope is around 10 R_*, and that the electron density is around 10^{13}. These methods and results are still used, in spite of their very approximate nature. The radii found by Burbidge and Burbidge are of the same order as those obtained from much more complicated ad hoc models, but the electron density, assumed to be constant, is higher by about a factor of 10. In a series of articles, Kitchin (1970b, 1973a, 1973b) proposed a method of determining the size of Be-star envelopes from the intensity ratios of the inner and outer parts of the emission lines. Assuming that the envelope has only rotational motion, he found a typical value of 10 to 15 R_*.

Considering the much larger values of the dilution factors and the larger densities in the envelopes of Be stars, as compared with those of planetary nebulae, it is not justified to assume for the Be stars that the ionization in the envelope occurs only from the ground level; a realistic treatment should also take into account ionization from the excited levels. This was clearly shown by Miyamoto (1950).

The radiation field in an atmosphere with the parameters generally adopted for the envelopes of Be stars has been the subject of many studies. Two different points of view have been adopted one assuming that the envelope is static, and the other trying to deal with the fact that the extended atmospheres are in motion. But in no case has there been applied a self-consistent solution of the equations of statistical equilibrium, radiative transfer, and gas-dynamic equations of motion, in order to interpret the observed spectrum of a Be star.

The Static Envelope. The system of equations for statistical equilibrium has been solved to determine the populations of the various levels, without taking into account the effect of the velocity field in the envelope on the radiative transfer (Miyamoto, 1949, 1952; Kogure, 1959, 1961, 1967, 1969; Pottasch, 1961) These various works consider different cases of opacity, represent the hydrogen atom by a different number of levels, and adopt different values for the temperature (which is assumed to be uniform), so that they are generally not directly comparable. In all these works, the problem of determining the source function at each point of the envelope has been treated approximately; rather, the various physical processes to which the stellar radiation gives rise at a point in the envelope have been studied, more or less completely.

The Moving Envelope. We have seen in the third section, Variability of the Line Spectrum and the Continuous Spectrum, that the velocities observed in the visible region were much smaller than the escape velocity at the surface of the star. However, they are generally larger than the thermal velocity, so that their effects cannot be ignored. In such a situation, the radiation field in the lines depends mainly on the velocity field in the envelope. Rottenberg (1952) studied the role played by the Doppler effect in the solution of the equation of transfer in the lines, in order to account for the line profiles in P Cygni-type stars. He studied the effect of the frequency change on the radiation, in the case where the star is surrounded by a geometrically thin system of expanding envelopes.

The works of Sobolev (1947, 1957) showed that in an atmosphere in motion, where there is a large velocity gradient, the treatment of the transfer problem is simplified because the medium tends to become optically thin through the leakage effect. The application of his method to emission-line stars, and especially to Be stars, which he outlines and recommends, is thus definitely indicated, since there is a velocity gradient in the direction of the observer, whether the motion of the envelope is rotation, expansion, or a combination of the two. Sobolev considered a homogeneous medium with a constant velocity gradient, which is transparent beyond the Lyman continuum but opaque in the lines. The absorption coefficient has a rectangular profile whose width, which is equal to the thermal velocity of the medium, is much smaller than the velocity gradient of the material. Under these conditions, the differential Doppler effect produces a frequency shift in the photons that allows a certain fraction of them, β_{ik}, to escape, not only from the edges of the medium, but also from the deeper layers of the envelope. Therefore, Sobolev introduces the concept of *escape probability*, which defines the probability β_{ik} that a photon emitted at a point in the atmosphere will escape from the medium without being absorbed along the way. The conditions in an envelope in motion are thus in between Baker and Menzel's cases A and B, which correspond to the two extreme situations $\beta_{12} = 1$ and $\beta_{12} = 0$, respectively. The solution of the statistical equilibrium equations then reduces to the solution of a set of nonlinear algebraic equations, in which the diffuse radiation emitted in the envelope does not enter explicitly. Thus, Sobolev's method makes it possible to solve the equations of statistical equilibrium while avoiding the real transfer problem in the lines. Considering an infinite homogeneous medium with a constant velocity gradient, Sobolev shows that grad u and W, the dilution factor, enter the equations only in the form of a ratio, so that the degree of excitation in the envelope remains the same if grad u and W vary proportionately. In particular, this shows that for a given dilution factor, grad u cannot be changed without also changing the excitation state of the envelope. On the other hand, the degree of ionization undergoes very little variation, because this is a situation dominated by photoionization. In order to determine the excitation and ionization state of the envelope, under these simplified conditions, one therefore has to know the ionizing radiation field, the ratio (grad u)/W, and the electron temperature in the envelope.

A comparison of the observed Balmer decrements (intensities of the Balmer-line emission normalized to Hβ) with the decrements computed in the case considered above show reasonable agreement, while the observed values are difficult to reconcile with the decrements computed by Kogure (1967) in the static case (Briot, 1971). In particular, it is possible with the Sobolev method to account for the great range in the values of the Balmer decrements observed in Be stars, by varying the velocity gradient in the envelope and its extension.

In order to compute the profiles, the geometry of the envelope and the emissivity as a function of depth are treated in an ad hoc fashion. As we have already said, there is no theory that allows us to determine the density distribution in the envelope. It is determined from the ad hoc velocity field, by applying the condition of the conservation of radial mass flux. The velocity field is "guessed at" and then improved by successive iterations, until a satisfactory agreement between observed and computed profiles is obtained.

The determination of the velocity field makes it possible to define surfaces of equal radial velocity, which give rise to the photons emitted at the same frequency in the direction of the observer. Figure 11-60 shows a set of these surfaces in the case of an envelope in rotation and decelerated expansion. These curves demonstrate the importance of the effects of the velocity gradients and of the geometry of the envelope. It can be seen at once that there is no longer a one-to-one correspondence between the radiation emitted at a given frequency and the depth at which it is emitted. Thus, it is impossible to deduce the depth dependence of the density by analyzing the observed profile. This shows, in particular, that the same profile can be obtained from different velocity distributions, and therefore from different

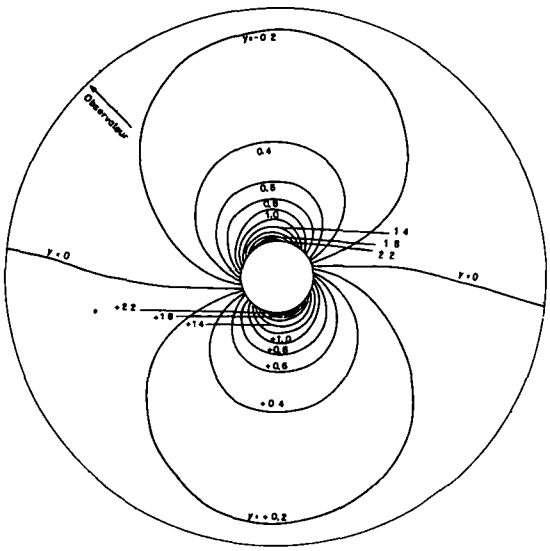

Figure 11-60. Curves of equal radial velocity for a rotating and expanding atmosphere, proposed to interpret the envelope of the Bep star HD 50138 (Doazan, 1965).

density distributions. The model constructed to interpret the profile of a line formed in the envelope will not be unique. In order to minimize the arbitrariness of the model, one tries simultaneously to compare the largest possible number of computed spectral features with those in the observed spectrum.

Aside from its ambiguities, the Sobolev method, or escape probability method (EPM), has been widely applied in the treatment of the transfer problem in the case where, for the chosen velocity field, the line of sight intersects the surfaces of equal radial velocity in only one point; this is the case for expanding motion that is not combined with rotation. In this case, Rublev (1961, 1964) showed that it is possible to obtain a very large variety of profiles by varying the appropriate parameters. But when rotation is combined with expansion or contraction, as is generally assumed in applying the method to Be stars, the line of sight intersects the surfaces of equal radial velocity in more than one point (see Figure 11-60). In this case, the interaction of the radiation in different regions of the envelope can have a large effect on the emergent flux (Noerdlinger and Rybicki, 1974; Surdej, 1977).

The Sobolev method, or EPM, has been an extremely useful tool in the investigation of atmospheres in motion. The method has been refined, stimulated by the demonstration of the generality of stellar winds, and the realization that this phenomenon is not restricted to peculiar stars, like the Be stars, for example, but that it is also observed in normal stars.

Ad Hoc Models of Be Stars

Because no solution has yet been found to the hydrodynamic problem of the formation of the envelope, all Be-star models are ad hoc, as such, they cannot and do not pretend to be physically self-consistent. In this respect, one must keep in mind the arbitrary nature of certain hypotheses on which their construction is based, and one must not expect this picture of reality to closely describe a real star.

There are a large number of Be-star models which can be grouped into two categories. (1) the models in which the envelope is formed as a result of the stellar wind; and (2) the binary model, in which the envelope is produced by mass transfer in a close binary system, where the companion fills its inner Lagrangian surface. We should also mention the static envelope models developed by Kogure according to the ideas of Miyamoto, as well as the elliptical ring model developed by Huang (1972, 1973, 1977, 1978) and Albert and Huang (1974), principally to explain the V/R variations (the ratio of the two emission peaks in the Balmer lines). Finally, we recall the series of models developed to interpret a more limited number of observations, such as the polarization or the infrared excess, which we have described as we presented the observations in the previous three sections. These models actually provided the first physical interpretations of these phenomena, which the more complete ad hoc models have adopted and assimilated.

The stellar wind models differ among themselves essentially in the ad hoc conditions adopted in the absence of a solution to the hydrodynamic problem, and in the methods used to determine the state of excitation in the envelope and the observed profiles. We recall that these models

were all constructed to represent only the observations made in the visible and infrared regions, and point out that they all produce good agreement between the observed and computed spectral features. This agreement is largely explained by the large number of free parameters that can be arbitrarily set. We have already noted that the same spectral feature could be reproduced by different models, and that the problem has no unique solution. It is therefore not surprising to see that different models constructed under different conditions can provide similar solutions. Finally let us say, anticipating Chapters 12 and 13, that none of these models is capable of integrating the observations made in the ultraviolet region without profound modifications, and even profound contradictions.

The stellar wind models differ not only in the ad hoc conditions imposed and the methods used, but also in the number of observable features that they interpret and reproduce numerically. Among the existing models, those developed by Marlborough and Poeckert, following the initial concepts of Limber, are doubtless the ones that have reproduced the largest number of observable features. This is the model we shall describe in detail. But let us also mention Doazan's (1965) model, the first one that has been constructed using Sobolev's method. It adopts two different velocity laws to represent the Hα profile in HD 50138: one in which the velocity decreases outward, and the other in which the velocity begins to increase between 1 and 2 R_* and then decreases. Hutchings' (1970, 1971) model adopts an increasing velocity law, and uses the populations computed by Baker and Menzel (1938), with certain modifications.

Limber's Model. As summarized earlier, it was Struve who proposed the idea of a rotation at the critical velocity leading to an equatorial ejection of material, and thus causing the extended atmosphere of Be stars. A series of papers by Limber, Marlborough, and Poeckert gave the idea quantitative form, and used it to predict various observable spectral features. Limber's investigations started (1964, 1967, 1969) as a wholly theoretical inquiry into the atmospheric extension expected when that critical point, where centrifugal force just balances gravitational force, occurs somewhere in the normal atmosphere—that is, where densities are large enough that this region contributes to the observed photospheric spectrum. The subsequent evolution of these studies proceeded, more and more, as simply ad hoc modeling, adjusting various parameters, quite independently of theory, to get the best match to visual observations. The theoretical aspects are interesting especially those regarding their ideas on the origin of the mass flux for such stars, and on a nonspherically symmetrical outer atmosphere. The ad hoc modeling exhibits well the effect of changing various parameters on the observed spectral features.

Limber's original theoretical focus lay on the idea that rotational instability is a consequence of stellar evolution, and thus is probably characteristic of other kinds of stars, rather than simply the Be stars. Thus, he attributed the existence and size of a mass flux from these stars to a configuration of the subatmosphere, rather than to some atmospheric effect alone, contrary to most other theories of mass flux origin. We believe the observations, especially those of the Be stars, increasingly support this idea of subatmospheric origin for the mass flux, although the origin does not necessarily lie wholly in the rotation. Furthermore, the basic demand of the model is for some departure from spherical symmetry, induced by a rotational decrease in gravity toward the equatorial plane. Polarization observations apparently demand such an asymmetry, without, of course, making precise the cause. Thus, as summarized below, although the thermodynamic consistency of aerodynamic solutions and modeling algorithms is lacking, these two attractive features—the subatmospheric origin of the mass flux, and the required asymmetry—make it useful to understand clearly what observational features models constructed from this viewpoint can represent, and how the model could possibly be modified to support other observational features.

The basic premise of Limber's work is that the Be phenomenon, presumably encompassing the three phases of Be, B shell, and quasi-normal B, somehow arises in those atmospheric configurations induced when the rotational velocity of the

star reaches its critical value somewhere in the atmosphere. How the rotational velocity varies with distance from the rotation axis is specified arbitrarily. Limber adopts a rotational velocity law, $u(r)$, such that the acceleration due to rotation everywhere balances gravitation in the equatorial plane; that is,

$$u_\phi^2(r) = GM/r. \tag{11-9}$$

Thus, there is no net force except the pressure gradient on an atmospheric element (barring, that is, any accelerations associated with gradients in the nonthermal velocities). Because no general treatment of such a nonlinear dynamic configuration exists, Limber restricted his investigations to the simplified steady-state situation, axisymmetric rotation, with no velocities greater than thermal velocities in the radial direction (ϖ), or in the direction (z) perpendicular to the plane of the equator, and obtained the density distribution, in the case of an isothermal atmosphere. Adopting hereafter a cylindrical coordinate system ϖ, θ, z, and with r denoting the radius ($r^2 = z^2 + \varpi^2$), the density, $\rho(\varpi, z)$, as a function of ϖ and z is expressed as

$$\frac{\rho(\varpi, z)}{\rho_0(\varpi_0, z=0)} = \exp\left\{\frac{-1}{Q}\left[\frac{2\alpha-1}{2\alpha} + \frac{1}{2\alpha}\left(\frac{\varpi_0}{\varpi}\right)^{2\alpha} - \frac{\varpi}{\left(\varpi^2+z^2\right)^{1/2}}\right]\right\}, \tag{11-10}$$

under the assumption that the rotational velocity varies with distance from the rotation axis as

$$u_\phi^2(\varpi) \,/\, u_\phi^2(\varpi_0) = (\varpi/\varpi_0)^{-2\alpha}, \tag{11-11}$$

where α is arbitrarily chosen. The condition $\alpha = 0.5$ imposes a critical rotational velocity everywhere in the atmosphere, $\alpha = 1$ conserves angular momentum. Also,

$$Q = \frac{kT_0}{\mu}\frac{\varpi_0(=r_0)}{GM} = \frac{q_0^2}{w_0^2}\frac{\varpi_0}{r_0}, \tag{11-12}$$

where q is the one-dimensional thermal velocity, w is the critical rotational velocity, equal to $2^{-1/2}$ times the escape velocity and r_0, the photospheric radius. We note that in an isothermal, spherically-symmetric, nonrotating atmosphere, the density-distribution is

$$\frac{\rho(r)}{\rho_0(r_0)} = \exp\left[-\frac{w_0^2}{q_0^2}\left(1-\frac{r_0}{r}\right)\right]. \tag{11-13}$$

Consider the case $\alpha = 0.5$: the rotational velocity always has its critical value, at all points in the equatorial plane. This is the case which was further developed by Marlborough. In this case, it can be seen from Equation (11-10) that the density distribution in the equatorial plane is constant: the atmosphere extends outward to infinity. The reason is physically clear: the "effective gravity" vanishes and the atmosphere here has a constant density in the equatorial plane. The density is fixed by conditions, at greater depth, where $\alpha = 0.5$ no longer holds; but the overlying atmosphere is wholly opaque.

Let us interpret this result strictly, in terms of the spectrum we should see in the equatorial plane, in the visual, at the lowest possible opacity which gives the photospheric spectrum. Clearly, for the LTE portions of the spectrum, we will see a blackbody at the boundary temperature, T_0. In the non-LTE portions—those lines formed under non-LTE conditions—we will see absorption lines with central intensities corresponding, roughly, to (sink-term) $^{1/2}B_\nu(T_0)$. Any of the standard references on non-LTE conditions in stellar atmospheres will give the solution to the transfer problem in a constant density atmosphere; this is the most simple solution possible. If we choose

$T_0 \sim 1.0 \times 10^4$ K, as did Marlborough, following Struve, we will see an A0 spectrum in the equatorial plane; if we choose $T_0 \sim 2.0 \times 10^4$ K, following Poeckert and Marlborough, we will see more nearly a B-type spectrum.

Let us continue this strict interpretation outside the equatorial plane. Then, near the axis, Equation (11-10) becomes

$$\rho(\varpi, z) = \rho_0 \exp\left[\frac{-1}{2Q}\left(\frac{z}{\varpi_0}\right)^2\left(\frac{\varpi_0}{\varpi}\right)^3\right]. \tag{11-14}$$

Thus, the farther one goes from the star, the less rapidly the density decreases away from the equatorial plane. So, when observing in or near the equatorial plane, one will "see" only a spectral type corresponding to T_0. In the extreme case of the polar direction, for $\varpi \sim \varpi_0$, Equations (11-10) and (11-12) yield

$$\rho(z) = \rho_0 \exp\left[-\frac{w_0^2}{q_0^2}\left(1 - \frac{r_0}{r}\right)\right], \tag{11-15}$$

which is the spherically symmetrical density distribution around a star with density ρ_0 at the base of the isothermal photosphere. Since there is no reduction of gravity at the pole, ρ_0 and T_0 should be fixed by the standard atmosphere solutions under hydrostatic equilibrium and radiative equilibrium. Thus, it is difficult to justify, in these polar regions, a boundary temperature, T_0, much below the standard atmosphere solution. At the equator, it might have been argued in Struve's day (before non-LTE) that the radiative flux decreased as r^{-2}; then, far enough from the star, T_0 could drop, while retaining the radiative equilibrium. We know, however, this is not the case; one simply reaches the asymptotic, non-LTE values given by the various standard, but non-LTE, models So, either the condition that T_0 can have a constant value throughout the atmosphere—the non-LTE asymptotic boundary value—must be imposed, or some other method for fixing a different value of T_0—possibly a distribution of T_0 (z,ϖ)—must be introduced In summary, it is difficult to avoid for T_0 a value as high as $\sim 2.0 \times 10^4$ K, for a Be star of $T_{\text{eff}} \sim 2.5 \times 10^4$ to 3.0×10^4 K In order to obtain $T_0 \sim 1.0 \times 10^4$ K in the equatorial region, as implied by the presence of Fe II, something beyond Limber's model or its extensions is required.

As we have mentioned, the value of the constant density in the equatorial plane, under this hypothesized static situation, is fixed by the density at the depth where the rotational velocity drops below critical. Usually, solid-body rotation is assumed in the subatmosphere: $u_\phi = r\dot{\theta}$, with $\dot{\theta}$ constant. If r_c is that radius where critical rotation is first reached, as in Equation (11-9), one can calculate the depths corresponding to various fractions of the "normal" gravity (undisturbed by rotation). Assuming this normal value to be $\log g = 4$, we obtain the following results: a gravity 80 percent normal is reached at 0.2 stellar radii in the direction of the center of the star, for 50 percent normal, 0 1 radii, for 10 percent normal, or $\log g = 3$ for this star, 0.03 radii. For a star with $T_{\text{eff}} \sim 3.0 \times 10^4$ K, $\log g = 4$, and radius $10 R_\odot$, the density scale-height is about 5000 km, or about 10^{-3} photospheric radii The normal atmosphere covers about 10 density scale-heights The depth where gravity is 10 percent of normal is about one normal atmospheric thickness below the critical point, and the depth where gravity is 50 to 80 percent of the normal gravity, is about 100 normal atmospheric thicknesses. Clearly, if this postulated static solution were to extend throughout the "unstable" region, and nothing removed material from the outer atmosphere, we would never see through to the regions of normal gravity, hence we would never see that quasi-normal B-star spectrum on the basis of which the star was originally classified. If "magically" one could remove more and more of the atmospheric material from the outside inward, we would see, progressively, all the varieties of spectra from supergiant through giant to main-sequence as effective gravity varied from nearly zero to normal. Such "magic" is of course not possible, Limber's resolution of the density-distribution problem, followed by Marlborough and his coworkers in

their ad hoc modeling, was simply to recognize that such a zero-force situation is unstable, and to postulate a forced ejection of matter, of an arbitrary amount, into the subatmosphere at the equator. Then the density-distribution becomes dynamic, as soon as the ejection-velocity is large enough to perturb the static solution. That is, Limber postulated the imposition of a mass flux, for which the velocity increases outward in those atmospheric regions where the density is not constant. The postulatory approach, rather than attempting to predict the value of the mass flux arising from this unstable situation, was adopted simply because of the difficulty of the complete aerodynamic problem. Indeed, this problem has never been solved, and remains outstanding today. From our concluding Chapter 13, it will be clear that we are sympathetic to this approach, believing that it is all that is possible today, if we desire to interpret the data in terms of empirical modeling. We believe only that such a mass flux should not be restricted wholly to the equatorial plane. It is then possible to have two extreme ejection patterns: only in the plane, or in a spherically symmetrical pattern, or, of course, any desired, ad hoc, distribution with polar angle.

Limber discussed the solution for this cylindrically-symmetrical outflow in the equatorial plane, in terms of two equally-imposed distributions: T_e (ϖ), which gives the thermal energy of the atmosphere, and A (ϖ), the radial component of the cross section of the flow. Thus, the equation of mass conservation is

$$u_\varpi \rho(\varpi) A(\varpi) = u_\varpi(\varpi_0)\rho(\varpi_0)A(\varpi_0) = \text{Const.} \quad (11\text{-}16)$$

under the approximation that

$$A(\varpi) = A(\varpi, p) = \frac{\varpi}{\varpi_0}\left(\frac{\varpi}{\varpi_0} - p\right), \quad (11\text{-}17)$$

with $p < 1$ and $\varpi \gtrsim \varpi_0$. p is not the pressure, it is simply assumed to be a constant parameter. The meridional projections of the streamlines characterized by A (ϖ, p) are straight lines radiating from $\varpi/\varpi_0 = p$ in the equatorial plane. The case of $p = 0$ corresponds to a simple outward flow, in a slab of constant cross section in the plane, replacing cylindrical flow with spherical flow simply corresponds to replacing ϖ with r as the variable. By combining momentum and mass conservation, neglecting any radiative, viscous, or hydromagnetic effects, and setting terms in $u_z\, d/dz$ to be negligible, one obtains the usual "stellar wind" equation, including the effect of a rotation which reaches the critical value at some location r_c, following Equation (11-9):

$$\frac{1}{2}\frac{du^2}{d\varpi}\left[\frac{q^2}{u^2} - 1\right] = \frac{1}{\varpi}\left[w_\varpi^2 - u_\phi^2 - q^2\left(\frac{d\ln A}{d\ln\varpi} - \frac{d\ln T}{d\ln\varpi}\right)\right] \quad (11\text{-}18)$$

By assuming that $A(\varpi, p)$ is a given function of ϖ, any z effect is bypassed. Limber assumed also that T, and hence q^2, can be taken as a specified function of ϖ. He asserted that any effect of "turbulence" can be incorporated into the above formalism simply by adding a mean square turbulent velocity to q^2 As already remarked, this suffices for the "kinetic temperature" aspect, but not for the "excitation/ionization temperature" effect.

One can use Equation 11-18, plus (11-10) to (11-12) and (11-17), to put into focus just how far beyond the preceding, purely static solution, Limber developed that quasi-theoretical basis upon which the further ad hoc models of Marlborough and his coworkers rest. One can also judge its internal physical consistency, and that of the ad hoc models.

First, as mentioned, by imposing Equation (11-17) with the constant p as a parameter, and adopting Equation (11-10) and Equation (11-11), one imposes the condition that only thermal processes fix the density distribution perpendicular to the plane. This requires that the velocity in the z direction does not exceed about $q/3$; for a temperature of 2.0×10^4 K (the maximum T_0

considered), this means that u_z is less than 6 km s^{-1}. Furthermore, one cannot, as Limber asserted, take account of any "turbulent" velocities by simply combining their mean square velocity with q^2 to redefine T_0. Especially at our epoch, T_e is completely mixed, in its dual aspects as kinetic temperature, which enters Equation (11-10), and as collisional excitation temperature, which enters the discussion of the spectral level–collisional sub-ionization as for Fe II, or superionization as for O VI, etc. Hence, any observations which show velocities perpendicular to the equatorial plane to be greater than 6 km s^{-1}, or any observations showing T_0 to lie outside the range fixed by radiative processes alone, negate the conditions imposed by this first point a quasi-static density distribution orthogonal to the plane, and a flow-pattern in the z direction fixed by a prespecified law for $A(\varpi)$.

Second, Limber sought solutions for Equation (11-18) in the plane for the flow, $u(\varpi)$, and hence the density distribution by Equation (11-16), which are compatible with. (1) u_ϕ^2, fixed a priori by some variety of Equation (11-11), with no effect of u on u_ϕ, (2) $T(\varpi)$ specified a priori, with $dT/d\varpi < 0$, (3) $A(\varpi)$, specified a priori, with $dA/d\varpi > 0$ and approaching $(\varpi/\varpi_0)^2$ asymptotically, and (4) all nonthermal velocities, except u_ϕ, much smaller than critical rotational velocity. Restriction (2) prohibits, a priori, the occurrence of any chromospheres-coronas and superionization in the equatorial plane Restriction (4) is too weak for the solutions that Limber imposed; it should be that all nonthermal velocities must be less than q, for the following reasons.

If one imposes the condition that the star rotates everywhere at the critical speed–the condition imposed in the rotationally forced ejection model–$(w^2 - u_\phi^2)$ vanishes in Equation (11-18), leaving just the coefficient of q^2 on the right-hand side. Then by assumptions (2) – (3) above, the right-hand side is always < 0. Any flow in which u is less than q initially can only decelerate, there is no problem so long as this condition is maintained in the ad hoc modeling Unfortunately, velocities up to 100 km s^{-1} are indeed adopted in such modeling, for T_0 less than 2×10^4 K, so the ad hoc parameters of the model are not consistent. On the other hand, if an initial velocity u greater than q is imposed in those regions where the rotational velocity is critical, the flow continually accelerates. And, because it is everywhere superthermic, shocks occur, energy dissipates, and condition (2) is violated. If one does not impose the condition that u_ϕ^2 has the critical value, one has precisely the solar wind situation, but with the requirement for the wind to be cold, modified by the presence of the rotational velocity. An initially small u is amplified, it reaches the critical point where $u \sim q$ and the right-hand side of Equation (11-18) vanishes, at larger w than in the case without rotation. Indeed, given condition (2) that w^2 is equal to 35×10^{14}, and that T_0 is equal to 2.0×10^4 K so that q^2 is equal to 3×10^{12}, the right-hand side vanishes only at some 1000 photospheric radii without rotation. To have it vanish, and thus to have u reach q, within 10 radii, requires the $(w^2 - u_\phi^2)$ term to be $10^{-2}\, w^2$ at such a value of T_0. Such a necessity is, of course, the reason for demanding near-critical rotation in such modeling, the observations alone, as already mentioned, do not suggest this condition. Clearly, if one drops condition (2), thus really approaching the solar situation, it becomes possible to produce a wind with non-trivial velocity. Trivial means $u < q/3$; such velocities do not extend the atmosphere, but allow it to remain hydrostatic.

Third, the theory, with all the above restrictions, is, in practice, set aside, and one models the flow by an ad hoc choice of the mass flux. Limber discussed some of the properties of the solutions for $u(\varpi)$, essentially in the isothermal case. However, in his own application of the approach to an actual star, a consideration of the 1938 to 1954 shell episode of Pleione, Limber (1969) stated: "It appears that the determination of $u(\varpi)$ in a deductive manner from the physics of the problem is at present beyond us" This situation has not changed 15 years later. We note, however, the contradictions mentioned above, when one actually introduces the ad hoc values of $u(\varpi)$ which, within this framework, are necessary to model the observations In practice, all these ad hoc models assume a distribution of $u(\varpi)$; but if one assumes that the base of the model, in the photo-

sphere, has a density distribution in agreement with standard modeling, then the choice of u and of the mass flux are equivalent. We return to this point in Chapter 13. We note only that both accelerating and decelerating $u(\varpi)$ are discussed, with minimum velocities near 0, and maximum velocities ranging up to 50 km s^{-1} in some models, and to 300 km s^{-1} in others (Limber, 1969); (100 km s^{-1}, for Marlborough, 1969; and 200 km s^{-1}, Poeckert and Marlborough, 1978a). Marlborough's models have u much greater than q only for distances greater than some 20 radii, with $u > q$ over most of the atmosphere. Poeckert and Marlborough deal with much the same conditions. Limber's models are more exploratory, covering the full range of u/q. In any event, all these ad hoc models adopt $u(\varpi)$ laws which, aerodynamically, simply contradict the conditions stated in (2). Moreover, the assumed hydrostatic density law perpendicular to the plane is clearly a postulate. Basically the chief criticism of these models lies in the assumed thermal and symmetry conditions which are contradicted by the observations made from space in the ultraviolet region and which show superionization and highly superthermal velocities in stars with high and low values of v sin i.

Marlborough and Poeckert's Model. Marlborough's model, which he later developed in collaboration with Poeckert, is, like all Be star models, ad hoc, and thus does not pretend to represent a real Be star. Its main advantage lies in the large number of observable features it manages to compute and reproduce satisfactorily. From this point of view, the model can be said to be very effective. However, the effectiveness of a model should also be judged by the number of hypotheses adopted, the number of parameters fixed arbitrarily, and also its physical self-consistency. Here, we shall describe the following: first, the methods used to construct the model; second, its application to a real star, γ Cas; and third, the influence of a change in the various parameters on the observed features.

The Construction of the Model. The model is based on the ideas of Limber (see the previous subsection). It adopts the hypothesis of rotationally forced ejection—that is, it assumes that all the Be stars rotate at the critical velocity. On the basis of this concept, it adopts a geometry in which the envelope is highly confined to the equatorial plane. We shall see that this geometry has the strongest effect on the observable features. The principles of the construction of the model are given in Marlborough (1969)

The physical parameters describing the underlying star are assumed to be known; they are those of a normal star, of the same spectral type as the Be star, whose radiative flux is given by the classical atmospheric models. The envelope is assumed to be isothermal, with a temperature T_e fixed in advance and lower than T_{eff}. The models have been constructed for $T_e \approx 10^4$ K (Marlborough, 1969) and $T_e \approx 2 \times 10^4$ K (Poeckert and Marlborough, 1978a).

1. The density and velocity distribution. The model sets the density distribution in the z-direction by assuming that there is hydrostatic equilibrium in the envelope in this direction. This implies that the z-component of the velocity is much smaller than the thermal velocity and entails the condition that there is no coupling between the velocity in the equatorial plane and the velocity in the z-direction. In a meridional plane, the expansion of the material takes place along streamlines, which may be approximated by straight lines converging at a point located at a distance p from the axis of rotation; it is defined by Equation (11-17). This distance p is one of the model parameters to be fixed in an ad hoc fashion. It enters the equation given by Marlborough (1969), which describes the density distribution in the (ϖ, z) plane, considering a cylindrical system of coordinates (ϖ, φ, z) with the origin at the center of the star, z the axis of rotation, φ the azimuthal angle, and ϖ the distance from the rotation axis

$$N(\varpi, z) = N(1,0) \frac{\exp\left\{\frac{-1}{Q}\left[\frac{1}{\varpi'} - \left(\frac{1}{\varpi'^2 + z'^2}\right)^{1/2}\right]\right\}}{\frac{u_\varpi(\varpi)}{u_\varpi(1)} \frac{\varpi(\varpi - p)}{1 - p}} \tag{11-19}$$

where the distances are expressed in units of stellar radii and ϖ' is a distance from the axis of rotation that is arbitrarily chosen in the model The density distribution in the envelope is then completely determined if one fixes. (1) the density at one point in the envelope; (2) the distance p, (3) the distance ϖ', (4) the expansion velocity function u_{ϖ} (ϖ). These four parameters are set in an ad hoc manner. Figure 11-61 shows the curves of equal density in the model of γ Cas, which is described in the following subsection.

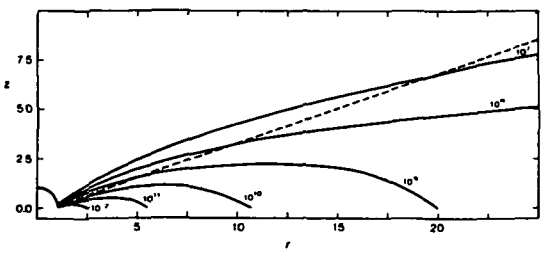

Figure 11-61. The curves of equal density of the atmosphere of γ Cas in Poeckert and Marlborough's model (1978a) (solid lines). The dashed line is the upper limit of the envelope used for the numerical computations. The distances are in units of stellar radius.

The velocity distribution in the envelope results from a combination of rotation and expansion. In Marlborough's (1969) model, it was assumed that the envelope was supported by centrifugal force modified by some viscous force—that is, a critical rotational velocity everywhere in the equatorial plane in the envelope. Poeckert and Marlborough (1978a) use an ad hoc parameter, β, which was introduced by Marlborough and Zamir (1975) and which allows a transition from the case in which the rotation is critical everywhere in the equatorial plane of the envelope to the case in which angular momentum is conserved. The expansion velocity function is also chosen in an ad hoc manner, as was pointed out above. In the end, the velocity function is "guessed," after making several iterations to obtain reasonable agreement between the computed and observed spectral features.

2. Calculating the population of the H I levels. The symmetry of the envelope permits a simplification of the problem by studying only selected points in one quadrant of the meridional plane. The details of the envelope grid used in the computation are given in Marlborough (1969). The adopted model of the hydrogen atom has five levels plus the continuum. The statistical equilibrium equations are solved at various points in the envelope, taking into account photoionizations from all the energy levels and collisional transitions. The radiation density considered in the continuum is produced only by the star, the diffuse radiation field produced by the envelope in the various continua has been neglected. In determining the optical depth, only bound-free absorption processes have been taken into account. However, electron scattering may be a greater source of opacity for $n \gtrsim 3$. The effects of mass motions and thermal motions are neglected, except near the Lyman limit. Poeckert and Marlborough (1978a) use the solution obtained for the first four levels by Marlborough (1969); an LTE solution, based on the population of the fifth level, is calculated for the fifteenth and twenty-fifth levels. This procedure was used because the populations of the fifth level were too high. Three cases for the determination of the populations are considered in Marlborough (1969), and five cases in Poeckert and Marlborough—from the classical nebular case in which the envelope is optically thin for all the lines, to the case in which it is optically thick for all the lines The final populations are determined by taking weighted means of the populations in two neighboring cases. The details of these means are given in Marlborough (1969).

3. Computation of the line profiles and the polarization. In principle, one should compute the emission per unit volume at each point in the envelope, take into account the absorption along its path, and correct for the frequency shifts of the photons due to mass motions. The existence of velocity gradients simplifies the transfer problem. The radiation transfer is computed along a line of sight, including the effects of the continuum, the thermal line-broadening, and the polarization in the line. For each line of sight, the emitted flux

and the Stokes parameters, which define the linear polarization, are determined by linearizing the expression for the optical depth and the source function. The computations are performed for 200 frequencies in the line, along approximately 2000 lines of sight.

4. The energy distribution and the polarization in the continuum. The same linear approximations are used But in this case, the treatment is simplified because the mass motions in the envelope can be neglected.

Poeckert and Marlborough's Model of γ Cas. Here we summarize the principal results of the model as given by Poeckert and Marlborough (1978a) The parameters that define the model of γ Cas are given in Table 11-1, and as can be seen, there are many of them. Their values have been fixed after a certain number of iterations (80), varying the velocity function (and thus the density distribution), the temperature, and the density scale height. The initial parameters were taken from Marlborough (1969). But there is a difference in the temperature of the envelope—1×10^4 K for Marlborough (1969) and 2×10^4 K for Poeckert and Marlborough (1978a). The rate of mass loss implied by this model is $4.4 \times 10^{-8} M_\odot$ per year. The choice of parameters in the model rests essentially on the agreement obtained between the computed and observed Hα profile, and the con-

Table 11-1
Model Parameters for γ Cas

Stellar Parameters						
Mass		$17 M_\odot$				
Radius		$10 R_\odot$				
log g		3.5				
T_{eff}		2.5×10^4 K				
v_{equ}		569 km s^{-1} (solid body rotation)				
Envelope Parameters						
T_e		2.0×10^4 K (isothermal)				
Composition		hydrogen				
N (1,0)		3.33×10^{13} cm^{-3}				
p		$0.8 R_*$				
r'		$15.0 R_*$				
Maximum extent of envelope		$50 R_*$ (line profiles)				
		$250 R_*$ (continuum)				
Inclination		45°				
Velocities*	r/R_*	1	2	6	18	40
	u_r (km s^{-1})	7.5	8.0	25	125	200
	β	0	0	0.5	1	1

Source Poeckert and Marlborough (1978a, table 1)

tinuum polarization.

The density in the envelope was fixed when the computed Hα intensity was in reasonable agreement with the observed value The final profile of Hα is shown in Figure 11-62, where it is compared with the observed profile; the profile of Hβ is given in Figure 11-63. The agreement is satisfactory for Hα, but for Hβ there is considerable disagreement in the line width. The Hβ line in the model is much too broad, by around a factor of 2 with respect to the observed line. This specific example reflects an observational fact that has already been pointed out: Hα is much too broad with respect to Hβ, if it is assumed that the broadening of the lines is principally due to rotation. We consider this a serious disagreement, for the matching of the Hα line is the first step in the construction of a model Poeckert and Marlborough adopt an inclination of 45° for γ Cas, and assume that the star rotates at the critical velocity (569 km s^{-1}). Hutchings and Stoekley (1977) determined an inclination of 47° and a rotation velocity equal to 75 percent of the critical value (427 km s^{-1}). Other things being equal, such a velocity leads to an Hα profile that is much too narrow—the width changes from 17.3 to 13 3 Å—while the agreement with Hβ is much better.

Note also that γ Cas exhibited a shell spectrum during its spectacular variation phase in 1937 and 1941 In Poeckert and Marlborough's model for γ Cas, it would be difficult to produce such a spectrum for an inclination lower than 70°. As we shall see in the following section, v sin *i*—a nonadjustable stellar parameter—has a decisive effect on the width and the nature (Be or shell) of the Hα line. The examples previously described

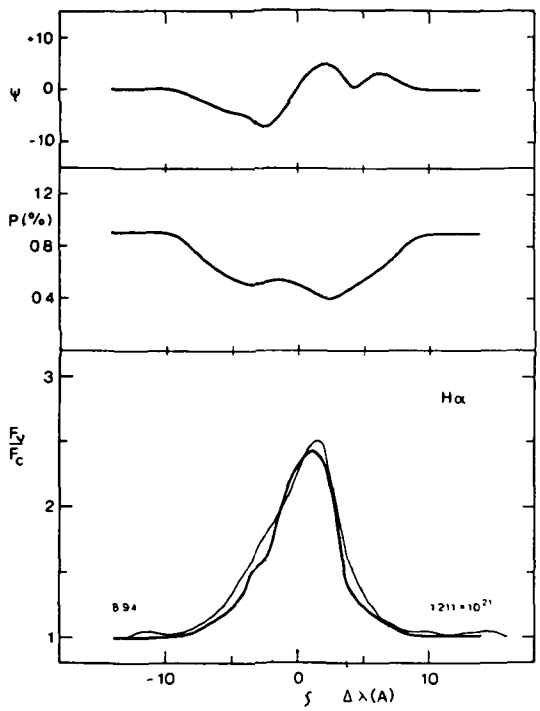

Figure 11-62. Position angle of polarization; polarization and Hα profile of Poeckert and Marlborough's model of γ Cas. The number to the left of the profile is the equivalent width of the line (in Å) and the number to the right is the continuum flux (in ergs s^{-1} Hz^{-1}) The light line is the observed profile of γ Cas on November 1, 1976 (from Poeckert and Marlborough, 1978a).

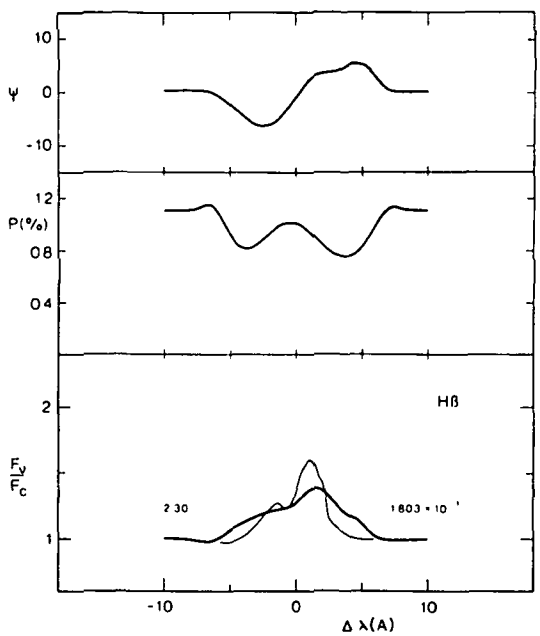

Figure 11-63. Position angle of polarization, polarization and Hβ profile of Poeckert and Marlborough's model of γ Cas (figure from Poeckert and Marlborough, 1978a). Note that the observed profile (light line) is much narrower than the computed one. A typical difficulty of the models is to account for the width of the Hα line as well as the higher Balmer lines.

in the third section amply demonstrate that the same star can exhibit very different emission-line widths, as well as either Be or shell characteristics, depending on its epoch of variation. The constraints imposed by the hypotheses and the geometry adopted in the model appear, in the example of γ Cas, to be much more restrictive than required by the observations

Figure 11-64 shows the energy distribution in the continuum, which is made up of the stellar flux and the free-free, free-bound, and scattered flux in the envelope. The continuous emission due to the envelope is a significant fraction of the total flux for all wavelengths greater than 2000 Å. At 5500 Å, it represents 10 percent of the total flux, implying that the equivalent widths of the photospheric lines would be about 10 percent larger if the envelope were not present. The resulting veiling of the lines must be seriously considered if we want to understand the significance

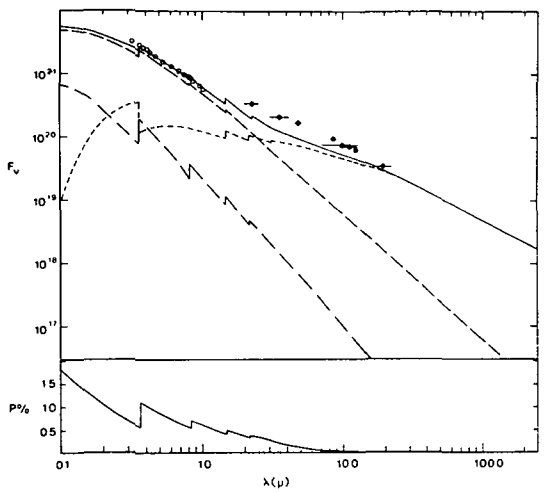

Figure 11-64. Energy distribution in the continuum from Poeckert and Marlborough's model of γ Cas. The solid line represents the total flux, short dashes, the free-free and free-bound emission in the envelope, the long dashes, the stellar continuum, dot-dashes the scattered flux, all in ergs s^{-1} sr^{-1} Hz^{-1}. The open circles are the data from Schild (1976), the filled circles are from Gehrz et al (1974). At the bottom is shown the polarization in the continuum (figure from Poeckert and Marlborough, 1978a).

of the v sin i values for Be stars. The flux of the star and that of the envelope are comparable at 2.5 μ For longer wavelengths, the flux from the envelope is greater than the stellar flux.

Poeckert and Marlborough note that the matching of the energy distribution shows the greatest disagreement at the Balmer jump, where the calculated discontinuity equals 0.15 mag in absorption, while the observations exhibit a zero discontinuity. In order to improve the agreement, the volume of that part of the envelope that is optically thin in the ultraviolet region ($\lambda < 3600$ Å) would have to be increased, thus increasing the continuous flux emitted by the envelope in this spectral region. This can be achieved by increasing the density in the envelope, that is, either by choosing a smaller expansion velocity or a larger scale height in z. Of course, these two changes will also affect the other observable quantities.

In the infrared region, the flux observed by Gehrz et al. (1974) is much higher than the model flux. Poeckert and Marlborough explain this disagreement by the variation of the star between the dates of Gehrz et al 's observations in the infrared region and their own observation at Hα. In the radio region, the envelope is optically thick out to 150 R_*.

The stellar flux scattered by the electrons in the envelope is mainly affected by bound-free absorption, which determines the wavelength dependence of the polarization, as Coyne and Kruszewski (1969) first showed (see the previous section) The emission in the envelope plays a negligible role for the polarization in the ultraviolet and visible regions, but longward of 1μ it begins to "dilute" the polarization. Figure 11-65 illustrates the polarization computed by the model, we note that it is much higher than the observed value. Poeckert and Marlborough point out that in order to obtain better agreement, one would have to decrease either the inclination, which would decrease the width of Hα, but improve the fit with the width of Hβ, or to decrease the density, which would entail a smaller decrease in the drop in polarization across the Balmer jump.

To summarize, in the model of γ Cas, the major contribution to the formation of the Hα line emission comes from the part of the envelope

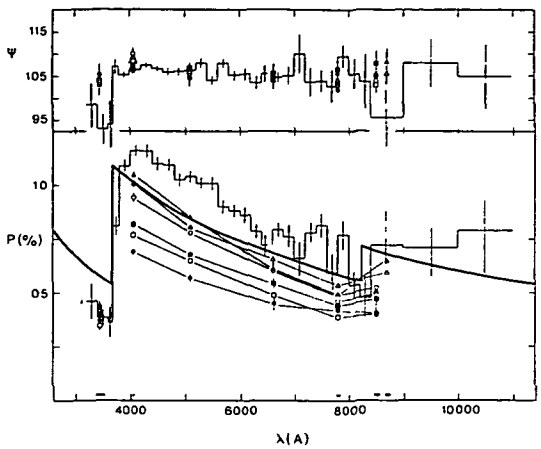

Figure 11-65. Position angle and polarization versus wavelength from the Poeckert and Marlborough's model of γ Cas. The thin solid line represents the data obtained by Landstreet and Angel (1973), measurements of Poeckert and Marlborough are open circles for January 1976, filled circles for September 1976, open squares for November 1976, filled circles for December 1976, open triangles for January 5, 1977, filled triangles for January 12, 1977 The solid bars at the bottom of the figure represent the filter FWHM (figure from Poeckert and Marlborough, 1978a)

located between 3 and 15 stellar radii. On the other hand, most of the polarization in the continuum (70 percent of the polarized flux) is produced close to the star, between 1 and 3 stellar radii. As for the radio emission, it is produced only at distances greater than $150\,R_*$.

The Influence of the Model Parameters on the Computed Spectrum. We summarize, here, the results of Poeckert and Marlborough (1978b) who have studied in great detail the influence of the parameters used in their model on the computed spectrum; Marlborough (1970) did the same kind of analysis, but in a more limited fashion. As we have said, the most important parameter is i, the inclination of the axis of rotation to the line of sight, because of the geometry adopted for the envelope, then come the density and the temperature of the envelope This study involves around 60 models; the method consists of varying one of the parameters while keeping all the others constant. The original parameters are those adopted to represent the spectrum of γ Cas, as described in the preceding section and listed in Table 11-1. The models have been computed with a density at the base of the envelope varying from 10^{12} cm^{-3} to 10^{14} cm^{-3}, and the mass loss rate range from 10^{-9} $M_\odot$ per year to 10^{-7} $M_\odot$ per year. We shall now summarize the main conclusions reached by Marlborough and Poeckert concerning the Balmer lines, the polarization, and the energy distribution in the continuum.

- The Balmer lines. Figure 11-66 shows the dramatic effect on the Hα profile of varying the inclination, i, of the rotation axis to the line of sight. We recall that i is determined by assuming that the star rotates at the critical velocity. This figure clearly shows that the width of the emission line depends very strongly on i, as does the Be or shell nature of the line. Shell lines appear for $i > 75°$. Note that these shell absorption lines are much broader than the observed ones. Poeckert and Marlborough propose to define shell lines as those in which the center of the absorption line drops below the continuum. Such a definition is not unambiguous, for it is precisely in the center of the shell lines that the velocity gradients are smallest and the radiation transfer effects are most important. This definition is also ambiguous for the observed spectrum, since the recognition of an observed shell line depends on the resolution used and the strength of the feature (see the section on The Visible and Infrared Line Spectrum).

The influence of the density on the shell feature is very important. The density must be 10 times greater to form a shell line at H25 than at Hα A shell spectrum in Marlborough and Poeckert's models has a negative Balmer progression; that is, the Balmer lines from the higher levels have larger expansion velocities than that of Hα. When the expansion velocity increases with radius the Balmer progression can only be negative or zero, while Balmer progressions of the opposite sign are also observed in Be stars. Similarly, the adopted velocity function makes it possible to obtain only Hα profiles having V/R < 1 (where V/R is the ratio of the violet and red emission

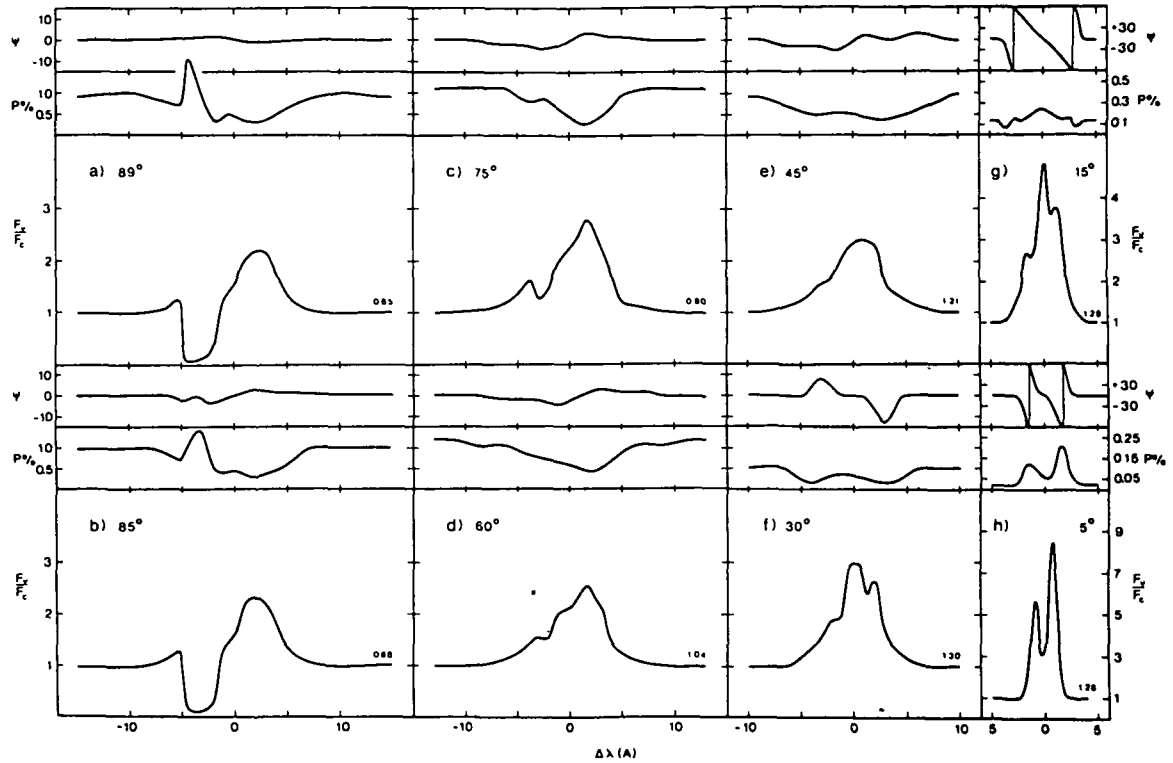

Figure 11-66. Position angle, polarization, and Hα profile for the standard model of γ Cas, for various inclination angle i (from Poeckert and Marlborough, 1978b).

peaks), while the observed ratio can change sign several times for a given Be star. In general, these two results indicate that the constraints imposed by the model are much more restrictive than required by the observations.

The quantity of emission in the Hα line depends on a large number of parameters, so that this quantity alone can define a large range of models. The Hα emission increases when the electron temperature in the envelope decreases, because the rate of recombination increases, and the degree of ionization is always high for the envelope temperatures in question (1.5×10^4 to 2.5×10^4 K). This effect is shown in Figure 11-67. The Hα emission also increases when the effective temperature of the star decreases from 3.0×10^4 K to 2.0×10^4 K. This is clearly seen in Figure 11-68. Of course, the Hα emission also increases when the density increases, as can be seen in Figure 11-69. Changing the density at the base of the envelope results only in changing the scale factor in the density distribution of the initial

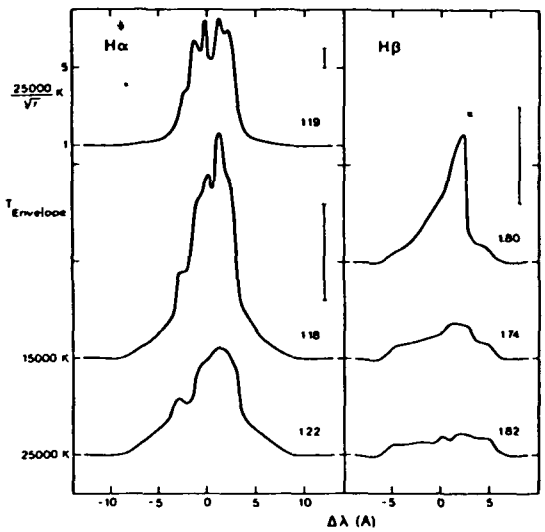

Figure 11-67. Hα and Hβ profiles for various temperatures of the envelope, the inclination is 45°. The bars indicate the scale of the continuum; the numbers to the right are the continuum level ($\times 10^{-21}$ ergs s^{-1} sr^{-1} Hz^{-1}) (from Poeckert and Marlborough, 1978b).

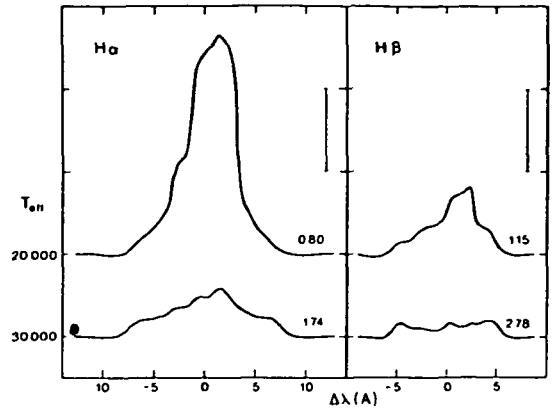

Figure 11-68 Hα and Hβ profiles for various stellar effective temperatures, the inclination is 45°. The bars indicate the scale of the continuum, the numbers to the right are the continuum level (X 10^{-21} ergs s^{-1} sr^{-1} Hz^{-1}) (from Poeckert and Marlborough, 1978b).

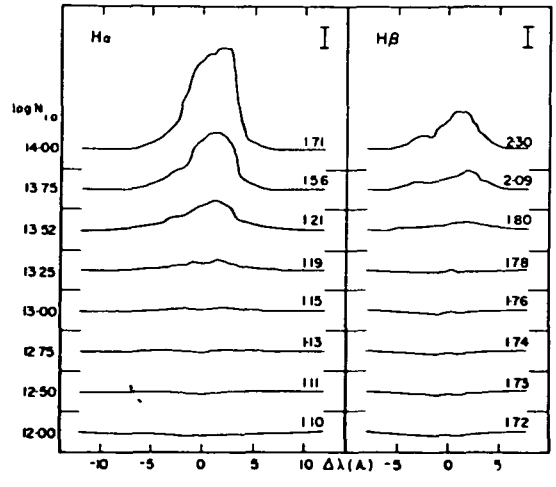

Figure 11-69. Hα and Hβ profiles for various densities of the envelope, the inclination is 45°. The bars indicate the scale of the continuum, the numbers to the right are the continuum level (X 10^{-21} ergs s^{-1} sr^{-1} Hz^{-1}) (from Poeckert and Marlborough, 1978b).

model. On the other hand, keeping the same density at the base and modifying the velocity function results in a change of the general shape of the density distribution with radius. Finally, the emission increases when the inclination decreases (Figure 11-66), so that pole-on stars should be more easily detected as Be stars than equator-on stars. Poeckert and Marlborough suggest this effect as an explanation for the excessive number of pole-on stars noted by Schild (1973).

- The polarization. The degree of polarization depends strongly on the inclination of the axes of rotation on the line of sight, i, and on the density The inclination determines the degree of asymmetry of the envelope with respect to the observer, while the density determines the number of scattering particles. These effects are shown in Figures 11-70 and 11-71. An increase in the T_e of the envelope from 1.5 X 10^4 K to 2.5 X 10^4 K is accompanied by an increase in polarization due to the increase in scattered radiation. An increase in the T_{eff} also increases the polarization by increasing the degree of ionization (and thus the number of scattering particles) and decreasing the bound-free absorption. An increase in the density is also accompanied by an increase in the bound-free absorption, which produces a Balmer discontinuity in the polarization. The polarization in Hα exhibits a complex structure in which the combined effects of absorption and emission play an important role. Figure 11-66 shows examples of the variation of the polarization across Hα as a function of the inclination.
- The energy distribution in the continuum. The energy distribution in the continuum depends

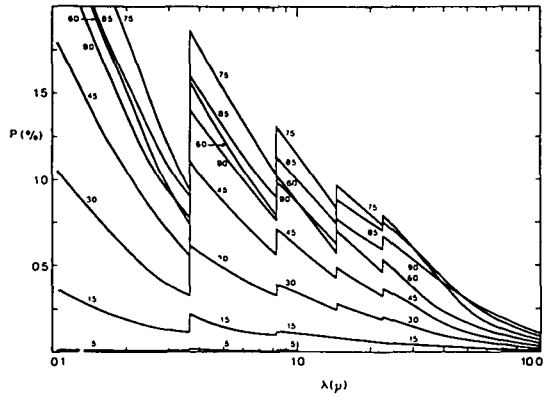

Figure 11-70. The continuum polarization for various angles of inclination; all other parameters are those of the model of γ Cas (from Poeckert and Marlborough, 1978b).

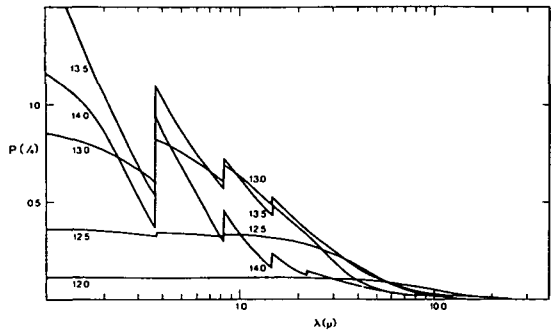

Figure 11-71. The continuum polarization for various densities of the envelope; all other parameters are those for the model of γ Cas (from Poeckert and Marlborough, 1978b).

strongly on the inclination, the density, and the electron temperature in the envelope. The total flux is the sum of the stellar flux, attenuated by absorption in the envelope, the flux emitted in the envelope, and the scattered stellar flux. The stellar flux and the scattered flux increase when the inclination decreases, because the optical depth decreases. The same is true for the free-free and free-bound emission. Figure 11-72 shows the changes in the continuous flux distribution with inclination. The infrared flux increases strongly and the Balmer jump gets smaller when the inclination decreases. However, we recall that there is no observed correlation between v sin *i* and the observed infrared radiation or the Balmer discontinuity (see the section on The Continuous Spectrum, from the Near Ultraviolet to the Radio Region). For large inclinations, the Balmer jump is large on account of the absorption of the stellar flux by the envelope. For small inclinations, the discontinuity is smaller because of the filling in due to the free-bound emission of the envelope.

Density effects are also important for the energy distribution in the continuum. If the density at the base of the envelope is low, of the order of 10^{12} cm^{-3}, the stellar flux is practically unchanged, because the envelope is optically thin out to 20 μ. When the density increases, the flux emitted by the envelope increases rapidly until the envelope becomes optically thick, especially in the infrared, as is shown in Figure 11-73. An increase in the electron temperature in the envelope produces an increase in the infrared and ultraviolet flux, especially below 2500 Å. An increase in T_{eff} also increases the flux, especially in the ultraviolet and the visible spectral regions.

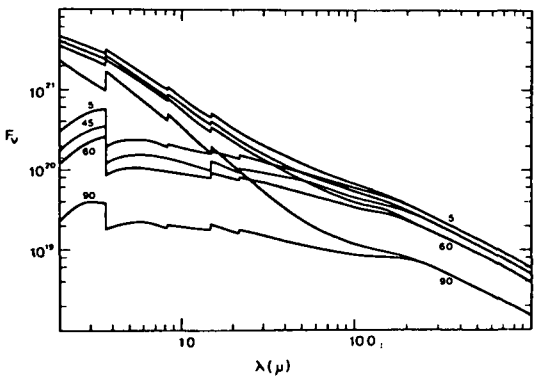

Figure 11-72. The energy distribution in the continuum for various inclinations; all other parameters are those of the model of γ Cas (from Poeckert and Marlborough, 1978b).

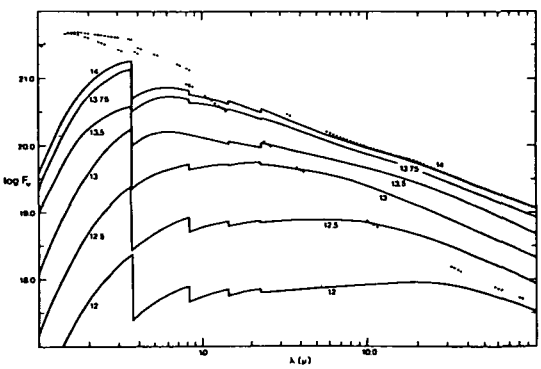

Figure 11-73. The energy distribution in the continuum for various densities in the envelope; all other parameters are those of the model of γ Cas (from Poeckert and Marlborough, 1978b).

12

DATA OBTAINED FROM SPACECRAFT

THE LINE SPECTRUM OF THE Be STARS IN THE ULTRAVIOLET

Observations in the ultraviolet region have brought to light four points concerning the spectra of hot stars, both normal and peculiar, which are of basic importance for the theory of stellar atmospheres.

1. Resonance lines are present arising from ionization states as high as O VI and N V—much higher than the level predicted at the effective temperatures of these stars under conditions of radiative equilibrium. A nonradiative energy source is required to explain their formation. This source of nonthermal heating necessarily entails the existence of a chromosphere-corona, as these regions are generally called

2. The large shifts of the superionized lines, which reach velocities of -3000 km s^{-1} and exceed the escape velocity at the surface of the star, prove the existence of a mass flux.

3. The intensities, profiles, and shifts of the superionized lines can be different for two normal or peculiar stars of the same spectral type and luminosity class (Morton, 1979). In other words, the velocity and density distributions in the superionized regions can be different for two stars characterized by the same values of T_{eff} and g_{eff}. Stars belonging to the same taxonomic box retain a certain individuality, implying that these two parameters used to describe the photosphere of a star are not sufficient to describe its outer layers.

4. The variability of the shifts, intensities, and profiles of the superionized lines is a phenomenon observed in normal stars as well as in peculiar stars.

None of these four observational points was predicted by the classical theory of stellar atmospheres. Up to now, none of these four points has been satisfactorily interpreted within the framework of that theory.

Although the spectrum of the Be stars is strikingly different from that of the normal B stars in the visible, there is no specific distinction between them in the ultraviolet region. Few emission features are observed, on the whole, in a sample of ultraviolet spectra—from 1000 to 3000 Å—of Be and normal B stars belonging to all luminosity classes. Those that are observed occur mainly among the hottest supergiants and among certain Be shell stars For the supergiants, the principal emission features are the red emission wings of the P Cygni profiles of the superionized lines. For certain Be shell stars and Bep stars, the emission features form a more or less even border on the low-excitation resonance lines such as those of Mg II, Al II, and the Fe II lines located in the mid-ultraviolet region.

The presence of emission lines in the visible is the principal phenomenon distinguishing Be stars from normal B stars, and demonstrating that one or more of the equilibrium conditions that are assumed, a priori, by the classical theory of stellar atmospheres are violated in these stars. In the ultraviolet region, the important phenomenon is the *presence* of superionized lines, for their formation requires a nonradiative energy flux, whose

existence constitutes an anomaly with respect to thermal models. The fact that the superionized lines may be strong, with a pronounced P Cygni profile having a red emission wing, or weak, with an absorption profile, does not reflect the existence of different phenomena; it reflects only a difference in the degree of the same anomaly among different groups of stars relative to thermal models

The existence of a nonradiative energy flux in the majority of the Be stars and in the hottest normal B stars strongly suggests that their atmospheres have the same overall radial-temperature structure This means that for these two types of stars, the regions above the photosphere are the chromosphere, the corona, and the post-coronal region, in that order. The fact that they have the same radial-temperature structure does not mean that the temperature distribution is identical for all the B stars. It implies only that the temperature increases from the photosphere to the corona, and then decreases due to radiative losses in the post-corona, the decrease can be more or less rapid, depending on the value of the nonradiative energy flux and on the density in these regions.

The existence of a mass flux in the Be stars and in certain normal B stars also suggests that their atmospheres have the same pattern of radial-density structure. This does not mean that these two types of stars must have the same density distribution, the same degree of symmetry or asymmetry, or the same fine structure in any inhomogeneities that may exist. It means only that, for these two types of stars, the exponential density decrease in the photosphere gives way to a slower decrease, varying roughly as r^{-2}, out to the coronal and post-coronal regions (Chapter 13).

Unlike the cases of the novae and the Wolf-Rayet stars, one of the problems facing the interpretation of the Be phenomenon in the visible region was the absence of information from the photosphere on the ejection of the material that forms the extended atmosphere. The expansion velocities of the cold regions observed in the visible range are too small to explain the formation of a very extended atmosphere. It was the observation of the superionized lines in the ultraviolet range that demonstrated the existence of large expansion velocities, capable of forming the extended envelope observed in the visible spectra.

The radial-velocity structure corresponds to the temperature structure out to the corona. The velocities increase from subthermal values in the photosphere to transthermal and superthermal values in the corona. In the hot post-coronal region, where the material is superionized, the ions receive an additional acceleration due to radiation pressure or other forces. But in the cold parts of the post-coronal region, which are subionized and form the extended envelope observed in the visible region, the velocities are low, thus indicating that the material has already undergone a deceleration. Such a deceleration could be produced in a rather strong interaction between a variable stellar wind and the interstellar medium, or local interstellar matter, forming a shock wave.

In the hot, low-luminosity normal B stars, only the first of these regions is observed, indicating that the cold regions of the post-corona must be less dense and less extended than those in Be stars. Thus, the outer atmospheres of the Be stars differ from those of the normal B stars essentially in the presence of denser, and extended, cold, low-velocity regions in the post-corona.

Before the ultraviolet observations, the basic question raised by the existence of the Be phenomenon was: Why, among all the B stars, do only the Be stars have an extended atmosphere? Now, we know that the presence of an atmosphere outside the photosphere is a property of both normal and peculiar stars in the HR diagram, and that an outer atmosphere does not constitute an anomaly. The Be stars are distinguished from the normal B stars, not by the presence of an outer atmosphere, but by the presence in the post-corona of cold regions, sufficiently dense and/or sufficiently extended for their emission lines to be observable in the visible. One condition for the formation of these dense regions is that the value of the mass flux must be higher in the Be stars than in the normal B stars. The few observations of Be stars in the ultraviolet suggest, as do the observations in the visible, that their mass flux is highly variable as well (as discussed in the section

on The Variability of Be Stars in the Ultraviolet Region).

Superionization in the Ultraviolet Spectra of Be Stars

The presence of the resonance lines of atoms having high degrees of ionization, like O VI and N V, and their large displacements or asymmetries, exclude the possibility of locating them in the photospheres of the stars; they are evidence for the existence of an atmosphere outside the photosphere. Lamers and Snow (1978) have studied the ionization equilibrium conditions in the outer atmospheres of O and B stars. They considered two different cases: one in which the outer atmosphere is cold, with $T_e \approx 0.8\ T_{eff}$, and the other in which the outer atmosphere is hot, with $T_e > T_{eff}$. In both models, the outer atmosphere was assumed to be optically thin. They showed that the ionization equilibrium cannot be radiatively dominated, and that the temperature in the outer atmosphere must be greater than the effective temperature of the star. They concluded that the outer atmospheres of the stars that exhibit the O VI and N V resonance lines must have a T_e of about $4 \pm 2 \times 10^5$ K, and those that exhibit the Si IV resonance lines, but not those of O VI and N V, must have a T_e of around $7 \pm 3 \times 10^4$ K

There is a tendancy for the hottest, most luminous stars to exhibit the highest degrees of ionization (Snow and Morton, 1976), but it is also clear that the superionization is not a function of M_{bol} alone or of T_{eff} alone. Counter-examples to this general trend are increasingly observed, in which the less luminous star exhibits a greater degree of ionization, or stars of the same spectral type exhibit different degrees of ionization (Morton, 1979, Costero et al., 1981). This is the most direct indication that the properties of the outer atmosphere do not depend only on the location of the star in the HR diagram—that is, on the parameters T_{eff} and g_{eff} that describe the stellar photosphere.

Observations made by Snow and Marlborough (1976) and Marlborough (1977a) with Copernicus (resolution 0.2 Å) show that superionization in the Be stars does not depend only on M_{bol} or T_{eff} either. The O VI resonance lines are present in 59 Cyg and HD 28497, type B1.5 Ve, while they are absent in γ Cas (B0.5 IVe) and χ Oph (B1.5 Ve). The N V resonance lines are present in γ Cas, φ Per(B1 III – Ve) HD 28497, 59 Cyg, and probably α Eri (B3 IVe); they are suspected in 31 Peg (B2 IVe) and absent in χ Oph.

Although the ultraviolet spectra obtained with Copernicus made it possible to observe the resonance lines of O VI ($\lambda\lambda$ 1038 – 1032 Å), whose ionization potential is 113.9 eV, the IUE spectra do not extend so far toward short wavelengths. The observed ion with the next highest ionization potential (77.4 eV) is N V, whose resonance lines are at 1238.8 Å and 1242.8 Å. These lines, located in the last orders of the IUE echelle spectrum (at high resolution), are often difficult to identify because of problems in extracting the signal in this spectral region. The N V resonance lines must therefore be used with a great deal of caution, in making a survey of the highest degree of ionization observed on these spectrograms. On the other hand, the C IV resonance lines, whose ionization potential is 47.9 eV and which are located in the most favorable region of the IUE spectrum, can be advantageously chosen to study the superionization in B and Be stars.

Dachs (1980) observed eight Be/shell stars with IUE; they had spectral types from B1 5 to B4, and v sin i values from 85 to 400 km s^{-1}. There was no particular tendency for the ionization to vary either with T_{eff} or with v sin i The N V and C IV resonance lines are strong and asymmetric in HD 120991, which has a spectral type of B2 V and a small value of v sin i, around 85 km s^{-1}; they are similar to those in 59 Cyg (B1.5 Ve), at some epochs of its variation, and whose v sin i is 450 km s^{-1}. The C IV resonance lines are observed in the spectrum of θ Cr B (B6 Ve), with v sin i = 450 km s^{-1} (Figure 12-1) and in the spectrum of HD 50138 (B7 – 8 V, IVe), with v sin i = 150 km s^{-1} (Figure 12-2). The C IV resonance lines cannot possibly be confused with the Fe III lines in this star, for its spectrum is completely dominated by nearly 2000 lines of Fe II, while the few Fe III lines are faint (Doazan and Zorec, 1981).

Henize et al. (1976) studied the intensity ratio

Si IV/C IV in 34 B0 to B2 stars, including 11 Be stars, using observations made with Skylab S019 (resolution 2 Å at 1400 Å). They found that this ratio is, statistically, smaller for some Be stars than for normal B stars of the same spectral type, as is also the case for the supergiants. Panek and Savage (1976) used observations made with OAO-2 (12 Å resolution) to study the equivalent width of the Si IV and C IV resonance lines in 118 stars, including 20 Be/shell stars. They found that the Si IV resonance lines in the Be/shell stars are comparable to those in normal main-sequence B stars, while the C IV resonance lines are stronger for several Be stars, as for the supergiants. They noted that the Si IV and C IV lines in γ Cas varied considerably in the space of a few months, changing their equivalent width from the dwarf range to the supergiant range. Molnar (1975) had also observed perceptible variations in the Si IV resonance lines in γ Cas within a day, using the Mariner 9 UVS spectrograph (resolution 7.5 Å). This is a clear indication that these results can represent only a trend, and that there is no close correlation between the equivalent width of C IV and the spectral type of the Be stars.

Taken as a whole, these results show that superionization is observed in both normal B stars and Be stars. However, the Be stars exhibit a more pronounced superionization than normal

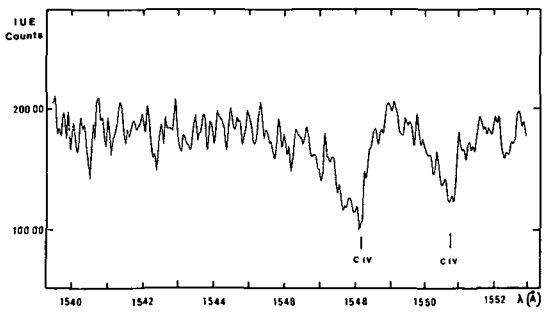

Figure 12-1. The C IV resonance lines of θ Cr B (B6 Ve, v sin i = 450 km s^{-1}) observed in May 1980 when the spectrum was quasi-normal in the visual region Note the extended wing toward the short wavelength. The bars indicate the position of the laboratory wavelengths of the C IV doublet

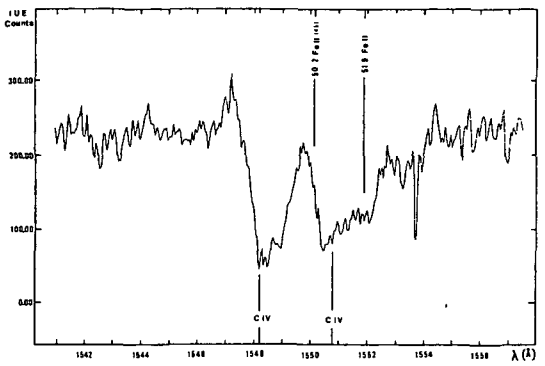

Figure 12-2 The C IV resonance lines in HD 50138 (B7-8 IV-Ve, v sin i = 150 km s^{-1}) in December 1978. In the ultraviolet region, the star exhibits a complete Fe II shell spectrum, while in the visual spectrum, no metallic shell line is seen The Fe III lines are very weak in the ultraviolet The blends due to Fe II are indicated. The bars show the position of the laboratory wavelengths

main sequence B stars, and this phenomenon is more conspicuous and persists toward the latest B subtypes. All these observations show that it is impossible to avoid a region heated by a nonradiative energy flux, above the photosphere in a Be star; this is the very definition of a chromospheric region. Moreover, the detection of X-ray emission from stars of all the spectral types in the HR diagram shows that the chromosphere is continued by a corona with a temperature of a few million degrees. This coronal region is followed by a post-coronal region in which radiative losses cool the atmosphere. The existence of superionization for both normal B stars and Be stars suggests that they have the same radial structure in the superionized regions. However, that does not mean that the relative size of the various regions is the same—that is, that the density and temperature distributions are identical—but only that above the photosphere, the temperature must increase outward and then decrease. Nor does this mean that the geometry of the outer atmosphere is identical for these two types of stars, although up to now there is no indication that the superionization depends on v sin i. All kinds of asymmetries or inhomogeneities, such as

is proposed in Part I of this volume, can be included in such an overall radial temperature structure, if they are required by the observations.

Observational Evidence for Mass Flux in Be Stars

The resonance lines of O VI, N V, C IV, and Si IV in the hot stars exhibit a great variety of profiles (Snow and Morton, 1976; Morton, 1979), which can be roughly classified into three types: (1) the type I P Cygni profile (Beals, 1951), with an emission component having little or no displacement and a shortward-displaced absorption component, (2) a shortward-displaced absorption profile, without an emission component; (3) an asymmetric absorption profile, with little or no displacement of the absorption minimum, exhibiting an extended wing toward shorter wavelengths Of these three profiles, only type (2) constitutes direct evidence of mass loss, when the radial velocity of the center of the absorption line is greater than the escape velocity. In the case of profile (1), the model of an expanding, extended envelope, optically thin to the continuous radiation of the photosphere, provides a simple interpretation of the profile. The absorption component is produced in the part of the expanding envelope that the observer sees projected on the stellar disk, while the emission component arises from the entire extended envelope, except for the region occulted by the photosphere In case (3), it is generally assumed that the asymmetries of the lines are formed in a low density, optically thin expanding gas, so that the position of the extreme shortward edge indicates the maximum expansion velocity at which the ions move in the radial direction. When this edge is sharp, its position is often interpreted as the terminal velocity of the gas leaving the star, ignoring the existence of the cool and low velocity envelope where the emission lines observed in Be stars in the visible, orignate Thus, in cases (1) and (3), the existence of mass loss depends on the validity of the model

The most luminous and hottest B stars tend to exhibit the strongest superionized lines with P Cygni profiles, and the greatest displacements. All these features indicate that in a statistical sense, the mass loss is higher for these stars than for the less luminous main sequence stars, for which these lines are fainter and exhibit a smaller displacement. The value of $\dot{M}$ is found to be of the order of 10^{-6} to 10^{-7} $M_\odot$ per year for the B supergiants, it is of the order of 10^{-7} to $10^{-9} M_\odot$ per year for the Be stars, and of the order of 10^{-8} to 10^{-9} $M_\odot$ per year for the earliest-type normal main-sequence B stars, like τ Sco. But this tendency to observe larger rates of mass loss for greater luminosities is not a one-to-one relation, and there is more and more evidence to show that two stars of the same spectral type and luminosity class can have superionized lines with very different profiles and displacements (Morton, 1979; Costero et al., 1981) This necessarily implies a different density and temperature distribution in the outer atmospheres of two stars that have the same M_{bol}. This can result only from a difference between the values of the mass flux and/or the nonradiative energy flux in these stars (for a complete discussion, see R. N Thomas, 1983).

For the Be stars, the superionized resonance lines generally do not exhibit P Cygni profiles Up to now, the only counter-example is the P Cygni profile in the C IV resonance lines of γ Cas, observed in 1968 and reported by Bohlin (1970). More often, absorption lines are observed with displacements and degrees of asymmetry that are more or less pronounced, depending on the star and, for a single star, on its epoch of variation.

The Displacements of the Superionized Lines. Displacements of the N V and C IV resonance lines that exceed the escape velocity at the photosphere have been reported for four Be stars 59 Cyg (B1.5 Ve), γ Cas (B0.5 IVe), 66 Oph (B3 IIIe), and ω Ori (B2 Ve), their values of $v \sin i$ are 450, 300, 275, and 190 km s^{-1}, respectively Thus, we can consider that in going from 59 Cyg to ω Ori, we are going from an equator-on Be star to a Be star viewed at a small angle to the rotation axis, on the rotation model. The observed displacements of the C IV or N V lines for these four stars (depending on the epoch of variation for 59 Cyg and γ Cas) are. -200 to -1200 km

s^{-1} for 59 Cyg, −150 to −1500 km s^{-1} for γ Cas, and −750 km s^{-1} for 66 Oph and ω Ori. It is clear that there is no apparent correlation between the observed displacements and the values of v sin i. On the contrary, there are much greater differences between the displacements observed for the same star, depending on its epoch of variation, than between two stars, one of which is viewed equator-on and the other at a small angle to the rotation axis. The existence of strong, highly displaced superionized lines for Be stars with small values of v sin i shows that the ejection of material is not restricted to the equatorial regions, and that it also occurs in high latitude regions, near the pole. The study of the ultraviolet spectra of pole-on stars leads to the same conclusion, because of the presence of many shell lines of ionized metals (Snow, 1975; Peters, 1976, Snow et al., 1979)

In 59 Cyg, there is, at certain epochs, a very clear progression between the displacement of the lines and their ionization potential, as well as between the degree of asymmetry and the ionization potential. The Si IV lines are quasi-symmetric and quasi-undisplaced, while the C IV and N V lines are highly asymmetric and displaced by −750 km s^{-1} to −1000 km s^{-1} (Doazan et al., 1980a, 1980b) At other times, this progression is much weaker: it goes from −100 km s^{-1} for the Si IV lines to −200 km s^{-1} for the N V lines (Snow and Marlborough, 1980). The profiles and displacements of C IV and N V in 59 Cyg undergo the largest variations that have been observed to date in the ultraviolet region for hot stars These variations suggest that the mass loss and its variations are greatest when the star changes from a quasi-normal B phase to a new Be phase with increasing emission (see the section on The Variability of the Be Stars in the Ultraviolet Region). For γ Cas, the resonance lines of N V, C IV, and Si IV exhibit two components at certain phases· the broader one has a low velocity (−100 km s^{-1}), while the narrower one, which is highly displaced at around −1500 km s^{-1}, undergoes large depth variations in a few days (Henrichs et al., 1980; Doazan et al., 1980c). Large displacements are observed for 66 Oph and ω Ori, about −750 km s^{-1} (Peters, 1981), ω Ori, which is considered to be a pole-on star, exhibits a larger expansion velocity than 59 Cyg and γ Cas at some phases of their variation. The C IV resonance lines in ω Ori, which are depicted in Figure 12-3, exhibit three components at −545, −750, and −855 km s^{-1}, similar to those observed at certain epochs of variation in 59 Cyg. For 66 Oph (Figure 12-4), which Slettebak also considers to be a pole-on star, two components are observed in the C IV resonance lines, one at −250 km s^{-1} and the other at −700 km s^{-1}.

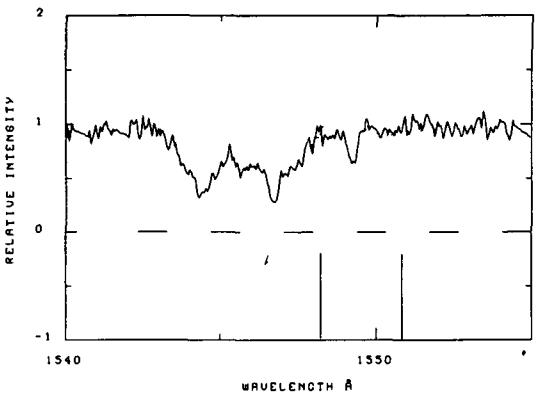

Figure 12-3 The C IV resonance lines in the pole-on star, ω Ori (B2 Ve, v sin i = 160 km s^{-1}). Three components are distinguished at −545, −750, and −855 km s^{-1} (from Peters, 1981). The bars indicate the position of the laboratory wavelengths

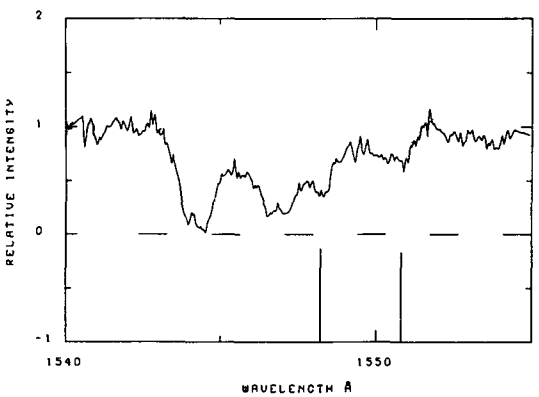

Figure 12-4. The C IV resonance lines in the pole-on star, 66 Oph (B2 Ve, v sin i = 220 km s^{-1}) Two components are distinguished, at −250 and at −700 km s^{-1} (from Peters, 1981). The bars indicate the position of the laboratory wavelengths.

All the other reported displacements, until now, are less than −240 km s^{-1}. Heap (1975) measured displacements of the order of −100 km s^{-1} in the C IV, Si IV, and Si III lines on a rocket spectrogram (resolution 0 1 Å) of the Be shell star ζ Tau The wavelength scale was calibrated from the circumstellar lines, mainly due to Fe III, assuming them to have zero shift. On a spectrogram observed simultaneously from the ground, the shell lines in the visible, which are mainly due to Fe II and are certainly formed in different regions from the Fe III lines, were displaced by −20 km s^{-1} with respect to the stellar lines. If it is assumed that the Fe III shell lines in the ultraviolet and those of Fe II in the visible have the same shifts, then the lines of C IV, Si IV, and Si III are displaced by −120 km s^{-1}, this is evidence for a high expansion zone, which was not detected in the visible at this epoch of variation.

Marlborough (1977a) measured the radial velocities of six Be stars on Copernicus spectra (resolution 0.2 Å). He noted that for four Be stars with large v sin i (α Eri, 59 Cyg, γ Cas, and HD 28497), the resonance or low excitation lines (excitation potential less than 0.10 eV) had a radial velocity that was systematically more negative than that of the lines arising from excited states (excitation potential greater than 0.5 eV); the largest shifts were as great as −240 km s^{-1}. On the other hand, for the two Be stars with low v sin i, 31 Peg and χ Oph, which are considered to be pole-on, the shifts of the resonance lines were smaller (−50 km s^{-1}) and were not different from those of the excited states As is shown by Peters' (1981) observations of 66 Oph and ω Ori, these low velocities are not characteristic of Be stars with low values of v sin i

Asymmetries in the Superionized Resonance Lines Snow and Marlborough (1976) and Marlborough and Snow (1976) discovered on Copernicus spectra that the profiles of the resonance lines in Be/shell stars exhibit large asymmetries. If these lines are formed in an optically thin, low-density atmosphere, then the position of the extreme edge of the wing, on the short-wavelength side, indicates the presence of ions in the atmosphere that move faster than the escape velocity at the surface of the star. These greatly extended blue wings constitute evidence for the existence of mass loss in the Be stars, but the evidence depends on the validity of the hypothesis that the atmosphere is optically thin in the superionized regions of the stellar wind. Subsequent observations have fully confirmed those of Snow and Marlborough, they show that the majority of the Be stars exhibit asymmetric resonance lines with wings that extend shortward to high velocities, greater than the escape velocity at the surface of the star (Marlborough, 1977a, Lamers and Snow, 1978; Dachs, 1980).

The observations of Snow and Marlborough (1976) seemed to suggest some correlation between the existence of mass loss and a large value of v sin i. Such a correlation would have indicated that the mass loss is channeled by rapid rotation, and that the mass flux takes place mainly in the equatorial plane. But, as the authors remarked, their observations were not sufficient to support firm conclusions In fact, later observations do not confirm this suggestion. Figure 12-5, based on a much larger sample, shows that there is no tendency for the mass loss to vary with v sin i (Doazan et al., 1981c; Snow, 1981) We see that mass loss is observed for all values of v sin i, and

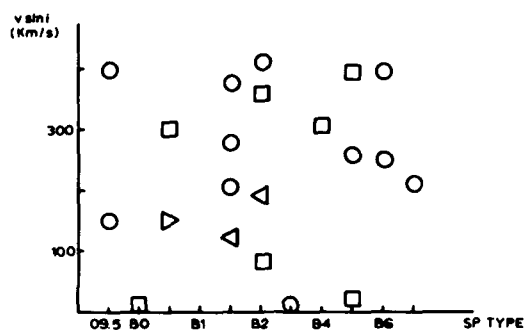

Figure 12-5 Lower values of mass loss rates in a v *sin i versus spectral type diagram for 15 Be/shell stars and 6 normal B stars The symbols indicate values of* $\dot{M} < 10^{-12}\ M_{\odot}\ yr^{-1}$ (◁), $10^{-12} < \dot{M} < 10^{-11}$ (○), $10^{-11} < \dot{M} < 10^{-10}$ (□), $\dot{M} < 10^{-10}$ (▷) *There appears to be a complete lack of any correlation between the lower limits of mass loss and* v *sin i (from Doazan et al., 1981c)*

that the equator-on stars do not behave differently from the pole-on stars. This means that the ejection of material is observed in Be stars viewed from the pole, and that matter is not ejected only in the equatorial plane of the Be stars.

Snow and Morton (1976) showed that mass loss was generally observable for stars brighter than $M_{bol} = -6$—that is, up to type B0.5 for main-sequence stars, and that it was usually not observed for low-luminosity stars. However, Snow and Marlborough (1976) observed this phenomenon up to type B1.5 Ve in the Be stars. They suggested that for these low-luminosity stars, the mass loss was linked to the Be or shell characteristics. Lamers and Snow (1978) improved this result by reobserving some of Snow and Marlborough's stars at higher resolution (0.05 Å) with Copernicus, and adding six new Be stars and some normal stars (at 0.2 and 0.05 Å resolution) with luminosities around the suggested limiting value for mass loss ($M_{bol} = -6$) proposed by Snow and Morton. The adopted criterion for mass loss was the shift or asymmetry of the Si IV resonance lines. In some cases, the improvement in resolution enabled them to move a star from the group without mass loss into the group with mass loss. With these new observations, mass loss is observed for normal B stars up to $M_{bol} = -5.3$ (B2 IV) and suspected up to $M_{bol} = -4.2$ (B2.5 V); but for Be stars, mass loss is observed up to $M_{bol} = -3.6$ (B5 Ve) The presence of shifted, asymmetric resonance lines of Si IV and C IV in θ Cr B (B6 Ve) pushes this limit out to $M_{bol} \simeq -3.2$ (Figure 12-1). Finally, we note that Lamers and Snow's conclusions are based only on an examination of the Si IV resonance lines, and that their criterion for the existence of mass loss is an asymmetry and/or a shift in these lines. Now, although this is a sufficient condition, it is not a necessary condition. The Si IV resonance lines may be symmetrical and unshifted, thus simulating an absence of mass loss, while on the same spectrogram, the C IV and N V resonance lines are highly displaced and asymmetrical. This is what is observed in 59 Cyg, at certain epochs of its variation (as discussed in the next section).

Determining the Mass Loss in Be Stars from Ultraviolet Observations. To determine mass loss in Be stars from ultraviolet observations, one would have to construct a realistic model, taking into account the observations made at all wavelengths, to represent the temperature, velocity, and density distribution in the entire outer atmosphere. Snow and Marlborough (1976) made an approximate estimate of the mass loss observed in 59 Cyg in 1972, using the observed asymmetry of the Si IV resonance lines. The excess absorption in these lines, which arises in the stellar wind, provides a value of the column density of the Si IV ions above the photosphere. They assumed a state of ionization such that one-tenth of the silicon ions are in the Si IV state; this enabled them to determine the total column density above the photosphere, assuming the silicon abundance to be normal. The observed shift in the Si IV lines leads to a systematic velocity of the material in the stellar wind, amounting to around -100 km s^{-1}. Assuming that the stellar wind extends over 20 R_*, they found a mass loss of 10^{-9} to 10^{-10} $M_\odot$ per year. Hammerschlag-Hensberge et al. (1980) determined the mass losses in γ Cas and X Per in two different ways. First, they compared the resonance lines observed in these stars with those of τ Sco, and adapted the model of τ Sco constructed by Lamers and Rogerson (1978) to γ Cas and X Per; that is, they used essentially the same velocity law. Second, they compared the observed profiles to the grid of profiles computed by Castor and Lamers (1979). Both methods lead to similar results, namely 5.5×10^{-9} $M_\odot$ per year for γ Cas and 1.5×10^{-8} $M_\odot$ per year for X Per.

These determinations of mass loss lead to values that are of the same order of magnitude, or smaller than, those obtained in the visible region. Here it is assumed that the mass flux is spherically symmetrical, while a disk-shaped envelope has been assumed generally in the ad hoc models constructed to interpret the visible spectrum. This difference in geometry would increase the disagreement between these mass flux values and those determined in the visible. In some cases, with such small mass flux values, the ad hoc models would not be capable of accounting for the large Hα emission intensity observed at this epoch in these

three stars. Finally, note that a major uncertainty on these values of mass loss comes from the assumed state of ionization of the considered ions.

The Cool Extended Envelope Observed in the Ultraviolet Region

The ultraviolet spectra of some Be/shell stars exhibit deep, sharp absorption lines similar to the shell lines observed in the visible, and arising from atoms that have a degree of ionization or excitation comparable to, or smaller than, that of the photosphere. This is an indication that these lines are produced in the cool post-coronal regions that we have called the extended envelope, as are the emission lines observed in the visible spectrum. The prinicpal lines observed are those of doubly ionized metals—such as Fe III, Cr III, and Ti III—and singly ionized metals, especially those of Fe II. The resonance lines of Al III, Al II, and Mg II are often very strong. Depending on the star, the lines of the first or second ionization state dominate the spectrum from 1200 to 3000 Å. The simultaneous presence of the two ions indicates large variations in the degree of ionization in the envelope.

The Fe II lines, which are very numerous throughout the ultraviolet spectral region observed with IUE (1200 to 3000 Å), exhibit emission wings on both sides of the sharp absorption, in some shell spectra (Dachs, 1980). These emission components are visible only from about 1600 Å to the long-wavelength region. Figure 12-6 illustrates three regions of the spectrum of HD 45677 (B2ep)—1260, 1780, and 2740 Å—in which the emission wings can be seen to appear at 1780 Å and increase greatly at 2700 Å. This increase in the emission with wavelength may be caused by a visibility effect, produced by the rapid flux drop in B stars longward of about 1600 Å. The same effect is observed in the spectrum of HD 50138 (Doazan and Zorec, 1981). The existence of emission in the wings of the mid-ultraviolet Fe II lines in some Be stars simulates an Fe II absorption feature at 2548 Å, which is statistically weaker in these stars than in normal stars, when observed at low resolution. This is the result obtained by Lamers et al. (1980) from a study of

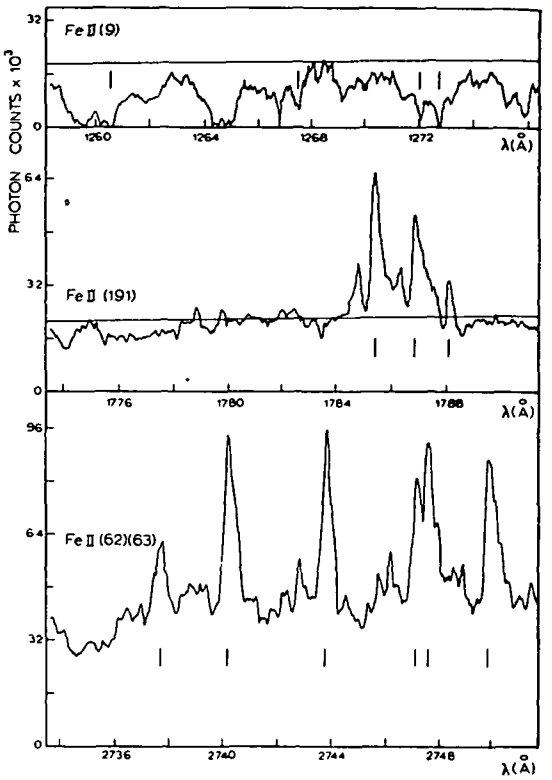

Figure 12-6. Three spectral regions of the spectrum of the B2ep star HD 45677, in which the emission wings in the Fe II lines can be seen to appear at λ 1780 Å and increase in strength toward longer wavelengths (from Selvelli and Stalio, 1980).

the S 59 spectra (resolution 1.8 Å) of 11 Be stars. These authors found that the feature near Fe III λ 2078 Å is also statistically weaker in the Be stars

The Mg II Resonance Lines. The Mg II doublet near 2800 Å exhibits emission wings in some Be/shell stars (de Jager et al., 1979; Slettebak and Snow, 1978) The behavior of this doublet has been studied by Lamers and Snijders (1975) for O-, B-, and A-type stars, including 14 Be and shell stars, and by Lamers et al. (1980) for 15 Be/shell stars observed with TD1 (resolution 1 8 Å). The Mg II lines in the Be/shell stars are statistically either weaker than those of normal B stars, with a suggestion of unresolved emission in their spectra, or stronger, indicating additional absorption in the cold envelope. The situation is actually

more complicated, since emission and absorption from the envelope can be present at the same time in these lines.

Morgan et al (1977) tried to demonstrate the existence of mass flux in the Be stars by observing the Mg II resonance lines For γ Cas, they observed a second narrow component, shifted by -215 km s^{-1}, next to each of the lines in the doublet; for ζ Tau, both the resonance lines and the subordinate lines were shifted by -75 km s^{-1} Two years later, large changes were observed on BUSS spectrograms (resolution 0.1 Å) by de Jager et al (1979); the subordinate lines, which were clearly present in the observations of Morgan et al., had practically disappeared, while the resonance lines were much stronger The non-interstellar component was shifted by around +50 km s^{-1}, indicating that the material was falling back. This is in contrast with the behavior of the hot regions of the outer atmosphere, where shifts of -120 km s^{-1} were observed for the C IV lines by Heap (1975). It is obvious that an interpretation of the motion of the outer atmosphere of Be stars requires simultaneous observations over the greatest possible wavelength range.

The Shell Spectrum and the Supergiant Spectrum in the Ultraviolet Region. The observations made with OAO-2 (resolution 12 Å) for six supergiants and the shell star ζ Tau showed that the depressions centered at 1720 Å (Underhill et al., 1972) and at 1920 Å (Thompson et al., 1974) were characteristic of these stars, while they did not appear in the spectra of normal main-sequence B stars. By analyzing a rocket spectrum of ζ Tau (resolution 0.1 Å), Heap (1975) showed that the depression at 1720 Å was composed mainly of lines of Fe II, Fe III, Ni III, and Al III, and that the depression at 1920 Å was due essentially to Fe III As Heap noted, one must be careful not to take certain spectral features observed in the supergiants for luminosity indicators, when they are really indicators of an extended atmosphere.

The similarity between supergiant spectra and shell spectra is an extension of what is observed in the visible region. It indicates that the ionization and density conditions in their cool extended envelope are similar in these two kinds of objects. This similarity has been clearly demonstrated by Snow et al. (1979) in the spectral range from 1120 to 1140 Å, which they observed with Copernicus. Figure 12-7 shows this region of the spectrum in two Be shell stars, ζ Tau and 48 Lib, and two supergiants, ρ Leo and η CMa; for both types of stars the lines of Fe III, Cr III, and Mn III dominate the spectrum.

The Shell Spectrum of Some Be and Pole-On Stars in the Ultraviolet Region. Shell lines in the ultraviolet region do not appear only in stars that exhibit a shell spectrum in the visible. They have also been observed in a certain number of Be

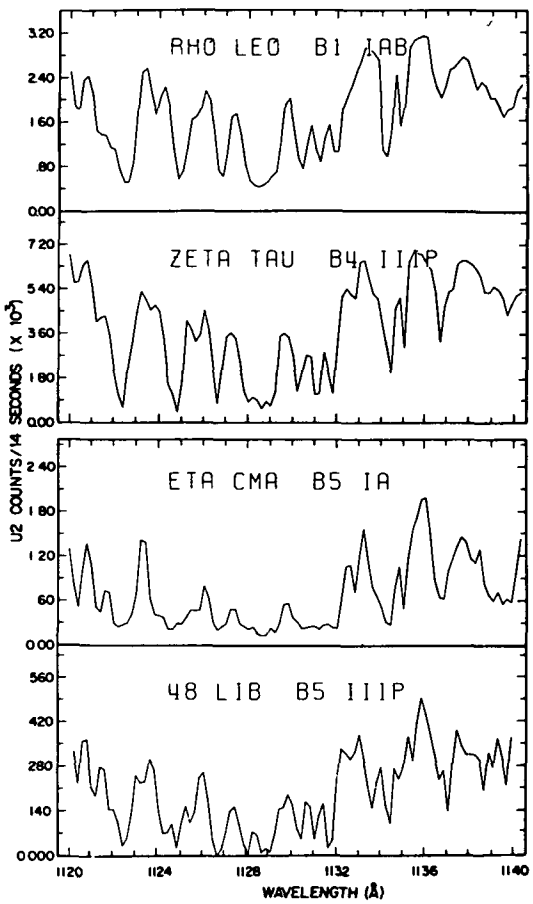

Figure 12-7. Comparison of supergiant spectra with those of shell spectra (ζ Tau and 48 Lib) in the 1120 to 1140 Å region. The similarity of the spectral features observed indicates that the origin of the lines is, for both types of stars, an extended atmosphere (from Snow et al., 1979)

spectra, including some that are considered to be pole-on. If the rotation model of the Be stars is accepted, a close correlation should be observed between the strength of the shell lines and the value of v sin i, since this model assumes that all the Be stars are rapid rotators. If the envelope is concentrated at the equator, the strength of the shell feature depends on the direction between the axis of rotation and the line of sight.

A visual inspection of the Fe III shell lines at 1131 Å in nine Be/shell stars observed with Copernicus strongly suggests that the strength of these lines is not correlated with v sin i in the Be stars (Peters, 1976b). This result has been refined by the observation of 17 Be/shell stars between 1120 and 1140 Å with Copernicus (Snow et al., 1979) which show that the correlation between these two quantities is very low. In particular, it is noted that a few pole-on stars (ω C Mi, η Ori, 31 Peg) have fairly strong shell lines; this implies that there are appreciable column densities in their polar regions, such as Snow (1975) had previously observed for χ Oph, in complete contradiction with the hypothesis of the rotation model. Nor has any correlation been found between the intensity of the emission in the visible region and the strength of the shell lines in the ultraviolet region. On the other hand, Peters (1979) did not observe any shell lines for two pole-on stars, ν Cyg (v sin i = 280 km s^{-1}) and μ Cen (v sin i = 190 km s^{-1}), for which she performed a complete analysis of the ultraviolet spectrum by means of model atmospheres

THE ENERGY DISTRIBUTION OF THE Be STARS IN THE ULTRAVIOLET CONTINUUM

In Chapter 11, we saw that the Be phenomenon—which is defined by the presence of emission lines in the visible region—is accompanied by an energy distribution that is different from those of normal B stars of the same spectral type, from the near ultraviolet ($\approx$ 3200 Å) to the infrared region ($\approx$ 20 μ). This difference in the energy distribution shows itself in two different ways.

1. On the average, the Be stars are observed to have higher luminosities than the normal B stars, by about 1 magnitude in the V band and over the whole infrared wavelength range. If the continuous spectrum of the Be stars were produced only in the photosphere, their high visual luminosity with respect to normal B stars of the same spectral type could result from the fact that their effective radius is greater than that of the B stars. Such an interpretation of the excess luminosity is consistent with the explanation of the Hα emission as a volume effect. But if the visual characteristics persisted throughout the spectrum, the Be stars would also have a brighter average value of M_{bol} than the normal B stars; such a result would have profound implications both for the internal structure of the star and for its evolution. In particular, it would have to be explained how the luminosity of the star could change as rapidly as it does, given the variability of the Be stars. Thus, it is essential to know whether the excess luminosity is limited to the visible and infrared regions, which represent a small fraction of the energy emitted by the B stars, or whether it also extends to the far ultraviolet, where the maximum energy is emitted.

2. The energy distribution in the visible range shows that the color temperature of the Be stars is, on the average, lower than that of normal B stars of the same spectral type, as was shown in Chapter 11, the Be stars have an intrinsic reddening. The excess luminosity and the reddening can be explained by free-free and free-bound emission in the outer atmosphere, if this region is optically thin. If it were optically thick, one would not see the photosphere of the underlying B star. If it were not known that the flux in the visible continuum of the Be star is greater than that of the normal B star, the color could be interpreted as a flux deficiency in the short-wavelength regions, instead of a flux excess in the long-wavelength regions. Data on the color of the star alone do not allow us to draw conclusions concerning the flux differences between the B and Be stars.

Thus—and this is very important for the study of the ultraviolet flux—it cannot be assumed that a Be star and a B star of the same spectral type and same visual magnitude are located at the same distance. Similarly, it cannot be assumed that a

B star and a Be star of the same color have undergone the same interstellar reddening.

The Problem of Determining the Ultraviolet Flux of the Be Stars

The study of the ultraviolet spectrum of the Be stars should lead, first, to a knowledge of the energy distribution of the Be stars, and second, to a comparison of the energy distribution of the Be stars with that of normal B stars of the same spectral type. For the first problem one must compute the interstellar extinction correction to be applied to the flux of the Be stars observed in the ultraviolet. For the second, one must compare the ultraviolet flux of Be stars to that of normal B stars of the same spectral type that are located *at the same distance* As we have pointed out, *normalizing the flux of B and Be stars to the same V magnitude is not equivalent to placing the stars at the same distance*, because of their intrinsic luminosity difference in the visible.

How have various studies proceeded to solve these two problems?

The Correction for Interstellar Extinction We know that the Be stars exhibit an intrinsic reddening in the visible region, which affects the (B − V) index. The existence of this reddening makes it impossible to apply to Be stars the methods of dereddening used for normal B stars, if the effects to be demonstrated are small If the effects are large, like those observed in the infrared, the relative error introduced will be small, and the conclusions of the comparison will be unchanged If the color excess E (B − V) is used, the correction applied is too large, and *the ultraviolet flux of the Be stars is overestimated*. Most studies have used E (B − V) to correct for interstellar extinction. Beeckmans (1977b, 1978) attempted to avoid this index and used the absorption bump at 2200 Å to make the correction.

The Comparison of the Flux of the Be Stars to That of Normal B Stars of the Same Spectral Type. All the studies made so far have failed to take into account the higher luminosity of the Be stars in the visible region with respect to the normal B stars, or have done so inadequately. Instead of comparing the flux of B and Be stars located at the same distance, the fluxes have been normalized to the same V magnitude. When such a procedure is used, the *ultraviolet flux of the Be stars is underestimated with respect to the B stars.*

Thus, neglecting the intrinsic reddening of the Be stars in the visible region leads to an overestimate of the ultraviolet flux of the Be stars with respect to that of the B stars, normalizing the fluxes at the same V magnitude amounts to underestimating the ultraviolet flux of the Be stars with respect to that of the B stars. These remarks show why some studies find flux excesses in the Be stars with respect to normal B stars in the ultraviolet region, while others find flux deficiencies. It could even be said that the results are less biased by not taking into account the intrinsic reddening in the visible region, if the flux of the B and Be stars are to be normalized to the same V magnitude. For these two procedures introduce compensating errors, while if the intrinsic reddening is taken into account and the fluxes are reduced to the same V magnitude, the ultraviolet flux of the Be stars *is sure to be underestimated* with respect to the normal B stars. These are, in fact, the conclusions of the various studies of the ultraviolet flux of the Be stars.

The case of the shell spectra deserves special attention Indeed, the study of individual stars (Chapter 11) shows that the shell phase corresponds to a phase of lower luminosity in the visible region than the Be phase. Observations of Pleione and 59 Cyg (Chapter 11; see also the next section of this chapter) show that the same is true in the ultraviolet region. This raises the question of whether the shell phase is intrinsically fainter in the visible and the ultraviolet regions than the normal B phase. This question cannot be answered by the determinations of M_V that have been made up to now using statistical methods, because they have made no distinction between the Be and shell phases. In the case of Pleione and 59 Cyg, the shell phases are less luminous than the normal or quasi-normal B phase. For γ Cas, the highest color temperature in the visible region

($\approx 3.0 \times 10^4$ K) is observed at the time of maximum development of the shell spectrum, and the lowest color temperature at the time of maximum intensity in the Be phase. The color temperature of Pleione, on the other hand, varies little between these two phases. Thus, for the moment, no general conclusions are apparent that are applicable to all the shell stars, each individual case must be examined separately. One can only make the following remarks in the case of the shell spectra. if the color of the shell phase is bluer than the normal B phase, the use of E (B − V) to correct for interstellar extinction leads to an underestimate of the ultraviolet flux of the shell stars. On the other hand, if the shell phase corresponds to a fainter intrinsic visual luminosity than that of the normal B phase, normalizing the flux of the normal stars and the shell stars to the same V magnitude results in an overestimate of the ultraviolet flux of the shell stars. Thus, the effects are opposite to those in the Be phase.

We have dwelt at some length on these problems in order to reach a better understanding of the contradictory results of the studies made in this area.

The Results

Bottemiller (1972) used OAO-2 observations to compare the ultraviolet continuous flux distribution of 25 B stars with that of 15 Be/shell stars; the latter group was made up of shell and Be stars, preferably with an infrared excess. From the values of E(B − V) obtained in the usual way—that is, without taking into account the intrinsic reddening of the Be stars—the excesses in the three colors (1690 − V), (2390 − V), and (3320 − V) were computed, using the relation for $E(\lambda - V)$ versus E(B − V) of Bless and Savage (1972) to correct for interstellar extinction in the ultraviolet region. The color-color diagrams obtained by Bottemiller do not reveal any systematic difference between the samples of B and Be stars he considered, nor was there any significant difference between the "shell" and "infrared excess-Be star" categories.

In their study of interstellar extinction from 3600 to 1100 Å, using OAO-2 observations, Bless and Savage (1972) concluded that Be stars with strong emission lines in the visible exhibit a flux excess for $\lambda > 2000$ Å, in comparison with normal B stars of the same spectral type, while for $\lambda < 2000$ Å they observed no difference.

Lamers et al. (1980) studied the intrinsic color (m_{2500} − V) for 15 Be/shell stars, using S 59 observations, and compared it to the color of normal stars. They found that the Be and shell stars have normal colors.

Two studies, one by Briot (1978) and the other by Beeckmans (1977b, 1978), used observations from TD1-S2/68. These authors used different methods to correct for interstellar extinction, and arrived at contradictory results. A comparison of these two studies shows that a final conclusion concerning the relative luminosity of the Be and B stars in the ultraviolet region cannot yet be given.

Briot (1978) used the TD1-S2/68 observations of the largest possible samples: 117 Be stars and 167 normal B stars. The interstellar extinction in the ultraviolet region was computed from the relation derived by Nandy et al. (1975), who tied this correction to E(B − V). Since no allowance was made for the intrinsic reddening of (B − V) in the Be stars, Briot overestimated the ultraviolet flux of the Be stars. Using the F_λ versus $1/\lambda$ curves obtained in this way, and normalizing the flux of the B and Be stars at the same V magnitude—which now underestimates the ultraviolet flux of the Be stars with respect to the B stars—Briot concluded that Be stars later than B3 were indistinguishable from normal B stars. For the types B0 to B3, the Be stars exhibit a very small flux excess with respect to normal stars of the same spectral type for wavelengths greater than 1900 Å, while for wavelengths less than 1900 Å there is neither a systematic excess, nor a deficiency. Thus, Briot recovered the conclusion of Bless and Savage (1972).

Beeckmans (1977b, 1978) also used the TD1-S2/68 observations to compare the flux of 72 Be stars to that of normal B stars. In order to avoid using E(B − V), which is corrupted by intrinsic reddening for the Be stars, she chose to use the 2200 Å interstellar absorption band as a criterion of interstellar extinction. The method of Nandy

et al. (1975), which was derived for the normal B stars, cannot be applied directly to Be stars, since it is based on differential measurements of reddened and unreddened stars of the same spectral type, having the same spectral features, which is not the case for the B and Be stars. Beeckmans used the index Δm_{2200} defined by Malaise et al. (1974), which corresponds to the magnitude difference between the intensity observed at 2190 Å in the absorption bump, and that of the pseudo-continuum, based on the flux maxima at 1670 and 2500 Å. The quantity Δm_{2200} is well correlated with the equivalent area W_{2200} of the 2200 Å absorption bump, measured by Nandy et al. (1975) for normal stars. Beeckmans used the index Δm_{2200} to characterize the interstellar absorption in all cases, for both the normal B stars and the Be stars. Thus, she assumed that the 2200 Å bump is produced only by the interstellar medium, and is not at all influenced by the outer atmosphere of the Be stars. She used the index $(m^i_{2100} - V)$ to characterize the ultraviolet flux of the stars she studied.

In order to understand Beeckmans' hypotheses, one must follow the steps in her analysis (1) She determined the intrinsic colors of the normal B stars by means of diagrams of $(m^i_{2100} - V)$ versus Q, where $Q = (U - B) - 0.72(B - V)$, and made the hypothesis that the observed excess $E(m^i_{2100} - V)$ is due only to interstellar extinction. She found a high correlation between $E(m^i_{2100} - V)$ and $E(B - V)$ for the normal B stars. However, there was a large scatter for the stars located in reflection nebulae, for which the ultraviolet extinction was smaller than for normal stars. (2) Then she determined a relation between $E(m^i_{2100} - V)$ and Δm_{2200} for the normal B stars. The scatter was large, especially around the origin ($\Delta m_{2200} = 0$), where the reddening is negligible and where the errors of measurement should be smallest, since the nearly unreddened stars are the brightest. This effect was interpreted, as in Malaise et al. (1974), by the presence of two components, mingled in variable proportions in the interstellar medium. The mean relation from the diagrams of $E(m^i_{2100} - V)$ versus Δm_{2200} for the normal B stars was used to correct for the interstellar extinction in the Be stars, using the measured values of Δm_{2200}, and to construct diagrams of $(m^i_{2100} - V)$ versus Q for these stars. A comparison of the position of the Be stars in this diagram, with the relation obtained for the normal B stars, led Beeckmans to the following conclusions: (a) the earliest-type Be stars have an ultraviolet flux deficiency with respect to the normal B stars, the deficiency seems to be connected with the intensity of the emission lines in the visible region and with the strength of the absorbing envelope; (b) the latest-type Be shell stars also have an ultraviolet flux deficiency with respect to the normal B stars, while the other Be stars have either a normal ultraviolet flux or an ultraviolet flux excess. Beeckmans interpreted the reddening of the $(m^i_{2100} - V)$ index as an indication of an ultraviolet flux deficiency at 2100 Å in the Be stars.

In this study, Beeckmans proposed a method of evaluating the interstellar extinction correction in the Be stars. the use of the absorption bump at 2200 Å. This method assumes that the spectral features of the Be stars are always the same in this spectral region. But the observation of high-resolution ultraviolet spectra shows that the presence of shell lines can significantly modify the spectral features in this region, as well as the definition of the continuum. Moreover, there are some problems with the use of the relation between Δm_{2200} and $(m^i_{2100} - V)$, as obtained for normal stars, to correct for the interstellar extinction in Be stars on the basis of measurements of Δm_{2200}. Although the correlation between W_{2200} and $E(B - V)$ is high for normal stars (Nandy et al., 1975), there are several stars that exhibit an anomalous intensity in the 2200 Å band (Willis and Wilson, 1975, 1977). The cause of this anomaly is not yet well understood (Millar, 1979). Smyth and Nandy (1978) extended the observations made in the ultraviolet with S2/68 out to 2.2 μ in the infrared, for 57 hot stars. In the diagram of $E(2190 - 2500)$ versus $E(V - K)$, where $E(2190 - 2500)$ is a measure of the band at 2200 Å, they noted that three shell stars diverged from the mean relation found for the normal stars. They suggested that the 2200 Å band may behave abnormally in these stars.

Most of the results from Beeckmans' thesis (1978), concerning the Be stars, can be found in

Beeckmans and Hubert-Delplace (1980), where the reddening of the index ($m^i_{2100} - V$) is again interpreted as an ultraviolet deficiency in the Be stars with respect to the B stars. In this study, the authors attempted to account for the emission of the envelope in the Paschen continuum, but they corrected only the V magnitude for the intrinsic reddening of the (B − V) index. This correction takes care of only part of the excess, it assumes that the luminosity of the B and Be stars is the same in the B band, which is not the case. The correction made by these authors brings the B and Be stars closer together, but not close enough, the ultraviolet flux of the Be stars is still underestimated. However, note that already this partial correction reduces the fraction of Be stars having an index reddened by more than 0.2 mag, from one-half to around one-third.

Finally, let us return to an essential point. *in all these studies, the conclusions refer to "deficiencies" or "excesses" of the ultraviolet flux in the Be stars with respect to the normal B stars, while the methods used can yield results only on the redness or blueness of some index ($\lambda_{uv} - V$) in the Be stars, with respect to the normal stars* In each of these conclusions, the word "deficiency" should be replaced with "redder ($\lambda_{uv} - V$) index," and "excess" with "bluer ($\lambda_{uv} - V$) index." In order to understand this distinction, we have only to recall the observations made in the visible, which show that the Be stars have redder indices than do the normal B stars, but in spite of this reddening the Be stars have a flux excess. At present it seems that, as long as we are not sure how to evaluate correctly these two effects—the correction for interstellar extinction and the difference in intrinsic luminosity between the B and Be stars in a given wavelength region—the conclusions drawn from a statistical study of the Be stars can be certain only if the effects under consideration are large with respect to the errors introduced by certain approximations. In the opposite case, the results will essentially reflect the effects of the approximations themselves. This is what we observe in the conclusions of the preceding studies As long as no accurate methods for evaluating these two corrections exist, and given the difficulties inherent in a statistical treatment of the Be stars—for each individual star introduces its own error which is difficult to estimate—it is preferable to study the behavior of a few individual stars over different epochs and phases of variation, in the greatest detail and over the longest wavelength range possible. The differential effects observed can then be unambiguously connected with other spectral features. As we have seen in the case of γ Cas, 59 Cyg, Pleione, and 88 Her, the study of these correlations can provide a much better outline of the Be phenomenon than the study of statistical properties, whose interpretation is uncertain (see the section on Variability in Chapter 11).

In addition to these two large effects—the correction for interstellar extinction and the intrinsic luminosity difference between the B and Be stars in the V band—other sources of error can influence the results, such as an error in the spectral type of the Be stars. Considering that the Be stars are always more or less variable, another large error is, of course, introduced by the fact that the V magnitudes and the ultraviolet fluxes have not been measured simultaneously.

The Ultraviolet Flux in the Shell Phase– ζ Tau

Beeckmans (1976a) compared the ultraviolet flux of ζ Tau from 1350 to 2550 Å with that of normal stars, using S2/68 spectra. One of the difficulties in this study was the uncertainty in the spectral type of the star. The MK classification criteria are difficult to use, for this shell spectrum—which is especially well developed in the visible region—disturbs a large number of photospheric lines. The spectral types that have been determined vary from B1 to B4, depending on the authors and the criteria they used. Beeckmans adopted the type B3 IIIp given by Jaschek She showed that the gradient of ζ Tau in the ultraviolet region is bluer than what would correspond to the spectral type determined in the visible region, and that it is similar to that of much hotter normal stars, of type 09.5 V or B1 II-III She interpreted the blueness of ζ Tau in the ultraviolet region as an indication of an earlier spectral type Normalizing the flux at the V magnitude, she

found that ζ Tau has an ultraviolet flux deficiency with respect to normal stars of types 09.5 II and B1 II-III, and also with respect to a standard model atmosphere for T_{eff} = 27,500 K and log g = 4. These values of T_{eff} and g were used because they are the ones proposed by Heap (1975) to interpret her high-resolution (0.1 Å) ultraviolet spectrum of ζ Tau. Heap studied the ionization equilibrium of C III versus C IV and Si III versus Si IV, using the Mihalas models. However, the observed Si IV and C IV resonance lines were shifted by around −120 km s^{-1}, showing that there can be no legitimate comparison with theoretical profiles computed under the static conditions of the classical theory of stellar atmospheres.

Hubert-Delplace and van der Hucht (1978) studied the ultraviolet flux of ζ Tau in the 2100 to 2800 Å region, using spectra from TD1. The ultraviolet flux was dereddened by using $E(B-V)$ as for normal stars, and the comparison with normal stars was made by normalizing the fluxes to the same V magnitude. These authors found that if ζ Tau has a spectral type of B3 V-IV, its ultraviolet flux is similar to that of normal stars of the same type; if the spectral type is B2, the ultraviolet flux of ζ Tau is deficient by around 0.35 mag. Note also that the ultraviolet flux of ζ Tau is highly variable. In a period of 6 months, Beeckmans (1976a) observed color and flux variations of as much as 0.4 mag.

For the moment, the safest conclusions concerning the ultraviolet flux of shell stars can be drawn from a comparison of the flux measured at different phases in the variation of a single star. Of course, a comparison of the flux of the same star in all three phases—Be, B shell, and normal B—would produce the most interesting results Up to now, only the Be and shell phases have been compared. Golay and Mauron (1977) observed Pleione from 2000 to 6000 Å during the Be and shell phases, demonstrating the existence of a large flux decrease in the ultraviolet and visible region during the shell phase. Beeckmans (1976b) compared the ultraviolet flux of 59 Cyg, from 1200 to 2300 Å, during the Be and shell phases. She also found a large drop in the ultraviolet flux, of the order of 1 mag.

A luminosity decrease during the shell phase has been observed for several stars in the visible region. The ultraviolet flux seems to behave similarly. It is quite obvious that the observation of a single star in different phases, over the greatest wavelength range possible, is essential for an understanding of the behavior of the continuous spectrum in the Be shell stars.

THE VARIABILITY OF THE Be STARS IN THE ULTRAVIOLET

In spite of the short baseline of the ultraviolet observations from space, it has quickly been established that the Be stars are also variable in this spectral region. Perceptible variations can take place on time scales of the order of hours, days, months, or years, depending on the epoch of variation of the star. But these variations are much greater than those that are observed in the visible region. For example, the shifts of the N V and C IV resonance lines in 59 Cyg have been observed to vary from around −200 to −1000 km s^{-1}, such large variations have never been detected in the visible. Before the space age, the outer atmosphere of the Be stars could have been considered static in comparison with other stars, like the Wolf-Rayet stars, in which large expansion velocities are observed in the visible region. The relative calm of the cold extended envelope is in striking contrast to the violent, high-amplitude variations of the superionized regions, which the ultraviolet observations have discovered in Be stars.

In order to construct an empirical model of the atmosphere of a star, one must know the behavior of all the regions of the outer atmosphere, simultaneously, from the chromosphere-corona to the cold regions of the post-corona. Relations between the variations in the ultraviolet and visible spectral regions must be determined—that is, relations between the rapidly expanding, superionized regions and the low-velocity subionized regions. Thus, the variability—which created difficulties in the study of the Be phenomenon in the visible, because it could not be connected to any of the parameters that describe the photosphere—becomes a means of investigating this phenomenon, once it can be

related to variations in the mass flux. The relations that can be determined between these various atmospheric regions will be constraints on the model which should not, a priori, contain any constraints that are not justified by the observations. In order to construct such a model, simultaneous observations of the various regions of the outer atmosphere, that is, observations over the greatest possible wavelength range, are necessary.

The observations of 59 Cyg suggest that the beginning of a new Be phase is the result of a very great increase in the mass flux, and that the Be phase with weak, increasing emission is accompanied by very strong, apparently erratic variations in the mass flux. It also seems that the value of the mass flux can be very different, depending on the epoch of variation observed in the visible region. Such information cannot be provided by statistical studies which cover a limited region of the atmosphere, such as the visible spectral range, it can result only from regular, simultaneous observations of the various regions of the outer atmosphere in individual stars.

We shall make use of the examples of γ Cas and 59 Cyg once again, to show what information is contributed by this new direction in the observations. A detailed summary of the observations of these two stars, which have been followed for nearly a century in the visible region, has been given in Chapter 11. We recall that at various epochs, these stars have exhibited different phases of variation from those in which we see them today. Figures 11-33 and 11-41 enable us to pick out striking similarities in the long-term behavior of these stars, but we have also noted differences in the amplitude, duration, and details of the variations, thus demonstrating the individuality of the Be phenomenon. Aside from the rich body of visible observations, γ Cas and 59 Cyg would have been chosen to illustrate the ultraviolet variations of the Be stars, because, among all the hot stars, they have exhibited the largest variations in this new spectral region. These variations involve mainly the shifts and profiles of the superionized lines, that is, precisely the lines that are used in the ultraviolet region to determine the mass loss of these stars, thus, indicating that the mass flux is highly variable. Any physical interpretation of the Be phenomenon and the origin of the mass flux in these stars must necessarily take this conclusion into account.

Variations of γ Cas in the Ultraviolet Region

γ Cas was observed many times in the ultraviolet region between 1968 and 1980, that is, during the long Be phase which began in 1946 (see Figure 11-33). One of the striking results from the body of ultraviolet observations is the fact that the superionized lines have varied with much greater amplitude than had the emission lines in the visible region at the same time. Moreover, systematic observations have made it possible to detect rapid variations (hours) and short-term and medium-term variations (weeks or months).

A description of a rocket spectrum (resolution 2 Å) of γ Cas, recorded in 1968, is given by Bohlin (1970). It is the only spectrum of γ Cas, or of any Be star, in which the C IV resonance lines have been reported with a P Cygni profile; the expansion velocity of the absorption component is around 450 km s^{-1}. Lillie et al (1972) also indicated shortward displacements of at least 500 km s^{-1} for the C IV lines. Working at low resolution (12 Å) with OAO-2, Panek and Savage (1976) noted a variation of a factor of two in the intensity of the C IV and Si IV lines, in the space of a few months.

The spectrum of γ Cas was observed several times with Copernicus and IUE at high resolution (0.2 and 0.1 Å, respectively) by Snow and Marlborough (1976), Marlborough (1977a), Marlborough et al (1978), Slettebak and Snow (1978), Hammerschlag-Hensberge et al. (1980), Henrichs et al. (1980), and Doazan et al. (1980c). Marlborough (1977a) and Hammerschlag-Hensberge et al. (1980) give a list of the identified lines, including lines of P V, N V, C IV, C III, C II, Si IV, Si III, Si II, N III, N II, Al III, and P II.

Rapid variations of the Si IV and Mg II lines

were detected by Slettebak and Snow (1978), who scanned these two regions with Copernicus continuously for 64 hours, and simultaneously observed Hα from the ground during two successive nights (at a resolution of 3 Å). They discovered a flare-type event with a total duration of around 100 minutes, during which the intensity in the violet emission wing of the Mg II resonance lines increased significantly, at the same time as the Hα emission

Both medium-term and rapid variations were detected by Marlborough et al. (1978), who used the Copernicus satellite to observe the resonance lines of N V, Si IV, and Mg II in 1974 and 1976. Figure 12-8 shows the resonance doublet of Mg II, in which variations of the red and violet emission wings are clearly visible. The Si IV lines exhibit only small changes in structure, while the spectrum undergoes the strongest variations in the N V region, as shown in Figure 12-9. In some Be/shell stars, this region is rich in lines, and the short extent of the scans made it impossible for the authors to identify the N V doublet with certainty Subsequent observations made with IUE have confirmed the presence of strongly displaced N V resonance lines, indicating that these lines were shifted by -1050 km s^{-1}. Hα observations, made by these authors at epochs close to those of the ultraviolet observations, show the asymmetry variations in this line. However, the very low resolution (3 Å) used for the ground-based observations is not sufficient to detect structural variations in the profile.

Marlborough et al. (1978) discussed the variability of the visible and ultraviolet spectra of γ Cas, and concluded that no existing model was capable of interpreting all the observations. They proposed a coronal model in which the terminal velocity of the stellar wind depends on the distance from the equatorial plane. the velocity is small in the plane, and much larger at large distances from the plane. The emission lines in the visible and the ultraviolet emission wings of the resonance lines of Mg II, the infrared excess, and the intrinsic polarization are produced in the dense equatorial regions, close to the star The mass flux from the star is produced by an unspecified physical mechanism. It is assumed that

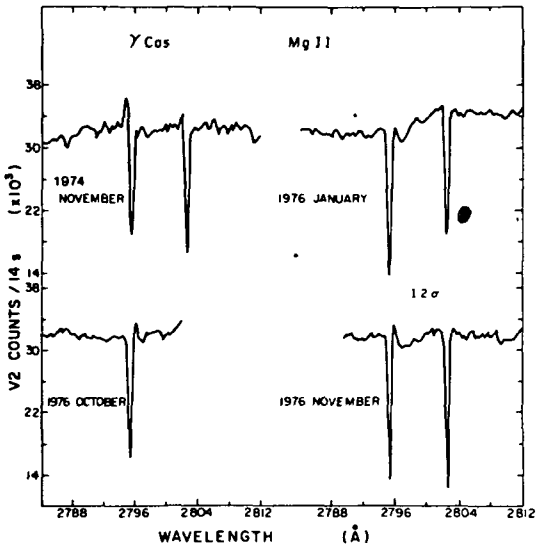

Figure 12-8. The V/R variations of the emission wings of the Mg II resonance doublet of γ Cas (from Marlborough et al , 1978)

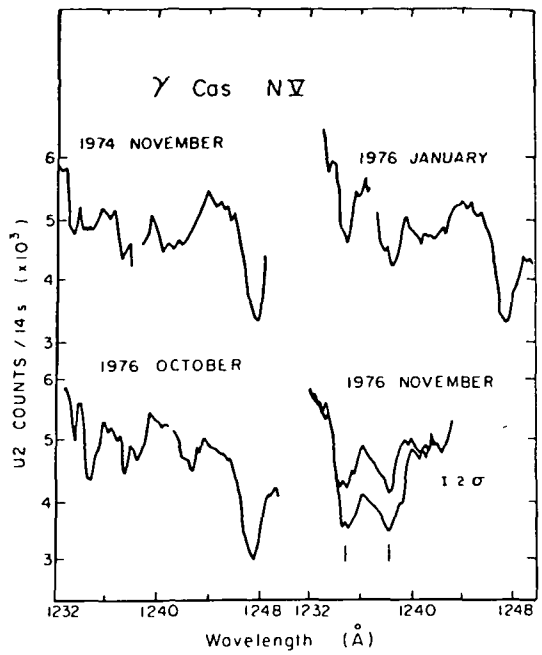

Figure 12-9. Copernicus U2 scans of the N V region in γ Cas Note the long-term variation in the scans from 1974 to 1976 and the short-term variation in November 1976 where appreciable changes occur in 2 hours (from Marlborough et al., 1978)

differential rotation produces turbulence in the regions close to the equatorial plane, which, in turn, produces a coronal layer at large distances from the plane. This coronal layer is accelerated to large terminal velocities by radiation pressure, produced mainly by the radiation field in the polar regions. In order to account for the V/R variations of the visible emission lines and the ultraviolet Mg II emission wings, Marlborough et al. postulated the existence of a compact companion, a neutron star. Because of the gravitational asymmetry of the system, the envelope would be elongated toward the companion. This compact object is supposed to produce the observed V/R variations, and to create the X-ray emission by the accretion of material from the equatorial regions of the stellar wind, where the terminal velocity is small

The proposed model is an ad hoc generalization of Poeckert and Marlborough's stellar wind model (see Chapter 11); it is not, and does not claim to be, physically self-consistent. Nor does it claim to be applicable to all the Be stars. This model can only postulate the existence of a compact companion, for it has never been shown that the V/R variations have a period, strictly speaking, although a great deal of research has been performed along this line. These V/R variations seem to take place on a time scale of 3 to 4 years, but it has never been possible to reduce them to a single period Marlborough (1977b) has proposed also a model, for γ Cas, where X-ray emission originates in the corona of the star (see the next section)

On the basis of a sequence of high-dispersion IUE observations, Hammerschlag-Hensberge (1979) announced that γ Cas was entering another shell phase. The reason for this alert was the observation of sharp secondary absorption components in the N V, C IV, and Si IV resonance lines which Hammerschlag called shell lines. However, the author's observations in the visible region did not indicate any significant change in the spectrum, except for the V/R variations that are typical of the present Be phase in γ Cas. We recall that the shell spectrum in the visible region is defined by the following spectral features: (1) sharp, deep absorption cores in the Balmer lines, and (2) sharp absorption lines of the singly ionized metals. The presence of these metallic lines, which are not ordinarily observed in B stars, implies the existence of regions of lower ionization than that predicted for the effective temperature of a B star. On the other hand, the "shell" lines of N V and C IV refer to lines of atoms that are superionized with respect to the effective temperature of the stellar photosphere. Thus, the shell spectrum of the Be stars as they have been defined in the visible, and the "shell" lines observed in the ultraviolet for superionized atoms, refer to regions in which the physical conditions are diametrically opposed. In order to avoid confusion, another term should be found. The term ultraviolet shell lines has been proposed to denote the sharp components of the superionized lines observed in the ultraviolet; but this term is also ambiguous, because there exist low-ionization shell lines in the ultraviolet which originate in the same cool envelope as the shell lines observed in the visible.

Spectra taken with IUE between April 1978 and October 1979 show large variations in the depth of the narrow absorption components of the N V, C IV, and Si IV resonance lines (Henrichs et al., 1980) In addition to the broad, asymmetrical, low-velocity (≈ -100 km s^{-1}) absorption lines, these authors observed, at four different epochs, sharp absorption components of variable depth, highly displaced at velocities between -1200 and -1500 km s^{-1}. The shifts in the sharp secondary absorption components of N V, C IV, and Si IV have the same velocity for all three ions. Their full width at half maximum have varied from 30 to 250 km s^{-1}, and the intensities of the two components of the resonance doublets are in agreement with their oscillator strengths. The sharp secondary absorption lines seem to be formed in less than 7 days, and to disappear in less than 2½ months. Moreover, at intermediate velocities (-900 to -1200 km s^{-1}), the absorption is negligible. Figure 12-10 shows an example of the N V, C IV, and Si IV lines observed by Henrichs et al. (1980).

Henrichs et al. interpreted the observed phenomenon in terms of transitory shells. They assumed that the stellar wind can exist in two

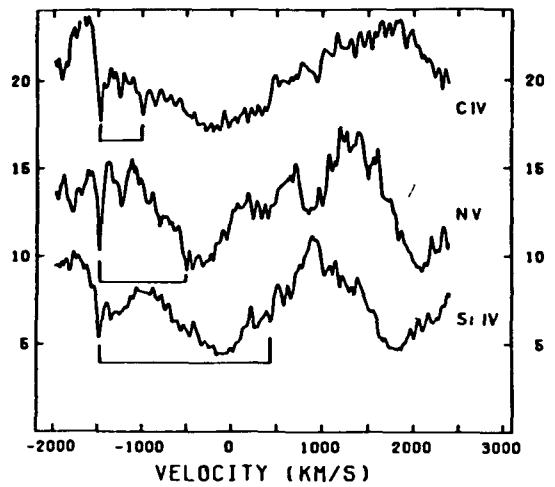

Figure 12-10. The sharp secondary absorptions in the resonance lines of N V, C IV, and Si IV of γ Cas are all displaced by −1500 km s^{-1} (from Henrichs et al, 1980).

phases: a quiet phase, in which only the broad, asymmetrical, low-velocity components are observed; and an active phase, in which the mass flux is multiplied by a factor p. The rate of mass flux is regulated in the photosphere, at the point where the velocity becomes supersonic. The authors did not specify the reason for the change in conditions at this point.

In this interpretation, only the ultraviolet observations—that is, the superionized regions of the outer atmosphere—are taken in account. Such a model, in which the outer atmosphere leaves the star at high terminal velocities after undergoing its final acceleration, cannot produce the cold, low-velocity regions in which the emission lines observed in the visible are formed. This interpretation makes the basic assumption that the observed variations can be approximated by fluctuations about a certain constant value. But there are enough observations of γ Cas to show that at other epochs, the N V lines exhibited very different displacements from those observed from 1978 to 1980. Marlborough et al.'s (1978) observations, which we gave in Figure 12-9, show that, in 1974 and 1976, the N V lines were shifted by −1050 km s^{-1}, into spectral regions where no absorption at all was detectable from 1979 to 1980. The variations in the shifts of these lines, from −1000 to −1500 km s^{-1}, seem difficult to explain in terms of only fluctuations. Moreover, it is impossible to neglect the history of γ Cas in the visible, which strongly suggests that the mass flux of this star is highly variable, and not merely fluctuating (see Chapter 11).

These same sharp absorption components were observed in γ Cas in October 1979 and May 1980 by Doazan et al. (1980c, 1981d), who interpreted them very differently. Their interpretation is based on the fact that the same object can exhibit three phases—Be, Be shell, and normal B—and that the classical parameters T_{eff} and gravity cannot represent such an object. The ultraviolet observations strongly suggest that it is necessary to introduce two other parameters, the mass flux and the nonradiative energy flux. These parameters can be specified only from the general thermodynamic relations. These authors proposed an empirical model to represent the ultraviolet and visible observations of γ Cas, which led them to the following conclusions. (1) the presence of superionized ions like N V and C IV implies the existence of a nonradiative energy flux, and therefore the existence of a chromospheric region; (2) the absence of absorbing ions at intermediate velocities between the low- and high-velocity components indicates that there is a region hot enough—that is, a corona—to eliminate them at the points corresponding to these velocities, because the temperature there is too high, the detection of X-ray emission from γ Cas strongly supports this idea, (3) the low velocity components in these lines refer to the chromosphere-corona transition region, where T_e is increasing, while the high-velocity components refer to the post-coronal region, in which T_e is decreasing, (4) the presence of emission in the Balmer lines, and the low velocities of these lines, imply that the atmosphere has been decelerated and cooled. Such a deceleration could take place following the formation of a shock wave, owing to the interaction of a variable stellar wind with the denser local interstellar medium, which was formed by the preceding lower velocity wind. If the interaction takes place only with the normal interstellar medium, it occurs too far, at 0.1 to 1 pc (Conti and

McCray, 1980). For the Be stars, the deceleration must be produced much closer to the star, at a distance of around 10 R_* or 10^{-6} pc. The analogous problem for the planetary nebulae was discussed by Kwok (1981), in terms of a stellar wind that was much weaker and slower at an earlier time, thus producing a denser interstellar medium in the neighborhood of the star. The details of the process are not yet clear, but it seems that such an approach is necessary This apparently limits the picture of a stationary stellar wind, and replaces it with the picture of a "cavity" whose capacity is a function of the magnitude of the mass flux not only at the epoch in question, but also in the past—that is, a function of its history (see Chapter 13)

In this interpretation, the atmospheric structure is described by means of at least four independent parameters T_{eff}, g_{eff}, the mass flux, and the nonradiative energy flux. In the first approximation, the mass flux determines the density structure of the atmosphere and the energy flux determines its temperature structure By varying the values of the mass flux and the nonradiative energy flux simultaneously, it should be possible to obtain different configurations of the density and temperature structures that can produce the observed variations in the ultraviolet and visible spectrum. The necessity of introducing the mass flux and nonradiative energy flux as independent parameters is strongly suggested by the observations made in the ultraviolet and X-ray regions, in which both normal and peculiar stars exhibit the characteristics of individuality and variability. We shall see that in the case of 59 Cyg, the variability of the mass flux is even more strongly required to explain the observations.

Variations of 59 Cyg in the Ultraviolet Region

Unlike the case of γ Cas, the observations of 59 Cyg from 1972 to 1981, were made during and after the episode of spectacular variations in the visible, which was characterized by a rapid succession of different phases (Figure 11-41). The first ultraviolet observation took place at the end of the long Be phase or at the beginning of the first shell phase, and the second took place at the end of the second shell phase. A long, regular series of ultraviolet observations—which began in 1978 and is still being actively pursued within a broad, international program—covered the beginning of the new Be phase. This phase succeeded the quasi-normal B phase of 1977, which marked the end of the episode of spectacular variations in the visible region

The high-resolution ultraviolet observations of 59 Cyg most directly show the variability of the mass flux and its relation to the phase of variation in the visible spectrum. Although the period of spectacular variations of 59 Cyg in the visible was only very partially covered by the ultraviolet observations, it is possible to draw the appropriate conclusions, thanks to the large amplitude of the variations in the ultraviolet and the monitoring of the development of the spectrum in the visible.

Snow and Marlborough (1980) and Marlborough (1977a) studied the ultraviolet spectrum of 59 Cyg as observed by Copernicus (resolution 0.2 Å) in October 1972, at an epoch for which no simultaneous observation in the visible region is available. It is known, however, that in July 1972 the Hα emission was very intense, and in June 1973 the shell spectrum was highly developed. Considering the very low intensity of the circumstellar absorption lines observed in the ultraviolet region, it seems likely that this observation took place during an emission phase, or perhaps at the beginning of the formation of a very weak shell. These authors identified the resonance lines of O VI, N V, P V, Si IV, Si III, C III, Si II, and Cl III in the ultraviolet region; as well as lines arising from excited levels of C III, S III, Si IV, Si III, and Si II. The resonance lines of N V clearly exhibited a double structure, with a first, deep minimum at -50 km s^{-1} and a second, shallower minimum at -300 km s^{-1}. This same structure was suspected for Si IV, which exhibited a first minimum with little or no displacement, and a second, much weaker minimum at -300 km s^{-1}. Thus, there was little or no velocity progression as a function of the ionization potential. The violet edges of these lines, which were highly asymmetrical, extended to

−800 km s^{-1} for Si IV, and to values between −850 and −1250 km s^{-1} for N V

The second observation of 59 Cyg, made with Copernicus by the same authors on November 18, 1975, took place after the second shell phase, but it also lacks a simultaneous observation in the visible region. However, Doazan's observations show emission at Hα and the absence of shell lines from October 10 to 23, 1975, and weaker emission from December 17 to 21, 1975. Thus, this second ultraviolet observation was apparently made during the Be emission phase that succeeded the second shell phase that occurred from 1974 to 1975. Certain differences were observed, in comparison with 1972. The N V lines were deeper than in October 1972, and the absorption minimum was located at −180 km s^{-1}. The double structure of these lines was no longer visible; asymmetric lines were observed, with violet wings extending out to −800 km s^{-1}. The Si IV resonance lines were much weaker, and poorly defined. The Si III resonance line at 1206 Å, which was asymmetric in 1972, was quasi-symmetric in 1975. No velocity progression as a function of the ionization potential of the ions was observed in 1975, as in 1972.

Since December 1978, the ultraviolet spectrum of 59 Cyg has been regularly observed with IUE, and with Copernicus for 1979 This period covers the new Be phase with increasing emission in the visible range, which followed the quasi-normal B phase of November 1977. Simultaneous ground-based observations were made to follow changes in the visible spectrum, from Hα to the end of the Balmer series.

Figure 12-11 shows the variations in the Hα line, characterized by V/R variations, during this period of low-intensity, increasing emission. According to McLaughlin's (1948) description of the behavior of 59 Cyg–"long periods of quiescence and short periods of activity"–this epoch of weak emission observed in the visible should be considered a quiet, inactive phase. We may add that in the photographic region used for classification, it would be difficult to distinguish the spectrum of 59 Cyg from that of a normal B star. But it is precisely during this phase that the greatest mass ejection activity ever observed for this star has been detected in the ultraviolet region. Thus, the period of greatest activity in the ultraviolet corresponds to a period considered uninteresting in the visible spectrum–a calm, quiescent period. This shows–as if it were still necessary to do so–that any description of the activity in the Be stars must combine the ultraviolet and visible observations, and that any

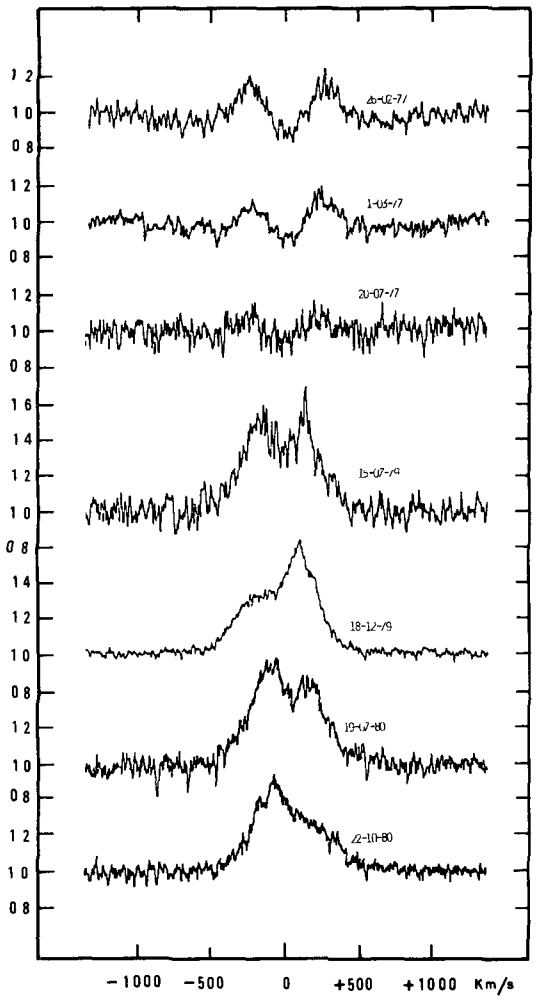

Figure 12-11. Variation of the Hα line in 59 Cyg from 1977 to 1980 (original dispersion 12.2 and 20 Å mm^{-1}, Haute-Provence Observatory). Note the decreasing emission at the end of the spectacular variation to a quasi-minimum, in July 1977. The largest variations observed in the ultraviolet region have occurred during the time where emission at Hα increased irregularly, but remained at a very low level.

interpretation of the Be phenomenon based only on data from the visible region can be completely misleading.

The first ultraviolet observations of this new Be phase with increasing emission were made with IUE, at high resolution, in December 1978 (Doazan et al., 1980a). They showed, for the first time, that the expansion velocities of the C IV and N V resonance lines were greater than the escape velocity at the surface of the star. These velocities were measured at the deepest points in the profile and not at the extreme edge of the violet extended wing of the lines. The IUE and Copernicus observations made in 1979 (Doazan et al., 1980b) showed velocity variations in these lines, but always at high velocities (−400 to −800 km s^{-1}). Figure 12-12 shows the profile of the N V resonance lines for the period 1972 to 1979. It can immediately be seen that there is a great difference in behavior between the period 1972 to 1975, which was described above, and the period 1978 to 1979, when the greatest mass flux activity was observed.

Subsequent observations, made with IUE, were characterized by very strong variations in the profile and displacement of the C IV resonance lines, indicating a strong variability in the ejection of material. These variations were also observed in the N V resonance lines, but on account of the compression of the orders of this region of IUE spectra, it is much more difficult to analyze the variations in these lines. Figure 12-13 illustrates the variations in the C IV resonance lines of 59 Cyg during the period 1978 to 1980. Large variations in the displacement, profile, and strength of the lines were observed. The position of the extreme violet edge varied from −900 to −1200 km s^{-1}. Most of the spectra show two components, one with an expansion velocity of the order of 100 km s^{-1}, which is usually also the weaker component, and the other with a high expansion velocity, of the order of 600 to 1000 km s^{-1}, which is generally also the stronger component. At least once, however, the stronger component was observed to have the lower velocity. In May 1980, the lines had a different configuration, with a broad profile on which were superimposed

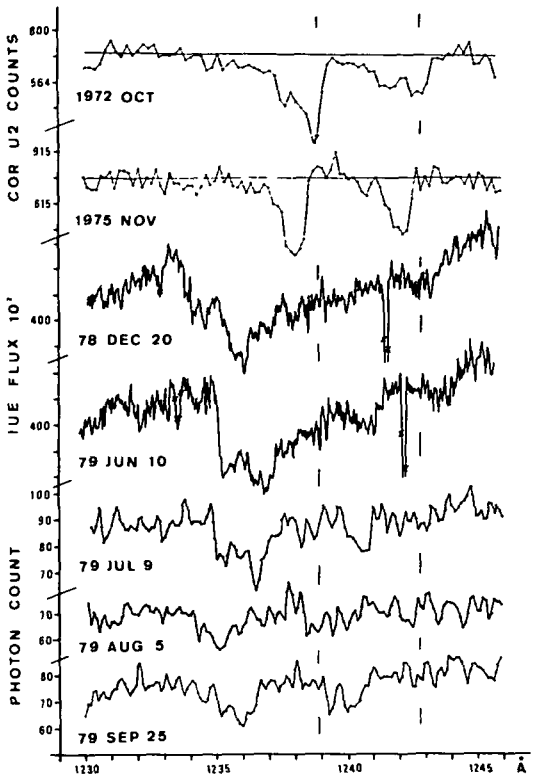

Figure 12-12. The behavior of the N V resonance lines in 59 Cyg from 1972 to 1979 The 1972 and 1975 observations made by Snow and Marlborough (1980), at the epoch of spectacular variation in the visual spectrum, show small displacements in the N V lines (about −180 km s^{-1}). From 1978 to 1979, the largest displacements of these lines are observed (from −400 to −800 km s^{-1}). The bars indicate the position of the laboratory wavelengths. All observations come from Copernicus (figure from Doazan et al., 1980b).

at least three narrow components. These components can be identified by noting their similar features and their separation, which is equal to the velocity difference of the two lines in the doublet. Large variations are observed on time scales of the order of months, but spectra taken 1 or 2 days apart also exhibit variations, characterized by gradual changes.

In striking contrast to the behavior of the C IV lines, the Si IV lines exhibit practically no variations. Their profile is quasi-symmetric, almost undisplaced and nonvariable, as shown in

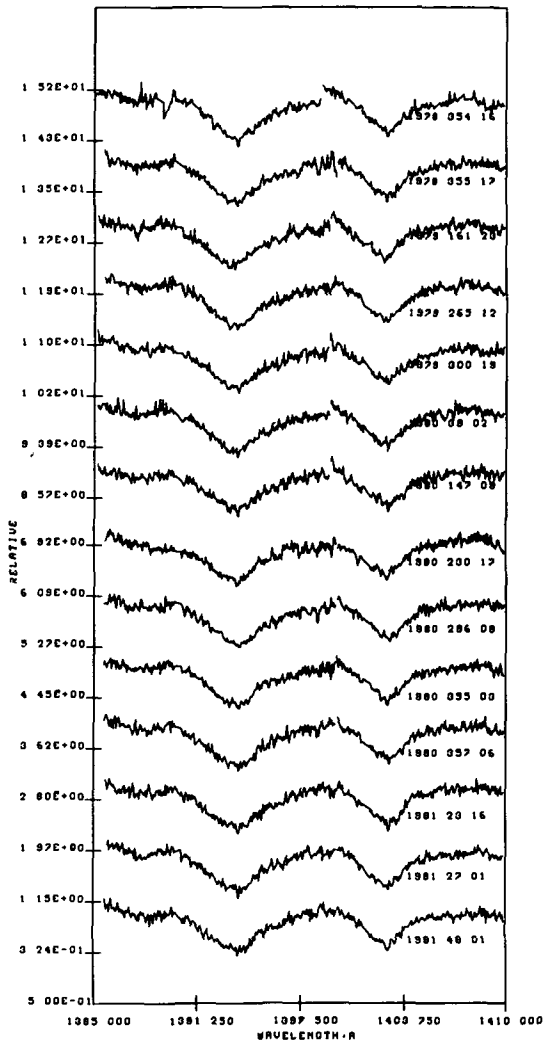

Figure 12-13. Variations in the C IV resonance lines of 59 Cyg during the period 1978 to 1980 observed with IUE. Most of the spectra show 2 components, the high velocity of which varies from about −600 to −1000 km s^{-1}. Note the changes in the profile (from Doazan et al., 1982).

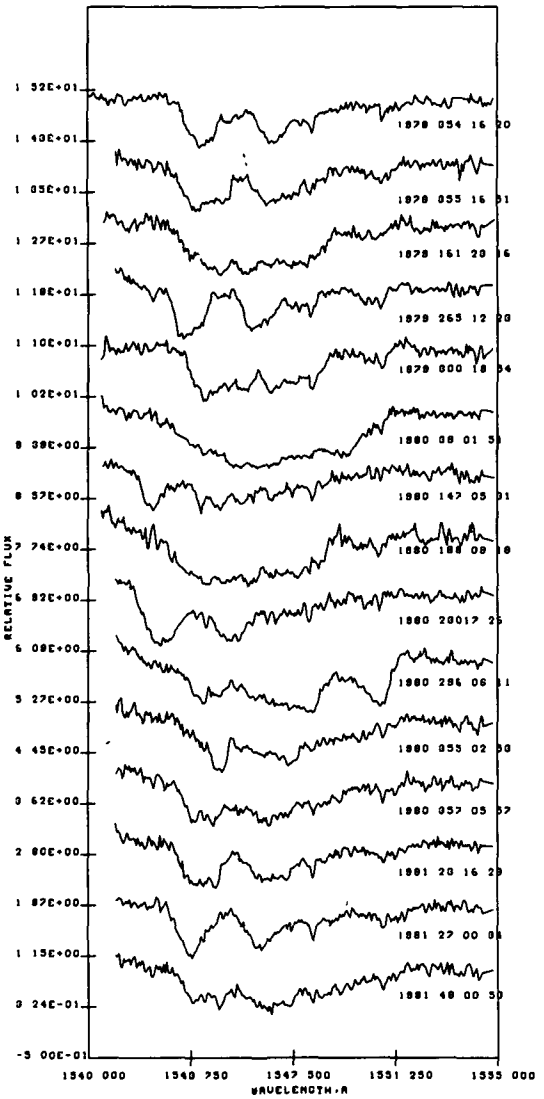

Figure 12-14. In striking contrast to the behavior of the C IV resonance lines, the Si IV resonance lines in 59 Cyg exhibit practically no variations during the period 1978 to 1980; their profile is quasi-symmetric, almost undisplaced and non-variable (from Doazan et al., 1982).

Figure 12-14. However, at the end of 1980 a certain asymmetry is detected in the ultraviolet wing of these lines. These observations show very clearly that the existence of a mass flux cannot be detected by observing the Si IV resonance lines alone, as was done in the survey of Lamers and Snow (1978); the C IV and N V lines must also be included.

The long time baseline over which 59 Cyg has been observed, both in the visible and the ultraviolet regions, enables us to draw four conclusions for an understanding of the Be phenomenon (Doazan et al., 1980a, 1980b; Doazan et al., 1981a):

1. The variations of the ejection velocities observed in 59 Cyg are so large—more than a factor of 10 in the displacements of the superionized lines—that they cannot be interpreted in

terms of fluctuations in the mass flux. They imply, on the contrary, that the mass flux is variable, and that it depends on the epoch of variation of the star. This implies, in particular, that the mass flux cannot depend only on the parameters T_{eff} and g_{eff} of the star.

2. The observations of 59 Cyg from 1978 to 1980 also suggest that the beginning of a new Be phase corresponds to the largest values of the mass flux; that is, the interaction between the variable stellar wind and the interstellar medium has to be very strong to begin "filling up" the extended atmosphere.

3. The activity of a Be star consists of a veritable cycle, from the beginning of the "filling up" of the extended atmosphere until its complete dispersion in the interstellar medium. It is impossible to describe this cycle on the basis of observations made in the visible alone; it is necessary to observe the star in the ultraviolet as well. The behavior of the subionized regions, which are observed in the visible, cannot be understood if the regions in which the mass flux is detected in these stars—the superionized regions—are not observed at the same time. The mass ejection activity of the star cannot be described on the basis of observations made in the visible region alone. The old description of the activity of a star, which was concerned only with the epochs of strong Hα emission, neglecting the weak emission phases, which were considered to be uninteresting, can lead to a completely false description of the Be phenomenon. This description, which might have been justifiable before the ultraviolet observations, can no longer be supported.

4. Similarly, it is not possible to construct a Be-star model on the basis of observations made only in the visible wavelength region. These observations lead to a representation of the star as having a "cool" outer atmosphere, where only the Balmer emission lines and the subionized lines, like those of Fe II, could be formed. Likewise, it is not possible to model the Be stars on the basis of the ultraviolet observations alone, for they would lead to a representation of the star as having a superionized outer atmosphere (like in the case in which the subionized shell lines are not observed, as for 59 Cyg from 1978 to 1981). An empirical model must, necessarily, be based on the phenomena that take place in both regions. Moreover, given the importance of the entire cycle of activity, an interpretation of the Be phenomenon must necessarily be based on the history of the cycle; that is, any Be-star model must be *time-dependent*

OBSERVATIONS OF Be STARS IN THE X-RAY REGION

The observations in the far ultraviolet region, described in the preceding sections of this chapter, demonstrated the existence of a mass flux and a nonradiative energy flux in the atmospheres of the Be stars These two fluxes are also observed in the normal B stars, and in a conspicuous way in the hottest ones. The resonance lines of the most highly ionized species that are formed in the ultraviolet spectra of these stars, in the wavelength range investigated up to now (from 3000 Å to around 900 Å) are those of O VI (on Copernicus spectra) and N V (on IUE spectra). The presence of the resonance lines of these two ions implies the existence of regions with temperatures of the order of 10^5 K.

Such a temperature rise, to values much higher than the effective temperature of the B stars, shows that these stars have a chromosphere-corona. However, these ultraviolet observations do not let us know the maximum temperature in the outer atmosphere, because the resonance lines of the abundant ions with higher ionization potential are found at shorter wavelengths than those that have been observed The measurement of the flux emitted in the X-ray range makes it possible to detect the coronal regions and to determine the maximum temperature in the outer atmosphere. Thus, observations in both the ultraviolet and X-ray regions are necessary to determine the temperature distribution in the superionized regions of the outer atmosphere.

The observations made with the Einstein satellite essentially changed our view of the structure of stellar atmospheres in general, with the detection of low luminosity ($<10^{35}$ ergs s^{-1}) X-ray emission in the 0.2 to 3.5 keV range, from stars

of all the spectral types in the HR diagram. The principal results of the observations made with this satellite can be found in Rosner and Vaiana (1979), Vaiana et al. (1980, 1981), and Vaiana (1981a). The most important conclusion from the survey of 143 normal stars is that X-ray emission from the stars, far from being an anomaly, is a normal characteristic. Consequently, as Rosner and Vaiana (1979) remark, "it appears that there is no category of stars to be called X-ray stars; that is, the data are consistent with the hypothesis that *all* stars are X-ray stars at *some* level, so that the two categories of stars and stellar X-ray sources may be essentially coextensive." The emission of soft X-rays has been detected in stars as hot as O3, of all luminosity classes (Seward et al., 1979; Cassinelli et al., 1981; Harnden et al , 1979), as well as in A stars–both those, like Sirius and Vega, in which no theoretical mechanism for the production of nonradiative energy could be identified, and those considered to be "active" because of the presence of Ca II emission. Such a conclusion complements the one that has already been derived from the observations in the far ultraviolet, where stellar winds and superionized regions (chromospheric-coronal regions) were shown in a more or less pronounced fashion to exist among the hot stars (with the Copernicus satellite) and then among stars located throughout the HR diagram (with IUE).

The characteristic of individuality with respect to the parameters T_{eff} and g_{eff}, which was already apparent from the ultraviolet observations, is distinctly sharper in the X-ray region, this is indicated by the large scatter of the emission levels about the median value, of the order of 3 to 4 magnitudes. As a result, the classical parameters are very poor indicators of the level of X-ray emission. The early-type stars have an X-ray luminosity that lies between 10^{28} and 10^{33} ergs s^{-1}. However, the number of stars that have been observed is still small, one dozen main-sequence stars from type O3 to A3, to which must be added the results of individual studies, which have not yet been published. For the moment, there are no outstanding differences in behavior between the B and Be stars (Vaiana, 1981). For example, the level of X-ray emission in the 0.2 to 3.5 keV range is 10^{33} ergs s^{-1} for τ Sco (B0 V) and 10^{32} ergs s^{-1} for ζ Oph (O9.5 Ve) (Lucy and White, 1980).

While the observations in the soft X-ray range rapidly demonstrated the generality of the existence of stellar coronae throughout the HR diagram, those in the hard X-ray range (>3 keV) have generally been interpreted as the result of a dynamic interaction in a binary system, according to the model proposed by Schklovski (1967). In this model, a mass-transfer binary, composed of a normal star and a compact object–white dwarf, neutron star, or black hole–is considered. The accretion of material by the compact object is the mechanism for the heating of the regions which emit the X-rays to temperatures of the order of 10^7 to 10^8 K, by the transformation of gravitational energy into thermal energy. Thus, in this model, the X-ray emission is only a result of the material transferred from the massive star to its compact companion. This transfer can take place in two ways: (1) the primary may have a stellar wind strong enough to be accreted by the secondary; (2) the primary may fill its Roche lobe and transfer material through the interior Lagrange point. The model of a compact X-ray source, thus, does not imply that the system is a close binary. A third mechanism is also mentioned in the literature, in which the X-ray source (the secondary) heats the outer layers of the primary star and produces a stellar wind, which, in turn, transfers material to the secondary and maintains the initial X-ray emission. In this model, the original X-ray emission from the secondary must be explained by some mechanism other than accretion. Blumenthal and Tucker (1974) and Bahcall (1978) have written reviews of compact X-ray sources.

In the hard X-ray range, the catalogue of Bradt et al. (1979) contains 96 sources, for which 65 supposedly reliable identifications have been made. As the authors note, these identifications are the result of a "gradual and subjective process." The acceptance of an identification depends both on the coincidence of the position of the object within the error box, and on the evidence for an anomaly in the nature of the opti-

cal object, such as the presence of emission lines, especially λ 4686 of He II in the visible region, or an excess ultraviolet flux. The identification is most reliable when simultaneous "flaring" has been observed in the X-ray and optical ranges. The great majority of the optical objects identified have one or both of these characteristics. Eleven Be stars appear in this catalogue, including γ Cas, whose variations in the visible and ultraviolet ranges have been described in detail in Chapters 11 and 12, and X Per. Both of them exhibit "classical" Be spectra which have been especially well observed in the visible region, unlike the other nine Be stars. For the latter, the spectral type is often very inaccurate and the luminosity class is poorly known The data for these stars, taken from the catalogue of Bradt et al., are listed in Table 12-1.

The X-ray luminosities of these stars fall between 10^{33} and 10^{37} ergs s^{-1}, and the behavior of the X-ray emission can have various characteristics A rough distinction can be made between the stars whose X-ray emission is more or less stable, undergoing only small variations, and those whose emission is transient in nature, with large intensity variations of the order of a factor of 10. Maraschi et al. (1976) considered the Be stars to be especially interesting candidates for the optical counterparts of transient X-ray sources. They suggested that the transient nature of the emission is due to abrupt changes in the rate of mass ejection from the Be star, which is part of a binary system containing a compact object. Of course, such a suggestion must be confronted with observations made simultaneously in the X-ray, far ultraviolet, and visible regions.

It has been possible to confirm the binary nature of a transient X-ray source, 4U0115 +

Table 12-1
Be Stars Appearing in the Catalogue of Bradt et al. (1979)

Source Star	Spectral Type	Period Binary	Period-Pulse	L_x (2 to 6 KeV) ergs s^{-1}	L_x/L_{op}
0050 − 727 SMC X-3 transient	OBe			7×10^{37}	0 5
0052 − 739 SMC X-2	B1e			10^{38}	3
0053 + 604 γ Cas	B0 5 IVe			3×10^{33}	6×10^{-6}
0114 + 650 LSI 65°010	B0 5 IIIe				$1\,5 \times 10^{-4}$
0115 + 634 transient	Bem ?	24 3 d	3 61s	3×10^{37}	2
0352 + 309 X Per	B0 IVe	581 d ?	13 9 m	$1\,2 \times 10^{34}$	10^{-4}
0535 + 262 HD 245770 recurrent	B0 Ve	$\geq$ 20 d	104 s	2×10^{37}	8×10^{-2}
1118 − 615 transient	Be		405 s		2
1145 − 619 HD 102567 Hen 715	B1 Vne		297 s and 292 s	6×10^{36}	0 2
1258 − 613 GX 304-1	B6 − 9ep		272 s	$2\,1 \times 10^{36}$	0 3

s = seconds, m = minutes, d = days.

63, by measuring the phase-lag in the arrival times of its X-ray pulses, which have a period of 3.615 s (Rappaport et al., 1978) The mass function of the system, with a value of 5 $M_\odot$, implies that the primary has a mass $\gtrsim 5\ M_\odot$ if the secondary is a neutron star. In conjunction with the probable identification of the source with a highly reddened, early-type star (Johns et al., 1978) and with the hypothesis of Maraschi et al., this conclusion led Rappaport et al. to suggest that the companion of this source is a Be star.

Peters (1981) analyzed the measurements made with the UHURU satellite in the 2 to 6 keV range, in order to detect hard X-ray emission in the 32 classical Be stars observed By using a point summation technique, she detected three Be stars—γ Cas, HR 4009, and HD 187399—at an emission level of 3.3σ or more, of these three stars, only HD 187399 is considered to be a spectroscopic binary. Other Be stars considered to be possible X-ray sources were π Aqr, κ Dra, 48 Per, and HD 45314 For the remaining Be stars observed, it is possible only to set upper limits on their emission Peters' results appear in Table 12-2

Among the Be stars for which X-ray emission has been detected, the only ones whose behavior in the visible has been studied over a baseline of several decades, or even a century or more, are uncontestably γ Cas and X Per, whose level of emission in the hard-X-ray range is among the lowest observed ($< 5 \times 10^{33}$ ergs s^{-1}) To illustrate the behavior of the Be stars in this spectral region, we shall describe the properties of these two stars, keeping in mind however, that given the diversity of the observed features, they should not be considered as prototypes.

MX 0053 + 60/ γ Cas

γ Cas was identified with the hard X-ray source MX 0053 + 60 by Jernigan (1976). Peters (1981), analyzing the observations made with UHURU from 1970 to 1973, pointed out that X-ray emission from this source was detected throughout the lifetime of the satellite, albeit at a variable level, and that its omission from the third UHURU catalogue had been wrongly interpreted as an absence of emission The observations made from 1970 to 1973 show that the X-ray flux of γ Cas varied by about a factor of 3; but an analysis of the measurements made during the longest observing run (May 8 to 16, 1972) did not reveal the existence of any short period that could suggest a possible pulsation period. Using observations made with Copernicus from 1973 to 1979, Polidan et al. (1981) showed that during this period γ Cas exhibited a variable behavior similar to that described by Peters, with an absence of detection on two occasions, demonstrating the variable nature of the object. A flare-type event was also reported by Slettebak and Snow (1978)

Cowley et al (1976) analyzed a large number of spectra taken between 1941 and 1969, in order to examine the behavior of the star and to seek observational evidence from the radial velocities for the existence of a compact companion. Their measurements were made on the broad, photospheric hydrogen absorption lines. No significant period between 2.5 and 4000 days, with an amplitude greater than 10 km s^{-1}, was found from the radial-velocity analysis. The authors noted that the standard deviation was about the same for all the computed "orbits," suggesting that they are all equally improbable and that the velocity is probably constant, and equal to -3.46 km s^{-1} $\pm$ 5.8 km s^{-1}. In the absence of a true periodicity, the authors set a limit on the mass of the hypothetical companion, adopting an upper limit of 10 km s^{-1} for the amplitude of the radial-velocity curve. For a period $P \approx 10$ days, $M_2 < 1\ M_\odot$; for $P \approx 100$ days, $M_2 < 2\ M_\odot$, for $P \approx 3$ to 4 years, $M_2 \approx 6\ M_\odot$ However, in the same article the authors reported radial-velocity measurements made on spectra taken from 1975 to 1976, which yielded very different values for hydrogen, -57 ± 6 km s^{-1}, or 52 km s^{-1} smaller than the mean value obtained for the interval 1941 to 1969. This result eliminates the possibility of drawing any valid conclusion from the upper limit on the velocity amplitude, 10 km s^{-1}, which was suggested in this study It is, in fact, difficult to explain such a discrepancy by the perturbation introduced by the small increase in emission at

Table 12-2
X-Ray Flux From Be Stars

Star	Spectral Type	Distance (pc)	$F_{2\text{-}6\ \text{ergs}\ s^{-1}}$
γ Cas	B0IVne	220	4.0×10^{32}
HD 45314	B0IVne	550	6.5×10^{32}
HD 53367	B0IVne	670	$<8.1 \times 10^{32}$
HD 153261	B0IVne	800	$<2.2 \times 10^{33}$
HD 161306	B0IVne	910	$<2.4 \times 10^{33}$
HD 203374	B0IVne	700	$<1.2 \times 10^{33}$
HD 204116	B0IVne	950	$<1.6 \times 10^{33}$
HD 206773	B0IVne	900	$<1.8 \times 10^{33}$
HR 2855	B0IVpne	760	$<1.2 \times 10^{33}$
AX Mon	B0pe	560	$<5.7 \times 10^{32}$
ϕ Per	B0.5IV-Vnne	200	$<1.2 \times 10^{32}$
π Aqr	B0.5Vne	325	5.0×10^{32}
HR 2142	B1IV-Vnne	400	$<4.5 \times 10^{32}$
HD 173219	B1pe	900	$<3.1 \times 10^{33}$
υ Cyg	B1.5IV-Ve	290	$<1.5 \times 10^{32}$
HR 4009	B1.5IVe	715	9.8×10^{32}
HD 7636	B2Ve	305	$<1.8 \times 10^{32}$
μ Cen	B2IVe	180	$<6.9 \times 10^{31}$
η Cen	B2IVe	100	$<3.4 \times 10^{31}$
66 Oph	B2Ve	280	$<4.2 \times 10^{32}$
48 Per	B3.Ve	175	2.2×10^{32}
HD 218393	B3IVne	550	$<6.8 \times 10^{32}$
HD 51480	B3pe	500	$<4.6 \times 10^{32}$
α Eri	B5IV(e)	39	$<3.0 \times 10^{30}$
ψ Per	B5pne	160	$<5.7 \times 10^{31}$
o And	B6pn(e)	100	$<1.8 \times 10^{31}$
κ Dra	B7IVe	100	1.5×10^{31}
28 Tau	B8pne	130	$<7.4 \times 10^{31}$
β Lyr	B8IIe	200	$<1.4 \times 10^{32}$
HD 187399	B8IIIe	450	3.7×10^{32}
17 Lep	B9pe	100	$<2.5 \times 10^{31}$
3 Pup	A2Ibpe	600	$<6.1 \times 10^{32}$

Source: Peters (1981)

Hα and Hβ between 1969 and 1975, especially since the authors measured, on the average, 11 lines per spectrum, and the higher members of the Balmer series did not exhibit emission during the two intervals in question. At present, it can be said only that there is no observational evidence to indicate that γ Cas may be a spectroscopic binary. This conclusion obviously does not exclude such a possibility, it means only that any model based on the assumed binary nature of the star must either postulate the binarity without putting forward any observational justification, or else justify it by further observations, measurements, or studies. Such a model has no foundation in the data published up to now.

Marlborough (1977b) has discussed the consequences of the identification of γ Cas with the X-ray source MX 0053 + 60, considering the lack of evidence for binarity in this star, and also noting that an analysis of the data concerning X-ray sources in general supports the conclusion that 30 to 50 percent of them do not belong to binary systems (Gursky and Schreier 1975). γ Cas is known to have a visual companion, ADS 782B,

located at a distance of 2.2 arcseconds and fainter by 8 magnitudes. Marlborough estimated the distance of the companion to be $10^5 R_\odot$ and its absolute magnitude to be around 3 or 4, which would indicate that the X-ray emission is not due to accretion onto the visual companion. He proposed to explain this emission by the presence of a coronal region surrounding γ Cas. Such a region would be a logical continuation of the superionized regions lying above the stellar photosphere, which have been brought to light by far ultraviolet observations. With the results of the observations made by the Einstein satellite, the existence of stellar coronae now seems to be a normal feature of the structure of stellar atmospheres, rather than an anomaly

Marlborough assumed that the X-ray emission of γ Cas was produced by bremsstrahlung in an optically thin Maxwellian plasma surrounding the star and composed of completely ionized hydrogen, at a given temperature T and density. Based on the observed X-ray luminosity, $2\,5 \times 10^{33}$ ergs s^{-1} or 6×10^{-5} times the total luminosity of the star, Marlborough expressed the X-ray emission from this envelope in terms of its temperature, density, n_e, and radius, r Then he fixed the constraints on the solution in the (r, n_e) plane, on the basis of the following conditions (1) the corona is optically thin for electron scattering, (2) the total energy emitted by the volume of the envelope cannot exceed the luminosity of the star, (3) the upper limit on the flux emitted by this region at radio frequencies is 0.01 Jy (Purton, 1976b), (4) the flux emitted in the soft X-ray range is very small, as suggested by the absence of a detection in this range at this epoch. This last condition is the most restrictive for the solution. A complete recapitulation of the X-ray measurements of γ Cas is clearly still necessary. Taking all these conditions into account, Marlborough showed that the X-ray emission of γ Cas can be explained by the presence of a corona with a temperature greater than 2×10^7 K and an electron density smaller than 10^{11} cm^{-3}, lying above the photosphere, the upper limit on the density depends essentially on the radius of the emitting volume

Marlborough considered the variability of the X-ray flux of γ Cas to be a weak point in his model. We note that variability of this kind can result either from a variation in the nonradiative energy flux necessary for the existence of the corona, or from variable opacity in the outer atmosphere, owing to a variation in the mass flux. Observations of Be stars have amply demonstrated that the most striking characteristic of their spectra is their variability. This has been shown in all the other spectral regions that have been investigated It would have been surprising for the X-ray region to be an exception

3U 0352 + 30/X Per

The identification of X Per with the X-ray source 3U 0352 + 30 has been proposed by Braes and Miley (1972), Brucato and Kristian (1972), and van den Bergh (1972), based on the fact that X Per is the brightest star in the error box defining the position of the source, and especially because X Per is known to have exhibited emission lines in its visible spectrum and a flux excess in the near ultraviolet region. We recall, however, that these features are not permanent, as is often the case with the Be stars. The column densities of interstellar absorption measured in the ultraviolet and X-ray regions are in sufficient agreement to satisfy the criterion for the identification of an X-ray source, and are compatible with the interstellar absorption deduced from the reddening of the (B − V) index (Mason et al., 1976) We should point out, however, that X Per is not the only proposed optical identification for 3U 0352 + 30 (Moffat et al., 1973; Haupt and Moffat, 1973). However, it is the generally accepted identification and, in this case, it is, like γ Cas, a low-luminosity source in the hard X-ray region, with $L_x = 4 \times 10^{33}$ ergs s^{-1}.

Characteristics of the X-Ray Source 3U 0352 + 30/X Per. Working in the 2 5 to 7.5 keV region, White et al. (1976) found a pronounced peak in the power spectrum of 3U 0352 + 30, with a period of 13 9 minutes; this period remained stable to within 0.024 minutes for around 2½ years. The amplitude of the variations undergoes a mean modulation of the order of 40 percent.

A 13.9-minute periodic component has also been observed in the low energy ranges, 0.6 to 1.9 and 1.0 to 3.1 keV, with a modulation comparable to that observed at high energies. The 13.9-minute period has been fully confirmed by all the subsequent measurements (White et al., 1977). The observations of White et al. (1976) also indicated a possible modulation of the 13.9-minute period of the X-ray flux with a period of 22 hours or even 11 hours. These latter periods were not confirmed by White et al. (1977); they noted, however, that their data are not incompatible with a period of 581 days, the value proposed by Hutchings et al (1974) for the period of the radial velocities of X Per in the visible region (as discussed in the next subsection).

Becker et al. (1979) observed 3U 0352 + 30/X Per in the high-energy range, 2 to 60 keV, for 20 days in February 1976 and February 1977. They compared the shape of the spectra they obtained at these two epochs with several simple continua—thermal bremsstrahlung, power law, blackbody—and concluded that the observations were in best agreement with thermal bremsstrahlung emission. They pointed out, however, that at both epochs, the observed spectrum exhibited a strong high-energy excess with respect to the best theoretical solution, as was also noted by Mushotzky et al. (1977). The shape of the observed spectrum varied in the course of the 13.9-minute period, exhibiting the highest temperature ($kT \approx 20$ keV) at the time of minimum X-ray luminosity; the mean value was $kT \approx 13$ keV. This effect was detected throughout the observed energy range. Moreover, Frontera et al. (1979) noted a variation of the X-ray flux by a factor of 2.6 in the space of a single day, during observations carried out in July 1977 in the very high energy range, 20 to 150 keV. The existence of such events had already been suggested by the observations of White et al (1976).

Becker et al. (1979) noted that the characteristics of the X-ray emission of 3U 0352 + 30 differ strongly from those of the other X-ray sources considered to be binary pulsars The latter exhibit an X-ray spectrum that is well represented by a power law. In general, these sources have strong lines of iron in emission between 6.4 and 6.9 keV, which are not observed in 3U 0352 + 30. Their low-energy cut-off varies strongly, while 3U 0352 + 30 exhibits a strong, variable excess on the high-energy end. Finally, as we have said above, the low-energy X-ray luminosity of 3U 0352 + 30 is much smaller than that of most binary X-ray sources.

Characteristics of X Per in the Visible and the Far Ultraviolet Regions. X Per is a well-observed Be star in the visible range; its spectral type, determined in the BCD classification system at a time when the Hα emission was very weak, is B0 IV (Divan, 1979). This star has been the object of renewed interest since its identification with the X-ray source 3U 0352 + 30 was proposed. Its variations in the visible region have been summarized by Wackerling (1972), Cowley et al. (1972) summarized the V/R variations in Hβ from 1913 to 1972. Large-amplitude, often abrupt variations have been observed in the Balmer-line emission and that of the singly ionized metals, mainly Fe II; in the V/R ratio of the emission peaks, in the gradient of the continuum in the visible, near ultraviolet, and infrared regions; and in the magnitudes in the UBV bands (Persi et al., 1977). X Per has most often exhibited strong emission in the Balmer lines, with a more or less centrally located reversal, as well as weak, intermittent emission in the 4686 Å line of He II and in the He I lines Hutchings et al. (1974) pointed out that the broad hydrogen absorption lines indicate a v sin i value of 500 km s^{-1}, implying that the rotation axis of the star is viewed at an angle of around 90°, on the rotation model—that is, assuming that all Be stars rotate at the critical velocity. However, the photospheric hydrogen lines are not adequate to determine the rotation velocity of the star, for they are broadened mainly by the Stark effect. A much lower value of v sin i, 200 km s^{-1}, is indicated by the He I lines (Hutchings et al., 1975). But, as these authors pointed out, these lines are perturbed by emission from the envelope, so that this value must be considered rather uncertain.

From 1957 to 1961, a very large increase in the emission was observed and reported by Wackerling (1972). Moreover, at certain epochs

X Per has exhibited a normal or quasi-normal B-type spectrum. The behavior of X Per in the visible region is not very different from that of the other Be stars, except for the fact that its very strong emission has persisted long enough—several years—at certain times, to be followed and observed by several observers.

Since X Per has been proposed as the optical identification for the source 3U 0352 + 30, the most frequently investigated aspect of its behavior has undoubtedly been its variability. There has been a search for periodicity in any of its spectral features, which might be in phase with the period, or periods, that have been detected in the X-ray flux. The behavior of the radial velocities has been studied by Hutchings and his coworkers in a series of articles (Hutchings et al., 1974, 1975, Hutchings, 1977). The velocities were measured in the broad Balmer absorption lines, at the violet emission peak of these lines, and in the He I absorption lines at λ 4026 and λ 3819 Å, which exhibit little emission on the spectrograms in question. Fifty spectrograms taken between 1920 and 1960, and 55 taken between 1967 and 1974, were measured. Hutchings et al. (1974, 1975) noted that the greatest velocity variations were derived from the hydrogen lines, with an amplitude varying from 68 to 48 km s^{-1}, as a function of the epoch under consideration The velocities of the He I lines were in phase with those of the hydrogen lines, but with a much lower amplitude, 7 km s^{-1}; those of the violet emission peaks, on the other hand, were in antiphase. If these variations are interpreted as orbital motion, with a period of around 580 days, the mass function is $f(m) \simeq 18$, this is the largest value known. Such a value would indicate that the companion has a mass $M_2 \approx 40\ M_\odot$, corresponding to a black hole. However, the velocities for the period 1920 to 1960, which were measured on prism spectrograms, differ by −50 km s^{-1} from those for the period 1967 to 1974. According to the authors, this difference can be explained by the difference in the slope of the continuum as seen on prism and grating spectrograms. The well-known difficulty of measuring the broad absorption lines is also reflected in the differences in radial velocity obtained by different authors, which can be as great as 30 km s^{-1} for spectrograms taken at the same epoch. The radial velocities for the epoch 1975 to 1976 pose an additional problem for they do not closely follow the period proposed previously, and are not in themselves sufficient to define a new period (Hutchings, 1977). These new measurements suggest a reduction in the mass function to $f(m) \approx 3.2$; if the mass of the primary is 20 $M_\odot$, this implies a secondary of mass 16 $M_\odot$, if the observed variation is due to orbital motion This new data set reduces the velocity variations in the He I lines to 5 km s^{-1}, which is not significant for lines that are so difficult to measure. The new values of the velocities for the violet emission peak indicate possible periods of 637 and 592 days, with almost equal probability. Hutchings (1977) concluded that the evidence for a 580-day period is still prevailing, but that the velocity amplitude is less and less well defined. It is to be noted, however, that the velocity amplitude tapers off as the Balmer-line emission decreases. In 1977, the very weak emission was visible only at Hα, and the Balmer jump was in absorption, corresponding to that of a normal B0 IV star (de Loore et al., 1979), this kind of variability is frequently observed among the Be stars.

In addition to the radial-velocity measurements, the variations of the He II line at 4686 Å and of the continuum in the visible, the near ultraviolet and infrared have been investigated (Liller, 1975, Hutchings and Walker, 1976, Margon et al., 1976, Ferrari-Toniolo et al., 1977); no well-established correlations with the X-ray flux variations were obtained. However, it has been shown that the visible and infrared luminosities decrease when the Balmer-line emission decreases; these long-term variations are unconnected with any of the periods advanced in the X-ray or visible regions. But Galkina (1978) has analyzed spectrograms of X Per taken between November 1974 and March 1978, on which the velocities of the violet and red emission peaks at Hα seem to exhibit two types of variability, one with a period of 22.4 hours and the other with a period of 581 days.

In the far ultraviolet region, X Per exhibits superionization (from the presence of N V and

CIV) and a mass loss of about $10^{-8}\ M_{\odot}$ per year (Hammerschlag-Hensberge et al., 1980), these features are not very different from those of other B and Be stars, such as τ Sco (B0 V), 59 Cyg, or γ Cas. Its variability in this spectral range has not yet been studied.

The Interpretation of 3U 0352 + 30/X Per. The source 3U 0352 + 30 has at least one period, 13.9 minutes, that has been confirmed by all the observations in the X-ray range This period is the basis for most of the models proposed to interpret the X-ray emission. All the models assume that the emission is produced by accretion onto a compact companion. The most frequently invoked explanation is that the X-ray pulses are due to the spin period of a magnetic neutron star (Garavoglia and Treves, 1976; Milgrom, 1976, White et al., 1977, Henrichs and van den Heuvel, 1977; Persi et al., 1977; Galkina, 1978, Becker et al , 1979). Under these conditions, the accreted material is channeled toward the magnetic poles of the neutron star, whose rotation axis is not parallel to the magnetic axis. From this point on, the models diverge, depending on the value adopted to define the orbital period. In some models, the orbital period is given by the 22-hour period of the X-ray emission, while the 580-day period is due to the apsidal motion of the elliptical orbit. In this case, the system is very compact, close to the point of tidal instability. In other models, the 580-day period defines the orbit of the system. The neutron star is then located in a low-density region, very far from the Be star. Finally, in still other models, the system is triple, with a neutron star revolving about X Per with a period of 22 hours, while the double system itself revolves about a distant, unseen companion, with a period of 580 days.

It is obvious that the best indirect evidence for the orbital period of the proposed system will be derived from a study of the X-ray emission, if it is possible to determine periodic variations in the arrival time of the pulses. The situation is much more confused in the optical region, as we have shown above. During most of the interval over which X Per has been investigated, its spectrum has been very strongly perturbed by the presence of emission lines, making it difficult to interpret the radial velocities of the hydrogen lines The possibility that the observed variations reflect the motion of the envelope, in a manner that is hard to quantify, cannot and should not be excluded. Moreover, the absence of variations in the He I lines has never been satisfactorily explained, and has no place in any of the adopted orbital solutions. Finally, it would be natural to assume that, at least, part of the X-ray emission comes from X Per itself, and that, at least, part of its variation is connected with the coronal activity of the star The differences between the binary X-ray sources and X Per, that Becker et al have noted, could be explained by the peculiar properties of the outer atmosphere of X Per. Obviously, simultaneous measurements in all the spectral regions are still necessary to give a more reliable interpretation of the emission of 3U 0352/X Per

Finally, we note that similarities between X Per and γ Cas are occasionally mentioned, without specifying the reasons. If we examine the characteristics of the X-ray emission from these two stars, the available observations show that the similarity is only in the low level of emission in the 2 to 6 keV range. But no short-period variations have yet been detected in γ Cas, like those in X Per. If we examine the behavior of these stars in the visible region, we note that both of them have exhibited strong variations at certain epochs. The main difference that has been emphasized is the presence of λ 4686 of He II in emission, weakly and intermittently, in X Per, unlike the case of γ Cas The few examples of variability described in Chapter 11 show that the Be stars can exhibit very different behavior during phases of very high activity in the visible (e.g., Pleione, EW Lac). For X Per, the very strong emission phase in 1957 – 1961 was no doubt spectacular, but it was not followed by two brief shell phases, as was the case for γ Cas and 59 Cyg. Thus, rather than saying that γ Cas and X Per are similar, we should rather say that their behavior differs greatly in the development of the phase sequences during their period of high activity in the visible region.

13

GLOBAL PICTURE OF A Be STAR

in collaboration with R. N Thomas

PERSPECTIVE ON MODELING Be STAR ATMOSPHERES

In this chapter, we try to abstract, synthesize, and order the observational material on Be stars, which was collected in preceding chapters of this Part II, into an *empirical pattern* of atmospheric structure for these stars. We also try to draw some conclusions on how that structural pattern arises, and what is its linkage to the subatmospheric structure of the star, and to the environment of the star.

General Considerations

As summarized in Part I, modern observations in the far ultraviolet and X-ray spectral regions show that standard atmospheric models, based only on radiative energy flux and gravity as parameters, subject to the thermal conditions of hydrostatic and radiative equilibria, producing a single-region atmosphere called a photosphere, are inadequate to describe even normal B stars· main-sequence, giants, and supergiants. Essentially, these standard models are inadequate to describe the *high-energy* spectrum of such normal B stars for the same reason they fail for normal stars of other spectral types. They cannot represent the *hot* chromospheric-coronal regions ubiquitously found enveloping stellar photospheres; nor can they accommodate to their structure the macroscopic outward flow of the atmosphere, which is universally called a stellar wind, and whose velocities pass, progressively outward, through subthermal, thermal, and superthermal values. Thermodynamically, this "wind" is simply a mass flux from the star. Thus, even a normal real star is an open thermodynamic system; while the standard model refers to a closed system. Thermodynamically, such a difference is basic; its actual effect on atmospheric structure, and relation of star to its environment, depend upon the "degree of openness," measured by size of mass flux.

But as summarized in Chapter 11, even classical observations in the visual spectral regions have shown, for a century, the inadequacy of such standard models to represent the full atmospheric structure of the Be stars. Essentially, these standard models fail to represent the *low-energy* spectrum of Be stars because such models cannot produce those very extended, low-velocity, dynamic rather than static, regions lying above the photosphere that are *colder* than the temperatures predicted under radiative equilibrium. And now, at our epoch, as summarized in Chapter 12, for the Be as for the B stars, modern far ultraviolet and X-ray observations demand that there also be some regions above the photosphere that are *hotter* than radiative equilibrium permits, statistically, and particularly at certain phases of variation, these regions in Be stars show stronger mass flow than do such regions in the B stars. So the Be stars are doubly discordant with standard models, and stronger in their "degree of openness."

Thus the Be stars, when compared to the normal B stars, strikingly exhibit one of the theses

of the monograph series (i) in the visual spectral region, the peculiar stars exhibit a greater range and amplitude of nonthermal characteristics than do the normal stars, (ii) outside the visual region, both the peculiar and normal members of the particular MK class exhibit a greater variety and amplitude of nonthermal phenomena than they do in the visual region. In these nonvisual regions, indeed, the distinction between normal and peculiar is often, observationally, blurred or lost. It now remains to be seen whether another thesis of the series, that *there exists a common general pattern of atmospheric structure*, embracing both peculiar and normal stars, and all nonthermal phenomena observed in them, is correct

Then the first empirical objective, using the Be observational data, is to try to establish the geometrical distribution of the hot and cold regions of the preceding paragraph, relative to the photosphere, and relative to each other. One seeks the same, for the macroscopic velocities, and for any empirical relation between T_e and U One asks whether one can find an ordered distribution of thermodynamic variables—that is, particle concentrations, T_e, macroscopic velocities—which can reproduce these data, or whether one can only represent the distribution of hot and cold, moving and static, regions stochastically, in a generalization of the classical, ad hoc, parameters of "astronomical turbulence." A priori, we must admit the possibility of radial, nonradial, and certainly temporal distributions Because of the strong dissipative processes accompanying any random superthermic motions, a wholly stochastic modeling seems unlikely; but, again, it cannot be excluded a priori. Only observational diagnostics and inference, not a priori speculation and imposition of a pattern, can lead to the actual distribution of these thermodynamic variables Only then can we turn to the complementary empirical-theoretical problem of interpreting and explaining how this empirically-determined distribution arises Otherwise, even what we try to explain is only speculation.

Such an empirical, and empirical-theoretical, formulation of the immediate goal of this chapter follows the general spirit of the monograph series, which is to ask for each "kind" of star studied, and which is specified in the visual region by its spectral subclass MK (1) *Can we identify*, essentially from the observations alone, but demanding thermodynamic self-consistency in both their diagnostics and synthesis, *a general pattern of atmospheric structure* for this kind of star? (2) *Can we identify those thermodynamic parameters which are necessary and sufficient to specify the details of such a structural pattern*, by showing how they do so? (3) *Can we* then show how to use the observations of any particular star to *construct a specific atmospheric model for that star*, which still falls into the general atmospheric pattern? (4) Finally, *can we understand* how *the particular values of these thermodynamic parameters are fixed*, for a particular star, by the particular structure of that star as a whole?

We could pose this general set of questions without ever having observed a Be star Indeed, they are posed for each kind of star, normal and peculiar, across the HR diagram, in the several monographs of the series, but with a variety of characteristics coming from the observed peculiarities of each class of stars At our epoch of knowledge, such variety does *not* lie in the simple existence, or nonexistence, of a chromosphere-corona and of a wind, the features common to both normal and peculiar stars across the HR diagram that were cited at the outset as obvious deficiencies of standard models Thermodynamically, one infers that such general *existence* of chromospheres-coronae and winds corresponds, respectively, to the general *existence* of nonradiative energy, and mass, fluxes. Such universal *existence* of these two features was possibly controversial a decade ago, especially among those astronomers who persisted in regarding the star as a closed thermodynamic system; from modern observations, the controversy is dead. So this phenomenological variety of characteristics arises mainly from the *sizes* of these fluxes, which cannot, a priori, be assumed to be the same for all spectral subgroups nor within such groups. Such variety can also arise from other characteristics, which may or may not be linked to the sizes, and interactions, of these two fluxes For Be stars, and stars observationally similar to them, a strong aspect of the variety lies in the character-

istics of the post-coronal, low-velocity, subionized regions summarized in earlier chapters. In addition to clues on the empirical structural pattern of the atmosphere, such aspects of variety also give us constraints on the basic physics which any modeling theory must satisfy. Any modeling which violates or ignores them can, a priori, be rejected.

In the remainder of this section on Perspective, in the problems of modeling Be star atmospheres, we abstract this variety of characteristics for the Be stars, to restate questions (1) to (4) for them and "similar" stars. In the second section, Empirical Pattern of Atmospheric Structure for Be Stars, we first place these characteristics in focus by abstracting the observational and conceptual evolution of atmospheric patterns for the Be stars. We then synthesize and order these modern data, collected in preceding chapters, to exhibit how they demand an atmospheric pattern which is a blend of (a) following Struve's (1942) attempt to model, empirically, the atmospheres of Be and "similar" stars according to the observed solar scheme, (b) satisfying the simultaneous presence of superthermic, superionized regions and low-velocity, subionized regions, (c) incorporating variability of mass flux to understand McLaughlin's characterization of Be stars as "little planetary nebulae " In the final section of this chapter, we ask the subatmospheric significance of such an empirical model

Variety of Characteristics Enhanced in Be and Similar Stars, to be Incorporated into Empirical Modeling

Be stars are defined by their showing, at *some* epoch, medium-energy spectral lines—at least the Hα line of hydrogen—in emission, in the visual spectral range. In common with other normal and peculiar stars, Be stars show superionization in the far ultraviolet and X-ray spectra, for Be stars, such lines exhibit displacements and profiles implying wind velocities from small up to some 1500 km s^{-1} In common with some other peculiar stars—notably the symbiotic, planetary nebulae, and some novae—they show subionization, very extended atmospheric phenomena, and evidence for lower velocity of the mass flow in the subionized regions. They often show evidence of emission excesses in the continuum, across the observed spectrum from the near ultraviolet to the infrared and radio regions, sometimes there is evidence for "veiling" of the line spectrum in the visual Some lines in the visual spectrum, notably those of He I, show profiles whose shape suggests that rotation at high velocities is a common characteristic of Be stars. However, one also notes that for every Be star with a given inferred rotational velocity, a normal B star showing the same observational appearance of the He I lines can be found

If all the details of these phenomena were common to all Be stars, and to a given Be star at all epochs, the atmospheric pattern would be clear To a classical photosphere, one would adjoin a chromosphere-corona, across which an outward mass flow was continuously accelerated Somewhere outside the corona, the flow would cool and decelerate. The empirical details would come from combining all observations of all Be stars at all epochs. Then one could proceed to an empirical-thermodynamic modeling in terms of some set of parameters, and to an explanation of how and why such an atmospheric configuration should occur The problem of such modeling would differ from the current problem of normal atmospheric modeling—which is to describe the superionized, high-velocity regions—by the necessity to account for an additional outer-atmospheric region—the subionized, low-velocity, very extended envelope It differs from the classical Be problem—which is to describe the subionized, low-velocity, very extended envelope beginning just above the photosphere—by the necessity to insert the superionized, high-velocity region between photosphere and cool envelope. Combining the two kinds of regions would not be trivial, even in this oversimplified situation

However, the details of the above general phenomena are *not* the same for all Be stars, nor are they the same for a given star at different epochs. Such details can be abstracted into several, more model-restricting, characteristics, which are at least enhanced in Be stars over normal stars, and some of which are even stronger in

stars similar to the Be. Possibly, such characteristics may be universally present, in all stars, only to a less conspicuous degree. The comparison of Be to similar stars suggests this possibility. The suggestion is hardly new; summaries by Beals (1939) and Struve (1942) place its background and proposal into perspective. Now, as then, only observations bringing new and more extensive data can ultimately decide. So we abstract what we know today, which should be regarded simply as an updating of the material and thinking in Struve's (1942) summary. There, Struve suggested using the detailed observations of a nearby, *normal, cool* star—the Sun—to obtain a first approximation to the atmospheric structural pattern of a class of *peculiar, hot* stars—the Be and similar The detailed modifications of this first-approximation pattern were to be established by the detailed observations of this class of stars We proceed, by first reformulating points (1) to (4) noted above, in a way peculiar to the Be and similar stars.

(1) *In addition to the common, gross characteristics of Be stars summarized above, we recall the following detailed characteristics of their individual spectra, hence of the atmospheric regions producing them, which the observations over all spectral regions continuously put into focus* (a) *Variability* of those spectral features originating in any part of the outer atmosphere exists, to some degree, in all Be stars (b) *A Be star spectrum falls into one of three types, which we have called phases—the Be, B shell, and quasi-normal B* The largest aspect of Be variability is passage from one phase to another, some Be stars have exhibited all or several of the phases at different epochs (c) *Individuality*, or differences to some significant degree in observed spectral features are exhibited in stars of the same MK spectral subclass and phase. (d) *Progressiveness in amplitude*, from zero to large, in those spectral features which distinguish. stars of the same MK spectral subclass exhibiting different phases, different stars, exhibiting the same phases; and spectra of the same star, exhibiting the same phase but observed at different epochs. (e) *The apparent necessity to know the history of a given Be star*, over a time interval of the order of a century, in order to model, even empirically, even in an ad hoc manner, its whole atmosphere at a given epoch. Given this set of five characteristics, which certainly negate the idea that stars within a given MK subclass, and the same star at different epochs, can be modeled as "identical" to even gross degree, we ask whether we can identify a general pattern of atmospheric structure, which suffices to represent all Be stars, at all epochs, whatever are the amplitudes of their spectral features. Within this general pattern, the highly individual characteristics just summarized must be accommodated, in order to model a particular star, at a particular epoch.

By defining stars similar to the Be as those often displaying characteristics similar to some of the above, but more extreme, and with some features such as phases sometimes not clearly identifiable, a question arises whether this general pattern for the Be stars—if it is found—can be extended to cover these "similar" stars also Conversely, we can ask whether the observations of these similar stars can be adjoined to those of the Be stars proper, to extend the empirical range of atmospheric phenomena For example, we shall see that McLaughlin's description of Be stars as "little planetary nebulae" can, when viewed against current ideas on the origin of the visual nebulae, be very useful in both empirical modeling and its translation into cause.

(2) We note that these five characteristics, (a) to (e), can no more be incorporated into those "wholly-thermal, standard models" current in the literature than can chromospheres-coronae and winds, nor the subionized and low-velocity regions So *we realize that the classical thermodynamic parameters of radiative energy flux and gravity are inadequate for a general atmospheric model, the question is how many, and which, others are sufficient and necessary* Clearly, one must add a nonradiative energy flux and a mass flux to describe chromospheres-coronae and winds. The debate in the current literature centers on three alternatives Can both these added fluxes be predicted from the two classical parameters, taking proper account of subatmospheric or atmospheric instabilities to produce them? Must we specify just *one* of these additional

fluxes from subatmospheric stellar structure, as we specify radiative flux and gravity, with the other of the new fluxes being predictable from these three? Or, must we specify *both* the additional new fluxes, their values being fixed by a subatmospheric nonthermal structure? In addition to these questions on *existence* of chromosphere-corona and wind, we must also ask what do the above characteristics, (a) to (e), add in the way of either clarifying the independence of nonradiative energy flux and mass flux as parameters, and/or requiring additional ones; for example, a magnetic field and flux, and of course, stellar rotation. Again, the observational data plus thermodynamic consistency must provide the answers.

Again, we ask for stars similar to the Be Do the parameters found necessary to model Be stars' atmospheres suffice to model the atmospheric structure of the similar stars, or do the more extreme phenomenological ranges of such stars demand other parameters?

(3) *Given that set of thermodynamic parameters specified in (2),* which suffices to model the general pattern of atmospheric structure found in (1), *we ask how to determine a set of values for these parameters, and thus, model the atmosphere of a particular star, at a particular epoch.* There are three alternatives either we need a complete empirical model of the particular atmosphere to determine these values, or we can determine all the values observationally but without knowing the whole atmospheric structure empirically; or we cannot, observationally, determine a complete set of values for the parameters In the last case we may not be able to specify, empirically, a complete atmosphere for all stars. We can only decide empirically among these three alternatives. Unlike the closed-system, thermal, alternative we have no a priori knowledge in this open-system, nonthermal case, of what observables, if any, uniquely measure any of the thermodynamic parameters. So in some situations, we may have to be resigned to the fact that for some stars, for which the data are too poor or incomplete, we have no way of assigning a value to some of these necessary thermodynamic parameters So we may not be able to be sure of the existence of some region of the general atmospheric pattern in some stars A useful example arises among some cool stars, where there seems to be some indication, observationally, that stars can have either a strong chromosphere with a feeble mass flux, or a feeble chromosphere and strong mass flux The situation is puzzling, because the most generally accepted theory for mass flux from such stars predicts a larger mass flux, the stronger the corona. One alternative is simply to decide the theory is incorrect, another alternative is that, when amplitudes of nonthermal effects are weak, the observations necessarily give incomplete information. We will see the same for the Be stars.

The problem is even more serious among the similar stars if, indeed, they represent more extreme situations Given the prominence of circumstellar nebulae and dust shells among them, one would expect to assign values to whatever are the parameters controlling nebulae, etc. that enter the Be star configuration.

(4) *Finally, we must consider the problem of the relation of these thermodynamic parameters to whatever, in the structure of the star, the atmosphere, and the environment fixes their values, for any particular star* One is accustomed to think in terms of stellar structure and evolutionary state fixing the radiative energy flux, and gravity, but the stellar structure is quasi-thermal One is also familiar with a small perturbation on this quasi-thermal internal structure producing an appreciable atmospheric effect For late-type stars, instabilities in the subatmospheric hydrogen ionization zone can produce, variously (i) through an induced convective instability, a flux of nonradiative energy which may produce chromospheres-coronae; (ii) through the kappa-mechanism on opacity, a pulsation of the outer stellar envelope which distends the star—both the atmosphere as a whole, and differentially Each of these phenomena—chromosphere-corona and atmospheric pulsation—has been classically modeled to produce no mass ejection from the star. It remains to be seen whether, as speculated presently, the observed mass fluxes can be adequately represented only in terms of an atmospheric phenomenon, or whether self-consistency

requires that the instability problem be solved with the mass flux as a free parameter.

Current ideas on planetary nebulae suggest their origin in an enhanced "burst" of mass flux when the internal structure of the star traverses the He "flashpoint"; so there is no dispute on a relation with an internal structure which, at least transiently, becomes nonthermal We have already summarized the classical, rotational instability source for a suggested equatorial mass ejection in the Be stars (Chapter 11). There, we noted that the ejection was linked to an unspecified, but nonthermal, subatmospheric configuration; lacking a theory for such, the ad hoc modelers simply took the mass flux as a free parameter, not constrained by any other thermodynamic parameters. As already summarized in Chapter 12, later, empirical, investigations have shown, thus far, no correlations between mass flux and rotation for these Be stars; nor correlations with any other parameters; only some trends. So, throughout the discussion in this chapter, we must remain aware of a possible linkage of these outer atmospheric characteristics of the Be and similar stars to a subatmospheric departure from thermal structure. In this chapter and Part II, we present no theoretical basis for such subatmospheric nonthermal structure We only ask the implication of the empirically determined atmospheric structural pattern, and the fluxes responsible for creating it, on the subatmosphere, whence come such fluxes.

In the same way, we should ask the possible influence of the interstellar medium on any characteristics of the Be atmosphere, especially in the aspect (1-e) above. From the standpoint of similar stars, especially for the planetary nebulae, the problem is even more significant. There have been many recent discussions in the literature on "interstellar bubbles," or veils of nebulosity, which, according to some authors, result from the interaction of stellar winds from hot stars with the interstellar matter Long ago, a similar origin was postulated for the planetary nebulae. One notes that the distances at which such interactions supposedly occur, which depend on the concentration of the interstellar matter in the vicinity of the star, are of the order of parsecs. Both the dimensions of the Be extended atmosphere—McLaughlin's "little planetary nebulae"—and the location of the nebula in the planetary nebulae, occur at distances much less than parsecs, ranging from some hundreds of stellar radii, 10^{14}cm, to 10^{15} or 10^{16}cm. It will appear that the Be stars manufacture their own nebular environment, under the influence of a variable mass flux, as is currently thought to be the case for the planetary nebulae. So, again, we return to the question of the preceding paragraph. What structural property of a star as a whole must be linked to such variability of mass flux: that of the atmosphere, or that of the subatmosphere; and how deep in the subatmosphere does such nonthermal structure have significant amplitude? We have the three usual alternatives for the production of stellar variability: a phenomenon in the energy-producing core, a phenomenon in the envelope, subatmospheric but above the core; a wholly atmospheric phenomenon. A decision between these must come from asking which is the most compatible with the data, and with thermodynamics.

EMPIRICAL PATTERN OF ATMOSPHERIC STRUCTURE FOR Be STARS

We first abstract the historical evolution of thinking on such a pattern, then synthesize the data into a particular pattern, and finally attempt to give quantitative estimates of the locations of some of the regions comprising this particular pattern.

Historical Evolution of Pattern

From the detailed discussion of observations in the visual spectrum, and attempts to fit them into an atmospheric model, summarized in Chapter 11, we see that there have been two distinct conceptual approaches to an outer atmospheric structural pattern for the Be stars based on such data. Both were introduced by Struve (1931b and 1942), the earliest has been extensively applied; the later has been mainly neglected. The former focused on Be stars alone, offered a conjecture as to the cause of the extended atmosphere, and consequently

imposed a particular geometry on the atmospheric pattern. The latter focused on Be and similar emission-line stars and asked, empirically, what could be an atmospheric pattern common to all these stars? Some attempts have been made to adjust the earliest pattern to match modern far ultraviolet, X-ray, far infrared, and radio data. The latter pattern has been mainly ignored in this respect; differences among the similar types, rather than similarities, have been stressed in modern discussion. In this monograph series, we have offered a third conceptual approach to establish, empirically, an atmospheric pattern—a contrast of peculiar to normal stars, speculating that the chief difference between these two classes of stars lies in the amplitudes of nonthermal phenomena. To us, this approach bears many similarities to Struve's (1942) approach to the Be and similar stars modeling So we consider that our attempts at constructing, empirically, an atmospheric pattern for the Be stars is not something startlingly new, but is rather an evolution of the "Be plus similar" star approach (a) by considering all the modern data which have accumulated since the time that Struve proposed the approach; and (b) by regarding the differences among Be and similar stars as similar to the difference between normal and peculiar stars, which these latter all are. In this viewpoint, the differences arise from differences in sizes, time scales, and other characteristics of the nonthermal properties of the stars exhibiting such phenomena. Possibly evolutionary questions also enter; we think it is premature to speculate on such until the structural pattern, and its origin, have been clarified.

We introduce our modeling scheme by first summarizing the historical conceptual evolution of the two preceding approaches, originally due to Struve.

Struve's Atmospheric Pattern I: The Be Stars Alone. *This pattern, which is historically the oldest, represents Struve's conjecture that an extended atmosphere simply represents the locus of material ejected in an equatorial plane because the rotational velocity of the star lies near its critical value equal to the photospheric escape value.* Struve's original picture was a one-time ejection of material, which formed a planetary-like equatorial ring. Subsequent development of the model permitted an essentially continuous ejection from the subatmosphere at the epoch when, by stellar evolution, the rotational velocity reaches the critical value, resulting in a quasi-steady unstable configuration—as we have already summarized in discussing Limber's formulation of the problem in Chapter 11.

The *first basic data* are *the observations of emission lines*, and their interpretation as requiring an extended atmosphere. The *second basic data* are *the dish-shaped appearance of the He I absorption lines, suggesting high rotation, and the trend showing greater emission-line widths accompanying, statistically, greater He I absorption-line widths*. The latter data were once interpreted to mean that the emission-line breadths were also fixed by the rotation; hence, the line origin was confined to an equatorial disk. However, such relations between absorption and emission-line widths constitute general trends rather than strict correlations, given the observed variability in line widths of a given Be star, and the differences between stars having the same $v \sin i$ as discussed in Chapter 11. A simple elaboration of the rotating, equatorial-disk model, following Gerasamovic's original, and Limber's later, demand for an equatorial outflow, removed the need for the emission profiles to be fixed wholly by rotation, hence wholly correlated to the He I absorption profiles. In such an atmospheric structural pattern, all nonstandard, nonthermal features were confined to an equatorial disk, and arose wholly from an instability induced by the star's critical rotation. The essential characteristics of this model are its focus only on Be stars, and its being based wholly on rotational instability. It is not so important, whether the model is considered in Struve's original form of a one-time ejection of material, or in Limber's later modification to demand a continuous ejection, as regards an equatorial concentration of material The distinction is, however, important relative to the ability to include variability. In Struve's version, it cannot be included; in Limber's, it can. Currently the far ultraviolet observations showing superescape velocities in stars classified as pole-on, as well as

in equator-on stars, and the absence of any correlation between size of expansion velocity and v sin i for other stars, contradicts the basic feature of this model.

Thus, the basic data underlying this model are of two kinds (i) one considers only the Be stars, not also those "similar" stars which share the two defining features of emission lines and variability, but not high rotation, nor does one consider the normal B stars, many of which do share the high rotation but neither the emission lines nor such pronounced variability, (ii) one uses just this limited amount of data, emission lines and rotation, to conjecture a cause of the whole Be phenomenon, without first considering all the other data (1) to (4) of the preceding section. *The strong innovative feature in Limber's modification was his attributing the basic feature demanded by the data used–the extended atmosphere required by the emission lines–to a continuous mass flux from the star, with the size of the flux being fixed wholly by a nonthermal instability and structure of the subatmosphere*, and not by some property of atmospheric conditions alone. Moreover, Limber's work clearly emphasized the necessity for a variable mass flux, thus presumably a variable subatmospheric structure, to model the observations of Pleione.

The preceding comments refer to the structure and the dynamic state of the outer atmosphere. To infer its thermal and spectroscopic state, one considered mainly the Balmer lines and those of Fe II Then one notes that in the B star class (i) Hydrogen lines are strong in absorption, decreasing in strength from B9 to B0; they reach maximum strength near A0-A2. (ii) Fe II lines do not appear, they are seen in A0 and later stars. Consequently, when one observes strong hydrogen emission lines in the Be stars, especially the hot stars like γ Cas and 59 Cyg, there is little basis to explain such emission by a superexcitation in a chromosphere-like atmospheric region hotter than the photosphere Such explanation is tempting for at least part of the Balmer emission in T Tauri stars, and for emission components of Ca II in the Sun. However, in the Be stars, such Balmer emission lines suggest simply an atmospheric region that is large relative to the photosphere, which produces the adjacent continuum. However, this Balmer-line emission alone does not suffice to give a good estimate of either the T_e or the excitation mechanism in these extended, exophotospheric, atmospheric regions, if the atmospheric extent is allowed to be a free parameter.

The presence of sharp, deep, absorption cores of Balmer lines, and of singly ionized metallic lines, which define the Be shell phase, which give that similarity to the spectrum of the A2 supergiant, α Cyg, was often stressed by the early observers. This similarity led them to conjecture that first, T_e must lie closer to the 1×10^4 K of α Cyg than to the 2×10^4 K of an early B photospheric boundary, in whatever atmospheric region produces these spectral features; second, particle concentrations, n, are closer to those of supergiants than main-sequence photospheres; third, these regions are more exterior than those producing the emission wings. BCD spectrophotometry at the head of the Balmer series, with its apparent delineation of several different regions contributing to both the BaC and the lines, appears to reinforce this historical, observationally-inferred pattern of T_e and n.

The Fe II lines, often appearing in Be spectra in emission, and in Be shell spectra with sharp and deep absorption cores, add strong, independent evidence for $T_e \sim 1 \times 10^4$ K, rather than 2×10^4 K, in the regions where such ions are concentrated. In some Be shell spectra, one observes a progressive narrowness in absorption linewidths, from He I permitted lines to Si II and Mg II, then through Fe II, and finally to the cores of the Balmer lines and He I, λ 3965. If, as did Struve, one uses such line-widths as a measure of the rotational velocity, and assumes this velocity to decrease outward and to conserve angular momentum, then the Fe II lines are produced quite far outward, nearly in the region of Balmer-line absorption cores and He I, λ 3965. Using Struve's estimates of dilution factors for He I, λ 3965, $W \sim 0.1$, and the various estimates for the radius of the regions of formation of the Balmer emission lines, one concludes that these low temperature regions exist at least at 3 to 5 stellar radii out.

In abstract, the formation of the Balmer emission lines in Be stars requires an extended, outer

atmospheric region, the Be shell spectrum suggests that T_e has dropped by about a factor of 2 in the even lower density region where the shell absorption cores are produced, the Fe II enhancement at the Be shell phase suggests equally low T_e and density, the forbidden, low-excitation lines observed in the Bep spectrum demand a further decrease in T_e in regions of decreasing density. Thus, in the radial distribution of T_e, and excitation/ionization, demanded by Struve's model, there would appear to be no place for hotter regions until at least some 5 radii above the photosphere. For this reason, ad hoc models, which follow Struve's Atmospheric Pattern I; have attempted to model the superionization regions as occurring only in the polar directions.

Struve's Atmospheric Pattern II: The Be and Similar Stars. *This was the first wholly empirical attempt to use all available observational data on Be and similar hot, peculiar stars to ask, free from theoretical preconception· What actually is an outer atmospheric pattern common to all these stars*? Furthermore, no preconception that hot and cool stars might differ in such a pattern was imposed. The detailed observations of the cool star, the Sun, were adopted as a conceptual guide. Because this solar guide was adopted at an epoch when solar chromosphere-corona were thought, for reasons analogous to those outlined above for the Be stars, to be cooler than the photosphere, we can call the result "the cool chromosphere-corona model" for Be and similar stars

This second approach of Struve focused on exploiting the inadequacies of the first: (i) it *added variability to emission lines as the basic characterization of the class of stars considered, ignoring rotation as a major distinguishing characteristic*, (ii) it *defined the "fringes" of the class in terms of other sequences of characteristics*, upon which we proceed to remark. Within such sequences, some features are shown weakly, some strongly, and some differing at different epochs among the stars in the sequence. *Thus, in addition to the property of variability, we have that, of gradualness of strength of the peculiar spectral features* stressed for the Be stars—now applied generally across this "broad-Be" class of stars

Realizing that there are several types of features and sequences, we can understand that it is not only imprecise classification that has caused some stars to appear previously in one spectral class, now in another Thus, we note that Z And has variously, at different epochs, been called nova, Be, Bp, and symbiotic, and that P Cyg, the prototype star of its class, was historically a nova, and is now the extreme fringe—sometimes called the only example—of that class of B supergiants with extreme velocities in the visual, but only moderate in the far ultraviolet. Moreover, while the outer atmosphere always "veils" the photosphere to some extent, it appears that, in these peculiar stars, the veiling can sometimes be large enough so that the MK classification that refers to the photosphere in normal stars becomes confused by the effect of the outer atmosphere

The great range in Balmer emission-line intensity and profile across the Be and Be shell phases, and especially among the stars variously labeled Bp, and sometimes symbiotic—such as Z And—led Beals (1939) to see a continuous taxonomic progression of such line profiles from the supergiant, α Cyg, through the Be stars to P Cygni-type supergiants. The progression embraced the Be, the Be shell, the Bp, the symbiotic. On one end, one finds the purely-absorption, static, sharp and deep lines of α Cyg, which the absorption cores of Be shell spectra resemble, on the other end, the distinctive, kinematic, P Cygni profiles which, by extension, quasi-embrace Wolf-Rayet, Be, Bp, and symbiotic spectra Noting that both P Cyg and Z And were observed, long ago, as novae, Beals included the novae among this broad class of similar peculiar stars Noting the customary interpretation of the classical P Cygni profile in terms of an expanding atmospheric region, the above taxonomic sequence also suggested a dynamic, probably expanding character, rather than a static character, of some of these extended outer-atmospheric regions. We note that in these historical atmospheric patterns, expansion velocities inferred from the visual classical P Cygni profiles, in P Cyg itself, exceeded those in any other stars except the Wolf-Rayet and the novae, these latter show values of the order of 1000 to 3000 km s^{-1}, a few hundred km s^{-1} in

P Cyg, about 100 km s^{-1} in the Be stars, Bp, and symbiotic.

As a postscript, because it was largely ignored in these historical atmospheric patterns, except by its authors (McLaughlin, 1931, and Beals, 1939), we have a description of the Be stars as little planetary nebulae. Such would imply an appreciable region around the star which does not contribute to the visual spectrum; visually, a "hole" around the star, which is either actually a hole, or a region so hot, or one so cold, as to be invisible in that spectral region. Surrounding the "hole", one has the emission nebula producing the Balmer emission lines, and also low-excitation, forbidden lines in emission. In earliest history, the "actual hole" alternative was adopted, thence the nebulae themselves were classified among phenomena of the interstellar medium. But later, and especially today, we recognize the "hole" as a very extended region of an even hotter (upward of 10^5 K) central star, possibly it is the very extended chromosphere-corona of an object resembling a Wolf-Rayet central star. The variety of central stars classified in planetary nebulae gives to the planetary nebulae that same strong aspect of individuality emphasized in the Be stars.

The essential link among this broad class of stars, for which Struve proposed to find, *empirically*, a common atmospheric pattern, is that community of features stressed among the Be stars—especially if one takes account of their individuality—which appears to define all kinds of extended atmosphere. These exo-photospheric regions can range from an apparently negligible extent at quasi-normal B phase to a much larger extent in Be, Be shell phases, and very much larger in the Bep, novae, and planetary nebulae configurations. A basic question is. What causes the *variable* extent? Is it the size of the mass flux at a given epoch, or its size at a given epoch along with its interaction with the matter ejected at other epochs? We have already rejected an interaction with the interstellar medium alone, because it would occur too far from the star.

We do not imply, nor did Struve, that any given star can, at some epoch, possibly take on *any* of the phases or configurations exhibited in this "Be and similar" class of stars. The conceptual basis of this approach to a general structural pattern of the outer atmosphere was well expressed, in 1942, by Struve. "Some of the peculiar phenomena generally attributed to a tenuous outer atmosphere in some early-type stars are not confined to a few freaks, but are probably characteristic, in at least small degree, of the majority of stars, in some phases of their evolution." At that point, Struve cited the sequence proposed by Beals and already mentioned. Wolf-Rayet, P Cyg, Be, and α Cyg. Struve further stressed that the rationale of this second conceptual approach was to focus on determining what the structural pattern is, before one even asks what causes it. So, one uses as much and as wide a variety of data as possible

Besides the observed characteristics—emission lines, variability, individuality, and gradualness—for this class of stars with extended atmospheres, Struve introduced as a major indicator of atmospheric pattern the dynamic criteria mentioned above, that is, some extended atmospheres appear quasi-static, any observed velocities being distinctly subthermic, other atmospheres appear dynamic, expansion velocities being distinctly superthermic The sequential range from α Cyg to P Cyg is illustrative So then, simply as an empirical basis for guidance, Struve stressed that the Sun, that star for which we have the most details on an extended atmosphere, just because of its proximity, exhibits precisely such a division into two extended-atmospheric regions. The lower outer-atmosphere, or the chromosphere, gives a quasi-static appearance, even though its emission scale-heights are a factor 6 larger than an isothermal, hydrostatic-equilibrium, scale-height at the photospheric boundary temperature. By contrast, the upper region, or corona, gives every appearance of a dynamic state, including outflow

One can understand a dynamic, outflowing extension of the chromosphere; a static one is harder to understand, if radiative equilibrium applies. Most solar astronomers in the pre-1942 epoch were content to think in terms of some kind of random, or "turbulent," macroscopic motions in the chromosphere, which kept it quasi-static, but distended McCrea, Rosseland, Unsold, had proposed various models of such a "turbu-

lent" chromosphere. Struve was familiar with the problem and its conceptual resolution, from his and Elvey's studies of the non-Stark broadening of supergiant line profiles, and their anomalous widths: a turbulence, occasionally superthermic, had been proposed to produce such line-broadening. So, in harmony with his speculation that those phenomena of the hot, peculiar stars that produced an extended atmosphere were hardly peculiar to them alone, Struve proposed a conceptual pattern based on a variety of kinds of observed phenomena in these hot, peculiar stars. The cool, quasi-static but turbulent chromosphere, and the cool, but dynamic corona, of the Sun would give the overall structural pattern. The observed characteristics of the peculiar, hot stars, would give the variety of details. Possibly the details would vary from star to star, and, for a given star, from epoch to epoch, but the main distinguishing characteristics among stars and epochs would be the opacities of the chromosphere and of the corona—the static and dynamic atmospheric components Struve conjectured that, to a first approximation, the pattern was spherically symmetric, the outer atmosphere did not consist of a series of prominence-like structures, between which one might see to the photosphere. He suggested that while the photospheric parameters, T_{eff} and g, vary considerably from star to star—main sequence, giants, supergiants, normal, peculiar—there might be a community of outer-atmospheres, all following the same structural pattern, which are distinguished by different values of the opacities of chromosphere and corona, and by the velocity of the outflowing material. We see well how the *individuality* stressed in preceding chapters for the Be stars is incorporated into such an empirical, conceptual pattern.

This "Be and similar" conceptual pattern of the cool chromosphere-corona *almost* satisfied Struve's basic characterization of it: find, empirically, what is there before asking for cause. *Almost*, because of its basic characterization of "cool," which was empirically introduced for the reasons already given: subionization in the visual spectra of most stars in the class, in most aspects. The standard model restriction of hydrostatic equilibrium was dropped, because of observational necessity, that of radiative equilibrium was not, because of a neglect of some observational data, and of thermodynamic consistency with the kind and size of departures from hydrostatic equilibrium that were admitted. However, O VI in the Wolf-Rayet end of the Beals sequence, and coronal lines in the novae and symbiotic stars, were the superionization phenomena suggesting that radiative equilibrium should not have been imposed. The interaction between the "turbulent" elements to void radiative equilibrium was the thermodynamic omission. So, just as rotation-alone and radiative-equilibrium conditions were the weakness of the equatorial-concentration concept, so were radiative equilibrium and a "turbulent" support of the chromospheric part of the outer atmosphere the weakness of the cool chromospheric-coronal concept

These weaknesses removed that interest which should have been maintained in the chromosphere-corona plus post-coronal concept of an atmospheric pattern for the Be and similar stars. Edlen's (1942) identification of the solar coronal lines as superionized species, hence also the same in the other stars showing them, and Redman's (1942) demonstration that solar chromospheric line-breadths were essentially thermal, showed that the anomalously-large chromospheric scale-heights were thermal, not "turbulent." These identifications came within a few years of Struve's introduction of the model. The chromospheric, quasi-static, thermal distension was placed on a very firm basis, disentangling the effects of self-absorption and thermal broadening, by Thomas, Athay, and collaborators (1961) from the 1952 solar eclipse. This last is very important as laying the basis for an *empirical* specification of those regions of the solar outer-atmosphere which have wholly thermal, but without radiative equilibrium, extension; and those which have non-thermal, dynamic, extension. In effect, such an empirical approach separates those regions where only a nonradiative energy flux, and those where both a nonradiative energy flux and a mass flux, control the atmospheric distension. We use this point later, in our approach to the actual Be star atmospheric mapping. It has not been well appre-

ciated in the literature, especially for the hot stars, where for so many years after Struve's model a nonradiative heating of a chromosphere was denied, because no mechanism to produce the required nonradiative flux was known. Once again, the observational evidence of the existence of such a chromosphere-corona in *peculiar* hot stars, the Wolf-Rayet, was simply set aside; the stars were judged too peculiar to be considered (cf., Avrett and Jordan, 1973).

With observations in the far ultraviolet region from space, and with the discovery of the ubiquitous superionization in the hot stars—including the Be and similar class—Struve's "*cool* chromosphere-corona" abruptly experienced the shock which the solar cool chromosphere-corona met in 1942. The configuration became the "*hot* chromosphere-corona." But in distinction from the strictly solar pattern of atmospheric regions, and probably illustrative of the more extended pattern of atmospheric structure accompanying a very much stronger mass flux than the solar, one recognizes the existence of important additional atmospheric regions which are "subionized and slow." These provide the emission-line Hα, the cool far infrared, cool radio, and possibly dust shell spectra.

Combined Atmospheric Pattern from Struve's Pattern II, and the Normal vs. Peculiar Star Approach. On the basis of the summary of Struve's two atmospheric patterns, and the observations summarized in Chapters 10 to 12, we abstract an atmospheric pattern of a modern, wholly-empirical, model that attempts, as first approximation, to follow the three principal concepts of Struve's cool chromospheric-coronal model without imposing that the outer atmospheric regions be restricted to being either chromosphere, or corona, or cool. That is we *follow the three concepts*: (i) *focus on the Be and similar stars, not the Be alone, to obtain a wider data base,* (ii) *adopt the working hypothesis that all such stars, while differing in the photospheric properties of T_e and g, have the same outer atmospheric pattern of structure*, which includes the solar pattern, but is possibly expanded from it because of larger values of nonthermal parameters such as mass flux; (iii) *find what is, empirically, the atmospheric pattern before trying to explain it* or speculate on its origin.

Immediately, because of the added data since Struve's epoch in the X-ray, far ultraviolet, far infrared, radio regions, we recognize that we need a broader structural pattern than just the two extended atmospheric regions of Struve: one quasi-static, one dynamic, both cool. Observationally, these far ultraviolet data on Be and similar stars require a variety of regions, as implied by the wide range of the observed ionization and velocities. In some regions, T_e has values corresponding to photospheric boundary T_e and small velocities; in others, T_e has risen sufficiently to produce C IV, N V, O VI lines, showing absorption minima displaced over a range of velocities from 0 to 1500 km s^{-1} There are apparently regions similar in ionization, but widely differing in velocity, as shown by Si IV, C IV, N V, O VI lines with multiple components, some with small, some with large velocities over the 0 to 1500 km s^{-1} range. Moreover, X-ray observations suggest the existence of other regions for which $T_e \sim 10^6 - 10^7$ K, but for which we have no information on their velocity. All these data are highly individual, there are no definitely established correlations, only some few trends with MK class And, as of today, their relation to the Balmer and Fe II data pertaining to subionized regions are not well defined. Later, we will stress this point, as strong evidence for the existence, and effect, of variable mass flux, needed to obtain that observed dependence of some outer-atmospheric properties upon the history of the variability. It appears that the density distribution is not fixed only by a simple outward mass flow at the given epoch, nor does the planetary nebula-like structure at the outer boundaries of the atmosphere appear to follow from a simple, constant, mass flux. So *the basic problem, already stressed, is to establish locations of hot and cold, fast and slow, regions. Because there are no correlations of T_e and speed with* v *sin i, the data strongly suggest that the distribution of these various regions is radial, not in sectors* as polar versus equatorial. As we see in the following section, this distribution is precisely in the spirit of Struve's (1942) model: a radial

distribution of regions; not a network of prominences, between which one sees to different atmospheric levels. So the problem is to delineate radial trends in ionization (i e., T_e) and acceleration.

Almost concurrently with the high-energy observations of the spatial decade, there has been a surge of low-energy studies in the far infrared and radio regions. As summarized in Chapter 11, infrared excesses in Be stars can be interpreted by free-bound and free-free emission from the ionized outer-atmospheric regions, both hot and cold. But mainly, until now, Be star models have focused on the cool regions, ionized by the thermal radiation from the star For some stars, showing large infrared excesses, a contribution from circumstellar dust has been postulated, even though the silicate signatures have not yet been observed. Such a suggestion is by analogy with similar stars, where the silicate signatures are observed, such as symbiotic and Herbig Ae, Be stars Again, we have as yet no observational detection of the Be stars in the radio region, although we do for some Bep and symbiotic stars But whatever the origin of the infrared excesses, their existence implies atmospheric extents out to some thousands of photospheric radii, stars detected in the radio wavelength must have even larger atmospheres. For a Be star radius of some 10^{12} cm, such extreme far infrared, and radio, data suggest atmospheric extents of some 10^{15} cm, which is indeed the dimension of the smallest planetary nebulae

If one needs *a succinct label for such an empirical model*, probably *Solar-Planetary-Nebular model of Be and similar stars* is at least pictorial. *Solar*, to focus attention on the fact that, as for the Sun, the first region above the photosphere is a nonradiatively-heated one, with the atmospheric distension being thermal hydrostatic-equilibrium, but at a T_e raised above the radiative-equilibrium boundary temperature, T_0, by dissipation of that nonradiative energy flux. *Planetary-nebular*, to focus attention on the fact that the last region we distinguish of this outer atmosphere is a cool, quasi-static one, as for the planetary nebulae And, as in current ideas on how such a cool nebula is formed for these objects at the observed distances, the mass flux must be variable, to provide an interaction between mass flows at different epochs. By contrast with the planetary nebulae, where current thinking links such variability in mass flux to an evolutionary change, most stars in the Be and similar class exhibit mass-flux variability over time scales far shorter than evolutionary. We apparently need such an interaction between mass flows of different epochs to make the Be star outer atmosphere resemble more a filled cavity—a "balloon," which is alternately filled and exhausted—than a steady outward flow. In the rest of this section, we abstract the conceptual pattern of this modern Struve-type model; in the next section, we summarize its observational basis; following that, we ask what can and what cannot be actually fixed, quantitatively, in this structure. We will see that the basic problem is insufficient knowledge of the time history of the mass flux to specify the distribution of n, T_e, U within the "balloon" structure and its time variation.

Then *we identify, in first approximation, a radial sequence of atmospheric regions*. We focus on such a wholly radial, gross structure for two reasons. First, for a typical Be star, we note that the particle concentration decreases, from some 10^{15} in the photosphere, through some 10^{13} at the beginning of the chromosphere, through some $10^{12} - 10^{11}$ in the region where the mass flux dominates and imposes a dynamic density distribution, to some 10^4 in "nebular" regions, and finally to about 1 in the interstellar medium Second, we note that T_e increases from some $2\,5 - 3 \times 10^4$ K in the outer photosphere of the hottest Be stars, through some 10^5 K where the far ultraviolet lines are produced, to some $10^6 - 10^7$ K in the regions of X-ray production, descending to some 1×10^4 K in the region where most of the Balmer emission, and certainly the Fe II emission/absorption arises, to about 1000 to 2000 K where any dust grains exist If we use the Sun as analogy, we have the same range in radial density and T_e gradients, with small lateral differences relative to these radial changes Density fluctuations are some few percent in the photosphere, fluctuations in T_e are the same, except in sunspots where 20 percent differences can be reached. Some authors stress the distinction between "cool"

coronal regions—the coronal holes—and the quiet corona. Yet the two regions differ, in the corona proper, by only a factor of 2 in density, while T_e for both lies in the range $1 - 2 \times 10^6$ K, the "hole" being only some 0.5×10^6 K, or 30 percent, cooler (Vaiana and Rosner, 1978). These two regions cover more than 95 percent of the solar surface; the much smaller "active" regions can be a factor of 100 more dense and show T_e to be a factor of 10 higher. A conjecture that active regions and flares dominate over "quiet" star and coronal holes for Be stars remains only that, until *observations* demand something else.

We stress that by this emphasis on the very small size of lateral gradients in physical quantities relative to radial, we do not imply their unimportance, particularly in the significance of whatever causes them. Here, we simply ask what is the gross atmospheric structure, and what causes it to depart from that structure expected for a closed, thermal, thermodynamic model of a star. Thus, to a first approximation, we set aside the lateral structure accompanying, for example, a nonradial oscillation which produces that nonradiative energy flux responsible for a structure deviating from a radiative equilibrium one. The approach has some hope of success, because such a nonradial oscillation, having lateral density fluctuations of a few percent, can, by heating, result in a difference by a factor of 100 in radial scale-height of density. This nonradial oscillation is important in terms of explaining the origin of the nonradiative flux. It is not important in specifying, empirically, the T_e, density, and velocity distribution along a sequence of outer atmospheric regions.

So, *we then have the following radial sequence of atmospheric regions*:

1. *A PHOTOSPHERE*, characterized by hydrostatic equilibrium and radiative equilibrium. For the Be stars, T_{eff} ranges from 3.5×10^4 K to 1×10^4 K; T_0, from 3×10^4 K to 8×10^3 K.

2. *A CHROMOSPHERE*, defined by a rise in T_e coming from nonradiative heating, so $T_e \gtrsim T_0$. In this region, the density distribution is quasi-static, hence in hydrostatic equilibrium.

3. *A CORONA*, characterized by a T_e increasing outward, but in this region, the density distribution is dynamic, rather than quasi-static. We distinguish the *LOWER-CORONA* as those regions, beginning with the thermal point, where flow velocity essentially equals the local one-dimensional thermal velocity; and *the UPPER-CORONA*, where flow velocity reaches the escape velocity and exceeds it.

4. *A POST-CORONAL TRANSITION-REGION* between the hot, rapidly moving corona and the cool, slowly moving regions demanded by the Balmer and Fe II observations.

5. *The COOL, EXTENDED ENVELOPE* where most of the contribution to the Balmer emission lines arises. Flow velocity is less than some 100 km s^{-1}. T_e lies in the range of 0 5 to $2\,0 \times 10^4$ K.

6. *A COOL SHELL* above the cool, Balmer emission envelope, where are formed the narrow, deep absorption cores of hydrogen and Fe II lines In its outer regions, the low excitation, forbidden lines of the Bep spectrum arise, so concentrations have dropped to some 10^5 cm^{-3}. Velocities and T_e are lower than in region (5).

7. For Bep, symbiotic, novae, and possibly other similar stars, but not the "conventional" Be stars, we *have possibly a dust shell*. T_e would be of the order of 1 to 2×10^3 K.

We now proceed to summarize the observational basis for this scheme of atmospheric regions.

Observational Basis for the "Solar-Planetary-Nebular" Empirical Sequence of Atmospheric Regions for Be Stars

We simply follow the numerical sequence of regions listed in the last section, in this observational summary of the evidence for the relative location of each region.

1. *PHOTOSPHERE*. This region exists, by definition, at the base of the atmosphere. It is the origin of the visual continuum, and the wings of the medium and strong absorption lines, and possibly the cores of some weak lines, formed in the visible region, on the basis of which that spectral classification which defines B, Be, and similar stars is made. Here, we do not enter a discussion of the difference between B and Be photospheric spectrum—for example, of the difference in

photospheric nonthermal velocities coming from larger values of the mass flux, and its effect on line profiles. Our only interest lies in those spectroscopic features, and changes in the apparent photospheric spectrum, coming from outer-atmospheric phenomena, and ascribing them to one or several of the outer-atmospheric sequence of regions, to order that sequence.

2. *CHROMOSPHERE. The primary question one asks is whether the first outer-atmospheric region above the photosphere is hotter or cooler than T_0, the photospheric boundary value of T_e under non-LTE, radiative equilibrium and hydrostatic equilibrium.* We have three kinds of observational evidence to guide the choice..

First, there is a continuous progression of superionization level, from the most highly ionized photospheric lines up through O VI, all appearing in absorption, all very broad. By contrast, the subionized species observed are in emission, if they are broad, like the Balmer lines of hydrogen, or, if in absorption, the lines are quite narrow, as the shell lines of Fe II and the shell cores of hydrogen. This comparison strongly suggests that the subionized species exist exterior to the superionized, thus arguing for an initial outward increase of T_e.

Second, the total emission from Hα gives an estimate of the product of emitting volume and particle concentration. Given that both the cool regions producing Hα, and the regions too hot to produce it, coexist, we have another argument for relative location of the region. If Hα originates in the lowest exophotospheric region, then the various calculations for the equatorial model, summarized in Chapter 11, require particle concentrations of some 10^{13} at the lower boundary of the emitting region, falling only to some 10^{12} to 10^{11} at 2 to 5 photospheric radii, and some 10^{10} at some 20 radii, which still contribute significantly to the emission. A spherically-symmetric model can be satisfied by densities less by a factor of about 40 In the lowest part of the region, if conditions are quasi-static, the scale-heights are so small at the $1 - 2 \times 10^4$ K values of T_e, some 0.0003 photospheric radii, as to cause an initial concentration of 10^{13} to drop to 10^9 in the next 0.003 radii, for $\log g = 4$. To maintain the concentrations at the 10^{12} to 10^{11} level, one requires either the "superthermic turbulence" postulated by the early investigators–which provides a larger, kinematic but quasi-static, scale-height–or the differential, superthermic, mass flow introduced by the equatorial-concentration modelers–which replaces the quasi-static scale-height by a dynamic, $\sim r^{-2}$, density distribution. However, each of these two alternatives results in a dissipation of mechanical energy, hence a rise in T_e, when they are treated physically consistently; and there is no basis to assume that some unspecified mechanism inhibits such dissipation. In abstract, locating the cool region low either gives particle concentrations too small to produce the observed Hα emission, or destroys the "cool" characteristic. Although an ignorance of some mechanism is never a strong argument for its absence, it is nonetheless significant that we do not know of any mechanism to decrease T_e, by the required factor of about two, within the required fraction of a photospheric radius. By contrast, dissipation of a nonradiative energy flux is quite sufficient to raise T_e by factors of 10 to 1000. So if the Hα region is located high, then the larger scale-heights of the low, hot chromosphere, and the dynamic density distribution, r^{-2}, of a corona, maintain the particle concentrations at those values necessary to produce the Hα emission exterior to the chromosphere-corona. We give numerical details in the following section.

Third, we have already remarked on the absence of understanding what are the nature and origin of the possible nonradiative energy fluxes in these Be stars. But the existence of mass fluxes is known, observationally, and was postulated in the early, equatorial-concentration, models. As we demonstrate in the next section, one can combine a value of mass flux–observational or hypothetical–with a photospheric model to set an upper boundary, in height, where a nonradiative heating must have already begun. Such an estimate gives an absolute height value to adjoin to the relative heights just discussed in the previous two paragraphs. Such upper-boundary heights are very low relative to the radii of the region where the hydrogen emission lines are

formed. The upper boundary on heating occurs a few hundredths of a photospheric radius above the surface, or less; the hydrogen emission regions require tens of radii.

Given these observations, *we conclude that the first post-photospheric atmospheric regions resemble the solar in two respects: (a) an outward increase in T_e; (b) a density gradient specified wholly by hydrostatic equilibrium under this gradient in T_e*, such that macroscopic motions, and flow velocity satisfy $U \lesssim q/3$, where q is the one-dimensional thermal velocity *These two characteristics are our definition of a chromosphere*

3. *CORONA*. Observations of C IV, N V, and O VI at velocities exceeding 1000 km s^{-1} show the existence of regions with $T_e \sim 10^5$ K, with velocities exceeding both thermal velocity and escape velocity of the atmosphere, in *some* Be stars at *some* epochs. Observations of both soft and hard X-rays in *some* Be stars leave equally-small doubt that regions of $T_e \sim 10^6$ to 10^7 K also exist, at *some* epochs, in some Be stars Those Be stars exhibiting these phenomena also exhibit the chromospheric regions summarized above in (2), the Hα emission regions, and occasionally, the Fe II absorption regions. For those Be and similar stars exhibiting all these phenomena, even if Fe II absorption is absent, there is no doubt that there exist regions satisfying our definitions of upper and lower corona, which are located between the chromosphere, region (2), and the cool, Hα-producing regions of (5) We stress that all Be stars do not show such a complete range of phenomena

Some of these regions showing superionization, and superthermic and superescape velocities, lie exterior to the radius of T_e (max) In γ Cas, there are some components of Si IV, showing $U \sim -100$ km s^{-1}, apparently superthermic, if $T_e \lesssim 0.5 \times 10^6$ K, but not superescape, and some showing $U \sim -1500$ km s^{-1}, definitely superthermal and superescape. These components occur in the same spectrum and are well separated. Moreover, the observed presence of C IV and N V and of X-rays in this star show that T_e (max) is too large in such regions to permit the Si IV ions to occur everywhere in the atmosphere. Thus, we cannot interpret the Si IV velocity spectrum as resulting from a continuous presence of Si IV ions, accelerated from less than 50 km s^{-1} to some 1500 km s^{-1}. Rather, these Si IV ions must occur in distinct regions, below and above the T_e (max). Thus, such data gives evidence of the existence of cooling regions in the coronae of such stars.

When we consider stars for which observations are more limited, we must be more cautious. Since some degree of superionization seems ubiquitous, all stars exhibit at least chromospheres. Lack of X-ray observed emission removes any conclusive evidence of regions at 10^6 to 10^7 K We are sure only of those T_e (max) corresponding to the observed superionization features. Since we discuss only Be stars, and those similar as defined by, among other things, the presence of Hα emission, they all must have some kind, and size, of mass flux which is sufficient to produce an atmosphere extended enough to give the observed Hα emission. In view of our discussion in previous chapters, we are cautious in implying whether it is the size of the mass flux at a given epoch, or the history of its variation preceding that epoch, which gives those properties of the extended atmosphere which are necessary to produce the observed Hα emission But we note that if the outflow velocity only reaches thermal values very far out in the atmosphere, that radius where an r^{-2} density distribution takes over from a thermal hydrostatic equilibrium will be so large, that the densities will be too low to produce a significant Hα emission. We give various examples, as a function of mass flux size, in the next section. However, the solar and T Tauri comparison provides the most direct observational example. Observationally, from detailed eclipse studies (Thomas, 1983), the solar thermal point does not occur until some 2 photospheric radii, where concentrations have dropped to some 10^6; there is no extended Hα-emitting envelope. By contrast, in the T Tauri stars, effectively the same spectral type as the Sun, the thermal point is much lower in the atmosphere, and one has an Hα-emitting envelope. Both types of stars show superionization and X-ray emission, although it is not clear that

the T_e distributions in the upper-corona are similar.

Thus, *we conclude that this observational condition of Hα emission requires a low-lying thermal point in the Be, and similar stars; hence, that they exhibit a LOWER-CORONA, a region where* $U \sim q$*–i.e., a transthermal region of flow–and* T_e *increases outward.* Its beginning height depends upon the size of the mass flux Whether such a steady-state treatment suffices for describing further atmospheric regions, remains to be considered.

The general existence of an UPPER-CORONA, as we define it, depends upon whether the mass-flow velocity continues to accelerate outward between the thermal and escape points. For those Be, and similar, stars discussed above, in which photospheric escape velocities are exceeded, from the evidence of line displacements, there is clearly no problem. But for some Be and shell spectra, neither far ultraviolet lines, nor visual lines, show significant line displacements, certainly not more than some 100 km s^{-1}. Yet the Hα emission can be very strong. So here, one has two alternatives for investigating the existence of an upper-corona, both leading to the same result: such an upper-corona exists.

In the first alternative, one recognizes, from the ad hoc model calculations summarized in Chapter 11, that one needs expansion velocities of some 100 km s^{-1} to match the observed Hα emission-line profiles, and that the region of strongest contribution to the total emission lies some 5 to 10 radii from the star. Given a photospheric escape velocity of some 500 km s^{-1} for such stars, the 100 km s^{-1} flow velocities are clearly superescape in the region of Hα formation.

In the second alternative, we note that most of the inferences of velocities from far ultraviolet lines are based on diagnostics of asymmetric line profiles, not on line displacements. The extended violet wings, whose interpretation is clearly model-dependent, leads to velocities exceeding the photospheric escape value. In each of these alternatives, the evidence for far ultraviolet velocities much exceeding those in the Hα region is, most often, model-dependent, and highly circumstantial. But, one is led to velocities exceeding the escape velocity somewhere in the outer atmosphere. Under the Struve modeling scheme, where the corona was cold, we would indeed have an upper-corona, for all these stars. Under our present scheme, it is not clear that we can satisfy an upper-corona which is hot. We can only state the problem, clearly, much investigation remains to be done, especially in the X-ray region, and in the detection of weak superionized lines in the far ultraviolet region.

Finally, we should comment on the dynamic versus thermal aspects of the corona. Above, *our indirect evidence for the existence of a corona, lower and upper, in the Be stars, rests on the dynamic aspects: the necessity for a nonthermal density distribution in order to give that extended atmosphere which produces emission lines.* Some of the Be stars also exhibit, observationally, the thermal aspects: the presence of CIV–NV–OVI, and of X-ray emission. But these last aspects are also present in normal B stars, such as τ Sco. *We ask the basic question: Why is there such an extended atmosphere for Be stars, but not for normal B stars? If such an atmospheric extent were caused by, or isomorphically linked to, wholly thermal properties, then we should not observe two classes of stars, the normal B and the Be. So the existence of these two classes in the same thermal-taxonomic box is certainly basic evidence* for understanding the extended atmosphere, and the mass flux linkage to fundamental nonthermal properties of stellar structure. We do not pretend, in any way, to resolve this problem in this monograph we only hope to delineate its various aspects.

The problem in empirically modeling the upper-corona is simple. how to model the velocities exceeding q at T_e (max), their variation within a given star, and between two stars of the same luminosity. If one interprets their large values as implying radiative acceleration, then one must explain the variation in their size, within a given star, without simultaneous variation of the radiation field, and between two stars showing the same radiation field. That the radiative acceleration is not the only possibility is made clear by the solar situation, where observed veloc-

ities up to 800 km s^{-1} occur, at some epochs, and radiative acceleration seems hardly plausible. So here, we defer the problem to more complete observational resolution and make no attempt to model it other than as a *pattern* which exists.

4. *POST-CORONAL TRANSITION REGION. This region has two primary functions* (i) *to decelerate the gas* from whatever is its outward flow velocity in the corona to the velocities $\sim$ 100 km s^{-1} that are observationally characteristic of the Hα-emitting region; (ii) *to cool the gas* from whatever is its T_e before the deceleration begins to the values characteristic of the Hα-producing region, which are in the range $1 - 2 \times 10^4$ K. These properties are mainly imposed, from observations of some Be and similar stars, by the coronal region, which precedes, and the Hα-producing region, which follows, this transition region—which is itself very inadequately observed directly. We summarize such observational imposition.

For those stars where one observes simultaneously: (i) lines from superionized species like C IV and O VI displaced by velocities $U \gtrsim 200$ to 300 km s^{-1}; and (ii) Hα emission profiles, with displacements—themselves, or absorption cores—$\lesssim$ 100 km s^{-1}, and sometimes also Fe II absorption lines with these same velocity characteristics, there is no doubt as to the existence of this intermediate region (4) in the framework of our model; that is, assuming a radial structure of the atmospheric pattern.

For those stars exhibiting these same Hα, possibly Fe II, characteristics, but for which no displacements in the far ultraviolet lines of the above size are observed, an observational justification of this region (4) is model-dependent. As summarized, it depends on the inference of velocities from asymmetries in the line profile· "asymptotic" velocities inferred from "blue-edge velocities"; generally, these exceed 200 to 300 km s^{-1}.

For those stars where far ultraviolet velocities, no matter how inferred, are similar to Hα and Fe II velocities, we can make neither inference nor comment, except possibly that a cooling is required, but this could occur in the corona.

There is one final kind of evidence for the existence of this transition region Some stars, at some phases, Be and similar, show three, possibly more, sets of superionized line components. We associate one of these with the chromospheric-coronal region of rising T_e. We associate the largest velocity component with the upper-corona. There remains intermediately-displaced components, which possibly can be associated with a decelerating region. One can associate the enhanced concentration of ions necessary to distinguish a separate line component with the density rise, velocity fall which accompany a shock deceleration.

All these pieces of evidence are suggestive rather than conclusive. Conceptually, the most striking evidence lies in the historical planetary-nebular similarity. Before the epoch of observations made from space, models of planetary nebulae represented the nebula itself as the *beginning* of a dynamic region; the H I boundary of the star's Strömgren-sphere being accelerated outward. Modern, far ultraviolet, observations show superionized species filling the central hole of the nebula, with line displacements observed up to values of the order of 1000 km s^{-1}. Thus, the picture has changed drastically. Instead of being the beginning of an accelerated region, the nebula is an outer fringe of a decelerated, far-outer atmosphere of these objects. Moreover, the very extent of the hole suggests a very extended chromosphere-corona. Some central stars of planetary nebulae show Wolf-Rayet type spectra, suggesting that one sees a *Wolf-Rayet phenomenon* in them—not a *Wolf-Rayet object*, there being a large mass discrepancy between Wolf-Rayet stars, and Wolf-Rayet central stars of planetary nebulae. Thus, the conjecture would be that we do not see a central star, in the conventional sense; rather, we see a "thick" corona, as in the Wolf-Rayet stars proper. The H II regions associated with the Wolf-Rayet and the Be and similar stars cannot be viewed as the classical Strömgren-sphere of such stars, radiatively controlled by the photospheric far ultraviolet spectrum. Rather, these outer atmospheres represent a modified Strömgren-sphere; fixed by the dynamic effect of the mass flow, and the radiative effect of the chromosphere-corona, produced

jointly by the nonradiative energy flux and the mass flux. Then, our "decelerating, cooling" region (4) would, for the planetary nebulae, be graphically present: invisible in the visual but observable in the far ultraviolet region. High-resolution, far-ultraviolet studies will provide the best observational test for the existence of this transition region, which seems difficult to avoid.

We can try to put in focus two other aspects of this picture by combining observational evidence for other members of the Be and similar group with that of the planetary nebulae. One aspect combines Wolf-Rayet stars and planetary nebulae data, to exploit an idea proposed by Sahade, to focus on the interior of region (4). The second aspect combines the Bp and planetary nebulae observations and cooling models, to explore the boundary of region (4) and the interior of region (5). We consider the former to conclude this section (4), the latter, to open (5)

Sahade (1980) has recently contrasted the contradictory indications from visual and far ultraviolet observations of the Wolf-Rayet stars on the outward evolution of ionization/excitation level. The classical visual data (Beals, 1939; Kuhi, 1968) indicate an outward decrease in ionization, but outward acceleration of the mass flow. The more recent far ultraviolet data suggest the contrary, an outward rise in ionization. Sahade proposes to resolve the problem by having two maxima of T_e in the atmosphere. one near the surface, the other at some distance. The origins of these maxima are not discussed, only their possible existence. We note a possible interpretation in terms of: (i) such a dense chromosphere-corona that one sees only it; and (ii) a shock deceleration in region (4), from the 2 – 3000 km s^{-1} flow observed from these stars, to whatever is necessary to produce the nebular region. Sahade discusses extensively the nebulae associated with the Wolf-Rayet stars, and stresses their similarity to the planetary nebulae. Contrary to the Be stars, where the Hα-emitting region begins at 3 to 5 radii, so that the H II-H I interface is relatively near, this nebular region of the planetary nebulae and Wolf-Rayet stars occurs far away—implying for these stars, as above, an extended region which embraces the chromosphere-corona and this cooling-decelerating region (4). We note other "tracers" of this second region of maximum temperature in both symbiotic stars and novae, such as the presence of high ionization/excitation forbidden lines of Fe VII, etc. For these Be and similar stars, where beginning regions of chromosphere-corona occur at much higher density than for the Sun, such forbidden coronal lines would more likely be associated with the low-density, second maximum T_e region of Sahade than with the low-lying, normal corona. Finally, we note that X-ray results from a variety of stars are represented in terms of two thermal emissivities, one near some 10^6 K, another at 10^7 K or larger. We note that if the maximum flow velocities have been accelerated beyond the thermal value of whatever is T_e (max) in the atmosphere—which is likely in terms of existing literature on the subject—stopping such a flow will produce a second T_e (max), larger than the first. For example, putting all the energy into a wholly-kinetic T_e gives a $T_e \simeq 10^8$ K with $\gamma \simeq 5/3$, which is, of course, an upper limit Clearly, such wholly-thermal representations and discussions must be justified.

In summary, if one considers that the existence and extent of this cooling, decelerating region (4) is mainly established by the necessity to match, on either end, the properties of the coronal region (3) and the Hα-emitting region (5), and if one uses the data on Be and similar stars to exhibit its range of properties, one can put together a significant amount of circumstantial evidence for its existence. In addition, this set of Be and similar stars gives a very wide range in size of the region if we use the beginning of the Hα-emitting region for the Be stars, and the nebulae for planetary nebulae and Wolf-Rayet stars, as a measure of the extent of (4).

When we consider the problem of empirical modeling of this transition region, it is clear that the present data are insufficient. To decelerate a flow, whose velocity is of the order of 1000 km s^{-1}, to a value of the order of 100 km s^{-1}, at a few radii from the star, we apparently need a variable mass flux from the star. The only star for which such data are partially complete is 59 Cyg (see Chapter 12). And that star has been ob-

served during the beginning of only one episode of increasing emission, that is, at the moment of the building up of the cool outer envelope.

5. *COOL, EXTENDED ENVELOPE.* In Chapter 11, we have already summarized the evidence for a low velocity region with a temperature of 1×10^4 to 2×10^4 K, where the Balmer and Fe II lines in the Be and shell phases are produced. These are regions (5) and (6). It is primarily the low-velocity character which associates the Hα-producing region to the chromosphere rather than corona in the Struve (1942) model. And, it was these low velocities which caused some authors to persist in placing this hydrogen region below the region of that strong acceleration which produces the OB star large wind velocity. In our summary of region (2), we gave the observational reasons for placing this region (5) exterior to the chromosphere-corona. In our preceding summary of the observational evidence on region (4), we presented what might be the deceleration pattern that can indeed produce this low-velocity character of the Hα and Fe II regions (5) and (6).

One of the major problems in the Struve cool chromosphere-corona model was the cooling below the $T_e \sim 1\,0 \times 10^4$ K level, especially if the Hα regions are placed contiguous to the photosphere. The problem is more pronounced at our epoch, when it is generally recognized that non-LTE effects cause T_e to be fixed by the quality, not quantity, of the radiation field (cf., the extensive tables for early-type stars by Auer and Mihalas, 1970). One should, of course, note that this effect was recognized, and demonstrated, by Baker and Menzel (1938) in treating the planetary-nebular problem, following Eddington (1930) who used this case to distinguish between gas and dust temperatures in the interstellar matter. It was rediscovered, and emphasized, by Cayrel (1966). Gebbie and Thomas (1970) have extended the approach to include the effect of impurity cooling and mechanical heating via a parameter called the "temperature-control bracket" (cf., also Thomas, 1983). Various authors (cf., Cassinelli, 1979) have argued for thin coronae in terms of a rapid radiative cooling when coronal densities are as high as demanded by the large mass fluxes for these early-type stars. In the same way, Marlborough (private communication) has argued for superionization effects to be confined to polar regions in the equatorial models, because of the much-larger density gradients at the pole relative to the equator. The larger densities in the equatorial regions will cool the gas more rapidly than in the polar regions. But again, in all these cases, *T_e will not fall below T_{e0} for the large densities existing when the Hα region is placed just above the photosphere.*

However, when we place the region of Hα emission in this region (5), and continue to follow the planetary-nebular analogy, the physical picture of such cooling becomes clear. It was outlined in the Planetary-Nebular series of papers by Menzel and collaborators in the 1930's, following the Bowen suggestion of the impurity cooling of the forbidden lines of O, N, etc. More modern summaries provide more modern values for T_e and its distribution (for example, Williams, 1967). In regions very close to the star, the populations of the metastable levels are collisionally depopulated, removing the thermostat action of the forbidden transitions from them.

We note that the characteristic feature of the Bep spectrum—low-excitation forbidden lines—supports this picture. Presumably, the Bep star differs from the ordinary Be star by a more extended atmosphere. The data summarized in Chapter 11 on the stronger far-infrared excesses and the measurable radio excesses in some of these stars relative to the ordinary Be star, support the picture of this cooling and its mechanism.

Clearly, the primary problem is to decide whether a simple, time-independent outflow is sufficient to model this region, or whether the cavity or "balloon-" type configuration is required. In the next section we illustrate the problem of estimating the density at the base of this region if the simple flow configuration suffices—which the 59 Cyg data led us *not* to believe. We consider that there are, at the moment, insufficient data to model, empirically, any balloon-type configuration, for the reasons given in discussing region (4) above. We consider that this balloon

problem is the major one in Be star modeling, bearing in mind the "little planetary nebula" analogy, which we think very useful.

6. *COOL SHELL: producing absorption cores of hydrogen and Fe II lines. The observational evidence for such a region lies wholly in the distinction between the Be and Be shell spectrum.* The shell lines are deep and narrow, suggesting large column-density and low T_e of low-excitation material, hydrogen and Fe II. Just what the onset of the shell spectrum implies has been long-debated. Some authors consider it to imply an increased density in the outer atmosphere, associated with a greater mass flux. Another possibility is simply a greater impurity-cooling rate, for the same density. Clearly, the transition between the Be shell and Bep spectrum, with the implication of lower densities for the latter because of the forbidden spectral lines, gives important information. In our opinion, until one resolves the question of how to construct at least an ad hoc model of the balloon-type configuration versus the simple radial flow, a good diagnostics of the observations is difficult. We have stressed the individuality of the pattern of variability for Be stars. Nonetheless, we regard the pattern shown by 59 Cyg in its most recent change from Be to B quasi-normal as having some kind of implication, if we were wise enough to see it: the rapid sequence of two Be shell phases following two strong emission phases and ending by a collapse to the B quasi-normal spectrum, the beginning of a new Be phase within which a gradual buildup of the cool envelope is observed at the time of the maximum rate and variability of mass flow

7. *COOL DUST SHELL. Evidence comes wholly from the Be-similar stars*, and it is not too profitable to dwell on this atmospheric region in this focus on the Be stars. Discussion is best deferred to other volumes in the monograph series.

Empirical-Numerical Estimates of Location and Structure of the Several Atmospheric Regions

1. **The Method.** Clearly, the easiest regional structure of a gas to model, after the degenerate homogeneous one of Thermodynamic Equilibrium, would be that where each region is adiabatically isolated from every other one, the configuration is static, and conditions within each region are homogeneous. Each such region would be locally in Thermodynamic Equilibrium; hence, its energy would be wholly thermal, which we would characterize by specifying the temperature and particle concentration (or density), plus chemical composition. If such regions were in some kind of external field, such as being part of a self-gravitating system like a star, the energy content of each region would be the sum of thermal plus "field"—for example, gravitational— energies. In the gravitational case, the static condition would order the (density, temperature) sequential structure of the regions according to hydrostatic equilibrium and the adiabatic condition. There is no basic physical difference between regions, as regards dominant storage and transport mechanisms, linear versus nonlinear configurations, etc.· in these respects, the regions are identical. They differ only in numerical values of the same set of state parameters. Such was the original modeling of stellar structure by Emden (1907) for an adiabatic polytrope. The nonadiabatic polytropes permitted some energy interchange between and within the regions of the star, and between star and environment—still under the restriction to quasi-static configurations. The complication was how to include more general energy exchange within and between regions, energy loss at the boundary, energy generation in the interior, and that nonlinearity at the boundary which invalidates LTE thermal distribution functions and requires those of non-LTE there.

So long as the quasi-static restriction is maintained, a broadening of the energy transport to include radiation maintains the local energy content of a region as thermal and gravitational but removes any pretense of even quasi-adiabaticity. The distributions of state parameters—temperature and density—are determined by the thermal (static) conditions of hydrostatic and radiative equilibria (HE and RE). Away from the boundary, there is but one main region, the LTE photosphere There are what have been called "opacity subregions" (Rudkjøbing, 1947), between which

the dominant opacity source differs, but there is no basic difference among them in storage and transport properties. Near the boundary, the necessary nonlinearity in radiative transport processes, and the change in relative importance of radiative and collisional microscopic interaction rates, necessitate non-LTE rather than LTE distribution functions. Thus, one can also distinguish a non-LTE photospheric region But again, the restriction to radiative transport, and quasi-static configurations, prohibits other boundary effects. So the whole standard photospheric model remains thermal, in both its LTE and non-LTE regions Adding a strongly subthermic convection does not change this thermal character.

The observations summarized in this monograph, which we have ordered into the sequence of regions summarized in the preceding section, make it clear that there is a basic difference between photospheric regions and outer atmospheric regions, in storage and transport of energy and mass. In essence, the distinctions we have introduced to define the several regions rest on such a difference. The predominant storage and transfer of matter and energy in the photosphere is quasi-static thermal: HE and RE are not perturbed. Thus, we do not, for these Be stars, consider pulsating, not quasi-static, photospheres such as exist in cepheids. Possibly this is an error; but as yet, observations have not demanded such. Hence, in the photosphere, while there is energy stored in the nonradiative energy flux which does not transport mass and in the mass flux, and while energy and mass propagate as well as being stored, and while such propagation is neither adiabatic nor isenthalpic, none of these affect the existence of HE and RE for describing the observable, mean photospheric structure; *by definition*, based on the observations.

The same configuration for storage and propagation characterizes the mass flux in the chromosphere: the mass flux propagates; its velocity is fixed by mass conservation, via Equation (13-1), using a density, T_e distribution fixed by HE but not RE, its thermal state and velocity are therefore completely coupled, *given* the value of the mass flux F_M as the coupling parameter, but there is no nonradiative dissipation of energy from this mass flow, by definition, based on the size of the flow velocity as defining the upper boundary of the chromosphere. Within the chromosphere, RE is perturbed by the nonradiative energy flux, part of whose energy dissipates.

In the lower-corona, the density distribution is fixed by the mass flow velocity. The mass flow accelerates outward, by taking energy from the thermal energy of the atmosphere (which *is* the mass flow). This thermal energy is fixed by the radiation field, by the nonradiative energy flux dissipation, and by some dissipation from the mass flow. This energy interchange process does not imply anything on the *source* of the mass flux, it only describes its *propagation.* In the upper-corona, the mass flow needs no further acceleration to be a true flux from the star, it may be, but need not be, accelerated.

Finally, in the post-corona, apparently a simple, time-independent flow pattern is perturbed to decelerate and cool the gas. Apparently, such deceleration and cooling requires an interaction between mass flows of differing sizes at different epochs; the extreme, observable features of such interaction are planetary-nebular-like configurations.

We proceed to show how some of this can be described quantitatively, in terms of initial values of radiative, nonradiative, and mass fluxes, plus gravity and a rotational velocity, given at the base of the photosphere. As already emphasized, if eventually it turns out that one can predict one or more of these parameters from the others, then the range of possible alternative configurations is simply reduced. Clearly, that individuality among stars of the same gravity and radiative fluxes which we have continually stressed, simply reflects our conclusion that these several parameters are indeed independent. How their values arise is another matter, to which we return, speculatively, in the last section. But the following description of atmospheric properties, based on these fluxes, has no dependence on any theory of their origin.

2. **The Equations.** We first consider the simple, time-independent, spherically-symmetric outflow corresponding to a mass flux whose value is given

a prion. Also, we consider that the value of the nonradiative energy flux which does not transport mass is given, as well as the way it dissipates energy. Then the equations describing the storage and transport of mass, macroscopic energy or momentum, and microscopic energy are as follows (cf., Cannon and Thomas, 1977, where the significance of the various terms are discussed).

Mass:

$$\frac{d}{dr}\left(4\pi r^2 U\rho\right) = 0 \qquad (13\text{-}1)$$

Macroscopic energy or momentum:

$$\rho U\left(\frac{dU}{dr}\right) + \frac{d}{dr}(p + p') = \rho g + \frac{\rho V^2}{r} + \frac{\rho}{c}\int F_\nu K_\nu \, d\nu \qquad (13\text{-}2)$$

Microscopic energy:

$$\frac{d}{dr}(U\epsilon) + (p + p')\frac{dU}{dr} + \frac{dh}{dr} = -4\pi\rho\int K_\nu (J_\nu - S_\nu)\, d\nu + \frac{dQ}{dr} \qquad (13\text{-}3)$$

where

- W^2 = GM/r, W = escape-velocity/$2^{1/2}$;
- q^2 = kT_e/μ, q = one-dimensional thermal velocity;
- U = mass flow velocity; V = rotational velocity of the star;
- p = gas pressure, p' = viscosity = $-\theta\, dU/dr$, θ depends slowly on T_e;
- ϵ = internal energy of the gas; generally, it depends on non-LTE distribution-functions over these internal energy states,
- ρ = density; κ is mass absorption coefficient;
- μ = mean particle mass of the gas;
- Q = the nonradiative energy flux, dQ/dr is the essential quantity,
- h = heat-conductive flux = $-\lambda\, dT_e/dr$

The radiative-acceleration approach developed by Castor et al. represents the last term on the right in Equation (13-2) in the form

$$\frac{\rho}{c}\int F_\nu K_\nu d\nu = \rho K\left[(\rho q)^{-1}\frac{dU}{dr}\right]^\alpha, \qquad (13\text{-}4)$$

where K and α are parameters depending upon the details of the theory. As we remark in the next section, these authors prefer $\alpha = 0.8$ to represent the mass flux data; they prefer $\alpha = 0.9$ to represent the "terminal velocity." They make no attempt to justify differences in these values in the two applications. Also, they offer neither explanation nor comment on why τ Sco should differ so significantly from ζ Oph and γ Cas in mass flux behavior, nor what are the possible mechanisms of variability of a mass flux, which does not correlate with any variation in the radiation field We make these comments to say that we include the above expression for radiative acceleration, but treat it with some skepticism in the following empirical approach. Here, we simply do not want to exclude a priori, any terms representing possible physical effects.

Then we combine Equations (13-1) and (13-2) to obtain the usual kind of expression for the evolution of the mass-flow velocity, where the distribution T_e (r) is considered as a parametric function. If we know at least something about Q (r), we can possibly evaluate T_e (r); if not, we are forced to such a parametric approach, in discussing the behavior of U (r) from the following Equation (13-5).

$$U\frac{dU}{dr}\left(\frac{q^2}{U^2} - 1\right) + K\left(\frac{1}{\rho U g}\right)^\alpha\left(U\frac{dU}{dr}\right)^\alpha + \frac{d}{dr}\left(\theta\frac{dU}{dr}\right) = \frac{1}{r}\left[W^2 - V^2 - 2q^2\right]. \qquad (13\text{-}5)$$

We ask what can be said, quantitatively, about the properties of the several regions established in the previous section.

3. Application to Delineating Boundaries of the Several Atmospheric Regions.

PHOTOSPHERE. The region is defined by requiring $U \lesssim q/3$, and dQ/dr to be negligible. This condition on U is set by realizing that U always enters Equations (13-2), (13-3), and (13-5) in the form $(U^2 \pm q^2)$. Thus, this condition establishes that the perturbation by neglecting U^2 is no more than about 10 percent. We illustrate this by writing that expression for density gradient which corresponds to Equation (13-5) for the velocity gradient—for expository simplicity dropping the radiative acceleration and viscosity terms

$$\left(1-\frac{U^2}{q^2}\right)\left(\frac{d\ln\rho}{dr}\right)= -\frac{\mu g}{kT_e}+$$

$$\frac{V^2+2U^2}{rq^2}+\frac{d\ln q^2}{dr} \qquad (13\text{-}6)$$

So, in those parts of the atmosphere which are not near any "critical" point where rotational velocity equals escape velocity, the error in evaluating $d\ln\rho/dr$ goes directly as $(1 - U^2/q^2)$. For $U/q \lesssim 1/3$, this error falls below the 10 percent level, as remarked However, when $U/q \gtrsim 1/3$, approaching 1, the density distribution changes nearly discontinuously, since the change from $U/q \simeq 1/3$ to $U/q \simeq 1$ occurs in a density scale-height. So here, the conditions defining a photosphere break down, and one enters another atmospheric region.

The situation is similar for the terms in U and Q in Equation (13-3). The photospheric definition imposes these to be negligible; and, under stellar atmospheric conditions where an RE gradient in T_e holds, the thermal conductivity is negligible. So, the $(J_\nu - S_\nu)$ term fixes the distribution of T_e, under such RE.

We specify the top of the photosphere simply by asking where the imposed conditions on U and Q break down. Equally simply, by observing spectral line displacements, and their profiles, we have some direct measure of U in atmospheric regions where most of the absorbing ions of that species are concentrated, hence, because the mass flux is conserved, we have some direct estimate of its value (granted a large uncertainty). Then, from this value and Equation (13-1), we can estimate U (r). But we have no such direct estimate of either Q or dQ/dr, or of the nonradiative energy flux underlying them; indeed, for most stars, we have only vague speculation on the source of Q. We can observe various emission excesses, and superionization, but to determine the size of Q and the region where $dQ/dr \neq 0$ requires a complete atmospheric model, which is a bootstrap operation. The exceptions are those stars where eclipse observations give some measure of the height distribution of excitation/ionization and of atmospheric density. The Sun has been the most explicitly exploited; only a beginning has been made on other stars (Thomas and Athay, 1961; Jordan, 1981; Thomas, 1983). Lacking such detail on Q, one can only proceed to place bounds on the top of the photosphere and on the bottoms of the chromosphere and lower-corona—the latter depending, respectively, on the breakdown of RE and HE—by a set of limits on such breakdown. We proceed by considering two alternative situations. (i) there exists no nonradiative energy flux that does not transport mass, and (ii) such a flux does exist. Situation (ii) is, a priori, the situation we must expect, simply because the observed presence of a nonthermal mass flux defines the star as an open thermodynamic system, which is generally characterized by radiative and nonradiative energy fluxes of arbitrary variety, and the mass flux. However, observationally, situation (i) gives us a directly computable upper limit, (ii) does not, unless we can find a way to specify what is the nonradiative energy flux not transporting mass, and its amplitude So we consider them in turn, establishing specific heights via (i), then recognizing these are only limits, via (ii).

(i) If there were *no* nonradiative heating by a nonradiative energy flux that does not transport mass, the photosphere would have its T_e distri-

bution fixed by RE, and its density distribution fixed by HE with that T_e determined under RE, up to that region where $U/q \simeq 1/3$. In this photospheric region, U would be determined from this (HE, RE) density distribution, using Equation (13-1) and some observed or assumed value for the mass flux, F_M. That is, we have, for steady-state, spherically symmetric flow

$$F_M = 4\pi r^2 U(r)\rho(r) = \text{constant}, \quad (13\text{-}7)$$

which, in an RE, HE photosphere becomes

$$F_M = 4\pi r^2 U(F_M, \rho)\rho(r), \quad (13\text{-}8)$$

or, explicitly in this photosphere, and using particle concentration instead of density

$$U[F_M, n_H(r)] = 0.642 \times 10^{20} F'_M \times$$

$$\times \left[n_H(r) \left(\frac{r}{R_p} \right)^2 \right]^{-1} \text{km s}^{-1}, \quad (13\text{-}9)$$

where R_p is the stellar photospheric radius, which, for these Be stars, we take as 10 solar photospheric radii, or 0.7×10^{12} cm. F'_M is the mass flux expressed in units of solar masses per year. Under these conditions, and especially in the outer parts of the photosphere which are effectively isothermal with about a 10 percent variation in T_e coming from non-LTE effects, n_H decreases outward quasi-exponentially, under a scale-height $H = kT_e/\mu g$ as in Equation (13-6). Consequently, U increases outward exponentially under the same scale-height. Because the scale-heights, in these photospheres, are so small relative to the stellar radius—$H/R \sim 0.0005$ for $\log g = 4$; $H/R \sim 0.005$ for $\log g = 3$—the r/R term in Equation (13-9) is unimportant. *The value of U at a given radius is fixed by the mass flux, so long as the condition $U/q \lesssim 0.3$ is satisfied.* Table 13-1 illustrates the situation for Be stars with $T_{eff} = 2.5 \times 10^4$ K and 3.0×10^4 K, $\log g = 4$ and 3, and arbitrary F'_M. To exhibit U relative to q, we choose points in the atmosphere where $T_e = T_{eff}$, $T_e = T_0$ (minimum), $T_e = T_{0x}$ (non-LTE maximum). We also give the value of the asymptotic T_e, T_{00}, which is less than T (max). T_e and n_H values are from Mihalas (1972a).

We see that we require $F'_M \gtrsim 10^{-6}$ for a thermal photosphere to become invalid as low as the point $T_e = T_0$. For $F'_M \sim 10^{-7}$ and these models, the photosphere ends very near the point $T_e = T_{0x}$ (max) The range of F'_M for Be stars given in

Table 13-1
U/F'_M at Location of Various T_e*
(velocity in km s^{-1})

T_{eff} / $\log g$		3.0 X 10^4 K				2.5 X 10^4 K			
		T_{eff}	T_0	T_{0x}	T_{00}	T_{eff}	T_0	T_{0x}	T_{00}
4	T_e	30,000	20,340	23,190	22,100	25,000	15,750	18,430	17,920
	q	22.3	18 4	19.7	19.2	20.4	16.2	17.5	17 2
	U/F'_M	1.0 X 10^5	4.0 X 10^6	6.0 X 10^7	–	9.0 X 10^4	6.0 X 10^6	1.9 X 10^8	–
3	T_e	30,000	22,800	25,570	23,800	25,000	16,850	18,970	18,500
	q	22.3	19.5	20.6	19.9	20.4	16.8	17.7	17.5
	U/F'_M	1.3 X 10^6	1.4 X 10^7	2.1 X 10^8	–	6.4 X 10^5	1.2 X 10^7	3.3 X 10^8	–

*T_e, n_H values from Mihalas (1972a)

the literature is 10^{-7} to 10^{-9} $M_\odot \mathrm{yr}^{-1}$, so we choose $r\ (T_{0x})$ as a reference point We note that these conditions refer to the invalidation of the HE condition. However, when U^2/q^2 becomes significant in the momentum equation, it also becomes important in the energy equation Physically, a gas within which there are differential motions with velocities near the thermal value dissipates energy mechanically in the simplest form, acoustic waves arise. (For a discussion of this point, see Thomas, 1983.) So if one is sure that there exist mass fluxes large enough to invalidate the condition $U/q < 1/3$ at some atmospheric point, then one can be sure that, at this point, there will be a nonradiative dissipation of energy, coming at least from this mass flow. Then, at this point, the condition of RE will be violated as well as that of HE.

We stress that if, in addition to the mass flux, there is also some nonradiative energy flux which does not transport mass, then the photosphere ends lower, because the condition of *RE will already have been violated at some lower height* due to dissipation of this nonradiative energy flux. And, it may well be that the mass flux takes much of its energy from this dissipation of energy and heating of the atmosphere by this nonradiative energy flux. Nonetheless, the mass flux, itself, will dissipate energy at this thermal point where flow velocity reaches the range $q/3 - q$. The value of q will be either the photospheric one, if no nonradiative flux exists other than the mass flux, or it will be a higher value, if the nonradiative flux exists. So we come to alternative (ii).

(ii) There exists a nonradiative energy flux, which does not transport mass. Then, very simply, T_e will be raised at every atmospheric point where $dQ/dr \neq 0$. The density distribution entering Equation (13-7) will give, everywhere, higher densities; hence, Equation (13-9) will yield lower U. So, while the breakdown of photospheric conditions will occur lower in the atmosphere than in case (i), from a violation of RE, the violation of HE, because of Equation (13-9) being satisfied, will occur higher in the atmosphere. How much lower in the atmosphere the photospheric conditions break down, and how much higher in the atmosphere the condition of HE is violated, we do not know from present observations except in the case of certain stars observed at eclipse, as already stressed.

Thus, we start from a photospheric model; under alternative (i), we calculate the ratio at which HE breaks down if there is no nonradiative energy flux not transporting mass, by using the value of the mass flux in Equation (13-9). Next, from the realization, by (ii), that these calculations under (i) provide only a limiting value where RE breaks down, we have established bounds on the top of the photosphere. From these, we establish similar bounds on the bottoms of the chromosphere and lower corona.

CHROMOSPHERE. We have defined the chromosphere as the region where RE fails, but HE continues to be satisfied. As in the above, a nonradiative heating must occur somewhere below that point where such a heating would occur from the mass flux alone. So this latter point only fixes an upper limit in height where nonradiative heating, hence the chromosphere, begins And, this upper limit is fixed by setting $U = q\ (T_e)$ Up until such heating begins, $q\ (T_e)$ is fixed by photospheric values, as is the density distribution. So, we compute this upper height limit by setting $U = q$ in Equation (13-7), then choosing $q\ [T_e\ (r)]$ and $n_H\ (r)$ iteratively, for self-consistency from the values given by the photospheric models, to satisfy Equation (13-7), which we write as

$$n_H(r) = 0.642 \times 10^{20} F'_M \left(\frac{\left(\frac{R_p}{r}\right)^2}{q[T_e(r)]} \right) \mathrm{km\ s^{-1}}. \quad (13\text{-}10)$$

Again, because the photospheric density gradient is quasi-exponential in these outer regions of the photosphere, with very small scale-height (in units of the photospheric radius), the term R_p/r is effectively 1 and does not enter the iteration. We obtain the results in Table 13-2, corresponding to the range of values for T_{eff}, g, F_M already used in Table 13-1. For comparison, we adjoin

the corresponding values for the Sun $R_p = r(T_{eff})$.

We see that the value of the atmospheric density at this upper height limit on the beginning of the chromosphere is directly proportional to the mass flux, and varies by only a few percent with gravity and T_{eff}. But the atmospheric height of this point varies inversely as the log of F_M, and inversely proportional to gravity In accordance with what we have already said, these heights are not very large, $r/R \lesssim 1.05$ for log g between 3 to 4 and $\lesssim 1.01$ for the most probable gravity of about 3.7. We have, at present, no reliable way to estimate the nonradiative energy flux not transporting mass, hence, to estimate how much lower actually begins a nonradiative heating. Table 13-2 gives the empirical beginning height for the Sun, compared with the above kind of estimate, we note the difference is very significant, especially in terms of the atmospheric density.

LOWER-CORONA We defined the corona as the region where both RE and HE fail, the former having already failed in the chromosphere. The latter fails in the corona, because U increases upward with the decreasing density; from its value specified at some arbitrary photospheric point, r_0, by photospheric model and the value of F'_M, to the value of $q\ [T_e(r)]$ at some r (LCB), the *lower-coronal-beginning*. Actually, LCB is a region, defined by $q[T_e(r)]/3 < U(r) \sim q[T_e(r)]$. If we knew T_e within this LCB, we would know, numerically, the ratio U (photosphere, r_0)/q (chromosphere, LCB), hence, by Equation (13-7) applied at r_0, and at r (LCB) where U(LCB) = q(LCB), the numerical value of the ratio $(n_H r^2)/(n_{H0} r_0^2)$, hence $n_H r^2$(LCB). So, a knowledge of *either* $n_H(r)$ *or* $T_e(r)$ would locate the LCB in terms of n_H and T_e, in the Be chromosphere we know neither, lacking a specification of the nonradiative flux, or an empirical $T_e(r)$, or $n_H(r)$ such as we have for the solar chromosphere. So, we adopt an iterative scheme to estimate Δr (n_{Hr}/n_{H0}) sufficiently well to place upper and lower limits on n_H and r at LCB.

First, we again emphasize that if there were indeed no source of heating other than that from the mass flux, the lower-corona would begin immediately after the photosphere. The computation of beginning heights of the chromosphere and the lower-corona would coincide, we would need no iteration to set limits on an $(n_{Hr}, \Delta r)$ relation. Both would begin at U(photosphere)$\sim$ q (photosphere) (Table 13-2); the chromosphere, from heating to destroy RE; the lower corona, from momentum input to destroy HE. Observationally, the superionization and superexcitation phenomena would begin, effectively, at the same height where the density gradient departs from quasi-exponential. Observationally, this does not appear to be true. It is definitely not true for the Sun (Thomas and Athay, 1961). For the Be stars we observe some components of the C IV and N V superionized lines with displacements which are small compared with thermal velocities corresponding to the T_e values necessary to produce such ions. (To state, as in some parts of the literature, for example, Cassinelli, 1979, that C IV, N V, and O VI are produced by Auger ionization from coronal X-rays begs the question; one needs to produce the corona, and in the rise of T_e to it, from the photosphere and chromosphere, one passes through those T_e capable of producing these ions.) So, the beginning heights of the chromosphere and corona do not appear, observationally, to coincide. In the Sun, the characteristics of the two regions, separately, can be directly measured at eclipse. In these Be stars, we have only the indirect inference just stated.

So, to estimate this beginning height of lower-corona, we look again at Equations (13-7) to (13-9), from the viewpoint of asking where the condition $U = q\ (T_e)$ is satisfied at the top of a chromosphere that is hotter than the photosphere. RE has already failed; we ask where HE fails. We apply the same Equation (13-10), but use the $q\ (T_e)$ corresponding to chromospheric T_e. Note that these need not be solar chromospheric T_e. Note also that, under our definition, the solar chromosphere would include T_e up to some 10^6 K, because it is there that the lower-corona, measured by our definition in terms of a $U \sim q$, begins, empirically (cf., the various discussions in Jordan, 1981, and Thomas, 1983). So, to compute the density range where the lower

Table 13-2
Upper Height Limit on Beginning of Chromosphere

T_{eff} (10^4 K)	log g	F'_M	n_H	T_e (10^4 K)	$\Delta r/R$ above T_{0x}	r/R
			Be Stars[a]			
3.0	4	10^{-9}	3.3×10^9	2.21	0.0031	1.0066
		10^{-8}	3.3×10^{10}	2.21	0.0018	1.0053
		10^{-7}	3.3×10^{11}	2.27	0.0006	1.0041
		10^{-6}	3.4×10^{12}	2.19	−0.0006	1.0030
3.0	3	10^{-9}	3.2×10^9	2.47	0.027	1.057
		10^{-8}	3.2×10^{10}	2.50	0 013	1.043
		10^{-7}	3.2×10^{11}	2.55	0	1.030
		10^{-6}	3.3×10^{12}	2.30	−0.014	1.016
2 5	4	10^{-9}	$3 7 \times 10^9$	1.79	0.0019	1.0051
		10^{-8}	$3 7 \times 10^{10}$	1.81	0.0010	1.0042
		10^{-7}	3.7×10^{11}	1.84	0	1.0032
		10^{-6}	3.9×10^{12}	1.64	−0.0010	1.0022
2.5	3	10^{-9}	3.6×10^9	1.85	0.018	1.045
		10^{-8}	3.6×10^{10}	1.87	0.007	1.034
		10^{-7}	3.6×10^{11}	1.88	0.003	1.030
		10^{-6}	3.8×10^{12}	1.69	−0.012	1.015
			The Sun[b]			
0.6	4.4	3×10^{-14}	3×10^7	0.42	–	1.004
			Actual, empirical, beginning height of solar chromosphere			
		10^{-14}	1×10^{15}	0 45		1.0007

[a] T_e, n_H values from Mihalas (1972a).
[b] Values from Thomas and Athay (1961)
Dash (–) represents no data at this entry

corona begins, from Equation (13-10), we simply cover the estimated range of T_e Clearly, the photospheric values of Table 13-2 set a lower limit, in the range $2.5 - 3.0 \times 10^4$ K, and the table gives the corresponding n_H where $U = q$. The range $0.5 - 2.0 \times 10^5$ K corresponds to the presence of C IV, N V, O VI. While we have no observations of lines from more highly ionized atoms than these, in the Be stars, we do have observations of some of the forbidden solar coronal lines in "Be-similar" stars, as already remarked. Furthermore, we observe X-rays from

some of these Be stars, so we must consider T_e up to some 10^7 K. We cannot impose, a priori, conditions on the way T_e might vary—impose a T_e (r)—but we can note the solar-inspired suggestions of T_e plateaus rather than a simple monotonic rise (Thomas and Athay, 1961; Athay, 1976, 1981 for summaries) Roughly, plateaus might occur at $0.5 - 1.0 \times 10^4$ K (hydrogen energy loss), $2\,0 - 5\,0 \times 10^4$ K (H Lα and He I, II energy loss), and some 2×10^5 K (free-free, O VI, etc. impurity cooling). The Cox-Tucker (1969) stability calculations suggest a plateau near 1.5×10^6. All plateaus except the 2×10^5 K plateau are observed in the Sun (cf., Athay, 1981; Zirker, 1981 summaries). So, one could manufacture arguments for representing the density variation as that across a series of isothermal plateaus, as the above, separated by jumps. With such a scheme, one could do almost anything one wants. Here, we take the simplest-minded approach. We use either a scale-height corresponding to the photosphere, effectively a 2.5×10^4 K plateau, or a scale-height corresponding to the particular T_e (chromosphere) for which we compute n_{Hr}. The former approximation gives a lower limit on the Δr corresponding to the density change; the latter gives an upper limit.

To apply the method, we need a value of r at the thermal point. We estimate it by asking the relation between Δr and the ratio n_r/n_{0x}, then iterating for r Because the chromosphere is defined as HE, we approximate the density distribution as an isothermal one; we obtain a range of solutions corresponding to the T_e value used for the scale-height. So long as Δr is sufficiently small, the plane-parallel approximation suffices. Set H_p equal to the scale-height from *photospheric* gravity and *chromospheric* T_e; H_{pp} corresponds to *photospheric* g and T_e Then for the density change within any isothermal "plateau," of length Δr, and base concentration n_{0x},

$$\Delta r_p = H_p \ln\left(\frac{n_{0x}}{n_r}\right) . \qquad (13\text{-}11)$$

In Equation (13-11), the value of n_r is that computed from Equation (13-10), using the actual q_r corresponding to $T_e(r)$ of the isothermal plateau. So, clearly an extreme lower limit on the LCB location is that given in Table 13-2 the r where, were there no nonradiative heating below this point, n_r would have decreased sufficiently to raise U (ox) to q (photosphere) As already mentioned, in this situation the beginnings of chromosphere and lower-corona coincide, a chromosphere does not exist; the atmosphere jumps from photosphere to lower-corona.

A nonradiative heating below the reference level r (T_{0x}) simply. (1) raises n_{0x}, and thus decreases U_{0x}, and (2) increases q_{0x} Conditions (1) and (2) combine to doubly increase the ratio $q(\text{LCB})/U_{ox}$, which fixes the ratio $(n_r r^2)/(n_{0x} r_{0x}^2)$ at which LCB occurs. Because we classify the Be stars by their photospheric spectrum, n_{0x} cannot increase above $n_r(T_{eff})$, which is about 200 to 2000 times n_{0x}. Table 13-3 gives the characteristics of these several points r (T_{eff}), r (T_0), r (T_{0x}) in the Mihalas models. A factor 10^2 corresponds to 4 5 density scale-heights, or a $\Delta r/R_p$ of about 0.002 to 0.003, as shown in Table 13-3. So adding this correction (1) does not change significantly the situation from that of Table 13-2 because the Δr comes from a photospheric scale-height. However, correction (2) has a much greater effect because the Δr comes from a chromospheric scale-height; its value depends upon the choice of T_e (chrom).

So we try to approximate an upper-limit on the location of the LCB by assuming that once heating begins, T_e jumps discontinuously to a chromospheric value, and then enters a plateau at that T_e, which lasts to the LCB. Such a jump in T_e, in these regions where $U \ll q$, is roughly hydrostatic, so we take the n_{0x} at the chromospheric beginning to be T_e (phot)/T_e (chrom) times n_{0x} in the photosphere. Since, as above, n_{0x} (photosphere) lies in the range n_{0x} (Table 13-3) to $n_r(T_{eff})$; and since $n_r(T_{eff})$ shows a small range with T_{eff} but a factor 10 as g changes by that factor; and since we simply want to set upper limits; we take n_{0x} where heating starts to be $10^{-1}\, n_r(T_{eff})$ For the Sun, the factor is, empirically, nearer 10^{-2}. The higher is n_{0x} where heating begins, the larger is the nonradiative energy

Table 13-3

. Reference Point Data

$\log g$	T_{eff} (10^4 K) n_H	T_0 n_H	T_{0x} n_H	T_{00} n_H
4	3.0	20,340	23,190	22,100
	6×10^4	1.72×10^{13}	1.06×10^{12}	
4	2.5	15,750	18,430	17,920
	7×10^{14}	$1\ 15 \times 10^{13}$	3.37×10^{11}	
3	3 0	22,850	25,570	23,800
	5×10^{13}	4.64×10^{12}	$3\ 00 \times 10^{11}$	
3	2.5	16,850	18,970	18,500
	1×10^{14}	$5\ 25 \times 10^{12}$	1.96×10^{11}	

$\log g$	T_{eff} (10^4 K)	$\delta r\,(T_{eff}, T_0)/R_p$	$\delta r\,(T_0, T_{0x})/R_p$	$\Sigma\delta r/R_p$
4	3.0	0 002007	0.001453	0.003460
	2.5	0 001786	0.001463	0.003249
3	3.0	0.001382	0.001620	0.003002
	2 5	0 001390	0.001413	0.002803

Source Mihalas (1972a).

dissipation required to change T_e significantly. Finally, we simply take a common T_0 of 2.0×10^4 K, because it is a reasonable average of the model values and because it lies at the lower end of the 2.0 to 5.0×10^4 K plateau. So combining these effects we have for n_{0x} at the base of the chromospheric isothermal plateau (using g–4 means $\log g = 4$)

$$n_{0x}\ (\text{Equation 13-10}) = 2\,0 \times 10^4/T_{chrom}) \times 10^{-1} \times (6 \times 10^{14},\ g\text{–}4, 6 \times 10^{13}, g\text{–}3), \quad (13\text{-}12)$$

also, $r\,(n_{0x})/R_p \sim 0.0001$ for g–4, $\sim 0\,001$ for g–3.

One quickly sees, especially for the small F_M, that for large enough T_e (chromosphere), the Δr requires the spherically symmetric HE relation between Δr and n_{0x}/n_r, even under the isothermal approximation. This HE, isothermal approximation to the chromospheric density distribution is then

$$n_r = n_{0x} \exp\left\{-\left(\frac{\mu g_p}{kT_e}\right) \times \times \frac{(r - R_p)}{(r/R_p)}\right\}, \quad (13\text{-}13)$$

which replaces Equation (13-11) by

$$\Delta r_S \left[1 - \left(\frac{\Delta r_p}{R_p}\right)\right] = \Delta r_p, \quad (13\text{-}14)$$

with Δr_p given by Equation (13-11) and Δr_S being the correct Δr in Equation (13-13). In Equations (13-10) and (13-13), the value of n_r is that from Equation (13-10), and n_{0x} is that from Equation (13-12). One iterates for consistent values of r and n_r between Equations (13-10) and (13-14), with T_e (chrom) as the parameter fixing both q and H_p, for given gravity. From Equation (13-13) we see that ln (n_{0x}/n_r) cannot exceed R_p/H_p; that is, $\Delta r_p/R_p \leq 1$. This limitation is a significant one, under this approximation of the chromosphere consisting of a *single* plateau. For example, at T_e (chromosphere) = 1.10^7 K, and log g = 3, H_p/R_p = 2.4; even at 1×10^6 K, H_p/R_p = 0.24. So, there is possibly only a very small decrease of density, hence increase in U, within this single chromospheric plateau. For very small F_M, which gives small U (r_{0x}), the combination of initial T_e jump and single, but high T_e, chromospheric plateau is inadequate.

For example, a rough model of the actual solar atmosphere consists of the following (1) a photosphere, with n_H $(T_{eff}) \sim 10^{17}$, (2) a chromosphere, beginning at $n_H \sim 4 \times 10^{15}$, whose first part lies in the hydrogen plateau, with T_e rising very slowly from some 5.0×10^3 K to 7.0×10^3 K, over about 1000 km ($\Delta r/R_p \sim 0.001$), and more rapidly, to about 1.0×10^4 K in the next 400 km, with a total density drop of a factor 10^4 across this first plateau; (3) a rapid rise from 1×10^4 K to some $1 - 2 \times 10^6$ K, $n_H \sim 10^9$, with a very small plateau at about 2.5×10^4 K; (4) a "coronal" (chromospheric, under our definition) plateau at this $1 - 2 \times 10^6$ K, across which n_H drops by a factor 10^3, reaching about 10^6 at some 2 radii. The lower-corona begins, and the upper-corona begins—under our definition—between 2 and 3 R_p. Our above, single-plateau, representation would attempt to model the n_H decrease, from some 4×10^{15} to some 10^6, by a product of the factors (T_0/T_{chrom}) and the exponential drop, at scale-height H_p, across the chromosphere For $T_{chrom} \sim 1\,5 \times 10^6$, and $T_0 \sim 5.0 \times 10^3$ K, the first factor is 300, leaving a factor about 1×10^7 to be matched by the change in $(n_H r^2)$ At this T_{chrom}, the limiting ratio for n (n_{0x}/n_H) from Equation (13-13), R_p/H_p, is some 7.6, leaving a factor some 10^4 to be matched by the change in r^2. So, one decreases the maximum T_{chrom}, thus H_p, as seen in Table 13-4, and the single-plateau model is inadequate for this low F_M.

This Table 13-4 presents the results of these upper and lower limits on the LCB, as a function of F'_M and g, for the range of T_e considered. Again for comparison, the solar predictions from the single-plateau modeling are given. Before commenting on the results of this table, taken in conjunction with the lower height limits of Table 13-2, it is useful to consider the beginning point of the upper-corona, given by the condition that $U^2 = q^2 = W^2/2$. In the present approach, where the mass flux is taken as a parameter, one has explicit expressions for both r/R_p and n_H, namely

$$r/R_p = 2.08 \times 10^3 (10^{-4} T_e)^{-1} \times \times (10^{-4} g_p)(R_p/10R_\odot), \quad (13\text{-}15)$$

and

$$n_{Hr} = 1\,15 \times 10^{12} F'_M (10^{-4} T_e)^{3/2} \times \times (10^{-4} g_p)^{-2} (R_p/10R_\odot)^{-4}. \quad (13\text{-}16)$$

Table 13-5 exhibits sample values, corresponding to the chromospheric-coronal T_e values used in computing the beginning point of the lower-corona Again, the Sun is included for comparison. Likewise, we consider the case $F'_M = 10^{-6}$.

Consider, now, these results from Tables 13-2, 13-4, and 13-5 to delineate the distinctions between the regions chromosphere, lower-corona, upper-corona, and their locations. Clearly, all this must be in the context of what we understand on conditions in post-coronal regions. We arrange our comments in terms of the approximations underlying these tables

A. *Conclusions under the assumptions leading to Tables 13-2, 13-4, and 13-5*: namely, neglect of radiative acceleration and stellar rotation, single-plateau representation of chromosphere, and a photospheric reference point set at $n_H = 10^{-1}$ $n_H(T_{eff})$.

Table 13-4
Lower Coronal Beginning Height

Log F'_M	log g	T_{eff} (K)	T_{chrom} (K)	n_H Lower Limit	r/R_p Lower Limit	n_H Upper Limit	r/R_p Upper Limit
−9	4	30,000	5×10^4	3.5×10^9	1.005	2.16×10^9	1.01
			2×10^5			1.02×10^9	1.04
			8×10^5			3.95×10^8	1.19
			1.5×10^6			1.99×10^8	1.43
			3.0×10^6			2.68×10^7	3.27
	3	30,000	5×10^4	3.3×10^9	1.038	1.84×10^9	1.10
			2×10^5			4.77×10^8	1.53
			3×10^5			1.80×10^8	2.26
			1.5×10^6				
−7	4	30,000	5×10^4	3.6×10^{11}	1.003	2.19×10^{11}	1.006
			2×10^5			1.07×10^{11}	1.022
			8×10^5			4.87×10^{10}	1.07
			1.5×10^6			3.17×10^{10}	1.13
			3.0×10^6			1.72×10^{10}	1.30
			5.0×10^6			7.61×10^9	1.71
			6.0×10^6			3.53×10^9	2.40
	3	30,000	5×10^4	3.5×10^{11}	1.015	2.08×10^{11}	1.03
			2×10^5			9.14×10^{10}	1.10
			8×10^5			2.24×10^{10}	1.58
			9×10^5			1.23×10^{10}	2.07
−6	4		5×10^4	3.5×10^{12}	1.001	2.20×10^{12}	1.003
			2×10^5			1.09×10^{12}	1.008
			8×10^5			5.36×10^{11}	1.020
			1.5×10^6			3.85×10^{11}	1.027
			3.0×10^6			2.72×10^{11}	1.029
			5.0×10^6			2.18×10^{11}	1.012
	3		5×10^4	3.5×10^{12}	1.004	2.20×10^{12}	1.002
			2×10^5				<1.0001
			1.5×10^6				

Table 13-4 (Cont.)
Lower Coronal Beginning Height

The Sun. $F'_M = 3.0 \times 10^{-14}; n_0 = 3.8 \times 10^{15}\ (6000/T_{chrom})$

T_{chrom}	1.0×10^4	2.5×10^4	5.0×10^4	2.0×10^5	4.0×10^5	4.5×10^5
n_H	1.44×10^7	8.68×10^6	5.61×10^6	1.53×10^6	2.54×10^5	9.17×10^4
r/R_p	1.018	1.043	1.088	1.47	3.06	4.93

1. From Tables 13-2, 13-4, and 13-5 we see that the thermal-point, where $U \sim q$ for the first time, always comes before the escape point, $U^2 = q^2 = W^2/2$, and that the two points are sufficiently separated so that the lower-corona has a very significant extent. A complete coverage of the range in T_{chrom} for the given range in F'_M is inhibited for two reasons

a The inadequacy of the single-plateau representation already discussed, via the solar example. To try to improve the representation by introducing two plateaus requires guessing the transition point between plateaus, so this is not useful at this point. But this uncertainty does not change any conclusions, so widely separated are thermal and escape points for the Be F'_M.

b. Some entries in Table 13-4 for F'_M of 10^{-6} and 10^{-7} are marked "< 1.0001" for r/R_p. The point here is that for these large F_M, $U \gtrsim q$ already at the adopted reference point. We can extend the solution by dropping the reference point to $r(T_{eff})$, thus increasing n_{0x}; but even here, for the larger F_M, one obtains $U \gtrsim q$ already at the $\tau = 1$, photospheric level. The interpretation is clear: at such large F'_M, the star ceases to be observed as having a normal photosphere: one sees only a chromosphere, at least because of the mass flux heating, even if from no other nonradiative energy flux. We have argued for some time (Thomas, 1968), that such a phenomenon is the underlying cause of the Wolf-Rayet phenomenon; that is, a Wolf-Rayet spec-

Table 13-5
Characteristics at the Escape Point

T_e (chrom) K	5.0×10^4	2.0×10^5	8.0×10^5	1.5×10^6	5.0×10^6	1.0×10^7
Be stars						
$(10^{-4} g_p)^{-1} (r/R_p)$	410	104	26	13.9	4.2	2.0
$(10^{-4} g_p)^2 (F'_M)^{-1} n_H$	1×10^{13}	1×10^{14}	8×10^{14}	2×10^{15}	1×10^{16}	4×10^{16}
the Sun						
r/R_p	110	29	7.1	3.8	1.13	–
n_H	5.0×10^2	4.0×10^3	3.0×10^4	8.0×10^4	5.0×10^5	–

trum, in either a standard Wolf-Rayet star, or those central stars of planetary nebulae showing a Wolf-Rayet type spectrum. Such interpretation follows the logic of the Struve-Beals sequences which were discussed earlier. That is, conditions in the outer atmosphere, and the physical parameters (especially mass and nonradiative energy fluxes) fixing them, are responsible for the "variety" among the stars in the sequence. Also, of course, they are responsible for the individuality.

2. Superficially, from Table 13-2 and Table 13-4, one would conclude that the way to get the large n_H (10^{11} to 10^{12}) demanded by the usual Hα emission models is to try to construct a model having no chromosphere, only an abrupt rise from photosphere to lower-corona, but a cool lower-corona, possibly remaining in the lower T_e end of the $2.0 - 5.0 \times 10^4$ K plateau. After all, one does observe in the Sun a short plateau at 2.5×10^4 K. The advantage of the suggestion is that one would start the r^{-2} density variation of the lower-corona at values of n_H sufficiently large to match the above n_H required by the Hα observations. (Note that the Marlborough et al. equatorial concentration models start with an $n_H \sim 10^{13}$ at the base of their r^{-2} region. By going to a spherically-symmetrical model, one can reduce n_H by about a factor of 40, hence, the above values.) The problem of the suggestion is two-fold. how to avoid excessive heating associated with the $U \sim q$ flow or how to reconcile the model with the Fe II observations on the one hand, and those of the superionized ions on the other, as already discussed.

The nonradiative heating occurs at least by the flow $U \sim q$, probably also by a nonradiative flux not transporting mass. Because the Be photospheric radiation field keeps hydrogen ionized, for these stars, the mechanical heating in this plateau need only keep He I and He II ionized. On the other hand, the observed/inferred small Δr for the solar $2.0 - 5.0 \times 10^4$ K plateau is not a fatal argument against a longer extension in the Be stars. In the Sun, the $n_H \sim 10^9$ to 10^{10} in this plateau; for the Be stars, one would have the 10^{12} to 10^{11} to 10^{10} required by an Hα emission out to some $10R_p$. Since cooling goes as n^2, one has a factor 10^2 to 10^6 increase in the cooling rate. One could also understand the low, $U \leq 100$ km s^{-1}, velocities associated with Hα emission, since q in this plateau ≤ 30 km s^{-1}. To us, the principal arguments against this alternative are those already stated, relative to the presence of Fe II and the superionized ions from Si IV through O VI. There may or may not be advantages in separating the Hα and Fe II regions, because one cannot produce Fe II in this $2.0 - 5.0 \times 10^4$ K plateau, and so, it must arise in the post-corona. But we would require the superionized ions to begin at the end of the plateau, at some $10R_p$, as well, of course, as the X-ray emitting regions. This seems difficult to accomplish in the ordinary Be stars; the distinction between τ Sco and ζ Oph, γ Cas, 59 Cyg is even more difficult. The argument would have to be that a smaller F'_M for τ Sco prohibits such a low lying $2.0 - 5.0 \times 10^4$ K plateau. The r^{-2} density variation, begins higher; cooling rates are lower, for τ Sco. We dwell on this alternative for completeness; we do not favor it, for the reasons given.

3. The solar comparison, especially with the results for the smaller F'_M, shows the reason that the assumption in the Parker theory—that thermal and escape point, hence, lower and upper corona, coincide—appears adequate for the Sun but is actually not true. As F_M decreases, the two points move closer together. As mentioned, our modeling approximation of a single-plateau chromosphere does not suffice to represent the solar situation.

One should be very clear just what kind of physical theory actually is in the Parker approach. Given a value of T_e (corona), one predicts r/R_p from Equation (13-15). With this T_e and a value of n_{H0} at the base of the coronal plateau, one predicts a value for F'_M, by inverting our present procedure, from Equation (13-16). One chooses the value n_{H0} observationally, not from any theory of the atmospheric structure in the corona and below. To construct the latter, one would need a theory of the nonradiative energy flux in the Sun. Approximations to this exist, but for some 40 years astronomers have been debating what it actually is, and to what nonradiative

energy dissipation it leads. One is not even certain, observationally, what this dissipation is, to an order of magnitude or so. Various authors have attempted to predict the mass flux "theoretically," by assuming values for coronal T_e, and the base pressure of the corona—or of the underlying chromosphere, and applying the kind of jump condition for n_H at the top and bottom, in terms of the T_e ratio which we have used. The difference is that this representation, under the Parker approach, is a multi-plateau model, in which attention is restricted to just the last plateau, that at some $1.0 - 2.0 \times 10^6$. In abstract, the Parker theory consists of an application of Equation (13-5), as we do, under the speculation that beginning points of lower and upper corona coincide. The validity of this speculation remained to be shown. The underlying aerodynamics of it and the observational evidence for coincidence or noncoincidence in the Sun, are discussed in Thomas (1983) Here, we have simply asked what the observational evidence on the Be stars says about the approach, and we do not find it applicable to them. We have already mentioned theoretical investigations of Hearn and Vardavas (1981), which are unsuccessful at producing large F'_M, as predictable from the preceding paragraph. All this is one of the reasons that we think that Be star atmospheric modeling must, at present, be restricted to an empirical approach. As we continue to emphasize, *especially* in the post-coronal regions, we have too little observational insight for even a satisfactory empirical modeling.

B *The effect of including rotation* clearly, the effect is essentially a modification of the equatorial gravity without modifying the polar. However, as summarized in Chapter 11, there is little evidence that the rotational velocity has the critical value, so that gravity is greatly reduced. We saw that a rotational velocity of 300 to 400 km s^{-1} is indeed a large value. W (photosphere) for a Be star with gravity 4 and the 10 $R_\odot$ radius used is some 830 km s^{-1} Hence, the *effective* W, at the equator, is 775 to 735 km s^{-1}, or the equatorial gravity is modified to some 0.87 to 0.77 times the polar value. From Table 13-4, we see the effect on the location, and the density there, of such a slight modification of gravity; from either Table 13-5 or Equations (13-15) and (13-16), we see the effect on the location of, and density at, the escape point. It is hardly major, although large enough to give the small polarization actually observed. One also recalls from Chapter 12 that no gross differences are observed in mass flow or superionization.

C. *The effect of including the radiative acceleration* terms can be seen from Equation (13-5). We can rewrite it in the form

$$U \frac{dU}{dr} \left[q^2/U^2 - (1 - K\left(U \frac{dU}{dr}\right)^{-1+\alpha} \times \times [\rho Uq]^{-\alpha}) \right] \qquad (13\text{-}17)$$

= right-hand side of Equation (13-5).

Our discussion of the flow in the lower-corona, based on this equation without the radiative-acceleration term, rests on laboratory experience in the trans-sonic flow regime. As U approaches q, the left-hand side of the equation has the bracket approach zero. Because the right-hand side has no zero at this point, unless the flow is at the escape point $W^2 = 2q^2$, which it is not in the lower-corona, either dU/dr becomes arbitrarily large, or one must introduce the time-dependent terms in $\delta U/\delta t$. Physically, the flow oscillates about a mean flow $U = q$; locally, the time-dependent terms keep the left-hand side of the equation from vanishing. One can observe various flow patterns, where $U \sim q$, and can see a system of acoustic waves produced by the fluctuations (see, for example, Charters and Thomas, 1945, and the extensive series of photographs at the Aberdeen Ballistic Research Laboratory on which the article is based. The phenomenon is equally well known from a variety of other experiments in a variety of aerodynamic/ballistic laboratories). We discuss this at greater length in Thomas (1983). Here, however, we ask the influence of the radiative-acceleration term upon this rough picture of the flow without the term.

Since the right-hand side of neither of the Equations (13-5) or (13-17) involves the radiative-acceleration term, its presence does not affect them So, by the above logic, one enters the same kind of fluctuating configuration, but about a

mean flow $U = q\ (1 - \delta)^{-1}$, where δ is the radiative-acceleration term, hence positive; so U exceeds q Also, since $0 < \alpha < 1, \delta$ is the smaller, the larger is dU/dr, and the larger are U and q. Hence, for given K, which is fixed by the radiative-flux in the accelerating spectral lines, δ is the smallest, near where U enters the transthermal regime. So, we do not expect a large δ, especially deep in the atmosphere, where the lower-corona begins, from the preceding discussion. Rather, we expect radiative acceleration to be the most effective in the post-T_e (max) regions.

We should note the interesting dilemma if we try again to make the best case for a cool lower-coronal, post-photospheric region. Within the 2.0 $- 5.0 \times 10^4$ K plateau, one can find the ions the radiative-acceleration proponents need; indeed, it is this T_e region which they consider, under their cool, radiative equilibrium flow models. But then, the radiation field tries to accelerate U and meets the above problem So the rate of mechanical dissipation of energy rises, and one is forced out of the cool coronal plateau by this effect alone. Unfortunately, the radiative-acceleration theories do not include such dissipation terms, preferring, as a first approximation, to ignore such effects (Abbott, 1980).

UPPER-CORONA The problems of locating the beginning height of the upper-corona have already been summarized. Since the region ends on entering the transition-region where acceleration and cooling occur, it is clear that the extent of the upper-corona is, observationally, very vague. Clearly, the gas does cool, as evidenced by the observed Si IV, C IV, N V, and O VI line components, in various stars, at velocities of the order of 1000 km s^{-1}. This is really all we know, hardly sufficient for empirical modeling.

TRANSITION-REGION. By analogy with current planetary-nebular observations, one thinks the gas can only decelerate by interaction with a slower mass flux from an earlier epoch So one produces something akin to the planetary nebula; but from all evidence, the production of nebular-like regions bounding the mass flow must occur much more often than in the planetary nebulae case. In 59 Cyg and γ Cas, one observes the disappearance and reappearance of Hα emission characteristics in "cycles" of 30 to 100 years, if one can misuse the word "cycle" so badly. For ζ Oph, the corresponding times are 2 to 10 years. Clearly, there is little empirical guidance as to characteristics of such behavior, let alone clues as to its origin. But it seems clear that we need to model the Hα-emitting region as more nearly a balloon, or a cavity which is filled and voided, rather than as a steady-state, outward mass flow.

Current observations of 59 Cyg offer the best hope that we can develop some insight into these post-coronal regions, empirically. 59 Cyg dropped to its nearly normal B phase in 1977. Today, almost 4 years later, the level of Hα emission is only some one-twentieth of what it was in the pre-1977 years of normal, and bright, Be phase. For the observed outflow of some 1000 km s^{-1}, one would, in a year, reach $\pi \times 10^{10}$ km, or 5000 photospheric radii. Clearly, we are looking at a cavity or balloon–filling process rather than a simple outflow. So, one is curious as to how reliable are our above glib demands for concentrations near 10^{13} to 10^{11} at the base of the Hα-producing region. Possibly we can indeed model the Be stars as "little planetary nebulae" in the location of their Hα "shell" as well as of the forbidden nebular lines in the Bep spectra. A simple calculation illustrates the point.

The models of a Be star like γ Cas, by Marlborough (1969) and Poeckert and Marlborough (1978a) are among those requiring densities of some 3×10^{13} just at the end of the photosphere, in order to represent the observed Hα emission under their model. These models are of an equatorial concentration; so a spherically symmetrical model is satisfied by somewhat smaller densities. Other estimates–the references are cited in Chapter 11–also estimate such densities as lying in the 10^{13} to 10^{12} range, for a more vaguely defined distribution of emitting material Clearly, a major uncertainty is the excitation state–the value of n_3 for an optically thin gas, or of the Hα source-function for a thick gas. But given all these uncertainties, one can give a rough, order-of-magnitude, com-

parison of the equatorial-concentration, to the spherically-symmetric, model, in terms of what concentrations are demanded for the Hα-emitting region

Hydrogen is strongly ionized everywhere in the Poeckert-Marlborough model ($T_{eff} \sim 2.5 \times 10^4$ K; $T_{envel} \sim 2.0 \times 10^4$ K), but this is so only interior to r/R about 1.5, and only about half-ionized in the remainder of the 10^4 K envelope, in the Marlborough model. Roughly,

$$n_3 \sim 10^{-20} n_e^2 \quad \text{Poeckert-Marlborough model}$$

$$n_3 \sim 10^{-20} n_H^2 \quad \text{Marlborough model,} \quad (13\text{-}18)$$

n_H is total (hydrogen) concentration. In each model, an n varying as r^{-2} is a reasonable approximation, and it is roughly exponential in z, perpendicular to the equatorial plane, with a scale-height increasing roughly as 0.1 r/R. Thus, roughly

$$n_3 = n_3\left(\frac{r}{R} = 1, z = 0\right)\left(\frac{r}{R_0}\right)^{-4} \exp\left(-\frac{2z}{0.1r}\right) \quad (13\text{-}19)$$

So for the equatorial concentration model, we have for the total number of hydrogen atoms:

$$N_3 = \int_0^\infty n_3\left(\frac{z}{R_0}, \frac{r}{R_0}\right) dz \int_{R_0}^{r} 2\pi r\, dr, \quad (13\text{-}20)$$

so

$$N_3 = n_3\left(\frac{r}{R} = 1, z = 0\right) 0.1\pi\left(1 - \frac{R_0}{r}\right) R_0^{-1}, \quad (13\text{-}21)$$

while for the spherically symmetrical distribution, under the same $(r/R)^{-2}$ law for total density, we have

$$N_3 = \int_{R_0}^{r} 4\pi r^2\, n_3\left(\frac{r}{R}\right) dr, \quad (13\text{-}22)$$

so

$$N_3 = n_3\left(\frac{r}{R} = 1\right) 4\pi \left(1 - \frac{R_0}{r}\right) R_0^{-1} \quad (13\text{-}23)$$

Thus we have, if we require the same value for N_3,

$$\frac{n_3\left(\frac{r}{R} = 1, z = 0\right)}{n_3\left(\frac{r}{R}\right)} = 40. \quad (13\text{-}24)$$

So, if the equatorial concentration requires 3×10^{13} for the concentration at its base, the spherically symmetrical distribution can survive on a concentration of 10^{12}

This last conclusion is what underlies the remarks, in discussing the lower-corona, that it would be easiest in reproducing the Hα emission, if the star could produce just a photosphere plus a cool lower corona on the $2.0 - 5.0 \times 10^4$ K plateau. We have discussed this alternative sufficiently. Rejecting it, one has problems in getting an n_H larger than some 10^{11}, even in a lower-corona just hot enough to produce the observed C IV-N V-O VI, at U about a few hundred km s^{-1}. This means one arrives, just marginally, at about 10^{10} as a concentration at a few radii. From Equation (13-23), it is clear that it really does not make much difference how far the Hα region extends, *except* for the dependence of excitation upon r, for an order-of-magnitude estimate of N_3 And unless one abruptly introduces a sufficient drop in hydrogen ionization to increase strongly the Hα opacity, the excitation of the n_3 level must decrease outward. Each of these considerations, plus that requiring Hα to be formed in a region where $U \lesssim 100$ km s^{-1}, suggests that the "interaction" with the F_M of an earlier epoch occurs within these few radii from the star That is, the "balloon" begins already, within these few radii As already noted in the previous section, further speculation is unwarranted until we have more observational

guidance. If the reader does want to speculate, we suggest that he focus his attention on this problem of what is required, compatible with existing observations, to produce a "balloon" compatible with all these requirements on concentration level and variability, especially in their linkage with the two nonthermal fluxes mass flux, and nonradiative energy flux not transporting mass

INFERENCES ON THE GENERAL STELLAR STRUCTURE REQUIRED TO GENERATE THE NONTHERMAL FLUXES WHICH PRODUCE THE OBSERVED ATMOSPHERIC PATTERN

We began this chapter with a succinct abstract of the inadequacies of the standard atmospheric model for *normal* stars like the B stars, but also extending throughout the HR diagram, and for *peculiar* stars, of which our present examples are the Be and some similar stars, but which also cover the HR diagram. In essence, from the observational material summarized in this volume, the inadequacies are striking and definitive *For both normal and peculiar stars, observations demand nonthermal fluxes of nonradiative energy and mass*, for the peculiar stars, evidence is noncontroversial that such fluxes are strongly variable, and can differ strongly among stars of the same MK taxonomic class having the same radiative energy flux and gravity so, classically, considered as identical The standard atmospheric model rests on the assumptions that its properties are fixed only by a radiative energy flux coming from the subatmosphere, and a gravity, and by applying the thermal (static) conditions of hydrostatic equilibrium and radiative equilibrium. The only kind of a subatmospheric structure compatible with such restrictions is that of a thermal (static) star, that is, a closed thermodynamic system, with no fluxes other than energy, and these are forbidden to vary over nonevolutionary time scales. For an isolated system, such as the star under this model, the energy flux can only be radiative So, observations contradict the thermodynamic basis of the standard model, not just some of its details.

In this chapter, synthesizing the observational material into an empirical pattern of atmospheric structure, and noting the characteristics of variability and individuality among stars of the same MK class, *we found it necessary to treat radiative energy flux, nonradiative energy flux, and mass flux as independent parameters*. We found it necessary to take each of them as given, at the top of the subatmosphere. We found some trends among them, but no correlations *We found no indications among them or among atmospheric phenomena, that one or several of the parameters could be predicted from the others plus gravity, or even the others plus a rotational velocity*. The inference is clear. Not only is there a basic thermodynamic difference between a standard model (closed, thermal system) and an actual star (open, nonthermal system), but there appears to be no simple way to slightly perturb the closed system of the model to produce the open system of the actual star So, if one wants to go farther than we did in the preceding section—try to predict, rather than simply measure or assume, values of these three fluxes and gravity—*one must apparently ask what are the nonthermal configurations of the subatmosphere, whence these fluxes arise.*

This viewpoint is not very widespread. Apart from our own efforts, there is only the example of Limber's work and its implicit realization in all the nonstatic ad hoc modeling of the atmospheres of Be stars the mass flux was chosen as an empirical parameter, presumably imposed, in some unknown way, by the subatmosphere. Unfortunately, such mass flux was, generally, restricted to the equatorial plane, contradicting recent observations, but this is irrelevant, as regarding the origin of the mass flux In the more current literature, there have been, grossly, two approaches which consider the mass flux to be predictable from atmospheric characteristics alone A *Radiative-origin*, B. *Coronal-origin*.

Atmospheric Origin of Mass Flux

A. Radiative-origin: The more restrictive was the resurrection, by Lucy and Solomon (1970), then by Castor et al (1972 et seq.), of a radiative ejection of material, originally popularized by

Milne, for the Sun, in the 1920's, and by Gerasamovic, for the hot stars, a few years later. In these efforts, a nonradiative energy flux is ignored, and several ad hoc conditions on the mass flux are imposed to predict the mass flux as a function of radiative field, gravity, and chemical composition of absorbing species. Neither mechanical heating, hence superionization, nor variability are allowed. In spite of the initial promise of this type of theory, it does not seem useful here to linger on its details. We can do no better than abstract parts of a very recent review article by Lamers (1981c), which summarizes the impact of modern observations made from space on the predicted models We reorder different aspects of his critique for greater coherence, but otherwise use his own descriptive summary. We do make several comments at the end of the following paragraphs, which are quoted from Lamers (1981c).

Lamers on Mass Loss Rates

"The most extended set of mass loss rates for early-type stars prior to IUE was from Barlow and Cohen (1977) based on the infrared excess of 44 luminous O, B, and A stars, ranging in temperature from 8500 to 50,000 K. The rates derived by these authors show a correlation with luminosity $\dot{M} \sim L^{1.15}$ These observations provided a very strong argument in favor of the radiation-driven wind theory from Castor et al. (1975), which predicted $\dot{M} \sim L^{1/\alpha}$ with $\alpha \sim 0.80$ and a very weak dependence on gravity. However, the stars studied by Barlow and Cohen were only supergiants and there was some indication that at least one main-sequence star (τ Sco, B0 V) had a much smaller rate

"Obviously, the luminosity is not the main parameter which determines the mass loss rate, contrary to the predictions of the radiation-driven models. This suggests very strongly that we may have to look for an alternative mass loss mechanism which should be closely connected to the evolution stage of the star and thus its interior structure."

Lamers on the Acceleration of the Stellar Wind

"Whatever the mechanism may be that determines the mass loss rate from a star, the large outflow velocities which have been observed in the ultraviolet resonance lines are most likely due to radiative acceleration (e g., Cassinelli et al , 1978). One way to determine the acceleration is to measure the terminal velocity, u_∞, reached in the wind at a large distance from the star. (This should not be confused, as is often done, with the edge velocity u_{edge}, measured from the extension of the violet wings of the ultraviolet resonance lines; for stars with a small mass loss rate u_{edge} can be much smaller than u_∞)

"The most extensive study of terminal velocities, prior to IUE, was made by Abbott (1978), who found $u_\infty \sim 3 \times u_{esc}$ This agreed very well with the radiation-driven wind models, which predict $u_\infty = u_{esc}\, \alpha/(1-\alpha)^{1/2}$, with $\alpha \simeq 0.90$. The IUE observations of late B- and A-type supergiants show that the ratio u_∞/u_{esc} decreases toward the cooler stars and reaches a value of about 0.5 for A-type supergiants (Lamers et al., 1980, figure 3)" (see comment 1)

"This suggests that not only do we have to look for another mass loss mechanism for hot stars, but also for an additional mechanism to accelerate the winds, at least in Wolf-Rayet stars.

"The winds of early-type stars are variable on a time scale of hours-to-years. The observations of a few early supergiants and of Be stars show that stars may go through active phases in which puffs or shells are ejected frequently. For one star, ζ^1 Sco, the active phase was found to coincide with a decrease in visual magnitude" (see comment 2)

Lamers on the Heating of Stellar Envelopes

"The Copernicus observations have shown that the stellar winds are superionized, i e., the degree of ionization is higher than can be accounted for by a wind in radiative equilibrium with the photospheric flux. In particular Snow and Morton (1976) and Lamers and Snow (1978) have shown

that there is a one-to-one correlation between superionization and mass loss (including the Be stars), suggesting that the two phenomena are in some way connected to each other. The origin of this superionization is unknown, but its presence indicates that somewhere above the photosphere, the stellar gas is heated considerably" (see comment 3a).

"Secondly, the IUE observations of the two extreme supergiants P Cyg (B1 Ia) and ζ^1 Sco (B1 Ia – 0) which have a mass loss rate of about 2×10^{-5} $M_\odot yr^{-1}$ show the presence of narrow absorption features or P Cygni profiles of low ions (Fe II, Al II, Mg II) in the wind (Hutchings, 1979; Cassatella et al., 1979; Wolf and Appenzeller, 1979). Although the winds of early type supergiants are generally superionized, the winds of extreme supergiants with very large mass loss rates have a low degree of ionization. This behavior might be explained by assuming that the dissipation of nonthermal energy in the stellar envelopes is not sufficient to heat the very dense winds of extreme supergiants because of the high radiative cooling rate. This situation resembles the presence of low ionization stages such as Fe II in the spectra of early-type shell stars" (see comments 3a and 3b).

"The presence of hot gas in the stellar winds as first suggested by the UV lines from high ionization stages such as N V and O VI, is confirmed by the observed x-ray fluxes The winds of the extreme B-supergiants with $\dot{M} \simeq 2 \times 10^{-5}$ $M_\odot$ yr^{-1} and the dense shells of shell stars, however, have low ionization and excitation temperatures" (see comments 3a and 3b).

Lamers' Summary

"The examples which I have given are in a way extremes in terms of variability or mass loss. It is *possible* that we can explain the physics of the more normal mass losing stars by ignoring these extremes I am afraid, however, that this is not very *likely*."

It is useful to adjoin the following comments to Lamers' summary, simply for clarification, mainly from additional data One can debate the details of the rest of what he says, but any changes only aggravate that disagreement between observations and the theory of radiative-acceleration *origin* of mass flux and heating which Lamers emphasizes.

1. Surprisingly, it seems almost habitual for advocates of the radiative-acceleration origin theory to quote $\alpha = 0.8$ to match mass-loss data, and $\alpha = 0.9$ for terminal velocity data; clearly, *one* value of α should be used for both. Note $\alpha = 0.8$ applied to terminal velocities gives u_∞ / u_{esc} of 2 rather than the 3 quoted from the data. But we also note the fit with the data is much worse, with much more scatter, than Abbott claims But more important, note also from our preceding discussions that the *idea of a terminal velocity*, especially when values inferred from far ultraviolet data are applied to radio measures, *seems invalidated* by the observations. Velocities in the region of origin of the far ultraviolet lines reach values of the order of 1000 km s^{-1}; in the overlying Hα regions, velocities are of the order of 100 km s^{-1}, our empirical atmospheric scheme places the cool, far infrared and radio, regions even more exterior, thus being characterized by an equally low velocity. Any *terminal* velocity can hardly exceed these low velocities

2. We recall our extensive discussion of the mass flux active phases versus the brightest Hα emission phases.

3. We must distinguish between the relation of superionization to mass loss, and the relation of subionization to both these quantities

(a) We have discussed in Chapter 12 the present status of the suggestion, by Snow and Morton (1976) and Lamers and Snow (1978), of any one-to-one relation between superionization and mass loss. Here, Lamers himself contradicts the relation by emphasizing the *lower* degree of superionization to the *higher* mass flux in the supergiants, P Cyg and ζ^1 Sco. We have summarized that evidence, from individuality and variability, among the Be stars which also invalidates any idea of such a one-to-one relation. Furthermore, at our epoch, the immediate origin of superionization seems well established; it and the associated X-ray emission from the coronal

regions correspond to that dissipation of a nonradiative energy flux which produces chromospheres and coronae throughout the HR diagram.

(b) The presence of Fe II in supergiants *may* imply similar physical conditions to those producing it in Be star shell phases, but the origin is hardly an insufficiency of nonradiative heating As we discussed at length, it is a manifestation of subionization in such stars, far exterior to the regions of mechanical heating As we have stressed, the presence of Fe II in such hot stars reflects the same phenomena as does the presence of strong Hα emission in stars showing O VI, N V, C IV.

B. Coronal-origin: This theory is less restrictive than the radiative origin, in that it admits one more parameter a nonradiative energy flux Again, it also imposes an extra condition to be able to predict the size, and velocity at a specific point, of the mass flux. It *imposes* that the flow velocity first becomes thermal at the same point where it reaches the escape velocity. Thus, under our definition, such a theory requires the beginning point of the lower-corona to coincide with the beginning point of the upper-corona. Clearly, there is no a priori physical reason for such imposition. In the empirical modeling of the preceding section, we illustrated the inconsistencies arising from its imposition, both a priori physically, and observationally for Be stars. And finally, for the large mass fluxes, 10^{-6} and greater, one requires T_e of some 10^7 K at very high densities; whether a source for the required large nonradiative energy fluxes can be found, remains to be seen. The problems encountered in the work of Hearn and Vardavas (1981) cited illustrate the point. And, apart from this work, no serious attempts have been made to apply the theory to actual observations. Again, the problems of variability and individuality have not been addressed by the advocates of this theory.

Then, if one rejects both the radiative-origin and coronal-origin theories for predicting the size of the mass flux, rejects them because of strong observational discord with the assumptions defining them, one is left with the conclusion that the star is an open thermodynamic system, in full nonthermal nondegeneracy That is, observations show the star to have a mass flux which is nonthermal· that is, the mass loss is not a simple, linear, "boiling off" of materials, from the outer atmospheric layers. This defines the star as being an open thermodynamic system, from which, generally, one must expect radiative, nonradiative, and possibly other energy fluxes, and a mass flux. Equally generally, such fluxes must, a priori, be allowed to be an independent system, produced, independently but in parallel, by the properties of the thermodynamic object as a whole Under the classical stellar modeling of a star as a closed thermodynamic system—no mass flux—the properties of the single remaining flux, the radiative flux, were set by the internal structure of the star. Because this structure was thermal, one did not need to know any storage modes for matter and energy, only the total mass of the star, and its composition. The radiative flux did not vary except in evolutionary times.

The exception was cepheids, and similar stars, for which nonthermal oscillation modes arose from an opacity instability, but thermal in origin. A thermal, linear, instability amplified to a nonlinear one. Classically, such cepheids were not modeled as having any significant mass flux; what effect a very large mass loss might have on the system has never been investigated.

The radiative-origin theories of mass loss proceeded on the assumption that one still needs a knowledge of *only* the radiative energy flux, the mass flux is predictable from it. The first discord with observations was the presence of superionization, implying a nonradiative energy flux as well as radiative. These radiative-origin theories did not predict such a flux, presumably, their basic assumptions must be modified to include such a nonradiative flux as an independent quantity. So their thermodynamic conditions become less restricted, as in the coronal-origin theory.

The coronal-origin theories of mass loss start from the premise that the stellar kind of open system has a mass flux which is predictable from a knowledge of its energy fluxes; so it is also a *restricted* open system. While such a system can

be variable, and not necessarily periodic in any sense, one must *either* find all stars of the same luminosity, gravity, and composition to be the same, in their coronal and wind properties, *or* one must admit some kind of structural individuality which produces the observed coronal and wind individuality. So, the limitation on open-system generality of this coronal-origin model founders, observationally, on the individuality characteristic.

Subatmospheric Origin of Mass Flux

So, very simply, one arrives at the conclusion that the two types of fluxes, energy and mass, are not determined one by the other, but in parallel, by structural characteristics of the star as a whole, which must admit the possibility of a strong individuality among stars of the same radiative flux and gravity, thus, among stars of the same mass and chemical composition We have seen that over very significant time intervals, but short relative to evolutionary times, it is the history of the star which describes much of its outer atmosphere, at least above some 5 photospheric radii We are curious what parameters might be introduced which depend upon even longer historical developments. Suggestions have been made, relative to solar-type, cool stars that it is the history of the magnetic field, and a coupled rotational state, which is important relative to chromospheres and coronae (cf., Jordan, 1981, Summary by Cram and Rutten). Under the original Parker theory, this would also imply that the wind would also depend upon such history. Thus far, any association of magnetic fields with Be-star structure is only speculative, not to be a priori excluded, but difficult to include in any other than equally speculative way.

It appears that the focal point should lie on asking what kinds of internal structural, non-thermal, configurations characterized by a variable mass flux could be found. Until this is done, any atmospheric modeling must remain empirical. And until we can obtain sufficiently coordinated observations: across the broad spectral ranges from the X-ray region, as measuring the maximum coronal temperature, as perturbed by overlying extended atmospheres, the far ultraviolet as measuring the variable, maximum-velocity pattern, polarization, as measuring atmospheric asymmetry probably linked to rotation, far infrared and radio, as measuring the truly asymptotic properties of the nebular H I region, with the forbidden nebular spectrum as tracer; and the not yet clearly observed second corona, or second ionization peak, associated with the deceleration process---until this observational program has advanced much further, even our empirical modeling will proceed by halting steps, not by models based on setting apart from consideration those strong observational characteristics summarized in this Be part of this volume. Most astronomers are becoming increasingly disillusioned by those theories of winds from hot stars which set aside, as a first approximation, coronal and superionization effects and consider a region some few radii from the star. We hope to see the same disillusion with theories, and empirical models, which set aside, to any degree of approximation, the cool region of low velocity which extends to 1000-10,000 radii from the star. In brief, theories which set aside from consideration the role of the star, as an open system, in creating its own local environment, should be suspect.

A star condenses from the interstellar medium, producing initial-value properties which may be highly individual. As it condenses and evolves, it passes through a series of internal configurations which return mass, as well as energy, to the parent medium, oftentimes in sufficiently large amount to profoundly alter our conclusions on what is the final state of the star, and of the adjacent interstellar medium. In considering here the Be stars as one member of a sequence of stars, reflecting the variety of their outer atmospheric structures, we think we are just beginning the study of the significance of the exophotospheric regions of the star. The comment that the study of stellar atmospheres is a mature discipline, unlikely to contain future surprises (Mihalas, 1974) refers to the purely mathematical theory of the "standard" atmospheric model enveloping a star as a closed system. This subject is mature because

it excludes the implications of new observations. *The real stars reveal, each day, something startlingly new—in this age of rapidly expanding observational horizons, and demands, equally unsettlingly, the development of new physical theory, and insight.*

Page intentionally left blank

Page intentionally left blank

REFERENCES

Abbott, D.C. 1978, *Astrophys J*, **225**, 893.

Abbott, D.C. 1980, *Astrophys J.*, **242**, 1183.

Abbott, D C., Bieging, J.H., Churchwell, E., and Cassinelli, J.P 1980, *Astrophys J.*, **238**, 196.

Abt, H.A., and Golson, J.C. 1966, *Astrophys J.*, **143**, 306

Abt, H.A., and Levato, H. 1977, *Pub Astron Soc. Pacific*, **89**, 797

Adams, W.S., and Dunham, T. 1938, *Astrophys J*, **87**, 102.

Adelman, S.J 1973, *Astrophys J.*, **182**, 531

Adelman, S.J. 1975, *Astrophys. J*, **195**, 397

Adelman, S.J. 1977a, *Pub Astron. Soc Pacific*, **89**, 650

Adelman, S J. 1977b, *Mon Not Roy. Astr. Soc.*, **181**, 667

Adelman, S.J. 1978, *Astrophys J*, **222**, 547

Adelman, S.J , and Wolken, P.R. 1976, *Astrophys J.*, **207**, 159

Adelman, S J., and Pyper, D.M 1979, *Astron J*, **84**, 1603.

Aizenman, M L., Hansen, C.J., and Ross, R R. 1975, *Astrophys. J.*, **201**, 387

Aizenman, M.L., Smeyers, P , and Weigert, A. 1977, *Astron. Astrophys* , **58**, 41.

Albert, A., and Huang, S.S. 1974, *Astrophys. J.*, **189**, 479.

Allen, C.W. 1973, *Astrophysical Quantities*, 3rd ed. (London· Athlone Press).

Allen, D.A., and Swings, J.P. 1972, *Astrophys Lett.*, **10**, 83.

Allen, D A 1973, *Mon Not Roy Astr Soc* , **161**, 145.

Allen, D.A , and Swings, J.P. 1976, *Astron Astrophys* , **47**, 293.

Allen, M.S. 1977, *Astrophys J*, **213**, 121.

Aller, L H., Elste, G., and Jugaku, J. 1957, *Astrophys J. Supplement*, **3**, 1.

Aller, L H , and Jugaku, J. 1959, *Astrophys J Supplement*, **4**, 109

Aller, L H , and Jugaku, J. 1969, *Pub. Obs Univ Michigan*, **9**, 203.

Allison, A.A , Glaspey, J W., and Fahlman, G.G. 1977, *Astron. J* , **82**, 283

Altenhoff, W.J , Brais, L L.E., Olnon, F.M., and Wendker, H J 1976, *Astron. Astrophys* , **46**, 11.

Ambartzumian, V A., Mirzoyan, L., and Snow, T.P 1979, *Astrophys J* , **227**, 519.

Andersen, J 1975, *Astron Astrophys* , **44**, 355

Andrews, P.J. 1968, *Mem. Roy Astron. Soc* , **72**, 35.

Andrillat, Y., and Houziaux, L 1967, *J Observateurs*, **50**, 107

Andrillat, Y., and Houziaux, L. 1972, *Astrophys Space Sci.*, **15**, 240.

Andrillat, Y , and Houziaux, L. 1975, *C.R Acad. Sci Paris*, **B281**, 321

Andrillat, Y , and Swings, J.P. 1976, *Astrophys J (Letters)*, **204**, L123.

Appenzeller, I., and Hiltner, W.A. 1967, *Astrophys J.*, 149, 353.

Appenzeller, I., and Wolf, B. 1979, *Astron Astrophys Supplement*, 38, 51.

Athay, R.G. 1972, *Radiation Transport in Spectral Lines* (Dordrecht: Reidel).

Athay, R.G. 1976, *The Solar Chromosphere and Corona· Quiet Sun* (Dordrecht· Reidel)

Athay, R.G. 1981, in *The Sun as a Star*, ed. S. Jordan, NASA SP-450, p. 85.

Auer, L.H., and Mihalas, D. 1972, *Astrophys. J. Supplement*, 24, 193

Auer, L.H., and Mihalas, D. 1973a, *Astrophys J. Supplement*, 25, 433.

Auer, L H , and Mihalas, D. 1973b, *Astrophys. J.*, 184, 151.

Avcioğlu, K. 1979, *Pub. Istanbul Univ. Obs.*, No. 108.

Avcioğlu, K. 1980, *Pub Istanbul Univ Obs* , No. 111.

Avrett, E H. 1964, in *Proc First Harvard-Smithsonian Conf on Stellar Atmospheres*, Smithsonian Astrophys. Obs. Special Report No. 167, p. 83.

Aydin, C., and Faraggiana, R. 1978, *Astron Astrophys. Supplement*, 34, 51.

Baade, D. 1980, *The Messenger*, 19, 4.

Baade, D. 1981, preprint.

Bahcall, J.N. 1978, *Ann Rev. Astron. Astrophys.*, 16, 241.

Bahng, J.D.R. 1971, *Astrophys. J (Letters)*, 168, L75.

Bahng, J.D.R. 1976, in *Proc IAU Symp. 70, Be and Shell Stars*, ed. A Slettebak (Dordrecht. Reidel), p. 41.

Baker, J.B., and Menzel, D.H. 1938, *Astrophys. J.*, 88, 52.

Baldwin, R.B. 1939, *Astrophys J.*, 89, 255.

Baldwin, R.B. 1940, *Astrophys J.*, 92, 82.

Baldwin, R.B 1941, *Astrophys. J.*, 94, 283.

Baliunas, S.L., Ciccone, M.A., and Guinan, E.F. 1975, *Pub. Astron. Soc. Pacific*, 87, 969

Balona, L.A. 1975, *Mon. Not Roy Astr Soc.*, 173, 605.

Balona, L.A., and Crampton, D. 1974, *Mon. Not. Roy. Astr. Soc.*, 166, 203.

Balona, L.A., and Feast, M.W. 1975, *Mon. Not. Roy. Astr. Soc* , 172, 191.

Bappu, M K., and Menzel, D.H. 1954, *Astrophys J.*, 119, 508.

Barbier, D. and Chalonge, D 1939a, *Ann. Astrophys* , 2, 254.

Barbier, D., and Chalonge, D. 1939b, *Astrophys. J.*, 90, 627.

Barbier, D., and Chalonge, D. 1941, *Ann. Astrophys* , 4, 75.

Barker, P.K. 1979, Ph.D. Diss., Univ. Colorado, Boulder

Barker, P.K. 1981, *Astrophys J.*, in press.

Barlow, M.J. 1979, in *Mass Loss and Evolution of O-type Stars*, ed. P.S. Conti, and C W.H. de Loore (Dordrecht Reidel), p. 119.

Barlow, M.J., and Cohen, M. 1977, *Astrophys. J.*, 213, 737.

Baschek, B. 1975, in *Problems in Stellar Atmospheres and Envelopes*, ed. B. Baschek, W.H. Kegel, and G. Traving (Berlin· Springer-Verlag), p. 101.

Batten, A H., Fletcher, J.M., and Mann, P.J. 1978, *Pub. Dom. Astrophys. Obs.*, 15, No. 5, (*7th Cat. Spectrosc. Bin*).

Beals, C.S. 1929, *Mon. Not Roy Astr. Soc.*, 90, 202.

Beals, C.S. 1930, *Pub. Dom. Astrophys. Obs.*, 4, 294 and 297.

Beals, C S. 1931, *Mon Not Roy Astr. Soc* , 91, 966.

Beals, C S. 1939, *Proc. Colloq. Intl. Astrophys., Novae and White Dwarfs* (Herman Co.), p. 113.

Beals, C.S. 1951, *Pub. Dom. Astrophys. Obs* , 9, 1.

Beals, C.S. 1951, *Pub. Dom. Astrophys. Obs.*, 9, 119.

Beardsley, W.R., Worek, T.F., and King, M.W. 1980, in *Current Problems in Stellar Pulsation Instabilities*, ed. D. Fischel, J.R Lesh, and W.M Sparks, NASA TM-80625, p. 409.

Becker, R.H., Boldt, E.A., Holt, S.S., Pravdo, S.H., Robinson-Saba, Serlemitsos, P J., and Swank, J.H. 1979, *Astrophys J. (Letters)*, 227, L21.

Beeckmans, F. 1976a, *Astron. Astrophys.*, 49, 263.

Beeckmans, F. 1976b, *Astron Astrophys* , 52, 465.

Beeckmans, F 1977a, *Astron. Astrophys.*, 60, 1.

Beeckmans, F. 1977b, *Bull Soc. Roy. Sci Liège*, 9-10, 306.

Beeckmans, F. 1978, Thesis, Univ. Liège, Belgium.

Beeckmans, F., and Burgher, M. 1977, *Astron. Astrophys.*, 61, 815.

Beeckmans, F., and Hubert-Delplace, A.M 1980, *Astron Astrophys.*, 86, 72

Behr, A. 1959, *Nach Akad. Wiss Cottingen 2, Math-Phys*, K1, 7185.

Berger, J., Fringant, A.-M., Rebeirot, E. 1974, *C.R. Acad. Sci. Paris*, 278, 227.

Berger, J., and Fringant, A.-M. 1978, *Astron Astrophys.*, 64, L9.

Bernacca, P.L. 1968, *Contr. Oss. Astr. Asiago*, No. 202.

Bernacca, P.L., and Molnar, M.R. 1972, *Astrophys. J.*, 178, 189

Bernat, A.P., and Lambert, D.L. 1978, *Pub. Astron. Soc. Pacific*, 90, 520.

Bijaoui, A., and Doazan, V. 1979, *Astron. Astrophys.*, 70, 285

Blaauw, A 1963, in *Basic Astronomical Data*, ed. K.A. Strand (Chicago. Univ. Chicago Press), p. 383.

Blaauw, A. 1964, *Ann Rev. Astron. Astrophys*, 2, 213.

Blackwell, D.E., and Shallis, M.J. 1977, *Mon. Not. Roy. Astr. Soc*, 180, 177.

Blanco, V M, Demers, S., Douglass, G.G., and FitzGerald, M.P. 1968, *Pub. U S. Naval Obs.*, 2nd Series, 21.

Bless, R.C., and Savage, B.D. 1972, *Astrophys J*, 171, 293.

Bless, R.C., Code, A.D., and Fairchild, E.T. 1976, *Astrophys J.*, 203, 410.

Blumenthal, G.R., and Tucker, W.H. 1974, *Ann. Rev. Astron. Astrophys.*, 12, 23.

Bohlin, R.C 1970, *Astrophys. J.*, 162, 571.

Bohlin, R.C., and Holm, A.V 1980, in *International Ultraviolet Explorer (IUE) Newsletter* (Greenbelt: NASA), p 37.

Bohlin, R.C., Holm, A.V., Savage, B.D., Snijders, M.A.J., and Sparks, W.M. 1980, *Astron. Astrophys.*, 85, 1.

Boksenberg, A., Evans, R.G., Fowler, R G., Gardener, I.S.K., Houziaux, L., Humphries, C M., Jamar, C., Macau, D., Macau, J.P., Malaise, D., Monfils, A., Nandy, K., Thompson, G I., Wilson, R., and Wroe, H. 1973, *Mon. Not Roy Astr Soc.*, 163, 291.

Bond, H 1973, *Publ Astron Soc. Pacific*, 85, 405.

Bond, H.E., and Levato, H. 1976, *Pub. Astron. Soc Pacific*, 88, 905.

Borra, E.F., and Landstreet, J.D. 1979, *Astrophys. J.*, 228, 809.

Bottemiller, R.L. 1972, in Scientific results from OAO2, ed Amherst A.D. Code, p. 505.

Bottenmiller, R.L 1972, in *Scientific Results from the Orbiting Astronomical Observatory (OAO-2)*, ed. A.D. Code, NASA SP-310, p 505

Bowen, I.S. 1947, *Pub. Astron Soc Pacific*, 59, 196.

Bradt, H.V., Doxsey, R E., and Jernigan, J.G. 1979, in *IAU/COSPAR Symposium on X-ray Astronomy*, ed. W.A. Baity and L.E Peterson (Oxford Pergamon), p. 3.

Braes, L.L.E., and Miley, G.K. 1972, *Nature*, 235, 273.

Braes, L.L.E. 1974, in *Galactic Radio Astronomy*, ed. F.J. Kerr, and S.C. Simonson (Dordrecht: Reidel), p. 377.

Breger, M. 1976a, *Astrophys. J. Supplement*, 32, 1.

Breger, M. 1976b, *Astrophys. J. Supplement*, 32, 7.

Briot, D. 1971, *Astron. Astrophys.*, 11, 57.

Briot, D. 1977, *Astron. Astrophys*, 54, 599.

Briot, D. 1978, *Astron. Astrophys*, 66, 197.

Brocklehurst, M. 1971, *Mon. Not. Roy. Astr. Soc.*, 153, 471

Brown, J.C., and McLean, I.S. 1977, *Astron. Astrophys*, 57, 141.

Brucato, R., and Kristian, J. 1972, *Astrophys. J. (Letters)*, 173, L105.

Brune, W.H., Mount, G.H., and Feldman, P.D. 1979, *Astrophys J.*, 227, 884.

Brunet, J.P 1975, *Astron. Astrophys.*, 43, 345.

Burbidge, G.R., and Burbidge, E.M. 1953, *Astrophys. J.*, 117, 407.

Burki, G., Maeder, A., and Rufener, F. 1978, *Astron. Astrophys.*, **65**, 363.

Buser, R. 1978, *Astron. Astrophys* , **62**, 411.

Buser, R., and Kurucz, R.L. 1978, *Astron Astrophys.*, **70**, 555.

Buta, R.J., and Smith, M.A. 1979, *Astrophys J.*, **232**, 213.

Cameron, A., and Mock, M. 1967, *Nature*, **215**, 464.

Campos, A.J., and Smith, M.A. 1980, *Astrophys. J* , **238**, 250

Cannon, C.J., and Thomas, R.N. 1977, *Astrophys. J.*, **211**, 910.

Capps, R.W., Coyne, G.V., and Dyck, H.M 1973, *Astrophys. J.*, **184**, 173.

Carroll, J.A. 1928, *Mon. Not Roy. Astr. Soc.*, **88**, 548.

Carruthers, G.R. 1969, *Astrophys. Space Sci.*, **5**, 387.

Carson, T.R. 1976, *Ann. Rev. Astron. Astrophys.*, **14**, 95.

Carson, T.R., and Hollingsworth, H.M. 1968, *Mon. Not. Roy. Astr. Soc.*, **141**, 77.

Carson, T.R., Mayers, D.F., and Stibbs, D.N.W. 1968, *Mon. Not. Roy. Astr. Soc.*, **140**, 483.

Carson, T.R., and Stothers, R. 1976, *Astrophys. J.*, **204**, 461.

Cash, W., Snow, T.P., and Charles, P. 1979, *Astrophys. J.*, *(Letters)*, **232**, L111.

Cassatella, A., Beeckmans, F., Benvenuti, J., Clavel, J., Heck, A., Lamers, H.J.G.L.M., Macchetto, F., Penston, M., Selvelli, P.L., and Stickland, D. 1979, *Astron. Astrophys.*, **79**, 223.

Cassinelli, J.P. 1979, *Ann. Rev. Astron. Astrophys.*, **17**, 275.

Cassinelli, J.P., and Hummer, D.G. 1971, *Mon. Not. Roy. Astr. Soc.*, **153**, 9.

Cassinelli, J.P., and Haisch, B.M. 1974, *Astrophys. J.*, **188**, 101.

Cassinelli, J.P., and Hartmann, L. 1977, *Astrophys. J.*, **212**, 488.

Cassinelli, J.P., Olson, G.P., and Stalio, R. 1978, *Astrophys. J* , **220**, 573.

Cassinelli, J.P., and Olson, G.P. 1979, *Astrophys. J.*, **229**, 304.

Cassinelli, J.P., Waldron, W.L., Sanders, W.T., Harnden, F.R., Rosner, R., and Vaiana, G.S. 1981, *Astrophys. J.*, **250**, 677.

Castor, J.I. 1970, *Mon. Not Roy. Astr. Soc.*, **149**, 111.

Castor, J.I., Abbott, D.C., and Klein, R.I. 1975, *Astrophys. J.*, **195**, 157.

Castor, J.I., and Lamers, H.J.G.L.M. 1979, *Astrophys. J Supplement*, **39**, 481.

Cayrel, R. 1966, *C R Acad. Sci. Paris*, **B257**, 3309.

Cester, B., Giuricin, G., Mardirossian, F., Puccillo, M., Castelli, F., and Flora, U. 1977, *Astron. Astrophys. Supplement*, **30**, 1.

Chalonge, D., and Divan, L. 1952, *Ann. Astrophys.*, **15**, 201.

Chalonge, D., and Divan, L. 1973, *Astron. Astrophys.*, **23**, 69.

Chalonge, D , and Divan, L. 1977, *Astron. Astrophys.*, **55**, 121.

Chalonge, D., and Safir, H. 1936, *C.R. Acad. Sci. Paris*, **203**, 1329.

Chandrasekhar, S. 1935, *Mon. Not. Roy. Astr Soc.*, **94**, 444.

Chandrasekhar, S. 1939, *An Introduction to the Study of Stellar Structure* (Chicago: Univ. Chicago Press, Dover Paperback, 1957).

Chandrasekhar, S. 1945, *Rev. Mod. Phys.*, **17**, 138.

Chandrasekhar, S. 1950, *Radiative Transfer* (Oxford· Clarendon Press).

Chiosi, C., and Summa, C. 1970, *Astrophys. Space Sci.*, **8**, 478.

Chiosi, C., and Nasi, E. 1974, *Astron. Astrophys.*, **34**, 355.

Chiosi, C., Nasi, E., and Sreenivasan, S.R. 1978, *Astron. Astrophys.*, **63**, 103.

Ciatti, F., d'Ordorico, S., and Mammano, A. 1974, *Astron. Astrophys.*, **34**, 181.

Ciatti, F., and Mammano, A. 1975, *Astron. Astrophys.*, **38**, 435.

Ciatti, F , Bernacca, P.L., and D'Innocengo, A. 1978, *Astron Astrophys.*, **69**, 171.

Clarke, D., and McLean, I.S 1974, *Mon. Not Roy. Astr. Soc*, 167, 27p.

Clarke, D., and McLean, I.S. 1975, *Mon. Not. Roy. Astr Soc.*, 172, 545.

Clarke, D., and McLean, I S. 1976, *Mon. Not Roy Astr Soc*, 174, 335.

Code, A.D. 1960, in *Stellar Atmospheres*, ed. J.L. Greenstein (Chicago Univ. Chicago Press), p. 50.

Code, A.D., Houck, T.E., McNall, J.F., Bless, R.C., and Lillie, C.F. 1970, *Astrophys. J*, 161, 377.

Code, A D., Davis, J., Bless, R.C., and Hanbury Brown, R. 1976, *Astrophys J.*, 203, 417.

Code, A.D., and Meade, M.R. 1979, *Astrophys J. Supplement*, 39, 195.

Code, A.D., Holm, A.V., and Bottemiller, R.L. 1980, *Astrophys J Supplement*, 43, 501.

Cohen, M. 1973a, *Mon. Not. Roy Astr Soc.*, 161, 85.

Cohen, M. 1973b, *Mon. Not Roy. Astr. Soc.*, 161, 97.

Cohen, M. 1973c, *Mon Not. Roy. Astr. Soc.*, 161, 105.

Cohen, M. 1980, *Mon. Not Roy. Astr. Soc.*, 191, 499.

Cohen, M., Barlow, M.J., and Kuhi, L.V. 1975, *Astron. Astrophys.*, 40, 291

Collins, G.W. 1966, *Astrophys. J*, 146, 914.

Collins, G.W 1970a, *Astrophys. J.*, 159, 583.

Collins, G.W. 1970b, in *Proc. IAU Colloq. 4, Stellar Rotation*, ed. A. Slettebak (Dordrecht: Reidel), p. 107.

Collins, G.W. 1974, *Astrophys. J.*, 191, 157.

Collins, G.W., and Sonneborn, G.H. 1977, *Astrophys. J. Supplement*, 34, 41.

Conti, P.S. 1973, *Astrophys J*, 179, 161.

Conti, P.S. 1978, *Astron Astrophys*, 63, 225.

Conti, P., and McCray, R. 1980, *Science*, 208, 9.

Costero, R., Doazan, V., Stalio, R., and Thomas, R.N. 1981, in *Proc IAU Colloq. 59, Effects of Mass Loss on Stellar Evolution*, ed. C. Chiosi, and R. Stalio (Dordrecht: Reidel), p. 131.

Cowley, A.P., and Marlborough, J.M 1968, *Pub Astron. Soc Pacific*, 80, 42

Cowley, A.P., McLaughlin, D.B., Toney, J., and MacConnell, D.J. 1972, *Pub. Ast. Soc. Pacific*, 84, 834.

Cowley, A.P., and Gugula, R. 1973, *Astron. Astrophys*, 22, 203.

Cowley, A.P., Rogers, L., and Hutchings, J.B. 1976, *Pub. Astron. Soc. Pacific*, 88, 911.

Cowley, C.R., and Aikman, G.C.L. 1975, *Pub Astron. Soc. Pacific*, 87, 513.

Cox, A.N., and Stewart, J N. 1965, *Astrophys. J Supplement*, 11, 22.

Cox, A.N., and Stewart, J.N. 1970, *Astrophys. J. Supplement*, 19, 243.

Cox, D.P., and Tucker, W.H. 1969, *Astrophys. J*, 157, 1157.

Cox, J.P. 1980, *Theory of* Stellar Pulsation (Princeton: Princeton Univ. Press).

Cox, J.P., and Stellingwerf, R.F. 1979, *Pub Astron. Soc. Pacific*, 91, 319.

Coyne, G.V. 1971, *Spec. Vatican Ric Astron.*, 8, 201.

Coyne, G.V. 1974, *Mon. Not. Roy. Astr. Soc.*, 169, 7.

Coyne, G.V. 1975, *Spec. Vatican Ric. Astron.*, 8, 533.

Coyne, G.V. 1976a, in *Proc. IAU Symp. 70, Be and Shell Stars*, ed. A. Slettebak (Dordrecht: Reidel), p. 233.

Coyne, G.V. 1976b, *Astron Astrophys*, 49, 89.

Coyne, G.V., and Kruszewski, A. 1969, *Astron. J.*, 74, 528.

Coyne, G.V., and McLean, I.S. 1975, *Astron. J.*, 80, 702.

Coyne, G.V., and Vrba, F.J. 1976, *Astrophys. J.*, 207, 790.

Coyne, G.V., and McLean, I.S. 1981, in *Proc. IAU Symp. 98, The Be Stars*, in press.

Cramer, N., and Maeder, A. 1979, *Astron. Astrophys.*, 78, 305.

Crampin, J., and Hoyle, F. 1960, *Mon. Not. Roy. Astr. Soc.*, 120, 33.

Crawford, D.L. 1973, in *Problems of Calibration of Absolute Magnitudes and Temperatures of Stars*, ed. B. Hauck, and B.E. Westerlund (Dordrecht: Reidel), p. 93.

Crawford, D.L. 1975a, in *Multicolor Photometry and the Theoretical HR Diagram*, ed. A.G. Davis Philip, and D.S. Hayes, Dudley Observatory Report No. 9, p. 17.

Crawford, D.L. 1975b, *Astron J*, 80, 955.

Crawford, D.L. 1978, *Astron J.*, 83, 48.

Crawford, D.L., and Mander, J.V. 1966, *Astron. J*, 71, 114

Crawford D.L., and Barnes, J.V. 1970, *Astron. J.*, 75, 978.

Crawford, D.L., and Barnes, J.V. 1974, *Astron. J.*, 79, 687.

Cucchiaro, A., Jaschek, M., Jaschek, C., and Macau-Hercot, D. 1976, *Astron. Astrophys. Supplement*, 26, 241.

Cucchiaro, A., Macau-Hercot, D., Jaschek, M., and Jaschek, C. 1977, *Astron. Astrophys Supplement*, 30, 71.

Curtis, R.H. 1923, *Pub. Univ. Michigan*, VIII, 1.

Dachs, J. 1980, in *Proc. Second European IUE Conference*, ESA-SP157, p. 139.

Dachs, J., and Schmidt-Kaler, T. 1975, *Astron. Astrophys Supplement*, 21, 81

Darius, J., Giddings, J.R., and Wilson, R. 1979, in *The First Year IUE*, ed. A.J. Willis (London: Univ. College), p. 363.

Dearborn, D.S.P., Blake, J.B., Hainebach, K.L., and Schramm, D.N. 1978, *Astrophys. J.*, 223, 552.

Dearborn, D.S.P., and Blake, J.B. 1979, *Astrophys J.*, 231, 193.

de Groot, M. 1969, *Bull. Astron. Inst. Netherlands*, 20, 225.

de Jager, C., Hoekstra, R., van der Hucht, K.A., Kampermann, T.M., Lamers, H.J., Hammerschlag, A., Werner, W., and Emming, J.G. 1974, *Astrophys. Space Sci.*, 26, 207.

de Jager, C., Lamers, H.J.G.L.M., and van der Hucht, K.A. 1975, *Astrophys Space Sci*, 38, 313.

de Jager, C., Kondo, Y., Hoekstra, R., van der Hucht, K.A., Kampermann, T.M., Lamers, H.J.G.L.M., Modisette, J.L., and Morgan, T.H. 1979, *Astrophys J.*, 230, 534.

de Loore, C., de Grève, J.P., and Lamers, H.J.G.L.M. 1977, *Astron. Astrophys.*, 61, 251.

de Loore, C., de Grève, J.P., and Vanbeveren, D. 1978, *Astron. Astrophys.*, 67, 373.

de Loore, C., Altamore, A., Baratta, G.B., Bunner, A.N., Divan, L., Doazan, V., Hensberge, H., Sterken, C., Viotti, R. 1979, *Astron. Astrophys*, 78, 287.

Delplace, A.-M. 1970, *Astron. Astrophys*, 7, 68.

Delplace, A.M, and Chambon, M. Th. 1976, in *Proc. IAU Symp. 70, Be and Shell Stars*, ed. A. Slettebak (Dordrecht Reidel), p. 79.

Deutsch, A.J. 1970, *Astrophys. J*, 159, 985.

Dinger, A.S. 1970, *Astrophys. Space Sci.*, 6, 118.

Divan, L. 1966, in *Spectral Classification and Multicolour Photometry*, ed. K. Loden, and U. Sinnerstad (London: Academic Press), p. 311.

Divan, L. 1979, in *Proc IAU Colloq. 47, Spectral Classification of the Future*, ed. M.F. McCarthy, A.G.D. Philip, and G.V. Coyne (Citta del Vaticano· Specola Vaticana), p. 247

Divan, L., Zorec, J., and Briot, D. 1981, in *Proc IAU Symp. 98, The Be Stars*, in press.

Divan, L., Doazan, V., and Zorec, J 1982, unpublished results.

Doazan, V. 1965, *Ann. Astrophys*, 28, 1.

Doazan, V. 1970, *Astron. Astrophys.*, 8, 148.

Doazan, V. 1973, *Astron. Astrophys.*, 27, 395.

Doazan, V. 1976, in *Proc. IAU Symp 70, Be and Shell Stars*, ed. A. Slettebak (Dordrecht: Reidel), p. 37.

Doazan, V., and Peton, A. 1970, *Astron. Astrophys*, 9, 245.

Doazan, V., and Briot, D., and Bourdonneau, B. 1975, *Astron. Astrophys*, 42, 161.

Doazan, V., Kuhi, L.V., and Thomas, R.N. 1980a, *Astrophys J (Letters)*, 235, L20.

Doazan, V., Kuhi, L.V., Marlborough, J.M., Snow, T.P., and Thomas, R.N. 1980b, in *Second IUE European Conference*, ESA-SP157, p. 151.

Doazan, V., Selvelli, P., Stalio, R., and Thomas, R.N. 1980c, in *Second IUE European Conference*, ESA-SP157, p. 145.

Doazan, V., and Zorec, J. 1981, in preparation.

Doazan, V., Grady, C., Kuhi, L.V., Marlborough, J.M., Snow, T.P., and Thomas, R.N. 1981a, in *The Be Stars IAU Symp. 98*, in press.

Doazan, V., Stalio, R., and Thomas, R N. 1981b, in *The Be Stars, IAU Symp. 98*, in press.

Doazan, V., Franco, M.L., Stalio, R., and Thomas, R.N. 1981c, in *The Be Stars, IAU Symp. 98*, in press.

Doazan, V., Stalio, R., and Thomas, R.N. 1981d, in *The Universe at Ultraviolet Wavelengths*, NASA CP-2171, p. 141.

Doazan, V., Harmanec, P., Koubsky, P., Krpata, J., and Zdarsky, F. 1982, in preparation.

Drilling, J.S. 1978, *Astrophys J. (Letters)*, **223**, L29.

Dufton, P.L. 1979, *Astron. Astrophys* , **73**, 203.

Dufton, P.L., and McKeith, D.C. 1980, *Astron Astrophys.*, **81**, 8.

Dupree, A.K. et al. 1980, *Astrophys. J* , **238**, 969.

Durney, B.R., and Hundhausen, A.J. 1974, *J. Geophys. Res.* 79, 3711.

Duval, M., Lacoarret, M., Herman, R., and Hubert, H. 1975, *C.R. Acad. Sci. Paris*, **B280**, 193.

Duval, P., and Karp, A.H. 1978, *Astrophys J.*, **222**, 220.

Dyck, H.M., and Milkey, R.W. 1972, *Pub. Astron Sci. Pacific*, **84**, 597.

Ebbets, D. 1980, *Astrophys. J.*, **235**, 97.

Eddington, A.S 1930, *The Internal Constitution of Stars* (Cambridge: Cambridge Univ. Press).

Edlén, B. 1942, *Z. Astrophys* , **22**, 30.

Edwards, D.L. 1956, *Vistas in Astronomy*, **2**, 1470.

Eggen, O.J. 1974a, *Astrophys. J* , **188**, 59.

Eggen, O.J. 1974b, *Pub Astron. Soc. Pacific*, **86**, 241.

Eggen, O.J. 1975, *Astrophys. J.*, **198**, 131.

Eggen, O.J. 1976, *Quart. Jour Roy Astr. Soc.*, 17, 472.

Eggen, O.J. 1977, *Pub Astron. Soc Pacific*, **89**, 187.

Eggleton, P.P., and Percy, J.R. 1973, *Mon Not Roy. Astr. Soc* , **161**, 421.

Emden, R. 1907, *Gaskugeln* (Leibzig and Berlin: B.G. Teubner).

Erro, B.I. 1969, *Bol. Obs. Tonantzintla y Tacubaya*, **5**, 89.

Faraggiana, R., and van der Hucht, K.A. 1975, *Astron. Astrophys.*, **38**, 455.

Feautrier, P. 1967, *Ann Astrophys.*, **30**, 125, and 604.

Feautrier, P. 1968, *Ann Astrophys.*, **31**, 257.

Feinstein, A. 1968, *Z f Astrophys* , **68**, 29.

Feinstein, A. 1970, *Pub. Astron. Soc. Pacific*, **82**, 132.

Feinstein, A. 1974, *Mon. Not. Roy. Astr. Soc.*, **169**, 171.

Feinstein, A. 1975, *Pub Astron. Soc. Pacific*, **87**, 603.

Fernie, J.D. 1969, *Pub Astron. Soc. Pacific*, **81**, 168.

Ferrari-Toniolo, M., Natali, G., Persi, P., and Spada, G., 1977, *Astron. Astrophys.*, **61**, 47.

Ferrari-Toniolo, M., Persi, P., and Viotti, R. 1978, *Mon. Not Roy. Astron Soc.*, **185**, 841.

Fischel, D., and Sparks, W.M. 1972, in *Scientific Results from the Orbiting Astronomical Observatory (OAO-2)*, ed. A D. Code, NASA SP-310, p 475.

Fischel, D., and Klinglesmith, D.A. 1973, *Astrophys J.*, **181**, 841.

Fischel, D., and Sparks, W.M. 1981, in *The Universe in Ultraviolet Wavelengths The First Two Years of IUE*, ed. R.D. Chapman, NASA CP-2171, p. 217.

Fitch, W.S. 1967, *Astrophys J.*, **148**, 481.

Fitch, W.S. 1969, *Astrophys. J.*, **158**, 269.

FitzGerald, M.P. 1970, *Astron. Astrophys* , **4**, 234.

Flower, P.J. 1977, *Astron. Astrophys.*, **54**, 31.

Frank, Z., Meisel, D.D., and Saunders, B. 1980, *Bull. Am. Astr. Soc.*, **12**, 751.

Frogel, J.A., and Stothers, R. 1977, *Astron. J.*, **82**, 890.

Frontera, F., Enlighi, F., Morelli, E., and Ventura, G. 1979, *Astrophys J* , **229**, 291.

Furenlid, I., and Young, A. 1980, *Astrophys. J. (Letters)*, **240**, L59.

Galkina, T.S. 1978, *Inf Bull Var. Stars*, 1461.

Garavoglia, M., and Treves, A. 1976, *Astron. Astrophys.*, **49**, 235.

Garrison, L.M., and Anderson, C.M. 1977, *Astrophys. J* , **218**, 438.

Garrison, R.F. 1967, *Astrophys J.*, **147**, 1003.

Garrison, R.F , and Hiltner, W.A. 1973, *Astrophys. J. (Letters)*, **179**, L117.

Garrison, R.F., Hiltner, W.A., and Schild, R.E. 1977, *Astrophys. J. Supplement*, 35, 111.

Gebbie, K.B., and Thomas, R.N. 1970, *Astrophys. J*, 161, 229.

Gehrz, R.D., Hackwell, J.A., and Jones, T.W. 1974, *Astrophys. J.*, 191, 675.

Geisel, S.L. 1970, *Astrophys. J. (Letters)*, 161, L105.

Gerasimovic, B.P. 1929, *Harvard Circ.*, 339.

Gerasimovic, B.P. 1934, *Mon. Not. Roy. Astr. Soc.*, 94, 737.

Gerasimovic, B.P. 1935, *Observatory*, 58, 115.

Gillet, F.C., and Stein, W.A. 1971, *Astrophys. J.*, 164, 77.

Gingerich, O. 1969, *Theory and Observation of Normal Stellar Atmospheres* (Cambridge, Mass. M.I.T. Press).

Golay, M., and Mauron, N. 1977, *Astron. Astrophys.*, 59, L1.

Goldberg, B.A., Walker, G.A.H., and Odgers, G J. 1974, *Astron. Astrophys.*, 32, 355.

Goldberg, B.A., Walker, G.A.H., and Odgers, G.J. 1976, *Astron. J.*, 81, 433.

Goy, G. 1977, *Astron. Astrophys.*, 57, 449.

Goy, G. 1980, *Astron. Astrophys.*, 88, 370.

Grabowski, B. 1969, *Acta Astron.*, 19, 23.

Gray, D.F. 1976, *The Observation and Analysis of Stellar Photospheres* (New York J. Wiley and Sons).

Greaves, W.M.H., and Martin, E. 1938, *Mon. Not Roy Astr. Soc.*, 98, 435.

Greenstein, J.L., and Wallerstein, G. 1958, *Astrophys J*, 127, 237.

Groote, D., and Hunger, K. 1976, *Astron. Astrophys.*, 52, 303.

Groote, D., and Hunger, K. 1977, *Astron. Astrophys.*, 56, 129.

Groote, D., Kaufmann, J.P., and Hunger, K. 1978, *Astron. Astrophys.*, 63, L9.

Groote, D., Hunger, K., and Schultz, G.V. 1980, *Astron. Astrophys.*, 83, L5.

Guerrero, G., and Mantegazza, L. 1979, *Astron. Astrophys. Supplement*, 36, 471.

Gulliver, A.F. 1977, *Astrophys. J Supplement*, 35, 441.

Gursky, H., and Schreier, E. 1975, in *Neutron Stars, Black Holes and Binary X-Ray Sources*, ed. H. Gursky, and R. Ruffini (Dordrecht: Reidel), p. 175.

Gurzadyan, G.A. 1974, *Astron. Astrophys* , 35, 493.

Gurzadyan, G.A. 1975, *Space Sci. Rev.*, 18, 95.

Gurzadyan, G.A., Kashin, A.L., Krmoyan, M.N., and Oganesyan, D.B. 1974, *Astrofizika*, 10, 177 (in Russian); English translation in *Astrophysics*, 10, 109.

Gutiérrez-Moreno, A. 1975, *Pub. Astron. Soc. Pacific*, 87, 805.

Gutman, F. 1967, *Pub. Astron. Soc. Pacific*, 79, 5.

Hack, M. 1967, in *Modern Astrophysics*, ed. M. Hack (New York: Gordon and Breach), p. 163.

Hack, M., and Struve, O. 1970, *Stellar Spectroscopy, Peculiar Stars* (Dordrecht: Reidel).

Hack, M., and Stalio, R. 1976, in *Physics of Ap Stars*, ed. W.W. Weiss, H. Jenker, and H.J. Wood (Vienna: Univ. Sternw.), p. 503.

Hadrava, P., Harmanec, P., Koubsky, P., Krpata, J., and Zdarsky, F. 1978, *IAU Circ.*, 3317.

Haefner, R., Metz, K., and Schoembs, R. 1978, *Inf. Bull. Var. Stars*, 1472.

Haisch, B.M., and Cassinelli, J.P. 1976, *Astrophys. J.*, 208, 253.

Hammerschlag-Hensberge, G. 1979, *IAU Circ.*, 3391.

Hammerschlag-Hensberge, G., van den Heuvel, E.P.J., Lamers, H.J., Burger, M., de Loore, C., Glencross, W., Howarth, I., Willis, A.J., Wilson, R., Menzies, J., Whitelock, P.A., Van Dessel, E.L., and Sanford, P. 1980, *Astron. Astrophys* , 85, 119.

Hanbury Brown, R., Davis, J., and Allen, L.R. 1974, *Mon. Not. Roy. Astr. Soc.*, 167, 121.

Hansen, C.J., Cox, J.P., and Van Horn, H.M. 1977, *Astrophys. J.*, 217, 151.

Hardorp, J., and Scholz, M. 1970, *Astrophys. J Supplement*, 19, 193.

Hardorp, J., and Strittmatter, P.A. 1970, in *Proc. IAU Colloq. 4 Stellar Rotation*, ed. A. Slettebak (Dordrecht: Reidel), p. 48.

Harmanec, P. 1981a, in *Proc. IAU Symp. 98, The Be Stars*, in press.

Harmanec, P., Koubsky, P., and Krpata, J. 1972, *Bull. Ast. Inst Czech.*, 23, 218.

Harmanec, P., Koubsky, P., and Krpata, J. 1973, *Astron. Astrophys* , 22, 337.

Harmanec, P., Koubsky, P., and Krpata, J. 1974, *Astron. Astrophys.*, 33, 117.

Harmanec, P., Horn, J., Koubsky, P., Kriz, S., Zdarsky, F., Papousek, J., Doazan, V., Bourdonneau, B., Baldinelli, L., Ghedini, S., and Pvalovski, K. 1978, *Bull Astron Inst. Czech.*, 29, 278.

Harmanec, P., Horn, J., Koubsky, P., Zdrasky, F., and Kriz, S. 1979, *Inf. Bull. Var Stars*, 1555.

Harmanec, P., Horn, J., Koubsky, P., Zdarsky, F , Kriz, S., and Pavlovski, K. 1980, *Bull. Astr. Inst. Czech.*, 31, 144.

Harnden, F.R., Branduardi, G., Elvis, M., Gorenstein, P., Grindlay, J., Pye, J.P., Rosner, R., Topka, F., Vaiana, S. 1979, *Astrophys J. (Letters)*, 234, L51.

Hartmann, L. 1978, *Astrophys. J.*, 224, 520.

Hartoog, M.R., and Cowley, A.P. 1979, *Astrophys. J* , 228, 229.

Hatchett, S., and McCray, R. 1977, *Astrophys. J.*, 211, 552.

Haupt, W., and Moffat, A.F J. 1973, *Astrophys. Lett* , 13, 77.

Haupt, H.F., and Schroll, A. 1974, *Astron Astrophys. Supplement*, 15, 311.

Hayes, D.P. 1975, *Pub Astron. Soc. Pacific*, 87, 609.

Hayes, D.P. 1980, *Pub. Astron Soc. Pacific*, 92, 661.

Hayes, D.P., and Illing, R.M.E. 1974, *Astron J* , 79, 1430.

Hayes, D.S., and Latham, D.W. 1975, *Astrophys. J.*, 197, 593.

Hayes, D.S. 1979, in *Problems of Calibration of Multicolor Photometric Systems*, ed. A.G. Davis Philip, Dudley Obs. Report No. 14, p. 297.

Heap, S.R. 1975, *Phil. Trans Roy. Soc. London A.*, 279, 371.

Heard, J.F., Hurkens, R.J., Percy, J.R., and Porco, M. 1976, *J. Roy. Astr. Soc Canada*, 70, 213.

Hearn, A.G. 1972, *Astron. Astrophys.*, 19, 417.

Hearn, A.G. 1973, *Astron. Astrophys.*, 23, 97.

Hearn, A.G. 1975a, *Astron Astrophys.*, 40, 277.

Hearn, A.G. 1975b, *Astron. Astrophys* , 40, 355.

Hearn, A.G. 1977, *Solar Phys.*, 51, 159.

Hearn, A.G., and Vardavas, A.M. 1981, *Astron. Astrophys.*, 98, 230, 241, and 246.

Heintze, J.R.W. 1973, in *Problems of Calibration of Absolute Magnitudes and Temperatures of Stars*, ed. B. Hauk and B.E. Westerlund (Dordrecht: Reidel), p. 231.

Henize, K.G., Wray, J.D., Parsons, S.B., Benedict, G.F., Bruhweiler, F.C., Rybski, P.M., and O'Callaghan, F.G. 1975, *Astrophys J. (Letters)*, 199, L119.

Henize, K.G., Wray, J.D., Parsons, S.B., and Benedict, G.F. 1976, in *Be and Shell Stars*, ed. A. Slettebak (Dordrecht: Reidel), p. 191.

Henrichs, H.F. 1980, in *Highlights of Astronomy*, 5, 541.

Henrichs, H., and van den Heuvel, E.P.J. 1977, *Astron. Astrophys* , 54, 817.

Henrichs, H.F., Hammerschlag-Hensberge, G., Lamers, H.J.G.L.M. 1980, in *Second IUE European Conference*, ESA-SP157, p. 147.

Henry, R.C., Weinstein, A., Feldman, P.D., Fastie, W.G., and Moos, H.W. 1975, *Astrophys. J.*, 201, 613.

Herbig, G.H. 1960, *Astrophys. J Supplement*, 4, 337.

Hertzsprung, E. 1923, *Bull Astr Netherl.*, 1, 217.

Herbison-Evans, D., Hanbury Brown, R., Davis, J., and Allen, L.R. 1971, *Mon. Not. Roy. Astr. Soc.*, 151, 161.

Hesser, J.E., Walborn, N.R., and Ugarte, P. 1976, *Nature*, 262, 116.

Hesser, J.E., Moreno, H., and Ugarte, P. 1977, *Astrophys J. (Letters)*, 216, L31.

Higginbotham, N.A., and Lee, P. 1974, *Astron Astrophys.*, 33, 277.

Higginbotham, N.A., Schiffer, F.H., and Dufour, R.J. 1974, *Pub Astron. Soc. Pacific*, 86, 272.

Hill, G. 1967, *Astrophys. J Supplement*, 14, 263.

Hill, I., and Adelman, S.J. 1978, *Astrophys J. Supplement*, 37, 265.

Hiltner, W.A. 1947, *Astrophys. J.*, 105, 212.

Hiltner, W.A., Garrison, R.F., and Schild, R.E. 1969, *Astrophys. J.*, 157, 313.

Hirata, R. 1978, *Inf. Bull Var. Stars*, No. 1496.

Hirata, R., and Kogure, T. 1976, *Pub. Astron. Soc. Japan*, 28, 509.

Hirata, R., and Kogure, T. 1977, *Pub Astron. Soc. Japan*, 29, 477.

Hjellming, R.M., and Wade, C.M. 1971, *Astrophys. J (Letters)*, 168, L115.

Hopp, U., and Witzigmann, S. 1980, *Inf Bull. Var Stars*, 1782.

Huang, S.S. 1972, *Astrophys. J.*, 171, 549.

Huang, S.S. 1973, *Astrophys. J.*, 183, 541.

Huang, S.S. 1977, *Astrophys. J.*, 212, 123.

Huang, S.S. 1978, *Astrophys. J.*, 219, 956.

Huang, S., and Struve, O. 1960, in *Stellar Atmospheres*, ed. J.L. Greenstein (Chicago: Univ. Chicago Press), p. 321.

Hubert-Delplace, A.M., and van der Hucht, K.A. 1978, *Astron. Astrophys.*, 67, 399.

Hubert-Delplace, A.M., and Hubert, H. 1979, *Atlas d'étoiles Be* (Paris: Obs. Paris).

Huffer, C.M. 1939, *Astrophys. J.*, 89, 139.

Hummer, D.G. 1976, in *Proc. IAU Symp. 70, Be and Shell Stars*, ed. A. Slettebak (Dordrecht: Reidel), p. 281.

Humphreys, R.M. 1978, *Astrophys. J. Supplement*, 38, 309.

Humphreys, R.M. 1979, *Astrophys. J Supplement*, 39, 389.

Humphreys, R.M., and Davidson, K. 1979, *Astrophys J*, 232, 409.

Humphries, C.M., Nandy, K., and Thompson, G.I. 1973, *Mon. Not. Roy. Astr. Soc.*, 163, 291.

Humphries, C.M., Nandy, K., and Kontizas, E. 1975, *Astrophys. J.*, 195, 111.

Humphries, C.M., Jamar, C., Malaise, D., and Wroe, H. 1976, *Astron Astrophys.*, 49, 389.

Hundt, E., Kodaira, K., Schmid-Burgk, J., and Scholz, M. 1975, *Astron. Astrophys.*, 41, 37.

Hunger, K. 1974, *Astron. Astrophys.*, 32, 449.

Hunger, K. 1975, in *Problems in Stellar Atmospheres and Envelopes*, ed. B. Baschek, W.H. Kegel, and G. Traving (Berlin: Springer-Verlag), p. 57.

Hunger, K., and Klinglesmith, D.A. 1969, *Astrophys. J*, 157, 721.

Hunger, K., and Kaufmann, J P. 1973, *Astron. Astrophys.*, 25, 261.

Hunger, K., and Kudritzki, R.P. 1980, *Astron Astrophys.*, 88, L4.

Hutchings, J.B. 1967, *Observatory*, 87, 289.

Hutchings, J.B. 1968a, *Mon. Not. Roy. Astr Soc.*, 141, 219.

Hutchings, J.B. 1968b, *Mon. Not. Roy. Astr. Soc.*, 141, 329.

Hutchings, J.B. 1969a, *Mon. Not. Roy Astr. Soc.*, 144, 235.

Hutchings, J.B. 1969b, in *Non-Periodic Phenomena in Variable Stars*, ed. L. Detre (New York: Academic Press), p. 191.

Hutchings, J.B. 1970a, *Mon Not Roy. Astr. Soc.*, 147, 161.

Hutchings, J.B. 1970b, *Mon. Not. Roy. Astr. Soc.*, 150, 55.

Hutchings, J.B. 1971, *Mon. Not. Roy. Astr. Soc.*, 152, 109.

Hutchings, J.B. 1976a, *Astrophys. J.*, 203, 438.

Hutchings, J.B. 1976b, *Pub. Dom. Astrophys. Obs.*, 14, 355.

Hutchings, J.B. 1976c, *Astrophys J. (Letters)*, 204, L99.

Hutchings, J.B. 1976d, in *Proc. IAU Symp. 70, Be and Shell Stars*, ed. A. Slettebak (Dordrecht: Reidel), p. 13.

Hutchings, J.B. 1977, *Mon. Not. Roy Astr. Soc*, 181, 619.

Hutchings, J.B. 1979, *Astrophys. J.*, 233, 913.

Hutchings, J.B. 1980, *Astrophys J.*, 235, 413.

Hutchings, J.B., Auman, J.R., Gower, A.C., and Walker, G.A.H. 1971, *Astrophys. J. (Letters)*, 170, L173.

Hutchings, J.B., Cowley, A.P., Crampton, D., and Redman, R.O. 1974, *Astrophys. J. (Letters)*, 191, L101.

Hutchings, J.B., Crampton, D., and Redman, R.O. 1975, *Mon. Not. Roy. Astron. Soc.*, 170, 313.

Hutchings, J.B., and Walker, G.A.H 1976, *Mon. Not. Roy. Astr. Soc.*, 176, 217.

Hutchings, J.B., and Hill, G. 1977, *Astrophys. J.*, 213, 111.

Hutchings, J.B., and Stoekley, T.R. 1977, *Pub. Astron. Soc. Pacific*, 89, 17.

Iben, I. 1965, *Astrophys J*, 142, 1447.

Iben, I. 1966a, *Astrophys. J*, 143, 483.

Iben, I. 1966b, *Astrophys. J.*, 143, 505.

Iben, I. 1966c, *Astrophys. J.*, 143, 516.

Iben, I. 1967a, *Astrophys J*, 147, 650.

Iben, I. 1967b, *Ann. Rev. Astron. Astrophys.*, 5, 571.

Iben, I. 1974, *Ann. Rev. Astron. Astrophys.*, 12, 215.

Inglis, D.R., and Teller, E. 1939, *Astrophys. J.*, 90, 439.

Isserstedt, J. 1970, *Astron. Astrophys*, 8, 168.

Jakate, S.M 1979, *Astron J.*, 84, 1042.

Jakate, S.M. 1980, *Astron. Astrophys*, 84, 374.

Jamar, C., Macau-Hercot, D., Monfils, A., Thompson, G.I., Houziaux, L., and Wilson, R. 1976, *Ultraviolet Bright-Star Spectrophotometric Catalogue*, ESA SR-27.

Jamar, C, Macau-Hercot, D., and Praderie, F. 1978, *Astron Astrophys.*, 63, 155.

Jarzebowski, T., Jerzykiewicz, M., Le Contel, J.-M., and Musielok, B. 1979, *Acta Astron*, 29, 517.

Jaschek, C., Jaschek, M., Morgan, W.W., and Slettebak, A. 1968, *Astrophys. J (Letters)*, 153, L87.

Jaschek, C., and Ferrer, L. 1971, *Pub. Astron. Soc Pacific*, 83, 346.

Jaschek, C., Ferrer, L., and Jaschek, M. 1971, *Obs. Astron. Univ. La Plata Ser Astron.*, 37.

Jaschek, M., and Jaschek, C. 1974a, *Astron. Astrophys.*, 36, 401.

Jaschek, M., and Jaschek, C. 1974b, *Vistas in Astronomy*, 16, 131.

Jaschek, M., Hubert-Delplace, A.M., Hubert, H., and Jaschek, C 1980, *Astron. Astrophys. Supplement*, 42, 103

Jefferies, J.T. 1968, *Spectral Line Formation* (Waltham, Mass Blaisdell).

Jernigan, J.G. 1976, *IAU Cir*, 2900.

Jerzykiewicz, M. 1978, *Acta Astron.*, 28, 465.

Jerzykiewicz, M., and Sterken, C. 1979, in *Changing Trends in Variable Star Research*, ed. F.M. Bateson, J. Smak, and I.H. Urch (Hamilton, N.Z.: Univ. of Waikato), p. 474.

Johns, M., Koski, A., Canizares, C., and McClintock, J. 1978, *IAU Circ*, 3171.

Johnson, H.L. 1958, *Lowell Obs. Bull.*, 4, 37.

Johnson, H.L. 1963, in *Basic Astronomical Data*, ed. K.A Strand (Chicago: Univ. Chicago Press), p. 204.

Johnson, H.L. 1965a, *Astrophys. J.*, 141, 923.

Johnson, H.L. 1965b, *Comm. Lunar and Planetary Lab.*, 3, 73.

Johnson, H.L. 1966, *Ann Rev Astron. Astrophys.*, 4, 193.

Johnson, H.L. 1967, *Astrophys. J. (Letters)*, 150, L39.

Johnson, H.L. 1978, *Rev. Mexicana Astron. Af.*, 4, 3.

Johnson, H.L., and Morgan, W.W. 1953, *Astrophys. J.*, 117, 313.

Johnson, H.L., Hoag, A.A., Iriarte, B., Mitchell, R.I., and Hallam, K.L. 1961, *Lowell Obs Bull.*, 5, 138.

Johnson, H.L., Mitchell, R.I., Iriarte, B., and Wiśniewski, W.Z. 1966, *Comm. Lunar and Planetary Lab.*, 4 99.

Johnson, H.L., and Mitchell, R.I. 1975, *Rev Mexicana Astron. Af.*, 1, 299

Johnson, H L, Wiśniewski, W.Z., and Fay, T.D. 1978, *Rev Mexicana Astron Af*, 2, 273

Johnson, M. 1958, *Etoiles à raies d'émission* (Liège Institut d'Astrophysique), p. 219.

Jones, D.H.P, and Shobbrook, R.R. 1974, *Mon. Not Roy. Astr. Soc.*, 166, 649.

Jones, T.J. 1979, *Astrophys J*, 228, 787

Jones, T.J., and Wolff, S.C. 1980, *Pub Astron Soc. Pacific*, 92, 84.

Jordan, S.D. 1981, *The Sun as a Star*, NASA SP-450.

Kamp, L.W. 1973, *Astrophys J.*, 180, 447

Kamp, L W. 1976, *Statistical Equilibrium Calculations for Silicon in Early-Type Model Atmospheres*, NASA TR R-455.

Kamp, L.W. 1978, *Astrophys J. Supplement*, 36, 143.

Karp, A.H. 1973, *Astrophys. J.*, 180, 895

Karp, A.H. 1975a, *Astrophys J*, 199, 448

Karp, A.H. 1975b, *Astrophys J.*, 200, 354.

Karp, A.H. 1975c, *Astrophys J*, 201, 641.

Karp, A.H 1978, *Astrophys. J.*, 222, 578.

Kaufmann, J.P., Schonberner, D., and Rahe, J. 1974, *Astron. Astrophys*, 36, 201

Kaufmann, J.P., and Hunger, K. 1975, *Astron. Astrophys.*, 38, 351.

Kaufmann, J.P., Schonberner, D. 1977, *Astron. Astrophys.*, 57, 169.

Keenan, and Morgan 1951, in *Astrophysics*, ed. J.A. Hynek (New York McGraw Hill Book Co.).

Kharnitov, A.V. 1963, *Soviet Astr -A.J.*, 7, 258.

Kitchin, C.R. 1970a, *Astrophys Space Sci.*, 8, 3.

Kitchin, C R. 1970b, *Mon Not. Roy. Astr. Soc*, 150, 455.

Kitchin, C.R. 1973, *Mon. Not Roy. Astr. Soc*, 161, 381 and 389.

Kitchin, C.R, and Meadows, A.J. 1970, *Astrophys Space Sci.*, 8, 463.

Klein, R.I., and Castor, J.I. 1978, *Astrophys J.*, 220, 902.

Klinglesmith, D.A., Hunger, K., Bless, R.C., and Millis, R.L. 1970, *Astrophys. J*, 159, 513.

Klinglesmith, D.A. 1971, *Hydrogen Line Blanketed Model Stellar Atmospheres*, NASA SP-3065.

Kodaira, K. 1970, *Astrophys. J.*, 159, 931.

Kodaira, K., and Scholz, M. 1970, *Astron. Astrophys.*, 6, 93.

Kogure, T. 1959, *Pub. Astron Soc. Japan*, 11, 127, and 278.

Kogure, T. 1961, *Pub Astron Soc. Japan*, 13, 335.

Kogure, T. 1967, *Pub. Astron. Soc. Japan*, 19, 30.

Kogure, T. 1969, *Astron Astrophys*, 1, 253.

Kondo, Y., Modisette, J.L., and Wolf, G.W. 1975, *Astrophys. J.*, 199, 110.

Kondo, Y., Modisette, J.L., Dufour, R.J., and Whaley, R.S. 1976, *Astrophys J.*, 206, 163.

Kopylov, I.M. 1958, *Pub. Crimean Astrophys Obs*, 20, 156.

Kosirev, N A. 1934, *Mon. Not. Roy. Astr. Soc.*, 94, 430.

Krautter, J., and Bastian, U. 1980, *Astron. Astrophys*, 88, L6.

Kruszewski, A. 1974, in *Planets and Nebulae Studied with Polarimetry*, ed. T. Gehrels (Tuscon Univ. Arizona Press), p. 845.

Kuan, P., and Kuhi, L.V. 1975, *Astrophys. J.* 199, 148.

Kubiak, M. 1972, *Acta Astron.*, 22, 11.

Kubiak, M. 1973, *Acta Astron*, 23, 23.

Kubiak, M. 1978, *Acta Astron.*, 28, 153.

Kudritzki, R.P., and Simon, K.P. 1978, *Astron. Astrophys.*, 70, 653.

Kudritzki, R.P., Hunger, K., Gruschinske, J., Simon, K.P., and Kaufmann, J.P. 1980, *Second European IUE Conference*, ed. B Battrick and J. Mort, ESA SP-157, p. 307.

Kuhi, L.V. 1968, in *Wolf-Rayet Stars*, ed. K.B. Gebbie, and R.N. Thomas, NBS Special Publ. 307, p. 103.

Kunasz, P.B., Hummer, D.C., and Mihalas, D. 1975, *Astrophys J.*, 202, 92.

Kunasz, P.B., and van Blerkom, D. 1978, *Astrophys. J*, 224, 193.

Kurucz, R.L. 1970, *ATLAS A Computer Program for Calculating Model Stellar Atmospheres*, Smithsonian Astrophysical Observatory Report No. 309.

Kurucz, R.L. 1979, *Astrophys J Supplement*, 40, 1.

Kurucz, R L., Peytremann, E., and Avrett, E.H. 1974, *Line-Blanketed Model Atmospheres for Early-Type Stars* (Washington. Smithsonian Inst.).

Kurucz, R.L., and Schild, R.E. 1976, in *Be and Shell Stars*, ed. A. Slettebak (Dordrecht Reidel), p. 377

Kwok, S. 1981, in *Proc. IAU Colloq 59, Effects of Mass Loss on Stellar Evolution*, ed. C. Chiosi, and R. Stalio (Dordrecht· Reidel), p. 347.

Lacoarret, M. 1965, *Ann Astrophys.*, 28, 321.

Lacy, C.H. 1977, *Astrophys. J.*, 212, 132.

Laget, M. 1972, in *The Scientific Results from the Orbiting Astronomical Observatory (OAO-2)*, ed. A.D. Code, NASA SP-310, p. 283.

Lamb, S.A., Iben, I., and Howard, W.M 1976, *Astrophys. J*, 207, 209.

Lamers, H.J.G L.M. 1974, *Astron. Astrophys.*, 37, 237.

Lamers, H.J.G.L.M. 1981a, in *Effects of Mass Loss on Stellar Evolution*, ed C. Chiosi, and R. Stalio (Dordrecht: Reidel), p. 181.

Lamers, H.J.G.L.M. 1981b, *Astrophys. J.*, 245, 593.

Lamers, H.J.G.L.M. 1981c, in *The Universe at Ultraviolet Wavelengths*, NASA CP-2171, p. 93.

Lamers, H J.G.L.M., and Snijders, M.A.J. 1975, *Astron. Astrophys.*, 41, 259.

Lamers, H.J.G.L.M., and Morton, D.C. 1976, *Astrophys. J. Supplement*, 32, 715.

Lamers, H.J.G.L.M., and Snow, R.P. 1978, *Astrophys. J*, 219, 504.

Lamers, H.J.G.L.M., and Rogerson, J.B 1978, *Astron Astrophys.*, 66, 417.

Lamers, H.J.G.L.M., Muller, E.A., and Llorente de Andrés, F. 1978a, *Astron Astrophys Supplement*, 32, 1.

Lamers, H.J.G.L.M , Stalio, R., and Kondo, Y. 1978b, *Astrophys. J.*, 223, 207.

Lamers, H.J.G.L.M., Faraggiana, R., and Burger, M 1980, *Astron. Astrophys.*, 82, 48.

Landolt, A.U. 1975, *Astrophys J.*, 196, 789.

Lane, M.C., and Percy, J.R. 1979, *Astron. J*, 84, 831.

Laskarides, P.G. 1973, *Astron. Astrophys.*, 26, 91.

Laskarides, P.G., Odgers, G.J., and Clumenhaga, J.L. 1971, *Astron. J.*, 76, 363.

Leckrone, D.S. 1971, *Astron. Astrophys.*, 11 387.

Leckrone, D.S. 1973, *Astrophys J.*, 185, 577.

Leckrone, D.S. 1980, *Highlights of Astronomy*, 5, 277

Leckrone, D.S., Fowler, J.W., and Adelman, S.J. 1974, *Astron. Astrophys.*, 32, 237.

Leckrone, D.S., and Heacox, W.D. 1978, *Pub. Astron. Soc. Pacific*, 90, 492.

Leckrone, D.S., and Snijders, M.A.J. 1979, *Astrophys. J. Supplement*, 39, 549.

Ledoux, P. 1947, *Astrophys. J.*, 105, 305.

Ledoux, P. 1958, in *Hb. d. Physik*, ed. S. Flugge (Berlin: Springer-Verlag), 51, 605.

Ledoux, P. 1965, in *Stellar Structure*, ed. L.H. Aller and D.B. McLaughlin (Chicago: Univ. Chicago Press), p. 499.

Ledoux, P., and Walraven, Th. 1958, in *Hb. D. Physik*, ed. S. Flugge (Berlin. Springer-Verlag), 51, 353.

Lee, K.-M. 1979, *PhD Thesis*, State Univ. of New York at Stony Brook (Ann Arbor, Mich: Univ. Microfilm International).

Lee, P., and O'Brien, A. 1977, *Astron. Astrophys.*, 60, 259

Lesh, J.R. 1968, *Astrophys J. Supplement*, 17, 371.

Lesh, J.R. 1972, *Astron. Astrophys. Supplement*, 5, 129.

Lesh, J R. 1976, *Astrophys. J.*, 208, 135.

Lesh, J.R. 1977, in *Highlights of Astronomy*, 4, pt. II p. 339, with additional unpublished material.

Lesh, J.R. 1978a, *Astrophys J*, 219, 947.

Lesh, J.R. 1978b, in *High Resolution Spectrometry*, ed. M. Hack (Trieste: Astron. Obs.), p. 344.

Lesh, J R. 1979, in *Spectral Classification of the Future*, ed. M.F. McCarthy, S.J., A.G.D. Philip, and G.V Coyne, S.J. (Citta del Vatican: Specola Vaticana), p. 81

Lesh, J.R. 1981, in *Workshop on Pulsating B Stars*, ed. C. Sterken, and J.M Le Contel (Nice: Observatory), in press.

Lesh, J.R., and Aizenman, M.L. 1973, *Astron. Astrophys*, 22, 229.

Lesh, J.R., and Aizenman, M.L. 1974, *Astron Astrophys.*, 34, 203.

Lesh, J.R., and Bohlin, R.C. 1975, *Pub. Astron Soc. Pacific*, 87, 587.

Lesh, J.R., and Aizenman, M.L. 1976, in *Multiple Periodic Variable Stars*, part 1, ed. W.S. Fitch (Dordrecht Reidel), p. 11.

Lesh, J.R., and Karp, A.H. 1977, *Veroff. Remeis Sternw. Bamberg*, 11, 625.

Lesh, J.R., and Aizenman, M.L 1978, *Ann Rev. Astron. Astrophys*, **16**, 215.

Lesh, J.R., and Wesselius, P R. 1979, *Astron. Astrophys.*, **79**, 115.

Lester, D.F. 1975, *Pub Astron Soc. Pacific*, **87**, 177.

Lester, J.B. 1976, *Astrophys J.*, **210**, 153.

Lillie, C.F, Bohlin, R.C, Molnar, M.R., Barth, C.A., and Lane, A.L. 1972, *Science*, **175**, 321.

Liller, W. 1975, *IAU Cir.*, 2888.

Limber, D.N. 1964, *Astrophys. J.*, **140**, 139.

Limber, D.N. 1967, *Astrophys. J.*, **148**, 141.

Limber, D.N. 1969, *Astrophys. J*, **157**, 785.

Limber, D.N. 1974, *Astrophys. J.*, **192**, 429

Limber, D.N. 1976, in *Be and Shell Stars*, ed. A Slettebak (Dordrecht Reidel), p. 371.

Limber, D.N., and Marlborough, J.M. 1968, *Astrophys. J*, **152**, 181.

Lomb, N.R. 1978, *Mon. Not. Roy. Astr. Soc*, **185**, 325.

Low, F.J., Johnson, H.L., Kleinmann, D.E., Latham, A.S., and Geisel, S.L. 1970, *Astrophys. J*, **160**, 531.

Lucy, L.B. 1971, *Astrophys. J.*, **163**, 95

Lucy, L.B., and Solomon, P.M. 1970, *Astrophys. J.*, **159**, 79.

Lucy, L.B., and White, R.L. 1980, *Astrophys J.*, **241**, 300.

Luud, I.S. 1967, *Astrophysics*, 3, 172; (*Astrofyzika*, 3, 379, in Russian).

Luud, L, and Sapar, A. 1980, Preprint A-1(1980) (Acad. Sci. Estonian SSR, Div. Phys., Math., Tech. Sci.,), Tartu Astrophys. Obs Contr. No. 60.

Lynds, C.R. 1959, *Astrophys. J*, **130**, 577.

Lynds, C.R. 1960, *Astrophys. J.*, **131**, 390.

Macau-Hercot, D., Jamar, C., Monfils, A., Thompson, G.I., Houziaux, L, and Wilson, R. 1978, *Supplement to the Ultraviolet Bright-Star Spectrophotometric Catalogue* (Paris: ESA).

MacGregor, K.B., Hartmann, L., and Raymond, J.C. 1979, *Astrophys. J*, **231**, 514.

Magalashvili, N.L., and Kumsishvili 1980, *Inf. Bull. Var. Stars*, 1968.

Magee, N.H., Merts, A.L, and Huebener, W.F. 1974, *Astrophys. J.*, **196**, 617.

Maillard, J.P. 1973, *C.R. Acad Sci. Paris, série B*, **277**, 127.

Malaise, D., Beeckmans, F., and Jamar, C. 1974, *Mem. Soc. Astron. Italiana*, **45**, 233.

Maraschi, L., Treves, A., and van den Heuvel, E.P.J. 1976, *Nature*, **259**, 292.

Margon, B., Bowyer, S., Penegor, G. 1976, *Mon. Not. Roy. Astr. Soc.*, **176**, 217.

Marlborough, J.M 1969, *Astrophys. J.*, **156**, 135.

Marlborough, J.M. 1970, *Astrophys. J.*, **159**, 575.

Marlborough, J.M. 1976, in *Proc. IAU Symp. 70, Be and Shell Stars*, ed. A. Slettebak (Dordrecht: Reidel), p. 335.

Marlborough, J.M. 1977a, *Astrophys. J*, **216**, 446.

Marlborough, J.M. 1977b, *Pub. Astron. Soc. Pacific*, 89, 122

Marlborough, J.M, and Zamir, M. 1975, *Astrophys. J*, **195**, 145.

Marlborough, J.M., and Snow, T.P. 1976, in *Proc. IAU Symp. 70, Be and Shell Stars*, ed. A. Slettebak (Dordrecht: Reidel), p. 179.

Marlborough, J.M, Snow, T.P., and Slettebak, A. 1978, *Astrophys. J*, **224**, 157.

Marsh, K.A. 1975, *Astrophys. J*, **201**, 190.

Marsh, K.A 1976, *Astrophys. J*, **203**, 552.

Marsh, K.A., Purton, C.R., and Feldman, P.A. 1976, *Astron. Astrophys.*, **49**, 211.

Marti, F., and Noerdlinger, P.D. 1977, *Astrophys. J.*, **215**, 247.

Mason, K.O., White, N.E., Sanford, P.W., Hawkins, F.J., Drake, J.F., and York, D.G. 1976, *Mon. Not Roy. Astr. Soc.*, **176**, 193.

Mattis, J.S., 1957, *Astrophys. J.*, **125**, 318.

McCrea, W.H. 1928, *Mon. Not. Roy. Astr. Soc.*, **88**, 729.

McCrea, W.H. 1962, *Quart. Jour Roy. Astr. Soc.*, 3, 63.

McLaughlin, D.B. 1931, *Pub. American Astron. Soc* , 7, 31.

McLaughlin, D.B. 1932, *Pub Obs Univ. Michigan*, 4, 198.

McLaughlin, D.B. 1933, *Proc Nat. Ac. Sci.*, 19, 44.

McLaughlin, D.B. 1936, *Astrophys J.*, 84, 235.

McLaughlin, D.B. 1937, *Astrophys. J* , 85, 181.

McLaughlin, D.B. 1948, in Merrill and Burwell 1948, *Astrophys. J.*, 98, 163.

McLaughlin, D.B. 1961, *J R. Astron Soc Canada*, 55, 13, and 73.

McLean, I.S. 1979, *Mon. Not. Roy Astr. Soc.*, 186, 265.

McLean, I.S., and Clarke, D. 1976, in *Proc IAU Symp 70, Be and Shell Stars*, ed. A. Slettebak (Dordrecht. Reidel), p. 261.

McLean, I S., and Brown, J.C. 1978, *Astron. Astrophys.*, 69, 291.

McLean, I.S., Coyne, G V., Frecker, J.E., and Serkovski, K. 1979, *Astrophys. J.*, 228, 802.

McLean, I.S., and Clarke, D 1979, *Mon. Not Roy Astr Soc.*, 186, 245.

Meade, M.R., and Code, A.D. 1980, *Astrophys. J. Supplement*, 42, 283.

Meisel, D.D. 1968, *Astrophys. J.*, 73, 350.

Meisel, D.D. 1971, *Pub. Astron. Soc. Pacific*, 83, 49.

Mendoza, V.E.E. 1958, *Astrophys. J.*, 128, 207.

Menzel, D.H. 1929, *Pub. Astron Soc. Pacific*, 41, 344.

Menzel, D.H. 1937, *Astrophys. J.*, 85, 330.

Merrill, P.W. 1952, *Astrophys. J.*, 115, 145.

Merrill, P.W., and Burwell, C.G. 1933, *Astrophys J* , 78, 87.

Merrill, P W., and Burwell, C.G. 1943, *Astrophys J* , 98, 153.

Merrill, P.W., and Burwell, C.G. 1948, *Astrophys J.*, 98, 163.

Merrill, P.W., and Burwell, C.G. 1949, *Astrophys. J.*, 110, 387.

Merrill, P.W , and Burwell, C.G 1950, *Astrophys J.*, 112, 72.

Michaud, G. 1970, *Astrophys. J.*, 160, 641.

Mihalas, D. 1965, *Astrophys. J. Supplement*, 9, 321.

Mihalas, D. 1966, *Astrophys. J. Supplement*, 13, 1.

Mihalas, D. 1970a, *Astrophys. Space Sci.*, 8, 50.

Mihalas, D 1970b, *Stellar Atmospheres* (San Francisco: W.H. Freeman and Co).

Mihalas, D. 1972a, *Non-LTE Model Atmospheres for B and O Stars*, NCAR-TN/STR-76.

Mihalas, D. 1972b, *Astrophys J.*, 176, 139.

Mihalas, D. 1972c, *Astrophys. J* , 177, 115.

Mihalas, D. 1973a, *Astrophys. J.*, 179, 209.

Mihalas, D. 1973b, *Astrophys. J.*, 184, 851.

Mihalas, D. 1974, *Astron. J.*, 79, 1111

Mihalas, D 1978, *Stellar Atmospheres*, 2d ed. (San Francisco. W.H. Freeman and Co.).

Mihalas, D. 1980, *Mon. Not Roy. Astr. Soc* , 189, 671.

Mihalas, D , and Hummer, D.G. 1973, *Astrophys J* , 179, 827.

Mihalas, D., and Hummer, D G. 1974, *Astrophys J. Supplement*, 28, 343.

Mihalas, D., Barnard, A.J., Cooper, J., and Smith, E.W. 1974, *Astrophys. J* , 190, 315.

Mihalas, D., Heasley, J N., and Auer, L.H 1975, *A Non-LTE Model Stellar Atmosphere Computer Program*, NCAR-TN/STR-104.

Mihalas, D., and Kunasz, P.B. 1978, *Astrophys. J* , 219, 635.

Milgrom, M 1976, *Astron. and Astrophys* , 53, 321.

Milkey, R.N., and Dyck, H.M 1973, *Astrophys J.*, 181, 83.

Millar, T.J. 1979, *Mon. Not Roy. Astr. Soc.*, 189, 507.

Milne, E A. 1926, *Mon Not. Roy. Astr Soc.*, 87, 697.

Miyamoto, S. 1949, *Jap J. Astr.*, 1, 17.

Miyamoto, S. 1950, *Astrophys. J.*, 113, 181.

Miyamoto, S. 1952, *Pub. Astron. Soc. Japan*, 4, 1 and 28.

Moffat, A F., Haupt, W., and Schmidt-Kaler, Th. 1973, *Astron. Astrophys.*, 23, 433.

Molnar, M.R. 1972, *Astrophys. J.*, **175**, 453.

Molnar, M.R. 1974, *Astrophys J.*, **187**, 531.

Molnar, M.R. 1975, *Astrophys. J.*, **200**, 106.

Morgan, T.H., Spear, G.G., Kondo, Y., and Henize, K.G. 1975, *Astrophys J.*, **197**, 371.

Morgan, T.H., Kondo, Y., and Modisette, J.L 1977, *Astrophys. J.*, **216**, 457.

Morgan, V.W., Code, A.D , Whitford, A.E. 1955, *Astrophys J. Supplement*, **2**, 41.

Morgan, W.W., and Keenan, P.C. 1973, *Ann. Rev. Astron. Astrophys.*, **11**, 29.

Morton, D.C. 1968, *Astrophys. J.*, **150**, 535.

Morton, D C. 1979, *Mon. Not. Roy. Astr. Soc.*, **189**, 57.

Morton, D.C., and Adams, T.F. 1968, *Astrophys. J*, **151**, 611.

Mushotzky, R.F., Roberts, D.H., Baity, W.A., and Peterson, L.E. 1977, *Astrophys J (Letters)*, **211**, L129.

Mustel, E.R. 1940, *Astron. Zh.*, **17**, No 2.

Mustel, E.R. 1941, *Astron Zh.*, **18**, 297.

Mustel, E.R. 1944, *Astron. Zh.*, **21**, 133.

Nagirner, D.T 1962, *Trudy Leningrad Astron. Obs*, **19**, 79

Nakagiri, M., and Hirata, R. 1979, *Inf. Bull Var. Stars*, 1565.

Nandy, K., Thompson, G.I., and Humphries, C M 1974, *Mon. Not Roy. Astr. Soc.*, **166**, 297

Nandy, K., Thompson, G.I , Jamar, C , Monfils, A., and Wilson, R. 1975, *Astron. Astrophys.*, **44**, 195.

Nandy, K., Thompson, G.I., Jamar, C., Monfils, A., and Wilson, R 1976, *Astron Astrophys* , **51**, 63

Navach, C 1973, *Astron Astrophys.*, **22**, 371.

Navach, C., Lehmann, M., and Huguenin, D. 1973, *Astron. Astrophys.*, **22**, 361.

Neckel, T., and Klare, G. 1976, *Astron. Astrophys.*, **52**, 77.

Nelson, G D., and Hearn, A.G. 1978, *Astron. Astrophys.*, **65**, 223.

Noerdlinger, P.D., and Rybicki, G.B. 1974, *Astrophys. J.*, **193**, 651.

Nordh, H.L., and Olofsson, S.G. 1977, *Astron. Astrophys.*, **56**, 117.

Norris, J. 1971, *Astrophys J. Supplement*, **23**, 193.

Norris, J , and Strittmatter, P.A. 1975, *Astrophys. J.*, **196**, 515.

Oblak, E., Cosidère, S., and Chareton, M. 1976, *Astron. Astrophys. Supplement*, **24**, 69.

Odell, A.P. 1974, *Astrophys. J* , **194**, 645.

Odell, A.P. 1979, *Pub. Astron. Soc. Pacific*, **91**, 326.

Odell, A.P. 1981, *Astrophys. J* , **246**, L77.

Oergle, R.W. 1977, PhD. Thesis, Univ. Massachusetts (Ann Arbor· Univ. Microfilms International).

Oergle, W.R., and van Blerkom, D. 1976, *Astrophys. J.*, **208**, 453.

Oke, J.B. 1965, *Ann Rev Astron Astrophys.*, **3**, 23.

Olnon, F.M. 1975, *Astron. Astrophys.*, **39**, 217.

Olsen, E.H. 1972, *Astron. Astrophys* , **20**, 167.

Olson, G P. 1978, *Astrophys. J.*, **226**, 124.

Opolski, A., and Ciurla, T 1961, *Acta Astron.*, **11**, 231.

Osaki, Y. 1971, *Astrophys J* , **189**, 469.

Osaki, Y 1975, *Pub Astron Soc Japan*, **27**, 237

Osaki, Y 1979, in *Changing Trends in Variable Star Research*, ed. F M. Bateson, J. Smak, and I.H. Urch (Hamilton, N Z. Univ. of Waikato), p. 467.

Osmer, P.S 1973, *Astrophys J. (Letters)*, **184**, L127.

Osmer, P.S , and Peterson, D.M. 1974, *Astrophys. J* , **187**, 117.

Osterbrock, D.E. 1974, *Astrophysical Processes in Gaseous Nebulae* (San Francisco W.H. Freeman and Co), chap. IV.

Ozemre, K. 1978, *Pub. Istanbul Univ. Obs* , No. 101.

Paczynski, B. 1970a, *Acta Astron* , **20**, 47.

Paczynski, B 1970b, *Acta Astron.*, **20**, 195.

Paczynski, B. 1971, *Acta Astron* , **21**, 271.

Paerels, F.B.S., Lamers, H.J.G.L.M., and de Loore, C. 1980, *Astron Astrophys* , **90**, 204.

Pagel, B E.F. 1960, *Vistas in Astronomy*, **3**, 203.

Pallavicini, R., Golub, L., Rosner, R., Vaiana, G S., Ayres, T., and Linsky, J. 1980, *Astrophys J*, 248, 279

Panagia, N. 1973, *Astron. J.*, 78, 929.

Panagia, N., and Felli, M 1975, *Astron. Astrophys*, 39, 1.

Panek, R J., and Savage, B.D 1976, *Astrophys J*, 206, 167.

Pannekoek, A. 1936, *Pub. Astron. Inst Amsterdam*, 4, also addendum published in 1936.

Papaloizou, J.C.B., and Pringle, J.E 1978, *Mon Not Roy. Astr Soc.*, 182, 423.

Parker, E N. 1958, *Astrophys J.*, 128, 664.

Parsons, S.B., Wray, J.D., Henize, K.G., and Benedict, G.F 1977, *Bull. Am. Astron Soc.*, 9, 307.

Pecker, J.-C. 1950, *Ann. Astrophys*, 13, 433.

Pecker, J.-C. 1962, *Space Res*, 3, 1076.

Pecker, J.-C 1963, *Space Sci. Rev.*, 1, 729.

Pecker, J.-C. 1965, *Ann Rev. Astron. Astrophys.*, 3, 135.

Pecker, J.-C. 1972, *Mém. Soc. Roy. Sci. Liège*, 6th Ser, III, 243.

Pecker, J.-C, and Thomas, R.N 1961, in *Aerodynamic Phenomena in Stellar Atmospheres*, ed R.N. Thomas, *Suppl. Nuovo Cim.*, 22, No. 1, p. 1.

Pedersen, H. 1976, *Astron Astrophys.*, 49, 217.

Pedersen, H. 1979, *Astron Astrophys. Supplement*, 35, 313.

Pedersen, H., and Thomsen, B. 1977, *Astron. Astrophys Supplement*, 30, 11.

Percy, J.R 1971, *Astron. J.*, 76, 1105.

Percy, J.R 1979, *Inf Bull Var. Stars*, 1530.

Percy, J.R. 1980, *Space Sci. Rev*, 27, 313.

Percy, J.R., and Madore, K. 1972, *Astron J.*, 77, 381

Percy, J.R., and Lane, M.C. 1977, *Astron J*, 82, 353.

Persi, P., Viotti, R., and Ferrari-Toniolo, M. 1977, *Mon Not Roy. Astr Soc*, 181, 685.

Peters, G.J. 1976a, *Astrophys J Supplement*, 30, 551.

Peters, G J. 1976b, in *Proc. IAU Symp. 70, Be and Shell Stars*, ed. A. Slettebak (Dordrecht Reidel), p 209.

Peters, G.J 1979, *Astrophys J Supplement*, 39, 175.

Peters, G J. 1981, in *The Be Stars*, IAU Symp. 98, in press.

Peters, G.J., and Aller, L.H 1970, *Astrophys. J.*, 159, 525

Peterson, D.M., and Strom, S.E. 1969, *Astrophys. J*, 157, 1341

Peterson, D.M., and Scholz, M. 1971, *Astrophys. J.*, 163, 51.

Peterson, D.M., and Shipman, H L 1973, *Astrophys J*, 180, 635.

Peton, A., Bigay, J H, Garnier, R, and Paturel, B 1972, *Astron. Astrophys*, 17, 47

Petrie, R.M 1952, *Pub Dom. Astrophys. Obs*, 9, 251.

Petrie, R M 1965, *Pub Dom. Astrophys Obs.*, 12, 317.

Peytremann, E 1975, *Astron Astrophys*, 39, 393.

Peytremann, E, and Davis, R.J. 1974, *Astrophys. J. Supplement*, 28, 211.

Phillips, A.P. 1977, *Mon Not Roy Astr Soc.*, 181, 777.

Plavec, M. 1976, in *Proc IAU Symp. 70, Be and Shell Stars*, ed. A Slettebak (Dordrecht Reidel), p. 1 and 439.

Poeckert, R. 1975, *Astrophys. J.*, 196, 777

Poeckert, R 1980, *Pub Dom. Astrophys. Obs.*, 15, 357.

Poeckert, R. 1981, in *IAU Symp 98, The Be Stars*, in press.

Poeckert, R, and Marlborough, J M. 1976, *Astrophys J.*, 206, 182.

Poeckert, R., and Marlborough, J M 1977, *Astrophys. J*, 218, 220.

Poeckert, R., and Marlborough, J.M. 1978a, *Astrophys J.*, 220, 940.

Poeckert, R, and Marlborough, J.M 1978b, *Astrophys J Supplement*, 38, 229.

Poeckert, R., and Marlborough, J.M 1979, *Astrophys. J*, 233, 259.

Poeckert, R, Bastien, P., and Landstreet, J.D. 1979, *Astron J.*, 84, 812.

Polidan, R.S. 1976, in *Proc. IAU Symp. 70, Be and Shell Stars*, ed. A. Slettebak (Dordrecht Reidel), p. 401.

Polidan, R S., and Peters, G.J. 1976, in *Proc IAU Symp. 70, Be and Shell Stars*, ed. A. Slettebak (Dordrecht Reidel), p. 59.

Polidan, R.S , Locke, M., and Parmar, A.N. 1981, quoted by G J. Peters (1981)

Popper, D.M 1974, *Astrophys. J* , **188**, 559.

Popper, D.M 1978, *Astrophys. J (Letters)*, **220**, L11.

Pottasch, S.R. 1961, *Ann Astrophys* , **24**, 159.

Prendergast, K., and Burbidge, G. 1968, *Astrophys. J.*, **151**, L83.

Preston, G.W 1974, *Ann. Rev Astron Astrophys.*, **12**, 257.

Purton, C.R 1976a, in *Proc. IAU Symp. 70, Be and Shell Stars*, ed. A. Slettebak (Dordrecht Reidel), p. 157.

Purton, C.R. 1976b, as quoted by Marlborough, J M 1977a.

Rappaport, S , Clark, G.M., Cominsky, L , and Joss, P.C., Li, F. 1978, *Astrophys. J. (Letters)*, **224**, L1.

Redman, R O 1942, *Mon Not Roy Astron Soc.*, **102**, 134, and 140.

Relyea, L.J , and Kurucz, R L 1978, *Astrophys J Supplement*, **37**, 45.

Richter, D 1971, *Astron. Astrophys* , **14**, 415

Roark, T.P. 1971, *Astron. J* , **76**, 634.

Robertson, J.W. 1972, *Astrophys J.*, 177, 473.

Rogerson, J.B., and Lamers, H.J G L.M 1975, *Nature*, **256**, 19.

Rosendhal, J.D. 1973a, *Astrophys J* , **182**, 523.

Rosendhal, J.D. 1973b, *Astrophys J (Letters)*, **183**, L39.

Rosendhal, J.D. 1973c, *Astrophys. J* , **186**, 909

Rosner, R., Golub, L., Coppi, B., and Vaiana, G.S 1978, *Astrophys. J* , **222**, 317

Rosner, R., and Vaiana, G.S 1979, in *Proc Intl School of Astrophys* , ed G Sette, and R. Giacconi (Erice)

Rosner, R., Seward, F., Topka, K., and Zwaan, C 1981, preprint

Rosseland, S. 1926, *Astrophys J* , **63**, 218.

Roth, M.L., and Weigert, A. 1979, *Astron Astrophys* , **80**, 48

Rottenberg, J.A. 1952, *Mon Not. Roy. Astr Soc* , **112**, 125.

Rublev, S.V 1961, *Soviet Astron* , **4**, 780.

Rublev, S V 1964, *Soviet Astron* , **7**, 492.

Rucinski, S M. 1966, *Astron Obs Warsaw Univ.*, Reprint 208

Rucinski, S.M 1967, *Warsaw Univ. Obs* , Reprint 231.

Rucinski, S.M. 1970, *Acta Astron* , **20**, 1.

Rudkjøbing, M 1947, *Pub mind. medd Københavens Obs.*, No. 145.

Rudy, R.J , and Kemp, J.C. 1978, *Mon Not Roy. Astr Soc* , **183**, 595.

Rufener, F. 1976, *Astron Astrophys Supplement*, **26**, 275

Rufener, F , Maeder, A., and Burki, G. 1978, *Astron. Astrophys Supplement*, **31**, 179.

Rybicki, G C 1970, in *Spectrum Formation in Stars with Steady-State Extended Atmospheres*, ed. H.G Groth, and P. Wellmann, Nat. Bur. Stds Special Pub. 332, p. 87.

Rybicki, G B , and Hummer, D G. 1978, *Astrophys J* , **219**, 654.

Sackmann, I J., and Anand, S.P.S. 1970, *Astrophys J* , **162**, 105.

Sahade, G. 1980, *Collège de France Lectures, The Wolf-Rayets Stars* (Collège de France Publ.)

Sapar, A., and Kuusik, I 1978, *Pub Tartu Astrophys Obs* , **46**, 71

Sareyan, J -P 1979, Thesis, Univ. of Nice.

Sargent, W.L W., and Searle, L. 1968, *Astrophys. J* , **152**, 443

Sargent, W L.W., and Strittmatter, P.A. 1966, *Astrophys J.*, **145**, 938.

Savage, B D., and Jenkins, E B. 1972, *Astrophys J* , **172**, 491

Savage, B D., Wesselius, P R., Swings, J P , and Thé, P S 1978, *Astrophys J* , **224**, 149

Savage, B.D , and Mathis, J S. 1979, *Ann. Rev Astron. Astrophys* , **17**, 73.

Scargle, J D., Erickson, E.F , Witteborn, F.C , and Strecker, D W. 1978, *Astrophys J.*, **224**, 527

Schafgans, J.J , and Tinbergen, J 1979, *Astron. Astrophys Supplement*, **35**, 279

Schild, R E. 1965, *Astrophys J* , **142**, 979.

Schild, R E. 1966, *Astrophys. J.*, **146**, 142.

Schild, R.E. 1973, *Astrophys J* , **179**, 221

Schild, R E. 1976, in *Proc IAU Symp. 70, Be and Shell Stars*, ed. A Slettebak (Dordrecht Reidel), p 107

Schild, R E 1978, *Astrophys. J. Supplement*, **37**, 77

Schild, R.E., Peterson, D.M., and Oke, J.B 1971, *Astrophys. J* , **166**, 95

Schild, R.E., Chaffee, F., Frogel, J., and Person, E 1974, *Astrophys. J.*, **190**, 73.

Schild, R E., and Chaffee, F H 1975, *Astrophys J* , **196**, 503.

Schild, R E , and Romanishin, S. 1976, *Astrophys J* , **204**, 493.

Schklovski, I S 1967, *Astrophys J (Letters)*, **148**, L1.

Schmid-Burgk, J. 1975, *Astron Astrophys* , **40**, 429

Schmid-Burgk, J., and Scholz, M 1975, *Astron Astrophys.*, **41**, 41

Schmidt-Kaler, Th. 1964, *Z f Astrophys* , **58**, 217

Schmidt-Kaler, Th 1965, in *Landolt-Bornstein Tables*, Group VI (Berlin· Springer-Verlag), p. 298.

Scholz, M 1967, *Zeit f Astrophys.*, **65**, 1

Scholz, M 1972, *Vistas in Astronomy*, **14**, 53.

Schonberner, D 1977, *Astron Astrophys* , **57**, 437

Schonberner, D., and Wolf, R E.A. 1974, *Astron Astrophys* , **37**, 87.

Schultz, G V., and Wiener, W. 1975, *Astron. Astrophys* , **43**, 133.

Schwarzschild, K 1906, *Akad. Wiss Gottingen, Math. -Phys. Klasse Nachrichten*, p 41.

Schwarzschild, M 1958, *Stellar Structure and Evolution* (Princeton. Univ. Princeton Press), p 44 et seq.

Sears, R.L , and Brownlee, R.R. 1965, in *Stellar Structure*, ed L.H. Aller, and D B. McLaughlin (Chicago Univ. Chicago Press), p 575.

Selvelli, P.L., and Stalio, R. 1980, in *Second IUE European Conference*, ESA SP-157, p. 155

Serkowski, K. 1968, *Astrophys J.*, **154**, 115.

Serkowski, K. 1970, *Astrophys. J* , **160**, 1083.

Seward, F.D , Forman, W.R., Giacconi, R., Griffiths, R.E., Harnden, F R., Jones, C., and Pye, J P , 1979, *Astrophys. J (Letters)*, **234**, L55.

Shajn, G., and Struve, O. 1929, *Mon. Not. Roy. Astr. Soc.*, **89**, 222.

Shakhovskoi, N.M. 1962, *Astron Circ USSR*, 228.

Shakhovskoi, N.M 1964, *Soviet Astron* , **8**, 83.

Shakhovskoi, N M 1965, *Soviet Astron* , **8**, 833.

Shapley, H , and Nicholson, S B. 1919, *Proc Nat Acad. Sci.*, **5**, 417

Sharov, A S., and Lyuty, V M. 1976, in *Proc. IA U Symp. 70, Be and Shell Stars*, ed. A. Slettebak (Dordrecht: Reidel), p 105.

Shaw, J.S 1975, *Astron. Astrophys* , **41**, 367.

Shibahashi, H., and Osaki, Y 1976, *Pub. Astron Soc. Japan*, **28**, 533.

Shobbrook, R R. 1976, *Mon Not. Roy. Astr Soc* , **176**, 673

Shobbrook, R R 1978a, *Mon Not Roy. Astr. Soc* , **184**, 43.

Shobbrook, R R 1978b, *Mon Not Roy. Astr Soc* , **184**, 825.

Shobbrook, R R. 1979a, in *Changing Trends in Variable Star Research*, ed. F.M. Bateson, J. Smak, and I H. Urch (Hamilton, N.Z.: Univ. of Waikato), p. 512.

Shobbrook, R.R 1979b, *Mon. Not Roy Astr Soc.*, **189**, 571.

Simon, K.P 1979, Thesis, Kiel Univ.

Sistla, G , and Hong, S S. 1975, *Astron. Astrophys* , **44**, 477

Sitko, M L., and Savage, B.D 1980, *Astrophys J* , **237**, 82.

Slettebak, A. 1949, *Astrophys. J* , **110**, 498.

Slettebak, A. 1966, *Astrophys J* , **145**, 121.

Slettebak, A. 1975, *Astrophys. J.*, **197**, 137.

Slettebak, A. 1976, in *Proc. IAU Symp. 70, Be and Shell Stars*, ed. A Slettebak (Dordrecht: Reidel), p. 123.

Slettebak, A. 1979, *Space Sci Rev.*, **23**, 541.

Slettebak, A., and Howard, R.F. 1955, *Astrophys J*, **121**, 102.

Slettebak, A., Collins, G.W., Boyce, P.B, White, N.M., and Parkinson, T D. 1975, *Astrophys. J Supplement*, **29**, 137.

Slettebak, A, and Reynolds, R.C. 1978, *Astrophys. J Supplement*, **38**, 205.

Slettebak, A., and Snow, T.P. 1978, *Astrophys J (Letters)*, **224**, L127

Smith, A.M. 1967, *Astrophys. J*, **147**, 158.

Smith, M.A. 1977, *Astrophys. J.*, **215**, 574.

Smith, M.A. 1978a, in *High Resolution Spectrometry*, ed M. Hack (Trieste: Astron. Obs.), p. 356.

Smith, M.A. 1978b, *Astrophys. J*, **224**, 927.

Smith, M.A. 1980a, *Astrophys J. Supplement*, **42**, 261.

Smith, M.A. 1980b, *Astrophys. J.*, **240**, 149.

Smith, M.A. 1980c, in *Nonradial and Nonlinear Stellar Pulsation* (Lecture Notes in Physics, vol. 125), ed H A Hill, and W.A. Dziembowski (Berlin: Springer-Verlag), p. 60.

Smith, M.A. 1981a, *Astrophys. J*, **248**, 214.

Smith, M.A. 1981b, *Astrophys J*, **246**, 905.

Smith, M.A., and Buta, R.J. 1979, *Astrophys J (Letters)*, **232**, L193

Smith, M.A., and Ebbets, D. 1981, *Astrophys. J*, **247**, 158.

Smith, M.A., and Karp, A.H. 1976, in *Proc. Los Alamos Conf. on Solar and Stellar Pulsation*, ed. A.N. Cox, and R.G. Deupree, LA-6544-C, p. 289.

Smith, M.A., and Karp, A.H. 1978, *Astrophys. J*, **219**, 522.

Smith, M.A., and Karp, A.H. 1979, *Astrophys J*, **230**, 156.

Smith, M.A., and McCall, M.L. 1978a, *Astrophys. J*, **221**, 861.

Smith, M.A., and McCall, M.L. 1978b, *Astrophys. J.*, **223**, 221.

Smith, M.A., and Stern, S.P. 1978, *Astron. J.*, **84**, 1363.

Smyth, M J., and Nandy, K. 1978, *Mon Not. Roy. Astr. Soc.*, **183**, 215.

Snijders, M.A.J. 1975, *Bull. Am Astron. Soc.*, **7**, 469.

Snijders, M.A.J. 1977, *Astron. Astrophys.*, **60**, 377.

Snijders, M A.J., and Lamers, H.J.G.L.M. 1975, *Astron. Astrophys.*, **41**, 245.

Snijders, M.A.J., and Underhill, A.B. 1971, *Mon Not Roy. Astr. Soc*, **151**, 215.

Snow, T.P. 1975, *Astrophys. J*, **198**, 361.

Snow, T P. 1981, *IAU Symposium 98, The Be Stars*, in press.

Snow, T.P., and Marlborough, J.M. 1976, *Astrophys J. (Letters)*, **203**, L87.

Snow, T.P., and Morton, D.C. 1976, *Astrophys. J. Supplement*, **32**, 429.

Snow, T.P., and Jenkins, E.B. 1977, *Astrophys. J. Supplement*, **33**, 269.

Snow, T.P., and Marlborough, J.M. 1980, *Astrophys. J.*, **235**, 85.

Snow, T.P., and Hayes, D.P. 1978, *Astrophys. J.*, **226**, 897.

Snow, T.P., Peters, G.J., and Mathieu, R.D. 1979, *Astrophys J. Supplement*, **39**, 359

Sobolev, V.V. 1947, *Moving Envelopes of Stars*, Thesis, Leningrad State Univ. (in Russian); transl. by S. Gaposchkin, 1960 (Cambridge, Mass. Harvard Univ. Press).

Sobolev, V.V. 1957, *Soviet Astron.*, **1**, 678.

Spitzer, L. 1962, *Physics of Fully Ionized Gases* (New York Interscience Publishers), p. 148.

Sreenivasan, S.R., and Wilson, W.J.F. 1978a, *Astrophys. Space Sci.*, **53**, 193.

Sreenivasan, S.R., and Wilson, W.J.F. 1978b, *Astron. Astrophys*, **70**, 755

Stalio, R., Selvelli, P.L., and Crivellari, L. 1977, *Astron. Astrophys.*, **60**, 109.

Stamford, P.A., and Watson, R.D. 1977, *Mon Not Roy Astr. Soc.*, **180**, 551.

Stamford, P.A., and Watson, R.D. 1979, in *Changing Trends in Variable Star Research*, ed. F.M. Bateson, J. Smak, and I.H. Urch (Hamilton, N.Z.: Univ. of Waikato), p. 504.

Stecher, T.P. 1968, in *An Introduction to Space Science*, ed. W N. Hess, and G D. Mead (New York: Gordon and Breach), p. 285.

Sterken, C. 1976, Thesis, Vrije Univ. te Brussel.

Sterken, C. 1977, *Astron. Astrophys.*, **57**, 361.

Sterken, C., and Jerzykiewicz, M. 1980, in *Nonradial and Nonlinear Stellar Pulsation Proceedings* (Lecture Notes in Physics, vol. 125), ed. H.A. Hill, and W.A. Dziembowski (Berlin· Springer-Verlag), p. 105.

Sterken, C , and Wolf, B. 1978, *Astron. Astrophys.*, **70**, 641.

Stibbs, D.N.W. 1950, *Mon. Not. Roy Astr. Soc.*, **110**, 395.

Stoeckley, T.R., and Mihalas, D. 1973, *Limb Darkening and Rotation Broadening of Neutral Helium and Ionized Magnesium Line Profiles in Early-Type Stars*, NCAR-TN/STR-84.

Stothers, R. 1972, *Astrophys. J.*, **175**, 431.

Stothers, R. 1974, *Astrophys. J.*, **194**, 695

Stothers, R. 1976, *Astrophys. J.*, **209**, 800.

Stothers, R., and Chin, C.-w. 1975, *Astrophys. J.*, **198**, 407.

Stothers, R., and Chin, C -w. 1976, *Astrophys. J.*, **204**, 472.

Stothers, R., and Chin, C.-w. 1977, *Astrophys. J.*, **211**, 189.

Stothers, R., and Chin, C.-w. 1978, *Astrophys. J.*, **226**, 231.

Stothers, R., and Chin, C.-w. 1979, *Astrophys. J.*, **233**, 267.

Stothers, R., and Chin, C.-w. 1980, *Astrophys. J.*, **240**, 885.

Strom, S.E., and Avrett, E.H. 1965, *Astrophys. J. Supplement*, **12**, 1.

Stromgren, B. 1940, *Pub mind, medd Kϕbenhavens Obs.*, No. 127.

Stromgren, B 1944, *Pub mind, medd. Kϕbenhavens Obs* , No. 144.

Strömgren, B. 1966, *Ann. Rev. Astron. Astrophys.*, **4**, 433.

Strongylis, G.F., and Bohlin, R.C. 1979, *Pub. Astron. Soc. Pacific*, **91**, 205.

Struve, O. 1931a, *Astrophys J.*, **74**, 225.

Struve, O. 1931b, *Astrophys. J.*, **73**, 94.

Struve, O. 1939, *Astrophys. J.*, **90**, 699.

Struve, O. 1942, *Astrophys. J.*, **95**, 134.

Struve, O. 1951, in *Astrophysics*, ed. J.A. Hynek (New York: McGraw-Hill Book Co.).

Struve, O., and Swings, P. 1932, *Astrophys. J* , **75**, 161.

Struve, O., and Elvey, C.T. 1934, *Astrophys J.*, **79**, 409.

Struve, O., and Roach, F.E. 1939, *Astrophys. J.*, **90**, 727.

Struve, O., and Wurm, K. 1938, *Astrophys J.*, **88**, 84.

Surdej, J. 1977, *Astron. Astrophys.*, **60**, 303.

Surdej, J. 1979, *Astron. Astrophys.*, **73**, 1.

Swings, J.P 1973, *Astron. Astrophys.*, **26**, 443.

Swings, P. and Struve, O. 1941, *Astrophys. J.*, **94**, 291.

Swings, P. and Struve, O. 1945, *Astrophys J.*, **101**, 224.

Swings, J.P., and Allen, D.A. 1971, *Astrophys. J (Letters)*, **167**, L41.

Swings, J.P., Klutz, M , Vreux, J.M., and Peytremann, E. 1976, *Astron. Astrophys. Supplement*, **25**, 193.

Takada, M. 1977, *Pub Astron. Soc Japan*, **29**, 439.

Tanaka, Y. 1966, *Pub. Astron. Soc. Japan*, **18**, 47.

Tebbe, P.L. 1969, *Astron J* , **74**, 920.

Thomas, R.N , and Athay, R.G. 1961, *Physics of the Solar Chromosphere* (New York Inter-Science Publ)

Thomas, R.N. 1968, in *Wolf-Rayet Stars*, ed. K.B. Gebbie, and R.N. Thomas, NBS, SP-307, p. 239.

Thomas, R.N. 1973, *Astron. Astrophys.*, **29**, 297.

Thomas, R.N. 1983, *Stellar-Atmospheric Structural Patterns*, to be published.

Thompson, G I., Humphries, C.M., and Nandy, K. 1974, *Astrophys J (Letters)*, **187**, L81.

Thompson, G I., Nandy, K., Jamar, C., Monfils, A , Houziaux, L , Carnochan, D J., and Wilson, R. 1978, *Catalogue of Stellar Ultraviolet Fluxes* (U K. The Science Research Council).

Thomsen, B. 1974, *Astron. Astrophys.*, **35**, 479

Traving, G. 1955, *Zeit f Astrophys* , **36**, 1

Uesugi, A., and Fukuda, I. 1970, *Contr. Inst. Astrophys Kwasan Obs Univ. Kyoto*, No. 189.

Underhill, A.B. 1948a, *Astrophys. J.*, **107**, 247.

Underhill, A.B. 1948b, *Astrophys J.*, **107**, 337.

Underhill, A.B. 1948c, *Astrophys. J* , **107**, 349.

Underhill, A.B. 1948d, *Astrophys J.*, **108**, 476.

Underhill, A.B. 1950, *Pub mind. medd, Kϕbenhavens Obs.*, No. 151.

Underhill, A.B. 1951, *Pub. Dom. Astrophys Obs* , **8**, 357

Underhill, A.B., 1953, *Mon. Not. Roy. Astr Soc.*, **113**, 477.

Underhill, A.B. 1960, *Pub. Dom. Astrophys. Obs* , **11**, 353.

Underhill, A.B. 1961, in *Aerodynamic Phenomena in Stellar Atmospheres*, ed. R.N. Thomas, *Suppl Nuovo Cim.*, **22**, No. 1, p. 69.

Underhill, A.B. 1962, *Pub Dom. Astrophys Obs.*, **11**, No. 23, No. 24.

Underhill, A.B. 1963, *Bull. Astron. Inst. Netherlands*, **17**, 161.

Underhill, A.B. 1966a, *The Early Type Stars* (Dordrecht. Reidel).

Underhill, A.B 1966b, *J. Quant Spectrosc. Radiat. Transfer*, **6**, 675

Underhill, A. B. 1966c, *Vistas in Astronomy*, **8**, 41.

Underhill, A.B. 1968, *Bull. Astron. Inst Netherlands*, **19**, 526.

Underhill, A.B. 1969, in *Spectrum Formation in Stars with Steady-State Extended Atmospheres*, ed. H.G. Groth, and P. Wellmann, NBS Special Pub. 332, p. 3.

Underhill, A.B. 1970, *Astron Astrophys.*, **6**, 114.

Underhill, A.B. 1972, *Vistas in Astronomy*, **13**, 169.

Underhill, A.B. 1973a, *Astron. Astrophys.*, **25**, 161.

Underhill, A B. 1973b, *Astron. Astrophys.*, **25**, 175

Underhill, A.B. 1975a, *Phil. Trans. Roy Soc. London, Series A* , **279**, 429.

Underhill, A.B 1975b, *Astrophys J* , **199**, 691.

Underhill, A.B. 1979a, unpublished results.

Underhill, A.B. 1979b, *Astrophys J.*, **234**, 528.

Underhill, A.B. 1979c, *Astrophys. J (Letters)*, **235**, L149.

Underhill, A.B. 1980a, *Astrophys. J.*, **239**, 220.

Underhill, A.B. 1980b, *Astrophys. J.*, **240**, L153.

Underhill, A.B. 1980c, unpublished results.

Underhill, A.B. 1981a, *Astrophys J.*, **244**, 963.

Underhill, A.B. 1981b, *Astron Astrophys.*, **97**, L9.

Underhill, A.B., Leckrone, D.S., and West, D.K. 1972, *Astrophys. J.*, **171**, 63.

Underhill, A.B., and Fahey, R.P. 1973, *Astrophys J. Supplement*, **25**, 463.

Underhill, A.B., Fahey, R.P., and Klinglesmith, D.A. 1975, *Astrophys. J.*, **197**, 393.

Underhill, A.B., and Silversmith, E. 1976, *Astrophys. J.*, **206**, 156.

Underhill, A.B., and Adelman, S.J. 1977, *Astrophys. J. Supplement*, **34**, 309.

Underhill, A.B., and van der Hucht, K.A. 1977, *Astron. Astrophys* , **54**, 393.

Underhill, A.B., Divan, L., Prévot-Burnichon, M.-L., and Doazan, V. 1979, *Mon Not Roy Astr. Soc.*, **189**, 601, and Microfiche MN 189/1.

Underhill, A.B., and Divan, L. 1983, *O, Of, and Wolf-Rayet Stars*, to be published.

Unno, W., Osaki, Y., Ando, H., and Shibahashi, H. 1979, *Nonradial Oscillations of Stars* (Tokyo: Tokyo Univ. Press).

Unsold, A. 1942, *Zeit f Astrophys.*, **21**, 22.

Unsold, A. 1955, *Physik der Sternatmospharen* (Berlin: Springer-Verlag).

Upson, W.L., and Rogerson, J.B. 1980, *Astrophys J. Supplement*, **42**, 175.

Vaiana, G.S. 1981b, in *Proc. Eslab Conference* (Amsterdam), in press.

Vaiana, G.S., Cassinelli, J.P., Fabbiano, G., Giacconi, R., Golub, L., Gorenstein, P., Haish, B.M., Harnden, F.R., Johnson, H.M , Linsky, J.L , Maxson, C.W., Mewe, R., Rosner, R., Seward, F., Topka, K , and Zwaan, C. 1981, *Astrophys J.*, **245**, 163.

Vaiana, G.S., and Rosner, R. 1978, *Ann Rev. Astron. Astrophys.*, **16**, 393.

van Blerkom, D. 1970, *Mon. Not. Roy Astr. Soc.*, **149**, 53.

van Blerkom, D. 1978, *Astrophys. J.*, **221**, 186

van den Bergh, S., 1972, *Nature*, **235**, 273

van Duinen, R.J., Aalders, J.W.G., Wesselius, P.R., Wildeman, K.H., Wu, C.C., Luinge, W., and Snel, D. 1975, *Astron. Astrophys* , **39**, 159.

van Helden, R. 1972, *Astron. Astrophys.*, **19**, 209.

van Schewick, H. 1968, *Zeit f Astrophys.*, **68**, 229.

Vilhu, O. 1978, *Inf. Bull Var Stars*, No 1378.

Vilhu, O., Tuominen, I.V., and Boyarchuk, A.A. 1976, in *Physics of Ap Stars*, ed. W.W. Weiss, H. Jenker, and H.J. Wood (Vienna Univ. Sternw.), p 563.

Vrba, F.J. 1975, *Astrophys J.*, **195**, 101.

Wackerling, L.R. 1970, *Mem Roy Astron. Soc.*, **73**, 153.

Wackerling, L.R. 1972, *Pub. Astron. Soc. Pacific* , **84**, 827.

Wade, C.M., and Hjellming, R.M. 1971, *Astrophys. J. (Letters)*, **163**, L105.

Walborn, N.R. 1971, *Astrophys. J Supplement*, **23**, 257

Walborn, N.R. 1972, *Astron. J.*, **77**, 312.

Walborn, N.R. 1973, *Astron. J* , **78**, 1067.

Walborn, N.R. 1974, *Astrophys. J (Letters)*, **191**, L95

Walborn, N.R. 1975, *Pub Astron. Soc Pacific*, **87**, 613.

Walborn, N R 1976, *Astrophys. J.*, **205**, 419

Walborn, N.R., and Hesser, J.E. 1976, *Astrophys. J (Letters)*, **205**, L87.

Walker, M F 1953, *Astrophys. J.*, **118**, 481

Walker, H.J., and Kilkenny, D. 1980, *Mon. Not. Roy. Astr. Soc.*, **190**, 299.

Wallerstein, G 1971, *Pub. Astron. Soc. Pacific*, **83**, 664.

Warren, W H. 1976, *Mon Not. Roy. Astr Soc.*, **174**, 111.

Watson, R D. 1971a, *Astrophys J.*, **169**, 343.

Watson, R D. 1971b, *Astrophys J* , **170**, 345.

Watson, R.D. 1972, *Astrophys J Supplement*, **24**, 167.

Weber, S.V., Henry, R.C., and Carruthers, G.R. 1971, *Astrophys J* , **166**, 543.

Wellman, P. 1952, *Z. f Astrophys.*, **30**, 7.

Wendker, H.J , Baars, J.W M., and Altenhoff, W.J. 1973, *Nature, Phys Sci.*, **245**, 118.

Wesselius, P R , van Duinen, R.J., Aalders, J.W.G., and Kester, D 1980a, *Astron Astrophys* , **85**, 221.

Wesselius, P R , van Duinen, R.J., and de Jonge, A.R.W. 1980b, *A Catalogue of ANS Observations* (The Netherlands Space Research Dept , Univ. of Groningen)

White, N.E , Mason, K.O., Sanford, P.W , and Murdin, P 1976, *Mon Not. Roy Astron. Soc.*, **176**, 201.

White, N.E , Mason, K.O., and Sanford, P W. 1977, *Nature*, **267**, 229.

Williams, E G. 1934, *Astrophys J* , **79**, 280

Williams, I.P 1967, *Mon. Not Roy Astr Soc* , **136**, 341.

Willis, A.J , and Wilson, R 1975, *Astron Astrophys.*, **44**, 205.

Willis, A.J., and Wilson R. 1977, *Astron Astrophys* , **59**, 113.

Wilson, O C. 1935, *Astrophys J* , **82**, 233.

Winzer, J.E. 1974, *Astron. J* , **79**, 45

Wolf, B., and Appenzeller, I 1979, *Astron Astrophys* , **78**, 15

Wolf, R.E A. 1973, *Astron Astrophys.*, **26**, 127.

Wolff, R.J., and Wolff, S.C. 1976, *Astrophys J* , **203**, 171

Wolff, S.C 1983, *A Stars*, to be published.

Wolff, S C., Kuhi, L.V , and Hayes, D.S. 1968, *Astrophys. J* , **152**, 871.

Wolff, S C , and Morrison, N.D. 1974, *Pub Astron. Soc. Pacific*, **86**, 935

Wolff, S.C., and Wolff, R.J. 1976, in *Physics of Ap Stars*, ed. W W. Weiss, H. Jenker, and H.J. Wood (Vienna Univ. Sternw.), p 503.

Woodsworth, A W., and Hughes, V.A 1977, *Astron. Astrophys.*, **58**, 105.

Woolf, N J., Stein, W.A., and Strittmatter, P.A. 1970, *Astron. Astrophys.*, **9**, 252.

Wright, A E , and Barlow, M.J. 1975, *Mon. Not. Roy. Astr Soc.*, **170**, 41.

Wright, K.O , Lee, E K , Jacobson, T.V., and Greenstein, J.L 1964, *Pub Dom. Astrophys Obs* , **12**, 173.

Zellner, B., and Serkowski, K. 1972, *Pub. Astron. Soc Pacific.*, **84**, 619.

Zirker, J B. 1981, in *The Sun as a Star*, ed. S. Jordan, NASA SP-450, p. 135.

INDEX

Page intentionally left blank

Page intentionally left blank

LIST OF CONTRIBUTING AUTHORS

Morris L. Aizenmann *Division of Astronomical Science*
National Science Foundation
1800 G Street, N.W.
Washington, D.C. 20550

Vera Doazan *Observatoire de Paris*
61 Ave. de L'Observatoire
75014 Paris, France

Janet Rountree Lesh *Laboratory for Astronomy and Solar Physics*
Goddard Space Flight Center
Greenbelt, Maryland 20771

Richard N. Thomas *Institut d'Astrophysique*
98 bis, Boulevard Arago
75014 Paris, France

Anne B. Underhill *Laboratory for Astronomy and Solar Physics*
Goddard Space Flight Center
Greenbelt, Maryland 20770

National Aeronautics and
Space Administration

Washington, D.C.
20546

Official Business
Penalty for Private Use, $300

SPECIAL FOURTH CLASS MAIL
BOOK

Postage and Fees Paid
National Aeronautics and
Space Administration
NASA-451

NASA

POSTMASTER: If Undeliverable (Section 158
Postal Manual) Do Not Return